CYCLOTRONS 2010

The 19th International Conference on Cyclotrons and their Applications

CYCLOTRONS 2010

September 6 - 10, 2010, Lanzhou, P.R.China

• Topics

- Cyclotron applications
- Facilities under construction
- High beam intensity operation
- Ion sources , strippers and targets
- Beam transport, diagnostics and control system
- Newly operating cyclotrons
- Projects and proposals
- Radioactive beams
- Radio frequency systems
- Operational cyclotrons: developments and status
- FFAG accelerators
- Beam dynamics
- Magnet and vacuum

• International Organizing Committee

P.Bertrand, GANIL; R. Bhandari, VECC; S.Brandenburg, KVI; L.Calabretta, INFN-LNS; J. Conradie, iThemba LABS; M. Craddock, TRIUMF; G.Dutto, TRIUMF; S.Gales, GANIL; K. Hatanaka, RCNP; P. Heikkinen, JYFL; Y. Hirao,NIRS; Y.Jongen,IBA; M. Loiselet,UCL; C.Lyneis, LBNL; R. Maier, FZ-JüLICH; F.Marti, NSCL/MSU; D.May, TEXAS A&M UNIV; Y.Mori, Kyoto Univ; L.Onischenko,JINR; H.Schweickert,FZK; M. Seidel,PSI; Y.Yano, RIKEN; W. L. Zhan, IMP (Chairman)

• Program Committee

P. Bertrand,GANIL; S.Brandenburg, KVI; L.Calabretta, INFN-LNS; M. Craddock, TRIUMF; A.Goto,RIKEN; Y.Jongen,IBA; C.Lyneis, LBNL; F.Marti, NSCL/MSU; Y.Mori, Kyoto Univ; M.Seidel, PSI; W. L. Zhan, IMP; T.J. Zhang, CIAE; H.W. Zhao, IMP(Chairman)

• Local Organizing Committee

X.H.Cai; H.LChen; H.F. Hao; Y.He; Z.G.Hu; Q.Liang(Secretary); Y.Liu; L.J. Mao(Scientific secretary); M.T. Song; B.Wang; J.W.Xia; M.Xie; Z.Xu; H.W.Zhao; X.D.Yang; Y.J.Yuan(Chairman)

Http: //cyclotrons10. impcas. ac. cn
Email: cyclotrons@impcas.ac.cn
Tel: 86-931-4969210/221
Fax: 86-931-8272100
Hosted by: Institute of Modern Physics (IMP), Chinese Academy of Sciences

Preface

The 19th International Conference on Cyclotrons and their Applications, CYCLOTRONS'10, was organized and hosted by Institute of Modern Physics (IMP), Chinese Academy of Sciences in Lanzhou, P.R.China. This Conference was held in the Ning-Wo-Zhuang Hotel of Lanzhou, China, on September 6-10, 2010. It's the first time for a conference of this series held in China. We would like to express our hearty thanks to all the participants.

This conference was attended by 170 participants from 21 countries. About 144 contributions were presented in talks, including 31 invited oral reports, 21 contributed oral reports and 92 posters. All the contributions were structured in 16 sessions with two sessions in the morning and two sessions in the afternoon, which was very compact. And the poster session was on the first two days with two hours each day.

The contributions in this conference covered most of the hot spot and frontier problems on cyclotrons and their applications, for example, FFAG accelerators and high beam intensity operation. Furthermore, the development and status of some operational cyclotrons, as well as newly operating cyclotrons and those facilities under constructions were also presented. Beyond these, more detailed topics were discussed in this conference, such as radioactive beams, beam dynamics, ion source, strippers and targets, radio frequency systems, magnet and vacuum, beam transport, diagnostics and control and so on.

Besides the significant scientific program of the conference, a reception evening in Ning-Wo-Zhuang Hotel, a conference banquet near the Yellow River, a technical tour of IMP facilities and a half day excursion to Water Wheel Park were also given. All this activities not only provided participants a well comfortable environment to relax themselves, but a further extension for free discussion.

The organizers would like to thank IMP, National Natural Science Foundation of China, Chinese Academy of Sciences, Thamway Co.Ltd (Japan) and Sumitomo Heavy Industries, Ltd (Japan) for sponsoring this conference.

Special thanks should be given to the conference secretaries Qiang Liang, Lijun Mao, Xiaohong Cai, Zhenguo Hu, Xiaodong Yang, Honglian Chen, Jinjie Liang, who prepared and managed the conference with high efficiency and great enthusiasm. Great thanks go to the editors Youjin Yuan, Lijun Mao and Lina Sheng for successfully applying the Scientific Programme Management System (SPMS) of Joint Accelerator Conference Website (JACoW) for the processing and publication of the conference and for their editorial work.

Chair: Wenlong Zhan
Co-Chair: Hongwei Zhao

September 06, 2010

Contents

International Program Committee

Patrick Bertrand	Grand Accëlërateur Nat. d'Ions Lourds (GANIL)
Rakesh Kumar Bhandari	Department of Atomic Energy (DAE/VECC) Variable Energy Cyclotron Centre
Sytze Brandenburg	Kernfysisch Versneller Instituut (KVI) Rijksuniversiteit Groningen
Luciano Calabretta	Istituto Nazionale di Fisica Nucleare (INFN/LNS) Laboratori Nazionali del Sud
Jacobus Conradie	iThemba LABS
Michael Craddock	TRIUMF Canada's National Laboratory for Particle and Nuclear Physics
Gerardo Dutto	TRIUMF Canada's National Laboratory for Particle and Nuclear Physics
Sydney Gales	Grand Accëlërateur Nat. d'Ions Lourds (GANIL)
Kichiji Hatanaka	Osaka University (RCNP) Research Center for Nuclear Physics
Pauli Heikkinen	University of Jyvaskyla (JYFL) Department of Physics
Yasuo Hirao	National Institute of Radiological Sciences (NIRS) Division of Accelerator Physics and Engineering
Yves Jongen	Ion Beam Applications SA (IBA)
Marc Loiselet	University College London (UCL) Department of Physics and Astronomy
Claude M Lyneis	Lawrence Berkeley National Laboratory (LBNL)
Rudolf Maier	Institut für Kernphysik, Forschungszentrum Jülich (FZJ)
Felix Marti	Michigan State University Cyclotron Laboratory (NSCL) Michigan State University (MSU)
Donald Philip May	Texas A&M University Cyclotron Institute
Yoshiharu Mori	Kyoto University Research Reactor Institute (KURRI)
Leonid Onischenko	Joint Institute for Nuclear Research (JINR/DLNP) Dzhelepov Laboratory of Nuclear Problems
Hermann Schweickert	Forschungszentrum Karlsruhe GmbH (FZK) Institute for Synchrotron Radiation
Mike Seidel	Paul Scherrer Institute (PSI)
Yasushige Yano	RIKEN Nishina Center
Wenlong Zhan	Chinese Academy of Sciences Institute of Modern Physics (IMP,CAS)

Local Organizing Committee

Youjin Yuan (Chairman)	Institute of Modern Physics (IMP,CAS)
Qiang Liang (Secretary)	IMP,Lanzhou,China
Xiaohong Cai (STD)	IMP,Lanzhou,China
Zhengguo Hu (STD)	IMP,Lanzhou,China
Honglian Chen (STD)	IMP,Lanzhou,China
Lijun Mao (Sci. Secretary)	IMP,Lanzhou,China
Lina Sheng (Editor)	IMP,Lanzhou,China
Hongwei Zhao	IMP,Lanzhou,China
Jiawen Xia	IMP,Lanzhou,China
Ming Xie	IMP,Lanzhou,China
Xiaodong Yang	IMP,Lanzhou,China
Mingtao Song	IMP,Lanzhou,China
Yuan He	IMP,Lanzhou,China
You Liu	IMP,Lanzhou,China
Bing Wang	IMP,Lanzhou,China
Zhe Xu	IMP,Lanzhou,China
Huanfeng Hao	IMP,Lanzhou,China

The 19th International Conference on Cyclotrons and Their Applications
9. 6. 2010 lanzhou


The 19th International Conference on Cyclotrons and Their Applications


The 19th International Conference on Cyclotrons and Their Applications


The 19th International Conference on Cyclotrons and Their Applications

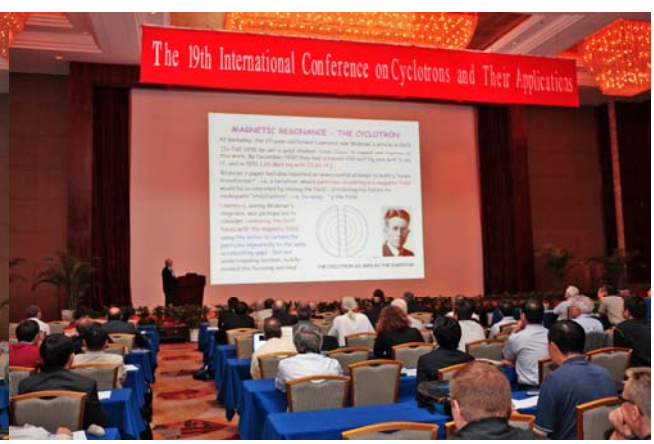
The 19th International Conference on Cyclotrons and Their Applications


The 19th International Conference on Cyclotrons and Their Applications
Cast steel for the top/bottom yokes and return yoke were accomplished in 2008.
The yokes are formed from 5 pots molten steel pouring together.


The 19th International Conference on Cyclotrons and Their Applications
4th Generation ECR Ion Source

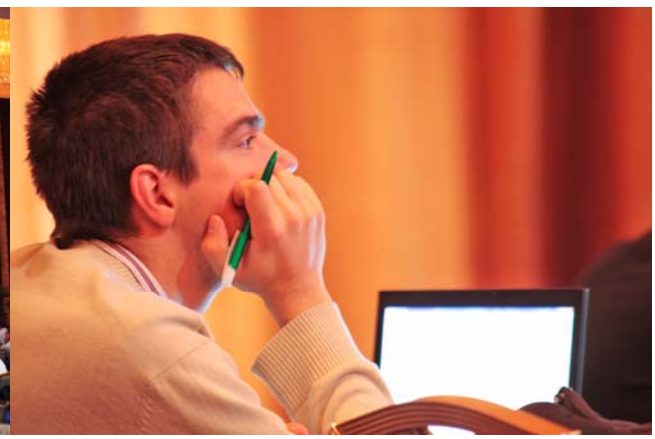

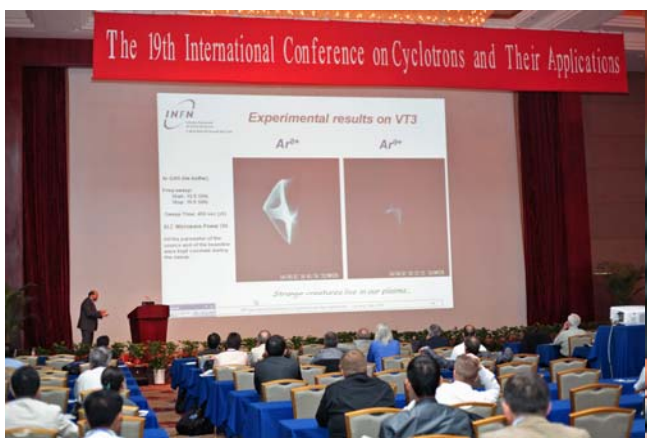
The 19th International Conference on Cyclotrons and Their Applications
INFN
Experimental results on VT3


The 19th International Conference on Cyclotrons and Their Applications


The 19th International Conference on Cyclotrons and Their Applications


The 19th International Conference on Cyclotrons and Their Applications
Multi-Gradients Method
Layout


The 19th International Conference on Cyclotrons and Their Applications
Dose delivery techniques: Depth


The 19th International Conference on Cyclotrons and Their Applications
ISAC RIB Facility - 2001




























Uniqu driver for dev
Un er for stu


上迷真
下怪美




large extent by
yclotron SC ma






SERVICE
PANTECH


Micromatter ™
μm


cromatter ™
μm
stom Coating Services
OMATTER™ provides
m coating services for









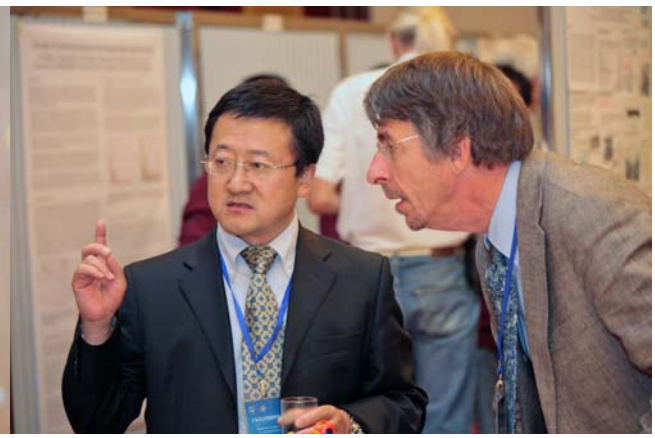
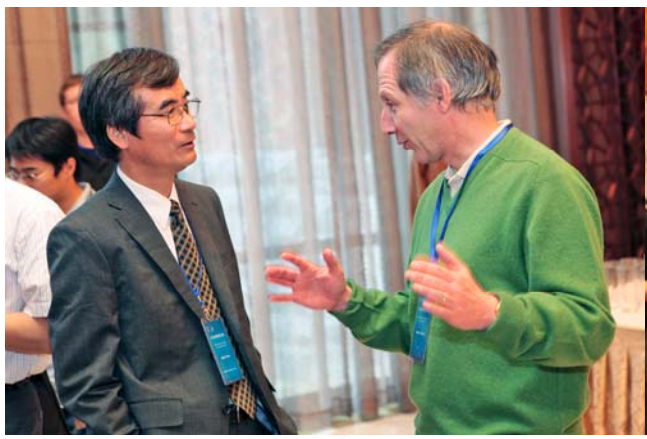



matter ™
μm
tion Standards
onitoring agencies
ve manufacturers
l laboratories


ating Services
ring agencies
facturers
tories

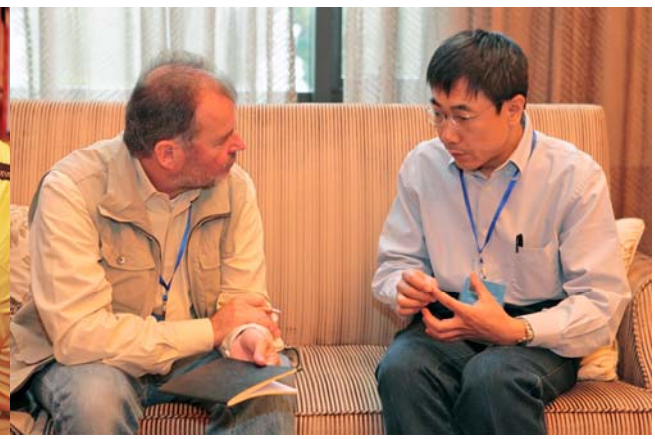


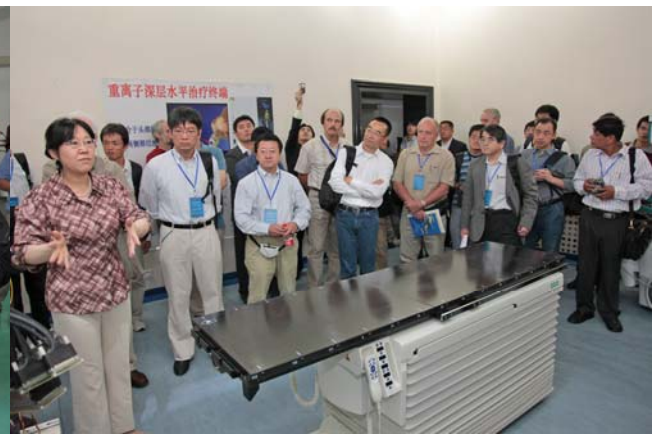
重离子深层水平治疗终端

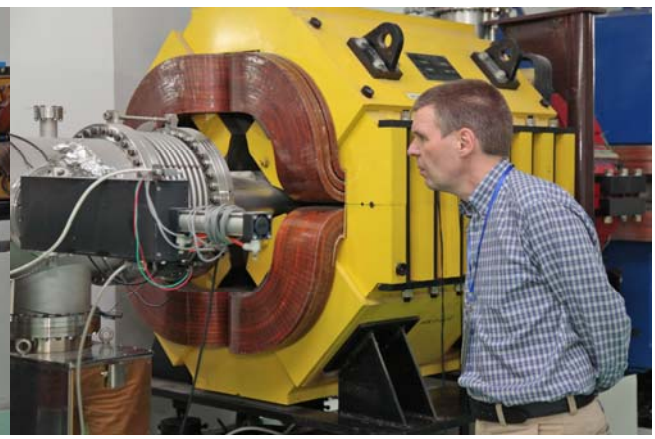
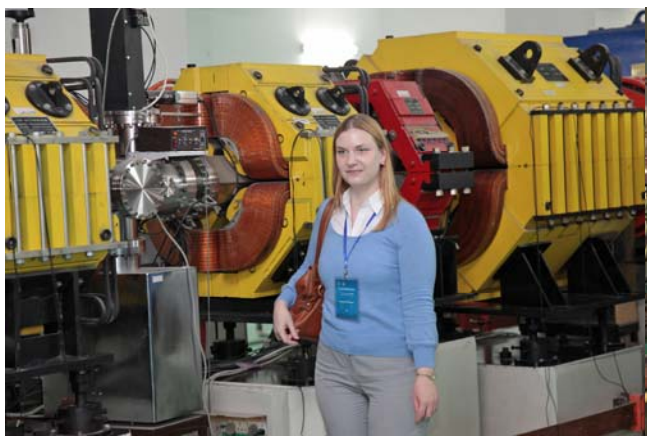
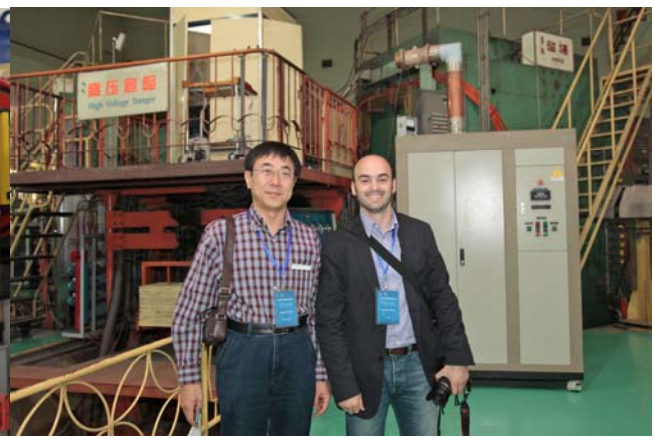
高压舱室
High Voltage Tamper
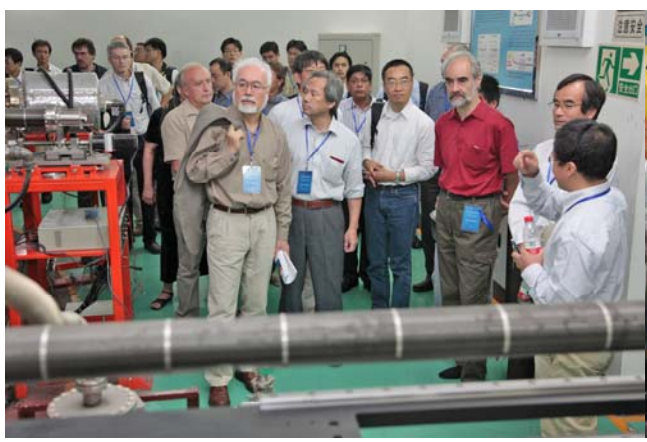


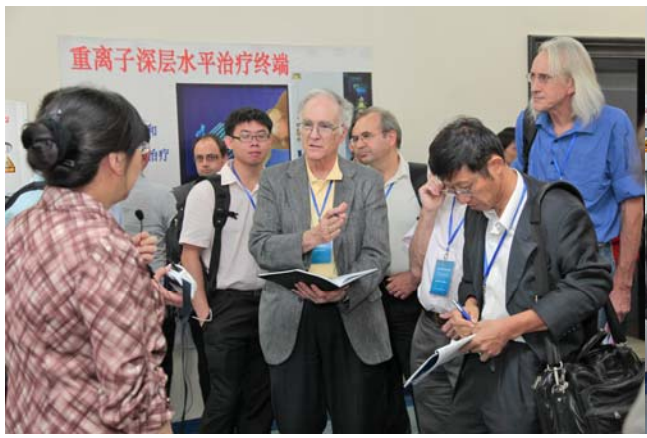
重离子深层水平治疗终端

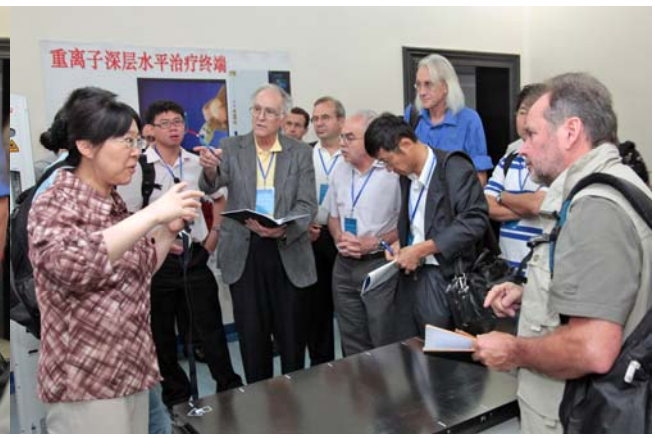
重离子深层水平治疗终端

EIGHTY YEARS OF CYCLOTRONS

M.K. Craddock, University of British Columbia and TRIUMF, Vancouver, B.C., Canada

Abstract

Lawrence's invention of the cyclotron in 1930 not only revolutionized nuclear physics, but proved the starting point for a whole variety of recirculating accelerators, from microtrons to FFAGs to synchrotrons, that have had an enormous impact in almost every branch of science and several areas of medicine and industry. Cyclotrons (i.e. fixed-field accelerators) themselves have proved remarkably adaptable, incorporating a variety of new ideas and technologies over the years: frequency modulation, edge focusing, AG focusing, axial and azimuthal injection, ring geometries, stripping extraction, superconducting magnets and rf... Long may they flourish!

INTRODUCTION

It was 80 years ago this month that Ernest Lawrence [1] first announced successful tests of a "magnetic resonance accelerator" - what was later to become known by its nickname "cyclotron". We can also celebrate the round-number anniversaries of a couple of cyclotron family members (counting from experimental demonstration):

- 60 years of isochronous cyclotrons (1950)
- 10 years of proton FFAGs (2000).

In the space available it's been impossible to do justice to the achievements of the whole 80 years at the same level of detail. Instead, I will concentrate on the earlier, perhaps less familiar, years, and only mention highlights from the later ones. For those seeking more detail, I recommend my sources [2-7] and also [8].

INVENTION

Lawrence had moved from Yale to Berkeley in 1928, hoping to advance from research on the photoelectric effect to nuclear physics – the exciting new field promised by Rutherford's 1919 Manchester discovery that nuclear reactions could be induced by MeV particles – and especially exciting if radioactive sources could be replaced by intense beams accelerated artificially!

In the 1920s dc voltages >200 kV were hard to produce and control. But perhaps energy could be added in a series of low-voltage steps, using pulsed or ac voltages, synchronized to the particle's arrival at the accelerating gaps: "resonance acceleration"?

The first such proposal, by Gustav Ising in Stockholm (1924), was to feed high-voltage pulses by transmission line to a series of drift tubes. But nothing was built, and publication in Swedish had little impact. His work was however noted by a Norwegian grad student in Germany, Rolf Widerøe, who in 1928 built a two-gap linac powered by a 1-MHz 25-kV oscillator, accelerating Na^+ and K^+ ions to ~50 keV [9]

At Berkeley, the 27-year-old Ernest Lawrence came across Widerøe's article in 1929. Interestingly, the paper had also reported an unsuccessful attempt to build a "beam transformer" - i.e. a betatron, where particles circulating in a magnetic field would be accelerated by raising the field – attributing his failure to inadequate "stabilization" – i.e. focusing – by the field. Perhaps this juxtaposition led Lawrence to consider combining the drift tubes with the magnetic field, using the latter to return the particles repeatedly to the same accelerating gaps - but not understanding German, he luckily missed the focusing caveat.

When Lawrence worked out the dynamics, he found an unexpectedly favourable result: for a particle with mass *m*, charge *q*, moving with velocity **v** normal to uniform magnetic induction **B**, the Lorentz Force $\mathbf{F} = q\,\mathbf{v} \times \mathbf{B}$ produces a circular orbit, and

$$q \cancel{r}\omega B = m \cancel{r}\omega^2 = m\omega.$$

"*r* cancels *r*", as Lawrence explained excitedly to each of his students, so that the "cyclotron frequency" is independent of *v* and the orbits are "isochronous":

$$\omega = \frac{qB}{m}$$

The electrodes can therefore be excited at a fixed rf frequency, the particles will remain in resonance throughout acceleration, and a new bunch can be accelerated on every rf voltage peak, allowing continuous-wave (cw) operation. Also radius is directly proportional to velocity: $r = mv/qB$.

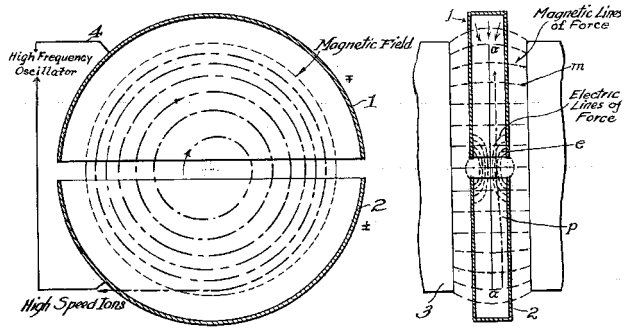

Figure 1: The cyclotron concept, from Lawrence's patent.

Early in 1930 Lawrence persuaded Nels Edlefsen, who had just completed his Ph.D., to join him in experimental work. Two rather crude models were built, one with dees formed by silvering a flattened glass flask, the other with copper "duants". They observed signals on a detector at the outer edge, though no definite resonance, but by September felt able to publish an optimistic report [1].

That month two new students arrived: Dave Sloan, who was set to work on a linac (and by December had achieved 200-keV Hg ions with 11-kV rf, and in 1931 1.26-MeV Hg with 25-kV rf), and Stanley Livingston, on the cyclotron. He also had rapid success, building a new all-brass 4-inch model (Figure 2), finding clear evidence of magnetic resonance in November, and 13-keV protons. By January 1931 Lawrence had obtained a stronger magnet and the energy was raised to 80 keV.

Figure 2: The 4-inch cyclotron vacuum chamber, showing the single dee, the deflector, and G. Seaborg's left hand.

Several people had considered the cyclotron idea before Lawrence: Gabor (1924), Flegler (1926, discouraged by Widerøe's doubts about orbit stability), Steenbeck (1927) – but none had published or built anything. Szilard filed a patent (1929), but the only experimental work was by Thibaud in Paris following Lawrence's publication, and he did not report any success. The credit for an invention does not lie just in having an idea - but in going on to show that it works! On that basis, Lawrence's claim is secure - an important one, as the cyclotron principle is the basis of all circular accelerators except the betatron.

EARLY CLASSICAL CYCLOTRONS

In what became a familiar style, Lawrence quickly moved to acquire larger and stronger magnets. First came the 11-inch (referring to the pole diameter), with which he and Livingston were able to achieve a world-record of 1.22-MeV protons in January 1932. Interestingly, their publication [10] shows a clear understanding of the importance of axial focusing, and how the magnetic and electric fields provide it (*cf.* Figure 1). But with no nuclear physics experience, in April 1932 they lost the race for nuclear disintegration to Cockroft and Walton, who had used a mere 600-keV cascade generator.

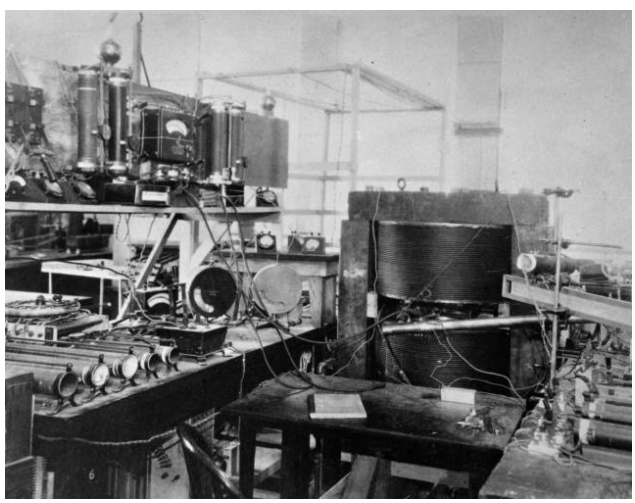

Figure 3: The 11-inch cyclotron and lab bench equipment.

This was followed in 1933 by the 27-inch, based on a war-surplus Federal Telegraph Co. Magnet, (Figure 4) which by 1936 was producing 20-μA beams of 6.3-MeV deuterons. A larger 37-inch pole was then installed, yielding 100-μA beams at 8.5 MeV in 1938. This was the workhorse for Berkeley nuclear physics in the 1930s, and also the provider of radioisotopes as tracers for novel studies in chemistry, botany, zoology and medicine - and for medical treatments too, led by Lawrence's brother John. In 1938 it could be claimed that "More new isotopes have been made artificially than occur in Nature".

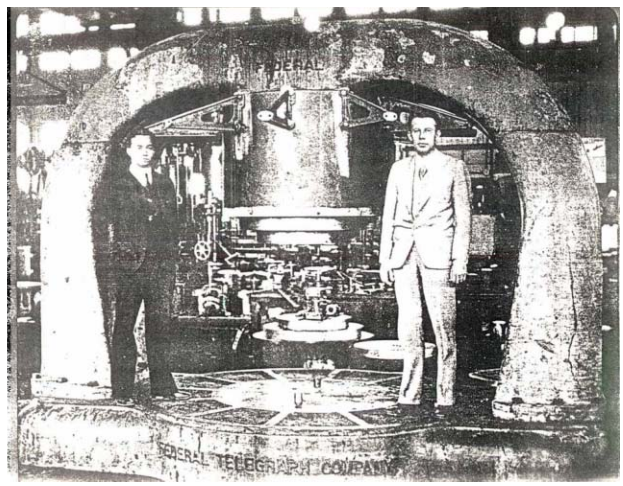

Figure 4: Livingston (left) and Lawrence with the 27-inch (later 37-inch) cyclotron.

The medical work got results. A local philanthropist helped to fund the Crocker Medical Laboratory and cyclotron – a 200-ton 60-inch machine that by 1940 was yielding 200-μA beams of 16-MeV deuterons. Not only was the nuclear physics reach extended (it produced the first six transuranic elements) but the first neutron therapy program was established, with ~200 patients being treated.

Figure 5: Setting up a patient for neutron therapy.

Berkeley's success of course led to interest elsewhere. By 1940 there were 24 cyclotrons operating in the U.S., 3 in Japan, 2 each in Britain and the USSR, and one each in Denmark, France, Germany and Sweden.

The late 1930s yielded a firmer theoretical understanding of cyclotron beam dynamics. Rose [11] and Wilson [12] almost simultaneously produced analyses of the axial focusing provided by the electric and magnetic fields. For the latter, *H(r)*, each of them showed that the axial tune (as it was later named) is given by:

$$\nu_z = \sqrt{-\frac{r}{H}\frac{\partial H}{\partial r}}.$$

Radial motion was apparently of no concern. If they had treated that as well, maybe today we'd be speaking of "cyclotron oscillations", not "betatron oscillations".

Bethe and Rose [13] also studied the effect on the longitudinal motion of an ion's relativistic increase in mass as it gains energy. They concluded that the phase drift resulting from the drop in angular frequency ω would limit deuteron energies to $8\sqrt{[V(\text{kV})/50]}$ MeV. Buoyed up by a Nobel Prize, Lawrence's plans for a huge 184-inch cyclotron were unaffected – he would just run the dees at 1 or 2 MV – and work began on the 4,300-ton magnet.

Figure 6: The 184-inch magnet with the UCRL staff.

SYNCHROCYCLOTRONS

World War II did what Bethe couldn't, though, and prevented installation of the vacuum tank and rf. By its end Veksler and MacMillan had proved that phase stability was possible for a changing rf frequency, and the way was open to try doing that so as to match the decreasing ω of an accelerating ion. This was first tried by Richardson, Mackenzie *et al.* [13] in 1946, by shimming the 37-inch magnet to simulate the frequency drop expected for deuterons being accelerated to 200 MeV, and installing frequency-modulated rf. When told of their success, Reg Richardson recalled [4], Lawrence "... rushed out... and [seeing] a truck carrying one of the huge dee stems necessary for 1 MV....told the driver to turn around and take the tank back to storage – or maybe the dump!"

The rf system for the 184-inch was immediately redesigned and by the end of 1946 it had been brought into operation as a synchrocyclotron, delivering 190-MeV deuterons, 380-MeV alphas and (later) 350-MeV protons - revolutionary steps in ion energy. The 37-inch was also fully converted to operate as a synchrocyclotron, and was later moved to UCLA.

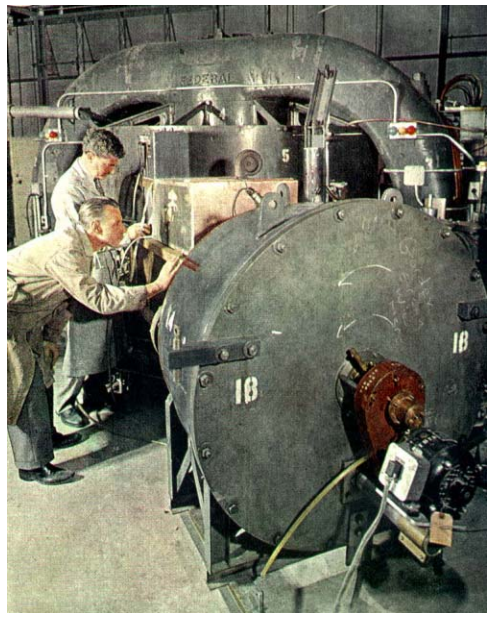

Figure 7: Lawrence and Richardson (rear) with the 37-in., showing the large rotating capacitor for fm operation.

The high energies they made available, together with their ease of operation, led to 10 more large synchrocyclotrons being built from 1946-54 (Table 1). They made possible controlled experiments with pions and muons, opening up the new field of particle physics. They also provided the first programmes of ion beam therapy, which was pioneered at Berkeley (1952), Uppsala (1954) and Harvard (1961). The price for their high energies, though, was pulsed operation and low (<1 μA) intensities, so that, for physics research at least, the advent of cw isochronous cyclotrons left them uncompetitive,

Table 1: Large synchrocyclotrons

Institute	Pole diameter (m)	Magnet wt. (t)	Proton energy (MeV)	Date first operated
UCRL Berkeley	4.70	4300	350	1946
			740	1957
U. Rochester	3.30	1000	240	1948
Harvard U.	2.41	715	160	1949
AERE Harwell	2.80	660	160	1949
Columbia U.*	4.32	2487	380/560*	1950
McGill U.	2.29	216	100	1950
U. Chicago	4.32	2200	450	1951
GWI Uppsala*	2.30	650	187	1951
Carnegie I.T.	3.61	1500	450	1952
U. Liverpool	3.96	1640	400	1954
LNP Dubna*	6.00	7200	680	1954†
CERN Geneva	5.00	2560	600	1958
NASA SREL	5.00	2765	590	1965
PNPI Gatchina	6.85	7874	1000	1967†
IPN Orsay	3.20	927	200	1977†

* Later modified with spiral sectors. † Still in operation

ISOCHRONOUS CYCLOTRONS

Back in 1938 Llewellyn Thomas [14] (reacting to Bethe's predicted energy limit) had pointed out a way to allow cyclotrons to be run isochronously (and thus with intense cw beams) at relativistic energies: the axial (z) defocusing associated with rising field $\langle B_z \rangle = \gamma B_0$ (and field index $k = -\beta^2\gamma^2$) may be countered by an azimuthally varying field (AVF)

$$B_z(\theta) = \langle B_z(\theta) \rangle (1 + f \cos N\theta).$$

This produces a non-circular 'scalloped' orbit, and a $qvrB_\theta$ component of F_z, everywhere a restoring force, to counter the defocusing $qv_\theta B_r$ (though unstable for $N < 3$):

$$\nu_z^2 = -\beta^2\gamma^2 + \tfrac{1}{2} f^2$$

- a simple result arising from some intimidating algebra.

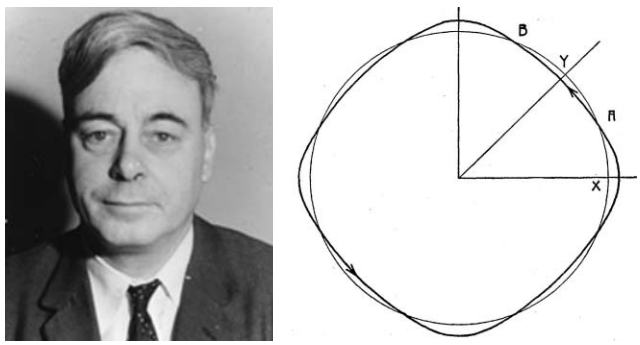

Figure 8: Left: L.H. Thomas; Right: Scalloped orbits.

Thomas's idea was neglected for 12 years, possible reasons being the perceived difficulty of creating pure $cosN\theta$ fields, the onset of World War II, and the success of synchrocyclotrons. But in 1950 an apparent lack of uranium reserves led to a crash US program to breed fissile isotopes by neutron irradiation. The Livermore Materials Test Accelerator was to be a 350-MeV, 500-mA cw deuteron linac (and estimated to cost $300M). Alvarez built Mark I, the first 18-m-diameter 18-m-long section (the biggest vacuum tank ever?), achieving 50 mA at 10 MeV in 1953, with 18 MW rf.

Back at Berkeley, Richardson argued that a 300-MeV Thomas cyclotron could be built at much lower cost. In 1950, he and some colleagues built two 3-sector electron models [15] (Figure 9). Like classical cyclotrons they required very precise shaping of the magnetic field, but 54 circular trim coils enabled this to be done more efficiently than with clumsy steel shims. Electrons were successfully accelerated to $\beta = 0.5$ (the same as 300-MeV deuterons) and extracted with 90% efficiency – but the work was not declassified till 1956.

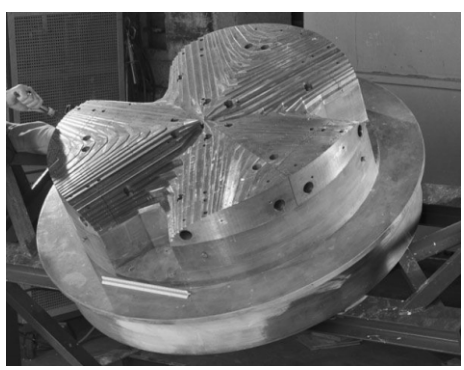

Figure 9: Reg Richardson and one pole of the second electron model, showing the harmonically-contoured hills.

Radial-sector Cyclotrons

Several classical cyclotrons were modified with radial sectors in the 1950s to provide stronger axial focusing and higher beam intensity (Los Alamos, MIT,..) - but were not made isochronous. The first sector-focused ion cyclotron was completed by Heyn and Khoe at Delft in 1958 [16]. It had 4 sectors, a pole diameter of 86 cm and a top proton energy of 12.7 MeV. The hill pole-tips were carefully shaped (Figure 10).

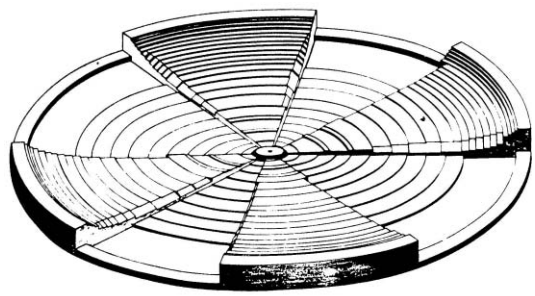

Figure 10: Hill and valley "shims" on the Delft cyclotron.

Others quickly followed (Table 2). Notice that their energies are limited to ~50 MeV/u by the difficulty of achieving high flutter in a compact magnet. To reach higher energies for physics research, designers turned to spiral sectors. Nevertheless, there has proved to be an enormous market for low-energy cyclotrons for radio-isotope production for industry and medicine. Over 300 radial-sector cyclotrons are now installed around the world, produced by at least 8 companies.

Table 2: Early radial-sector cyclotrons.

Location	Pole diameter (m)	Sectors	Energy (MeV/u)	First beam
Delft	0.86	4	12.7 (p)	1958
Birmingham	1.02	3	5.5 (d)	1961
Moscow	1.50	3	16 (d)	1961
Karlsruhe	2.25	3	25 (d)	1962
Orsay	1.20	3	17 (α)	1965
Milan	1.66	3	45 (H^-)	1965

Spiral-sector Cyclotrons

In 1955 Kerst [17] had suggested using spiral sectors to provide "strong" alternating edge focusing in FFAGs. His idea was quickly adopted for sectored cyclotrons. For an isochronous field the axial tune formula becomes:

$$\nu_z^2 = -\beta^2\gamma^2 + \frac{N^2}{N^2-1} F^2\left(1 + 2\tan^2\varepsilon\right)$$

where the magnetic flutter $F^2 \equiv \left\langle [B_z(\theta) - \langle B_z\rangle]^2 \right\rangle / \langle B_z\rangle^2$,

ε is the spiral angle, and there are N sectors. The powerful $2\tan^2\varepsilon$ term enhances the flutter focusing ×3 for ε = 45°. Spiralling is now used for most proton machines >40 MeV, and has allowed designs up to 12 GeV. The earliest spiral-sector cyclotrons are listed in Table 1.

Table 3: Early spiral-sector cyclotrons

Institute	Pole diameter (m)	Sectors	Max$^{m.}$ spiral	Energy (MeV)	Date first operated
UCLA	1.25	4	47°	50 H^-	1960
UCRL Berkeley	2.24	3	56°	60 p	1961
U. Colorado	1.32	4	45°	30 H^-	1962
Oak Ridge NL	1.93	3	30°	75 p	1962
U. Michigan	2.11	3	43°	37 p	1963
U. Manitoba	1.17	4	48°	50 H^-	1964
Michigan S.U.	1.63	3	10°	56 p	1965
V.U.Amst'dam	1.40	3	37°	33 p	1965
AERE Harwell	1.78	3	45°	53 p	1965

The first to come into operation was the UCLA 50-MeV cyclotron [18] (Figure 11), notable for its very compact design, its use of spiral in-valley rf electrodes, and adoption of Colorado's innovation of accelerating H^- ions [19], making it possible to extract the beam with 99% efficiency by stripping.

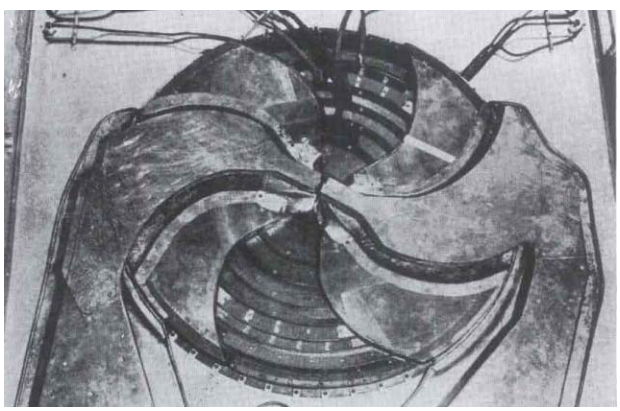

Figure 11: The UCLA 50-MeV cyclotron, with spiral dees.

The most relativistic spiral-sector cyclotron ever to operate was the Oak Ridge Analogue II [20] (Figure 12), an electron model for the proposed Mc^2 Cyclotron meson

Figure 12: The Oak Ridge Analogue II electron model.

factory, in which protons were to be accelerated to 810 MeV in an 8-sector magnet with 12-m diameter poles. In the model the electrons reached the corresponding energy of 465 keV (β = 0.86), and were extracted with 80% efficiency with the help of the ν_r = 2 resonance.

Isochronous cyclotrons have been remarkably receptive to adaptations, the most notable being:

- External injection of beam
- Injection or extraction by stripping
- Separate sector magnets
- Superconducting technology.

Axial injection, in particular, makes it possible to inject beams at low energy from the large or complex sources needed to produce negative, polarized or heavy ions. Two types of 90° electrostatic deflector were developed, the mirror inflector by Powell [21] in Birmingham (8-kV for 10-keV deuterons), and the spiral inflector by Belmont [22] in Grenoble (15-kV for 50-kV protons).

Stripping is an effective tool for both heavy ions and negative hydrogen ions. For H^- ions it not only makes possible very efficient extraction, but the extraction of multiple beams – a feature often employed in isotope-production cyclotrons. The TRIUMF 70-520 MeV cyclotron routinely extracts 3 beams simultaneously at different energies [23], and plans to add another (Figure 13).

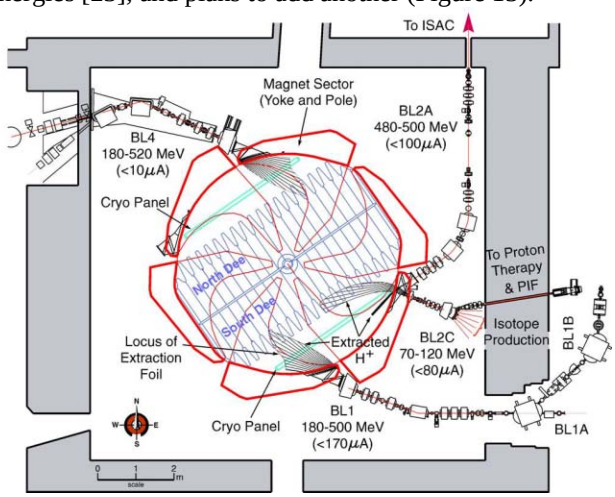

Figure 13: The TRIUMF cyclotron permits simultaneous extraction of four beams at different energies.

Separate-sector Ring Cyclotrons

This powerful concept was first proposed by Hans Willax [24] for the 590-MeV Swiss meson factory (Figure 14). Each sector magnet (hill) has its own yoke and coil, while the valleys are field-free and available for rf, injection, extraction and diagnostic equipment.

With small pole gaps the magnets are very efficient and produce hard-edge fields with flutter $F^2 \geq 1$, making it possible to reach $\beta\gamma \approx 1$ (≈400 MeV/u) with radial sectors. This has made the design popular for large heavy-ion cyclotrons, such as the Lanzhou K450 and the four at RIKEN, ranging from K540 to K2600 (the last with the additional novelty of using superconducting magnets).

In the case of PSI it was serendipitously found possible to obtain almost complete turn separation at extraction,

where $\nu_r \approx 1.5$, by using high energy-gain per turn with very short bunches, and injecting off centre. With 99.97% extraction efficiency, 2-mA external beams are routine, and 3-mA beams are planned. PSI's current 1.3-MW beam remains the world's most powerful.

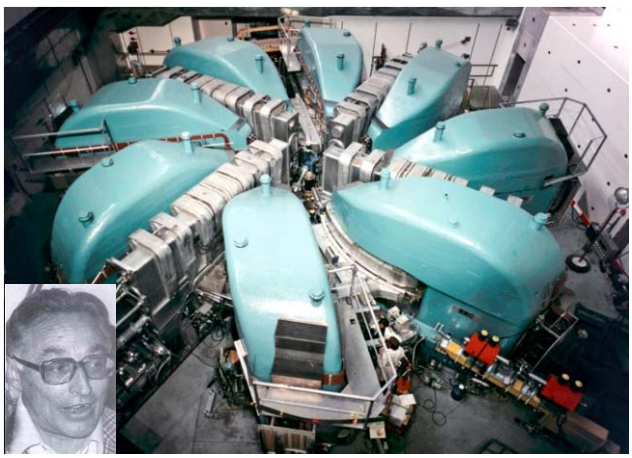

Figure 14: The PSI 590-MeV ring cyclotron, showing the 8 spiral magnets and four rf cavities. Inset: Hans Willax.

Compact Superconducting Cyclotrons

Superconducting coils can provide magnetic fields at least 3 times higher than those of conventional magnets, allowing the dimensions to be reduced by the same factor for a given ion momentum, and the cost even more (not to speak of the power bill). The pioneers responsible for this development were Bigham *et al.* [25] at AECL, Chalk River, and Blosser *et al.* [26] at MSU (Figure 15). The main coil is typically housed in an annular cryostat), while the conventional room-temperature components, including pole tips, rf accelerating system, vacuum system, and ion source, are inserted in the warm bore of the cryostat from top and bottom. The largest compact superconducting cyclotron, the K1200 at MSU, is only 2.9 m in overall diameter, but can accelerate heavy ions to energies as high as 200 MeV/u.

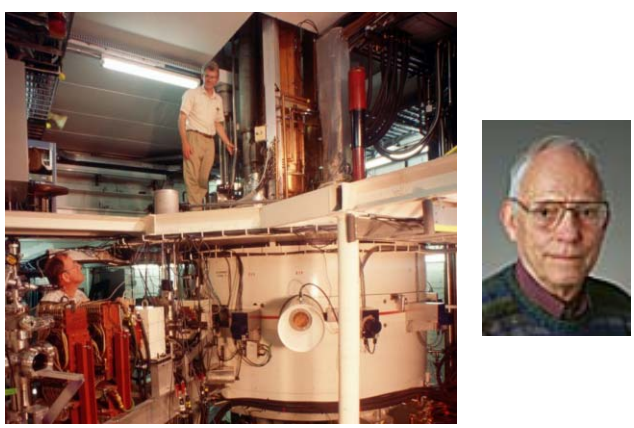

Figure 15: Left: The first superconducting cyclotron to operate, the MSU K500; Right: Henry Blosser.

Besides the several superconducting cyclotrons built for nuclear physics, an increasing number are being produced for particle therapy. The first was modest but innovative, a 50-MeV deuteron machine for neutron therapy, small enough to be mounted on a gantry and rotated around the patient. Now Varian-Accel produces a 250-MeV machine for proton therapy, while IBA's C400 will also deliver 400-MeV/u carbon ions.

Separated Orbit Cyclotrons

The separated-orbit cyclotron (SOC), in which the bending and focusing fields of the sector magnets are specially tailored for each orbit, was proposed by Russell [27] in the early 1960s for the acceleration of high-current (~50 mA) proton beams to GeV energies. Its complexity and cost, using normal magnets, deterred potential builders. However, a prototype superconducting SOC, the K85 TRITRON, was built and demonstrated in Munich [28]. This was the ultimate in superconducting cyclotron design, since the six rf accelerating cavities as well as the magnet were superconducting. The entire cyclotron was enclosed in a 3.5-m diameter vacuum chamber, with the vacuum being maintained by cryogenic pumping. The magnets were very modest in size, consisting of 12 sectors, each 6 cm high, about 90 cm in radial extent, and containing twenty 2-cm × 2-cm channels containing the coils, copper shielding and a 1-cm diameter beam aperture (Figure 16). A 40-MeV S^{14+} ion beam from an MP tandem was accelerated through six turns to 72 MeV.

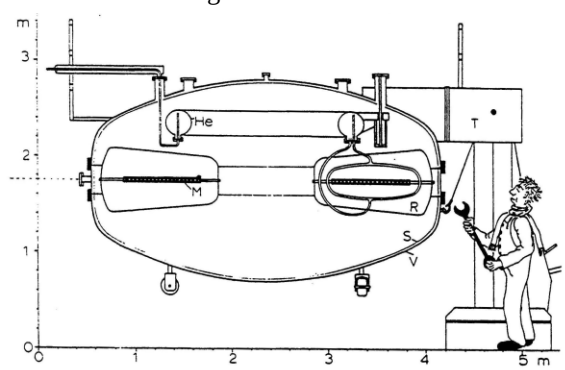

Figure 16: The K85 TRITRON SOC. The thin black bar M indicates a magnet; R is an rf cavity.

FFAG ACCELERATORS

Fixed-Field Alternating-Gradient (FFAG) accelerators occupy the missing niche in the family of fixed magnetic field (cyclotron) accelerators [29] (Figure 17). They share

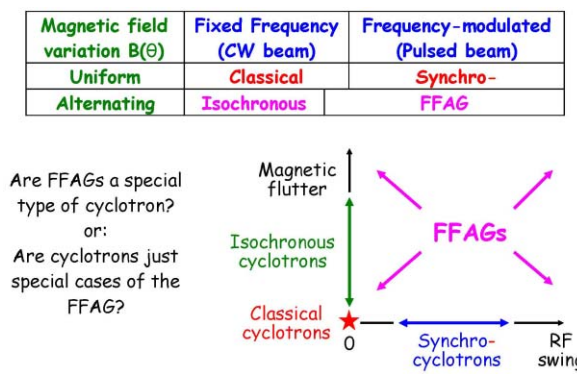

Figure 17: The cyclotron (fixed-field) accelerator family.

the features of both synchro- and isochronous cyclotrons, operating in pulsed mode with fm rf, and acquiring axial focusing through azimuthal field variation.

The basic idea, conceived independently by Ohkawa [30], Kolomensky [31] and Symon [32] in 1953-4 , was to introduce "strong" AG focusing to fixed-field accelerators for the GeV region, either by alternating positive and negative gradient magnets with radial edges (Figure 18), or by using spiral sector magnets (Kerst [17]).

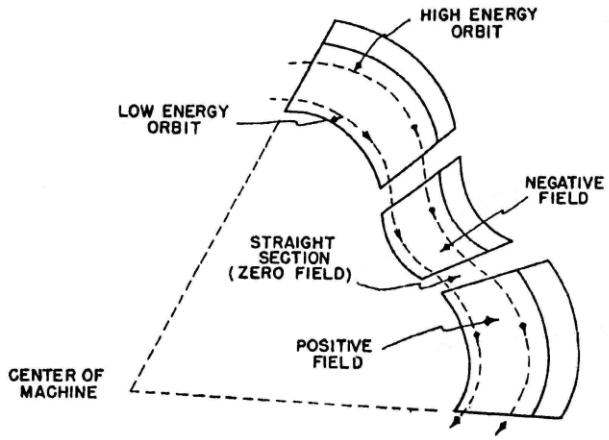

Figure 18: Radial-sector FFAG magnets and orbits.

Compared to AG synchrotrons they would have larger acceptances and pulse repetition rates, and hence much higher beam currents. Their spiral orbits would require wider magnets, rf cavities and vacuum chambers, but the width would be limited by using high field gradients k. The most intensive studies were carried out at the Mi-West Universities Research Association (MURA), where the "scaling" principle was adopted and several successful electron models built (Figure 19).

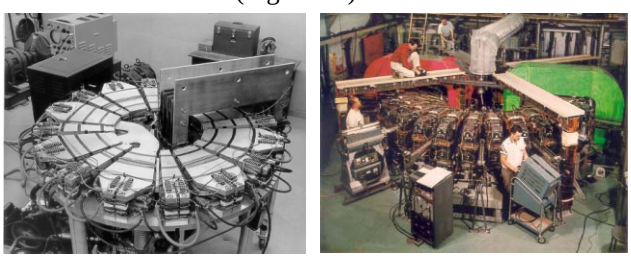

Figure 19: MURA radial-sector electron model FFAGs: left: 400-keV; right: 50-MeV two-way accelerator.

"Scaling" means keeping the orbit shape, optics and tunes fixed for all energies, and thus avoiding crossing any betatron resonances with possible loss of beam current or quality. To first order, for many cells (N >>1):

$$\nu_r^2 \approx 1+k \qquad \nu_z^2 \approx -k+F^2(1+2\tan^2\varepsilon),$$

so the MURA scaling recipe was to keep the field index k, flutter F^2, and spiral angle ε constant for all radii, resulting in the field and momentum (p) laws:

$$\langle B_z \rangle = B_0(r/r_0)^k \qquad p = p_0(r/r_0)^{k+1}.$$

In spite of the success of the electron models, none of MURA's proposals for proton FFAGs (0.5, 10, 15, and 20 GeV) were funded. Nor were Argonne's and Jülich's later proposals for 1.5-GeV 4-mA spallation neutron sources.

The first proton FFAG was Mori's 1-MeV radial-sector machine at KEK in 2000 [34]. Proton FFAGs are more challenging than those for electrons, as frequency modulation cannot be avoided. The mechanical modulators used in synchrocyclotrons had been notoriously unreliable. Mori instead loaded his cavities with Finemet alloy, producing high fields with low Q (≈1), allowing broadband operation. He followed this with a 12-cell 150-MeV FFAG at KEK and a 3-stage FFAG complex at Kyoto University Research Reactor Institute (KURRI) that is now in use for the world's first tests of Accelerator-Driven Subcritical Reactor (ADSR) operation (Figure 20). Three more scaling FFAGs have been built in Japan (one for electron irradiation, one for BNCT neutron therapy and the third for muon momentum cooling), and several others are being studied.

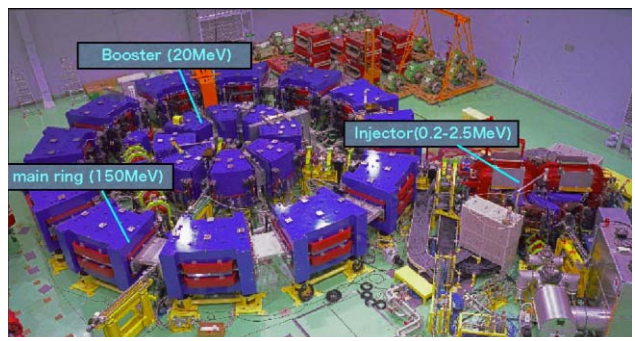

Figure 20: The 3-stage FFAG complex at KURRI.

Non-scaling FFAGs

The recent resurgence of interest in FFAGs stems not only from the above work but also from Mills's [34] and Johnstone's [35] 1997 suggestion of building non-scaling FFAGs for the muon accelerators in a neutrino factory – muons being so short-lived that the rapid acceleration required leaves no time for resonances to spoil the beam. Johnstone proposed a "linear" non-scaling (LNS) design using constant negative-gradient magnets (Figure 21). This offers a number of advantages: greater momentum compaction (hence narrower radial apertures); minimal orbit-time variation (allowing cw operation at fixed rf frequency); no multipole field components to drive higher-order betatron resonances; simpler construction (quadrupolar rather than $B \propto r^k$). LNS-FFAGs have been chosen for the 12.5-25 and 25-50-GeV muon stages of the Neutrino Factory International Design Study. EMMA, a 10-20-MeV electron model of a 10-20-GeV muon FFAG is currently undergoing beam commissioning at Daresbury.

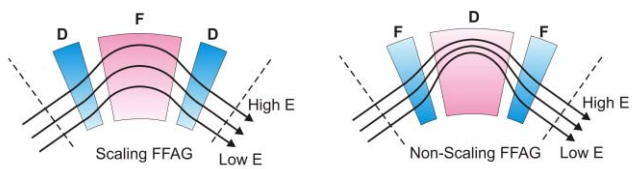

Figure 21: Orbits in scaling and linear non-scaling FFAGs (colour density denotes field strength).

Non-linear non-scaling designs are also being studied, particularly for cancer therapy. But the most interesting for a cyclotron audience is perhaps one of Rees's designs using 5-magnet "pumplet" cells: an 8-20-GeV isochronous muon accelerator (Figure 22) with nearly radial magnet edges that remains vertically focusing up to γ=190 (and $\beta^2\gamma^2$ = 36,100)! Using three magnet types per cell, rather than two, provides extra degrees of freedom, so that the axial focusing term is no longer restricted to $F^2(1+2\tan^2\varepsilon)$.

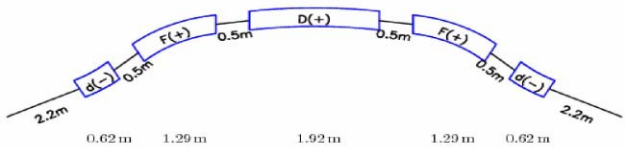

Figure 22: Five-magnet "pumplet" cell.

FINAL THOUGHTS

Over 80 years, Lawrence's magnetic resonance principle has proved remarkably productive as the basis for all modern "circular" accelerators. Classical cyclotrons opened up nuclear physics, and synchrocyclotrons particle physics, while isochronous cyclotrons have provided ion beams of unrivalled intensity in the 10-600 MeV/u range not only for physics but increasingly for other sciences and medicine. FFAGs too are enjoying a resurgence in their original scaling form, and have recently been discovered to offer interesting possibilities in a variety of non-scaling forms. Let's wish the fixed-field accelerator family another productive 80 years!

REFERENCES

[1] E.O. Lawrence, N. Edlefsen, *Science*, **72**, 376 (1930).
[2] J.L. Heilbron & R.W. Seidel, *Lawrence and His Laboratory*, v.1 (U. California Press, 1989); http://ark.cdlib.org/ark:/13030/ft5s200764/
[3] M.S. Livingston, *The Development of High-Energy Accelerators* (Dover, 1966).
[4] M.S. Livingston, *The History of the Cyclotron* , Proc. 7th Cyclotron Conf., 635 (Birkhaser Verlag, 1975)
[5] J.R. Richardson, *A short Anecdotal History of the Cyclotron*, Proc. 10th Cyclotron Conf., 617 (IEEE, 1984).
[6] F.T. Cole, *Oh Camelot! A Memoir of the MURA Years*; Proc. Cyclotrons 2001, Supplement; http://www.jacow.org
[7] L. Jones, F. Mills, A. Sessler, K. Symon, D.Young, *Innovation Was Not Enough* (World Scientific, 2009).
[8] M.K. Craddock, K.R. Symon, *Cyclotrons and FFAGs*, Rev. Acc. Sci. Tech. **1**, 65 (2008).
[9] R. Wideröe, *The infancy of particle accelerators* (Braunschweig: Vieweg, 1994) p.41.
[10] E.O. Lawrence, M.S. Livingston, *Phys. Rev.* **40**, 19 (1932).
[11] M.E. Rose, *Phys. Rev.* **53**, 392-408 (1938).
[12] R.R. Wilson, *Phys. Rev.* **53**, 408-20 (1938).
[13] J.R. Richardson, K.R. MacKenzie, E.J. Lofgren, B.T. Wright, *Phys. Rev.* **69**, 669 (1946).
[14] L.H. Thomas, *Phys. Rev.* **54**, 580-8 (1938).
[15] E.L. Kelly, R.V. Pyle, R.L. Thornton, J.R. Richardson, B.T. Wright, *Rev. Sci. Instr.* **27**, 492 (1956).
[16] F. Heyn, K.T. Khoe, *Rev. Sci. Instr.* **29**, 662 (1958).
[17] D.W. Kerst, K. M. Terwilliger, K.R. Symon, and L.W. Jones, *Phys. Rev.* **98**, 1153 (A) (1955).
[18] D.J. Clark, J.R. Richardson, B.T. Wright, *Nucl. Instr. & Meth.* **18-19**, 1-24 (1962).
[19] D.A. Lind, J.J. Kraushaar, R. Smythe, M.E. Rickey, *Nucl. Instr. & Meth.* **18-19**, 62 (1962).
[20] J.A. Martin, J.E. Mann, *Nucl. Instr. & Meth.* **18-19**, 461-8 (1962).
[21] W.B. Powell, B.L. Reece, *Nucl. Instr. & Meth.* **32**, 325 (1965).
[22] J.L. Belmont, J.L. Pabot, Proc. 5th Cyclotron Conf., IEEE Trans. NS-13, 191 (1966); http://www.jacow.org
[23] J.R. Richardson, E.W. Blackmore, *et al.*, *Proc. PAC'75*, IEEE Trans. **NS-22**, 1402 (1975).
[24] H. Willax, *Proc. 3rd Cyclotron Conf.*, CERN 63-19, 386 (1963); http://www.jacow.org
[25] J. Ormrod, C.B. Bigham *et al.*, *Proc. PAC'77, IEEE Trans.* **NS-24**, 1093-5 (1977); http://www.jacow.org
[26] H.G. Blosser, F. Resmini, *Proc. PAC'79, IEEE Trans.* **NS-26**, 3653-8 (1979); http://www.jacow.org
[27] F.M. Russell, *Nucl. Instr. & Meth.* **23**, 229 (1963).
[28] A. Cazan, P. Schütz, U. Trinks, *Proc. EPAC'98*, 556-8 (1998); http://www.jacow.org
[29] E.M. McMillan, *Particle accelerators*, in *Experimental Nuclear Physics* ***III*** (Wiley, 1959) 639.
[30] T. Ohkawa, Phys. Soc. Japan Symp. Nucl. Phys. (Tokyo, 1953).
[31] A.A. Kolomensky, V.A. Petukhov, M. Rabinovich, *Lebedev Phys. Inst. Report* RF-54 (Moscow, 1953).
[32] K.R. Symon, Phys. Rev. **98**, 1152(A) (1955).
[33] M. Aiba *et al.*, *Proc. EPAC'00*, 581-3 (2000).
[34] F. Mills, *Proc. 4th Int. Conf. Physics Potential and Development of $\mu^+\mu^-$ Colliders, 1997*, 693 (1998)
[35] C. Johnstone, *ibid.*, 696.
[36] G.H. Rees, *ICFA Beam Dynamics Newsletter* **43**, 74 (2007); http://www-bd.fnal.gov/icfabd/Newsletter43.

REVIEW OF HIGH-POWER CYCLOTRONS FOR HEAVY-ION BEAMS

A. Goto#, RIKEN Nishina Center, Wako-shi, Saitama 351-0198, Japan

Abstract

Since the development of heavy ion cyclotrons in the 1980s for use in the field of radioactive beam physics considerable effort has been made to upgrade these cyclotrons in terms of beam intensity and beam energy. This paper presents an overview of cyclotrons that provide heavy-ion beams with powers in the range of several hundred W and above. Some technological issues related to high-power heavy-ion beams are also discussed on the basis of the experiences of those cyclotrons.

INTRODUCTION

Several cyclotrons producing a wide range of heavy-ion beams were developed in 1980s to meet the increasing demand for heavy-ion beams [1]. They were designed to accelerate ions typically in the range of Q/A=1/2-1/3 at 50-100 MeV/nucleon and very heavy ions like uranium at 10-15 MeV/nucleon. Two types of cyclotrons were developed for this purpose: superconducting AVF cyclotrons and separated-sector cyclotrons (ring cyclotrons). The advent of ECR ion sources dramatically improved the performance of these cyclotrons [2,3]. These sources replaced the PIG-type ion sources that were originally used for the production of heavy ions. The use of ECR ion sources resulted in beams with higher intensities. Furthermore, the requirements for radioactive ion (RI) beam have promoted us to obtain much higher intensities as well as higher energies.

At present, several facilities worldwide operate cyclotrons with beam powers of approximately equal or greater than 1 kW. This paper describes the general features and status of six facilities that operate such cyclotrons along with some technological issues related to high-power heavy-ion beams.

HIGH POWER CYCLOTRONS NOW OPERATING FOR HEAVY ION BEAMS

In this section, the general feature and status of six facilities worldwide that operate high-power heavy-ion cyclotrons, along with their upgrade history, are described.

Table 1 lists the key parameters of the main cyclotrons at these facilities, and Figure 1 shows the statistics of beam power for the heavy ion beams produced.

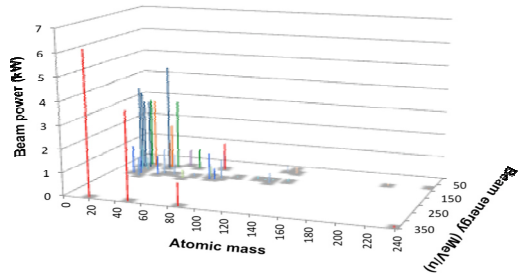

Figure 1: Statistics for the beam power of heavy ion beams obtained from high power cyclotrons so far.

GANIL

The Grand Accelerateur National d'Ion Louds (GANIL) in France is a heavy-ion accelerator facility that accommodates an accelerator complex consisting of three cyclotrons in series: a compact cyclotron (C01 or C02, K=30 MeV) and two separated-sector cyclotrons (CSS1 and CSS2, K=380 MeV) [4-7]. The first beam from the CSS2 was extracted in 1982. The number of sector magnets of the CSS2 is 4, and its maximum sector field, extraction radius and total magnet weight are 1.6 T, 3.0 m and 1,700 t, respectively. The facility delivers a wide spectrum of high intensity ion beams ranging from C to U at energies up to 95 MeV/nucleon.

The GANIL accelerator complex was originally designed taking into consideration the characteristics of PIG ion sources. However, several years later after its commissioning, it was redesigned and modified in order to meet the demands for very heavy ions with higher energies (OAE project) [8]. With these modifications, the output energies of the CSS2 for very heavy ions were increased by a factor of approximately two from 10 MeV/nucelon.

RI beams are obtained using two complementary methods: the projectile fragmentation method and the ISOL method. The RIs produced by the ISOL method are post-accelerated with a K265 compact cyclotron (CIME) at energies from 1.2 MeV/nucleon to 25 MeV/nucleon (SPIRAL1)[9,10]. The first beam from the CIME cyclotron was obtained in 1998. Upgrade in terms of beam intensity for the SPIRAL1 facility was performed [11-13].

Table 1: Key parameters of the six high power cyclotrons for heavy ion beams.

Facility	Main cyclotron	K-value (MeV)	Type	Main coil	No. of sectors	R_{ext} (m)	B_{max} (T)	Magnet weight(t)
RIBF	SRC	2,600	SS	SC	6	5.36	3.8	8,100
NSCL	K1200	1,200	AVF	SC	3	1.01	6.1	260
KVI	AGOR	600	AVF	SC	3	0.89	5.1	390
FLNR	U400M	550	AVF	RT	4	1.6	2.6	2,300
HIRFL	SSC	450	SS	RT	4	3.21	1.6	2,000
GANIL	CSS2	380	SS	RT	4	3.0	1.6	1,700

(SS: separated-sector, SC: superconducting, RT: room-temperature)

#goto@riken.jp

At present, more than 10 primary beams with powers exceeding 1 kW are available; 3-5 kW beams of C, N, O, Mg and Ar ions and 1-2 kW beams of S and Kr ions are available for experiments [6,7,14].

NSCL/MSU

Two superconducting AVF cyclotrons, K500 and K1200, are operated at the National Superconducting Cyclotron Laboratory (NSCL) at Michigan State University (MSU), U.S.A. [15-21]. This facility can deliver a wide range of primary beams from hydrogen to uranium at energies up to 200 MeV/nucleon. Various kinds of RI beams, which are produced via the projectile fragment method using the superconducting fragment separator A1900, are used for experiments.

The K500 cyclotron (K=500 MeV) is the first superconducting cyclotron, and the K1200 (K=1,200 MeV) is the largest superconducting AVF cyclotron. The first beams from the K500 and K1200 cyclotrons were obtained in 1982 and 1988, respectively. The number of sectors of the K1200 is 3, and its maximum magnetic field, extraction radius and total magnet weight are 6.1 T, 1.01 m and 260 t, respectively. A superconducting ECR ion source SuSI recently became operational.

The K1200 cyclotron was operated in the stand-alone mode (direct injection of beam from the ECR ion source into the K1200) at the beginning by using the highly charged ions then available from the ECR ion source, although the original proposal was to use the K500 with an internal PIG ion source as an injector [18]. Then, the Coupled Cyclotron Facility (CCF) project was started in the early 1990s with the objective of increasing the beam intensity by coupling the K500 and K1200 [19,20,22]. Ion beams extracted from the K500 are transported and injected into the K1200 by stripping using a carbon foil located near its center. The beam energies for very heavy ions can be increased with this scheme, although those for light heavy ions are maintained at 200 MeV/nucleon. In this project, the K500 cyclotron was refurbished and a new beam injection system was installed in the K1200 cyclotron accordingly. The first beam from the coupled cyclotrons was obtained in 2000.

A continuing program of beam development in the low energy beam transport (LEBT) has been performed [23]. At present, beams of O, Ne, Mg, Ar, ^{48}Ca, Kr ions, etc. are available at energies from 120 to 170 MeV/nucleon with a beam power of approximately 1 kW [24].

FLNR/JINR

Four isochronous cyclotrons are operated at the Flerov Laboratory of Nuclear Reactions (FLNR) at the Joint Institute for Nuclear Research (JINR) in Russia: U400, U400M, U200 and IC100 cyclotrons [25-30]. The U400 and U400M cyclotrons are used for the acceleration of high-power heavy-ion beams (DRIBs project). The first beams from the U400 (K=625 MeV) and U400M (K=550 MeV) cyclotrons were obtained in 1978 and 1991, respectively. The number of sectors of the U400M cyclotron is 4, and its maximum magnetic field, extraction radius and the total magnet weight are 2.6 T, 1.6 m and 2,300 t, respectively. The internal PIG ion sources in the U400 and U400M cyclotrons were replaced by ECR ion sources in the mid 1990s. Beams are extracted from both the cyclotrons using a thin stripping foil with an efficiency of approximately 40 %, for example for ^{48}Ca beams.

About 66 % of the total operation time is used for the acceleration of ^{48}Ca ions to synthesize new superheavy elements. Another characteristics of this facility is that RI beams produced by the ISOL method using primary beams extracted from the U400M are transported along a 120-m transfer line and post-accelerated by the U400.

At present, various kinds of ions, O, Ar, ^{48}C, Ti, Fe, Kr, Xe, etc. are obtained from the U400M. The energies of these beams range from several to about 15 MeV/nucleon, among which the beam power of oxygen ions exceeds 1 kW and the beam intensity of ^{48}Ca ions is 1.2 pμA. An upgrade project for upgrading from U400 to U400R, and increasing beam intensities up to 2.5-3 pμA, and increasing the available energy variation by a factor of 5 for ^{48}Ca, ^{50}Ti, ^{54}Cr, ^{58}Fe and ^{64}Ni ions is planned to start in 2010 and end in 2011.

HIRFL

The Heavy Ion Research Facility in Lanzhou (HIRFL) in China, consists of an injector AVF cyclotron (SFC, K=69 MeV), a separated-sector cyclotron (SSC, K=450 MeV) and two newly constructed electron cooler synchrotrons, CSRm and CSRe [31-34]. The first beam from the SSC was obtained in 1988. The number of separated sector magnets of the SSC is 4, and its maximum sector field, extraction radius and total magnet weight are 1.6 T, 3.21 m and 2,000 t, respectively. The commissioning of the CSRm started before the end of 2005 and a $^{12}C^{4+}$ beam at 7 MeV/nucleon from the SFC was injected and accumulated in the CSRm for the first time in 2006.

In the beginning of 2000s, a series of upgrades were performed: the replacement of the vacuum chamber of the SFC, installation of a new rebuncher between the SFC and the SSC, increasing the RF voltage for both the SFC and the SSC, improvement of the control and diagnostic systems, and replacement of all the power supplies in the facility. A dramatic enhancement of the HIRFL performance was achieved by this upgrade. The use of the superconducting ECR ion source SECRAL, which has been operational since 2005, further increased the HIRFL performance [35].

At present, various kinds of ions up to Bi are available from the SSC at energies from 10 to 100 MeV/nucleon. The available beam power is generally low except for $^{36}Ar^{18+}$ beam at 22 MeV/nucleon (350 W), which is used for the injection into the CSRm, since the beam transmission mainly through the SSC is still somehow poor. On the other hand, the beam power from the SFC is the highest among such cyclotrons, as high as 100-300 W for O-Xe ions with beam energies of several MeV/nucleon [36]. This implies that the beam power

from the SSC can be easily increased above 1 kW by improving the beam transmission through the SSC.

KVI

A superconducting isochronous cyclotron called AGOR is operated at the Kernfysisch Versneller Instituut (KVI) at University of Groningen, the Netherland [37-40]. The AGOR cyclotron (K=600 MeV) was designed and constructed through the collaboration between l'Institut de Physique Nucleaire (IPN), Orsay and KVI, Groningen, and the first beam at KVI was obtained in 1996. The number of sectors of the AGOR cyclotron is 3, and its maximum magnetic field, extraction radius and total magnet weight are 5.1 T, 0.89 m and 390 t, respectively. The facility delivers heavy-ion beams at energies from several to 90 MeV/nucleon as well as protons up to 190 MeV.

In the early stages of operation, the AGOR cyclotron suffered internal beam losses due to the large coherent vertical motion of the proton beam with the highest energy; this was not observed in the case of heavy-ion beams [41]. The reason for this problem was determined by the careful measurement of the vertical beam position as a function of radius and a detailed study of the beam dynamics. The internal beam losses disappeared by the shifting of the main coil position by -0.34 mm.

A beam power of 1 kW has been achieved so far for Ne ion beams of 23 MeV/nucleon. An upgrade project for increasing the beam intensity in order to obtain a beam power of ~1 kW for all beams up to Bi is underway. The upgrade includes the construction of a new ECR ion source, improvement of the LEBT system, reconstruction of a part of the extraction system, and development of a beam loss monitoring and control system.

RIBF

The RI Beam Factory (RIBF) at RIKEN Nishina Center, Japan, is a heavy-ion accelerator complex consisting of two different types of injectors – a unique variable-frequency heavy-ion linac (RILAC) and an AVF cyclotron (K=78 MeV) – and four ring cyclotrons, the RRC, fRC, IRC and SRC with K-values of 540, 570, 980 and 2,600 MeV, respectively, from the upstream [42-47]. The facility can deliver a variety of ion beams from hydrogen to uranium at a wide range of energies from several to several hundreds MeV/nucleon.

The RILAC, AVF cyclotron and RRC are used in the old facility that is in operation since 1986 when the first beam from the RRC, injected from the RILAC, was obtained. The maximum energy of ion beams from the RRC is 135 MeV/nucleon for ions such as C, N, O and around 15 MeV/nucleon for very heavy ions. A projectile fragment separator, RIPS [48], in combination with these accelerators produces the intense RI beams with atomic masses of around 50 or less.

The RIBF project was started in the mid 1990s with the aim of increasing beam energies in order to meet the strong demands from users for different kinds of RI beams up to uranium. First, the pre-injector of the RILAC was upgraded in an attempt to increase the beam intensities of very heavy ions. The pre-injector system consisting of an 8 GHz NEOMAFIOS and a 450-kV Cockcroft-Walton terminal was replaced with a new system consisting of an 18 GHz ECR ion source and a variable-frequency FC-RFQ linac [49,50]. The construction of new cyclotrons for the RIBF project then started in late 1990's. The construction of three new ring cyclotrons, fRC, IRC and SRC was completed in 2006, and the first beam from the SRC was obtained at the end of 2006.

The SRC is the world's first and world's most powerful superconducting ring cyclotron [51]. The number of the separated sector magnets of the SRC is 6, and its maximum sector field, extraction radius and total magnet weight are 6, 3.8 T, 5.36 m and 8,100 t, respectively. The RIBF accelerator complex provides various modes of acceleration. The maximum energy of the beams from the SRC thus obtained is 440 MeV/nucleon for ions with Q/A=1/2 and 345 MeV/nucleon for all kinds of ions up to uranium. The target beam intensity is set to be 1 pμA, which is limited by the radiation shielding power around the primary beam dump. Radioactive ion beams are produced using a superconducting fragment separator, BigRIPS [52], via two methods: the projectile fragmentation of stable heavy ions or in-flight fission of uranium ions.

The SRC have so far delivered polarized deuterons and ^{14}N beams at 250 MeV/nucleon; α beams at 320 MeV/nucleon; and ^{18}O, ^{48}Ca, ^{86}Kr, ^{238}U beams at 345 MeV/nucleon. The beam intensities of the α and ^{18}O beams were 1 pμA, which is limited by the safety regulation rule. Their beam powers were 1.3 kW and 6.2 kW, respectively. The beam intensities of the ^{48}Ca and ^{238}U beams were 230 pnA and 0.8 pnA, respectively. Their beam intensities were limited by the beam loss at the electrostatic deflector of the SRC and the beam intensity of the ECR ion source, respectively. A search for new isotopes was carried out in 2008 by employing the in-flight fission of a 345 MeV/nucleon ^{238}U beam with an average beam intensity of 0.2 pnA, which is 5,000 times less than the target intensity, and 45 new neutron-rich isotopes were observed [53]. This result verified the potentiality of the RIBF.

A new injector linac, RILAC2, consisting of a 28 GHz superconducting ECR ion source, an LEBT system, an RFQ linac and three DTLs is under construction [54,55]. It will be ready for commissioning by the end of 2010. Uranium beam with intensities of 50-100 pnA are expected to be obtained from the SRC by the use of this new injector in the near future.

SOME TECHNOLOGICAL ISSUES RELATED TO HIGH-POWER HEAVY-ION BEAMS

This section discusses some technological issues concerning high-power heavy-ion beams, based on the experiences in operating the above-mentioned facilities.

ECR Ion Sources

One of the challenging tasks for ECR ion sources is to produce more than 500 eμA U^{35+} ions, which are necessary to attain the beam intensity of 1 pμA from the SRC at the RIBF. Fortunately, the performance of ECR ion sources has been remarkably increased with the development of 3rd generation superconducting ECR ion sources (SC-ECRISs) such as VENUS [56], which is the first among them, and SECRAL [35], which has a unique magnetic structure with all the axial solenoid coils located inside a superconducting sextupole magnet. The VENUS, for example, has already produced 175 eμA U^{35+} ions, which means that the value of 500 eμA is within arm's reach. A 28 GHz superconducting ECR ion source has recently been developed at the RIBF [57,58]. The main features of this ion source are as follows: (1) it has six solenoid coils for producing magnetic mirrors in the axial direction, and (2) the magnetic field gradient and ECR zone size can be changed independently using this configuration. Production tests using 18 GHz microwaves showed that a smaller field gradient and a larger size of the ECR zone gave a higher beam intensity as expected. Therefore, this ion source is expected to produce a U^{35+} beam with the intensity of more than 500 eμA.

LEBT

It is very important to control the quality of beams in the LEBT system from the ECR ion source to the injector. At NSCL, for example, an intensive study of the behavior of beams in the LEBT was carried out using BaF_2-coated viewing plates and an Allison-type emittance scanner [59]. The image of the beam on the viewing plate showed a hollow shape when a significant fraction of the unanalysed beam had a higher charge-to-mass ratio than the desired beam. By attributing this result to the effect of space charge forces from the unanalysed beam, a solenoid located between the ECR ion source and the analyzing magnet was replaced with an electrostatic lens. As a result, the net beam transmission efficiency was improved by 400 % over the period 2003-2006.

A more detailed study involving both simulations and experiments has to be carried out to further elucidate the mechanism of beam motion in the LEBT system. Neutralization and the initial condition at the extraction of the ion source etc. are important factors to be investigated.

Extraction

A key factor limiting cyclotron output beam intensity is beam loss at electrostatic deflectors. The problem is serious for heavy ion beams, which have high power density in the Bragg peak of them, leading to greater damage to the septum electrode. Therefore, the beam extraction should be carefully tuned. In the SRC at RIBF, for example, the temperature of the septum electrode and the radiation from it are constantly monitored using thermocouples attached to the electrode and loss monitors located in the neighbourhood of the deflector, respectively. Here, the temperature rise is kept below the value that corresponds to a beam loss of 300 W.

Some of the ways to reduce the beam loss at the deflector are increasing the RF voltage, using a flattop resonator and collimating the beam at the upstream [23]. In addition, a deflector that can endure higher values of beam loss, say 1,000 W, would also be necessary [60].

Charge Strippers

Another set of components that strongly limit output beam intensity, and thus availability (mentioned later), are the charge strippers used for very heavy ions. In the acceleration of a uranium beam at RIBF, two major problems occur with the first of the two carbon foil strippers – the 0.3 mg/cm2 foil at 11 MeV/nucleon (from U^{35+} to U^{71+}) and the 17 mg/cm2 foil at 51 MeV/nucleon (from U^{71+} to U^{86+}) - used after the RRC and the fRC, respectively. One is their finite lifetime and the other is the energy spread due to the non-uniformity in foil thickness [47]. In the experiment carried out in 2008 and 2009, the lifetimes were as short as 10-12 h with a beam intensity of 14 pnA and 10 h at the longest with a beam intensity of 80 pnA [61], respectively. Different kinds of carbon foils, including diamond-like carbon and multi-layer carbon [62], have been tested with no satisfactory results. The non-uniformity in foil thickness is approximately 30 %, as estimated by comparing the longitudinal widths of the beams generated with and without the carbon foil. Thus, a switch to 0.2 mg/cm2 carbon foils (to U^{69+}) is planned, together with minor modifications to the fRC power supplies, in order to mitigate the energy spread.

The target intensity for the uranium beam at RIBF is approximately 1,000 times higher than what is currently available. It is necessary, therefore, to develop charge strippers that can endure such high intensity uranium beams as soon as possible. For this purpose, one of the possibilities being investigated is that of using a gas stripper [63]. The use of a liquid-Li stripper foil [64] is another such possibility.

An experiment recently performed in the K1200 cyclotron at NSCL using a Pb ion beam showed that the beam transmission through the cyclotron decreased significantly at 10^{14} ions in the beam spot area of 4 mm^2 and that the carbon foil experienced significant changes after irradiation [65]. It was concluded that carbon foils are not practical to use for very heavy ions at the present time.

Beam Diagnostics/Safety System

Non-destructive beam diagnostic devices are indispensable for high-intensity operations. At GANIL, in the operation of high-power beams, the machine is tuned step by step by reducing the beam-chopping rate and monitoring the beam losses using two types of diagnostics [66]: interceptive diaphragms or copper plates located at the entrance and exit of dipole magnets as well as the entrance of the inflectors and deflectors inside the cyclotrons, and current transformers located in the beam

lines. During the delivery of the beam to the experiment, the beam loss is continuously monitored and if it exceeds a threshold, the safety system quickly stops the beam with the chopper. At RIBF, a monitoring system of beam phases and RF fields using lock-in amplifiers (LIAs) has recently been developed [67]. The system constantly monitors fluctuations in the voltages and phases of 25 RF resonators in total, the output signals of 13 phase pickup probes placed along the beam transport lines and those of 69 phase pickup probes in total placed in the RRC, fRC, IRC and SRC. An automated beam alignment system using inductive beam position monitors (BPMs), such as the one adopted in iThemba LABS [68], is also useful.

Stability

One of the issues concerning cyclotrons is the instability of the magnetic fields due to the huge size of the magnets. The magnetic field strength of the RRC at RIBF drifts particularly fast, at a rate of approximately 1 ppm/h, for the first 600 h, whereas those of the IRC and SRC are stable. It is expected for this drift to be suppressed by the procedure similar to that adopted for the Takasaki AVF cyclotron [69,70]; that is, by controlling the temperature of the magnet iron, by thermally isolating the main coil from the yoke and by precisely controlling the cooling water temperature of the trim coils attached to the pole surfaces.

Availability/Reliability

Operational statistics at every facility show that the availability of the machine, defined as the ratio of the delivered beam time to the scheduled beam time, is now as high as 90 % [14,40,71]. In the operation of 345 MeV/nucleon ^{48}Ca beam carried out at RIBF in May and June, 2010, an availability of approximately 80 % was achieved, which was an improvement over the 60 % availability achieved in 2008 [55].

It is important to note that an electric power co-generation system (CGS) with the maximum output of 6.5 MW is operated at RIBF in order to increase the reliability and overall energy efficiency of the power supply to the entire facility [72,73]. Apparatus requiring non-stop operation, such as the He refrigerator for the superconducting sector magnets of the SRC, are powered by the CGS. When the CGS stops, the equipment is immediately switched over to the commercial power grid. The CGS also contributes to the increase in the availability of the facility.

Space Charge Effect

There has been little study until now on the space charge effects on heavy ions in cyclotrons, whereas considerable research has been devoted to space charge effects for high-intensity protons, for example, in the PSI cyclotrons [74,75]. However, it has become necessary to take these effects into account in simulations since the recent high power cyclotrons are required to accelerate high-intensity, highly charged heavy ions. In Ref. 76, the phenomenon of "round beam" formation, which was observed and has been studied [77] in the PSI proton cyclotron, Injector II, and its matching condition for heavy ion beams are discussed both analytically and numerically. Recently, a numerical simulation demonstrates that beams of U^{35+} ions with an intensity of 0.5 emA form a "round beam" in the RRC at RIBF [78]. Another simulation shows that the intensity limit due to the longitudinal space charge effects for the U^{88+} ion beam in the SRC at RIBF is approximately 2 pμA, which is twice the target intensity [79]. Further simulations are necessary to understand and control the behavior of high-intensity heavy ion beams.

SUMMARY

High power cyclotrons for heavy ion beams have played an essential role in RI beam sciences. In this paper, six such cyclotrons are reviewed by describing their general features and status. In addition, some of the technological issues related to them are discussed. High-power heavy-ion cyclotrons are expected to be more and more useful for RI beam sciences.

ACKNOWLEDGEMENTS

The author acknowledges with great pleasure the following people for helping him prepare for the talk: S. Adam, S. Brandenburg, F. Chautard, B. Gikal, D. Leitner, F. Marti, M. Seidel, J. Stetson, S. Vorozhtsov and H. Zhao.

He would also like to express his sincere thanks to all the members of the Accelerator Group, RIKEN Nishina Center.

REFERENCES

[1] M. Craddock, "Cyclotrons in 1986", Cyclotrons'86 (1986) 756.
[2] R. Geller, "Multiply Charged ECR Ion Sources for Particle Accelerators", Cyclotrons'86 (1986) 699.
[3] C. S. Lyneis, "Operational Performance of the LBL 88-inch Cyclotron with an ECR source", Cyclotrons'86 (1986) 707.
[4] J. Ferme et al., "Status Report on GANIL", Cyclotrons'81 (1981) 3.
[5] A. Joubert et al., "Status Report on the GANIL Facility", Cyclotrons'84 (1984) 3.
[6] F. Chautard et al., "Status Report on GANIL-SPIRAL1", Cyclotrons'07 (2007) 99.
[7] F. Chautard et al., "Operation Status of High Intensity Ion Beams at GANIL", HIAT'09 (2009) 54.
[8] J. Ferme, "Project "OAE" at GANIL a project for increasing the heavy ion energies",Cyclotrons'86 (1986) 24.
[9] M. Bourgarel et al., "SPIRAL Facility: First Results on the CIME Cyclotron obtained with Stable Ion Beams", Cyclotrons'98 (1998) 311.
[10] M. Lieuvin et al., "Commissioning of SPIRAL, the GANIL radioactive beam facility", Cyclotrons'01 (2001) 59.

[11] E. Baron et al., "Upgrading the GANIL Facilities for High-Intensity Heavy Ion Beams (T.H.I. Project)", Cyclotrons'95 (1995) 39.
[12] E. Baron et al., "Experience with High Intensity Operation of the GANIL Facility", Cyclotrons'98 (1998) 385.
[13] E. Baron et al., "High intensity heavy ion beams for exotic nuclei production at GANIL", Cyclotrons'01 (2001) 431.
[14] F. Chautard, "Intense Beam Operation at GANIL", Cyclotrons'10, Lanzhou, Sept. 2010, MOM2CIO02.
[15] H. Blosser, "The Michigan state university super-conducting cyclotron program", Cyclotrons'79 (1979) 2040.
[16] H. Blosser et al., "Advances in Superconducting Cyclotrons at MSU", Cyclotrons'86 (1986) 157.
[17] P. Miller, "The MSU Superconducting Cyclotron Program", Cyclotrons'84 (1984) 11.
[18] J. Nolen et al., "Commissioning experience with the NSCL K1200 superconducting cyclotron", Cyclotrons'89 (1989) 5.
[19] F. Marti et al, "Commissioning of the Coupled Cyclotron System at NSCL", Cyclotrons'01 (2001) 64.
[20] P. Miller et al., "Status of the Coupled Cyclotron Facility at NSCL", Cyclotrons'04 (2004) 62.
[21] http://www.scholarpedia.org/article/The_NSCL_laboratory_and_the_FRIB_facility.
[22] The K500-K1200, A Coupled Cyclotron Facility at the NSCL, MSU, MSUCL-939, July 1994.
[23] J. Stetson et al., "High-Transmission Operation of the NSCL Accelerators", Cyclotrons'07 (2007) 340.
[24] J. Stetson, "Intense Beam Operation of MSU Cyclotrons", Cyclotrons'10, Lanzhou, Sept. 2010, MOA1CIO01.
[25] R. Oganessian et al., "The Flerov Laboratory of Nuclear Reactions JINR Radioactive Ion Beam Project with the U400M-U400 Cyclotron Complex", Cyclotrons'95 (1995) 659.
[26] G. Gulbekyan et al., "New Development at the JINR Heavy Ion Cyclotron Facility", Cyclotrons'92 (1992) 11.
[27] B. Gikal et al., "Recent Developments at Dubna U400 and U400M Cyclotrons", Cyclotrons'98 (1998) 587.
[28] B. Gikal et al., "Dubna Cyclotrons – Status and Plan", Cyclotrons'04 (2004) 100.
[29] G. Gulbekyan et al., "Status Report and Future Development FLNR JINR Heavy Ions Accelerator Complex", HIAT'09 (2009) 59.
[30] B. Gikal et al., "Status of the FLNR JINR Cyclotrons", PAC'09 (2009) FR5REP099.
[31] B. Wei et al., "HIRFL Separated Sector Cyclotron Progress", Cyclotrons'86 (1986) 176.
[32] B.Wei, "Commissioning of HIRFL", Cyclotrons'89 (1989) 9.
[33] H. Zhao et al., "HIRFL Operation and Upgrade", Cyclotrons'04 (2004) 121.
[34] W. Zhan et al., "Commissioning of CSR in Lanzhou", Cyclotrons'07 (2007) 110.
[35] H. Zhao, "World-wide Development of Intense Highly Charged Superconducting ECR Ion Sources", IPAC'10 (2010) 31.
[36] H. Zhao, "IMP Cyclotron Status and Development", Cyclotrons'10, Lanzhou, Sept. 2010, MOA1CIO03.
[37] S. Gales et al., "AGOR A Superconducting Cyclotron for Light and Heavy Ions", Cyclotrons'86 (1986) 184.
[38] H. Schreuder et al., "AGOR: Initial Beam Tests, Transport and Commissioning", Cyclotrons'95 (1995) 6.
[39] S. Brandenburg et al., "AGOR Status Report", Cyclotrons'04 (2004) 90.
[40] S. Brandenburg et al., "High Intensity Operation of the AGOR-Cyclotron for Rib-Production", Cyclotrons'07 (2007) 493.
[41] S. Brandenburg et al., "Vertical Beam Motion in the AGOR Cyclotron", EPAC'04 (2004) 1384.
[42] M. Odera et al., Nucl. Instrum. Methods 227 (1984) 187.
[43] H. Kamitsubo, "Progress in RIKEN Ring Cyclotron Project", Cyclotrons'86 (1986) 17.
[44] M. Kase et al., "Present Status of the RIKEN Ring Cyclotron", Cyclotrons'04 (2004) 160.
[45] Y. Yano, "RI Beam Factory Project at RIKEN", Cyclotrons'04 (2004) 169.
[46] A. Goto et al., "Commissioning of RIKEN RI Beam Factory", Cyclotrons'07 (2007) 3.
[47] N.Fukunishi et al., "Operating Experience with the RIKEN Radioactive Isotope Beam Factory", PAC'09 (2009). M03GRI01.
[48] T. Kubo et al., Nucl. Instrum. Methods B70 (1992) 309.
[49] A. Goto et al., "Construction of a New Pre-Injector System for the RILAC", Cyclotrons'89 (1989) 202.
[50] O. Kamigaito et al., "Design of a New Type of Variable-Frequency Radio-Frequency Quadrupole Linac with a Folded-Coaxial Resonator", Jpn. Journal Appl. Phys. 33 (1994) L537.
[51] H. Okuno et al., "Magnets for the RIKEN Superconducting Ring Cyclotron", Cyclotrons'04 (2004) 373.
[52] T. Kubo et al., Nucl. Instrum. Methods B204 (2003) 97.
[53] T. Ohnishi et al., J. Phys. Soc. Jap., Vol. 79, No. 7 (2010) 073201.
[54] O. Kamigaito et al., "Intensity-Upgrade Plans of RIKEN RI-Beam Factory", HIAT'09 (2009) 21.
[55] O. Kamigaito et al., "Status of RIBF Accelerators at RIKEN", Cyclotrons'10, Lanzhou, Sept. 2010, TUM2CIO01.
[56] D. Leitner et al., "Progress and Perspective for High Frequency, High Performance Superconducting ECR Ion Sources", Cyclotrons'07 (2007) 265.
[57] T. Nakagawa et al., Rev. Sci. Instrum. 81 (2010) 02A320.
[58] T. Nakagawa et al, "28 GHz SC-ECRIS at RIBF", Cyclotrons'10, Lanzhou, Sept. 2010, WEM1CIO02.

[59] J. Stetson et al., "A Comparison of Electrostatic and Magnetic Focusing of Mixed Species Heavy Ion Beams at NSCL/MSU", Cyclotrons'04 (2004) 483.
[60] S. Alfredson et al., "Electrostatic Septum for Kilowatt Heavy Ion Beams", Cyclotrons'01 (2001) 133.
[61] H. Hasebe et al., 25th World Conference of the International Nuclear Target Development Society, Vancouver, BC, Sept. 2010.
[62] H. Hasebe et al., Nucl. Instrum. Methods A613 (2010) 453.
[63] H. Kuboki et al., Phys. Rev. ST Accel. Beams, 13 (2010) 093501.
[64] S. Kondrashev et al., "Upgrade of the FRIB Prototype Injector for Liquid Lithium Film Testing", PAC'09 (2009) TU6RFP048.
[65] F. Marti et al., "Stripper Foil Developments at NSCL/MSU, Cyclotrons'10, Lanzhou, Sept. 2010, THN2CCO03.
[66] G. Senecal et al., "GANIL High Intensity Transport Safety System", HIAT'09 (2009) 291.
[67] R. Koyama, "Beam Phase and RF Fields Monitoring System using Lock-in Amplifier for RIKEN RIBF", EPAC'08 (2008) 1173.
[68] J. Dietrich et al., "Operational Experience with Beam Alignment and Monitoring Using Non-destructive Beam Position Monitors in the Cyclotron Beam Lines at iThemba LABS", DIPAC'05 (2005) 96.
[69] S. Okumura et al., "Temperature Control of a Cyclotron Magnet for Stabilization of the JAERI AVF Cyclotron Beam", Cyclotrons'01 (2001) 330.
[70] S. Okumura et al., "Magnetic Field Stabilization by Temperature Control of an Azimuthally Varying Field Cyclotron Magnet", Rev. Sci. Instrum. 76 (2005) 033301.
[71] D. Sanderson, "Availability at the NSCL", ARW'09, Vancouver, Jan. 2009.
[72] T. Fujinawa et al., "Cogeneration System for RI Beam Factory", RIKEN Accel. Prog. Rep. 36 (2003) 310.
[73] T. Emoto et al., "Co-Generation System for RIBF", Cyclotrons'04 (2004) 163.
[74] W. Joho, "High Intensity Problems in Cyclotrons", Cyclotrons'81 (1981) 337.
[75] T. Stammbach, "High Intensity Problems, Revisited or Cyclotron Operation Beyond Limits", Cyclotrons'98 (1998) 369.
[76] P. Bertrand et al., "Specific Cyclotron Correlations under Space Charge Effects in the Case of a Spherical Beam", Cyclotrons'01 (2001) 379.
[77] S. Adam, "Space Charge Effects in Cyclotrons – from Simulations to Insights", Cyclotrons'95 (1995) 446.
[78] H. Okuno, private communication.
[79] S. Vorojtsov et al., "Beam Space Charge Simulation in the RIKEN SRC", RIKEN Accel. Prog. Rep. 36 (2003) 299.

GANIL OPERATION STATUS AND DEVELOPMENTS

F. Chautard, Bd Henri Becquerel, BP 55027, 14076 CAEN Cedex 05, France

Abstract

The GANIL (Grand Accélérateur National d'Ions Lourds) produces and accelerates stable ions beams since 1982. The first radioactive beam post-accelerated with the CIME cyclotron happened in 2001. In 2013, stable beams with higher intensities and new energy range will be available from the new superconducting linear accelerator SPIRAL2. In 2014, new exotic beams will be accelerated with the existing cyclotron CIME. This paper will show how GANIL facility is preparing the arrival of SPIRAL2 accelerator. To achieve this goal two main objectives have to been set:

- Continuing the delivery of high intensity and exotic beams.
- Pursuing the developments of the machine capabilities in a project structure in order to keep equipments running with a high reliability yield and still responding to physics demands.

The progress in ion source production (both beam intensities and new species) will be presented together with the foreseen GANIL beam delivery capabilities when SPIRAL2 will be in operation.

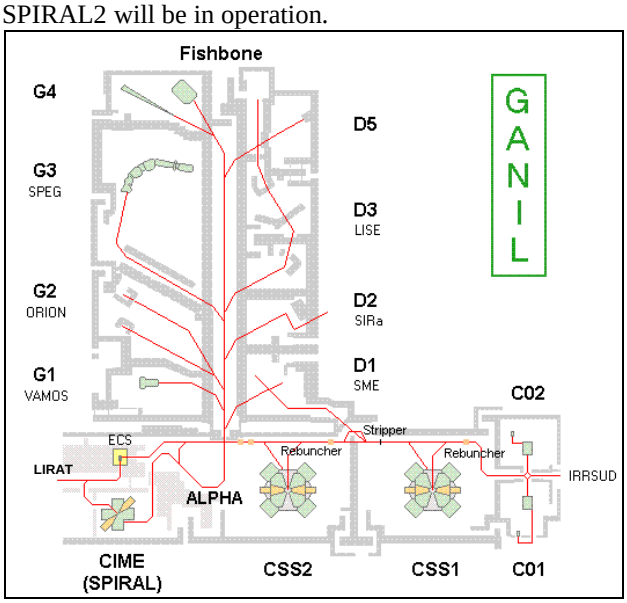

Figure 1: GANIL layout

RUNNING MODES AND BEAM REVIEW

Multi-beam delivery is routinely done at GANIL using its 5 existing cyclotrons. Up to five experiments can be run simultaneously in different rooms with stable beams:

- Beams from C01 or C02 are sent to an irradiation beam line IRRSUD (<1MeV/u).
- A charge state of the ion distribution after the ion stripping downstream CSS1 is sent to atomic physics, biology and solid states physics line D1 (4-13MeV/u).
- A high-energy beam out of CSS2 transported to experimental areas (<95MeV/u).
- An auxiliary experiments shares the previous CSS2 beam (10% of the pilote experiment time)
- Finally, stable beams from SPIRAL1 source can be sent to LIRAT (<34keV/A) or post-accelerated by CIME and given to detector tests for example.

During radioactive beam production with SPIRAL1, the combination are reduced to the four first and with radioactive beam sent to the 2 experimental areas.

Intense Primary Beams

The facility delivers a wide spectrum of high intensity ion beams ranging from ^{12}C to ^{238}U accelerated ranging from 95MeV/u for the lighter ones (12C) to 24MeV/u for Uranium beams. The acceleration scheme lies on the use of three cyclotrons in line. One compact injector cyclotron (C01 or C02, K=30) and two separated sector cyclotrons (CSS1 and CSS2, K=380). Those accelerators and beam lines have been adapted to transport intense ion beams. More than 10 beams are available at a power exceeding 1kW (Table 1) over the 50 stable beams available from the GANIL sources [1]. The beam losses detectors, beam transformers and control system allow the transport of intense stable beams with power exceeding 3kW in routine operation. The main limitations come now from the SPIRAL1 target ability to withstand beam power greater then 3kW and the GANIL safety limitations rules (beam < 2 10^{13}pps or 6kW).

Table 1: The GANIL high intensity beams

Beams	Imax [µAe]	10^{13} [pps]	Emax [MeV/u]	Pmax [W]	Used with Spiral
$^{12}C^{6+}$	19	2	95	3 600	planned
$^{13}C^{6+}$	18	2	75	2 900	X
$^{14}N^{7+}$	15	1.6	95	3 400	planned
$^{16}O^{8+}$	16	1	95	3 000	X
$^{18}O^{8+}$	2.3	0.18	75	400	
$^{20}Ne^{10+}$	15.7	1	95	2 400	X
$^{22}Ne^{10+}$	15	1	80	2 600	planned
$^{24}Mg^{12+}$	20	1	95	3 800	planned
$^{36}S^{16+}$	11	0.43	77.5	1 900	X
$^{36}Ar^{18+}$	24	0.8	95	4 600	planned
$^{48}Ca^{19+}$	4.5	0.15	60	700	X
$^{58}Ni^{26+}$	4	0.1	75	700	
$^{76}Ge^{30+}$	3.5	0.07	61	500	
$^{78}Kr^{34+}$	7	0.13	70	1 200	X
$^{124}Xe^{44+}$	2	0.03	50	300	

Exotic Beam Production

Exotic beams are produced with two complementary methods. The ISOL (Isotope Separation On Line) method with SPIRAL1 where the primary heavy ion beam is fragmented into a thick carbon target. The fragments produced are ionized by an ECR source and post-accelerated with the cyclotron CIME (K=265) from 1.2 to 25MeV/u. Table 2 gathered the exotic beam produced by SPIRAL1 and sent to physics. The production of the isotopes is very dependant of the charge state [2]

Table 2: Radioactive beam produced and post-accelerated from 2001 to 2009

ions	*W* [MeV/u]	[pps]	ion	*W* [MeV/u]	[pps]
6He	3.8	$2.8\ 10^7$	20F	3	$1.5\ 10^4$
6He	2.5	$3.7\ 10^7$	17Ne	4	4.10^4
6He	5	3.10^7	24Ne	4.7	2.10^5
6He	34 keV/A Lirat	2.10^8	24Ne	7.9	$1.4\ 10^5$
6He	20	5.10^6	24Ne	10	2 105
8He	3.5	1.10^5	26Ne	10	3.10^3
8He	15.5	1.10^4	31Ar	1.45	1.5
8He	15.4	$2.5\ 10^4$	33Ar	6.5	3.10^3
8He	3.5	6.10^5	35Ar	0.43	4.10^7
8He	3.9	8.10^4	44Ar	10.8	2.10^5
14O	18	4.10^4	44Ar	3.8	3.10^5
15O	1.2	$1.7\ 10^7$	46Ar	10.3	2.10^4
19O	3	2.10^5	74Kr	4.6	$1.5\ 10^4$
20O	3	4.10^4	74Kr	2.6	$1.5.10^4$
20O	4	4.10^4	75Kr	5.5	2.10^5
18Ne	7	1.10^6	76Kr	4.4	4.10^6
18F	2.4	2 104			

The production of exotic beam by an In Flight method is also possible with the new rotating , high power target system installed in the LISE beam line, called CLIM (Cible LISE à Intensité Maximale). This devise allows the fragmentation of high energy and intense primary beams onto a rotating target. The equipment is located in the LISE experimental room (Figure 3). The exotic cocktail beam after the target is purified with the following fragment separator spectrometer. A 2kW beam can be sent to the 2000rpm target with a maximum of 800W beam power deposited. This is an alternative to the device SISSI (Superconducting Intense Source for Secondary Ions) [3] which operation had been stopped in 2007. The energy beam produced is comparable to the primary beam (max 95MeV/u)

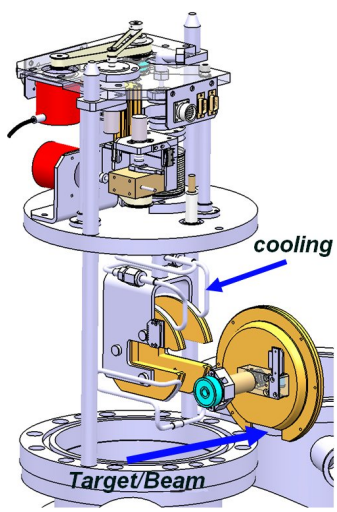

Figure 2: Schematic view of rotating target CLIM before insertion in the module for irradiation.

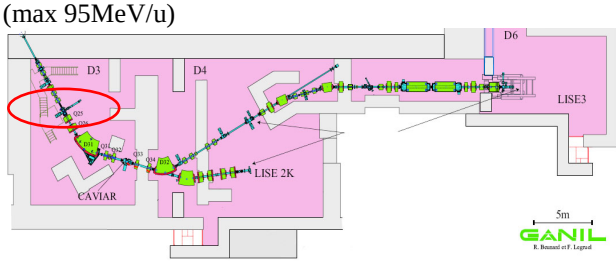

Figure 3: LISE experimental room (D3, D4 and D6) where In Flight exotic beams are produced

2001-2009 GANIL OPERATION STATUS

Since 2001, (Figure 4) more than 26400 hours of beam time was delivered by GANIL to physics. 16700 hours of beam time have been delivered to physics from the CSS cyclotrons and 9700 hours from SPIRAL1. The total beam time for physics (tuning and maintenance excluded) is on the average around 3000 hours a year.

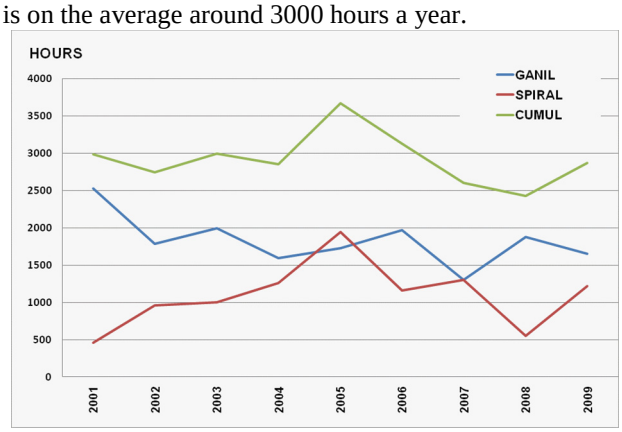

Figure 4: Beam time repartition between SPIRAL and GANIL beams over 9 years.

The number of beam delivered per year (Figure 5) has increased but the tuning time requiered impacts on the time dedicated to physics. Campagne of physics with similar ion beam is tempted to reduce tunings.

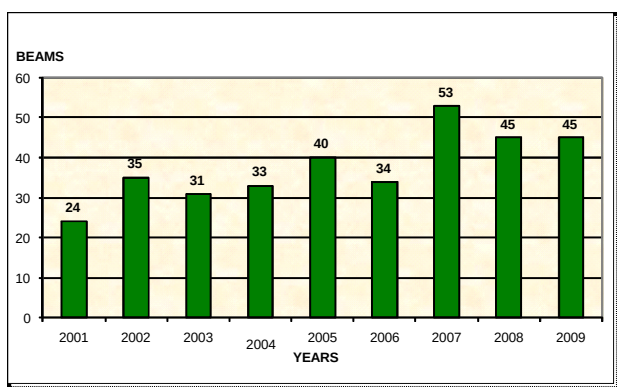

Figure 5: Number of beams tuned between 2001 and 2008

Finally, maintenance on a 27 year old accelerator is a main concern. Recently:

- 36 power supplies of the fishbone and entrance of few experimental rooms have been changed. This allows us to test also in operation the future equipment and command-control system for the SPIRAL2 project.
- All of the flexible cooling water pipes (600) of the magnets and RF systems (except experimental area) have been replaced.

Those actions are manpower consuming but the Figure 6 shows such maintenance actions have given rise to a higher availability time.

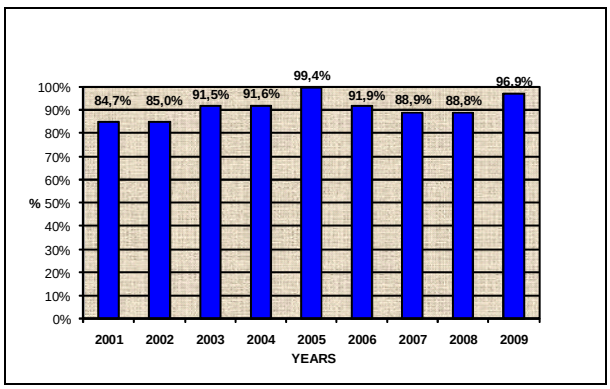

Figure 6: Ratio between the beam time available to the physics to the scheduled beam time online.

STABLE BEAM DEVELOPMENTS

The GANIL source activity [4] is focused to improve the reliability of the actual beams delivered (~30 chemical species + isotopes) as well as the intensities within the safety range limitations (2.10^{13}pps or 6kW beam out of CSS2). It goes with an improvement of the oven for the metallic ion production. Two different steps are under study. First, a modified version of the existing micro-oven at high temperature (1700°C max) to a higher capacity oven (Figure 7) but at a lower average temperature (1100°C max). In a second step build a large capacity and high temperature oven. Above the 1700°C temperature limit, development with induction oven is foreseen. Those developments are coherent with the beam needs expressed by the SPIRAL2 project for the production of $^{48}Ca^{16+}$ and $^{58}Ni^{19+}$.

Table 3: GANIL recent stable beam developments

Beams	Imax [µAe]	10^{13} [pps]	Emax [MeV/u]
$^{64}Zn^{28+}$	1.2	0.03	74
$^{127}I^{45+}$	0.23	0.03	49.5
$^{133}Cs^{47+}$	0.08	0.01	49.3
$^{238}U^{34+}$	0.04	0.01	7.8

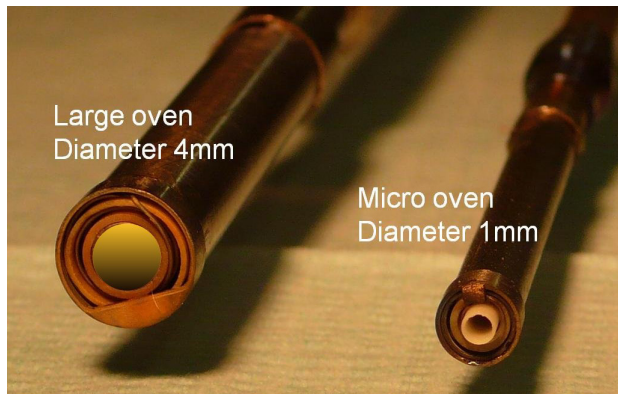

Figure 7: Example of large and micro oven developments

EXOTIC BEAM DEVELOPMENTS

The recommendations of "GANIL 2015", a prospective study on the possible evolution of the SPIRAL1 facility driven by letters of intent from the physicist community have emphasized the importance of broadening the range of the exotic and stable ion beams from the SPIRAL1 target ion-source system. Today, only gaseous elements can be produced (see Tableau 2) due to the use of a cold transfer tube installed between the production target and the ECR source. To overcome this limitation a new project is launched to modify the SPIRAL1 cave in term of power and connectors. No modification on the remote system is foreseen as well as the modification of the storage of used target-ion sources. But it is showed that solutions for remotely install new types of ion sources to permit the production of other elements are possible. It is then expected to have by the end of 2013 the first new 1+ exotic beams produced out of the actual SPIRAL1 thick carbon target. These 1+ beams are further stripped by a charge breeder downstream before the post-acceleration by the CIME cyclotron.

Charge Breeder

Because of strong constraints on the SPIRAL1 Target and Ion Source units (TIS) dimensions, the choice was made to start with compact 1+ sources such as FEBIAD (Forced Electron Beam Induced Arc Discharge) source producing various 1+ metallic ions.

This new 1+ beam could be sent to LIRAT line but a charge breeder has to be inserted between the TIS unit and CIME to reach the N+ charge of the ion required for acceleration with the CIME cyclotron. A collaboration with ISOLDE (CERN) has been set up to install their phoenix 1+N+ test bench at GANIL[5]. It will be mechanically adapted to be inserted in the actual low energy line (fig 3). It is foreseen that by the end of 2013 the first new SPIRAL1 exotic beam is produced.

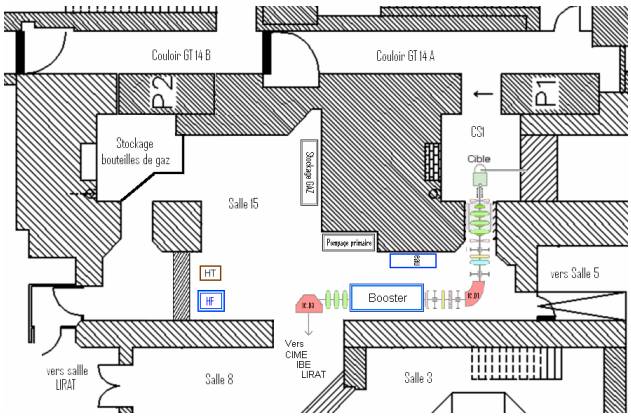

Figure 8: SPIRAL1 low energy beam modifications to insert a new charge-breeder.

Intense R&D activities are being pursued in the framework of this new project to define other possible source types such as surface ionization source, EBIS source or advanced N+ source with high density plasma.

SPIRAL1 Beam Purification System

Even if the present ion source of SPIRAL1 is too selective from the physicist point of view, the exotic beam is nevertheless sometimes accelerated with CIME polluted by ions with a ratio mass over charge (M_2/Q_2) close to the ion of interest (M_1/Q_1) and then be extracted and sent to the physics. The condition to eliminate an undesired ion corresponds at first order to:

$$\left[\frac{M_2}{Q_2}-\frac{M_1}{Q_1}\right]\Big/\frac{M_1}{Q_1}>\frac{1}{2\pi\ H\ N_{turn}} \qquad (1)$$

Where N_{turn} and H are respectively the number of turns and the harmonic in the cyclotron. Hence the mass resolution of a cyclotron is defined as $R=1/2\pi\ H\ N_{turn}$. The mass resolution of CIME can reach 2 10^{-4}. But even with this resolution beam tail may exit. For example, isobars are of main concern because purification around 10^{-4} or 10^{-5} would be needed and is out of reach of the cyclotron. Similarly, in a close future, SPIRAL2 beams will also be affected by the same problem more dramatically mainly due to the production mode. Thus, an upgrade of the diagnostics station for beam detection and purification will be installed at the exit of CIME in the fall of this year (Figure 9). Composed of remotely controlled silicon detectors for identification and 7 thin targets for purification by stripping or by energy loss in a degrader. The drawback can be an important intensity loss for beam energies below 3MeV/u.

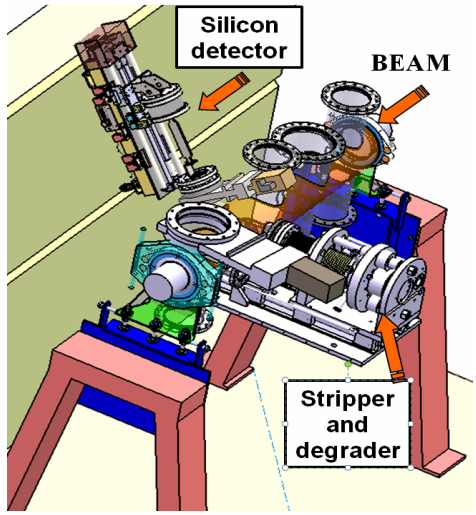

Figure 9: New diagnostics vessel at the extraction of CIME to improve the identification of post accelerated exotic beams and their purification by stripping and energy degrader remotely inserted.

Another way explored since few years, is the development of an electrostatic vertical deflector (Figure 10). An elegant solution is to insert an electrostatic vertical deflector around the 10 last trajectory paths of the beam in the cyclotron. The amplitude of the sinusoidal electric wave between the deflector plates will be zero for the beam of interest (isochronous) and increase with the mass/charge ratio difference. The efficiency of such a device is measured and is able to reduce by a factor 10 beams which have difference of M/Q as low as 310^{-4}. It is expected to test this device in 2011.

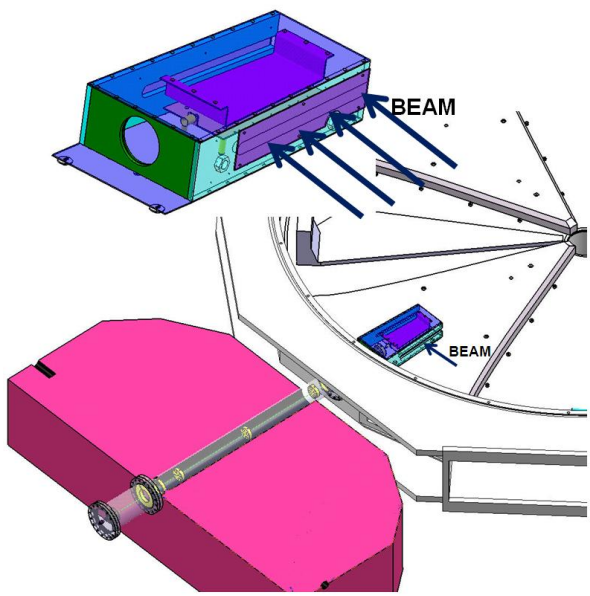

Figure 10: Electrostatic vertical deflector used to purify exotic beam from polluant beam.

FORSEEN OPERATION

The SPIRAL2 machine [6] will increase the capability of GANIL in term of beam time. It is possible to use at

the same time the new SPIRAL2 beams and the existing ones (Figure 11). 44 weeks for SPIRAL2 and 36 weeks for GANIL a year are foreseen. The Figure 11 shows the possible sequences between accelerators:

- Stable beams :
  - LINAG
  - CSS1 and 2
  - CSS1 solo
  - SME
  - IRRSUD
- Exotic beams :
  - SPIRAL1
  - SPIRAL2
    - UCx target
    - Other targets

Again along with GANIL 2015 conclusions [7], one of the main recommendation was to ask for detailed studies to allow the high intensity beams of SPIRAL2 into specifically identified caves have to be carried out with very specific constraints from the radioactive beams.

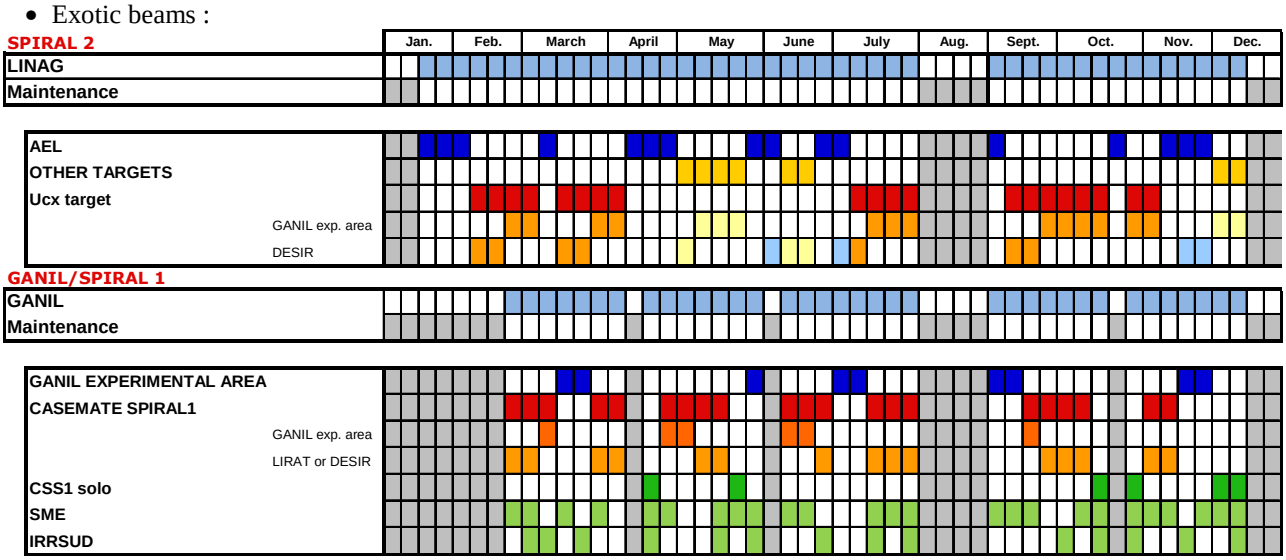

Figure 11: GANIL operation potential with the SPIRAL1, SPIRAL2 and CSS

CONCLUSIONS

The first beam of GANIL was sent to an experimental room in 1983. Since then, the variety and intensity of the ion beams available has continuously evolved. Progresses in the ion source domain make possible to potentially the transport of kW beams. The cyclotrons and the beam lines had to be upgraded to handle such a new constraint. In 2001, the first exotic beam of SPIRAL1 was produced with the existing cyclotron used as a driver. The exotic ion production was then strongly dependant of the target power capabilities and of the increase of the primary beam power. The developments made led to the production of 3kW target for SPIRAL1 and meanwhile increase the primary beam power within the safety limits (<6kW).

The diversity of the ion species (stable and exotic) is now the main concern at GANIL. The present selective ECR ion source should be replaced by alternative ion sources in order to access to metallic beams.

The great care given to the maintenance of the 27 years old allows us to still expect to increase its performances and be competitive until the completion of the SPIRAL2 facility.

ACKNOLEGEMENTS

This paper being an overview of the GANIL operation, the author would like to thank particularly P. Leherissier, P. Delahaye, P. Jardin and Y. Georget for their valuable contributions and discussions.

REFERENCES

[1] http://pro.ganil-spiral2.eu/users-guide/accelerators/available-stable-ion-beams-at-ganil/view.
[2] http://pro.ganil-spiral2.eu/users-guide/accelerators/spiral-beams.
[3] E. Baron et al., “The High Power Target System for SISSI”, NIM A 362 (1995) 90-93.
[4] P. Jardin, et al, “Latest developments at GANIL for stable and radioactive ion beam production”, Rev. Sci. Instrum. Vol. 81, 02A909 (2010).
[5] P. Delahaye et al., "Potentials of the ECR 1+ n+ charge breeding for radioactive ions”, Rev. Sci. Instrum. B, Vol. 266, Issues 19-20, (2008), [4429-4433].
[6] P. Bertrand et al., “Post-acceleration of high intensity RIB through the CIME cyclotron in the frame of the SPIRAL2 project at GANIL”, this conference.
[7] Report on prospective for GANIL 2015. DIR_059_2009.

PROGRESS TOWARDS HIGH INTENSITY HEAVY ION BEAMS AT THE AGOR-FACILITY*

M.A. Hofstee#, S. Brandenburg, J.P.M. Beijers, V. Mironov, H.R. Kremers, J. Mulder, M.A. Hevinga, A. Sen , S. Saminathan
Kernfysisch Versneller Instituut, University of Groningen, 9747AA Groningen, the Netherlands

Abstract

The AGOR-facility has an on-going upgrade program aiming at intensities beyond 10^{12} pps for heavy ion beams up to Pb. The main elements of the program are: further development of the ECR-source, improvement of the transmission into and through the cyclotron, and protection of equipment against excessive beam loss. Further improvement of the ECR ion source is facilitated by the installation of a second source. Redesign of the Low Energy Beam-line, to compensate for aberrations, is in progress; simulations predict a significant increase in transmission. A new, cooled, electrostatic extractor is being commissioned and the beam loss control system has been completed. The main remaining issue is vacuum degradation induced by beam loss caused by charge exchange on the residual gas. Tracking calculations of the distribution of the beam losses over the vacuum chamber to determine the optimum location of scrapers are underway. A gold coating was recently applied to relevant parts of the vacuum chamber aiming at reduction of beam loss induced desorption.

INTRODUCTION

The AGOR-facility delivers heavy ions beams up to Pb for experiments in the framework of the TRIμP programme on fundamental symmetries.

Experiments on violation of time reversal symmetry in β-decay are performed with beams up to ^{40}Ar at energies between 20 and 30 MeV per nucleon. The objective for the beam intensity during the final production runs of these experiments is around 10^{13} pps, corresponding to a beam power of around 1 kW. Currently the beam intensity for these experiments is limited to 4×10^{12} pps (300 W) by constraints in the experimental setup. During test experiments we have achieved an extracted beam intensity of 1.3×10^{13} pps for a $^{20}Ne^{6+}$ beam at 23.5 MeV per nucleon, corresponding to 1 kW beam power.

For experiments on permanent electric dipole moments and atomic parity violation in Ra-atoms and –ions, beams of various Pb-isotopes with an energy in the range 7 – 10 MeV per nucleon are used. In the on-going development phase of these experiments beams with an intensity up to 3×10^{11} pps (100 W) have been delivered. For the production phase of these experiments we aim at a beam intensity exceeding 10^{12} pps. In this paper we describe the on-going improvements, in several areas that directly or indirectly limit the beam intensity for these beams, which are needed to achieve this goal.

ION SOURCES AND LEBT

Following the phasing out of the experimental programme with polarized proton en deuteron beams the polarized ion source POLIS was decommissioned. The source and the associated Lamb shift polarimeter have been transferred to PNPI, Gatchina for experiments in low energy nuclear physics. At the location of POLIS we have now installed a 14 GHz Supernanogan ECR source that we have obtained on a long term loan from HZB, Berlin. The source will be used to produce the beams of gaseous compounds, while the 14GHz AECR-source will be dedicated to the production of metal beams.

The performance of the 14 GHz AECR-source has been significantly improved during the last years by a number of modifications that are elaborated in ref. 1. We now routinely produce 50 μA of Pb^{27+} beams and more than 500 μA of $^{16}O^{6+}$ and $^{20}Ne^{6+}$.

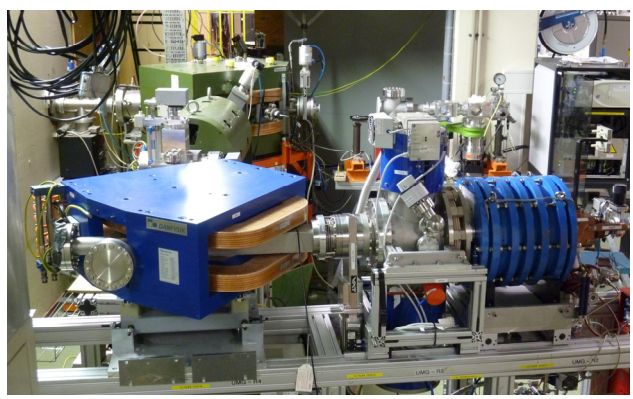

Figure 1: Supernanogan ECR source and beam line.

In the 20 m long beam transport line between the ECR ion sources and the cyclotron up to 50 % of the beam is lost. Detailed simulations and emittance measurements show that these are mainly due to the aberrations in the various magnets, which lead to an increase of the apparent emittance [2]. The beam line is currently being redesigned on the basis of these findings. The redesign of analyzing magnet of the AECR-source, similar to that developed at LBNL [3] has been completed; production of the new magnet poles is about to start.

*This work is part of the research programme of the 'Stichting voor Fundamenteel Onderzoek der Materie (FOM)', which is financially supported by the 'Nederlandse Organisatie voor Wetenschappelijk Onderzoek (NWO)' It was supported by the European Commission within the Sixth Framework Programme through I3-EURONS (contract no. RII3-CT-2004-506065).
#hofstee@kvi.nl

For the Pb^{27+} beams losses in the low energy beam line due to charge exchange are non-negligible. In the horizontal part of the beam line the vacuum was improved to 3×10^{-8} mbar by baking the components and removing some parts with high outgassing. In the 5 m long vertical beam line into the cyclotron the vacuum is in the 10^{-7} mbar range due to lack of pumping speed. The high stray fields preclude the use of turbomolecular pumps and cold heads. We are investigating the possibilities to install NEG-pumps [4] to improve the vacuum and thereby the transmission for the Pb beams.

The AGOR-cyclotron is equipped with a single harmonic sinusoidal buncher at 0.5 m from the median plane. A bunching efficiency of 35 % has been deduced from measurements using the phase probes [5] and from the gain in intensity obtained with the buncher. A substantially higher bunching efficiency can be achieved with a multi-harmonic bunching system. We are currently working on the conceptual design of a new buncher system, preferably including the existing buncher.

VACUUM DYNAMICS

The desorption caused by beam particles impinging on the walls of the acceleration chamber and the acceleration electrodes after a charge changing collision with the residual gas leads to a degradation of the vacuum and thereby to an increase in the losses [6, 7]. Due to this mechanism the extracted beam intensity for heavy ion beams exhibits a maximum as a function of the injected intensity: injecting a higher intensity results in a lower extracted current. The actual value of the maximum intensity strongly depends on ion species and final energy. For heavy ion beams up to Ar with energies above 20 MeV per nucleon a degradation of the vacuum and consequently the transmission has been observed but the intensities requested for the experiments can be delivered. For the Pb-beams in the energy range 7 – 10 MeV per nucleon operational experience and calculations show that the maximum achievable intensity is below the value requested for the experiments.

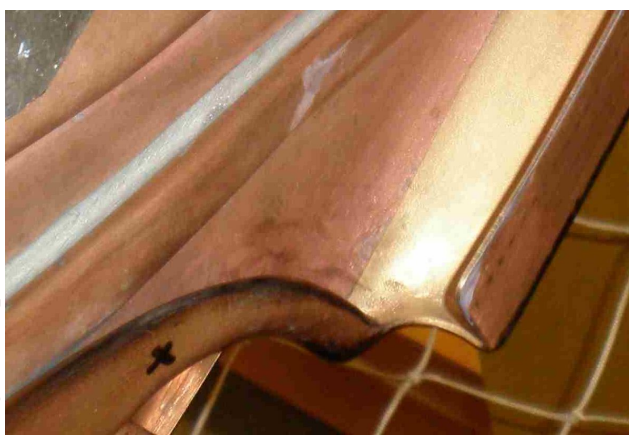

Figure 2: Detail of the gold coated outer perimeter of the acceleration electrodes.

The pumping speed in the acceleration chamber is due to the 18 mm height of the acceleration chamber conductance limited even with the internal cryopumps in use. Improvement of the beam transmission can thus only be achieved by reducing the desorption. On the basis of the work described in ref. 6 we applied a gold coating to the outside perimeter of the acceleration region. This is expected to reduce the local high energy beam loss induced outgassing by a factor 10.

UV-stimulated outgassing, improved cleaning procedures and the additional pumping speed of a third internal cryopump will further reduce both the base pressure and the desorption yield, thus enabling higher beam intensities.

EXTRACTION SYSTEM

The extraction efficiency for the relevant heavy beams from the AGOR cyclotron typically exceeds 85 % and has been found to depend only weakly on the beam intensity. The beam losses occur mainly in the electrostatic deflector, with minor losses in the subsequent electromagnetic channels.

The losses in the second, superconducting channel do not lead to quenching as the (relatively low energy) particles are stopped in the inner 20 K-shield of the channel. The temperature increase of the shield has turned out to be a useful diagnostic to optimize the transmission through the channel. Minimizing the beam losses in the channel is also important because of the important outgassing from the cold surface they induce.

The original electrostatic deflector is not actively cooled. With a septum with a V-groove at the entrance it has operated very reliably for the intensities delivered up to now. For the operation at the higher intensities anticipated for the production phase of the experiments, an upgraded electro-static deflector with cooling has been developed, which is currently being completed and will be installed in the cyclotron at the end of 2010.

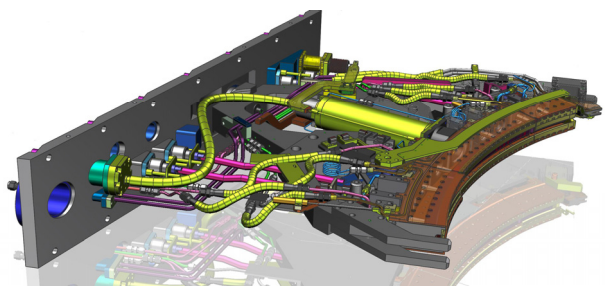

Figure 3: New electrostatic deflector

The tungsten septum has a V-groove to spread beam losses and is cooled via a cooling circuit in the upper part of its support structure. Geometrical constraints prevented the lower part to be cooled as well. In order to reduce beam losses on the septum even further a tungsten pre-septum with V-groove has been installed up stream of the septum as part of the collimator at the entrance of the deflector, which is shown in fig. 4.

The cathode is cooled via conduction through the aluminium nitride insulators, which are internally water cooled at the ground side. Extensive testing showed that the new insulators reliably operate at voltages up to at least 60 kV, while the maximum voltage required is 46 kV. Breakage of insulators due to stresses introduced by the brazing of their titanium endcaps was remedied by minor modifications of the brazing procedure.

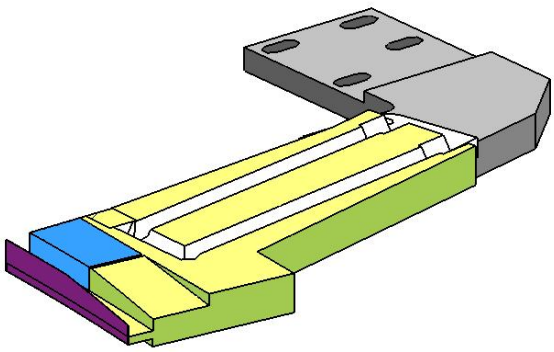

Figure 4: Cross section of the pre-septum of the electrostatic inflector. Violet: 0.2 mm tungsten foil; blue: tungsten block to stop protons; green/yellow: copper block with direct water cooling

BEAM LOSS CONTROL

Beam losses in the extraction system and high energy beam line cause power densities up to 1 kW/mm^3 in the materials in which the beam is stopped. Such power densities result in damage to components at the 10 – 100 ms timescale. Therefore a system for fast beam loss monitoring and control is essential for safe operation. We have developed and commissioned such a system based on previous developments at GANIL [8] and GSI [9]. It is described in more detail elsewhere in these proceedings [10]; here we only mention the main characteristics.

The beam losses in the cyclotron and high energy beam line to the entrance of the fragment separator (split up in six sections) are assessed by measuring the beam intensity at the entrance and exit of each section with non-destructive inductive pick-ups and the localized losses on collimators and slits. The non-localized losses in each section are determined from a current balance. Localized or non-localized losses in the cyclotron or any section of the high energy beam line exceeding an individual preset limit cause the duty cycle of a chopper in the injection beam line to be reduced stepwise until the losses are again within safe limits. Losses exceeding a second, higher limit, typically related to error conditions, cause the beam to be interrupted within 10 ms.

Increasing the duty cycle of the chopper or switching the beam on again after remedying the cause of the too high losses requires operator intervention.

The system also protects the semi-interceptive beam profilers. Inserting a beam profiler under normal operating conditions causes the beam to be interrupted. After inserting a pepperpot in the injection line to reduce the primary beam intensity to a safe level the operator can switch the beam on again.

CONCLUSION

We have demonstrated that the AGOR cyclotron can deliver beams with an intensity exceeding 10^{13} pps for elements up to Ar accelerated to an energy in the range 20 – 30 MeV per nucleon. The beam loss monitoring and control system needed for safe operation has been completed and the new electrostatic deflector that can withstand such beams for long periods is nearly completed.

For the heavy elements such as lead, the maximum obtained beam intensity of 3×10^{11} pps is due to limitations related to ion optics, injection efficiency and vacuum. The obtained intensity is still a factor three below the ultimate requirements for the experiments. With the on-going improvements on all these aspects the requested intensity is well within reach.

REFERENCES

[1] V. Mironov *et al.*, Cyclotrons2010, MOPCP053; http://www.JACoW.org
[2] S. Saminathan *et al.*, ECRIS2010, THCOAK03; http://www.JACoW.org
[3] M. Leitner *et al.*, ECRIS02 workshop, Jyväskylä, June 2002
[4] www.saesgetters.com
[5] S. Brandenburg and T.W. Nijboer, KVI Annual report 2003, p. 89
[6] C. Omet, H. Kollmus, H. Reich-Sprenger, P. Spiller, Proc. EPAC08(2008)295; http://www.JACoW.org and references therein
[7] A. Sen, M.A. Hofstee and S. Brandenburg, Cyclotrons2010, MOPCP083; http://www.JACoW.org
[8] C. Jamet *et al.*, Proc. DIPAC2005 p 169; http://www.JACoW.org
[9] H. Reeg, J. Glatz, N. Schnieder H. Walter, Proc. EPAC06 p.1025; http://www.JACoW.org
[10] M.A. Hevinga *et al.*, Proc. Cyclotrons2010, paper MOPCP087; http://www.JACoW.org

RECENT PROGRESS ON THE FACILITY UPGRADE FOR ACCELERATED RADIOACTIVE BEAMS AT TEXAS A&M *

D. P. May, G. J. Kim, R. E. Tribble, H. L. Clark, F. P. Abegglen, G. J. Derrig, G. Tabacaru, G. G. Chubaryan, Cyclotron Institute, Texas A&M Univ., College Station, TX 77843 USA

Abstract

The Cyclotron Institute at Texas A&M University is involved in an upgrade, one goal of which is to provide radioactive ion beams accelerated to intermediate energies by the K500 superconducting cyclotron. The old 88" cyclotron, now the K150, has been refurbished to be used as a driver and also to provide higher intensity, low-energy, primary beams for experiments. Two external ion sources, an electron-cyclotron-resonance ion source (ECRIS) and a multi-cusp negative ion source, have been installed on a new axial line to inject beams into a modified K150 central region. Acceleration of negative ions of protons and deuterons with stripping for extraction will be used in order to mitigate activation of the K150. Beams from the K150 will be used to create radioactive species via a light-ion guide and a heavy-ion guide. Singly charged ions from either ion guide will be transported to an ECRIS that is configured to capture these ions and further ionize them. One charge-state from this second ECRIS will be selected for subsequent acceleration by the K500. Progress on the upgrade, including the acceleration and extraction of both negative and positive beams by the K150, is presented.

INTRODUCTION

Since 2005 the Texas A&M Cyclotron Institute has been extensively upgrading its facility (fig. 1). Described previously [1] this upgrade involves the axial injection of beams from both a 14.5 GHz ECRIS and a multi-cusp negative ion source for acceleration by the recommissioned K150 cyclotron. Although K150 beams will not be as energetic as beams from the K500 superconducting cyclotron, the K150 will be capable of providing much more intense beams for experiments and for the creation of radioactive ions that will then be accelerated by the K500 into an energy range unique for such beams. Two immediate goals for the refurbished K150 are 14 μA of 30 MeV protons and 0.9 pμA of 13.7 AMeV ^{40}Ar. Using intense beams from the K150, radioactive ions will be produced by stopping products from beam-target collisions in helium-filled cells in a light-ion guide, utilizing p, d and α beams, and in a heavy-ion guide. Low-charge-state radioactive ions collected from such a cell will be transported to a charge-boosting electron-cyclotron-resonance ion source (CB-ECRIS). Higher charge-state ions from the CB-ECRIS will then be injected into the K500 cyclotron for acceleration. The CB-ECRIS and its analysis line have been installed and are now being tested [2]. The analysis line will become the first leg of the low-energy-beam transport leading to the existing axial line for injection into the K500 cyclotron.

*Work Supported by U. S. Dept. of Energy Grant DE-FG02-93ER40773

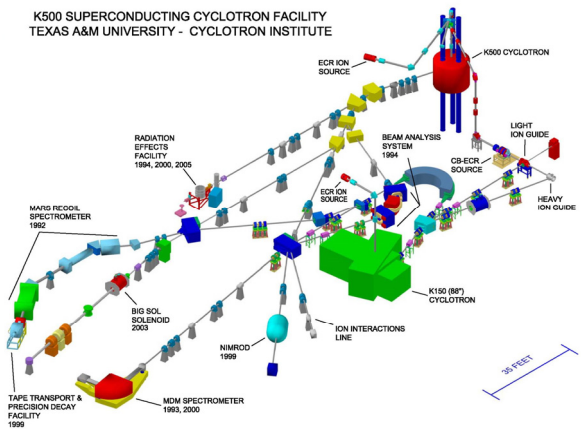

Figure 1: Overview of the Cyclotron Institute Facility.

K150 CYCLOTRON

In late 2007 a beam of protons was axially injected, accelerated to 20 MeV by the K150 and extracted at an intensity of 25 nA with an extraction efficiency of ~10%. This provided a first trial of the extensively refurbished K150, including its new rf system, new magnet power supplies, new vacuum system and new axial injection system as well as its original rf panels and dee, its original mirror inflector and deflector and its original beam probe. A substantial fall-off in intensity from the center to outer radius was observed, presumably due to poor matching in the center region. After some tests the axial injection system, including the upper central steel plug, and the dee were removed so that modifications could be made to improve the transmission. Most recently, a negative-ion, multi-cusp source along with an extraction-by-stripping system were added to the K150.

Axial Injection Line

The injection line (fig. 2) was augmented by the addition of a Glaser lens and steering coils to a new upper steel plug in order to improve beam injection. The upper and lower steel plugs shape the central magnetic field so particular care was taken in alignment with respect to the median plane. Also, extra focusing einzel lenses were added to accommodate the new multi-cusp, negative ion source which was mounted on axis directly above the 90º analysis magnet which bends the beam from the ECRIS onto cyclotron axis.

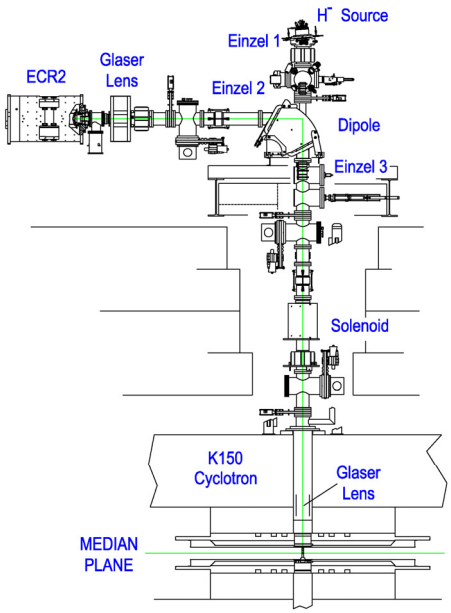

Figure 2: Injection line for the K150.

Central Region Modification

Before the K150 was decommissioned in 1986, beams from polarized ion sources were axially injected, but since internal, off-axis filament and PIG ion sources were still being used, the central region was not optimized for the injected beams. To improve the initial electric focusing and orbit centering, a set of titanium dee inserts, following the design for the LBNL 88" cyclotron [3], were recently constructed and installed (fig. 3). A great deal of effort was devoted to proper alignment of the inserts, both due to its importance to beam acceptance and to the fact that the inserts had to be manipulated from a distance of 1.6 m inside the cyclotron-pole clearance of 15 cm. The dee inserts provide a well-defined electric field near the center of the cyclotron and reduce the gap between the dee and the dummy dee in this region from 5 cm to 0.64 cm. Center region acceleration was studied using the NSCL code Z3CYCLONE with 3D electric field maps produced with TOSCA and magnetic field maps from the LBL orbit code CYDE (fig. 4). It was found that reasonable dee voltages lead to well-centered orbits.

After installation of the dee inserts several test beams were run. Table I lists these beams and compares them to the October 2007 proton beam. All these beams were unbunched and accelerated to an outer radius close to the extraction radius. What is striking is the improvement in the intensity-versus-radius profile for the 20 MeV proton beam as well as a much lower optimized rf voltage. Most of the beams exhibit a good I vs R profile except for the more vacuum sensitive $^{16}O^{5+}$ beam.

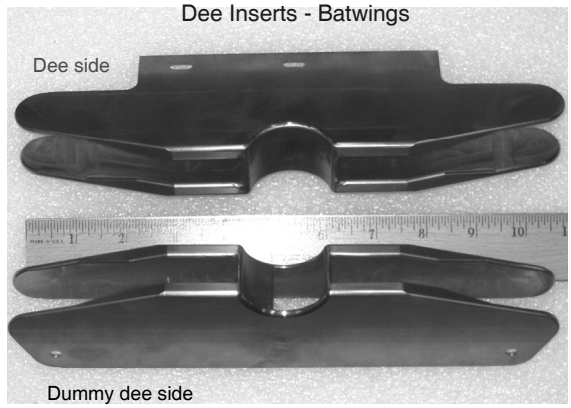

Figure 3: Dee inserts, before installation.

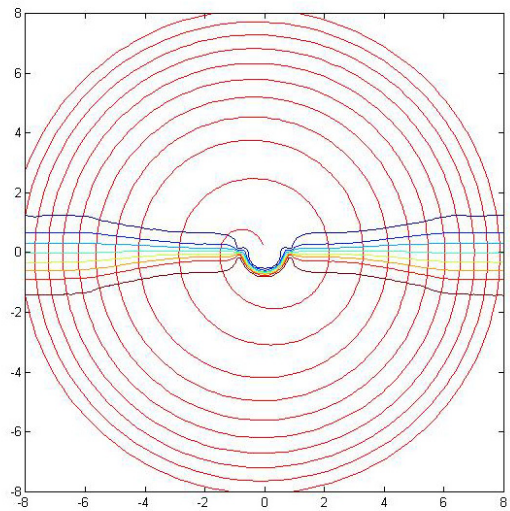

Figure 4: Centered orbits calculated with dee inserts. Scale is inches.

Table 1: First Beams

T/A MeV/u	Ion	Vdee (kV)	I@inj (eμA)	I@infl (eμA)	I@10" (eμA)	I@35" (eμA)
20	P (Oct07)	73 (w/o inserts)			0.65	0.22
20	P	45	29	10	0.33	0.32
25	P	46	23	8	0.56	0.54
30	P	52	25	9	0.40	0.37
7.5	$^{16}O^{5+}$	53	89	35	3.1	1.9
10	$^{16}O^{6+}$	56	132	62	3.9	3.5
12	$^{16}O^{6+}$	65	130		5.0	4.7
14	$^{16}O^{6+}$	65	110		3.4	2.9
14	$^{16}O^{7+}$	65	22	12	0.74	0.67

Negative Ion Beams

Radiation simulations confirmed that the high intensity light-ion beams required for radioactive ion production would cause high levels of activity in the K150 deflector, which would be a troublesome maintenance issue. Following the successful scheme for H- acceleration by the JYFL cyclotron laboratory [4], it was found that a similar approach would work for the K150: a multi-cusp ion source produces intense H- and D- beams which are accelerated to full radius and then stripped to protons or deuterons and then directed along the exit beam-line by a dipole magnet. Studies showed that there would be sufficient clearance in the K150 beam chamber with the deflector moved to its maximum radius, that an existing port near the exit could be used for the insertion of a moveable carbon foil, that a surplus dipole could be refurbished to provide the maximum 18º deflection required to bring the beam unto the exit beam-line (fig. 5) and that the existing vacuum in the K150 (10-5 torr in the center to 2X10-6 torr near extraction radius) would not cause significant beam loss with resulting activation.

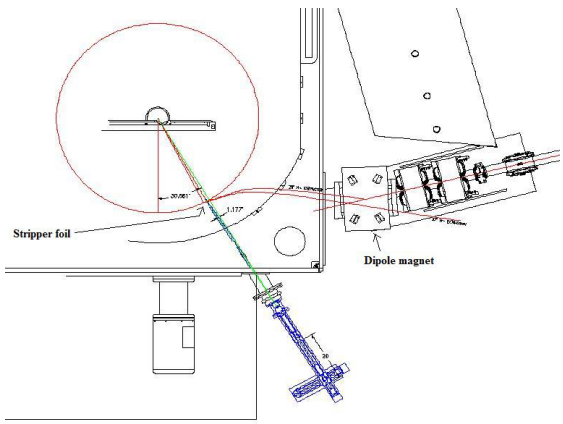

Figure 5: Extraction for H^- and D^- beams.

Testing at JYFL showed that their unused prototype multi-cusp source could produce a sufficient amount of H^- beam for our project. This source was acquired for the K150. With a new source extraction system designed and built by Texas A&M, testing at JYFL showed that the ion source produced up to 1 mA of H^- ions and with an emittance less than 8π mm-mrad. Injection of the H^- beam was studied with the code SIMION (transport plus space charge effects) and two einzel lenses were added to the injection line. The source was mounted and a 1.0 mA current was measured at the analysis faraday cup in the vertical section of the line.

Recently, H^- and D^- acceleration and strip extraction were tested. For H^- the currents in the main and trim coils were reversed and set to the values from the earlier 20 MeV proton run. After some optimization, beams of ~10 μA of H^- were stripped and extracted from the cyclotron onto the faraday cup after the exit dipole. Next, 30 MeV H^- ions were accelerated, and up to 24 μA was obtained on the exit Faraday cup, but this value would slowly decrease to approximately 18 μA as the cyclotron vacuum degraded due the beam heating. In a similar fashion ~1.2 μA of 10 AMeV deuterons was extracted.

With the 30 MeV H- extracted and stopped on the external faraday cup of the K150 cyclotron, secondary radiation levels from neutrons and gamma rays were measured in the cyclotron vault and at the injection line above the K150 cyclotron. Levels of ~1 Rem/hr were measured inside the cyclotron shielding and 2 – 3 mRem/hr were measured at the injection line outside the shielding. These are low values with regard to the safety of the staff working around the cyclotron facility.

FUTURE PROGRESS

Transporting beams from K150 to target for experiments is planned for the near future. An internal LHe cryopanel is being constructed for installation in 2011. The next series of tests will focus on beam-loss of injected negative ions, on extraction of positive ions through the electrostatic deflector, on magnetic field and rf voltage limits for beams and on the ability to predict accurately main-magnet and trim-coil current values for a wide variety of beams. The acceleration of radioactive beams by the K500 is scheduled for late next year.

ACKNOWLEDGMENTS

We are grateful to Claude Lyneis and Daniela Leitner of LBNL for help with the design of the axial injection line and the dee inserts, and to Juha Arje, Taneli Kalvas, Tommi Ropponen and Olli Tarvainen from JYFL of the University of Jyvaskyla for their help with the negative ion source. We would also like to thank Pauli Heikkenen of JYFL and Felix Marti of NSCL for their help and advice.

REFERENCES

[1] D. P. May *et al.*, Proc. of the 18th Int. Conf. on Cyclotrons and their Applications. Giardini-Naxos, Italy, Oct. 2007, p. 505.

[2] "Design of a Charge-Breeder Ion Source for Texas A&M Univ.", W.D. Cornelius, accelconf.web.cern.ch/AccelConf/ecris08/papers/weco-b01.pdf.

[3] D. J. Clark and C. M. Lyneis, Proc. of the 11th Int. Conf. on Cyclotrons and their Applications, Tokyo, Oct. 1986, p.499.

[4] P. Heikkinen and E. Liukkonen, Proc. of the 16th Int. Conf. on Cyclotrons and their Applications, East Lansing, May 2001, p. 89.

INTENSE BEAM OPERATION OF THE NSCL/MSU CYCLOTRONS*

Jeffry Stetson#, Guillaume Machicoane, David Poe, Felix Marti, NSCL/MSU, East Lansing, MI 48824, USA

Abstract

Intense heavy-ion beam acceleration by superconducting compact cyclotrons presents significant challenges since surfaces impacted by lost beam are subject to high thermal loads and consequent damage. High transmission efficiencies allow 0.7 – 1.0 kW beams to be routinely delivered for experiment at the NSCL, with minimal negative impact on reliability. Net beam transmission measured from just before the K500 to extracted beam from the K1200 is often about 30% and usually above 20% depending on the ion used (factoring out the unavoidable loss due to the charge stripping foil in the K1200). Results, techniques and examples are discussed.

INTRODUCTION

The National Superconducting Cyclotron Laboratory (NSCL) consists of two coupled cyclotrons, the K500 and K1200 [1], which accelerate ion beams produced by an ECR-type ion source (ECRIS). For the majority of running time, the machines are used as "drivers", impacting the beam onto a target at the object of the A1900 particle separator to produce fragments which are then purified and sent downstream as a rare ion beam (RIB) suitable for nuclear science experiments with exotic nuclei.

Presently, two ECRIS's are available for axial injection into the K500. Besides providing a measure of redundancy in the event of a failure of one source, being able to alternate between two sources is a significant benefit to operations overall in that the next beam can be prepared while the present experiment is running. This is particularly important when the ions come from a solid rather than gaseous material, which may require venting the source, special hardware, cleaning the plasma chamber, or long periods of conditioning. The older source, called ARTEMIS-A (Advanced Room Temperature Ion Source), is a modified version of the Berkeley AECR-U operating at a frequency of 14.5 GHz. (A duplicate, ARTEMIS-B, located on an independent test stand is used for development purposes.) A new, 3rd generation, ECRIS named SUSI (SUperconducting Source for Ions), presently operates at 14 or 18 GHz [2], [3]. Both sources run with extraction potentials ranging from 18 – 27 kV depending on the K500 injection requirements.

Beams in the range of 8 – 15 MeV/u from the K500 are injected mid-plane into the K1200 through a 200 - 800 μgm/cm^2 stripper foil (usually amorphous carbon) located at a radius of about 32 cm. Transport dynamics require the ratio of beam charge going into the foil to the charge coming out to be between 2.3 and 2.7.

In the evolution of the NSCL to a provider of RIB's almost exclusively, the emphasis has shifted from "maximum energy" to "maximum intensity". Development toward producing higher-power beams continues, but must remain consistent with an active experimental physics program which requires reliability, consistency, and the avoidance of unscheduled downtime that may result from running at high power.

PRESENT LIMITS

A list of most of the NSCL beams, together with their present estimated intensity limits and the reason for those limits, is provided in Tables 1, 2 and 3 below. These intensity restrictions fall into the general categories of power-limited, source-limited, and stripper foil-limited. Several additional NSCL-run beams are not listed because they have not yet been developed to their full potential, due either to being only recently introduced (^{82}Se, for example) or due to limited user demand. About half of the NSCL running time uses five beams (^{48}Ca, ^{40}Ar, ^{78}Kr, ^{76}Ge, and ^{86}Kr) of the 22 ion species available, so consequently, these beams are the most thoroughly developed. The values given in theses tables are generally not the peak recorded intensities, nor are they what is guaranteed to experimenters for planning purposes (those are made available on the NSCL website), but are values considered reasonably achievable and maintainable for some hours. However, days-long RIB production using beam powers greater than that presently run will require additional machine protection features than are presently available in order to limit damage in the event of beam position excursions. It will also require active feedback from non-intercepting probes to precisely monitor and maintain the high extraction efficiency obtained in the initial tune throughout the duration of the high-power run.

Table 1: Beams presently limited by ECRIS output.

Ion	Mev/u	pnA	Watts
58-Ni	160	40	370
64-Ni	140	15	134
76-Zr	120	3	37
112-Sn	120	10	120
118-Sn	120	3	38
124-Sn	120	3	44

Refractory-metal beams are an area of experimental interest, but are difficult to produce in the ion source because of the high temperatures required. Continued

*Supported under National Science Foundation Grant PHY-0606007
#stetson@nscl.msu.edu

SUSI and associated oven development is expected to rapidly raise the existing output of the present beams and to make other ion species available at useable intensities in the future.

Table 2: Beams presently limited by power issues.

Ion	MeV/u	pnA	Watts
16-O	150	500	1200
18-O	120	500	1080
22-Ne	150	220	726
24-Mg	170	200	816
36-Ar	150	150	810
40-Ar	140	200	1120
48-Ca	140	140	941
78-Kr	150	100	1170
86-Kr	140	70	843
124-Xe	140	25	434

For most of the beams shown in Table 2, the limiting factor is beam loss on the K1200 deflector. While the K500 deflectors are not as well-cooled, no heat-related problems have been noted up to double the chosen loss-limit of 100 W, nor have there been any beam-related failures. The K1200 deflectors are water-cooled, with a planned loss-limit of 1000 W, but there have been failures well below that level, so losses much greater than 200 W are avoided. Deflector limits in practice however, are not only determined by the value of the power lost, but also by the energy density created by beam hitting the (tungsten) septum. Oxygen, with a range of 4.1 mm, causes less material damage at a given beam power than xenon which has a range of 0.7 mm at the NSCL energies. An additional source of K1200 deflector heating can be the large-angle impact of injected beam that is not charge-stripped from its starting value. (This factor is a problem for some beams and not others, depending on the details of the injection dynamics.)

Separate from other considerations, the subset of medium-heavy beams capable of ~1 kW power, presently argon, calcium, and krypton, are also restricted by potential damage to the A1900 production target during the course of an experiment. Experience has shown that sustained, full-power exposure over the course of an experiment can damage these targets (usually beryllium) within the 1 mm diameter beam impact region, causing an unacceptable reduction in both the resolution of and transmission through the A1900 separator. This effect occurs even when the overall heating of the target material is significantly less than its 500 W cooling limit. Replacement of the present fixed target with a rotating version is planned and should greatly curtail this problem.

The uranium, lead, and bismuth beams share both low stripping efficiency characteristics and short ranges in materials. A thinner foil absorbs less energy, but may be far away from the equilibrium thickness required for best stripping efficiency. A thicker foil may give better stripping efficiency, but absorb more power and increase beam emittance. Such conditions make optimization of these heavy beams difficult.

Table 3: Beams presently limited by stripping-foil issues.

Ion	MeV/u	pnA	Watts
208-Pb	85	2	36
209-Bi	80	2	34
238-U	80	0.3	6
238-U	45	0.1	1

In the case of the 80 MeV/u uranium beam, an injected beam of 7.7 MeV/u $^{238}U^{30+}$ at a current of 20 pnA, will noticeably degrade the foil in about 15 seconds and make it totally unusable after a few minutes. Even reducing this incoming beam intensity by ½ or more will only extend the foil lifetime to at most to 3 or 4 hours. It is not clear that there is a solution to the foil lifetime problem for the heaviest ions within the constraints of the present machines. A detailed discussion of stripper-foil performance is presented in this conference [4].

Improvements in High-Intensity since 2006/07

The trend toward higher transmission efficiencies through the cyclotrons has continued. A comparison of four selected beams normalized to the same output power is given in Table 4 and Table 5.

Transmissions for the K1200 are given with the unavoidable losses due to the stripping efficiency of the foil factored out; this allows comparison of machine tune quality across the range of 22 different ions presently used at NSCL. The efficiency of stripping into the desired charge state for acceleration are experimentally-determined results from measurements taken on a test setup in the K500 to K1200 coupling beam line. Each ion type used for acceleration is tested for stripping ratios at the required energy with the particular foil thicknesses and, in some cases, materials used. The selection of foil thickness to be used is made based on these measurements as well. A sample of such results is given in Table 6.

Most remarkable in this comparison has been the improvement in the K500 total transmission (measured in the injection beam line ~ 2 m upstream of the K500 inflector and on the first Faraday cup in the K500 - K1200 coupling beam line). Presently, the expectation of this value for normal tunes is 40-50%.

The transmission efficiency of beam through the K1200 has also improved over this period, with the effect of improving the net transmission through both machines by about a factor of two and generally reducing losses on the deflectors at comparable intensities.

Table 4: High-power beam transmissions and related deflector losses in 2006/2007. Unacceptably high deflector losses are indicated by red shading.

2006/2007	^{16}O	^{48}Ca	^{78}Kr	^{124}Xe
Final E (MeV/u)	150	140	150	140
Beam Power (W)	1500	1000	1000	400
K500 out / K500 in	21%	37%	15%	28%
K500 Deflector Loss (W)	113	78	180	79
K1200 out / K1200 in	34%	63%	49%	53%
K1200 Deflector Loss (W)	484	111	380	110
K1200 out / K500 in	6%	22%	6%	14%

Table 5: High-power beam transmissions and related deflector losses in 2009/2010.

2009/2010	^{16}O	^{48}Ca	^{78}Kr	^{124}Xe
Final E (MeV/u)	150	140	150	140
Beam Power (W)	1500	1000	1000	400
K500 out / K500 in	50%	51%	36%	43%
K500 Deflector Loss (W)	106	37	68	36
K1200 out / K1200 in	66%	66%	61%	57%
K1200 Deflector Loss (W)	290	140	112	88
K1200 out / K500 in	20%	33%	30%	25%

Table 6: Stripping efficiencies into the desired charge state for K1200 acceleration using a 600 μgm/cm^2 thick amorphous carbon foil.

	^{16}O	^{48}Ca	^{78}Kr	^{124}Xe	^{238}U
Charge In, Out	3+ 8+	8+ 20−	14+ 34+	19− 45−	30− 69−
Efficiency	95%	69%	53%	26%	9%

HARDWARE MODIFICATIONS 2007-2010

A number of hardware changes contributed to increased beam powers over this period including, (1) installation of a beam chopper, (2) adding a second harmonic to the K500 buncher, (3) repair of a polarity error with one pair of K500 centering bump coils, (4) the replacement of an older 6.4 GHz ECRIS with SUSI, and (5) replacement of a cylindrical-type electrostatic bender under the K500 with one of a spherical-electrode design.

A 2-plate electrostatic beam chopper was installed on the K500 injection beam line in January of 2008. While not directly a performance enhancement, it greatly enhances exploration of high beam intensities by reducing the likelihood of thermal damage during optimization of the machine tune, but still allows evaluation of machine performance at high burst intensity. Previous to this time, control of the injected beam intensity was entirely done with attenuator grids and/or slits, giving results that were often not scalable to the full-intensity tune.

Second-harmonic capability was added to the buncher in August of 2008, with immediate improvements observed in accelerated beam intensities in rough agreement with expectations (a gain over DC of a factor of 5 assuming 40 degrees of phase acceptance) [5]. This compares to a gain of about 3 for first harmonic bunching alone.

In April 2009, a long-standing wiring error in the K500 resulting in a reversed polarity on one of the three inner trim coil sets used to generate an adjustable field bump for beam centering was discovered and remedied. This repair resulted in better extraction and lower losses for a given beam intensity, as well as less “scatter” in parameter settings from run-to-run.

First beam through the cyclotrons from SUSI occurred in October 2009. The development and injection of beams from this source is in its early stages and is hence yet to be fully optimized. Initial results are however encouraging (showing improved final beam powers with krypton and oxygen beams, to date) and SUSI is already in reliable rotation with ARTEMIS as a producer of beams used in the NSCL experimental program.

The last 90 degree bend of the injection line is upwards onto the center axis of the K500. Until recently, this was accomplished with a cylindrical-plate electrostatic bender, which has strong vertical focusing and no horizontal focusing, making it difficult (or impossible) to pass a symmetrical beam to the K500 for injection. This bender was replaced by a spherical-electrode bender in April 2009. The requirement for a large electrode gap of 64 mm and a small bending radius of 200 mm, plus the restriction of fitting into the existing small vacuum chamber, demanded a rather unique design in order to keep aberrations at a minimum and to get the bent beam simultaneously on-axis and with the proper 90 degree angle. The general configuration of this device is shown in Fig. 1.

The overall better matching possibilities provided by this double-focusing design have allowed transmissions through the K500 with injected beam emittances of 10π mm×mrad (rms) achieved before this change, to be achieved with double that emittance afterwards..

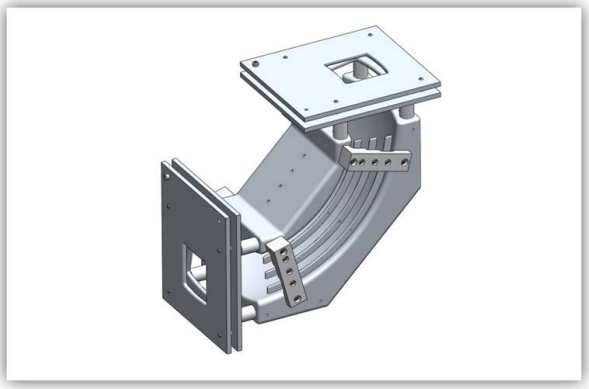

Figure 1: The electrode configuration of the high-acceptance, low aberration, spherical bender is shown. The entrance and exit aperture plates can be biased and aid in precise shaping of the electric field at the ends of the main electrodes. Since sides of the main electrodes come as close as 10 mm to the grounded vacuum chamber, the pair of 3 "arc" electrodes are provided to act as a voltage-divider for straightening the field on both sides. The bend radius and main electrode gap are 200 mm and 64 mm, respectively.

DEFLECTORS

A measure of beam loss on the extraction deflectors of heavy-ion superconducting compact cyclotrons is unavoidable. The turn separation of the outer orbits in the K500 is about 1.3 mm center-to-center and half that in the K1200, even when not taking into account the "arc" created by sine-wave acceleration over a significant phase width. The detrimental effects of such loss are compounded by the short penetration depth of heavy ions in materials. For the NSCL beams of significant power, their ranges in tungsten (the chosen septum material) vary from 0.03 to 0.08 mm in the K500 and from 0.7 to 4.1 mm in the K1200, depending on the ion being accelerated and its energy. These losses, the high power density per watt created upon beam impact, and the high electric fields required (up to 75 kV/cm in the K500 and 115 kV/cm in the K500) conspire to make reliable deflector operation a difficult challenge. Some specific engineering considerations to meet these challenges are described in Ref. [6]. Additionally, experience has led to a procedure whereby all new or repaired deflector assemblies are conditioned for several days to run at high voltage without sparking or significant current draw. This is done in a vacuum chamber kept in a magnetic field provided by a retired bending dipole permanently installed in an x-ray shielded area. After conditioning, the deflectors are kept in a sealed container until use. This minimizes the time from their mounting in the cyclotron until they are fully ready to run, and guarantees that a serviceable spare is immediately available in case of a failure.

A further requirement of successful deflector function is the continuous introduction of oxygen during intense beam operation. Stress on the deflector appears either as an increase in the spark rate or an increase in the drawn current (over minutes or hours) which eventually results in the power supply no longer being able to generate the high voltage required. Small amounts of oxygen gas fed along the high-voltage connections directly into the deflector housing seem to mitigate these effect. For K1200, the normal flow rate is about 0.2 standard cubic centimeters per minute (sccm). (The K500 deflectors generally require flow rates under the 0.1 sccm limit of the present mass-flow controllers, so their flow is pulsed on and off at about once per minute).

For difficult K1200 cases, the flow rates may be raised significantly up to 2 sccm, until the deflector responds and the current draw drops, whereupon the flow can be reduced to a more-normal value. It's desired to keep the flow rates as low as possible because the increased pressure in the vacuum chamber causes increased attenuation of the accelerated beam, however for flows under 1 sccm and for all but the heaviest ion species, this effect is minimal.

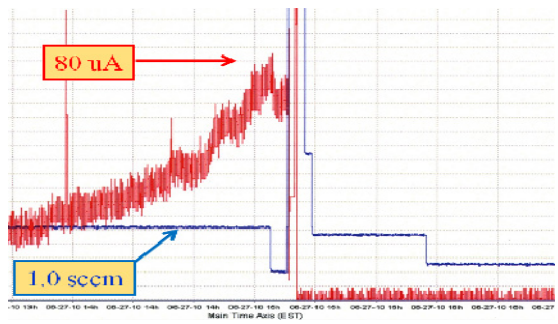

Figure 2: Oxygen gas-flow rate in sccm (blue) and K1200 deflector power supply current in μA (red) as a function of time are shown. Normal operation is interrupted by a rise of the drain current to a level (here ~80 μA) where full voltage cannot be maintained. A "high-pressure gas treatment" is applied as described above, dropping the drain current to low levels and allowing normal operation to resume after a 20 minute interruption. The total period shown is 3 hours.

For severe cases, when the K1200 deflector has essentially failed and is unable to maintain voltage, another technique, called a "high-pressure gas treatment", is used. First beam is stopped upstream, and the RF is shut off. Then, with the deflector still set for the desired voltage, the mass-flow controller is opened to deliver its maximum flow of about 12 sccm. This raises the chamber vacuum from its base value of around 2 μTorr to about 50 μTorr. The current normally will drop quickly. If this doesn't work, then a manual bypass valve is opened to increase the flow even further, inducing a high-current, low-voltage corona discharge in the deflector. After period of discharge for as long as 30 minutes, the deflector will then usually return (upon reducing the gas flow) to the desired low-current, high-voltage state and

normal operation can be resumed. An example of this process is given in Fig. 2 above.

Why this process works and why oxygen seems to be effective is not clear, but it may be similar to oxygen plasma cleaning techniques becoming common in industry.

To achieve reliable operation, the K500 deflector loss limits are set to about 100 W and the K1200 at 200 – 300 W, conditional on housing temperatures remaining under 110 degrees C. (Limits on the xenon beams tend to be considerably lower.) Design engineering, pre-conditioning, oxygen gas flow, and loss-limit restriction taken together have made interruptions of beam delivery caused by deflector failure, rare events.

OTHER CONSIDERATIONS

A well-established requirement for good performance from the NSCL cyclotrons is a beam of low emittance and minimal "tails" injected into the K500. The intrinsic emittance of an ECRIS beam is about 200π mm×mrad, while best K500 performance is achieved with beams less than 20π mm×mrad.

Besides the clear relationship between injected transverse phase space and maximally-separated turns for good extraction efficiency, there is a strong cross-coupling across the injected transverse phase ellipse to the phase spread of the bunched beam as it passes though the spiral inflector. While it is possible to pass a 100π mm×mrad beam from the axial injection path into the K500 cyclotron midplane for acceleration, particles on one side of the transverse phase ellipse can be shifted into a phase 40 degrees different than particles located on another side [7]. A reduction in the injected emittance minimizes this effect. K500 performance continues to improve as emittance is reduced to levels that become difficult to measure with the available instrumentation (2 – 5π mm×mrad).

A system of collimation techniques for ARTEMIS-A and its associated beam line achieves this and still allows up to about 30% of the ECRIS beam intensity to pass through. A thorough discussion of these techniques is given in Ref. [8]. Once established, the quadrupole settings are quite consistent between different ion species and scale well by rigidity. The collimation scheme for SUSI is quite different and still being optimized. A discussion of those techniques is given elsewhere during this conference [9].

Reproducible and stable ECRIS tunes are important in both the initial setup of high-power beams for RIB production and keeping that intensity at high levels for the duration of the experiment. The high sensitivity of the K500 to any shift in beam position or any increase in injected emittance puts increased stability constraints on source operation. A general and effective technique to aid stable running, made possible by the availability of two sources, is that the one to be used for the next scheduled beam is run for at least 24 hours beforehand at the output required for that experiment.

Still, source changes affecting cyclotron beam output do occur over the course of a run and can be difficult to detect as they do not always involve clear changes in the source output current or in other easily-measurable parameters. Quickly isolating source issues from a myriad of potential other reasons for a reduction in cyclotron output can be a difficult task. To solve this problem and potentially aid as a tool for source optimization and physical understanding of sources in general, a new tool is being explored.

Using a signal take directly (except for a resistor to drop the voltage created by the ~ 25 kV beam potential and a low-pass filter to eliminate spurious < 1 MHz noise from various unrelated devices), one can see with an oscilloscope that the beam produced by the ECRIS is not pure DC but contains AC components ranging from near zero to around 10% for tunes that otherwise appear reasonably stable. For the most part, the AC components also have defined characteristic frequencies which can be analyzed real-time via the scope's FFT function (if available). Varying normal source parameters such as microwave power or feed gas flow may either smoothly change the characteristic frequencies seen, or they may remain rather unaffected over a wide range, only to flip suddenly into a new mode frequency with tiny further changes. The output beam intensity may or may not change between mode transitions.

An example of sudden transitions is shown in Fig. 3 where the source, in this case ARTEMIS, exhibited three distinctly different oscillation modes over the small range of 305 to 315 W in microwave power, with the settings of all other devices remaining unaltered.

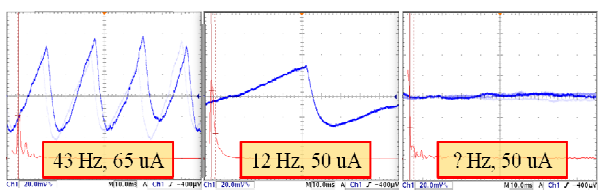

Figure 3: A beam of $^{40}Ar^{7+}$ at a 24.43 kV extraction potential is shown on an FFT oscilloscope for microwave powers of 305, 310, and 315 W. The AC coupled signal is shown as the upper trace in blue, with the AC component of the DC signal being 2.7%, 1.9%, and < 0.1%, respectively.

To date, only one attempt to correlate various source modes with K500 performance has been made, but it proved interesting in an unexpected way. After a day of tuning different-mode beams through the K500, the source was left in a chaotic frequency, low-noise mode, similar to that shown on the right in Fig. 3 above, for the overnight hours. By morning, with the exact same device settings as before, and with similar source output current, the K500 output was down by about 50%. The source had drifted into a distinctly different mode with 75 Hz oscillations. Very slight changes to the gas flow and

microwave power restored the original condition and simultaneously restored the original tune quality. With tweaking of the injection line steering and focusing, both conditions gave good results from the K500, but each mode required a somewhat different beam line tune to transmit properly into the cyclotron. It is suspected that source mode changes may be responsible for some otherwise-unexplained needs to "peak up" the machine tune over several-day running periods. Monitoring the state of the source using this technique (which, if the signal comes from a wire put into the injected beam path, can be easily done without beam interruption) is expected to reduce the need for such retunes.

Investigation of these effects is continuing, but some very preliminary observations are as follows: (1) The sensitivity to source parameters is greater for the heavier ions, (2) The modes vary between different charge states of the same ion (with source parameters kept constant), (3) For a given ion and charge, there seem to be a set of modes < 100 Hz, a set of modes >1 kHz, and a range of "quiet chaos" in between, and (4) Mode shifts may occur at or near peak source output. (This last point, in particular, is in line with operational experience where the operators often shift the source tune away from peak intensity, most often using a change in gas flow, to achieve best long-term stability.)

Low-emittance injection, in addition to its intrinsic benefits, helps make evident other effects that were hidden before. An example is the influence of a steering effect of the leads powering the innermost trim coil (TC01) of the K500 became evident. Unlike the other trim coil leads which are fed in through the caps, the TC01 leads run along the injection beam path near the machine center. It was found empirically that by setting this coil to zero and roughly compensating with TC02, that the centering bump magnitude could be reduced. Upon this discovery, the predicted trim coil settings were recalculated with TC01 forced to zero. In terms of trim coil settings, this feedback loop of hand-tuning improvements, determining what those settings represent in terms of a radius vs. phase history, then using that history to guide a new calculation, has proven quite productive. Ideally, one would also measure the resulting phase history, but the long-standing absence of a functional phase probe makes that impossible at present. A certain degree of confidence in the predictions is warranted however, because, to date, every such feedback cycle has worked; the predicted new values of trim and main coil settings based on the calculated phase history of an empirically-determined trim coil set seem to give identical results as far as the beam is concerned.

Through a similar process, it was discovered that increasing the phase error at injection right to the edge of vertical focusing limits, resulted in consistently better extraction efficiency when compared to smaller offsets. By injecting well off-phase, then bringing the beam back to zero phase at a larger radius, the energy gain per turn increases over the region, and is believed to result in a phase compression effect along the lines described in Ref. [10].

THE FUTURE

In principle, further gains in beam intensities can be achieved. (The progression would be along the path of increased beam collimation at critical points and compensating with increased source output that is anticipated with SUSI.) However, the "easy" gains have already been made, considering the limitations inherent in the design of the present machines. In addition, the planned retirement of the cyclotrons and their replacement by a much higher intensity heavy-ion linac driver means that the cost/benefit of any major future cyclotron improvements must be carefully considered.

CONCLUSIONS

After a series of upgrades to hardware and improvements in tuning techniques, the NSCL coupled cyclotrons are reliably producing heavy-ion beams at powers up to 1 kW. Improvements with the intention of increasing present power limits will continue, but progress is likely to be incremental.

ACKNOWLEDGEMENTS

The authors wish to thank the Operations Department at NSCL, S. Adam at PSI, and P. Spädtke at GSI for their contributions and productive discussions.

REFERENCES

[1] F. Marti, P. Miller, D. Poe, M. Steiner, J. Stetson, and X.Y. Wu, in Cyclotrons and their Applications, AIP Conf. Proc. 600 (2001) p. 64.
[2] P. Závodszky, *et.al.* in Rev. Sci. Instrum. 79, Issue 2 (2008) 02A30.
[3] G. Machicoane, D. Cole, and P. Závodszky, in Proc. of ECRIS08 (JACoW), Chicago, USA, (2009) p. 14.
[4] F. Marti, S. Hitchcock, P. Miller, J. Stetson, J. Yurkon, *this conference*.
[5] F. Marti and A. Gavalya, in Proc. of the 11th Intl. Cyclotron Conf., Tokyo, Japan, (1987) p. 484.
[6] A. Alfredson, F. Marti, P. Miller, D. Poe, and G. Stork, AIP Conf. Proc 600 (2001) p. 133.
[7] F. Marti, J. Griffin, and V. Taivassalo, IEEE Trans. On Nucl. Sci., Vol. NS-32, No. 5 (1985) p. 2450.
[8] J. Stetson, in Proc. of ECRIS08 (JACoW), Chicago, USA, (2009) p. 208.
[9] G. Machicoane, D. Cole, M. Doleans, T. Ropponen, J. Stetson, L. Sun, X. Wu, *this conference*.
[10] A. Chabert, G. Gendreau, P. Lapostolle, and P. Yvon, in IEEE Trans. of Nucl. Sci., Vol. NS-28, No. 3, (1981).

HIGH INTENSITY CYCLOTRONS FOR SUPER HEAVY ELEMENTS RESEARCH OF FLNR JINR

G.Gulbekyan, B.Gikal, I.Kalagin, S.Bogomolov, Joint Institute for Nuclear Research, FLNR, Dubna, Moscow region, Russia

Abstract

Main theme of FLNR JINR is super heavy elements research. From 2000 up to 2010 more then 40 isotopes of elements 112, 113, 114, 115, 116, 117, 118 were synthesized in the laboratory. As a target we used 243Am, 242Pu, 248Cm, 249Bk, 249Cf et al. Total flux 48Ca ion beam was on the level $5 \cdot 10^{20}$ ion. 48Ca matter consumption in ion source averaged 0.4 mg/hour at the beam intensity of 1 pμA .

According plan after U-400 cyclotron modernization (2012) 48Ca beam intensity will be increased up to 3pμA on the target and 48Ca. New cyclotron DC-200 planed to be put in to operation in 2014 will allow to reach 10 pμA of 48 Ca beam intensity.

INTRODUCTION

At present four isochronous cyclotrons: U-400, U-400M, U-200 and IC-100 are under operation at the JINR FLNR. Total operation time is about 71 000 hours per year. In the DRIBs project for production of accelerated exotic nuclides as 6He, 8He etc. the U-400M is used as radioactive beam generator and U-400 is as postaccelerator. Layout of FLNR accelerators complex presented at fig.1 [1].

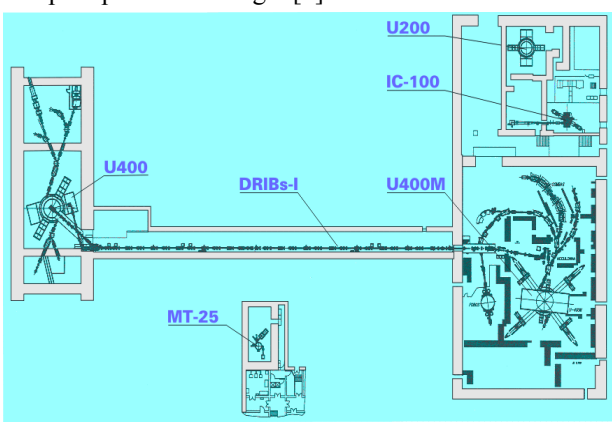

Figure 1: Layout of FLNR JINR accelerator complex

U400→U400R CYCLOTRON MODERNIZATION

The cyclotron U-400 (pole diameter 4 m) has been in operation since 1978 [2], [3]. In 1996, the ECR-4M ion source (GANIL) was installed at the U-400. The axial injection system with two bunchers (sin and linear) and spiral inflector was created to inject ions in cyclotron Fig.2. Since 1997 total operation time of the U400 amounts 71 000 hours. About 66% of the total time was used for acceleration 48Ca5+,6+ ions for synthesis of new super-heavy elements. Within the mentioned period elements with number of 113, 114, 115, 116, 117, 118 were synthesized. Chemical properties of 112 element were studied. The 48Ca beam intensity on the target was 8·1012 pps (1.2 pμA) at 0.4 mg/hour 48Ca substance consumption. Extraction efficiently of 48Ca beam by stripping foil was on the level 40% due to charge spread. The U-400 modernization in to U-400R is planned to start in 2011 and finishing in 2012. The aim of the modernization:

- increasing 48Ca, 50Ti, 54Cr, 58Fe, 64N, beam intensity on the target up to 2.5÷3 pμA;
- providing the smooth ion energy variation by factor 5 by magnetic field variation in the range of (0.8 - 1.8) T instead 1.93÷2.1 T now;
- improvement of the energy spread in the ion beam at the target up to 10^{-3};
- improvement of the ion beam emittance at the target up to 10π mm·mrad.

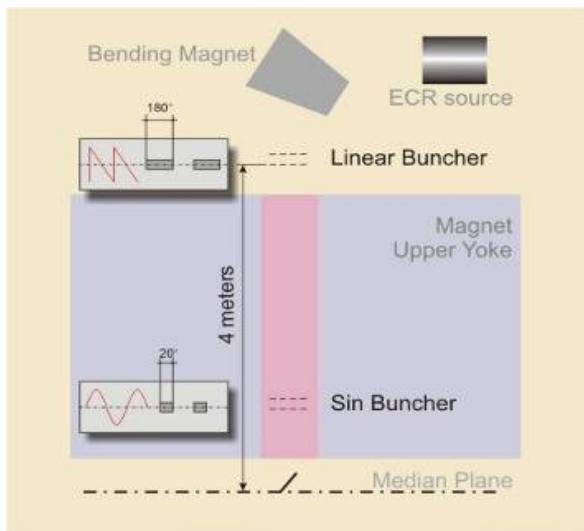

Figure 2: Scheme of the beam bunching system

The project of modernization intends changing axial injection system, magnetic structure, vacuum system, RF system, power supply system, beam diagnostic system and additionally electrostatic deflector instillation. The main comparative parameters of U-400 and U-400R are presented in Table 1.

The working diagram of the U-400R cyclotron with 48Ca beams intensities presented on Fig.3.

Scheme of the ion beam extraction from U-400R by stripping foils in two opposite directions A and B and by deflector in direction A are presented on Fig.4.

Table 1: Comparative parameters of U-400 and U400R

Parameters	U-400	U-400R
Mass to charge ratio of accelerated ions	5÷12	4÷12
Magnetic field	1.93÷2.1 T	0.8÷1.8 T
K factor	530÷625	100÷500
RF modes	2	2, 3, 4, 5, 6
Injection potential	10÷20 kV	10÷50 kV
Ion energy range	3÷20 MeV/n	0.8÷27 MeV/n
Number of sectors	4	4
Number of dees	2	2
Flat – top system	-	+
Beam extraction	stripping	Strip. deflector
Power consumption	~1 MW	~0.4 MW

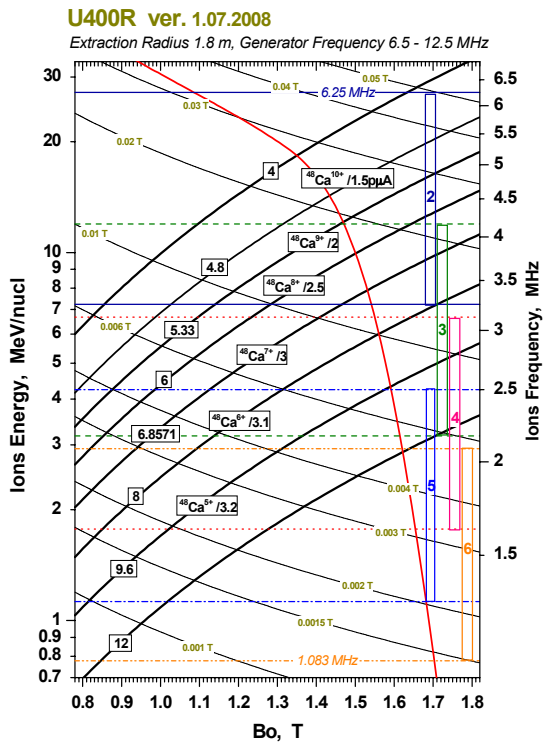

Figure 3: Working diagram of the U400R cyclotron

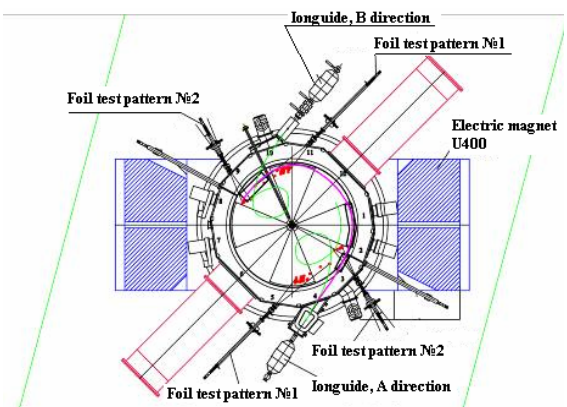

Figure 4: Scheme of the beam extraction from U400M in two selected directions.

U-400M CYCLOTRON

The 4 sectors and 4 dees cyclotron U-400M has been in operation since 1991 [3]. The cyclotron was originally intended for ion beam acceleration with A/z =2÷5 at energies of 20÷100 MeV/n. Now the ion beams are extracted from cyclotron by stripping with stripping ratio Z_2/Z_1= 1.4÷1.8. It defines energy range of extracted beams from 30 up to 50 MeV/n. The light ion beams from U-400M are used for radioactive beams production. The intensity of light ion beams as 7Li or 11B on the targets $(3\div5)10^{13}$ pps. Tritium ions are accelerated as molecular $(DT)^{1+}$ with intensity $6\cdot10^{10}$ pps and energy 18 MeV/n. For generation of $(DT)^{1+}$ ions special RF ion source is used. In 2008 the U-400M possibilities were widened by acceleration of ion beams with mass to charge ratio of 5÷10 with energies of 4.5÷20 MeV/n. This low energy ion beams (as 48Ca) will be used for synthesis and study of new elements.

Scheme of low and high energy beam extraction from U-400M in two opposite direction are presented on Fig.5.

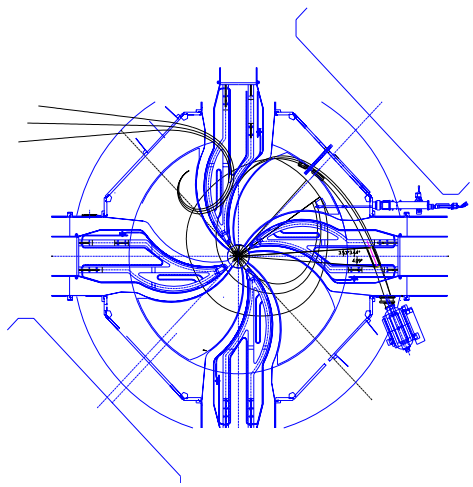

Figure 5: Scheme of beam extraction from U400M

DRIBS PROJECT

The DRIBs (Dubna RIB) project has been running at Lab since 2002 [3] (Fig.1.). The primary ion beams (7Li or 11B) from U-400M used for production nuclides as 6He, 8He in the target (Be or C). The produced radionuclides come from hot catcher into ECR (2.45 GHz) ion source by diffusion, where they are ionized. After separation, extracted from ECR radioactive ion beam are transported through 120 m transport line into the U-400 for acceleration. At present 6He2+ ions with energy of 11 MeV/n are available for physical experiments. DRIBs possibilities will be widened after carrying out U-400 modernization (see Table 2).

DUBNA ECR ION SOURCES (DECRIS) AND INJECTION SYSTEMS [4]

For the last 15 years 6 units room temperature 14 GHz ECR sources have been developed in Lab. Two superconducting ECR (DECRIS-SC) have been designed for IC-100 and U400M cyclotrons. Three permanent magnet 2.45 GHz ECR have been created in Lab especially for generation single-charge stable and radioactive ions. Effective axial injection systems have been developed to inject the beam into cyclotron for acceleration. As example, the scheme of U-400R axial injection channel is shown at Fig.6. The results of the capture efficiency for 40Ar4+ are presented in Fig.7. Decreasing efficiency of bunchers effect with increasing intensity can be explained by influence of space-charge effect. In the future, we are planning to increase the injection voltage from 13÷20 up to 50÷100 kV, it means shift of the space charge limits by factor 6÷20.

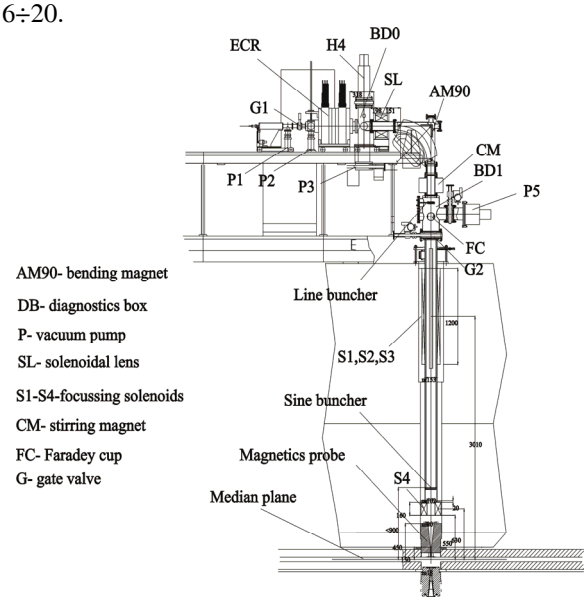

Figure 6: Scheme of U-400R axial injection system.

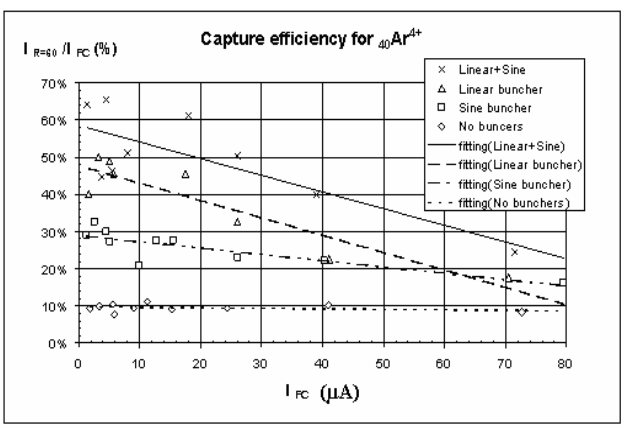

Figure 7: The afficiency of beam capture to acceleration versus injecting beam current and bunchers.

NEW FLNR ACCELERATOR – CYCLOTRON DC-200

In order to improve efficiency of the experiments it is necessary to obtain the accelerated ion beams with following parameters.

Energy	4÷8 MeV/n
Masses	10÷238
Intensity (for 48Ca)	10 pμA
Beam emittance	less 30 π mm·mrad
Efficiency of beam transfer	>50%

Main parameters and goals DC-200 cyclotron are in the Table 3.

Table 3.DC-200 cyclotron - main parameters and goals

	Parameter DC200	Goals
1.	High injecting beam energy (up to 100 kV)	Shift of space charge limits by factor 30
2.	High gap in the centre	Space for long spiral inflector
3.	Low magnetic field	Large starting radius. High turns separation. Low deflector voltage
4.	High acceleration rate	High turns separation.
5.	Flat-top system	High capture. Single orbit extraction. Beam quality.

Main technical parameters of the DC-200 cyclotron are presented in Table 4.

Table 4. Main parameters of the DC-200

Injecting beam potential	Up to 100 kV
Pole diameter	4000 mm
A/Z range of accelerated ions	4÷7
Magnetic field	0.65÷1.27 T
K factor	220
Gap between plugs	320 mm
Valley/hill gap	400/300 mm/mm
Magnet weight	915 t
Magnet power	270 kW
Dee voltage	2x130 kV
RF power consumption	2x30 kW
Flat-top dee voltage	2x14 kV
Beam turns separation	10 mm
Radial beam bunch size	3 mm
Efficiency of beam transferring	60%
Total accelerating potential	up to ~ 40 MV

Working diagram of DC-200 presented at Fig.8. New resources and research opportunities of the Lab are presented in Table 5.

Table 5: New resources and research opportunities.

	U-400M A/Z=3÷3.6,E=34÷50MeV/u A/Z=8÷10,E=4.5÷9 MeV/u		U-400R A/Z=4÷12, E=0.8÷27 MeV/u		DC-200 A/Z=4÷7, E=3.6÷8 MeV/u		
beam	E/A (MeV)	intensity	E/A (MeV)	intensity	E/A (MeV)	intensity	Physics
light RIB 6He 8He 24Ne			2.8 ÷ 14.4 1.6 ÷ 8 0.8 ÷ 20	10^8 10^5 ?			structure of light exotic nuclei, reactions, sub-barrier fusion, astrophysics
6<A<40 7Li 18O 40Ar	 35 33 40	 6×10^{13} 10^{13} 10^{12}	 2÷17 2÷19 0.8÷8	 1×10^{14} 1×10^{14} 3×10^{13}	 4÷6 4÷8 4÷8	 1×10^{14} 1×10^{14} 6×10^{13}	production of light RIB, fragmentation, transfer, structure of light exotic nuclei
A ~ 60 48Ca 54Cr 58Fe	 5 5 5	 6×10^{12} 3×10^{12} 3×10^{12}	 4÷7 4÷7 4÷7	 2×10^{13} 6×10^{12} 6×10^{12}	 4÷8 4÷8 4÷8	 6×10^{13} 4×10^{13} 4×10^{13}	superheavy elements, spectroscopy of SHE, fusion-fission, quasi-fission, etc.
A ~ 150 124Sn 136Xe	 5 5	 2×10^{11} 4×10^{11}	 3÷7 3÷7	 2×10^{12} 3×10^{12}	 4÷7 4÷7	 2×10^{12} 2×10^{13}	DIP, multi-nucleon transfer, new neutron rich nuclei, shell effects
A ~ 240 238U	 7	 2×10^{10}	 3÷7	 10^{11}	 4÷7	 10^{11}	neutron-rich SHE, new heavy isotopes, ternary fission, super strong electric fields, e^+ e^- formation
	2011		2012		2014		

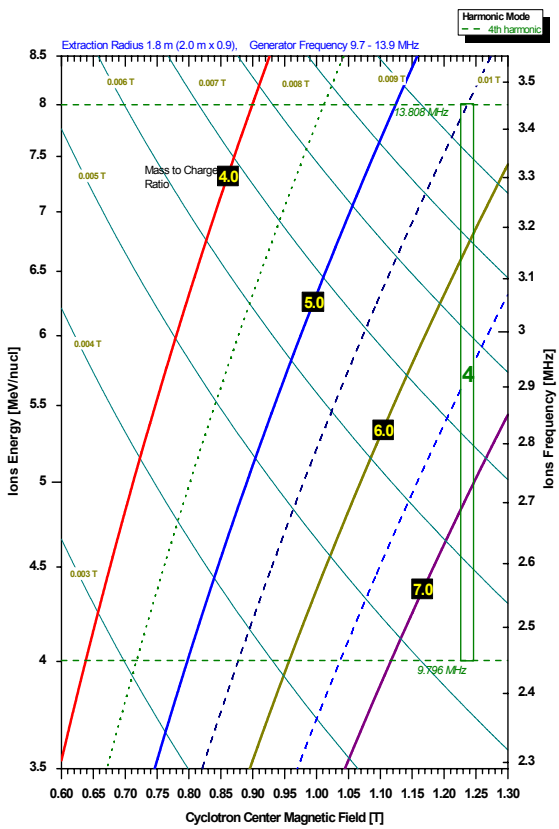

Figure 8: Working diagram of DC-200.

REFFERENCES

[1] Gulbekian G. and CYCLOTRONS Group, "Status of the FLNR JINR Heavy Ion Cyclotrons" in Proc. of 14th Int. Conf. On Cyclotrons and Their Applications, Cape Town, South Africa, pp. 95-98,1995.

[2] Yu. Ts. Oganessian, G.G. Gulbekyan, B.N. Gikal, I.V. Kalagin et al.,"Status report of the U400 cyclotron at the FLNR JINR ", in Proc. of APAC2004, Gyeongju, Korea, pp.52-54, 2004.

[3] B.N. Gikal, S.L. Bogomolov, S.N. Dmitriev et al., "Dubna cyclotrons- status and plans", in Proc. of Cyclotron04 Int. Conf., Tokyo, Japan, 2004. accelconf.web.cern.ch/accelconf/c04/data/CYC2004_papers/20A1.pdf.

[4] Efremov A.A., Bekhterev V.V., Bogomolov S.L. et al., "Status of the ion source DECRIS-SC", Review of Scientific Instruments, V. 77, P.235–239, No.03A320,2006.

[5] B.N.Gikal et al., "U200 cyclotron operating experience and upgrade". JINR preprint, 9-83-311, Dubna, 1983.

[6] B.N.Gikal, S.N.Dmitriev et al., " IC-100 Accelerator Complex for Scientific and Applied Research ". ISSN 1547-4771, Physics of Particles and Nuclei Letters, Vol. 5, No. 1, pp. 33–48. © Pleiades Publishing, Ltd., 2007.

[7] N.Yu. Kazarinov. Non-linear distortion of multi-component heavy ion beam emittance caused by space charge fields. In: Proceedings of the 14th International Conference on Ion Sources, Dubna, Russia, 2003, Review of Scientific Instruments, 75, 1665, (2004).

HIRFL-CSR FACILITY STATUS AND DEVELOPMENT*

Y.J. Yuan#, H.W. Zhao, J.W. Xia, X.D. Yang, J.C. Yang, H.S. Xu, Y. He, X.W. Ma, X.H. Cai
X.L. Tu, D.Q. Gao, W. Zhang, Z. Xu, X.T. Yang, Y.W. Su, R.S. Mao, L.Z. Ma, Y.P. Yang

Institute of Modern Physics (IMP), CAS, Lanzhou, 730000, P.R. China.

Abstract

The HIRFL-CSR facility come into operation by the end of 2007. During operation in recent years, CSR supplied beam for experiments at several terminals and inside both CSRm and CSRe rings. The experiments covers high resolution mass measurement, cancer therapy research, neutron wall, atomic physics using electron target and internal gas target, using injection beam mainly from the SFC of cyclotron injector. New methods and further developments are required to improve the performance of CSR system including multi-gradients measurement method for beam spot commissioning and beam transfer, nonlinear effect correction and stabilization of isochronous mode of CSRe. For suppling of heverier ion beam with proper ernergy, the cyclotron complex should be enhanced and new injector is proposed to replace SFC as injector of SSC.

INTRODUCTION

The layout of HIRFL-CSR project including injector system is shown in Figure 1[1,2,3]. The main parameters are listed in Table 1. For injection and acceleration of low energy beam(<10MeV/u) directly from SFC, as the span of RF cavity is insufficient, harmonic capture and acceleration (H=2 or 3) is adopt.

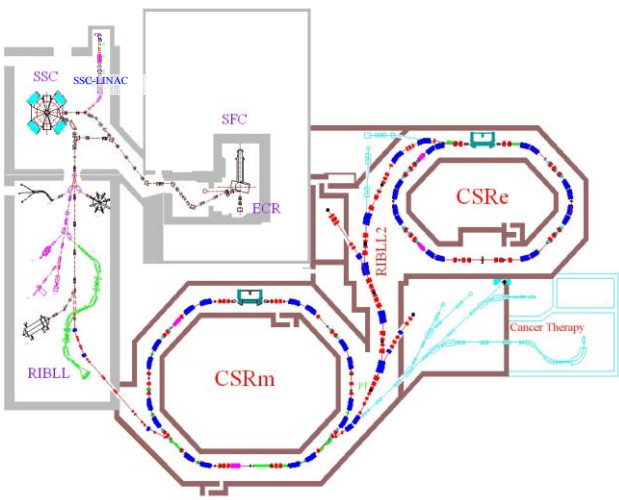

Figure 1: Layout of HIRFL-CSR.

The HIRFL-CSR facility come into operation by the end of 2007. During operation in recent years, CSR supplied beam for experiments at several terminals and inside both CSRm and CSRe rings. The operation parameters of supplied beams are listed in table 2. The operation time with HIRFL-CSR took about half of the total running time of HIRFL.

Table 1: Major Parameters of CSR

	CSRm	**CSRe**
Length	161.0m	128.8m
Ion species	Carbon~Uranium	Carbon~Uranium
Magnet rigidity	0.7~11.5Tm	0.6~9.4Tm
Acceptance		Normal mode
ε_x (π mm-mrad)	200(ΔP/P =±0.15 %) 50(ΔP/P =1.25%)	150(ΔP/P =±0.5%) 10(ΔP/P =±1.3%)
ε_y (π mm-mrad)	30	75
Tunes	3.63/2.62	2.53/2.58
e-Cooler	2-35kV (3-50MeV/u)	50-300kV (70-420MeV/u)
Vacuum Pressure	$<6\times10^{-11}$mbar	$<6\times10^{-11}$mbar
RF cavity	0.24~1.7MHz 7kV	0.5~2MHz 2×10kV
Injection	Multi-turn Charge exchange	Single turn
Extraction	Fast Slow(RF KO)	-

Table 2: Major parameters of CSR operation

Beam	$^{12}C^{6+}$	$^{36}Ar^{18+}$	$^{78}Kr^{28+}$	Xe^{27+}
Injector	SFC	SFC+SSC	SFC	SFC
Accumulation Scheme	Charge exchange	Multi-turn	Multi-turn	Multi-turn
Energy(MeV/u)	150~300/600	368~500	300~500	197~235
Extraction Scheme	Slow/fast extraction	Fast ext.	Fast ext.	Fast ext.
Intensity(ppp)	2×10^8/7×10^9	4×10^8	2×10^8	1×10^8
Exp. Terminal	Cancer Therapy/ Neutron Wall	CSRm/ CSRe mass spect.	CSRe mass spect.	CSRe internal target

*Work supported by NSFC(10921504) and National Laboratory of Heavy Ion Research Facility in Lanzhou, China
#yuanyj@impcas.ac.cn

OPERATION WITH SLOWLY EXTRACTED BEAM

Basic Design and Performance

In CSRm, the 1/3 integer resonant in horizontal plane is designed for slow extraction[4]. For slow extraction at the energy flattop, the horizontal tune value is set to 3.663, the chromaticity is corrected to zero in both plane and the dispersion function at first extraction inflector is set zero. The area of stable separatrix triangle for all momentum deviation (<0.1%) is designed as 13 π.mm.mrad.

By using RF Knock-out as resonance exciter, the amplitude of horizontal betatron motion increases gradually, finally particles cross the stable separatrix and extracted. The excitation frequency is usually set to 1.663 times of the revolution frequency. The field strength is modulated during extraction to get smooth spill. The main frequency in spill structure is 50Hz due to the power supply ripple, filling factor is about 0.6 presently(Fig. 2). Spill structure will be improved by feedback system later. The extraction efficiency ranges from 15% to 60%, further study of slow extraction is being done to improve it.

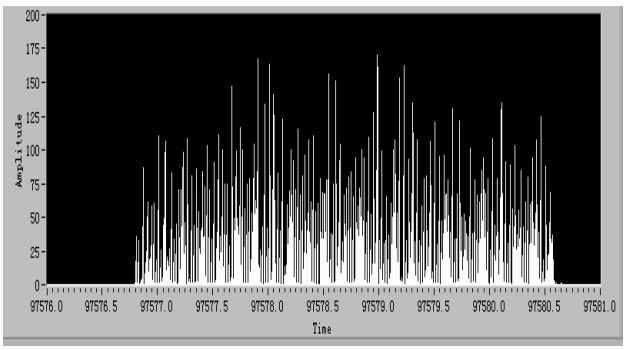

Figure 2: Time structure of slowly extracted beam from CSRm, detected by plastic scintillator. (Spill length is 3.5s)

Beam Spot and Improvement

The time structure of beam spill is not the only one, but the beam spot size is important for cancer therapy to get required dose distribution. The FWHM of beam spot is 10~20mm presently. To reach smaller beam spot in CSR cancer therapy terminal, new method is being developed. The beam parameters, both transverse and longitudinal, can be measured using the multi-gradient method. Figure 3 shows the basic layout of multi-gradient method.

The three-gradient emittance measurement method is well known, but it depends on the assumption of negligible momentum spread and dispersion. When multi-gradient method is used, the longitudinal beam parameters can be easily revealed by fitting of spot sizes to focusing strength of the quadrupole. It's expected to be helpful in target spot forming.

Single-time Charge Stripping Injection

For cancer therapy, single-time charge stripping injection is tested, without electron cooling but with RF bucket on; over 10^9 carbon particles are injected every machine cycle. The result shows the possibility of using cyclotron as injector for HITFiL(Heavy Ion Therapy Facility in Lanzhou, shown in Fig.4), which will be constructed in 3 years.

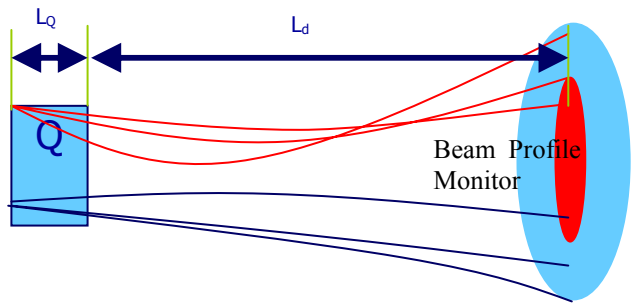

Figure 3: Basic layout of multi-gradient method to measure beam parameters.

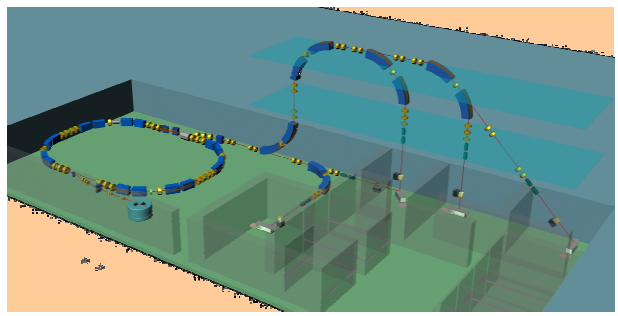

Figure 4: Layout of heavy ion therapy facility in Lanzhou

Conformal Ion Beam Treatment

The treatment in CSR extended the therapy research to deep-seated tumour; two batches including 10 patients were treated. The location depth of tumours was in the range of 3 to 10cm. Most of the tumours were treated with passive energy variation longitudinally and uniform scanning transversely.

The active energy variation and spot scanning technologies are developed and being tested. CSR has the possibility of active energy variation with 255 steps in the energy range of 100~430MeV/u for C^{6+}. It's difficult in commissioning of the energy steps since the hysteresis effect influenced the injection field level (~1%) and efficiency. This effect can be eliminated by ramping of the magnet field to its maximum of treatment every machine cycle. The spot scanning results show good position precision (<1mm) and dose distribution (>80% uniformity, detected by irradiation films). An online dose distribution monitor using 2 sets of slitting ionization chambers (2mm resolution) for both horizontal and vertical direction was built up. A measured particle counting distribution result is shown in Figure 5. The scanning area is 12×12cm^2.

Neutron-Wall Experiment

For testing of the detector matrix at stationary target area, C^{6+}-600MeV/u was slowly extracted and transported through Be foil to a stationary target outside the vacuum

chamber. The test experiment observed and distinguished mesons for the first time in IMP. The stability of beam position on the target should be improved to increase the resolution of spectrum.

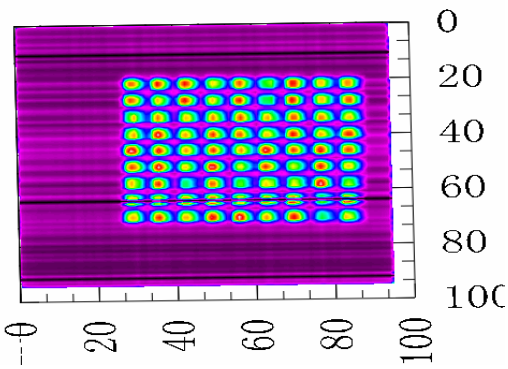

Figure 5: Result of spot scanning test. The black lines show detector failure.

OPERATION OF CSRE MASS SPECTROMETER

The isochronous mode of CSRe is designed with γ_{tr} =1.3953 and acceptance $\Delta P/P \cong \pm 0.35\%$ ($\varepsilon_{x,y}$ = 20, 75 π mm mrad). Lacking of proper testing method, the mode is tested with Shottky spectrum of primary beam. Later test experiments with $^{36}Ar^{18+}$ as primary beam[5], the mass resolution reached 10^{-5} for the measurement of ^{32}S, ^{28}Si, ^{34}Cl and ^{30}P.

Aiming at the precise mass measurement of ^{65}As, ^{78}Kr was chosen as primary beam. In every machine cycle (~15s), 2×10^{8} primary particles hit the 15mg/cm^2 Beryllium target. The experiment takes two runs, 10 days for the first run and 15 days for the other. For the first run, 10 target-events are recorded [6], 50 events for the later.

All the data recorded are used to check the whole experiment set. As the first result, by proper fitting method, the magnet rigidity of centre closed orbit is revealed and checked with continuous field measurement of one dipole. Figure 6 shows the fitted centre rigidity offset to the measured data of magnet field in one hour.

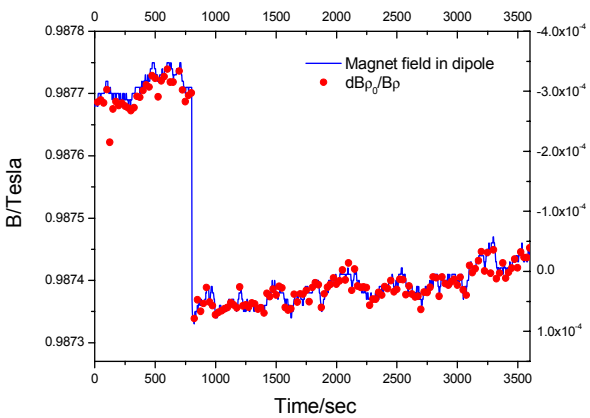

Figure 6: The fitted centre rigidity offset to the measured data magnet field during one hour. The big change is intentional.

The magnet field data are recorded during the second run of 15 days. Figure 7 is the waterfall chart of the data. By removing of the artificial field shift, the field drift is clearly periodic by day, as shown in Figure 8, and reveals the influence of human activity on power supply system. the field drift about 10Gs(0.05%) every day. The influence on experiment is large, this can be seen in the period data. Nine hours of the period data are shown in Figure 9, the period fluctuation is very large. The data are reconstructed to designed condition (red dots in figure 9).

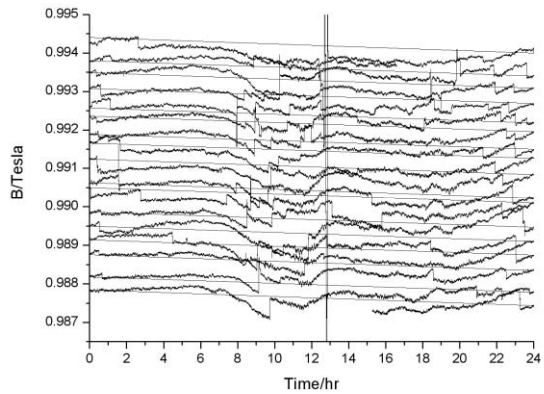

Figure 7: Waterfall plot of recorded field drift of dipole from midnight to midnight.

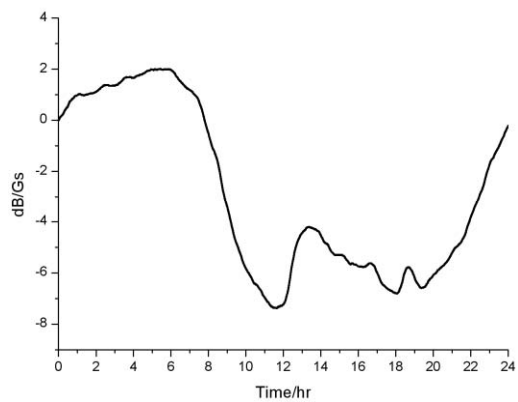

Figure 8: Periodic field drift of dipole field from midnight to midnight.

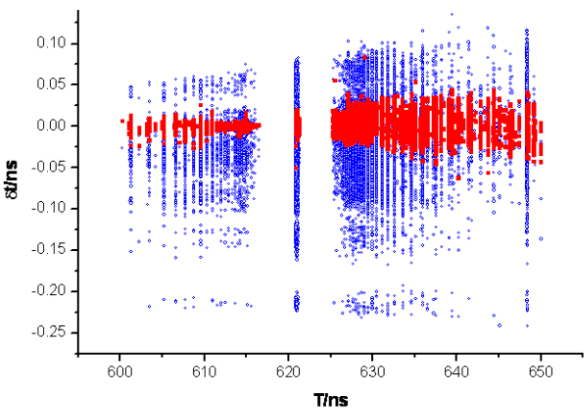

Figure 9: Data of the measured periods of identified nuclides in 9 hrs(blue) and the distribution after reconstruction (red).

Further study of isochronous mode of CSRe shows the correction of nonlinear effect is necessary. The lattice investigation shows the dependence of transition energy on momentum offset at different conditions (Figure 10).

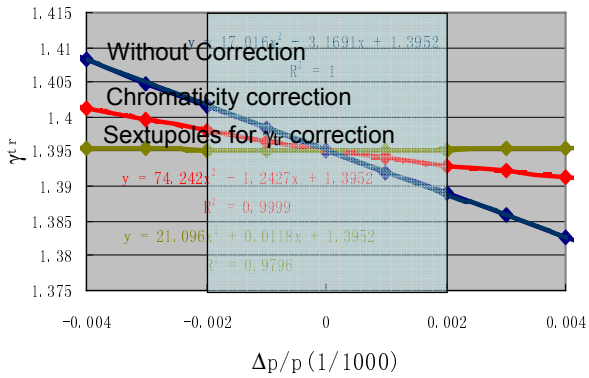

Figure 10: The dependence of transition energy on momentum offset at different conditions.

The experiments up to now were done without transition energy corrections. That's limits the time resolution to 1×10^{-5} for the target nuclei as isochronous mode. With precise corrections, we can expect 1×10^{-7} time resolution. The key point to acheive such a high resolution is the testing method, it's now under investigation.

OPERATION OF ELECTRON COOLER AND EXPERIMENTS OF ATOMIC PHYSICS

The e-cooler for CSRm was in function by the end of 2006[7,8], the performance is very good for the accumulation of heavy ions. However, there is still trouble in the positioning of electron beam and ion beam to be parallel and coaxial between each other; it results in less efficiency of the accumulation.

The modification of high voltage power supply and control system of CSRm cooler is done to change the electron beam energy rapidly. Based on further test of it, modification of the e-cooler in CSRe will be done for atomic physics with higher energy highly charged ions.

The e–cooler of CSRe is now works stably in cooling of high energy heavy ion up to energy of 400MeV/u[9], where it is also difficult to position then electron beam. With the e-cooler of CSRe, the first REC experiment with internal target is done.

In the REC experiment, $^{129}Xe^{54+}$ is produced with thick target in RIBLL2 transfer line, injected in CSRe and hits on the Nitrogen gas target (~$10^{12\text{-}13}$atoms/cm^2). By using of high purity Ge detectors the energy distribution of X-rays is recorded with good resolution (Figure 11).

It's observed from total signals count rate that the beam closed orbit shifts during the target period and affects the brightness and resolution. A slow feedback system should be used to keep the closed orbit and maintain high brightness.

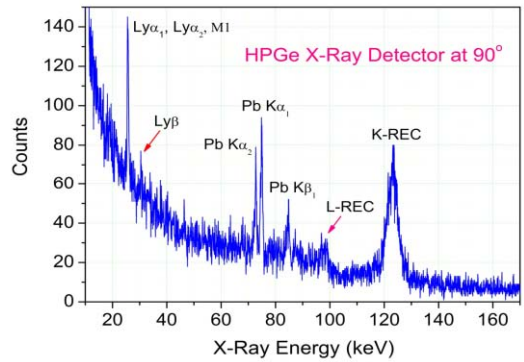

Figure 11: X-ray spectrum detected by HPGe detectors in first REC experiment of CSRe.

THE INJECTOR COMPLEX

By using of cyclotron complex of SFC and SSC as injector system, CSR successfully provided beams of C, Ar, Kr and Xe beams for experiments. But its disadvantage in beam intensity is obvious too.

Usually, the SFC cyclotron alone is used as the injector as its intensity is about one order higher than SSC. But the energy from SFC is not enough to get high charge to mass ratio for heavy ions. It limits the maximum energy can be reached in CSRm.

Bismuth beam is tried this year, the intensity from SSC is about 70~300enA, and is unstable. To get higher intensity of heavy metallic ion beams, the stabilization of machine operation is the first thing to overcome in HIRFL.

It's planned to build a linear accelerator as injector of SSC. The SSC-LINAC is designed to provide heavy ion beam up to Uranium with energy of 1MeV/u. the plan is shown in Figure 12. The major parameters are shown in Table 3.

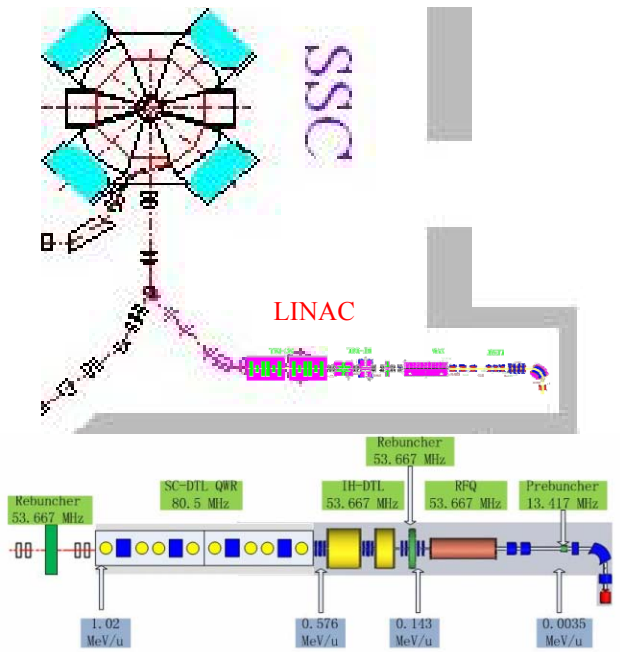

Figure 12: The layout of SSC-LINAC plan

Table 3: Main Parameters of SSC-LINAC

Total Length(m)	18.5
Ions	C~U
Energy(MeV/u)	0.576/1.025
Bunch Frequency (MHz)	13.4167
RFQ Frequency (MHz)	53.6667
Rt-DTL Frequency (MHz)	53.6667
SC-DTL Frequency (MHz)	80.5
$\delta P/P$	$\pm 5\times10^{-3}$
$\Delta\phi$(deg)	± 6
$\varepsilon_h/\varepsilon_v$ (π mm.mrad)	15/15

OTHER ASPECTS OF HIRFL-CSR IMPROVEMENT

An automatic commissioning system is developed and tested for the commissioning of transfer line. By using beam intensity measured from faraday cup, the commission cycle repeated automatically to improve transfer efficiency. It's expected to reduce workloads if the system is spread over the whole HIRFL injector system.

For mass measurement of secondary nuclei with Shottky spectrum, in addition to the existing electron cooler of CSRe, a stochastic cooling system is also proposed to be designed and installed. To make the span wider and cooling time shorter, a new lattice structure is designed to reduce the flipper factor η to about 0.2, meanwhile the acceptance is reduced to $\delta P/P=\pm5\times10^{-3}$ with emittance $\varepsilon_h=50\pi$ mm mrad. The cooling time simulated is about 4s.

A molecule injector of CSRe is also proposed. It will supply beam of molecule with mass number up to 100 to CSRe. After it's accelerated to maximum magnet rigidity, it will interact with new developed electron target. The injection system, beam detection and diagnosis system will be reformed for this purpose too.

REFERENCES

[1] Y.J. Yuan, H.W. Zhao, J.W. Xia et al, "Status of HIRFL-CSR Project",COOL 2009 Proceedings, 31 Aug - 4 Sep. 2009, Lanzhou, China.

[2] W. L. Zhan, H. S. Xu, G. Q. Xiao etc., "Progress in HIRFL-CSR", Nuclear Physics A, 834 (2010) 694c–700c, March 2010. NN2009, Beijing, China, 16-21 August 2009.

[3] W.L. Zhan, J.W. Xia, H.W. Zhao, et al, "HIRFL today", Nuclear Physics A, 805: 533C-540C, June 2008, 23rd International Nuclear Physics Conference，Jun 03-08, 2007, Tokyo, Japan.

[4] Y.J. Yuan, "Injection and slow extraction for carbon ion therapy at IMP",NIRS-IMP Joint Symposium on Carbon Ion Therapy, August 2009, Lanzhou, China.

[5] Tu Xiao-Lin, Xu Hu-Shan, Xia Jia-Wen, et al, "A pilot experiment for mass measurement at CSRe", Chinese Physics C, 33(7): 516-520, July 2009.

[6] H.S. Xu, X.L. Tu, Y.J. Yuan, et al, "First mass measurement of short-lived nuclides at HIRFL-CSR", Chinese Science Bulletin, 54 (24): 4749-4752, Dec 2009.

[7] X.D. Yang, V.V. Parkhomchuk et al, Proceedings of COOL 2007, Bad Kreuznach, Germany, pp.59-63.

[8] L.J. Meng, X. Ma, H.P. Liu et al, "The first test experiment performed at the electron cooler of storage rings in Lanzhou", (HCI 2008), IOP Publishing, Journal of Physics: Conference Series 163 (2009), doi:10.1088/1742-6596/163/1/012031.

[9] X.D. Yang, L.J. Mao, G.H. Li, et al, "Commissioning of electron cooling in CSRe", COOL 2009 Proceedings, 31 Aug - 4 Sep. Lanzhou, China.

CURRENT STATUS AND FUTURE PROJECTS OF THE ITHEMBA LABS CYCLOTRON FACILITIES

J.L. Conradie, L. Anthony, A.H. Botha, J.G. de Villiers, J.L.G. Delsink, W. Duckitt, D.T. Fourie, M.E. Hogan, C. Lussi, I.H. Kohler, A. Crombie, H. Mostert, R. McAlister, S.S. Ntshangase, J.V. Pilcher, P.F. Rohwer, M. Sakildien, N. Stodart, R.W. Thomae, M.J. van Niekerk and P.A. van Schalkwyk
iThemba LABS, P.O. Box 722, Somerset West 7129, South Africa
Z. Kormany, ATOMKI, P.O. Box 51 H-4001 Debrecen, Hungary
J. Dietrich*, Forschungszentrum Jülich, D-52425 Jülich, Germany
C. Boehme, University Dortmund, D-44221 Dortmund, Germany

Abstract

The cyclotron facilities at iThemba LABS have been utilized for isotope production, nuclear physics research, proton therapy and neutron therapy for nearly 25 years. The upgrading and replacing of redundant systems is essential, in order to keep the interruptions due to equipment failure to a minimum. The computer control system will be replaced by an Experimental Physics and Industrial Control System (EPICS) and the analogue low-level RF control systems will be replaced with digital systems. The Minimafios ECR ion source is being replaced with an ECR source that was used at the former Hahn Meitner Institute. Another source, based on the design of the Grenoble test source, will be commissioned later this year. To increase the production of radioisotopes, the 66 MeV proton beam is split with an electrostatic channel to deliver two beams simultaneously. The first results with the beam splitter will be reported. A phase measuring system for the separated-sector cyclotron, comprising 21 fixed probes, has been installed. The progress of these projects and the status of the facilities will be presented. Plans for new facilities for proton therapy and radioactive beams will also be discussed.

EPICS CONTROL SYSTEM

During the past 2 years iThemba LABS has been developing an EPICS-based control system, which will eventually replace the current control system that was developed during the 1980's. The current system is based on a LAN of PCs with an in-house developed distributed database, in which portions of the database reside on PC nodes close to the equipment. This is very much the philosophy of EPICS with the EPICS process variables (PVs) implemented in Input/Output Controllers (IOCs) constituting a distributed database. Our I/O structure is defined by a series of crates and I/O cards. The various types of cards allow a range of controls, including analogue and digital signals, power supply, stepper motor and actuator control. There are approximately 25000 variables connected in this way. EPICS driver software has been developed to connect to this I/O structure.

So far EPICS has been installed on a rotating wire scanner, the beam splitter devices, slits, pneumatic actuators and vacuum system components and also constitutes 90% of the controls of the tandem Van de Graaff at iThemba LABS Gauteng.

During the transition phase when both the old and the new control systems have to run concurrently, it was necessary to develop bridging programs that allow operator screens to access both systems. So far the IOCs which are running on standard PCs with Ubuntu Linux ver. 10.04 have proved to be very stable.

RF CONTROL SYSTEM

A prototype of a digital low-level RF control system has been successfully developed at iThemba LABS. The system as illustrated in Fig. 1 utilizes a Xilinx Virtex 5 FPGA that is interfaced with high speed 16 bit 500MHz DACs from Analog Devices to synthesize the RF signals. Amplitude and phase information is extracted from the feedback signals using quadrature demodulation. A closed loop controller within the FPGA is utilized to keep the phase and amplitude at an operating point and to reject system disturbances. Amplitude and phase information as well as system parameters can be streamed to a LabVIEW client via Ethernet allowing monitoring and diagnostics of the RF signal to be performed in real time. The system has the capability to generate, under closed loop conditions, an RF signal with an intrinsic amplitude and phase accuracy of 0.006% and 0.005 degrees respectively.

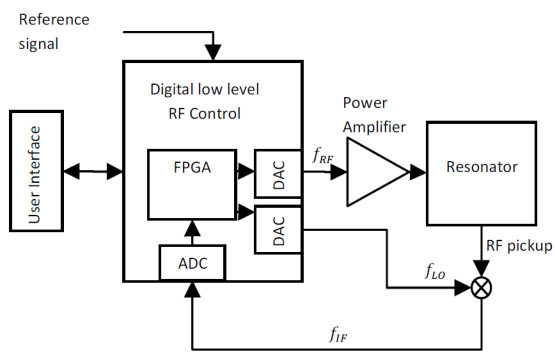

Figure 1: New prototype digital low-level RF control system

*Supported by BMBF and NRF, project-code 39.1.B0A.2.B

ELECTRON CYCLOTRON RESONANCE ION SOURCES (ECRIS)

Grenoble Test Source 2 (GTS2)

iThemba LABS is in the process of assembling an ECRIS (GTS2) that was originally designed by CEA Grenoble in France [2] which is based on the same design as the heavy-ion ECRIS in use at the Large Hadron Collider (LHC) facility at The European Organization for Nuclear Research (CERN) facility in Europe. Consequently a collaboration was proposed by CERN and a Letter of Intent was signed between iThemba LABS and CERN that outlines the terms and conditions of the collaboration agreement. It involves the initial commissioning of the GTS2 ECRIS at iThemba LABS, followed by the study of specific heavy-ion beams as requested by the fixed target experiment group (NA61) of CERN. Construction of the source is on schedule for completion by the end of 2010. Fig. 2 shows the partially assembled source.

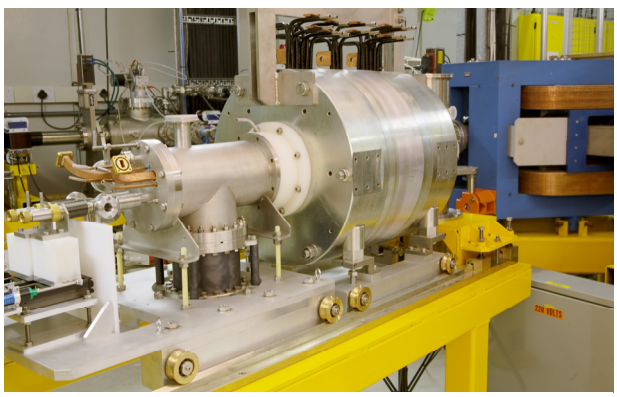

Figure 2: Partially assembled GTS2 ECRIS.

Hahn Meitner Institute (HMI) ECR Ion Source

The HMI ECRIS, donated by the Hahn Meitner Institute, was fully commissioned and put into service during 2009. Since then the source has been used to deliver beams of various ion species for nuclear physics experiments. The beams are very stable and with higher charged states and intensities than can be achieved with the Minimafios ECRIS. The Minimafios source will be decommissioned by end of September 2010, after more than 20 years of operation.

BEAM SPLITTER

The beam splitter system [1] was commissioned during the course of the year. To allow simultaneous irradiation of two targets for isotope production, an electrostatic channel (EC) and a magnetic channel (MC), similar to those at the Paul Scherrer Institute, are used to obtain two separate beams. During the beam development phase some components in the beam line section between the EC and MC had to be rearranged and after careful optimization of the beam optics, beam was delivered to both the vertical and the horizontal beam line targets simultaneously. The beam profiles in front and behind the electrostatic channel are shown in Fig. 3. Beam transport parameters were fine-tuned while the intensity of the split beam was increased, and so far 80 µA has been split and delivered to the horizontal line while 140 µA has been delivered to the vertical beam line, with negligible beam loss. Additional precautionary modifications have been implemented, e.g. in the beam line section between the EC and MC, quadrupole magnets with larger apertures and a beam pipe with a larger diameter were installed in order to reduce the setup time of the beam splitter and to practically eliminate all beam losses. Full radionuclide production with the beam splitter will start in September 2010.

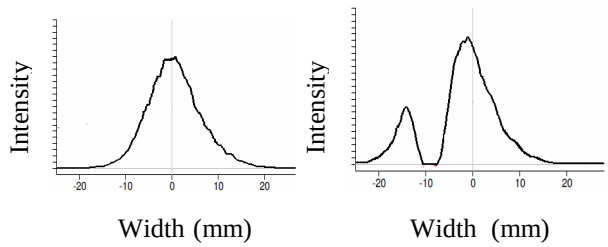

Figure 3: The beam profile in the horizontal plane in front of the electrostatic channel (left) and 100 mm behind the electrostatic channel (right), showing clear separation between the deflected part and the main beam.

PHASE MEASURING SYSTEM FOR THE SSC

The radial moveable phase probe in the SSC injection valley vacuum chamber, which also contains the flat-topping resonator, a pulse selector and a beam stop, was recently replaced with 21 non-destructive fixed phase probes. They could not be installed on the centre line of the valley vacuum chamber and therefore have the shape of parallelograms instead of rectangles. Each probe consists of two double shielded electrodes, symmetrically arranged with respect to the median plane. Each electrode is connected to a semi-rigid cable through a coaxial, non-floating feedthrough mounted on a conflat flange. All the probes have the same radial and azimuthal width of 70 mm and 120 mm, respectively. Outside the vacuum chamber the semi-rigid cables are connected, via quarter-inch coaxial cables with solid outer conductors, to two multiplexers. Fig. 4 shows the phase probes and their support structure being installed into the vacuum chamber of the SSC.

Commercial multiplexers with suitable specifications could not be found. Consequently RF coaxial, terminated relays, with a specified life-time of ten million cycles were selected for the multiplexers. They are situated in the cyclotron vault below one of the sector magnets. Tests verified that the switches function satisfactorily in the low stray field of the magnet.

These multiplexers are connected, via half-inch coaxial cables with solid outer conductors and low-noise wideband amplifiers, to an oscilloscope in the control

room to display signals. Initial measurements with these phase probes are very promising; the pulse shapes are exhibiting very limited reflections. When the signals from the upper and lower electrodes that comprise one phase probe are summed, the RF pick-up components from the resonators, being 180 degrees out of phase on the two electrodes, effectively cancel each other while the sum of the beam induced signal is doubled.

In the future the signals will also be routed through filters for phase measurement with a lock-in amplifier, controlled by LabVIEW software. It is possible to select various combinations of probes and operating modes for phase measurement.

Figure 4: The phase probe structure, supporting the 21 fixed probes, during installation in a vacuum chamber of the SSC.

BEAM STATISTICS

The cyclotron performance over the past 8 years is shown in Table 1. The improved statistics achieved during 2009 can be partially attributed to the excellent condition of the 4.4 MW uninterruptable power supply, resulting in zero interruptions due to power dips. Interruptions as a result of ageing equipment still remain a concern, but an ongoing program of replacing and upgrading obsolete equipment and the concerted effort of all operational and support staff generally ensured speedy recovery after break-downs.

Table 1: Operational statistics of the SSC for the past 8 years

Year	Beam supplied as:		% of scheduled beam time for:	
	% of total time	% of scheduled time	Energy changes	Inter-ruptions
2002	72.29	82.69	7.50	7.28
2003	70.93	82.79	6.87	8.08
2004	72.0	84.9	6.7	5.9
2005	71.3	83.6	5.5	6.4
2006	66.1	80.3	5.5	7.9
2007	67.1	79.28	5.4	10.4
2008	62.0	75.17	4.0	14.3
2009	70.5	83.7	6.9	7.9

FUTURE PROTON THERAPY AND RADIOACTIVE ION BEAM PROJECTS

Facilities for proton therapy, based on a 200 MeV cyclotron, with three new vaults, of which two will be equipped with gantries, were proposed in 2004 [3]. The third vault was envisaged for the implementation of the scattering method of treatment, with a horizontal beam line as well as a beam line at 30 degrees with respect to the vertical. A business plan has now been produced indicating the viability of this project. This project, if realized, will be in private partnership with iThemba LABS.

iThemba LABS is considering the establishment of a Radioactive Ion Beam (RIB) facility to provide additional beam time, which will meet the needs for human resource development, maintain and develop research at the international forefront, as well as increase radioisotope production.

It is proposed to divide the project into several phases. During the first phase a new cyclotron will be installed for isotope production and neutron therapy. This accelerator should be a H- machine capable of simultaneously supplying two proton beams in the energy range of 30 to 70 MeV and with a maximum current of about 400 μA for each of the two beams. These beams will fulfil future demand for isotope production and the creation of radioactive ion beams. Removing neutron therapy and isotope production from the SSC beam schedule will immediately double the beam time available for nuclear physics research with the advantage of a more stable beam.

The second phase is the development of radioactive beams using the new cyclotron as driver. The production target and ion-sources for radioactive beam production will be installed. These beams will have multidisciplinary applications, being used not only for nuclear physics but also astrophysics and material science research. A new injector and the existing SSC will be used to accelerate the radioactive beams to their final energy.

REFERENCES

[1] J.L. Conradie et al., “Improvements to the iThemba LABS Cyclotron Facilities”, Cyclotrons’07, Catania, October 2007, p. 140.

[2] D. Hitz et al., “Grenoble Test Source (GTS): A Multi-purpose Room Temperature ECRIS”, ECRIS’02, Jyväskylä, June 2002, p. 53.

[3] J.L. Conradie et al., “Cyclotrons at iThemba LABS”, Cyclotrons’2004, Tokyo, October 2004, p. 105.

STATUS OF THE LBNL 88-INCH CYCLOTRON HIGH-VOLTAGE INJECTION UPGRADE PROJECT

K. Yoshiki Franzen, P. Casey, A. Hodgkinson, M. Kireeff Covo, D. Leitner, C. Lyneis, L. Phair, P. Pipersky, Lawrence Berkeley National Laboratory, 1 Cyclotron Road, Berkeley, CA 94720, U.S.A.

Abstract

The goal of the project is to design and install a new center region that allows external beam injection at voltages between 20 and 30 kV for high intensity beams. This new center region will make use of a spiral inflector to eliminate the use of a gridded mirror for high intensity beams. At the same time the mechanical design must be flexible enough to allow use of the existing center region for less intense beams. The use of two or more different center regions is necessary to cover the wide range of operation parameter space utilized by the 88-Inch Cyclotron nuclear science and applied research programs. The project also includes HV upgrades to the external injection lines and HV insulation of the AECR and VENUS sources with the goal to provide focusing for beams up to 25 kV or if feasible up to 30 kV. The current spiral inflector design is based on extensive 3D FEM simulations for which results will be presented. In addition results from ongoing efforts to improve on the transport efficiency from the AECR ion source to the current mirror inflector will be discussed.

INTRODUCTION

Beam development experiments at the LBNL 88-Inch Cyclotron using the AECR-U injector source and particularly when using the high intensity beams available from the fully superconducting 28 GHz ECR ion source VENUS have demonstrated that for high intensity beams the space charge effect reduces the injection efficiency into the 88-Inch Cyclotron. At injected currents above 100 eμA the ion beam transmission decreases due to beam losses in the center region of the cyclotron and injection line. While for many experiments conducted at the 88-Inch Cyclotron, ion beam intensity on target is not a limiting factor, luminosity is crucial for the super-heavy element research program. Therefore, this upgrade is mainly focused on increasing the beam intensity of key ion beams in the mid mass range (A=20 to A=136) for the heavy element program at energies around the Coulomb barrier, in particular for ^{48}Ca and ^{50}Ti ion beams.

The goal of the four year upgrade project is to increase the injection energy into the cyclotron to take full advantage of the high intensity beams available from the VENUS ECR ion source. In addition, the project includes an upgrade to the external cyclotron injector beam line. While this upgrade is focused on the BGS ion beam requirements in the mid mass range, a crucial requirement is to preserve the versatility and wide parameter space of beams, intensities and ion beam energies available at the 88-Inch Cyclotron.

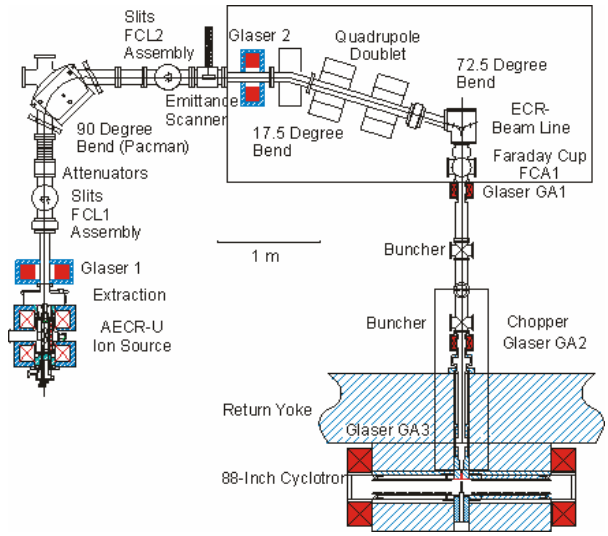

Figure 1. Schematic view of the AECR ion source, the injection beam line and the 88-Inch Cyclotron at LBNL.

DESIGN

Overview

During operation a beam is extracted from either one of the three ion sources and transported through an injection beam line system until it reaches the center region of the cyclotron; see Figure 1 for a schematic view. At the cyclotron mid plane it is necessary to redirect the beam horizontally which presently is done by the use of a mirror inflector. The great advantage of the mirror inflector is its versatility to support all the requested beams of the 88" Cyclotron. As mentioned above the goal of the project is to increase the injection voltage of the beam in order to improve on transmission efficiency at high current operation and reduce the required maintenance time of the inflector. However, due to limitations in vacuum it is not possible to operate the current mirror inflector at higher potentials required for beams injected at higher voltages. The plan is thus to temporary replace the mirror inflector during high intensity operation with a spiral inflector which can be operated at significantly lower voltages. The spiral inflector also does not utilize a grid which in the case of the mirror inflector requires frequent replacement during high current operation. Another equally important advantage of the spiral inflector is that it can be designed to better center the beam which is critical at higher injection energies. It should be emphasized though that the spiral inflector has a limited operating range so the goal is to quickly be able to switch between the two systems by utilizing the existing ion source mechanism which before the early 1990's was regularly used in a

similar fashion when switching between an internal and an external ion source. However, using this mechanism put a severe constraint on the maximum size of the spiral inflector since it has to fit within the existing diameter of the shaft which is only 2.125".

Spiral Inflector Design

As our target beam we chose Ar^{9+} injected at 25 kV in a magnetic field configuration set to support cyclotron acceleration to 200 MeV. The reason for this choice of ion beam is that the magnetic rigidity and final energy per nucleon is similar to $^{48}Ca^{11+}$ which is one of the most important beams for the heavy element program and is also often used for beam development at the 88-Inch Cyclotron.

The design of the spiral inflector was based on models using the computer code CASINO [1]. This code produces a set of coordinates which describes the center ray trajectory of a particle with a given mass-over-charge ratio and kinetic energy traveling through a spiral inflector situated in a defined magnetic field. By stepping through the spiral inflector parameter space of height (A), magnetic radius (R_m) and tilt (k') it was possible to find a combination which defines a configuration which 1) fits within the diameter of the shaft, 2) provides a beam which clears the inflector during the first revolution and 3) is centered enough to reach full acceleration. The final parameters are listed in Table 1.

Table 1. Parameters of spiral inflector optimized for injection of 25 kV Ar^{9+} ions into a 14.2 kG center region field.

Parameter	Value
A	30.0 mm
R_m	32.1 mm
k'	1.0

From the calculated trajectory data the next step was to define three-dimensional representations of electrodes that produce an electric field distribution which together with the magnetic field would steer the beam into the cyclotron mid plane. A code was developed in Matlab which produced a representation of these surfaces. In addition to the top and the bottom electrodes, grounded entrance and exit electrodes were added to the model. The electrode volumes were represented in STL file format which is commonly used in various CAD and FEM programs, see Figure 2 for an example visualization.

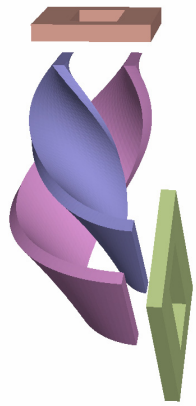

Figure 2. Spiral inflector electrodes (blue: top, pink: bottom, brown: entrance, green: exit).

The next step was to test the defined set of electrodes by using a FEM software package AMAZE [2]. This software creates a mesh representation of the spiral inflector electrode volumes and from the result a corresponding 3D field map was produced. Ar^{9+} ion trajectories were then calculated for 25 kV injection into the system and the results were compared with the output of CASINO. See Figure 3 for an example of trajectories plotted together with a field map solution. When a feasible design was found that fits into the available space of the 88-Inch Cyclotron center region, the STL file representations were used as a basis to produce a model in SolidDesigner compatible with the rest of the system, see Figure 4. In addition, the system was optimized for vacuum compatibility and voltage holding capability.

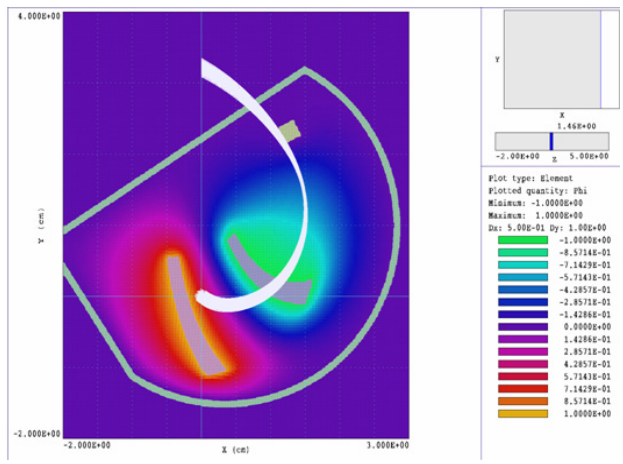

Figure 3. Field map solutions (top view) and 25 kV Ar^{9+} trajectories starting at x=0 cm, y= 0 cm travelling in the negative z-direction. The initial beam diameter is 2 mm. The applied voltages to the top and bottom electrodes are -7.75 and 7.75 kV respectively.

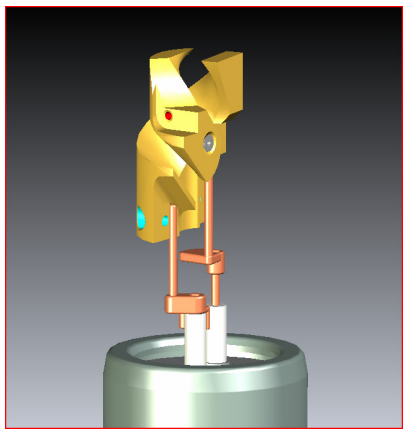

Figure 4. Model of spiral inflector prototype showing the tip of shaft, the high voltage feedthroughs and the spiral electrodes.

Cyclotron Center Region Design

In order to fit the new spiral inflector on the 2.125" shaft the entrance has to be positioned off the shaft axial center. The shaft itself thus has to sit off center from the cyclotron axis and subsequently the present Dee and Dummy Dee inserts have to be modified. Therefore, the original (mirror) center region design was adapted to accommodate the geometry of the spiral inflector, see Figure 5. One major difference is that the space available for the inflector housing is now half-moon shaped in order to position the first accelerating gap closer to the cyclotron center axis. The design was imported into the AMAZE FEM meshing software and an electric potential solution was calculated.

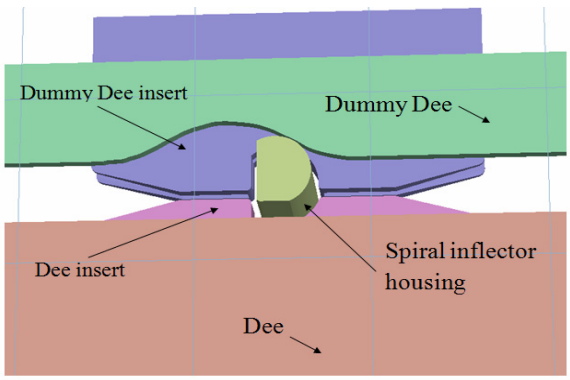

Figure 5. Upgraded Dee and Dummy Dee inserts compatible with the spiral inflector housing.

A magnetic field map was obtained from a code called CYDE which computes the predicted frequency and magnetic field settings (main coil, trim coils) for the 88-Inch Cyclotron from the input data m/q, Dee voltage, harmonic number and desired final energy.

The acquired electric and magnetic field maps were used as input data for the Z3CYCLONE code [3] which calculates the trajectories from the exit electrode of the spiral inflector to the cyclotron extraction radius, see Figure 6 for example results of such calculation.

With the Z3CYCLONE trajectory data it was possible to iteratively optimize the performance of the spiral inflector and the center region. More detailed results will be published elsewhere.

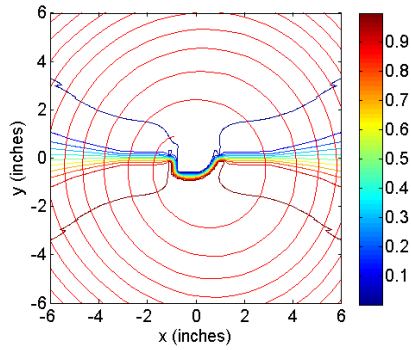

Figure 6. The first few turns of a 25 kV Ar^{9+} ion beam in the new center region of the 88-Inch Cyclotron and equipotential contours of the electric field. Colorbar indicates fraction of Dee voltage.

ONGOING WORK AND INSTALLATION PLAN

The AECR ion source and the injection beam line are presently being tested by 19.5 kV extraction of Ar^{9+} ions followed by transportation down to the mirror inflector. In addition to the goal of increasing the beam current this work aims to verify the current beam line model.

The spiral inflector prototype design is close to being sent off for manufacturing. When ready it will be tested by applying the required voltages while being positioned inside the cyclotron at high vacuum and tuned magnetic field. In addition the new Dee and Dummy Dee inserts will be manufactured and positioned with Dee RF voltage applied. The goal is to have these tests done by the end of the year 2010.

During the spring of 2011 injection will be tested using the spiral inflector. In addition an additional buncher will be installed.

During fall/winter of 2011 the complete system will be tested and improved upon as needed.

CONCLUSION

A design of a spiral inflector together with a matching center region has been produced using a series of simulation codes. The design is optimized to support transmission of a 25 kV Ar^{9+} beam. Manufacturing and testing will begin in the fall of 2010.

REFERENCES

[1] B. F. Milton and J. B. Pearson, CASINO user's guide and reference manual, TRIUMF, TRI-DN-89-19
[2] Field Precision LLC (http://www.fieldp.com/)
[3] F. Marti, private communication

THE ISOCHRONOUS MAGNETIC FIELD OPTIMIZATION OF HITFIL CYCLOTRON*

Q.G. Yao#, L.Z. Ma, S.F. Han, X.Y. Zhang, W. Wu, B.L. Guo, H.F. Hao, B. Wang
Institute of Modern Physics, Chinese Academy of Sciences, 730000, Lanzhou, China

Abstract

A new project named HITFiL（Heavy Ion Therapy Facility in Lanzhou）is being constructed. In this project, a 7Mev C125+ cyclotron is selected as the initial injector providing a 10 uA carbon beam. The isochronous magnetic field optimization of the cyclotron is introduced in this paper. Optimization result shows that the deviations between calculation values and theory are smaller than 5Gs. In the design process, the sofware OPERA has been utilized for the field calculation and optimization.

INTRODUCTION

At present, the activities on the development of isochronous cyclotron for the HITFiL are carried out at IMPCAS (Fig.1). This project include cyclotron, synchrotron and four high energy beam lines, which intended for obtaining the carbon beam to treat tumors. The cyclotron magnet has the pole diameter size of 1.68m and provides the maximum magnetic fields 1.8T between sectors. Its main parameter is shown in table1 [1].

Table1: Main parameters of the cyclotron

Maximum energy, [Mev]	7
Beam species	C_{12}^{5+}
Number of sectors	4
Ion source	outer
Hill angle, [°]	56
Valley angle, [°]	34
Maximum average magnetic field,[T]	1.2
Harmonic number	4
Cyclotron frequency,[MHz]	7.755
Magnet aperture, [mm]	50
Injection radius, [mm]	27
Extraction radius, [mm]	750
Extraction beam current, [uA]	10

The main magnet has a round yoke, four pairs of straight-line sectors. The relation of the distance in the "valley" to the distance in the "hill" is equal d_{valley}/d_{hill} =7.2. In this paper, we introduce the main magnet with particular emphasis on the isochronous mangetic field design. It is the important criterion of the designing of the cyclotron magnetic structure.

*Work supported by HITFiL
yaoqinggao@impcas.ac.cn

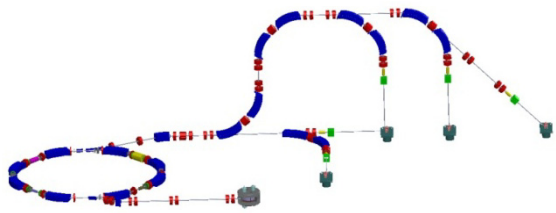

Fig.1 the layout of HITFiL

MAGNETIC FIELD DESIGN

The shape of the magnet yoke is optimized by OPERA-2D and 3D magnetic field calculation [2], Fig.2 shows the 2D cross section along the radial direction of this magnet. As the result of simulation, the straight line sectors with the flat surface are used. The sectors are placed on the magnet pole with the radial displacement with 10mm from the centre of magnet. In addition, for the axial injection of the beam, a cylinder which diameter is 200mm (is used to settle two solenoids) and a cone is designed in the center of magnet. For magnetic field calculation in the valley region, which is obtained with the help of OPERA-2D program [Fig.3]. Total current per each coil is 68734.4 ampere-turens and the current density is about 3.4A/mm2.

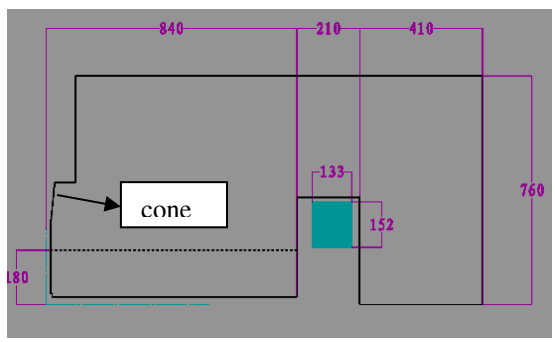

Fig.2：The cross section of cyclotron

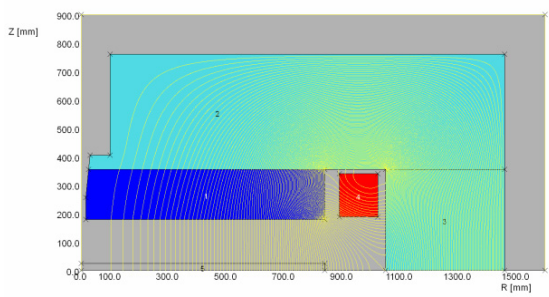

Fig.3 Opera-2D calculation (valley region)

The OPERA-3D program was used to calculate the theree-dimensional field. In the Modeller, the 1/16 model is created according to the symmetry of the magnetic field. Fig.4 shows the geometry of the cyclotron modeled by the OPERA. There are four holes at the valley center which designed for the vacuum and RF systems, they distort the field greatly, a step by step optimization of the magnet geometry is thus needed. Fig.5 shows the radial magnetic field along the "hill" median line at the centre plane, the field seen by accelerating beam is increased in radial direction. We have been able to obtain a reasonable isochronism by some optimization methods.

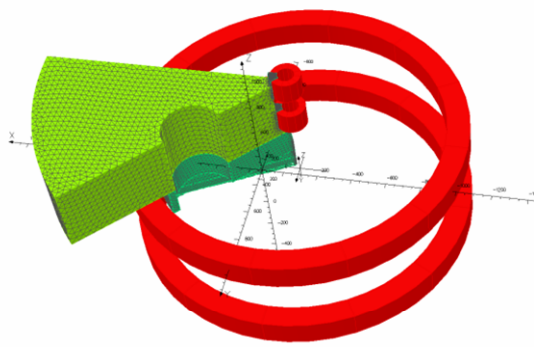

Fig.4 OPERA 3D model (conclude two solenoid).

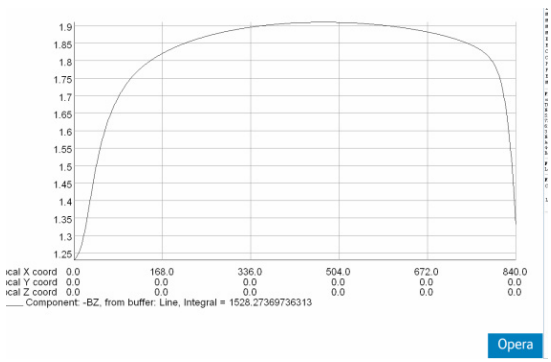

Fig.5 Radial magnetic field distribution

THE ISOCHRONOUS MAGNETIC FIELD OPTIMIZATION

The theoretical isochronous magnetic field $\overline{Bt}$ of carbon is calculated by a fomula as follows:

$$\overline{Bt} = \frac{2\pi mf}{q} \bullet \sqrt{1 - \frac{4\pi^2 \bar{r}^2 f^2}{c^2}}$$

Where $\bar{r}$ is the average radius of orbit, $\frac{m}{q}$=12/5, f is the cyclotron frequency.

The calculation value $\overline{Bc}$ is obtained by OPERA software. Firstly, to take the mapping magnetic field of cyclotron center plane from post-processor; secondly, to calculate the radius of static balance orbit (fig.6); thirdly, to take the magnetic field in the orbits and calculate their average value.

The aim of magnetic field optimization is to make the $\Delta B = \overline{Br} - \overline{Bc}$ approaches zero as much as possible. There are several shimming methods which optimizing its isocoronous field [3], here we adopted an effective method that is cutting air trim slot and chamfering cover plate of sector. This makes the cyclotron operation simpler, avoiding complicated optimization procedure with trim coils. The optimization method is introduced as follows:

1) Cutting air trim slot: cut a slot along the radial direction (35mm≤R≤782mm) by using several frustum of cones to deal with the sector; it could adjust the magnetic field in large measure and make the error between the calculation value and theory in isochronous field smaller than 30Gs (Fig.7 b) .

2) Chamfering the cover plate(the deep is 5mm): by chamfering the pole plate, it could adjust the magnetic field in a limited range and make the error between the calculation value and theory in isochronous field smaller than 5Gs (Fig.7 c) .

3) Changing the total current: by adjusting the total current, the magnetic field could be optimized as a whole.

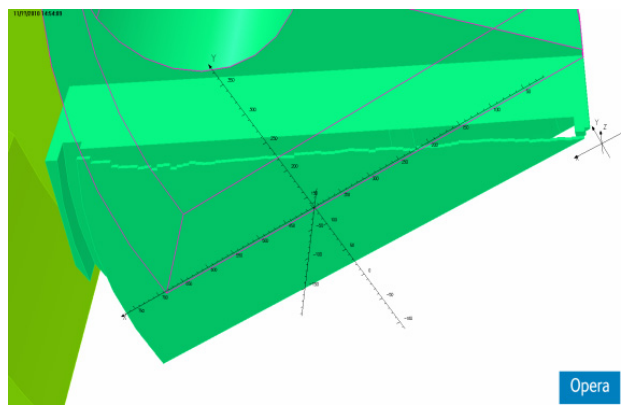

Fig.6 the optimized shape of pole

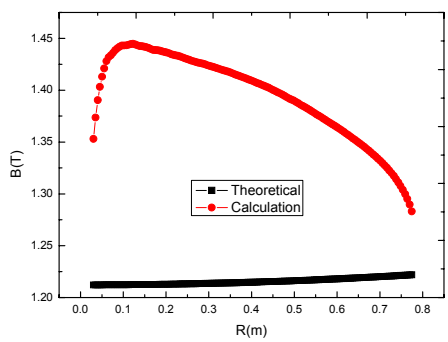

(a) Without any optimization

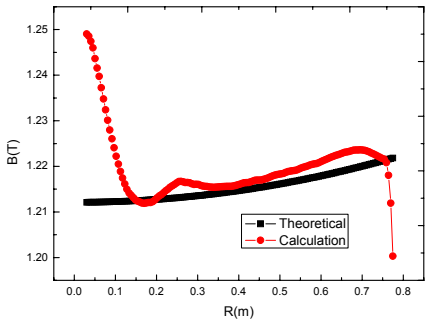

(b) only cutting air trim slot

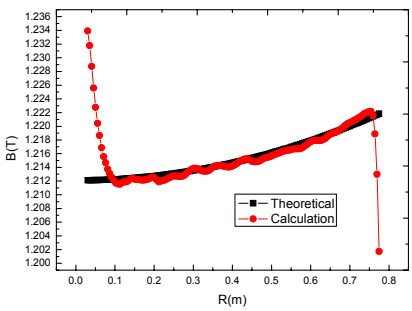

(c) Cutting air trim slot and chamfering pole plate

Fig.7 Magnetic field optimization procedure

The Fig.6 shows the final optimized pole, the complicated chamfer shape could be seen. The comparison between the calculation and theory is shown in the Fig7, it gives the optimization procedure: the deviation between calculation values and theory is very big before optimization (Fig. 7 a), but after the magnetic field optimiztion, the result shows the deviation does not exceed 5Gs over a large area.

In addition, horizontal and vertical focusing frequencies are also obtained from the equilibrium orbit calculation. Generally we hope the focusing frequency sufficently away from the resonances, especially the vertical focusing frequency. The fig.8 shows the two focusing frequencies, the vertical focusing frequency is below 0.5 except some points in final radius.

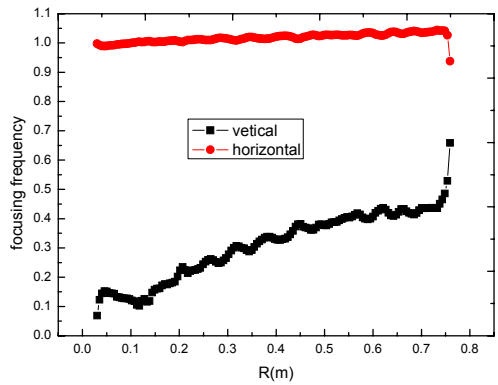

Fig.8 Focusing frequency

Conclusion

Magnetic field calculation of main magnet for a 7Mev C_{12}^{5+} cyclotron have been finished.The purpose of the work is to obtain the resonable isocoronous magnetic field, an effective method has been carried out. By complicated chamfering, the isocoronous magnetic field could satisfy the design requirements.

REFERENCES

[1] HITFiL design parameter handbook
[2] Cobham Technicals Services, www.cobham.com/technicalservices
[3] I.Ivanenko, G.Gulbekian, J.Franko, A. Semchenkov, "The model of DC72 cyclotron magnet. The research of the sector shimming methods for obtaining the working magnetic field for light and heavy ions acceleration." In: Proceedings of the 8th European Particle Accelerator Conference, 3-7 June 2002, Paris, p.p 2349-2351

APPLICATION OF CYCLOTRONS IN BRACHYTHERAPY

P.Saidi, Islamic Azad University (PPRC) Science and Research Branch, Tehran, Iran
M.Sadeghi, Agricultural, Medical & Industrial Research School, Tehran, Iran
A.Shirazi, Tehran University Faculty of Medicine Department of Biophysics, Tehran, Iran

Abstract

Cyclotrons are particle accelerator machines which have many applications in industry, technology and medicine. Cyclotrons play an important role in medicine and about 50% of the all particle accelerators running in the world are used in medicine for radiation therapy, medical radioisotopes production, and biomedical research. In this short review the use of cyclotrons for a radiation therapy method, brachytherapy, is discussed.

Brachytherapy is a form of radiotherapy where a radioactive source placed on or in the tissue to be irradiated. For a long period the production of radioactive isotopes for medical applications was essentially done in nuclear reactors but due to some advantages of radioisotopes production with cyclotron over a nuclear reactor, in the last two decades several types of cyclotrons have been developed to meet the specific demands of radionuclide production.

This talk will briefly explain the technical design, beam transfer and beam delivery systems of cyclotron for brachytherapy radioisotope production; and also will shortly describe some detail of 103Pd production in the following: production, targetry, radiochemical separation and seed fabrication.

INTRODUCTION

Brachytherapy is a special form of radiotherapy where a radioactive source is carefully placed on or inside the area to be treated. Brachytherapy sources are usually encapsulated; they can be used within the body cavities close to the tumor, placed in a lumen of organs, implanted in to the tumor or placed over the tissue to be treated. Depending on the dose rate of the sources at the dose specification point, brachytherapy treatment classified in three categories: high dose rate sources (HDR) >12 Gy/h, high energy photon emitters s like ^{137}Cs, 60Co, ^{192}Ir, ^{198}Au are used, medium dose rate (MDR) 2-12 Gy/h, is not common use; and low dose rate sources (LDR), less than 2 Gy/h with low energy photon emitters such as ^{125}I and ^{103}Pd. The use of radioactive sources for treatment of cancerous tumours started shortly after the discovery of radium (^{226}Ra) in 1898 by Madame Curie. Quantities and forms of radioactivity useful for brachytherapy were not available until 1940s, when civilian applications of nuclear reactors were encouraged, and also after for a long period the production of radioactive isotopes for medical applications was mainly based on neutron induced nuclear reactions. This was essentially done in nuclear reactors but their availability is slowly decreasing so that the accelerators based production facilities are growing up. The development of particle accelerators started in the past century and various radio-isotopes which are suitable for medical applications, produced.

In this study the accelerator production method for ^{103}Pd, is investigated. The production of 103Pd is carried out via the ^{103}Rh(p,n)^{103}Pd reaction which is well suited to low-energy cyclotrons. The irradiation of the electroplated Rh target was performed in a cyclotron (Cyclone-30, IBA) at 18 MeV energy [1-2] of proton and a beam current intensity of 200 μA at the Agricultural, Medical and Industrial Research School (AMIRS) [3].

The main problem in the 103Pd radiochemical separation stage is dissolution of target material due to extremely low chemical reactivity of rhodium metal. The other problem is the high quantity of rhodium in solution. Well known palladium extractor is dimethylglyoxime, but to prevent the decrease of extraction yield, the α-furyldioxime is used [5]. Pure obtained 103Pd is then absorbed in to resin; the active resins are encapsulated inside the titanium brachytherapy seed.

MATERIALS AND METHODS

According to Sadeghi et al. [4] manuscript, to prepare copper backing for proton bombardment, $RhCl_3$.3H2O was dissolved in water. sulfamic acid (stress reducing agent) was added to this solution followed by filtration to remove any solid particles. The resultant solution was transferred to the plating vessel, heated up to 40 °C and then a DC current was applied to the electrodes. The plating continued for 24 hours to complete Rh depletion. The copper carriers of electroplated ^{103}Rh targets were dissolved in concentrated nitric acid. A mixture of alcoholic solution which contains dimethylglyoxime (DMG) and chloroform as the organic phases were added to the Rh/^{103}Pd/HCl solution. The mixture was vigorously stirred for 10 minutes. The separated organic phase was washed with HCl. After complete degradation of organic compounds, in order to remove the residue oxidizing agent and form 103Pd chloride, the residue evaporated in hydrochloric acid, this process repeated for two times. The final product was dissolved in hydrochloric acid with desired concentration. ^{103}Pd radioactivity was measured by HPGe detector coupled with a CanberraTM multi-channel analyzer and the extraction process was repeated several times in the same conditions. Produced paladium-103 is then absorbed in (20-50 mesh) IRA-93 resin beads to encapsulate inside the titanium brachytherapy seed. Generally brachytherapy are packed inside a titanium cylinder of 4.8 mm length, 0.7 and 0.8 mm internal and external diameter respectively, in different format like resin beads or loaded on silver or copper rods. Because low energy photon emitting sources, such as ^{103}Pd, are sensitive to specifications and fabricating practices, according to American Association of Physicists

in Medicine (AAPM) TG-43U1 recommendation, the dosimetric characteristics of the source must be determined to provide reliable data for clinical use. Few different brachytherapy seed models have been developed the Agricultural, Medical and Industrial Research School. All the dosimetric parameters following the TG43-U1, determined (experimental and theoretical) [7-10]. Table 1 show a comparison between the dose rate constant of the seeds with other commercial brachytherapy seeds, which are in acceptable range. Figure 1 depicts radial dose function, of developed seeds at AMIRS with commercial sources.

Table 1: Monte Carlo calculated dose rate constant, Λ, of the IRA1-103Pd, IR01-103Pd and IR08-103Pd seeds in compare with the measured and calculated values of model MED3633 and Theragenics200 and best double-wall sources.

Source type	Method	Medium	Λ (cGy h^{-1} U^{-1})
IR01-^{103}Pd	MC simulation[8]	Liquid water	0.69±0.05
	TLD dosimetry[8]	Perspex	0.83±0.05
IRA1-^{103}Pd	MC simulation[7]	Perspex	0.669±0.001
IR08-^{103}Pd	MC simulation[9]	Liquid water	0.695±0.021
Theragenics 200	MC simulation[11]	Liquid water	0.686±0.03
	TLD dosimetry[12]	Solid water	0.650±0.08
MED3633	MC simulation[13]	Liquid water	0.677±0.02
	TLD dosimetry[14]	Liquid water	0.680±0.05
Best® double-wall	TLD dosimetry[15]	Solid water	0.69±0.08
	Monte Carlo simulation[15]	Liquid water	0.67±0.02

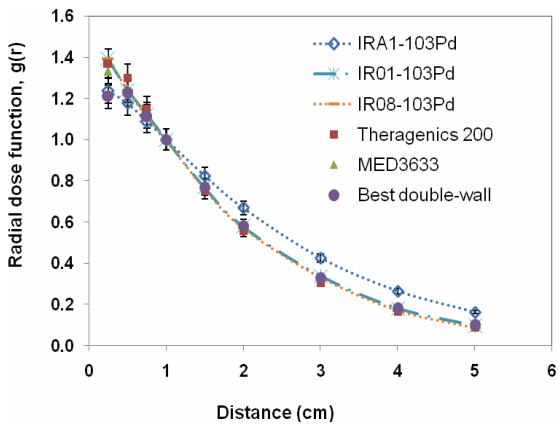

Figure 1: Comparison of the Monte Carlo calculation radial dose function of IRA1-103Pd [7], IR01-^{103}Pd [8], and IR08-^{103}Pd [9] seeds with the three model commercial sources [6].

RESULTS

The rhodium target for production of 103Pd can be prepared by an electro-deposition technique. Produced palladium is loaded on resin or absorbed on silver of copper core for use in brachytherapy seeds. Three new models brachytherapy seeds developed and fabricated at

AMIRS, the dosimetric parameters of them compared with three commercial sources [6]. The dose rate constant values of the seeds are in good agreement with other sources. Comparison between the radial dose rate function values show a good agreement with the exception for IRA1-103Pd model due to different internal component in compare with others.

REFERENCES

[1] A. Hermanne, M. Sonck, S. Takacs, F. Tárkányi, FY.Shubin,"Study on alternative production of 103Pd and characterisation of contaminant sin the deuteron irradiation of 103Rh up to 21 MeV", Nucl Instrum Methods B 187:3–14, (2002).

[2] S. Sudar, F. Cserpak, SM. Qaim, "Measurements and nuclear model calculations on proton-induced reactions on Rh-103 up to 40-MeV-evaluation of the excitation function of the Rh-103(p,n)Pd-103 reaction relevant to the production of the therapeutic radionuclide Pd-103", Appl Radiat Isot 56:821–831, (2002).

[3] M. Sadeghi, B. Shirazi, "Extraction separation of no-carrier-added 103Pd from irradiated Rh target, Cu and Zn using α-furyldioxime, dimethylglyoxime and α-benzildioxime", Appl Radiat Isot 66:1810–1813, (2008).

[4] M. Sadeghi , P. Van den Winkel , H. Afarideh, M. Haji-Saeid , "A thick rhodium electrodeposition on copper backing as the target for production of palladium-103", J. Radioanal Nucl Chem 262:665–672, (2004).

[5] M. Sadeghi, B. Shirazi, N. Shadanpour, "Solvent extraction of no-carrier-added 103Pd from irradiated rhodium target with α-furyldioxime", J Radioanal Nucl Chem 269:223−225, (2006).
[6] M. J. Rivard, B. M. Coursey, L. A. DeWerd, W. F. Hanson, M. S. Huq, G. S. Ibbott, M. G. Mitch, R. Nath, and J. F. Williamson, "Update of AAPM Task Group No. 43 Report: A revised AAPM protocol for brachytherapy dose calculations," Med. Phys. 31, 633-674 (2004).
[7] M. Sadeghi, GH. Raisali, S. H. Hosseini, A. Shahvar, "Monte Carlo calculations and experimental measurements of dosimetric parameters of the IRA-103Pd brachytherapy source" Med. Phys. 35, 1288-1294 (2008).
[8]Gh. Raisali, MG.Ghonchehnazi, P. Shokrani, M. Sadeghi, "Monte Carlo and experimental characterization of the first AMIRS 103Pd brachytherapy source", Appl. Radiat. Iso. 66: 1856-1860, (2008).
[9] P. Saidi, M. Sadeghi, A. Shirazi, C. Tenreiro, "Monte Carlo calculation of dosimetry parameters for the IR08-103Pd brachytherapy source", Med. Phys. 37: 2509-2515, (2010).
[10] M. Sadeghi, SH. Hosseini, Gh. Raisali, "Experimental measurements and Monte Carlo calculations of dosimetric parameters of the IRA1-103Pd brachytherapy source." Appl. Radiat. Isot. 66, 10,1431–1437, (2008).
[11] JF. Williamson "Monte Carlo modelling of the transverse-axis dose distribution of the model 200 103Pd interstitial brachytherapy source", Med. Phys 2000; 27: 643-654.
[12] R. Nath, N. Yue, K. Shahnazi, and P. J. Bongiorni, "Measurement of dose-rate constant for 103Pd seeds with air kerma strength calibration based upon a primary national standard," Med. Phys. 27, 655-658 (2000).
[13] Z. Li, JR. Palta, JJ Fan, "Monte Carlo calculations and experimental measurements of dosimetry parameters of a new 103Pd source." Med. Phys. 27: 1108-1112, (2000).
[14] RE. Wallace, JJ. Fan, "Dosimetric characterization of a new design 103palladium brachytherapy source." Med. Phys. 26: 2465-2470, (1999).
[15] AS. Meigooni, Z. Bharucha , W. Yoe-Sein M, et al. "Dosimetric characteristic of the best double –wall 103Pd brachytherapy source". Med. Phys. 28: 2568-2575 (2001).

KHARKOV COMPACT CYCLOTRON CV-28: PRESENT AND FUTURE STATUS

Yuri Petrusenko[1], Dmytro Barankov[1], Sergii Shkyryda[1], Denys Irzhevskyi[1], Rainer Hoelzle[2]
1 - CYCLOTRON Science & Research Establishment, NSC KIPT, 61108 Kharkov, Ukraine,
2 - Institut für Festkörperforschung, FZJ, 52425 Jülich, Germany

Abstract

Reported are the present and future statuses of the Kharkov Compact Cyclotron CV-28 donated to the National Science Center - Kharkov Institute of Physics & Technology (NSC KIPT) by the Forschungszentrum Juelich (Germany). The cyclotron configuration and special features of new installation at the NSC KIPT are described. Consideration is given to the use of the cyclotron beam as a promising means for investigation and development of materials for fusion reactors and generation-IV nuclear reactors, investigation and production of medical radionuclides, possible applications of a high-energy neutron source based on a deuteron beam and a thick beryllium target.

INTRODUCTION

A compact isochronous cyclotron CV-28, supplied by Cyclotron Corporation (USA) to the Jülich Research Center (Germany) provides the generation of light ion beams (H^+, $^2H^+$, $^3He^{++}$, He^{++}) in the continuous mode of operation with output energies adjustable in a sufficiently wide range [1].

Table 1 gives the performance characteristics of cyclotron CV-28.

Table 1: Cyclotron CV-28 performance characteristics

Particles	Beam energy range	External Current at Minimum Energy	External Current at Maximum Energy	Internal Current
H^+	2-24 MeV	70 μA	70 μA	500 μA
D^+	3-14 MeV	100 μA	100 μA	500 μA
$^3He^{++}$	5-36 MeV	15 μA	70 μA	150 μA
He^{++}	8-28 MeV	10 μA	50 μA	100 μA

It should be noted that the above-mentioned advantages of the cyclotron are supported by the fact that it can be readjusted for ion production with different energies or for acceleration of ions of other species more than once per working shift, i.e., sufficiently promptly.

The cyclotron is really operated as a multi-particle and variable-energy machine, as it is common practice with it to have several different beams a day, mostly on different targets, too. The general view of the compact cyclotron CV-28 is shown in Fig. 1.

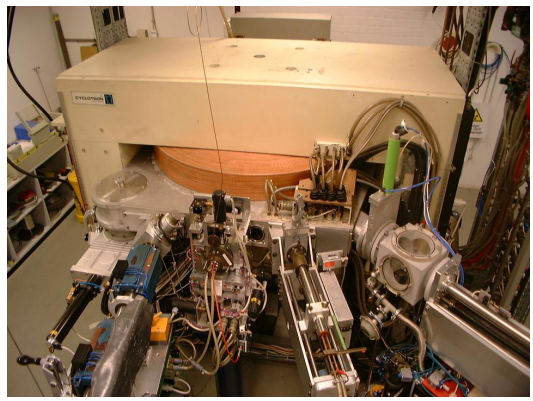

Figure 1: View of cyclotron

An accelerated beam can be guided to the target located inside the acceleration chamber, and can be extracted by means of the deflector and the magnetic channel outside the acceleration chamber.

The ion guide with ion-optical elements arranged on it directs the beam to the switching electromagnet.

PRESENT STATUS OF CV-28

In 2006, the cyclotron complex CV-28 equipment (except ventilation and water-cooling systems) was dismantled, packed and, by the end of 2006, was brought to the NSC KIPT. The layout of the cyclotron complex equipment is shown in Fig. 2

We have designed a new scheme of locating the cyclotron in a specially assigned building at the NSC KIPT. This scheme follows the German version of the equipment arrangement in many ways. The main feature consists in the ejection of the accelerated ion beam to three radiation-isolated target rooms, which accommodate five channels altogether. Two more ion beam channels are located in the cyclotron room.

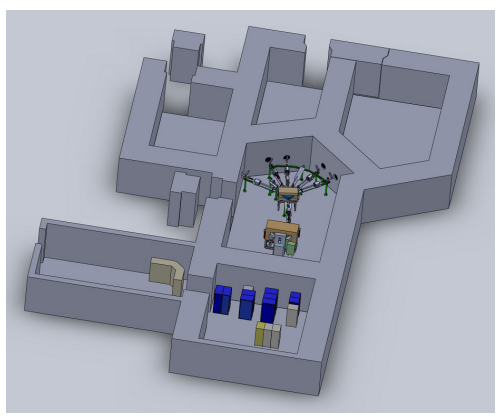

Figure 2: Layout of the cyclotron complex equipment

Currently, the work on installing the components and units of the cyclotron is under way. The cyclotron chambers with main magnetic coils as well as the switching magnet are installed in their working places. Assemblage of the major ion channel has been started. Installation of service cables and air channels is carried out. The work is in progress on the preparation of the main and backup power supply of the cyclotron. The 3D picture of the cyclotron and switching magnet is presented in Fig. 3.

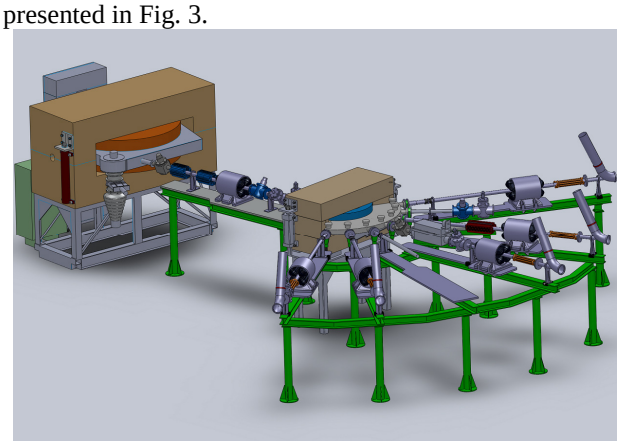

Figure 3: The cyclotron with switching magnet

FUTURE STATUS

The main lines of research at the NSC KIPT with the use of cyclotron CV-28 include: nuclear physics, production of medical isotopes, investigation of radiation damages in structural materials of nuclear power reactors [2].

Medical Radionuclide Production

The cyclotron CV-28 offers the challenge of producing isotopes for PET and SPECT diagnosis, as well as for radionuclide therapy of cancerous growths (brachytherapy, radioimmunotherapy, targeted alpha therapy, Auger-therapy) [3]. The possibility of production of medical radionuclides ^{123}I, ^{124}I, ^{125}I at the cyclotron CV-28 with the use of Te targets has been investigated

The Neutron Source

As regards the creation of a neutron source on the beam of deuterons with a thick beryllium target, it has been shown that with a deuteron beam having energy of 14 MeV and current of 100 mA, one can obtain neutron beams with a maximum density of 10^{12}·n/sm^{2}sec. The calculated energy spectrum of neutron flux is shown in Fig. 4.

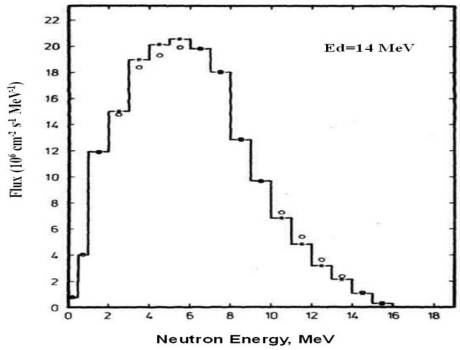

Figure 4: The energy spectrum of neutron flux

The main areas of application of the neutron source based on the cyclotron are as follows:

- development and testing of neutron detectors;
- element analysis;
- neutron effects on biological materials.

The neutron collimator is shown in Fig.5.

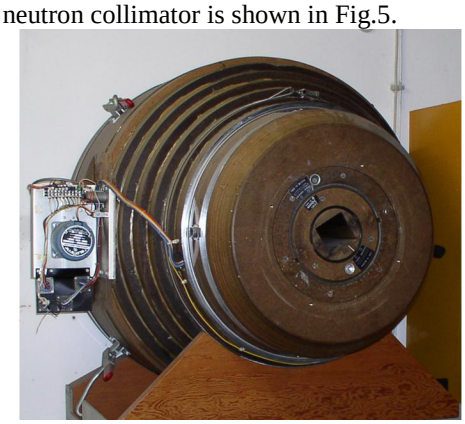

Figure 5: The neutron collimator

Study of Radiation Damage in Structural Materials of Nuclear Power Reactors

The main research areas are: radiation creep, high-temperature radiation embrittlement; effects of implantation of H, He; vacancy swelling; the role of nuclear reaction products in the change of mechanical and other properties of reactor vessel and fuel cladding. The maximum doses and dose rates attainable for different ion beams were calculated and are presented in Table 2.

Table 2: Calculated maximum damage by different particles

Particles	Max Beam Energy	Average Current	Max Dose Rate	Max Dose
H^+	24 MeV	50μA	~$5\cdot10^{-6}$ dpa/sec	~0.25 dpa
D^+	14 MeV	50μA	~10^{-4} dpa/sec	~5.0 dpa
$^3He^{++}$	36 MeV	50μA	~$2\cdot10^{-4}$ dpa/sec	~10 dpa
$^4He^{++}$	28 MeV	50μA	~10^{-3} dpa/sec	~50 dpa

The depth of proton penetration into nickel has been calculated (see Fig. 6).

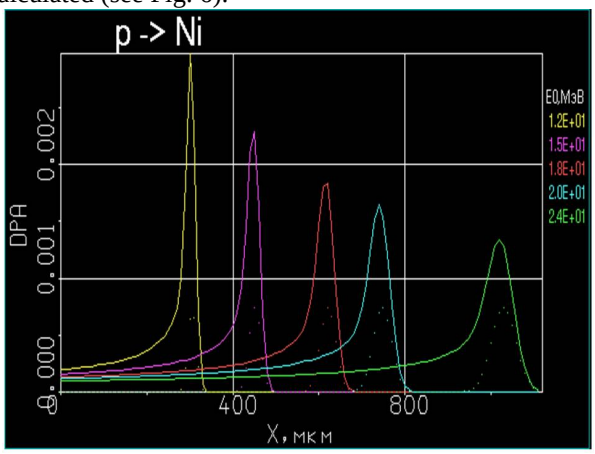

Figure 6: Profiles of defect accumulation in nickel irradiated with a proton beam.

ACKNOWLEDGEMENTS

We thank V. Gann at National Science Center – Kharkov Institute of Physics & Technology for calculation of damage profiles in nickel irradiated with a proton beam.

REFERENCES

[1] J. Hemmerich, R. Hoelzle,W. Kogler. The Juelich compact cyclotron – a multi – purpose irradiation facility // Kerntechnik. 1977, No 2.

[2] A.M. Yegorov, A.G. Lymar, I.M. Nekludov, Yu.T. Petrusenko. Compact cyclotron CV-28 and prospects its usage //Problems of atomic science and technology, 2008. No 5. Series: Nuclear Physics Investigations (50), p.12-15.

[3] V.V. Sotnikov, V.A. Voronko, Yu.T. Petrusenko, D.Yu. Barankov // The Potential of medical radioisotopes production by cyclotron CV-28, Problems of atomic science and technology. 2010. No 3. *Series:* Nuclear Physics Investigations (54), p.168-172.

CONTROL SYSTEM OF CRYOGENIC PLANT FOR SUPERCONDUCTING CYCLOTRON AT VECC

Umashankar Panda*, Sandip Pal, Ranadhir Dey, Tanushyam Bhattacharjee, Aditya Mandal
Variable Energy Cyclotron Centre, 1/AF, Bidhan Nagar, Kolkata – 700064, India

Abstract

Cryogenic Plant of Variable Energy Cyclotron Centre consists of two Helium refrigerators (250W and 415W @ 4.5K), valve box with sub-cooler and associated sub systems like pure gas storage, helium purifier and impure gas recovery etc. The system also consists of 3.1K liters of liquid Nitrogen (LN_2) storage and delivery system. The plant is designed to cater the cryogenic requirements of the Superconducting Cyclotron. The control system is fully automated and does not require any human intervention once it is started. EPICS (Experimental Physics and Industrial Control System) architecture has been adopted to design the Supervisory control and data acquisition (SCADA) module. The EPICS Input Output Controller (IOC) communicates with four Programmable Logic Controllers (PLCs) over Ethernet based control LAN to control/monitor 618 numbers of field Inputs/ Outputs(I/O). The plant is running very reliably round the clock, however, the historical data trending of important parameters during plant operation has been integrated to the system for plant maintenance and easy diagnosis. The 400 KVA UPS with 10 minutes back up time have been installed to keep the cryogenic system running with one 160KW cycle compressor during utility power interruptions.

PROCESS DESCRIPTION

Superconducting Cyclotron at VECC requires a dedicated Helium Refrigerator for operation of the Superconducting Cyclotron Magnet at a temperature of about 4.2 K. The process diagram is as shown in Figure 1.

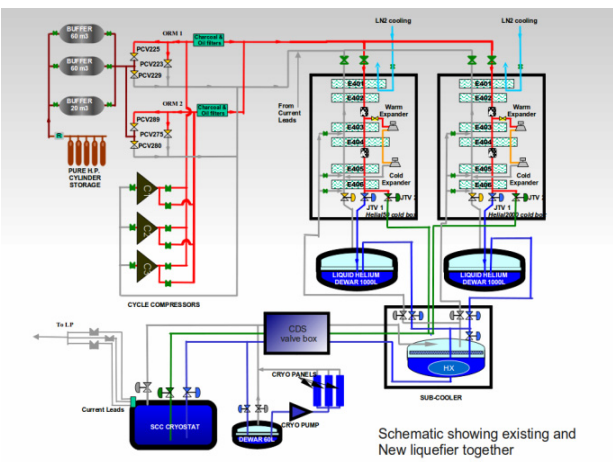

Figure 1: Process Diagram

The heat load of the liquid Helium(He) Cryostat of superconducting cyclotron system is around 160W @ 4.2K. One of the existing two helium liquefiers is connected at a time to the cryostat through a sub-cooler. Each liquefier is having Dewar of 1K litres capacity each. Liquid helium is transferred by keeping a constant pressure of 1.4 bar at Dewar and 1.2 bar at Cryostat. The liquefiers are operating in modified Claude Cycle with two turbo expanders running in series. There are six heat exchangers and two Joule-Thompson expansion valves in the system. The bigger liquefier requires 85 gm/s compressed helium gas at 14 bar pressure and the smaller one requires 50 gm/s. The system is having two Oil Removal Modules (ORM) (100gm/s and 50gm/s capacity) and three numbers of helium screw compressor of 50gm/s capacity each. The high and low pressure lines are common to both the liquefiers and the compressor selection with the ORM has been made flexible so that any compressor can be operated with any liquefier. The higher size liquefier requires two compressors running for its operation cycle. The advantage of such arrangements gives the benefit of compressor isolation for maintenance without stopping the operating liquefier. One 20 m^3 and two 60 m^3 of water capacity helium buffer gas storage tanks at a maximum working pressure of 14 bar are connected to the system.

Four liquid nitrogen storage Dewars of 2x2KL, 1x12.5KL and 1x14.5KL are also operating to receive LN_2 from the supplier tanker and the stored LN_2 is transferred to the Superconducting Cyclotron radiation shield cooling system. LN2 cooled external helium purifier of 20m^3/hr @ 140 bar, pneumatic air system for control valve, turbo-expander water cooling system and impure helium gas recovery system are also connected for the proper operation of the plant.

Out of the three, one compressor is powered through 400 KVA UPS. This has been done because in case of normal power failure the liquefier which is connected to the cryostat keeps operating. However, in case the bigger liquefier is in operation, the second compressor is started from the normal power or Diesel Generator (DG) power automatically after 5 minutes. This facility provides the non interruption of the cryogenics operation and also saves the restoration time and pure helium gas loss. Highly skilled manpower need not to be deputed round the clock for restoration job.

CONTROL SYSTEM OVERVIEW

Control architecture of our cryogenic system control is a three layer architecture comprising of device layer, IOC server layer and user Interface layer. The device layer consists of PLCs which controls the automatic process

*usp@vecc.gov.in

sequence operations. The PLCs and the process components are configured to satisfy fail-safe operation. The user interface layer consists of the control computers where the operators issue the set points and the mode of operation commands. The alarm and historical archiver are also running in this layer. Figure 2 represents the overview of the control system.

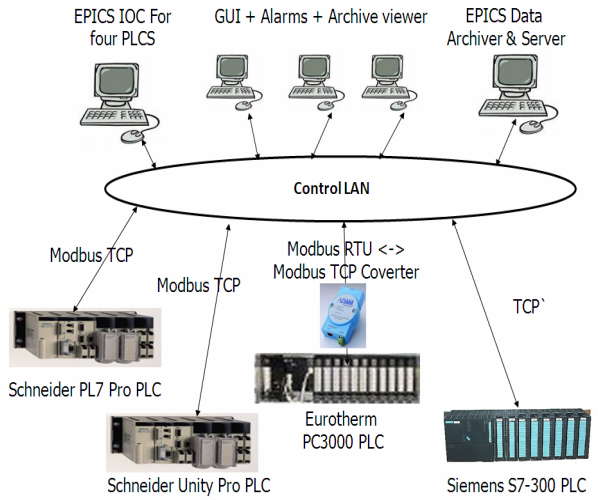

Figure 2: Control system overview

The smaller helium liquefier is controlled by means of Eurotherm PC3000 PLC which is handling 130 field I/Os. The bigger liquefier and the sub-cooler valve box are controlled by Siemens S7-300 PLC having 144 field I/Os. Both liquefiers are designed in such a manner that there is only few initial commands is required to be issued by the operations [1],[2]. For example, to operate with the cryostat in cooled down condition the operator gives only the commands of start liquefier and connection to cryostat. Liquid helium level to be maintained in the 1KL Dewar and the maximum allowed turbine speed are set in the set point and can be modified in certain range by the operator. The plant automatically adjusts the refrigeration power according to the demand by varying the turbine speeds to keep a constant level in the Dewar. Once the liquefier is operating in steady state there is no human intervention is required for the operation of the plant.

The impure gas handling, turbine cooling, buffer tanks, liquid nitrogen Dewars and transfer system and turbine water cooling system are controlled by Schneider PL7 PLC which is having 292 field I/Os. [3]. All the systems related to Schneider PL7 PLC are operated based on mode of operation commands from the operator. All sequence, set points and safety features are programmed in the PLC logic.

The external helium purifier operating at 140 bar, 77K and 20 m^3/hr is controlled by Schneider Unity Pro PLC having 52 field I/Os. Operators have to select and issue command of the Purification or Regeneration mode and rest sequences are automatic. Sequential Flow Chart (SFC) language is used for all PLC programming.

SUPERVISORY CONTROL

Supervisory control is the user interface layer part. In this layer four different PLCs of three different manufacturers are being monitored and controlled through Ethernet based control LAN. We felt a requirement of a SCADA which can give user interface at a common platform as well as exchange data between systems. Also the user interface computers were required to be put at different locations spread over two buildings.

After evaluation of requirements, we selected Experimental Physics Industrial Control System (EPICS) [4] as suitable system which fulfil our need.

We first tested EPICS IOCs (Input-Output Controllers) on simulator software for Modbus TCP protocol for communicating with Schneider and Eurotherm PLC. After testing successfully we implemented this in a linux PC in our network to run the IOC to communicate with Eurotherm and Schneider PLCs. We also used IOC for Siemens PLC with TCP communication. There was no Ethernet port in Eurotherm PLC. So we have put a Modbus RTU to Modbus TCP converter module of Advantech make. Watch dog program is also implemented to generate alarm to operator when there is a communication failure for more than 5 seconds.

The Graphical User Interface (GUI) is made by using EPICS Motif Editor and Display Manger (MEDM) tool. All the process parameters of all the systems are displayed here for monitoring with a proper navigation buttons. Same GUIs are running in three different PCs so that different systems can be monitored together. Process line colour change occurs according to the process so that the process can be viewed at a glance. Figure 3 shows the GUI of liquid helium system overview.

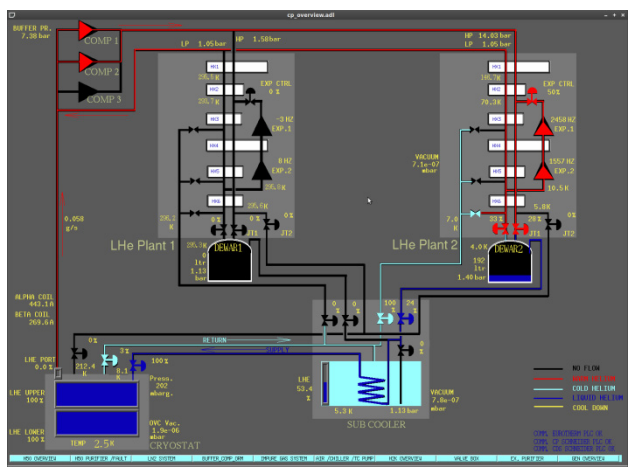

Figure 3: GUI of liquid helium system overview

EPICS Alarm Handler is used to handle the Alarms of the channels observed from all four IOCs to sound an alarm to the operator to take preventative action. For example if the water level in the turbine cooling system tank then the alarm handler sounds an alarm with red coloured indication against the particular alarm. The operator then acknowledges it and takes necessary action to fill up water or change the pump or repair the gland

packing leakage etc. Screenshot of alarm handler is shown in Figure 4.

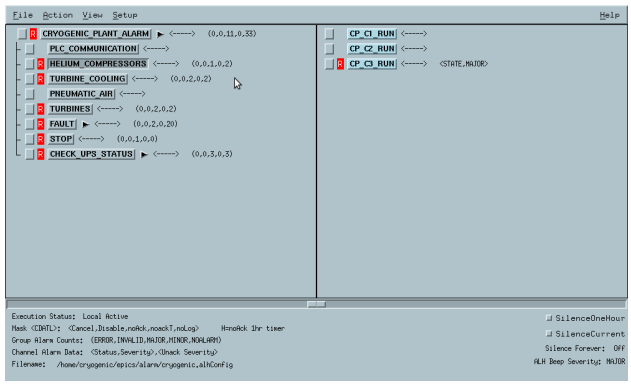

Figure 4: Screen shot of Alarm Handler

EPICS Channel Archiver is used to archive the values of 376 important parameters from all four IOCs. The archive values are stored to hard disk only when the value changes. Standalone archive server is used to host the data for viewing in EPICS Archive Viewer. EPICS Archive Viewer is available at three computers in the network. Process sequence step numbers are also achieved to diagnose the system behaviour for understanding the system dynamics.

Pure gas stock calculation is continuously done by EPICS IOC by monitoring parameters from different systems like pressure and temperature from gas storage tanks, liquid helium level of Dewars, valve box and cryostat etc. The calculated value is the pure gas stock in normal m^3 and archived in the Archiver. The trend gives us the idea of helium gas leak rate from the total installation. Screen shot of Archive Viewer is shown in Figure 5.

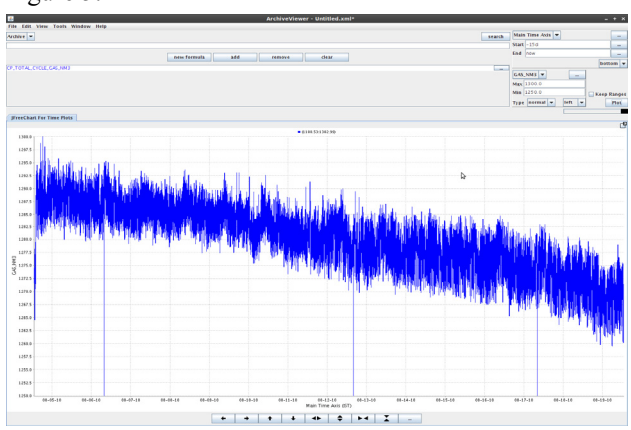

Figure 5: Screen shot of Archive Viewer

All the applications are set in the start up script so that in case the PC got switched off due to UPS power fail or some other problem all the applications get restarted. PCs BIOS are also set such that PC restarts itself after the power failure.

CONCLUSION

We had operated the system continuously for 22 months and 13 months without any interruption with the small liquefier. Presently total control system is running undisturbed and without any human intervention since 19th July 2010 with the new helium liquefier and valve box commissioned. The superconducting magnet of the cyclotron had been cooled down to 4.2K, and filled up with liquid helium and plant is operating in refrigeration mode. The required current is applied in the superconducting magnet and Ne3+ beam tuning in progress. The cryogenic control system is integrated with the main cyclotron control system through EPICS so that cyclotron operator can also monitor cryogenic system status from the central control room.

REFERENCE

[1] U. Panda et al, “Modifications For Optimum Operation Of Helium Liquefier – Refrigerator at VECC, Kolkata”, Indian Cryogenics Journal Vol 33 No 1 2008.

[2] R Dey et al, “Operational Experience of Helium Liquefier-Refrigerator after interfacing with K-500 Superconducting Cyclotron”, Indian Particle Accelerator Conference, VECC, Kolkata, March 1-5, (2005).

[3] Sandip Pal et al, “PLC-based Helium Gas Management and Liquid Nitrogen Delivery Control System for K-500 Superconducting Cyclotron at VECC, Kolkata”, DAE BRNS Symposium on Nuclear Physics, December 12-16, (2005).

[4] EPICS website : http://www.aps.anl.gov/epics.

DEVELOPMENT OF POWER SUPPLIES FOR 3-Φ, 240 KW RF SYSTEM WITH CROWBAR PROTECTION FOR SUPERCONDUCTING CYCLOTRON AT VECC

S. K. Thakur*, T. P. Tiwari, J. S. Prasad, A. De, Y. Kumar, S. Som, S. Saha, R.K. Bhandari
Variable Energy Cyclotron Centre, Kolkata, India.

Abstract

RF system of K-500 Super-conducting Cyclotron at VECC is a complex three phase system operating in the frequency range of 9 MHz to 27 MHz with maximum acceleration potential of around 100KV feeding to each of three Dee cavities placed in median plane of cyclotron 120º apart through coupling capacitors. Each phase consists of chain of amplifiers and resonator operating in synchronization and at final stage of each phase, high power water cooled Tetrode Tube (Eimac4CW150,000 E) is used as high power amplifier each capable of delivering 80 KW of RF power. Individual power supplies for biasing Anode, Filament, Grid and Screen for all three high power Tetrode Tubes are designed and developed in house. Anode supply is common to all three tubes, rated at 20KV, 22 Amp, 450 kW along with fast acting crowbar protection using Ignitron. All these power supplies are commissioned and have been in operation for more than one year successfully. This paper describes about the technical aspects of the power supplies for RF Amplifier Tubes and special features of protection systems.

INTRODUCTION

For three RF amplifiers, which uses Tetrode Tube (Eimac 4CW 150,000E), three set of power supplies each for Filament (15.5V, 215A), Grid (-500V, 0.1 A), Screen Grid (1600V, 0.5 A) and a common power supply (20KV, 22 Amp) for Anode are designed and developed in house. Each of the power supplies are equipped with control and monitor systems with Local/Remote control facility, power switchgear with interlocking, protective systems etc as shown in Fig-6. A PLC system is interfaced with individual power supplies by which each power supplies can be controlled as well as interlocking and monitoring of parameters can be done in Remote mode of operation.

FILAMENT POWER SUPPLY

A variac controlled, voltage regulated power supply with a regulation of ± 1%. This consists of a step down 3-ph transformer with full bridge rectifier followed by a filter. A control circuit added with variac auto zero and soft start feature in the power supply adjusts the variac, corresponding to its set value. The input 415V, 50 Hz, 3-ph ac supply ramps up in steps through variac from zero to around 80% voltage corresponding to output 15.5 V dc in approximately 3 minutes. Soft start is an added feature to limit the filament current during cold condition. Heater current is approximately 210 A corresponding to 15.5 V.

GRID POWER SUPPLY

It is a series regulator type power supply that uses IGBT as series element for voltage regulation as shown in Fig-1. A low ripple and highly regulated power supply with adjustable voltage which ranges from -200 V to -500V for setting the Grid biasing of amplifier.

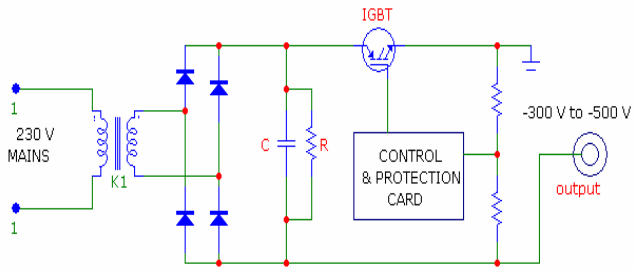

Fig-1: Schematic of Grid Power Supply

SCREEN POWER SUPPLY

Screen Grid power supply (1600V, 0.5 Amp, 60 ppm) is a series regulator type which uses water cooled tetrode tube (Eimac 4CW2000) as regulating element connected in common cathode mode. Three individual regulator tubes with their respective circuitry are used except their common anode voltage which is kept at around 2500Vdc. Part of output voltage is sampled and fed back to an error amplifier which ultimately drives the transistor for adjusting Grid biasing of series regulator tube as shown in Fig-2. A very stable power supply with very low ripple voltage is designed and developed along with fast crowbar protection feature which is initiated by either main anode crowbar as well as screen over current.

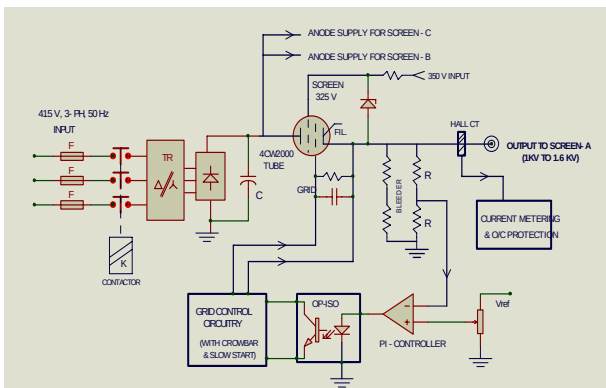

Figure 2: Schematic of Screen power supply.

*thakur@vecc.gov.in

Tube may exhibit reverse screen current depending upon the operating condition which may lead to high plate current. In order to suppress this problem, adequate amount of bleeder resistance is used. Suitable interlocking facility such as water, main Anode ON, phase fail etc are employed along with crowbar and over current (reverse / forward) in each power supply. Output voltage and current is monitored by individual hall CTs and being displayed at Local control panels as well as in control room.

ANODE POWER SUPPLY

All three High Power Amplifiers (HPA) are powered by a single Anode power supply rated at 20 kV, 22 Amp (Fig.-3). EHT uses two high power transformers, each 250KVA, 415V / 3700V & 3700 V rating, forced air cooled whose primary connected in delta and secondary connected in star & delta for 12 Pulse mode output. The 3-ph power system is connected to each of two transformers via air core choke in each line and fast interrupting circuit breaker. “Siemens” make circuit breakers are used which disconnects from mains ac lines within 4-5 cycles. Chokes are employed to restrict input line current in the event of crowbar or short circuit.

A primary SCR based soft start feature is added in one transformer in order to reduce inrush current. In second transformer, a primary online voltage regulating oil cooled motorised Variac is used to adjust output voltage from 10KV to 20 KV. Forced air cooled 3-Ph full wave bridge rectifier assembly is used in each of four secondaries of both Transformers. Each rectifier assembly gives output 5 KV dc connected in series making a 20 KV dc voltage with ripple frequency 600 Hz. A capacitor filter is used to smoothen output ripple.

Various protection like over-voltage, over current, phase failure, thermal overload, over temperature, spark/arc protection have been incorporated in this power supply. Various fault conditions were simulated in this power supply and all above-mentioned protection features were checked reliably before putting with actual load.

RF and microwave tubes are prone to internal arc that can lead to a permanent damage if excessive energy is dissipated. So, a shunt diverter topology was chosen in which stored energy in electrical system is diverted to the ground by quick shorting the output terminals of power supply through Ignitron (NL7703) as a Crowbar switch followed by tripping of mains Circuit Breakers. Internal arcing in the tube is a common phenomena which depends upon operating conditions. Thus crowbar protection is the most critical part in the power system used for the protection of high power very expensive RF and microwave devices. Three final power amplifier Tubes which feed RF power to 3 nos of main cavities placed in the cyclotron through individual coupling Capacitors and quarter wave coaxial transmission line in each halves. Thus HPA is main constituent of RF system which needs to be protected reliably through a Mercury filled Ignitron (NL7703). The Crowbar switch system should meet following requirements:-

Operating voltage:- 20 KVdc
Full load current :- 22 Amp
Peak current :- 900 A (during discharge)
Stored Energy in filter capacitor :- 6000 Joule
Energy transfer per shot < 50 Joule
Operating time :- < 5 µsec
CB tripping time :- 0.15 sec
Charge transfer :- < 1 Coulumb.

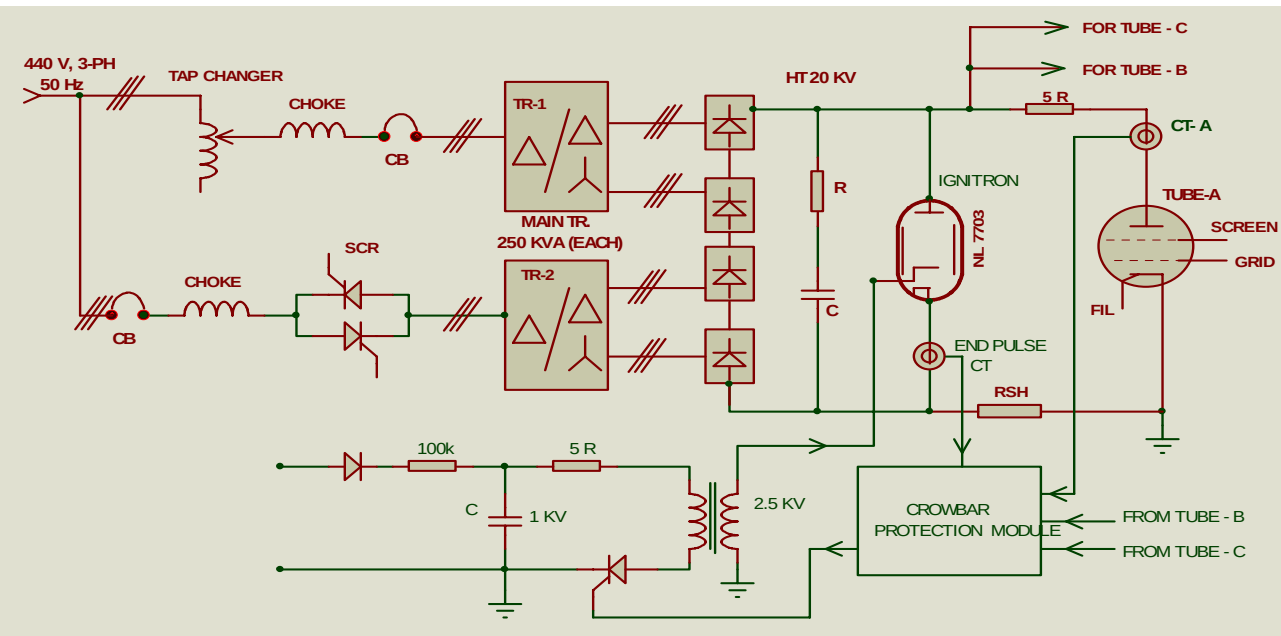

Figure 3: Schematic of Anode Power Supply (20 KV, 22 Amp) with Ignitron Crowbar Protection scheme.

Summary of Measurements

Crowbar system performance was thoroughly tested at various voltage level and ultimate protective capability is performed by wire survivability test. The wire provides an approximately calibrated measure of energy deposition for fusing. As per the manufacturer, the energy deposition in tube should be limited to less than 50 Joule during a fault. Empirical test result with a 6 inch long piece of 30 AWG copper wire indicates almost same energy deposition for fusing.

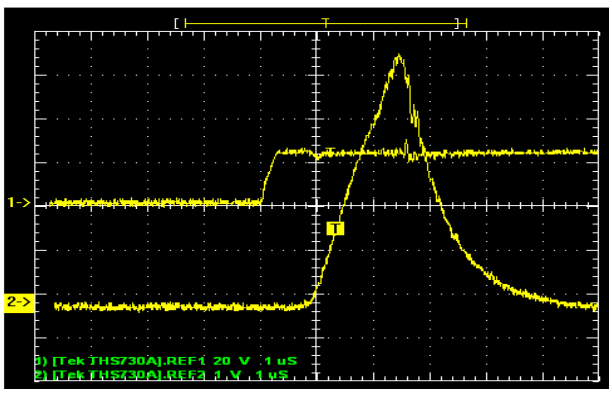

Figure 4: Crowbar measurement, Ch-1-Fault current & Ch-2 Trigger signal to Ignitron and time delay around 3 µs.

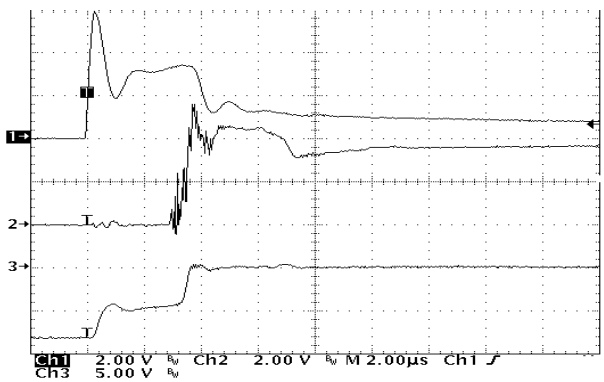

Figure 5: Fault current (ch-1), Crowbar current(ch-2) sensed by pearson CTs (1V=100 Amp) and Load Voltage (ch-3) 5V=10KV.

To conduct the test, a high voltage relay is connected in series with the wire and connected across the output terminals of the power supply. The fault is initiated by closing the relay and wire survival test was performed. The current flowing through the wire is sensed by the fast acting Pearson CTs. The signal is sent to the fault processing circuitry which issues the triggers signal to the Ignitron and finally main CBs opens. Fig-4 shows that a trigger signal is generated within 3 µs. Fig-5 shows the output voltage comes to zero within 4 µs when Ignitron fires. For reliability, this test was performed several time for few days and not a single time wire was blown.

Figure 6: Anode Transformers & Local Control Panel showing monitoring, fault indications & controls.

Challenges and Experience

During the design & development of such a high power system at high voltage, a reliable and robust protective Crowbar system became the most significant challenge. Initially wire survivability test could not pass even at lesser voltage. Noise & grounding problems creates spurious triggering & delayed response time as well. Then with modified protection system hardware architecture, final crowbar circuitry was designed and proper layout of switch assembly, system response time was improved after 2-3 attempts and subsequently wire survivability test could pass.

ACKNOWLEDGEMENT

The authors would like to thank Mr. Amiya Mitra, TRIUMF, Vancouver, Canada for his valuable guidance. The authors would also like to thank each and every Technical staffs of HVPS Section, VECC for their sincere effort for the development & installation of power supplies for RF system successfully.

REFERENCES

[1] A. K. Mitra, “Measurements of Crowbar Performance of the 20 kV, 130 A dc Power Supply of the TRIUMF rf System” IEEE, 1991.
[2] S. G. E. Pronko and T. E. Harris, “A New Crowbar System for the Protection of High Power Gridded Tubes and Microwave Devices”. IEEE Int. Vac. Elec. Conf., 2001.
[3] Eimac 4CW150,000E data sheet, published in May, 1983.
[4] Richardson Electronics application notes for Ignitron mounting and maintenance.
[5] Various VECC reports and News Letters published in VECC.
[6] S. Som, Dr. R. K. Bhandari, “Development of RF system for K-500 Cyclotron” presented in 18th International conf. on Cyclotron and their applications.

ACTIVITIES AT THE COSY/JÜLICH INJECTOR CYCLOTRON JULIC

R. Brings, O. Felden, R. Gebel*, and R. Maier, Forschungszentrum Jülich, 52425 Jülich, Germany
Institute for Nuclear Physics (IKP), Jülich Center for Hadron Physics (JCHP)

Abstract

The operation and development of the accelerator facility COSY is based upon the availability and performance of the isochronous cyclotron JULIC as the pre-accelerator. The cyclotron has been commissioned in 1968 and exceeded 241 000 hours of operation. In parallel to the operation of COSY the cyclotron beam is also used for irradiation and nuclide production. A brief overview of activities, performance, new and improved installations und procedures is presented.

INTRODUCTION

The institute for nuclear physics at the Forschungszentrum Jülich is dedicated to fundamental research in the field of hadron, particle, and nuclear physics. The aim is to study the properties and behaviour of hadrons in an energy range that resides between the nuclear and the high energy regime. Main activities are the development of the high energy synchrotron ring HESR, operation and improvement of the Cooler Synchrotron COSY-Jülich [1], with the injector cyclotron JULIC [2-4], as well as the design, preparation, and operation of experimental facilities at this large scale facility, and theoretical investigations accompanying the scientific research program.

The accelerator HESR, part of the GSI FAIR project [5], synchrotron is dedicated to the field of high energy antiproton physics with high quality beams over the broad momentum range from 1.5 to 15 GeV/c to explore the research areas of hadron structure and quark-gluon dynamics. An important feature of the new facility is the combination of phase space cooled beams with internal targets which opens new capabilities for high precision experiments. The tools to reach the required quality are tested at COSY. The cooler synchrotron COSY offers excellent research opportunities for hadron physics experiments and for essential preparatory studies for the machine development of HESR. A 2 MeV electron cooler is under construction, Detector tests for PANDA and polarization build-up studies for PAX are performed.

EXPERIMENTS AT COSY

The cooler synchrotron and storage ring COSY delivers unpolarized and polarized beams of protons and deuterons with momenta up to 3.7 GeV/c for three internal experiments — ANKE, PAX and WASA — and one experiment — TOF — at an external target position. All four detection systems are operated by large international collaborations [6].

At ANKE, Apparatus for Studies of Nucleon and Kaon Ejectiles, is a large acceptance forward magnetic spectrometer at an internal target station in the COSY ring. First double polarized experiments have been performed with a polarized internal target with a storage cell.

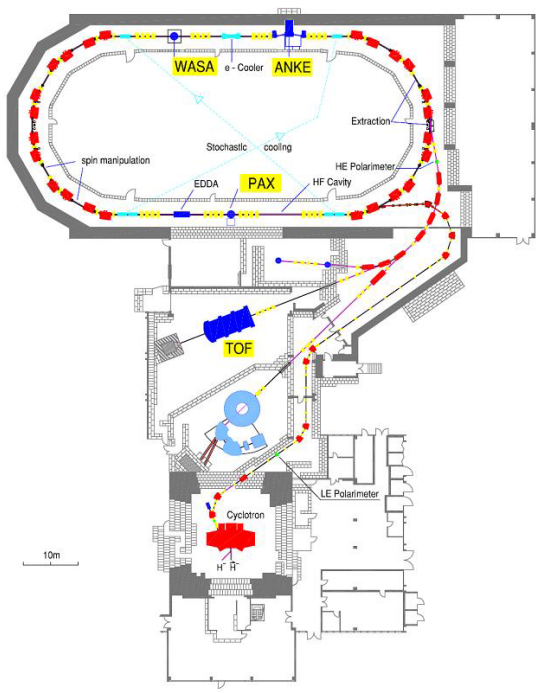

Figure 1: Layout of the COSY facility.

The 4 pi spectrometer for neutral and charged particles, WASA, Wide Angle Shower Apparatus, is operated also with the internal COSY beam. The barrier bucket cavity of COSY was successfully used to optimize the compensation of the main energy loss, which is introduced by the WASA frozen-pellet target.

An advanced grant of the European Research Council has been obtained for the polarization of anti-protons. Additionally installed quadrupoles in the mid of the straight target section provides the needed low beta values for the newly installed former HERMES polarized target as a polarized internal gas target. This is an important step to provide polarized antiprotons for FAIR.

In addition, the unique COSY capabilities are used by the SPIN@COSY-, dEDM- and PAX-collaborations to investigate spin-manipulations, to build a dedicated EDM-storage ring experiment, and to prepare experiments on polarization build-up in storage rings.

NEW METHODS AT COSY

The 2 MeV electron cooler project for COSY is funded and is expected to boost the luminosity in the presence of

*r.gebel@fz-juelich.de

beam heating by high density internal targets. In cooperation with the Budker Institute of Nuclear Physics, BINP Novosibirsk (Russia), the manufacturing has been started. The cosy section has been prepared to insert the cooler at the former position of the rf cavity [7].

Theoretical investigations of stochastic momentum cooling for the HESR clearly reveal that the strong mean energy loss induced by the interaction of the beam with an internal pellet target can not be compensated by cooling alone. At COSY stochastic cooling and internal targets are available similar to those which will be operated at the HESR. A barrier bucket cavity is routinely in operation. The COSY machine is exquisitely suited for beam dynamic experiments in view of the HESR. Important feasibility studies to compensate the large mean energy loss induced by an internal pellet target similar to that being used by the PANDA experiment at the HESR with a barrier bucket cavity (BB) have been carried out [8, 9].

CYCLOTRON OPERATION

The operation and development of the accelerator facility COSY is based upon the availability and performance of the isochronous cyclotron JULIC used as the pre-accelerator. The cyclotron has been commissioned in 1968 and exceeded 241000 hours of operation in 2010. A fraction of the run time since 2000 is shown in the upper part of fig. 2. The lower part shows the distribution of the available beam species, protons and deuterons, polarized or unpolarized.

Table 1: Runtime and failures

Year	Available / h	Unavailable / h
2007	6590	300
2008	7303	156
2009	6716	164
2010/07/01	3621	40
Since 1989	132800	-
Since 1968	241000	-

Table 1 reflects the high availability of the cyclotron from 2007 to mid 2010. Only about 3 % of the scheduled beam time could not be provided to experiments, due to failures at the cyclotron. Excluded were short events, like spark recovery, which are fixed automatically or by the operator. The most common reasons for such events were power drops, shortage in water cooling, septum exchange and failures in the rf subsystems.

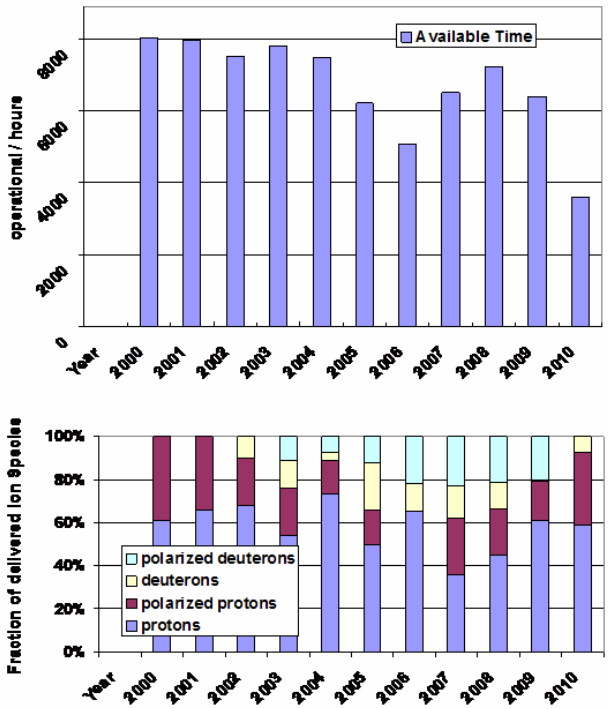

Figure 2: Beam usage statistics.

A special effort went into having replacement parts for critical systems and systems with limited lifetime. The electrostatic septum has to be replaced about once every year. Especially run periods with elevated voltages or irradiation with continuous operation are detrimental for the septum. So we have two spare septa under vacuum for quick exchange. At least one replacement is provided for motor-driven tuning elements and capacitor set-ups.

IRRADIATION FACILITIES

The cyclotron is equipped with 5 ports for radial moveable targets. Today two targets are used routinely. The target behind the septum provides special support for fast exchange of irradiated target constructions. For tuning of the beam extraction one needs the two targets behind the electrostatic septum and the magnetic extraction elements. An inherent problem is the contamination by out gassing of the target material. Accompanying detail improvements the external target station is extended to use production targets for radio isotopes. The principal user of the external target station investigates radiation defects on semiconductors and electronic elements for space missions. The focus of the user with internal targets for radiopharmaceutical products is data measurement and production of longer living PET isotopes at higher beam energies. A new external target station, adopted from one of the cyclotrons of the on-site nuclear chemistry institute, was developed to irradiate solid state targets. Table 2 gives an overview of irradiations at JULIC. Additional activities are planned for the second half of 2010 to get the new target station fully operational. The included helium-cooled double

window separates the vacuum around the target from the cyclotron chamber. That provides fast recovery to routine injector operation.

The new target set-up is shown schematically in fig. 3. By replacing the target by an appropriate aluminium window the situation for the other users is kept unchanged. The reduction of beam path length in air is compensated by proper selection of the thickness of the window.

Table 2: Irradiations at JULIC

Year	internal	external
2007	4	-
2008	7	6
2009	7	6
2010/07/01	4	3
Since 1973	233	29

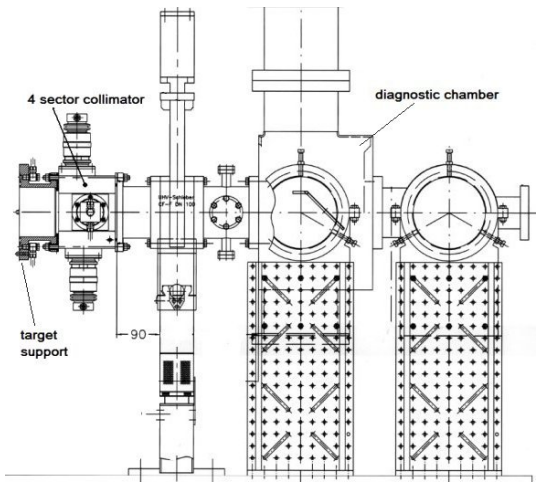

Figure 3: Layout of the actual high current target station.

POLARIZED BEAMS

During the last years the demand for precise polarization measurements, especially for deuterons with various polarization states is increasing. Another motivation has been an observed reduction of polarization for experiments. To exclude effects in the vicinity of the cyclotron and in the path to the synchrotron additional polarimeters have been constructed. There was no significance for polarization losses there.

Since 2009 data from the routine polarimeter can be collected by controlled transmission of beam from the source to the polarimeter. The beam is dumped behind the polarimeter. This monitoring feature enables the judgment of stability up to the polarimeter. Fig. 4 shows an example for polarized deuterons; the data is collected over a period of 11 days. The current status of the polarized ion source and polarimetry at the injector were described in a contribution to the workshop for Polarized Sources, Targets and Polarimetry at Ferrara, Italy [10].

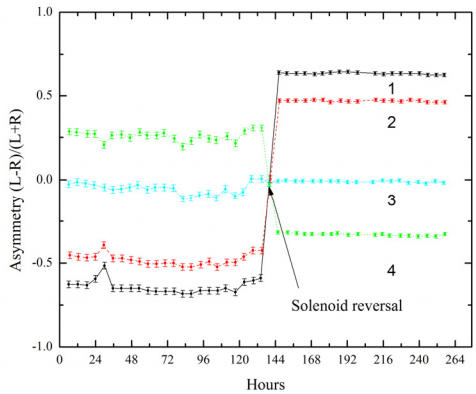

Figure 4: Monitoring the polarized beam behind JULIC. The averages of the measured left-right asymmetries from four different states are plotted.

REFERENCES

[1] R. Maier, Cooler Synchrotron "COSY – performance and perspectives", NIM A 390, (1997) p. 1.
[2] W. Bräutigam et al; "H- operation of the cyclotron JULIC as injector for the cooler synchrotron COSY-Jülich; Proc. of Cyclotrons 1998, Caen, IOP (1999) p. 654.
[3] W. Bräutigam et al.; "Extraction of D- beams from the cyclotron JULIC for injection into the cooler synchrotron COSY". Proc. of Cyclotrons 2001, East Lansing, AIP 600, (2001) 123.
[4] R. Gebel et al.; "Negative ion sources at the injector cyclotron JULIC for the cooler synchrotron COSY". Proc. of Cyclotrons 2004, Tokyo, Particle Accelerator Society of Japan, (2005) p. 287.
[5] http://www.gsi.de/fair.
[6] http://www.fz-juelich.de/ikp/en.
[7] J. Dietrich et al., Status of the 2 MeV Electron Cooler for COSY Jülich, Proc. COOL 2009, Lanzhou, China.
[8] H. Stockhorst et al., Compensation of Mean Energy Loss due to an Internal Target by Application of a Barrier Bucket and Stochastic Momentum Cooling at COSY, Proc. COOL 2009, Lanzhou, China
[9] R. Stassen et al., COSY as ideal Test Facility for HESR RF and stochastic cooling hardware, Proc. PAC09, Vancouver, Canada.
[10] O. Felden, „The COSY/ Jülich Polarized H- and D- Ion Source", PSTP 2009, Ferrara (Italy), 7.9.-11.9.2009.

25 YEARS OF CONTINUOUS OPERATION OF THE SEATTLE CLINICAL CYCLOTRON FACILITY

R. Risler, S. Banerian, J.G. Douglas, R.C. Emery, I. Kalet, G.E. Laramore and D. Reid
University of Washington Medical Center, Seattle, WA 98195-6043, USA.

Abstract

The clinical cyclotron facility at the University of Washington Medical Center has now been in continuous operation for over 25 years. It is highly reliable, and fast neutron therapy remains its primary application, mostly for salivary gland tumors. Neutron therapy accounts for about 85% of the facility use time. In cases where the tumor involves the base of the skull, significant improvements of patient outcome have been achieved by combining the neutron treatment with a Gamma Knife® boost to areas where the neutron dose is limited by adjacent healthy tissue.

Production of 211-At and 117m-Sn with alpha particles at 29.0 and 47.3 MeV and currents between 50 and 70 μA have become routine. These isotopes are used for medical applications presently under development.

The introduction of a new control system using EPICS (Experimental Physics and Industrial Control System) is progressing systematically. All the user interfaces are up and running, and several accelerator subsystems have been migrated to the new controls. No interruption of therapy or isotope production operation is planned for the conversion to the new control system.

INTRODUCTION

The cyclotron facility at the University of Washington Medical Center in Seattle has now been in clinical operation for over 25 years. It is fully integrated in the Radiation Oncology Department, together with four linear accelerators used for standard external beam radiation therapy. Initially it was designed and built to treat tumors with fast neutrons. This remains its primary application. However, the production of certain radioisotopes for medical applications has become an important part of today's operation.

For fast neutron therapy, a 50.5 MeV proton beam is transported from the cyclotron vault into a treatment room with an isocentric gantry with 360 degree rotation capability. Neutrons are produced in a semi-thick beryllium target with copper backing. The neutrons are collimated by a 40-leaf variable collimator to achieve the desired treatment field shape. From the first day of operation in 1984, all the set-up information for patient treatments has been transferred to the neutron therapy system electronically via a network connection from the treatment planning computer, and the set-up has been verified by the control system.

Fast neutron therapy has turned out to be effective for just a few special tumor sites, primarily inoperable salivary gland tumors. Great progress has been achieved in situations where the neutron dose is limited by adjacent structures in the base of skull region by adding a precision photon boost delivered by a Gamma Knife®.

The Scanditronix MC-50 cyclotron is designed for multiple particles and variable energy. Initially, only deuteron operation was envisioned besides the protons, primarily to produce fast neutrons having a different energy spectrum. This was only used rarely. However, as demand for alpha beams emerged, the internal ion source and the central region were optimized to improve the performance for this modality. Isotope production with alpha beams has now become routine.

Over the years many components have been upgraded, in particular power supplies and other electronic parts. A major effort is in progress to replace the original Scanditronix control system based on a PDP11/23 computer and a proprietary I/O system. The new system is based on EPICS and commercially available components. Migration to the new system is being done in stages with both systems controlling part of the facility at this time.

FAST NEUTRON THERAPY

Fast neutron therapy remains a niche therapy, primarily for inoperable salivary gland tumors and sarcomas or after surgical intervention for these tumors, where gross disease is left behind. It remains the treatment of choice for these cases. Apart from the new light ion treatment beams, neutrons are the only high LET (Linear Energy Transfer) radiation available for the clinical treatment of tumors. While the local control rate and survival is excellent for certain patients with good prognostic factors, there are subgroups of patients where success is elusive. In some of these cases the cancer extends to areas where the neutron dose must be kept sub-optimal to protect adjacent anatomical structures. Because of scatter within the patient's tissues, the field edge for neutrons is intrinsically not as sharp as would be desirable. In particular for patients with salivary gland tumors involving the base of the skull, recurrences in this region were frequent. When a Gamma Knife® unit became available to the oncologists, a photon boost was added to the fast neutron treatments to supplement the radiation to the underdosed area. Several years of data are now available. The local/regional control rate for these patients

is shown in figure 1. The outcome for patients with base of skull involvement receiving a Gamma Knife® boost has now become comparable to patients without this complication [1]. This boost is now standard practice for these patients.

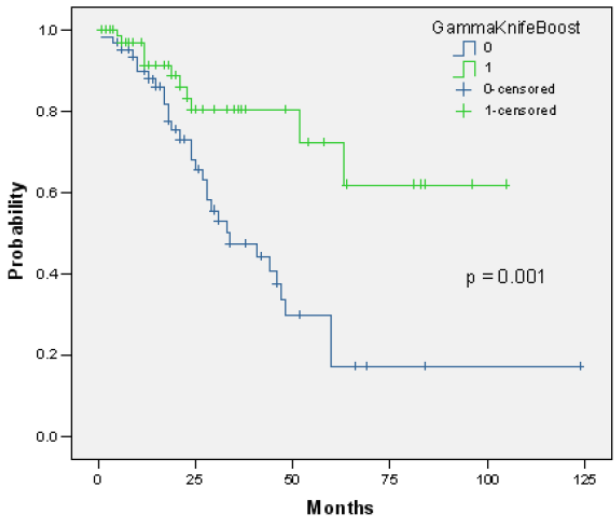

Figure 1: Local/regional tumor control for salivary gland patients with base of skull involvement. The control rate for patients receiving a Gamma Knife boost is compared to patients without a boost.

OPERATIONAL STATISTICS AND EQUIPMENT PERFORMANCE

The cyclotron system and the fast neutron radiation therapy equipment has an excellent history of reliability. Over the past three years only seven patient sessions had to be rescheduled on a subsequent day because of technical problems. Three were caused by an I/O system failure, three because of treatment head problems with mechanically damaged wiring, and one because of the RF system. Fig. 2 shows facility downtime, counted during scheduled therapy days (Tuesday – Friday, 08:00 to 18:00). Downtime events lasting four hours or longer are more serious as patients have to be postponed to a later date. For shorter events patients can frequently wait or be rescheduled later in the day.

During the whole life of the facility there has never been a scheduled downtime period more than an extended weekend (Friday – Monday). These periods were primarily required for mechanical or wiring upgrades and/or repairs of the therapy unit. All support work is being performed by local staff with excellent support from various on-campus shops. Only on one occasion did we request support from the manufacturer for a mechanical problem with the leaf collimator.

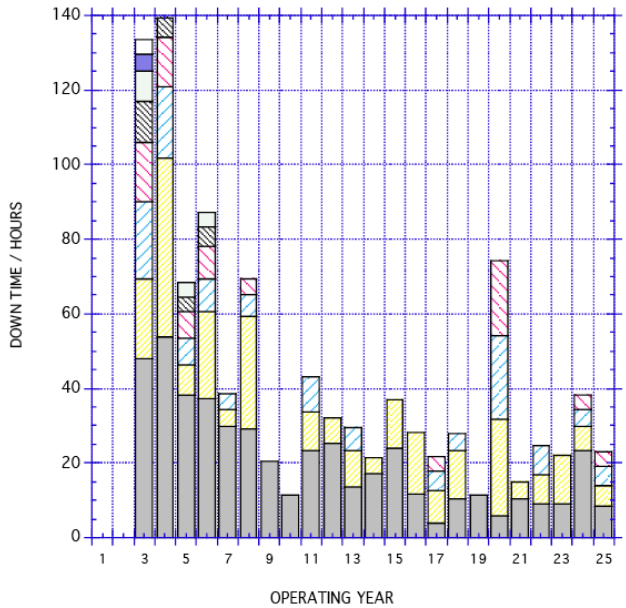

Figure 2: Facility downtime for each operating year. Downtime events lasting four hours or more are shown individually.

ISOTOPE PRODUCTION WITH ALPHA BEAMS

Initially, operation with alpha particles was not part of the program and was added when demand for 211-Astatine emerged. This alpha emitter with 7.2 hour half-life is promising for radio-labeled compounds to target distributed tumors. Several groups at the University of Washington and the Fred Hutchinson Cancer Research Center are involved in these studies [2].

After the addition of a new beam line at the zero degree port of the switching magnet, a dedicated target station for isotope production with alpha beams became available a few years ago. It is designed for solid targets installed at a 10 degree slant. They are retrieved manually after irradiation and an appropriate waiting time. Operation with alpha particles has now become routine with one run per week for 211-At, typically on Monday morning. Presently the produced 211-At is used for animal studies and chemistry development. Typical run times are under one hour. This can easily be expanded when demand rises as is expected for clinical trials. Average current on target is 50 μA at 29 MeV. There is poor transmission, around 65%, between the first Faraday Cup after the machine and the target, because there are no further focusing elements in this line and the beam is broad.

The second isotope produced is 117m-Sn using the 116-Cd(α,3n) reaction. It is produced for Clear Vascular Inc., an outside company. The customer delivers the enriched targets to the facility where they are irradiated and returned for processing. 117m-Sn has 13.6 days half life and is investigated for imaging and potentially treating vulnerable plaque, a type of plaque in the arterial wall that

can produce sudden heart attacks or a stroke [3]. Human clinical trials are presently in progress. This isotope requires typical run times of 8 to 16 hours at the maximum available energy of 47.3 MeV. These runs occur about monthly, on Friday/Saturday, with shipping on Monday after short lived byproducts have decayed. The average beam current for the most recent 20 runs is 70 μA. At the higher energy the transmission from the cup to the target is better, 85%.

The target station is open to the beam line with no vacuum window. While this is convenient for operation, it also creates a potential contamination hazard. The vacuum pumps in this line and at the switching magnet are equipped with activated carbon exhaust filters to catch any undesired air emissions. The filters are monitored after each run and have proven to be very effective, in particular for 211-At. There are additional filters in the exhaust duct from the cyclotron vault.

UPGRADE OF THE CONTROL SYSTEM TO EPICS

The aging PDP11/23 and the Scanditronix I/O system are being replaced. The new system is based on EPICS (Experimental Physics and Industrial Control System, [4]) and has been described previously [5]. At this time, the user interface is fully operational. It is similar to the original Scanditronix interface with two terminal screens at the cyclotron control console, one for interacting with the system and one for display of subsystem information only. There are six tuning module knobs which can be used to control any of about 80 analog parameters. In addition there are some dedicated knobs, pushbuttons and indicator lamps at the cyclotron control console. The necessary utilities for user login, error log files, for stopping and rebooting EPICS I/O controllers, and for storing and retrieving parameter settings are fully functional.

Presently the new system controls the cyclotron magnet subsystem, the ion source subsystem and part of the extraction subsystem. It also monitors all vacuum pump groups. The cyclotron console has temporarily been expanded to accommodate both the old and new control system components. The changeover to the new system is being performed in small steps, a few parameters at a time. The ongoing therapy and isotope production operation cannot be interrupted by this work.

CONCLUSIONS

After 25 years the cyclotron facility is running well and continues its mission to treat cancer patients with fast neutron therapy as one of the few centers worldwide, and to provide beam time in support of other medical applications, specifically production of 211-At and 117m-Sn with alpha particles.

REFERENCES

[1] J. G. Douglas, R. Goodkin and G.E. Laramore, “Gamma knife stereotactic radiosurgery for salivary gland neoplasms with base of skull invasion following neutron radiotherapy”, Head Neck (2008) Apr; 30(4), 492.

[2] S. Wilbur, MK. Chyan, D.K. Hamlin and M.A. Perry, “Preparation and in vivo evaluation of radioiodinated *closo*-decaborate(2-)derivatives to identify structural components that provide low retention in tissues”, Nucl. Med. Biol. 37 (2010), 167.

[3] N.R. Stevenson, “The Production and Applications of High Specific Activity Sn-117m”, CAARI 2010, Fort Worth, August 2010.

[4] http://www.aps.anl.gov/epics/index.php

[5] R. Risler, S. Banerian, R.C. Emery, I. Kalet, G.E. Laramore and D. Reid, “Recent Improvements and Operational Status of the Seattle Clinical Cyclotron Facility”, Cyclotrons and Their Applications, Catania 2007 p. 134.

MAGNETIC FIELD CALCULATION AND MAGNET SHIMMING SIMULATION FOR CYCHU-10 CYCLOTRON

Z. H. Chen*, D. Z. Chen, B. Qin
Huazhong University of Science and Technology, Wuhan 430074, P. R. China

Abstract

The compact internal ion source cyclotron CYCHU-10 developed in Huazhong University of Science and Technology (HUST) is in magnet machining, and will be assembled soon later. The accuracy of the finite element analysis (FEA) prediction of the magnetic field compared to the measurement is an important guarantee for virtual magnet shimming. In this paper, a further study on magnet field computation using FEA is implemented. Both An 1/8 and a 1/4 models are established to make a comparison. Based on the computation, researches on virtual magnet shimming are also carried out. A new shim tool using an improved matrix method combining the multiple linear regressions is employed to simulate the virtual shimming process. With the aid of 3D finite element code and beam dynamics code, an iterative shimming process has been accomplished successfully. The results verify the feasibility and effectiveness of the shimming method.

INTRODUCTION

Commercial cyclotrons are widely applied in medical field, especially for proton therapy and isotopes production in recent years [1]. A compact H- cyclotron with 10MeV extraction energy CYCHU-10 is being developed in HUST, which is designed for short-life isotopes production in PET system. The essential parameters of the cyclotron are exhibited in Table 1. Some details of the model are optimized by iterative computation, and a good isochronism of the magnetic field is observed.

Table 1: Parameters of the cyclotron

Number of pole	4
Extraction energy	10MeV
Extraction radius	27.2cm
RF frequency	100.12MHz
Dee voltage	35KV
Dee angle	40°
Average flux density	1.64Tesla

When machining of the main magnet is completed, measurement of the magnetic field using mapping system will carried out to confirm if it meets the requirement for particle accelerating [2]. According to experience, the initial machining will not reach the goal of a good isochronism, for there exists about ±0.5% difference by TOSCA software comparing to the real magnetic field, so magnet shim work should be put on the agenda [3][4]. Generally, there are mainly two ways to shim the magnetic field: (1) adjust the trim coils; (2) change the shape of the magnet pole. To CYCHU-10, only primary coil is employed to supply excitation, so method (2) will be adopted [5].

*chenzihao576@163.com

CALCULATION OF THE MAGNET

The model of the main magnet of CYCHU-10 cyclotron has been constructed by using pre-processor of TOSCA. To reduce the amount of elements, an 1/8 model was formerly adopted, and periodic symmetric boundary condition is applied on the edge of the magnet pole. Nevertheless, the periodic symmetric boundary condition is actually an approximate dispose in this model, since the magnet yoke of the cyclotron is not strictly periodic symmetrical. What we concerned is whether it will bring unpredictable error to the calculated magnetic flux density ***B***. In fact, we could gain a more accurate field result by using a 1/4 model in theory. So a 1/4 magnet model is created for a comparison. Fig. 1 shows the 1/8 and 1/4 models of the CYCHU-10 with scalar plot of magnetic field, which are meshed by 190,000 and 450,000 quadratic hexahedra elements, respectively.

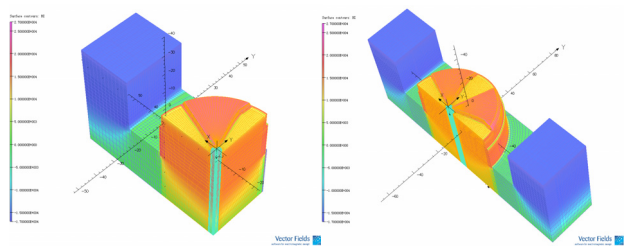

Figure 1: 1/8 and 1/4 models of the main magnet.

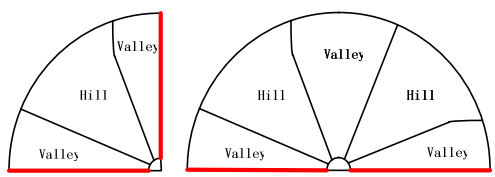

Figure 2: The periodic symmetric edge on two models

The periodic edges on the two models are shown in Fig. 2 decorated with red-thick line. Fig. 3 gives the calculated circular magnetic field difference between 1/8 and 1/4 models at various radiuses. We can obtain that the influence is smaller at the hill of the pole. And the subtraction of the two fields at different radius is about 13 Gauss on average.

Fig. 4 exhibits the isochronous ***B*** in mid plane of the

models, and the difference between the two isochronous magnet fields is about 12 Gauss at most radius, which is a small change compared to the integral average magnetic flux density 1.64T. It indicates that the periodic symmetric condition and mesh grid will not bring enormous influence.

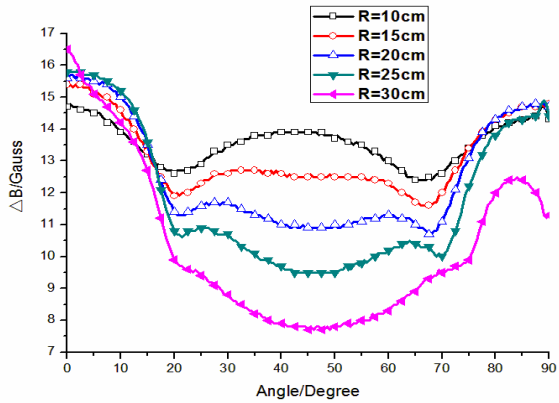

Figure 3: Circumferential △B at various radius

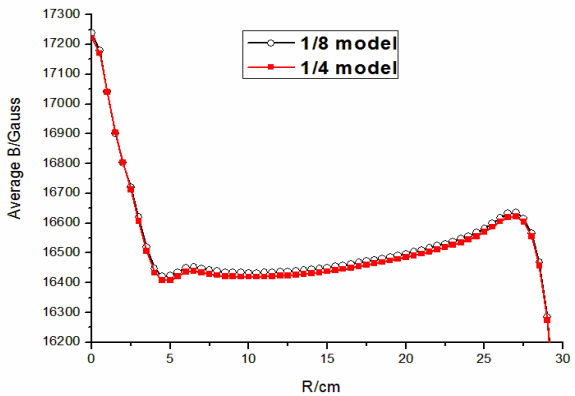

Figure 4: Isochronous magnet field of two models

According to analysis of the calculation result, we finally summarize that the magnet field difference between the two models is about 0.08% which means the frequency error is less than 0.1%. In consideration of the calculation error of TOSCA software, this will not arouse a large influence to accuracy of magnetic flux density ***B*** and beam dynamics simulation result. So the virtual shim work on the 1/8 magnet model is reliable.

MAGNET SHIMMING SIMULATION

When the initial machining of the magnet is completed, magnetic field should be measured for estimating its deviation from isochronal field. The task is to minimize the deviation of the field by magnet shimming.

Cutting strategy is adopted as the magnet shimming method for CYCHU-10. In general, our magnet shimming is an iterative process containing two main steps: (1) to qualify the isochronous field error; (2) to predict the magnet pole shape modification according to the calculated field error in the first step [6]. We plan to employ a matrix method with nonlinear radial fringe field effect, which is based on multiple linear regressions to predict cutting quantity. A shim tool code based on MATLAB has been developed. Commonly, the shim tool will provide cutting quantity at each radius and TOSCA COMI files when we input the local phase slip of particle which is calculated by beam dynamic calculation software CYCLOP. With the aid of shim tool, the general procedure of magnet shim work is shown in Fig. 5.

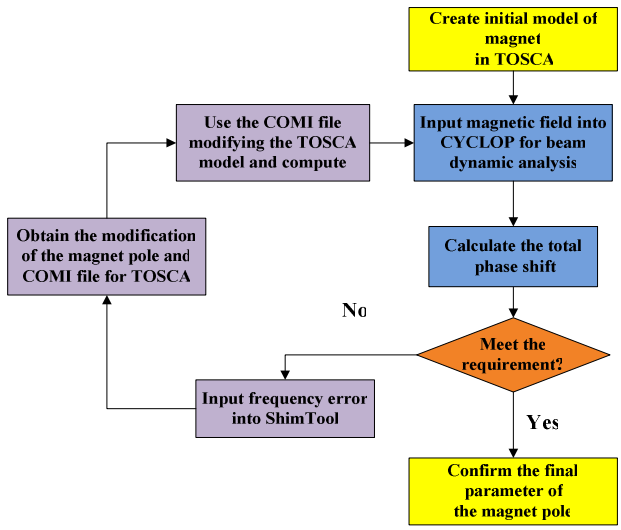

Figure 5: General procedure of magnet shimming

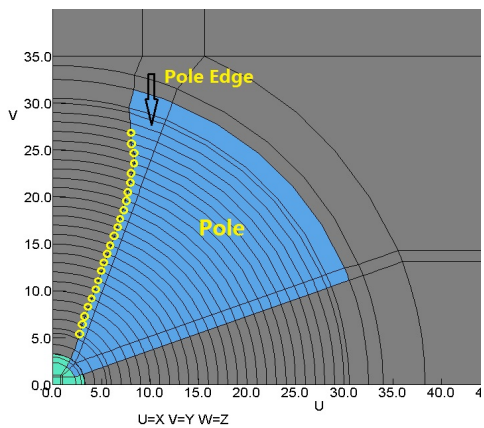

Figure 6: The cutting pole edge of the model

A virtual shim process is simulated on the 1/4 model. Firstly, an initial model with some allowance on the pole edge is established. As shown in Fig. 6, we leave some alterable key points distributed at different radiuses from 6cm to 28cm on the pole edge (marked by circles). The model will be modified when coordinates of these points are transformed. Then it will lead to changes to the average magnetic field at various radius. When the moderate RF frequency is set, we make the average magnetic field a bit higher than ideal isochronous magnet field by leaving a margin on the pole edge, so cutting strategy must be taken to lessen the error between our actual field and ideal field. The shim tool will automatically give the quantity should be cut.

Generally in engineer, a conservative strategy will be employed, for once an excessive quantity is cut, there is no compensational measure. So a cutting factor is also introduced in shim tool. By multiplying a cutting factor no more than 1.0, the cutting amount will be under control. Here are the experimental results of the magnet shim on computational models shown in Fig. 7-9.

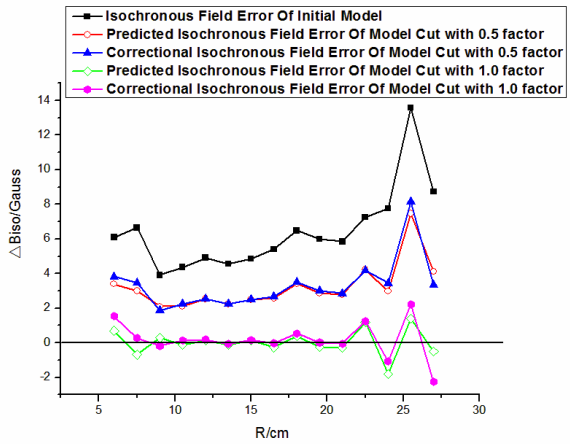

Figure 7: Isochronous field error of iterative models

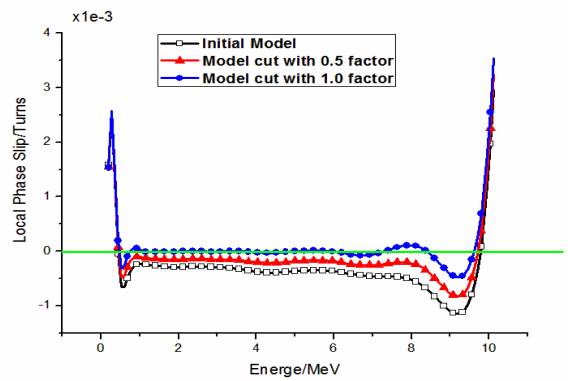

Figure 8: Local phase slip of iterative models

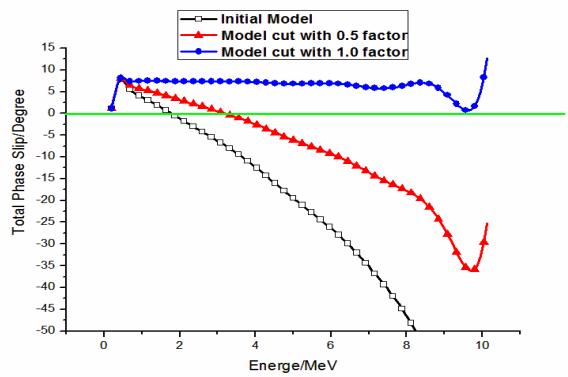

Figure 9: Total phase slip of iterative models

We cut the pole edge of initial model by shim tool separately with 0.5 and 1.0 cutting factor. Fig. 7 gives the isochronous field error of initial model, the predicted isochronous field error and the correctional isochronous field error after shimmed with cutting factors. Obviously, by modifying magnet model, the isochronous field error has decreased, when the 1.0 cutting factor is adopted, the deviation of correctional field from ideal field is minimized nearly to zero Gauss, this means good a isochronism have reached.

The change of field will definitely improve the phase slip of particles. Fig. 8, 9 respectively exhibit the local phase slip and the total phase slip of the three models. It's clear that the local phase slip decreased with the increase of the cutting factor. And we find that the total phase slip of initial model has exceeded 50 degree when the energy comes to 8 MeV, particles will drop into decelerating zone rapidly. By cutting the pole edge, this situation has been changed. The total phase slip is under control after shimming work. After cutting with 1.0 factor, it finally don't exceed 10 degree in the whole accelerating procedure which shows a good shimming result.

Anyhow, those studies above are based on the computational magnetic field. When it comes to practical engineering, measured magnetic field will be used for magnet shimming instead.

CONCLUSION

By implementing a comparative magnetic field calculation, we finally eliminate some unpredictable factors in models, which will be beneficial to our magnet shim work. A shimming scheme using a shim tool has been verified, the result proved its feasibility and reliability, and this method will be employed in practical shim work later on.

REFERENCES

[1] Y. Jongen. Review of Compact Commercial Accelerator Products and Applications. Proceedings of the IEEE Particle Accelerator Conference 1997, Vancouver, B.C., Canada, May 1997, pp, 3770-3774.

[2] J. Yang et al. "Magnetic Field Measurement system for CYCHU-10", these proceedings.

[3] C. Baumgarten, et al., Nucl. Instr, and Meth.A 570 (2007) 10.

[4] OPERA-3D User Guide, Vector Fields Limited, England.

[5] B. Qin, et al., Main magnet and central region design for a 10 MeV PET cyclotron CYCHU-10. PAC09, Vancouver, BC, Canada.

[6] B. Qin, et al., An improved matrix method for magnet shimming in compact cyclotrons. Nucl. Instr. And Meth. A (2010), doi:10.1016/j. nima. 2010.03.135.

ACTIVATION OF A 250 MEV SC-CYCLOTRON FOR PROTON THERAPY

G. Steen, B. Amrein, N. Frey, P. Frey, D. Kiselev, M. Kostezer,
R. Lüscher, D. Mohr, O. Morath, A. Schmidt, M. Wohlmuther, J.M. Schippers
Paul Scherrer Institut, Villigen, Switzerland

Abstract

Beam losses in dedicated 230-250 MeV cyclotrons for proton therapy cause radioactivity in machine parts. A systematic study has been performed of the activation of PSI's 250 MeV SC-cyclotron for proton therapy. Since the start of the cyclotron operation dose rate measurements have been made as a function of time at several locations in and around the cyclotron. Gamma ray spectra have been measured of selected iron inserts in the pole and of copper disks in the liner of the RF system. The isotopic composition of the activation has been derived and compared with activations calculated with Monte Carlo calculations (MCNPX). The data and beam history of the cyclotron allow predictions of the dose rate during service activities shortly after beam interruption as well as after a specified period of operation.

INTRODUCTION

Dedicated Cyclotrons of 230-250 MeV have been used at proton therapy facilities since ~12 years [1]. Beam losses during the acceleration and extraction cause build up of radioactivity in the cyclotron, having consequences for accessibility, service and decommissioning. At the Center of Proton Therapy at PSI a dedicated 250 MeV SC-cyclotron [2,3] is in operation since 2007. Although the cyclotron is compact, the design has been optimized to achieve an extraction efficiency of 80%, which is achieved routinely at PSI.

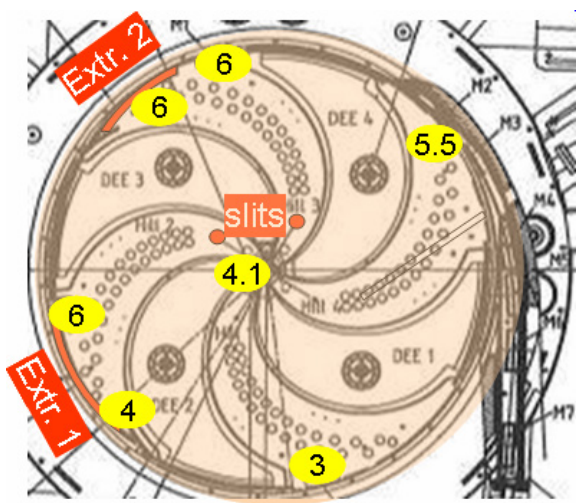

Figure 1: Dose rates (mSv/h) at different locations in the cyclotron, 10 cm from the surfaces, measured in 2010. The two phase slits and the two electrostatic extraction channels are indicated. The beam direction is clock wise.

The 20% beam loss at extraction will result in activation of the cyclotron. The other source of activation is the set of phase slits at 20 cm radius. Depending on the beam emittance from the source, 20-80% of the 11 MeV protons are intercepted by these slits. The here created neutrons and scattered protons thus also cause activation. The (tungsten) slits themselves (~6 mSv/h at 10 cm, 1 h after beam stop) can be retracted into the pole and therefore hardly contribute to the dose to the service staff. In order to estimate the activity and dose rates during future service tasks and at decommissioning of the cyclotron after many years of operation, a systematic study is going on since the first beam has been extracted.

METHODS AND MATERIALS

At every service activity that needs opening of the cyclotron, the dose rate is measured routinely with a standard dosimeter at several locations in the cyclotron, see fig.1. The measurements are performed at 10 cm distance from the surfaces and, as an indication for the dose to service staff, in between the pole caps in their open position.

At three occasions, dose rates at several locations have been measured as a function of time during 48 hours after beam switch off, using Genitron GammaTRACERs. The first time was in 2006 during the commissioning phase of the cyclotron, just after an acceptance test at which a beam with an intensity of 500 nA was extracted during 1 hour. The integral of all extracted beam until the moment of the measurement was only 2 μAh. The other two measurements have been done at service weekends, scheduled since the start of the patient treatment program. In 2010 an isotopic analysis has been made of the activation produced in iron inserts in the pole and in copper disks in the liner covering the pole. Gamma spectra from these samples have been measured in a calibrated HPGe setup at the Radiation Safety and Security Department at PSI. The spectra have been analysed automatically, yielding absolute activities of the gamma-ray emitting isotopes in each sample, at the reference moment in time: 1 hour after switching the beam off. The sample locations have been selected at different proton energies (radii).

A Monte Carlo calculation has been made with MCNPX 2.5.0 [4] to calculate the activity of created isotopes. A very simple model was used: 1 m^3 of iron or copper was hit by 10^6 protons of 50, 100 and 200 MeV or 10^6 neutrons of 6, 10, 50,100 and 200 MeV. The data generated by MCNPX have been processed with CINDER'90 [5,6] to obtain the activation at different moments in time, assuming a certain beam history.

RESULTS AND DISCUSSION

Dose Rate inside the Cyclotron

Figure 1 shows the top view of the lower cyclotron pole with the dose rates measured 50 minutes after stopping the beam in August 2010. The beam integral at that moment was 805 µAh. The dose rate at the exit of extraction channel Extr1 is higher than at the entrance. Also the dose rates at Extr2 and at the entrance of the channel through the SC-coil are relatively high (6 mSv/h), although beam measurements with foil burns have clearly shown that no beam is lost at these locations and that the beam leaves Extr1 without touching the septum or cathode. Therefore these dose rates must be caused by scattered protons and neutrons created in the first septum. These are forward peaked and will cause activation downstream. The relatively low dose rate of 3 mSv/h at 45° in front of Extr1 supports this assumption.

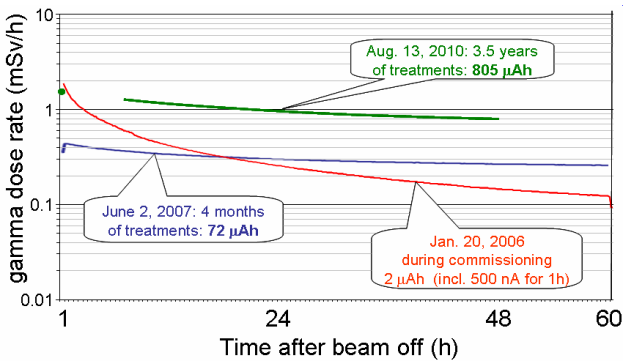

Figure 2: Dose rate in between the pole caps, after switching the beam off.

The measured dose rates in between the open pole caps as a function of time, are shown in figure 2. Contrary to the rather constant dose rates measured in 2007 and 2010, the measurement during the cyclotron commissioning in 2006 shows a strong contribution of isotopes with a short half life. This is due to both the low activity accumulated during the preceding beam history (2 µAh) and to the high extracted beam intensity during one hour just before opening the cyclotron. In normal operation, however, the beam intensity averaged over the day is 20-40 nA, yielding much lower contributions of short living isotopes.

Observed Isotopes in Iron and Copper

The distribution of measured gamma emitting isotopes 1 h after beam switch off, is shown in figure 3. Apart from the strong Cu^{64} and Cu^{61} contributions, the distribution of the isotope types is broader in copper than in iron. In iron the $Mn^{52,54,56}$ isotopes dominate the distribution. The total specific dose rate at 10 cm, calculated from the specific activities, is larger from copper (180 nSv/h.g) than for iron (74 nSv/h.g). In copper more than 90% of the dose rate is due to the decay of Cu^{64} (~70%) and Cu^{61} (~20%), with half life of 12 h and 3.4 h respectively. Most of the isotopes in iron and copper have a half life time of less than 100 days. Exceptions are Mn^{54} (312 d) in iron, Zn^{65} (243 d) in copper and Co^{60} (5 y) in both iron and copper. All isotopes show an increase of specific activity with the radial location of the sample. This correlates with the higher beam density and the higher energy of the protons and eventually created neutrons at large radius.

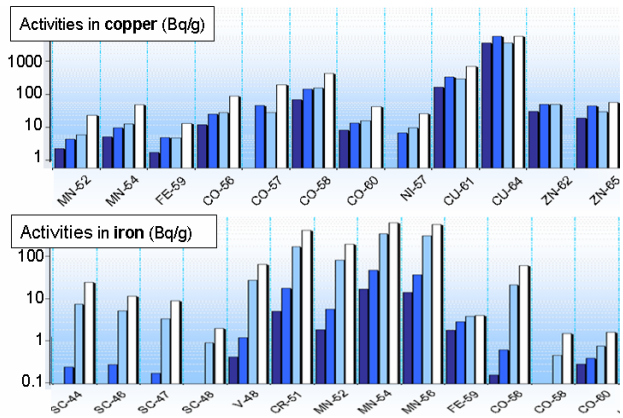

Figure 3: Measured specific activities of the most important isotopes in copper (top) and iron (bottom). The different bars at each isotope reflect the sample locations in the cyclotron: the brighter the line colour, the larger the radius of the location in the cyclotron.

Calculation of the Activation of Iron and Copper

From the MCNPX calculations with protons or neutrons at the different energies, the amount of the isotopes created in copper and in iron has been calculated. From these results the relative activity per isotope has been calculated at the reference moment. The calculations also yield isotopes that do not emit (measurable) gamma rays. The obtained distributions (fig. 4) look very similar to the measured data in figure 3.

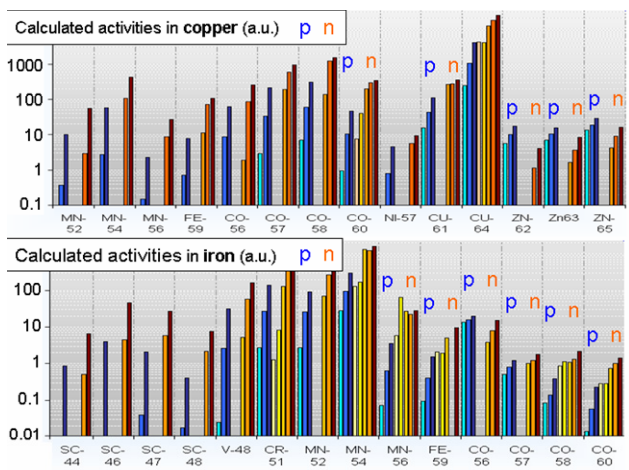

Figure 4: Calculated specific activities (a.u.) of the most important isotopes in copper (top) and iron (bottom). The colours of the different bars at each isotope reflect the incident particle (blue: p, red: n). Darker colours indicate higher energy.

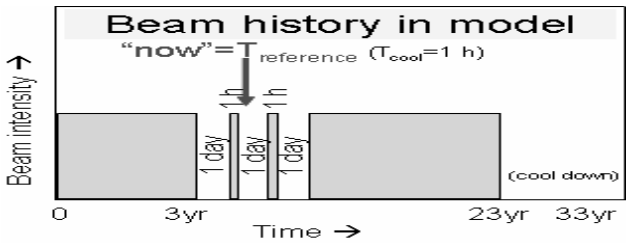

Figure 5: Beam intensity as a function of time, as used in the calculations of the activity.

In fig. 4 it can be seen that in most cases the activities created by protons are less than those created by neutrons. In general a larger specific activity is observed when higher energies (p or n) are used, which is consistent with the experimental observations.

ANALYSIS

Estimation of Future Activation

Despite the very coarse model and the lack of any energy spectrum usage, the close resemblance between the calculations and the measurements allows a normalization of the calculated distribution to the measured distribution. Separate scale factors have been calculated for iron and copper, each defined as the ratio between the integral of the calculated activity distribution and the integral of the measured activity distribution.

The thus obtained factors will also be used to scale the calculated distributions at later moments in time, given the assumed history of beam usage shown in figure 5. Figure 6 shows the remaining activity after a running period of 23 years with a continuously extracted 250 μAh per year, followed by a cool down time of 1, 10 and 100 years. The specific activity in copper is higher than that in iron. Fortunately the volume of the copper parts is smaller and easier to process than the big iron pole pieces.

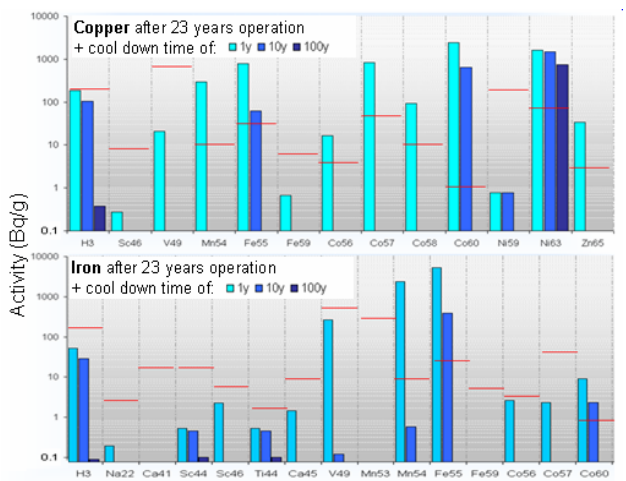

Figure 6: Calculated specific activities of the isotopes in copper (top) and iron (bottom) after 23 years of continuous operation, followed by a cool down time of 1, 10 and 100 years. The horizontal lines indicate the legal limits for non radio-active disposal.

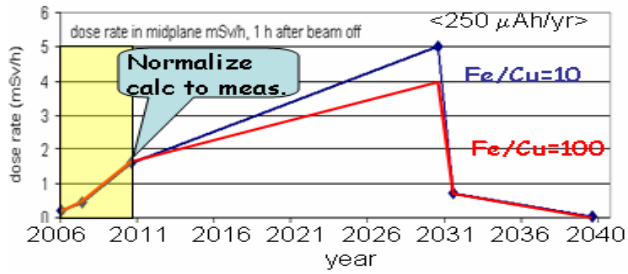

Figure 7: Estimated dose rate in the mid plane between open pole caps, based on the 2010 measurements and scaled calculated dose rates, assuming 250 μAh/y.

Scaled to the 2010 measurement of the dose rate at the mid plane between the poles (fig. 2), the calculated dose rates from iron and copper have been extrapolated into the future. In figure 7 the results are shown. Since the contribution to the total dose rate of iron with respect to the one of copper is not yet known, curves with different contribution (weight) ratios are shown. The total dose rate is estimated to rise from 1.5 mSv/h in 2010 to 4-5 mSv/h in 2030. Of course a more intensive beam usage will increase this value.

CONCLUSIONS

After 3 years of patient treatments the typical dose rate close to the pole has grown to 3-4 mSv/h, with local hot spots of 6 mSv/h. Already after a few months of daily patient treatments, the dose rate at the mid plane of the opened cyclotron is hardly decreasing shortly after beam off. Therefore waiting times until a few days will not help to limit the dose to the staff. The calculations and the measurements show that the activation increases with the radius in the cyclotron and that it is mainly due to activation by neutrons. A shift of the slits more into the cyclotron centre is expected to reduce the rise in dose rate. The calculation model, although very crude, indicates good qualitative agreement with the measurements of the isotopic content of the iron and the copper. By scaling the calculations to the measurement results, a prediction can be been made of the isotopic content, activity and dose rate at any moment in the future; a method that could be employed at other cyclotrons as well.

REFERENCES

[1] J.M. Schippers, Rev. Acc. Science and Techn., vol II (2009) 179-200
[2] M. Schillo et al., Proc. 16th Int Conf. Cycl. Appl., 2001, pp. 37–39
[3] J.M. Schippers et al., Nucl. Instr. and Meth. B 261 (2007) 773-776
[4] D.B. Pelowitz, ed., MCNPX Users Manual, Version 2.5.0, LA-CP-05-0369, Los Alamos, (2005).
[5] W.B. Wilson et al., Proc. GLOBAL'95, Versailles, France (1995).
[6] F.X Gallmeier et al, Proc. of AccApp'07, Pocatello Id, USA (2007).

STATUS OF THE HZB# CYCLOTRON: EYE TUMOUR THERAPY IN BERLIN

A. Denker*, C. Rethfeldt, J. Röhrich, Helmholtz-Zentrum Berlin, Germany
D. Cordini, J. Heufelder, R. Stark, A. Weber, BerlinProtonen am Helmholtz-Zentrum Berlin

Abstract

The mission of the ion beam laboratory (Ionenstrahllabor) ISL was the provision of fast ions for solid state physics, materials analysis and medical applications in basic as well as applied research. Eye tumours are treated since 1998 with 68 MeV protons in collaboration with the University Hospital Benjamin Franklin, now Charité - Campus Benjamin Franklin. In autumn 2004 the board of directors of the HMI decided to close down ISL at the end of 2006. In December 2006, a cooperation contract between the Charité and the HMI was signed to assure the continuity of the eye tumour therapy, at this moment being the only facility in Germany.

We have now experienced the first three years under the new boundary conditions; treating more than 600 patients in that time. The main challenge is to supply protons for the therapy with less man-power but keeping the same high reliability as before. The conversion process is not yet finished. The installation and commissioning of a new, facile injector for protons will be discussed. In addition to the routine treatment, proton therapy of ocular tumours for very young children under general anaesthesia was performed.

ACCELERATOR OPERATION

Since 2007, the cyclotron was operated for the most part for medical purpose. Hence, the scheduled beam time hours decreased tremendously (fig. 1). The new financial boundary conditions lead to a reduction of the man-power for accelerator operation to a third of the original crew. Hence, the accelerator operation was changed from a three-shift to a two-shift mode. Over night the machine idles, monitored by new control programmes.

Nevertheless, operation continued smoothly. The reliability of the machine was kept at a high level: Beam time losses due to break-downs were between 2% and 5%. Due to the small number of scheduled beam time hours, single major breakdowns have huge impacts on the beam statistics. An example is an internal water leak in the RF system of the cyclotron, leading, for the first time since 1998, to an interruption of the therapy week. In 2008, one fifth of the unscheduled down time was caused by failures in the electric power supply of the laboratory. Some of these failures lasted for almost 1 sec. Beam tests were performed for the change from the three-shift to two-shift mode in order to test the monitoring control programs. Further tests were made for the commissioning of the tandetron (see below).

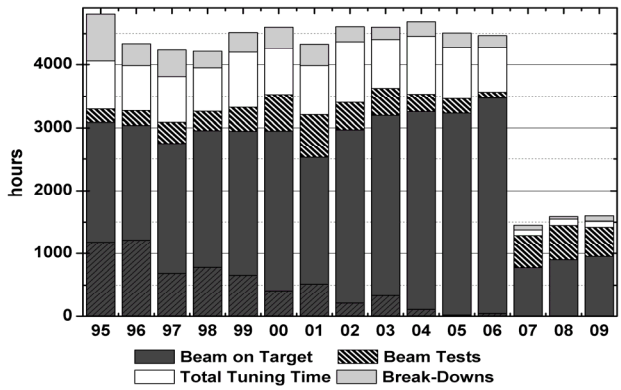

Figure 1: Operation statistics of ISL (1995-2006) and the HZB cyclotron (since 2007)

EXPERIMENTS

The increase of beam time as shown in fig. 1 in the past two years is due to an increasing patient number. In addition, a small number of experiments were carried out. These experiments comprised radiation hardness tests for the Deutsches Zentrum für Luft- und Raumfahrt as well as detector tests and dosimetry.

In addition, a new way to correlate the axis of the proton beam to the x-ray positioning system was developed: The patient positioning is performed with the aid of tantalum tumour position markers observed by two, orthogonal X-ray systems. Usually one X-ray system is mounted in the axial direction, anti parallel to the proton beam, creating an inverse beams eye view. For patient positioning it is important that the axes of the proton beam as well as the axial X-ray system are identical. With a CCD system [1] consisting of a scintillating foil, a mirror, and a CCD camera, the two dimensional dose distributions can be measured and analysed with high precision in a very fast way. The CCD system is mounted on the patient chair thus allowing the checking of position and direction of the proton beam. A 0.2 mm tantalum cross-hair is mounted in front of the CCD camera. By moving the patient chair both cross-hair and CCD camera are moved. The chair is brought into a position where the centre of the mounted cross-hair superimposes the centre of the beam-line's cross-hair, as observed by the axial X-ray system. Thus the centre of the mounted cross-hair lies on the central axis of the axial X-ray system. In this position the dose distribution is measured by the CCD camera. The tantalum cross-hair in front of the CCD can be seen clearly in the resulting CCD image.

* denker@helmholtz-berlin.de
[#] The Helmholtz-Zentrum Berlin für Materialien und Energie has been formed by the merger of the Hahn-Meitner-Institut Berlin (HMI) and the Berliner Elektronenspeicherring-Gesellschaft für Synchrotronstrahlung

Its centre can be evaluated, thus transferring the centre of the X-ray system to the CCD. The cross-hair is removed and the dose distribution is measured anew, enabling the determination of the centre of the proton beam. From the two CCD images differences between the two centres can be calculated.

With this method it is possible to ascertain the differences between the X-ray axis and the proton axis with an accuracy of up to 0.1 mm. The whole procedure takes less than 10 minutes. The former method – looking for the field centre with two one-dimensional high resolution diode scans, positioning the diode in the field centre and checking the centre with the axial X-ray system – required nearly one hour.

INSTALLATION OF A TANDETRON

The injector for light ions, the Van-de-Graaff, provided steadily over more than 30 years a wide variety of ion species over a broad energy range. Although the 5 Ghz ECR-source itself runs very reliable, the position of the source on the high-voltage terminal including a RF bunching system, the moving belt, and the elaborated fast high-voltage regulation system require careful maintenance. In order to reduce the required manpower, a 2 MV tandetron accelerator was bought from the Bundesanstalt für Materialforschung und -prüfung (Federal Institute for Materials Research and Testing). It was dismantled and transported to the cyclotron vault. The installation took place on the position of the former heavy ion injector, the RFQ. Thus, the installation of the tandetron could be executed without interruptions of the therapy schedule. This position will reduce the length of the injection line by more than 20 m. The beam emittance of the RFQ and the tandetron are different, the latter having larger beam spot and emittance [2,3]. Furthermore, the size of the tandetron made it impossible to maintain the focus on the same position in the beam line, requiring a different focusing into the beam line to the cyclotron.

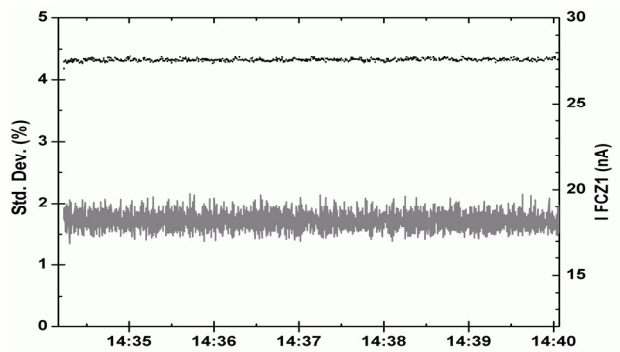

Figure 2: Short term beam stability (grey line) and beam intensity (black line) of the proton beam from the tandetron-cyclotron combination

Fig. 2 shows the extracted beam of the cyclotron using the tandetron as injector with the typical intensity used for therapy. The beam was scanned with 10 kHz and the update rate was about 10 Hz. The short-term stability is excellent; the beam changes only for 2 %. Slow variations over longer times, e.g. several hours, are in the order of 5 %.

When comparing the proton beam delivered either by the Van-de-Graaff-cyclotron or the tandetron-cyclotron combination, they are similar: Differences in the dose distribution are negligible (fig. 3).

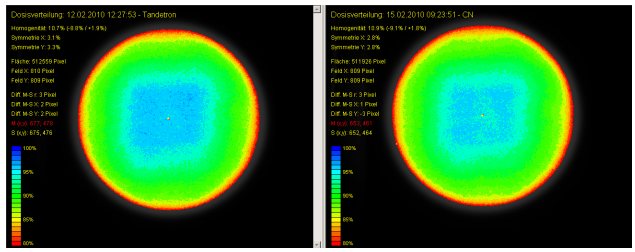

Figure 3: Dose distribution at the therapy station measured for both injectors: Van-de-Graaff (right) and tandetron (left)

The single Bragg peak of the 68 MeV proton beam was determined for both injectors, and they are identical. Due to the acceptance of the cyclotron, small changes on the tandetron voltage will not affect the energy, i.e. the range, of the extracted beam. The distal fall off from 90 % of the dose to 10 % of the dose is in both cases 0.95 mm. This sharp distal fall off provides best possibilities to spare healthy tissue.

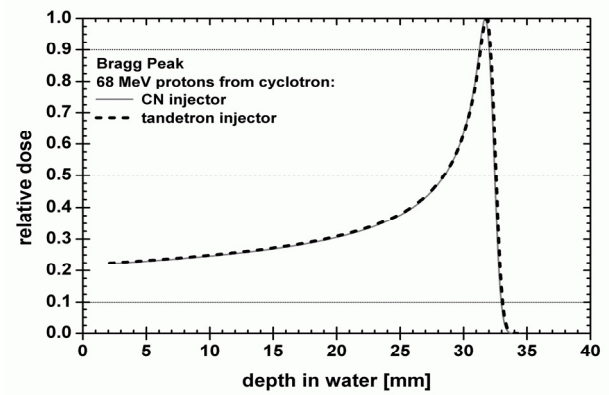

Figure 4: Bragg peak at the therapy station determined for both injectors: Van-de-Graaff (solid grey) and tandetron (dashed black)

INDICATIONS, DEVELOPMENT OF PATIENT NUMBERS AND SPECIAL CASES

In 2007, eleven therapy weeks were scheduled: Quality assurance is performed on Monday, whereas the patients receive their irradiation in four fractions of about 40 s from Tuesday to Friday. The number of patients rose to more than 210 per year (fig. 5). Hence, the number of therapy weeks was increased to twelve. More than 90% of the indications are choroidal melanomas. The case-subgroup of large uveal melanomas increased, mostly followed by surgical removal (endoresection or

transscleral resection) of the inactivated tumour mass to prevent toxic reactions.

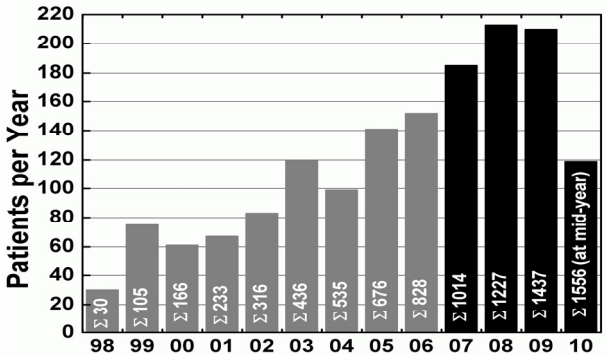

Figure 5: Patient figures treated per years (bars) and in total (white numbers).

In the treatment of ocular melanomas, the cooperation of the patient is absolutely necessary. As small children are unable to cooperate in the appropriate way; they must be treated under general anaesthesia. The treatment room was equipped with a mobile anaesthesia workstation. Car seats, for different body sizes, were modified to fit to the treatment chair.

The anaesthesia procedure has to take place in the treatment room on a separate couch for anaesthesia. The anaesthetised child is transferred into one of the modified car seats. Within the seat the child is still in a lying position, fixed by seat belts. A thermoplastic mask attached to the car seat immobilizes the head. The car seat with the child is then mounted at the treatment chair and moved into a nearly sitting position. In treatment position the eyelids are kept out of the irradiation field by lid retractors. A suction cup is attached to the cornea to adjust the gazing angle of the eye for treatment (see fig. 6). After verification of the localization the irradiation takes place. The position of the eye and the vital signs are continuously monitored in the treatment and in the control room. Following irradiation the child is transferred to the couch for recovery from anaesthesia. As soon as the child can breathe by itself and has protective reflexes, it is transported to a recovery room for observation until an ambulance carries the patient back to the eye hospital.
Prior to the treatment course a simulation session with the child under general anaesthesia is necessary to fit the immobilization mask and test the feasibility of the treatment plan. The treatment procedure itself takes about two hours: one hour for anaesthesia and positioning, one minute irradiation, few minutes dismounting and roughly 45 minutes for recovery from anaesthesia. Simulating an emergency situation showed that the child can be dismounted in less than a minute, giving full access of the anaesthesiologist to the child for emergency procedures.

With this set-up we treated three children (10 months, 5 years, and 7 months). Treatment was tolerated well. With the frontal irradiation approach we can use the benefits of a dedicated eye beam line: sharp lateral penumbra and sharp distal fall-off, enabling us to spare the bones of the skull completely.

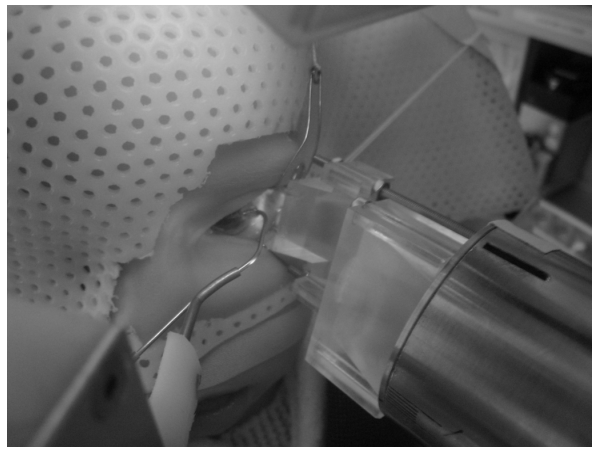

Figure 6: One of the children in treatment position. The proton beam arrives from the lower right. A suction cup fixes the eye in the desired position.

SUMMARY

This activity is based upon more than 10 years of accelerator development and common R&D of the accelerator scientists and the Eye Clinic of the Benjamin Franklin University Hospital within the Charité. The joined effort created Germany's only facility for this kind of therapy. In spite of major structural changes we could keep a high quality standard and even increased the number of treated patients. Proton therapy of ocular tumours for complicated cases like very young children under general anaesthesia is feasible on a horizontal eye beam line.

We have now experienced the first three years under the new boundary conditions; treating more than 600 patients in that time. The conversion process from a multi-purpose, multi-ion machine to a single ion, single energy accelerator is not yet terminated. Nevertheless, the accelerator operation went quite smoothly. A tandetron was installed as new injector and the beam tests were successful. As the beam tests of the tandetron-cyclotron combination have been successful, we now apply for the permit to use it for patient treatment.

We will continue to provide unique therapeutic possibilities for the patients in Germany.

ACLNOWLEDGEMENTS

The authors wish to thank the accelerator crew for their endeavours and endurance.

REFERENCES

[1] S.N. Boon, P. van Luij, T. Bohringer T, et al. Med Phys, 2000 (27) 2198-208
[2] O. Engels, et al., Proc. of the 1999 Particle Accelerator Conference, Eds.: A. Luccio, W. MAcKay, Piscataway, NJ, USA: IEEE, (1999) p.3519-21 vol.5
[3] V. Gressier, private communication

PRESENT STATUS OF THE RCNP CYCLOTRON FACILITY

K. Hatanaka*, M. Fukuda, M. Kibayashi, S. Morinobu, K, Nagayama, T. Saito, H. Tamura, T. Yorita,
RCNP, Osaka University, 10-1 Mihogaoka, Ibaraki, 567-0047 Osaka, Japan

Abstract

The Research Center for Nuclear Physics (RCNP) cyclotron cascade system has been operated to provide high quality beams for various experiments in nuclear and fundamental physics and applications. In order to increase the research opportunities, the Azimuthally Varying Field (AVF) cyclotron facility was upgraded recently. A flat-topping system and an 18-GHz superconducting Electron Cyclotron Resonance (ECR) ion source were introduced to improve the beam's quality and intensity. A new beam line was installed to diagnose the characteristics of the beam to be injected into the ring cyclotron and to bypass the ring cyclotron and directly transport low energy beams from the AVF cyclotron to experimental halls. A separator is equipped to provide RI beams produced by fusion reactions at low energy and by projectile fragmentations at high energy. A muon capture beam line (MUSIC) was constructed in this spring Developments have been continued to increase secondary beams as white neutrons, ultra cold neutrons, muons and unstable nucleri.

INTRODUCTION

The Research Center for Nuclear Physics (RCNP) is a national user's facility founded in 1971 and is the major research institute for nuclear physics in Japan. RCNP, as a national laboratory, is open to all users in Japan and from abroad. The cyclotron facility is its major facility and consists of an accelerator cascade and sophisticated experimental apparatuses. Research programs cover both pure science and applications. Demands for industrial applications have been growing more and more.

A schematic layout of the RCNP cyclotron facility is shown in Fig. 1. The accelerator cascade consists of an injector Azimuthally Varying Field (AVF) cyclotron (K=140) and a ring cyclotron (K=400). It provides ultra-high-quality beams and moderately high-intensity beams for a wide range of research in nuclear physics, fundamental physics, applications, and interdisciplinary fields. The maximum energy of protons and heavy ions are 400 and 100 MeV/u, respectively. Sophisticated experimental apparatuses are equiped like a pair spectrometer, a neutron time-of-flight facility with a 100-m-long tunnel, a radioactive nuclei separator, a super-thermal ultra cold neutron (UCN) source, a white neutron source, and a RI production system for nuclear chemistry. A pion capture beam line was installed to provide muons. Such ultra-high-resolution measurements as $\Delta E/E=5x10^{-5}$ are routinely performed with the Grand-Raiden spectrometer by utilizing the dispersion matching technique. The UCN density was observed to be 19 UCN/cc at the experimental port at a beam power of 400 W. The white neutron spectrum was calibrated and the flux was estimated to be 70 % of that obtained at Los Alamos Neutron Science Center (LANSCE) in the USA. Neutrons are used for the radiation effect studies on integrated circuits and so on.

*hatanaka@rcnp.osaka-u.ac.jp

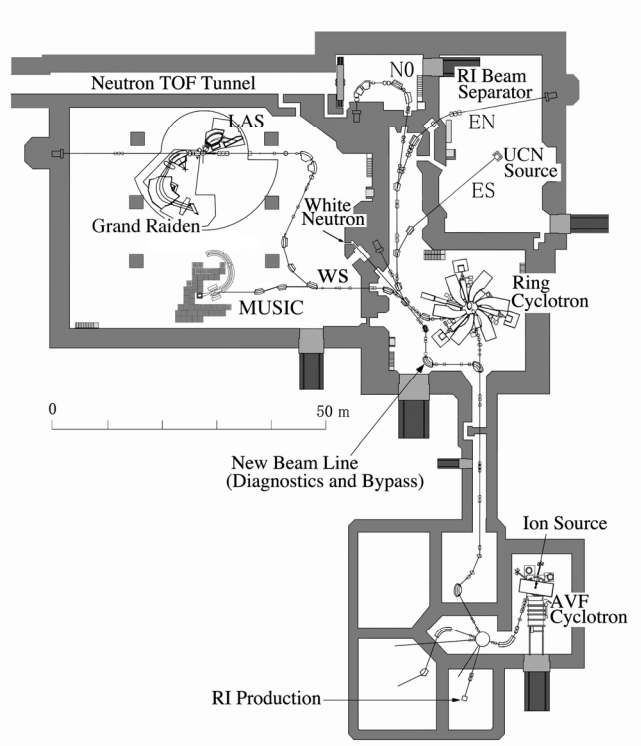

Figure 1: Layout of the RCNP cyclotron facility.

ACCELERATOR DEVEPOLMENTS

User's demands on the beam characteristics are expanding rapidly: ultra-high resolution, high intensity, a variety of heavy ions. Since there are no slits or collimators in the beam lines downstream of the ring cyclotron, the beam quality on targets is determined by the characteristics of the injected beam. The AVF upgrade program for these items is in progress [1-3]: Some of them are presented in these proceedings [4,5].

ECR Ion Source

An 18-GHz superconducting ECR ion source was installed in order to increase beam currents and to extend the variety of ions, especially for highly-charged heavy ions, which can be accelerated by RCNP cyclotrons. The production development of several ions beams and their acceleration by the AVF cyclotron has been performed since 2006.

Figure 2 shows a cross sectional view of the source. The source was designed based on RAMSES [6] at RIKEN, but the inner diameter of the hexapole magnet and of the plasma chamber were extended to 90 and 80 mm, respectively, based on the experience during their developments. The mirror magnetic field is produced with four liquid-helium-free superconducting coils, which are cooled by two Gifford-McMahon refrigerators and which are installed in a cryostat chamber covered by iron magnetic shields. Upstream coil 1 (U1) and downstream coil (D) are of the same size and are excited in series by using a common power supply. Central coil (C) and upstream coil 2 (U2) are excited by using independent power supplies, and the mirror magnetic field distribution is controlled quite flexibly. Typical operating currents are 36.3 A, 36.9 A, and 60.5 A for the U1+D, C, and U2 coils, respectively. The maximum current for each coil is 66 A. The permanent magnet hexapole is of the Halbach type, with 24 pieces of NEOMAX-44H material. The radial field strength is 1.0 T on the stainless-steel plasma chamber's inner diameter. The diameter and the length of the plasma chamber are 80 mm and 380 mm, respectively.

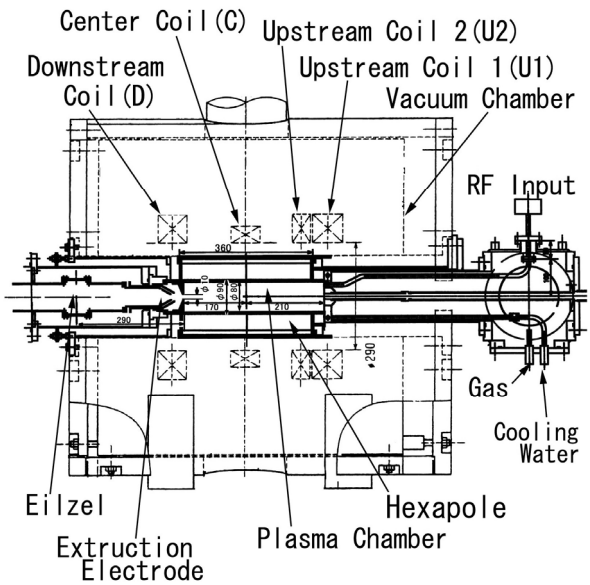

Figure 2: Cross-sectional view of a liquid-helium free18-GHz superconducting ECR ion source.

In order to improve the performances of the source, a liner was inserted. A bias probe was installed on the beam axis on the injection side. The maximum applicable voltage is -500 V relative to the plasma chamber, and the probe position is variable between 120 and 220 mm from the center of the C coil. The optimum position is located at 170-190 mm, which corresponds to the position of the maximum mirror field. The extraction system is composed of two electrodes and can be moved along the beam axis. An einzel lens is placed downstream of the extraction electrode.

The ion beams extracted from the source are analyzed by using a dipole magnet and are measured in a Faraday cup placed at the image focal point of the analyzing system. Detailed performance of the source is presented somewhere in these proceedings [4]. 8.5 MeV/u $^{86}Kr^{23+}$ beams were accelerated by the AVF cyclotron and were delivered to user's experiments. In order to produce metallic boron-ions, a test by using the MIVOC (Metal Ion from VOlatile Compounds) method [7] was performed using o-carborane ($C_2B_{10}H_{12}$). Its vapour pressure was around 1-2 Torr at the room temperature. The stable flow of the vapour from the o-carborane powder to the plasma chamber enabled us to produce a fully stripped boron ions. The o-carborane was put in a glass vessel directly connected to the plasma chamber via a buffer tank. A helium gas was used to generate plasma..

2.45 GHz ECR Proton Source

A proton source is under development to supply high currents with a low emittance. It consists of three ring permanent magnets and no multipole magnets are employed. Performance tests were finished and 0.6 mA protons were extracted at 15 kV and with a relatively low RF power of 200 W. The source has been installed in the injection beam line. On-line tests will start this fall.

Flat-Topping Acceleration System

A schematic layout of the main and the flat-top resonators of the AVF cyclotron is shown in Fig. 3. An additional flat-top cavity of a coaxial movable-short type is inductively coupled to the main resonator on the opposite side of the main power feeder for fundamental-voltage production. The flat-top cavity has a length of 700 mm and an outer diameter of 170 mm. A full stroke of the shorting plate of the flat-top cavity is 100 mm. The coupler electrode and the inner conductor of the flat-top cavity are shown in Fig. 3. The gap between the coupler electrode and the inner tube of the main cavity can be changed from 0 to 155 mm. Fine adjustment for 50Ω impedance matching is accomplished by using a tuner with a full stroke of 40 mm.

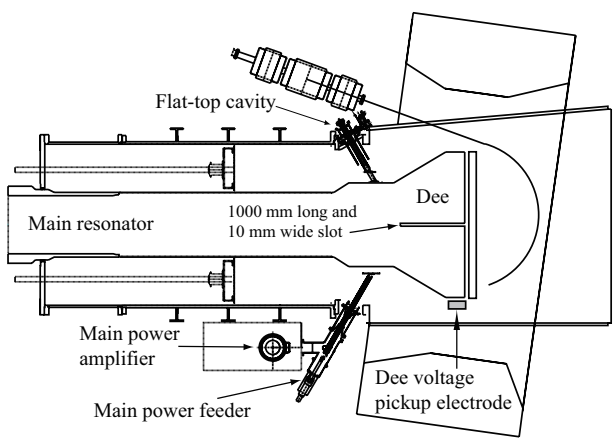

Figure 3: Cross-sectional view of a liquid-helium free18-GHz superconducting ECR ion source.

A flat-topped dee voltage waveform can be generated by superimposing a harmonic voltage on the fundamental

one [8]. The RF power from a 10-kW transistor amplifier is transmitted to the flat-top resonator. through a coaxial waveguide (WX39-D) and is inductively fed to the Dee electrode. Impedance matching of the 50Ω transmission line from the flat-top cavity to the main resonator is optimized by adjusting the positions of the coupler, the shorting plate, the tuner, and the feeder capacitor. Impedance matching can be achieved over a wide range of harmonic frequencies from 50 to 80 MHz. Hence, the fifth, seventh, and ninth harmonic modes are available for production of the flat-topped voltage waveform. Such higher order harmonic modes have an advantage of saving power for the harmonic voltage production, because the *n*-th harmonic voltage required for flat-toped waveform production is $1/n^2$ of the fundamental one [5, 9]. For the present structure of the Dee electrode, a parasitic resonance mode is known to exist around 76 MHz. This resonance is generated in the transversal direction of the dee electrode axis. There is some possibility of the parasitic resonance's interference with the fifth harmonic voltage production for the flat-top acceleration of higher energy protons. In order to shift the transversal resonance frequency to around 55 MHz, we put a 1000-mm-long and 10-mm-wide slot along the electrode axis, as shown in Fig. 3. Beam developments are on-going with the FT system [5].

RESEARCH PROGRAMS

Beams are available on targets for 5000-6000 hours in a year. A wide range of research programs are performed at the RCNP cyclotron facility as listed below.

- Few-body problem
- Nucleon and nuclear interactions in nuclear medium
- Proton/deuteron elastic & inelastic scattering (p,2p), (p,n) reactions
- Charge exchange reactions relevant to the astronuclear physics: (^{4}He,^{6}He), (^{4}He,^{8}He)
- Giant resonance excited by （p,p'）, (^{3}He,t), (α,α'), (^{7}Li,^{7}Be γ) reactions
- Fragmentation of deep hole states in light nuclei
- Proton-proton Bremsstrahlung (p,p'γ) reaction
- Weak hyperon nucleon interaction by the pn → pΔ reaction
- Heavy ion physics with rare isotopes
- Fundamental physics with ultracold neutrons
- Applications (neutrons)
  Material science
  Biological science
- Nuclear chemistry

Intensive studies have been performed on the spin and isospin excitation by charge exchange (p,n) and (n,p) reactions around 300 MeV. The στ nucleon-nucleon interaction has the maximum strength at this energy region. The mechanism of these reactions is simple, as well. We can extract the spin and isospin excitation strength with least ambiguities. Recent result showed the strength distribution in the nuclei relevant to 2ν double β decays [10].

A beam line was installed to bypass the ring cyclotron and to directly deliver low-energy, high intensity beams from the AVF cyclotron to experimental halls, It increases research opportunities at the cyclotron facility as well as diagnoses the quality of the beam injected into the ring cyclotron. With this line, low energy heavy ions are delivered to the rare isotope separator and are used to study high spin isomeric states in nuclei. Owing to low backgrounds at the second target area, decaying γ rays can be clearly observed form isomeric states. A new beam line was installed to capture pions by superconducting solenoid magnets. Muons are produced in succeeding decay channel.

REFERENCES

[1] Hatanaka, T. Itahashi, M. Itoh, M. Kibayashi, S. Morinobu, K. Nagayama, S. Ninomiya, T. Saito, Y. Sakemi, K. Sato, A. Tamii, H. Tamura, and M. Uraki, Proceedings of the 17th International Conference on Cyclotrons and their Applications, Tokyo, Japan, pp. 115-117 (2004).

[2] Fukuda, H. Tamura, T. Saito, T. Yorita, and K. Hatanaka, Proceedings of the 18th International Conference on Cyclotrons and their Applications, Giardini Naxos, Italy, pp. 470-472 (2007).

[3] Hatanaka, M. Fukuda, M. Kibayashi, S. Morinobu, K.Nagayama, H. Okamura, T. Saito, A. Tamii, H. Tamura, and T. Yorita, Proceedings of the 18th International Conference on Cyclotrons and their Applications, Giardini Naxos, Italy, pp. 125-127 (2007)

[4] T. Yorita et al., in these proceedings, MOPCP051

[5] M. Fukuda et al., in these proceedings, MOPCP056.

[6] T. Nakagawa, T. Aihara, Y. Higurashi, M. Kidera, M.Kase, Y. Yano, I. Arai, H. Arai, M. Imanaka, S. M. Lee, G. Arzumanyan, and G. Shirkov, Rev. of Sci. Instru. 75, 1394 (2004).

[7] H. Koivisto, E. Kolehmainen, R. Seppala, J. Arje, and M. Numia, Nucl. Instr. Meth. Phys. Res. B117, 186 (1996).

[8] J. L. Conradie, A. H. Botha, J.J.Kritzinger, R. E. F. Fenemore, and M. J. Van Niekerk, Proceedings of the 14th International Conference on Cyclotrons and their Applications, Cape Town, South Africa, pp. 249-251 (1995).

[9] M. Fukuda, S.Kurashima, S. Okumura, N. Miyawaki, T. Agematsu, Y. Nakamura, T. Nara, I. Ishibori, K. Yoshida, W. Yokota, K. Arakawa, Y. Kumada, Y. Fukumoto, and K. Saito, Rev. Sci. Instru., 74, 2293 (2003).

[10] K. Yako, M. Sasano, K. Miki, H. Sakai, M. Dozono, D. Frekers, M. B. Greenfield, K. Hatanaka, E. Ihara, M. Kato, T. Kawabata, H. Kuboki, Y. Maeda, H. Matsubara, K. Muto, S. Noji, H. Okamura, T. H. Okabe, S. Sakaguchi, Y. Sakemi, Y. Sasamoto, K. Sekiguchi, Y. Shimizu, K. Suda, Y. Tameshige, A. Tamii, T. Uesaka, T. Wakasa, and H. Zheng, Phys. Rev. Lett. 103 (2009) 012503.

NEW HIGH INTENSITY COMPACT NEGATIVE HYDROGEN ION CYCLOTRONS

V. Sabaiduc, D. Du, T. Boiesan, J. Zhu, K. Suthanthiran, R.R. Johnson,
BCSI, Springfield, VA 22153, U.S.A.
W. Gyles, Ladysmith, Canada, W. Z. Gelbart, ASD, Garden Bay, Canada,
E. Conard, PAC sprl, Belgium

Abstract

Best Cyclotron Systems Inc (BCSI) has been established in Springfield, Virginia, US, for the design and production of commercial cyclotrons. The company is a subsidiary of Best Medical International renowned in the field of medical instrumentation and radiation therapy. Cyclotrons are manufactured and tested at Best Theratronics, Ottawa. BCSI is initially focusing on three different energy cyclotrons 14, 35 and 70MeV negative hydrogen ion accelerators.

CYCLOTRON CHARACTERISTICS

Various small cyclotrons had successfully been developed with compact structure for isotopes production in 1990s. CIAE has dedicated to the exploration of the cyclotron physics and key technologies with the compact structure remained and the energy range extended to 70~100 MeV since late 1990s. The cyclotrons developed by BEST began with referring to 10 MeV CYCIAE-CRM, as well as the advanced design of CYCIAE-14[1] and CYCIAE-70[2]. As preceded by CIAE, the sophisticated technologies on compact cyclotrons with high intensity and relatively high energy have taken the lead in the developing trends to some extent, as the case of BEST.

All BEST's cyclotrons have room temperature magnets, deep valley design with four radial sectors, two dees in opposite valleys, external ion source and simultaneous beam extraction on opposite lines. The BEST 14 cyclotron is designed for both internal and external ion source configuration. The cyclotrons are illustrated in Figure 1.

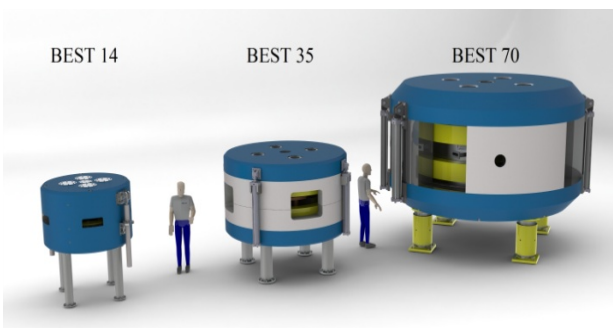

Figure 1: BCSI Cyclotrons

The main characteristics of the cyclotron magnets are shown in Table 1 with power specifications, including four beam lines each for the 35 and 70MeV cyclotrons.

Table 1: Comparative Specifications

Energy	Dimension (dia. x height)	Weight	Electric power
14MeV	1.7 m x 1.0 m	14 t	60KVA
35MeV	2.7 m x 1.5 m	55 t	280KVA
70MeV	4.5 m x 2.2 m	195 t	400KVA

BEST 14 CYCLOTRON

The BEST 14p cyclotron system is designed for negative hydrogen ion (H^-) acceleration and fixed energy 14MeV dual beam extraction using multi-foil extraction carousel. The cyclotron has the unique feature of compatibility between the uses of an internal or external ion source. The design allows for field upgrade from internal to external ion source.

Main Magnet

A strong axial focusing magnet design has been chosen to allow for future beam intensity increase with $\nu_z > 0.5$ and $> \nu_r/2$ as shown in Figure 2.

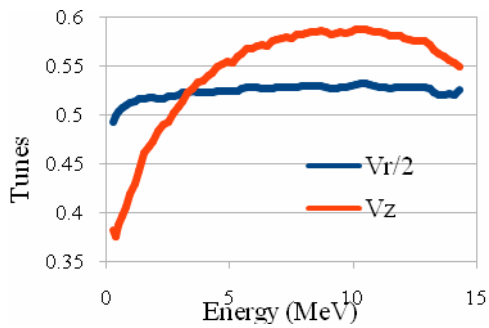

Figure 2: Tune diagram

Table 2: Magnet parameters

Number of sectors	4
Sector angle	52°
Average magnetic field	1.2T
Radius of sector magnet	50.0cm
Hill gap	2.6cm
Magnet coil	100kAT
Coil power	20kW

Ion Source

The internal ion source option is based on a PIG source as shown in Figure 3, designed to provide an extracted beam current in excess of 100μA.

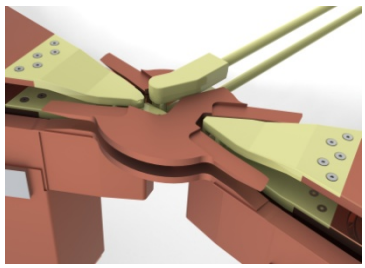

Figure 3: Internal ion source

The external ion source option is based on a multi-cusp ion source with a DC capability of 5mA ensuring a minimum of 400μA of extracted beam at an injection energy of 27keV. The plots in Figure 4 were obtained by accelerating the beam from the injection point after the inflector to the extractor and then to the target outside of the magnet. Ellipse containing 95% of the beam have normalized emittance of **Z**=6.2 mm mr, **X**=3.8 mm mr.

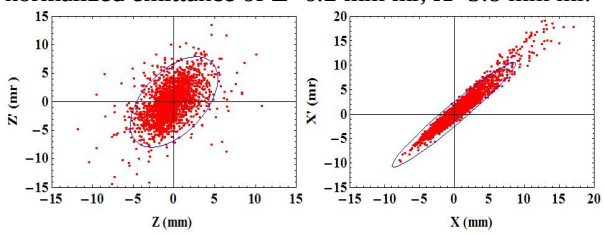

Figure 4: **Z** and **X** normalized emittances at target

The centre region magnetic field configuration is capable of accelerating beam from both internal and external sources with minimal changes (factory mapped for both options). The upgrade to an external ion source requires replacing two magnet shims, the centre region assembly and ion source. The centre region includes the inflector and new dee tips.

RF System

The resonator is composed of two λ/4 resonant cavities connected at the centre as shown in Figure 5. This option optimises the resonator power dissipation with minimum dee voltage off balance between the lower and upper dee plates.

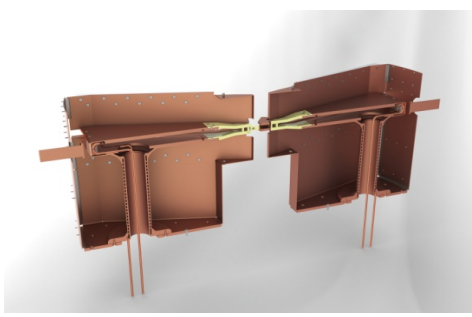

Figure 5: RF Resonators

Table 3: Main characteristics of the RF System

Frequency	73MHz, 4th harmonic
Dee angle	30^{o}
Dissipated power	8kW
Dee voltage	40kV
Quality factor	7000

The resonant cavity has been simulated with CST MWS to optimise the resonator characteristics and continues with coupling and tuning optimization. The final design will ensure identical resonator characteristics when replacing the centre region and dee tips for the external ion source.

Extraction Mechanism

The beam can be simultaneously delivered to two of the four target stations (two on each side) installed at the end of the vacuum wall extraction horns. Beam extraction is achieved with two diagonally opposite extraction probes each probe being equipped with two four-foil carousels as shown in Figure 6.

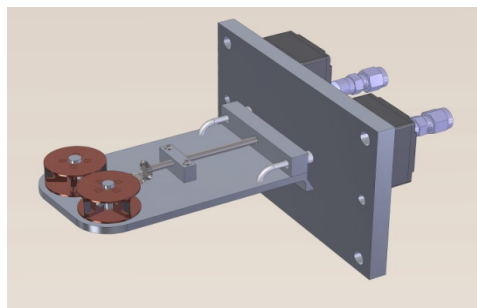

Figure 6: Extraction probe

Carousel rotation moves the beam in the horizontal plan and radial movement adjusts the beam ratio between extractors.

CONTROL SYSTEM

The main purpose of the Control System is to provide a fully integrated real-time operation and monitoring of the cyclotron systems, interlock and safety signals. The controller consists of a Siemens-based Programmable Logic Controller that analyzes all input and output signals. The graphical user interface, built on WinCC software, links the operator with the PLC as shown in Figure 7.

The daily operations of the cyclotron are simplified through built-in automated procedures like machine start-up, or machine shutdown for the basic users. Manual operation of the cyclotron is also available to fine-tune the machine by more experienced operators based on higher security level access.

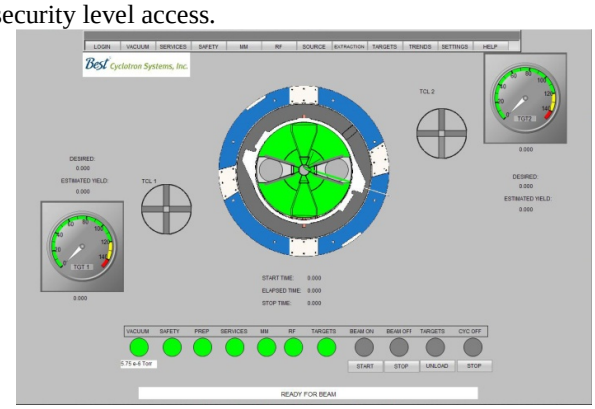

Figure 7: Control system interface

BEST 35 CYCLOTRON

The BEST 35p cyclotron is designed for negative hydrogen ion (H^-) acceleration and variable beam extraction between 15 and 35MeV. There is a broad range of single photon emitters that are used in nuclear diagnostic imaging and therapy that are accessible in this energy range. Typical characteristics of the cyclotron are presented in Table 4.

Table 4: BEST 35p Main characteristics

Main magnet	four sectors coil current: ≈ 98000AT
RF resonators	two resonators connected frequency: 70MHz harmonic: 4th dissipated power: 20-22kW dee voltage:50kV
External ion source and injection line	multi-cusp H^-, 15mA DC combined beam current in excess of 1.5mA axial injection, spiral inflector
Vacuum	ion source: < 1 x 10^{-5} Torr main tank: < 5 x 10^{-7} Torr
Extraction	simultaneous dual beam 2 stripping multi-foil carousels variable energy 15-35MeV
Beam lines	2 or 3 way switching magnet 4 to 6 beam lines

BEST 70 CYCLOTRON

The BEST 70p cyclotron is designed for negative hydrogen ion (H^-) acceleration and variable energy extraction up to 70MeV with a combined beam current of 800μA. It may be used as a research accelerator as well as a radioisotope production cyclotron.

Typical characteristics are presented in Table 5.

Table 5: BEST 70p Main characteristics

Main magnet	B_{max} field: 1.6T coil current: ≈ 127kAT 4 sectors, deep valley hill sector angle: 50° varying hill gap: 6 – 4.69 cm
RF resonators (two resonators connected)	frequency: 58MHz, harmonic: 4th dissipated power: 28kW dee voltage: 60 - 81kV dee angle 36°
External ion source and injection line	multi-cusp H^-, 15-20mA DC beam current: 800μA axial injection, 40kV spiral inflector
Vacuum	ion source: < 1 x 10^{-5} Torr main tank: < 1.5 x 10^{-7} Torr
Extraction	simultaneous dual beam 2 stripping multi-foil carousels variable energy 35-70MeV
Beam lines	2 way switching magnet Up to 4 beam lines

The illustration in Figure 8 shows the cyclotron, one side switching magnet and beam line.

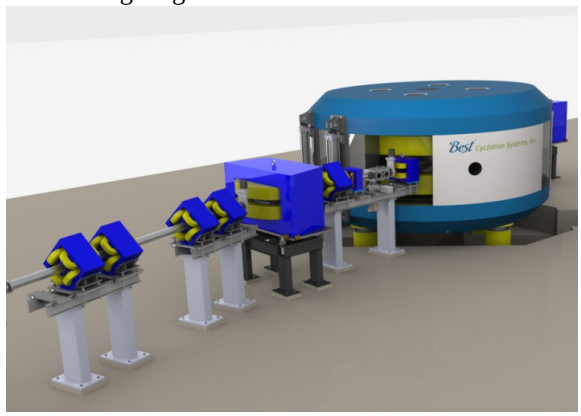

Figure 8: BEST 70p Cyclotron and beam line

Stripping Losses

The design goal is to keep the total H^- vacuum and E.M. stripping losses ≤2%. At 70MeV the gas stripping losses approximates at 2% and E.M. stripping losses at 0.2%, as shown in Figure 9.

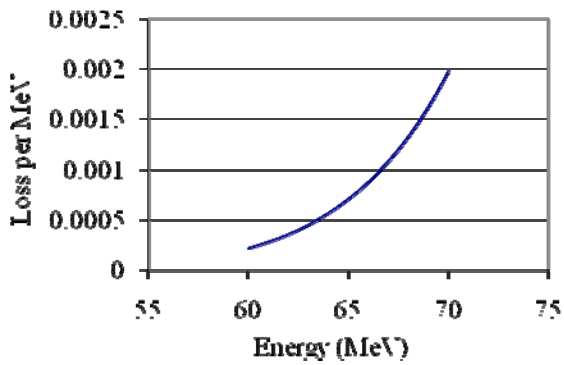

Figure 9: E.M. Stripping losses

RF Resonators

A two separated cavities solution has been chosen driven by individual amplifiers and LLRF digital control. The cavity design adopts the "triangular" stem structure for increase dee voltage distribution toward outer radii (reduce Lorentz stripping).

ACKNOWLEDGMENTS

We would like to thank Dr. Gerardo G. Dutto and Dr. George H. Mackenzie for their contribution to our cyclotron design studies.

REFERENCES

[1] Tianjue Zhang, Yinlong Lu, Zhiguo Yin, et al., "Overall Design of the CYCIAE-14, a 14MeV PET Cyclotron", Proc. of 10th ECAART 2010, Athens

[2] Tianjue Zhang, Shizhong An, Chuan Wang, et al., "Physics design of a 70MeV High Intensity Cyclotron, CYCIAE-70", Proc. of 10th ECAART 2010, Athens

[3] George H. Mackenzie, *private communications*

EXPERIENCE OF CYCLOTRON OPERATION WITH BEAM SHARING AT TSL

D. M. van Rooyen[1], E. Blomquist*, K. Gajewski, E. Grusell*, B. Gålnander, B. Lundström, M. Pettersson, A. V. Prokofiev, C. Vallhagen Dahlgren*
The Svedberg Laboratory, Uppsala University, Box 533, S-75121, Uppsala, Sweden
*Department of Oncology, Radiology and Clinical Immunology, Uppsala University, S-751 85 Uppsala, Sweden

Abstract

Following a reorientation in 2005/2006, the focus of activities at TSL was shifted from nuclear physics to proton therapy and radiation testing with protons and neutrons. In order to use the beam as efficient as possible beam sharing is employed. The paper describes the development of a range of control system utilities, for example switching of the beam between users by the principal user instead of being controlled via a cyclotron operator.

INTRODUCTION

The Gustaf Werner cyclotron, completed in the early 1950s as a fixed-energy 185 MeV proton synchrocyclotron was converted during the eighties to a variable-energy multi-purpose sector-focused cyclotron and has been since then in use for a wide range of applications. An interesting feature of the accelerator is that it is operated both as an isochronous cyclotron and as a synchrocyclotron.

The principal users are now the proton therapy facility of the Academic Hospital, Uppsala, as well as accelerated testing of electronics at the neutron and proton irradiation facilities. Other applications are detector development and calibrations, as well as nuclear data measurements. Heavy ion beams are produced mainly for biomedical research [1].

THE GUSTAF WERNER CYCLOTRON

With a k-value of 192, non-relativistic ions can be accelerated up to an energy of 192 x Q^2z/A MeV, whereas the maximum energy for protons is limited to 180 MeV. In the isochronous cyclotron mode proton energies between 25 and 100 MeV can be delivered, whereas the synchrocyclotron mode is employed for proton beams with energies between 100 and 180 MeV. In this mode beam stretching is often used to provide a beam (macroscopic) duty factor of about 15%. This is achieved by reducing the *df/dt* and the accelerating voltage during extraction. More details may be found in [2, 3].

Heavy ion beams are mostly utilized for the biomedical research program where the most frequently used beams are fully stripped ^{12}C and ^{14}N with a highest achievable energy of 40 MeV/nucleon. The ECR ion source is of an older generation and was upgraded in 2002 in collaboration with JYFL [4], which resulted in a significant improvement of the performance of the source.

IRRADIATION *FACILITIES*

Proton Therapy

The average number of radiation fractions given per treatment week for 2009 was 28. This includes mainly treatments of intracranial tumors and cancer of the prostate [5]. Prostate cancer patients are treated with protons in combination with photons. Treatments of eye melanomas have been given but occur less regularly depending on the need. Experience indicates that the technical design of the switching procedure functions well.

Facilities in the Blue Hall

There are three irradiation facilities in the Blue Hall: ANITA, QMN, and the proton facility.

The ANITA facility (Atmospheric-like Neutrons from thIck TArget) provides a neutron beam with atmospheric-like spectrum (”white”, ”spallation”, cosmic-ray induced neutrons), primarily for studies and testing of electronic components and systems for neutron-induced single-event effects (SEE), which cause one of the major reliability concerns in semiconductor electronic components and systems [6], [7]. The proton beam is guided to a tungsten target, which fully stops the incident protons. The resulting neutron beam is formed geometrically by a collimator aperture. A modular design of the aperture allows the user to select the size of the neutron beam spot between 1 and 120 cm. The highest neutron flux is available at the Standard User Position (SUP), located 250 cm downstream of the production target. The energy-integrated neutron flux above 10 MeV amounts to $\approx 10^6$ $cm^{-2} \cdot s^{-1}$ for “the standard ANITA neutron field”, defined as the field at the SUP for the standard incident proton beam current of 200 nA on the production target. The user can choose lower flux at any time, down to ≈200 $cm^{-2} \cdot s^{-1}$ at the SUP and further down to ≈5 $cm^{-2} \cdot s^{-1}$ at the downstream end of the beam path. At a given position, the available range of immediate flux variation amounts to a factor of at least 150, which is achieved by altering the repetition frequency of the beam macropulses. All mentioned features are fully compatible with the beam sharing mode. Further details can be found in Ref. [8], [9].

1 Corresponding author: daniel.vanrooyen@tsl.uu.se

The Quasi-Monoenergetic Neutron (QMN) facility shares the beam line with the ANITA facility and uses the ^{7}Li(p,n) reaction for neutron production. The energy of the peak neutrons is selectable in the 20–175 MeV range. The flux of high-energy peak neutrons amounts to $3{\cdot}10^{4}$ - $3{\cdot}10^{5}$ cm$^{-2}{\cdot}$s^{-1} at the SUP, dependent on energy. In addition to SEE testing and studies (see the previous section), the QMN facility is employed for nuclear data measurements and detector calibrations. Further details can be found in Ref. [9], [10].

The accelerated proton beam, with the energy selectable in the range 20-180 MeV, can be guided to another beam line in the Blue Hall. Most of applications (testing for SEE and total ionisation dose effects, detector development and calibrations) utilize broad uniform proton fields, obtained by scattering of the primary beam on a tantalum foil. The produced scattered proton beam of Gaussian shape is geometrically limited using a set of graphite collimators. The diameter of the resulting beam spot can be chosen in the range 0.4-20 cm. The highest available proton flux amounts to $5{\cdot}10^{7}$ - $5{\cdot}10^{9}$ cm$^{-2}{\cdot}$s^{-1} for the scattered beam and to 10^{11} - 10^{12} cm$^{-2}{\cdot}$s^{-1} for the unscattered one, dependent on the proton energy. The proton flux is controllable within a range of ≈10 orders of magnitude. Further details can be found in Ref. [9].

BEAM SHARING TECHNIQUES

Due to the predominant use of beam time by proton therapy since 2005/2006, it became crucial to develop a method that could allow other users access to the beam in parallel with therapy treatments. While practised at TSL in specific situations during the last 10 to 15 years, beam sharing's possibilities were considered from a new perspective realizing that it is the only workable solution that would allow the laboratory to continue offering proton and neutron irradiation services for non-therapy users from industry and science, as well as to develop new irradiation facilities, as e.g. ANITA (see the respective section). A second motivation for exploring a new beam sharing approach, is related to the fact that reduced manpower motivated an operatorless control room solution.

A suitable beam sharing technique was therefore developed in 2006, which enables the beam to be switched between different irradiation areas by the principal user, instead of being controlled via the cyclotron operator. This enables a more efficient use of beam time and manpower. The duty of being operator is still assigned to one of the cyclotron personnel. The installation of mobile telephone repeaters throughout the facility enables users to contact the "operator" (who may be performing other duties), should the need arise.

The control system group at TSL developed a range of features that help the users to evaluate the beam quality.

Beam Sharing Scenario

During a run in the beam sharing mode, the beam is made available alternately for proton therapy, as the primary user, and for one of the irradiation facilities (IF) in the Blue Hall, as the secondary user.

Before the beam sharing can be operated by users, it has to be set up by the cyclotron operator. This procedure is usually performed on Mondays and the resulting settings are used during the following week. Depending on the beam charachteristics requested by the primary and secondary users, the following decisions are made:

- Selection of parameters that will be changed when switching the beam between the users.
- Choice of the delay time between requesting and granting the beam switching.
- Setting up alarm limits for the beam current.

After the beam switching is set up and all necessary quality assurance measurements are done, the control of the beam switching can be handed over to the therapy staff. From this moment on the cyclotron operator does not need to be in the control room, provided the operational status is normal. If the beam characteristics deviate from the preset range, the programs run by the primary and/or secondary users send alarm message(s) to the operator's mobile telephone.

Therapy, as the primary user, has full and exclusive control over the switching of the beam from the irradiation facility to the therapy area and vice versa. The switching of the beam is done using a dedicated program available only to the therapy staff and the cyclotron operators. The sequence for switching from the irradiation facility to therapy consists of the following steps:

- The therapy operator initializes the beam switch after selecting the number of irradiation fields and possibly adjusting the expected duration of the therapy beamtime slot.
- A voice message is sent to the cyclotron and IF control rooms to inform about the scheduled beam switching.
- After the preset delay, the beam is switched to the therapy area.
- After passing the beam current check, the beam is available for the therapy.

Switching the beam from therapy to IF includes the following actions:

- The therapy operator initializes the beam switch after selecting the expected time the beam will be available at the irradiation facility.
- The switching is performed.
- After passing the beam current check, the beam is available at the IF with a voice message sent informing that the beam is available for the specified expected time.
- If the secondary user has enabled the beam, it is put on target, otherwise the beam is turned off. The secondary user may turn on the beam again at any time.

Features Available for Users

The sets of available features are different for the therapy and IF users. The therapy operator controls the beam switching process and can monitor the beam

parameters (beam current, beam shape and position on viewers, beam position and angle using two multisector ionization chambers). The therapy operator also controls the access to the therapy room and the total dose delivered to the patient. The therapy staff is responsible for the dose control and patients' safety.

After the specified number of irradiation fields is completed, the therapy operator is reminded by the program to switch the beam back to the secondary user.

IF users have limited access to the control system via the Automated Workplace (AWP) with a simple graphical user interface, where the following features are available:

- Control of access to the irradiation facility area.
- Enabling/disabling the beam.
- Monitoring the beam current and other parameters.
- Monitoring the expected remaining duration of the beam slot for therapy or IF.
- Viewing the status of the beam switching (i.e. showing which beam line the beam is directed to).
- Viewing graphical plots of the beam current or particle beam flux density, as well as the event log.

In addition, the AWP allows the user to preprogram an irradiation so that it is automatically terminated after accumulation of a preset particle fluence on the user's object or device under test. This application makes use of real-time readings coming from one of calibrated proton or neutron monitors.

SCHEDULE AND USERS OF THE BEAM

A typical operation schedule has a four-week cycle, as detailed in Table 1.

Table 1: Available time slots with 180 MeV beams.

Week #	Time slots			
	07-09	09-18	18-22	22-07
1	Trim/QA	PT [+ IF]	-	-
2	Trim/QA	PT + IF	IF	-
3	Trim/QA	PT + IF	IF	-
4	Trim/QA	PT + IF	IF	IF

Abbreviations: PT = Proton Therapy, IF = Irradiation Facilities in the Blue Hall, QA = Quality Assurance. "PT + IF" indicates slots in the beam sharing mode.

The average share of the beam time available for IF in the beam sharing mode (between 09:00 and 18:00) amounts to ≈70%, or ≈6 hours. In weeks 2, 3 and 4 (see Table 1), IF users may continue running even after 18:00 in the single-user mode.

In addition, there are 3-4 weeks per year when the cyclotron can be run in a mode dedicated to the needs of a specific user, thus not necessarily using 180 MeV protons. Beams of heavy ions can be delivered, as well as protons with energy below 180 MeV (down to about 25 MeV).

The beam usage statistics for 2008 and 2009 shows a 36% increase for proton therapy and a 6% increase for the irradiation facilities.

ONGOING DEVELOPMENTS

A new diagnostic system is under development, which includes replacing the existing Vidicon-camera system with solid-state cameras.

The following developments are in progress at the irradiation facilities in the Blue Hall:

- A variable energy degrader, which would allow us to offer proton beams with controllable energy without re-tuning the cyclotron.
- Interactive user control of the beam intensity, compatible with the beam sharing mode.
- A shed for shielding of user's out-of-beam equipment from thermal and epithermal neutrons.

CONCLUSIONS (AND OUTLOOK)

The accelerator and irradiation facilities are continually developed and rebuilt according to users' demands.

Beam sharing between proton therapy and alternative radiation facilities has proven to function reliabely and safely.

REFERENCES

[1] Fakir, H., Sachs, R. K., Stenerlöw, B. and Hofmann, W., Clusters of DNA double-strand breaks induced by nitrogen ions for varying LETs and doses: experimental measurements and theoretical analyses. *Radiation Research,* **166,** 917-927 (2006).

[2] S. Holm, *Status report on the Gustaf Werner cyclotron in Uppsala*, Proc. 13th Int. Conf. on Cyclotrons and their Applications, Vancouver, Canada, July 6-10, 1992, p.106.

[3] D. Reistad, *Recent developments at the Gustaf Werner Cyclotron and CELSIUS*, Proc. 15th IEEE Particle Accelerator Conference, Washington, DC, USA, 17 - 20 May 1993, pp.1744.

[4] D.M. van Rooyen, D. Wessman, *The TSL 6.4 GHz ECR ion source - status, improvements and measurements*, Nukleonika 48, p. 99 (2003).

[5] A. Montelius, *et al*, The narrow proton beam unit at the The Svedberg Laboratory in Uppsala, Acta Oncol. **30** 739-45 (1991).

[6] JEDEC Standard JESD89A, "Measurement and reporting of alpha particle and terrestrial cosmic ray-induced soft errors in semiconductor devices", October 2006, http://www.jedec.org/download/

[7] T. Nakamura, *et al*, Terrestrial neutron-induced soft errors in advanced memory devices, 1st ed., Singapore, World Scientific, 2008, ISBN-13 978-981-277-881-9.

[8] A. V. Prokofiev, *et al*, "Characterization of the ANITA neutron source for accelerated SEE Testing at The Svedberg Laboratory", 2009 IEEE Radiation Effects Data Workshop, Quebec, Canada, July 20-24, 2009, pp. 166-173.

[9] http://www.tsl.uu.se/radiation_testing/

[10] A.V. Prokofiev, *et al*, "The TSL Neutron Beam Facility", Rad. Prot. Dosim. v. 126, pp. 18-22 (2007).

PRESENT STATUS OF JAEA AVF CYCLOTRON FACILITY

T. Yuyama *, Y. Yuri, T. Ishizaka, S. Kurashima, I. Ishibori, S. Okumura, K. Yoshida,
N. Miyawaki, H. Kashiwagi, T. Nara, W. Yokota
Japan Atomic Energy Agency, 1233 Watanuki, Takasaki, Gunma 370-1292, Japan

Abstract

In order to supply ion beam stably we have recently constructed an all-permanent-magnet type ion source. Ion beams such as H, O and Ne were produced stably. A beam attenuation system with metal meshes has been improved. By using new meshes with denser hole arrangement and lengthening the space of meshes, beam intensity can be controlled more precisely with maintaining the beam profile. The power supplies of the magnet coils used in the cyclotron were modified to stabilize the coil current with the stability $\Delta I/I$ of the order of 10^{-6}. In addition, developments of new irradiation techniques such as quick change of microbeam by cocktail beam acceleration technique and large-area uniform beam irradiation using multipole magnets are in progress.

INTRODUCTION

The JAEA AVF cyclotron with a *K* number of 110 MeV accelerates various ions, 5 to 90 MeV protons and 2.5 to 27 MeV/n heavy-ions at TIARA (Takasaki Ion accelerators for Advanced Radiation Applications) facility. TIARA is a very unique accelerator facility established for utilization of ion beams exclusively for the research in the field of biotechnology and materials science; for example, estimation of radiation hardness of space-use devices and plant breeding using ion-induced mutation. We have been developing ion sources, acceleration techniques and beam irradiation techniques for providing useful irradiation fields to researchers.

MACHINE OPERATION

Scheduled irradiation experiments were completely accomplished in fiscal year 2006 and 2008 without any serious troubles. Integration of operation time since the first beam in 1991 reached 60,000 hours on May 2010. Table 1 shows the detail of the cyclotron operation in fiscal year 2009. We usually operate the cyclotron from Monday morning to Friday evening through day and night, and the yearly operation time amounted to 3148.3 hours. The number of switching ion species, energy, or beam course amounts to 547 times, the number of changing acceleration harmonics 56 times. The number of machine troubles including minor breakdowns was 130 times. The severest trouble in 2009 was a breakdown of a high voltage power supply of the RF system. Cancellation of experiments in fiscal 2009 resulted from only this trouble.

Table 1: Statistics for cyclotron operation in fiscal 2009

Beam time	2461.8 h
Machine tuning	620.9 h
Beam development	65.6 h
Total operation time	3148.3 h
Switches of particle and/or energy	238 times
Change of beam course	309 times
Change of harmonic number	56 times
The number of experiments	633
Experiment cancelled due to machine trouble	2(8.5h)

* E-mail: yuyama.takahiro@jaea.go.jp

NEW ION SOURCE

The AVF cyclotron has three external ion sources; Multicusp ion source for H^+ and D^+, OCTPUS (ECR) for gaseous heavy ions, and Hyper nanogan (ECR) for highly- charged heavy ions including metal ions. In addition to them, a new ECR ion source has been developed to provide highly-stabilized beams [1]. Since this source is of all-permanent-magnet type, fluctuation of beam current intensity is less than that of ECR ion sources with room temperature coils, which cause considerable heat transfer to the plasma chamber and the sextupole magnets. The mirror magnetic field distribution of the new ECR ion source is adjustable by radially moving the permanent magnets in order to form the magnetic field suitable for various ion species. Highly stable ion beams such as H, O and Ne can be produced by this ion source. Figure 1 shows the stability of the $^{16}O^{6+}$ beam intensity, which is better than 3.2% for 8 hours.

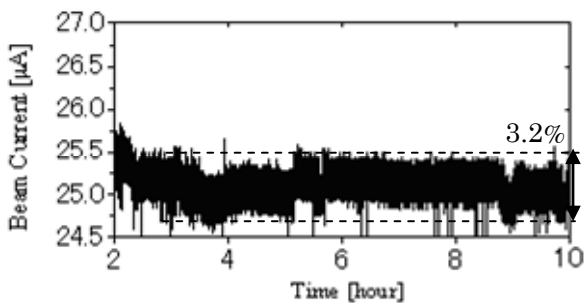

Figure 1: Stability of the $^{16}O^{6+}$ beam intensity produced by the all-permanent-magnet ECR ion source. The long-time stability of the beam is better than 3.2%.

BEAM ATTENUATOR IMPROVEMENT

A beam attenuation system using thin metal meshes, which have many regularly-arrayed holes, is installed in the injection line for quick attenuation of beam intensity with the beam size and the emittance almost maintained. Each metal mesh has the opening ratio of 1/2, 10^{-1}, 10^{-2} or 10^{-3}. However, when single mesh with low opening ratio of 10^{-2} or 10^{-3} or combined meshes were used for high beam attenuation, the beam profile changed or vanished at

the target point, as shown in Fig. 2 (a) and (b). The cause of this phenomenon is thought that the beam was not attenuated uniformly due to the scattering distribution of the mesh holes and/or the too-short installation interval of meshes.

The beam attenuation system has been improved. By using a new meshes with denser hole distribution and lengthening the maximum interval of meshes from 120 mm to about 1100 mm, beam intensity can be controlled more precisely with maintaining the beam profile [2]. As a result, the beam profile on the target barely changes even by use of combined meshes. Figure 2 (c) shows the effect of new meshes; the beam profile was maintained.

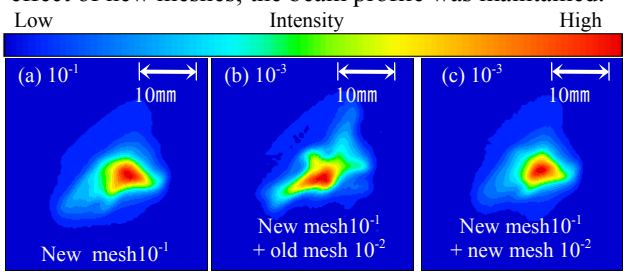

Figure 2: Comparison of beam intensity profiles on the target with a previous short interval of meshes: (a) standard for comparison with only a new mesh of opening ratio of 10^{-1}, (b) added an old mesh of opening ratio of 10^{-2} (ϕ 0.1 mm), (c) added a new mesh of opening ratio of 10^{-2} (ϕ 0.01 mm). These profiles were obtained from the optical density of irradiated radiochromic films, GAFCHROMIC films (HD-810, International Specialty Products) [3].

STABILIZED POWER SUPPLIES

A number of developments of acceleration technique are in progress. For production of a focused heavy-ion microbeam [4], an energy spread of the beam has to be reduced to $\Delta E/E = 2 \times 10^{-4}$ to diminish the effect of chromatic aberration at the lens which focus beam to a micrometer in diameter. The energy spread is reduced by introducing a flat-top (FT) acceleration system [5]. A highly-stabilized magnetic field of the cyclotron with a stability $\Delta B/B$ within 10^{-5} is also indispensable to realize FT acceleration because slight change of the magnetic field strength has significant influence on beam phase and trajectory in the cyclotron.

The required stability of the magnetic field was achieved by keeping temperature of the magnet constant [6]. In addition, the power supplies of the magnet coils used in the cyclotron were modified to stabilize the coil current with a stability $\Delta I/I$ of the order of 10^{-6}. The current feedback circuits with a digital-to-analog converter (DAC) are mounted in thermostatic chambers, temperature in which was formerly kept at 50 ±1°C by an electric heater. However, such high temperature precipitates degradation of electric parts in the DAC. The heater was therefore replaced with a Peltier device to keep temperature of the circuit at 27 ±1°C in ambient temperature over around 30°C. Moreover, the DAC circuit with Peltier device for main magnet coil was put in a incubator, a high-precision temperature controlled bath at 20 ±1°C, because of the high contribution to the magnetic field strength, while the other DAC's put on power supplies were at room temperature. The shunt resistance to measure the main magnet coil current for feedback control in the power supplies were replaced with direct current current transformer (DCCT). Figure 3 shows a change of the main magnet coil current. The stability $\Delta I/I$ was within $\pm 1.5 \times 10^{-6}$.

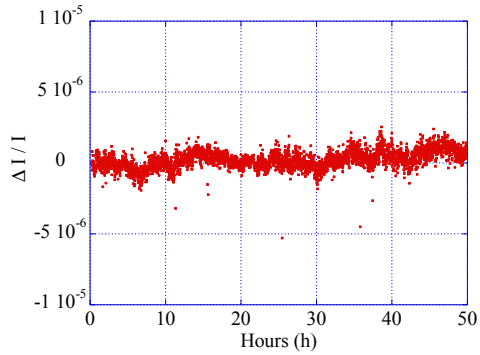

Figure3: Stability of main magnet coil current measured by DCCT.

QUICK CHANGE OF HEAVY-ION MICROBEAM

A microbeam of 260 MeV $^{20}Ne^{7+}$ with a spot size of 1 μm in diameter is available. Users of the microbeam require irradiating at plural values of linear energy transfer (LET) in one experiment. To do so, we have to change the ion species and/or kinetic energy of the microbeam in short time. Forming the microbeam, however, takes about 8 hours or more because the ion source, the cyclotron, and the focusing lenses must be tune very carefully. A microbeam of one species is provided in a beam time for this reason.

On the other hand, a cocktail beam acceleration technique is often used to change the ion species quickly. In this technique, beams of cocktail (mixture of plural species) having almost the same mass to charge ratio (M/Q; M is ion mass in the atomic mass unit, Q ion charge state) are injected into a cyclotron simultaneously, and one of them is extracted by slightly shifting the acceleration frequency. The magnetic rigidity of extracted beams is the same; therefore, lens parameters in the beam transport line do not need to be changed in principle.

This technique with microbeam formation has enabled

Table 2: Series of the cocktail beam with M/Q ≈ 2.85

Ion	M/Q	RF (MHz)	Energy (MeV/A)	LET in water (keV/μm)
$^{11}B^{4+}$	2.75178	18.1337	14.01	90.71
$^{14}N^{5+}$	2.80007	17.8210	13.54	186.6
$^{20}Ne^{7+}$	2.85551	17.4750	13.01	387.2
$^{28}Si^{10+}$	2.79714	17.8397	13.56	684.7
$^{40}Ar^{14+}$	2.85391	17.4848	13.03	1143

us to change microbeam from 260 MeV $^{20}Ne^{7+}$ to 520 MeV $^{40}Ar^{14+}$, which have M/Q ≈ 2.85, within 30 minutes. In the near future, $^{11}B^{4+}$, $^{14}N^{5+}$ and $^{28}Si^{10+}$ as shown in Table 2 will be added to the series of the 'cocktail microbeam' with M/Q ≈ 2.85 [7].

FORMATION OF LARGE AND UNIFORM BEAM PROFILE

The raster scanning method is widely used for large-area uniform irradiation of beams. In TIARA, the beam is swept at 50 Hz in one direction and 0.25~2.5 Hz in the other so as to obtain a uniform field. Irradiation time much longer than the scanning period is necessary to achieve a good uniformity. That is, this method is less suitable for short-time irradiation or low-fluence irradiation. Therefore, we have been developing a multipole-magnet beam profile uniformization system, MuPUS, based on the nonlinear focusing method as a new large-area and uniform irradiation technique [8].

The system can form a uniform beam by folding the tail part of the beam profile using the nonlinear magnetic field of octupole magnets. This method needs a simple and smooth profile such as a Gaussian or parabolic one as a precondition. Therefore, the beam from the cyclotron, which usually has a complicated profile, is multiply-scattered by a thin foil to form the profile close to Gaussian. Figure 4 (a) shows a quasi-Gaussian profile of the scattered beam on the target, measured by GAFCHROMIC film. The quasi-Gaussian profile was transformed to a uniform profile by octupole magnets of MuPUS as shown in Fig. 4 (b). A uniform beam of 10-MeV H^+ was successfully formed over 6 cm square, and is already supplied to research experiments.

At present, the uniform beam is extracted into the air through a 30-μm-thick titanium foil for quick change of target samples. The uniformity of the beam is affected by scattering and energy loss in the air. Thus, distance from the titanium foil to the target must be as short as possible.

REAL TIME MEASUREMENT SYSTEM OF BEAM PROFILE AND UNIFORMITY

MuPUS can form a stationary and broad uniform profile on the target, while the beam spot is moving fast in the raster scanning method. We have to confirm the large-area profile and the uniformity on the target before the beam is supplied to users. However, measurement of the profile using radiochromic films takes time to scan and analyze the irradiated films. Therefore, a real-time measurement system is being developed using a fluorescent screen.

A few kinds of Tb-doped Gd_2O_2S fluorescent screens called DRZ (Mitsubishi Chemical Co.) are used in this system. Compared with an Al_2O_3 fluorescent screen, the DRZ screen has much shorter decay time of light emission and higher sensitivity to ion beams. The light emitted from the DRZ screen on the target is detected by a CCD camera, and the fluorescent signal is analyzed by a LabVIEW (National Instruments Co.) system on a Windows PC. Figure 5 is a screen shot of the measurement program, which can show relative 1D and 2D beam profiles and uniformity of the irradiation area in real time. The uniformity is calculated as the root-mean-square (rms) error of the average beam intensity in arbitrary regions of interest. We have confirmed that the rms uniformity of the fluorescent has a similar tendency to that of GAFCHROMIC films. In order to monitor the uniformity of a large-area beam precisely, the installation location of the camera has been optimized.

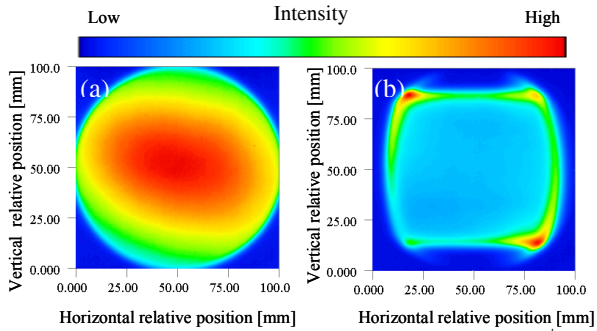

Figure 4: 2D intensity distributions of a 10 MeV H^+ on the target. (a) A quasi-Gaussian beam. (b) A uniform beam.

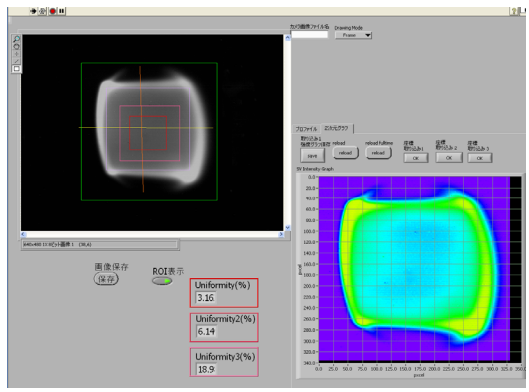

Figure 5: An image of the beam profile measured by the real-time measurement system. The uniformities of three different areas can be calculated automatically. Note that the deformation of the beam profile is because the light emitted from the screen is monitored from the approximately 27° direction.

REFERENCES

[1] K. Yoshida, et al., Rev. Sci. Instrum. 81, 02A312 (2010).
[2] T. Ishizaka, et al., JAEA-Review 2008-55 184 (2008).
[3] T. Agematsu, et al., RADIOISOTOPES, 57, 2, 87 (2008).
[4] M. Fukuda, et al., Nucl. Instrum. Methods Phys. Res. B 210, 33 (2003).
[5] S. Kurashima, et al., Nucl. Instrum. Methods Phys. Res. B 260, 65 (2007).
[6] S. Okumura, et al., Rev. Sci. Instrum. 76, 033301 (2005).
[7] S. Kurashima, et al., Nucl. Instrum. Methods Phys. Res. B 267, 2024 (2009).
[8] Y. Yuri, et al., Proc. IPAC'10, 4149 (2010).

BEAM EXTACTION SYSTEM FROM DC60 CYCLOTRON

O.N. Borisov, B.N. Gikal, G.G. Gulbekyan, I.A. Ivanenko, V.N. Melnikov, V.I. Mironov, A.V. Tikhomirov, E.V Samsonov, V.V. Seleznev, A.I. Sidorov
Joint Institute for Nuclear Research, Dubna, Moscow region, Russia

Abstract

The results of numerical simulation of the heavy ions beam extraction system (A/Z=6÷12, W=0.35÷1.77 MeV/amu) from the DC60 cyclotron are presented. The parameters of the extraction system elements (electrostatic deflector and focusing magnetic channel) and diagnostic elements are chosen. The experimental extraction efficiency of $^{14}N^{2+}$ and $^{84}Kr^{12+}$ beams is equal to 60÷65% with intensity 1.5÷2.5 μA.

INTRODUCTION

The DC60 is a sector cyclotron with variation of the magnetic field level at range Bo=1.25÷1.65 T. The energy range of the accelerated and extracted ion beams W is continued with interval 0.35÷1.77 MeV/amu for ratio of the ion mass (A) to ion charge (Z) A/Z=6÷12. The main parameters of DC60 cyclotron are given in Table 1.

Table 1. Main parameters of the DC60 cyclotron

Pole diameter [mm]	1620
Number of the sectors	4
Azimuthal width of sector [deg]	52
Valley gap [mm]	176
Sector gap [mm]	33
Bo [T]	1.25÷1.65
Number of dee	2
Azimuthal width of dee [deg]	35
Udee [kV]	50
Frot [MHz]	1.83÷4.35
q	4 , 6
Frf [MHz]	11.0÷17.4
A/Z	6÷12
W [MeV/amu]	0.35÷1.77

For beams extraction from the cyclotron is used the electrostatic deflector. The extraction system of the DC60 cyclotron consist a next elements:

1. Electrostatic deflector (ESD);
2. Focusing magnetic channel (MC);
3. Elements of diagnostic
   a) Extraction probe;
   b) profilometer.

NUMERICAL SIMULATION OF THE BEAM EXTRACTION

For numerical simulation the 5 test ions in accordance with working diagram are used. The parameters of there ions are given in Table 2.

Table 2. Parameters of the test ions

N	A/Z	W [MeV/amu]	Udef [kV]	Bo [T]
1	6	1.07	30.8	1.25
2	10	0.38	18.6	
3	8	0.79	29.4	1.45
4	6	1.77	51.9	1.65
5	12	0.46	25.6	

The extracted trajectory is shown in Figure 1. The average radius of the maximal accelerated orbit is equal ≈70 cm (Figure 2).

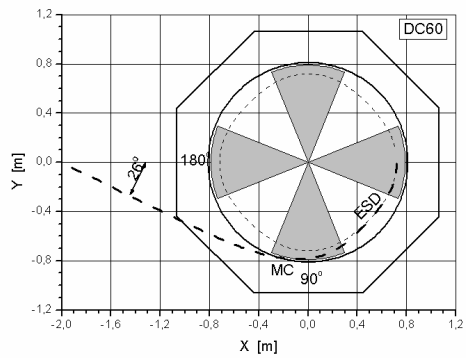

Figure 1. Trajectory of the test ion (A/Z=8, Bo=1.45T) extracted from DC60 cyclotron

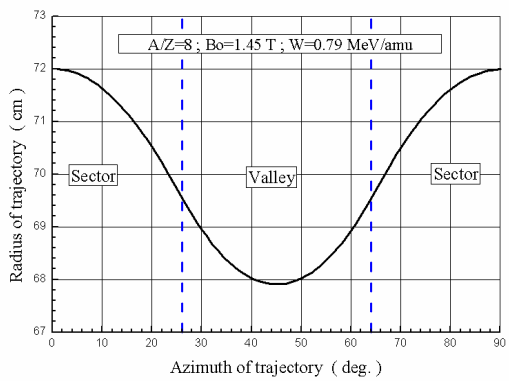

Figure 2. The maximal accelerated orbit for test ion

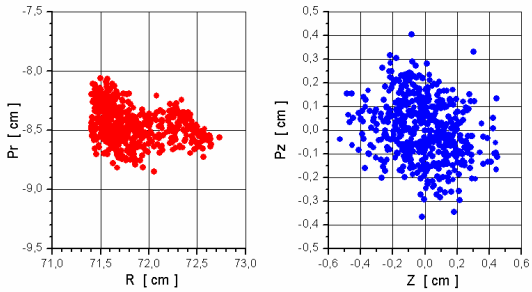

Figure 3. The horizontal and vertical beam emittances at the deflector entrance (A/Z=8, Bo=1.45 T)

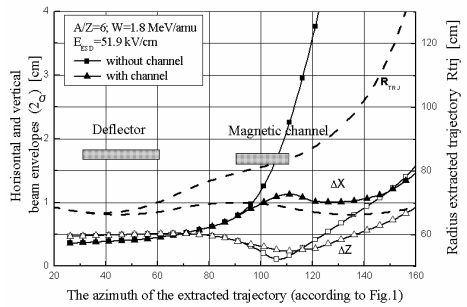

Figure 4. The horizontal and vertical beam envelopes

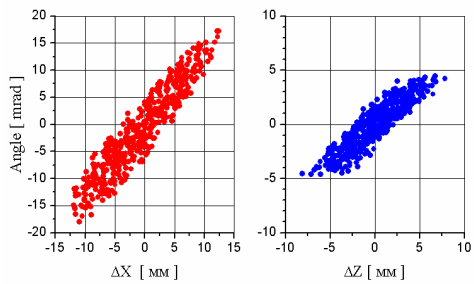

Figure 5. The horizontal and vertical emittances of the extracted beam (A/Z=8, Bo=1.45 T)

ELECTROSTATIC DEFLECTOR

The main parameters of the electrostatic deflector are given in Table 3. The electrostatic deflector is shown in Figure 6.

Table 3. Parameters of the electrostatic deflector

Azimuthal position [deg]	84÷112
Max. voltage [kV]	65
Length of the “potencial” plate [mm]	400
Length of the “septum” plate [mm]	440
Thickness of the “septum” plate [mm]	0.3÷1.0
Curvature of the plate [mm]	1800
Gap between plates [mm]	10
Displace of the deflector edges [mm]	± 15
Material of the “potencial” plate	Ti
Material of the “septum” plate	Mo

FOCUSING MAGNETIC CHANNEL

The main parameters of the magnetic channel are given in Table 4. The magnetic channel is shown in Figure 7.

Table 4. Parameters of the magnetic channel

Azimuthal position [deg]	84 ÷ 112
Length of the channel [mm]	≈400
Curvature of the plate [mm]	≈ 860
Aperture [mm] horizontal	25
vertical	15
Displace of the edges [mm]	± 15
Focusing gradient of the magnetic field [T/m]	35÷40

THE ELEMENTS OF DIAGNOSTIC

The extraction probe is placed between electrostatic deflector and magnetic channel. It has 10 lamels with thickness 5 mm for measurement of the beam intensity and horizontal distribution. The extraction probe is shown in Figure 8.

The profilometer is placed at the vacuum chamber exit. It has 15 vertical and 15 horisontal wires with step 5 mm and is used for measurement of the beam intensity, horizontal and vertical distribution. The profilometer is shown in Figure 9.

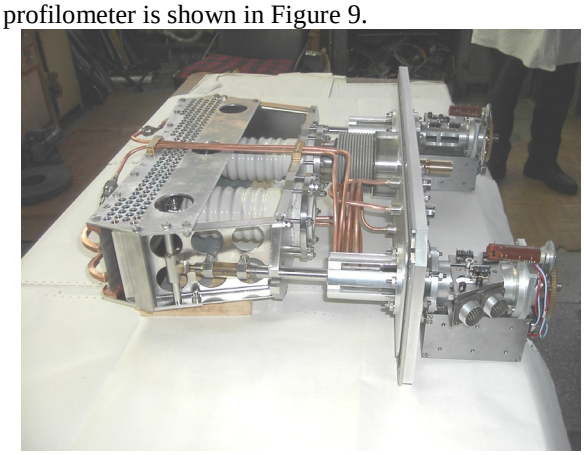

Figure 6. Electrostatic deflector

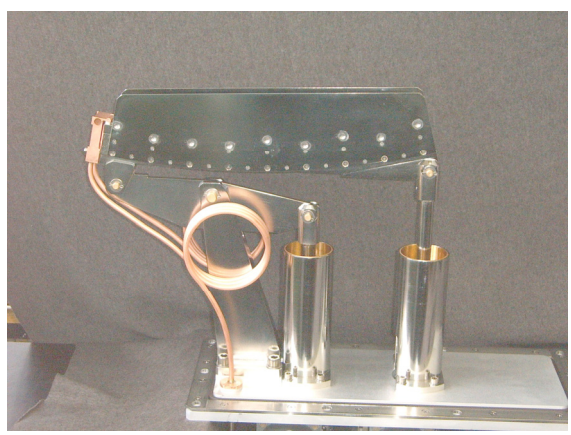

Figure 7 Magnetic channel

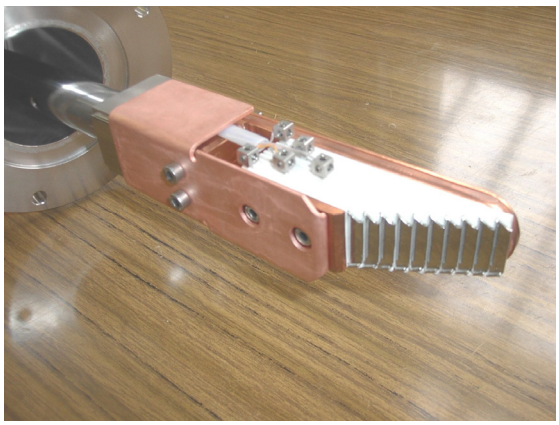

Figure 8. Extraction probe

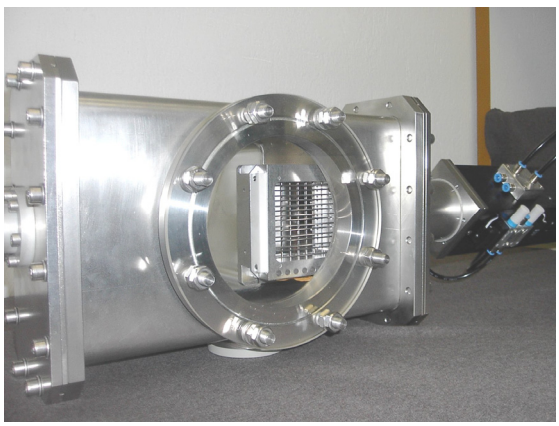

Figure 9. Extraction chamber with profilometer

EXPERIMENTAL RESULTS

The first extracted beams was obtained at December 2006. The parameters of the first extracted beams are given in Table 5.

Table 5. Parameters of the extracted beams

Ion	$^{84}Kr^{12+}$	$^{14}N^{2+}$
A/Z	7	7
Bo [T]	1.42	1.64
Rfr [MHz]	12.67	14.4
Buncher	Yes	No
Accelerated beam currency [μA]	2.5	1.46
Extracted beam currency [μA]	1.65	0.9
Extraction efficiency [%]	66	61.6

CONCLUSION

Extraction of the heavy ion beams from DC60 cyclotron is realized. The extraction efficiency is is equal to 60÷65% with intensity 1.5÷2.5 μA.

REFERENCES

[1] B.N. Gikal et al., “Project of the DC-60 cyclotron with smoothly ion energy variation for researcn center at L.N. Gumilev EuroAsian State University in Astana (Kazakhstan)”, Cyclotrons and their applications, 2004, pp.205-207.

AUTOMATED OPERATION AND OPTIMIZATION OF THE VARIAN 250 MeV SUPERCONDUCTING COMPACT PROTON CYCLOTRON

T. Stephani#, H. Röcken, U. Behrens
VARIAN Medical Systems Particle Therapy GmbH, Bergisch Gladbach, Germany
C. Baumgarten, PSI, Villigen, Switzerland

Abstract

The 250 MeV superconducting compact proton cyclotron of Varian Medical Systems Particle Therapy is specially designed for the use within proton therapy systems. During medical operation typically no operator is required. Furthermore, several automated control system procedures guarantee a fast, simple and reliable startup as well as beam optimization after overnight shutdown or regular service actions. We report on the automated startup procedures, automated beam centering and automated optimization of extraction efficiency. Furthermore we present an automated beam current setting as used during medical operation by means of an electrostatic deflector located at the cyclotron center at low beam energies.

INTRODUCTION

The VARIAN medical proton accelerator is a compact four sector AVF isochronous cyclotron incorporating a superconducting main coil. The design of this compact machine, proposed by Henry Blosser and his team [1] and further developed and manufactured by VARIAN, proved to be very successful. The beam energy is 250 MeV, the maximum beam current during medical operation is 800 nA and the typical extraction efficiency is 80%. More detailed technical information and dedicated cyclotron parameters are provided in our last status report [2] which dealt with the commissioning of VARIAN's superconducting 250 MeV proton cyclotrons at PSI, Switzerland and RPTC, Germany.

Both machines are fully operational and are used to provide beam for proton therapy treatment systems with scanning techniques. Since the last report considerable progress has been made in the field of automation procedures for the control system. The announced optimization procedures for beam centering and extraction are operational and have proved reliable. For power saving reasons the standby condition of the RPTC cyclotron has been modified. Furthermore, a fast beam current variation procedure has been implemented and several new automatic characterization procedures are implemented in the cyclotron control system.

AUTOMATED CYCLOTRON STARTUP

Five cyclotron states have been defined and automatic transition routines have been introduced to guarantee reproducible system settings and a fast startup especially following overnight shutdown. Tab. 1 gives an overview on these cyclotron states and a short explanation of the respective cyclotron condition. An operator can easily change between the states by using automated transition procedures.

Table 1: Cyclotron States

Off	cyclotron vented, magnet off ⇒ cyclotron can be opened
Standby 1	cyclotron closed and evacuated ⇒ long shutdown period
Standby 2	additionally magnet energized, cooling water temperature increased ⇒ access to bunker, overnight shutdown
RF ready	additionally RF operating at reduced power ⇒ short standby period, alternative overnight shutdown
Beam ready	all active cyclotron components operating at predefined set values ⇒ cyclotron ready for beam operation

At RPTC currently "Standby 2" is used as overnight shutdown state. To reduce the power consumption of the system, all active components except the cryo-cooling, the superconducting magnet system, and the vacuum system are switched off. To maintain the thermal stability of the magnet iron the cooling water is set to an increased temperature. This minimizes the transient effects caused by heating from RF losses when coming back to standard beam operation. In addition this state enables access to the bunker to allow service actions if necessary.

Starting from "Standby 2" beam operation is possible within several minutes. With the transition to the state "RF ready" the RF amplifier is switched on and the RF system is set to operation at a reduced power of about 75 kW. A subsequent transition to the state "Beam ready" sets all other active components (ion source, extraction deflectors, …) to their nominal values. The time flow diagram in Fig. 1 illustrates this startup procedure for the important subsystems. The transition algorithm computes and sets the required magnet current as a function of the iron temperature. After setting the voltage of the vertical deflector – an electrostatic component located at the center of the cyclotron – to $U_{VD} = 0$ V (Fig. 1 at 8 min) beam is extracted from the cyclotron. A phase feedback loop ensures the optimal fine setting of the magnet current and also tunes the extraction efficiency and the beam current stability to its optimal values to ensure reliable and stable beam operation. The feedback system utilizes the signal of a non-destructive beam phase detector [4], mounted as the first beam line element. This phase pickup is designed to measure and quantify the effect of beam phase shifts due to magnetic field drifts.

thomas.stephani@varian.com

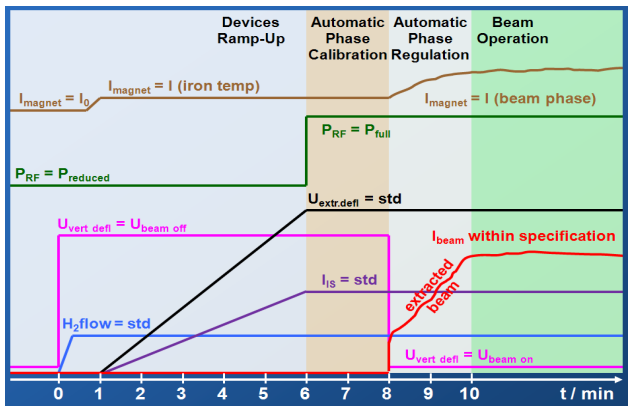

Figure 1: Timing diagram of the transition "RF ready" to "Beam ready".

Using the automatic transition procedures it takes only 10 minutes to extract a quality proton beam starting from the overnight shutdown while only 2 buttons at the control system have to be pressed. It is expected that further optimization of the timing parameters will reduce this startup time to approximately 5 minutes.

AUTOMATED CYCLOTRON OPTIMIZATION

To ensure a stable and reliable cyclotron operation with a minimum of downtime the cyclotron settings have to be optimized after service of major components. Several automatic procedures have been implemented in the control system that enable a fast optimization of the cyclotron.

Automated Beam Centering

Beam centering is one key issue in optimization of the cyclotron performance. Only with a well centered beam a reliable operation is possible and high extraction efficiency can be reached.

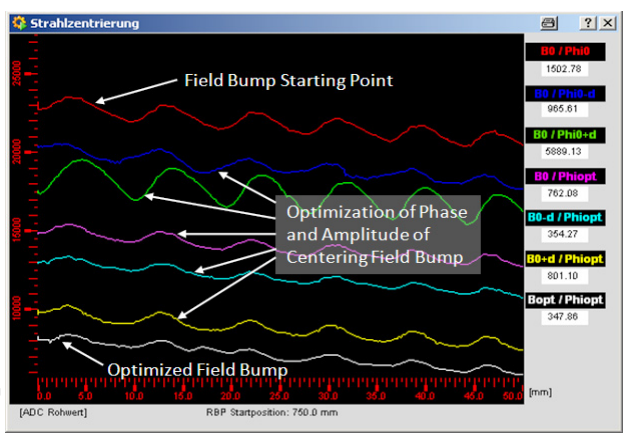

Figure 2: Graphical output display of the automatic beam centering procedure.

The beam is centered by proper positioning of 8 iron trim rods near the center of the cyclotron (inner trim rods). These rods are used to adjust the amplitude and the phase of the first field harmonic which allows minimizing the radial beam precession. A measure of the beam precession is the oscillation of the beam current as measured with a radial probe. The automation procedure takes several probe scans and computes the optimal inner trim rod settings based on these measurements using a dedicated algorithm [3]. Fig. 2 shows a graphical output display of this procedure with the beam current signals for the different scans.

Automated Optimization of the Extraction Efficiency

The extraction efficiency is also automatically optimized. A second set of movable trim rods placed at the extraction radius (outer trim rods) is used to excite some beam precession before extraction in order to increase the turn separation at the two electrostatic deflectors. Together with an automated optimization of the extractor voltages this procedure reliably optimizes the extraction efficiency up to 80% and sometimes above, see Fig. 3.

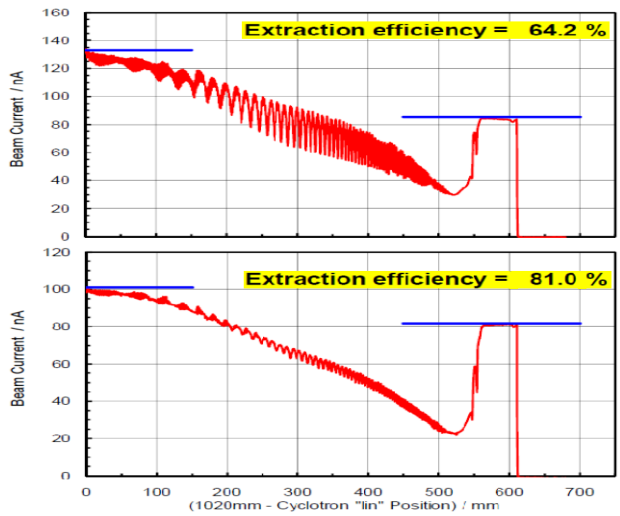

Figure 3: Radial beam probe scan with non-optimized (upper) and optimized (lower) cyclotron settings.

Automated Optimization of the Radial Phase Slit Positions

Internal beam losses can be minimized by proper positioning of two movable phase slits that are used for beam current adjustment during medical operation. A control system procedure measures the beam currents captured by the phase slits with respect to their radial positions. The optimal radial positions for the phase slits are computed and they are positioned automatically by the control system.

AUTOMATED CYCLOTRON CHARACTERIZATION

A predefined set of performance characterizations is recorded on a regular basis. The data are part of the

quality checks and enable prediction of upcoming service actions required to keep the beam quality at the desired level. The following cyclotron characterization measurements are automated in the control system:

- beam current dependence on phase slits positions
- beam current dependence on vertical deflector voltage
- beam current dependence on RF power
- beam phase dependence on magnetic field settings
- plausibility check for current losses on center slits

AUTOMATED CYCLOTRON OPERATION

All the presented procedures help to set up the cyclotron in a well defined state that supports the automated operation of the system.

During medical operation the complete beam handling is managed by a higher level control system including the requests for dedicated beam currents. There are no planned interventions of an operator during the standard operation of the cyclotron after setting up the system.

The maximum beam current for each patient treatment is adjusted by means of two movable phase slits based on an automatically generated look-up table. Beam current adjustment starts by setting the slit widths to defined values. The slits are then opened and allow a precise tuning of the maximal beam current in the range between 1 nA to 800 nA. After the adjustment of the phase slits the dependency of the beam current on the voltage of the vertical deflector is recorded online at the RPTC machine. The complete sequence takes about 20s. Based on this suppression curve later on the beam current can be changed within milliseconds over a wide dynamic range by changing the voltage setting of the vertical deflector during the irradiation. Fig. 4 shows the extracted beam current during an irradiation.

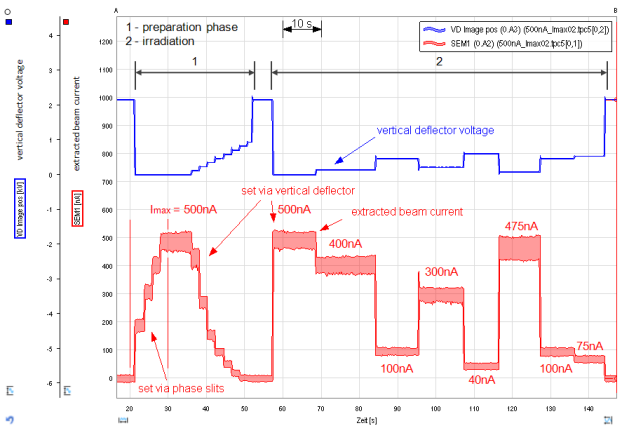

Figure 4: Sequence of the beam current setting procedure.

Fig. 5 gives a more detailed view on the timing behavior when the beam current is changed.

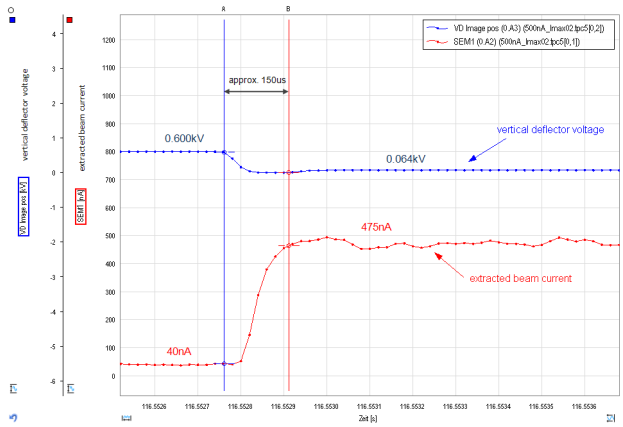

Figure 5: Fast beam current setting using the vertical deflector.

CONCLUSION

We have optimized the accelerator control system to ensure a reproducible and reliable beam operation during daily patient treatment and especially after service actions. The implementation comprises several software routines: an automatic routine for beam centering; an automatic optimization of the beam extraction efficiency; an automatic optimization of the radial positions of the two movable inner phase slits and a fast beam current setting procedure based on an automatically generated look-up table for slit widths and the vertical deflector induced beam suppression.

In addition we have successfully implemented and tested automatic routines for daily startup and regularly system characterization. All these routines have a simple user interface and allow a non-expert operator to perform a morning startup including standard QA procedures. During regular medical operation usually no operator interactions are necessary. As a result, the VARIAN 250 MeV superconducting compact proton cyclotron can be operated as a real “turn-key system”.

REFERENCES

[1] H. Blosser et al., “Proposal for a Manufacturing Prototype Superconducting Cyclotron for Advanced Cancer Therapy”, NSCL internal report MSUCL-874, East Lansing, Mi USA (1993).

[2] A.E. Geisler, J. Hottenbacher, H.-U. Klein, D. Krischel, H. Röcken, M. Schillo, T. Stephani, J.H. Timmer, “COMMISSIONING OF THE ACCEL 250 MEV PROTON CYCLOTRON”, Proc. of 18th Int. Conf. on Cycl. and their Appl., Giardini Naxos, Italy, p. 9-14 (2007).

[3] C. Baumgarten, “Beam Centering Calculation Algorithm”, Internal Report, ACCEL Instruments GmbH, Bergisch Gladbach, Germany (1997, unpublished).

[4] J.H. Timmer, H. Röcken, T. Stephani, C. Baumgarten, A.E. Geisler, “Automated cyclotron tuning using beam phase measurements”, Nucl. Instr. and Meth. A 568 (2006) 532 - 536.

PRESENT OPERATIONAL STATUS OF NIRS CYCLOTRONS (AVF930, HM18)

M. KanazawaA), S. HojoA), A. SugiuraA), T. HonmaA), K. TashiroA), T. OkadaB), T. KamiyaB), Y. TakahashiB, H. SuzukiA), Y. UchihoriA), and H. KitamuraA)
A)National Institute of Radiological Sciences, 4-9-1 Anagawa, Inage, Chiba, Japan
B) Accelerator Engineering Corporation, 2-13-1 Konakadai Inage Chiba Japan

Abstract

Since Japanese government launched a new program of the "Molecular Imaging Research Program" in 2005, the NIRS AVF930 cyclotron has been mainly operated to produce radio-isotopes together with a small cyclotron (HM18) for PET imaging. There are also machine operations of the AVF930 for physical experiments and tests of radiation damage on electric devices. To carry out cyclotron operations for these purposes, some improvements have been done in the facility. In this report, we will present recent operational status of the NIRS cyclotron facility (AVF930, HM18), and its improvement points.

INTRODUCTION

In 1974, operation of the NIRS (National Institute of Radiological Sciences) isochronous cyclotron (AVF930) was started, which was for clinical trial of radio-therapy with fast neutron. Besides this main purpose, production of short-lived radio-nuclides and proton radio-therapy were intended to study. In June 1994, because a new facility of heavy ion accelerator complex of the HIMAC (Heavy Ion Medical Accelerator in Chiba) has started its operation for carbon ion radio-therapy, the fast neutron therapy with the AVF930 had been terminated. In conjunction with start of the HIMAC operation, a new small cyclotron (HM-18 by Sumitomo heavy industry) was installed just beside the AVF-930 as shown in Fig. 1. With the HM18, short-lived radio-isotopes of ^{11}C and ^{18}F are produced to get radio-pharmaceuticals for PET diagnosis before and after carbon ion radio-therapy in the HIMAC. Corresponding this change of situation, the utilization of the AVF-930 also has been shifted to general experiments and radio-isotope productions except for above common isotopes such as ^{11}C, ^{13}N, ^{15}O and ^{18}F. The axial injection system has been installed to provide various kinds of heavy-ions for general experiments, where an ECR ion source with permanent magnets has been equipped. With this ECR ion source, we can supply not only proton but also light ions for cyclotron user.

In 2005, MEXT (Ministry of Education, Culture, Sports and Technology) of Japan launched a new program called the "Molecular Imaging Research Program", and the NIRS was selected as one of centre in Japan. One purpose of this program is the application of imaging technology with PET by use of radio-pharmaceuticals with super-high specific activity. For this purpose, an old RF system of the AVF930 cyclotron has been replaced to a new one for its stable operation[1].

For production of common short-lived radio-isotopes such as ^{11}C, ^{13}N, ^{15}O and ^{18}F, the target stations of C1 and C2 can be used, where the beams are provided from both cyclotrons, but not simultaneously (see Fig. 1). With the AVF930 cyclotron, beam will be transported to target stations of C4 and C9, where radio-nuclides with longer life times will be produced. Physical experiments will be arranged in the target stations of C3, C6, C8, and C10 according its requirements.

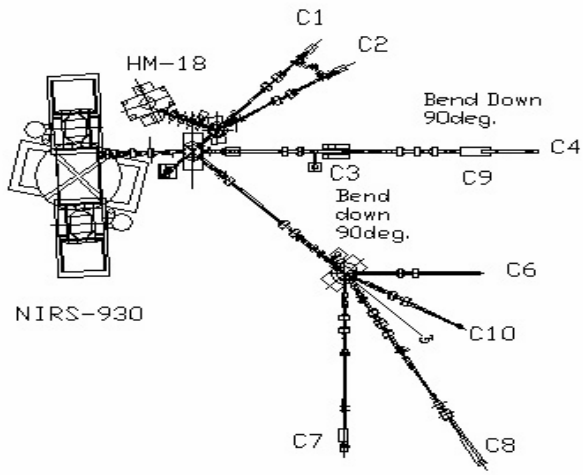

Figure 1: Layout of cyclotrons and beam lines.

OPERATIONS

In annual schedule of the AVF930 and the HM18 cyclotrons operations, there are two maintenance periods, which are planed in March and August with two or three weeks. Weekly maintenance is scheduled in Monday with full and half day every two weeks. Though the main purpose of the AVF930 cyclotron is RI production, there is about one day for general experiments in a week. Daily operations of the AVF930 and the HM18 cyclotrons will start at 9 am until evening. With those operational conditions, annual operation times in recent several years are shown in Fig. 2. Last year, there was no serious break-down in the AVF930 and the HM18, and both cyclotrons could be operated about 1500 hours as scheduled. In 2005 and 2006, operation times were short, which was due to renewal of an acceleration system of the AVF930, where D-electrodes, resonators, RF amplifiers, and control systems have been replaced[1]. With this renewal,

operation of the AVF930 has become stable to supply beam for RI production.

In a control system of HM18, a PC9801 computer of NEC was used to control the devices in the cyclotron by use of UDC's (Unit Device Control), which was a control system made by Sumitomo Heavy Industry. These system was used since 1994, and becoming difficult to repair due to its non-compatibilities of the control computer and the UDC's. Considering these situations, we have replaced the control system of the HM18 together with power supplies and stepping motors in the end of 2007 financial year. In the new system, a personal computer with windows XP is used in a man-machine interface, and PLC's are used to control the each device in the HM18 cyclotron.

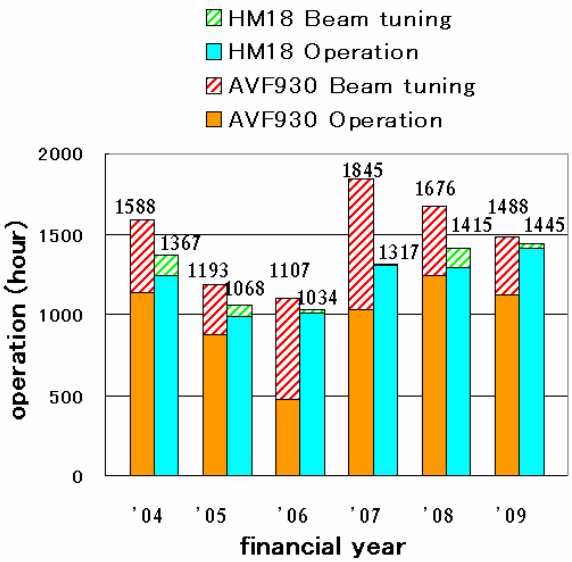

Figure 2: Operation time of the AVF930, and the HM18.

Experimental Fields with the AVF930

Since 2006, largest fraction of the AVF930 machine time was used for RI productions to study PET diagnosis with produced radio-pharmaceuticals. As shown in Table 1, its operation occupied about 37% of AVF930 machine time. Radiation dosimeter developments, physical experiment, radiation damage tests with neutron, biological experiments, and radiation damage tests with proton were also studied as in table 1. If there is requirement for machine operation such as new particle or new energy value, we will test the required operational condition that is classified as "Tuning operation and machine developments".

Beam Energy and Particles in the AVF930 Operation

Accelerated particles and energies in the AVF930 operation are summarized as in Table 2. For the RI production, proton was used, where lower energy proton (lower than 40MeV) was usually required. If there were requirements for higher beam current, we have accelerated H_2^+ beam to increase beam current. For the radiation damage tests, proton energy of 70 MeV was usually selected. In the case of damage test with neutron, deuteron was accelerated up to 30 MeV, and Be target in C3 course was used to generate neutron. Including other experiments, used AVF930 operation times of each energy and particle are summarized as in Table 2.

Table 1: AVF930 operation times for classified fields

RI productions for radiopharamaceutical	547.8h(36.8%)
Studies on radiation dosimeters	329.9h(22.2%)
Physical experiments	124.0h(8.3%)
Studies on radiation damage with neutron	30.4h(2.0%)
Biological experiments	14.8h(1.0%)
Radiation damage tests (Pay experiments)	78.3h(5.3%)
Tuning operation and machine developments	362,3h(24.4%)
Total	1487.5h

Table 2: Particles and energies of AVF930 operation

proton		carbon (6+)		other particles		
energy (MeV)	operation (h)	energy (MeV)	operation (h)	energy (MeV)		operation (h)
80.0	11.5	180.0*	4.0	H_2^+	27.0	288.9
70.0	273.9	156.0*	3.5	H_2^+	28.0	166.0
50.0	9.0	144.0	28.0			
40.0	34.3	120.0	24.5	d^+	30.0	39.6
30.0	163.9	72.0	173.5			
18.0	65.3	48.0	32.8	α	40.0	10.5
16.0	23.0					
12.0	74.0			$^{13}C^{4+}$	104.0	24.3
10.0	26.0			$^{13}C^{4+}$	143.0	11.0
	680.9		266.3			540.3
*』without beam extraction				total time (h)		1487.5

IMPROVEMENTS

Experimental Course of C8

Beam course of C8 is utilized for experiments that require laterally uniform beam distribution. To fulfil this requirement, wobbler magnets are equipped at 3m upstream of target point. These wobbler magnets can rotate beam direction with 12Hz, and we can obtain uniform beam distribution at the target point in combination with aluminium scatterer of 0.18mm thick at upstream of wobbler magnets. Beam uniformity was checked in the experiments with 70MeV proton, and the obtained uniformity of ±5% in the region of ±4cm in lateral direction. With this uniformity of beam distribution, detector tests, biological experiments, and radiation damage tests of electronics have been performed. To control exposure dose more accurately, a beam monitor and a quick shutter have been equipped at the end

of beam line and upstream of wobbler magnets, respectively. This quick shutter can be closed manually, and also with a TTL gate signal. A closing speed was estimate with extra beam quantity after the closing gate signal, and a closing time of 200ms was obtained with this measurement[2].

Though experiments have been performed well, high energy operation has problem recently in a magnetic channel. We could not excite the magnet with required field strength due to increasing cooling water temperature. Replacement to a new magnetic channel[3] is planned in this financial year.

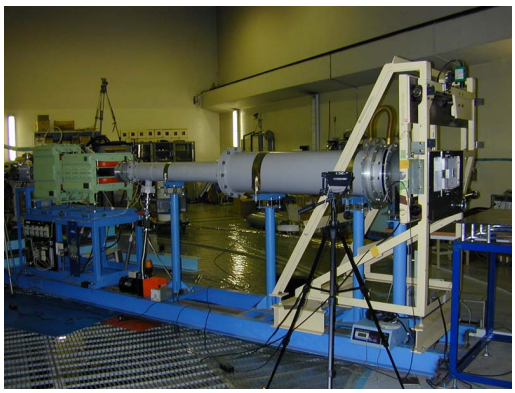

Figure 3: Beam course of C8 for physical experiments with wobbler magnets and scatterer to obtain uniform lateral distribution.

Horizontal Irradiation Course of C4.

The C4 course can be used for metal target irradiation to produce RI, where a robotic system and a target transport system to a hot cell are equipped to produce radio-pharmaceuticals. With this irradiation course, collaborative studies on the usefulness of [^{62}Cu]ATSM for tumor hypoxia imaging had been performed among NIRS, and other three laboratories from 2007 until summer of 2009. Produced ^{62}Zn/^{62}Cu generator, a source of ^{62}Cu for [^{62}Cu]ATSM labelling, has been produced in NIRS and delivered to collaborative laboratories. Production of ^{62}Zn can be achieved by the irradiation with 30 MeV proton beams on natural Cu target via the ^{nat}Cu(p,xn)^{62}Zn reaction. This collaborative study is planed to restart at the end of 2010, and several improvements were taken in this course. First one is installation of quadrupole and stirring magnets (see Figure 4) at the end of this C4 course to adjust beam shape and center easily. Second one is replacement to new target port where a collimator divided in four parts will be equipped to get information of beam position during irradiation. Target cooling is also reinforced with increase of cooling water pressure and good thermal contact by an aluminium target holder.

Other Improvements.

Increase of beam intensity will be desired in several cases. For example, in the operation for ^{62}Zn/^{62}Cu generator production, required irradiation time is 10h (9:00-19:00) with beam intensity of 20μA to use ^{62}Cu-ATSM in four laboratories. After irradiation, chemical process to produce ^{62}Zn/^{62}Cu generator, including purification of ^{62}Zn, filling in generator column and quality control must be performed to ship produced generators at 24:00. If we can supply higher beam intensity, operation schedule of the cyclotron become flexible and easy to manage with shorter irradiation time. For this purpose, a single gap buncher with higher harmonic waves in an injection line is planned to install[4]. With this new buncher, we expect better bunching ratio and extraction efficiency, with which we can increase the beam current on the target.

Figure 4: Horizontal irradiation course of C4 without target station.

To reduce residual radiation level in the cyclotron facility, we have replaced a beam shutter that is made of a copper plate. New one is a Faraday cup that has a cooled graphite of 10mm thick and a cupper plate of 0.2mm thick at entrance. With this structure, proton of lower energy than 47 MeV can be stopped in the graphite. This choice of the graphite thickness is practical because high intensity proton operation is usually with lower energy than 40MeV.

Replacement of a control system for the injection line is undergoing, where a PLC will be used instead of current potentiometers.

ACKNOWLEDDDGMENTS

The authors would like to express their thanks to members of the Div. of Accelerator Physics and Engineering at NIRS for helpful discussions and also their supports in cyclotron operations of the AVF930 and the HM18.

REFERENCES

[1] T.Honma et al., Proc. Of 18th Int. Conf. on Cyclotrons and their Applications 2007, Oct. 1-5, Giardini Naxos, Italy, p137-139.
[2] H.Kitamura, Annual report of NIRS cyclotrons 2009.
[3] S.Hojo et al., in this conference.
[4] A.Sugiura et al., Annual meeting of Particle Accelerator Society of Japan, Himeji-shi, 2010.

DESIGN OF RF SYSTEM FOR COMPACT AVF CYCLOTRON*

J.H. Oh, B.N. Lee, H.W. Kim, J.S. Chai#
Accelerator and Medical Engineering Lab. , SungKyunKwan University, Suwon, 440-746, Korea

Abstract

RF system is one of the most important parts for producing good and efficient accelerator system. The ion beam will be derived by a K100 SSC (Separated-Sector-Cyclotron). 8 MeV SF(Sector-focused) Cyclotron which produces 8 MeV proton beam is used as injector of K100 SSC cyclotron. In this paper, we designed RF system including RF cavity. The total specification of system is on the following. The frequency of this RF system is 70 MHz coaxial type cavity. Also we applied 4th harmonic, dee voltage of 50KV. We simulated the RF system using commercially available simulator, CST Microwave studio.

INTRODUCTION

A design research about RF system of 8MeV cyclotron was recently conducted. This cyclotron produce 1 mA proton beams at 8 MeV for K100 SSC. The high-intensity beam will be derived to SSC of above 1 mA. Then this extracted beam of this cyclotron goes to ISOL target

This paper mainly describes a development study of 8 MeV injector Sector-Focused cyclotron RF system. RF system is designed to have a few thousand of Q value with resonance frequency of 74.33MHz which based on the magnet design. Because of the limitation caused by magnet, we satisfied the condition of λ/2 by adjusting stem, liner, gap of Dee and so on. H^- particles having 24KeV for average energy are safely supplied in middle plane of poles through inflector and accelerated from central region by 50KV Dee voltage. Then accelerated particles having same angular frequency by isochronous magnetic field are ejected from final extraction stage with 8MeV energy. 3D modelling process was done by 3D CAD system, CATIA P3 V5 R18 [1] and analyzed by CST-MWS. By repeating this process, we completed the fully satisfied design.

RF SYSTEM DESIGN

The RF system has total 4 vertical stems. [2] Before designing this RF system, magnet design was preceded. Almost parameters of whole size are decided from magnet design. Material of RF Cavity is OFHC copper to get electric conductivity better and not affect magnetic field intensity. OFHC copper (model name : NBM C11000) has good electric conductivity($5.91\times10^7 S/m$) compare with electric conductivity of normal copper ($5.8\times10\ \ S/m$) .

Dee angle is 40° which is located both of valleys. Total length of each dee is about 30cm. Cavity is coaxial type which has λ/2 resonant mode:

$$\lambda = \frac{c}{f} \tag{1}$$

Where c is the light velocity and f is frequency of RF system. Supposed resonance frequency of RF system is 70MHz, the wavelength, λ, is 4.28m. We set the length of whole inner conductor to half-wave length for resonance mode of λ/2. Based on this, the length of the stem which becomes an inner conductor is set to 36.5 cm.

This value, 36.5 cm, is applied for magnet design and the length of inner conductor approaches to 2.14 m, the value of half-wave length through 4 stems.

The radius of outer conductor is 40 cm based on the size of magnet. Liner is designed to have 39 cm height along the valley gap and exactly fit into the valley. Then the outer conductor which has 7.5 cm for radius is constructed by a hole in the valley of magnet. Particles are accelerated in E-field formed by two 5cm length dummy dees attached at both sides of outer conductor.

Table 1: Specification of RF system for 8MeV Cyclotron

Parameters	Values
Resonant Frequency	74.33MHz
Harmonic Number	4^{th}
Dee Voltage	50kV
Resonant mode	λ/2
Material	OFHC Copper
Pole radius	0.40 m
Hill/Valley gap	0.03 / 0.39 m
Dee angle	40°
Number of Sector/Dee	4 / 2

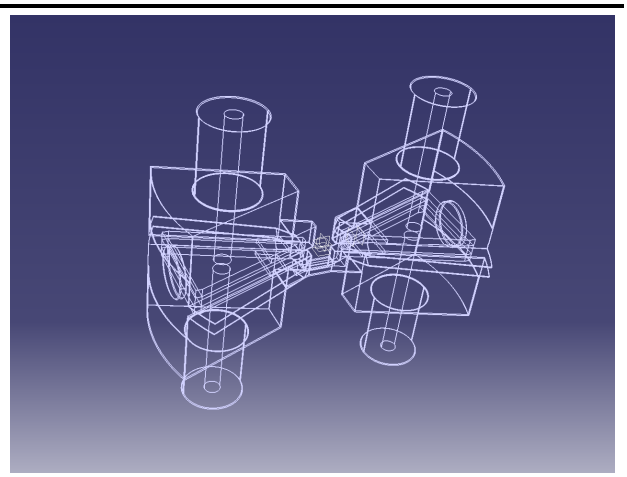

Figure 1: Wireframe of RF cavity basic model

*Work supported by Ministry of Education, Science and Technology, Republic of Korea and Department of Energy Science and School of Information and Communication Engineering of SungKyunKwan University
#jschai@skku.edu

RF SYSTEM SIMULATION

CST Microwave studio is one of special tool for 3D electromagnetic of RF system. [3] It can show E-field and H-field in the 3-dimensional. To optimize 70MHz RF frequency, various method is used. Especially, the stem position and shape is a primary key to decide resonant frequency and field distribution.

We suppose that the frequency is strongly influenced by the thickness of stem. Besides, it also affects Q value so the optimization of stem thickness is very important. If thickness of stem is so thin, the stem would be melted by RF power and Q value is decreased.

On the contrary to this, the frequency becomes higher with thick stem.

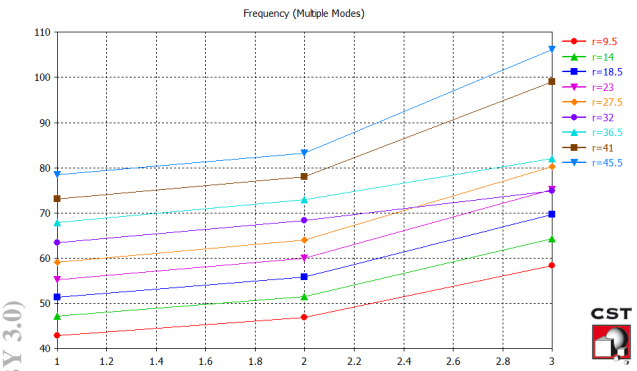

Figure 2: Frequency range following the radius of stem.

In Figure 2, vertical axis is resonance mode at each frequency and horizontal axis is RF frequency (MHz). The 'r' is radius of vertical stem. In this study, mode 3 is chosen due to suitable field distribution. So we optimized the stem figure and location as shown in Figure 3.

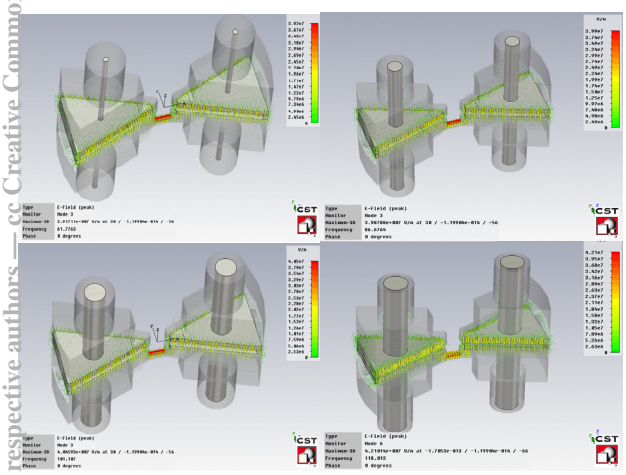

Figure 3: Frequency optimizing process.

By an optimization process, the radius of stem was decided to 2cm and the electric and magnetic field of final model was shown in Figure 4,5.

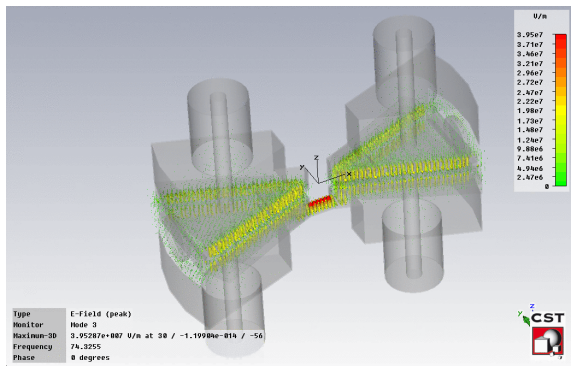

Figure 4: Electric field distribution.

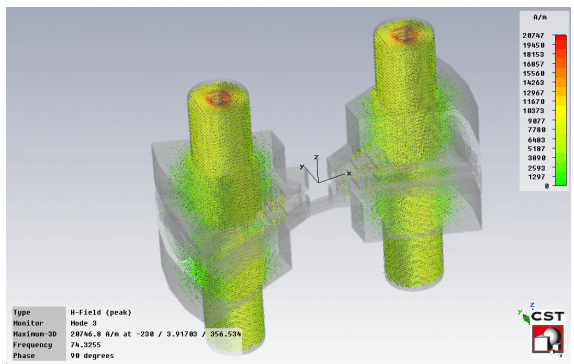

Figure 5: Magnetic field distribution

The resonant frequency of this RF system is 74.33MHz. H^- particles are accelerated by E-field direction which occurred to dee from dummy dee or opposite direction. A marginal error of frequency with targeted value can be adjusted by fine tuner.

We can calculate the Q value of resonant mode using Micro Wave Studio, CST. The equation for the calculation is shown below. [4]

$$Q = \frac{2\pi \cdot Stored\_Energy}{Energy\_Consumed\_per\_period} = \frac{2\pi \cdot f \cdot W}{P_{rms}} \quad (2)$$

Applying the method, the Q value of this RF resonator calculated by MWS is 5981.

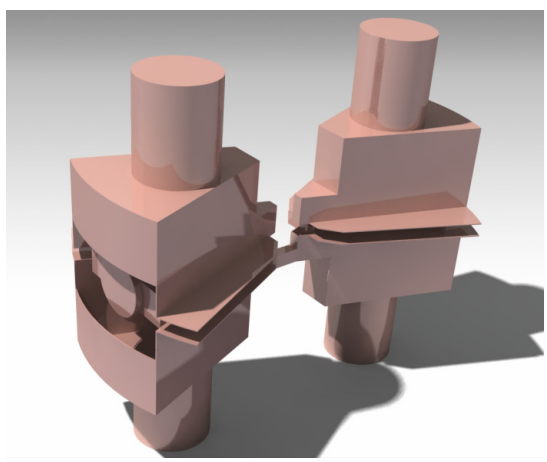

Figure 6: Final RF cavity design using CATIA V5

SUMMARY

This paper has explained the features of 8 MeV injector cyclotron RF cavities. we could acquire the optimal Q value and resonant frequency after iterated simulation many times. Designed cavity has proper RF frequency and Q value. Marginal error of RF frequency will control by RF tuner next process. It is expected that full conception design of 8 MeV cyclotron, included magnet, RF system ,etc, will be finished in November,2010

REFERENCES

[1] Dassualt Systems, FR.
[2] I.S. Jung, “Design of the RF SYSTEM FOR A 30 MeV Cyclotron”, EPAC’06, June 2006, Edinburgh, WEPCH080.
[3] Computer Simulation Technology, Germany, http://www.cst.de.
[4] C.Pagani, “Cyclotron Cavities”,CERN 92-03, CAS, April 1991, Oxford, UK

CONSTRUCTION OF NEW INJECTOR LINAC AT RIBF

K. Yamada*, S. Arai, M. Fujimaki, T. Fujinawa, H. Fujisawa, N. Fukunishi, A. Goto, Y. Higurashi, E. Ikezawa, M. Kase, M. Komiyama, K. Kumagai, T. Maie, T. Nakagawa, J. Ohnishi, H. Okuno, N. Sakamoto, Y. Sato†, K. Suda, H. Watanabe, T. Watanabe, Y. Watanabe, Y. Yano, S. Yokouchi, and O. Kamigaito,
RIKEN Nishina Center, Wako, Saitama 351-0198, Japan

Abstract

A new injector linac called RILAC2 has been constructed in order to enable the independent operation of the RIBF experiments and super-heavy element synthesis. Construction of the RILAC2 started at the end of FY2008. The RFQ linac and three DTL tanks were installed in the AVF-cyclotron vault and the excitation of rated voltage have succeeded. Two rebunchers are in fabrication and alignments of LEBT and HEBT are performed now. We plan to start the beam commissioning in December 2010.

INTRODUCTION

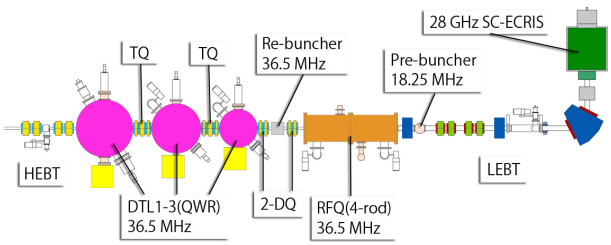

Figure 1: Schematic-layout view of the RILAC2.

A new additional injector linac called RILAC2 has been constructed at the RIKEN Nishina Center for performing independent RIBF [1] experiments and super-heavy-element synthesis [2]. As shown in Fig. 1, RILAC2 consists of a 28-GHz superconducting ECR ion source (SC-ECRIS) [3], a low-energy beam transport (LEBT) [4] with a pre-buncher, a four-rod RFQ linac, three drift-tube linac tanks (DTL1-3), a rebuncher between the RFQ and DTL1, a high-energy beam transport (HEBT) from the DTL3 to the RIKEN Ring Cyclotron (RRC) [5], and strong quadrupole magnets between the acceleration cavities for transverse focusing. Another rebuncher is located at the HEBT to focus the longitudinal phase spread at the injection of RRC by a combination of the rebuncher and an existing rebuncher. Very heavy ions with mass-to-charge ratio (m/q) of 7, such as $^{136}Xe^{20+}$ and $^{238}U^{35+}$, are accelerated up to an energy of 680 keV/u in the cw mode and injected into the RRC without charge stripping. The rf resonators excluding the pre-buncher are operated at a fixed rf frequency of 36.5 MHz, whereas the pre-buncher is operated at 18.25 MHz. The basic design of the RILAC2 was finished in 2006 [6] and the construction has started since the budget was approved at the end of FY2008. We decided to relocate the SC-ECRIS, which was originally fabricated for the existing linac called RILAC and tested in the RILAC, to a new room for the ion source of RILAC2. Other equipments for the RILAC2 are placed in the existing AVF-cyclotron vault. This article mainly presents the details for the construction of linac part.

* nari-yamada@riken.jp
† Present affiliation is KEK.

CONSTRUCTION OF RF CAVITIES

RFQ Linac

To save construction cost, we decided to recycle a four-rod RFQ linac which was originally developed by Nissin Electric Co., Ltd. in 1993 [7] for ion implantation. In November 2007, the RFQ system was transferred to RIKEN through the courtesy of Kyoto University. The RFQ linac can accelerate heavy ions with an m/q of 16 up to 84 keV/u in the cw mode with an rf frequency of 33.3 MHz. The maximum rf input power was designed to be 50 kW(cw). If the RFQ resonator is so modified to have a resonant frequency of 36.5 MHz, ions with an m/q of 7 can be accelerated to 100 keV/u for RILAC2 without changing the vane electrodes. The intervane voltage required for RILAC2 is 42 kV, which is less than the originally designed value of 55 kV. The basic parameters corresponding to the RFQ linac after the conversion are listed in Table 1; the parameter values were obtained by scaling the original values.

For modification of the resonant frequency, we inserted a block tuner into the gaps between the posts supporting the vane electrodes. The size of the block tuner was optimized by 3D electromagnetic calculations using the computer code Microwave Studio 2009 (MWS) and rf measurements using cold-model test pieces made of aluminum. The rf power required to excite the intervane voltage of 42 kV was evaluated to be 17.5 kW by taking into account 80% derating of the shunt impedance (63 kΩ) determined by the MWS calculation.

The heat load distribution was also evaluated by MWS calculations to decide the cooling conditions. The Maximum current density in the block was 32 A/cm, which was very small. The total heat load estimated for the five blocks was approximately 2.1 kW. The size of the cooling

Table 1: Basic parameters corresponding to RFQ linac.

Frequency (MHz)	36.5
Duty (%)	100
m/q ratio	7
Input energy (keV/u)	3.28
Output energy (keV/u)	100.3
Input emittance (mm·mrad)	200π
Vane length (cm)	225.6
Intervane voltage (kV)	42.0
Mean aperture (r_0:mm)	8.0
Max. modulation (m)	2.35
Focusing strength (B)	6.785
Final synchronous phase (deg.)	-29.6
Unloaded Q	4500 (MWS)
Shunt impedance (kΩ)	63 (MWS)
Required rf power (kW)	17.5 (80%-Q)

water channel was so chosen that the flow rate of water was approximately 16 L/min; at this flow rate, the water temperature increases only by 2 °C. The cooling capacity was found to be sufficiently high if the value of the shunt impedance degraded to 70%.

The block tuner was made of oxygen-free copper; three types of blocks were required by the mounting position. Intricate cutting was carried out on the block in order to reduce the weight of block to half the original value. The blocks were mounted on a base with an rf contact provided by coil springs. The water channels in the blocks were connected in series by copper pipes. Figure 2 shows the internal structure of the RFQ linac after mounting the block tuner and water pipe.

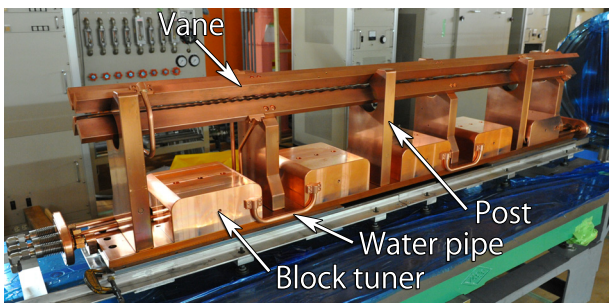

Figure 2: Internal structure of RFQ after mounting the block tuner.

Figure 3 shows the present aspect in the AVF vault. A low-power test was performed to evaluate the rf characteristics, and the resonant frequency was found to be changed to 36.5 MHz successfully. Vacuum level reached 8×10^{-6} Pa with the cooling-water flow. After the electric-wire and water-pipe connection, high power test was performed in August 2010, and the excitation with rated voltage of 42 kV has been achieved successfully.

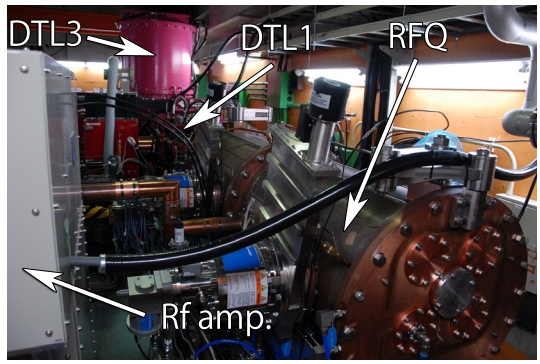

Figure 3: RILAC2 located in the AVF vault. DTLs can be seen behind the RFQ.

Drift-tube Linac

The structure of DTLs is based on a quarter-wavelength coaxial-cavity resonator. Table 2 shows the design parameters of DTLs. The cavity dimensions were determined by MWS calculations to optimize the rf characteristics. Figure 4 shows a DTL1 model used in the MWS calculation. The distribution of rf-power dissipation in the cavity was also evaluated by the MWS calculations to determine the amount of cooling required.

Table 2: Design parameters of three DTL tanks.

	DTL1	DTL2	DTL3
Frequency (MHz)	36.5	36.5	36.5
Duty (%)	100	100	100
m/q ratio	7	7	7
Input energy (keV/u)	100	220	450
Output energy (keV/u)	220	450	680
Cavity diameter (m)	0.8	1.1	1.3
Cavity height (m)	1.32	1.43	1.89
Gap number	10	10	8
Gap length (mm)	20	50	65
Gap voltage (kV)	110	210	260
Drift-tube aperture (mm)	17.5	17.5	17.5
Peak surface field (MV/m)	8.9	9.4	9.7
Synchronous phase (deg.)	-25	-25	-25
Max. power of amp. (kW)	25	40	40

In order to reduce the construction cost and the space occupied by the equipments, a direct coupling scheme was adopted for the rf amplifier. A plate electrode of a 4CW50000E vacuum tube was directly connected to the capacitive coupler, which was mounted on the cavity. The load impedance of the vacuum tube can be adjusted by changing the position of the coupler electrode. When the coupler and vacuum tube were mounted on the cavity, the resonant frequency decreased because of their series/parallel capacitance. Thus, we had to set the target frequency of the cavity such that this decrease in the resonant frequency was compensated. The decrease in the resonant

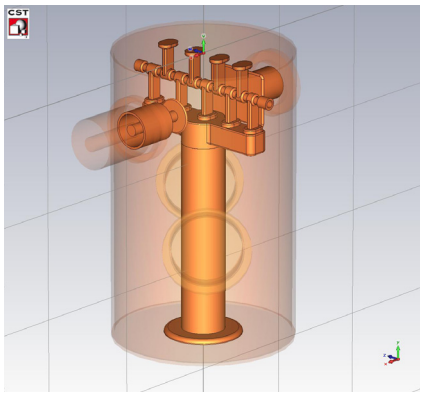

Figure 4: A DTL1 model used in the MWS calculation; the model includes a tuner and coupler.

frequency was estimated by comparing the result of MWS calculations with the measurement results obtained using the DTL3 with a 50-Ω coupler. Since the DTL3 was obtained by modifying a decelerator resonator that was developed for a Charge-State-Multiplier system [8], we were able to use it for the comparison. For example, the cavity length of DTL1 was determined to actualize the target frequency of 36.725 MHz. The coupler was designed such that the load impedance could be adjusted to approximately $1000 + j0\ \Omega$ with using vacuum tube. The default position and radius of the coupler electrode were determined by the MWS calculation using a frequency-domain solver.

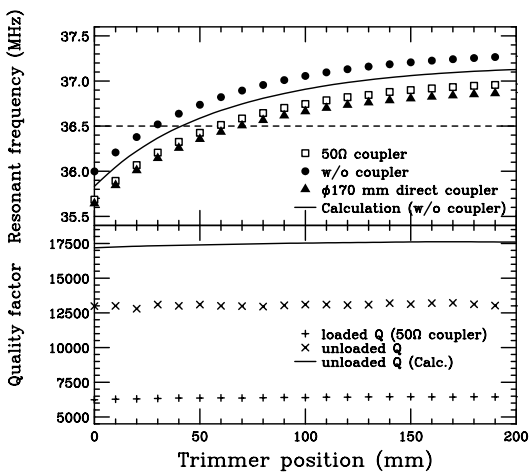

Figure 5: Frequency response of DTL1 as a function of trimmer position.

The results of the low-power test measurements for the DTL1 carried out using a network analyzer are indicated in Fig. 5. The frequency response as a function of trimmer position is plotted in the upper panel of Fig. 5. The lower panel presents the quality factors. As shown in the figure, an operation frequency of 36.5 MHz was achieved at the trimmer position of 68 mm by using a ϕ 170 mm direct coupler for the DTL1, that is consistent with the estimation by MWS calculation. The load impedance can be adjusted from 600 to 1300 Ω for the DTL1 by moving the coupler electrode over a distance of 40-mm. The electric-field distribution along the beam axis was measured using a ϕ 12 mm TiO_2 bead by the perturbation method. The shunt impedance was evaluated from the integral of the result, and the required rf power was determined. The rf characteristics of DTLs are listed in Table 3.

Table 3: Measured rf characteristics of DTLs.

	DTL1	DTL2	DTL3
Unloaded Q	13000	20350	22500
Shunt impedance (MΩ)	0.94	1.65	1.72
Effect. shunt imp. (MΩ/m)	135	176	102
Required rf power (kW)	6.5	13.4	19.6

A high-power test was performed with a load impedance setting of 700-1000 Ω depending on the tank. After one day of conditioning, the rated voltages were successfully achieved for every tank. Further conditioning and re-tunes to improve the long-term stability are performed now.

Rebuncher

The structures of rebunchers are also based on the quarter-wavelength cavity resonator with four gaps. The total required voltage of the rebuncher between the RFQ and DTL1 is 100 kV, which is driven by a 1 kW transistor amplifier. The cavity is now in fabrication and it will be installed in November 2010. For the rebuncher in HEBT, total 200 kV is required and a 3 kW transistor amplifier is used. It is now in mechanical design and will be installed in January 2011. Low-level circuits, power amplifiers, and control systems are ready.

OUTLOOK

The 28-GHz SC-ECRIS has been installed and cooled. Beam test will be performed before long. The LEBT and HEBT have been installed in the AVF vault and being aligned to the beam line now. Beam diagnosis and control system are also in preparation. We plan to start the beam commissioning of RILAC2 in December 2010.

REFERENCES

[1] Y. Yano, Nucl. Instr. Meth. B 261 (2007) 1009.
[2] K. Morita et al., J. Phys. Soc. Jpn. 73 (2004) 2593.
[3] T. Nakagawa et al., Rev. Sci. Instrum. 79, 02A327 (2008).
[4] Y. Sato et al., Proc. of PASM6, FOBTA01, (2009) 801.
[5] Y. Yano, Proc. 13th Int. Cyclo. Conf., 102 (1992).
[6] O. Kamigaito et al., Proc. of PASJ3-LAM31, WP78, (2006) 502.
[7] H. Fujisawa, Nucl. Instrum. Meth. A 345 (1994) 23.
[8] O. Kamigaito et al., Rev. Sci. Instrum. 76, 013306 (2005).

BEAM EXTRACTION SYSTEM DESIGN FOR CYCIAE-14

Sumin Wei, Ming Li, Tianjue Zhang, Shizhong An, Huaidong Xie, Tao Cui, Weiping Hu,
Jiuchang Qin, Zhiguo Yin, Yinlong Lu, Lipeng Wen, Jiansheng Xing
China Institute of Atomic Energy, Beijing, 102413, P.R. China

Abstract

A 14MeV medical cyclotron is under design and construction at CIAE (China Institute of Atomic Energy). H^- ion will be accelerated in this cyclotron and proton beam will be extracted by carbon strippers in dual opposite direction. Two stripping points are chosen in each extracting direction to extract proton beams to different targets to extend the use of the machine and the stripping points can be selected only by rotating the stripping foil. Two modes have been considered of the extraction system, one is designed to be installed on the wall of the vacuum chamber, the other is designed to be inserted vertically from the sector poles. Final choice will depend on the agility, the simpleness and the results of the experimentation. The angle between the stripper and the beam orbit is optimized to improve the extracted beam quality. Numerical simulation shows the two stripping points, the beam orbit and the beam characteristic at each extraction direction. The optimized azimuth of the stripper is also presented in this paper to show its influence for the beam quality. Based on the concept design, the mechanical design and the correlative experimentation have been done; the results are shown in the paper.

PACS: 29.20.HM CYCLOTRON;
Key words: cyclotron, proton beam, extraction system, stripping foil

INTRODUCTION

Since the incidence of cancer and cardiovascular disease is increasing, the domestic demand for PET cyclotrons in China is increasing rapidly. For productions of medical radioactive isotope, a compact cyclotron is under design and construction at CIAE. H^- ion is accelerated up to 14MeV in this machine. Except the radioactive isotopes usually produced by PET cyclotrons such as ^{18}F and ^{201}Tl, this cyclotron is also designed to produce the isotopes that usually produced by reactors such as ^{99}Tc, so the intensity of the extracted proton beam is up to 400 μA. In most PET cyclotrons, stripping method is used [1, 2] for high extraction efficiency. CYCIAE-14 [3] will use carbon foils to extract proton beam in dual opposite direction. In each extraction direction, two beams are extracted to extend the use of the machine, as shown in figuer 1: in primary design, the beam 2 is to hitting the liquid target directly for ^{18}F production, the beam 1 is to be sent to a beam line to hit the solid target to produce medical radioactive isotope such as ^{124}I and ^{201}Tl. Two stripping points in each extracted direction can be selected only by rotating the stripping foil to allot beam to different target or beam line easily.

For the cyclotrons whose extraction energy can be changed, the combination magnets are necessary in the extraction region. But for most PET cyclotrons with single extraction energy, there is no combination magnet, as shown in figure 1.

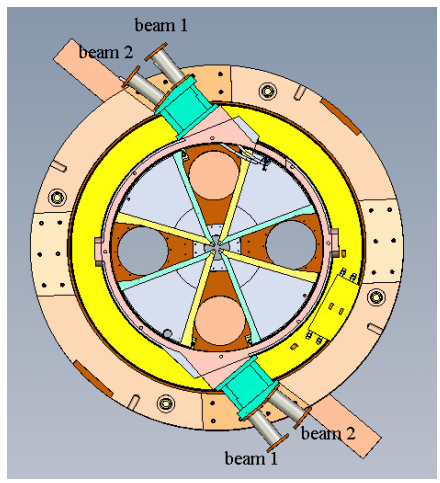

Fig.1 The extracted proton beams of CYCIAE-14

Two types of mechanical design for extraction system have been accomplished, one is designed to be installed transversely on the vacuum chamber and the other one is vertically from the sector poles, the design and the corresponding experimentation are also shown in this paper.

STRIPPING POINT AND THE BEAM DISTRIBUTION

Stripping Points on Each Direction

There are two stripping points in each extraction direction to allot proton beam to different targets, they can be calculated under the affirmatory magnetic field and target. Table 1 shows the radius and angles of two points in one direction, in which the point 1 is the right one shown in figure 1, they are calculated by using the code GOBLIN [4].

Table 1 Stripping points of CYCIAE-14

Points	Radius/ cm	Angle/ deg
1	45.69	57.09
2	45.22	61.38

weisumin@tsinghua.org.cn

Beam Distribution

Beam distribution on the foil have been calculated by using the code COMA and shown in figure 2 (left pictures in figure 2), only the beam 1 has been selected as an example.

GOBLIN is a common particle tracking computer code, with the help of the TRIUMF scientists, CIAE had been extended the function of this code, new subroutine had been added to calcualte the transfer matrix from stripper to the combination magnet. The upgraded code had been used for extraction optics simulation of several cyclotrons in CIAE. CYCIAE-14 also use this upgraded code to calculate the extraction optics. With the affirmatory magnetic field, the transfer matrix including the dispersion forms the stripping foil to the outside of the return yoke (about 70 cm after stripping foil) had been obtained and shown in the next section. The particles distribution outside of the return yoke then can be obtained by matrices multiplication, also shown in the right pictures of figure 2. The horizontal beam dimension increased from 4 mm to about 10 mm without any focusing elements.

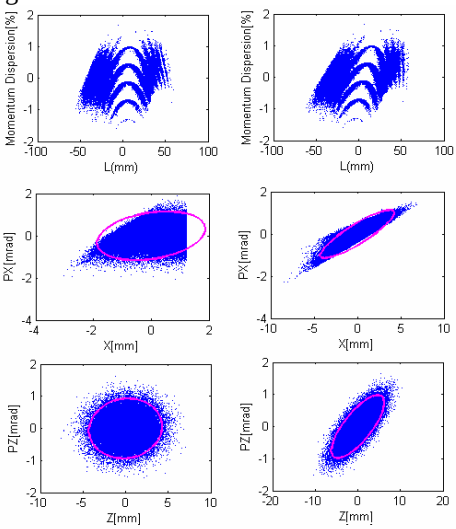

Fig.2 Beam distribution on the foil and out of the return yoke

TRANSFER MATRIX, DISPERSION AND THE BEAM CHARACTER IN EXTRACTION REGION

Transfer Matrix and Dispersion in Extraction Region

Through the fringe field of the main magnet, the transfer matrix with dispersion of the two extracted beams can be obtained [5]. Take the extracted beam 1 as an example, its transfer matrix is shown in table 2. The elements R_{16} and R_{26} in the matrix are the dispersion in mm/% and mrad/%, it is indicate that for the extracted beam 1, a momentum dispersion of 0.5% may bring a 1.36mm displacement of the beam in horizontal plane out of the return yoke, as shown in figure 2, form the foil to the outside of the return yoke, the beam distribution in horizontal plane is changing from 4 mm to almost 10 mm.

Table 2 the transfer matrix from stripping foil to the outside of the return yoke of beam 1

$$\begin{bmatrix} 0.1078 & 0.6350 & 0 & 0 & 0 & 2.7191 \\ -1.4257 & 0.8767 & 0 & 0 & 0 & 4.2401 \\ 0 & 0 & 1.0592 & 0.7240 & 0 & 0 \\ 0 & 0 & 0.1370 & 1.0377 & 0 & 0 \\ -0.4334 & -0.0310 & 0 & 0 & 1 & 6.8540 \\ 0 & 0 & 0 & 0 & 0 & 1 \end{bmatrix}$$

Beam Character

By using the code GOBLIN and COMA, the beam distribution on the foil and the transfer matrix along the extracted beam orbit can be obtained. Then the beams envelop and the emittance can be got by multiplying these matrices. The envelop from the foil to the target are shown in figure 4, and he figure 3 shows the transverse emittance, the emittance will increased a little in the horizontal plane because of the dispersion, and keeped constant in the vertical plane.

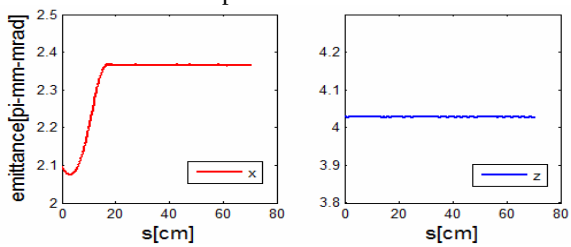

Fig.3 Emittance of the extracted beam

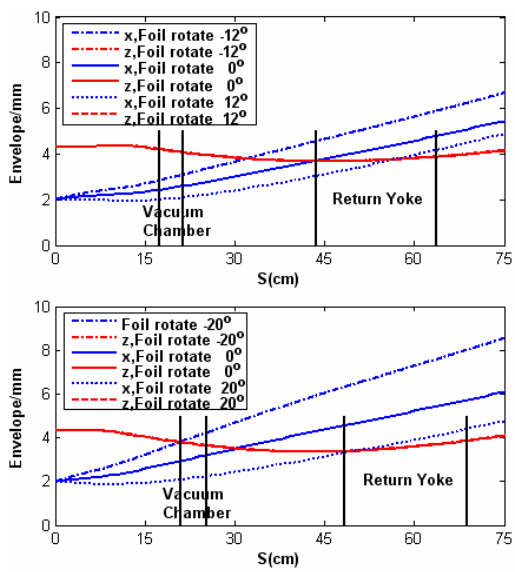

Fig.4 Beam envelope with and without foil rotate (upper:beam 1, nether: beam 2)

Usually the stripping foil is perpendicular to the beam orbit, when rotating the foil for a small angle, the extracted beam envelop will be changed in radial direction, just like the edge angle of a dipole magnet.

Numerical simulation shows that the horizontal envelop changes sensitively to the rotating angle, but the vertical envelop almost the same. Figure 4 shows the beam envelop with and without a rotating angle of the two extracted beam, from which we can see that the envelop in horizontal plane can be optimized by this angle. Beam 1 is transported to beam line and will be focused by quadrupoles out of the return yoke as soon as possible; beam 2 will hit the liquid target directly inside the return yoke. For this calculation, the initial emittance of the two beam are 4 π mm·mrad, usually the emittance of the injected beam is better than 4 π mm·mrad, so we can adjust the beam spot as Φ8mm, if various beam sizes are needed, then we can adjust the foil angle, as shoen in figure 4.

MECHANICAL DESIGN AND EXPERIMENTATION

Two mechanical types of extraction system have been designed based on the optics simulation mentioned above. Figure 5 shows the two types, the upper one is designed to be installed transversely on the vacuum chamber; the nether one is vertically from the sector poles.

The transverse one which is installed on the vacuum cavity wall is drove by motor, the motor and the potentiometer used for feedback are put between the main coils, in where the magnetic field is about several hundreds Gauss. The experiment of the DC motor and the step motor working in the magnetic field had been carried out, the results shows that the DC motor can still work at the field of 2000 G normally, but when the field is above 620G, a 1.5 Nm step motor stop working.

The advantages of the transverse one are: 1) the foil can be rotated to the stripping point easily only by using a motor; 2) no need to drill the pole, so the isochronous field would not be broken. The disadvantages are: 1) the potentiometer can't be installed directly on the rotating axes of the stripping foil, so the control precision can't be so high; 2) this configuration is hard to water-cooling.

The advantages of the vertical one are: 1) the foil can be rotated to the stripping point easily, too; 2) can be water cooled easily; 3) the potentiometer can be installed directly on the rotating axes of the stripping foil; 4) the motor and the potentiometer are out of the magnetic field and the radiant field. The disadvantages are: 1) needed to drill on the pole, which means to influence the isochronous field.

For CYCIAE-14, the extracted proton beam intensity is up to 400 μA, water-cooling for the extraction system is necessary, so the vertical type is selected as the final design. Now this system is under manufacturing based on the design above. But for those PET cyclotrons with low extraction intensity, the transverse one can be used too.

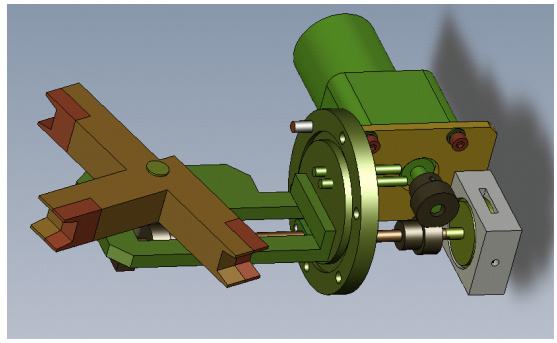

a) transverse type

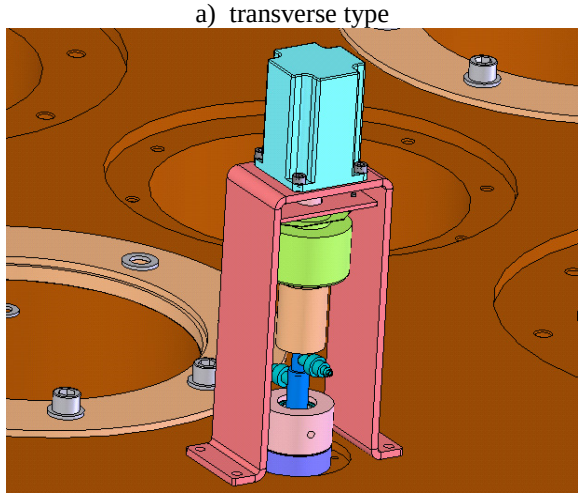

b) vertical type

Fig.5 Mechanical design of extraction system for CYCIAE-14

CONCLUSION

The extraction system of a 14 MeV PET cyclotron have been designed and is under machining, the proton beam is extracted in dual opposite direction by using carbon foil. In each extraction direction, two beams are extracted only by rotating the foil to allot beam to different target or beam line. The stripping points, particles distribution, beam envelop and transfer matrix are calculated. Two types of mechanical design are carried out and the vertical one is selected as the final design. Now this system is under manufacturing based on these design.

REFERENCES

[1] Alexandr Papash, TR13 cyclotron extraction studies, TRI-DN-93-5

[2] CERN Accelerator School Cyclotrons, Linacs and their Applications, (CERN96-02),1996

[3] Tianjue Zhang, Overall Design of CYCIAE-14, a 14MeV PET Cyclotron, to be published.

[4] B.F.Milton, GOBLIN User Guide and Reference V3.3, TRI-CD-90-01

[5] Sumin Wei, Shizhong An, et al., beam optics study on the extraction region for a high intensity compact cyclotron, PAC 09, Vancouver, 2009

FACILITY FOR MODIFICATION AND ANALYSIS OF MATERIALS WITH ION BEAMS (FAMA)*

A. Dobrosavljević#, P. Beličev, V. Jocić, N. Nešković, I. Trajić, V. Vujović, Lj. Vukosavljević,
Laboratory of Physics, Vinča Institute of Nuclear Sciences, Belgrade, Serbia

Abstract

The facility for modification and analysis of materials with ion beams (FAMA) is the low energy part of the TESLA Accelerator Installation, in the Vinča Institute of Nuclear Sciences, Belgrade, Serbia. It presently comprises two machines: a heavy ion source (M1) and a light ion source (M2), and two experimental channels: a channel for analysis of ion beams (C1) and a channel for surface modification of materials (C2).

In April 2009 the Vinča Institute signed a contract with the Joint Institute for Nuclear Research, Dubna, Russia, on the upgrading of FAMA. The contract comprises: (i) the refurbishment of the M1 and M2 machines and the C1 and C2 channels, (ii) the construction of a channel for surface physics (C3) and a channel for deeper modification of materials (C4), (iii) the construction of a small isochronous cyclotron (M3), and (iv) the construction of a channel for analysis of materials in vacuum (C5) and a channel for analysis of materials in air (C6). This presentation is devoted to the upgraded FAMA and its research program.

PRESENT STATUS OF FAMA

The facility for modification and analysis of materials with ion beams (FAMA) is the low energy part of the TESLA Accelerator Installation (TAI), in the Vinča Institute of Nuclear Sciences, Belgrade, Serbia. It has been used by several user groups performing experiments in different basic and applied research projects. FAMA presently comprises two machines and two experimental channels: a heavy ion source (M1), a light ion source (M2), a channel for analysis of ion beams (C1) and a channel for surface modification of materials (C2). Fig. 1 gives a scheme of present FAMA without M2 machine.

The M1 machine is an ECR ion source providing different kinds of multiply charged ions from gaseous and solid substances [1]. It operates at 14.5 GHz, while the maximal extraction voltage is 25 kV. This machine was designed and constructed jointly by the Flerov Laboratory of Nuclear Reactions of the Joint Institute for Nuclear Research (JINR), Dubna, Russia, and the Laboratory of Physics of the Vinča Institute. It is in operation since 1998.

The C1 channel is used for analysis of heavy ion beams produced with the M1 machine. It comprises a beam emittance meter of the pepper-pot type. This channel was put in operation in 2003 [2].

The C2 channel is used for surface modification of materials with heavy ion beams produced with the M1 machine [3]. It includes a beam scanning system, enabling uniform irradiation of the samples inside the interaction chamber. The main components of the vast (1 m^3) interaction chamber are the following: (a) the target holder enabling positioning and rotation of the samples, (b) a low energy (2 keV) argon gun enabling one to employ the technique of ion beam assisted deposition (IBAD), (c) an electron-beam evaporation source for thin film deposition, (d) a sample heater (T_{max} = 800 ºC) and separate cooling unit with liquid nitrogen, (e) a quadrupole mass spectrometer (1-100 amu). The channel was constructed by Danfysik, Jyllinge, Denmark and commissioned in May 1998.

In addition, there is a separate multicusp ion source (M2 machine) that produces positive or negative light ions (H^-, H_2^+, H_3^+, D^-, D_2^+, D_3^+, He^+). The maximal extraction voltage is 30 kV. It was constructed by AEA Technology, Abingdon, UK and commissioned in July 1997. Initially, this machine was planned to be an injector to the main cyclotron of TAI, but after the TESLA Project has been stopped, it has been occasionally used for surface modification of materials with light ion beams.

UPGRADING THE FAMA FACILITY

The experience of the user groups of FAMA has shown that the facility needs several improvements. These improvements should be (i) to integrate the M2 machine in FAMA and provide irradiation of targets with light ion beams in parallel with heavy beams, (ii) to enable irradiation of targets to high fluences (above 10^{17} cm^{-2}) in relatively short period of time, (iii) to enable one to bombard single crystals, (iv) to increase the beam energy, and (v) to introduce some techniques for analyzing the modified targets.

In April 2009 the Vinča Institute signed a three-year contract with the Joint Institute on the upgrading of FAMA. The contract comprises: (i) refurbishment and upgrading of the M1 and M2 machines and C1 and C2 channels, (ii) construction of a channel for surface physics (C3) and a channel for deeper modification of materials with post-accelerated ion beams (C4), (iii) construction of a set-up for analysis of materials comprising a small isochronous cyclotron (M3) providing proton beams for analysis of materials in vacuum (channel C5) and for analysis of materials in air (channel C6), and (iv) purchasing of a scanning probe microscope. These jobs are performed on the basis of the concepts made by the Laboratory of Physics of the Vinča Institute, in accordance with the previously mentioned necessary improvements of FAMA. Figure 2 gives a scheme of the upgraded FAMA without the M3 machine and the C5 and C6 channels.

*Work supported by the Ministry of Science and Technological Development of Serbia through the project 151005
#alexd@vinca.rs

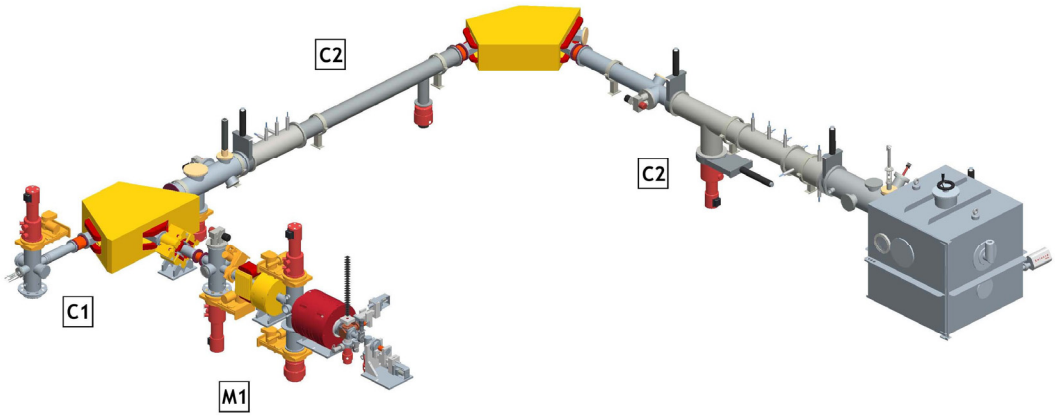

Figure 1: Present experimental facility for surface modification of materials.

The main highlights of the upgraded FAMA are the following:

- Reconstructed ECR ion source (M1) with new hexapole, larger plasma chamber and improved injection chamber should have better performances (higher charge states and higher beam intensities).
- Channel C1 will be used for the ion beam analysis using new emittance meter and for irradiation of samples to high fluences, above $10^{17}cm^{-2}$, usually obtained within one day. Homogenious irradiation will be obtained by mechanical x-y movement of the samples in front of the fixed ion beam [4]. In addition, the interaction chamber will have 6-axes target goniometer enabling one to perform implantation into single crystals.
- Channel C2 will be reconstructed in order to improve its ion beam transmission coefficient and to enable integration of light ion source (M2) into FAMA.
- Channel C3 will comprise an ultrahigh vacuum chamber for experiments in the field of surface physics.
- Channel C4 will provide additional acceleration of ions by biasing the target to the negative potentials of down to -100 kV, thus overriding the limitation in beam energy given by maximal extraction voltage of the ECR ion source (+25 kV). For example, we shall be able to bombard the target with the Xe^{24+} ion beam of the energy up to 3 MeV, instead of 600 keV without the biasing system [5].

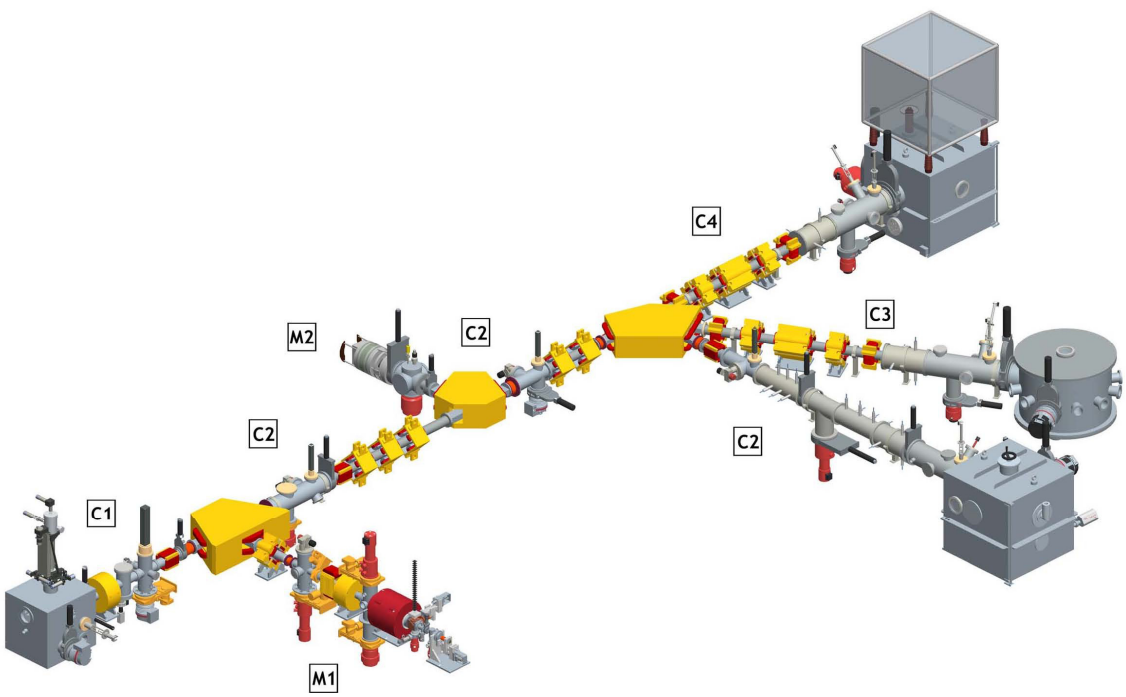

Figure 2: The scheme of upgraded FAMA.

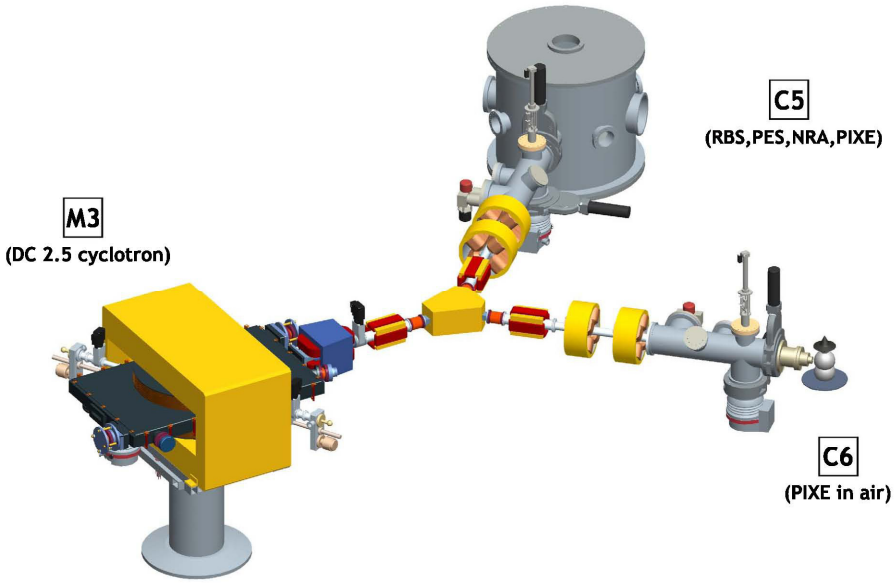

Figure 3: Set-up for analysis of materials using different techniques (RBS, PES, NRA, PIXE).

The scheme of the set-up for analysis of materials (e.g. irradiated samples) is shown in Fig. 3. It comprises a small isochronous cyclotron (machine M3) based on the DC 2.5 cyclotron prototype whose concept was made in JINR few years ago. It has 52 cm diameter of poles, four pairs of straight sectors, internal PIG ion source and extraction by stripping foil system, delivering proton beams of energies between 1 and 2.7 MeV. These beams will be used for different techniques of material analysis, realized in channels C5 and C6. In the C5 channel one will be able to perform the analysis of materials in vacuum by Rutherford backscattering spectrometry (RBS), proton elastic scattering (PES) spectrometry, nuclear reaction analysis (NRA), and proton induced X-ray emission (PIXE) spectroscopy. In the C6 channel one will be able to perform the analysis of materials in air by PIXE spectroscopy.

CONCLUSION

We hope that in a few years the upgraded FAMA should become regional user facility for different basic and applied research programs in the field of nanotechnologies and investigation of new materials with improved properties, offering advanced techniques for modification and analysis of materials with ion beams.

REFERENCES

[1] A. Dobrosavljević et al., Rev. Sci. Instrum. 71 (2000) 915.
[2] M. Šiljegović, 'A Pepper-Pot Emittance Meter for Low Energy Ion Beams', the Fifth General Conference of the Balkan Physical Union, Vrnjačka Banja, Serbia and Montenegro, August 2003, p. 2057 (2003).
[3] A. Dobrosavljević et al., Rev. Sci. Instrum. 71 (2000) 786.
[4] M. Šiljegović et al., Rev. Sci. Instrum. 77 (2006) 03A313.
[5] A. Dobrosavljević et al., Nucl. Instr. and Meth. A 597 (2008) 136.

THE INJECTION LINE AND CENTRAL REGION DESIGN OF CYCIAE-70*

Jianjun Yang#, Tianjue Zhang, Xianlu Jia, Chuan Wang, Ming Li, Hongjuan Yao, Yinlong Lv
China Institute of Atomic Energy, Beijing, 102413, China

Abstract

A 70MeV compact cyclotron is under design at CIAE, which is aimed to provide both proton and deuteron by stripping two electrons from H^- beam and D^- beam respectively. Both of the negative charged beams are produced in a single external multi-cusp ion source, injected axially by a low energy beam injection line and bent onto the median plane through a spiral inflector. In the central region, the electrode structures and the shape of Dee tips are constructed and optimized to achieve matching at the inflector exit and to maximize the acceptance of the central region. The preliminary design results of the injection line, the spiral inflector and the central region are elaborated in the paper.

INTRODUCTION

China Institute of Atomic Energy (CIAE) is carrying out the physics design of a multi-purpose 70MeV compact cyclotron, CYCIAE-70[1], which will be applied in radioactive ion-beam production and nuclear medicine. This machine adopts a compact structure of four straight sectors. It will be capable of accelerating both H^- and D^- beam and extracting proton and deuteron beam in dual opposite directions by charge exchange stripping devices. The energy of the extracted proton beam is in the range 35~70MeV with a beam intensity up to 700μA. The energy of the extracted deuteron is 18~35MeV and the required beam intensity is only 40μA. For both particles, the energy is continuously adjustable.

As is well known, the internal PIG ion source is incapable of providing the high intensity beam of milliampere level, therefore the external ion source, and accordingly, the beam injection line and inflector are essential for this cyclotron. Considering the fact that a single multi-cusp ion source is capable to provide both H^- beam and D^- beam by filling with H_2 gas and D_2 gas respectively, only a single ion source and a single beam injection line are needed. After extracted by the ion source located underneath the cyclotron, the beams are injected into the cyclotron axially by an injection line upwards to the spiral inflector which bends beam by 90° onto the median plane of the central region. The detailed design methods and results of the central region, the spiral inflector and the injection line are reported in the following sections.

CENTRAL REGION DESIGN

The central region is one of the most challengeable sub-systems of a compact isochronous cyclotron. The principle of the design is that the central region is capable of accepting both 40keV H^- beam and 20keV D^- beam without replacing any components.

The approach for central region design is as follows:

(1) Build a 3D finite element model of the cyclotron main magnet and create the isochronous field maps on the median plane for both H^- and D^- particles respectively. The conversion between the two isochronous fields can be achieved by moving 8 additional shimming bars and tuning the ampere-turns of the main coils. Orbit centering in the central region is achieved by tuning the ampere-turns of the centering coil.

(2) Draw a preliminary geometry of the central region in AUTOCAD, which is then imported into RELAX3D[2] with the help of the pre-processing code Pre_Relax3D[3], that can read the geometry information and generate the finite difference grid with the boundary conditions. Then the 3D electric potential map around the median plane can be calculated. The central region structure must be compatible with the main magnet and the electrode of inflector. In order to avoid voltage breakdown, the accelerating gap was chosen not smaller than 6mm.

(3) Search the AEOs of a given energy points W_0 at the high energy region for H^- and D^- beam. Then do the backtracking from the AEOs of high energy towards the central region.

(4) Observe and analyze the backtracking results of H^- and D^- particles and check whether the following conditions are fulfilled: (a) The two orbits cross just before entering the first accelerating gap, the crossing point is the matching point (MP1) with inflector; (b) the energy of H^- and D^- particles at MP1 are approximately equal to 40keV and 20keV respectively; (c) in the central region the distances between the H^- orbit and the posts of two sides are approximately equal.

(5) In case the above conditions in item (4) is not fulfilled, try to do the following changes in sequence: (a) adjust the starting energy W_0; (b) adjust the structure of central region; (c) adjust the magnetic fields by adjusting the magnet structure or tuning the ampere-turns of main coils.

(6) Once the above conditions in item (4) is fulfilled, track the H^- and D^- particles of different phases. Check that whether the phase acceptance of central region is larger than 40º for H^- beam and 20º for D^- beam, and the normalized axial acceptance for both beams are larger than 0.5π mm-mrad. Otherwise optimize the structure of central region.

The iteration of orbit tracking and structure adjusting were performed according to the above approach. Figure 1 shows the final layout of the central region including the electrode structure and accelerating gaps. The

*Work supported by the NSFC, under contract 10775185, 10775186
#yangjianjun00@ tsinghua.org.cn

reference orbits of H^- beam and D^- beam for the first 3 turns are obtained and the results are shown in Fig. 2. The energy increase in the 3 turns is shown in Fig. 3. The parameters of the reference particle after the first 3 turns are listed in Table 1. To obtain these results, RF frequency of the resonator can maintain the same value (56.265MHz) for both beams. Nevertheless, the price we have to pay is that the voltages of Dee tip must be different, i.e., V_{Dee} = 60kV for H^- beam and V_{Dee} = 70kV for D^- beam. Figure 2 shows that the reference orbit for D^- beam is not well centered during the first 3 turns. Since the required beam current for H^- beam is much higher than D^- Beam, H^- beam has higher priority for beam centering in order to diminish the beam loss caused by off-centering injection. However, the centering coil will be capable to construct beam centering for D^- beam after the first turn, where we have enough space to install the components of the trim-coil.

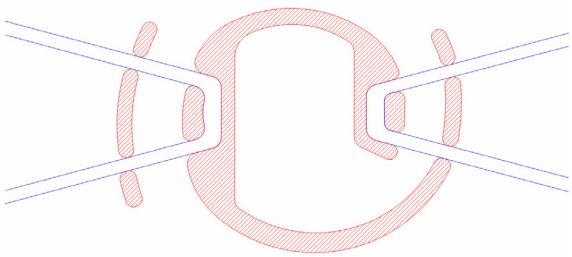

Fig. 1: The layout of the central region including the electrode structure and accelerating gaps

Table 1: Parameters of the Reference Particle after the First 3 Turns (azimuth: 345°)

	H^- beam	D^- beam
Energy E (keV)	652.48	524.57
Radius r (cm)	12.53	17.29
Momentum Pr (cm)	-0.84	-2.09
RF time τ (°)	7.88	41.81

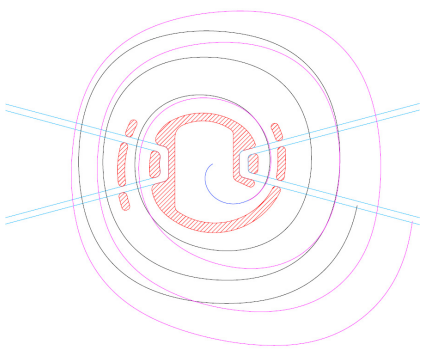

Fig. 2: The reference orbits of H^- particle (black) and D^- particle (pink) in the central region for the first 3 turns, plotted with the projection of the central orbit in the inflector onto the median plane (blue).

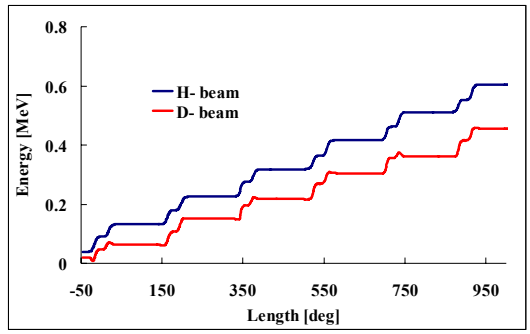

Fig. 3: Energy increase in the first 3 turns

INFLECTOR DESIGN

The central region design provides the matching point closely to the exit of the spiral inflector and the reference parameter at the inlet of central region, which should be used as the confinement conditions for inflector design. Therefore the central region and the inflector must be considered as a whole and the design work must be carried out simultaneously.

The principle of the design is that a single inflector should be capable of bending both H^- and D^- beam onto the median plane by only adjusting the voltage with the transmission efficiency higher than 80%. In order to obtain the same trajectory for the reference particles, the injection energy of D^- beam must be a half of H^- beam. This is because the ratio of charge and mass of D^- beam is only a half of that of H^- beam. For this cyclotron the kinetic energy of the injected H^- and D^- beam are 40keV and 20keV. It is also important that at the match point, both types of reference particles must be accepted by the central region of the cyclotron.

The inflector design was carried out by using CASINO[4] codes. Table 2 shows some key parameters of the inflector. The surface of the inflector electrodes and central trajectory of H^- beam (overlap with and D^- beam) are shown in Fig. 4 The projects of central trajectory onto the r-z plane is plotted in Fig.5 (a). The projection onto the median plane is plotted in Fig. 5 (b) and also in Fig. 2, from which we can see the orbits in the central region and inflector are matching well.

Table 2: Some Key Parameters of the Inflector

Parameter (unit)	Value
Electric bend radius A (mm)	58
Tilt parameter k'	-0.55
Electrode spacing d (mm)	8
Electrode width w (mm)	16
Orientation angle α (deg)	199.40
Voltage V (kV)	±6.90 (H^-) ±3.45 (D^-)

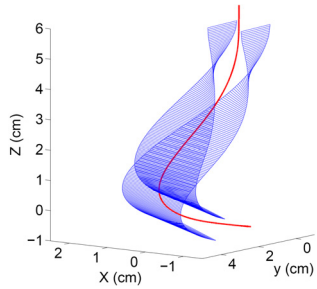

Fig. 4: The surface of inflector electrodes and the central trajectory of H^- beam (overlap with and D^- beam)

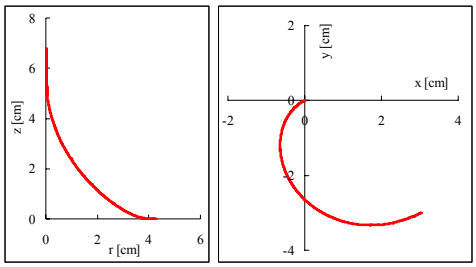

(a) (b)

Fig. 5: The project of central trajectory of H^- beam (overlap with and D^- beam) onto the *r-z* plane and median plane

INJECTION LINE DESIGN

The injection line layout of the 70MeV cyclotron obtained by preliminary design is shown in Fig. 6. The DC beam is injected from the ion source located below the magnet of the cyclotron. The injection line utilizes two solenoids and a triplet for transverse focusing and a two-gap buncher for longitudinal bunching. The total length of the injection line is about 2.5m. The effective lengths of two solenoids are 20cm and 40cm respectively, and the aperture diameters are 8cm. The effective lengths of the three quadrupoles are 10cm, 12cm and 10cm respectively, and the aperture diameters of the triplet are 6cm.

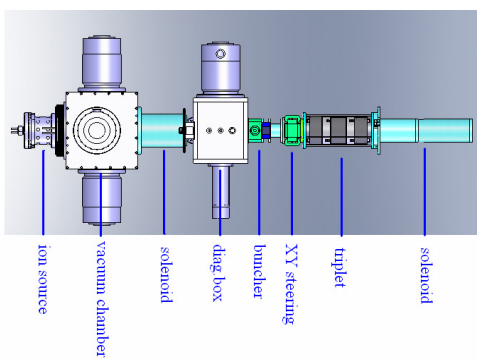

Fig. 6: The layout of the injection line

The ion source will provide the 40keV H^- beam with a current of about 8mA and 20keV D^- beam with a current of about 500μA respectively. Considering the H^- beam space charge effects will be significant, they need to be compensated by neutralization measure. The neutralization of 95% is assumed in the design, which can be achieved with a vacuum of more than 10^{-4}Pa. According to the measured results of phase space at the extraction outlet of the existing ion source[5] at CIAE, we selected the initial parameters of $\varepsilon_r = 48\pi$ mm-mrad, $r_{max} = 4$mm, $r'_{max} = 22$mrad, $R_{12} = 0.83$.

The beam optics design was performed using TRANSOPTR[6] code. During the design the constraints and fitting conditions were used, including the requirement that the beam sizes should be smaller than the inflector inlet sizes at the inflector entrance and the normalized circulating emittance in the central region should be minimized. Figure 7 shows the beam envelopes from the extraction outlet of the ion source to the first turn in the central region of the cyclotron under the conditions that the cyclotron was approximated by the dipole and the inflector was represented by a transfer matrix. It is indicated that larger envelope size is expected for D^- beam as a result of the larger space charge effects. However, the maximal size of envelope is still smaller than the aperture.

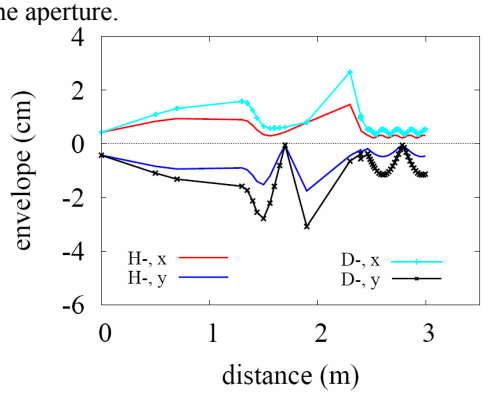

Fig. 7: The beam envelopes for the 8mA H^- beam with 95% neutralization and 500μA D^- beam without neutralization.

REFERENCES

[1] T.J. Zhang et al. Proceedings of ECAART2010, Athens, to be published.
[2] H. Houtman, F.W. Jones and C.J. Kost, Computer in Physics, Vol. 8, No. 4, p. 469, 1994.
[3] K. Hu et al. Atomic Energy Science and Technology, Vol.37, No.3, p. 268, 2003.
[4] B.F. Milton et al. CASINO User Guide and Reference Manual, TRI-DN-89-19, 1989.
[5] T.J. Zhang, et al. Rev. Sci. Instrum. 81, 02A705, 2010.
[6] E. A. Heighway and R. M. Hutcheon, Nucl. Instrum. Methods 187, 891981.

PHYSICS DESIGN OF CYCIAE-70 EXTRACTION AND BEAMLINE SYSTEM

SZ.An, SM.Wei, M.Li, TJ.Zhang, C.Wang, JQ.Zhong, FP.Guan, GF.Song, F.Yang
China Institute of Atomic Energy, Beijing, 102413, P.R. China

Abstract

A driver with beam power of 50KW (70 MeV, 0.75 mA) based on compact H-/D- cyclotron, CYCIAE-70, has been designed at CIAE in Beijing for the RIB production and application in the nuclear medicine recently. CYCIAE-70 is designed to be a dual particle cyclotron and it is able to deliver proton with energy in the range 35~70 MeV and deuteron beam with energy in a range of about 18~33 MeV. About 700μA for H+ and 40μA for D+ will be extracted in dual opposite directions by charge exchange stripping devices and the extraction beam energy is continuously adjustable. The physics design of CYCIAE-70 stripping system has been done and the optics calculation for the extraction proton and deuteron beam has been finished. The dispersion effects for the extracted beam are analyzed and the beam parameters after extraction are calculated. 6 beam transport lines and experiment target stations are designed for different applications. A wobbling magnet is used in one of the beam transport lines, which will rotate the beam to form a beam spot on the target with a size of Φ40mm and uniformity of better than 95%.

INTRODUCTION

In order to afford the applications in the radioactive ion-beam (RIB) production and the filed of nuclear medicine, a multi-functional compact cyclotron CYCIAE-70 [1] is completely designed at China Institute of Atomic Energy under the accumulated experience on the physical research and technology design of the H- high intensity cyclotron [2,3]. The machine adopts a compact structure with four straight sector poles, capable of accelerating two kinds of beams, i.e. H- and D-. The proton beam in the range 35~70 MeV with an intensity up to 700μA, and the deuteron beam with 18~33 MeV and 40μA will be extracted in dual opposite directions by charge exchange stripping devices. For both particles that are extracted, the energy is continuously adjustable.

The cyclotron will be equipped with two combination magnets, placed at 180° one respect to the other. Any proton beam extracted by the stripper in the energy range 35~70MeV, will be transported at a crossover point inside one of the extraction combination magnets. The crossover point is the starting point of the extraction line. One of the two extraction magnets has to be equipped with a beam transport line to transport the full power beam outside the cyclotron and inside the commissioning room. In order to reduce the time of changing foils, the stripping foil changing devices are put in the independent vacuum chamber. Two stripping probes with carbon foil are inserted radially in the opposite direction from the main magnet pole. By comparing the optic calculating results for the extracted beam, the combination magnet is fixed between the adjacent yokes of main magnet in the direction of valley region. To keep all the extracted beams with various energies can be transported through the same crossing point in the combination magnet, the stripping probe can be moved in the radial direction and rotated in the angular direction.

6 beam lines and experiment target stations in the design will meet different users' demands in a variety of application fields. High extraction efficiency and low beam loss are designed for the striping extraction beam lines. Optics matching of the beam lines with the matrix of fringe field and the dispersion effects are taken into account during the extraction. A wobbling magnet is used in one of the beam transport lines, which will rotate the beam to form a beam spot on the target with a size of Φ40mm and uniformity of better than 95%.

STRIPPING FOIL AND SWITCH MAGNET

The positions of the stripping points and the combination magnet are fixed by calculating the extraction trajectories of extracted proton beams and deuteron beams after stripping foil for different energy with the code CYCTR [4]. In order to reduce the envelope of extracted beam, the combination magnet is fixed at the adjacent yokes of main magnet in the direction of valley region. The main magnetic field used to calculate the extraction trajectories is assumed to have mid-plane symmetry. The extracted proton and deuteron beams energies are chosen by the corresponding static equilibrium orbits.

For 70MeV cyclotron, the radius of magnet pole is 1.4 m and the outer radius of magnetism yoke is 225 cm. The center of combination magnet is located at R＝200 cm and THETA=100o). Table 1 shows the stripping points for the extracted proton beam and deuteron beam for different energies.

Table1: Position of stripping foil at different extraction energies for H- and D-.

H^-			D^-		
Energy (MeV)	R (cm)	Theta (^{o})	Energy (MeV)	R (cm)	Theta (^{o})
70	126.81	58.70	35	132.23	58.39
50	109.18	57.15	25	112.72	56.74
35	92.59	55.97	18	96.07	55.68

Work supported by the NSFC, under contract 10775185, 10775186

In order to extract the H- and D- beams with different energies, the stripping probe is inserted in the radial direction from the sector pole to the cyclotron center along the line of 57.2°. The minimal inserted position of the stripping probes is at R=92 cm. In order to extract beams at different energies, the stripping probe can be moved along the radial direction and rotate along the angle direction with a swaying angle of ±5°. Figure 1 shows the position of combination magnet and the extracted trajectories of proton beams with energy of 35MeV, 50MeV, 70MeV respectively.

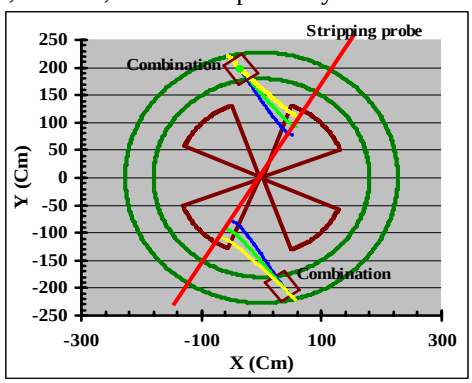

Fig.1 The stripping probe and extracted proton beam orbits with 35MeV, 50MeV, 70MeV.

In order to reduce the time of changing foils, the stripping foil changing devices are put in the independent vacuum chamber. Figure 2 shows the assembly of stripping extractor for H- and D- extraction and the foil changing system. The foil automatic changing machine is outside the magnetism yoke and 12 pieces foil can be changed in one time. For the stripping extraction system, the carbon foil will be used. For the extracted energy of 70MeV, the stripping efficiency is about 99.96% when the carbon foil thickness is 120 μg/cm^2 [4]. So, the foil thickness of 120 ~ 130 μg/cm^2 is enough for this machine.

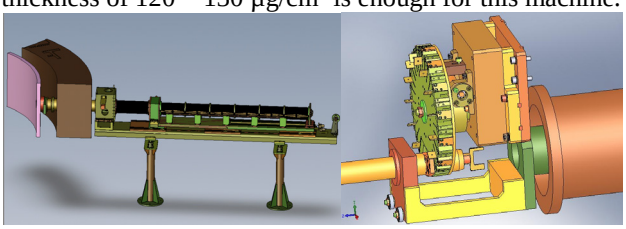

Fig. 2 Stripping Extractor and Foil changing devices.

The structure of the combination magnet is designed, and the main field 0.5T, Gap g=80 mm, Bending radius R=2968.2 mm, Effective length of the magnet Leff=300 mm, Maximum bending angle 5.79°, Uniform field range 80 mm, Mechanical length of magnetic pole 234 mm, $\Delta B/B<5.78\times10^{-4}$.

THE EFFECTS OF DISPERSION

The dispersion effects caused by the main magnet fringe field should be considered during the designs of the extraction system and beam transfer line. Due to the asymmetric magnetic field, the dispersion will be produced and this will lead to the emittance growth in x direction. The dispersion from stripping foil to the center of combination magnet (cross-over point) will be got from the modified code GOBLIN by CIAE [5]. Table 2 is the transfer matrix from stripping foil to the cross-over point with dispersion for different beam energy. Figure 3 shows the dispersion for the extracted proton beam from stripping point to the cross-over point. Not shown the case of D+ beam, which is very similar as the case of H+ beam.

Table 2 The transfer matrix from stripping points to the center of combination magnet.

Ion	H^+			D^+		
E/MeV	70	50	35	35	25	18
R_{11}/1	0.968	1.051	1.158	0.801	0.874	1.009
R_{12}/cm/mrad	0.163	0.178	0.190	0.156	0.171	0.185
R_{16}/cm/%	0.578	0.709	0.837	0.539	0.668	0.798
R_{21}/mrad/cm	-0.604	0.738	1.031	-2.117	-0.739	0.359
R_{22}/1	0.931	1.076	1.032	0.837	0.999	1.057
R_{26}/mrad/%	4.588	4.533	3.874	4.547	4.380	4.107
R_{51}/1	-0.479	-0.424	-0.362	-0.479	-0.432	-0.386
R_{52}/cm/mrad	-0.021	-0.004	0.013	-0.026	-0.008	0.009
R_{56}/cm/%	1.325	1.506	1.701	1.464	1.609	1.759
R_{33}/1	0.399	0.057	-0.415	0.601	0.278	-0.183
R_{34}/cm/mrad	0.148	0.145	0.141	0.154	0.153	0.147
R_{43}/mrad/cm	-4.155	-6.576	-9.313	-2.471	-4.858	-7.788
R_{44}/1	0.965	0.840	0.756	1.029	0.928	0.787

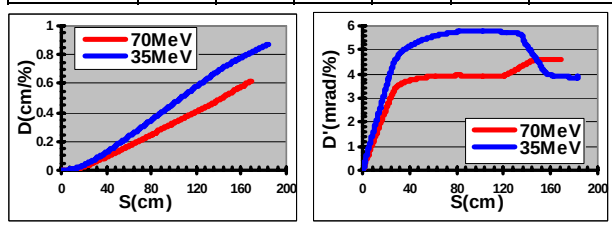

Fig.3 The dispersion for the extracted proton beam from stripping point to the cross-over point.

STRIPPING EXTRACTION SIMULATION

The extracted beam distribution just after stripping foil can be got from the modified multi-particle tracking code COMA by CIAE [6]. Not only the case of 180° dees in TRIUMF, but also accelerating gap with general dee geometry is includeded in COMA. Gaussian input distribution and linear space charge calculation are added for the modified code COMA.

Figure 4 shows 1.5 MeV H- input phase space distribution and the extracted 70 MeV H+ beam distributions on the stripping foil with the initial normalized emittance of 4.0π-mm-mrad, which is the transverse acceptance of cyclotron central region. The injected is H- bunch with phase extension of $\Delta\varphi=40°$, but zero energy spread. The input distribution is random in transverse direction and uniform in longitudinal direction. The beam parameters for the extracted H+ with different energies can be got from the distributions on the foil, this is the beginning point of the beam transport line for all

beam lines design. From the simulation results, the initial normalized emittance of $\varepsilon_x=\varepsilon_z=4\pi$-mm-mrad used in the calculation is reasonable [7]. For the CYCIAE-70, the phase acceptance is 40° to get high current and the energy spread for the extracted beam is about ±0.6%.

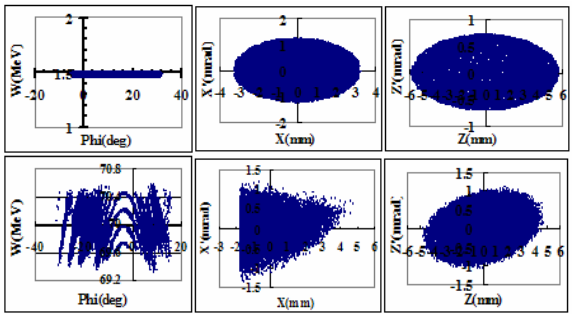

Fig.4 The phase space distributions of initial beam (upper), extracted 70MeV H+ beam on the stripping foil.

BEAM LINE DESIGN

6 beam lines and experiment target stations in the design will meet different users' demands. This system can transport 35-70 MeV, 700μA H+ beam or 18-35 MeV, 40μA D+ beam to the target. High extraction efficiency and low beam loss are designed for the striping extraction beam lines. The beam optics and the layout of the extraction beam line, designs of the main component like bending magnets, steerers, quadrupoles lens, diagnostic devices, vacuum pumps, vacuum-meter etc. have been finished. Figure 5 shows the layout of beamlines.

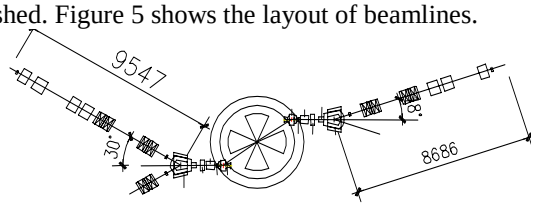

Fig. 5 The layout of beamlines.

The beam parameters as the beginning point of the whole beam line design can be got from the distributions on the foil. Figure 6 shows the beam envelope of one of beam lines. The beam current density uniformity must be better 95% on the target with a size of Φ40mm, so a wobbling magnet is selected. The position of wobbling magnet is about 4.8m before the target. The needed maximum filed is about 200 Gauss to get the beam offset 10.5 mm on the target. The spot on the target can be controlled to be 12mm×18mm and can reach Φ40 mm by using the wobbling magnet, as shown in Figure 7.

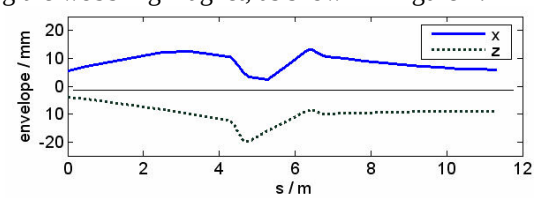

Fig. 6 Total beam envelopes along one beam line.

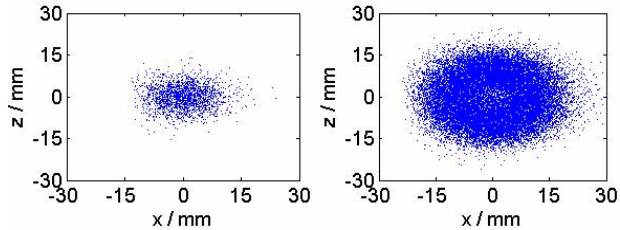

Fig.7 Particles distribution on target without (left) and with (right) wobbling magnet.

SUMMARY

CYCIAE-70, a compact cyclotron with high intensity, will produce proton beam with energy 35-70 MeV and deuteron beam with energy 18-35 MeV. The design intensity is up to 700μA for proton beam and 40μA for deuteron beam with the stripping foil. The positions of the stripping points and the combination magnet are fixed by calculating the extraction trajectories of proton beams and deuteron beams after stripping foil for different energy. The physics designs of CYCIAE-70 stripping system and the combination magnet have been done and the optics calculations for the extracted proton and deuteron beam have been finished. 6 beam lines and experiment target stations in the design will meet different users' demands. High extraction efficiency and low beam loss are designed for the striping extraction beam lines. Optics matching of the beam lines with the matrix of fringe field and the dispersion effects are taken into account during the extraction. A wobbling magnet is used in one of the beam transport lines, which will rotate the beam to form a beam spot on the target with a size of Φ40mm and uniformity of better than 95%.

REFERENCES

[1] Tianjue Zhang, Shizhong An et al., Physics Design of a 70MeV High Intensity Cyclotron, 10th European Conference on Accelerators in Applied Research and Technology, 13-17, Sep., 2010, Athens, Greece.

[2] Tianjue Zhang, et al., Research progress in high intensity cyclotron technology, Chinese Science Bulletin, Nov. 2009, Vol. 54, Iss 21, p3931-3939.

[3] Tianjue Zhang, etc, Research progress on several aspects of advanced high intensity cyclotron technology at CIAE, Atomic energy science and technology, Vol. 43, 2009.

[4] Stripping extraction system for CYCIAE-100, CYCIAE design note in Chinese, 2006.

[5] Sumin Wei, et. Al., Beam Extraction System Design for CYCIAE-14, this proceeding.

[6] Yuanjie Bi, et al., Cosine Gradient Theory in Cyclotrons with Gen-eral Dees, N.I.M A, Vol. 597, Issues 2-3, pp149-152.

[7] Shizhong An, etc, Stripping extraction calculation and simulation for CYCIAE-100, Chinese Physics C (HEP & NP), V33 (Suppl. 2), Jun. 2009.

DESIGN STUDY OF COMPACT CYCLOTRON FOR INJECTION K=100 SSC*

B. N. Lee,H. W. Kim, J. H. Oh,J. S. Chai†
Accelerator and Medical Engineering Lab., SungKyunKwan University, Suwon, 440-746, Korea

Abstract

The Compact cyclotron was designed for injection of K=100 Separated-Sector-Cyclotron (SSC) [1]. It has four magnet sectors with pancake type and maximum magnetic field is 1.92T. The magnet adopting 4 harmonics has three kinds of holes for beam injection, vacuum pumps and RF systems. The pole diameter was chosen about 80 cm with 50kV dee-voltage and 40˚dee-angles. The Injection system of this accelerator consists of a double gap buncher, Solenoid-Qaudrupole-Qaudrupole (SQQ) and a spiral inflector. It will provide a 4~8 MeV, ~1 mA of proton beams and 2~4 MeV, ~0.5mA of deuteron ion beam. In this paper we will describe the conceptual design of this machine including the design of Ion-source, Injection system, Magnet and RF system.

INTRODUCTION

In this research, we designed a cyclotron which can produce beam more than 1mA with relatively small energy, 8MeV. General specifications of this cyclotron are shown at Table 1. The particle of negative hydrogen is accelerated, in the end of the procedure it generates proton beam through a carbon stripper. The H- ion created from ion source runs into the injection system and is accelerated to 8MeV at the middle plane of upper and lower magnet poles. After this acceleration it is ejected to outside by drawn system. For the higher beam current the multicusp ion source of volume type is used and the injection system make DC beam have pulse type to have same phase with RF system. The magnet is designed to produce isochronous magnetic field by shimming and RF system is considered for easily occurring a resonance near 74.3MHz.These process supported by MicroWaveStudio(MWS)[2] andOPERA-3D TOSCA[3].

ION SOURCE

The high intensity and improved TRIUMF type DC Volume-Cusp H^- ion source is used for source of beam. It consists of three major parts: body assembly, lens assembly and vacuum box assembly. Lenses are plasma lens (first electrode) and extraction lens (second electrode) with magnet filter to remove the extracted electron and re-enter beam. Vacuum box is the third electrode and it consists of steering magnet for plasma confinement.

*Work supported by Ministry of Education, Science and Technology,Republic of Korea and Department of Energy Science and School of Information and Communication Engineering of SungKyunKwanUniversity
†Corresponding author: jschai@skku.edu

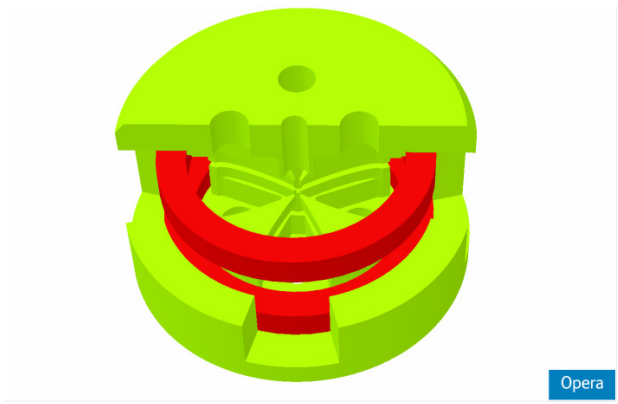

Figure 1:Model of magnet system and main coils.

Table 1: Specifications of 8MeV Cyclotron

Parameters		Values
Ionsource	Multi-cusp DC Type	
	Max. Extracted Beam Current	15mA
	Max. Arc Volt.	150V
	Type of Extracted Ion	H-, D-
Injector System	Buncher Max. E-potential	200 V
	Solenoid-Q doublet OP. power	35kW
	Inflectorelectrode potential	±10 kV
Magnet	Pole/Extraction Radius	0.4m / 0.35m
	Diameter	0.8 m
	Hill Angle	48˚
	Center field	1.15T
	Max./min B field	0.3T / 1.95T
RF System	Frequency/ Harmonics Number	74.3MHz/4th
	Dee Number/Dee angles	2 /40˚
	Dee Voltage/Q-value	50kV/5981

The 15mA H^- beam is extracted with a measured emittance of about 0.860 mm mrad. Beam kinetic energy is about 20 to 30 keV because of bias supply voltage (28 keV).

Filament current is about from 230A to 340A for the ionizing. The ion source is filled with hydrogen gas. When the filament current flows, the thermal electron is extracted from filament. This extracted thermal electron is accelerated to the cusp-body. In this situation thermal electrons are collided with cusp-body's hydrogen and generate H^- ions because of 150V arc voltage. The Ion-source is identical to TRIUMF one. [4]

INJECTION SYSTEM

Designed injection system consists of Double gap buncher, faraday cup, Solenoid-Q doublet lens andspiral inflector.The Beam pass along the way in the same order as above and the faraday cup plays ion particle detector. [5]

Buncher

The aim of Buncher is bunching of negative hydrogen from ion-source.It is composed of RF signal generator, RF amplifier, RF matching circuit, double gap buncher andfrequency tuner.Maximum electric potential at the centre pole is 200 V. Distance between gap is 18.7mm which is calculated by $(\beta \cdot \lambda)/2$.When the DC negative hydrogen beam incident into buncher, the energy distribution of ions is formed by double gap and then it becomes a kind of bunch shape with condensation and rarefaction of ion at specific distance by the difference of energy.

Solenoid-Q doublet

Solenoid-Q doublet is located at the centre hole of upper magnet yoke.Solenoid lens is used to convert the rapid magnetic field variation to gradual one. Spiral inflector acceptsreasonable beam size and transverse distribution by Q-doublet lens. The Maximum beam size in SQQ occurs at the centre of solenoid along the axial direction.

Spiral Inflector

To inject the pulsed beam which given in the magnetic field along the SQQ located at the upperyoke of magnet in horizontal orbit plane, we use spiral inflector. It is the main factor that minimizing distortion and loss of quantity with safe arrival in the middle plane including proper matching when the beam change its orbit.[6] Designed spiral inflector has 20 cm E-field radius and k'=0. Injected energy at the entrance of inflector is 24 keV.

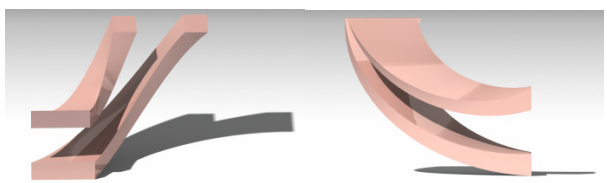

Figure 2: Spiral Inflector design using 3D CAD

MAGNET

Magnet using normal conductor with 4 sectors was designed for the radius of whole magnet and pole is 0.7m and 0.4m, respectively. The upper and bottom yokes have a two holes at each valley so that totally 4 holes are there and those are used for vacuum and RF system. The value of maximum field on the mid-plane is 1.95T while central region has 1.15T.

Fig.3 shows a longitudinal drawing and magnetic field characteristics of magnet of 8 MeV Cyclotron. To produce isochronous field, three stageswere weredone in this study. At First we define parameters such the kinds of like harmonic number and RF frequency. And then gamma value, magnetic rigidity at maximum beam energy and extraction radius was calculated. After the mathematical work, 3D CAD drawing with CATIA P3 v5 r18[6] and field simulation with OPERA-3D TOSCA were done.

In the central region the magnetic field decreases slightly with increasing radius and to make isochronous field shimming process and the method that changing hill-valley ratio along the azimuthal direction were used.[7]The average magnetic fields and radial and axial beam tunes of magnet were shown in Fig.4.

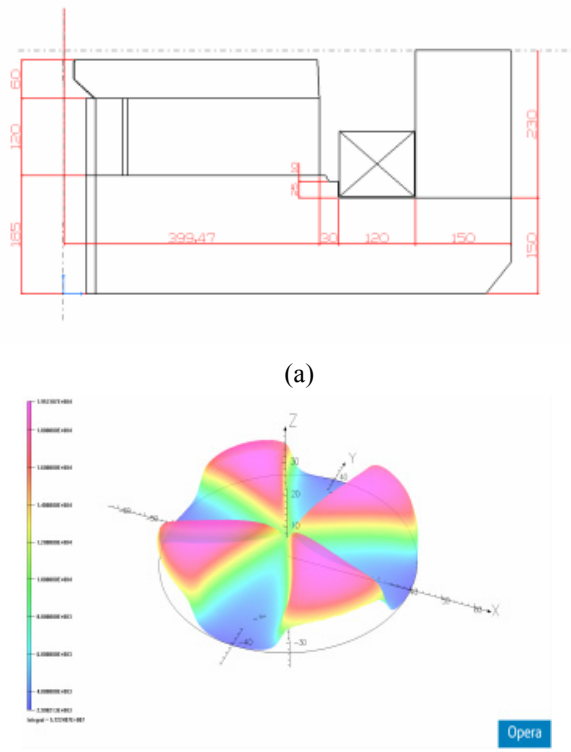

(a)

(b)

Figure 3: A longitudinal drawing (a) and Magnetic field characteristics (b) of 8 MeV cyclotron.

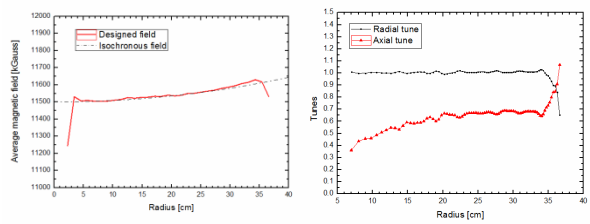

(a) (b)

Figure 4: Average magnetic field of magnet with idle isochronous field (a) and radial and axial beam tunes of

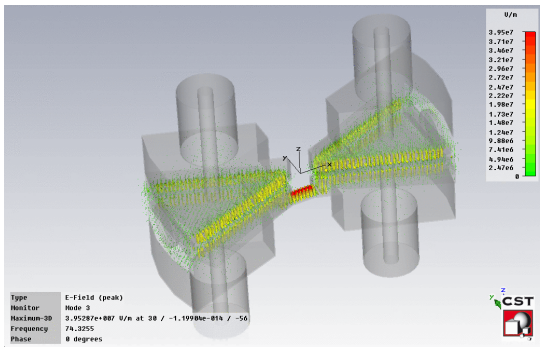

(a)

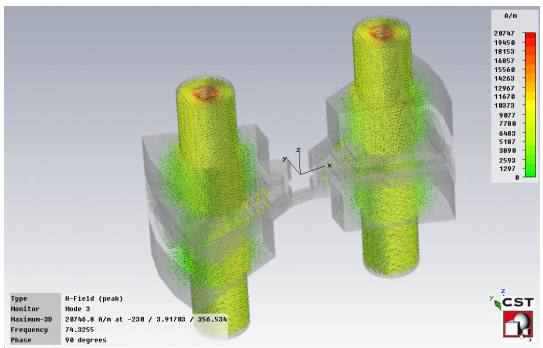

(b)

Figure 6: Electric field distribution (a) and Magnetic field distribution (b) of 8 MeV cyclotron magnet.

RF SYSTEM

H- particles exposed to middle plane through inflector run into an acceleration by Dee-voltage of 50KeV. These particles get there energy from resonance of 70MHz cavity frequency and are emitted with 8MeV energy from final extraction stage.

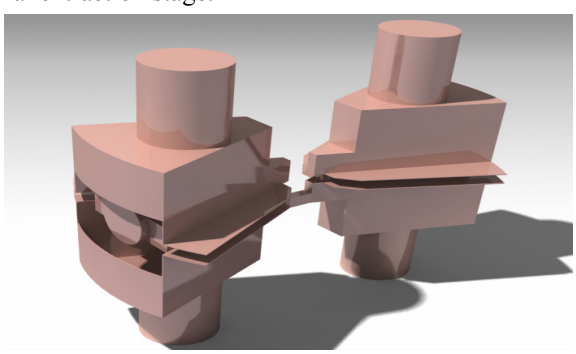

Figure 5: Cavity design using 3D CAD

A resonator mode of λ/2 is used in designed RF system. The sum of length of two Dees and four stems is roughly 2.15m which almost correspond with the half of wavelength of 70MHz. There was an adjustment through stem because of lack of space with magnet. The material for RF cavity is OFHC having better electrical conductivity ($5.91\times\frac{10^7 s}{m}$) than normal cupper.

Once the diameter was decided to 4 cm by repeating process using CST-MWS code, the Q value of RF resonator with same code was 5981.

CONCLUSION

We designed ion source, injection system, magnet and RF system of cyclotron as injector for K=100 SSC. To guarantee 1mA beam current, ion source produces a beam with more than 10mA and that supposed to be reached in orbit plane through spiral inflector. The magnet and RF system are designed for extraction of particles accelerated by 8MeV.

Based on this design, we will compose extraction and transporting system according to main cyclotron. This K=100 cyclotron will be able to accelerate particles up to 74.3MeV with the designed 8MeV cyclotron.

REFERENCES

[1] J.SChai et al., “Design Feature of K=100 cyclotron magnet for ISOL”,CAARI’10, FORTWORTH, August 2010, ID322
[2] CST, DE.;http://www.cst.com
[3] Cobham, Vector Fields Ltd, UK.; http://www.vectorfields.com
[4] T.Kou et al, "Development of a 15mA DC H- Multi-Cusp Source for Compact Cyclotrons", Proc, 14th Int'l Conf. on Cyclotrons & Their Applications, Capetown, 1995.
[5] J.S Chai et al. “Commissioning of KIRAMS-30 Cyclotron for nuclear science research”, Cyclotron and Their Applications 2007, October 2008, Sicily, Italy
[6] Dassualt Systems, FR.;http://www.3ds.com/
[7] John J. Livingood, “Principles of Cyclic Particle Accelerators”(1961)

MAGNET DESIGN OF 70 MEV SEPARATED SECTOR CYCLOTRON (KORIA)*

Khaled Mohamed Gad[1], Jong, Seo Chai[#], Electrical and Computer Engineering, SungKyunKwan University, 300 Cheoncheon – dong, Suwon Gyeonggido 440-746, Korea

Abstract

A K=100 separated sector cyclotron is being designed in SKKU in South Korea, this cyclotron is considered the main drive for ISOL to produce ~ 70MeV proton beam and 35 MeV deuteron beam for production of radioactive material as a basic nuclear research.

In this paper we will describe CST numerical simulation for determining the basic magnet parameters, magnet material, deformation, imperfection fields and preliminary ion beam dynamics study for verifying the focusing properties of the designed magnet.

INTRODUCTION

The purpose of this study is to design a separated sector cyclotron magnet for Korean National project, KORIA, which was started on April 2010 for radioactive ion beam (RIB) production using both ISOL and In Flight Fragmentation. KoRIA will contribute to the various research fields such as nuclear, atomic, material, bio and medical science. Its facilities consist of 3 blocks. Fig 1 is the layout of the KoRIA and the Fig 2 shows separated sector magnet layout.

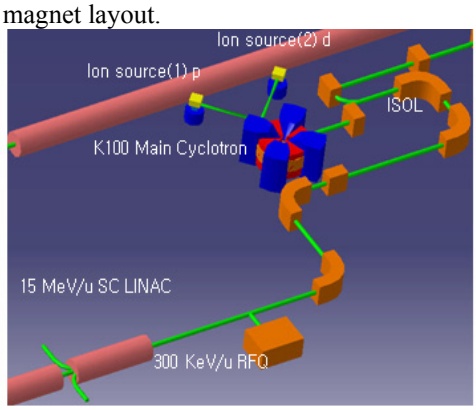

Figure 1: Block 1 layout of the KoRIA project

MAIN PARAMETERS AND DESCRIPTION OF SSC

SSC (Sector Separated Cyclotron) was selected for accelerating high beam current about 1~2 mA. The magnet diameter is 8.8 m, injection radius is 1 m, pole radius is 3.3m and approximately the total weight of iron is ~ 400 tons. For minimizing the energy dissipation at main magnet coil the minimal 3-cm gap between sectors was defined. Cyclotron Parameters cyclotrons are shown in Table 1.

*This work is mainly supported by Ministry of Education, Science and Technology, Republic of Korea. Also Department of Energy Science and School of Information and Communication Engineering of SungKyunKwan University

#jschai@skku.edu

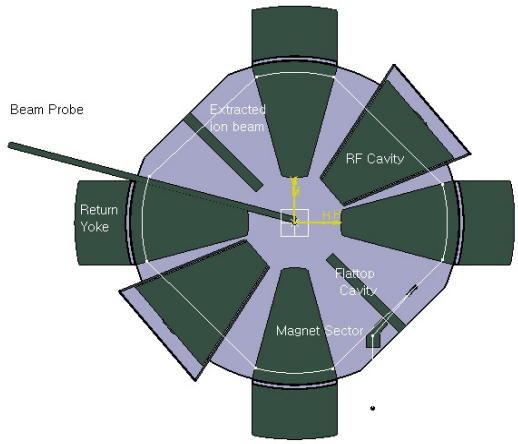

Figure 2: Separated Sector magnet Layout

Table 1: General cyclotron data

Parameters	Values
Energy	70MeV/35MeV
Ion Beam	H^+,D^+
Average field	0.385 T
Relative Field variation	0.38-0.415 T
Sector Gap	0.03m
Number of sectors	4

DESIGN REQUIREMENT FROM BEAM DYNAMICS

Acceleration of intense beams requires a very efficient focusing and extraction process free of beam loss. The main parameters of magnet design should satisfy the following criteria:

Single turn extraction: A large radial gain per turn is requested, i.e. a high energy gain per turn, in order to get an effective turn separation on the extraction radius.

Vertical and radial focusing: the problem of space charge effect is not fully understandable because of the very complicated nonlinearity of it, however many systems that have been designed were very successful for overcoming this problem, a deep valley sector focused cyclotron have been designed to be injector for a separated sector cyclotron.

SECTOR MAGNET DESIGN

One of the first decisions to be made in the design process is the number of sectors in the magnet and the angular width of each sector necessary to achieve the final energy of approximately 70 MeV. To avoid the effects of Resonances like $\nu_z = 1$ and $\nu_r = N/2$, we have selected four sectors and a magnet sector angle of 30 degrees ($\alpha = 30/90 = 0.333$).

The magnetic field of the sector magnets was studied with the finite element code CST. We have adopted a minimum magnet gap of 3 cm with the assumption that the magnet surface close to the median plane will be part of the vacuum chamber. We obtain an isochronous field by using 3 groups of trim coils

To achieve these goals, firstly hand calculations were done for determining the basic geometry of the magnet, the isochronous magnetic field was calculated by the equation [1],

$$B_{iso}(r) = \gamma \cdot B_c = (1 + T / E_0) \cdot B_C$$

Relativistic factor γ is a function of radius; we have calculated it from the equation [1]

$$B(r) / B_0 = \gamma(R) = [1 - (qB_c / m_i c)^2]^{-1/2}$$

2D simulation had been carried out for determining the basic magnet dimensions, trim coil. LANL Poisson 2D code had been used, the advantage of 2D simulation is the ability to use small mesh size for areas with high magnetic field gradient[2] , Fig (3)

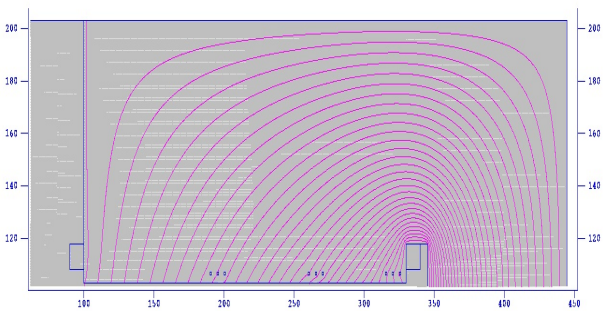

Figure 3: Poisson simulation (main magnet)

After determining the basic parameters of the magnet we draw the whole magnet using CATIA P3 V5 R18 [3] Fig (4), for drawing the whole magnet in 3D perspective, Followed by a 3D FEM (TOSCA and CST) code for the final calculations of the model [4] ,Fig (5).

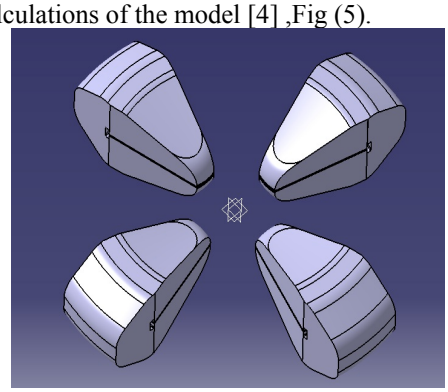

Figure 4: CATIA drawing

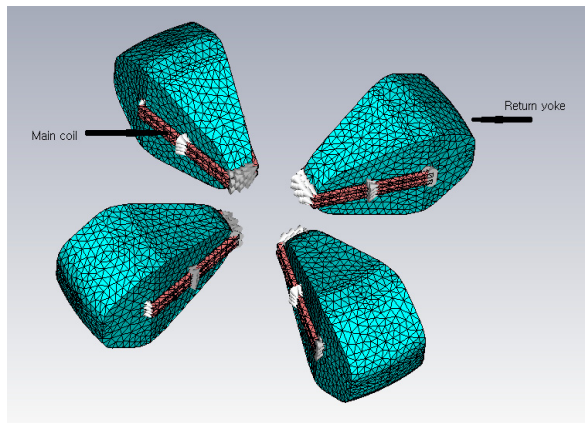

Figure 5: CST magnet simulation

SIMULATION RESULTS

After simulation of magnet using CST code , it was found that the average magnetic field of magnet was increasing with respect to radius fig(6) , this increase of the average magnetic can be adapted by using 3 set of trim coils which is feed by 3 separated power supplies.

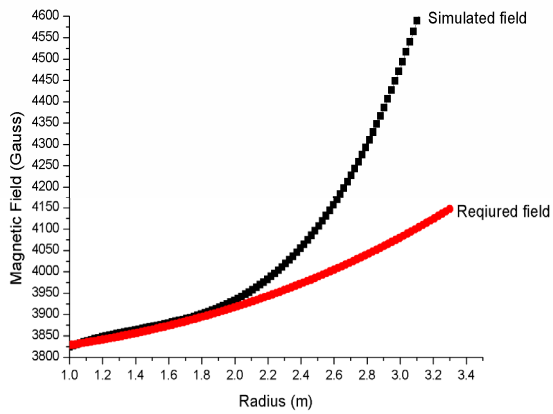

Figure 6: Simulated verse required field

Because of the small magnet gap, it was decided not to locate the trim coils in the gap space, but rather to place them inside the steel of the pole tip fig (7); it was impeded at a 5 cm distance from the pole surface.

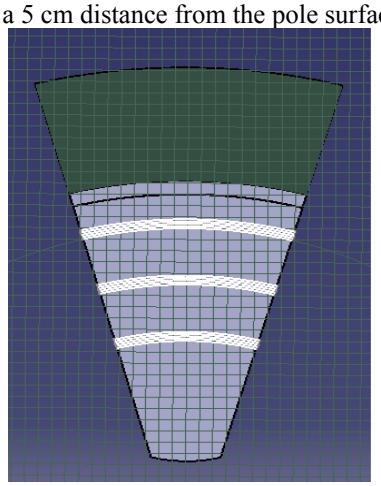

Figure 7: Trim coils position

Though not fully saturated, the field in the steel is nonlinear, and ultimately will require a nonlinear successive approximation technique to find the total field produced by the trim coils. However, in order to obtain a first estimate of the trim coil power requirements, linearity has been assumed. A 2D POISSON model was created consisting of a simplified azimuthally symmetric magnet with circular trim coils. The return path for the trim coils will either be on the outer radius of the magnet (for those at larger radii) or the inner radius (for those at smaller radii). This model gives an approximation to the 3D model that will later be constructed with TOSCA or CST program. To simplify the POISSON grid, the holes were represented by regions of 1cm by 10 cm. A small section of the POISSON model is shown in Fig 8.

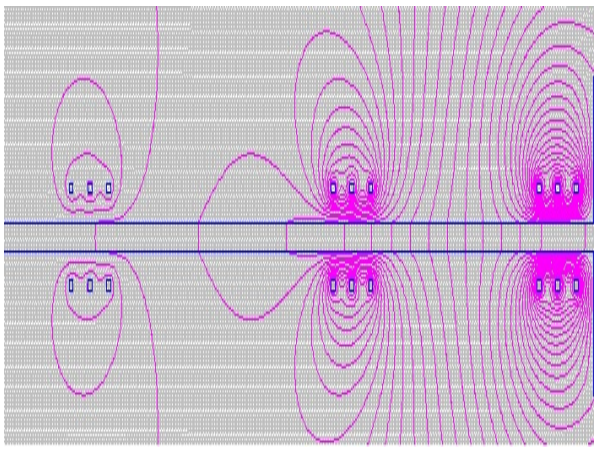

Figure 8: A vertical cross section of the POISSON model showing holes in the pole tip for the trim coils

By changing the direction and value of electric current in trim coils, we can obtain the required magnetic field which is isochronous for both Hydrogen and deuterium

TUNE DIAGRAMS

Calculations of betatron oscillations have been done by using simple homemade code the results is shown in fig .9.

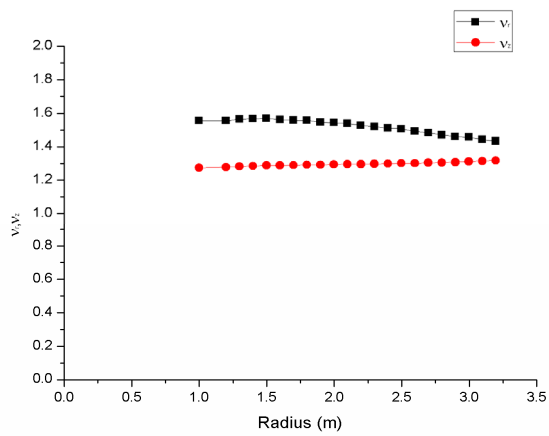

Figure 9: Radial and Axial beam tunes

Study of betatron resonance diagram Fig.10 we found that the work point of cyclotron is almost far away from dangerous resonance zones.

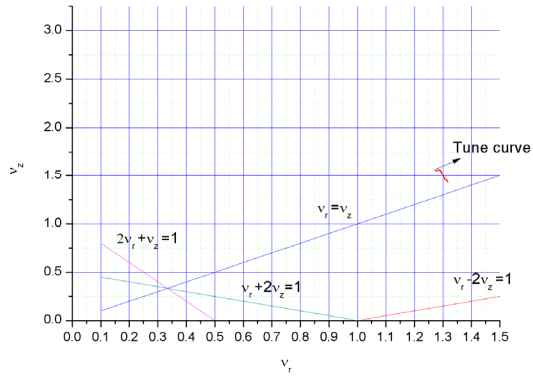

Figure 10: Tune diagram

CONCLUSION

The design study of 70 MeV separated sector cyclotron is almost done. The study of trim coils show that it is possible to obtain the isochronous magnetic field within high range of precision , harmonic coils will be studied in details to offer more stable magnetic field , it is expected that the whole system conceptual design will be finished on November, 2010.

REFERENCES

[1] Principle of charged particle accelerator, Stanley Humphiries ,Jr
[2] User's Guide for the POISSON/SUPERFISH Group of Codes, LA-UR-87-115, LosAlamos Accelerator Code Group
[3] Dassualt Systems, FR
[4] CST Microwave studio manual

BEAM OPTICS STUDY OF A FRAGMENT SEPARATOR FOR THE PLANNED RARE ISOTOPE BEAM FACILITY IN KOREA

W. Wan, Lawrence Berkeley National Lab., Berkeley, USA
Y.H. Park, J.W. Kim*, National Cancer Center, Gyeonggi-do, Korea

Abstract

A heavy-ion accelerator facility based on a linear accelerator is planned in Korea. The facility is designed to provide high-current radioisotope beams, and they will be utilized in the fields of nuclear, material and biomedical sciences. The primary beam energy is in the range of a few hundreds of MeV/u. A major mechanism to produce isotope beams is in-flight fragment separation. The separator system should have high mass resolution and particle identification method to separate and identify rare isotopes of interest, and also large momentum and angular acceptances for maximal utilization of produced isotopes. We are considering improved beam optics design to realize such a system, where second order aberrations are corrected. The study has been performed mainly using COSY Infinity.

INTRODUCTION

A plan to construct a heavy ion accelerator facility has been announced by the Korean government in January 2009. The primary accelerator is a superconducting linac to accelerate U ions to 200 MeV/u at a maximum beam power of 400 kW. It is planned to utilize both ISOL and in-flight fragmentation methods to produce rare isotope beams. In fact, considering the difficulties of using ISOL methods for some refractory elements and short-lived ions, in-flight fragment method is complementary in producing rare isotope beams [1].

The designs of two separators, which are in operation and under design, have been referred: the BigRIPS at RIKEN [2] and the separator design for the FRIB at Michigan State University [3]. BigRIPS is a two-stage fragment separator, which is actively utilized to search for new rare isotopes using heavy-ion beams from the cyclotron complex. We have studied the beam optics of a two-stage separation similar to that of the BigRIPS, also the possibility of symmetric lattice employing larger number of higher order multi-pole components.

The separator design for the FRIB facility, which is aimed to operate with the beam power of 400 kW while the beam power for BigRIPS is 100 kW, adopts a pre-separator to accommodate heavy shielding and remote handling capability. The primary beam not used for reaction is dumped in this area. The design of the FRIB separator includes vertical bending to account for the level difference between the accelerator and the beam lines for experiments. Our separator is designed to be at the same elevation considering technical and maintenance difficulties caused by the vertical bending.

*jwkim@ncc.re.kr

The use of wedge degrader is essential to separate the isotope with the same q/A ratio by Z-dependent energy loss. The wedge is located in the dispersive focal plane, and then the energy loss makes the beam achromatic at the focal point with appropiate wedge shaping. However, the effect of the wedge is not considered in the present work.

DESIGN OF A FRAGMENT SEPARATOR

The use of 400-kW beam power requires significant enhancement in radiation shielding compared to the usual nuclear science facility handling less than a few tens of kW. A pre-separator is needed to separate the primary beam and most of the unwanted isotope beams so as to dump them into water-cooled shielding structure. The design of pre-separator should consider radiation damage and shielding structures [4].

Configuration of the separator under consideration is given in Fig. 1 together with the beam envelope in the dispersive plane. The entire separator is located at the same level, and the locations of beam dump and shielding walls are schematically indicated. To accommodate the space for the shielding walls, we leave a long drift space of roughly 4 m in the middle of the pre-separator, a 2 m long drift space after the first dipole and a 1 m long drift between the pre- and the main separator.

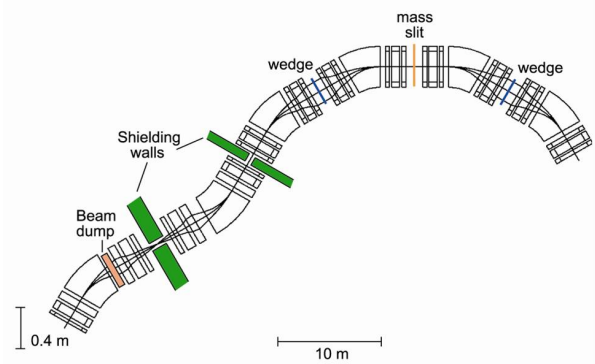

Figure 1: Configuration of a separator under consideration.

The optics of the separator was studied using COSY Infinity [5], including the pre-separator and the following main separator. The use of a matching section in between was considered but eventually dropped due to limited benefit and additional cost it brings.

OPTICS OF THE PRE-SEPARATOR

The pre-separator contains 2 dipoles and 12 quadrupoles, and its maximum magnetic rigidity is 8 Tm.

The dipoles bend to the opposite directions and the quadrupoles are symmetric about the centre. The dispersion is zero at the centre, which ensures the whole beamline is achromatic as shown in Fig. 2. An image in the horizontal plane is formed at the midpoint of the drift after the first dipole where the beam dump is located. Furthermore, in the first half, it is point-to-parallel in both planes and parallel-to-point in only the vertical plane. The one free parameter, the first quadrupole in our case, is used to adjust the ratio of the horizontal and vertical acceptance so that they are roughly the same.

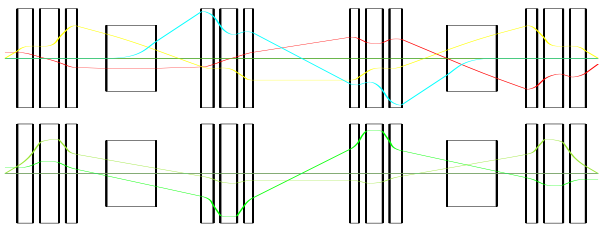

Figure 2: The sine-like, cosine-like and dispersive rays in the pre-separator. Upper envelop is for horizontal plane and the lower one is for vertical plane. The slope of the sine-like rays is 40 mrad; the amplitude of the cosine-like rays is 1.75 cm (beam radius 1 mm) and the momentum deviation of the dispersive ray is 9%. The total arc length is 26.3 m, and the radius of quadrupole aperture is 15 cm for all cases of this paper. The bending angle and arc length of the dipoles are 30° and 2.2 m, respectively.

The 4.3 m long drift in the centre of the pre-separator is to be occupied by the shielding wall. The beam dump is located in the 2 m drift space after the first dipole. A wedge can be placed in the symmetric position to the beam dump across the middle. There is a 1.3 m drift after the second bend magnet where additional shielding can be placed. The 1.1 m drift space at the end of the pre-separator is reserved for the second shielding wall shown in Fig. 1.

During the study, we have also considered the option of same bending direction with a large dispersion in the middle so that a wedge can further purify the beam. By splitting the dipoles, we achieved imaging in the horizontal plane between the split dipoles while keeping the entire pre-separator achromatic as displayed in Fig. 3. Hence the beam dump will be placed between the first two dipoles. Other constraints are the same as the above mentioned s-shaped pre-separator. The drift spaces at the middle, after the last bend and at the end of the c-shaped pre-separator are the same as those in the s-shaped one. In comparison, the c-shaped pre-separator has smaller dispersion at the beam dump (0.4 m in momentum deviation as oppose to 1.06 m). On the other hand, the large dispersion at the centre (1.0 m) makes it possible to either further reduce the momentum spread with a second slit or purify the beam with a wedge.

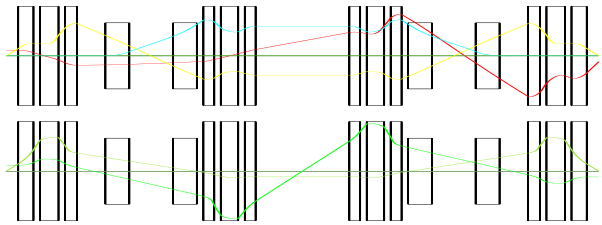

Figure 3: The sine-like, cosine-like and dispersive rays in the c-shaped pre-separator. The conditions of the rays are the same as those of Fig. 2. The total arc length is 27.2 m. The bending angle and arc length of the dipoles are 15° and 1.1 m, respectively.

If only linear dispersion is taken into account, the c-shaped pre-separator clearly has larger momentum acceptance. Yet the advantage vanishes when fringe field and high order aberrations are included. For ±40 mrad angular acceptance, the momentum acceptance for the c-shaped and the s-shaped pre-separators are ±1.5% and ±1.4%, respectively. The sizes of the image at the end are also similar. As a result, only the tracking result of the s-shaped pre-separator is shown in Fig. 4. Attempts to correct aberrations using multipoles have not been successful. It's clear that the size of the image at the end is dominated by aberrations. Furthermore, we found that the aberrations come mainly from the extended fringe field which is based on measured field data of the PEPII magnets [5, 6]. Therefore, magnets designed to limit the extent of the fringe field will help reduce aberrations.

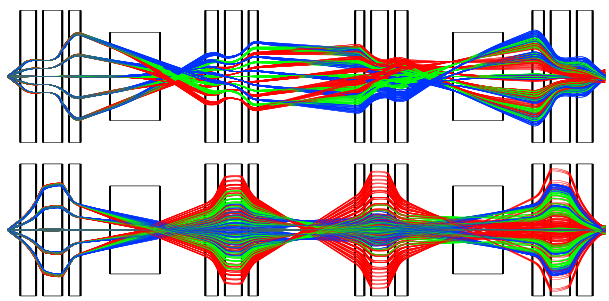

Figure 4: The element-by-element tracking result of the s-shaped pre-separator using 7th order Taylor map. Upper envelop is for horizontal plane and the lower one is for vertical plane. The maximum slope of rays is 40 mrad; the amplitude is 1 mm and the momentum deviation is 1.4%.

OPTICS OF THE MAIN-SEPARATOR

The use of high power primary beam allows the production of isotopes with small cross-sections near the drip-lines of the nuclear chart. To separate such isotopes requires more refined method than a single-stage separation using momentum dispersion by magnetic field to purify the isotope of interest. A profiled wedge degrader at the dispersive focal point is used to allow Z-dependent separation in addition to the dispersion by the magnetic field of the dipole. However, the use of a target material in the beam course adds background particles

and induces energy straggling. The main-stage separator can indentify isotope beam species by measuring the time of flight and energy loss of the beam as well as the magnetic rigidity.

Since the two stages of the main separator are identical, only one is shown in the proceeding figures. The Gaussian optics is somewhat similar to that of the first stage of the BigRIPS [1] or the c-shaped pre-separator. The main difference is that the first half is point-to-parallel in the horizontal plane as well. Apart from the marginal benefit of higher degree of symmetry, the main advantage is that it lowers the strongest quadrupole strength by about 8% compared to the solution of BigRIPS and reduces the magnification of the dispersive image from 1.7 to 1.3, resulting in higher momentum resolution. The disadvantage is that the angular acceptances of the two planes are no longer the same as shown in Fig. 5. The first-order momentum resolution is around 1760, which is expected to decrease around 15-20% when aberrations are included.

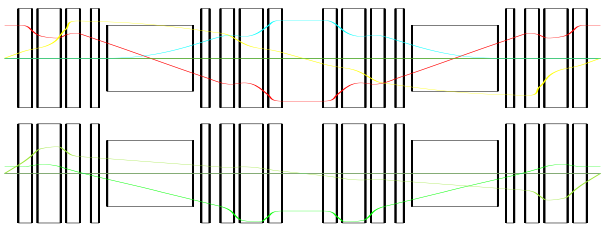

Figure 5: The sine-like, cosine-like and dispersive rays in the main-separator. The slopes of the sine-like rays in the horizontal and the vertical planes are 30 and 50 mrad, respectively; the momentum deviation of the dispersive ray is 5%. The total arc length is 21.8 m. The bending angle and arc length of the dipoles are 30° and 3.14 m, respectively. The four short magnets next to the dipoles are octupoles.

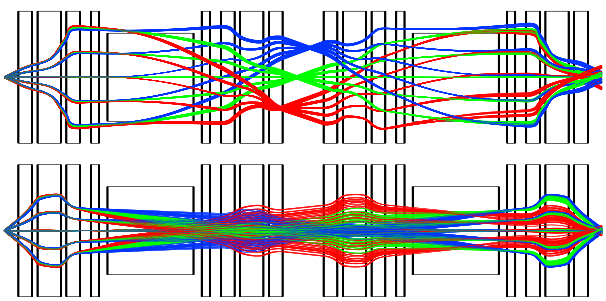

Figure 6: (Top) Effect of aberrations on the horizontal and (Bottom) the vertical planes without multipole correction. The maximum slopes of rays in the horizontal and the vertical planes are 30 and 50 mrad, respectively; the momentum deviation is 3%.

The effects of aberrations were analyzed through element-by-element tracking using the 7th order Taylor for each magnet. As shown in Fig. 6, the aberrations severely degrade the quality of the image both at the middle and at the end. One obvious effect is the change of focal length for different momentum at the middle due to chromaticity. To correct those most prominent terms, we added sextupole coils in the 3rd, 4th, 8th and 9th quadrupoles and octupole coils in the 2nd and 11th quadrupoles, together with four stand-alone octupoles next to the dipoles. The result is presented in Fig. 7, which shows significant improvement.

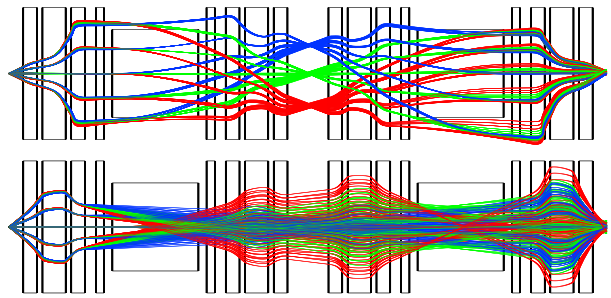

Figure 7: (Top) Effect of aberrations on the horizontal and (bottom) the vertical planes with multipole correction. The maximum slopes of rays in the horizontal and the vertical planes are 30 and 50 mrad, respectively; the momentum deviation is 3%.

CONCLUSIONS

The design of an in-flight fragment separator for the planned Korean heavy-ion beam facility is in the early stage taking into account the designs of existing and future facilities of other places. While the other separator designs have been constrained by the existing facility layout, the Korean facility may provide more freedom in adopting new schemes. Tracking result shows the role aberrations plays in determining the size of the image and the momentum resolution of the separator and the effectiveness of multipoles in aberration correction. Future work includes studying the impact of the wedges and optimizing the beamline based on detailed engineering design.

ACKNOWLEDGEMENTS

This work was supported by National Research Foundation Grant No. 20092006790. The authors want to acknowledge the helps of Dr. T. Kubo of RIKEN and Prof. B. Sherrill of Michigan State University.

REFERENCES

[1] B. Sherrill, Nucl. Instr. and Meth. B 204, 765 (2003).
[2] T. Kubo et al., IEEE Trans. Appl. Superconductivity 17, 1069 (2007).
[3] R. York et al., Proc. of SRF2009, Berlin, Germany, 888 (2009).
[4] I. Baek et al., Proc. of PAC07, New Mexico, USA 1763 (2007).
[5] K. Makino and M. Berz, Nucl. Instr. and Meth. A 558, 346 (2006).
[6] K.L. Brown and J.E. Spencer, IEEE Trans. Nucl. Sci. NS-28, 2568 (1981).

CENTRAL REGION DESIGN OF A BABY CYCLOTRON

He Xiaozhong, Yang Guojun, Zhang Kaizhi, Long Jidong
IFP, CAEP, Mianyang, Sichuan, China

Abstract

Baby cyclotrons are widely used in short lived β+ radioactive isotope production. A 11 MeV baby cyclotron for PET isotope production was designed and is in construction in CAEP now. Central region design is one of the most important parts of cyclotron design work. In this paper, central region design of the 11 MeV baby cyclotron, including design processes and design results, is reported.

INTRODUCTION

PET (Positron emission tomography) becomes more and more widely used in China. A project was started in the end of 2007 in CAEP, to design and construct a 11 MeV baby proton cyclotron for PET isotope production. Main design parameters of the 11 MeV cyclotron are listed below [1].

Table 1: Main design parameters of the 11 MeV cyclotron in CAEP

Mag-net	Number of sectors	4	Ion source	Type	H-, Internal PIG
	Hill gap /cm	3.8			
	Hill angle /Deg	58			
	Valley gap /cm	140			
	Radius of the pole /cm	45	Central region	Accepted RF Phase /Deg	0-40
	B_{avg} /Tesla	1.18	Extraction	Type	Carbon foil
RF	Number of Dees	2		Number of stations	2
	Dee voltage /kV	42 or 37		Radius /cm	40
	Frequency /MHz	72	Vaccum	Pressure /Pa	1×10^{-3}
	RF power /kW	~10		Pump speed /Ls^{-1}	⩾4000

CENTRAL REGION DESIGN

Firstly, the magnetic field map is calculated by Opera3D [2]. The magnetic field map is shown in Fig1. Then, a H- ion with equilibrium momentum starts to decelerate from the extraction radius to central region. Slightly adjusting the dee voltage, we can make that the ion decelerates to rest exactly at the center of the magnet. The position and direction of first several gaps, are recorded as the initial central region electrode position and direction. Then, the CAD model of the central region is constructed, and the electric field map is calculated by MAFIA. The electric field map of median plane is shown in Fig2. Particles are emitted from the slit of ion source, and the Dee serves as the puller. After that, the beam trajectories are calculated by a particle tracking code written in c++. Finally, the first several gaps are adjusted adaptively to improve the accepted RF phase and to improve the centralization.

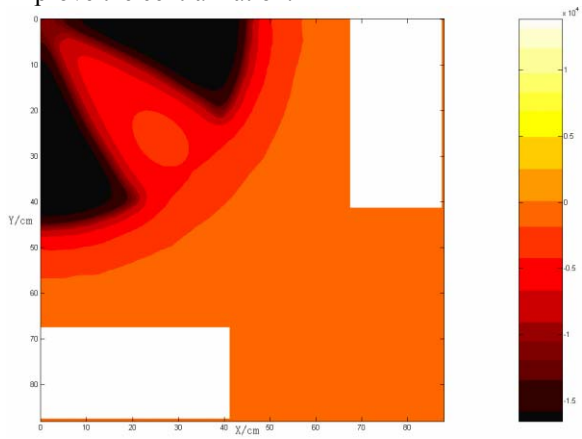

Figure 1: magnetic field map of the median plane

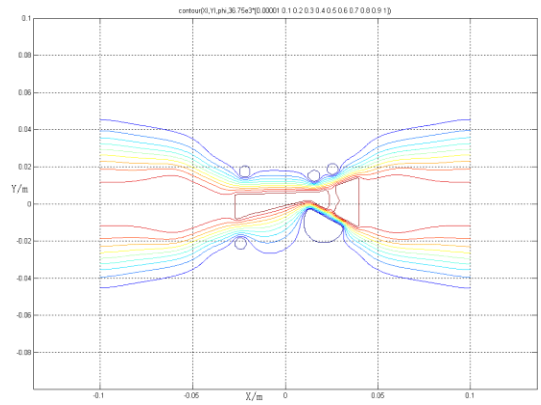

Figure 2: electric field map of the median plane

PARTICLE TRACKING

The beam tracking was done with a code written in c++ by our team. The code synchronizes the magnetic field computed by Opera and electric field computed by MAFIA, and tracks the particles by 4th order Runge-Kutta fixed step method.

H- ions start with zero momentum, from the position of the ion source slit. The width and height of the slit is .4mm and 5mm respectively. After optimization of the first several gaps, all particle emitted from the ion source slit and with initial RF phase of 0-40 degree can be accelerated in central region. The orbit, vertical motion, and energy gain are shown in figure 3-5. The vertical gap of the central region is 12mm, so the maximum expansion factor of the vertical beam size in central region is 2.5. Fig4 shows, the maximum expansion factor is only about 1.7 and all particles emitted with 0-40 degree RF phase will pass through the central region without loss due to vertical motion.

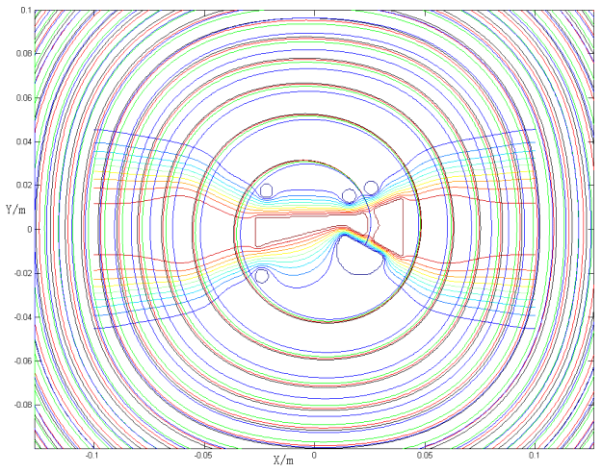

Figure 3: The trajectories of particles with initial RF phase of 0-40 degree. The black, red, green and blue are corresponding to 0, 20, 30, 40 initial RF phase respectively.

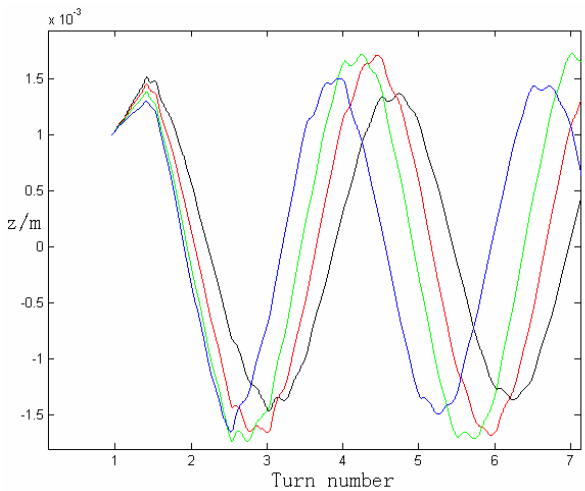

Figure 4: Vertical motion of particles with initial RF phase of 0-40 degree

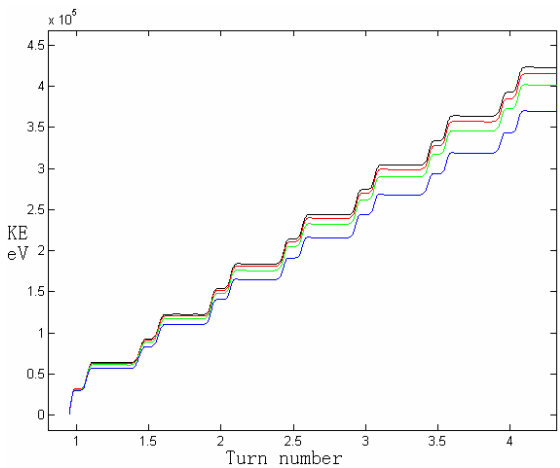

Figure 5: Energy gain of particles with initial RF phase of 0-40 degree

CENTRALIZATION OF THE ORBIT

(dr=r-re, rp) phase space at the center of magnet valley is used to indicate the extent of the centralization of beam trajectories. (dr, rp) phase space with initial RF phase of 0, 20, 30, 40 degree are shown in Fig6. As another indication of the centralization, RF phase at the valley of the magnet VS turn number, which is another indication of the extent of the centralization of beam trajectories, is shown in Fig 7. From the (dr, rp) phase spaces, we can find that particles with 0-30 degree initial RF phase move with quite small dr, so they move quite close to equilibrium particle. For all particles with 0-40 degree initial RF phase, the centralization offset is less than 1 millimeter. In Fig7, the curve with 40 degree initial RF phase oscillates with larger amplitude than that with 0-30 degree initial RF phase. It implies that particles with 40 degree initial RF phase centralized not well as 0-30 degree initial RF phase. This is agree with the (dr, rp) phase space.

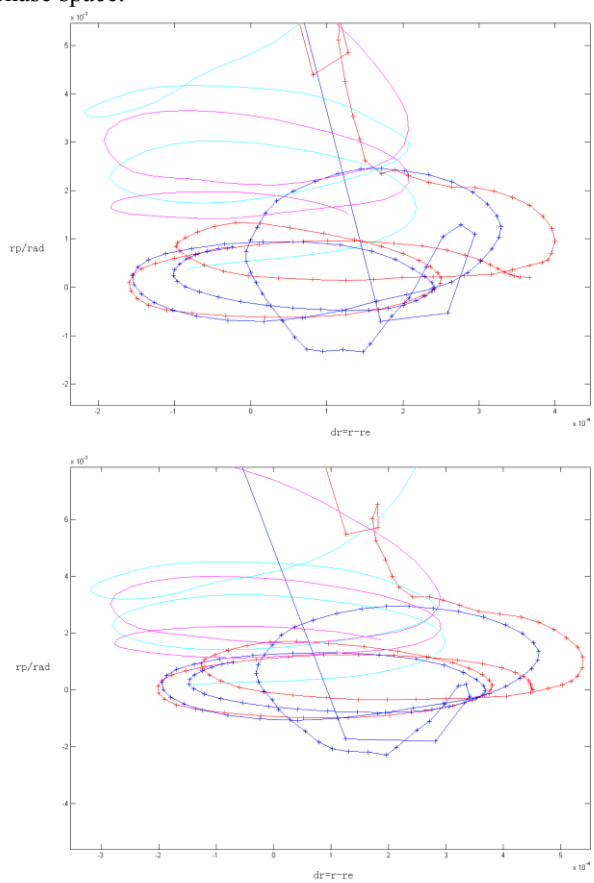

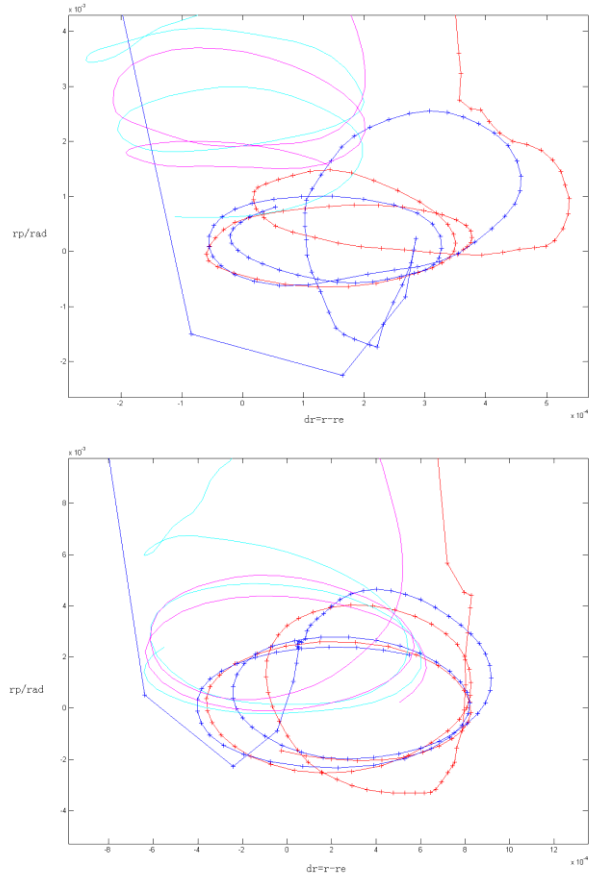

Figure 6: (dr, rp) phase space of the particle trajectories

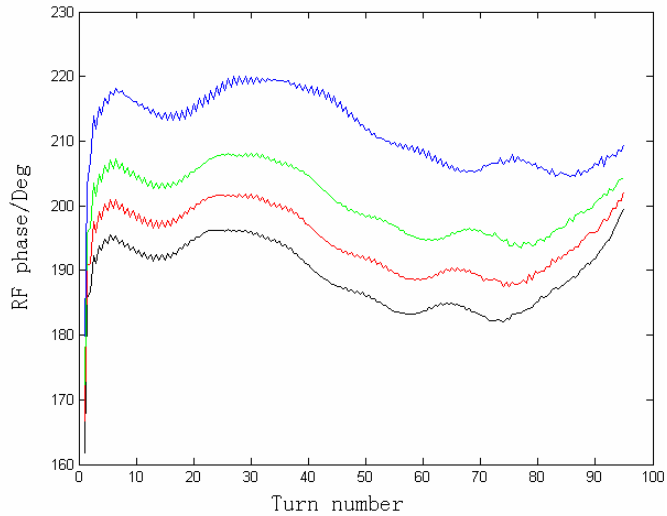

Figure 7: RF phase at the magnet valley VS turn number of the particle trajectories

DISCUSSION

Central region of a 11 MeV cyclotron was designed. Beam tracking was done with a code written in c++ by our team. The particles are emitted from the slit of ion source in rest. After several adaptive design processes, the accepted RF phase of the central region reached 40 degrees.

The beam dynamics in the first gap may be sophisticated because of the existence of the plasma in the first gap. But the beam tracking code neglects the plasma in the first gap, which may leads to errors of the simulation results.

REFERENCES

[1] He Xiaozhong et al. Annual Science and Technology Conference of CAEP, Mianyang, May, 2008.
[2] Opera user manual.

DESIGN OPTIMIZATION OF THE SPIRAL INFLECTOR FOR A HIGH CURRENT COMPACT CYCLOTRON

A. Goswami, P. Sing Babu and V. S. Pandit*
Variable Energy Cyclotron Centre, 1- AF, Bidhannagar, Kolkata-700 064, India

Abstract

This paper describes the design of a spiral inflector in an environment where magnetic field is not constant in the region occupied by it and results of studies done on its optical properties in the presence of space charge. We have used the magnetic field data obtained from a 3D code and analytical electric field. We have also checked the orbit centering of the injected beam using a central region code. The effects of linear space charge have been evaluated and optimization of the input beam parameters has been done to minimize the coupling effects.

INTRODUCTION

At the Variable Energy Cyclotron Centre, we are developing a 10MeV, 5mA compact proton cyclotron [1]. A 2.45 GHz microwave ion source presently under testing for beam characterization, will produce ~20mA of proton beam at 80 keV. The extracted beam will be first collimated using slits, bunched using a sinusoidal buncher and will be injected axially in the central region of the cyclotron where a spiral inflector [2] will place the beam on the proper orbit. Two delta type resonators, each having ~ 45 degree angle located in the opposite valleys, will be used for providing acceleration to the beam.

Due to low average magnetic field and large ratio of hill/valley fields (~7), the computed magnetic field in the central region near the axis of the cyclotron is slightly lower than the resonance field (6.89 kG) and it also varies with radius. This makes the design of the spiral inflector more complicated and challenging.

We have developed a code to calculate the central ray in the spiral inflector using the 3D magnetic field data. Results were compared with CASINO [3]. The output of the program was used in code INFLECTOR [4] to find the shape of the electrodes. The electric field in the inflector was calculated using RELAX3D [5]. We have computed the paraxial ion trajectory in the presence of space charge effect and optimized the initial starting conditions of the beam to get minimum coupling effects in two transverse phase planes at the inflector exit.

SPIRAL INFLECTOR

Details of the spiral inflector have been described in classical reference [2] and in many other papers. Here we briefly outline the formulations used to design the spiral inflector. We have used the right handed Cartesian coordinate system x, *y*, *z* whose origin lies on the cyclotron axis. The *z* axis is vertically opposite in the direction of the incoming ion and major component of the magnetic field (B_z) is opposite to the z direction and initial electric field is along the *x* direction. The components of Lorentz force equation in the combined electric and magnet field can be written as:

$$x'' = \frac{q}{mv_0^2}E_x + \frac{q}{mv_0}\left(z'B_y - y'B_z\right) \quad (1a)$$

$$y'' = \frac{q}{mv_0^2}E_y + \frac{q}{mv_0}\left(x'B_z - z'B_x\right) \quad (1b)$$

$$z'' = \frac{q}{mv_0^2}E_z + \frac{q}{mv_0}\left(y'B_x - x'B_y\right) \quad (1c)$$

where v_0 is the velocity, *m* is mass and q is the charge of the ion. Here the electric and magnetic fields both are the functions of coordinates *x*, *y*, *z* and the prime denotes the differentiation with respect to path length $s = v_0 t$ .The electric fields for tapered electrodes of a spiral inflector can be written as

$$E_x = E_0\left(-\frac{x'z'}{\sqrt{x'^2+y'^2}} - \frac{y'}{\sqrt{x'^2+y'^2}}\tan\theta\right) \quad (2a)$$

$$E_y = E_0\left(-\frac{y'z'}{\sqrt{x'^2+y'^2}} + \frac{x'}{\sqrt{x'^2+y'^2}}\tan\theta\right) \quad (2b)$$

$$E_z = E_0\sqrt{x'^2+y'^2} \quad (2c)$$

Here θ is the local tilt angle and E_0 is the magnitude of the electric field which is always constant and perpendicular to the direction of motion of the ion and decides the height parameter *A* of the spiral inflector;

$$A = 2T/qE_0 \quad (3)$$

T is the kinetic energy of the ion. In fact *A* is the electric radius of the ion in the absence of the magnetic field.

In the case of a tilted inflector a component of the electric field is used to generate a force in the plane of the magnetic force to modify the beam centering. The spacing between electrodes is narrowed gradually to maintain the electric radius constant. The local tilt angle θ is given by

$$\tan\theta = k'\frac{A - z(s)}{A} \quad (4)$$

*pandit@vecc.gov.in

where k' is a free parameter defines the maximum tilt angle $\theta_m = \tan^{-1} k'$ at the exit of the inflector (z = 0). Choosing a suitable value of A and k' one can easily solve the differential equations (1) to get the coordinates of central ion trajectory in a given magnetic field and hence the required shape of the spiral inflector.

We have written a computer code to analyze the central ion trajectory through the spiral inflector in the presence of 3D magnetic field and analytical electric field. We have performed all the calculations at injection energy of 80 keV. Important parameters of the inflector are listed in Table 1.

Table 1: Parameters of the inflector

Parameters	Values
Height (A)	8.6 cm
Tilt (k′)	0.65
Electric field	18.5 kV/cm
Off centering	4.1 cm
Electrode gap entrance/exit	1.4 cm/1.2cm
Position at exit (r,θ)	7.05 cm , 99.11°

The central trajectory data is used in the programme INFLECTOR to create the shape of the electrodes (shown in Figure 1) and mesh points for RELAX3D to calculate the electric field distributions in the spiral inflector.

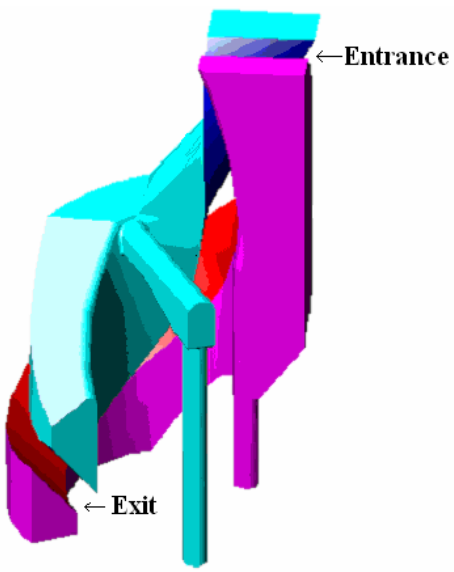

Figure 1: Optimized electrode geometry of the inflector.

Figure 2 shows the electric field calculated using RELAX3D on the axis along the central trajectories and compares with the analytical field (hard edge approximation). We can easily see that the effect of fringe field is very small due to the choice of comparatively large height A in the present design.

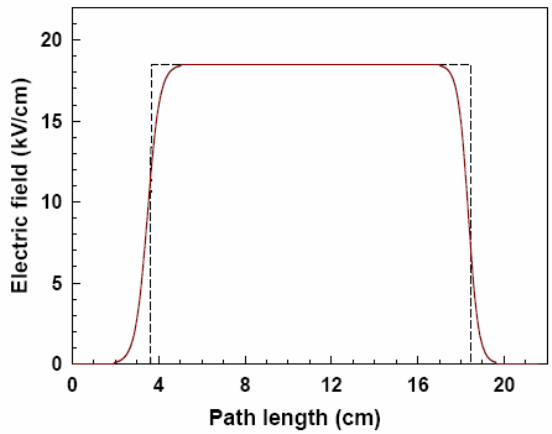

Figure 2: Comparison of analytic and computed electric field along the central trajectory inside the spiral inflector.

ORBIT CENTERING

The orbit centering of the injected beam to the central region of the cyclotron was checked using a central region code. The coordinates and velocity of the particle at the inflector exit are entered as an input to this programme. All calculations of the beam centering have been performed with following parameters: injection energy = 80keV, Dee Voltage = 125kV, gap width between dee and dummy dee = 2cm, dee height = 3cm and magnetic field obtained from 3D code. Figure 3 shows the position of the accelerating gaps in the median plane and accelerated orbits of protons.

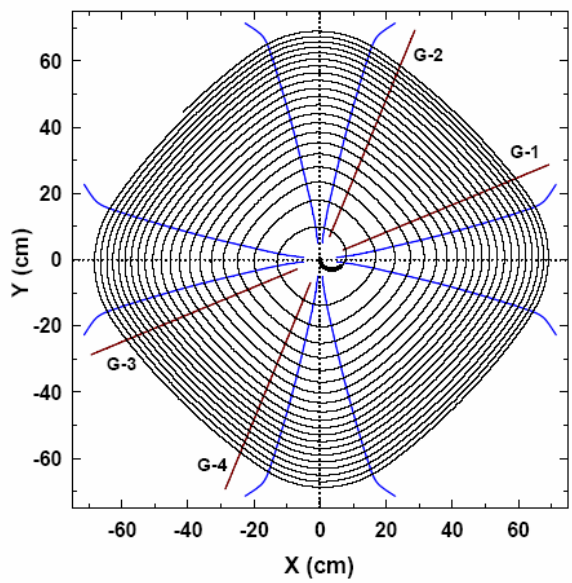

Figure 3: Position of the inflector, location of the accelerating gaps and optimized accelerated orbits for protons from 80 keV to 10 MeV.

INPUT BEAM OPTIMIZATION

Because of high intensity, it is necessary to study the effect of space charge on the beam transmission through the spiral inflector. In order to achieve the optimum

performance, the input condition must be optimized to minimize the dilution of the beam emittance at the inflector exit. We have used the paraxial ray trajectory equations given in reference [6] with some modifications in the space charge term. Since these equations are valid only for a constant magnetic field, we have found out a constant field B_0=5.15 kG (resonance field 6.89 kG) which gives almost identical central ray trajectory for fixed A and k' as shown in Figure 4. In our calculations we have neglected the effect of fringe field at the entrance and exit of the spiral inflector which is very small.

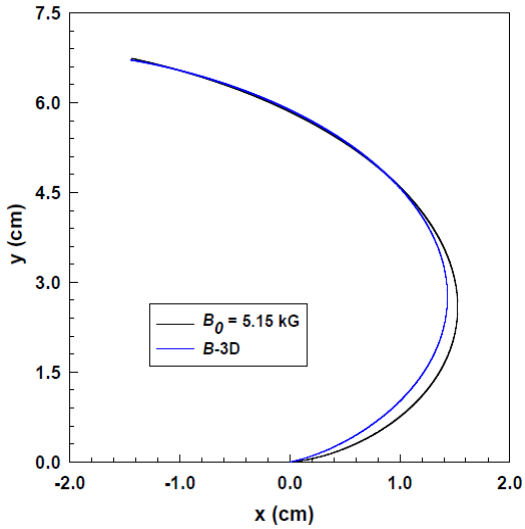

Figure 4: Central ray trajectories with 3D magnetic field and constant magnetic field of 5.15 kG.

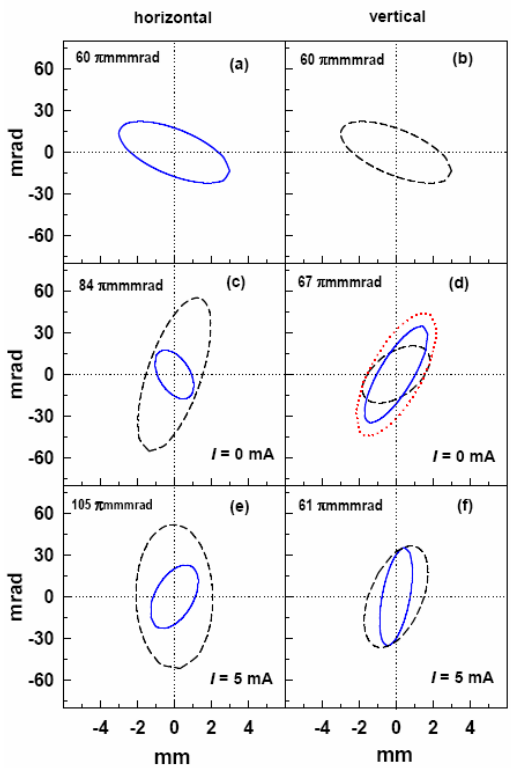

Figure 5: Phase space diagrams in horizontal and vertical planes: a) & b) at entrance; c) & d) at exit with I=0 mA, e) & f) at exit with I=5 mA (I_{peak} in the bunch~60mA)

The phase space ellipses, in the horizontal (h-plane) and vertical (u-plane) planes at the entrance and exit of inflector are presented in Figure 5 for two values of the beam current and of equal emittances 60 πmmmrad in both planes. We can clearly see the coupling effects between the horizontal and vertical motions. We have taken care that the effect of coupling on the emittance dilution should be minimum in the vertical plane because focusing forces are weak in this plane. The estimated effective emittances at the exit in the horizontal and vertical planes are indicated in Figure 5. The beam envelopes around the central ion trajectory obtained using twelve different initial conditions of the particles on entrance ellipse through the inflector is shown in Figure 6. The maximum beam size in both planes at the exit is within 5 mm, less than the gap between the electrodes at the exit (12 mm).

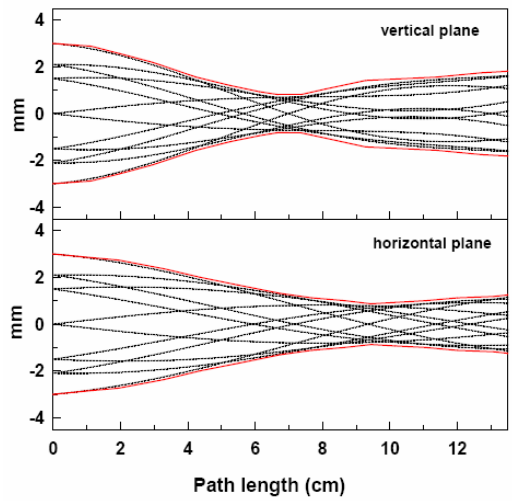

Figure 6: Beam envelop in the inflector.

CONCLUSION

We have presented the design of spiral inflector using 3D magnetic field data. The beam centering requirement forced us to chose tilt parameter k'= 0.65, making the fabrication a challenging job. Numerical simulations with linear space charge effects have been performed and input beam parameters have been optimised to have minimum coupling between the two transverse planes at the inflector exit.

REFERENCES

[1] V. S. Pandit, "Development of ion source and injection system for high current compact cyclotron" Indian Particle Accelerator Conference InPAC-05 (2005) 13
[2] L. Belmont, J. L. Pabot, IEEE Trans. Nucl. Sci. NS-13 (1966) 191
[3] F. B. Milton, J. B. Pearson, CASINO User's Guide and Ref. Manual, TRI-DN-89-19, Vancouver, 1989.
[4] Lj. M. Milinkovic, RELAX3D Spiral Inflectors, TR30-DN-89-21, Vancouver, 1989.
[5] C. J. Kost , F.W. Jones, RELAX3D User's Guide and Reference Manual, TRI-CD-88-01, Vancouver, 1988.
[6] D. Toprek, Nucl. Instr.& Meth. Phys. Res. **A453** (2000)501.

BEAM TUNING IN KOLKATA SUPERCONDUCTING CYCLOTRON

M. K. Dey, J. Debnath, J. Pradhan, A. Dutta, U. Bhunia, Z. Naser, S. Paul, Md. Haroon Rashid,
V. Singh, A. Agrawal, C. Mallik, and R.K.Bhandari
Variable Energy Cyclotron Centre, Kolkata, India

Abstract

The Superconducting cyclotron at VECC, Kolkata, has accelerated ion beams up to extraction radius successfully confirmed by the neutrons produced by the nuclear reactions. The internal beam tuning process started with beam parameters calculated using the measured magnetic field data [1]. Due to some mechanical and electrical problems we were forced to tune the beam with three major trim coils off. Accurate positioning of central region Dee-extensions ensuring the proper acceleration gaps in the first turn was required for successful acceleration of beam through the compact central region clearing the posts in the median plane. Here we present different aspects and results of initial beam tuning.

INTRODUCTION

The superconducting cyclotron at VECC, Kolkata, attained its major milestone in August 2009 when Ne^{+3} beam was accelerated to full extraction radius, after all the major subsystems were tested and operated synchronously. Beam acceleration involves following issues:

- Production of ion beam in the ECR ion source and transport the ion beam through 28 m beam line
- Transmission of beam through vertical beam line (~3 m) and axial cylindrical hole in the magnet yoke (~1.1 m) where high fringing field exists
- deflection of beam in the cyclotron median plane with a spiral inflector and clearing the central region by proper centering of the beam
- Obtaining isochronous magnetic field till extraction radius and accurate knowledge of beam dynamics in the cyclotron, which in turn required a very precise mapping of the guiding magnetic field inside the magnet and calculation of accelerating electric field.

Here we discuss the beam dynamical calculations using measured magnetic field data which helped in obtaining optimum settings for beam acceleration.

BEAM INJECTION

The ECR ion source operates at 14.4 GHz microwave frequency at maximum of 1 kW of power to produce light ion beams such as N, O, Ne, Mg, Al, S etc. and heavier ion beams like Ar, Kr, Xe etc. Till now Argon and Neon ion beams have been successfully injected and accelerated. The heavy ion beams, produced in ECRIS, are charge/mass separated by an analyzing magnet and then guided through horizontal beam line sections and bend downwards (~22 m length in total) to be injected into the cyclotron through its axial hole[2]. The beam injection system consists of solenoid magnets, steering magnets, diagnostics elements, vacuum pumps and the spiral inflector.

Figure 1: The ECR ion source and injection beam line in the high bay (top) and the superconducting cyclotron along with external beam line in cyclotron vault (bottom).

The injection beam line is designed for the maximum beam rigidity of 0.058 T-m, which corresponds to ions with specific charge (η=q/A) equals to 0.12 and energy equals to (20*η) keV/u.

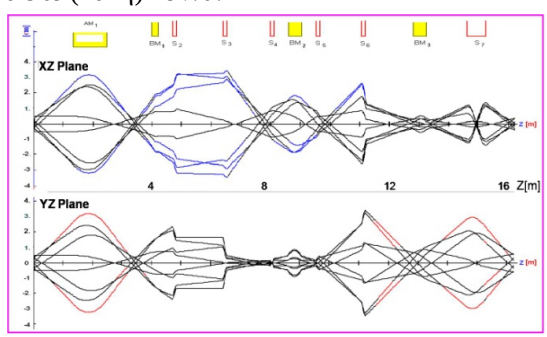

Figure 2: Beam profile along the injection beam line from ECRIS up to the matching point on the vertical beam line.

Along the axial hole large fringing field exists up to several meters from median plane (~10mT at 4m) which couples transverse motions of the charged particles resulting blow up or the beam. A long solenoid

(L_{eff}=63.5cm, B_0=1.57kG), placed just above the cyclotron yoke, is used for beam confinement and matching with the spiral inflector. The injected beam is bent into the median plane of cyclotron by a spiral inflector having aperture of 4 mm.

EQUILIBRIUM ORBIT PROPERTIES

The optimum isochronous field is produced by a pair of superconducting coils (main coils), the iron core and 14 trim coils. A field fitting code (TCFIT) is used to calculate the main coil and trim coil current settings required to produce an appropriate field for accelerating a beam to its desired final energy, with the constraint that the trim coils power consumption is minimum. The specific charge (Q/A), final energy and the energy vs. phase curve is given as input values. It also calculates the correct the RF frequency so that the energy spread is minimized at extraction radius. This is achieved by making $\int_{E0}^{E\,max} \sin\varphi\, dE = 0$, where, $\sin\varphi(E) = \sin\varphi_0 + \frac{2\pi h}{qV_{dee}} \int_{E0}^{E} W(E)dE$.

This is the well known phase-energy relation for an accelerated particle in the cyclotron. The simulation results from '*TCFIT*' for the ion species: $^{20}Ne^{3+}$, E = 4.4 MeV/u, Bo=30.9 kG, ν_{rf} =14 MHz, h=2, are shown in following figure.

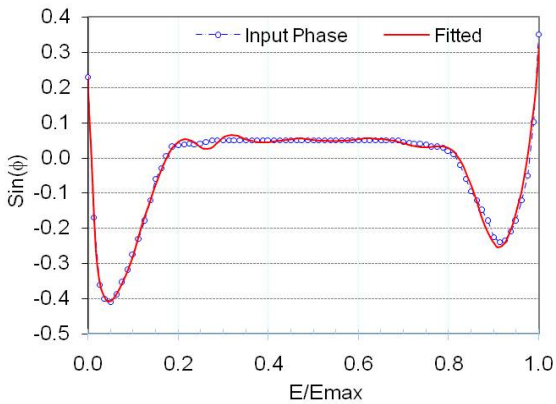

Figure 3: Input phase curve and fitted phase.

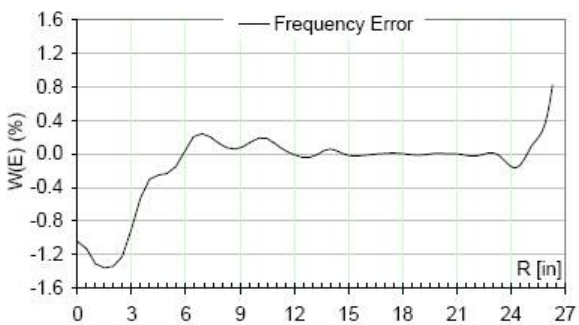

Figure 4: Frequency error along radius

The phase φ implies the particle timing relative to the RF accelerating voltage. The frequency error $W(E) = \frac{\omega}{\omega_0} - 1$, where $\omega_0 = 2\pi h \nu_{rf}$ and ω is the instantaneous particle angular frequency. This phase curve has been chosen to meet several important criteria. First the large initial positive phase is chosen to gain electric focusing (ν_z^2 =h Sinφ/2πn, n is the turn number) in the first few turns. The negative excursion and subsequent rise back to zero is a result of tailoring the magnetic field so that ν_z does not become too small (<0.1).

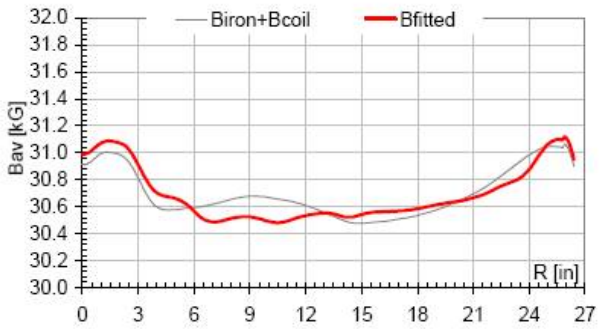

Figure 5: Field profile along radius at fitted current set

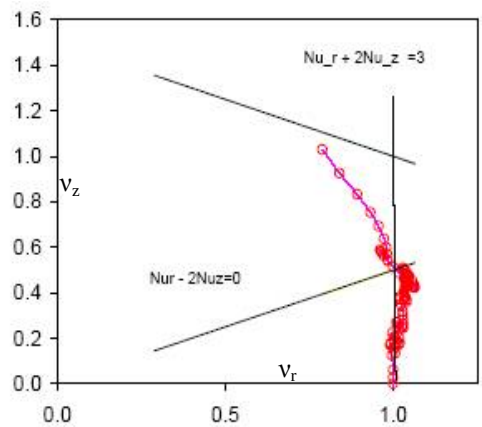

Figure 6: ν_r Vs ν_z plot

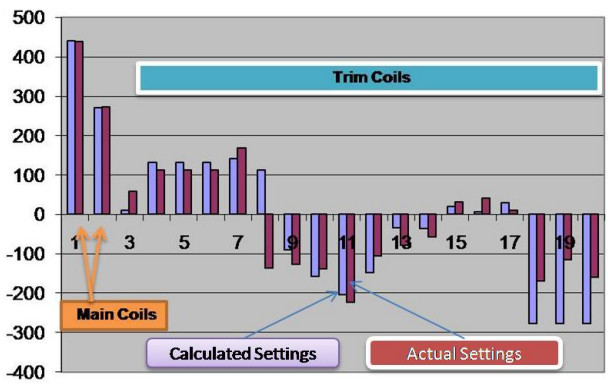

Figure 7: Comparison of the main coil & trim coil current settings

The frequency error W(E) corresponding to the optimized isochronous field is such that and the integral of sin(φ) near extraction is nearly zero ensuring minimum energy spread in the beam. The frequency error curve also shows that W(E) is nearly equal to zero from 6 to 24 inch radius suggesting good degree of isochronisms (fig 4). The initial large frequency error in the curve is

due to the 'cone field' necessary for providing axial stability to the beam in the region where flutter is not sufficient.

As shown, the magnetic field can provide satisfactory horizontal and vertical focusing all along the accelerating path (fig 6). Another important beam dynamical issue that needs careful study is to ensure that the beam does not meet any devastating resonance $\nu_r+2\nu_z=3$ before being extracted and it crosses the $\nu_r=2\nu_z$ zone quickly. The tune diagram (fig 6) shows that the investigating species meets these two criterions satisfactorily.

SIGNATURE OF ACCELERATED BEAM

Accelerated Ne^{3+} beam in the VECC superconducting cyclotron was observed on bore-scope beam viewer at 384 mm from centre for the first time on 14th August 2009. The beam was accelerated in 2nd harmonic mode. On 25th August 2009, the beam current up to 30 nA at 650 mm from centre was read by the main probe.

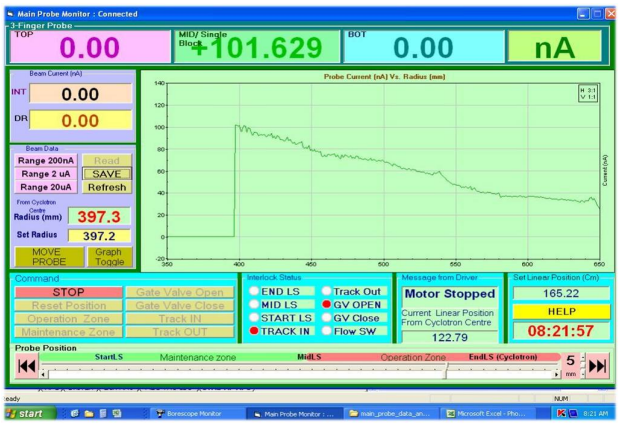

Figure 8: Ne3+ beam current variation with radius as seen on main probe control console.

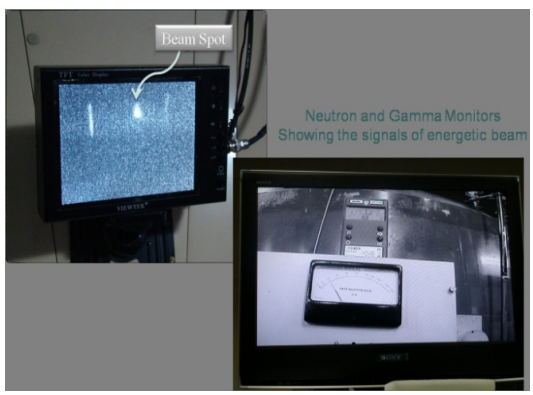

Figure 9: Beam spot on Borescope at 650 mm radius

SC cyclotron area is equipped with area neutron and gamma monitors. Neutron monitors are BF-3 based proportional counter with a paraffin moderator. Gamma Area monitors are based on GM tubes. Area neutron monitor placed near the exit port measured a neutron flux of 10 n/cm^2/sec, with Ne^{3+} accelerated beam of about 30 pnA beam current at the extraction radius with total energy of 88 MeV. A (5"x 7") BC-501A liquid scintillation was place along with standard Pulse Shape Discrimination Circuit (PSD) to detect both neutron and Gamma based on rise time dependent signals. The detector was place about 2 m away from the edge of the machine in the beam extraction direction. The following spectra show a clear evidence of neutron and gamma during operation of machine.

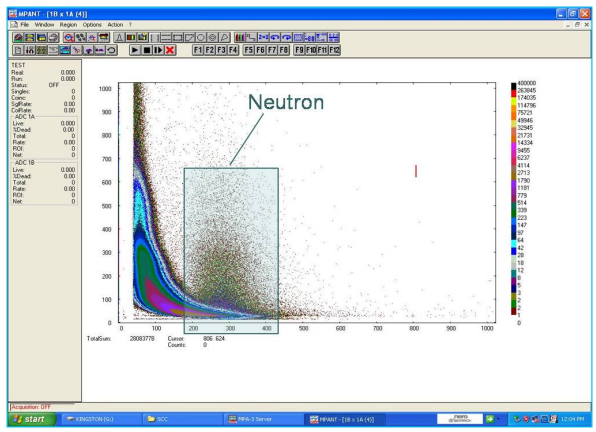

Figure 10: Neutron-Gamma discrimination with liquid scintillator.

CONCLUSION

The Kolkata superconducting cyclotron has been successfully commissioned with internal ion beams accelerated up to extraction radius producing neutrons via nuclear reactions. Shortly the beam will be extracted out of the cyclotron and transported to the experimental area for nuclear physics experiments.

REFERENCES

[1] C. Mallik, et. al., "Magnetic Field Mapping of Kolkata Superconducting Cyclotron", 18th International Cyclotron Conference, 2007, p.435.

[2] M. K. Dey, et. al., "Beam Injection System of the Kolkata Superconducting Cyclotron", 18th International Cyclotron Conference, 2007, p.346.

DETERMINATION OF ISOCHRONOUS FIELD USING CALCULATED MAP OF MAGNETIC FIELD IN CYCLOTRON MEDIAN PLANE

N. Kazarinov†, V. Kazacha, O. Borisov, JINR, Dubna, Moscow region, Russia

Abstract

In this work a new scheme for calculation of a cyclotron isochronous field using the previously calculated or measured map of the cyclotron magnetic field in its median plane is adduced. The calculating map of the cyclotron magnetic field was set by the matrix having the dimensions 201×181. The flutter part of the magnetic field obtained by subtraction of the zero azimuth harmonic from the magnetic field values was calculated in all net nodes. The magnetic rigidity value in the equation for the particle radius versus the angle was replaced by product of the mean radius and mean along the closed orbit magnetic field. The flutter function was interpolated with the help of the third order Lagrange's polynomials using 16 nodes of the net. At every given radius with the help of the nonlinear simplex method of optimization one can find such value of the isochronous field when the particle path is enclosed with accuracy of 10^{-9}. The results of the fulfilled calculations for the cyclotron DC-110 and their comparison with results of other calculations are given.

INTRODUCTION

A scheme for determination of a cyclotron isochronous field using the previously calculated or measured map of the cyclotron magnetic field in its median plane is adduced. The results of the fulfilled calculations for the cyclotron DC-110 [1] and their comparison with results of other calculations are given.

SCHEME OF CALCULATIONS

The cyclotron DC-110 has 4 "hills" and 4 "valleys". Therefore four full periods of the magnetic field $B(r,\theta)$ are kept within the circuit ($r = const$) when $0 \le \theta \le 2\pi$. The calculated map of the cyclotron magnetic field in its median plane was set by the matrix $Q_{i,j}$ having the dimensions 201×181. The values of the flutter part $F(r_i,\theta_j)$ were calculated in the net nodes (r_i,θ_j) by subtraction of the zero azimuth harmonic from the magnetic field values.

The distribution of the flatter versus radius is shown in Fig. 1. The calculated flutter versus the angle θ for r = 80 cm is shown in Fig. 2.

The following differential equation for a reference particle radius r [2] was used in our calculations.

$$\frac{d}{d\theta}\left(\frac{r'}{\sqrt{r^2+(r')^2}}\right)=\frac{r}{\sqrt{r^2+(r')^2}}+\frac{r[B(r)+F(r,\theta)]}{B\rho} \qquad (1)$$

†nyk@lnr.jinr.ru

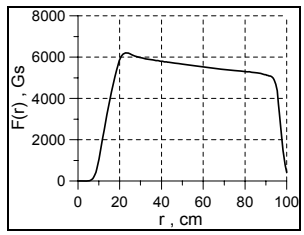

Figure 1: Flutter function $F(r)$ when $\theta = const$

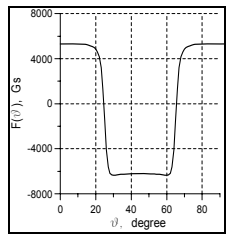

Figure 2: Flutter function $F(\theta)$ when r = 80 cm

The magnetic rigidity $B\rho$ value in (1) was replaced by product of the mean radius $\bar{r}$ and mean along the closed orbit magnetic field $\bar{B}$:

$$B\rho = \bar{r}\bar{B}(\bar{r}) \;\; ; \;\; \bar{B}(\bar{r}) = \frac{B_0}{\sqrt{1-(\bar{r}/r_\infty)^2}}$$
$$B_0 = \frac{A}{Z}\cdot\frac{M_p c^2}{e}\cdot\frac{1}{r_\infty} \;\; ; \;\; r_\infty = \frac{ch}{2\pi f} \qquad (2)$$

Here A is the ion atomic mass, Z is the ion charge, M_p is the atomic unit mass, c is the speed of light, e is the elementary charge, h is the harmonic number and f is the frequency of the cyclotron RF generator.

As a result the isochronous magnetic field was found by solving the following system of equations:

$$\begin{cases} \dfrac{d}{d\theta}\left(\dfrac{r'}{\sqrt{r^2+(r')^2}}\right)=\dfrac{r}{\sqrt{r^2+(r')^2}}+\dfrac{r[B(r)+F(r,\theta)]}{\bar{r}\bar{B}(\bar{r})} \\ \dfrac{d\rho}{d\theta}=\dfrac{r}{2\pi}\cdot\sqrt{1+\left(\dfrac{r'}{r}\right)^2} \\ 0 \le \theta \le 2\pi \end{cases} \qquad (3)$$

Here the function $\rho(\theta)$ defines the mean radius of the closed orbit $\bar{r} = \rho(2\pi)$. During calculation the value $\bar{r}$ was found by iteration with specified accuracy of 10^{-9}.

The function $B(r)$ is the varying magnetic field specified in the points w_i ($i = 1,...,N$) along the radius where $N = R_{extr}/\Delta r$ and Δr is the value of chosen radial step. When $r = 0$ then $B(r) = B_0$.

The function $B(r)$ in the range between two points w_i and w_{i+1} was found by means of the linear interpolation:

$$B(r) = B(w_i)\cdot\frac{r-w_{i+1}}{w_i-w_{i+1}} + B(w_{i+1})\cdot\frac{r-w_i}{w_{i+1}-w_i} \qquad (4)$$

The flutter function $F(r,\theta)$ was interpolated with the help of third order Lagrange's polynomials using 16 nodes of the net. Part of this net is shown in Fig. 3.

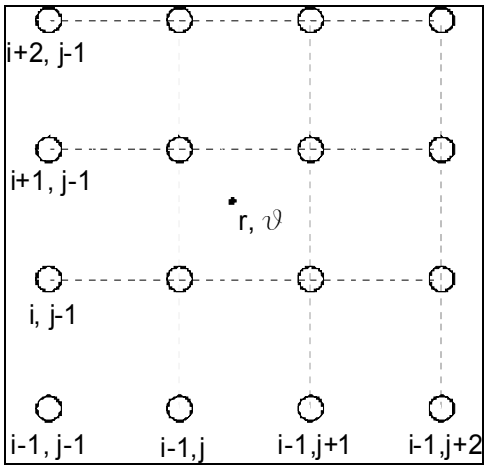

Figure 3: Part of the net

The flutter part of the magnetic field in an arbitrary point having the coordinates $\{r,\theta\}$ was found using the values of the magnetic field in 16 neighbours nodes (given in the matrix $Q_{i,j}$) in the following way. At first the value $F_k(\theta)$ was calculated on four horizontal layers of this part of the net.

$$\begin{aligned} F_k(\theta) = &-Q_{k,j-1}\cdot\frac{(\theta-h_\theta(j-1))\cdot(\theta-h_\theta j)\cdot(\theta-h_\theta(j+1))}{6h_\theta^3}+\\ &+Q_{k,j}\cdot\frac{(\theta-h_\theta(j-2))\cdot(\theta-h_\theta j)\cdot(\theta-h_\theta(j+1))}{2h_\theta^3}-\\ &-Q_{k,j+1}\cdot\frac{(\theta-h_\theta(j-2))\cdot(\theta-h_\theta(j-1))\cdot(\theta-h_\theta(j+1))}{2h_\theta^3}+\\ &+Q_{k,j+2}\cdot\frac{(\theta-h_\theta(j-2))\cdot(\theta-h_\theta(j-1))\cdot(\theta-h_\theta j)}{6h_\theta^3}\\ &k=i-1,i,i+1,i+2 \end{aligned} \quad (5)$$

Here h_θ = 1 degree. It is the value of the net step. The final value of the magnetic field in the given point one can get by formula:

$$\begin{aligned} B(r,\theta) = &-F_{i-1}(\theta)\cdot\frac{(r-h_r(i-1))\cdot(r-h_r i)\cdot(r-h_r(i+1))\cdot}{6h_r^3}+\\ &+F_i(\theta)\cdot\frac{(r-h_r(j-2))\cdot(r-h_r i)\cdot(r-h_r(i+1))\cdot}{2h_r^3}-\\ &-F_{i+1}(\theta)\cdot\frac{(r-h_r(i-2))\cdot(r-h_{r\theta}(i-1))\cdot(r-h_r(i+1))\cdot}{2h_r^3}+\\ &+F_{i+2}(\theta)\cdot\frac{(r-h_r(i-2))\cdot(r-h_r(i-1))\cdot(r-h_r i)\cdot}{6h_r^3} \end{aligned} \quad (6)$$

Here h_r = 5 mm is the value of the radial net step.

The system of equations (3) was solved by Runge-Kutta method with the step equal to 1/32 of degree.

In calculations the initial azimuth is chosen in the middle of the hill. Thereby the closed orbit has a maximum radius r_{max} at this point. The radius r_{max} is increased in our calculation from zero up to the extraction radius with the step 1 mm. At every subsequent step on the radius r_{max} one can found with the help of optimization algorithm (simplex method, for example) such value of the isochronous field $B_{is}(r_{max})$ when the particle orbit is enclosed with sufficient accuracy (10^{-9} in our calculation). During optimization process the values of the isochronous field at inner radii were found by formula (4) with values of isochronous magnetic field at the nodes w_i obtained in the previous steps of calculation.

To check-up the accuracy of our calculations the results were compared with ones obtained in [3] for $^{86}Kr^{13+}$ isotopes by means of Gordon's method [2]. The frequency of the RF-generator f = 15.506 MHz and r_∞ = 12.31 m. The calculated dependences of the isochronous magnetic field value versus radius, inferred in our calculations (black curve) and in [3] (red curve) are shown in Fig. 4.

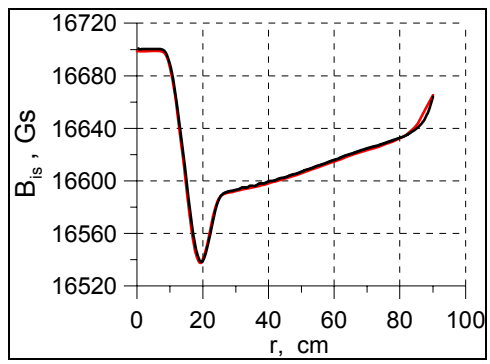

Figure 4: Isochronous magnetic field versus radius

The same curves calculated up to the radius r = 95 cm are shown in Fig. 5. As one can see from Fig. 4 and Fig. 5 the curves coincide practically completely except two regions of radius: $0 \le r \le 9$ cm and $81 \le r \le 90$ cm.

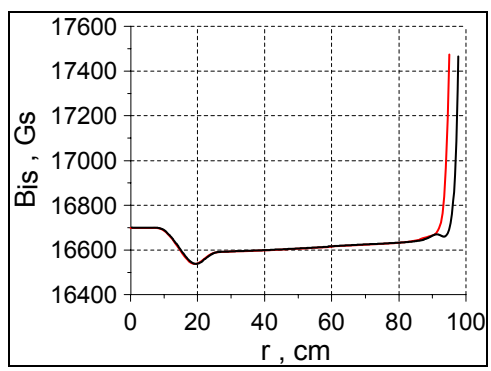

Figure 5: Isochronous magnetic field versus radius

Interpolation of the function $F(r,\theta)$ by the cubic Lagrange's polynomials in 16 nodes of the net (5 – 6) was

chosen because interpolation by linear or quadratic polynomials gives a calculation noise on some regions of the magnetic field curve connected with unstable work of the code (see Fig. 6).

This instability disappeared when we used the cubic interpolation (see Fig. 7). The calculated curves in both figures 6 and 7 are shown for the interval $25 \le r \le 40$ cm.

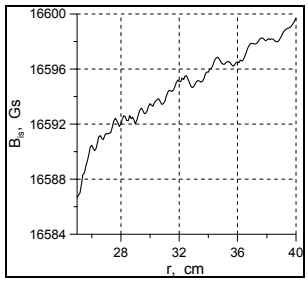

Figure 6: Noise on the calculated curve

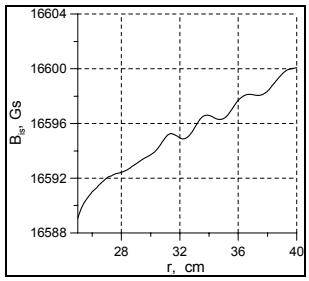

Figure 7: The curve without noise

The oscillations on the calculated curve $B_{is}(r)$ that are shown in Fig. 7 are not already connected with unstable work of the code but they are connected with peculiar properties of the calculated flutter magnetic field map of the cyclotron.

CONCLUSIONS

The obtained results show that the suggested scheme for calculation of the isochronous cyclotron magnetic field works and gives its correct values.

REFERENCES

[1] B.N.Gikal, G.G.Gulbekyan, S.N.Dmitriev et al., "The Project of the DC-110 Heavy Ion Cyclotron for Industrial Application and Applied Research in the Nanotecnology Field", Preprint JINR, P-9-2009-111, Dubna, 2009.

[2] Gordon M.M., "Calculation of Isochronous Fields for Sector-Focused Cyclotrons", Particle Accelerators, vol. 13, 1983 , p.p. 67 – 84.

[3] Ivanenko I.A., "Results of Magnetic Field Calculations, Step 3 ", FLNR report TOT-DC110-03-05_231, Dubna, 2009.

MODIFICATION OF THE CENTRAL REGION IN THE RIKEN AVF CYCLOTRON FOR ACCELERATION AT THE H=1 RF HARMONIC

S.B. Vorozhtsov#, V.L. Smirnov, JINR, Dubna, Russia
Akira Goto, RIKEN, Wako, Japan

Abstract

A highly advanced upgrade plan of the RIKEN AVF cyclotron is under way. The study is focused on the formulation of the new acceleration regimes in the AVF cyclotron by detailed orbit simulations. The extension of the acceleration energy region of light ions towards higher energies in the existing RF harmonic equal to 2 and the modification of the central geometry for the RF harmonic equal to 1 to allow an acceleration of protons at several tens of MeV are considered. The substantial redesign of the central electrode structure is needed to accelerate protons with reasonable values of the dee voltage. The new inflector geometry and the optimized central electrode structure have been formulated for the upgrade.

INTRODUCTION

A highly advanced upgrade plan of the RIKEN AVF cyclotron is under way [1]. The computer model of the AVF 3D electromagnetic field was prepared and successfully checked against the measurements [2].

The present study is focused on the formulation of the new acceleration regimes in the AVF cyclotron by detailed orbit simulations. Some experiments already conducted with the beams confirmed the selection of the machine parameters based on the beam dynamics simulations.

The new acceleration regimes include the extension of the acceleration energy region of light ions towards higher energies in the existing RF harmonic equal to 2 (H=2), and the modification of the central geometry for the RF harmonic equal to 1 (H=1) to make it possible an acceleration of protons at several tens of MeV. Clearly, with the realistic dee voltage of about 50 kV many particles would be lost in the channel of the Dee, since the existing structure of the central region (CR) was designed for the 2nd harmonic, not for the 1st one. Thus, the substantial redesign of the central electrode structure is needed to accelerate protons with reasonable values of the dee voltage.

The new inflector geometry and the optimized central electrode structure have been formulated for the upgrade.

PROTONS OF 20 MEV

In the H=2 regime the maximal experimentally available proton energy is 14 MeV for the existing electrode structure. It was found in simulations that under the restricted dee voltage of 50 kV acceleration of protons to the energy 23 MeV is also feasible there. Eventually, the energy of 20 MeV was selected for the detailed study, assuming application of the Flat Top (FT) system to suppress the energy spread in the extracted beam. Parameters of the regime are given in Table 1.

Table 1: Proton H=1 regime parameters. Structure S0 means the existing central geometry and S6 is the newly proposed geometry, which is shown in Fig. 5.

Structure	Final energy MeV	Frf MHz	Winj keV	Uinf, kV	Udee1 kV	Udee2 kV
S0	20	13.60	11.19	3.52	50	50
	23	14.54	11.41	3.71	50	50
S6	30	16.52	16.87	5.26	50	50

The main criteria for selecting the operational parameters of the regime were passing of the reference track as close as possible to the central line of the channel in the 1st Dee and clearance of the central electrodes to ensure maximal transmission of the ion bunch, and good centring of the particle trajectory in the following turns. Also, the RF phase excursion should provide the maximal possible energy gain per turn. For the 84º Dees and H=1 regime the RF phase should be as close as possible to 48ºRF. To ensure the conditions formulated above the Dee voltages and the RF particle phase in initial 4 acceleration gaps were varied.

The estimation of the bunch transmission started from preparing the initial particle distribution in the 6D phase space upstream of the inflector. In Fig. 1 the positions of the bunch at successive turns are given, black points being the lost particle locations. The main channel of the losses is the axial one. At the final radius, just at the entrance of the deflector, the projections of the particle 6D distribution are calculated. Rather large energy spread (~ 0.5 MeV) in the bunch can be explained below with the proposal of how to suppress it substantially.

SHARP TOP SYSTEM

The optimal particle RF phase at the entrance and exit of the Dee is shown schematically in Fig. 2 with the corresponding positions of the bunch (black ellipses) and the Dee voltage performance (red line).

Since the bunch does not sit at the top of the RF wave, the energy gain obtained by particles in the head and tail of the bunch substantially differs at the entrance of the Dee. But at the exit of the Dee the energy spread obtained at the entrance of the Dee gets compensated for to the same reason. The remnant energy spread in the bunch can be explained by the nonlinear dependence of the Dee voltage on time.

#vorozhtsov@jinr.ru

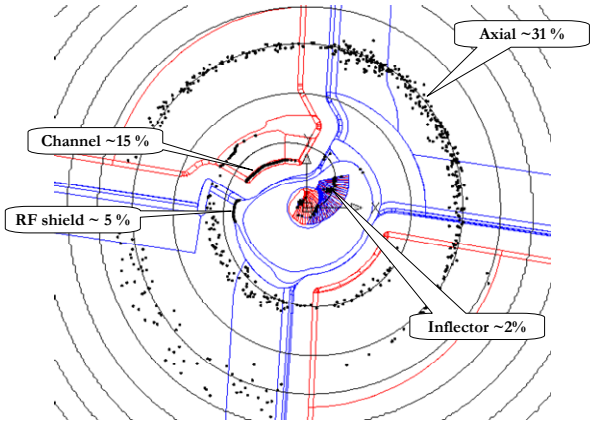

Figure 1: Total losses ~ 53% (Axial ~ 31 %)

The linearization of the Dee voltage performance with time could be reached by sharpening the red curve in Fig. 2 at the top by the FT system, which could be called now a Sharp Top (ST) system. The resulting Dee voltage performance is shown in Fig. 2 by a blue-dash curve. The optimal amplitude of the ST system is close to the FT regime but with the opposite sign wrt the main wave. The resulting energy spread at the final radius could be reduced by a factor of ~50. But considering small RF phase excursion during acceleration and also induced energy spread by some RF phase perturbation due to the radial betatron oscillation of the particles, the effect is just an order of magnitude. Some increase of the particle losses and the number of turns to reach the final radius accompany the effect. The resulting beam emittance at the final radius is shown in Fig. 3. There is striking reduction of the correlated radial emittance as compared to the main-wave-only regime.

INFLECTOR REDESIGN

The main limitation for increasing the proton energy in the existing central structure is the available maximal Dee voltage of 50kV. With this voltage, the particle with the energy higher than 23 MeV is not able to clear the central electrode structure at the 1st turn.

The size of the central structure is mainly determined by the existing inflector dimensions, and there is a substantial reserve in the RIKEN AVF cyclotron for miniaturization of the central electrode structure. Even some moderate minimization of the structure with the RF shield will permit an increase of the proton energy up to 30 MeV. But it would require some modification of the infrastructure around the inflector.

OPERATION DIAGRAM

The RIKEN AVF cyclotron operation diagram (Fig. 4) shows 3 regions, reflecting an advance in the energy for various accelerated ions: the yellow region presents the initial design stage of the cyclotron; the blue region is related to the recently proposed by the simulations and experimentally tested regimes, and finally, the green area reflects the energy advance in the present study, limited by the available maximal Dee voltage of 50 kV.

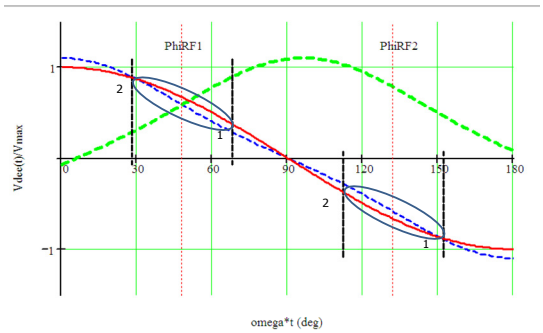

Figure 2: RF wave with the bunch positions at the entrance and exit of the dee. The principle of the energy compensation, PhRF1=48º.

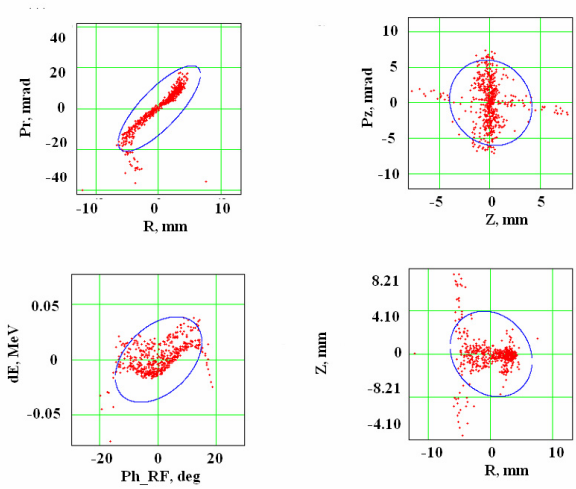

Figure 3: Beam emittance at the final radius, upstream of the deflector.

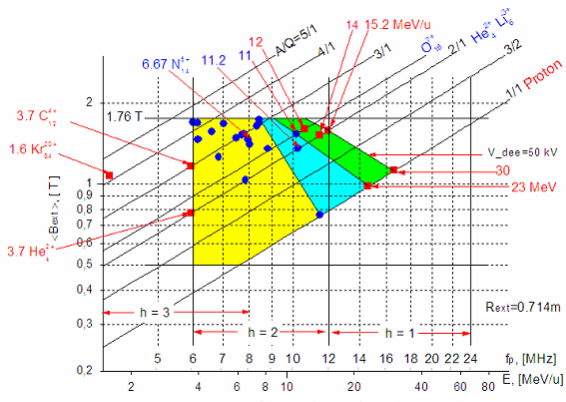

Figure 4: Acceleration performance of the RIKEN AVF cyclotron.

PROTONS OF 30 MEV

A set of the central configurations (S0 is the existing structure) were tried in an attempt to obtain good

centering and transmission for as high proton energy as possible, simultaneously retaining the possibility to accelerate ions at the H=2 RF harmonic. As a result, we arrived at the compromised configuration S6 (see Fig. 5), which was investigated in detail below.

In acceleration of protons of 30 MeV, similar to the previous regime for protons of 20 MeV, the major channel of the particle losses is axial ion motion.

$^6LI^{3+}$ OF 12.6 MEV/U

To check the viability of the eventually obtained S6 structure an acceleration of 6Li3+ with the maximal feasible energy was simulated. The lithium energy indicated in the operation diagram suggests the maximal Dee voltage 50 kV. But in reality there is some reduction of the Dee voltage dependent on the RF frequency of the regime. Experimentally available data on the issue show that in our case the maximal lithium energy at the acceleration at the H=2 RF harmonic is 12.6 MeV/u, and not 14 MeV/u, as was considered before. So, all subsequent studies for lithium are performed for this realistic energy. Presently, the experimentally tested regime corresponds to the lithium energy 11.2 MeV for the H=2 RF harmonic.

EMITTANCE PERTURBATION BY INFLECTOR

In the previous sections it was shown that the main channel of the particle losses in the central region is axial motion of ions. In reference [3] there is an attractive proposal as to how to mitigate the situation by modification of the inflector electrode surface in the manner presented in Fig. 6 (“bended” electrodes). This permits increasing the axial focusing in the inflector at the expense of some worsening of the radial focusing. The surface of the electrodes is not smooth as in the classical spiral inflector but folded at some optimal angle with the “valley” along the central line of the electrode surface. There is a compromised solution with the resulting reduction of the total losses [3].

The proposal was tested by simulations for the AVF Cyclotron, investigating an acceleration of 6Li3+ of 12.6 MeV/u. The “bended” inflector substantially reduces axial beam emittance at the exit of the inflector with some increase of the radial emittance.

An analysis of the overall losses during acceleration up to the final radius shows that there is simply redistribution of losses with the total losses staying at about the same level. Further optimization of the inflector electrodes and the regime parameters is needed to fully exploit the proposed modification of the inflector plates.

Figure 5: Comparison of the S6 structure with S0 (white lines).

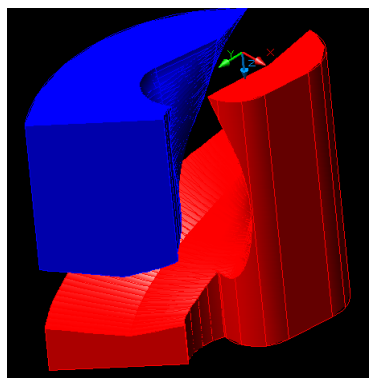

Figure 6: Inflector with the “bended” electrodes.

CONCLUSIONS

The final structure of the selected central region electrode for beam tests is presented in Fig. 5. The program of the forthcoming experiments with a beam is essentially based on these calculations.

ACKNOWLEDGMENTS

The authors would like to thank Dr. A. Vorozhtsov for making us acquainted with the electromagnetic model of the RIKEN AVF cyclotron, Dr. E. Perepelkin for explaining us the peculiarities of the CBDA program, Prof. F. Marti (MSU, USA) for detailed discussions and important suggestions.

REFERENCES

[1] S. Vorozhtsov et al. The Particle Accelerator Society of Japan (PASJ), Annual meeting, Aug. 5-7, 2009, Tokai, Japan.
[2] S.B. Vorozhtsov et al. CNS-REP-82, CNS Report. RIKEN-NC-AC-2. RIKEN, June 2009.
[3] B.N.Gikal et al. Proc. RuPAC 2008, Zvenigorod, Russia, p.127.

NEW MAGNETIC EINZEL LENS AND ITS BEAM OPTICAL FEATURES

M.H. Rashid# and C. Mallik, VECC, Kolkata, India

Abstract

Magnetic cylindrical lens is used mostly in beam lines to focus and transport low energy beam. It is well known that focusing power of a magnetic solenoid lens depends on the ratio of particle momentum and electric charge. A solenoid rotates also an ion beam while focusing it and the phase space areas of the beam in x- and y-plane get entangled and increased. The paper reported here describes an effort to design a new magnetic einzel lens (MEL) using a pair of Glaser solenoid lens (GSL) in anti-solenoid mode for the first time to get zero rotation of the exit beam. Analytical formulae have been generated to deduce the scalar magnetic potential and field along the central axis of the lens. Thereafter, beam optics and particle tracking is done using the combined field of a pair of GSL's constituting the MEL. The required focusing power of the designed lens is achieved for a beam of given rigidity.

INTRODUCTION

We know that an electrostatic einzel lens consists of three co-axial cylinders. The mid-cylinder is kept at some potential which can be varied while the end-cylinders at small gaps are kept at constant zero potential. This creates opposite fields at the two gaps giving accelerating and decelerating force on a charged particle beam passing through the gaps along the central axis. So, the overall energy gained by the beam is zero. The focusing and defocusing effects at the gaps due to the opposite radial components of the electric field give overall focusing to the beam, which depends on the energy of the beam also.

Two iron yoked solenoids create opposing magnetic field along the central axis if they are energized oppositely and equally. They resemble electrostatic einzel lens and so we call them MEL. One solenoid rotates the beam in one direction about the central axis while the other in the opposite direction. So the overall rotation of the beam is negligible and there is almost no coupling of the sub-phase spaces in the horizontal and vertical plane resulting null growth of the phase space area. But the radial component of the magnetic field at the rising and falling regions of the field give overall focusing to the beam, which depends on the momentum of the beam.

Earlier, properties of small such lens were studied for application in electron microscope to produce small rotation-less electron beam spot with little lens aberrations. General theory of MEL was studied by Baba and Kanaya [1]. We will use more simplified model of potential and field. It is easier to construct a solenoid to confirm the axial field distribution. The particles and beam are simulated for transportation to study its beam optical features.

#E-mail: haroon@veccal.ernet.in

MAGNETIC POTENTIAL AND FIELD

The sketch of the MEL formed from two GSL; kept attached or at small gap 2G, along the beam line and energized oppositely, is shown in Fig. 1. The hatched area is the iron yoke confirms the bell shaped field for the Glaser solenoid magnet. The diameter D and pole-to-pole distance S are given for the structure of the GSL. These parameters together with the magneto-motive force (NI) set the design of Glaser lens for certain focal lengths individually for a beam of given rigidity. Design and test of Glaser type of solenoid magnet have been presented in InPAC-2009 [2]. If O is the origin, the centre of the two solenoids are at d=(S/2+G) from the origin.

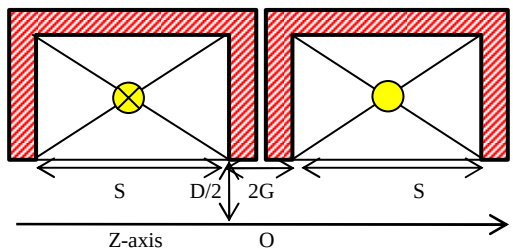

Figure 1: Cylindrically symmetric MEL in which electric current flows into and out of the page in the right and left solenoids respectively.

Magnetic Potential

The magnetic scalar potentials φ_i for a GSL are defined by eqs. (1), (2) and (3) in ref. [2] where subscript i stands for 1, 2 and 3. The forms of scalar potentials along the axis represented by φ_1, φ_2 and φ_3, which depend on the geometry of solenoid that is the pole to pole gap S and diameter D and magneto-motive force (MMF) and were expressed in detail therein.

Magnetic Field

The potential formulae for the magnetic Glaser lens are used to evaluate the field analytically. The net axial field $\varphi_i'(z)$ for a GSL is given in eqs. (1), (2) and (3) below using $\varphi_i'(z) = -\mu_0 d\varphi_i(z)/dz$. Now the magnetic field for a MEL as depicted in Fig. 1 is given by eq. (4) using the three fields from three potentials for i = 1, 2 and 3. The evaluated fields of the MEL for S=10 cm, D=10 cm, G= 0 cm, 5 cm, 10 cm and NI=37000 A-turn are shown in Figs. 2a and 2b. The GSL field is given by eq. (1) in ref. [3].

$$\varphi_1'(z) = \frac{-\mu_0 NI}{\pi S}\int_0^\infty \frac{2\sin(Sx/D)\cdot\cos(2xz/D)}{x\cdot I_0(x)}dx \qquad (1)$$

Where $I_0(x)$ is the modified Bessel function of first kind and order zero. The integration is in radial direction using the dummy variable x. Another field form is given by eq. (2) below.

$$\varphi_2'(z) = \frac{-\mu_0 NI}{\pi S}(P - Q) \quad (2)$$

$$P = \frac{z_+}{1+z_+^2} + \tan^{-1}(z_+) \quad (2a)$$

$$Q = \frac{z_-}{1+z_-^2} + \tan^{-1}(z_-) \quad (2b)$$

Where, $z_+ = (2z+S)/D$, $z_- = (2z-S)/D$, it is deduced from electric scalar potential form given by Szilagyi [4] for two apertures at the two solenoid pole ends. Complete and closed optical analysis of GSL is done by eq. (3).

$$\varphi_3'(z) = \frac{-\mu_0 NI}{b}\left(\frac{1}{1+(z/a)^2}\right) \quad (3)$$

Where, $b=\sqrt{(S^2+0.45D^2)}$ and $a=0.485b$ are the semi-empirical expressions to adjust the bell-shaped field due to an iron shielded solenoids and they are popularly known as Glaser model as the lens problem with this field configuration was solved by Glaser in [3, ch.VII] and [5].

$$B_i(z) = \varphi_i'(z-d) - \varphi_i'(z+d) \quad (4)$$

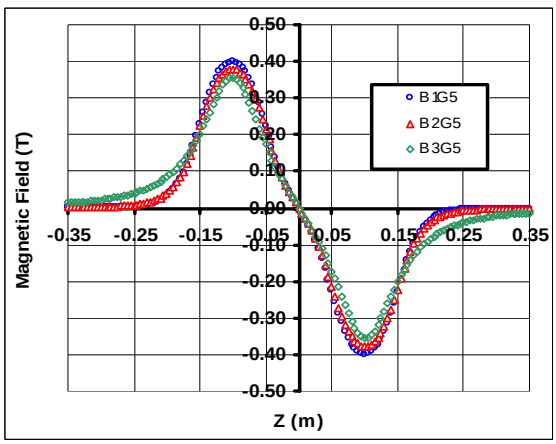

Figure 2a: Magnetic field B1 to B3 calculated from corresponding potential forms at gap G=5cm.

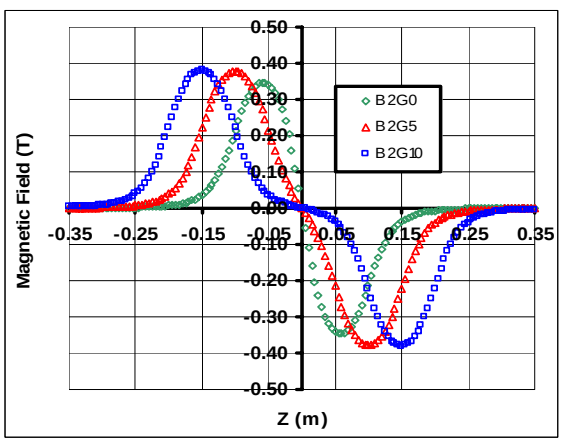

Figure 2b: Magnetic field B2 calculated for gap G=0, 5 and 10cm.

BEAM OPTICAL FEATURES

When a beam of magnetic rigidity B_ρ is launched para-axially through a GSL with a field distribution B(z) from the field free (low field) region, the general expression for focal length, f_m and beam rotation, θ are given by eqs. (5) and (6) respectively deduced from the equation of motion. The field free region for the integration limit can be approximated to the low field region fixed without any adverse effect up to the region z=-3S to +3S.

$$\frac{1}{f_p} = \frac{1}{4B\rho^2}\int_{-\infty}^{\infty} B(z)^2\,dz \quad (5)$$

$$\theta = \frac{1}{2B\rho}\int_{-\infty}^{\infty} B(z)dz + \theta_0 \quad (6)$$

The field formulae B3(z) gives the exact Glaser type of bell-shaped field and was used to obtain expressions for principal focal length (fp) and principal plane location (zp) as given in eqs. (7) and (8) respectively. The mid-focal length of the lens is found as zm=fp+zp, which is given by eq. (8) also if the factor 2 is replaced by 1 on the RHS.

$$\frac{1}{f_a} = \frac{1}{a}\sin\left(\frac{\pi}{\sqrt{K^2+1}}\right) \quad (7)$$

$$\frac{1}{z_p} = \frac{-1}{a}\tan\left(\frac{\pi}{2\sqrt{K^2+1}}\right) \quad (8)$$

Where $K=(B_0 a)/(2B_\rho)$ and B_0 is the peak magnetic field at the centre of a particular GSL. These parameters should be adjusted repeatedly to achieve appropriate design of the lens after confirmation of B_0 and 'a' by numerical evaluation of the field by some standard code for the same geometry and MMF. An expression for f_p in this case is obtained by direct integration of eq. (5) using field in eq. (3) and found to be $f_a=(2a)/(K^2\pi)$, which is also found by approximating eq. (7). This gives very crude value of focal length as the lens is not weak and there is a significant change in the distance of particle from the axis inside the lens [3, p. 270]. The focal length of a MEL having GSL and anti-solenoid is estimated using the optical lens relation, $1/f_p=1/f_1+1/f_2-(2G+S)/(f_1 x f_2)$.

A particle of Bρ=0.06 T-m is projected at r=5, 3 and 1cm parallel to the central axis at different conditions G=0, 10 and 20 cm. Motion of the particle is tracked using the same matrix method for the thin lens as described in reference [2]. The crossing point of the particle track with the z-axis gives the approximate point of focus which help in finding the principal focal length f_p, mid-focal length z_m and the position of the principal plane z_p according to the above equations.

The trajectory represented by G0 and G10 curves in Fig. 3 correspond to G=0 and 10 cm. The initial values of the distance and angle of the particle are r=3 cm and r'=0 mrad respectively. As the gap G increases the focal point moves towards the origin. The combined lens become stronger with a limit when G is increased keeping other

parameters constant. The net beam rotation of the beam depends on G, S and NI of individual solenoid but it is zero and independent of the gap G for overall solenoid system forming the MEL.

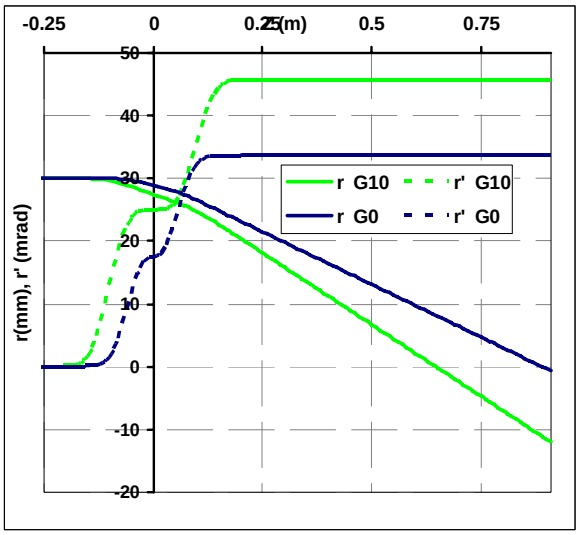

Figure 3: The distance r and angle r' of the particle are given by solid and dotted lines at different gap G=0 cm and 10 cm respectively.

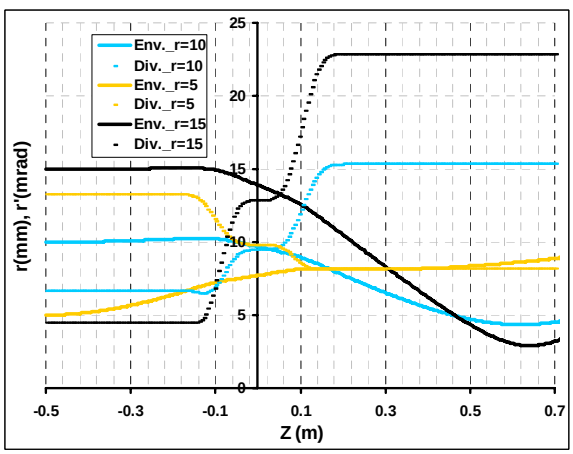

Figure 4: The beam envelops (Env.) and divergence (Div.) with initial beam width 2r and angular width 2r' of the beam of phase space area taken to be = rr'=200 mm-mrad passing through the MEL for G=5 cm gap.

$$\sigma_f = \prod_{1}^{f} M_i \sigma_i M_i^{T} \qquad (9)$$

Where M is the combined transport matrix of the i-th weak lens and a drift space in between the thin lenses and σ_i is the beam matrix at the i-th weak lens in the section model. Since the initial beam is assumed to be round, the transport of the beam is represented by a 2x2 matrix multiplication appropriately. Beam transport calculation is done in usual manner employing eq. (9).

For the upright initial beam of width 20 mm and 30 mm, it is seen that the beam waist occurs at ~62 cm from the origin and it gives proper focusing to the beam as the initial beam accounts to be almost parallel with a little divergence, which is calculated from the 200/π mm-mrad beam emittance. The beam depicted in black (dark) and blue (light) colour curves in Fig. 4 show this feature of the lens. The curves of beam envelopes and beam divergences are represented by smooth line and '-' marker respectively. But as we move towards the initial point object beam, the width goes on increasing while the divergence gradually decreasing. A beam with initial size of 10mm swells in size inside the lens as depicted in golden (lighter) curves in Fig. 4. This property of the lens can be used to properly control the divergence of the incoming beam by the lens to let pass through a small bore charge analyzing dipole system successfully by controlling the beam loss. The numerical values of analytical focal length (f_a), principal focal length (f_p), mid-focal length (z_m) and principal plane position (z_p) of the lens and the total beam rotation (θ) are listed for gap G, 0 , 5 and 10 cm, S and D, 10 cm and NI, 37000 A-turn in table 1 below.

Table 1: The cardinal points of the MEL using the calculated field above for different gaps G

G(cm)	$\mathbf{f_a}$(cm)	$\mathbf{f_p}$(cm)	$\mathbf{z_m}$(cm)	$\mathbf{z_p}$(cm)	**θ**(deg.)
0.0	85.3	89.3	89.0	-0.30	0.0
5.0	59.2	65.7	64.7	-1.0	0.0
10.0	57.7	67.3	65.0	-2.3	0.0

CONCLUSIONS

It describes the procedure of setting the MEL parameters for certain focusing power of the lens for certain beam rigidity. Since the overall rotation of the beam is zero, it curtails the effect of lens aberrations on the beam, which will be studied further in detail. The optical features were also studied to evaluate the focal length, principal plane and the beam envelop of a beam of certain phase space area. It is hoped that the study will prove to be beneficial for designing MEL for low energy beam focusing and transport more efficiently and easily.

REFERENCES

[1] N. Baba and K. Kanaya, J. Phys. E: Instrum. Vol. 12 (1979) p.525.
[2] M.H. Rashid et al., Proc. DAE-BRNS Indian Particle Accel. Conf. at RRCAT, Indore, India, InPAC-2009, Manuscript No. 115, Feb. 2009.
[3] A.B. Elkareh and J.C.J Elkareh, "Electron Beam Lenses and Optics", Vol. 1, Academic Press, London, 1970.
[4] M. Szilagyi, "Electron Ion Optics", Plenum Press, 1988, p. 84; G.H. Gillespie and T.A. Brown, 5th Intl. Conf. on Charged Particle Optics, Deft, The Netherlands, 1998.
[5] C. Fert and P. Durandeau, "Focusing of Charged Particles- Vol. 1", Ed. A. Septier, Academic Press, 1967, ch. 2.3.

TOWARDS QUANTITATIVE PREDICTIONS OF HIGH POWER CYCLOTRONS *

Y. J. Bi1,2,3, A. Adelmann2, J. J. Yang1, T. J. Zhang1, R. Dölling2, M. Humbel2, W. Joho2, M. Seidel2, C. X. Tang3 (1 China Institute of Atomic Energy, Beijing 102413, China; 2 Paul Scherrer Institut, Villigen, CH-5232, Switzerland; 3 Department of Engineering Physics, Tsinghua University, Beijing 100084, China)

Abstract

The large and complex structure of cyclotrons poses great challenges in the precise simulation of high power beams. However, such simulation capabilities are mandatory in the design and operation of the next generation high power proton drivers. The powerful tool OPAL enables us to do large scale simulations including 3D space charge and particle matter interactions. We describe a large scale simulation effort, which leads to a better quantitative understanding of the existing PSI high power proton cyclotron facility and predicts the beam behaviour of CYCIAE-100 under construction at CIAE.

INTRODUCTION

High intensity problems in cyclotrons draw a lot of attention because of the widely use of high intensity proton beams for palliation neutron sources and accelerator driven transmutation technologies. The 1.3 MW CW proton beam at the Paul Scherrer Institute (PSI) poses great challenges for high intensity beam simulations in cyclotrons [1]. With the fast development of HPC (High Performance Computing), the powerful tool OPAL [2] which includes 3D space charge and particle matter interactions enables us to perform large scale simulations in complex high intensity accelerators.

The Beijing Radioactive Ion-beam Facility (BRIF) is now in the construction phase at the China Institute of Atomic Energy (CIAE). The driving accelerator of this project, CYCIAE-100, a high intensity proton cyclotron, is designed to provide a 75 MeV~100 MeV, 200 μA~500 μA proton beam [3].

In this paper, we report on precise beam dynamic simulations of the PSI Ring Cyclotron. We present a new particle matter interaction model taking into account energy loss, multiple Coulomb scattering and large angle Rutherford scattering together with the 3D space charge. This model is used to obtain the necessary beam loss statistics during the acceleration process in CYCIAE-100 Cyclotron This data is indispensable in the design of an efficient collimation system.

THE 1.3 MW PROTON CYCLOTRON

The high intensity accelerator complex at PSI generates a 1.3 MW proton beam in routine operation. This gives us the unique opportunity to study the beam behavior of high intensity proton beam based on the experience with MW beam powers.

The simulation in this paper starts at the beginning of the 72 MeV transfer line between the Injector 2 and Ring Cyclotron. There are 18 beam profile monitors in both x and y direction. The initial distribution is obtained using Transport [4,5] and fitting the profile monitor data.

For the start of the Ring simulation, the emittance acquired at the end of the transfer line is used. The length of the bunch is measured using the time-structure probes [6]. For a 2 mA beam, the non-normalized radial emittance is $1.5\pi\ mm\cdot mrad$, vertical emittance is $0.6\pi\ mm\cdot mrad$, and the standard deviation of bunch length is $\sigma = 23\ mm$. A six-dimensional Gaussian distribution is used as the initial distribution of the Ring Cyclotron.

The beam intensity of the Ring Cyclotron is mainly limited by the beam losses at the extraction. To keep the extraction loss lower than 0.02%, the following effects must be considered.

- The turn separation at the position of extraction septum must be as large as possible.
- The radial beam size at the extraction region should be smaller than the turn separation and large amount of halo particles must be avoided.
- Since a long “pencil “ beam is used in the Ring Cyclotron, the space charge effect must be effectively compensated to avoid the formation of the S-shape beam which apparently increases the effective radial beam size.

In the original design of the Ring cyclotron, the beam will pass the coupling resonance $\nu_r = 2\nu_z$ four times at 490, 525, 535 and 585 MeV. A large horizontal oscillation is transformed into a large vertical one at the coupling resonances which can lead to beam losses. A trim coil TC15 was designed to avoid the resonance at 525 and 535 MeV. It provides an additional magnet field and field gradient in the radial direction. The effect is shown in Fig. 1. The trim coil provides a maximum magnetic field of 14 Gs. It has a long tail towards the smaller radii in order to make the integrated strength of the trim coil over the radius to zero.

A long beam with bunch length of $\sigma = 23\ mm$ is used in the Ring Cyclotron. To get a beam at the extraction turn with low losses, the flattop phase is adjusted to compensate the distortion caused by space charge forces. For an ideal flattop, the whole beam gains the same energy after one turn. In the case of high beam current, when the space charge force cannot be ignored, the head particle gains additional energy and the tail particle loses energy, so the beam will tend to show an s-shape in an isochronous cyclotron. Through the shift of

the flattop phase, the tail particle gains more energy than the head one, which can compensate the linear part of the space charge force. Consequently there exists an optimum flattop phase for an given intensity.

Since $\nu_r \approx 1.7$ in the region of extraction, adjusting the injection position and angle, results in the betatron amplitude being almost equal to the radius gain per turn. This is a special turn pattern because the last turn is well separated from the overlapping second, third and fourth last turns (see Fig. 2). In this case, the turn separation at the extraction turn is much larger than a width of the beam, hence it allows the extraction of high intensity beam with low losses.

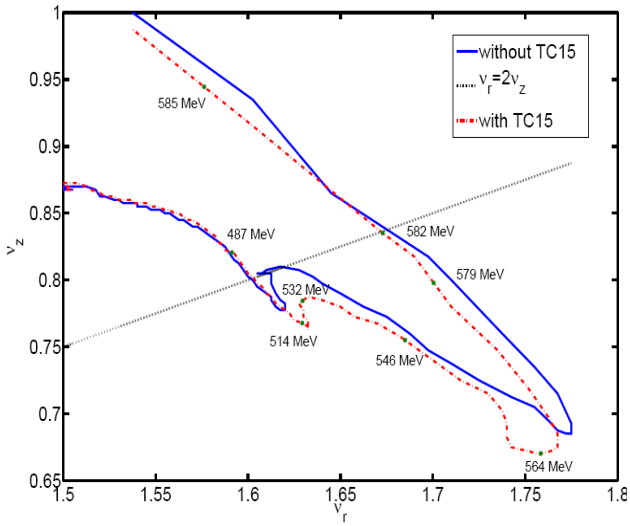

Figure 1: Tune diagram with and without TC15

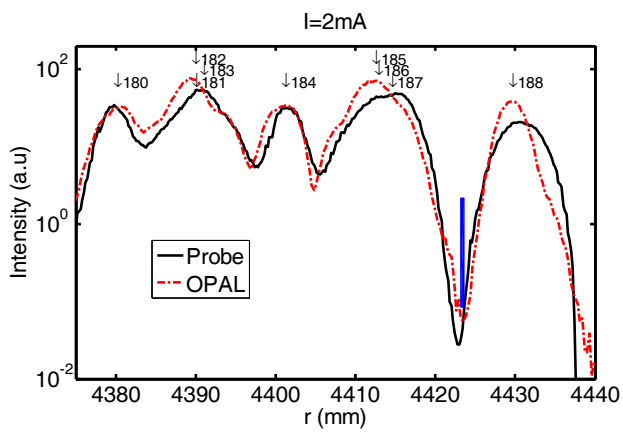

Figure 2: The formation of the turn pattern at extraction in the PSI Ring Cyclotron.

THE PARTICLE MATTER INTERACTION MODEL

General-purpose Monte Carlo codes, e.g. MCNPX [7], FLUKA [8,9], are developed to model the particle matter interaction, however, they have limited capabilities to track the particle in both complex external and space charge fields. We extend OPAL in order to handle efficient particle matter interactions, hence collimator systems in high intensity accelerators can be modeled together with space charge.

When the particle interacts with the matter, the energy loss is calculated using the Bethe-Bloch equation. Comparing the stopping power with the PSTAR program of National Institute of Standards and Technology (NIST), the error is found in the order of 10 % for copper, from several MeV to 10 GeV. For the application at PSI, the error is within 3% in the region from 50 MeV to 1 GeV. For relatively thick absorbers such that the number of collisions is large, the energy loss distribution is Gaussian [10]. If the energy of the particle is low enough to be absorbed after a certain distance, it is marked to be deleted and written to a file.

The Coulomb scattering is treated as two independent events: the multiple Coulomb scattering and the large angle Rutherford scattering, using the distribution given in [11].

As a benchmark of the collimator models in OPAL, the energy spectrum and angle deviation is compared against two general-purpose Monte Carlo codes, MCNPX and FLUKA, as shown in Fig. 3. A 72 MeV cold Gaussian beam with $\sigma_x = \sigma_y = 5\,mm$ is send through a copper elliptic collimator with the half aperture of 3 mm in both x and y direction from 0.01 m to 0.1 m. The deflected particles contribute to the energy spectrum and angle deviation after a collimator. These particles may be lost downstream.

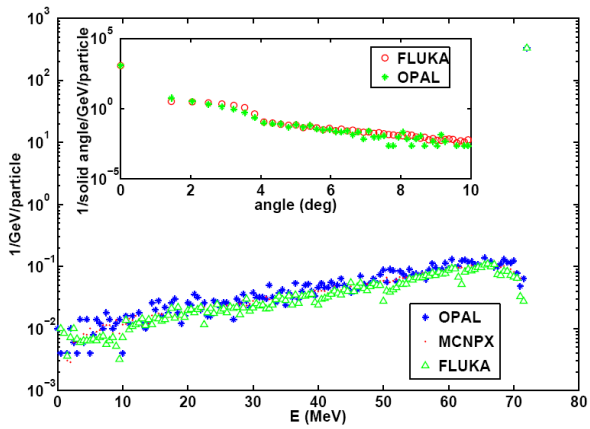

Figure 3: Energy spectrum and angle deviation (small plot).

THE COLLIMATOR SYSTEMS FOR CYCIAE-100

CYCIAE-100 is a compact isochronous cyclotron in which the vertical gap is limited. The half gap of magnet pole decreases from 30 to 24 mm with the radius. The two RF cavities with half gap of only 20 mm locate at the red line region as shown in Fig. 4. The revolution period is 90 ns and the bunch length is 2.5 ns.

The OPAL simulation including space charge effect and particle matter interaction starts with the initial energy of 1.49 MeV and normalized emittance of $4\,\pi\,mm\cdot mrad$.

The imperfect case is considered when simulating the vertical beam loss. Suppose the bunch is 3 mm off center in radial and vertical direction, and also a mismatch of the envelope is given as: $\sigma^*_{x,z} = 2\sigma_{x,z}, \sigma^*_{px,pz} = \sigma_{px,pz}/2$. When the beam intensity reaches 5 mA, the vertical beam loss is shown in Fig. 4. The lost beam concentrates at the position of RF cavity.

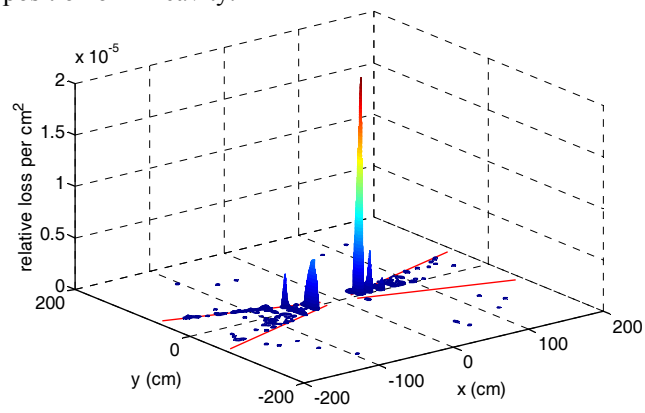

Figure 4: Vertical beam loss without collimator.

The collimator system is designed according to the following principle. Place the collimator at the low energy to minimize the radiation field. In general, collimation at high energies should be avoided, otherwise, large amount of additional radiation will be produced by the collimator itself. The simulations show that the best position for the collimator is at the entrance of the RF cavities, and the energy should limited up to 5 MeV. The material of the collimator is also carefully considered. The collimator material should not produce a large amount of neutrons when bombarded by protons. The release of gas in vacuum must keept to a minimum. Copper is selected as collimator material, also because of the good thermal conductance. The vertical beam loss with collimators is shown in Fig. 5. Comparing with Fig. 4, the losses are concentrated at the position of the collimators, and the RF cavities are well protected.

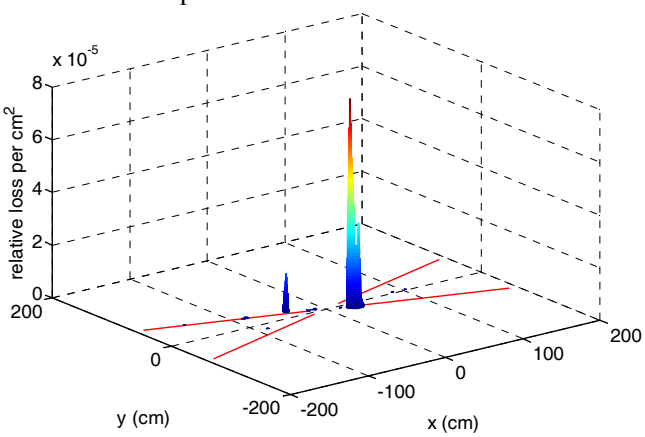

Figure 5: Vertical beam loss with collimator.

CONCLUSION

The beam power of 1.3 MW delivered by the PSI 590 MeV Ring Cyclotron together with stringent requirements regarding the controlled and uncontrolled beam losses poses great challenges with respect to predictive simulations. The comparisons with measurements show that OPAL can precisely predict the radial beam pattern at extraction with large dynamic range (3-4 orders of magnitude).

The ability of considering both space charge effect and the particle matter interaction in OPAL makes it a powerful and predictive tool for Cyclotron simulations. The design of the collimator system in CYCIAE-100 decreases the activity of the accelerator component and minimizes the radiation field inside the Cyclotron.

ACKNOWLEDGEMENTS

The authors thank the Accelerator Modeling and Advanced Computing group members C. Kraus and Y. Ineichen for many discussions regarding programming. We also thank D. Kiselev for the MCNPX simulations and fruitful discussions w.r.t. the particle matter interaction models, and H. Zhang for providing the element information in the IW2 line and Ring Cyclotron.

REFERENCES

[1] M.Seidel et al, Production of a 1.3MW Proton Beam at PSI, IPAC10, p.1309, Kyoto (2010).

[2] A. Adelmann, C. Kraus, Y. Ineichen (PSI), S. Russell (LANL), Y. J. Bi and J. J. Yang, The OPAL Framework (Object Oriented Parallel Accelerator Library) Version 1.1.61 User's Reference Manual, 2010.

[3] T. J. Zhang et al. Progress on Construction of CYCIAE-100, this meeting.

[4] K. L. Brown, D.C. Carey, Ch. Iselin and F. Rothacker, Transport, a Computer Program for Designing Charged Particle Beam Transport System, CERN 73-16 (1973) & CERN 80-04 (1980).

[5] U. Rohrer, PSI Graphic Transport Framework based on a CERN-SLAC-FERMILAB version by K.L. Brown et al. 2007.

[6] R. Döling, New time-structure probes between injector and Ring cyclotron, PSI - Scientific and Technical Report 2004 / Volume VI.

[7] D. Pelowitz ed., MCNPX User's Manual, Version 2.5.0 LA-CP-05-0369, 2005.

[8] G. Battistoni, S. Muraro, P.R. Sala, F. Cerutti, A. Ferrari, S. Roesler, A. Fasso`, J. Ranft, The FLUKA code: Description and benchmarking, roceedings of the Hadronic Shower Simulation Workshop 2006, Fermilab 6--8 September 2006, M. Albrow, R. Raja eds., AIP Conference Proceeding 896, 31-49, (2007).

[9] A. Fasso`, A. Ferrari, J. Ranft, and P.R. Sala, FLUKA: a multi-particle transport code, CERN-2005-10 (2005), INFN/TC_05/11, SLAC-R-773.

[10] William R. Leo, Techniques for nuclear and particle physics experiments, 2nd, Springer-Verlag, Berlin Heidelberg New York, 1994.

[11] J. D. Jackson, Classical Electrodynamics, 3rd, John Wiley &. Sons, New York, 1998.

ANALYSIS OF BEAM QUALITY OPTIMIZATION OF BUCKET ION SOURCE

Ya-hong Xie#, Chun-dong Hu, Li-zhen Liang, Sheng Liu, Yuan-lai Xie,
Cai-chao Jiang, Jun LI, Zhi-min Liu
Institute of Plasma Physics, Chinese Academy of Sciences, Hefei, 230031, China

Abstract

The bucket ion source is widely used as the high energy beam source on the high power neutral beam injector system. A hot cathode bucket ion source is studied. The main parameters which influence the performance of bucket ion source are arc voltage, filament voltage, gas inlet rate and extracted voltage. The proton ratio is the dominate parameter for the ion source. In the experiment, the characteristics of ion source are got by regulate the parameter setting. Based on this, the beam proton ratio, are analyzed and optimized. The proton ratio of extracted beam increased from 28 % to 40 %. It is very useful for the experimental operation and study about the bucket ion source.

INTRODUCTION

The high power neutral beam injection (NBI) is wildly used for the realization of controlled thermonuclear fusion sciences. The high current ion source is one of the most important parts on NBI, and it is characterized as high plasma density, large dimensions and high proton ratio. In order to promote the performance of ion source, the researchers did many study and experiments, one of them is the proton ratio.

The proton ratio is define the percentage of the number of atom ions in the over all species ions number. Consider the hydrogen as the experimental gas, it may generate ions of H1+, H2+, H3+, and the proton ratio[1] can be defined as

$$\eta = \frac{I_{H_1^+}}{I_{H_1^+} + I_{H_2^+} + I_{H_3^+}} \approx \frac{n_1}{n_1 + n_2/\sqrt{2} + n_3/\sqrt{3}} \quad (1)$$

Where, n1, n2, n3 is the ion density of H1+, H2+, H3+, respectively.

The ions are used to accelerate from the arc chamber to form the ion beam, but the energy of molecular ions only 1/2 and 1/3 compare with the atom ions, therefore, the number of atom ions in the plasma is expected as high as possible. That is means that, the proton ratio of ion source should be promoted.

The usual used ion source is hot cathode ion source, and also is the wide used, which can be seen in Figure 1. It contains plasma generator and beam extraction system. The plasma generator contains the filaments, and the gas inlet and arc chamber, which surrounded with permanent magnets to form cusp magnetic to confine the plasma.

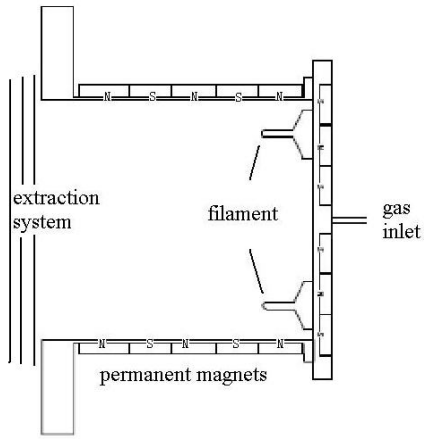

Figure 1: A sketch map of bucket ion source.

THE PHYSICAL MECHANISM OF PLASMA DISCHARGE

The ion source is a complicated device, including the plasma generate part and beam formation part. The particles in the plasma are used to form the ion beam, so, the ion species can decide the proton ration of extracted beam. And the plasma generation is only discussed. The principle of plasma generated in the hot cathode ion source can be described briefly as follows: The filament is supplied by a voltage and is then heated to emit thermo-electrons. When the arc voltage applied on the filament and arc chamber, the thermo-electrons are accelerated by the electric field. When the electrons energy large than the ionization potential of gas, the gas can be ionized and the plasma is generated. In case of hydrogen, it can generate atom ion H+ and molecular ions H2+, H3+. The formation of ions is a complicated thing, it contains many processes, and the collision cross-section of each process can decide the ion species which generated in the plasma. The electrons collide with the gas including one-collision and multi-collision. For the one-collision, mainly produce molecular ion H2+, the atom ion H+ almost produced in the second collision or more[2,3]. The collision processes are listed in Table 1. It can be seen that it including the molecules ionization, molecular ions dissociation, excitation and composition. The table also shows the threshold energy when the process take place, the collision cross-section and the optimize electron energy. Choose the big collision cross-section processes and give

*Work supported by the National Natural Science Foundation of China under Grant No. 10875146 and the Knowledge Innovation Program of the Chinese Academy of Sciences (The study and simulation on beam interaction with background particles in neutralization area for NBI).
#xieyh@ipp.ac.cn

Table 1 The processes of arc discharge in the arc chamber[4]

NO	Processes	Threshold energy (eV)	σ_{max} ($10^{-16}cm^2$)	E_{max}(eV)
Ⅰ	H_2 dissociation and excitation: $H_2 + e = H_2^* + e = H + H + e$	8.8	0.9	17
Ⅱ	H_2 ionization: $H_2 + e = H_2^+ + 2e$	15.4	0.98	70
Ⅲ	$H_2 + e = H^+ + H + 2e$	18	0.058	100
Ⅳ	H_2 dissociation and ionization: $H_2 + e = H^+ + H^+ + 3e$	46	0.005	120
Ⅴ	H_2^+ dissociation and excitation : $H_2^+ + e = H^+ + H + e$	12.4	4.3	≈24
Ⅵ	H_2^+ dissociation and composition: $H_2^+ + e = H_2^* = H + H$	Heat energy	(100)	≈0
Ⅶ	H_2^+ dissociation and ionization : $H_2^+ + e = H^+ + H^+ + 2e$	17	0.18	105
Ⅷ	H ionization: $H + e = H^+ + 2e$	13.6	0.7	64
Ⅸ	$H + e = H^*(2p) + e$	10.2	0.74	50
	$H + e = H^*(2s) + e$	10.15	0.14	12
Ⅹ	$H^*(2p) + e = H^+ + 2e$	3.3	17	9
	$H^*(2s) + e = H^+ + 2e$	3.3	9.4	13
Ⅺ	H_2 excitation: $H_2 + e = H_2^* + e$	11.5	0.16	60
Ⅻ	H_3^+ formation: $H_2^+ + H_2 = H_3^+ + H$	Heat energy	(100)	≈0
ⅩⅢ	H_2^+ charge exchange: $H_2^+(q) + H_2(s) = H_2(q) + H_2^+(s)$		7	3600
ⅩⅣ	H_3^+ dissociation and composition : $H_3^+ + e = H + H + H(=H_2 + H)$	Heat energy	(100)	≈0
ⅩⅤ	H_3^+ dissociation and excitation : $H_3^+ + e = H_2^+ + 2H + e$	15	3.5	17
ⅩⅥ	H_3^+ dissociation and excitation : $H_3^+ + e = H_2^+ + H + e$	12.4	4.3	≈24

the cross-section as a function of electrons, which show in Figure 2.

From Figure 2, we can seen that, when the electron energy achieve about 80eV, the collision cross-section to produce H+ and H2+ can reaches the maximum value. And when the electron energy increased, the collision cross-section decreased slowly. According the Schottky effect and double sheath stable theory[1], increase the arc voltage properly can increase the emission of thermo-electrons and got high arc current and plasma density.

According the literatures[5,6], the electrons with small energy can dissociation molecular ion H3+ to produce atom ion H+, it is an effective way to increase the proton ratio, especially in the extraction area. Besides, high arc current can easily to get high proton ratio[7].

EXPERIMENT RESULTS

In the experiment, a hot cathode bucket ion source is used and can generate hydrogen plasma. The ion source typical parameters setting are as follows:

- Arc voltage: 100V-200V
- Filament voltage:5V-8V
- Arc current: more than 100A
- Arc chamber pressure: ~4 mTorr
- Extraction voltage: 35kV-45kV
- Extraction current: more than 4A

The ion source operated with high temperature filament, but control the filament works in the emission limited regime [8]. The arc voltage is expected to high and gas inlet ratio should be regulated in a small range.

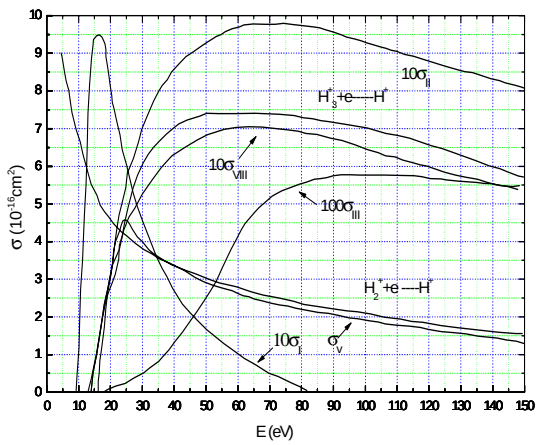

Figure 2: The collision cross-sections of main processes as a function of electron energy

The spectrometer is used to study the effect of operating parameters setting on proton ratio. Through regulate the parameters setting according to the theory and experimental experiences [9], the spectrum of the extracted beam emitted Hα light is measured and the typical spectrum is shown in Figure 3. The beam fractions of H+ : H2+ : H3+ : H2O+ is in the ratio of 40% : 34.7% : 9% : 16.3%.

The experiment studies the influence of beam current on the beam proton ratio. The arc current (beam extraction current) increased by regulate the ion source parameters, the beam ion species are measured and the

results shown in Figure 4. The proton ratio increased with the extraction current, which is in accord with the theory and experimental results.

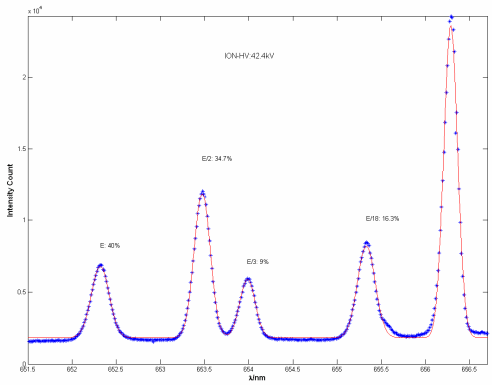

Figure 3: Spectrum of the H_α lines of ion beam

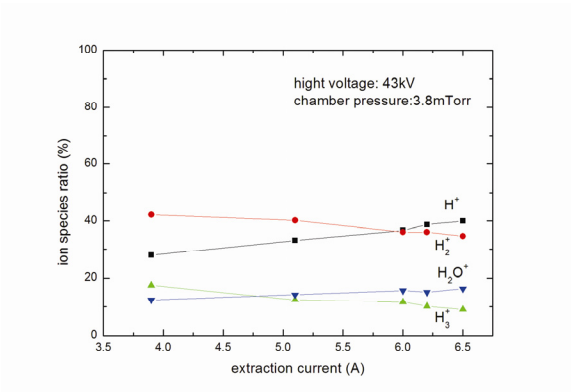

Figure 4: Proton ratio as a function of extraction current

SUMMERY

The proton ratio is an important parameter for high current ion source, which employed for NBI. It is mainly dominated by the collision cross-section between the electrons with different ion species in the arc chamber. Through analyze these collisions processes, gives the principle of arc discharge regulation. Even many researches were done to pursue high proton ratio, more studies need to do in the future.

REFERENCES

[1] H. S. Zhang. Ion Source and High Power Neutral Beam Source, Atomic Energy Press, Beijin, 1987 [in Chinese].

[2] J. P. Jiang, Cathode Electron Theory and Principle of Gas Discharge, National Defence Industry Press, Beijing, 1980 [in Chinese].

[3] A. J. T. Holmes, Intense H+ and H- sources, European Particle Accelerator Conf., London, 1994, 223-227.

[4] м.д.габович, The Physics and Technology of Plasma Ion Sources, Translated by C. H. Wan, Science Press, Beijing,1976 [in Chinese].

[5] A. J. T. Holmes, The development of high current singly charged ion sources, First European Particle Accelerator Conf., Italy,1988, 93-101.

[6] A. J. T. Holmes, T. S. Green, and A. F. Newman, Development of a high proton yield plasma source with multipole confinement and a magnetic filter, Rev. Sci. Instrum. 58 (1987) 1369-1376.

[7] Y. Okumura, H. Horiike, K. Mizuhashi. High Magnetic Field, Large-volume Magnetic Multipole Ion Source Producing Hydrogen Ion Beams with High Proton Ratio, Rev. Sci. Instrum. 55 (1984) 1-7.

[8] K. W. Ehlers and K. N. Leung, Characteristics of the Berkeley multicusp ion source. Review of scientific instruments, Rev. Sci. Instrum. 50 (1979) 1353-1361.

[9] Y.H. Xie, C.D. Hu, S. Liu, et al., Study of Beam Quality Optimization of Diagnostic Neutral Beam for the HT-7 Tokamak. Nuclear Instruments and Methods in Physics Research Section A., 620 （2010）585-588.

ION SOURCE RELATED RESEARCH WORK AT JYFL*

H. Koivisto#, V. Aho, T. Kalvas, J. Kauppinen, J. Komppula, T. Ropponen**, O. Tarvainen, V.Toivanen and J. Ärje, JYFL, Jyväskylä, Finland.

Abstract

In this article the work of the JYFL ion source group will be presented. New bremsstrahlung measurements were carried out in order to compare the results with different electron heating models. Especially attention was paid to study the effect of different heating parameters on the evolution of bremsstrahlung energy. A project to obtain new information about the ion temperatures and their time evolution has been initiated. The study will be performed using spectroscopic techniques measuring the ion temperature from the Doppler broadening of emission lines. The objective is to obtain accurate information about the evolution and the behaviour of highly charged ions in the ECRIS plasma. The work of the JYFL ion source team also includes frequency tuning experiments, beam quality experiments and tests with a so-called collar structure mounted on the plasma electrode. The beneficial effect of collar was first tested and noticed with the ECR ion sources by the KVI ion source group and has been shortly confirmed at JYFL. The JYFL ion source group is also developing a low power electron gun for the needs of spacecraft applications. The results of the development work can possibly be applied also with the ion sources in order to increase the density of cold electrons.

INTRODUCTION

The JYFL ion source group has studied the plasma physics of ECR ion sources. This includes for example the studies of plasma potential and evolution of electron energies via bremsstrahlung diagnostics. The intention is to extend the studies to cover the most of the energy range of the photon emission. In addition to the plasma studies, the ion source group also carries out the active research and development work for developing ion sources and their beams.

EXPERIMENTAL WORK AT JYFL

Electron Heating Limits of JYFL 6.4 GHz ECRIS

The high-energy bremsstrahlung emission generates an extra heat load to the cryostat of superconducting ECR ion sources [1]. An efficient shielding is very difficult to realize because of the limited space inside the ion source. In order to understand the parameters affecting the heating limits the experimental results were compared to the stochastic heating theory presented in ref. [2]. According to the theory the heating limit depends on the gradient of the magnetic field and the amplitude of the electric field E on the electron cyclotron resonance surface. The theory can be expressed as

$$W_s = 0.2\left[m_e L\left(1+\frac{l^2}{L^2}\right)\right]^{1/4} l\omega^{1/2}(eE)^{3/4} \qquad (1)$$

where $\omega = 2\pi f$ (f is the microwave frequency), m_e the mass of the electron, e is the unit charge, L is a parameter, which can be calculated from the axial magnetic field profile ($B = B_{\min}(1+z^2/L^2)$), where the resonances are at z = ± l. Here B_{min} is the minimum magnetic field and z the axial distance from this minimum. Adiabatic heating limit is defined to be $W_a = 5W_s$. The objective of the work was to found out if the end point energy of bremsstrahlung follows the behaviour of adiabatic heating limits.

Figure 1 shows the effect of magnetic field gradient on the bremsstrahlung spectrum extracted from the JYFL 6.4 GHz ECRIS. Both the end point energy and the yield of the emission increase. Using the values shown in Figure 1 and Table 1 it can be seen that Eq. (1) fails in predicting the behaviour of high-energy photon emission (compare $W_{end\text{-}point}$ and W_a in Table 1). A possible explanation is that the theory does not take into account the relativistic effect, which tends to move the resonance point towards higher magnetic field values. This is illustrated in Figure 2, which shows that the length l is longer for the relativistic electrons. The maximum length l for the relativistic electrons equals the distance between the B_{min} and extraction aperture and is independent on the magnetic field gradient. Table 1 shows the energy of electron when the resonance takes place at the extraction aperture of the ion source. According to the experiment it is possible that the energy of the electron is limited by the magnetic field configuration (for details see ref. [3]).

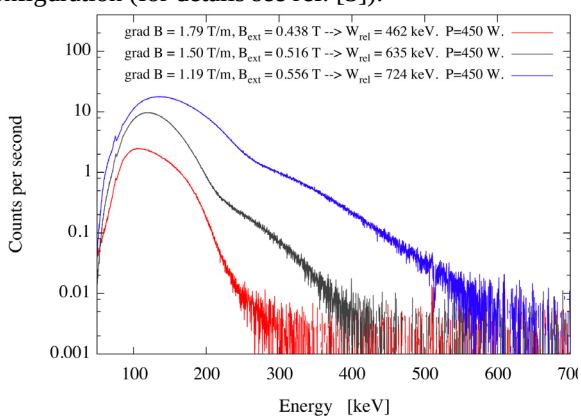

Figure 1: Effect of magnetic field settings on the bremsstrahlung energy and count rate.

* This work has been supported by the Academy of Finland and Magnus Ehrnrooth and Nyyssönen foundations

** Present affiliation NSCL/MSU

hannu.koivisto@phys.jyu.f

Table 1: Table shows the data corresponding to Figure 1.

$gradB_{re}$ $_s$ [T/m]	B_{min} [T]	B_{ext} [T]	l [mm]	$W_{end\text{-}point}$ [keV]	W_a [keV]	$W_{rel,max}$ [keV]
1.19	0.199	0.556	52.4	620	322	724
1.50	0.178	0.516	68.9	420	431	635
1.79	0.146	0.438	94.6	310	619	462

The energies $W_{end\text{-}point}$ are estimated from spectra shown in Figure 1, W_a is the adiabatic heating limit and $W_{rel,max}$ is the energy corresponding to resonance at B_{ext}.

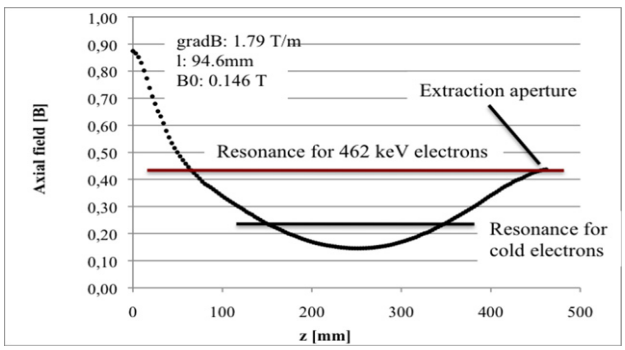

Figure 2: Resonance for cold and 462 keV electrons.

Spectrometer for Ion Source Plasma Diagnostics

A 1000 mm Fastie-Ebert type spectrometer has been built for ion source plasma diagnostic purposes. The spectrometer consists of a spherical mirror, stepper motor controlled 1800 lines/mm grating, interchangeable entrance and exit slits and an ET Enterprises 9406B photomultiplier tube. The device is vacuum compatible and can be used at a wavelength range of 200-600 nm. The control and readout of the spectrometer is computer controlled. The schematic of the monochromator can be seen in figure 3.

The instrument has tested by measuring spectra of He and Hg-Cd discharges. A detailed view of the helium spectrum can be seen in figure 4. The resolution of the device is sufficient for measuring the Doppler broadening of emission lines of light ions with ion temperatures around 1 eV. Other planned applications for the instrument are measurement of time development of ionization in an ECR plasma with different species and study of the effect of gas mixing on ion temperatures.

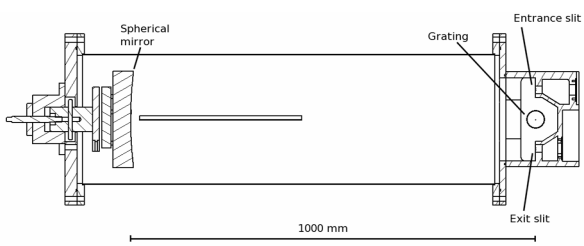

Figure 3. Schematic view of the monochromator.

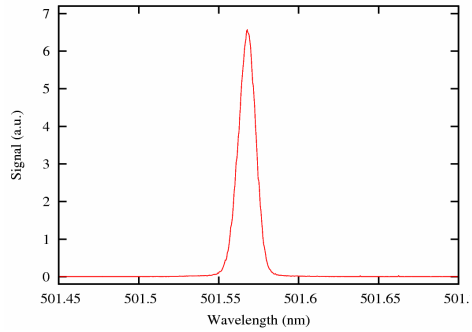

Figure 4. A preliminary helium spectrum of He discharge. The instrumental resolution of monochromator is 17 pm FWHM at 501.57 nm.

Time Evolution of Plasma Potential

ECR ion sources exhibit fast transient peaks of extracted ion beam currents at the leading and trailing edges of the applied microwave pulse [1,2]. The fundamental difference between these transients, called preglow and afterglow, is the charge state distribution (CSD) of extracted ion beams - low charge ions exhibit preglow while the afterglow boosts the beam currents of highly charged ions. Studies of the preglow are driven by the aim of creating a short-pulsed multi-charged ion source with high ionization efficiency. The afterglow mode is utilized e.g. for injection into circular accelerators as it offers intensive beams of highly charged ions. In order to gain understanding on the plasma processes associated with these transients the time evolution of plasma potential during the microwave pulse was measured with the JYFL 6.4 and 14 GHz ECR ion sources. The plasma potential was observed to increase 10-50 % during the preglow and 10-30 % during the afterglow compared to steady state. For detailed description of the experiment see reference 3. Plasma potential peaking during the preglow and afterglow implies that any application, relying on running an ECRIS in pulsed mode and utilizing either one of these transients, must take into account the increased energy spread of the ion beam causing the bending and focusing properties of the ion beam differ from those of a cw beam.

Table 1: Table shows the relative change of plasma potential in preglow and afterglow peaks.

Ion Source	Preglow/ cw plasma potential	Afterglow/ cw plasma potential
JYFL 6.4 GHz	1.06 – 1.12	1.09 – 1.14
JYFL 14 GHz	1.13 – 1.47	1.17 – 1.28

Frequency Tuning at JYFL 14 GHz ECRIS

Microwave frequency fine- tuning [7] of ECR ion sources has successfully been studied and developed by the INFN-LNS ion source group in Catania. This method, where the microwave frequency fed into the plasma chamber is varied in a narrow frequency range around the normal operation point to achieved improved source

performance, has been tested also at JYFL in collaboration with the LNS ion source group [8]. The latest results of the work have been presented in ref. [9] and in this proceeding [10]. Some frequency tuning experiments have been performed also in collaboration with the LBNL ion source group (please see. Ref. [12]).

Collar Experiments at JYFL 14 GHz ECRIS

The first very promising collar experiments with the JYFL 14 GHz ECRIS have been carried out. The collar structure developed and tested [11] by the KVI ion source group and shown in Figure 5 was used. In the preliminary tests the improvement of several tens of per cent was seen in the beam currents of high charge states of oxygen. At the same time the intensity of low charge states decreased. Further studies will be performed to optimize the collar geometry and to get more information about the physics related to its positive effect.

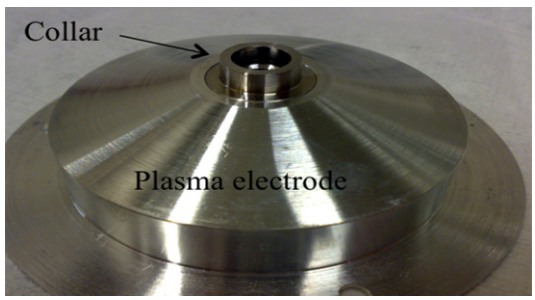

Figure 5: The collar structure used in the experiments at JYFL.

Low Power Electron Gun

The JYFL ion source group is participating in an E-sail project [12], which relates to a propellantless space travelling method using the momentum of solar wind flux. In the method so-called tethers (thin wires, some tens of µm in thickness, length several km) are biased to positive voltage in order to use the momentum of positive charges of solar wind to produce spacecraft propulsion. The positive charge of the tethers is maintained by an on-board electron gun.

The JYFL ion source group will test the durability of the tethers by bombarding them by electrons and ions. The group is also developing a low power electron gun for the test mission which main purpose is to observe and measure the E-sail effect in the ionosphere for the first time. The maximum power available during the test mission is about 1.5 W. The beam intensity of 2 mA is required at the electron energy of 500 eV. The power level available is not sufficient to use a thermionic cathode due to the high radiation losses. Consequently, a cold cathode electron gun is being developed at JYFL. This approach is based on electron field emission from a nanographite or a nanocellulose coated cathode. The gap between the cathode and anode has to be about 100 µm in order to make the field emission at the voltage of 500 V possible. The short gap between the electrodes sets very high requirements also for the anode structure. According to the tests the most viable configuration includes a silicon nitride anode with the mesh size of about 100 µm. The size of the cathode and anode is about 14 mm x 9 mm being capable of producing current of about 0.7 mA through the anode. This requires the emitted current of about 1.2 mA. Consequently three modules are needed to meet the current requirement of 2 mA, which at the moment slightly exceeds the power limit set by the mission.

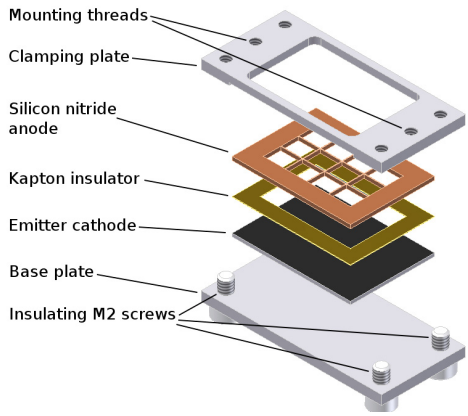

Figure 6: The drawing of the low power (1.5 W) field emitter electron gun developed at JYFL.

REFERENCES

[1] D. Leitner et al., Rev. Sci. Instrum. 79, 033302, (2008).
[2] N.C. Wyeth, A. J. Lichtenberg and M.A. Lieberman, Plasma physics, Vol. 17, p. 679, (1975).
[3] H. Koivisto et. al., to be published in Proc. 19th Intl. Workshop on ECR Ion Sources, Grenoble, France, (2010), JACoW.org
[4] I.V. Izotov, A.V. Sidorov, V.A. Skalyga, V.G. Zorin, T. Lamy, L. Latrasse, T. Thuillier, IEEE Transactions on Plasma Science, 36, 4, Part 2, (2008), p. 1494.
[5] G. Melin et al., Rev. Sci. Instrum. 61, 236, (1990).
[6] O. Tarvainen, H. Koivisto, T. Ropponen, V. Toivanen, Y. Higurashi and T. Nakagawa, to be published in Proc. 19th Intl. Workshop on ECR Ion Sources, Grenoble, France, (2010), JACoW.org.
[7] L. Celona et. al. Rev. Sci. Instrum. 79, 023305 (2008)
[8] V. Toivanen et. al., Rev. Sci. Instrum. 81, 02A319 (2010).
[9] V. Toivanen et. al., to be published in Proc. 19th Intl. Workshop on ECR Ion Sources, Grenoble, France, (2010), JACoW.org
[10] V. Toivanen et al., this proceeding.
[11] C. Lyneis et al., to be published in Proc. 19th Intl. Workshop on ECR Ion Sources, Grenoble, France, (2010), JACoW.org
[12] V. Mironov, H. Beijers, Private communications.
[13] P. Janhunen, J. Propulsion Power, 20 (2004), 763.

STUDIES OF ECRIS ION BEAM FORMATION AND QUALITY AT THE DEPARTMENT OF PHYSICS, UNIVERSITY OF JYVÄSKYLÄ*

V. Toivanen†, V. Aho, J. Kauppinen, H. Koivisto, T. Ropponen‡, O. Tarvainen, J. Ärje,
JYFL, Jyväskylä, Finland
L. Celona, G. Ciavola, S. Gammino, INFN-LNS, Catania, Italy
D. Mascali, INFN-LNS and CSFNSM, Catania, Italy
A. Galatà, INFN-LNL, Legnaro, Italy

Abstract

During the last couple of years a lot of effort has been put into studies concerning the ion beam formation and beam quality of electron cyclotron resonance ion sources (ECRISs) at the Department of Physics, University of Jyväskylä (JYFL). The effects of microwave frequency fine tuning on the performance of JYFL 14 GHz ECRIS have been studied with multiple experiments in collaboration with INFN-LNS (Instituto Nazionale di Fisica Nucleare, Laboratori Nazionali del Sud). Also, a number of measurements have been carried out to study the effects of space charge compensation of ion beams on the beam quality. In order to proceed further with these studies, a modified version of the beam potential measurement device developed at LBNL (Lawrence Berkeley National Laboratory) is under development. Simulations are used to study the possibility to improve the beam quality by biasing the beginning of the beam line upstream from m/q separation. With high voltage biasing the beam energy could be increased temporarily over the limit of the injection system of the accelerator. Latest results and current status of these projects will be presented and discussed.

INTRODUCTION

Improving the performance of ion sources is crucial for the future of accelerator facilities. However, increasing the amount of produced ion beam is not enough, as the beam quality determines what fraction of the beam can be utilized by the experiments. In addition, with high beam currents many of the beam quality problems, such as space charge effects, are more pronounced.

At JYFL a significant amount of effort has been put into understanding better the underlying problems of the beam quality, both at the ion source and during the beam transport. The effects of microwave frequency on the phenomena inside the ion source plasma chamber and on the formation of the ion beam and its consequent characteristics have been studied in collaboration with INFN-LNS. The space charge effects play an important role in the high beam current section between the ion source and the analyzing magnet. Possibilities to mitigate these effects have been studied from multiple points of view. One is enhancing the degree of the space charge compensation by decreasing the charge density during the transport by introducing electrons, the other is by altering the beam starting conditions, like energy.

FREQUENCY TUNING

By feeding microwaves into the plasma chamber of an ECR ion source it is possible to excite electromagnetic field structures, or modes, inside the chamber. If the microwave frequency is around 14 GHz, like with JYFL 14 GHz ECRIS, and the chamber has typical ECRIS plasma chamber dimensions, these modes only have separation in the order of some MHz [1]. Thus only a slight change in the feeding frequency can significantly alter the electric field structure inside the plasma chamber. It is not clear how the situation changes when the chamber is filled with plasma. However, if the clear mode structure remains, it should have an influence on the characteristics of the produced ion beam [2].

The measurements were conducted by setting a constant microwave power output and varying the frequency between 14.050 and 14.135 GHz, the normal operation frequency being 14.085 GHz. At the same time, the ion source

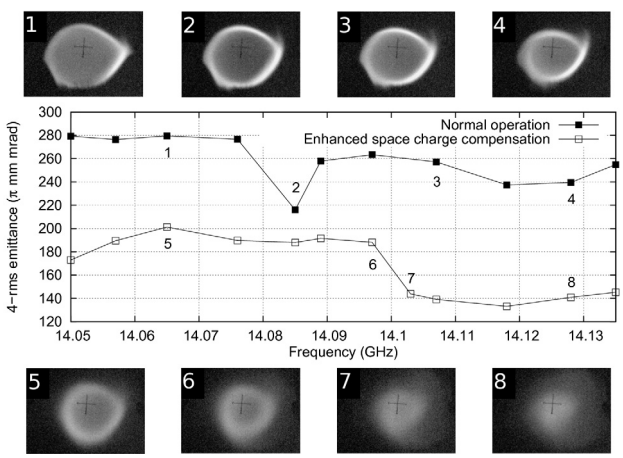

Figure 1: 4-rms emittance of Ar^{9+} with and without enhanced space charge compensation and beam viewer images at selected frequencies.

* Work supported by the Academy of Finland and Nyyssönen foundation. LNS team acknowledges the support of the INFN Strategic Project NTA-HELIOS.

† E-mail: ville.toivanen@jyu.fi
‡ Currently at NSCL/MSU, East Lansing, Michigan, USA.

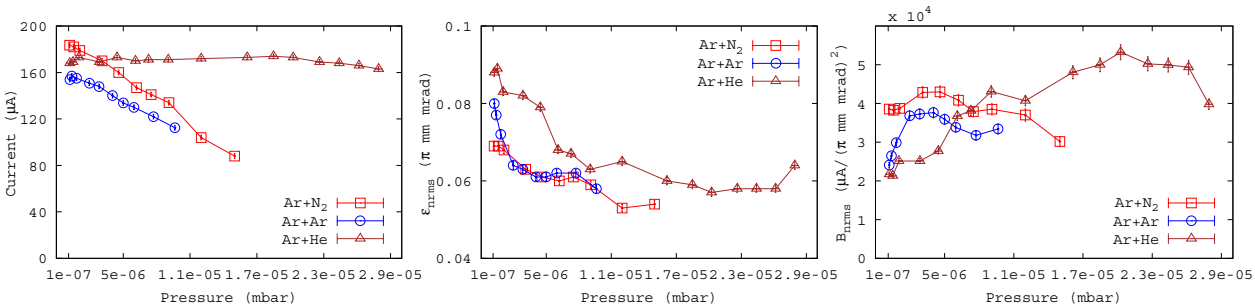

Figure 2: The current, emittance and brightness values of Ar^{8+} as a function of beam line pressure with different gas species injected into the beam line.

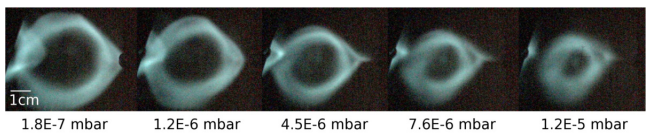

Figure 3: The beam viewer image of Ar^{8+} with various beam line pressures. N_2 as feeding gas. Part of the N^{3+} beam can be seen at the left edge of the viewer plate.

and beam parameters were recorded. In this article the focus is on the beam quality issues. A more complete presentation of the studies can be found in reference [3].

It was observed that the reflected power from the plasma chamber had a clear oscillating behavior which is caused by the wave guide system (see ref. [3]). These oscillating power fluctuations affected the measured beam currents and bremsstrahlung emission, making it difficult to see any underlying phenomena coming from possible mode variations. However, it was observed that the beam emittance exhibited clear variations with varied frequency which did not follow the power fluctuations. These variations correlated with changes in the beam profile and the effects were further strenghtened when additional enhancement of space charge compensation was introduced into the system (see next chapter). An example of the behavior is presented in Fig. 1. These changes in the emittance and profile were reflected in the beam transmission through the injection line and JYFL K-130 cyclotron. Compared to normal operation frequency, relative differencies of up to tens of percent were seen in the transmission efficiency.

SPACE CHARGE COMPENSATION

An extensive series of studies have been performed to study the effects of space charge compensation of ion beams on the beam quality. A more complete presentation of the method and results can be found in reference [4].

Enhancement of space charge compensation was achieved with neutral gas injection into the beam line section between the JYFL 14 GHz ECR ion source and its analyzing magnet. In this section all the ion species produced by the ion source are still present, yielding high total beam currents in the order of a few milliamperes. The ions in the beam interact with the neutral gas atoms and molecules, and the consequent ionization produces slow electrons and ions. The ions are repelled away and the electrons are trapped in the beam potential. The effective charge density of the resulting plasma is lower than the charge density of the original ion beam leading to a decrease in the beam potential. As a result, the radial electric field inside the grounded beam pipe is decreased, which weakens the undesired space charge blow up of the ion beam.

A significant reduction of beam emittance was achieved with this method. The measurements were conducted using helium, nitrogen and argon as feeding gases. With heavier gases (N_2, Ar) the drop of the emittance was steeper with increasing beam line pressure. This is explained with the fact that the ionization cross section in ion-atom collisions increases with the target atom element number [5].

The added neutral gas increases beam losses mainly via charge exchange reactions. It was observed that helium yields the least amount of losses and nitrogen the greatest, argon falling in between. This result is in a good agreement with the theory, which states that the charge exchange cross section decreases with increasing ionization potential [6, 7]. Even though the beam losses increased, the strong decrease in emittance leads to a substantial increase in the beam brightness, which exhibits a clear maximum in the 10^{-6} mbar or low 10^{-5} mbar region. An example of the beam current, emittance and brightness behavior is presented in Fig. 2.

The ion beam profile was measured after the analyzing magnet with a potassium bromide scintillation screen. It was observed that the beam size decreased considerably as the beam line pressure was increased (see Fig. 3). This is a strong indication of the enhancement of space charge compensation. As a further indication of this, no clear emittance decrease was seen when the gas was injected into the beam line section downstream from the analyzing magnet, where the beam current is significantly lower and the space charge effects much weaker. Measurements were conducted with varying ECRIS parameters and tunings, excluding the possibility that the observed phenomena originate from the ion source.

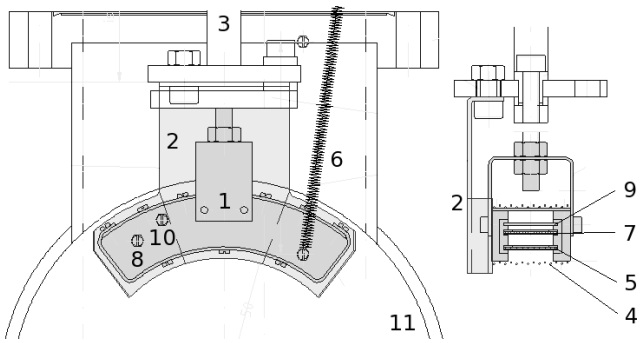

Figure 4: Schematics of the beam potential device. The device (1) is protected from primary beam ions with a cover plate (2) and can be retracted with a pneumatic actuator (3). (4) is the isolation mesh, (5), (7) and (9) are the retardation mesh, bias mesh and current reading plate with feedthroughs (6), (8) and (10). (11) is the vacuum chamber walls.

The improvement on the beam quality led to higher transmission efficiency through the injection line and the JYFL K-130 cyclotron. Unfortunately, because of the increased beam losses, this method does not offer a significant increase in the current of accelerated ion beam. If the beam losses can be decreased, these studies show that enhancement of space charge compensation can be a powerful tool to improve the quality of heavy ion beams on a practical level. Current studies aim to introduce compensating electrons into the beam line using other methods than gas feeding.

Beam Potential Measurement Device

In order to better quantify the changes in the space charge compensation, a device capable of measuring the beam potential is needed. It was decided to construct such an device based on the model developed at the Lawrence Berkeley National Laboratory [8], modified to better suit the beam line configuration at JYFL.

The working principle of the device is based on the determination of the energy of the ions which are produced via ionization of the rest gas. Initially these ions are practically at rest and are accelerated by the beam potential, thus having energy directly proportional to it. The device consists of a series of meshes. The first is used to isolate the device from the beam potential, a retardation voltage is applied to the second and the third is negatively biased to stop electrons. After the third mesh a plate exists for current measurement. The retardation voltage is ramped up linearly as the ion current is measured from the plate. When the current disappears, i.e. no ions reach the plate, the potential of the retardation mesh equals that of the beam potential. A schematic of the device is presented in Fig. 4. The device is constructed and is currently under testing.

HIGH VOLTAGE BIASING OF THE INJECTION LINE

Increasing the extraction voltage of an ion source mitigates the space charge effects, leading to improved beam quality. Also, if the ion source extraction is space charge limited, the increased voltage also leads to increased beam currents. However, the injection structure of the JYFL K-130 cyclotron sets severe limitations to the maximum ion beam energies coming from the ion sources, limiting the typical extraction voltages to values around 10 kV. One possible way to overcome these limitations would be to increase the beam energy only temporarily. The advantages of increased extraction voltages would be acquired at the beginning of the beam line where the beam currents are highest, thus yielding the strongest effects. After the m/q separation the beam would be slowed down making it possible to feed it into the accelerator. This would be done by biasing the first section of the beam line to negative high voltage, creating increased potential difference at the ion source extraction acceleration gap. After the analyzing magnet the beam line would return to ground potential through a lens structure providing additional beam focusing and adjustment.

A set of simulations have been carried out to study the effects of slowing down the beam with a simple cylindrical Einzel lens configuration. The simulations have been carried out with IBSIMU, a three-dimensional simulation software for charged particle optics [9]. The simulations indicate that such a system does not significantly increase the beam emittance or distort the beam shape. These results make this approach for beam quality improvement very promising. However, more studies are still needed to cover all aspects of the project.

REFERENCES

[1] F. Consoli, L. Celona, G. Ciavola, S. Gammino, F. Maimone, S. Barbarino, R.S. Catalano and D. Mascali, Rev. Sci. Instrum. 79, 02A308 (2008).

[2] L. Celona, S. Gammino, G. Ciavola, F. Maimone and D. Mascali, Rev. Sci. Instrum. 81, 02A333 (2010).

[3] V. Toivanen, et al., to be published in the Proceedings of the 19th International Workshop on ECR Ion Sources, Grenoble, France, 2010.

[4] V. Toivanen, O. Steczkiewicz, O. Tarvainen, T. Ropponen, J. Ärje and H. Koivisto, Nucl. Instrum. Meth. B 268 (2010) 1508-1516.

[5] I.D. Kaganovich, E. Startsev, R.C. Davidson, Proceedings of the Particle Accelerator Conference, Chicago, USA, 2001.

[6] A. Müller, E. Salzborn, Phys. Lett. A 62 (1977) 391-394.

[7] T. Kusakabe, T. Horiuchi, N. Nagai, H. Hanaki, I. Konomi, M. Sakisaka, J. Phys. B 19 (1986) 2165-2174.

[8] D. Leitner, Proceedings of the Beam Instrumentation Workshop, Santa Fe, USA, 2010.

[9] T. Kalvas, O. Tarvainen, T. Ropponen, O. Steczkiewicz, J. Ärje, H. Clark, Rev. Sci. Instrum. 81, 02B703 (2010).

ECRIS DEVELOPMENT AT KVI*

V. Mironov#, J.P.M. Beijers, H.R. Kremers, J. Mulder, S. Saminathan, S. Brandenburg
Kernfysisch Versneller Instituut, University of Groningen, The Netherlands

Abstract

This paper reports on work performed during the last two years to improve the performance of the KVI-AECR ion source, which is used as an injector for the AGOR cyclotron. We have installed stainless-steel screens at the injection and extraction sides and an additional collar around the extraction aperture resulting in better plasma stability and an increase of extracted ion currents. Source tuning is aided by continuously observing the visible light output of the plasma through the extraction aperture with a CCD camera. We now routinely extract 700 µA of O^{6+} ions and 50 µA of Pb^{27+} ions.

Source optimization is supported by extensive computational modelling of the ion transport in the low-energy beam line and measuring the transverse emittance of the extracted ion beam with a pepperpot emittance meter. These efforts have shown that second-order aberrations in the analyzing magnet lead to a significant increase of the effective beam emittance. Work is underway to compensate these aberrations.

INTRODUCTION

The Advanced Electron-Cyclotron-Resonance Ion Source at KVI (KVI-AECRIS) has been used as an injector of multiply-charged ions into the superconducting AGOR cyclotron for several years already. The main demands on the source are defined by the needs of the TRIµP program on fundamental symmetries (Ne^{6+} and Pb^{27+} beams), as well as by radiobiological studies (C^{6+} ions). The intensities of the neon and carbon beams are exceeding the user's requirements and the main concerns are beam stability and reproducibility. The lead intensity is significantly less than requested for the final production stage of the experiment (by a factor of two to three) and efforts are underway to improve both the source performance and the beam transmission through the low-energy beam transport line. The paper is organized as follows: first the KVI-AECRIS is briefly described together with the recent modifications to improve its performance. Then we discuss the visual diagnostics used to observe plasma light emission through the plasma electrode aperture and finally we report on our efforts to improve beam transport through and imaging properties of the analyzing magnet.

SOURCE DESIGN AND MODIFICATIONS

The KVI-AECRIS design is the same as AECRIS-U of LBNL and the 14 GHz source of Jyväskylä. The source is equipped with soft-iron plugs at the injection and extraction sides (B_{inj}=2.1 T, B_{extr}=1.1 T, B_{min}=0.36 T), has radial slits between the hexapole bars for better pumping, and an aluminium plasma chamber with a length of 300 mm and inner diameter of 76 mm. The radial magnetic field in this geometry is lower than for other 14 GHz sources and reaches 0.86 T at the plasma chamber wall.

In addition to the main 14.1 GHz RF heating system, the source is also equipped with a 11-12.5 GHz, 400 W Travelling Wave Tube Amplifier (TWTA), enabling two-frequency plasma heating. In normal operational conditions, however, no benefits of dual frequency heating have been observed.

In the original design the injection plug was shielded from the plasma by an aluminium screen. Also the plasma electrode was made of aluminium and had a cone-like shape. In these conditions the source output was unstable, with frequent changes in the operational modes and moderate extracted currents. We replaced both the injection screen and the plasma electrode with stainless steel ones and changed the shape of the plasma electrode to a flat one. This resulted in large improvements in source performance, with much better stability and reproducibility. We still see jumps in source output, but they are now more controllable. In addition, the extracted currents increased with e.g. typical outputs of Ne^{6+}, O^{6+} and Ar^{8+} ion currents of around 300 µA.

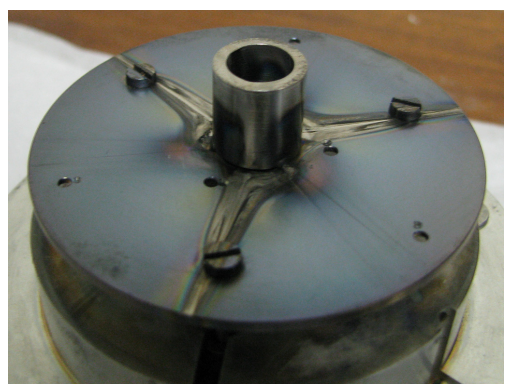

Figure 1: The plasma electrode with its collar.

An additional boost in performance was achieved by installing a collar around the extraction aperture. A picture of the collar is shown in Figure 1. The collar is a stainless steel cylinder with a length of 15 mm, inner diameter of 10 mm and outer diameter of 13 mm. In first instance installation resulted in a significant decrease of the output of the lower-charged ions (O^{4+} and lower). Output of the higher charge states on the contrary increased by a about 20 % The decrease in extracted low charged ions

*This work is part of the research programme of the 'Stichting voor Fundamenteel Onderzoek der Materie (FOM)', which is financially supported by the 'Nederlandse Organisatie voor Wetenschappelijk Onderzoek (NWO)' It was supported by the European Commission within the Sixth Framework Programme through I3-EURONS (contract no. RII3-CT-2004-506065).
#mironov@kvi.nl

decreased a load on the extraction electrodes; the total extracted current from the source goes down with increasing gas load beyond the level optimal for the high charge states. This is consistent with the point of view that the lower charged ions are less localized at the source axis compared to the higher charged ions.

Second, with the collar we are able to tune the source in such a way as to drastically increase the currents of the highest charge states ($O^{6+,7+}$). This is done by simultaneously applying the gas mixing and two-frequency heating techniques. The tuning is quite sensitive to the inputs (less than 0.1% changes in the magnetic field and input rf power destroy the high output mode). It is very reproducible, however. We are able to extract up to a record 700 µA of O^{6+} in this mode, with a reproducible level of 550 µA, as well as 500 µA of Ar^{8+}. Also the output of Pb^{27+} ions reached a level of 50 µA (estimated value, we measured 25 µA of Pb^{27+} at the end of the transport line). These values are comparable to the outputs of AECRIS-U and the 14 GHz source at Jyväskylä.

The reasons for this high output mode of operation remain unclear, though one can speculate about the formation of internal transport barriers in the plasma at sufficiently high input power analogous to H-mode operation in tokamaks.

VISUAL LIGHT DIAGNOSTICS

For a better understanding of source operation we installed a video camera behind the analyzing magnet, looking into the plasma chamber through the 8 mm diameter extraction aperture. Using a low depth-of-field objective we can distinguish different plasma shapes in the plasma centre (the characteristic six-arm star) and in the injection and extraction regions (three-arm stars). In the visual spectral range we do not observe a strong localization of the plasma inside the ECR zone, but rather a smooth intensity distribution along the source axis. The plasma is radially localized around the axis with FWHM less than 8 mm.

We also observe radial shifts of the plasma close to the extraction aperture that correlate with the jumps in the operational modes of the source, i.e. with abrupt changes in the extracted ion currents. Such shifts occur in the direction of one of the star arms. The extracted currents are clearly at their maximum when the plasma is nicely centred.

Changes in the biased-disk voltage result in changes of the plasma shape. The optimal voltage (which is around 200 V for neon/argon plasmas) corresponds to the smallest plasma size. This is illustrated in Figure 2, which shows the plasma shapes of an Ar plasma in false colours for the optimal biased disk voltage of -200 V (Fig. 2a) and for a floating voltage of -60 V (Fig, 2b). The maximum intensity of the light did not change significantly when varying the disk voltage (changes were around 10% only, with, typically, higher intensity for the lower disk voltage).

These observations are consistent with experiments reported in Ref. [1] that demonstrated a fast reaction of the extracted ion currents to changes in the biased disk voltage. This is not consistent with variations in ion population due to increased ion confinement or to an increase of the plasma density. The function of the biased disk is to reduce the ion radial losses by controlling e.g. the anomalous plasma losses in the radial direction.

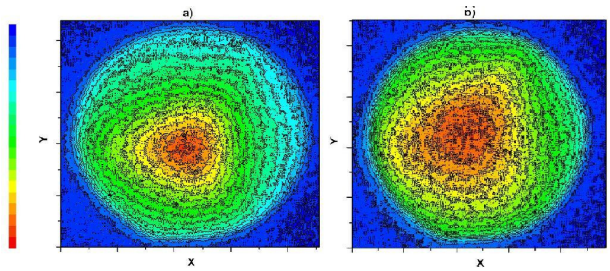

Figure 2: CCD images in false colours of an Ar plasma at the extraction region of the source. In a) the biased disk voltage is -200 V and the extracted Ar^{8+} current is 450 µA, while in b) the disk floats at -60 V and the extracted Ar^{8+} current is only 200 µA.

BEAM TRANSPORT OPTIMIZATION

Reduction of the ion beam losses in the low-energy beam transport line (LEBT) is at least as important as increasing the intensity of the extracted currents. We estimate the ion losses in the LEBT to be around 50%. To cure the problem we performed beam shape diagnostics using beam profile monitors such as harps and BaF_2 beam viewers located at different places along the beam line. We also installed a 4-D pepperpot emittance meter at the focal plane of the 110º analyzing magnet [2]. The measurements are accompanied with extensive computer calculations. For the simulations we use a home-made PIC-MCC Chaos [3] code to calculate the initial distribution of ions at the extraction aperture, and the ion tracking codes LORENTZ-3D [4] and COSY INFINITY [5]. The LORENTZ-3D code was also used to calculate the electric field in the extraction gap and the magnetic fields of the source and analyzing magnet. The simulations were done for He^{1+} ions at an extraction voltage of 24 kV and assuming full compensation of the beam space charge.

The beam profile measurements immediately after the extraction system confirm the initial triangular spatial distribution of the ions. No beam hollowing or filamentation was observed for normal operating conditions, only for some special tunings of the source with highly unstable output.

Further downstream the beam suffers from large second-order aberrations in the analyzing magnet. This magnet is an unclamped double-focusing magnet with straight 37º tilted edges. The magnet gap is 67 mm, bending radius 400 mm and the bending angle is 110º. According to the simulations, the initial beam emittance before entering the magnet is 65 π mm mrad, fully determined by the extraction of the ions in the solenoidal

magnetic field of the source. The beam emittance has grown by a factor of up to 5 after the analysing magnet. The estimated losses in the magnet are around 30%. The simulated and measured beam profiles in the focal plane of the analysing magnet are shown in Figure 3. The parabolic shape is a clear sign of the large second-order aberrations of the analyzing magnet. Agreement between the simulated and experimental profiles is satisfactory and shows that the dominant effects determining the beam transport are incorporated in our computational model.

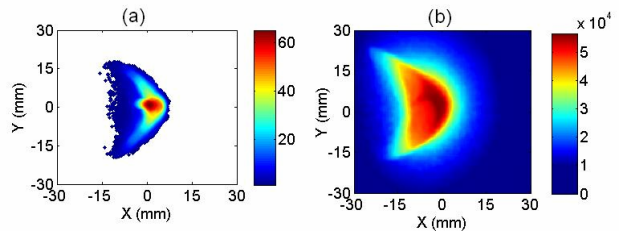

Figure 3: Simulated (a) and measured (b) spatial profiles of a 24 keV He^{1+} beam in the focal plane of the analyzing magnet.

In order to reduce the beam losses in and improve the ion-optical properties of the analyzing magnet we are using our simulation tools to calculate the effects of a modified magnet. The pole gap is increased from 67 to 110 mm and to compensate the second-order aberrations we added sextupole components to the main dipole field following the design of the VENUS analyzing magnet of LBNL [6]. The pole faces at the entrance and exit sections of the analyzing magnet have a positive parabolic curvature, while the pole face in the central region of the magnet has a negative parabolic curvature. In this way both the horizontal and vertical sextupole components of the fringe field are (partly) compensated. The modified pole face of the analyzing magnet is shown in Figure 4. To optimize the curvatures we first used COSY INFINITY to quickly estimate the required sextupole strengths and then LORENTZ-3D for the fine tuning. According to the simulations the full beam is transported without losses through the modified analyzing magnet and the beam emittance is decreased with a factor of two compared to the original magnet.

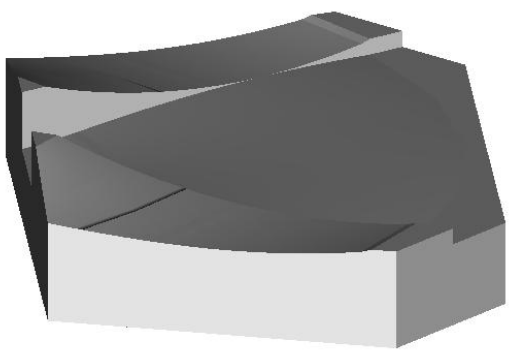

Figure 4: Modified pole face of the analyzing magnet with parabolic shapes to compensate the second-order aberrations.

CONCLUSIONS AND OUTLOOK

We have made good progress to improve the performance and stability of KVI-AECRIS. This was done by replacing the aluminium injection screen with a stainless steel one and the aluminium cone-shaped plasma electrode by a stainless steel flat electrode. We also attached a short cylindrical collar on the plasma-facing side of the plasma electrode. These modifications resulted in very stable source operation and large extracted currents, e.g. 700 µA of O^{6+}, 500 µA of Ar^{8+} and 50 µA of Pb^{27+}. The use of a CCD camera installed on the source axis behind the analyzing magnet to view the visible plasma emission through the plasma electrode aperture has proved to be a valuable tool to tune the source. We have also performed detailed simulations of beam extraction from the source and its transport through the analyzing magnet. The observed beam losses and emittance increase are caused by a too narrow pole gap and large second-order aberrations of the analyzing magnet. Our simulations show that these deleterious effects can be remedied by increasing the pole gap and adding sextupole corrections by modifying the pole face shape, respectively. We will implement these magnet modifications in the near future.

REFERENCES

[1] K. E. Stiebing, O. Hohn, S. Runkel, L. Schmidt, H. Schmidt-Böcking, V. Mironov, and G. Shirkov, Phys. Rev. ST Accel. Beams 2, 123501 (1999).
[2] H.R. Kremers, J.P.M. Beijers, and S. Brandenburg, Rev.Sci.Instrum. 77, 03A311 (2006).
[3] V. Mironov and J. P. M. Beijers, Phys. Rev. ST Accel. Beams 12, 073501 (2009).
[4] See home page of the code at http://www.integratedsoft.com.
[5] K. Makino and M. Berz, Nucl. Instrum. Methods Phys.Res. A 427, 338 (1999).
[6] M. Leitner et al., ECRIS02 workshop, Jyväskylä (FI), June 2002.

A COMPACT SOLUTION FOR DDS-GENERATOR, TURN-ON AND PROTECTIONS IN RADIO FREQUENCY ACCELERATOR SYSTEMS

A. Caruso#, F. Consoli, A. Spartà, INFN-LNS, Catania, Italy
A. Longhitano, ALTEK, S. Gregorio di Catania, Italy

Abstract

One single compact rack includes: Direct Digital Synthesizer (RF-generator), turn-on and protection devices. The system synthesizes a highly stable RF signal up to 120 MHz, turns the power on in the RF cavities through a step-ramp modulator, and protects the RF system against mismatching, sparks and multipactoring. A first prototype has been designed, assembled and tested on the RF system of the k-800 superconducting cyclotron at Infn-Lns. The hardware, the software, and the preliminary test results, are shown in this paper. This solution is part of the new computer-based RF control system.

CONCEPTUAL DESIGN

One of the most important aims in an RF control system is to supply the power to the cavities. Terms like conditioning and multipactoring are common in all the RF systems [1]. The conditioning, especially of a new cavity, can be really problematic. The stabilization of the right high voltage on the RF electrodes is often a difficult procedure [2]. Proper modulation of the RF signal in the initial conditioning phase is essential to reduce the risk of sparks, high reflected waves and multipactoring phenomena. In the general frame of the k-800 superconducting cyclotron [3] RF control system upgrade, a prototype single board has been developed. It is able to synthesize and modulate the output RF signal and to protect the system. The specific design can reduce the conditioning time remarkably. Moreover, a programmable modulation to bypass multipactoring has been introduced. Figure 1 shows the conceptual block diagram.

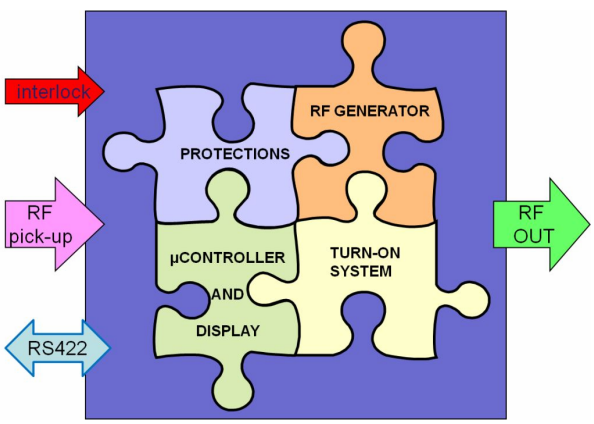

Figure 1: The block diagram of the system.

The puzzle components inside the box summarize the compact concept of the system. The main components inside the box are: the RF generator, turn-on system, protections, microcontroller and display unit. The RF output, the RF pick-up, the RS422 bus and the interlock line are the external connections of the box. The system is a sort of smart RF synthesizer including important and essential components of a radio frequency low level control system. For this reason we have called it the 'Low Level RF Box' (LLRF-Box). On its own it represents half of a typical RF control system. The addition of the stabilization loops (amplitude, phase and tuning) and the control interlock complete the low level RF system. The LLRF-Box can be compatible with most of the cyclotrons and accelerator RF control systems.

LOW LEVEL RF BOX APPLICATION

In general it is common practice that the RF generator, the turn-on system and the protections are placed in separate and independent racks. We came up with the idea of inserting all the components of Figure 1 in a single board during the upgrade of the low level RF system [4].

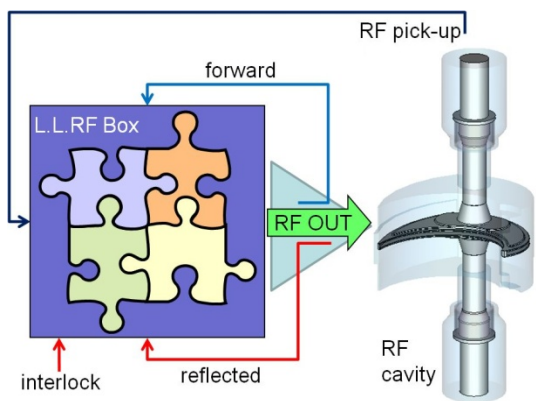

Figure 2: The LLRF-Box connected to the cavity.

The LLRF-Box can be used as a single apparatus for the conditioning of a RF cavity up to 120 MHz. This matches perfectly our RF devices frequency bandwidth at Infn-Lns. The prototype test has been performed on one cavity of the k-800 cyclotron. Figure 2 shows a simple layout where the LLRF-Box is connected to the RF cavity through the amplification section only. The RF box has three RF inputs: forward and reflected wave from the directional coupler and an RF pick-up from the cavity.

THE LOW LEVEL RF BOX

The Low Level RF-Box functions of protections, turn-on and RF-generator are based mainly on the following electronic components: the dsPIC30F4013 by Microchip and the AD9854 by Analog Devices [5,6]. The dsPIC is a

#caruso@lns.infn.it

high performance digital signal controller, 16 bit architecture, 80 MHz frequency clock. The AD9854 is the RF generator, based on DDS technique [7]. The bus RS-422 connects LLRF-Box and PC-unit while the SPI digital buses are used inside the block. The LLRF-Box block diagram is shown in Figure 3.

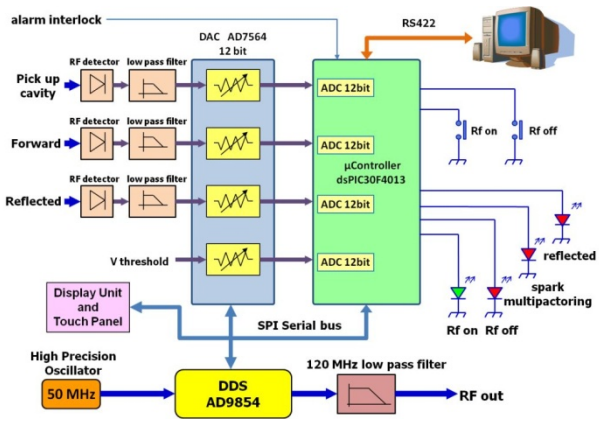

Figure 3: Low Level RF-Box block diagram.

Turn-on System and Protections

The RF inputs are the forward and reflected waves from the directional coupler and the RF pick-up from the cyclotron cavity. After the demodulators and the low pass filters the inputs meet the 12 bit DAC (AD7564). It is an analog attenuator with digital steps. At this stage the input signals are still analog. The reflected wave is compared with the reference threshold voltage, while the pick-up is compared with the forward one. The comparator function is carried out digitally by the dsPIC at the maximum resolution. The dsPIC analog-to-digital converters can exploit all the 12 bit of the comparators to manage the protection and turn-on operations. Under the multipactoring threshold, typically in the cyclotron resonators, the protections work at very low input signal levels, while exceeding this phenomenon the input levels are very high [1,2]. The input values, before the comparators, can be read by test points on the electronic board, displayed on the PC-control panel or directly on the RF-box display unit. In brief, if $V_{cavity} \leq V_{forward}$ the system produces an alarm of multipactoring and/or spark. If $V_{reflected} \geq V_{threshold}$ the system produces a reflected wave alarm. The thresholds can also be set automatically. In this way the comparison between the signals will follow a dynamic response: small signal levels means lowly attenuated thresholds, large signal levels means highly attenuated thresholds. A front panel cabinet hosts the main functions and indications, such as the main alarms and turn-on/off push-buttons. The resonator's multipactoring effects can be overcome by the proper setting of step and ramp envelope modulation. This is adjustable through the PC control panel, according to the resonance frequency. The pulse mode can be set, if necessary, in case of conditioning. The turn-on sequence, shown in Figure 4, generally feeds the RF power into the k-800 cavities, in one-shot, as shown in the frame *step-ramp-CW*. The *step-ramp* frame, in the same figure, shows a typical alarm condition: the cavity voltage is turned off and, after an interval of time, the system automatically tries again to turn on the voltage in the cavity. The superimposed signal power spectrums, after the step and the ramp sequences, are shown in the last frame of the figure. This kind of turn-on procedure and modulation technique is a copy of the old RF system. This digital upgraded version allows more freedom in setting and checking the protections and turn-on parameters.

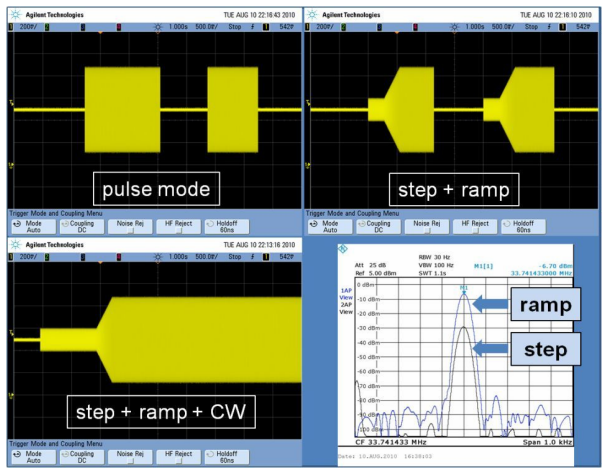

Figure 4: The RF output spectrum and turn-on sequence.

RF Generator

The RF generator is a high frequency source based on the Direct Digital Synthesis technique (DDS) [7]. The DDS technique has been adopted to generate the sine wave for the RF cavity or any other RF load. The initial frequency, amplitude and phase are set by the dsPIC control system without any phase shifter or linear attenuator. The DDS board are based on the electronic component AD9854 by Analog Devices [6]. The system provides a 48 bit frequency resolution together with a highly stable system clock of 300 MHz giving a resolution of 1 µHz, 0.02° in phase, 43 µV in amplitude with a maximum frequency output of up to 120 MHz. The clock source is based on an ultra low noise (-160 dBc/Hz @ 10kHz) high precision oscillator by Valpey Fisher Corporation [8]. A low pass filter is placed at the output stage of the DDS to avoid any residual trace of the waveform digitalization.

FULL POWER TEST

The Low Level RF-Box was successfully tested on March 2010 in the control system of one cavity of the k-800 superconducting cyclotron, at the frequency of 33.74 MHz, with a V_{dee} of around 65 kV. The other two cavities of the cyclotron remained under the traditional RF control system. We ran the RF system at full power with this hybrid configuration for more than one week. No difference was noticed on the accelerated and extracted beam for the whole testing time. The bandwidth of the k-800 cyclotron RF system is between 15 and 50 MHz. The

above test, performed at only one frequency, requires further checking in the near future. The beauty of this system, fully assembled in a three unit 19" rack, is that it is portable. It will soon be used for the complete conditioning of a coaxial cavity of a new chopping beam system at our Lab. It would be a good test bench to operate with the whole functions of the LLRF-Box.

The advantage of using the Box is evident if we focus on the high versatility of the control panel of Figure 5.

Figure 5: Low Level RF-Box control panel.

The in-house visual basic software manages all the functions of the LLRF-Box. During the present power test the control panel has been very useful in setting and reading all the main parameters. The operator can set frequency, amplitude and initial phase of the RF output. The turn-on operation modes can be set in *automatic*, *manual* and *one-shot*. The shape of the trapezoidal envelope signal can be modified in terms of step size, step duration and ramp slope (see Figures 4-6). The setting of the protections can be easily done as well. The control panel allows the setting and reading of $V_{forward}$, $V_{reflected}$, $V_{pick\text{-}up}$, $V_{threshold}$. The acquisition of these waveforms in the time domain, like an on-line oscilloscope, can facilitate the setting of the protection parameters to avoid sparks, multipactoring phenomena and mismatching. The setting of the RF system depends on the frequency. Since our cyclotron system is wideband (15-50 MHz), each frequency needs a proper and precise setting. With this control panel, a database can be stored for each frequency settings and the operator can easily recall them when necessary. The detected signal from the cavity pick-up, related to the turn-on sequence during the high power test at 33.74 MHz, is shown in Figure 6. The prototype electronic board is shown too.

The designed step envelope of the turn-on system is extremely fast, and the RF output rise time is equal to a few ns. The detected step of Figure 6 shows instead a rise time of 30 μs, which is the delay step response of the entire RF system (amplifier, coupler, cavity, etc). In any case, the modulated step has to be fast enough to overtake the multipactoring. From the same detector the step-ramp signal envelope has been acquired with two different settings of step size and ramp slope. After the step, a stabilization time has been introduced before the final modulation ramp sets the final power to the cavity.

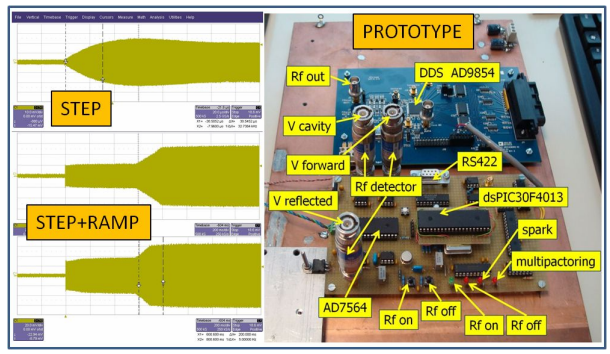

Figure 6: The LLRF-Box and the RF pick-up signal.

FINAL REMARKS

The LLRF-Box is installed in a standard 19" electronic rack and will be part of the cyclotron RF control system of one single cavity. A long time test at different frequencies of the cyclotron RF will be carried out. We are confident we can install the LLRF-Box in the cyclotron's two other cavities and all the INFN-LNS RF systems soon. A further programme of full power test has been scheduled on a new coaxial resonator. The LLRF-Box should be suitable with most of the accelerator RF systems. The versatility of the modulated output signal should match all the RF cavities operating up to 120 MHz. A higher performance version of the LLRF-Box is under study foreseeing a maximum operating frequency of 1 GHz. A more sophisticated programmable envelope modulation of the RF signal is under design, to achieve even higher peak voltages at given time intervals.

REFERENCES

[1] A. Wu Chao, M. Tigner, Handbook of accelerator physics and engineering, World Scientific Publishing (2009).
[2] J. Sura, A. Caruso, Multipactoring in the LNS Superconducting Cyclotron, Internal report INFN-LNS, Catania, Italy (1995).
[3] D. Rifuggiato et al, Japan 16th ICCA, 2004, p.118.
[4] A. Caruso et al, New PC-Based Control for the RF System at Infn-Lns, ICALEPCS 2009, Kobe, Japan.
[5] dsPIC30F4013 Microchip, www.microchip.com.
[6] AD9854 Analog Devices, www.analog.com.
[7] V. F. Kroupa, Digital Frequency Synthesizers, IEEE Press, 1998.
[8] Valpey Fisher Corporation, www.valpeyfisher.com.

COMMISSIONING EXPERIENCE OF THE RF SYSTEM OF K500 SUPERCONDUCTING CYCLOTRON AT VECC

S. Som*, Saikat Paul, Aditya Mandal, S. Seth, S. Saha, R.K. Bhandari,
P. Gangopadhyay, P.R. Raj & RF group
Variable Energy Cyclotron Centre, 1/AF, Bidhannagar, Kolkata-700 064

Abstract

Radio frequency system of Superconducting cyclotron at VECC, Kolkata, has been developed to achieve accelerating voltage of 100 kV max. With frequency, amplitude and phase stability of 0.1 ppm, 100 ppm and ±0.5o respectively in the frequency range of 9 – 27 MHz. Each of the three half-wave coaxial cavity is fed with rf power (80kW max.) from each of the three high power final rf amplifiers based on Eimac 4CW150,000E tetrodes. Initially, the whole three-phase RF system has been tuned for operation with RF power to the cavities at 19.1994 MHz and thereafter commissioned the cyclotron with neon 3+ beam at external radius at 14.0 MHz. In this paper, we present brief description of the rf system and behaviour observed during initial conditioning of the cavities with rf power and the way to get out of multipacting zone together with discussion on our operational experience. We have so far achieved dee voltage up to 57 kV at 14 MHz with 20 kW of RF power fed at each of the three dees and achieved vacuum level of 4.5 x 10-7 mbar inside the beam chamber. We also present discussion on the problems and failures of some RF components during commissioning stage and rectifications done to solve the same.

INTRODUCTION

The Radiofrequency system of k500 Superconducting Cyclotron including the development of high power rf amplifiers, design aspects of rf cavities and their coarse frequency tuning mechanism, low-level electronic controls like three-phase signal generation, phase detection, amplitude regulation, phase regulation etc. of the complete rf system and Programmable logic controller based interlocks for the safety of the rf system and personnel, have been thoroughly described in various status and review papers presented in a number of conferences [1-8]. In the following sections, we will discuss the commissioning experience of the rf system gained so far, some major problems we faced and finally the solutions or rectification we decided to incorporate in the system for better reliability.

RF AMPLIFIERS

Three high power rf amplifiers (each having 80kW output at 50 Ohm) for feeding power to the three main rf cavities have been installed at the vault of Superconducting cyclotron building (as shown in Fig.1) and are driven by solid-state wideband amplifiers in the specified frequency range.

* ssom@vecc.gov.in

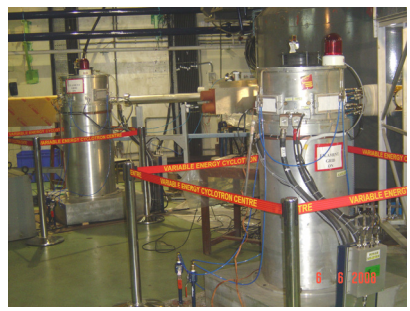

Fig.1. High power rf amplifiers installed at SCC Vault

Each of the high power rf amplifiers consists of Eimac 4CW 150,000E water-cooled tetrode as active device and with individual cavity tuneable by moving the sliding short, similar to that used for the main dee resonator cavity. The four identical Bridge-T network in the grid of the final amplifier are driven with equal power levels of up to 300 watts. PLC-based interlock system for all parameters like all water interlocks for main cavities, amplifier cavities and tetrodes, interlocks for DC power supplies related to RF amplifiers, airflow interlocks for dee-stem alumina window cooling, coupler alumina cooling and amplifier internal cooling etc. was in operation before putting on the rf system. DC power supplies for the tetrode – 3 nos. of Filament P/S (15.5V/215A), 3 nos. of Control Grid P/S (–400V to −200V), one no. of Anode P/S (20kV/22.5A) with fast crowbar protection for 3 amplifiers and 3 nos. of Screen Grid P/S (1.5kV/0.5A) were tested and installed. Amplifier cavity was tuned (with VNA connected at Anode pick-up port) by moving the position of its sliding short with the help of a PC-based stepper motor controlled drive system with positional accuracy better than 20μm.

PROBLEMS IN AMPLIFIERS

We encountered a problem in high power RF Amplifier-B after few months of operation with RF. Under DC condition with 2.5A anode current, suddenly we observed RF power appeared in the power meter. It seems the amplifier is oscillating and observed the oscillation at 1.083GHz on a 6 GHz Spectrum Analyzer. As this kind of high frequency oscillation can appear only from the tetrode itself, we replaced that particular tetrode with a new one and the problem got solved.

In one occasion, we found in one amplifier that as soon as screen grid power supply is put on, it trips. On close observation it was found that control-grid current is much higher than the usual operating value (bleeder current).

Finally it was detected that the grid terminal of the tetrode socket (Eimac SK-2011A) is electrically short with ground due to it's insulation breakdown. In another occasion, for the same initial observation, the control-grid terminal of the tetrode was detected electrically short with the ground under hot condition. However, in cold condition the shorting problem disappears. In the above two cases, the socket and the tetrode were replaced with new ones respectively.

MAIN RF CAVITIES

Before, energizing the cavity, we properly tuned the main RF cavity (two quarter-wave one-end short-circuited coaxial transmission line sections making half-wave resonant cavity of around 12 m length) first with the movement of two sliding shorts of two λ/4 sections for coarse frequency and the loaded Q of the cavity is measured (as shown in Fig.2) using Vector Network Analyzer (VNA).

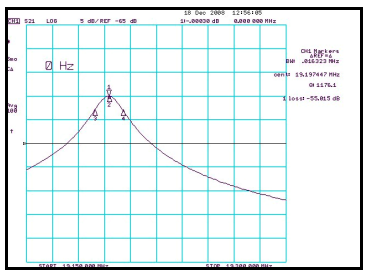

Fig.2.Measurement of main cavity parameters using VNA

It is to be noted that the position of the two sliding shorts (up and down) of one half-wave coaxial cavity is almost same, thus confirming the system symmetry good enough to use geometrical symmetry for positioning the sliding short. Three cavities, however, have slightly different parameters due to different dee capacitances. This is a consequence of the resonant extraction mechanism that requires different dee radial extensions.

The precise movement of sliding short is accomplished by the same mechanism as adopted in case of amplifier cavity. Then PC-PLC-based hydraulic drive system [9], which is developed at VECC for the movement of coupling capacitor (coupler) and trimmer capacitor, is operated to move the coupler upward or downward for matching (as shown in Fig.3) the high shunt impedance of the cavity close to 50Ω, which is the output impedance of the high power RF amplifier. Finally, Trimmer capacitor is also operated for fine tuning.

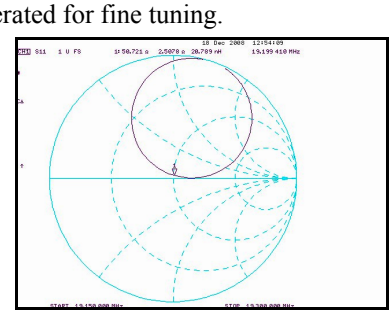

Fig.3. Measurement of impedance at the input coupler

LOW-LEVEL ELECTRONICS

The closed loop amplitude control is done by Dee Voltage regulator (DVR) unit. DVR is based on AD834JN RF Modulator [10] that modulates the RF drive signal according to the error signal between highly stable dc reference (REF01) and the feedback sample obtained from Dee pick-up signal.

Any deviation of sample phase from the reference phase is detected by the phase detector that produces dc error signal, which, in turn, controls online I&Q phase modulator and lock the phase to its reference within ±0.5°. Phase detectors, based on double balanced mixer, have been fabricated using MCL-RPD-1 having response of 8mV/degree in +8dBm saturated mode.

CAVITY CONDITIONING

With vacuum level inside the cavity having $1.0\text{x}10^{-6}$ mbar and magnetic field off, we started feeding RF power in the cavity at 19.2 MHz and immediately observed pressure increasing rapidly. When RF drive is put off, vacuum level improved very fast and came back to the original level. This indicates that the phenomena of multipacting occurred in the virgin cavity with a lot of trapped gases and they were getting ionized under the low power rf field. After some time we increased the power level to around 1kW and kept on feeding RF power to the cavity in pulsating mode for about 3 hours and thus finally we could overcome the multipacting zone and achieved steady RF field inside the cavity. Vacuum interlock was set at $5.0\text{x}10^{-6}$ mbar.

It is to be noted that to cross the multipacting level, pulsed input rf power of around 2kW is preferred in order to reduce the conditioning time. After few days of round-the-clock operation, we could achieve Dee voltage up to 45kV at 19.2 MHz, with forward input rf power of 20kW into the cavity measured with RF power meter of make-Bird Electronic Corp.,USA. The amplitude of the dee voltage is measured by dee-pick-up signal, once calibrated by Vector Network Analyzer according to the shunt impedance of the cavity.

COUPLER & DEE-STEM ALUMINA INSULATOR PROBLEMS

During first RF power test, we had one coupler failure. After initial conditioning of the cavities, when around 17 kW of RF power was fed to the cavity-C, suddenly pressure burst occurred with vacuum interlock operated and RF tripped. The vacuum level was not restored at all. Finally, it was identified that the ceramic (alumina) to copper brazing inside the coupler (as shown in Fig.4) has been damaged. The obvious mechanism of destruction is persistent arcing on the air side of alumina. However, the other two identical couplers for cavity-A & B are working fine each with 20 kW of RF power at 14 MHz till date. Probably, there was a manufacturing defect existing in that particular coupler. We have now incorporated reflected power interlock, which eventually withdraws RF power if the reflected power exceeds the set limit (100W).

We had encountered dee-stem alumina insulator damages few times for different cavities. The dee-stem upper and lower cavity with alumina insulators is shown in Fig.5, The alumina window got cracked twice for upper cavity-C, once each for lower cavity-B and C and upper cavity-B. The photo of cracked alumina for cavity-C is shown in Fig.6. We are analysing the causes of alumina failures. Probably, the local multipacting is taking place near the alumina (vacuum side). We are also thinking of thin coating of titanium on the alumina surface to minimize possible multipacting effect.

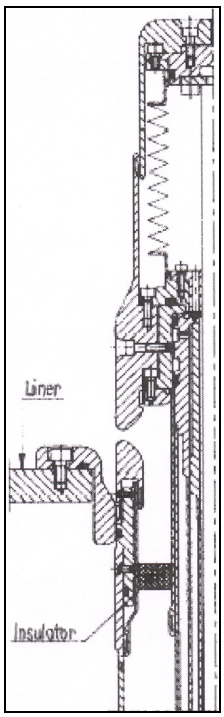

Fig.4.

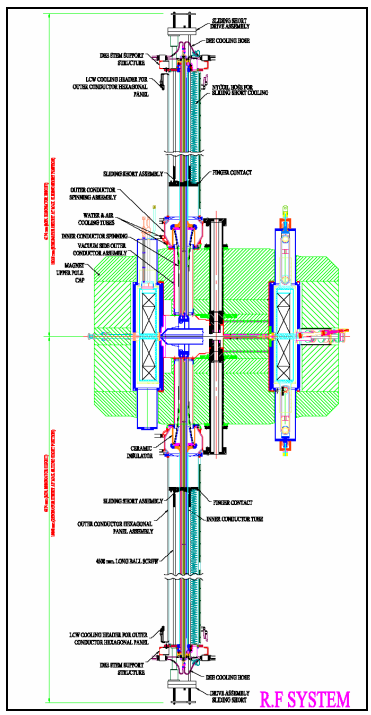

Fig.5.

Fig.4. Assembly of RF Power Coupler

Fig.5. Assembly of one cavity with dee-stem insulators

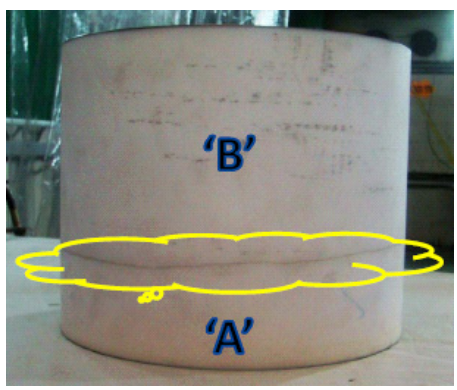

Fig.6. Cracked alumina insulator for cavity-C

CONCLUSION

Despite the problem in one coupler and few dee-stem alumina insulators, the general behaviour of the overall radio-frequency system during high power tests has been very satisfactory. The performance of major rf components were very well and reliable. The damaged coupler and dee-stem alumina insulators have been replaced by new ones and performed satisfactorily, without any further failure at 14 MHz RF frequency, with power level up to 20 kW. We have already obtained accelerated neon 3+ internal beam (40 nA) at the extraction radius with RF frequency 14 MHz from the k500 Superconducting Cyclotron successfully on 14th August, 2009. After that machine was shut down for installation of external beam lines, deflector etc. and now again the same neon3+ beam tuning is in progress and hoping to get the external beam very soon.

REFERENCES

[1] S. Som et. al, "An overview of the RF system of k500 Superconducting Cyclotron at VECC", InPac-2005, C-139, VECC, Kolkata, India

[2] S. Paul et. al, "Overview of control and power electronics of k500 RF system", InPac-2005, C-141, VECC, Kolkata, India.

[3] A. Mondal et. al, "RF interlock system for superconducting cyclotron", InPac-2005, C-140, VECC, Kolkata, India.

[4] S.Som, et. al, " Present Status of Radio-frequency System of Superconducting Cyclotron at VECC". InPac-2006, BARC, Mumbai.

[5] S. Som, et. al, "Development of 100kW RF amplifier for Superconducting Cyclotron at VECC", APAC-2007, RRCAT.

[6] S. Som, et. al, "Development of RF System for k500 Superconducting Cyclotron at VECC, Kolkata", Cyclotrons-2007, LNS, INFN, Italy.

[7] S. Som, et. al, "RF Cavity analysis using PC-SUPERFISH Code", 1997 IEEE – Russia Conference: MIA-ME'97.

[8] Aditya Mandal, et. al, "RF Tuning System for Superconducting Cyclotron", InPac-2009, RRCAT, Indore.

[9] Aditya Mandal, et.al., "Closed loop RF tuning for Superconducting Cyclotron at VECC", being presented in this conference Cyclotrons-2010, IMP, China.

[10] K.L. Erdman, et.al, "Some aspects of control and stabilization of RF accelerating voltage in TRIUMF Cyclotron", AIP Conf. on Cyclotron, 1972.

THEORETICAL ANALYSIS AND FABRICATION OF COUPLING CAPACITOR FOR K500 SUPERCONDUCTING CYCLOTRON AT KOLKATA

M.Ahammed#, A. Dutta Gupta, B.C. Mandal, B. Manna, B. Hemram, J. Chaudhuri, M.K. Dey, N. Mandal, P. Bhattacharyya, R.K. Bhandari, S. Saha, S. Murali, S. Sur, Y.E. Rao

Variable Energy Cyclotron Centre, Kolkata

Abstract

K500 SC cyclotron has already been constructed and commissioned after spiralling Ne^{3+} internal beam with 70 nA up to extraction radius (670mm) at variable Energy Cyclotron Centre at Kolkata, India. Several problems have been experienced related to the coupling capacitor of the radio frequency system including its sever burning during commissioning of the cyclotron. Making of the dissimilar joints between alumina ceramic and copper of the coupling capacitor demands the usage of vacuum furnace to avoid the cracking of the ceramic. Therefore exhaustive analysis has been carried out to facilitate the in-house fabrication of the coupling capacitor without using the vacuum furnace in case of emergency. The maximum allowable rate of temperature rise of the ceramic and the optimum thickness ratio of the copper to ceramic have been estimated. Finally, fabrication of the coupling capacitor has been carried out in-house without employing vacuum furnace. At present the coupling capacitor is performing well as maximum 57 KV DEE voltage were been achieved till date. This paper presents the details of the analysis and experiences gained during the fabrication of the coupling capacitor.

INTRODUCTION

K500 Superconducting Cyclotron was installed at VECC last year. After commissioning of all the individual sub-system and having spiralling internal beam up to extraction radius, beam extraction process is going on.

While commissioning of the cavity-C of the Radio Frequency (RF) system was going on, suddenly coupling capacitor of the same cavity was burnt with immediate effect of vacuum degradation to 10^{-1} mbar from $8x10^{-7}$ mbar. Whereas other two cavities were energized satisfactorily up to 15 kW RF power which is equivalent to 40 kV DEE voltage. Several arching marks at some places of the inner conductor of the coupling capacitor were observed. Copper made argon tube was charred and melted copper drop deposition on the ceramic insulator was noticed. The ceramic insulator acts both as electrical insulator between inner to outer conductor of the coupling capacitor and interface between beam space vacuum (around $8x10^{-7}$ mbar) to atmospheres. Subsequent helium leak testing of the burnt coupling capacitor revealed that ceramic to metal joint was leaking. Therefore in-house fabrication of the coupling capacitor was taken up on top priority basis to short cut the delay in commissioning of the K500 Superconducting Cyclotron.

Each author should submit all of the source files (text and figures), the postscript file and a hard copy version of the paper. This will allow the editors to reconstruct the paper in case of processing difficulties and compare the version produced for publication with the hard copy.

DESCRIPTION

Coupling capacitor of K500 Superconducting Cyclotron couples the RF power that is to be fed to the DEE of resonating cavity from amplifier. It is connected to the RF amplifier by coaxial transmission line. Inner conductor of the coupling capacitor is insulated by ceramic insulator made of alumina (99.99 % purity) from its outer conductor. It also acts as interface between beam space vacuum and atmosphere. Therefore the ceramic to metal joint of the insulator should have helium leak tightness of the order of 10^{-9} mbar.lit/s.

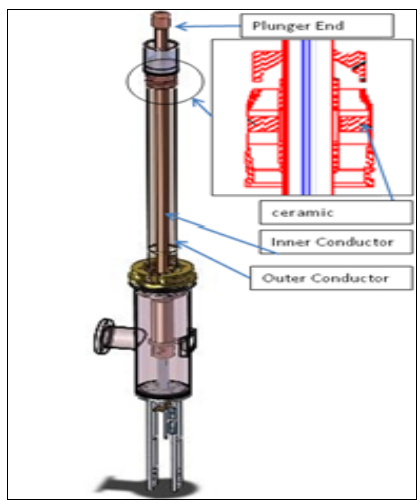

Figure 1: 3D view of the coupling capacitor.

Some part of it is located in the beam chamber vacuum and rest in air. Plunger end of it is positioned within the coupler cup of the DEE after penetrating beam space vacuum from atmosphere. Gap between the plunger and DEE coupler cup is adjusted by moving the inner conductor up and down by hydraulic drive system for the smooth transmission of power. Sliding electrical contact was fabricated by soldering be-cu made contact figure on

#manir@vecc.gov.in

outer conductor surface. Cooling water is circulated within the inner conductor for removing the heat generated in it. Figure 1 shows the 3D view of the coupling capacitor.

THERMOSTRUCTURAL ANALYSIS

Main criticality involve in fabricating the coupling capacitor is successful making of ceramic to metal joint and few neighbouring vacuum tight brazed joint. In the first few trial it has been revealed that ceramic was cracking repeatedly even though provision for maximum cooling was made available. Cracking of the ceramic might be due to the induced thermal tensile stress caused by the excessive heating rate of the ceramic regarding which we were complete ignorant.

Analytical

Therefore a comprehensive analysis to find out the thermal stress developed because of transient temperature gradient and differential thermal expansion coefficient between copper and ceramic was carried out.

A lumped model for the ceramic was considered and temporal variation of temperature (given by equation-1) was found out by solving the equation-2. Lumped modelling of this ceramic material is valid as the value of Biot number is 0.005 which very less than the criteria (i.e. 0.01) below which lump analysis is fairly valid.

$T = Ta + (To-Ta)\exp(-t/\tau)$ eq-(1)

$\rho C_p V(dT/dt) = h.A(Ta-T)$ eq-(2)

Where, ρ=Density, Cp=Specific heat, V=Volume, T=Temperature, t=Time, h=Heat transfer coefficient, A= Heat transfer area, Ta =Atmospheric Temp, h= Heat transfer coefficient, To=Initial Temp and τ is time constant given by [(ρ.Cp.V)/(h.A)].

Calculated time constant for our geometry and material is 15 minute. Heat transfer coefficient has been calculated using the empirical formula given by Churchill and chu for natural convection for horizontal plate as given by equation-3.

$$Nu = 0.36 + \frac{0.518\,R_a^{0.5}}{[1+(0.559/\mathrm{Pr})^{9/16}]^{4/9}} \qquad \text{eq-(3)}$$

Where, Nu= Nusselt no i.e.$\left(\frac{hL}{K}\right)$, R_a=Rayleigh no i.e. $(G_r.P_r)$, G_r= Grashof no i.e.$\left(\frac{g.\beta.\Delta T.L^3}{\nu^2}\right)$, P_r= Prandtl no i.e $\left(\frac{C_p.\mu}{K}\right)$, μ=Dynamic Viscosity, g= Gravitational Acceleration, β= Volume expansion coefficient and ν= Kinematic Viscosity (μ/ρ), μ = viscosity of liquid, L= Characteristic length, ΔT= Temperature deference, K= Thermal conductivity of copper.

Therefore to have quasi static heating process and to avoid cracking of the ceramic, pre-heating of the ceramic should be done continuously but temperature rise should not go beyond 40 K (calculation shown below) for length of time of duration of time constant i.e. 15 minute.

Now what should be the step of temperature rise for a time interval of each time constant? Maximum possible transient thermal stress is calculated using the formula given by equation-4.

$$\sigma = \frac{E*\alpha*\Delta T}{1-\Omega} \qquad \text{eq-(4)}$$

Where, E= Elastic Modulus, α=Liner Thermal Expansion, ΔT=Temperature gradient, Ω=Poison Ratio.

Equation-4 gives out the allowable maximum sudden rise of temperate without cracking the ceramic，i.e.

$\Delta T=\frac{\sigma_{t(1-\mu)}}{E.\alpha.\Delta T.FS}$ (ΔT is calculated putting $\frac{\sigma_t}{FS}$ in place of σ)

Where, σ_t = Ultimate tensile Stress, FS= Factor of Safety

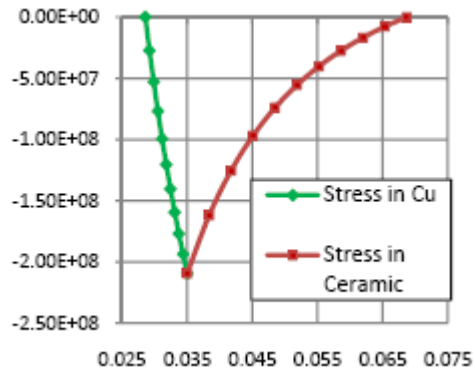

Graph-1: Radial stress in Pa along y-axis and radial distance in meter along x-axis

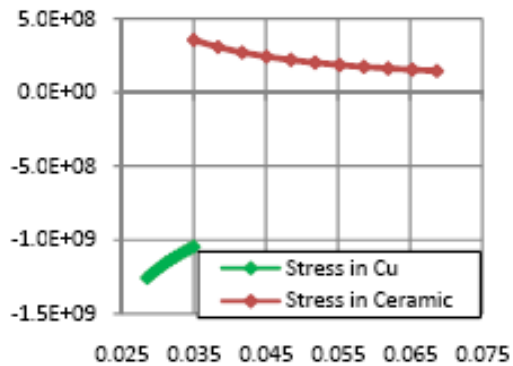

Graph-2: Tangential stress in Pa along y-axis and radial distance in meter along x-axis

Evaluated ΔT comes out as 40 K for FS=1.5.Therefore allowable rate of temperature rise is ΔT/ τ i.e. 2.66 K/min. And this rate of temperature rise also decreases (i.e as the brazing process goes on) as the stress induce due to the differential liner thermal expansion of the ceramic and copper increases with time. This increase in stress further eat away the available allowable stress.

Thermal Stress induces because of temperature gradient has also been calculated using equation-5, 6 along with the assumption made are infinite long cylinder and shear stress is neglected, All the material properties are isotropic.

$$\sigma_\theta=\frac{E}{1-\Omega^2}\left\{\frac{u}{r}+\Omega\frac{du}{dr}\right\} \qquad \text{eq- (5)}$$

$$\sigma_r=\frac{E}{1-\Omega^2}\left\{\frac{du}{dr}+\Omega\frac{u}{r}\right\} \qquad \text{eq- (6)}$$

Where, u=Radial displacement, r=Radial direction, σ_θ= Tangential (circumferential) stress, σ_r= radial stress

Radial displacement has been find out solving the equation-7 and the plot of the radial stress and circumferential has been presented by graphs-1 and 2

$$\frac{1}{r}\frac{d}{dr}\left\{r\frac{du}{dr}-\frac{u}{r}\right\}=0 \qquad \text{eq-(7)}$$

Maximum tangential stress induced in the ceramic is found to be 120 MPa, Therefore the rate of temperature rise reduced to 1.5 K/min.

Calculation has also been made to find out the minimum current of the TIG welding machine by which TIG brazing could be carried out. When the temp of the welding zone reaches to 600°C, the steady heat loss to the atmosphere due to convection and radiation is 500W. To maintain the temperature of the brazing material minimum 40A current is required to be set in the TIG welding machine at 10 to 12 V. Where ever at the first trial, current at which brazing was done was 100A which in turn resulting to higher rate of temperature rise than the allowable.

Finite Element Analysis

Also 3D finite element analysis has also been carried out using ANSYS software code to evaluate spatial temperature distribution and hence the thermal stress induced due to the temperature gradient. Simulation revealed uniform heating around the copper tube will reduce the induced stress from 100 MPa to 45 MPa. Therefore TIG brazing was preferred with pre-heating along with distributed heating with multiple torch instead of TIG brazing only. Figure-2a shows the model used in FEM analysis and Figure-2b shows the thermal stress induced in case of only TIG brazing is done.

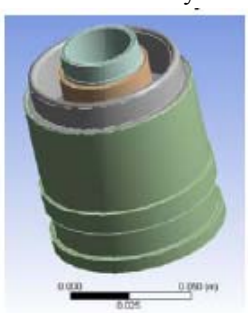

Figure-2a

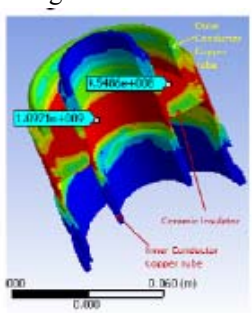

Figure-2b

FABRICATION

During fabrication, arrangements were made for monitoring the temperature of the alumina ceramic as well as copper tube using thermocouple temp. sensor.

Suitable fixture were made and employed to maintain the concentricity between inner and outer conductor of the ceramic as well as to control the brazing distortion. And it has been observed that by heating a copper tube by using one torch could not be sufficient to maintain the rise of temperature within the tolerable limit. Therefore preheating of the copper was carried out up to 200°C by using heater and multiple torch along the circumference and length of the tube. To avoid the contamination of the ceramic reduced atmosphere with argon gas is used.

Finally brazing (see Figure 3) of the copper along with their mating part has been performed. Melting point of the used brazing filler rod (i.e 43% Ag and 57% Cu) is 600°C. To carry out the single circumferential joint of 215 mm length, it took around 6 hours of time. Brazing of the joint was tried to performed with minimum current so that concentrate heating effect could be minimised. It was observed that current could be reduced to 40 A minimum value. After the joint was performed, cooling rate of the joint as well as ceramic was controlled using the heater. After each joint was performed, subsequent vacuum test was carried out and all the joints were pass the helium leak test successfully. Leak found was less than $1x10^{-9}$ mbar.lit/s.

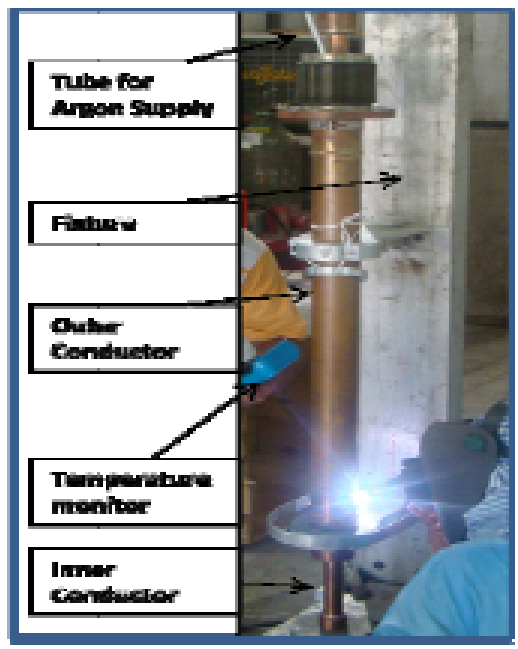

Figure 3: Gas brazing process is under progress

Presently the fabricated coupling capacitor is working satisfactorily with the cyclotron for more than a year and beam extraction using Ne^{3+} is under progress.

REFERENCES

[1] F.P. Incorpera, D.P. Dewitt, “Fundamentals of Heat and Mass Transfer”

[2] J. Kokavec and L. Cesnak, “Mechanical stress in cylindrical superconducting coils”, J. Phys. D: Appl. Phys. 10 NO 11 (1 Aug. 1451-1459).

[3] S. Timoshenko, “Strength of Material Part 2 Advance theory and Problem”, 3rd Edition, CBS Publication & Distributor.

[4] J.F. Harvey, P.E,“ Theory and design of pressure vessel", CBS Publications & Distributor.

[5] S.P. Sukhatme," A textbook on Heat transfer", 4th Edition, University Press.

DESIGN, CONSTRUCTION AND COMMISSIONING OF THE 100KW RF AMPLIFIER FOR CYCIAE-100

ZhiguoYin[1], Zhenlu Zhao[1], Shidong Wei[2], Yong Xie[2], Zhenguo Li[1], Bin Ji[1],
Haichao Xiao[2], Tianjue Zhang[1]
China Institute of Atomic Energy, Beijing, China
23rd Research Institute of the Second Academy of China Aerospace Science and Industry Corp.
Beijing, China

Abstract

As a major part of the BRIF project, CYCIAE-100, the 100MeV high intensity cyclotron being constructed at CIAE, will provide 200μA-500μA proton beam ranging from 75MeV to 100MeV for RIB production. Two identical 100kW RF amplifiers will be used to drive two cavities independently to accelerate H- beam up to 100 MeV. The detail technical specification has been investigated, fixed, and initial design has been finished by CIAE. Then, the construction design and manufacture is done by China Academy of Aero and Space. The on site test is successful by mutual efforts. The final commissioning is under way with a full scale prototype cavity at CIAE. A general description of the CYCIAE-100 RF system design will be given, as well as the review of 100kW amplifier design. In the commissioning of the amplifier with dummy load, different high order resonances are found when operated at different frequencies between 42MHz to 46MHz. An equivalent circuit model is carried out to hunt down the problems. The model and related analysis will be reported together with the process and results of high power test with the cavity load through about 35-meter 6-1/8" rigid coaxial line.

INTRODUCTION

For the RF system of CYCIAE-100, two 100kW amplifiers will be connected though about 35 meters 6 inch transmission line to power the two cavities individually. A set of digital low level controls will be used to ensure the amplitude of the each cavity, tuning of each cavity and regulation of the phase difference between the two cavities [1][2].

As planned years ago, a full scale OFHC test cavity was fabricated in year 2009, polished and assembled in early 2010. In the mean time, the two amplifiers were designed in year 2008, approved by CIAE, and manufactured by the 23th research institute of CASIC (Changfeng Broadcasting Co. Ltd.). In early 2010, the two amplifiers finished various kinds of factory tests, and one of them is shipped to CIAE cyclotron laboratory. With the full scale cavity and the amplifier on site, the cyclotron laboratory prepared the vacuum system, the water cooling system and the 150kW mains system for the amplifier test with the real cavity load. The amplifier design will be reviewed in Section 2, while the factory test and the on site test with cavity load will be reported in Section 3 and Section 4 respectively. To dump the transmission line high order mode at a frequency of 311.5MHz, a harmonic absorber will be promoted in Section 5 as next step.

AMPLIFIER DESIGN REVIEW

The amplifier chain consists of a 6kW solid driving stage, a 100kW final stage and necessary low level protection circuits.

The driving stage utilizes BLF287 MOSFET as core amplification unit. There are in total 32 these units in the driving stage. The combination of RF power is divided into three stages. Firstly, four 200W units was combined together making an amplification unit capable of delivering 800W power, taking 4U space in a 19 inch cabinet; Secondly, four 800W units combine their power together to get ~3kW RF power; eventually, the two 3kW units were combined together as the driving stage solid amplifier with a capability of delivering more than 6kW power.

The final stage uses a EMAIC 4CW150,000 power tube, a ground grid configuration is selected. To be more specific, both the grid and the screen are RF grounded to the tank wall. Though in ground grid configuration, certain amount of driven power will be directed to output, which in turn means more driven power. Yet, from stability point of view, still it is a good choice for high power amplifiers, especially in the case to power a high Q load, e.g. the cyclotron cavity.

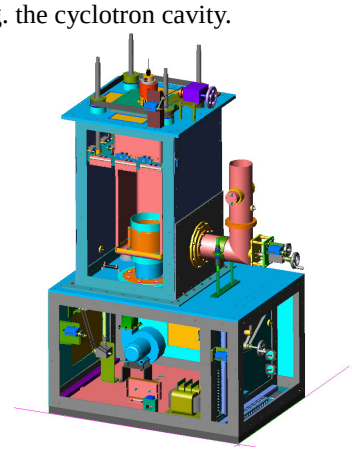

Figure 1: The final stage amplifier

As shown in Fig. 1, the anode tank uses a quarter-wave cavity with a movable short driven by four synchronized worm wheels. The inner conductor is made of copper while the outer is of copper clad aluminium. The output power of the amplifier is channelled out though a

COMET variable vacuum capacitor, connected at the voltage terminal of the resonator.

Tube Operating Parameters

Considering the efficiency, the tube is designed to operate in class C. Once the conductive angle is selected, the residual anode potential can be determined using formula 1.

$$E_{a(\min)} = 0.5 \cdot \left(1 - \sqrt{1 - \frac{8P}{0.5 \cdot S \cdot E_a^2 \cdot \alpha_1(\theta)}}\right) E_a \qquad (1)$$

Where E_a is the DC anode potential, P is the design output RF power, S is the transconductance of tube and θ is the conductive angle. In a similar way, one may find out the maximum current by

$$I_{a(\max)} = \frac{2P}{\left(E_a - E_{a(\min)}\right) \cdot \alpha_1(\theta)} \qquad (2)$$

Then the operating line can be fixed on tube constant-current curves, using point $A\left(E_{a(\min)}, I_{a(\max)}\right)$, and $P\left(E_a, I_{a(\min)}\right)$, as shown in Fig.2. It should be noted that $I_{a(\min)}$ is chosen by experience.

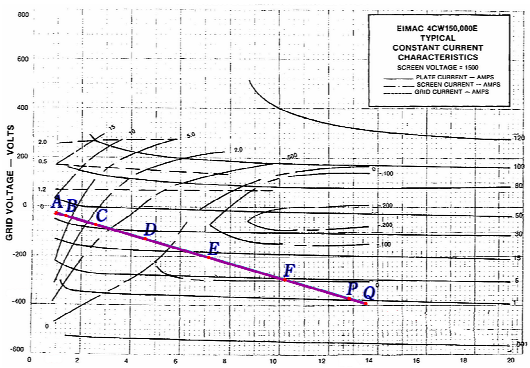

Figure 2: Tube operating line for 4CW150,000

The output power, DC meter readings as well as the fundamental RF peak current and tube anode impedance can be calculated out by applying Runge-Kutta method to the operating line. The result is tabulated as follows.

Table 1. Calculated parameters for the amplifier

Anode potential	13.5 kV
Screen potential	0.95 kV
Grid potential	-360V
Anode DC Current	10.55A
Anode RF Current	16.82A
Anode RF resistance	751 ohm
Output power	106 kW
Anode dissipation	36 kW
Gain	15dB

Input and Output Circuits Design

As the amplifier is designed to be driven from cathode, the input circuits need to adapt very low impedance (e.g. 6.2-9.5j ohm) to normal 50 ohm driving port. The circuit consists of 3 components, i.e. a shunt variable vacuum capacitor, a serial inductor and a parallel strip line inductor. The matching procedures are relatively easy can be well understood using smith chart.

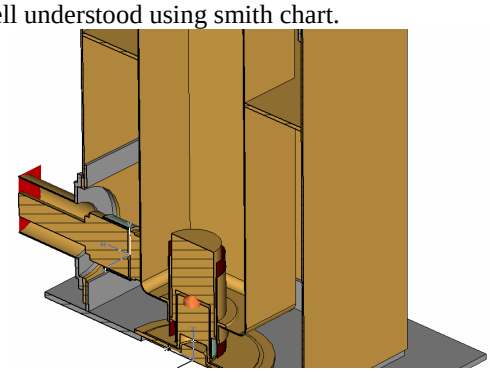

Figure 3: Amplifier Output circuits design

The output circuits design concerns modelling the anode tank structures in 3D electromagnetic software. As shown in Fig. 3, the model consists of a tube anode structure, a lumped element representing anode resistance, an anode Kapton® DC block capacitor, upper part of the tube socket including screen DC block capacitor, a rectangular coaxial resonator, a vacuum capacitor structure and the output port. The simulation is performed with the lumped resistor set to 751ohm. Several iterations with different output capacitance and short plate position had been done by time domain solver, for the evaluation of the tuning and matching of the anode tank. The results shows the S_{11} of output port could reach -35.82db when the output capacitance is set to 18.8pF, which is right in the middle of the COMET variable capacitor tuning range. In the mean time, the short plate travelling range is also determined to cover the whole amplifier frequency range.

HIGH POWER TEST

Test with Dummy Load

The power test with dummy load was done at the CASIC. During the seven hour endurance test, the amplifier worked in a reliable manner. Though there was small gain difference in the solid stage comparing the data acquired in noon and evening, it was believed to be caused by room temperature variation, and concluded as acceptable.

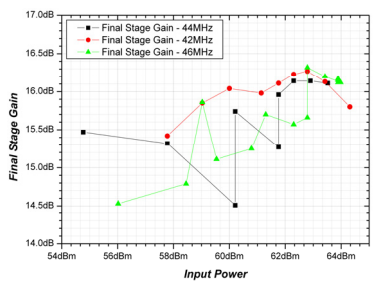

Figure 4: Final stage gain versus input power

Also, gain linearity with respect to different output power level has been checked during the factory test, the

final stage trends to have 1 db higher gain in high power, as shown in Fig.4. Note the gain jumping in the chart is for test purpose, cause by deliberately turning up or down the anode potential (700V each time) during the test.

For higher harmonics measurements, the amplifier has -28db for 2nd and -27db for 3rd. A reflective high power filter was promoted by 23th institute of CASIC and fabricated, installed in the transmission line during the power test with dummy load. After the installation, the 2nd and 3rd harmonic are well below -50db.

Test with Cavity Load

Though the waveform and the spectrum look clean and nice after the filter, the filter was not installed during the test with cavity after one of the amplifiers was shipped to CIAE site. To clarify this issue, a similar SPICE model including the filter and the cavity has been developed and studied, following the CRM cyclotron RF system model (reported in another paper of this conference). Afterward, the parasitic resonance has been confirmed by network analyzer measurements, thus both sides agreed to remove the filter from the transmission line.

After the vacuum, cooling and the AC mains input satisfied the hot test requirement, the real load test for the amplifier was carried on in summer of 2010. The major purpose of the high power test with the cavity is to check if instability exists in high power operation, meanwhile verification of Dee accelerating voltage is also important.

At the begin of the high power experiment, the conditioning progress takes longer time than expected, due to the fact that the vacuum is not so good and frequently the vacuum tank need to be opened for various reasons, e.g. changing water pipe sealing, installing new temperature sensor etc. As the carbon compounds are slowly but steadily built up on certain surface of the cavity, feed power to the cavity is easier time by time. After three weeks, continuous wave can be applied to the cavity after 2 to 3 hours of pulse conditioning.

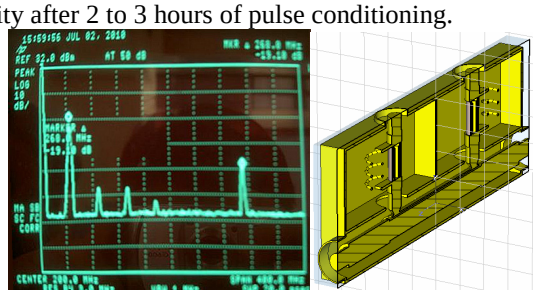

a) 7th harmonic b)promoted absorber

Figure 5: DC equivalent circuits and anode circuits

The amplifier has proved to be reliable in high power test. Even at the beginning, to feed power into the cavity, with low duty cycle in several microseconds, the amplifier was driven to its limit with reflect almost equal to forward power in level of 100kW, and no big issues emerged except that several small isolation transformer was broken down due to isolation material imperfection.

One issue to be confirmed and handled later is that the 7th harmonic is abnormally higher compare to the power test with dummy load. The spectrum taken from the transmission line is shown in Fig.5 a). A promotion of high harmonic absorber has been put forward by RF group, as shown in Fig.5 b). The centre frequency of the 3db coupler in the absorber is set to 318.5MHz, in the hope of lowering the transmission line Q at the 7th. The absorber is to be fabricated after the installation of trombone, in case the 7th harmonic resonance cannot be weakened or moved to other frequency by fine turning of the transmission line length.

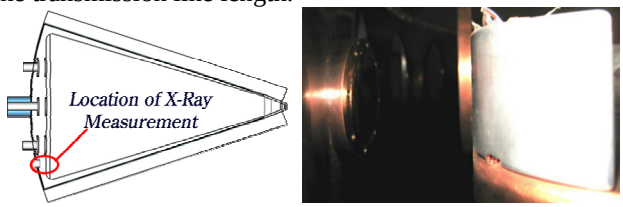

Figure 6: One of the X-ray measurement positions

Another major task is to verify the shunt impedance in high power, with the present of field emission electrons load and possible dark current load. It is planned to use X-Ray to calibrate the Dee voltage [3]. The difficulty of this task is related with finding a position with higher x-ray yields and good alignment [3] [4], considering the fact that the cavity for CYCIAE-100 has an unique voltage distribution [5]. To be more accurate in the measurement, the electron motion as well as photons yields curve has been calculated for this case, using the method in [3][6]. After these works done, considering the accessibility of the vacuum tank, around the middle plane, four different locations were selected to install AMPTEK XR-100SDD detector, one of which is shown in Fig.6. The experiment will be performed soon after the detector is available.

REFERENCES

[1] Tianjue Zhang, Zhenguo Li, Zhiguo Yin et.al., Design & construction status of CYCIAE-100, a 100 MeV H− cyclotron for RIB production, NIM-B, Volume 266, Issues 19-20, October 2008, Pages 4117-4122

[2] Xiulong Wang et.al., The alternative of RF system design for the 100 MeV cyclotron at CIAE, NIM-B, Volume 261, Issues 1-2, August 2007, Pages 70-74

[3] J. Sura, L. Calabretta, et.al. X-ray calibration of the Superconducting Cyclotron DEE-Voltage, INFN-LNS reports 1995

[4] J.H. Timmer, H. Röcken, P.A. Komorowski ,Dee voltage calibration for the ACCEL proton therapy cyclotron, ICAP 2006, Chamonix, France

[5] JI Bin, ZHAO Zhenlu, ZHANG Tianjue, et al., Theoretical and practical study on RF model cavity of 100 MeV H- cyclotron, Chinese Physics C, 2008, 32(Suppl.1): 160-162

[6] J.P.Duke, A.P.Letchford and D.J.S.Findlay, Measurements of RF cavity voltages by x-ray spectrum measurements, XX International Linac Conference, Monterey, California

RF CAVITY SIMULATIONS FOR SUPERCONDUCTING C400 CYCLOTRON

Y. Jongen, M. Abs, W. Kleeven, S. Zaremba, IBA, Louvain-la-Neuve, Belgium
A.A Glazov, S.V. Gurskiy, O.V. Karamyshev, G.A. Karamysheva, N.A. Morozov, JINR,Dubna, Russia

Abstract

The compact superconducting isochronous cyclotron C400 [1] has been designed by IBA (Belgium) in collaboration with the JINR (Dubna). It will be the first cyclotron in the world capable of delivering protons, carbon and helium ions for therapeutic use. $^{12}C^{6+}$ and $^{4}He^{2+}$ ions will be accelerated to the energy of 400 MeV/u energy and extracted by electrostatic deflector, H_2^+ ions will be accelerated to the energy of 265 MeV/u and extracted by stripping. It is planned to use two normal conducting RF cavities for ion beam acceleration in cyclotron C400. Computer model of the double gap delta RF cavity with 4 stems was developed in is a general-purpose simulation software CST STUDIO SUITE. Necessary resonant frequency and increase of the voltage along the gaps were achieved. Optimization of the RF cavity parameters leads us to the cavity with quality factor about 14000, RF power dissipation is equal to about 50 kW per cavity.

RF CAVITY GEOMETRY

Magnetic field modeling and beam dynamics have determined orbital frequency of the ions equal to 18.75 MHz. As RF cavities will be operated in the 4th harmonic mode resonance frequency must be 75 MHz. It is planed to use two normal conducting RF cavities [1] for ion beam acceleration in the C400 cyclotron.

The geometric model of the double gap delta cavity housed inside the valley of the magnetic system of the C400 cyclotron was developed in the CST STUDIO SUITE. We studied a number of models that differ in the width of the accelerating gap, the height of the dee; the final variant of the model is presented in Figure 1. The depth of the valley permits using the cavity with the total height 116 cm. The vertical dee aperture was 2 cm. The accelerating gap width was 6mm at the center increasing to 8 cm at R = 75 cm, and remaining constant to extraction region as shown in Fig. 3.

Distance between dee and back side of the cavity was equal to 50 mm. Cavities have a spiral shape similar to the shape of the sectors. The sector geometry permits azimuth extension of the cavity (between the middles of the accelerating gaps) equal to 45 deg up to the radius of 150 cm, (see Fig. 2). We inserted four stems with different transversal dimensions in the model. We studied different positions of the stems to insure increasing voltage along the radius of the accelerating gap, which should range from 80 kV in the central area up to 160 kV in the extraction region. It is important to have a high value of voltage beginning approximately at R = 150 cm before crossing the 3Qr = 4 resonance.

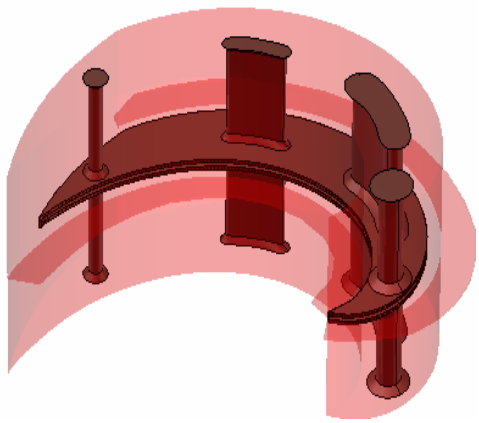

Figure 1. View of the cavity model.

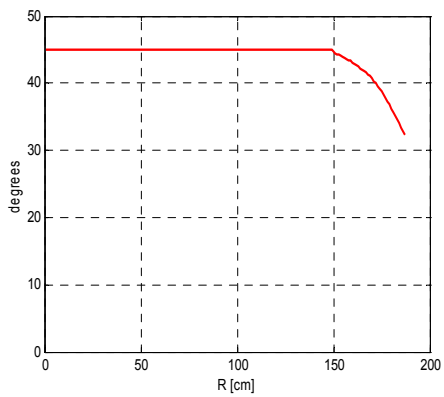

Figure 2. Azimuth extension of the cavities (between middles of the accelerating gaps).

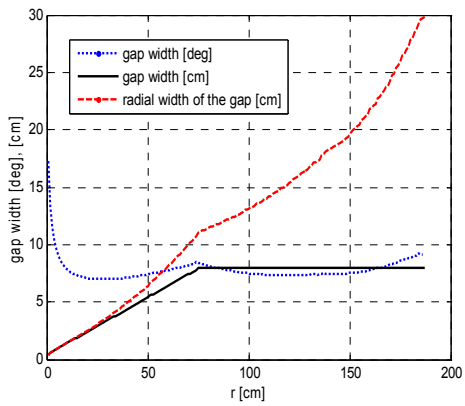

Figure 3. Gap width against radius. Dashed line- radial width in cm, dotted line-azimuth extension in deg, solid line-perpendicular in cm.

The thickness of the dee was 20 mm. The edges of the dees were 10mm thick and have a rounded form optimized from the 2D electric field simulations in order to minimize the electric field in the environment.

Each cavity will be excited with the RF generator through a coupling loop (which should be rotated azimuthally within small limits (+- 30 degrees). The active tuning system must be designed to bring the cavities to the frequency initially to compensate for detuning because of temperature variations due to RF heating and to provide frequency difference 450 kHz for C^{6+} and H_2^+ ions acceleration.

We analyzed effect from the tuner in the position R = 120 cm and at R = 70 cm with diameter 10 cm and 18 cm. One tuner with diameter 10 cm provides changing of frequency about 500 kHz. We found that the better position for the tuner is at radius R = 120 cm (see Fig. 4).

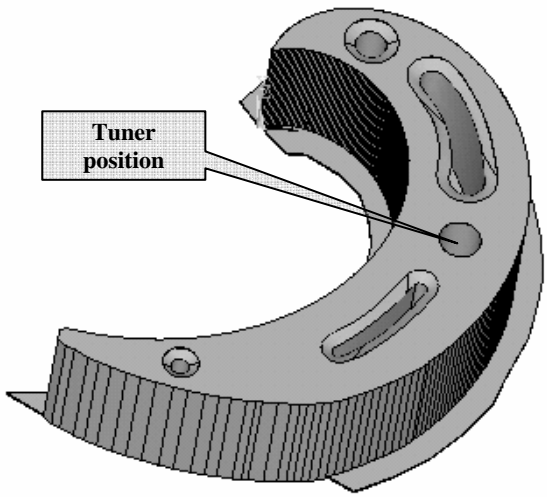

Figure 4. View of the ANSYS model with tuner.

SIMULATIONS IN CST MICROWAVE STUDIO AND ANSYS (MODAL)

CST STUDIO SUITE is a general-purpose simulator based on the Finite Integration Technique (FIT). This numerical method provides a universal spatial discretization scheme applicable to various electromagnetic problems ranging from static field calculations to high frequency applications in time or frequency domain. [2]. ANSYS is an engineering simulation software which mainly rely on the Finite Element Method (FEM). These are general-purpose finite element modeling packages for numerically solving mechanical problems, heat transfer and fluid problems, as well as acoustic and electro-magnetic problems. [3]. Calculations of the created model were performed using the eigenmode JD lossfree solver (Jacobi Division Method) in the CST Microwave Studio and the Block LANCZOS solver in ANSYS. For simulations in ANSYS we imported in ***.sat*** format the model created in CST Microwave Studio. The half structure model of the cavity was used where the vertical symmetry could be utilized and the accuracy of the solution was important (see Fig. 4).

In order to shape the radial voltage distribution we moved stems. In addition, we needed to change the transversal dimensions of the stems. The voltage value was obtained by integrating the electric field in the median plane of the resonant cavity. To fit the frequency of the cavity to the project value after rearranging stems positions we had to change horizontal dimensions of all stems by the same value. We found that variation of the horizontal dimensions of all stems by one percent changes the frequency by about 300 kHz and the value of the voltage along the radius does not change noticeably while the frequency is fitted by less than 1 MHz.

Simulations show that the frequencies from both programs are about the same beginning with the number of meshcells 7 million for CST and 3 million for ANSYS:

F_{rf} = 75.02 MHz, CST Microwave Studio.

F_{rf} = 74.80 MHz, ANSYS.

Now we can conclude that the accuracy of the calculations for the cavity frequency in our simulations is better than 0.3%.

From Fig. 5 one can see the difference between the acceleration gap voltage profiles in two programs is negligible. For these simulations we needed a powerful computer with the 8 GB RAM. Less meshcells number gives substantially bigger difference not only in frequency value but in voltage distribution.

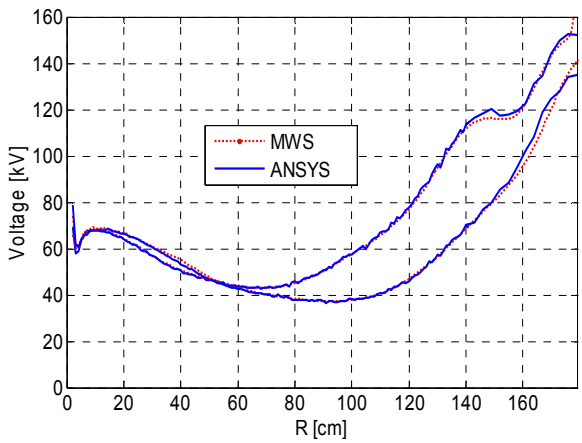

Figure 5. Voltage distribution along the radius.

Radial and azimuth electric field components and magnetic field maps in median plane were created for the beam dynamics simulation. This model simulation technique can be used to study central region of the accelerator.

Power dissipation in the model was calculated on the assumption that the wall material is copper with conductivity $\sigma = 5.8*10^7$ 1/(Ωm). The quality factor was about 14000 and power losses of the model were as follows:

For the storage energy 1 J the voltage at the center is 65 kV, and average losses are 35 kW

For the storage energy 1.5 J the voltage at the center is 80 kV, and average losses are 50 kW

Each cavity will be powered by a 75 MHz, 100 kW tetrode-based amplifier (as used in the current C235).

FITTING OF THE FREQUENCY OF THE CAVITY

As the accuracy of the cavity frequency calculations in our simulations is about 200 kHz (0.3%) we had to think of possible fitting of the cavity frequency by 300 kHz.

We analyzed fitting methods of the cavity frequency. In order to decrease the resonant frequency the pillar diameter could be changed. It was shown earlier that simultaneous variation of the transversal dimensions of stems changes frequency without changing the voltage behavior along radius. But machining so many stems of the real cavity is not a simple task. Also, second and third stems have rather complicated transversal shape. That is why we tested the influence of machining of round stems on the resonant frequency and voltage variation along the radius.

First of all we created a model with the resonant frequency 75.8 MHz and examined possibilities of decreasing resonant frequency in this model by modulating diameter of the first stem. Diameter of the first pillar was decreased by 1.9 cm. As the result resonant frequency decreased from 75.8 MHz down to 75.45 MHz i.e. the magnitude of frequency difference per diameter difference was about 19 kHz/mm pillar for the first pillar. It is too small value. In addition, the voltage in the center was changed too much – more than 10 kV.

Then in the model with frequency 75.8 MHz we changed diameter of the fourth stem. Initially diameter of the fourth stem was D_0 = 8 cm. We decreased diameter step by step in order to achieve frequency 75 MHz. The frequency difference per diameter difference is about 115 kHz/mm_{pillar} for the fourth pillar. Influence on voltage value in the center region was much smaller for the fourth stem diameter decreasing than for the first stem's. Practically, it is possible to decrease cavity's resonant frequency by 300 kHz, decreasing diameter of the fourth stem by 2.5 mm.

CONCLUSIONS

The computer model of the double gap delta RF cavity with 4 stems was developed, simulated and analyzed in CST Microwave Studio and ANSYS. The model had frequency 75 MHz, necessary voltage distribution from 80 kV in the center up to 160 kV (average) in the extraction region. It was shown that the voltage behavior along the radius depends substantially on positions and diameters of the stems. The frequency value can be changed by scaling transversal dimensions of all stems without essential voltage profile modification.

It was demonstrated that it was possible to change the resonant frequency of the cavity by varying of the diameter of the fourth stem. The frequency difference per diameter difference is about 115 kHz/mm. The capacitance tuners in position R = 120 cm will provide the necessary frequency tuning.

Optimization of the RF cavity parameters leads us to the cavity with quality factor about 14000, RF power dissipation is about 50 kW per cavity.

REFERENCES

[1] Yves Jongen et al, "IBA C400 Cyclotron Project for Hadron Therapy", The 18th International Conference on Cyclotrons and their Applications Cyclotrons 2007, Laboratori Nazionali del Sud, Giardini Naxos, Italy 2007.

[2] Yves Jongen et al, "Radio Frequency System of the Cyclotron C400 for Hadron Therapy", The 18th International Conference on Cyclotrons and their Applications Cyclotrons 2007, Laboratori Nazionali del Sud, Giardini Naxos, Italy 2007. http://felino.elettra.trieste.it/cyc07/papers/TUPPRA05.pdf

[3] CST STUDIO SUITE http://www.cst.com

[4] ANSYS http://www.ansys.com

TRIUMF CYCLOTRON BOOSTER FREQUENCY TUNING SYSTEM

Q. Zheng*, K. Fong, and M. Laverty, TRIUMF, vancouver, V6T 2A3, Canada

Abstract

For the auto frequency tuning of TRIUMF cyclotron booster, a new control module based on the VXI Bus has been designed, tested, and put into commission. This new auto tuning control module, which replaced the old analogue control box, has more features, including the implementation of PIC16C71 microprocessor to generate Pulse Width Modulation (PWM) pulse, the utilization of digital RF phase detector, and the most important aspect of computer control capability. Thus, the resonant frequency of the cyclotron booster RF cavity is tuned automatically by this control module, and the reflected RF power is kept at the minimum level in the operation.

INTRODUCTION

For an accelerator RF cavity, the auto frequency tuning system keeps the cavity at resonant frequency to achieve the desired RF voltage with minimum RF power input. If the RF cavity is out of tune, RF power is partially or totally reflected and the reverse power may damage the RF power amplifier or the transmission line, especially in cases of high power operation.

Thus, the auto frequency tuning system is essential for the RF resonant structure. The TRIUMF RF Booster operates at 92MHz with a nominal voltage of 150kV[1]. In order to realize the auto frequency tuning, two capacitor tuners called Master Tuner and Slave Tuner, are implemented in the TRIUMF cyclotron booster cavity to cover the resonant frequency excursion.

This design uses the microprocessor PIC16C71 to generate a PWM waveform to drive the DC motor of the cyclotron booster tuner. Such a design has good flexibility to adjust the PWM pulse width by using programming software. Furthermore, a digital type of RF phase detector is implemented in the new tuner control module and covers a wider phase error range. These new features make this control module more flexible and reliable.

PRINCIPAL CIRCUITS AND FUNCTIONS

Figure 1 shows the block diagram of the new booster tuner control module. It mainly consists of two logarithmic amplifiers, a RF phase detector, a PIC16C71 microprocessor, a RF amplitude detector, and a driver amplifier.

PIC16C71 Microprocessor

The PIC16C71 is a low-cost high-performance 8-bit micro-controller. It has 36 bytes of RAM and 13 I/O pins. Also, a 4-channel high-speed 8-bit A/D converter is provided within the chip. The 8-bit resolution is ideally suited for applications requiring low-cost analogue interface (e.g. tuner control, thermostat control, etc).

In the booster tuner control PCB, two PIC16C71 microprocessors are used to control the master tuner and the slave tuner separately. For the master tuner PIC16C71 controller, RB0 and RB1 of port B are set up as the PWM pulse output channels. Port A 4-channel A/D converter is set up like the following: RA0 is the RF phase input; RA1 is the RF amplitude input; RA2 is the master tuner position input; and RA3 is the standard ADC reference voltage input. As to the slave tuner PIC16C71 controller, Port B RB0 and RB1 are similarly set up as PWM pulse output channels. Port A RA0 is the master tuner position ADC and RA1 is the slave tuner position ADC.

For timing insensitive applications such as the RF cavity frequency tuning controller, the "RC" oscillator for the microprocessor is good enough to let the controller running. The RC oscillator frequency is mainly a function of the supply voltage, the external resistor (Rext), the external capacitor (Cext) values, and the operating temperature. For Rext values below 2.2kΩ, the oscillator operation may become unstable, or stop completely. For very high Rext values (e.g.1MΩ), the oscillator becomes sensitive to noise, humidity, and leakage. Thus, Rext values should be chosen between 3.3kΩ and 100kΩ. As to Cext, the oscillation frequency can vary dramatically due to residual capacitance with no or small external capacitance. Therefore, it is recommended to choose Cext values above 20pF for noise and stability reasons.

In this design, 3.3kΩ is selected as Rext value and 22pF is selected for Cext. The oscillation frequency is about 6MHz, including residual capacitance on the PCB board.

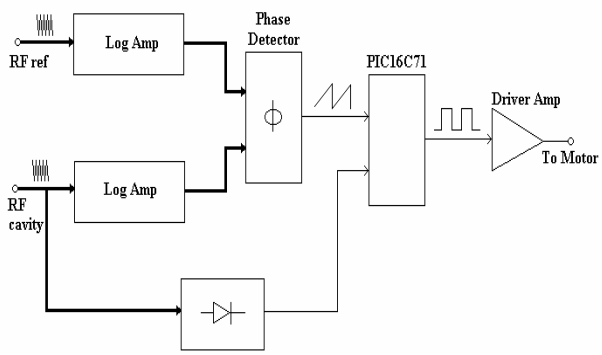

Figure 1: Block diagram of booster tuner control module.

RF Phase Detector

In the old booster tuner control unit, a SRA-1 mixer was used to detect the RF phase error. For the new tuner control module, a different type of phase detector is utilized. This phase detector uses two F100304 chips, which is a low power quintuplet AND/NAND gate chip.

*zhengqw@triumf.ca

This digital phase detector generates saw-tooth-waveform phase error output by applying two different RF signals into its inputs. This kind of phase detector is easier to get auto frequency tuning locked and more stable because of its wider phase coverage. The actual phase detector circuit is illustrated in Fig.2. The detected phase error is the output of TL082 and ranges between –2.5V and +2.5V.

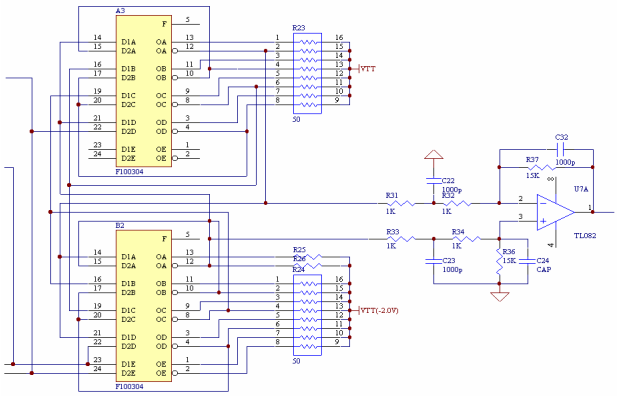

Figure 2: Phase detector circuit.

Logarithmic Limiting Amplifier

For a normal RF phase detector, the phase error signal is not only related to input signals phase difference, but also related to input signals amplitude level. In order to get an accurate phase error, the amplitude of input signals to the phase detector must be set to a fixed value. Therefore, limiting-logarithmic amplifiers are necessary at the RF input for every phase detector to achieve an accurate phase control. [2]

In this booster tuner control module, Log amplifier AD8306 is implemented. It has super high dynamic range and amplitude gain. Its operation frequency range is from 5 MHz to 400 MHz and its dynamic range is 100 dB, from –91dBV to +9dBV. The designed schematic circuit of the limiting-logarithmic amplifier is shown in Fig.3.

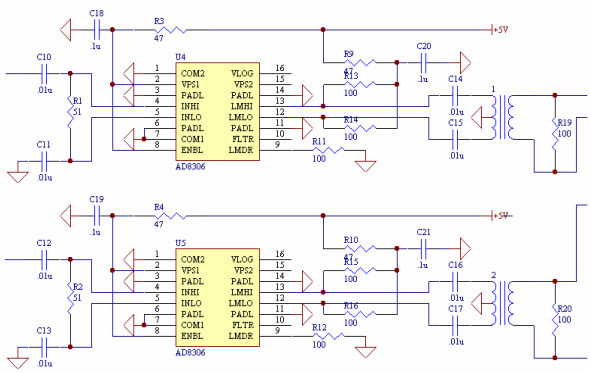

Figure 3: Logarithmic amplifiers circuit.

Amplitude Detector

The amplitude detector is used to monitor the booster cavity's RF voltage level. Only when the booster amplitude reaches a certain level is the booster auto-tuning control set to close-loop. During the power-up procedure, the cavity is firstly powered by RF pulse to pass through the multipactoring. So during start-up, the auto frequency tuning control is not operational. Only when the pulsed RF signal is switched to CW RF signal can the auto-frequency-tuning module work properly. After that, it is possible to set the tuner to close-loop when the appropriate RF amplitude level has been reached.

Driver Amplifier

The driver amplifiers are incorporated into the tuner control board to drive the DC motors of booster tuners. Each driver amplifier consists of a pair of power transistors, MJE340 and MJE350. MJE340 is a NPN silicon transistor and MJE350 is a PNP silicon transistor. Both transistors are useful for high-voltage general-purpose applications. The driver amplifier for the master tuner DC motor is indicated in Fig.4.

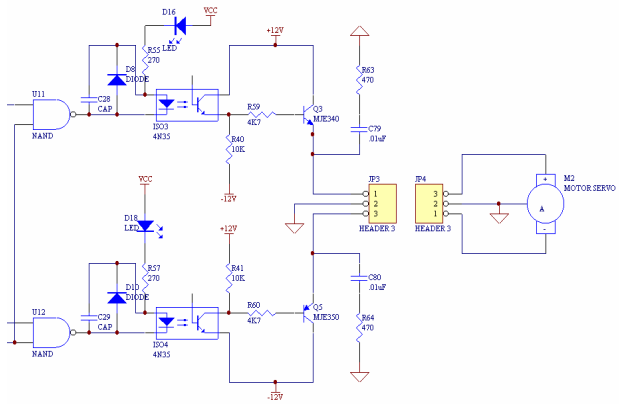

Figure 4: Driver amplifier for tuner DC motor.

SOFTWARE

For PIC16C71, a set of special instructions is used for programming. All instructions are recognized by the MPASM assembler or by the Integrated Development Environment MPLAB IDE. The program for the booster tuner control module is written in this assembly language. [3]

CONCLUSION

This auto frequency control module has already been put into commissioning. It has been installed in a VXI crate and can communicate with the local control computer to realize the booster tuner control properly. High power tests have been done for the booster cavity power level up to 40kW. The auto tuning system keeps the tuners moving and tracks the resonant frequency well.

REFERENCES

[1] K. Fong, M. Laverty, "RF Control for TRIUMF Booster Cavity", Proceedings of the Third European Particle Accelerator Conference, Berlin, March 1992, pp. 1176 - 1178.

[2] Q. Zheng, "High Performance Limiting-Logarithmic Amplifier", TRIUMF Design Note TRI-DN-02-25, Dec. 2002.

[3] Microchip Technology Inc, Microchip PIC16/17 Microcontroller Data Book, 1996/1997.

AMPLIFIER TEST STAND FOR THE CRM CYCLOTRON

Zhiguo Yin, Kai Fei, Guofang Song, Tianjue Zhang, Bin Ji, Pengzhan Li Gengshou Liu
China Institute of Atomic Energy, Beijing, China

Abstract

The final stage amplifier stability has proved to be an important issue in the commissioning of CRM cyclotron at CIAE. An air cooled 4CX15,000 tube final amplifier was designed to evaluate the anode circuit and neutralization, both of which are weak points of the CRM cyclotron amplifier. Instead of strip line, the new designed anode structure adopts coaxial form, resulting less chance of parasitic resonance in the circuits. A tuneable neutralization circuits was also included in the design, giving an opportunity to fine tune in high power operations. First, the instability in CRM RF system will be analyzed in this paper, followed with the new amplifier designs including the tube operating line calculations, input/output circuits designs and finite integral simulations. The mechanical design for tube socket and anode tank were successfully carried out using the data provided in this paper. The final stage amplifier was then manufactured, assembled and commissioned. In the power test with dummy load, more than 9.2kW RF fundamental power was provided at the frequency of 44.5MHz.

Key Words: RF Amplifier; neutralization; coaxial resonator

INTRODUCTION

In the commissioning of CRM cyclotron at CIAE[1], a parasitic resonance mode was found having significant influence to the RF system stability[2], showing an unreasonable screen current incensement of 200% once the amplifier output exceeds 6kW when driving cavity load. The reason of this parasitic mode concerns the interaction of the transmission line and cavity and will be analyzed in the following section. To solve the instability, the transmission line length was adjusted to multiple of half wave length, and the neutralization of the amplifier was tuned accordingly to have more stable gain margin considering the final stage taking ground cathode configuration[2]. As the plan of upgrading beam current to 1mA put forward, the amplifier anode transformer was changed to a bigger one giving more anode potential, from 7.5kV to 9.2kV, yielding extra 4.5kW output power. In such a case, the stability of the final stage once again is challenged. It was then decided to make an amplifier test stand to evaluate feasibility of high power tuneable neutralization circuits. In the same time, the test stand can be used to test new tubes before it is mounted on the CRM RF amplifier. The frequency of the test stand was decided as 44.5 MHz, in case the 1:1 scale cooper cavity return earlier, it can be used in the cavity power test for 100MeV cyclotron.

The original amplifier of CRM cyclotron was designed and manufactured by a local Chinese company, having 3 parallel strip lines in anode circuits. To have a different choice and expecting less parasitic in anode circuits, the coaxial structure was selected in the amplifier test stand design. Also, the design of the test stand amplifier takes advantage of modern 3D finite integral simulations. While calculation for the active components (e.g. the final stage tube) follows the traditional analytical way, as will be reported in Section 3 of this paper.

INSATBILITY IN THE RF SYSTEM OF CRM CYCLOTRON

The differences between amplifiers used in broadcasting and cyclotron is that for the latter, the amplifier was operated with a narrow band high Q load through a certain length of transmission line[3,4].

The instability showing up in CRM cyclotron RF system is that when the amplifier operated with a dummy load, there was no evidence of instability even at full power level, which is around 10kW[5]. Once connected through about 6 meters rigid 3-inch line to the cavity, it can be stable in low power level. However, if we try to increase power e.g. to 6kW, the screen current will increase rapidly. When continuing to increase the power, the tuning loop in LLRF control starts to tune the cavity in a wrong direction, which will eventually kill the resonance of the cavity.

To evaluate the situation, a set of differential equation model is developed. Specially, in electrical designs, the equation model is often represented as SPICE models.

SPICE Model of CRM RF System

Though modern 3D finite computation tools has offered an integral environment to interactive with electrical design tools, for simplicity, a cavity model was put forward using parameters identified in real operations. In general, the fundamental resonance of a cyclotron cavity can be represented as parallel RLC circuits. Another approach is to split the cavity into two parts: the Dee plate and the coaxial part.

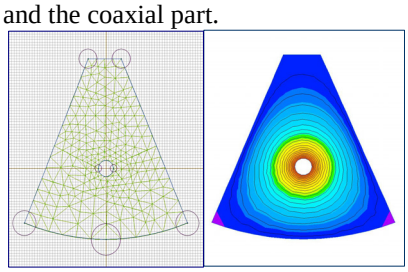

Figure 1: stem impedance calculation

According to the geometry of the cavity[6], in the cavity model, the impedance of two coaxial parts is calculated using analytical equations and 2D Laplace's solver respectively. Then the equivalent components for

the Dee plate are calibrated using measurements results, by means of checking Q value and resonance frequency.

In CRM cavity, the upper part of stem has a triangular shaped outer conductor. The impedance of this part can be evaluated using equ. 1.

$$Z_0 = \frac{1}{cC_{tri}} \qquad (1)$$

Where c is the speed of the light travelling in vacuum, and C_{tri} is the capacitance per unit length of the object, which can be calculated using electrostatic code, as shown in Fig. 1. The impedance for this part is calculated as 133.8ohm, and a cylindrical with outer diameter of 280mm is substituted for this triangular section (e.g. TL3, 4, 6, 7 in Fig. 2a). The other parameters included in the cavity model is taken from measurements and adjusted to have an identical resonance curve shown in Fig. 2 b), e.g. the coupling capacitor is set to 0.92pF, the Dee capacitance and dissipation is set to 30.68pF and 720ohm respectively. The connection bar that connects the two hot arms, was model as a section of transmission line as shown on the right side (TL9) of Fig. 2 a).

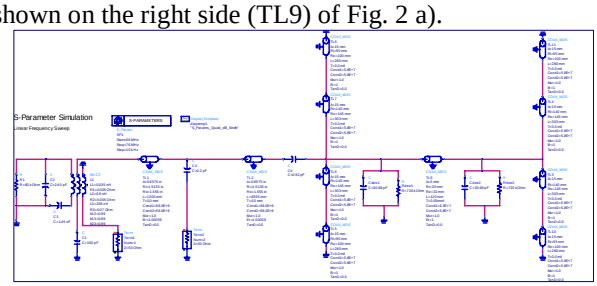

a) SPICE model of CRM RF System

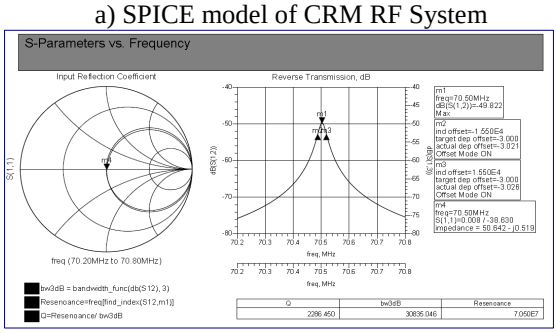

b) S parameter of the cavity model

Figure 2: CRM cyclotron RF system Model

The transmission line modelling takes advantage of TX-Line model in the SPICE software, in which an inner diameter of 1.315 inch and outer diameter of 3.027 inch is specified for 3 inch rigid line. In the middle of the transmission line, a capacitive pickup was connected to the inner conductor, together with a 50 ohm port, as to facilitate the extraction of S parameters.

The equivalent circuits for final stage tube amplifier in cold state includes the dissipation of the anode tank, tube output capacitor, shunt inductor, compensation capacitor etc. as shown on the left side of Fig.2 a). It should be noted that in the model an inductive loop with 50 ohm port was added to give stimulations.

The measurement using network analyser for CRM cyclotron RF system is shown in Fig. 3 b), as predicted using the above SPICE model. On the left hand of Fig. 3 b), about 0.4MHz lower than working resonance,

a) Simulation result (line length turned)

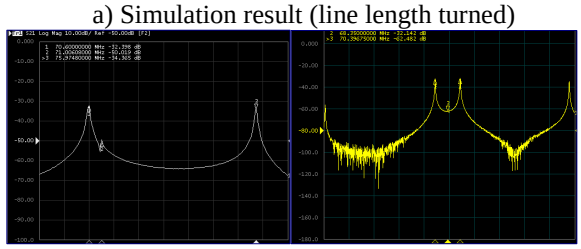

b) before adjusting c) after adjusting

Figure 3: Transmission line length effects on parasitic resonance mode, simulations and measurements

there is a parasitic resonance mode generated by incorrect transmission line length w.r.t. multiple of half wave length. This resonance is determined as the primary source of the CRM RF system instability. Using the SPICE model, the correct transmission line length was easily determined, as shown in Fig.3 a) and the two harmful resonances were turned to be symmetrical w.r.t. the cavity resonance, which in turn is a proof of having right line length.

The S parameter after tuning is shown in Fig. 3 c), from the figures it can be concluded that in frequency 68.35MHz and 72.35MHz, the parasitic resonances still has much higher impedance seen by the anode. Therefore, a hot tuneable neutralization or dumping method should be considered to get the final stage unconditional stable. As the nature of dumping method is to remove part of the output power to a dummy load, considering the CRM cyclotron is still short of power for its 1mA project, the better choice is to have a better neutralization, taking the fact that the amplifier is designed in ground cathode configuration.

AMPLIFER TEST STAND DESIGN

Ground cathode circuits have been adopted to minimize the driven power and to provide a higher gain in the final stage. The tube operating parameters was identified from the 4CX15,000A tube characteristic curves using EMAIC graphic method ”Tube Performance Computer”. A set of input and output RF circuits were designed according to the impedance determined from the working line, in which, a coaxial structure was selected as output due to the reduced chance of producing parasitic resonance for the anode. In order to give an accurate direction of the mechanical design, the finite integral method was selected to calculate the cavity. It is worth noting that, however, in the application of cyclotron RF systems, the tube

amplifier may suffer from the side resonance effect caused by the transmission taped with the high Q load. To achieve higher stability in this case, a high power tuneable neutralization circuit was included, as can be found as C_6 in Fig. 4(the DC equivalent circuits of the amplifier).

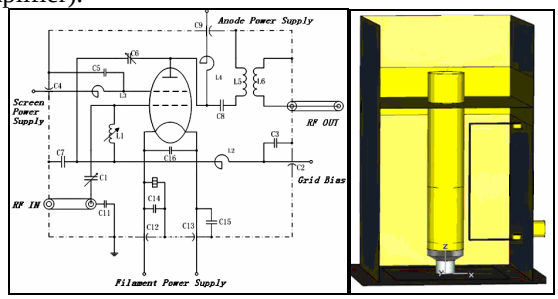

a) DC equivalent circuits b) CST model

Figure 4: DC equivalent circuits and anode circuits

Tube Operating Parameters

The anode DC power supply is designed to give 7.9kV potential, while the grid bias is set to -230V, letting a small DC current flowing through the tube, as a compromise of efficiency and linearity. The residual anode voltage was estimated as 1kV, giving a voltage swing about 6.9kV. These parameters are used to determine the load line in EMAIC tools, yielding the operating parameters, as listed in Tab.1.

Table 1. Calculated parameters for the amplifier

Anode potential	7.9KV
Screen potential	765V
Grid potential	-230V
Anode DC Current	1.7A
Anode RF Current	3.1A
Anode RF resistance	2.13kohm
Output power	10kW
Anode dissipation	3.8kW
Anode efficiency	63%
Gain	33dB

Input, Output and Neutralization Circuits

The output circuit was simulated using CST MWS, in which the output stage of the tube is treated as a vacuum capacitor. Load impedance of 2.13kohm is represented as a discrete component through the geometrical center of the capacitor. The simulation model is shown in Fig. 4 b).

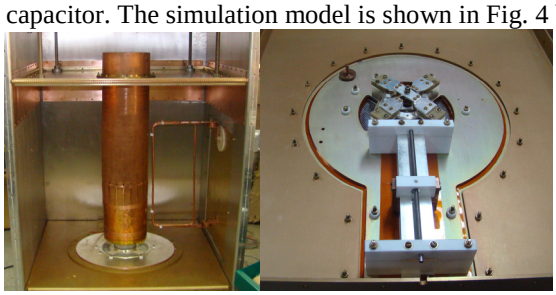

a) Anode tank b) Input and neutralization

Figure 5: Pictures of the amplifier test stand

The input circuits consist of a vacuum coupling capacitor and a strip line inductor. The strip line and the input capacitance of the tube form the resonance, and the coupling capacitor adapts it to 50omh. The neutralization circuits pick up small amount of output power, feedback to the ground side of the strip line. In such a case, the nature of the tube current conduction will ensure the feedback to be a negative one. These two sections are shown in Fig.5.

TEST OF THE AMPLIFIER

Low Level RF Measurements

The low level RF measurements are performed using vector network analyzer. Note that difference still exists between tube cold and hot parameters, the major task for low level measurements is to adjust the input, output and the feedback loop not far from its optimal status. The result of the cold tests with VNA is that, input S11=-52 db@44.5MHz; output S22=-41db@44.5MHz; input output transfer S21=-34.5db @44.5MHz.

High Power Tests

The high power test for the moment is only done with a 20kW dummy load. The 7 hours endurance test shows that the amplifier itself is stable for output 9.2kW fundamental RF power at 44.5MHz. Afterwards, when the driven power increases, it reaches a salutation state as the anode current increase slowly and screen current increases linearly with input power. It is believed the test stand amplifier can give more power once the anode potential is increased.

One of the authors ZhiguoYin would like to thanks Yuri Bylinsky and Joseph Lu from TRIUMF for their enlightening discussions and kind encouragement to build the amplifier test stand.

REFERENCES

[1] Tianjue Zhang, Zhenguo Li, Chengjie Chu, et al., Test Stand Design and Construction for High Intensity Cyclotron Development [J]. CHINESE PHYSICS C. 2008,Vol.32(z1)

[2] Zhiguo Yin, Zhenlu Zhao et.al., High power feedback in the CRM Amplifier, CIAE cyclotron Lab internal note, 2009

[3] R. Hohbach, Investigation on Stabilizing the 92 MHz,150 kW Booster Amplifier, TRIUMF Design Note TRI-DN-95-24, Sept. 94.

[4] Kevin J. Kleman, Improved RF System for Aladdin, PAC93, 17-20 May 1993, Washington, DC. 15th IEEE Particle Accelerator Conference, p.1235

[5] Marek Lipnicki, Investigation of the Radio Frequency System for the 10 MeV Cyclotron, CIAE cyclotron Lab internal Note, 2007

[6] JI Bin, ZHANG Tian-jue, PENG Zhao-hua et. al., Numerical Experiment of RF Performance for 70 MHz Cyclotron Cavity [J]. Atomic Energy Science and Technology.2004, Vol. 38 (2)

CLOSED LOOP RF TUNING FOR SUPERCONDUCITNG CYCLOTRON AT VECC

Aditya Mandal*, S. Som, S.Saha, Saikat Paul, S.Seth, R.K. Bhandari,P.R. Raj,
B.C.Mandal, B.K.Das, U.Panda & RF group
Variable Energy Cyclotron Centre, 1/AF, Bidhannagar, Kolkata-700 064

Abstract

The RF system of Superconducting cyclotron has been operational within 9 - 27 MHz frequency. It has three tunable half-wave coaxial cavities as main resonators and three tunable RF amplifier cavities. A PC-based system takes care of stepper motor driven coarse tuning of cavities with positional accuracy ~20μm and hydraulically driven three couplers and three trimmers. The couplers, in open loop, match the cavity impedance to 50 Ohm in order to feed power from RF amplifier. Trimmers operate in closed loop for fine tuning the cavity, if detuned thermally at high RF power. The control logic has been simulated and finally implemented with Programmable Logic Controller (PLC). Precision control of trimmer (~20μm) is essential to achieve the accelerating (Dee) voltage stability better than 100 ppm. and also minimizing the RF power to maintain it. Phase difference between Dee-in and Dee-pick-off signals and the reflected power signals (from cavity) together act in closed loop for fine tuning of the cavity. The closed loop PID control determines the final positioning of the trimmer in each power level and achieved the required voltage stability.

INTRODUCTION

The RF cavities are consisting of three numbers of half-wave (λ/2) coaxial sections. Three numbers of RF power amplifiers (each 80 kW) are designed to drive power in each of these RF cavities [4]. These RF amplifiers are narrow band and have to be tuned for the user-required frequency. Output section of each RF amplifier has stepper-motor controlled tuneable sliding short plunger movement system. Similar sliding short movement systems are also developed for the tuning of main resonant RF cavities. There are three numbers of amplifier-cavity and six numbers of main resonator cavities, i.e., nine sliding-short movement system has been developed.

RF TUNING

Because of high-Q (quality factor), both RF amplifier-cavities and main resonator cavities are narrow band structure [2]. From cavity simulation results [1] it is found that in case of main resonator cavities, frequency shift produced at the highest frequency (27 MHz) is around 22 kHz/mm and at the lowest frequency (9 MHz) is around 0.4 kHz/mm. Fine frequency tuning requirement for RF amplifier-cavities is less than that of Main resonator cavities as the former has much less loaded Quality factor (Q). The RF power is capacitively coupled to the dee (accelerating electrode) of the main resonant cavity through Coupler (Coupling capacitor). The coupler is used to match the high shunt impedance of the main resonant cavity to the 50 Ohm output impedance of final RF power amplifier [2]. There is a vacuum variable capacitor formed between a insert and DEE (in each main cavity) called "trimmer capacitor". Trimmer capacitor operates in closed loop for the adjustment of a small variation in tuned frequency due to thermal effect and beam loading of the cavity. Coupler can travel 100 mm. maximum and trimmer has a maximum of 20 mm. span of travel [5]. The Coupling capacitor and trimmer capacitor movement is based on hydraulic drive system. This system is responsible for the overall tuning of the system in closed loop [3]. Critical coupling between RF amplifier and RF cavity is achieved by analysing impedance matching and minimising VSWR. It also ensures minimal reflection at coupler port.

When RF power is fed to the cavity, it gets detuned because of thermal instability arising due to RF heating. The effect of the cavity tuning error results in decrease in dee voltages and change in phase. The precise movement of trimmer is necessary to compensate the change in volume of the cavity due to thermal expansion. The accurate position and stability depend on the lowest piston speed determined by minimum flow rate. The typical hydraulic valve has dead band and hysteresis error. The dead zone inevitably brings about steady-state position error, so the dead band is set according to position accuracy. The error due to this ultimately affects the stability of Dee voltage substantially. In addition to this variation in dynamic impedance of the RF cavity, increase the VSWR as well as reflected power which is harmful to the RF amplifier. The problem is further complicated as variation in vacuum level occurs due to variation of rf power inside the cavity.

PID CONTROL OF HYDRAULICALLY DIRVEN COUPLERS AND TRIMMERS

This system consists of a proportional-derivative-integral (PID) controller, hydraulic proportional control valve, position sensor and hydraulic drive system. A PID based feedback loop control system is implemented for the positioning of trimmer and coupler. The block

* E-mail: aditya@vecc.gov.in

diagrams of coupler control loop and trimmer control loop are shown in Fig.1 and Fig.2 respectively.

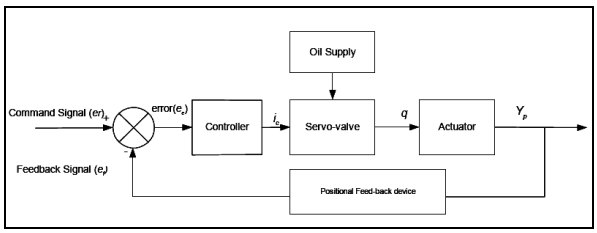

Figure 1: PID loop position control system for coupler

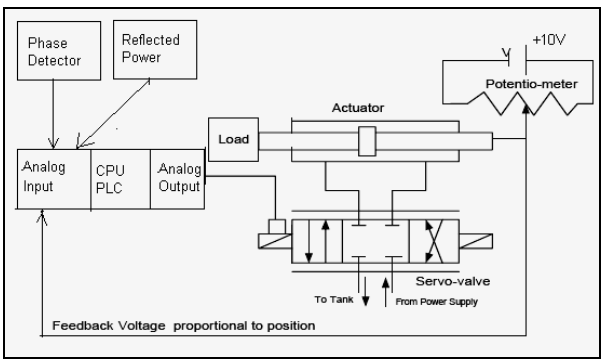

Figure 2: Control system for Trimmer

Under perfectly tuned condition, there will be a phase difference of 90 degree between dee-in pick-up and dee pick-up signal (as shown in Fig.3). A phase detector circuit detects this phase difference and phase error signal drive the trimmer to track the tuning condition of the cavity in closed loop operation. The error amplifier continuously monitors the input reference signal (U_r) and compares it against the actuator position (U_p) measured by a displacement transducer to yield an error signal (U_e).

$$U_e = U_r - U_p$$

The error is manipulated by the servo controller according to a pre-defined control law to generate a command signal (U_v) to drive the hydraulic flow control valve. The processing of the error signal in a controller is a function of the proportional, integral, and derivative gain compensation settings according to the control law.

$$U_o(t) = K_p \cdot U_e(t) + K_i \int U_e(t)dt + K_d \cdot \frac{dU_e(t)}{dt}$$

Where, K_p, K_i, K_d are the PID constants, U_e is the error signal and U_o is the controller output [6].

PHASE DETECTOR

The AD8302 based phase detector measures the relative phase between the Dee-in pick-off signal taken from the input of the coupling capacitor and the Dee pick-off signal from the cavity. The phase detector output signal acts on hydraulic valve which drives the movable plunger tuning into the cavity until there is resonance. Proper tuning is necessary in large dynamic range of the cavity voltages.

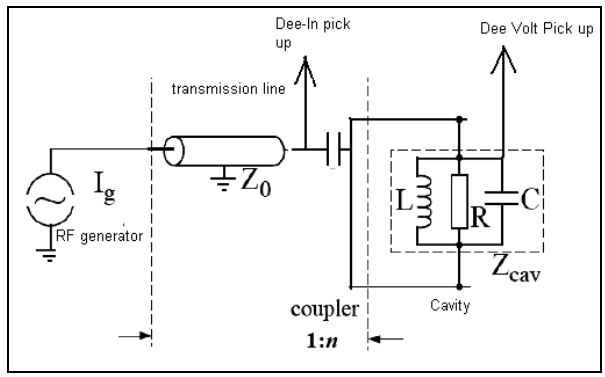

Figure 3: Block diagram of the trimmer control signal

THE EFFECT OF STATIC AND DYNAMIC FRICTION OF HYDRAULIC VALVE AND ACTUATOR

The tight sealing inside the valve and hydraulic cylinders enhances strong dry frictional effect. The static friction inside the valve and actuator possesses complex nonlinear behavior during the onset of the motion. It is modeled as a discontinuous nonlinear mapping between the velocity and static friction. The frictional force depends upon the velocity and direction of velocity. Coulomb and viscous frictional force restricts instantaneous movement of the spool of the valve. This stick-slip motion limits performance at movement accuracy of the valve. The high static friction and dynamic behavior of the frictional force impact significantly on the performance of the valve at low signals, results in chattering in the movement.

As a result of hysteresis, a large error signal is required to overcome the static friction of the valve and therefore the movement of the trimmer capacitor. Again, the large signal causes significant overshoot. Trimmer is unable to take correction at low error signal resulting in increase in reflected power. Detuning will result in the following undesirable effects (as shown in Fig.4).

- Reduce the cavity voltage and shift the cavity phase and so more input power will be needed to maintain the cavity voltage.
- Input phase should be changed to compensate the phase shift.
- High forward power is required to achieve the same dee voltages.
- The modified transmitter power (P) and resulting phase (ψ) are as follows.

$$P = P_0 \cdot \left(1 + \left(\frac{\Delta\omega}{\omega_{1/2}}\right)^2\right); \psi = \tan^{-1}\left(\frac{\Delta\omega}{\omega_{1/2}}\right)$$

Where, $P_0, \Delta\omega, \omega_{1/2}$ are power at tuned condition, change in frequency and half bandwidth of the cavity.

Both Dee voltage stability and relative phase stability between three dees are very important parameters for

beam acceleration. The Dee voltage regulator will maintain the dee voltages and therefore a portion of additional power will reflect back to the generator and increase plate dissipation. This situation lasts until the error is significantly large and valves starts responding to the input.

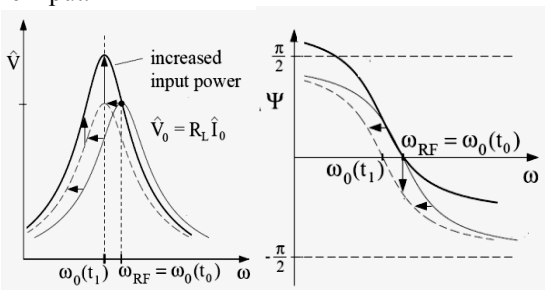

Figure 4: Effects of Detuning a) Increase in Power b) Change in Phase

CLOSED LOOP TRIMMER CONTROL

The closed loop control system is developed with the help of Siemens 315-2DP PLC to control trimmer. A 16 bit (15bit + 1 sign bit) analog input channel is used to sense the position of the trimmer. Linear potentiometer is used to measure the position of the trimmer. The PI controller works in a closed loop to minimise this error signal. The analog output channel is of 12 bit. This phase detector signal acts as an error signal for trimmer movement. It was observed that in case of small error signal, it takes longer time for the correction and some jittering effect in the movement of trimmer occurs due to the nonlinear behaviour of the valve and actuator at low flow condition. The dead-band of the valve causes the hysteresis resulting in variation in the reflected power.

To overcome the problem of jittering effect due to nonlinear behaviour of the valve and actuator at low error signal reflected power is also considered in the closed loop.

The square of the reflected power with suitable scaling factor is multiplied to the phase error. Now the sign of the product determines the direction of the movement and the error is magnified when there is substantial reflected power but the small phase error. Again total error reduced drastically when reflected power is small. It reduces the movement of trimmer when reflected power is small and provides large gain in case high reflected power. It mitigates the problem of nonlinear behaviour of friction and dead band of the valve. Substantial improvement is observed with introduction of this technique in the trimmer control loop and effect of jittering is completely eradicated [7].

INTEGRATED RF TUNING USER INTERFACE:

An integrated operational interface (as shown in Fig.5) is developed for the movement of nine stepper motors (for sliding shorts of three amplifier-cavities and six main resonator cavities), three couplers, three trimmer capacitors and frequency synthesizer. It has a feature to control each of the parameter independently and store in the database. An EPICS based data archiving system is also developed to monitor the effect of movement of trimmer on dee voltage, phase, forward power and reflected power.

Figure 5: User Interface of the RF Tune operation control.

CONCLUSION

The commercially available hydraulic drive based system has its limitation of precise movement at very low flow. Even response of the control system becomes critical for the high precision system. To overcome the effect jittering due to complex friction function inside the valve and actuator limits overall performance. The developed system has been operating satisfactorily round-the-clock with k500 superconducting cyclotron which has been commissioned with internal neon3+ beam in August, 2009.

REFERENCE

[1] S. Som and P.K. Khemka, "RF cavity analysis using PCSUPERFISH Code", IEEE Conf. (MIA-ME, 1997), p.179.

[2] S. Som et. al, "DEVELOPMENT OF 100 KW RF AMPLIFIER FOR SUPERCONDUCTING CYCLOTRON AT VECC".

[3] S. Som et. al, "An overview of the RF system of k500 Superconducting Cyclotron at VECC", InPac-2005, C-139.

[4] S. Som et. al, "DEVELOPMENT OF RF SYSTEM FOR K500 SUPERCONDUCTING CYCLOTRON AT VECC, KOLKATA".

[5] John J Vincent, "Modeling and Analysis of Radio Frequency Structures using an Equivalent Circuit Methodology with Application to Charged Particle Accelerator RF resonators".

[6] Texus Inst Application Report, SPRAA76–January 2005.

[7] S.Som et. al " Commissioning experience of the RF system of K500 Superconducting cyclotron at VECC", International Cyclotron Conference 2010,IMP, China.

DESIGN AND PRIMARY TEST OF FULL SCALE CAVITY OF CYCIAE-100

Bin Ji, Zhiguo Yin, Tianjue Zhang, Jiansheng Xing, Zhenlu Zhao, Jun Lin, Xia Zheng,
Pengzhan Li, Gengshou Liu, Zhenhui Wang,Gaofeng Pan, Suping Zhang,
China Institute of Atomic Energy, Beijing, 101213, P.R. China

Abstract

The engineering of the RF cavity for cyclotron concerns several aspects, including the vacuum, cooling, mechanical support etc. Sometimes it is even more complex than RF design itself. Given the space limit in a compact cyclotron, to have a voltage distribution of 60kV in central orbit and 120kV for outer orbit, a double stem double gap lambda by 2 cavity has been designed for CYCIAE-100[1]. The RF resonance of the cavity is simulated [1] by finite integral codes, while the thermal analysis and mechanical tolerance is studied using other approaches[2-3]. The mechanical design and fabrications is then carried out under these directions, resulting in a full scale testing cavity. The simulations and mechanical design will be reported in this paper, followed with low level measurement results of quality factor, shunt impedance curve along accelerating gap etc. After surface polishing, the measurement yields an unloaded Q value of 9300, which matches well with the simulation with a neglectable difference of several hundreds. The high power test of the cavity and will be presented in a separate paper of this conference.

INTRODUCTION

A 100 MeV H^- compact cyclotron, CYCIAE-100, is under construction at China Institute of Atomic Energy (CIAE). It will provide a 75 MeV~100 MeV, 200μA~500μA proton beam [1-2]. In the compact cyclotron, the two cavities are designed to be placed in the two opposite valleys. The operating frequency is in the range of 43MHz ~45MHz, which will be fixed after the magnet field mapping. The unloaded quality factor Q_0 should be not less than 8000. The Dee voltage distribution along radius of the accelerating gap is designed to be 60kV at the central region and 120 kV at the extraction region.[1]

The resonance of the cavity is simulated and the mechanical design has been done accordingly. A 1:1 scale cavity is fabricated using oxygen-free copper, with cooling pipes on the outer surface of the liner, cooling water grooves in the Dee plates and stems as well. The resonant frequency, matching, shunt impedance, etc. are measured and compared with the design value. The difference between them is small and acceptable.

DESIGN OF THE RF CAVITY

The structure of the RF cavity in CYCIAE-100 is complex and a large number of parameters of the structure need to be adjusted. The resonant frequency and the electromagnetic field have been taken into account in design of the cavity; the distribution of cavity power loss should not be ignored at the same time. The RF resonance of the cavity is simulated by finite integral codes.

The preliminary consideration is to adopt the two stems structure to control the voltage distribution well and adjust the frequency by changing the position and diameter of the stems[1]. The structure of cavity is shown in Figure 1[4]

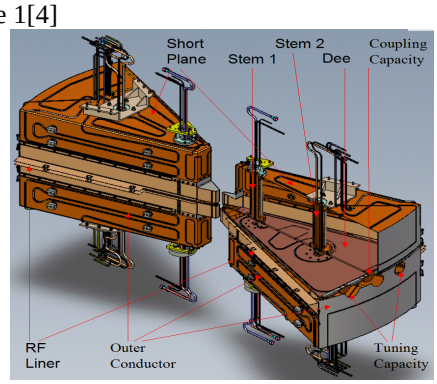

Figure 1: The structure of two stem cavity.

After optimization, the frequency of the cavity simulated to be 44.32MHz, the unloaded Q value is about 10100, Dee-voltage distribution from the center to the extraction area is 60kV to 120kV. The results of the simulation meet the design requirements. The results of the surface current are given by the simulation as well. The power loss distribution of the RF cavity is obvious. The arrangement of the cooling pipes is based on the power loss distribution and the surface current. The E field in the centre plane and the Dee voltage distribution vs. radius are shown in Figure 2.[5] The surface current of the outer conductor and Dee plate are shown in Figure 3.

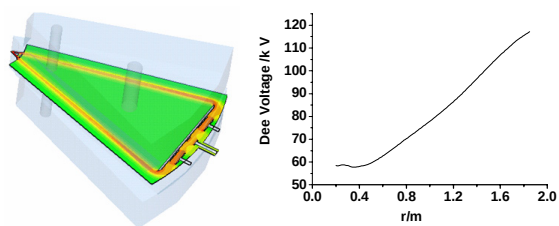

Figure 2: E-Field and the Dee voltage distribution

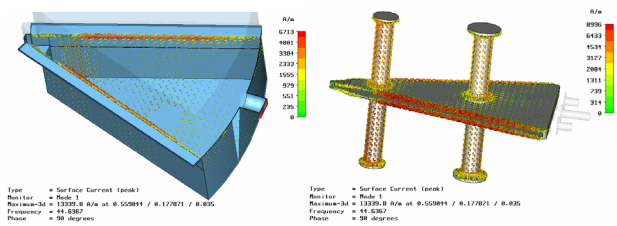

Figure 3: The surface current

Kilpatrick field E_K, as practical indication to breakdown voltages[6], which is known as Kilpatrick limit:

$$f = 1.64 \times E_K^2 \cdot e^{-8.5/E_K} \qquad (1)$$

Here, f is the frequency and E_K is the Kilpatrick electric field in megavolts per metre.

In the simulation of the RF cavity in CYCIAE-100, the maximum electric field is located in the gap between the head of the central region, it's about 9.5MV/m. It is less than the experienced limit.

PRIMARY TEST OF FULL SCALE CAVITY

The mechanical design and fabrications are then carried out after the simulation. Consequently, a full scale cavity model has been successfully manufactured. The mechanical design of the cavity is in accordance with the conditions in CYCIAE-100. The cooling pipes are soldered on the outer surface of the liner. The full scale cavity model is shown in Figure 4.

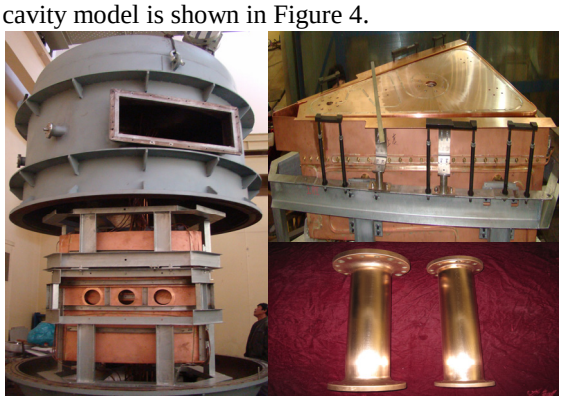

Figure 4: The full scale cavity model

The Test of the Q Value

Thermal deformation and oxidation caused by welding occur on the surface of the outer conductor, and the primary test has been done after simple handling. The unloaded quality factors is measured with the aid of Vector Network Analyser, by connecting two ports to pickups located in upper and lower half cavity. The coupling capacitor is not installed when measuring. The result shows the cavity has a very low Q of 4746, about only half of simulation. The same test is repeated again, after surface polishing according to the surface currents in the simulation and using finger contacts for connections. The new unloaded Q value is ~ 9300, which is 92% of the simulated value, as shown in Figure. 5.

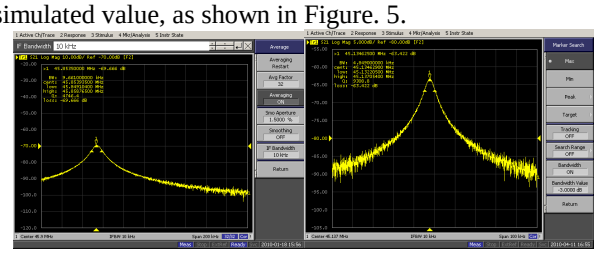

(Without finger contact) (With finger contact)

Figure 5: The unloaded Q value of the cavity

After the test of unloaded Q value, the two tuning capacitors and the coupling capacitor are put on the full scale cavity. The frequency of cavity is adjusted to 44.5MHz and the critical coupling is approached by changing the distance of the capacitance. The cavity is measured with the Network Analyzer, for which two ports are used, i.e. the sampling port on the upper short plate and the port connected with the coupling capacitance. The result from the Network Analyzer is shown in Figure 6.The loaded Q value is ~ 4404 from test and the unloaded Q value of 8808 can be calculated. The calculated unload Q value is closed to the one we get from two sampling ports directly.

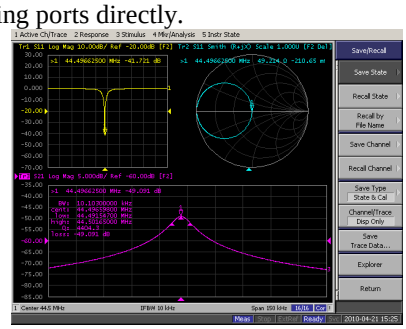

Figure 6: The loaded Q value of the cavity

Shunt Impedance Measurement

Power efficiency of the cavity is usually characterized by a parallel resistance defined as

$$P = \frac{V^2}{2R} \qquad (2)$$

Where, P is the power loss in the cavity to obtain the accelerating voltage, which is identified as V in the formula. The equivalent shunt impedance at the accelerating gap can be evaluated with low level measurements. The principle of the measurement is taking the cavity as a two-port network, and measuring the reversed transmission between the coupling and the gap. Detailed information about the method itself can be found in [7], in which the shunt impedance of the accelerating gap can be calculated from scattering parameter as following,

$$R = \frac{Z_0}{S_{21}^2} \qquad (3)$$

The probe (with 50Ω) is put on one accelerating gap, as stimulating port. The receiving port, port 2, is connected though transmission line to the coupling window. The measuring positions are selected along the gap from the central region to outer orbit, with an interval of 0.2m. The VNA measured S_{21} parameters are recorded for each position, as shown in table 1. The shunt impedance and the accelerating voltage (assuming input power of 33.7kW) across the gap can be obtained accordingly. Note that, the two gaps are specified as Gap A and Gap B, as shown in Figure 7.The comparison of

simulated voltage distribution and measured one is shown in Figure 8.

Table 1: Data of the test

S_{21} /gapA	R / k Ω	Vp / kV	S_{21} /gapB	Rp / k Ω	Vp / kV
-30.3	53.3	60.0	-30.3	53.3	60.0
-30.2	51.9	59.2	-30.2	51.9	59.2
-30.1	51.2	58.8	-30.1	51.4	58.9
-30.9	61.1	64.2	-30.9	61.7	64.5
-31.9	77.1	72.1	-31.9	78.0	72.6
-32.8	94.6	79.9	-32.9	96.8	80.8
-33.7	116.7	88.8	-33.8	119.7	89.9
-34.7	146.9	99.6	-34.8	150.0	100.6
-35.6	179.9	110.2	-35.6	182.4	111.0
-36.2	207.5	118.4	-36.2	209.9	119.0
-36.4	215.8	120.7	-36.4	218.3	121.4

The voltage distribution from the test is similar to the simulation. When the Dee voltage at the center is proportional to 60kV, the power loss of cavity is about 33.7 kW according to the measurement.

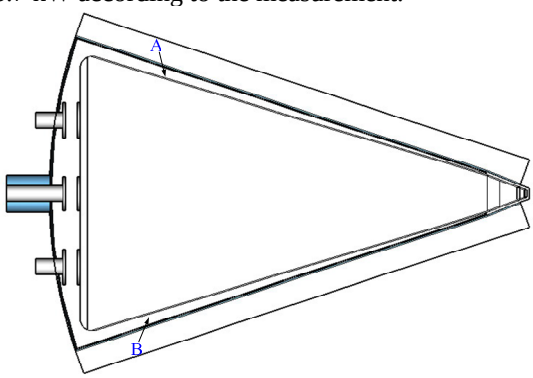

Figure 7: The accelerating gap

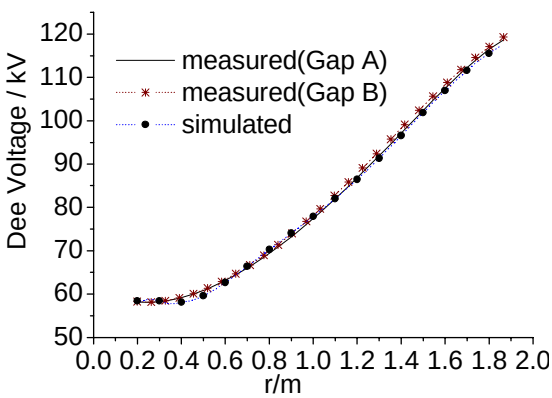

Figure 8: The Dee Voltage of the model cavity vs. the radius

The Test of the Tuning Range

The tuning range of cavity is measured in the test. When the distance between the capacitance plates is 17mm, the resonant frequency is 43MHz, corresponding to 38mm at 45MHz. The tuning rang meets the design requirements. The frequency curve is shown in Figure 9.

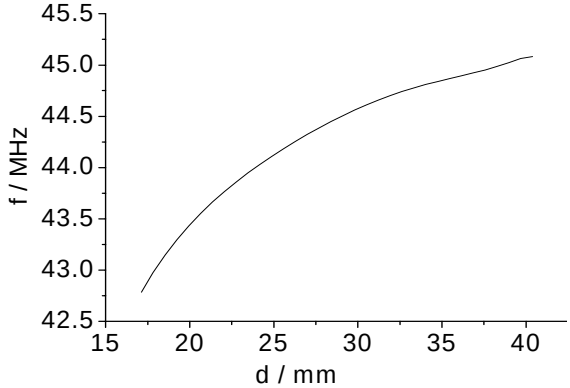

Figure 9: The frequency curve

SUMMARY

Following the simulation by finite integral codes, a full scale RF cavity has been made accordingly, and it is suggested that the test result agrees well with the simulation. Then improvements are made in terms of the design and fabrication technology based on the primary tests conducted on the full scale cavity. The high power test of the cavity will be presented in a separate paper of this conference.

ACKNOWLEDGEMENTS

The authors are very much grateful to a number of scientists from TRIUMF, e.g. Drs. Yuri Bylinsky, Ken Fong, Shuyao Fang and Qiwen Zheng, and those from PSI, e.g. Drs. Peter Sigg, Wolfgang Tron for their helpful discussion, suggestion and comment and very productive visit to the Cyclotron Lab at CIAE for scientific collaboration.

REFERENCES

[1] Tianjue Zhang,et al, 100 MeV H- Cyclotron as an RIB Driving Accelerator, CYC 2004
[2] Yuanjie Bi, et al, THE STUDY ON RF CAVITY TOLERANCE FOR CYCIAE-100, CYC 2007
[3] S.M. Wei, et al,THERMAL ANALYSIS OF RF CAVITY FOR CYCIAE-100, CYC 2007
[4] Tianjue Zhang,,et al, Design and construction progress of BRIF, Chinese Physics C Vol. 34, 2010
[5] Bin Ji, et al, Theoretical and Practical Study on RF Model Cavity of 100MeV H- Cyclotron, Chinese Physics C,2008
[6] Marco DI GIACOMO,RF Systems for Cyclotrons, ECPM 09 Tutorial session
[7] Jozef SURA,Shunt Impedance Measurement , INFN-LNS Report, Catania,1993.

STABLE OPERATION OF RF SYSTEMS FOR RIBF

K. Suda*, M. Fujimaki, N. Fukunishi, M. Hemmi, O. Kamigaito, M. Kase, R. Koyama, K. Kumagai, N. Sakamoto, T. Watanabe, K. Yamada

RIKEN Nishina Center for Accelerator-Based Science, Wako-shi, Saitama 351-0198, Japan

Abstract

At RIKEN RI-Beam Factory (RIBF), very heavy ion beams like uranium are accelerated up to 345 MeV/u by the RIKEN heavy ion linac (RILAC) and four ring cyclotrons, the RIKEN Ring Cyclotron (RRC), the fixed-frequency ring cyclotron (fRC), the intermediate-stage ring cyclotron (IRC), and the superconducting ring cyclotron (SRC) [1]. In order to provide high intensity beams up to 1 pμA, all the RF systems must be stable enough for a long term (a few weeks) within $\pm$ 0.1% in voltages and $\pm$0.1 degrees in phases. For a stable operation of RIBF, we have started to investigate a degree of stability of the RF systems using a newly developed monitoring system [2]. The efforts to improve the stability will be described.

INTRODUCTION

Since the first beam extraction from SRC in December 2006 [3], intense efforts has been made to increase intensities of several heavy ion beams (^{238}U and ^{20}Ca) with an energy of 345 MeV/u. The goal of beam intensity is 1 puA, whereas maximum beam intensity so far achieved is 0.8 pμA for ^{238}U. In order to achieve this goal, the loss of beams during the acceleration must be minimized. One of the most important factor which makes beams unstable is a fluctuation of accelerating RF. All the RF systems must be stable enough for a few weeks (during a period of operations) within $\pm$ 0.1% in voltages and $\pm$0.1 degrees in phases.

RF CONTROL SYSTEM

Injector Linac RILAC

RILAC consists of 6 tanks [4], and used as an injector for the accelerator complex of RIBF. A block diagram of the RF control system is shown in Fig. 1, which is similar as that for SRC [5]. The reference signal from a master oscillator is divided by a power divider, and is delivered to each tank of RILAC. The RF phase and voltage are stabilized by Auto Phase Control (APC) and Auto Gain Control (AGC), respectively. The grid and plate pickup signals are used to tune a resonant frequency of the tanks through Auto Tune Control (ATC). The main parts of the feedback control circuits (AGCs for tank #5 and #6, and all the APCs) are temperature regulated so that the circuits operates stably. These low level circuits for RILAC were designed to have a stability of $\pm$ 0.1% in voltages and $\pm$0.1 degrees in phases, which is the same specification as that for SRC. Four old type AGSs, which were without temperature control, were upgraded to the new type (the same as that used for #5 and #6) by September 2009.

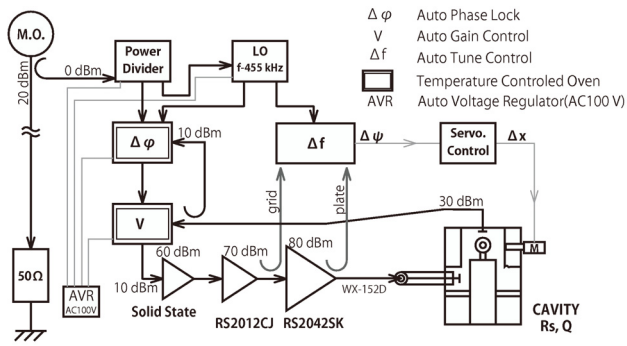

Figure 1: Block diagram of the RF system for RILAC.

Four Cyclotrons, RRC, fRC, IRC, and SRC

In the case of RRC, the low level circuits designed when RRC was constructed (in 1986) had been used until 2008. In order to maintain a relative RF phase between two cavities (#1 and #2), the phase of #1 is locked to the pickup phase of #2. This method was not applied for the other cyclotrons (each cavity is self-locked). It was found that this phase lock system for RRC fails to maintain relative phase in the uranium acceleration (see Fig. 5), which is partly due to a low dee voltage ($\sim$ 70 kV/gap) and low pickup signal. Therefore, all the low level circuits were upgraded to fulfill the stability requirement in September 2008.

The RF control systems for SRC, IRC, and fRC are essentially the same. For details of SRC, refer to Ref. [6].

MONITORING SYSTEM OF RF VOLTAGES AND PHASES

Since several accelerators are used in cascade at RIBF, it is important to maintain the accelerating RF and the matching of beam phases between accelerators. For a stable operation of accelerators in RIBF, a monitoring system using Lock-In-Amplifiers (LIA) SR844 [7] was developed to monitor continuously all the RF voltages and phases as well as the beam intensities and phases [2]. SR844 has a bandwidth of 25 kHz to 200 MHz, which is suitable for the operational RF frequency from 18 to 165 MHz at RIBF. The resolution of LIA was evaluated to be $\pm$ 0.1% in voltage and $\pm$0.03 degrees in phase.

* ksuda@ribf.riken.jp

REFERENCE SIGNAL DISTRIBUTION

Schematic diagram of the reference signal distribution is shown in Fig. 2. The upper panel shows the system used

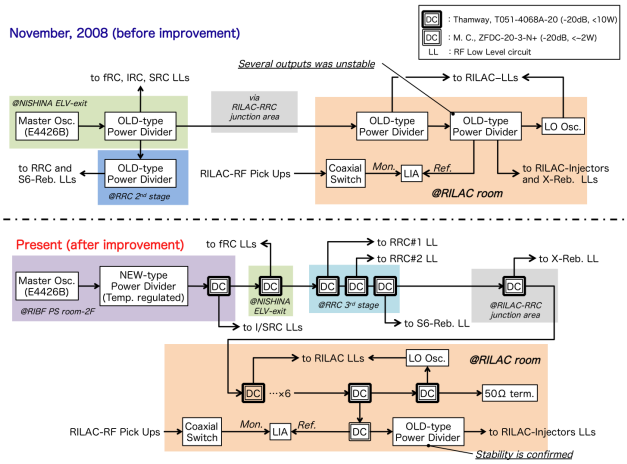

Figure 2: Schematic diagram of reference signal distribution. Upper and lower panel shows the method used in November 2008, and December 2009, respectively.

until 2008. The reference signal from the master oscillator was divided by the power divider and delivered to low level circuits of each accelerator. The master oscillator and the power divider of the first stage was located at where a large change of room temperature occurs ($\sim \pm 2°$C), and the power divider was not temperature regulated. Therefore, the output phases and voltages from power divider fluctuated depending on room temperature. As a consequence, a sudden change of RF phases for fRC was observed during the operation of RIBF on November 2008 [2].

Based on this experience, we have performed several modifications as follows: (a) relocate master oscillator to the room where low level circuits for SRC were placed [5]. The variation in room temperature was typically within $\pm 0.5°$C. (b) a temperature-controlled amplifier was introduced in the same room of (a) so that the reference signal from the master oscillator can be amplified up to 10 W. The output signal is delivered by a single, low-loss coaxial cable shielded by an aluminum pipe, and several single-port directional couplers are used to divide the signal for accelerators.

STABILITY OF RF PICKUP VOLTAGES AND PHASES

In the followings, the stability data for RILAC, RRC, and SRC obtained during uranium acceleration are shown. Figure 3 shows a long-term ($\sim$ 14 h) deviation of RF pickup voltages and phases in six tanks of RILAC observed in July 2008. The voltages for the last two tanks (#5 and #6) were relatively stable within 0.05%, whereas that for the rest tanks deviate more than 0.1%. The newer AGCs for #5 and #6 showed a better stability than others. The

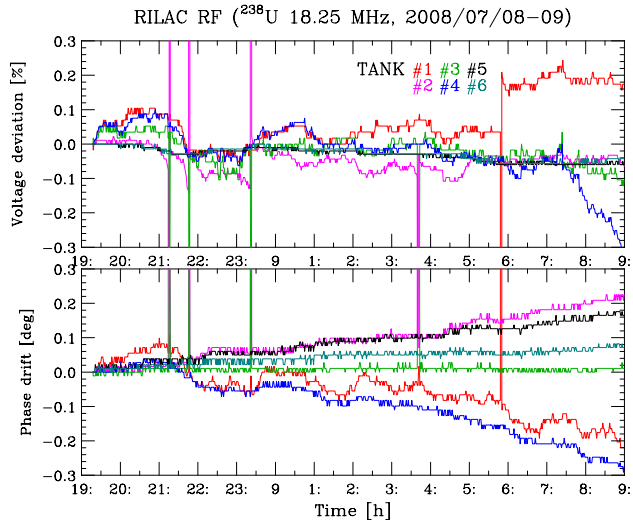

Figure 3: RF voltages and phases for 6 tanks of RILAC observed in July 2008.

phases were nearly monotonically increasing or decreasing. This instability was often observed, and it might be due to the temperature dependence of the power divider used for RILAC. After the modification mentioned above, the RF system of RILAC has been considerably stabilized in November 2009 as shown in Fig. 4. The deviation of

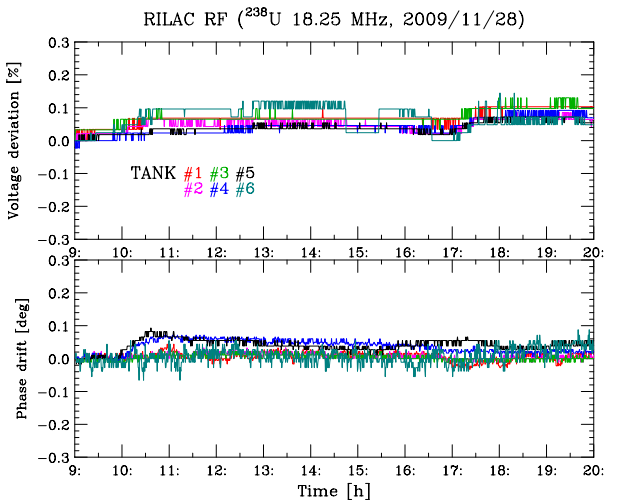

Figure 4: Same as in Fig.3, but observed in November 2009.

RF was within $\pm$ 0.05% in voltages and $\pm$ 0.08 degrees in phases for all tanks.

Figures 5 and 6 compare the data for RRC. Owing to the upgrade of low level circuits, a phase lock of the cavity #1 against #2 was improved, however, the stability became worse ($\pm$ 0.3% in voltage and $\pm$0.4 degrees in phase). The RF deviations of both voltages and phases between two cavities show inverse correlation. The further investigation is required to determine the source of this instability.

Figures 7 and 8 shows the data for SRC, observed in

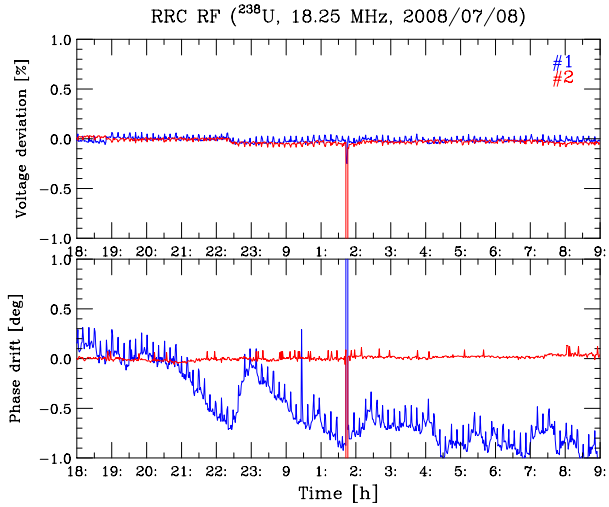

Figure 5: RF voltages and phases for 2 cavities of RRC observed in July 2008.

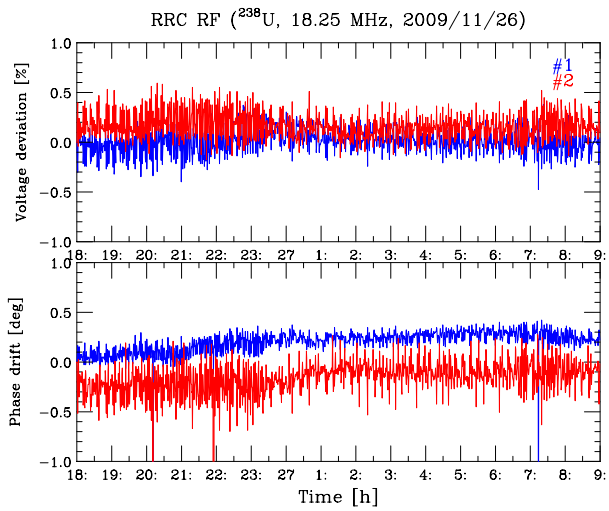

Figure 6: Same as in Fig. 5, but observed in November 2009.

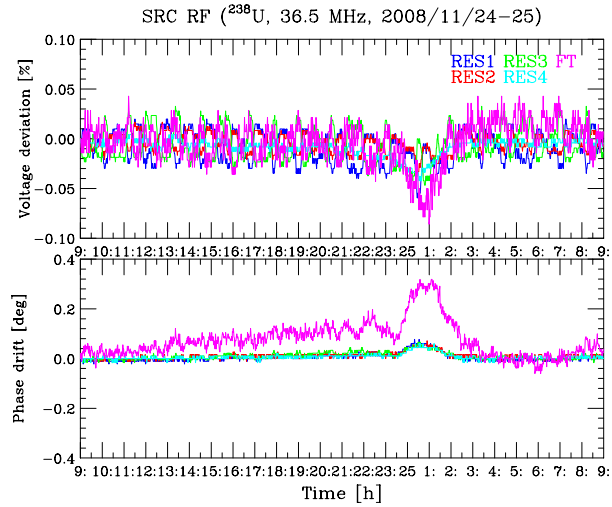

Figure 7: RF voltages and phases for 5 cavities of SRC observed in November 2008.

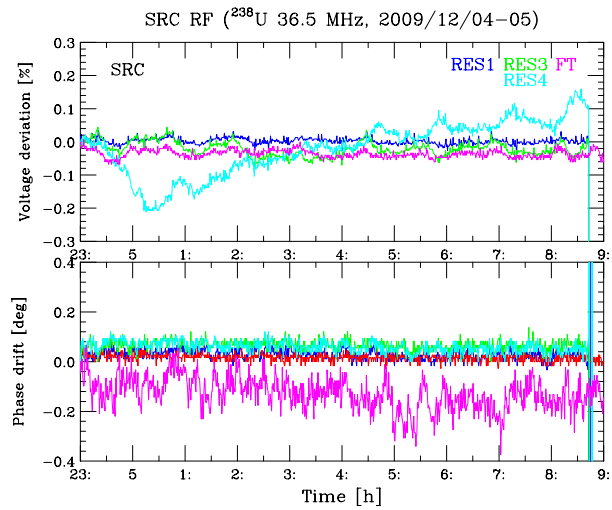

Figure 8: Same as in Fig. 7, but observed in December 2009.

November 2008 and December 2009, respectively. The four main cavities operated at the second harmonic (2f = 36.5 MHz), and one flattop cavity (FT) at the sixth harmonic (6f = 109.5 MHz). In Fig 8, the data for one of the main cavities, RES2 is missing because it was not operational due to a water leak from a tuner panel into vacuum. The instability of the voltage for RES4, and the phase for FT might be attributed to a failure of low level circuits.

PERSPECTIVE

Further modification of the reference signal distribution system is in progress. The local oscillator signal (LO), the 2f, and its LO (2f-LO) signals will be also distributed in the same manner as the reference signal. An eight-port directional coupler was introduced instead of using several single-port ones in series so that the number of connection and return loss are reduced. At first, two units were installed for the reference signal and LO to the low level circuits for SRC.

REFERENCES

[1] O. Kamigaito et al., *this conference*, TUM2CIO01.

[2] R. Koyama et al., EPAC'08, Genoa, Italy, p. 1173 (2008); R. Koyama et al., RIKEN Accel. Prog. Rep 42, p. xviii (2009).

[3] N. Fukunishi et al., PAC'09, Vancouver, M93GRI01 (2009).

[4] M. Odera et al., Nucl. Instrum. Methods A227, p. 187 (1984).

[5] N. Sakamoto et al., HIAT'09, Venezia, p. 85 (2009).

[6] N. Sakamoto et al., *this conference*, WEM2CCO02.

[7] http://www.thinksrs.com/products/SR844.htm, Stanford Research Systems.

DESIGN OF IBA CYCLONE® 30XP CYCLOTRON MAGNET

E. Forton, M. Abs, W. Kleeven, D. Neuveglise, S. Zaremba and B. Nactergal.
Ion Beam Applications s.a., Chemin du Cyclotron 3, Louvain-la-Neuve, Belgium

Abstract

IBA is currently developing an evolution of its famous Cyclone® 30 cyclotron. The Cyclone® 30XP cyclotron will be a multi-particle, multiport cyclotron capable of accelerating alpha particles up to 30 MeV (electrostatic extraction), deuteron (D^-) beams between 7.5 and 15 MeV and proton (H^-) beams between 15 and 30 MeV (stripping extraction). The magnet system has been updated with improved versions of IBA Cyclone 18/9 and Cyclone 70 features.

At first, coil dimensions have been updated in order to raise the free space in the median plane to allow mounting a retractable electrostatic deflector system for the extraction of the alpha particle beam. Gradient corrector pole extensions, have been added to ease the alpha beam extraction. Finally, compensation for relativistic effects between H^- (q/m=1/1) and D^-/alpha (q/m=1/2) beams is made by the use of movable iron inserts located in two valleys, as is done in IBA Cyclone® 18/9 cyclotrons.

These modifications could have an adverse effect on the flutter. In addition, the second harmonic induced by the movable iron inserts drives the machine in the $2.\nu_r=2$ resonance close to the extraction. As a consequence, modifications on the pole sectors and chamfers have been made in order to improve the flutter and eliminate harmful resonance up to extracted energies.

After the presentation of the magnet features, some results on beam extraction are also discussed.

INTRODUCTION

IBA, with more than 20 years of experience in building commercial cyclotrons is developing a new version of its first accelerator: the Cyclone® 30XP.

The Cyclone® 30XP will be able to accelerate beams of H^- ions up to 30 MeV, D^- up to 15 MeV and $^4He^{++}$ (α) to 30 MeV. At first glance, it is an extension of the Cyclone® 30 with Cyclone® 18/9 and Cyclone® 70 magnet features [1,2], but a closer look shows it is a bit more complex.

MAGNET FEATURES

As the α-beam will be extracted by means of an electrostatic deflector, the first modification with respect to classical Cyclone 30 was to reduce the height of the coils in order to allow for deflector and deflector movement mechanisms installation.

Then, movable iron inserts have been installed in two valleys out of four to compensate the differential relativistic mass increase between H^- and D^-/α.

Finally, gradient correcting pole-extension have been added in order to ease the extraction of α beam. Such pole extensions are installed on the IBA Cyclone® 70.

Figure 1 shows a schematic of the preliminary design with the added features.

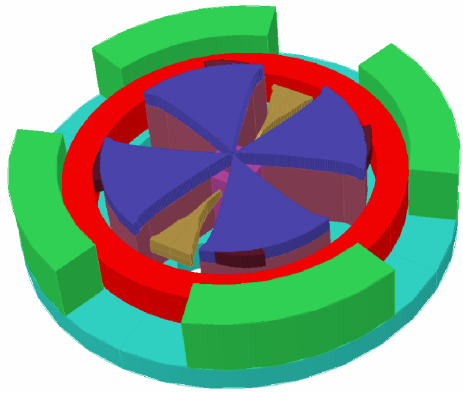

Figure 1: Early structure of the Cyclone® 30XP magnet. One can see the coils (red), poles (in purple), sectors (underneath the poles), movable iron inserts (light brown) and pole extensions (dark purple).

POTENTIALLY HARMFUL RESONANCES

Both the movable iron inserts and the pole extensions have a negative impact on the cyclotron beam optics.

Indeed, the magnetic field change obtained by the movable inserts is as high as 200 Gauss (Figure 2). This implies that the second harmonic of the field changes by the same amount. In addition, the flutter is also reduced when the magnet is in H^- configuration.

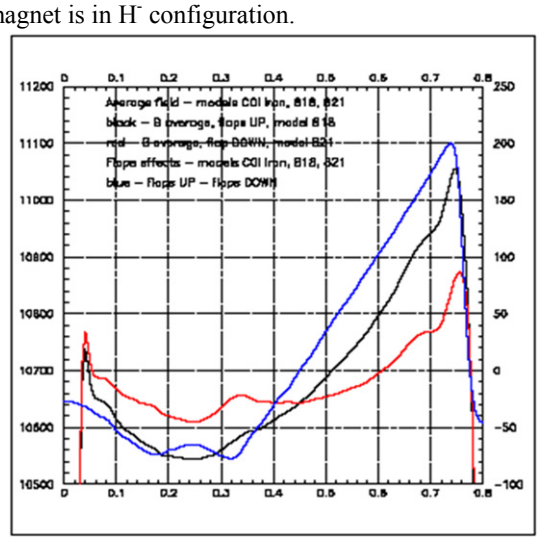

Figure 2: Average field with flaps up (black), down (red) and net effect of the flaps (blue, right scale).

The pole extensions further reduce the flutter by diverting part of the pole's magnetic flux. One can choose to have one, two or four pole extensions, trying to find a compromise between minimal field reduction or minimal impact on first and second harmonics.

Out first Cyclone® 30XP model had two movable iron inserts and four-fold symmetric poles and pole extensions. After isochronisation for the various particles, it has been found that the betatron oscillations of the H^- beam locked on the $2Q_r=2$ resonance. This effect is shown on Figure 3 and 4 and needs to be corrected to avoid high beam losses and high energy spread of the extracted beam.

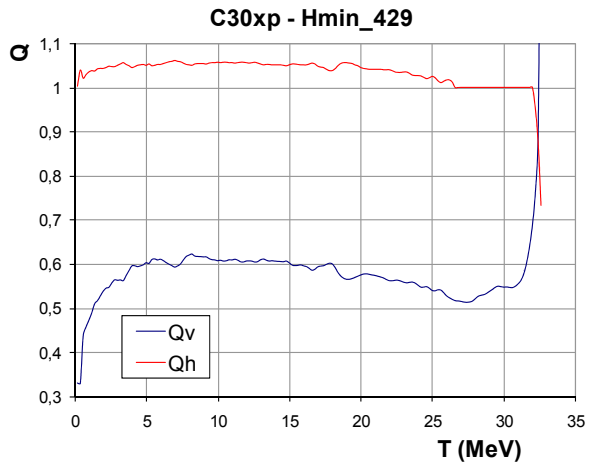

Figure 3: Locking on the 2Qr=2 resonance for H- on early Cyclone 30xp models (flat plateau on the red curve).

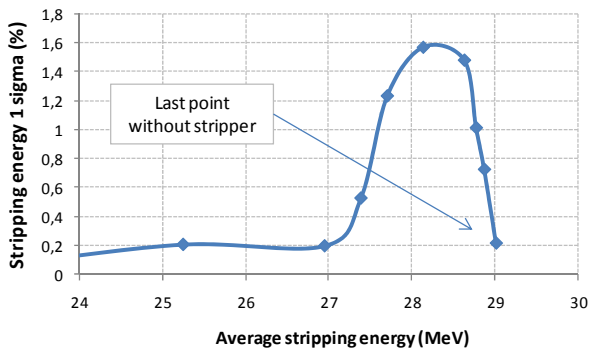

Figure 4: Effect of the 2Qr=2 resonance on the H- beam.

INCREASING THE FLUTTER AND AVOIDING HARMONICS

The flutter has been increased by reducing the azimuthal extension of the poles. This implies an increase in the number of ampere-turns in the Cyclone® 30XP with respect to the classical Cyclone® 30. This increase has been limited by keeping the sectors as they were and chamfering the pole outer radius (Fig. 5). It has also been decided to have only two pole extensions to limit their impact on the flutter.

To avoid resonance problems, the first and second harmonic imperfections from the magnetic field are corrected by an iterative process. This procedure has already been used during the development of IBA's Cyclone® 14 cyclotron [3].

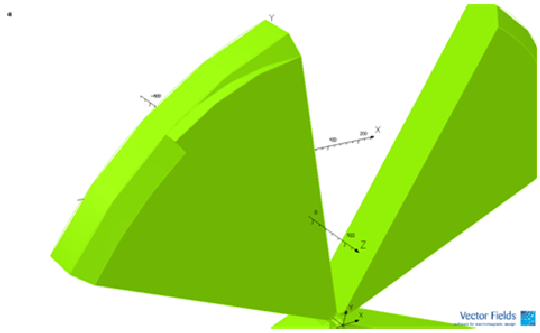

Figure 5: Chamfers on the outer radius of the pole.

Correction of the first harmonic requires the milling of δ_1 and δ_2 corrections, computed as:

$$\delta_1 = \left(\frac{\sin(\alpha_2-\varphi_1)}{\sin(\alpha_2-\alpha_1)}\right)\cdot\frac{\pi H_1}{B_h-B_v}$$

$$\delta_2 = \left(\frac{\sin(\varphi_1-\alpha_1)}{\sin(\alpha_2-\alpha_1)}\right)\cdot\frac{\pi H_1}{B_h-B_v}$$

Where: H_1 - amplitude of the first harmonic imper-fection error; φ_1 - azimuth or phase angle of the first harmonic imperfection error; α_1 and α_2 - azimuthal positions of two pole edges closest and around the azimuth of the first harmonic φ_1; B_h and B_v - the magnetic field in the hills and in the valleys of the cyclotron.

These equations assume a hard edge approximation of the magnetic field and the corrections should be applied on the two pole edges located around the azimuth of the first harmonic.

For the second harmonic, similar equations are used, but the milling of $\delta_1(\alpha_1)$ and $\delta_2(\alpha_2)$ should be applied on the four pole edges located close and around the phase of the second harmonic and on the opposite pole $\delta_1(\alpha_1+180^\circ)$ and $\delta_2(\alpha_2+180^\circ)$:

$$\delta_1(\alpha_1)=\delta_1(\alpha_1+180^\circ)=\left(\frac{\sin 2(\alpha_2-\varphi_2)}{\sin 2(\alpha_2-\alpha_1)}\right)\cdot\frac{\pi}{2}\cdot\frac{H_2}{B_h-B_v}$$

$$\delta_2(\alpha_2)=\delta_2(\alpha_2+180^\circ)=\left(\frac{\sin 2(\varphi_2-\alpha_1)}{\sin 2(\alpha_2-\alpha_1)}\right)\cdot\frac{\pi}{2}\cdot\frac{H_2}{B_h-B_v}$$

Applying this method at each radius for both the first and second harmonics significantly reduced the level of harmful harmonics. For instance, the second harmonic generated by the flaps can be reduced down to less than 10 Gauss for a given particle species. With such method, resonances can be pushed towards higher radii: energies of 31.2 MeV and 31 MeV are obtained for α and H^- acceleration, respectively, before the resonance appears.

EXTRACTION

Extraction studies for each beam of the Cyclone® 30XP are part of the magnetic design as they can affect the field harmonics and have a significant impact on the machine design.

The position of the stripper mechanisms have been determined by tracking H^- and D^- particles in the isochronous field. Particles are started on the equilibrium orbit. It has been found that the existing Cyclone 30 yoke allowed for the extraction towards the "internal" switching magnet (right part of Figure 6), but that it had to be modified for extraction to an "external" switching magnet in order to allow for vacuum chamber installation.

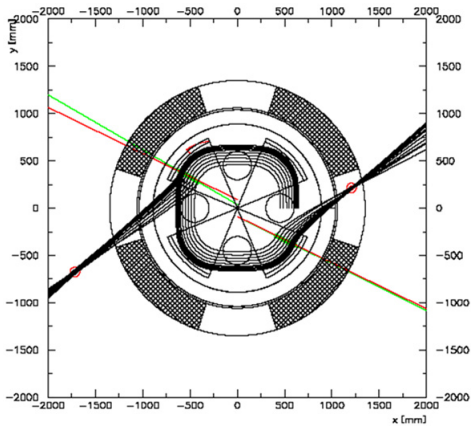

Figure 6: Equilibrium orbits and extracted trajectories for H- and protons respectively.

The position, length and shape of the electrostatic deflector have also been optimized by particle tracking. It has been found that, despite pole extensions, smooth extraction of the α-beam requires strong focusing before exiting the cyclotron yoke. A permanent magnet quadrupole doublet has been designed for this purpose. Figure 7 shows the position of that quadrupole doublet and the extracted α-beam.

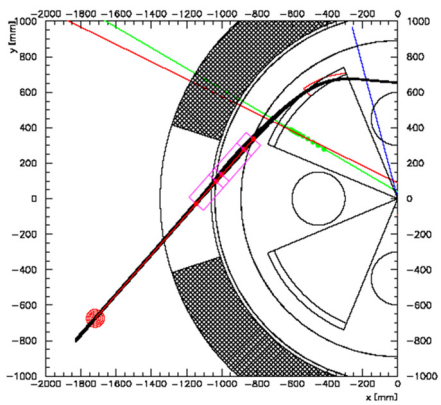

Figure 7: Trajectories for extracted alpha beam.

FINAL DESIGN AND CONCLUSIONS

The modification of the Cyclone 30 towards the Cyclone® 30XP was not as straightforward as was expected but thanks to previous experience with IBA's Cyclone® 30 and 70, important pitfalls have indeed been detected early in the design process. Several modifications have been made to the first design, leading to the geometry pictured below.

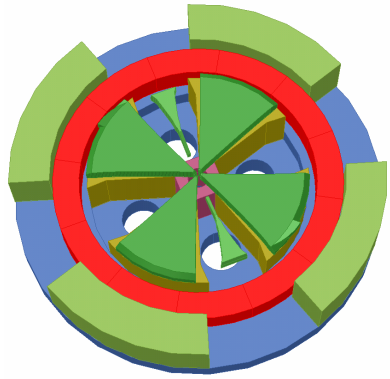

Figure 8: Final Cyclone® 30XP model.

REFERENCES

[1] Y. Jongen et al., "IBA C70 cyclotron development", proc. of the 18th international conference on cyclotrons and their applications, pp 54-56, 2007.

[2] S. Zaremba et al., "Magnetic field design and calculations for the IBA C70 cyclotron", proc. of the 18th international conference on cyclotrons and their applications, pp 75-77, 2007.

[3] W. Kleeven et al., "The self-extracting cyclotron", proc. of the 16th international conference on cyclotrons and their applications, pp 69-73, 2001.

DESIGN OF IBA CYCLONE®11 CYCLOTRON MAGNET

V. Nuttens,# M. Abs, W. Kleeven, B. Nactergal, D. Neuveglise, T. Servais, and S. Zaremba
Ion Beam Applications s.a., Chemin du cyclotron, 3, B-1348 Louvain-la-Neuve, Belgium

Abstract

The development of a new Cyclone®11 11MeV H- cyclotron is in progress at IBA. Such machine is designed for the production of radionuclides for nuclear medicine. This cyclotron is based on the existing Cyclone®10 that has been boosted to more than 11 MeV with as minor as possible change to the Cyclone®10 geometry. At first, the magnetic field has been raised by a small reduction of the valley depth. Additionally, the main coil current has been increased. Pole edge milling has been used to obtain the isochronous magnetic field shape. Beam optics in the magnet is excellent. Extraction is ensured by means of stripper foils mounted on carousels located at different azimuths allowing installation up to eight targets and dual beam extraction.

INTRODUCTION

To extend customer choice in the low energy range, IBA is developing the Cyclone®11. It is a fixed energy 11 MeV H- cyclotron for the production of PET isotopes. The cyclotron magnet is based on the well known Cyclone®10/5 [1,2] with the same yoke dimensions, which is compatible with the IBA self-shielding design [3]. The higher proton energy compared to the 10 MeV machine is beneficial for higher PET isotope production yield.

CYCLOTRON MODEL

The 3D model of the Cyclone®11 cyclotron is based on the Cyclone®10/5 geometry and is shown in figure 1. The movable inserts have been removed and the isochronous magnetic field is obtained by milling one pole edge on each pole. The 90° symmetry has been used for the magnetic field study and 180° symmetry for the extraction study.

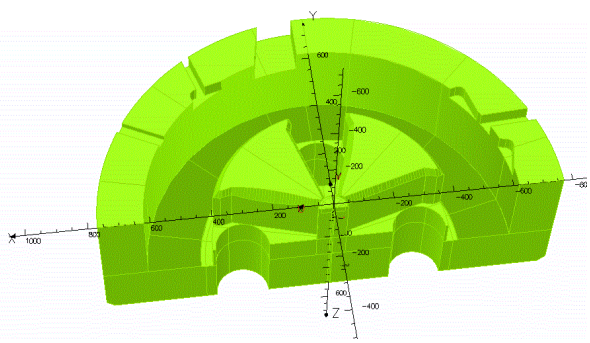

Figure 1: Opera-3D 180° symmetry model of the Cyclone®11 cyclotron.

#vincent.nuttens@iba-group.com

MAGNETIC FIELD REQUIREMENTS

The magnetic rigidity is proportional to the particle momentum. Therefore, the energy that can be extracted at a given radius in a cyclotron is proportional to the square of the magnetic field. Hence, the relative increase of energy ΔE/E is

$$\Delta E/E = 2\Delta p/p = 2\Delta B/B \qquad (1)$$

According to the Cyclone®10/5 mapping results, the magnetic field should be increased by at least 520 Gauss to be able to extract H- at 11.0 MeV instead of 10.2 MeV. The magnetic field increase can be provided by a higher main coil current and/or a reduced valley depth. The magnetic field study has been performed using the TOSCA magnetostatic solver of Opera-3D.

Effect of the Main Coil Current

To increase the average magnetic field, the current in the main coil can be increased. The 90° symmetry model without addition of iron in valleys has been simulated for different main coil currents (176 A, 186 A, 196 A). The resulting increase in the magnetic field is shown in figure 2. The average magnetic field gain at the level of the poles is about 160 Gauss per 10 A. The study has also shown that the quality of the iron has very little effect on the field gain.

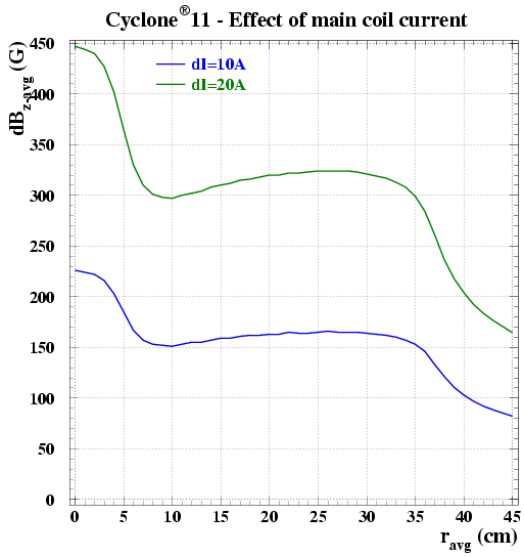

Figure 2: Magnetic field increase as a function of radius for different main coil current increase. The reference map (dI=0 is at IMC=176 A).

Effect of the Valley Depth

A second solution to raise the average magnetic field is to increase the field in the valleys. For that purpose, the valley depth has to be decreased and the effect on the flutter has to be checked. The 90° symmetry model has been simulated for different valley depth with a main coil current of 186 A. dD=0 mm is the Cyclone®10/5 valley depth, dD=-50 mm corresponds to a valley filled with 50 mm of iron and dD=-100 mm a valley filled with 100 mm of iron. The effect of the valley depth on the magnetic field is shown in figure 3. The average magnetic field gain at the level of the poles is about 180 Gauss with 50 mm of iron and 450 Gauss with 100 mm of iron. The effect on the flutter is less than 5% and do not affect the beam stability.

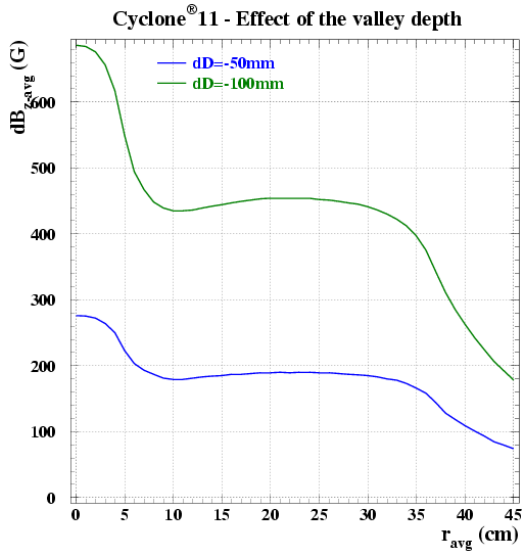

Figure 3: Magnetic field increase as a function of radius for different thicknesses of additional iron.

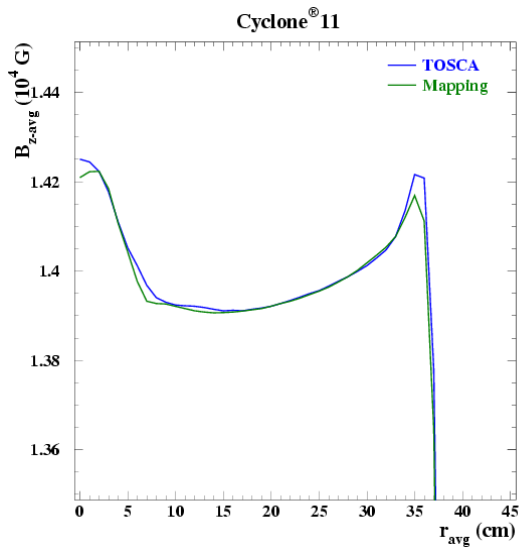

Figure 4: Comparison of the experimental magnetic field profile with the results of the TOSCA analysis.

Adopted Solution

Compared to the Cyclone®10, increasing the main coil current by 15 A and filling the valleys with 100mm of iron should provide an increase in the average magnetic field of about 690 Gauss which roughly correspond to an extracted energy of about 11.3 MeV. Both modifications were applied for the new cyclotron. The magnet has been made and has already been mapped. The TOSCA magnetic field at 185 A with the valley filled with 100 mm of iron is compared to the isochronous experimental map of Cyclone®11 on figure 4. The agreement is very good.

ISOCHRONISM

Isochronism of the cyclotron is obtained by milling one edge per pole. The BH curve used for the TOSCA analysis is directly provided by the iron supplier. It can be seen on figure 5 that the magnetic fields are isochronous with the (second harmonic mode) RF frequency of 42.877 MHz. The vertical and horizontal betatron frequencies are plotted on figure 6.

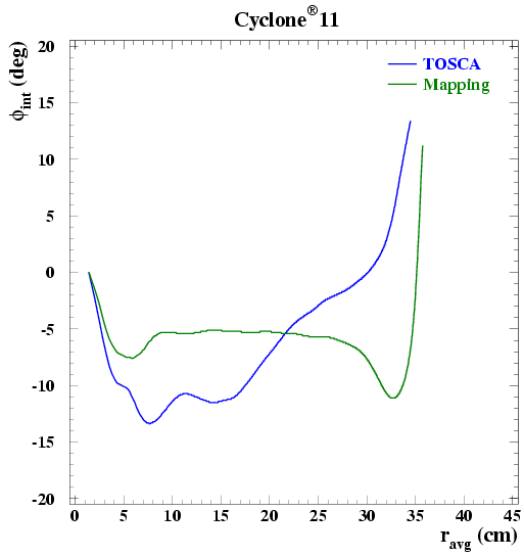

Figure 5: Experimental and simulated integrated phase shifts for the Cyclone®11.

EXTRACTION

Proton extraction is performed by stripper foils mounted on a carrousel (figure 7) with the same design as the Cyclone®18/9 carrousel with a fork length of only 25 mm. The fork length is 5 mm shorter than the one of the Cyclone®10 which allows for extraction of higher energy orbits. Each carrousel can accommodate two stripper foils to reduce the number of cyclotron openings. There are eight carrousels located at eight different azimuths.

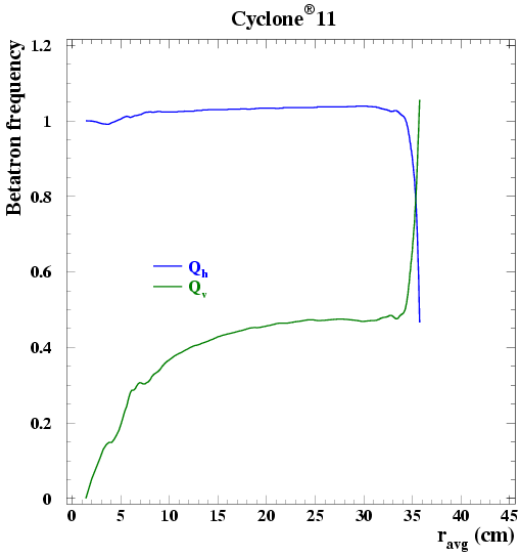

Figure 6: Horizontal and vertical betatron oscillation frequencies as a function of average orbit radius for the experimental map of the Cyclone®11.

The extraction study has been performed on the two first ports, the other being symmetric. As the experimental magnetic field measurement can be performed only up to a radius of 45cm, we extend the experimental map with the TOSCA map for radii from 46cm to 100cm. The particles are tracked in that map for different energies. It has been found that with the Cyclone®11 extraction system, the extracted beam has an energy of 11.5MeV (figure 8). Note that compared to the Cyclone®10/5, the position and direction of the exit ports in the vacuum chamber have been adapted to the new extracted orbits.

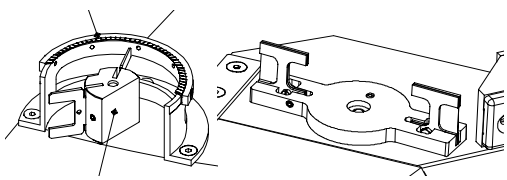

Figure 7: Carrousel for extraction: Cyclone®10/5 design (left); Cyclone®18/9 design used for Cyclone®11 (right).

PRESENT STATUS

The iterative procedure to obtain the isochronous magnetic field in Cyclone®11 was successfully finished in the mechanical workshop of IBA subcontractor. The installation of other subsystems of the cyclotron in the assembly hall of IBA is nearly completed and initial beam tests will follow.

CONCLUSIONS

Calculation results of the Cyclone®11 are in very good agreement with the experimental data. Compared to the Cyclone®10 (with movable inserts removed), increasing the current up to 185 A and filling the valley with 10 cm of iron allows to increase the energy above 11 MeV.

The experimental map of magnetic field shows that we manage to get the Cyclone®11 isochronous and the extracted energy can be expected to be close to 11.5 MeV.

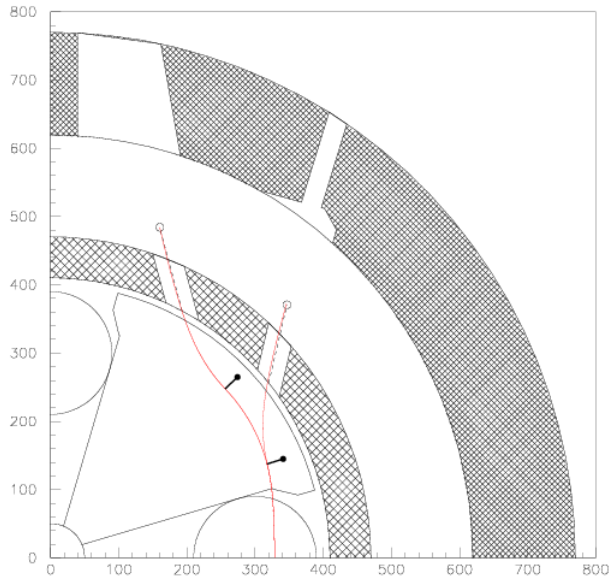

Figure 8: Particle track at the extraction in the experimental map of the Cyclone®11.

REFERENCES

[1] S. Zaremba et al. – Beam Dynamics in Newly Designed Cyclotrons at Ion Beam Applications; Proceedings EPAC 1990, p. 1774-1776.
[2] M. Abs et al. – RF Systems Developed for CYCLONE 3D and CYCLONE 10/5; Proceedings EPAC 1990, p. 967-969.
[3] F. Stichelbaut - Design of the Cyclone®11 Self-Shielding; IBA internal report.

VACUUM SYSTEM OF HIRFL'S CYCLOTRONS

X.T. Yang#, J.H.Zhang, Z.M.You, J.Meng and Vacuum group of IMP
Institute of Modern Physics, Chinese Academy of Sciences, Lanzhou 730000, P.R.China

Abstract

HIRFL has 2 cyclotrons: a sector focus cyclotron (SFC) and a separate sector cyclotron (SSC). SFC was built in 1957. In the past 50 years, the vacuum system of SFC has been upgraded for three times. The vacuum chamber was redesigned to double-deck at the third upgrade. The working pressure in beam chamber was improved from 10^{-6}mbar to 10^{-8}mbar. SFC has delivered Pb, Bi and U beams in the past few years since the last upgrading of its vacuum chamber. SSC began to operate in 1987. The vacuum chamber of SSC has a volume of 100m^3. 8 cryopumps keep the pressure from 5×10^{-7}mbar to 8×10^{-8}mbar depending on the used pump numbers (2~8). In the past 20 years, because of the contamination of oil vapour and leaks occurred in some components inside the SSC vacuum chamber, the vacuum condition has worsened than the beginning. It is a big problem to accelerate the heavier ions. The upgrade for the SSC vacuum system will be an urgent task for us. The rough pumping systems of both SFC and SSC have been rebuilt recently. As a result, the oil vapour in two cyclotrons will be eliminated and the vacuum condition of them will be improved.

A new small cyclotron will be built in HIRFL as an injector of the Heavy Ion Therapy Facility in Lanzhou (HITFiL). The brief introduction of the vacuum system design is given in the paper.

VACUUM SYSTEM OF SFC

SFC with the energy constant of 69 is the injector of SSC and HIRFL-CSR [1]. It was built in 1957. In the past 50 years, the vacuum system of SFC has been upgraded for three times. The working pressure was improved from 10^{-6}mbar to 10^{-8}mbar. At the third time, the vacuum chamber was redesigned to double-deck [2] (Fig.1). All components with large gas load such as magnet cores, coils and hundreds of electric wires were put into the insulation chamber where the pressure is 10^{-1}mbar pumped by a mechanical pump. Consequently, a pressure of 10^{-8}mbar can be obtained in the beam chamber by 2 cryopumps with a total pumping speed of 40000 l/s. Because the beam chamber was made of thin copper with a thickness of 4mm, the safety valves both in mechanical mode and electrical mode were installed between the two chambers, which are interlocked with the pressure sensors to protect the copper chamber from the damage.

After this upgrade of the vacuum system, 1.1 MeV/u $^{208}Pb^{27+}$ beam was accelerated to confirm the vacuum effect, which turned out that the upgrade of the SFC vacuum chamber was successful. SFC has delivered $^{208}Pb^{27+}$, $^{209}Bi^{31+}$, $^{238}U^{26+}$ beams in the past few years since the last upgrade of the SFC vacuum chamber. So, the heavy ions from C to U can be accelerated in SFC.

Figure 1: SFC double-deck vacuum chamber

VACUUM SYSTEM OF SSC

SSC with the energy constant of 450 began to operate in 1987. It provides beams to about 10 experimental terminals and is also the injector of the cooling storage ring (HIRFL-CSR). The vacuum chamber of SSC (Fig.2), which was made of 316L stainless steel with a permeability of 1.01, has a volume of 100m^3. The magnet cores, RF cavities, injection and extraction components were inside the vacuum chamber with a large gas load. 8 cryopumps with a pumping speed of 20000 l/s for each were installed in the chamber. Depending on the accelerated heavy ion species, 2~8 pumps were used to keep the pressure from 5×10^{-7}mbar to 8×10^{-8}mbar.

SSC has operated for more than 20 years. Because of the contamination of oil vapour and leaks occurred in some components inside the SSC vacuum chamber, which were very difficult to eliminate, at present the pressures in four vacuum gauges which were installed in different positions were $2\sim4\times10^{-7}$mbar with 6 cryopumps operating. It was a big problem to accelerate the heavier ions although the $^{209}Bi^{31+}$ beam was delivered recently. The upgrade for the SSC vacuum system will be an urgent task for us. In order to improve the vacuum condition, one measure is to change the old pumps which have exceeded the time limit by new ones; second measure is to try to reduce the system leaks and the third one is to eliminate the oil vapour contamination.

yangxt@impcas.ac.cn

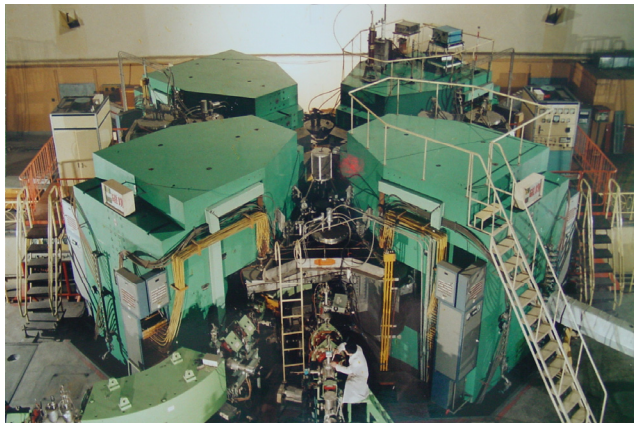

Figure 2: SSC (vacuum chamber is between the magnets)

ROUGH PUMPING SYSTEM UPGRADE

The oil mechanical pumps which cause the serious contamination to the vacuum chambers were used for the rough pumping systems of SFC and SSC for many years. In August, 2010, during the accelerators shutdown period, the rough pumping systems were rebuilt. The oil pump units were changed by large dry mechanical pumps with a pumping speed of 630m^3/h and 250m^3/h for SSC and SFC respectively (Fig.3). As a result, the oil vapour in two cyclotrons will be eliminated and the vacuum condition of them will be improved.

Figure 3: The new rough pumping stations of SSC and SFC

VACUUM SYSTEM OF 7MEV/U CYCLOTRON

The small cyclotron with the energy of 7 MeV/u is the injector of the Heavy Ion Therapy Facility in Lanzhou (HITFiL). The new project is under construction. The vacuum chamber of the cyclotron which is made of stainless steel has a dimension of ϕ1720mm ×760mm (D×H). The magnet yokes are used for the cover plates of the chamber. Same as SSC, the RF cavities, magnet cores, injection and extraction elements are designed inside the vacuum chamber. Since rusty surface will induce the significant increase of the gas load, the magnet cores made of DT4 material will be coated with TiN film to avoid getting rusty.

The vacuum equipment layout of the cyclotron is shown in Fig.4. The total gas load of the vacuum system is about 4×10^{-3}mbar.l/s. In order to obtain the working pressure of 5×10^{-7}mbar, the effective pumping speed for center plane of the machine has to be larger than 8000 l/s. Because of the limited room, 4 cryopumps with a pumping speed of 5000 l/s for each can only be installed in the upper and lower planes of the magnet yokes, where there are 4 holes with a diameter of 350mm and a length of 580mm. The pump-down station consists of a turbo molecular pump (TMP) with a pumping speed of 2000 l/s and a dry pump with a pumping speed of 300m^3/h. 5 vacuum gauges are installed in different positions of the chamber to read the pressures and interlock with the valves which fixed to each pump.

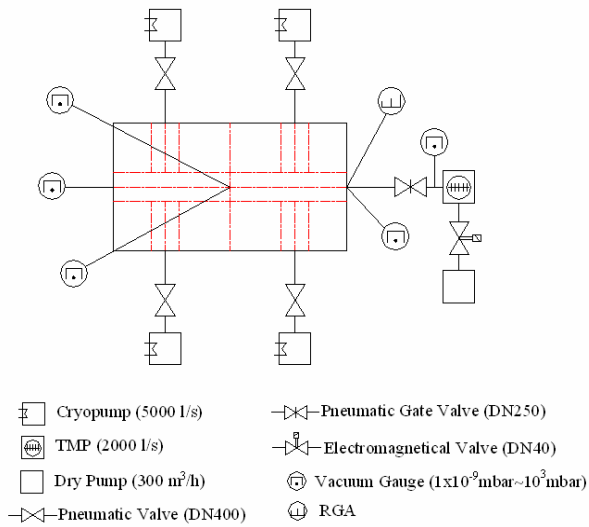

Figure 4: The vacuum equipment layout of the cyclotron

HITFiL project will be completed in 2013. The vacuum system of the new cyclotron will be finished in 2011.

REFERENCES

[1] J.W.Xia, W.L.Zhan, B.W.Wei, et al., "The Heavy Ion Cooler-Storage-Ring Project (HIRFL-CSR) at Lanzhou", NIM A 488(2002) 11-25.

[2] D.Z.Wu, Y.F.Wang, X.Q.Zhang, et al., "The upgrade of the vacuum chamber of SFC", Vacuum and Cryogenics, 2005 (1): 40-45 (In Chinese).

UPGRADE OF IBA CYCLONE® 3 CYCLOTRON

W. Kleeven, M. Abs, E. Forton, D. Neuveglise, S. Zaremba, B. Nactergal and Th. Servais
Ion Beam Applications s.a., Chemin du Cyclotron 3, Louvain-la-Neuve, Belgium

Abstract

Some specific applications of $^{15}O_2$ need a stand alone production machine to avoid disrupting the hospital main PET cyclotron. Due to recent renewal in interest, IBA has decided to improve the design of its Cyclone® 3 which accelerates D^+ ions to energy of more than 3 MeV and which was originally developed for this purpose.

The main improvement relates to the magnetic structure. In the existing design the vertical focusing is obtained by four straight pole-sectors that are mounted on the circular base of the pole. In the new design these are replaced by three spiralled pole sectors. This modification changes the rotational symmetry from four to three and improves the vertical focusing properties of the machine. Also the main coil and the return yoke were slightly modified. This allowed increasing the extraction energy by about 10 % from 3.3 MeV to 3.6 MeV.

This new design will improve the transmission in the cyclotron and will result in an extraction efficiency of more than 80% using an electrostatic deflector. For the prototype the goal is to obtain an extracted current of 50 µA. This value should rise to 70 µA for subsequent machines, representing a doubling of the existing performance.

In the paper, results of magnetic field optimization and extraction calculations are presented.

INTRODUCTION

The Cyclone® 3 has been developed in the early nineties [1-6] as a very compact cyclotron for stand alone production of Oxygen-15 in open flow. Even if still in use, only few machines have been sold. Recently, new markets have shown more interest in the Cyclone® 3 concept. An example is the promotion of new emergency-room evaluation of brain stroke and ischemic attack in remote centres.

As a consequence, IBA decided to review its Cyclone® 3 design and improve it. This paper describes the modifications made on the magnetic circuit of the cyclotron to improve its expected performances.

MAGNET FEATURES

In its first version, the Cyclone® 3 had 4 magnetic poles (fig. 1). That choice was rather natural to avoid impedance imbalance between the two RF cavities. The Cyclone® 3 is equipped with two 90 degrees dees. However, such design had two major drawbacks:

1. Due to the hill-valley small gap difference, the flutter was relatively low and vertical (axial) betatron frequency was about 0.15. This ensures the minimal axial focusing but is far from the axial focusing provided by IBA patented deep valley design.
2. Due to the size of the machine and available space between poles there was very limited place for the electrostatic deflector.

IBA took some distance with its habit to have four-fold rotational symmetry cyclotrons and proposed a new design with only 3 poles that are spiralled to increase the axial betatron oscillation frequency. This new design has the additional advantage to leave more room for the extraction system. The schematic view of the new magnet is shown on figure 2.

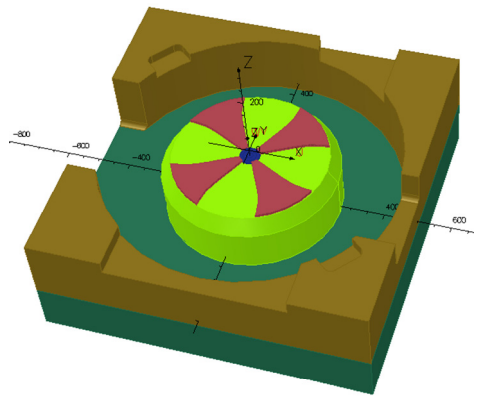

Figure 1: Previous design of the Cyclone® 3 (coils not shown).

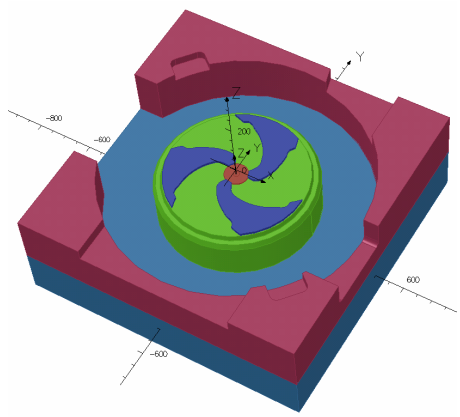

Figure 2: New design of the Cyclone® 3 (coils not shown).

It is also worth to mention that the outer contour of the cyclotron yoke has been modified to limit iron saturation effects.

CLOSED ORBIT ANALYSIS

The OPERA models have first been used to obtain a nominal configuration that is isochronous and shows reasonable frequencies of betatron oscillations.

After a classical correction of the field in the hard-edge approximation, the model proved to be isochronous with the (second harmonic mode) RF

frequency of 28.805 MHz (fig. 3). Closed orbits have been found up to an energy of 3.94 MeV.

The vertical (axial) betatron oscillation frequency (fig. 4) has been raised. A compromise on the spiral angle as a function of radius has been found in order to achieve that increase in axial betatron frequency while keeping the advantage of 3-fold rotational pole symmetry for deflector space. At an average radius of 15 cm, it is now about 0.21, to be compared with values around 0.17 for the previous design.

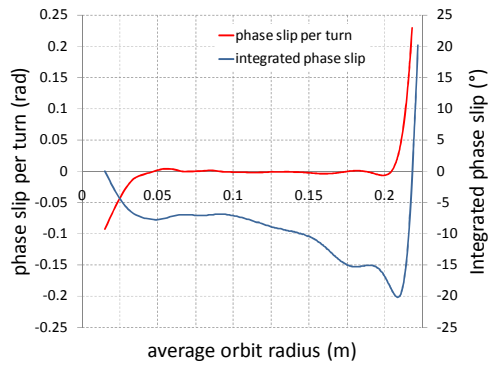

Figure 3: Isochronism of the Cyclone® 3 model.

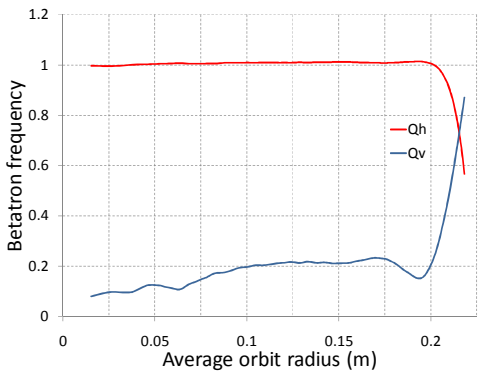

Figure 4: Horizontal and vertical (axial) betatron frequencies as a function of average orbit radius.

BEAM ACCELERATION AND EXTRACTION

The beam extraction has been studied by particle tracking, starting from the equilibrium orbit with kinetic energy of 1 MeV. Normalized horizontal and vertical emittances have been chosen to be 3π mm·mrad.

The electrostatic deflector has an entrance gap of 4 mm, an exit gap of 8 mm. It was modelled by the change of the magnetic field being the equivalent of the electric field in the deflector when the tracked particle reaches a given radius and azimuth.

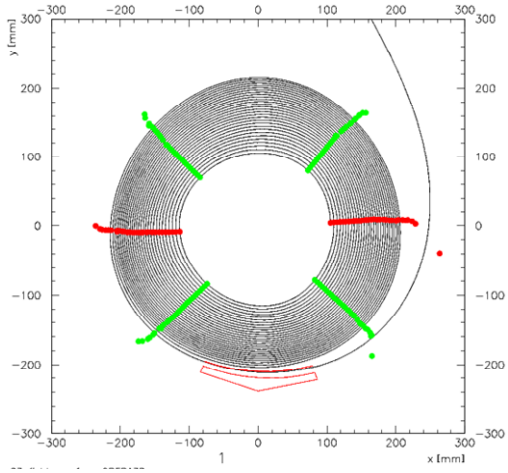

Figure 5: Single particle trajectory showing acceleration and extraction by the electrostatic deflector. 3-Fold symmetry and effect of the pole spiralization can be observed in the turn pattern.

Figure 5 shows an example of the particle trajectory from kinetic energy 1 MeV to extraction. Red and green dotted curves correspond to trajectory points where the dee voltage was 0 and 30 kV dee voltage, respectively. These dotted curves confirm the correct isochronism of the magnetic field.

At 3.5 MeV, the extraction radius is 202 mm and the deflector has an extraction efficiency of 87.8 %. 53.1 % of the total beam reaches the internal target.

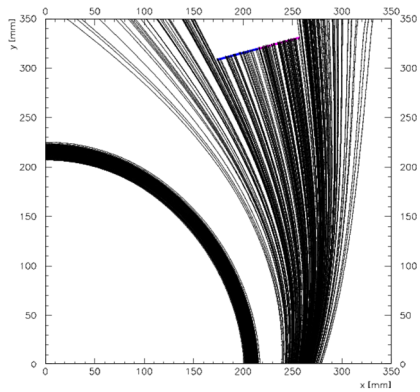

Figure 6: Multiple particle tracking for determination of efficiency on internal target.

Figure 6 presents last few turns of calculated trajectories for 500 tracked D^+ ions. In the region of the internal target one can see the important horizontal extension of the beam related to the passage by the fringing field of the cyclotron.

This could be improved by correcting optics between the deflector and the target, using for instance 3-bar correctors. It is difficult due to the present dee and vacuum chamber design which limits available

space and would need modifications to accommodate for such elements.

PRESENT STATUS

All iron parts of the newly designed magnet have been already machined. The magnet iron was assembled and is ready in IBA assembly hall for magnetic field measurements.

Figure 7: Cyclone® 3 being currently assembled at the Belgian IBA facility. One can distinguish the various vacuum chamber access in the return yoke: pumping and dee stems access (top), the deflector access (left) and the target hole (bottom).

CONCLUSIONS

This new development was unique at IBA due to the fact that for the first time the three-fold rotational symmetry was applied. This successfully contributed to increase of the modest vertical (axial) focusing in Cyclone® 3 cyclotron. The new design also increased the kinetic energy of extracted ions keeping the same pole diameter as before. This will boost production yield of Oxygen-15, especially at this energy range, where the production yield is rapidly going up.

REFERENCES

[1] J.L. Morelle et al., “An inexpensive ^{15}O labeled molecule delivery system for clinical flow studies”, proc. of the 3rd workshop on targetry, pp 62-65, 1989.

[2] IBA, “The Cyclone 3D – IBA presents an alternative to the ^{82}Sr->^{82}Rb generator”, proc. of the 3rd workshop on targetry, 1989.

[3] S. Zaremba et al., “Beam Dynamics in Newly Designed Cyclotrons at Ion Beam Applications”, proc. of EPAC 1990, p. 1774-1776.

[4] M. Abs et al., “RF Systems Developed for CYCLONE 3D and CYCLONE 10/5”, proc. of EPAC 1990, p. 967-969.

[5] M. Ladeuze et al., “Control Systems for Ion Beam Applications Baby Cyclotrons”, proc. of EPAC 1990, p. 827-829.

[6] E. Conard et al., “Current Status and Future of Cyclotron Development at IBA”, proc. of EPAC 1990, p. 419-421.

CYCLOTRON VACUUM MODEL AND H- GAS STRIPPING LOSSES

V. Nuttens,# M. Abs, J.-L. Delvaux, Y. Jongen, W. Kleeven, M. Mehaudens, L. Medeiros Romao, T. Servais, T. Vanderlinden, and P. Verbruggen Ion Beam Applications s.a., Chemin du cyclotron, 3, B-1348 Louvain-la-Neuve, Belgium

Abstract

A model to compute the vacuum in the different parts of IBA H^- cyclotrons has been developed. The pressure results are then used to compute the beam transmission through the cyclotron by integration of the residual gas stripping cross-section along the ion orbits. The model has been applied to the ARRONAX Cyclone®70 with the initial vacuum design and the results are compared to the experimental data. The pressure and the transmission are in good agreement with experimental data.

INTRODUCTION

Many proton cyclotrons use the advantage of stripping extraction, by accelerating H^- ions. However, before extraction, the negative ion beam can suffer losses from stripping by the residual gas. The higher is the pressure, the higher are the losses. Moreover, the stripped beam will be stopped on the inner wall of the cyclotron, inducing an additional degassing that increases the pressure and hence losses in the cyclotron. For high beam currents, degassing can be too large compared to the pumping capacity and the beam transmission can drop down to zero. The pressure inside the cyclotron has therefore a large impact on the current that can be extracted from the cyclotron. A simple model has been set up at IBA to determine the vacuum pressure in the hills and in the valleys of the Cyclone®70 and then deduce the beam transmission.

MODELS

A first model to compute the beam transmission through the cyclotron has been set up. The succession of hills and valleys leads to pressure inhomogeneities in the machine. Therefore, we have set up a model to compute the vacuum in the pole gaps and in the valleys.

Beam Transmission

The number dN of H^- ions that can be stripped by the residual gas is obtained from:

$$dN = -\sigma n N v dt \tag{1}$$

where N is the number of incident ions; dt is the time spent by the ions in the residual gas of atomic density n; v is the ion velocity; and σ is the total stripping cross section. We use the analytical fit proposed by the Nakai et al to compute the stripping cross section [1]. The beam transmission in an isobar region for particles with a transit time t is:

$$T = 1 - \frac{\Delta N}{N} = \exp(-v t n \sigma) \tag{2}$$

The residual gas analysis (RGA) performed on ARRONAX Cyclone®70 have shown that the residual gas was composed mainly by 70% of H_2O, 30% of air and 0.15% of rare gas. However, the parameters of the Nakai et al fit are not reliable for water in the Cyclone®70 energy range. Therefore, we consider the worst case scenario (i.e. largest stripping cross section) of 100% O_2. The cyclotron has been subdivided into three isobar regions: the poles at pressure p_1, the pumping valleys at pressure p_2 and the RF valleys at pressure p_3. The ion orbit is supposed straight segments in valleys and circular arcs in hills (figure 1). The particle track length in the hills and in the valleys is obtained from:

$$r_{magn} = (B\rho)/B_z \tag{3}$$

$$l_{hill} = \frac{\pi}{2} r_{magn} \tag{4}$$

$$l_{valley} = \frac{r_{magn} \tan(v)}{1 - \tan(v)} \tag{5}$$

The injection energy is 40keV. Acceleration is supposed to occur once a turn with an energy equal to the energy gain per turn defined by:

$$dE = q \cdot V_{RF} \cdot 2 \cdot n_{dee} \cdot \sin\left(\frac{\delta}{2} \cdot h\right) \tag{6}$$

where q=1 is the particle charge, V_{RF}=65kV is the RF voltage, n_{dee}=2 is the number of dees (two gaps per dee); δ=36° is the dee angle; and h=2 is the harmonic mode.
The total transmission is the product of the transmission in the eight regions (4 poles and 4 valleys) for each ion energy.

Vacuum

As the ion travels along its trajectory, it sees a series of vacuum chambers of infinite conductance (valleys) and conducts of finite conductance (hills). However, in the RF valley, the dees limit the conductance and have to be taken into account. The two-fold rotational symmetry allows us to consider only a half-cyclotron as shown on figure 1. Without the beam, the main contribution of

#vincent.nuttens@iba-group.com

outgassing is coming from the surface of the different parts of the cyclotron. In order to simplify the model, we consider that the surface outgassing is only located at different points in the machine as shown in figure 1:

- In the middle of each pole;
- In the accelerating gaps;
- In the middle of each dee;
- In the middle of the pumping valley;
- In the middle of the extraction vacuum chamber;
- At the exit of the switching magnet;
- A contamination at the end of each beam line (due to the target, …)

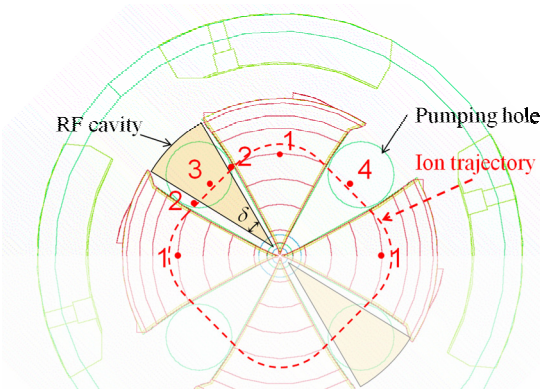

Figure 1: Outgassing points in the cyclotron.

The equivalent diagram used for the vacuum model is shown in figure 2. By symmetry, we can deduce that $P_1=P'_1=P''_1$ and $P_2=P'_2$.

The outgassing rates were taken from the literature [2]. RF cavities surfaces were supposed made of fresh copper, vacuum chamber of bright rolled aluminum and magnetic part of mild steel slightly rusty. We sum up all the surfaces surrounding each outgassing point multiplied by the corresponding outgassing rate depending on the material. Note that the ARRONAX Cyclone®70 contains correction coils surrounding the poles which are covered by epoxy which can be heated by Joule effect. These coils can therefore lead to a significant additional outgassing. However, in the throughput calculation, each interface between two pieces in contact is considered as two outgassing surfaces. Results of our calculations show that this method is sufficient to account for the outgassing contribution from correction coil epoxy. The gas throughputs considered in this calculation are listed in table 1.

We consider the stationary case where the pressure is constant in time everywhere in the cyclotron. The pressure is below 10^{-5}mbar and the molecular regime can be considered to determine the conductances. In this case, the conductance of a conduct can be written in the form:

$$C = aAv/4 \qquad (7)$$

where a is the transmission probability of the conduct; A is the cross-sectional area of the conduct; and v is the thermal velocity of the gas which depends on the composition of the gas and its temperature. We considered according to the RGA analysis that the gas is 100% of H_2O at 22°C, which lead to a thermal velocity v=586m/s. Many conducts (extraction vacuum chambers, pipes in the switching magnet) in the cyclotron can be considered as thin, rectangular slit-like pipes. The transmission probability for such a conduct can be fitted by an analytical function:

$$\log_{10} a = \sum_{i=0}^{6} b_i \left(\log_{10}(l/h)\right)^i \qquad (7)$$

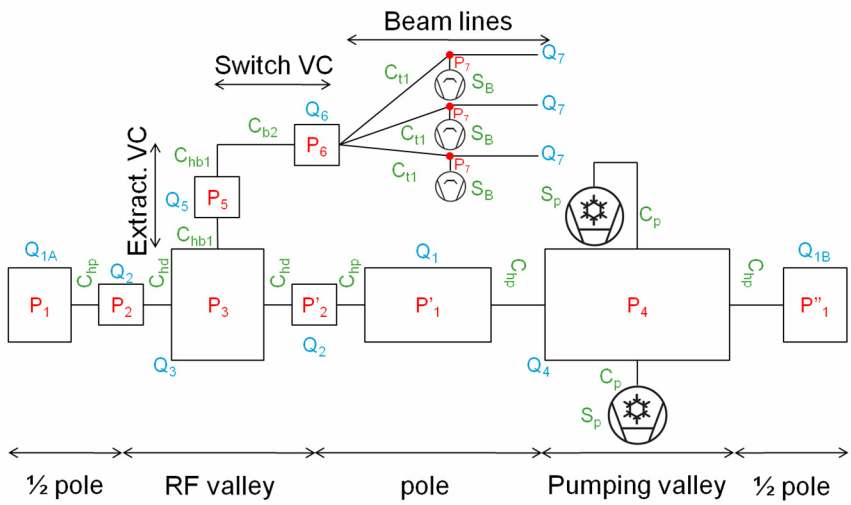

Figure 2: Equivalent diagram of the cyclotron vacuum model. Pi is the pressure at the point i in the cyclotron; Qi are the outgassing throughput, Ci are the conductance and Si are the pumping speed.

where b_0=-0,165; b_1=-0.288; b_2=-0.170; b_3=-6.84E-3; b_4=1.46E-2; b_5=-3.08E-3; b_6=2.08E-4. The poles and dees can also be seen as slit-like corner conduct with variable length while the radius increases (figure 3). As the transmission probability is independent of the width, we can approximate the slit-like corner by a series of slit-like tubes with no lateral wall. The conductance can then be computed by the integration of the transmission probability:

$$C = \frac{vh^2}{8\tan(\theta/2)} \int_{\lambda_1}^{\lambda_2} a(\lambda) \cdot d\lambda \qquad (7)$$

where $\lambda = l/h = 2l/h \cdot \tan(\theta/2)$. The conductance of half a pole/dee is the double of the pole/dee conductance.

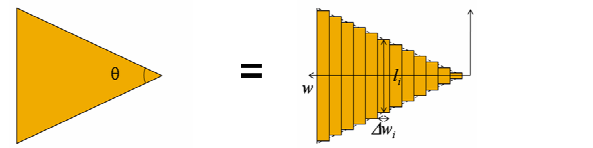

Figure 3: Model used for the conductance calculation of poles and dees.

The pumps are also considered as conduct with a zero pressure at one end. Conductances and pumping speeds used for this model are given in table 1.

Table 1: Gas throughputs and conductances

Throughput			Conductance		
Q_1	mbar-L/s	5.4×10^{-4}	C_{hp}	L/s	2236
Q_2	mbar-L/s	1.1×10^{-3}	C_{hd}	L/s	2624
Q_3	mbar-L/s	5.8×10^{-4}	S_p	L/s	17300
Q_4	mbar-L/s	1.2×10^{-3}	C_{hb1}	L/s	4734
Q_5	mbar-L/s	6.7×10^{-5}	C_{b2}	L/s	473
Q_6	mbar-L/s	1.0×10^{-4}	C_{t1}	L/s	76
Q_7	mbar-L/s	8.4×10^{-5}	S_B	L/s	300

RESULTS AND DISCUSSION

The computed pressures at the different points in the cyclotron are given in table 2. Experimentally, we have no information on the pressure in the hills and in the valleys (in the median plane). However, the pressure measured at the level of the cyclotron cryopumps can be compared to the pressure in the pumping valleys (P_3). Although there is a factor ~1.5 between these two pressures, it has little impact on the transmission results because the beam losses are mainly due to residual gas stripping in the poles and in the dees where the pressure is higher by a factor ~10. The pressure at the level of the extraction vacuum chambers agrees well. Finally, it can be seen that the total transmission through the cyclotron is in good agreement with the experimental data.

Table 2: Pressure and transmission results for the ARRONAX Cyclone®70: our model versus measurements.

Position			Model	ARRONAX
Pole	P_1	mbar	1.02×10^{-6}	-
Gap	P_2	mbar	1.65×10^{-6}	-
Dee	P_3	mbar	1.75×10^{-6}	-
Pump. Val.	P_4	mbar	1.47×10^{-7}	2.23×10^{-7} *
Extraction	P_5	mbar	1.74×10^{-6}	1.85×10^{-6} †
Switch	P_6	mbar	1.47×10^{-6}	-
BTL	P_7	mbar	5.20×10^{-7}	-
Transmission	T	%	86.7	87.7

*Average of the pressures measured close to the valley cryopumps.
† Pressure measured on the extraction vacuum chamber.

CONCLUSIONS

The models set up to compute the residual gas pressure and beam transmission are in good agreement with experimental data. They were used to compute the performance of the ARRONAX Cyclone®70 (with the initial vacuum design) with an agreement of 1% on the beam transmission.

REFERENCES

[1] Y. Nakai et al, "Cross sections for charge transfer of hydrogen atoms and ions colliding with gaseous atoms and molecules", Atomic Data and Nuclear Data Tables 37 (1987) 69-101.
[2] J.F. O'Hanlon, "A User's Guide to Vacuum Technology", Wiley, 3rd Edition.

OPERATIONAL EXPERIENCE OF SUPERCONDUCTING CYCLOTRON MAGNET AT VECC, KOLKATA

U Bhunia*, M K Dey, J Pradhan, Md. Z A Naser, U S Panda, C Nandi , T K Bhattacharyya, A Dutta Gupta, M Ahmed, S Paul, J Debnath, A Dutta, G Pal, S Saha , R. Dey, C Mallik and R K Bhandari
Variable Energy Cyclotron centre
1/AF Bidhan Nagar Road Kolkata-700064, India

Abstract

The Kolkata Superconducting cyclotron magnet has been operational in the Centre since last few years and enabled us to extensively map magnetic fields over a year covering the operating range of the machine and successful commissioning of internal beam. The magnet cryostat coupled with the liquid helium refrigerator performs satisfactorily with moderate currents (<550A) in both the coils. The superconducting coil did not undergo any training and over the years has not suffered from any quench. Author would share the experience and difficulties of enhanced overall heat load to the liquid helium refrigerator at higher excitations of coils. This creates instability in the operation of liquid helium refrigerator and finally leads to slow dump. Rigorous study has been carried out in this regard to understand the problems and operational logic of liquid helium refrigerator has been modified accordingly to alleviate from. Some other measures have also been taken from cryostat and cryogenic distribution point of view in order to reduce the heat load at higher excitations, optimize the current lead flow, etc.

INTRODUCTION

Variable energy cyclotron centre, Kolkata is successfully operating its superconducting cyclotron main magnet since 2006 that enables us to successfully map magnetic fields over a year covering the operating range of machine and successful commissioning of internal beam. The K-500 Superconducting Cyclotron (SCC) main magnet consists of two superconducting coils (alpha coil and beta coil), which has been energized to different current levels for extensive magnetic field measurement. An annular vacuum chamber, made of magnetic steel, referred as cryostat OVC, surrounds the stainless steel cryostat bobbin. In the following sections, several operational problems of cyclotron magnet encountered over the past few years have been explained.

EXPERIMENTAL OBSERVATIONS

OVC Vacuum during Liquid Helium Filling up

Moisture level in the cryostat was brought down to 20ppm before starting up of cool down process. During the process of cool-down tension in radial support link increases gradually. The positional adjustment is necessary, if the force approaches a maximum allowable level by tightening/loosening the support bolts attached with each link.

It was found that helium leakage would change as the cryostat was filled with liquid helium. Correlating the helium leakage rate with the liquid helium height of cryostat has allowed vertical location of leakage to be found as shown in figure 1.

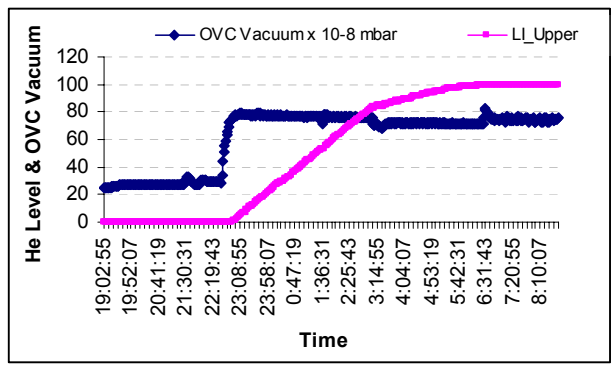

Figure 1: OVC vacuum during liquid helium filling up

Due to inaccessibility of the location of leak (~ low 10^{-4} mbar-lt/s) inside the cryostat, it was not feasible to repair it. However, there are several very small leaks found in the outer median plane region of cryostat and repaired those successfully.

OVC Vacuum during Energization

It is observed that the OVC vacuum deteriorates with current as shown in figure 2. It is interesting to note that the degradation of OVC vacuum is dependent mainly on the current in alpha coil, which is nearer to the median plane. In this regard, detail study has been carried out [1]. Being nearer to median plane, alpha coil has more contribution of magnetic field than beta coil, in the median plane region of OVC. For alpha current of 600 A and beta current of 400 A, OVC vacuum degrades to 3.0E-4 mbar.

Additional pumping module of pumping speed for He ~300 lt/s has been installed with the OVC annular space to improve the vacuum to low 10^{-5} mbar. In addition, observations are kept on cryogenic transfer line if any frostings occur over it and annular space is evacuated to a vacuum level better than 1E-6 mbar.

*ubhunia@vecc.gov.in

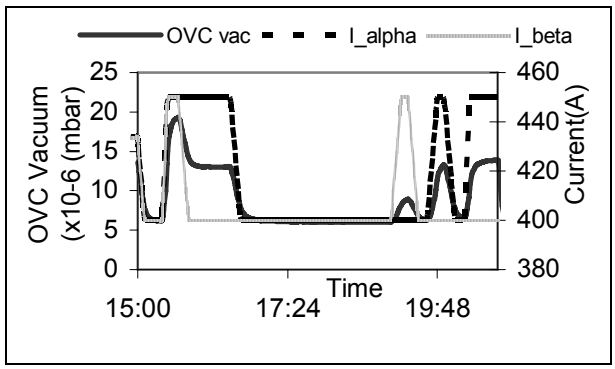

Figure 2: Variation of OVC pressure with coil current

Instability of Helium Refrigerator Expander Control Loop

Out of all control loops, expander control loop is very vital in the control of the helium liquefier performance. The control loop was affected partly due to temperature sensor problem and partly due to improper programming also. When we were coupling the plant with the cryostat with full current in the coils of the superconducting magnet, the expanders were unable to provide rated cooling. We were controlling the expander control valve mostly in manual mode by seeing the pressure in the cold expander outlet (LP), liquid helium level in the Dewar and pressure in the compressor outlet (HP) etc. This was troublesome and prone to error. So we were unable to handle even 100 W @ 4.5 K load in the cryostat and transfer lines.

The transients created during current ramping up or down and cryostat return valve operation was such that, it was creating a problem of pressure swing in HP and LP line of compressor. Sometimes even it was tripping by crossing the alarm limits. We were bound to have less opening of expander control valve to get rid of compressor tripping problem. Less opening of expander control valve was leading to less refrigeration power. So some modifications in the expander control loop had been implemented [2] to take care of the scenario previously done in manual mode.

Parameters	Old program	New program
Set point	14.00# (Bar abs.)	3000*X Attenuators(rps)
Feed back	Compressor high pressure	Warm expander speed
Prop. Band	6.5%	400 %
Integral time	1 min	15 sec

 # =usersettable

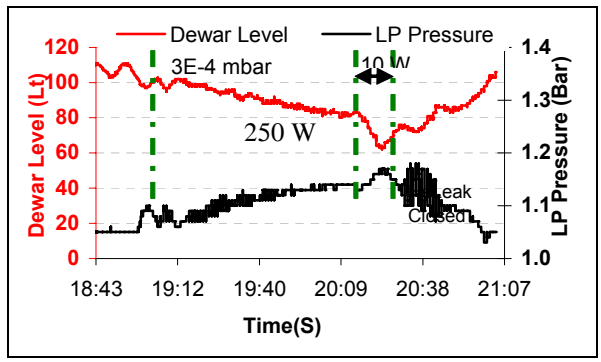

Figure 3: Heat Load study for OVC maintained at 3.0E-4 mbar.

Initially the expander control was based on compressor high pressure feed back. As the compressor high pressure was not changing according to cycle performance, the expander control valve was more or less constantly opened at a fixed value. So it was producing a constant cold power irrespective of the cycle refrigeration load. This was the root cause for instability in the system. Expander's speeds are the quick indication of change in the system thermodynamics. Therefore expander valve control operation has been modified to operate as per the warm expander speed feed back and the refrigerator is capable to handle even 3E-4 mbar vacuum in annular space (≅ 250 W @ 4.5 K) as shown in figure 3.

Optimization of Current Lead Helium Flow

Three vapour-cooled AMI current leads are used for the energization of the main magnet coil of K 500 cyclotron in VECC, Kolkata. Optimum helium mass flow rate at different operating currents, voltage developed across the current leads has been investigated since data were not available from vendors. Slow dump interlocks has been put to the power supply w.r.t. lead voltage drop of 100 mV.

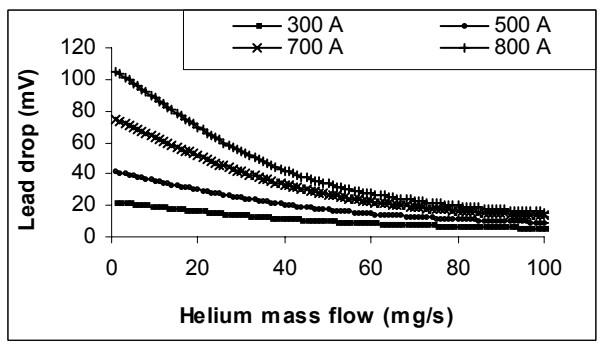

Figure 4: Simulated lead voltage drop for various excitations

Current lead voltage drop are also measured and compared with the theoretical study for 300 A of current in both the coils as shown in figure 5.

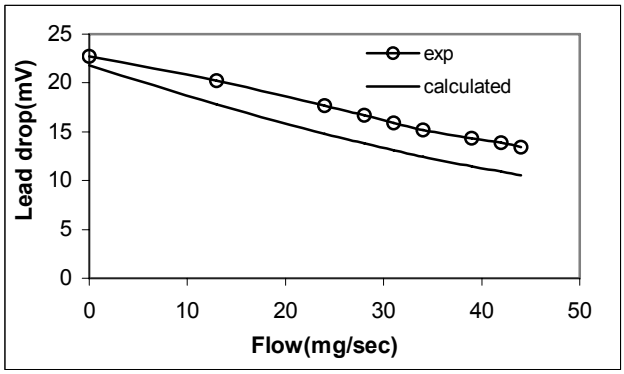

Figure 5: Comparison of lead voltage drop with experimental curve

Slow & Fast Dump Scenario

Each coil is protected by slow and fast dump resistor against any unusual scenario like low helium level in cryostat, excess pressure in cryostat, detoriation of OVC vacuum over a set value, excess lead voltage drop, etc. In several occasions, fast and slow dump occurred due to failure of preset interlocks value though there was no real quench like phenomena developed.

CONCLUSION

Over the past few years, we have encountered several problems corresponding to various subsystems and solved most of the difficulties such as extra heat load to cryostat, instability to helium refrigerator, etc. The superconducting cyclotron magnet is now operating quiet smoothly for ion beam acceleration.

ACKNOWLEDGEMENT

Authors express their sincere gratitude to all colleagues who has directly or indirectly involved for successful commissioning of superconducting cyclotron magnet.

REFERENCES

[1] Z.A.Naser, U.Bhunia et al., " Study of Vacuum Related Problems during energization of K500 SCC", in 4th Asian Particle Accelerator Conference (APAC-2007), Indore, Jan 31-Feb 02, 2007.

[2] U. Panda, U. Bhunia, R Dey et al., "Modifications for optimum operation of Helium Refrigerator", Indian Journal of Cryogenics, Vol.33, No. 1, 2008.

MEDIAN PLANE EFFECTS AND MEASUREMENT METHOD FOR RADIAL COMPONENT OF MAGNETIC FIELD IN AVF CYCLOTRONS

G. Karamysheva, N. Morozov, P. Shishlyannikov, JINR, Dubna, Russia

Abstract

The median plane of the magnetic field in AVF cyclotrons rather often does not coincide with the mid-plane of their magnetic system. The idea of an effective median plane formulated by J.I.M.Botman and H.L.Hagedorn [1] for the central region of the cyclotron is extended to the entire working region and tolerances for the horizontal components of the magnetic field are estimated. Equipment based on the search coils is proposed and used for measurement of the radial component of the magnetic field and for correction of the magnetic field median plane.

INTRODUCTION

The vertical deviation of the beam center from the median plane of the vacuum chamber was observed and corrected at some cyclotrons (AVF Cyclotron, Einhoven, Netherlands [1], AGOR, Groningen, the Netherlands [2], U-120M, Rzez, Chech Republic [3], AIC-144, Krakow, Poland [4], JINR Phasotron, Dubna, Russia [5]). Thus it is very important for the cyclotron design to be clear in knowing the tolerances for horizontal components of the magnetic field, their relation to the manufacturing tolerances for magnetic and current elements and the method of magnetic field measurement and correction.

EFFECTIVE MEDIAN PLANE AND TOLERANCES FOR HORIZONTAL COMPONENTS OF THE MAGNETIC FIELD

When the median plane of the magnetic field is symmetric, the equation of free vertical oscillations of the particle near the median plane of the vacuum chamber is:

$$z'' + \nu_z^2 z = 0 \qquad (1),$$

where ν_z^2 is the total vertical focussing force of the magnetic and electric field. When the symmetry of the magnetic system is lost, the horizontal components (B_r and B_φ) of the magnetic field appear in the vacuum chamber median plane. In this case the magnetic field median plane is not physically the plane where B_r and B_φ are equal to zero at the same time. Stable vertical oscillations exist now near the effective medial plane (EMP) (Z_{eff}):

$$z'' + \nu_z^2 (z - Z_{eff}) = 0 \qquad (2).$$

Physically the EMP is the plane in which the sum of all vertical forces acting on the particles is zero. If in the cyclotron there are some vertical forces with factor ν_{zi}^2 and zero point Z_i, the position of EMP can be evaluated as:

$$Z_{eff} = \Sigma_i (\nu_{zi}^2 \cdot Z_i) / \Sigma_i \nu_{zi}^2 \qquad (3)$$

or

$$Z_{eff} = \Sigma_i (\nu_{zi}^2 \cdot Z_i) / \nu_z^2 \qquad (4).$$

The main physical conclusion from (4) is that the influence of each vertical force in the AVF cyclotron on the vertical position of the EMP depends on the relative contribution of this force to the total vertical force ν_z^2.

In a classical cyclotron there is only one vertical force generated by the average radial component of the magnetic field, and the vertical beam position follows the position of the plane with $B_{r\ aver} = 0$. In the AVF cyclotron there are basically two vertical forces, the defocussing force generated by the average radial component of the magnetic field and the focussing force generated by the horizontal components of the magnetic field azimuth variation. When the plane with $B_{r\ aver}=0$ shifts, the vertical beam position follows the plane with the overall vertical force equal to 0 (Fig. 1).

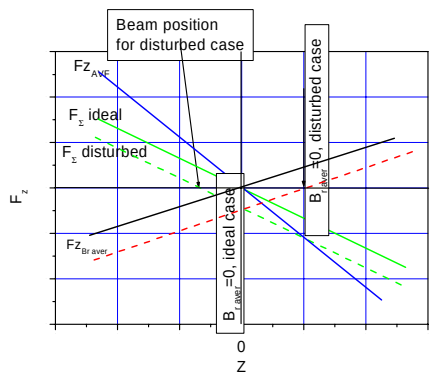

Figure 1: AVF cyclotron: vertical beam position follows the plane with zero overall vertical force

If the vertical component of the cyclotron magnetic field is written in the form

$$B_z = B_{zav} + \Sigma_i B_{zi} \cdot Cos[i(\varphi - \varphi_{zi})] \qquad (5),$$

the vertical beam center position, which arises due to the average radial field component (B_{rav}), and the main (N) harmonic of the radial and azimuth component (B_{rN} ,$B_{\varphi N}$), may be found as:

$$Z_{eff} = R/(B_{zav} \cdot \nu_z^2)[B_{rav} + 0.5(B_{zN}/B_{zav})B_{\varphi N}/N \cdot Sin\{N(\varphi_{\varphi N} - \varphi_{zN})\} - (B_{zN}/B_{zav}) \cdot B_{rN}\varphi'_{zN} R/N \cdot Sin\{N(\varphi_{rN} - \varphi_{zN})\}] \qquad (6).$$

If we take into account only the part of B_{rN} and $B_{\varphi N}$ in the form of their projections on the vector shifted by $\pi/2/N$ from the vector with the phase of the main vertical harmonic designated as B_{rNs}, $B_{\varphi Ns}$ (only these horizontal components of the magnetic field give the vertical force

acting on the accelerated particles), the latter formula may be written as:

$$Z_{eff} = R/(B_{zav}\cdot\nu_z^2)[B_{rav} \pm 0.5(B_{zN}/B_{zav})B_{\varphi Ns}/N \pm \pm((B_{zN}/B_{zav})\cdot B_{rNs}\varphi'_{zN}\cdot R/N)] \quad (7).$$

To find separately the allowable values (tolerances) for the horizontal field components from the allowable vertical beam offset the latter formula can be transformed into three ones:

$$B_{rav} = Z_{eff} B_{zav}\cdot\nu_z^2/R$$

$$B_{\varphi Ns} = Z_{eff} B_{zav}\cdot\nu_z^2/R\cdot 2N(B_{zav}/B_{zN}) \quad (8).$$

$$B_{rNs} = Z_{eff} B_{zav}\cdot\nu_z^2/R\cdot N/R(B_{zav}/B_{zN})/\varphi'_{zN}$$

TOLERANCES FOR THE HORIZONTAL COMPONENTS OF THE MAGNETIC FIELD OF THE C400 CYCLOTRON

For hadron therapy project, the C400 superconducting cyclotron [6] is proposed and designed. With the simulated magnetic field map and computed vertical betatron frequency, we can use formulas (8) (N = 4) to obtain the radial dependence of tolerance for the horizontal field components of this cyclotron per 1 mm of acceptable vertical offset of the beam (Fig. 2). By increasing the frequency ν_z at the extraction region of C400 close to 0.45, it was possible to increase the tolerances for the horizontal magnetic field components. For the extraction region those tolerances are B_{rav} <3-4 G, $B_{\varphi 4}$ <70-90 G and B_{r4} <15-20 G. The region most sensitive to B_{rav} is the central one (R <40 cm). To check the analytic formulas, the beam dynamic was simulated for separate C400 working regions. The result of the simulation for $B_{r\,4}$ = 50 G is presented in Fig. 3.

MEASUREMENT AND CORRECTION OF THE AVERAGE RADIAL COMPONENT

The average radial component of the AVF cyclotron's magnetic field is the first among the most dangerous causes for the vertical beam offset and the most difficult part of the magnetic field measurement procedure. The difficulties of the measurement are so great that the accelerator physicists very often prefer not to measure this component of the field but rather to correct it by the accelerated beam effect during the cyclotron commissioning. So, the accelerator physicists have to go along three ways:

- to use as high a vertical force (ν_z) as possible during the cyclotron design;
- to get and implement an accurate B_{rav} measurement method;
- to be prepared for correcting the vertical offset of the accelerated beam.

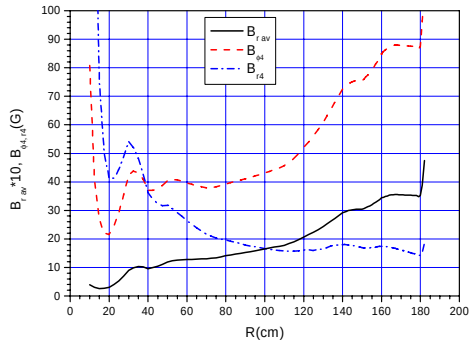

Figure 2: B_{rav}, B_{r4}, $B_{\varphi 4}$ for the possible vertical beam 1 mm offset

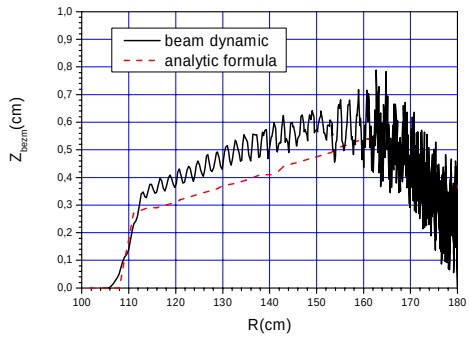

Figure 3: Vertical beam offset due to B_{r4} = 50 G according to the analytic formula and the beam dynamics simulation

The best solution for the B_{rav} problem is to have an accurate measurement method. Considering the available cyclotron design experience it is possible to distinguish two ways in the B_{rav} measurement:

- direct measurement of the radial component of the magnetic field;
- integration of the difference between the vertical components in two planes at the distances ± a from the median plane:

$$B_{rav}(R) = -\frac{1}{2aR}\cdot\int_0^R \Delta\bar{B}z(r)rdr \quad (9).$$

Measurements by the Hall Probe

Direct B_r measurements by the Hall probe reveal a very strong influence of the large vertical component of the magnetic field: $B_{r\,error} = B_z\bullet\delta$, where δ is the accuracy of the Hall probe orientation in the radial direction. It is impossible to have δ at the level better than 10^{-3}. To overcome the above difficulties the Hall probe was used in the way of a pendulum [8] or with laser alignment [9]. The accurate measurement by the Hall probe may be additionally complicated by the planar effect.

If the Hall probe is used to measure ΔB_z, the influence of the vertical component is less, it is ~ ½ $B_z\bullet\delta^2$ but additional problems arise:

- keeping the angle δ constant when the Hall probe shifts from one measurement plane to another;
- small measurement error at the inner radius gives a large overall effect at the outer radius after integration by (9).

Measurements by Search Coils

The use of search coils for the measurement of ΔB_z makes the measurement of $B_{r\ av.}$ more accurate due to high sensitivity of the coils and lower influence of the vertical component of the magnetic field than in the case of the Hall probes.

The first type of search coil use is the one of a small diameter. The measurements are performed in the polar grid, and for signal generation the coil is shifted in the vertical direction in positions ±a from the median plane of the cyclotron. The second possibility is the use of two similar coils (at the distance ±a) with opposite connection. The signal is generated as the probe moves radially from the center of the cyclotron to the final radius R. The signal can be processed in the floating mode to get the radial ΔB_z dependence. For this type of measurements the same hardware and software can be used as for the measurement of the vertical component of the magnetic field [10].

The AVF magnetic field was first measured by a small search coil (with vertical shift) at the JINR Phasotron [11]. It was demonstrated that for this type of measurements the systematic error is proportional to the gradient of the vertical component of the magnetic field:

$$\Delta_s \cdot (\Delta\overline{Bz}) = 2a\frac{d\overline{Bz(r)}}{dr}\delta \qquad (10)$$

and accumulation of the systematic error occures under integration of $\Delta\overline{Bz}$ by formula (9).

The second type of search coils is the one with radius R which is needed for measurement of the component $B_{r\ av.}$ of the magnetic field. The signal is generated during the vertical shift of the coil at the positions ± a from the median plane of the cyclotron. To get a full magnetic field map, it is required to use a set of coils with the designed set of radii. This method was tested and used at the JINR Phasotron [5]. It was shown that the influence of the vertical component of the magnetic field on the radial component is:

$$\Delta_{err}(B_{rav}) = ½ B_{zav} \cdot \delta^2 \qquad (11).$$

The practical accuracy of the measurement of $B_{r\ av.}$ is about 0.2-0.3 G. This measurement method was used for correcting the radial component of the magnetic field and the magnetic field responses of iron elements in the central part of the Phasotron. The value of the radial component was corrected from 15 G to 1-2 G.

To measure the radial component of the magnetic field at the IBA C235 cyclotron, a measurement equipment on the basis of a set of search coils was designed and tested. The system consists of the measurement disk with 35 search coils, alignment and pneumatic system for the vertical shift of the disk. The system at the test stand is shown in Fig.4. The search coil system is planned to be used for measuring of the radial component of the magnetic field at version V3 of the C235 cyclotron.

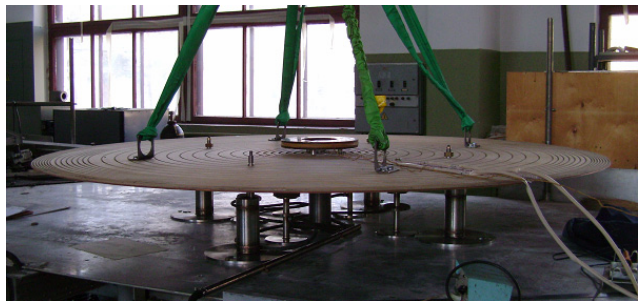

Figure 4: Measurement disk with search coils for the C235 cyclotron.

REFERENCES

[1] J.I.M.Botman, H.L.Hagedorn, "Median Plane Effects in the Eindhoven AVF Cyclotron", IEEE Trans. On Nucl. Science, Vol. NS-28, No.3, p. 2128.

[2] S.Brandenburg et al., "Vertical Beam Motion in the AGOR Cyclotron", Proc. of EPAC 2004, Lucerne, Switzerland, p. 1384-1386.

[3] J.Stursa et al., "The Axial Injection System of the Isochronous Cyclotron", Proc. of EPAC 2002, Berlin, Germany, p. 1513-1515.

[4] E. Bakevicz et al., "Extraction of Protons with the Energy of 35 MeV from the Upgraded AIC-144 Cyclotron", NUKLEONIKA 2001; 46(2), p. 51-57.

[5] N. Zaplatin et al., "Magnetic Field Median Plane Determination and Shaping for the JINR Phasotron", JINR, P9-82-925, Dubna, 1982.

[6] Y. Jongen et al., "IBA C400 Cyclotron Project for Hadron Therapy", Proc. of 18-th Cyclotrons and Their Application International Conference, 2007, Giardini Naxos, Italy, p. 151-156.

[7] Y. Jongen et al., "Computer Modeling of Magnetic System for C400 Superconducting Cyclotron", Proc. of EPAC 2006, Edinburgh, UK, p. 2589-2591.

[8] D.P. Vasilevskaya, Yu.N. Denisov, Instruments and Experimental Techniques, No.3, 1959.

[9] D. Vandeplassche, Y. Paradis, "Radial Field Mapping in C235", IBA internal report, January 6, 2006.

[10] A.Roy et al., "Median Plane Magnetic Field Mapping for Superconducting Cyclotron (SCC) in VECC", Proc. of APAC 2007, Indore, India, p. 652-654.

[11] N. Morozov, P. Shishlyannikov, "The Method of Experimental Determination of the Mean Radial Magnetic Field Component for the JINR Phasotron", JINR, P9-82-926, Dubna, 1982.

STUDY OF MAGNETIC FIELD IMPERFECTIONS OF KOLKATA SUPERCONDUCTING CYCLOTRON

J. Pradhan†, M K Dey, J Debnath, U. Bhunia, S Paul, C Mallik and RK Bhandari
VECC, Kolkata, India.

Abstract

Analysis of the magnetic data obtained during the magnetic field mapping of Kolkata superconducting cyclotron showed imperfections in the main magnetic field. Since the main magnet of the superconducting cyclotron is three fold rotationally symmetric, any deviation from this symmetry creates imperfections in the magnetic field. Generally, 1st and 2nd harmonic components are inherently present in the field due to assembling errors in iron/coil. A major portion of these imperfections is attributed to the misplacement/tilting of the iron pole tip with respect to coil. The error in positioning of main superconducting coil with respect to surrounding iron produces another imperfection. Pole tip deformation due to rise of temperature produces field imperfection. This paper reports the various possible sources of imperfection in general and their estimation. The calculation was compared with measured data to find out the actual cause of imperfections and necessary corrections have been carried out.

INTRODUCTION

The Kolkata superconducting cyclotron magnet was commissioned and detail magnetic field mapping and corrections was carried out [1]. Measured data is analysed for field imperfection studies. It is found that the imperfections exist and it is required to identify the actual cause of imperfection in order to carry out the necessary corrections. Magnetic field has three fold rotational symmetry with respect to its axis and mirror symmetry with respect to the median plane. Any deviation from these symmetries creates imperfections in the magnetic field and can be express in terms of different harmonics. A first harmonic of 2 or 3 gauss is sufficient to disturb the beam as it passes through a $\nu_r = 1$ resonance. This paper discusses the different sources of imperfections in general and it's analysis, which was carried out to estimate such errors. The calculation was compared with measured data to find out the actual cause of imperfections and necessary corrections have been carried out.

MODEL & ANALYSIS

Three-fold symmetry dominated magnetic field distribution is a characteristic feature of the three-sector geometry of this cyclotron. Deviation from the three-fold symmetry arises out of manufacturing tolerances and assembling errors, which create, unwanted harmonics (especially 1st and 2nd harmonics). The contribution of field imperfection comes from the positional errors of superconducting coil and sectored iron pole tips. A major portion of these imperfections is attributed to the misplacement/tilting of the iron pole tip, which produces the main azimuthal variation in the field. It is important to determine the positioning errors of the pole pieces by calculating field imperfections produced from combinations of simple displacement of pole pieces and comparing it with the measured data. The presence of very large magnetic field (~5T), in the superconducting cyclotron creates saturation of iron pole tips near the median plane. So, in the model used to calculate magnetic field produced by asymmetric pole tips, it is assumed that the iron is uniformly magnetised in the vertical direction. And the field can be represented in terms of surface current distribution flowing in the direction perpendicular to magnetization direction in a closed loop. The magnetization current density is given by $\vec{J} = \vec{\nabla} \times \vec{M}$, where $\vec{M}$ is magnetization vector of iron [2]. The accuracy of the calculated field is reasonably satisfactory and calculation of this type has long been used [3]. The uniform M calculations are faster and in view of the reasonable accuracy, we have adopted this method to compute the field of 3-dimensional pole tips.

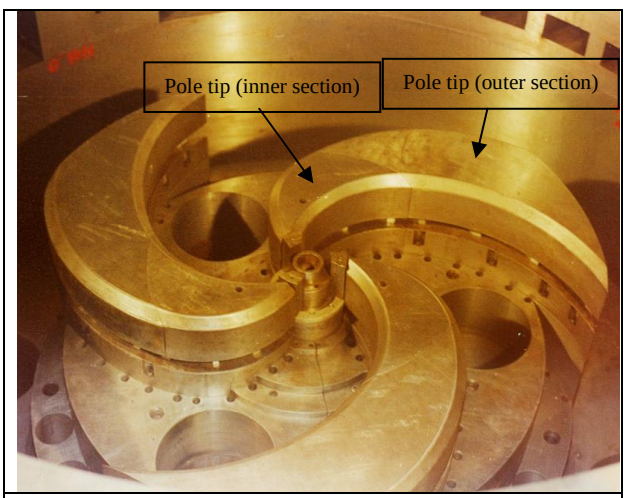

Figure 1. Pole tips view from the top

We have taken saturation magnetization M=21.4 kG. For a given geometry of the iron piece, the code generates the magnetic field using Biot Savart's law and carries out Fourier analysis to calculate field imperfections in terms of different harmonics.

The error in positioning of main superconducting coil with respect to the iron pole pieces produce 1st harmonic which is dominating at higher radius. Tilting of coils and

† jpradhan@veccal.ernet.in

measurement zig plane also produces field imperfections in the measured data. We introduced known shifts to 3-fold symmetric field at a particular direction and used 3rd order formula

$$Bz(r,\theta,z)=Bz(r,,\theta,0)-0.5 * z^2 *LBz(r,,\theta,0)$$

Where L is the 2-dimensional Laplace operator, to get the off-median plane field and carried out Fourier analysis in the shifted coordinate frame

We have simulated the thermal expansion of pole tip due to the rise of temperature, possibly because of water supply failure in the trim coils. Pole tip is assumed to be fixed at one side, where it is bolted. Magnetic field in the median plane is calculated using finite element code ANSYS™. We have considered pole tips with a constant and uniform magnetisation. Temperature variation of iron magnetisation is also considered in the simulation.

RESULTS & DISCUSSION

Subtracting the fields from the original position of the pole tips with the field from the displaced position has generated a number of imperfection fields. Such displacement fields are then superimposed to study the combined effect. Fourier analysis is performed to calculate different harmonics specially 1st and 2nd harmonic component of the field.

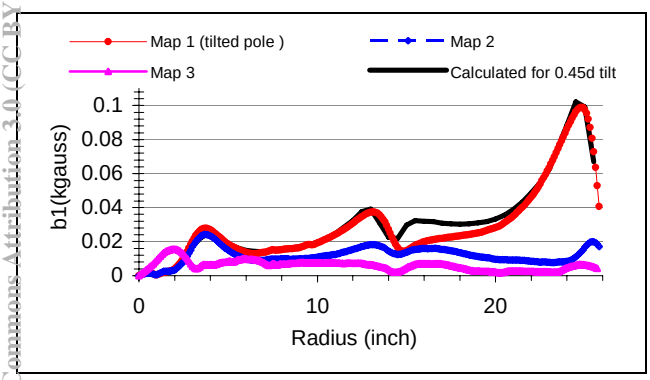

Figure 2. Comparison of 1st harmonic field amplitude for three successive measurements and calculation for 0.45° tilts of outer section of pole tip

We have studied number of imperfection caused by in-plane displacement, in-plane rotations, vertical displacement vertical tilts and so on and compare them with measurement. A series of measurement data taken initially has a 1st harmonic of about 100 gauss for all the grid points as shown in figure 2 as map 1(tilted one). Displacement fields are calculated for both the inner and outer section of pole tips. It is found from the calculation that a slight tilt of the outer section by about ~ 0.45° with respect to inner section of pole tip would create a similar 1st harmonic ~ 100 gauss to the main magnetic field data as shown in figure 2.

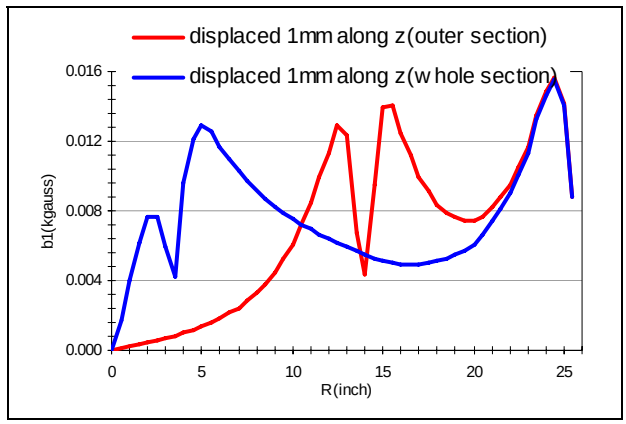

Figure 3. Radial distribution of 1st harmonic amplitude for pole tip displacement of 1mm along Z- direction

All the bolts were tightened properly, and further field mapping shows significant reduction of 1st harmonic imperfection in the magnetic field (map 2 in figure 2). The remaining imperfection of 1st harmonic component (~ 20 gauss) is from some other sources, which have been identified and reduced further by adding shims. Vertical displacements of 1mm along Z direction of the inner and outer section of the pole tip separately and combining the fields to get the first harmonic component is shown in figure 3.

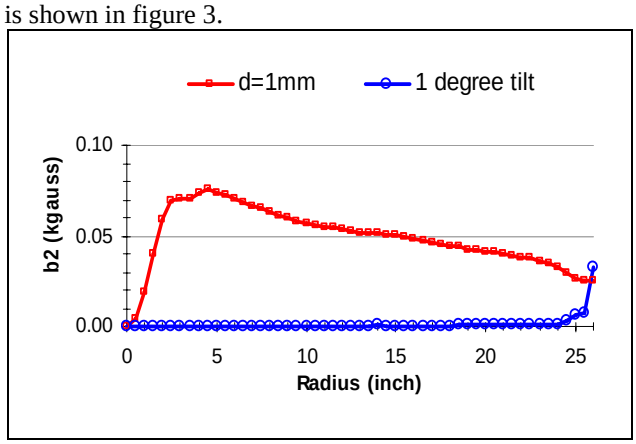

Figure 4. Radial distributions of 2nd harmonic distribution for a shift of 1mm and 1˚ tilt of measurement zig

The axis of measurement grid generally does not match with the symmetry axis of the magnetic field, and will introduce additional field imperfection. It is found that the 2nd harmonic component is more dominant, about 75 gauss for a shift of d=1mm compared to other harmonics and is shown in figure 4. The figure also shows 2nd harmonic imperfection due to 1° tilt of measurement zig about its axis. The symmetry axis required for field analysis is obtained by minimizing the 2nd harmonic component from the measured field by iterative search [4].

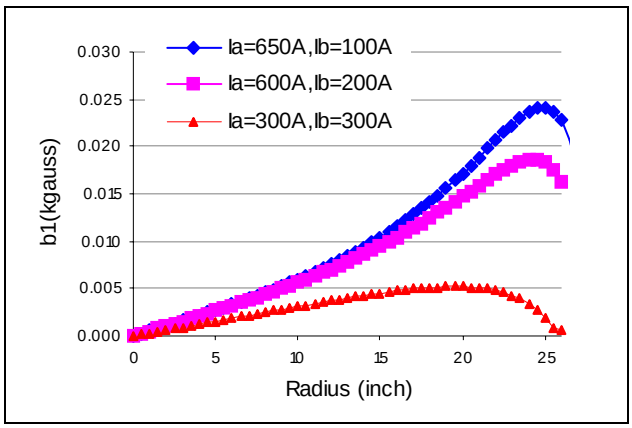

Figure 5. Radial distribution of 1st harmonic amplitude for 1mm shift of coil for different combination of α-coil and β-coil

In superconducting cyclotron two superconducting coils (α-coil & β-coil) should be well centred with respect to iron pole pieces, otherwise it produces 1st harmonic imperfection and also un-balanced forces. This is a variable term, which depends on the current settings of both the coils as shown in figure 5 for 1mm off-centre. Superconducting coils were centered with respect to iron pole pieces by reducing this 1st harmonic amplitude and knowing its phase.

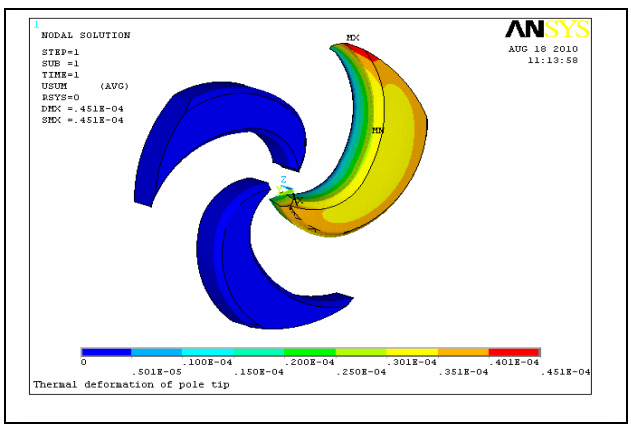

Figure 6. Thermal deformation of one of the pole tip due to temperature rise of 10˚ C

The rise of temperature in the pole tip will deform it and produce field imperfection in the median plane. We have estimated the 1st and 2nd harmonic amplitude for 10-degree rise of temperature and is shown in figure 7. It is observed that the harmonic amplitude is proportional to the rise of temperature.Pole tip deformation due to rise of 10˚ C is also shown in figure 6.

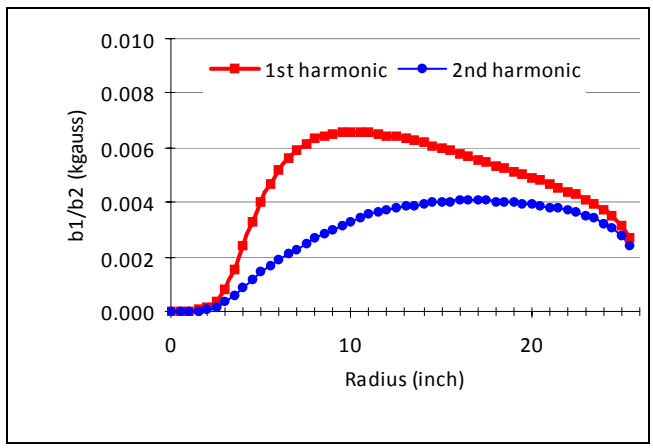

Figure 7. Radial distribution of 1st harmonic amplitude due to temperature rise of 10˚ C in the pole tip.

REFERENCES

[1] C. Mallik et al., "Magnetic field mapping of Kolkata superconducting cyclotron", presented in 18th International conference on cyclotrons and their applications CYCLOTRONS-2007, during Sept30-Oct5, 2007, Italy

[2] M M Gordan and D A Johnson, "Calculation of fields in a superconducting cyclotron assuming uniform magnetization of the pole tips" Particle Accelerators 1980 Vol. 10 pp 217-222.

[3] H G Blosser and D A Johnson, "Focussing properties of superconducting cyclotron magnet", Nuclear Instruments and Methods 121 (1974) 301-306

[4] M K dey, et al., "Determination of Symmetry Axis of Magnetic Field of K-500 Superconducting Cyclotron at VECC", Proc. of DAE-BRNS Symposium on Nuclear Physics (BARC), **Vol. 50**, 424 (2005).

OPTIMIZATION OF SECTOR GEOMETRY OF A COMPACT CYCLOTRON BY RANDOM SEARCH METHOD

P. Sing Babu, A. Goswami, P. R. Sarma and V. S. Pandit*
Variable Energy Cyclotron Centre, 1- AF, Bidhannagar, Kolkata-700 064, India

Abstract

This paper describes the procedure of optimizing the sector geometry of the magnet to obtain the desired isochronous field. The hill shape of the magnet is described in terms of a small number of parameters which are iteratively determined by random search technique geared to minimize the frequency error. 3D magnetic field data and results of equilibrium orbit code are used as input for the iterative optimization process.

INTRODUCTION

A 10 MeV, 5 mA four sector compact cyclotron for proton is under development at VECC Kolkata. Proton beam at 80 keV from 2.45 GHz microwave ion source (under testing) will be first collimated and bunched [1]. It will be injected axially in the central region where a spiral inflector will place the beam on the proper orbit. Two delta type resonators located in the opposite valleys will accelerate the beam and an electrostatic deflector will be used for the extraction. In general the magnet pole shimming is an iterative process [2,3]. Analytical formulas [4,5,6] are available for calculating the average magnetic field and betatron frequencies for a given configuration of the magnet geometry. But these formulas are not valid for high flutter field and particularly at the lower radii in the case of a compact cyclotron. Hence an equilibrium orbit code becomes necessary to obtain the frequency error. An acceptable phase shift of the particles with respect to rf determines the tolerance of the magnetic field isochronism. In this paper we present a shimming method, which gives smooth sector geometry of the hill. We have approximated the shape of the sector by a polynomial function of the radius, and minimized the frequency error by optimizing the coefficients of the polynomial by using random search technique.

METHOD OF OPTIMIZATION

We have used a 3D magnetic field code MagNet [7] to calculate the field in the median plane and obtained the frequency errors as a function of energy using equilibrium orbit code GENSPEO [8]. These frequency errors are then minimized by modifying the sector geometry.

For an N sector cyclotron, using hard edge approximation, we can write the following relations:

$$\theta_h(r)+\theta_v(r)=\frac{2\pi}{N} \tag{1}$$

$$\overline{B}(r)=\frac{\theta_h(r)\cdot B_h+\theta_v(r)\cdot B_v}{\theta_h(r)+\theta_v(r)} \tag{2}$$

$$\overline{B}(r)=\frac{B_0}{\sqrt{1-ar^2}} \tag{3}$$

where B_h and B_v are the hill and valley field respectively. B_0 is the isochronous field at the center of the cyclotron and $a=\left(\frac{qB_0}{m\cdot c}\right)^2$. Using equations (1-3) we can write

$$\theta_h(r)=\frac{2\pi}{N\cdot[B_h-B_v]}\left[\frac{B_0}{\sqrt{1-ar^2}}-B_v\right] \tag{4}$$

Expanding the above equation we get

$$\theta_h(r)=a_0+a_1r^2+a_2r^4+a_3r^6+\ldots+a_mr^{2m} \tag{5}$$

The polynomial coefficients a_0, a_1 etc. depend on B_h, B_v and average central field B_0. For the optimisation one has to start with an initial set of a_n values, and iteratively correct these to obtain the final optimized hill angle. At first the z-component of the magnetic field at the median plane is calculated for the initial sector geometry and frequency errors are obtained at n different discrete energies. The frequency error is defined as

$$\Omega(k)=\frac{\omega_0}{\omega(E_k)}-1 \tag{6}$$

where, ω_0 is the constant rotation frequency of the particle and $\omega(E_k)$ is the rotation frequency for the calculated magnetic field at energy E_k.

The second step involves the calculation of the elements of the $n\times(m+1)$ correlation matrix. For this it is required to calculate the magnetic field by slightly changing the coefficients say $a_i=a_i+\Delta a_i$ of the polynomial one at a time keeping all other coefficients and geometry constant. The same procedure is repeated for all other coefficients one by one. For the small change in polynomial coefficients Δa_i, the deviation in frequency errors $\Delta\Omega(1)$, $\Delta\Omega(2)$,… $\Delta\Omega(n)$ can be related linearly as

$$\Delta\Omega(k)=\frac{\partial\Omega(k)}{\partial a_0}\Delta a_0+\frac{\partial\Omega(k)}{\partial a_1}\Delta a_1+\cdots\frac{\partial\Omega(k)}{\partial a_m}\Delta a_m \tag{7}$$

and $$\frac{\partial\Omega(k)}{\partial a_i}=\frac{\Omega(k)\big|_{a_i+\Delta a_i}-\Omega(k)\big|_{a_i}}{\Delta a_i}. \tag{8}$$

*pandit@vecc.gov.in

While calculating the correlation matrix we have found that the values of the matrix elements at lower radii are very small. So for the optimisation of sector shape at lower radii we have added another term to the equation of hill angle $\theta_h(r)$. Now the modified hill angle becomes

$$\theta_h(r) = \sum_{i=0}^{m} a_i r^{2i} + g \cdot e^{-\alpha(r-r_0)^2} \quad (9)$$

Here, the parameter g controls the pole shimming in the central region, r_0 and α are chosen constant. Further, we have included the coil current as a parameter for the optimization so the total number of parameters becomes m+3 and the size of the correlation matrix is $n\times(m+3)$. The linear set of equations in the matrix form

$$\begin{bmatrix} \Delta\Omega(1) \\ \Delta\Omega(2) \\ \vdots \\ \Delta\Omega(n) \end{bmatrix} = \begin{bmatrix} \frac{\partial\Omega(1)}{\partial a_0} & \frac{\partial\Omega(1)}{\partial a_1} & \cdots & \frac{\partial\Omega(1)}{\partial a_{m+2}} \\ \frac{\partial\Omega(2)}{\partial a_0} & \frac{\partial\Omega(2)}{\partial a_1} & \cdots & \frac{\partial\Omega(2)}{\partial a_{m+2}} \\ & \vdots & & \\ \frac{\partial\Omega(n)}{\partial a_0} & \frac{\partial\Omega(n)}{\partial a_1} & \cdots & \frac{\partial\Omega(n)}{\partial a_{m+2}} \end{bmatrix} \begin{bmatrix} \Delta a_0 \\ \Delta a_1 \\ \vdots \\ \Delta a_{m+2} \end{bmatrix} \quad (10)$$

For the optimization of the parameters a_0, a_1,….a_{m+2}, we have used random search method. Here parameter a_{m+1} represents the coefficient g in equation (9) and a_{m+2} is the coil current parameter.

Random Search Method

In this method we have minimized the frequency error of the particle by a suitable combination of all the unknown parameters. The error term R is defined as

$$R = \sum_{k=1}^{n} \left(\Omega(k) - \sum_{i=0}^{m+2} \left(a_i \frac{\partial\Omega(k)}{\partial a_i} \right) \right)^2 \quad (11)$$

Here $\frac{\partial\Omega(k)}{\partial a_i}$ are the elements of the correlation matrix. Now the quantity R is minimized by varying the parameters a_i randomly. A set of parameters is chosen randomly within a small range for a_i, and the quantity R is calculated. This is done repeatedly until a small value of R is obtained. This gives an intermediate set of a_i. The process is repeated with random values chosen around the intermediate set of values. At each step the range for each parameter is decreased so that the search becomes faster. After a number of cycles of the process one obtains the minimum value of R and new values of parameters a_i. With this set of new parameters a_i, a new hill shape is obtained, and the magnetic field is calculated once again. The iterations are continued until the frequency error falls below the required tolerance. In random search technique one can include constraints in the problem such as maximum coil current, maximum and minimum hill angle etc. One can reject a solution if the constraints are not fulfilled.

RESULTS

The above iterative method has been applied to optimize the sector geometry of our 10MeV, 5mA four sector compact cyclotron for proton. The preliminary design of the magnet was obtained using hard edge approximation method [1,2]. We have chosen maximum hill field of 1.5T and valley field of 0.25T so that we can get high flutter. A high flutter provides strong focusing in the vertical direction. The main idea was to provide the vertical betatron tune > 0.5 at all radii for handling the space charge defocusing force of 5mA beam. The hill gap is 5 cm and the valley gap is 50 cm. We have used 3D MagNet code for the field calculation. Proper symmetry considerations allowed us to use only 1/16 portion of the magnet, as shown in Figure 1 for field calculation.

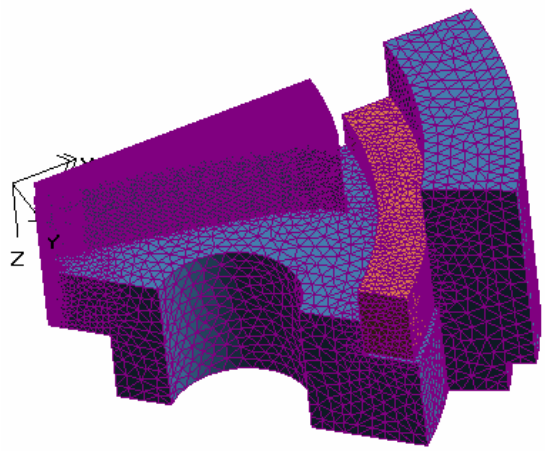

Figure 1: Model of the magnet with mesh.

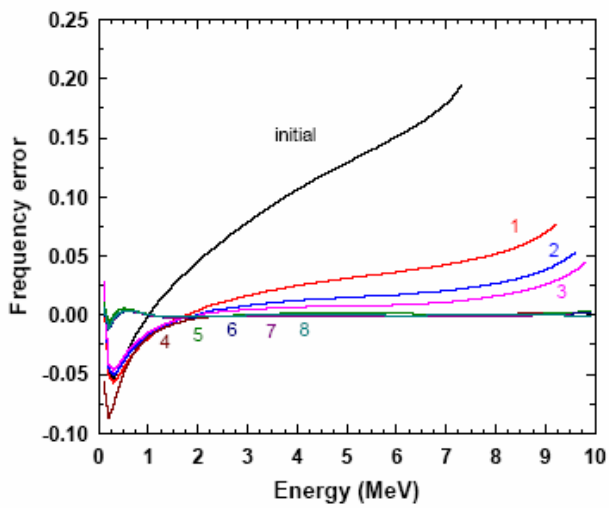

Figure 2: Decrease in frequency error as a function of energy at different iterations 1,2,3… .

In the optimization we have used six parameters a_0, a_1, a_2, a_3, a_4, a_9 from the polynomial and other two as coil current and g. We have started with constant angular width of the hill shape equal to 20 deg. and current in the coil is set equal to 500 A (total no. of turns ~200). The values of frequency error as a function of energy are shown in Figure 2 for successive iterations. After 8 iterations we achieved the magnitude of frequency error < 10^{-4} at all energies.

Figure 3 shows the variation of the mean square frequency error $\sigma_\Omega{}^2$ as a function of the iteration number.

$$\sigma_\Omega{}^2 = \frac{1}{n}\sum_{k=1}^{n}\Omega^2(k) \qquad (12)$$

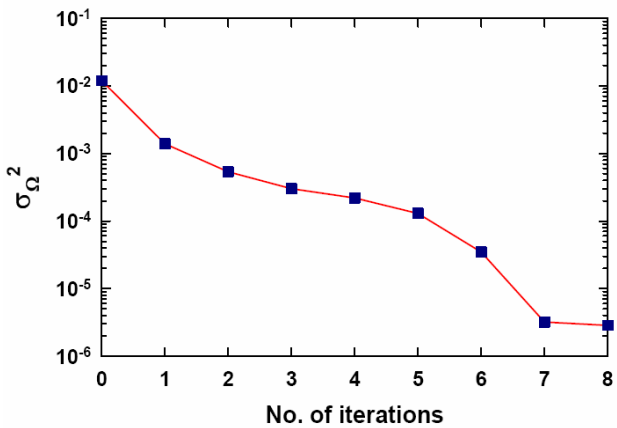

Figure 3: Mean square frequency error as a function of the number of iterations.

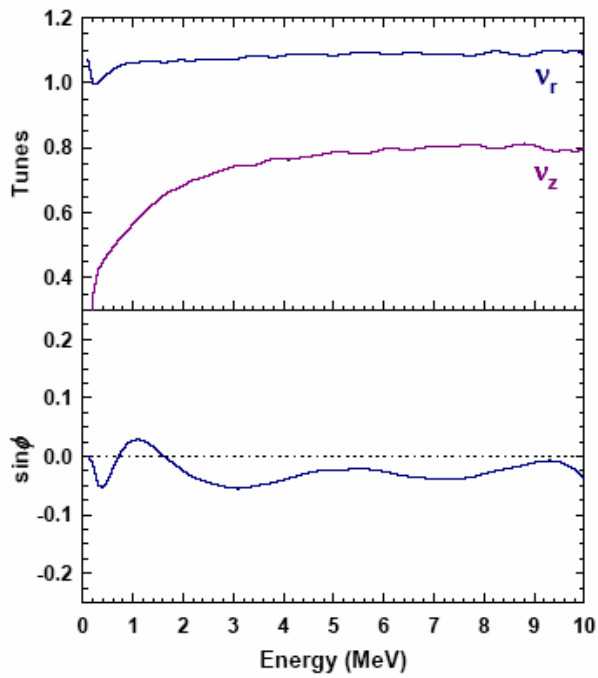

Figure 4: Variation of betatron tunes and phase slip sinϕ as a function of energy.

The radial and axial tunes, integrated phase shift etc. were found out for the optimized sector shape using the equilibrium orbit program as shown in Figure 4. The phase excursion in the entire region is limited within $\pm 2^0$.

We have also checked the centering of the accelerated orbits using the optimized magnetic field data. The electric field E in the accelerating gaps of the two resonators has been approximated by a Gaussian function. Figure 5 shows the position of the accelerating gaps (G-1 to G-4) in the median plane and accelerated orbits of protons up to the extraction radius.

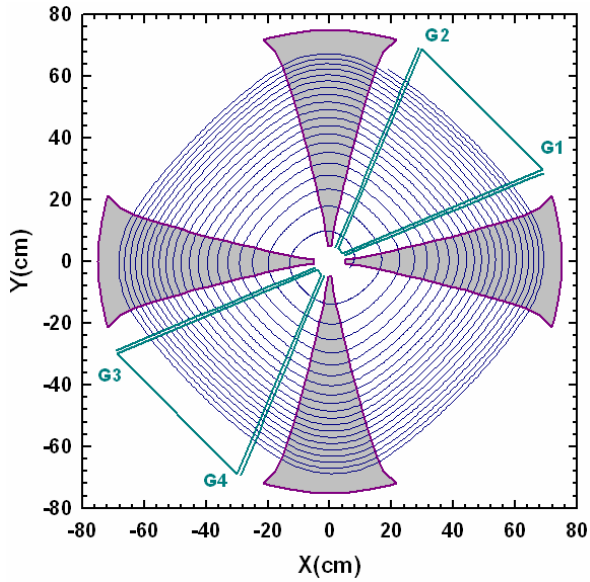

Figure 5: Location of the accelerating gaps and optimised accelerated orbits for proton from 80 keV to 10 MeV.

CONCLUSION

This paper describes a technique based on random search for obtaining the isochronous magnetic field for a 10MeV, 5mA compact cyclotron by optimization of pole profile of the hill. This method uses less number of parameters and convergence is fast.

REFERENCES

[1] V. S. Pandit, "Development of ion source and injection system for high current compact cyclotron" Indian Particle Accelerator Conference InPAC-05 (2005) 13

[2] B. Qin, D. Z. Chen, L. C. Zhao, J. Yang and M. W. Fan, Nucl. Instr. and Meth. A 620 (2010) 121.

[3] W. Kleeven *et.al*, "Magnetic Field Calculation & Shimming of the Self-Extraction Cyclotron" Proc. of the 16th Int. Conf. on Cyclotrons and Their Applications, East Lancing,USA (1986), p. 348.

[4] J. R. Richardson, "Sector Focusing Cyclotrons", Progress in Nuclear Tech. & Instru., Vol. 1, North Holland (1965)

[5] A. Goswami, P. Sing Babu and V. S. Pandit, Nucl. Instr. and Meth. **A 562** (2006) 34.

[6] H. L. Hagedoorn and N. F. Verster, Nucl. Instr. and Meth. 18,19 (1962) 201.

[7] MagNet User Guide, Infolytica Corporation.

[8] M. M. Gordon, Particle Accelerators, **16** (1984), pp. 39-62.

DESIGN STUDY OF MAGNETIC CHANNEL AT NIRS-AVF930

Satoru Hojo[A], Mitsutaka Kanazawa[A], Katsuto Tashiro[A], Toshihiro Honma[A], Nobuyuki Miyahara[A], Akinori Sugiura[A], Takanori Okada[B], Takashi Kamiya[B], Yuichi Takahashi[B], and Kouji Noda[A]
[A] National Institute of Radiological Sciences,
4-9-1 Anagawa, Inage-ku, Chiba 263-8555, JAPAN
[B] Accelerator Engineering Corporation,
3-8-5 Konakadai, Inage-ku, Chiba 263-0043, JAPAN

Abstract

In the NIRS-AVF930 cyclotron, a current magnetic channel has been used for ten years, and the flow of cooling water gradually decreases. Therefore, the high energy operation such as 70 MeV proton became recently difficult. As the design specification of this magnetic channel is very severe, the flow velocity of cooling water is very fast as 5.4 m/sec. The condition of the current magnetic channel and the design consideration of a new one will be presented.

INTRODUCTION

The NIRS (National Institute of Radiological Sciences) -AVF930 cyclotron is used mainly for RI production [1]. The other utilizations are the studies on radiation dosimeters and radiation damage tests, where height energy proton beam such as 70 MeV was frequently used. The proton energy of 70 MeV is almost maximum in NIRS-AVF930 operation. However, that high energy operation became difficult recently, and the source of this problem is decreases in cooling water of the magnetic channel. The magnetic channel is composed of eight coil units made with hollow conductor, and two coil units among them are cooled with a chiller system in the high energy operation. Those two coils are longest coil in the magnetic channel. Therefore, low power consumption and low temperature at the outlet of cooling water is needed for of high energy operation in the new design magnetic channel.

PRESENT STATE CONDITION OF THE MAGNETIC CHANNEL

In the current magnetic channel, the maximum design current is 1300 A, and the current density is 56.5 A/cm^2. This magnetic channel is composed of a hollow conductor type that size is 6×6 mm^2 and diameter of cooling water hole is 4 mmϕ. The A2 coil(see Figure 1) is the longest coil in a magnetic channel, and has the problem that is rises of the temperature at the outlet cooling water. In Figure 2, measured temperatures of the cooling water at outlet of the A2 coil were plotted against the current of the magnetic channel. The water temperature at the outlet was increased up to 70 degrees at 1000 A, where interlock of water temperature will work.

There are two causes of the temperature rise in the present magnetic channel. One of the causes is decreases in flow of cooling water. At the beginning, flow of cooling water in A2 coil was 3.0 L/min with pressure drop of 1.2 MPa, but that is 2.14 L/min at present with same pressure drop. Another cause is increase in resistance of magnetic channel. At beginning, resistance of magnetic channel was 48.9 mΩ, but now that value is 54.2 mΩ. Therefore, power consumption increased with this higher resistance.

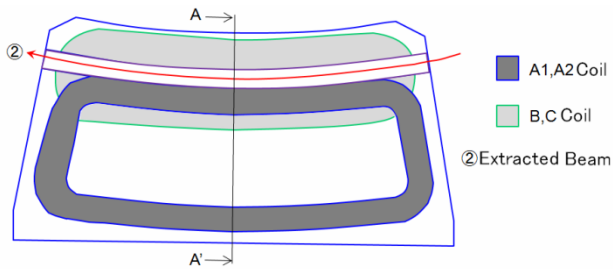

Figure 1a: The horizontal sectional view at median plane.

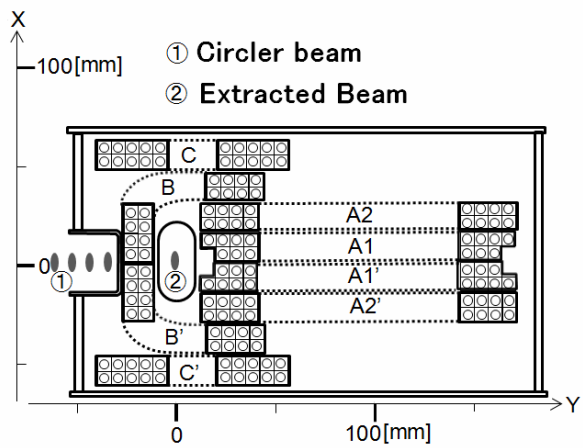

Figure 1b: The vertical sectionals view at a plane A-A'.

STRUCTURE OF THE MAGNETIC CHANNEL AND NEW DESIGN

Figure 1b shows the cross section of the current magnetic channel, which is composed from the eight coils with four types. Those eight coils are made of the hollow conductor that has cross section of 6×6 mm^2 with hole of 4 mmϕ in diameter.

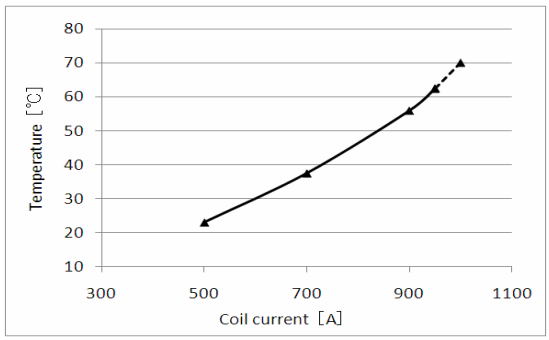

Figure 2: Temperatures of the cooling water at outlet of the A2 coil. Inlet 10 Deg, Flow rate 2.14 L/min

The temperature rise of cooling water is maximum at the A2 coil in those eight coils. The A2 coil was wound outside of the extracted beam orbit. The vertical space for the magnetic channel is limited at 140 mm with magnetic pole of the NIRS-AVF930.

In this design study, size of the A2 coil is 6×9 mm2 to decrease temperature of cooling water. The cross sectional area of conductor is expanded by a factor of 1.6 compared with the existing magnetic channel. The resistance at the A2 coil will be reduced by 40% and we can reduce its power consumption.

In addition, the cross sectional area of water flow is expanded by a factor of 1.4 compared with the existing magnetic channel, thereby the temperature rise is suppressed almost 50% at the outlet of cooling water in the A2 coil.

However, expansion of the conductor make problem that is influence to the magnetic field. Therefore, using POISSON/SUPERFISH programs from LAACG[2], the magnetic field is estimated for the updating design of the magnetic channel.

The polarity of leakage magnetic flax at orbit of circulating beam in the cyclotron is same a as cyclotron main magnetic flax. The leakage flax is very important because circulating beam passes several times on the line "P" in figure 4.

As the first step, the cross sectional area of A2 coil conductor was expanded, which is Figure 4(2), and calculated magnetic fields on the line "P" are plotted in Figure 5(2). This leakage magnetic field is high compared with the present magnetic channel, so that adjustment is necessary such as change of the B-coil position. In the new design, the B-coil position is moved to inside at the cyclotron, and turn radius in the B-coil conductor is smaller than the present design, it shown to the Figure 4(3). This result of calculated leakage magnetic field at new design is plotted in Figure 5(3).

The calculated leakage magnetic field with the new design is similar to the leakage field of the present magnetic channel.

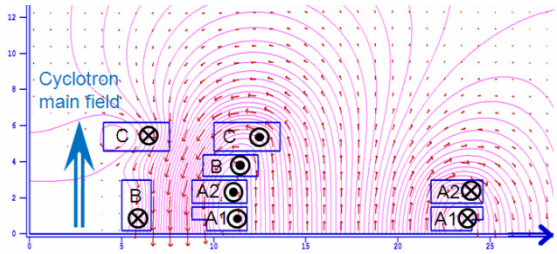

Figure 3: The magnetic field 2D-simulation by POISSON/SUPERFISH.

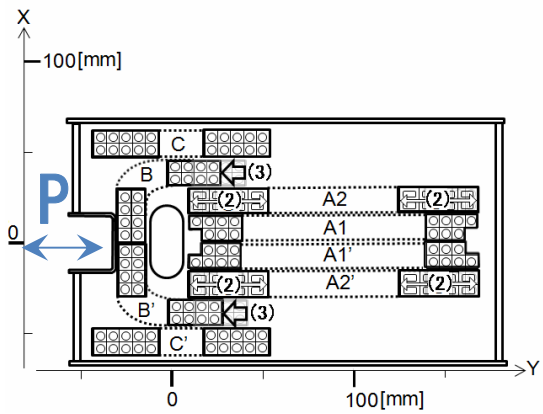

Figure 4: Conductor layout plan of magnetic channel.

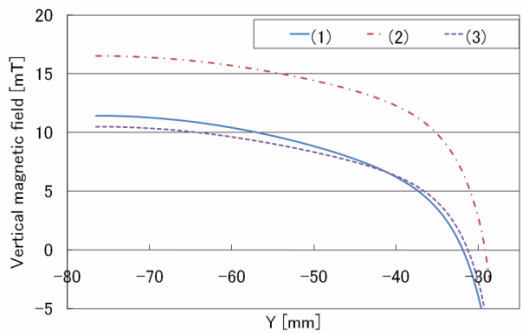

Figure 5: Vertical magnetic field at Line "P".

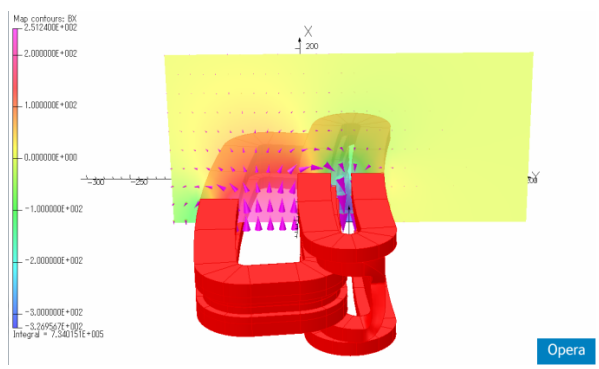

Figure 6: The magnetic field 3D-simulation by Opera-3D/TOSCA.

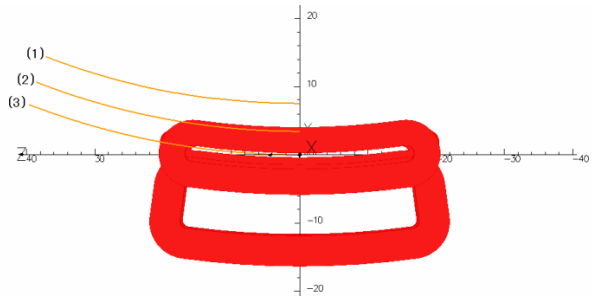

Figure 7: Arc orbit for comparing to magnetic field in OPERA-3D/TOSCA. (1) Radius 90cm from centre of cyclotron. (2) Radius 94cm from centre of cyclotron. (3) Radius 97.5cm from centre of cyclotron. (extracted beam orbit)

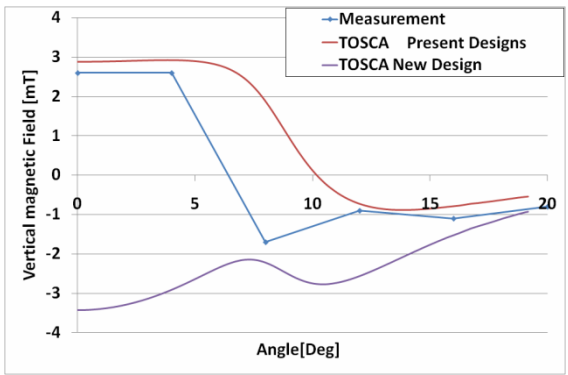

Figure 8: Magnetic field at arc orbit of radius 90 cm.

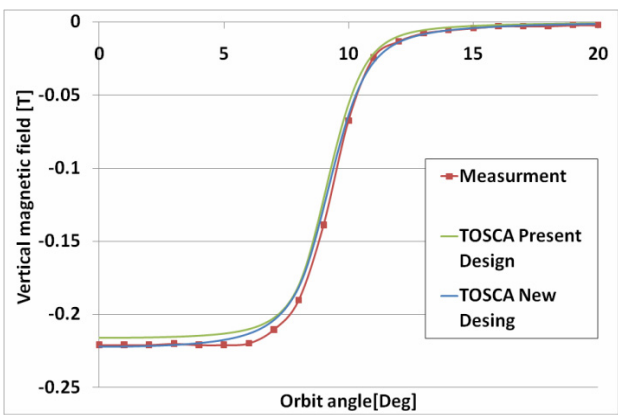

Figure 9: Magnetic field at extracted beam orbit of radius 97.5 cm.

In addition, using Opera-3D/Tosca programs from Vector Fields [3], the 3D magnetic field calculation was performed for updating the design of the magnetic channel. The calculated results of magnetic fields were compared between the present magnetic channel and the updated one.

In the magnetic field have two important points at the magnetic channel.

One is enough the magnetic fields for extracted beam at extraction orbit that has radius of 97.5 mm. The other important point is reducing the leakage field at orbit of

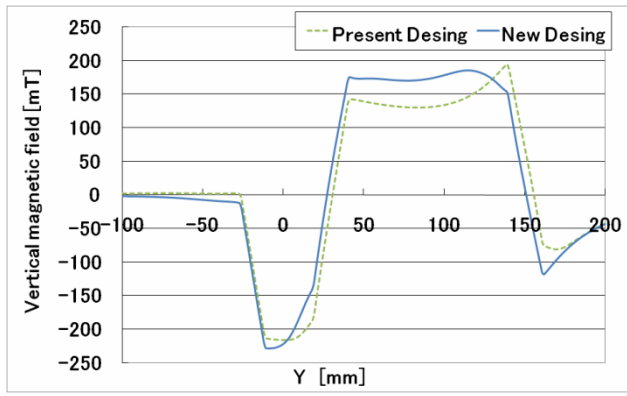

Figure 10: Magnetic field at centre of magnetic channel

circulating beam in the cyclotron. Therefore, the leakage field is compared in the orbit, where orbital radius is 90cm. These calculated magnetic fields with the both designs are plotted in figures 8, 9 and 10. Additionally, the measured leakage magnetic fields of the present magnetic channel are plotted in Figure 8.

At the circulating orbit, calculated magnetic field will agreed with measured magnetic field in the present magnetic channel. In contrast to this agreement, polarity of calculated magnetic field with the new design is inverse, and maximum value of new design is 3.4 mT and angular distribution of leakage magnetic field is broad.

At the extracted beam orbit, the calculated magnetic field in new design is enough for beam extraction.

Moreover, the magnetic fields at extracted beam position (Y=0) have a gradient with the new design, which is shown in Figure 10.

For this reason, the optimization of conductor arrangement is further required in order to low leakage magnetic field and smaller radial gradient in extracted beam position.

CONCLUSIONS

The magnetic field calculation is performed for the updating design of the magnetic channel, where the A2 coil was expanded the cross section area of conductor and cooling water hole. Calculating with Opera-3D/Tosca programs from Vector Fields, the radial distributions of the magnetic fields have a radial gradient at extracted beam area. Therefore, the further optimization of arrangement at conductor is necessary.

REFERENCES

[1] M. Kanazawa, S. Hojo, T.Honma, K.Tashiro, A. Sugiura, T. Okada, T. Kamiya, Y. Takahashi, “Present operational status of NIRS cyclotrons”, Proceedings of this conference, MOPCP022.

[2] POISSON/SUPERFISH Group of Codes, Available at the Los Alamos National Laboratory, LA-UR-87-126 (1987). http://laacg1.lanl.gov/laacg.

[3] TOSCA, Vector Fields Ltd., www.vectorfields.com, Software for electromagnetic design, Oxford, UK.

DESIGN STUDY OF AVF MAGNET FOR COMPACT CYCLOTRON*

H.W. Kim, J.H. Oh, B.N. Lee, J.S. Chai#
Accelerator and Medical Engineering Lab., SungKyunKwan University, Suwon, 440-746, Korea

Abstract

K=100 separated sector cyclotron and its injector cyclotron design is started on April, 2010 at Sungkyunkwan University. The main purpose of the K=100 separated sector cyclotron is producing proton and deuteron beam for ISOL which generate rare isotopes to accelerate RI beam for basic science research. In K=100 separated sector cyclotron facilities, two 8MeV sector focused cyclotrons will be used as an injector cyclotron for the main cyclotron.

In this paper, an Azimuthally Varying Field (AVF) magnet for the 8MeV injector cyclotron is designed to produce 8MeV proton beam and 4MeV deuteron beam. All field simulations have been performed by OPERA-3D TOSCA for 3D magnetic field simulation. The assignments of these injector cyclotrons are generating 8MeV, 1mA proton beam and 4MeV deuteron beam that inject to the main cyclotron.

INTRODUCTION

An 8 MeV H- injector cyclotron for K=100 separated sector cyclotron is being designed at Accelerator and Medical Engineering Laboratory (AMEL), SungKyun-Kwan University. It will provide an 8 MeV, 1 mA proton and 4 MeV deuteron beams for K=100 separated sector cyclotron and it is the main cyclotron which is located before ISOL for generating RI beam.

A design study of 8 MeV H- injector cyclotron magnets is described in this paper. This injector cyclotron has normal conducting magnet with 4 sectors so that is AVF and fixed RF frequency machine. The diameter of magnet is 1.4 m, pole is 0.4 m and height is 0.76 m. The top and bottom yoke of magnet has one hole at each valley (4 holes total) and those holes will be used for other subsystem devices - vacuum pumps and RF system [1]. The maximum field on the mid-plane is 1.95 T. Other magnet parameters are shown in Table 1 and the 1/8 model of designed magnet is shown in Figure 1.

3D modelling process was done by 3D CAD system, CATIA P3 V5 R18 [2] and whole field calculations were processed under computer simulation. Precise 3D field calculations had been performed by OPERA-3D TOSCA [3]. To reduce the field calculation time, batch files were developed which can generate model, mesh and field map automatically in TOSCA modeller and post processor. The beam dynamics program OPTICY [4] is used for calculation of the tunes.

*Work supported by Ministry of Education, Science and Technology, Republic of Korea. Also Department of Energy Science and School of Information and Communication Engineering of SungKyunKwan University supported this project.
#jschai@skku.edu

MAGNET DESIGN

Three steps were done to design isochronous cyclotron magnet. Some basic calculations were done first to determine parameters of magnet. Harmonic number and RF frequency was set before the calculation of gamma value, magnet rigidity at maximum beam energy and extraction radius. After the consideration of parameters 3D CAD drawing with CATIA P3 V5 R18 [2] is followed. 3D field simulation using OPERA-3D TOSCA [3] is done with those 3D drawings.

Table 1: Parameters of magnet

Parameters	Values
Maximum energy	8 MeV / 4 MeV
Beam species	H-, D-
Central field	1.15 T
Pole radius	0.40 m
Extraction radius	0.35 m
Number of sectors	4
Hill / Valley gap	0.03 / 0.39 m
Hill angle	48°
B-field (min.,max)	0.30, 1.95 T

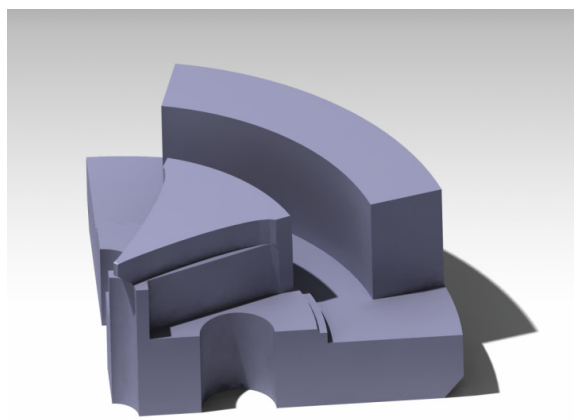

Figure 1: 1/8 model of designed magnet.

0.41 T-m magnet rigidity is needed at the extraction radius and the proton beam energy is 8 MeV at there. The RF frequency is set to 70 MHz, so central field of the magnet is 1.15 T.

3D CAD drawing can be converted to 2D drawings with CATIA P3 V5 R18 [2], and Figure 2 shows that

result. 3D drawing-Figure 1 is converted and specific magnet parameters are shown.

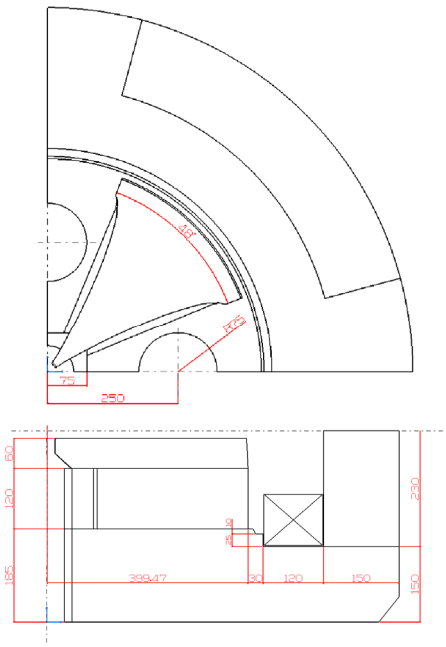

Figure 2: 2D drawings converted from 3D drawing

All 3D field simulation was done by OPERA-3D TOSCA [3]. The drawings from CATIA are imported to OPERA-3D modeller and modified to generate surface and volume mesh.

The material of magnet is determined on this step. Low carbon steel, ANSI 1008 and ANSI 1010, were considered to main material and ANSI 1008 is selected to main material of magnet. Both steels are good magnetic materials but saturation point of ANSI 1008 is slightly higher than ANSI 1010. The difference of saturation point between two materials is approximately 0.2 T.

Local mesh is used to increase accuracy of simulation. The mesh size adapted to pole part is much smaller than boundary part and return yoke part. Figure 3 shows the meshing result before start field calculation. Total number of calculated node is about 2.2 million and only 1/8 nodes were simulated because of the symmetrical model geometry. Dummy vacuum gap is used to check the precise magnetic flux density on mid-gap. It contains a lot of mesh so that can show the smooth field distribution on mid-gap plane.

After the field calculation, the results were reprocessed with OPERA-3D post processor to check the field on the surface of model, vector map of magnetic flux and field map of mid-plane. Figure 4 shows the result of post processing.

The batch files for OPERA-3D modeller and OPERA-3D post processor were made to accelerate the modelling process and reproducing time. Files for OPERA-3D modeller import the 3D CAD file automatically and modifies the model. After the modification, meshing is also automatically done by itself. Files for OPERA-3D post processor performed that generating field on the surface of model, vector map of magnetic flux and field map of mid-plane.

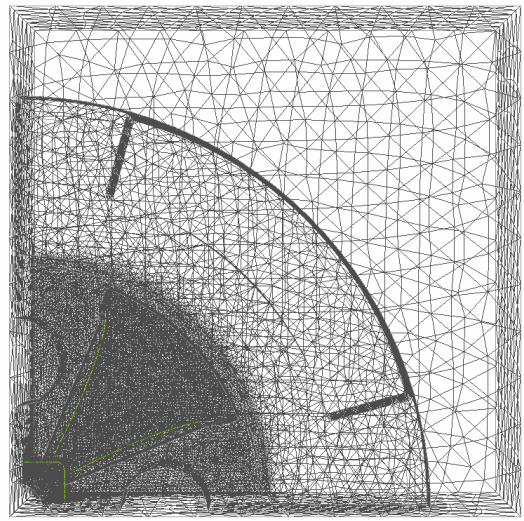

Figure 3: Local meshed model for precise simulation.

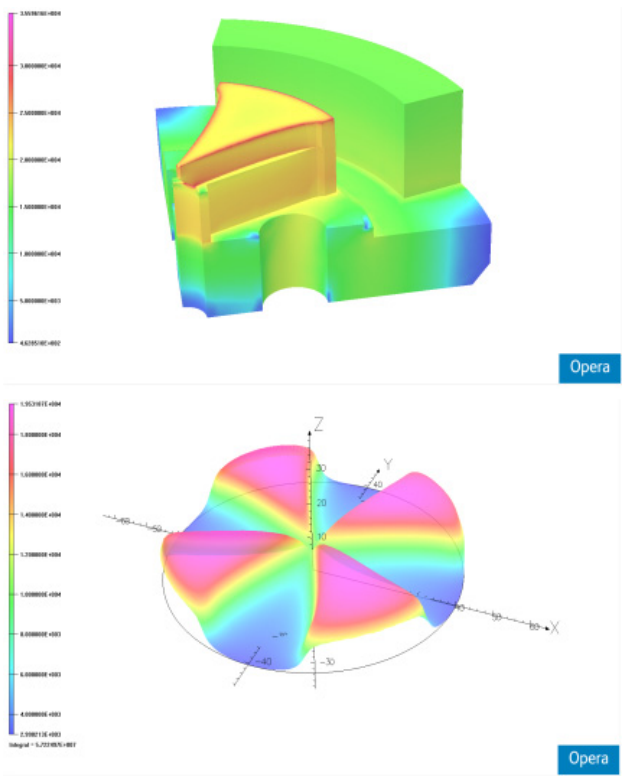

Figure 4: Results of post processing; field on the surface of model and histogram of magnetic field on mid-gap.

Shimming process is necessary to make isochronous field. The average magnetic field of mid-gap must increase gradually with radius of pole [5]. The method that change hill-valley ratio along the radius is a way to make isochronous field. Using the spline curve, 37 points were set along the pole radius and they have specific angles to make the isochronous field. Figure 5 shows the designed side shim.

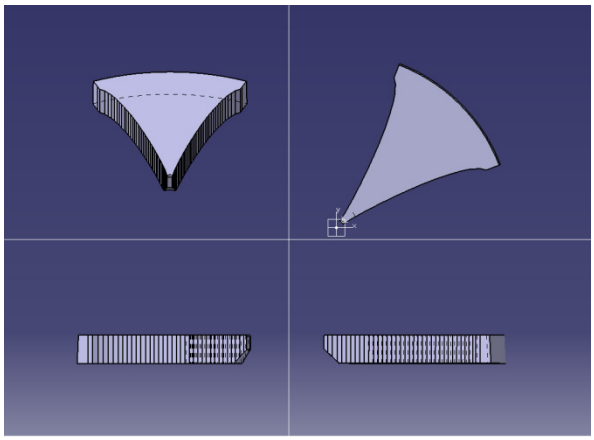

Figure 5: Side shim design using CATIA V5.

The designed isochronous field and calculated isochronous field are shown in Figure 6. Designed field is increased with pole radius and that field have 25 gauss error boundary.

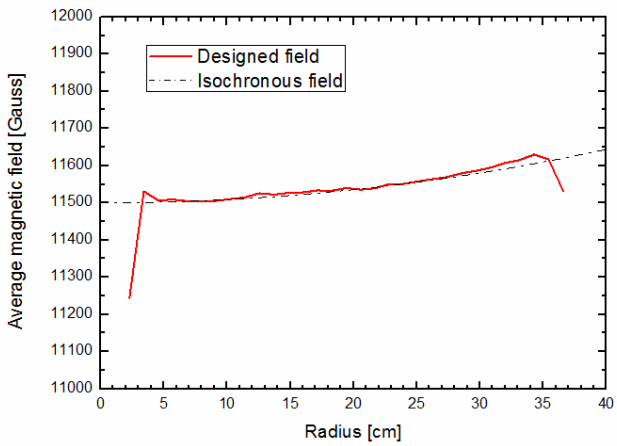

Figure 6: Average magnetic field graph of designed magnet with idle isochronous field.

The OPTICY [4] is own-made program to calculate the tunes and phase error for beam dynamics. Fig. 7 contains the tune diagrams from OPTICY.

CONCLUSION

The design study of 8 MeV injector cyclotron for K=100 separated sector cyclotron facility is almost done. Designed magnet shows isochronous field with high precision. The OPTICY [4] will be modified to be suitable for beam tracking calculation. It is expected that the full analysis and whole conceptual design report of 8 MeV injector cyclotron magnet will be finished in November, 2010.

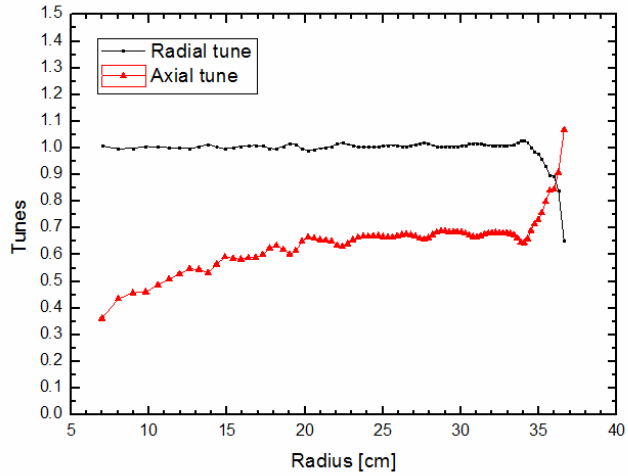

Figure 7: Radial and axial beam tunes.

REFERENCES

[1] J.S. Chai, “Commissioning of KIRAMS-30 cyclotron for nuclear science research”, 18th International Conference of Cylotrons and Their Applications, Giardini, 2007.
[2] Dassualt Systems, FR.
[3] Cobham, Vector Fields Ltd, UK.
[4] S.H. Shin, Pohang Accelerator Laboratory, POSTECH, Pohang, Korea, 2007.
[5] John J. Livingood, “Principles of Cyclic Particle Accelerators”, Chapter 13.

VACUUM SIMULATIONS FOR HEAVY ION BEAMS IN THE AGOR CYCLOTRON*

A.Sen#, M.J. van Goethem, M.A.Hofstee, S. Brandenburg.
Kernfysisch Versneller Instituut, University of Groningen, 9747AA Groningen, the Netherlands

Abstract

The TRIμP program at the KVI requires the development of high intensity heavy ion beams in particular $^{206}Pb^{27+}$ at 8.5 MeV/amu and $^{20}Ne^{6+}$ at 23.3 MeV/amu. For the Pb beam, losses in the cyclotron are one of the factors limiting the intensity that can be achieved. Charge changing collisions between the heavy ion beam and the residual gas cause subsequent desorption off the walls of the cyclotron which in turn leads to vacuum degradation. This causes a positive feedback loop leading to a reduced transmission with increasing beam intensity. We have developed a model to track the trajectory of the particles after a charge changing collision and 3D vacuum simulations to predict pressure profiles from desorption values. We have built and tested an experimental setup to measure beam induced desorption for relevant materials. Preliminary results are described.

INTRODUCTION

The TRIμP program at the KVI requires high intensity Pb beams for which transmission is to be maximized because of the limited intensity from the ion source. Primary beam loss in the cyclotron occurs when collisions of beam particles with the residual gas, mostly H_2O and N_2, lead to a change in the charge state of the ion. The cross-sections for the charge changing collisions depend on ion species and energy (Fig 1).

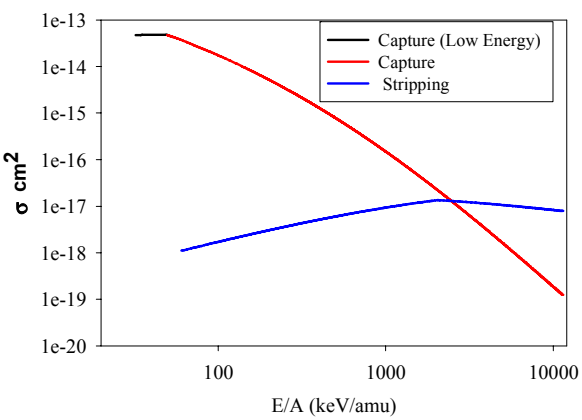

Figure1: Dependence of cross-section of capture and stripping processes on energy [1] [2] [3]

*This work is part of the research programme of the 'Stichting voor Fundamenteel Onderzoek der Materie (FOM)', which is financially supported by the 'Nederlandse Organisatie voor Wetenschappelijk Onderzoek (NWO)' It was supported by the European Commission within the Sixth Framework Programme through I3-EURONS (contract no. RII3-CT-2004-506065).
sen@kvi.nl

Using these cross-sections we predicted the transmission for a beam inside the AGOR cyclotron and the injection line for uniform pressure [4]. To study the effect of particles lost through charge exchange on the pressure, we simulated particle tracks after a charge changing collision. From there we calculated the angle of incidence of these particles when they hit the walls of the cyclotron causing desorption. The desorption is dependent on the energy of the particles, their angle of incidence on the wall, as well as the wall material. Desorption leads to a pressure increase and a different pressure distribution. This leads to increased beam loss creating a positive feedback loop.

We are developing a geometrical model to predict the pressure distribution for an arbitrary fixed value of desorption and outgassing. This will be used for further beam transmission calculations.

PARTICLE TRACK SIMULATION

The magnetic field used in the particle track simulation has a sinusoidal flutter term in addition to average magnetic field. This is a simplification of the actual field for a heavy ion in the AGOR cyclotron and has been used as a test case.

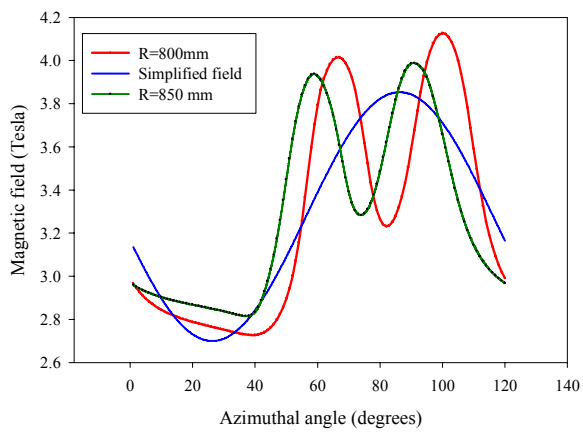

Figure 2: Dependence of the Magnetic field with azimuthal angle, showing actual field at a radius and simplified field as used in simulation.

The equations of motion [5] were solved using the RK4 method of integration for a fixed energy. From a calculated closed orbit, a charge change was simulated and subsequently the particles were tracked.

For a $^{206}Pb^{27+}$ ion, a charge changing collision gives a 4% change in the radius of curvature. Calculations show that the particle then moves in an off-centre orbit

close to the original orbit. The particles lost in the central region of the cyclotron do not contribute significantly to the hits on the outer boundary (defined as r =890 mm).

The main contribution to the desorption stems from the high energy particles near extraction (R >870mm), where also the orbit density is highest. Tracking these particles in our simplified preliminary model show that most hit the outer wall of the cyclotron at a grazing angle of incidence, below 8° (Fig 3).

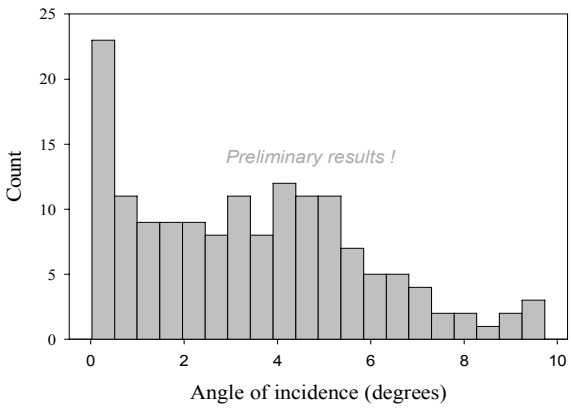

Figure 3: Calculated angle of incidence for particles hitting the walls of the cyclotron with initial radius greater than 870mm.

VACUUM SIMULATIONS

In earlier work we achieved good agreement between calculation and measurements of transmission in the injection line assuming a constant pressure [4]. For the interior of the cyclotron the agreement is not good, probably due to the assumption of a constant pressure profile inside the cyclotron. We developed a model with a simplified geometry to predict the pressure profile gradient for a given outgassing on all surfaces. The geometry is defined in STL format and the simulations are done using MOLFLOW [6]. For simplicity we have replaced the 3 hills and 3 valleys by a hexagon.

Figure 4 shows the density of hits on the top surface of the model. Three of the side walls of the extraction elements have a higher outgassing term to simulate beam loss induced desorption. The central projection (injection area) and other six holes act as the pumping units. The remainder of the walls have a fixed out-gassing term. The pumping areas are simulated by areas with unity sticking factor.

The pumping speed is limited by the surface area in MOLFLOW. We are working on a more realistic modelling of the cyclotron vacuum chamber to determine effect of desorption on the pressure distribution in more detail.

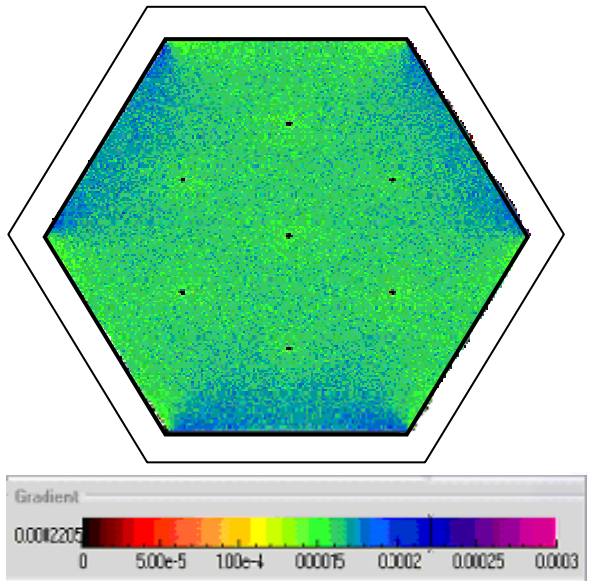

Figure 4: Output from a MOLFLOW simulation.

EXPERIMENT TO STUDY DESORPTION

The beamloss is increased by the vacuum degradation caused by desorption. The particle track simulation shows that the lost particles hit the walls at grazing angles. We therefore set up an experiment to determine the value of desorption for grazing angle of incidence for various beam energies and surfaces.

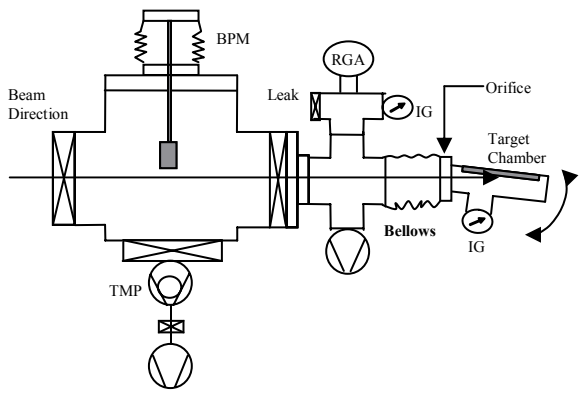

Figure 5: Experimental setup to measure desorption

The setup as shown in Figure 5 has been modified from the setup used by Mahner *et al.* in their desorption experiments [7]. The setup is attached to the AGOR high energy beam line. The target chamber is being differentially pumped by a turbo molecular pump unit of 150 l/s. The pumping speed of the test chamber is conductance limited by the shape of the orifice connecting the test chamber to the bellows. Pressure measurements are made by two ionization gauges (IG) and a quadrupole mass analyzer (RGA). In the main vacuum chamber is a ZnS beam position monitor viewed by a camera, to align the ion beam to the target chamber. The lid of the target chamber acts as the

target surface. It is detachable and can be replaced with a different material. The entire test chamber is welded at an angle of 4° to the flange attached to the bellows. Rotating the target changes the angle of incidence of the beam from 1° to 8°.

A first commissioning experiment of the setup has been performed with a $^{20}Ne^{6+}$ beam at 23.3 MeV per nucleon, which is a standard heavy ion beam used for the TRIμP experiments. The target surface was aluminium with no surface treatment. The angle of incidence was fixed at 4°. Beam current was varied from 12 nA to 890 nA. The base pressure in the target chamber was around 5×10^{-6} mbar. For the lower beam currents no rise in pressure above the base pressure was observed. However above 200 nA a measurable pressure increase inside the test chamber occurred. Figure 6 shows the response of the pressure to the intensity of the beam impinging on the target material.

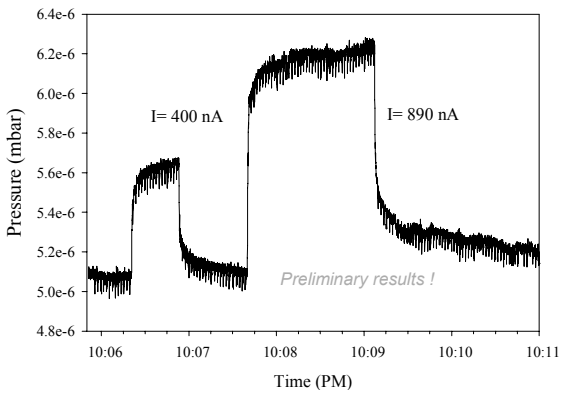

Figure 6: Pressure in test chamber for different beam intensities.

Beam induced desorption is not significant for the neon beam in the AGOR cyclotron. We used the beam for an initial proof of principle on the experimental setup. To measure desorption at lower beam currents a lower base pressure inside the test chamber is needed, which will be achieved by baking.

Further experiments are being designed with the standard $^{206}Pb^{27+}$ beam which does affect the vacuum in AGOR. We will also use different surfaces and surface treatments for a comparative study on desorption. We will in particular study the effectiveness of gold coating which has been shown to effectively reduce desorption [8].

OUTLOOK

The particle tracking simulation gives us the angle of incidence and energy of particles hitting the walls of the cyclotron. The desorption experiment aims to quantify desorption for different beams and surfaces. We will proceed with different surfaces and surface treatments to look for the desorption coefficient at grazing angles. This will be used as input for desorption in the vacuum simulation model to get desorption induced pressure profile inside the cyclotron. The pressure profile will be then used in the particle tracking model with the relevant cross sections to find out the number of particles being lost in charge changing collisions. The entire procedure is iterated till the pressure profile reaches equilibrium. Using the equilibrium pressure profile the final transmission of the beam can be calculated. These calculations will be used to predict and test results of the mitigation measures being implemented in the AGOR like gold plating of the interior of the cyclotron and implementation of scrapers.

REFERENCES

[1] A. Schlachter, “Charge changing Collisions”, Proc. 10th Int. Conf. on Cyclotrons and their Applications (1984), pg. 563

[2] H. Knudsen, H.K. Haugen and P. Hvelplund, Phys. Rev. A23(1981)567

[3] B. Franzke, IEEE Trans. on Nuc. Sci, NS-28 No-3(1981)2116.

[4] A.Sen, “Heavy Ion Beam induced Vacuum effects in the AGOR Cyclotron”, ECPM’2009, Groningen,October-2009; https://www.kvi.nl/~agorcalc/ECPM2009/Posters/11ECPM_Sen.pdf.

[5] F. Chautard, “Beam Dynamics for Cyclotrons”, CERN Accelerator School Zeegse, May 2005; http://cas.web.cern.ch/cas/Holland/PDF-lectures/Chautard/Chautard-final.pdf

[6] R. Kersevan,” Molflow Users Guide”, Sincrotrone Trieste Technical Note, 1991

[7] E. Mahner et al., “Ion-Stimulated gas desorption yields and their dependence on the surface preparation of stainless steel”, EPAC 2002, Paris, pg- 2568.

[8] C. Omet, H. Kollmus, H. Reich-Sprenger, P. Spiller, Proc. EPAC08(2008)295; http://www.JACoW.org

APPLICATION OF HTS WIRE TO MAGNETS *

K. Hatanaka#, M. Fukuda, J. Nakagawa, T. Saito, T. Yorita, RCNP, Ibaraki, 567-0047 Osaka, Japan
Y. Sakemi, CYRIC, Sendai, 980-8578 Miyagi, Japan
T. Kawaguchi, KT Science Ltd., Akashi, 673-0044 Hyogo, Japan
K. Noda, NIRS, Inage, 263-8555 Chiba, Japan

Abstract

We have been developing mgnets utilizing high-temperature superconducting (HTS) wire. A scanning magnet was designed, fabricated, and tested for its suitability as beam scanner. After successful cooling tests, the magnet performance was studied using DC and AC currents. In AC mode, the magnet was operated at frequencies of 30-59Hz and a temperature of 77K as well as 10-20Hz and 20K. The power loss dissipated in the coils was measured and compared with the model calculations. The observed loss per cycle was independent of the frequency and the scaling law of the excitation current was consistent with theoretical predictions for hysteretic losses in HTS wires. As the next step, a 3T dipole magnet is under construction now.

INTRODUCTION

More than two decades have passed since the discovery of high-temperature superconductor (HTS) materials in 1986 [1]. Significant effort went into the development of new and improved conductor materials [2] and it became possible to manufacture relatively long HTS wires of the first generation [3]. Although many prototype devices using HTS wires have been developed, these applications are presently rather limited in accelerator and beam line facilities [4].

Our previous study demonstrated a possibility to excite HTS magnets with alternating currents (AC) [5]. Since HTS systems have higher operating temperatures than low-temperature superconductor (LTS) systems, the cryogenic components for cooling are simpler and the cooling power of refrigerators is much larger than at 4K. Because the temperature range for superconductivity is wider than for LTS systems, a larger range pf operating temperatures is available. A high-frequency AC mode operation should be possible in spite of heating loads due to AC losses in the coils.

A two-dimensional scanning magnet was designed and built to model a compact system for such applications as ion implantation or particle cancer treatment. Two sets of single-stage GM (Gifford-McMahon) refrigerators were used to cool the coils and the thermal shields. After performance tests of the design parameters with direct currents (DC), the magnet was operated with AC current to investigate the dissipated losses in the coils. Observed AC losses are compared with theoretical predictions and model calculations.

A 3T dipole magnet is under construction to continue developments. It is a super-ferric magnet and the coil has a negative curvature..

* hatanaka@rcnp.osaka-u.ac.jp

SCANNING MAGNET

Design and Fabrication

A two-dimensional scanning magnet was designed to model a compact beam scanning system. The size of the irradiation field is 200mm by 200mm for 230MeV protons at the distance of 1.25m from the magnet center. The schematic layout of the coils is shown in Fig. 1. Both the B_x and B_y coils are centered at the same position along the beam axis. The required magnetic field length is 0.185 Tm. We selected the high temperature superconductor Bi-2223 [6] that is commercially available in lengths longer than 1000m. The HTS wire consists of a flexible composite of Bi-2223 filaments in a silver alloy matrix with a thin stainless steel lamination that provides mechanical stability and transient thermal conductivity. The wire, High Strength Wire, was supplied by American Superconductor Corporation [7] and is in thin tape-form approximately 4.2mm wide and 0.26mm thick.

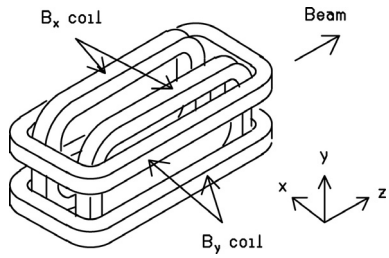

Figure 1: A schematic layout of the scanning magnet coils is shown. They generate the horizontal (Bx) and vertical (By) magnetic fields.

Table 1: Design parameters of the HTS scanning magnet.

Coils	Iner size	B_x: 150mm x 300mm.
		B_y: 150mm x 380mm
	Separation	70mm
	Maximum Field	0.6T
	# of tturns	420 x 2 for B_x and B_y
	Winding	3 Double pancakes/coil
	Inductance/coil	B_x: 75mH, B_y: 92mH
	Temperature	20K
	Rated current	200A
Cryostat	Cooling power	45W at 20K, 53W at 80K

The scanning magnet consists of two sets of two racetrack-type coils. Each coil is built by stacking three double pancakes. The design parameters are summarized in Table 1. Figure 2 shows a photograph of an as

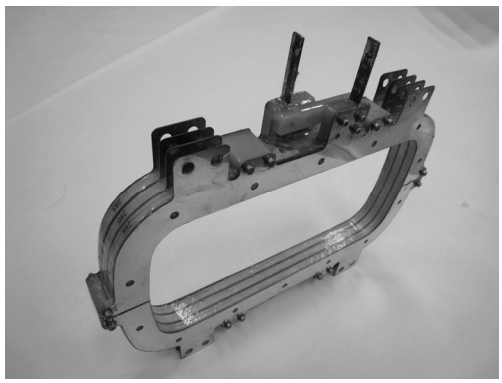

Figure 2: Photograph of single assembled Bx coil.

The critical current (Ic) of the HTS conductor depends on the operating temperature and the magnetic field at its surface. The magnetic field perpendicular to the conductor has larger effects on Ic than the horizontal component. Before winding, the Ic of the wire over the full length was measured at 77K in a 10m pitch and found to be between 125 and 140A corresponding to an electric field amplitude of 1μV/cm. The Ic values of the coils were estimated from the Ic ($B_\perp$) characteristics of the tape conductor and a magnetic field analysis using the finite element code TOSCA. The load line of the coil was found to cross the Ic ($B_\perp$) curve at 0.195T and a current of 39A corresponding to an Ic at 77K. In the present design, the maximum field was 0.6T in the center along the axis of the magnet and the required magneto-motive force is 8.4 x 10^4AT for each coil. The maximum field perpendicular to the tape surface is estimated to be 1T. From the specification of the temperature dependence of the I($B_\perp$) characteristics, the Ic value was estimated to be 260A at 20K. The rated current of the coil was designed to be 200A to generate the field length of 0.185Tm.

DC Performance Tests

The Ic value of each pancake was measured in a liquid nitrogen bath. They were 56-62A for all pancakes. After stacking three pancakes to form a coil, the self-field Ic of the B_x and B_y coils was measured separately. The Ic values were 40-43A and consistent with the design value of 39A described in the previous section. This demonstrated that the HTS wire was not damaged by the winding procedure and that we can expect operating currents larger than 200A at 20K.

After the installation of the magnet, the cryostat was evacuated by a turbo-molecular pump with a pumping rate of 300l/sec. Coil resistances and temperatures on the coil surfaces and shields were measured during the cooling procedure. HTS coils became superconducting at 105K after 10 hours of cooling. The final temperature below 20 K was achieved after one day of cooling. The temperature of the coils was measured by silicon diode sensors DT-670 of Lake Shore Cryotronics Inc. at several locations. The temperature of the thermal shields was measured by thermocouples. The equilibrium temperature was about 100K at the farthest point from the cold head of the refrigerator.

The Ic values measured at 20K were 257A and 282A for the B_x and B_y coils, respectively. They were consistent with the design values. The magnetic field distribution along the central axis (z) was measured at 100A using a Hall probe. The measured magnetic fields agreed with calculations by the code TOSCA very well.

AC Operation

Owing to the good thermal performance we can expect a large thermal operating range for the present coils. Such a large range suggests the possibility to excite the magnet in the AC mode while maintaining superconductivity as long as the AC loss in the HTS tape is acceptable. Several AC loss components are observed in both LTS and HTS magnets [8, 9]. They are (1) hysteretic magnetization losses in the superconductor material, (2) dynamic resistance losses generated by a flux motion in the conductor, (3) coupling losses through the matrix, and (4) eddy current losses in the matrix and metallic structures including cooling plates. For HTS magnets, there are Ohmic losses at exciting currents above the critical current as well. Each AC loss shows a different dependence on the frequencies (f), the amplitude of the external magnetic field (B) and the transport current (I_t). The power dissipation per cycle for each loss (1) - (4) listed above scales as

$$2\ln[\cosh x] - x\tanh x \quad (1)$$

$$BI^2 \quad (2)$$

$$fB^2 \quad (3)$$

$$fB^2 \quad (4)$$

where $x = B/B_{c0}$ and $B_{c0} = \mu_0 J_c d/\pi$. J_c is the critical current density and d thickness of the conductor tape. For such a geometry as discussed in the present study, the external magnetic fields are also generated by the transport current. In this case, the magnetic field amplitude can be expected roughly proportional to the transport current. AC losses due to the first two phenomena (1) and (2) are independent of the frequency. On the other hand, losses (3) and (4) depend linearly on the frequency.

In AC loss measurements, two B_x coils were connected in series in the cryostat and cooled down below 20K [10]. The power dissipated in the coils was measured at three frequencies, 10.5Hz, 15Hz and 21Hz. Measurements were performed using an electrical method where the voltage across coils was measured in-phase with the transport current using an oscilloscope. The system consisted of an inverter, an induction motor and a generator that was employed to convert the line frequency of 60Hz to the resonance frequencies. The inductance of a single B_x coil was measured to be 70 mH at 77K. The total inductance of two coils in series was estimated to be 170mH. Coils and condensers formed a series resonance circuit. The

capacitances of condensers in series were 1200μF, 600μF and 300μF. The resonance frequencies were roughly estimated to 10, 15 and 20Hz, respectively.

Figure 3 shows the measured AC power losses of the two B_x oils in series. The losses are roughly proportional to the 2.4th power of the transport current instead of the third power observed at 77K. The dashed curve in Fig. 5 presents the result of the finite element model analysis by T. King [10]. A close inspection of the result showed that the hysteretic and normal resistance losses were all reduced compared to calculations at 77K, but the eddy current losses in the silver alloy matrix and the brass cooling plates resulted in an overall increase of the losses. It was found that the predicted power was dominated by the losses due to eddy currents in the metallic materials. Consequently, the modelled losses were roughly proportional to the quadratic power of the transport current and the losses per cycle were linearly dependent on the frequency. In contrast, the observed dissipated power per cycle is again almost independent of the frequency of the transport current as seen in Fig. 3. The solid curve in the figure shows the theoretical Q_{hys} which is normalized to the measured value at 45A and 15Hz. At 20K, J_c of the present HTS wire is about 5 x 10^8A/m^2. The theory is found to reproduce the scaling law well as a function of the transport current, if we take account the temperature dependence of the critical current density of the conductors.

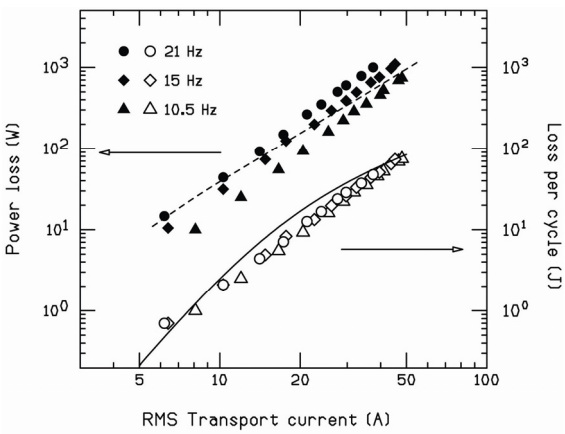

Figure 3: Measured AC losses at 20K of the Bx coils in series. Full symbols show the total power losses on the left side scale. Open symbols present losses per cycle on the right side scale. The dashed curve shows the model calculation by King [11]. The solid curve is a theoretical prediction normalized to the measured data.

3T DIPOLE MAGNET

In order to investigate feasibilities of synchrotron magnets using HTS wire, we are fabricating a super-ferric dipole magnet to be operated by lumping currents. The specifications are summarized in Table 2.

Table 2: Design parameters of the 3T HTS dipole magnet.

Magnet	Bending radius	400mm
	Bending angle	50deg.
	Pole gap	30mm
Coils	# of tturns	600 x 2
	Winding	3 Double pancakes/coil
	Temperature	20K
	Rated current	300A

Upper and lower coils were already fabricated. Each consists of 3 double pancakes of 200 turns. Figure 4 shows double pancakes for the upper coil. Critical currents were measured of wire measured at 77K. Self-field Ic of wire was higher than 160A. Ic values of double pancakes were 60-70A. After stacking, they were 47A and 51A for the upper and lower coil, respectively. There were no damages in wire during winding process.

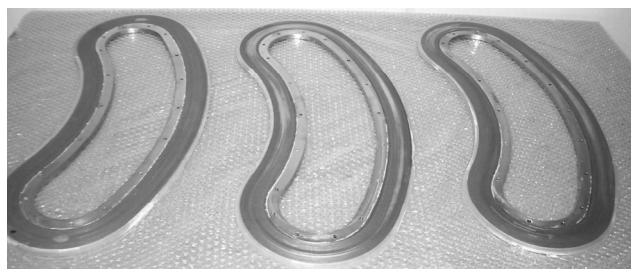

Figure 4: Photograph of double pancakes.

REFERENCES

[1] J.G. Bednorz and K.A. Müler, Physical B 64 (1986) 189.
[2] K. Sato, K. Hayashi, K. Ohkura, K. Ohmatsu, Proc. of MT-15, Beijing (1997) 24-29.
[3] L.J. Masur, J. Kellers, F. Li, S. Fleshler, E.R. Podtburg, Proc. of MT-17, Geneva (2001) 1-5.
[4] D.M. Pooke, J.L. Tallon, R.G. Buckley, S.S. Kalsi, G.Snitchler, H. Picard, R.E. Schwall, R. Neale, B. MacKinnon, Proc. o CIMTEC'98, Italy (1998).
[5] K. Hatanaka, S. Ninomiya, Y. Sakemi, T. Wakasa, T. Kawaguchi, N. Takahashi, Nucl. Instr. Meth. in Phys. Res. A 571 (2007) 583-587.
[6] A.P. Malozemoff et al., Proc. 1998 Applied Superconductivity Conference, Palm Desert, CA, 14-19, 1998.
[7] http://www.amsc.com/
[8] C. M. Friend, "Ac losses of HTS tapes and wires", Studies of High Temperature Superconductors, A. V. Narlikar, Ed. New York: Nova Science Publishers, 2000, vol. 32, pp. 1-61.
[9] E.H. Brandt and M. Indenbom, Phys. Rev. B 48 (1993) 12893-12906.
[10] K. Hatanaka, J. Nakagawa, M. Fukuda, T. Yorita T..Saito, Y. Sakemi, T. Kawaguchi, K. Noda, Nucl. Instr. Meth. in Phys. Res. A 616 (2010) 16-20.
[11] T. King, private communication.

BEAM LOSS MONITORING AND CONTROL FOR HIGH INTENSITY BEAMS AT THE AGOR-FACILITY*

S. Brandenburg#, M.A. Hevinga, T.W. Nijboer, H. Vorenholt,
Kernfysisch Versneller Instituut, University of Groningen, 9747AA Groningen, the Netherlands

Abstract

The experiments at the AGOR facility require intense heavy ion beams. Typical examples are 10^{13} pps of $^{20}Ne^{6+}$ at 23.3 MeV/A and $\geq 10^{12}$ pps $^{206}Pb^{27+}$ at 8.5 MeV/A. To prevent damage to components by the beam (power density up to 1 kW/mm^3 in unfavourable cases) a modular beam loss monitoring and control system has been developed for the cyclotron and high energy beam lines. The architecture of the system is described and the considerations for the major design choices discussed. The system uses the CAN-bus for communication and verification of system integrity. The injected beam is chopped at 1 kHz with a variable duty factor between 5 and 90 %. The beam intensity at injection and a number of locations in the high energy beam line is measured by inductive pick-ups. Furthermore, localized beam losses on slits and diaphragms are directly measured. When beam loss in any section exceeds the predefined maximum value, the duty factor of the beam is automatically reduced.

INTRODUCTION

The AGOR-facility delivers heavy ions beams up to Pb for experiments in the framework of the TRIμP programme on fundamental symmetries. Experiments on violation of time reversal symmetry in β-decay are performed with beams up to ^{40}Ar at energies between 20 and 30 MeV. The beam intensity in these experiments is currently limited by constraints in the experimental setup to 4×10^{12} pps (300 W). The cyclotron has demonstrated its ability to deliver the 1 kW beam aimed at by the experiment. For experiments on permanent electric dipole moments and atomic parity violation in Ra-atoms and ions beams of various Pb-isotopes with an energy in the range 7 – 10 MeV per nucleon and an intensity up to 3×10^{11} pps (100 W) are used. A further intensity increase by at least a factor 3 is requested, requiring improvement of both the experimental setup and the cyclotron output

The power density in materials hit by in particular the Pb-beams is up to 1 kW/mm^3, leading to damage at the ms time scale. Therefore a monitoring and control system for the beam losses, both in the cyclotron and in the high energy beam lines, is essential for safe operation of the AGOR-facility for this type of experiments.

*This work is part of the research programme of the 'Stichting voor Fundamenteel Onderzoek der Materie (FOM)', which is financially supported by the 'Nederlandse Organisatie voor Wetenschappelijk Onderzoek (NWO)' It was supported by the European Commission within the Sixth Framework Programme through I3-EURONS (contract no. RII3-CT-2004-506065).
#brandenburg@kvi.nl

SYSTEM SPECIFICATIONS

The beam loss monitoring and control system (BLMCS) has to ensure that the unavoidable beam losses in the cyclotron and high energy beam lines remain within preset limits by controlling the beam intensity injected into the accelerator. The system operates in a uni-directional way: deterioration of the transmission leads to automatic reduction of the beam intensity, but intensity increase made possible by improved transmission requires operator intervention. In case of more or less complete loss of the beam, as occurs due to equipment failure, the system suppresses the beam at injection within 10 ms.

The semi-interceptive beam profile monitors in the cyclotron and high energy beam lines can not withstand the full beam intensity. Therefore the system also supervises the status of all beam diagnostics equipment in the cyclotron and high energy beam lines. Under normal operating conditions insertion of a beam diagnostics device leads to immediate interruption of the beam by the BLMCS. After reducing the primary beam intensity to a safe level by inserting a pepperpot in the injection line and switching the BLMCS to tuning mode, beam can be injected into the cyclotron again. Removing the pepperpot while in tuning mode results in suppression of the beam in the injection line.

Lay-out

The path of the beam from the injection beam line below the cyclotron up to the experimental setup at the end of the high energy beam transport system has been divided in seven sections for which the transmission is measured individually. The experiments with high intensity beams are performed at one of the four experimental setups only, so there was no need to implement beam line selector logic. For each section of the high energy beam line and the cyclotron a Beam Loss Control Module (BLCM) has been installed that assesses the beam losses, verifies the status of the beam diagnostic devices and triggers actions if necessary. This modular structure is easily adapted to the operational experience.

The BLCM has six analog inputs for current measurements. Two of these are used for non-destructive pick-ups measuring the beam current at the entrance and exit of the section, the others are used to measure the current on diaphragms and/or slit jaws in the section that intercept part of the beam. The non-destructive pick-ups are shared between sections: the BLCM of section N receives its entrance current signal from the BLCM of section N-1 and sends its exit current signal to the BLCM of section N+1, where it serves as the entrance current

signal. The BLCM integrates the currents over each chopper cycle to determine the losses.

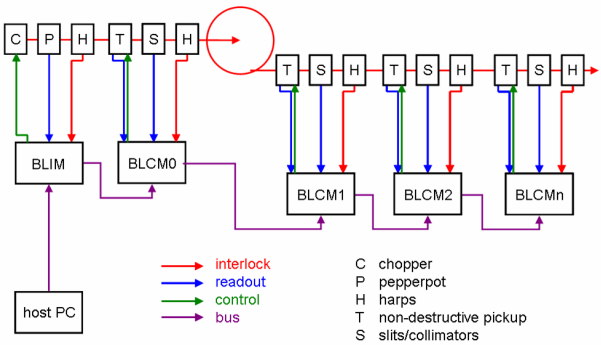

Figure 1: Layout of the Beam Loss Monitoring and Control System (BLMCS). The BLIM and BLCM0 modules are located in the injection beam line, the other modules in the high energy beam line. The bus contains the CAN-bus connection, the synchronization of the measurements with the chopper cycle and the transfer of the beam intensity measured by the non-destructive pick-up of a given BLCM to the next.

The BLCM compares both the localized losses on the diaphragms and slits and the non-localized loss, evaluated as the difference of the total loss determined with the non-intercepting probes and the localized losses, with individual preset high, low and alarm levels. Any loss exceeding the high level results in requests to the Beam Loss Interrupt Module (BLIM) that controls the chopper to reduce the duty cycle until the beam loss is lower than the low level. Beam loss exceeding the alarm level causes a request to the BLIM to completely suppress the beam.

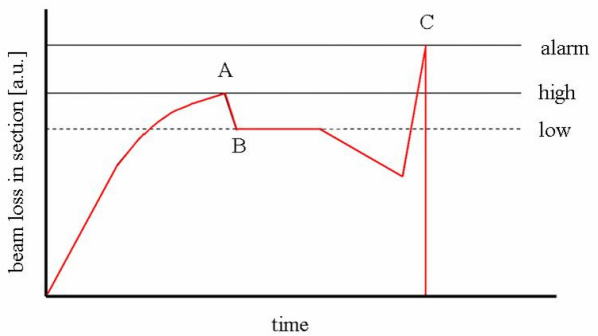

Figure 2: Principle of operation of the BLMCS. At time A the beam loss exceeds the "high" level and the system starts to reduce the duty cycle of the chopper until the loss is below the "low" level (time B). Decreasing losses do not result in a increase of the duty cycle. Losses exceeding the alarm level at time C result in complete suppression of the beam.

The BLCM also has eight digital inputs for the status of the (semi-)destructive beam diagnostics in the section of the beam line it supervises. Currently all beam profilers and beam stops in the high energy beam line have been connected to the system: thermal calculations indicate the aluminium core of the beam stop will be damaged by the 1 kW anticipated beam power.

System Architecture

Both the BCLMs that supervise the different sections of the beam lines and the BLIM that controls the chopper and the pepperpot are based on ARM7-processors. For the communication in-between the modules and with the PC supervising the system the CAN-bus has been adopted because of its robustness and real-time properties. The CAN-bus is used to load the limit values into the BLCMs and to transfer the request for reduction of the chopper duty cycle or suppression of the beam from the BLCMs to the BLIM. The software is loaded into the modules via a separate RS232-port.

A watchdog mechanism is used to verify the proper operation of the individual modules and the system as whole. Failures detected by the watchdog result in suppression of the beam via the “red line” of the radiation protection system.

The proper synchronization of the integration of the beam intensity over each chopper pulse is ensured by a separate PulseBus that distributes the trigger signal of the chopper. The synchronization pulse to the BLCMs in the high energy beam line has a variable delay to compensate for the propagation delay of the beam through the cyclotron, which varies between 50µs for a beam energy of 5.5 MeV per nucleon and 15 µs for 190 MeV protons.

BEAM INTENSITY MEASUREMENT

The extraction of heavy ion beams from the AGOR-cyclotron has an efficiency of ≥ 85 % up to the maximum intensities delivered so far. The beam loss during extraction mainly occurs in the electrostatic deflector, with minor losses in the subsequent electromagnetic channels.

The use of DCCTs or fast inductive or capacitive probes operating at the RF-frequency (24 – 62 MHz), which would have avoided continuous thermal cycling of the septum, was unfortunately not feasible. The inductive probes available had too low S/N-ratio at our intensities, whereas the capacitive probes required a rather complex signal treatment to ensure a sufficiently accurate relative calibration. Also for the DDCT to be installed in the injection line as a reference the S/N-ratio was marginal at our intensities. We therefore adopted the chopping scheme as used at e.g. GANIL [1] and GSI [2]. The 1 kHz chopper frequency and 90 % nominal duty cycle are the result of a compromise between the following aspects:

- fast response time of the system.
- minimal thermal cycling of the septum.
- up to 10 µs variation in cyclotron transit time.
- time needed for signal handling per chopper period.

Full 3D-simulations of the thermal transients of the septum including radiation show temperature variations of the septum below 10 K for a beam loss on the septum of 100 W, which was considered acceptable. During the first year of operation with beam losses on the septum up

to 25 W no deterioration of deflector operation has been observed.

Inductive Pick-up

The inductive pick-up and associated front-end electronics is based on that used at the UNILAC at GSI [3]. The reference pick-up in the injection line is integrated in a flange that also includes the required diversion of the wall current. The pick-ups in the high energy beam line are mounted in an electrically insulated magnetic shielding and slid over the aluminium beam tube. The diversion of the wall current is in this case realized by interrupting the electrical continuity of the beam tube at the nearest coupling point between sections of beam tube. As a result these pick-ups have a signal-to-background-ratio that is significantly lower than that of the reference pick-up, but this is not compromising the performance of the system.

The pick-ups consist of a Vitrovac 6025F core with four winding sets. The two winding sets for the measurement of the beam current are wound such that signals induced by currents not enclosed by the core are cancelled. The beam current signal is obtained by integrating the signal of the pickup. The integrator is reset after each chopper cycle to take into account drifts and low frequency background. Droop of the output signal is negligible thanks to the short integration period. The other two winding sets serve for calibration and offset compensation. The calibration windings of all cores are connected in series to so that the calibration current of all cores is identical.

OPERATIONAL EXPERIENCE

From operation of the system in test experiments we conclude that the measurement of the cyclotron transmission merits further consideration and can be improved. In the current layout the overall transmission between the non-destructive pick-ups in the injection beam line below the cyclotron and in the high energy beam line at the exit of the cyclotron and the losses on the collimators in front of the four extraction channels are measured and compared with the preset limits to control the beam intensity.

The transmission through the cyclotron is dominated by the injection efficiency of 25 % (mainly determined by the buncher) and for certain beams the losses due to charge exchange during acceleration, which strongly depend on the energy ion species, energy and intensity. Consequently the sensitivity of the overall transmission to changes in the extraction efficiency is rather limited. Furthermore the losses in the extraction channels, which are from the point of view of damage risks more important than those on the collimators, can not be assessed. Consequently rather tight limits on the losses have to be imposed to warrant safe operation.

We are investigating whether we can improve the assessment of the transmission through the cyclotron by using the innermost and outermost phase probes. By comparing the pick-up in the injection line and the innermost phase probe the injection efficiency can be determined, while the comparison of the two phase probes yields a measure of the internal beam losses. By combining the intensities measured with the outermost phase probe, the pick-up at the cyclotron exit and the losses on the collimator the losses in the extraction channels can be assessed.

The measurement of the beam intensity from the phase probes requires the development of a new multiplexer system to allow the dual use of the phase probes and a super heterodyne detector combined with a lock-in amplifier locked to the chopper drive signal.

ACKNOWLEDGEMENT

We would like to thank our colleagues P. Forck, W. Kaufmann and H. Reeg of the GSI Beam Diagnostics group for generously sharing their experience in developing beam loss monitoring and control systems with us.

REFERENCES

[1] C. Jamet et al., Proc. DIPAC2005(2005)169.
[2] H. Reeg, J. Glatz, N. Schnieder H. Walter, Proc. EPAC2006(2006)1025.
[3] H. Reeg et al., private communication.

THE SIMULATION ON BEAM INTERACTION WITH BACKGROUND PARTICLES*

J. L. Wei#, C. D. Hu and L. Z. Liang
Institute of Plasma Physics, Chinese Academy of Sciences, Hefei, Anhui, 230031, China

Abstract

A particle simulation with Monte Carlo was developed to study beam interaction with background particles in neutral beam injector (NBI). The collision processes associated with charge state change and reaction cross-section were analyzed for neutralization and re-ionization. Take the neutralization processes as a reference, for positive arc discharge ion source, there are three different original ion species in the energetic ion beam. In evolution, a fast particle will suffer kinds of collisions decided by the collision cross-section or no impact within the target gas. Classify those collisions and their cross-sections according the change of charge state and momentum. The neutralizer is divided into many extremely short segments averagely. So the gas density quantity at middle point can be regarded as that of each segment. According to the collision cross-section, select a random number to determine the evolution of particle states in each segment. With that particle simulation, the neutralization efficiency is estimated.

INTRODUCTION

A NBI system can produce an energetic neutral beam which is used to heat the plasma in the magnetic confinement fusion device [1]. A sketch of the NBI system is shown in Figure 1 [2]. A high energy ion beam from the ion source will undergo neutralization processes in a gas cell named neutralizer, in which part of the energetic ions turn into energetic neutral particles. And then, the mixed particles beam is separated into ions and neutral particles by the bending magnet. Finally, the energetic neutral particles pass through the drift tube and inject into the fusion device, while the residual ions are dumped into a target (i.e., residual ion dump). However, the produced neutral beam will suffer a re-ionization process, due to the limit of vacuum in the drift tube.

Take neutralization processes for example. In the neutralizer, atomic processes involving charge transfer and dissociation will change particles' charge state and momentum. Thus, these processes will determine the species evolution along the neutralizer downstream and the neutralization efficiency. Numerical calculations of this problem have been reported in [3]. Moreover, the functional forms of variation for all species are discussed later, which offer more detailed information of the species evolution [4]. However, both of the researches base on sets of the differential equations (DE) for each species. Although the same problem is considered here, we adopt Monte Carlo (MC) simulation to research instead.

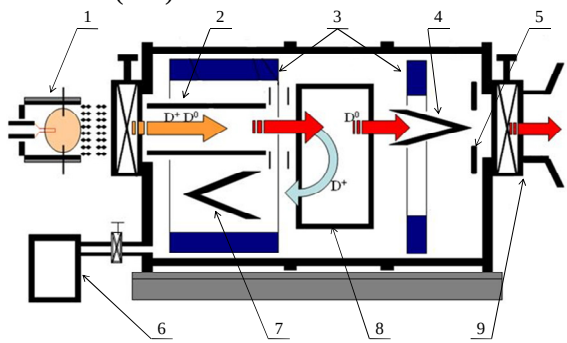

Figure 1: Sketch of NBI beamline: 1. Ion source; 2. Neutralizer; 3. Cryopumps; 4. Calorimeter; 5. Collimator; 6. Pump set; 7. Residual ion dump; 8. Bending magnet; 9. drift tube.

MODEL DESCRIPTION

Collision Processes

For a positive ion source, if the operating gas is deuterium, there are three different original ion species in the energetic ion beam, D^+, D_2^+ and D_3^+ [4]. In evolution these species are independent of each other, so we can analyze the particle species evolution respectively. Enough sample calculations and experiments have been carried out, however, to indicate that D_2 is representative of the better gas neutralizer for D species ion beam [3]. Based on the elementary MC principle, we select the relatively important collision processes between these fast species and slow molecule D and neglect the minute ones, which depend on the values of their corresponding cross sections.

Table 1 lists the various types of collision processes we take into account. From table 1 we can see clearly the close connection of these particles in their various collision processes. Except for the process of secondary D_2^+ production, most of the collisions will change the fast particles' charge state or momentum, which is more concerned for particle species evolution. Particularly, the tiny productions of D^- are considered here to show the rounded system of charge state. Thus, with the number of collisions increasing, the particles species evolution is dominated by inter-conversion between D^+ and D^0 in the neutralizer. Note that, some collision equations are generalized by several collision processes, such as production of fast D from fast D_2, which should be distinguished to avoid repeated calculation. These dates of the cross sections are all taken from [5].

*Work supported by the National Natural Science Foundation of China under Grant No. 10875146, and the Chinese Academy of Sciences Knowledge Innovation Project: the study and simulation on beam interaction with background particles in neutralization area for NBI.
#jlwei@ipp.ac.cn

Table 1: Margin Specifications

Particle	Process	New product
D	$D + D_2 \rightarrow D^+ + D_2 + e$	D^+, e
	$D + D_2 \rightarrow D^- + D_2^+$	D , D_2^+
	$D + D_2 \rightarrow D + D_2^+ + e$	D_2^+ , e
D^+	$D^+ + D_2 \rightarrow D + D_2^+$	D , D_2^+
	$D^+ + D_2 \rightarrow D^- + 2D^+$	D^-, D^+
	$D^+ + D_2 \rightarrow D^+ + D_2^+ + e$	D_2^+ , e
D^-	$D^- + D_2 \rightarrow D + D_2 + e$	D , e
	$D^- + D_2 \rightarrow D^+ + D_2 + 2e$	D , e
D_2	$D_2 + D_2 \rightarrow \sum$ D (fast, total)[a]	D
	$D_2 + D_2 \rightarrow \sum D^+$(fast, total)[a]	D^+
	$D_2 + D_2 \rightarrow \sum D_2^+$ (fast, total)[a]	D_2^+
	$D_2 + D_2 \rightarrow$ (destruction of D_2)[b]	
D_2^+	$D_2^+ + D_2 \rightarrow \sum$ D [a]	D
	$D_2^+ + D_2 \rightarrow \sum D^+$ [a]	D^+
	$D_2^+ + D_2 \rightarrow D_2 + D_2^+$	D_2 , D_2^+
	$D_2^+ + D_2 \rightarrow D + D^+$	D , D^+
D_3^+	$D_3^+ + D_2 \rightarrow$ (destruction of D_3^+)[b]	
	$D_3^+ + D_2 \rightarrow \sum D^+$ [a]	D
	$D_3^+ + D_2 \rightarrow \sum D_2$ [a]	D^+
	$D_3^+ + D_2 \rightarrow \sum D_2^+$ [a]	D_2
	${D_3^+}_f + D_{2s} \rightarrow \sum {D_2^+}_f$ [a]	D_2^+

[a] X (fast, total) indicates the sum of all processes leading to the creation of a fast species X.

[b] (Destruction of X) indicates the sum of all processes leading to the destruction of species X.

Physical Model

We will consider the idealized NBI system. We assume that (1) a monoenergetic ion beam is extracted and accelerated from the source in the x direction; (2) the ion beam is perfectly collimated, and the beam divergence is neglected; finally, (3) most of the collisions occur at large impact parameter, hence the fast particles hardly changing the direction and decelerate.

Under these hypotheses, we can create the following physical model. Consider the distribution of target gas density along the neutralizer is in an arbitrary form (shown in figure 2). Divide the neutralizer into k segments averagely, and ensure that the length of each segment Δl is less than $\lambda/20$, where λ is mean free path. If Δl is short enough, we can regard the gas density quantity n_i at middle point as that of each section. Furthermore, we postulate that every particle impacts with the target gas molecules no more than once in each segment. Thus, the probability of specific collision process in each segment is give by:

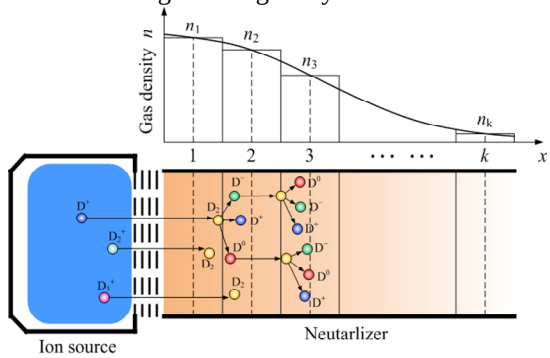

Figure 2: Sketch of neutralization processes.

$$P_{cd}^{ab} = \sigma_{cd}^{ab} \cdot n_i \cdot \Delta l \quad (1),$$

where σ_{cd}^{ab} is the reaction cross-section involving a mass change from a to b and a charge state change from c to d for fast particle.

Monte Carlo Simulation

According to the above analysis, we adopt Monte Carlo method to simulate the particle species evolution in the neutralizer. The collision type is stochastic, so we can use a random number to ascertain which processes the incident particle undergoes: construct an interval sequence $[0, z_1)$, $[z_1, z_2)$, … , $[z_{m-1}, z_m]$, $[z_m, 1]$, where $z_1 = P_1$, $z_2 - z_1 = P_2$, $z_{m-1} - z_m = P_m$. Obviously, each interval represents a corresponding collision type, and the interval $[z_m, 1]$ indicates a collisionless process. Afterwards, judge a random number (distributing uniformly between 0 and 1) yielded by computer, find out which interval it belongs to and fix on the collision process. Thus, we can learn what process the incident particle undergoes after traversing the first segment of the neutralizer, and the property of emergent particle. At the same time, the emergent particle for the first segment is just the incident particle for the second segment. Consequently, we can use the same method step by step to research this particle evolution in the following segments. Note that the possible collision types may be different for diverse incident particle. Finally, we accomplish the simulation on particle species evolution in the neutralizer of one ion injecting.

SIMULATION RESULTS

The required amount of target gas in the neutralizer (i.e., target thickness) varies with beam energy and species, and in turn affects the requirement of gas feeding system and large vacuum system. See the figure 3, multiplying the density values n_i by Δl, we get the gas line density for each section. And then, target thickness π of the neutralizer turns out to be:

$$\pi = \int_0^L n(x) \cdot dx = \sum_k n_i \cdot \Delta l \ . \ (2)$$

If the target gas density n is uniform along the neutralizer, the particles traversing each segment in sequence is the

same as particle species evolution in linear target thickness. So this MC method can be used to calculate the variation of the fraction of particle species with the target thickness as the DE method does. In the DE methods, the solutions to the relevant differential equations of each beam are given in [4], but we get the solutions by Runge-Kutta method here.

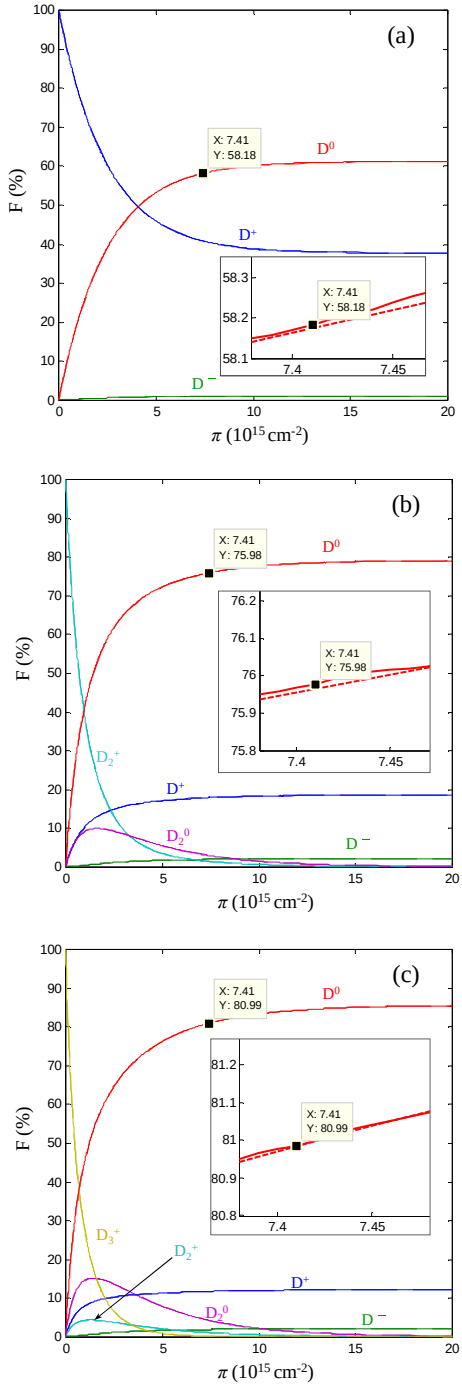

Figure 3: Fraction of particle species as a function of target thickness for (*a*) 80 keV D_3^+ beam, (*b*) 80 keV D_3^+ beam and (*c*) 80 keV D_3^+ beam (or 40 keV H^+, H_2^+ and H_3^+ beam) traversing D_2 (or H_2): (—) results of MC simulation; (- - -) results of DE simulation.

With two methods, the fraction of particle species vs. D_2 neutralizer target thickness for D^+, D_2^+ and D_3^+ beam at the energy 80 keV are shown respectively in figure 3. In those figures, the solid curves are the results of MC method, and the dash ones are given by DE method. We can see that, each pair of data curves are all fitting close with the target thickness increasing, and we cannot tell the difference in common dimension. To distinguish the two sorts of lines, the regions around the same value of target thickness for D^0 curve are zoomed in 100 times.

Particularly, the curve of D^0 for D^+ beam is just the variation of neutralization efficiency η with target thickness π. As target thickness increasing, the neutralization efficiency doesn't have a significant maximum but tends to equilibrium. The target thickness is usually set less than the equilibrium target thickness in a NBI system since the fraction of neutrals is slightly increasing near the equilibrium, and the excessive gas flowing to the drift tube will lead to more neutrals re-ionization losses [16]. We define optimum neutralizer thickness π_{opt}, which is the value of π required to achieve 95% of the equilibrium η. Acronyms should be defined the first time they appear.

CONCLUSION

The collision processes have been selected and classified in the beamline of the NBI system precisely, according to their collision cross sections and significance. Based on the relationships among responsible collision processes, a Monte Carlo simulation model is developed to analysis beam interaction with background particles in the neutralization processes, which are more complicated. The fractions of the major particles as a function of target thickness is given for 80 keV compared with the results of the differential equations method, which are fitting closely.

REFERENCES

[1] Wang J, Wu B and Hu C 2010 Plasma Sci. Technol. 12 289.
[2] Wesson J 2004 Tokamaks 3rd Ed. (Oxford, UK: Clarendon).
[3] Berkner D H, Plye R V and Stearns J W 1975 Nucl. Fusion 15 249.
[4] Kim J and Haselton H H 1979 J. Appl. Phys. 50 3802
[5] Barnett C F 1990 ORNL Technical Reports No. ORNL-6086.

PROGRESS IN FORMATION OF SINGLE-PULSE BEAMS BY A CHOPPING SYSTEM AT THE JAEA/TIARA FACILITY

S. Kurashima#, M. Taguchi, I. Ishibori, T. Nara, W. Yokota
Japan Atomic Energy Agency, 1233 Watanuki, Takasaki, Gunma 370-1292, Japan

Abstract

The intervals of beam pulses from a cyclotron are generally tens of ns and they are too short for pulse radiolysis experiments which require beam pulses at intervals over 1 μs (single-pulse beam). A chopping system, consisting of two types of high voltage kickers, is used at the JAEA AVF cyclotron to form single-pulse beam. However, we could not provide single-pulse beam stably over 30 min since the magnetic field of the cyclotron gradually decreased and the number of multi-turn extraction increased. The magnetic field is stabilized at present by keeping temperature of the cyclotron magnet constant. In addition, a new technique to measure and control an acceleration beam phase has enabled us to reduce the number of multi-turn extraction easier than before. The single-pulse beam of a 320 MeV $^{12}C^{6+}$ is successfully provided without retuning of the cyclotron over 4 h, as a result.

INTRODUCTION

A *K*110 AVF cyclotron at the JAEA/TIARA facility accelerates various kinds of heavy-ions up to 560 MeV mainly for research in biotechnology and materials science. The cyclotron has two RF resonators with a dee electrode whose span angle is 86°, and the acceleration harmonics *h* of 1, 2 and 3 are available. More than half of the heavy-ion beams are accelerated at *h* = 2. Beam pulses are extracted at intervals of 45.5 to 90.9 ns depending on an acceleration frequency ranging from 11 to 22 MHz. The ordinary intervals of beam pulses are too short for a pulse radiolysis experiment in radiation chemistry and for a time-of-flight measurement of secondary particles from a target. For example in a pulse radiolysis experiment [1], one cannot observe decay of a radical in a solution correctly since the following beam pulse hits the target before the radical, produced by the last beam pulse, goes out. We provide beam pulses spaced at intervals over 1 μs (single-pulse beam) using a chopping system as shown in Fig. 1 for the experiments [2].

The ion beam is extracted by multi-turn extraction for all acceleration harmonics in the original design of the cyclotron. In order to form single pulse beam, the number of multi-turn extraction is less than 5 to 9 by the chopping system design. It is very effective to narrow a beam phase width using a phase slit for limitation of the number of multi-turn extraction. However, the beam phase width could not be practically less than 40° in the cyclotron using two pairs of original phase slits in the case of *h* = 2.

E-mail: Kurashima.satoshi@jaea.go.jp

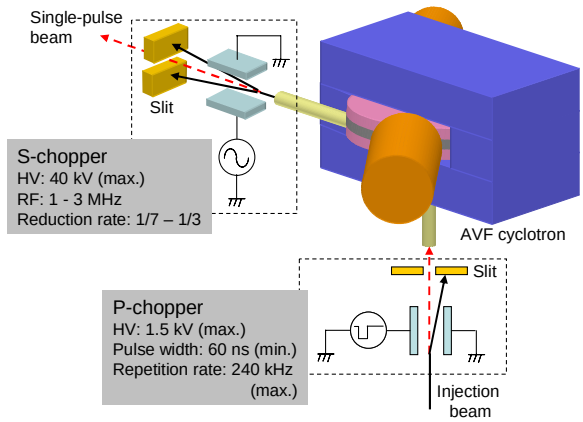

Figure 1: Layout of a chopping system consisting of two types of high voltage kickers: P-chopper and S-chopper.

The number of multi-turn extraction amounted over 30 when good isochronism was formed and the beam current was maximized at the exit of the cyclotron. The most effective way to reduce the number of multi-turn extraction was detuning the magnetic field from isochronism by changing coil current of the outermost trim coil. As a natural result, the beam current considerably decreased. We had formed single-pulse beam using the chopping system in this way. But the beam could not be provided for users stably over 30 min since the magnetic field gradually decreased by the order of 10^{-4} due to temperature rise of the cyclotron magnet, which led growth of the number of multi-turn extraction beyond the limitation.

The central region equipment was improved to precisely define the beam phase width [3], and the magnetic field was stabilized within $\Delta B/B = 1 \times 10^{-5}$ by keeping temperature of the magnet constant [4] mainly for reducing an energy spread of the ion beam using flat-top acceleration technique [5]. In addition, we have developed a new technique to measure and control an acceleration beam phase [6]. These improvements and technique greatly help us to form and provide single-pulse beam stably. In this paper, we describe the chopping system, control of the acceleration beam phase, and result of experiments for single-pulse beam formation of carbon ion.

CHOPPING SYSTEM

Figure 1 shows a layout of equipments of the chopping system consisting of two types of high voltage kickers. The first kicker (P-chopper) installed in the injection line generates beam pulses with repetition period of over 1 μs.

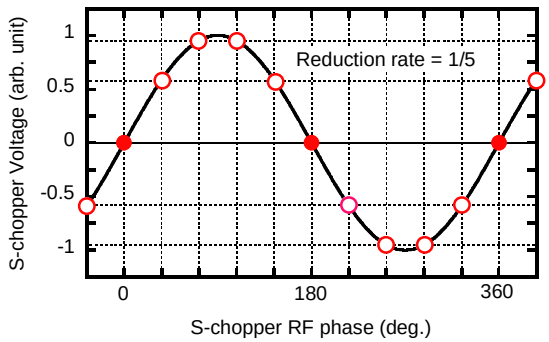

Figure 2: Distribution of beam bunches on the S-chopper RF phase for thinning out with reduction rate of 1/5. The beam bunches represented by open circles deflect from the beam transport axis, while ones represented by closed circles travel along the axis.

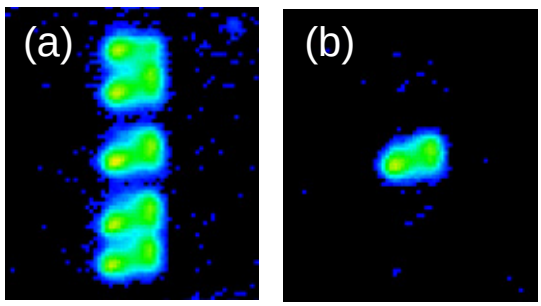

Figure 3: 2D deflection images of the 220 MeV $^{12}C^{5+}$ beam (h = 2) on the alumina scintillator obtained using the S-chopper with the reduction rate of 1/5: (a) no cutting beam, (b) cutting beam by the slit.

The pulse width is about a cycle length of acceleration frequency. A fast pulse generator (PVX-4150, Directed Energy, Inc.) is used as a main component of the P-chopper. The other kicker (S-chopper) in the transport line thins out needless beam pulses caused by multi-turn extraction. The S-chopper generates RF high-voltage ranging from 1 to 3 MHz, and vertically deflects most of the beam bunches. The deflected beam bunches are cut by a downstream slit. Reduction rate of the beam bunches is selectable from 1/7 to 1/3. When the reduction rate is 1/N, the operational frequency of the S-chopper f_{SC} is given by

$$f_{SC} = \frac{f_{RF}}{2N},$$

where f_{RF} is the acceleration frequency of the cyclotron and N is an integer between 3 and 7. We mostly use 5 or 6 as N.

An optimal relation between the beam bunches and the S-chopper voltage waveform with the reduction rate of 1/5 is shown in Fig. 2. Figure 3 shows 2D deflection images of a 220 MeV $^{12}C^{5+}$ beam (h = 2) on an alumina scintillator obtained using the S-chopper with N = 5. An RF phase of the S-chopper voltage was fine-tuned to obtain the 2D image of Fig. 3 (a). The beam current measured by a Faraday cup reduced to about 1/5 with cutting beam by the slit. When the number of multi-turn extraction is limited less than 9, we can obtain single-pulse beam using the P-chopper together with the S-chopper. In the case of h = 1, the number of multi-turn extraction is also allowed up to 9 when N equals to 5.

CONTROL OF ACCELERATION BEAM PHASE

A phase excursion, relative variation of the beam phase, is commonly measured by a phase probe to form the isochronous field. However, it is difficult to measure the acceleration beam phase θ which means the absolute value of the beam phase in an energy gain curve. The energy gain of the ion is the maximum at θ = 0°. In addition to defining the beam phase width, control of θ is also very effective to reduce the number of multi-turn extraction since radial spread of the beam bunch narrows due to reduction of the energy spread. Recently, we have developed an easy method to measure θ in the cyclotron. Beam current at a fixed radius before extraction is measured by a probe slightly varying the acceleration frequency within about $\Delta f_{RF}/f_{RF} = \pm 5 \times 10^{-4}$ to obtain a trapezoidal current pattern. The acceleration beam phase is obtained by analyzing symmetry of the beam current pattern; when θ equals to 0°, both absolute values of $\Delta f_{RF}/f_{RF}$ where the beam current disappears are the same. The beam phase width is also obtained by analyzing gradient of beam current decreasing part. Once θ is measured, we can control it by changing magnetic field of the central bump without breaking the isochronous field.

Figure 4 shows beam current distributions of the 220 MeV $^{12}C^{5+}$ measured by a deflector probe with a differential head. A clear turn pattern is seen when θ was estimated to be –3° (optimum condition). On the other hand, no clear turn pattern is seen when θ lagged by 15° by changing coil current of C2 trim coil which generates the central bump (C2 change). This result indicates that our method to control θ has enough reliability. The former instability of the magnetic field was simulated by changing coil current of the outermost trim coil (C12). The magnetic field reduction of 1×10^{-4} in the whole acceleration region lagged θ by about 20° at the extraction radius, and this operation also disappeared the clear turn pattern (C12 change). Compared with the

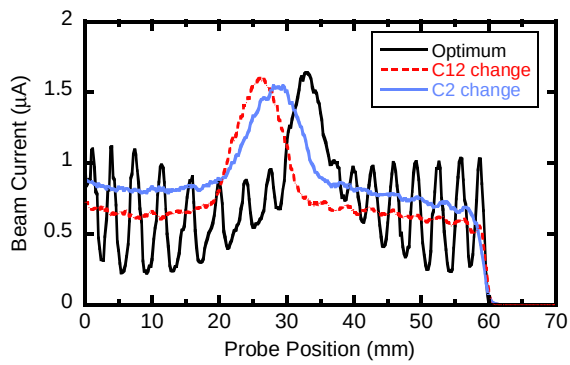

Figure 4: Beam current distributions of the 220 MeV $^{12}C^{5+}$ measured by the deflector probe for three conditions of acceleration.

optimum condition, the beam current at the exit of the cyclotron decreased to 58% and 18% for C2 and C12 trim coil current change, respectively. The beam phase width was estimated to be 6° in full width at half maximum in the cyclotron. This result, obtained without drastic beam cutting, indicates that the new central region has good performance for $h = 2$.

FORMATION OF SINGLE-PULSE BEAM

Experiments to form single-pulse beam were done with the reduction rate of the S-chopper of 5. First, we measured the number of multi-turn extraction by a plastic scintillation counter using only the P-chopper. Figure 5 shows beam pulse trains of the 220 MeV $^{12}C^{5+}$. Acceleration conditions are the same as those in Fig. 4. Quasi single-pulse beam was confirmed for the optimum condition of θ, and single-pulse beam has been formed easily using the two choppers. Although quasi single-pulse beam was obtained in the case of C12 change, the main pulse could not pass through the slit of the S-chopper because the bean bunch was extracted laggardly due to decrease of the energy gain. This change of the magnetic field must have made single-pulse beam lost on a user target. On the other hand, obvious multi-turn extraction was confirmed for C2 change, but the number of the beam bunches was less than 9. There is nothing difficult in forming single-pulse beam for the multi-turn extracted beam in this case.

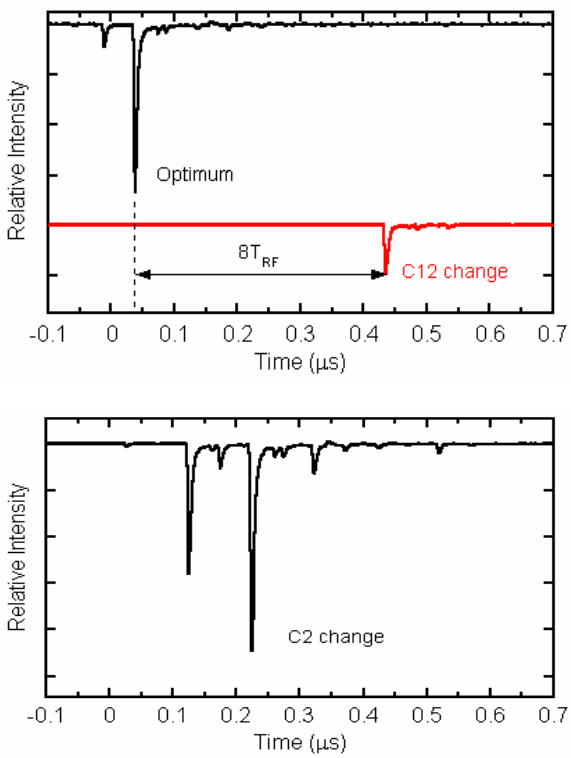

Figure 5: Beam pulse trains of the 220 MeV $^{12}C^{5+}$ (h = 2, T_{RF} = 49.0 ns) measured by the plastic scintillation counter. Beam pulses with duration of about a cycle length of the acceleration frequency were injected into the cyclotron using the P-chopper.

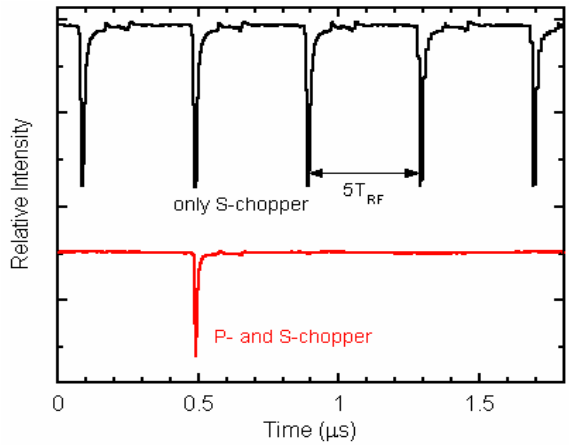

Figure 6: Beam pulse trains of the 320 MeV $^{12}C^{6+}$ (h = 1, T_{RF} = 80.3 ns) formed by the chopping system. The reduction rate of the S-chopper was 1/5.

Formation of single-pulse beam of a 320 MeV $^{12}C^{6+}$, a heavy-ion beam with the highest energy per nucleon at TIARA, was carried out at h = 1. Figure 6 shows pulse trains of the beam obtained using the chopping system. The S-chopper was operated with the reduction rate of 1/5, and the number of multi-turn extraction was limited to 7 by tuning the phase slit and the P-chopper. As a result, excellent single-pulse beam was obtained.

Main coil current of 900 A for the 320 MeV $^{12}C^{6+}$ is the highest value for all ion beams accelerated by the cyclotron. Therefore, the most serious magnetic field reduction arose before because temperature rise of the magnet originated from heat generation of the main coil. However, we have succeeded to provide single-pulse beam of heavy-ion with the highest energy stably over 4 h without retuning of the cyclotron.

ACKNOWLEDGEMENTS

This work was supported, in part, by a grant from the Ministry of Education, Culture, Sport, Science and Technology.

REFERENCES

[1] M. Taguchi, et al., Nucl. Instr. and Meth. B 132 (1997) 135.
[2] W. Yokota, et al., Rev. Sci. Instrum. 68 (1997) 1714.
[3] M. Fukuda, et al., Proc. 17th Int. Conf. on Cyclotrons and their Applications, Tokyo, Japan, 2004, 113.
[4] S. Okumura, et al., Rev. Sci. Instrum. 76 (2005) 033301.
[5] S. Kurashima, et al., Rev. Sci. Instrum. 80 (2009) 033302.
[6] S. Kurashima, et al., Rev. Sci. Instrum. 81 (2010) 033306.

BEAM DIAGNOSTIC COMPONENTS FOR SUPERCONDUCTING CYCLOTRON AT KOLKATA

S. Roy#, S. Bhattacharya, T. Das, T.K. Bhattacharyya, G. Pal, C. Mallik and R.K. Bhandari
Variable Energy Cyclotron Center, 1/AF Bidhan Nagar, Kolkata 700064, India.

Abstract

VEC Centre Kolkata has constructed a K500 superconducting cyclotron (SCC). Several beam diagnostic components have been designed, fabricated and installed in SCC. In the low energy beam line, uncooled slits, faraday cup, beam viewers, and collimators are used. The inflector is also operated in a faraday cup mode to measure the beam inside SCC. The radial probe and viewer probe are respectively used to measure beam current and to observe the beam size and shape inside SCC. The magnetic channels, electro-static deflectors and M9 slit are also used to measure beam current at the extraction radius. Water cooled faraday cup and beam viewers are used in the external beam line. The radius of curvature of the radial probe track was reduced to align the internal and external track during its assembly. It was observed that the probe did not functioning properly during beam trials. Different modifications were incorporated. But, problem with the probe persisted. The paper describes the beam diagnostic components used in the cyclotron, discusses the problems faced in operating the radial probe, modifications tried and outlines the future steps planned to operate the beam diagnostic components.

INTRODUCTION

Beam diagnostic components are used to detect various parameters of the beam of charged particle as it is transported from the ion source to the superconducting cyclotron, accelerated within it and finally extracted from the cyclotron.

BEAM CHAMBER DIAGNOSTICS

The charged particles are axially injected at the centre of the cyclotron and an electrostatic filed is applied across the electrodes of a spiral inflector to inflect the particles at the horizontal median plane of the cyclotron. The inflector can also be used in diagnostic mode to detect the beam injected at the cyclotron centre by measuring the beam current on the electrodes.

Main Probe

The main probe is the most sophisticated diagnostic instrument used for tuning the internal beam from central region up to extraction radius. It consists of a vertical array of three electrically isolated probe segments which measures the distribution of charged particles across the median plane and a differential wire which provides information on the centering of beam. The probe is inserted within the beam chamber along a curved path through the 27 mm aperture between liners along the center of the hill. The probe is a 1100 mm long assembly of several carts and links connected end to end using hinged joints and flexible enough to follow the slotted track. Two guide wheels are mounted at the bottom of each cart which are inserted into the 3.2 mm deep slot of the track so that the probe can follow the track contour as its rear end is pushed to and fro with a linear drive system [1]. The track consists of a curved and straight segment connected together with a transition track. Curved track is brazed on the liner and straight portion of track is laid through the radial penetration of the beam chamber. Probe carts are provided with a spring loaded top wheel which is kept in contact with the upper liner. The downward force due to compression of the spring prevents any upward movement of the probe from the track.

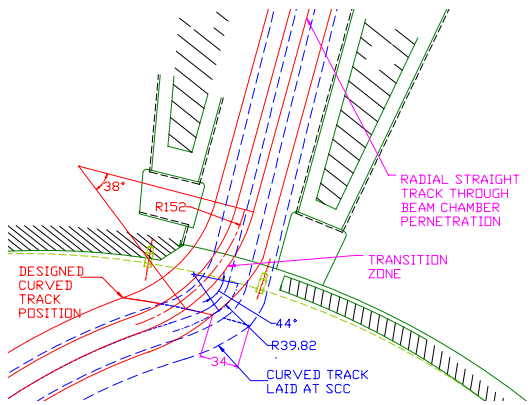

Figure 1: Change in main probe track

It was observed during assembly of magnet with cryostat that the curved track was shifted by 34 mm from the straight track (Fig.1). In order to accommodate this error, the radius of curvature of the transition track was reduced to 38 mm instead of its designed value 152 mm. It was found during initial operations of the probe that the guide wheels were severely worn and finally dislodged on track causing malfunction of probe. Design modifications e.g., change of material of the guide wheel shaft from phosphor bronze to stainless steel and use of larger circlip (6 mm) to clamp the guide wheel shaft with the probe carts were implemented to resolve the problem of disintegration of probe components. The modified probe used to go out of track (see Fig. 2) near the small curvature zone as it is pushed from the rear end and ultimately get trapped between the liners. The problem of derailed movement persists even after the probe was reconstructed with smaller link length so that it can negotiate smaller bend radius. The solid height of the probe was increased such that the space available in

#suvadeep@veccal.ernet.in

Figure 2: Main probe in derailed condition within the beam chamber.

between upper liner and probe top would not be sufficient for upward movement and subsequent failures. The modifications could not succeed due to variation of track height, varying inclination of the track and unevenness of the liner gap along the complete length of the track.

A theoretical analysis has also been carried out to assess the effect of lateral thrust on the probe near the transition zone. Lateral thrust would result in increase of frictional resistance against the probe motion and as it is pushed from rear end, the whole train tends to buckle and finally comes out of the track. The link angles are obtained corresponding to different position of link at the transition zone. The cosine components of this angle are multiplied to obtain the transmitted force (F2) and the remaining part causes lateral thrust only (Fig. 3). The lateral reaction force imparted by track on the probe links becomes significantly high as the radius of curvature is reduced (Table-1).

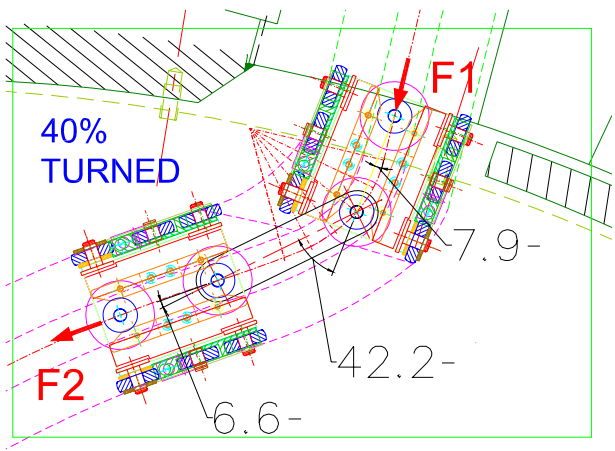

Figure 3: Component of link forces near transition zone

Viewer Probe

The viewer probe is used to observe the shape of the charged particle beam inside the cyclotron from 350 mm radius to extraction radius. A fluorescence is produced as the accelerated particles hit the zinc-sulphide (ZnS) screen of viewer probe and the illumination is brought out to the CCD camera placed out side the beam chamber using a small aperture borescope.

Table 1: Comparison of Thrust on Main Probe

Link Rotation	**Thrust component of driving force (F_1)**	
	At design curvature R = 152mm	At as built curvature R = 38mm
0% turned	0.19	0.24
20% turned	0.18	0.28
40% turned	0.15	0.27
60% turned	0.15	0.24
80% turned	0.15	0.23
100% turned	0.18	0.25

Magnetic Channels and M9 Slit

The electro-static deflectors, passive magnetic channels no. 1 to 8 are placed along the extraction path of the accelerated beam. These devices can be moved radially within a short span and current due to hitting of beam on these components can be measured to detect the beam trajectory.

M9 slit along with active magnetic channel no. 9 is placed within the yoke of the superconducting cyclotron magnet just before the external beam line. The gap between the slits determines the width of the beam to be delivered through the external line. The beam current measured from the electrically isolated slits can be used for optimising beam transport. M9 slit (Fig 4) is operated using a non conventional pneumatic circuit, since it is placed within a strong magnetic field. The slit opening can be varied from 2 mm to 26 mm through a closed loop control circuit consisting of a pneumatic cylinder, a current to pneumatic pressure converter, linear potentiometer and a control modules [2]. A pair of double acting pneumatic cylinders is used to move both slit jaws in either direction. Each cylinder is actuated by two current to pneumatic converter, which varies cylinder pressure according to the current input. The position of the slit is sensed by a linear potentiometer and fed back to the control module. The control unit compares the slit position with the set one and sends the forward signal to current to pneumatic converter.

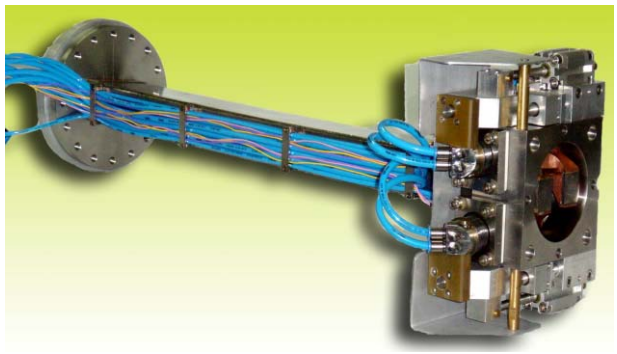

Figure 4: M9 Slit.

BEAM LINE DIAGNOSTICS

Beam diagnostic components installed at injection and external beam line are similar in principle except the addition of cooling circuit in the external line components to cater to the cooling required for higher beam energy.

Faraday Cup and Beam Viewer

Faraday cup is used to measure the beam current as well as deviation of beam from the center. when it is transported along the beam line. A nine segment disc with eight angular sectors and central one is used to detect the distribution of the beam in the injection line (Fig. 5).

Beam viewer is used to visualize the shape and size of beam at different locations of the beam transportation line. Fluorescence is produced when the beam strikes the zinc-sulphide disc. A camera placed at the view port helps to view the image in the control console

Faraday cup and beam viewer uses similar drive system comprising a double acting pneumatic cylinder of 100 mm stroke actuated by a two-way direction control valve. The diagnostic element is mounted on the carriage of linear drive system comprising three parallel guide shafts. It is inserted at the center during diagnostic mode and kept away from beam line during transportation of beam. End position feedbacks are obtained from two limit switches.

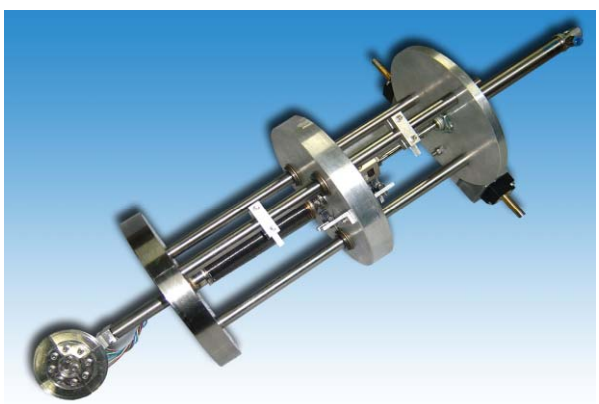

Figure 5: Faraday Cup used in low energy injection line.

Slit

Slits are installed at various locations of beam line to trim the beam width. Two electrically isolated copper jaws are mounted on two lead screws which are constrained to rotate but free to move axially (Fig. 6). The lead screw nuts are rotated by two independent motor drive and the lead screws along with the jaws slide over span of 20 mm from the mean position. Two rotary encoders are used to obtain the position feedback for each slit.

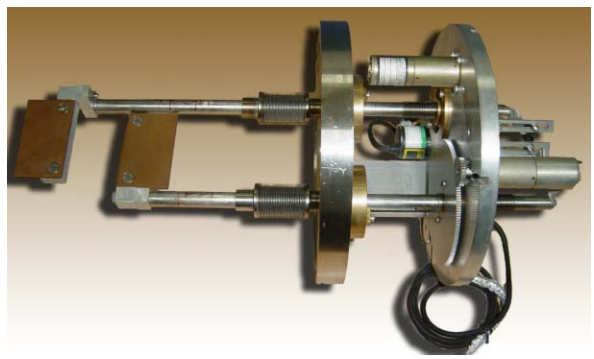

Figure 6: Un-cooled Slit.

CONCLUSION

- Problems were faced in operating the main probe. The following alternatives are planned.
  - A new cart has been designed, where welding has been completely eliminated and the downward spring force has been increased to restrain upward movement of the probe.
  - It is proposed to convert the open slot of the track in to a 'T' slot and design a new cart with its lower guide wheels moving inside the slot. The slot would not allow the probe to come out from the track.
  - Partial modification of contoured track on liner is also suggested. Feasibility of removing a part of curved track from the liner and reinstallation of the track with larger radius of curvature is also being studied.
- Viewer Probe having similar design as the main probe but without a track, M9 Slit, Faraday Cup, Beam Viewer and Slits are all functioning properly.

REFERENCES

[1] S. Roy, S. Bhattacharya, T. Das, T.K. Bhattacharyya, S. Pal, G. Pal, C. Mallik and R.K. Bhandari, "Fabrication of Beam Diagnostic Components for Superconducting Cyclotron at Kolkata", CREMC, Kolkata, June 2009, p. 102 (2009);

[2] T.K. Bhattacharyya, S. Roy, T. Das, C. Nandi, S.K. Mishra, G. Pal, C. Mallik, and R.K. Bhandari, "Kolkata Superconducting Cyclotron M9 Slit Control" National Symposium on Nuclear Instrumentation, Mumbai, February 2010.

STUDY ON PXI AND PAC-BASED HIL SIMULATION CONTROL SYSTEM OF CYCHU-10 CYCLOTRON

Xiao Hu#, Dong Li, Yongqian Xiong, Jun Yang, Tiaoqin Yu, HUST, Wuhan, China.

Abstract

Using the technology of hardware in loop (HIL), control system simulation model of the CYCHU-10 cyclotron is developed with real-time, simulation and statechart module under the LabVIEW environment. A prototyping design method based on NI PXI operation condition virtual platform and PAC controller is presented. The result indicates that the platform is feasible and effective in completing control system test under hardware virtual environment and shortening development time.

INTRODUCTION

The core problem of cyclotron control system design is how to ensure the high availability (HA) of the control system which involves the reliable operation study, failure mode and detection algorithm analysis, and avoidance of conflict strategy research. Hardware-in-the-loop (HIL) simulation is becoming a significant tool in prototyping complex, highly available system, especially when a portion of the given system is a simulation algorithm and a portion of the same system is a hardware implement. HIL technology is introduced into CYCHU-10 control system design, prototyping and testing because of the complex internal algorithms, possible catastrophe if failed in the testing, and difficulty in building a laboratory test environment with fully real system [1].

In order to improve efficiency and reduce risk, our team has accomplished the whole machine running simulation by use of virtual prototyping (VP) technology relied on the existing control design tool, experimental data and operating experience. But from off-line simulation to prototype test, it is impractical to proceed under fully real facility environment in consideration of safety, feasibility and cost. This paper describes a HIL simulation platform based on NI PXI, PAC and LabVIEW, which accelerating the controller validation test under hardware virtual environment, and shortening the design cycle.

THE HIL SIMULATION SYSTEM

The purpose of the HIL simulator is to achieve an interaction between a real implement of a closed-loop control system and a simulated plant. There are many commercial off-the-shelf (COTS) tools for HIL, such as dSPACE, xPC target, RT-lab [2], etc, which are widely used in the fields of auto industry, aerospace and weapon manufacturing. But dSPACE development tools are expensive while the data acquisition board of xPC Target may bring some inconvenience to user. With the evaluation of performance, learning time, acquisition cost and required coding, we choose NI LabVIEW to simulate a plant model with real-time hardware and add real-world I/O to the model created in Simulink software environment.

#huxiao_hust@163.com

Hardware Structure

The HIL simulation platform consists of host station, PAC controller, PXI simulator, and external actual auxiliary system (see Fig. 1).

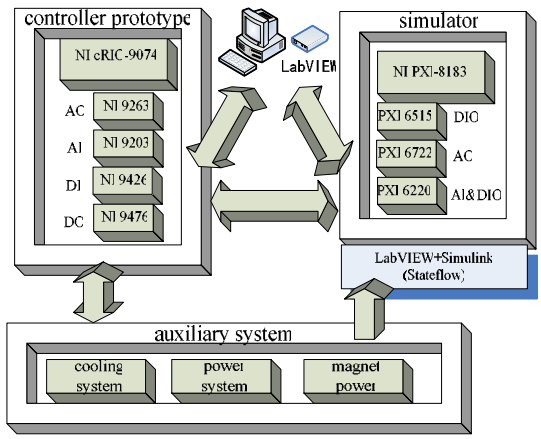

Figure 1: Hardware structure of HIL platform.

- The host station is an industrial PC with a Windows operation system, which serves as the user interface (see Fig. 2) adopting network sharing variable technique and allows user to edit and modify models with any popular model builder software such as LabVIEW. In addition, it also used in fault inserting, parameter configuring, and data recording.

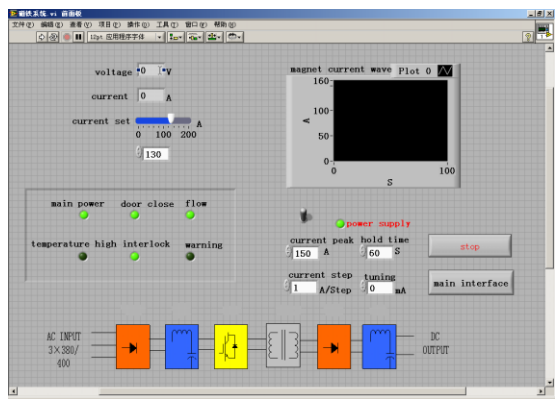

Figure 2: GUI of magnet power supply.

- NI compact RIO platform (Programmable Automation Controller) is used as rapid controller prototype running feedback control algorithm. NI 9203 module (AI board) reads not only the pressure,

vacuum degree, ion source voltage and current, motor position, beam amplified current, and phase load from cyclotron simulation model, but also the real temperature and conductivity signal from the existing cooling system. NI 9263 module (AO board) sets the parameter of Dee voltage, motor speed, flow of hydrogen and current in ion source. NI 9426 and 9476 (DIO board) mainly treat with the interlock signals, valve on/off, water flow switch and contactor in the power distribution system.

- PXI simulator builds up a whole model of CYCHU-10 cyclotron based on graphical programming language, which can reflect the system response under various conditions in the real time. In order to guarantee the fidelity of a real running cyclotron, PXI system needs to embody all kinds of working conditions such as automatic operation, manual operation and faults maintenance. Configurable parameters supplied by the simulator allow the user to rapidly investigate interactions between components or to explore the influence of design parameters on system performance.
- Auxiliary system includes power distribution system, high precision magnet power supply and water cooling system. In the HIL simulation, these equipments are connected to each load in close loops for the purpose of acquiring real time test data.

The host PC, controller and simulator exchanges data through the field bus and the auxiliary system transfers the real time signals to the PXI and PAC by means of sensors, actuators or serial communication module of its own. In addition, the PXI simulator also modifies the cyclotron model dynamically by inverse operation of the acquisition signals such as temperature, water level, conductivity, *etc*. One of the most important characters of the PXI simulator is the ability to change among different working conditions, even the extremely error pattern. For example, it can simulate the system response when Dee sparks, flow deficiency in RF subsystem, grid power supply error or diffusion pump temperature switch operation, *etc*. These test items are significant to improve the reliability of control system, and HIL simulation is beneficial in both cost reduction and risk control.

Software Design

As an effective and extensive use tool, Simulink is suitable for modelling, simulating, and analyzing complex dynamic system like cyclotron. Beside, its statechart module which complements Simulink with its handling of event-based system can describe the sequential control process of CYCHU-10 graphically. So we firstly create the finite state machine (FSM) off-line model of the subsystem of vacuum, RF, ion source and so on. Then separating the model into target part and main control logic part, and introducing respectively to the PXI and PAC real time HIL simulator via interactive environment between LabVIEW and Simulink. This hybrid programming method based on the comparative advantages of different development packages increases the efficiency and reduces the repeated work. The Simulation Interface Toolkit (SIT) Connection Manager in LabVIEW can connect real time signal to the input node of the Simulink model to ensure determinism and change the parameters or introduce parameters on text in the process of simulation, contributing to the regulation of multi-parameter complex system like cyclotron. Moreover, the use of statechart module is helpful to the control system modelling based on state transition and event driven.

HIGH AVAILABILITY OF HIL

The definition (see Eq. 1) shows that availability is proportional to the Mean Time Between Failures (MTBF). A failure has some Mean Time To Repair (MTTR). The key techniques used to build a high availability system are 1 modularity, 2 fail-fast (means either operate correctly or stop immediately), 3 independent failure mode, 4 redundancy [3] .These concepts embody both in the software design and the hardware construction. NI hardware itself has the outstanding performance of availability and the characteristic of modularity. So we put more emphasis on the part of software. The software structure in Figure 3 is modularized and the reboot files are a valuable tool for running infrastructures that provide services with high availability requirements. The Simulink (stateflow) model in Figure 4 indicates that special fault handling modes are designed to tolerate fault (means to detect the fault, report it, mask it, and then continue service while the faulty component is repaired offline).

$$\text{Availability} = \frac{\text{MTBF}}{\text{MTBF} + \text{MTTR}} \qquad (1)$$

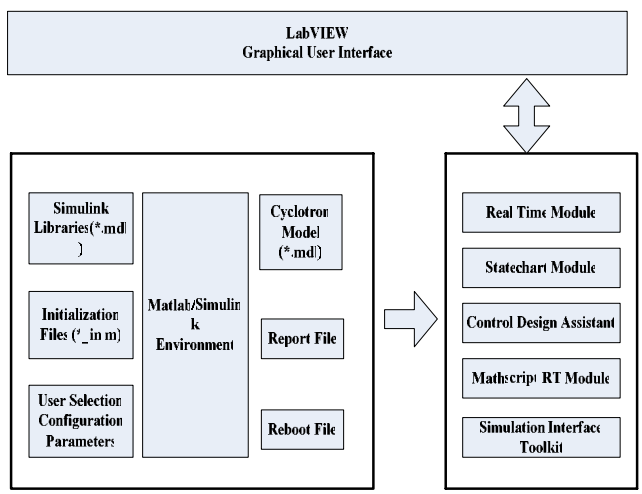

Figure 3: Software structure of HIL platform.

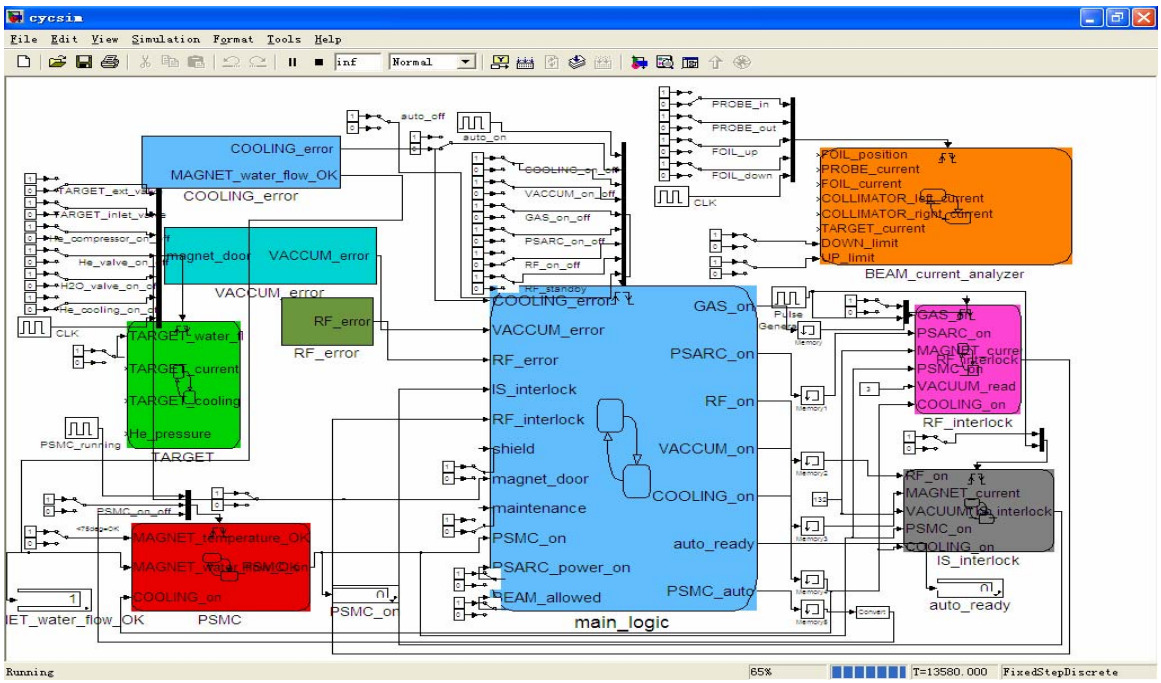

Figure 4: Simulink model of CYCHU-10 cyclotron

CONCLUSIONS

On account of the particularity of cyclotron, the reliability is the primary consideration for control system designer. NI software and hardware are widely used in accelerator measure and control field, such as LHC in CERN, KIRAMS-13 in Korea, XAFS experimental system in IHEP, etc. But we can not find many researches on cyclotron HIL simulation system. The HIL close-loop between controller rapid prototyping on the PAC platform and working condition simulation on the PXI hardware can avoid accidents within controlled extreme test environment. Furthermore, the components characteristic of high real-time property can verify the controller function precisely, correct the system design without delay and greatly reduce the development time.

REFERENCES

[1] Bacic, Marko, Neild, Simon, Gawthrop, Peter, "Introduction to the special issue on the hardware in-the-loop simulation", Mechatronics 19, p. 1041-1042(2009).

[2] Baracos, P., Murere, G., Rabbath, C.A., "Enabling PC-based HIL simulation for automotive applications", IEMDC 2001. IEEE International Electric Machines and Drives Conference 721-9(2001).

[3] Gray, J., Siewiorek, D. P., "High-availability computer system", Computer 24, p. 39-48(1991).

BEAM EXTRACTION SYSTEM AND EXTERNAL BEAM LINE OF KOLKATA SUPERCONDUCTING CYCLOTRON

J. Debnath#, S. Paul, M. K. Dey, U. Bhunia, J. Pradhan, P. S. Chakraborty, B. Shoor, Md. Z. A. Naser, C. Mallik, G. Pal, S. Bhattacharya, T. K. Bhattacharya, R. K. Bhandari
Variable Energy Cyclotron Centre, 1/AF, Bidhan Nagar, Kolkata 700064, India

Abstract

All the major components of the extraction system of the Kolkata superconducting cyclotron are installed and functional. It includes the Electrostatic deflectors, magnetic channels, M9 slit etc. Internal beam acceleration has already been done successfully and now we are on the verge of extracting and transporting the beam to the cave.

The external beam transport system has been designed comprising of quadrupole magnets, steering magnets, switching magnets, beam diagnostics etc.

One of the four beam lines has been installed, which extends 20 meters up to the experimental cave-1. Control and monitoring system for all these components have been developed and tested. All the beam dynamical and technical aspects of the beam extraction and beam transportation have been discussed.

INTRODUCTION

The extraction system of the Kolkata Superconducting Cyclotron consists of two electrostatic deflectors (the first one is 55o long and the second one is 43o long positioned in the successive hills of the magnet), eight passive magnetic channels, one active magnetic channel and two compensating bars. The active magnetic channel (M9) is located in the yoke hole of the main magnet. Except the active magnetic channel all the other elements are radially moveable as the beam dynamics demands that the extraction components must be moveable to suit extraction conditions of different beams and as the beam traverses almost 330o before being extracted out of the cyclotron. The computer controlled drive system can move the elements precisely.

The extracted beam from the super conducting cyclotron will be transported through four beam lines (channels) to the experimental area. Channel#1 will be at 0 degree. The external beam line layout is shown in figure 6. The beam optics calculation of channel#1 has been carried out. The cyclotron will be operating between 3 Tesla to 5 Tesla average magnetic field. The phase space characteristics of the extracted beam will have wide variations owing to passive magnetic channels being used in the extraction system. So different momentum particle will have different beam characteristics and these wide variations have been considered for beam optics calculation. The optics calculation has been done by Graphic version of Transport code [1].

jdebnath@vecc.gov.in

Extraction Elements

The extraction system layout is shown in figure 1. All the different parameter of the extraction elements that affects the beam behaviour is listed in Table 1. For the deflectors, the septum to electrode gap is set to 6 mm and the maximum voltage is set at 100 kV. To compensate the field perturbation effects of the magnetic channels on the inner orbits, two compensating bars (C_1 and C_2) are used, C_1 compensates the effect of M_1 while C_2 compensates the overall effect of the remaining magnetic channels.

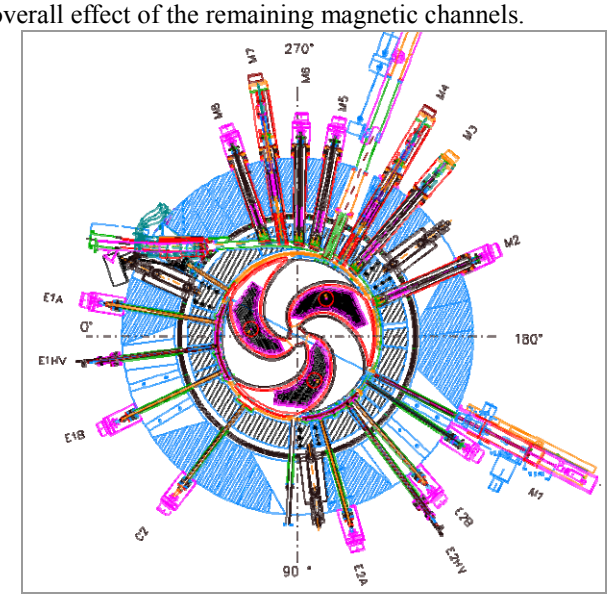

Figure1 Extraction system layout

Table 1: Extraction Element's parameters

	θ_I	θ_F	*R (min)*	*R (max)*	*Rbar (min)*	dR	B	dB/dx
			mm	mm	mm	mm	(kG)	(kG/cm)
E1 A	-23		672.4	678.5	-	6.1		
E1 B	32		678.2	686.4	-	8.2		
E2 A	94		682.2	690.8	-	8.6		
E2 B	137		698	707	-	9.0		
M1	140	153			*702.0*	13.8	1.14	3.46
M2	200	206			*711.0*	17.5	1.14	3.46
M3	226	232			*731.8*	64.0	1.05	5.24
M4	236	242			*730.3*	83.0	1.05	5.24
M5	256	262			*758.8*	18.0	1.05	5.24
M6	266	272			*776.4*	18.0	1.05	5.24
M7	276	282			*800.7*	86.0	1.14	3.46
M8	286	292			*836.4*	17.0	0.97	4.57
C1	320	334			705.5	2.5		
C2	46	58			735.3	6.4		

θ_I , θ_F : Initial and final azimuth of the element listed, Rbar gives the magnetic channel position with respect to cyclotron centre.

Calculations

The beam properties were calculated by the ray tracing method. The radial and axial phase space ellipses of the different beam species obtained by tracking the corresponding eigen ellipses from the deflector entry to the M9 slit passing through the extraction path were investigated as shown in figure 3. The initial ellipse is obtained by running the equilibrium orbit code GENSPEO [2]. The area of the phase space ellipse taken into account is 30 mm mrad.

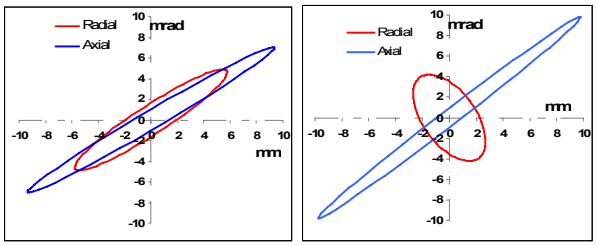

Figure 2. Phase Space Ellipse at (a) Deflector midpoint (b) M9 Slit for Ne3+, E/A=4.5 MeV/A, Bo=30.5 kG

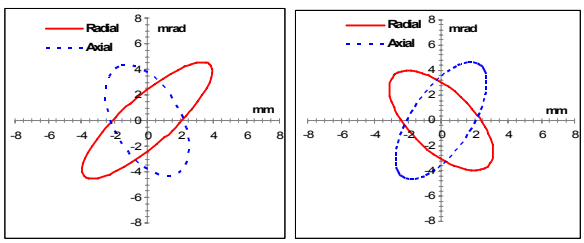

Figure 3. Phase Space Ellipse at (a) Deflector Entry (b) M9 Slit for He1+, E/A=20.1 MeV/A, Bo=38.3 kG

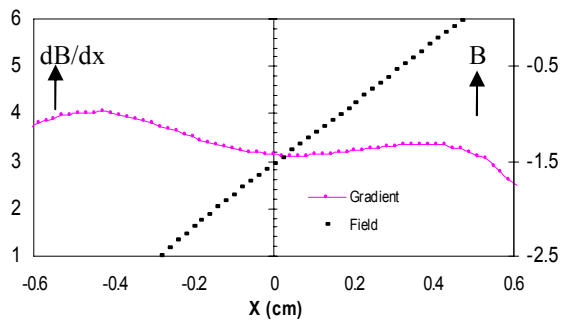

Figure 4. Field gradient (in kG/cm) and Field (in kG) across a magnetic channel.

Beam Transport Calculation

The maximum rigidity of the cyclotron beam is 3.3 Tesla metres hence momentum is about 1GeV/c. The emittance of the beam is considered to be 30 mm mrad. Four different ellipses are considered and the initial ellipses are not upright ellipse as correlation matrix has been introduced. Energy spread is considered to be 0.12%. High rigidity beam is focussed at the first beam viewer and slit size is kept according to the size of the beam to be obtained at the target position. To obtain a particular beam size, first quadrupole triplet may need slight variation in current because of different input beam parameters. The beam optics from first beam viewer to the image point at the second beam viewer in the vault is set as point to point and unity magnification. This is done by two sets of quadrupole triplet. The beam optics from the second beam viewer to the third beam viewer is also set as point to point and unity magnification. A required beam spot can be achieved with this beam optics configuration at the target positions. A beam input parameters is given in the Table 2.

Table 2: Input beam parameters

	Beam 1	Beam 2	Beam 3	Beam 4
X(cm)	0.90	0.89	0.95	0.54
θ (mr)	2.00	1.78	2.68	1.78
Y(cm)	0.94	0.56	1.23	1.13
Φ (mr)	8.94	8.06	1.12	5.58
l (cm)	0.00	0.00	0.00	0.00
δ(percent)	0.03	0.03	0.03	0.03
P(GeV/c)	1.00	1.00	1.00	1.00
R16 cm/(δp/p)%	4.0	-29.6	2.0	-20.0
R26 mrad/(δp/p)%	40.0	4.0	40.0	4.0

Various beam optics options have been tried to achieve required beam size at the target positions. At the same time it was also kept in mind to handle minimum number of parameters during beam transportation.

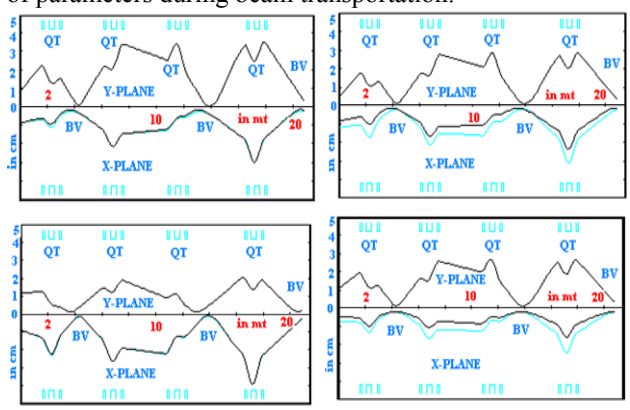

Figure 5. Beam envelopes for 4 types of Beam

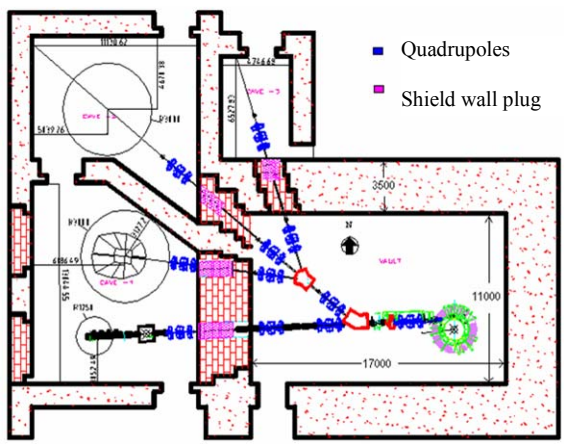

Figure 6: External Beam Handling System Layout

ACKNOWLEDGEMENTS

The authors would like to thank all the colleagues of the Accelerator Physics Group for their support and co-operation. Their contribution led to the successful commissioning of the superconducting cyclotron and first internal beam commissioning at VECC, Kolkata.

REFERENCES

[1] K.L.Brown, D.C.Carey, Ch. Iselin & F. Rothacker, "TRANSPORT, A Computer Program for Designing Charged Particle Beam Transport Systems", Yellow Reports, CERN 73 – 16 (1973) & CERN 80 – 04 (1980).

[2] M.M.Gordon, "Computation of closed orbits and basic focussing properties for sector-focussed cyclotrons and the design of CYCLOPS",Particle Accelerators, 1984, Vol. 16, p 39 – 62.

[3] J. Pradhan, et. al, "Characteristics of the magnetic channel in the yoke hole of K500 SCC", Presented in this conference.

[4] S. Paul, et. al, "Simulation Study of the Extraction System of K500 Superconducting Cyclotron in VECC, Kolkata", presented in InPAC'05 (2005).

[5] C. Mallik, et. al.,"First Beam Acceleration in Kolkata Superconducting Cyclotron and Its Present Status", presented in this Conference.

CONSISTENCY IN MEASUREMENT OF BEAM PHASE AND INTENSITY USING LOCK-IN AMPLIFIER AND OSCILLOSCOPE SYSTEMS

R. Koyama*[,1),2)], M. Fujimaki[1)], N. Fukunishi[1)], A. Goto[1)], M. Hemmi[1)], M. Kase[1)], N. Sakamoto[1)], K. Suda[1)], T. Watanabe[1)], K. Yamada[1)], and , O. Kamigaito[1)],
1) RIKEN Nishina Center, 2-1 Hirosawa, Wako, Saitama 351-0198, Japan
2) SHI Accelerator Service Ltd., 1-17-6 Ohsaki, Shinagawa, Tokyo 141-0032, Japan

Abstract

The phase probes (PPs) are installed in all cyclotrons and beam transport lines of RIBF, and the beam-bunch signals that are detected nondestructively by these PPs are used for tuning of isochronism of cyclotrons and for monitoring the beam phase and beam intensity. We mainly use a newly developed system that incorporates a lock-in amplifier (LIA) for those tuning and monitoring; however, a conventional measurement method using an oscilloscope (OSC) system is also used. In this study, we investigated the consistency in the measurements carried out using LIA and OSC systems by FFT analyzing the observed data. Additionally, we investigated the measurement accuracy of LIA and OSC.

INTRODUCTION

The RIKEN RI beam factory (RIBF) consists of four ring cyclotrons (RRC, fRC, IRC, and SRC) and two injectors (RILAC and AVF) which are all connected in cascade. RILAC, AVF, and RRC began operation in the 1980s, and fRC, IRC, and SRC were installed in 2006. Phase probes (PPs) are installed in all cyclotrons and beam transport lines of RIBF, and the beam-bunch signals that are detected nondestructively by these PPs are used for tuning of isochronism of cyclotrons and for monitoring the beam phase and beam intensity (Fig. 1). We mainly use a newly developed system that incorporates a lock-in amplifier (LIA; SR844, SRS) for those tuning and monitoring;[1] however, in AVF and RRC, a conventional measurement method using an oscilloscope system (OSC; DSO6052A, Agilent) is used. In this study, we investigated the consistency in the measurements carried out using LIA and OSC systems.

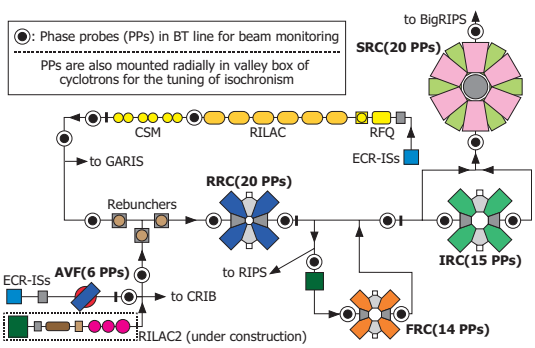

Figure 1: Schematic layout of RIBF.

* rkoyama@riken.jp

MEASUREMENT AND ANALYSIS

The block diagram of the measurement system is shown in Fig. 2. The beam-bunch signals from PPs are divided by a power divider and transported to the LIA and OSC and measured by them simultaneously. LIA use a technique known as phase-sensitive detection and outputs the beam phase and the beam intensity at a specific reference frequency. In order to investigate the consistency with OSC system, the phases and intensities for 1st to 10th frequency components (1f–10f) is calculated by performing FFT-analysis on the data from OSC.[2] These analysis were processed automatically by the LabVIEW program.

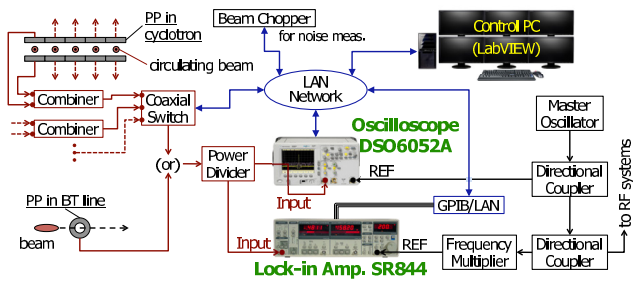

Figure 2: Block diagram of measurement system.

CONSISTENCY RESULTS

Consistency in ischronism of SRC

The comparison of the isochronism of SRC ($^{14}N^{7+}$ beam, Energy: 250 MeV/u, Frequency: 27.4 MHz) that was evaluated on the basis of the results of three measurement methods is shown in Fig. 3. This figure shows the relative beam phase observed by 20 PPs, which are radially mounted in the orbital region of SRC. Here, "LIA-3f"is the beam phase measured using LIA with the third harmonic of acceleration RF as its reference signal, "FFT-3f"is the third frequency component (3f) of FFT-analyzed phase of the beam-bunch signal measured using OSC, and "Zero cross"is the zero-cross points of the beam-bunch shape observed using OSC (conventional method).[2] We measured the 3f component of the beam-bunch signal because it had relatively good S/N ratio. It was observed that the phase differences between the three measurement methods are less than 0.2 ns (approximately 2° at fundamental acceleration RF).

Figure 4 shows the FFT-analyzed phase up to the 10f

component of the beam-bunch signal measured using OSC, together with "LIA-3f"and "Zero cross". Since in the LIA system, we can basically measure only one frequency component of the beam-bunch signal,[2] we need to investigate the other frequency components. However, from the measurements carried out in our work, it was found that the phase differences between ten frequency components are less than 0.5 ns (approximately 5° at fundamental acceleration RF).

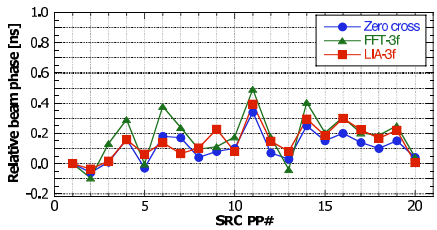

Figure 3: Comparison of isochronism of SRC on the basis of three measurement methods.

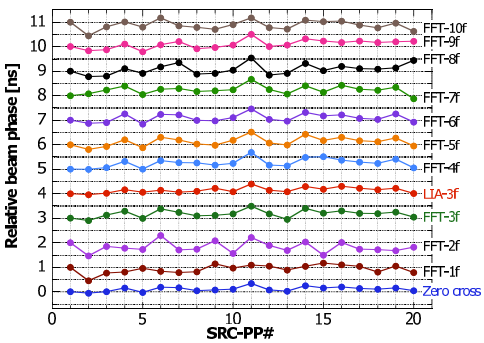

Figure 4: Comparison of isochronism of SRC for 1f–10f of FFT-analyzed phase.

Consistency in ischronism of RRC

On the other hand, relatively large discrepancy among three methods for RRC was observed especially in inner PPs. The results of measurement of RRC ($^{40}Ar^{17+}$ beam, Energy: 95 MeV/u, Frequency: 28.1 MHz) are presented in Fig. 5. This inconsistency is considered to depend on observed-bunch width on the beam orbital. Using OSC, different signal shapes were observed for PPs#1, #10 and #20 as shown in Fig. 6. For RRC, the inner-bunch width is narrower than the outer one unlike in the case of SRC. Figure 7 shows the FFT-analyzed phase of RRC-original data from OSC after the zero-cross points of all PPs of RRC are aligned at the same phase (for more detail, see [2]). The inconsistency between FFT-2f and zero cross is improved if the correction phase is subtracted from original phase as shown in Figure 8. However, the correction is still insufficient especially for PPs#1 and #3. The reason is considered to be the effect of 9f component. As shown in Figure 9, relatively large 9f component is observed in PPs#1 and #3 and is considered to affect the determination of zero-cross points.

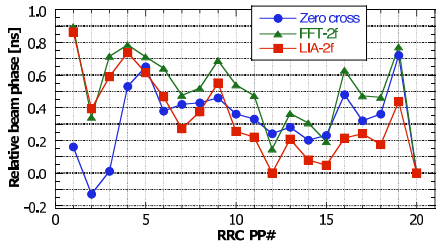

Figure 5: Comparison of isochronism of RRC on the basis of three measurement methods.

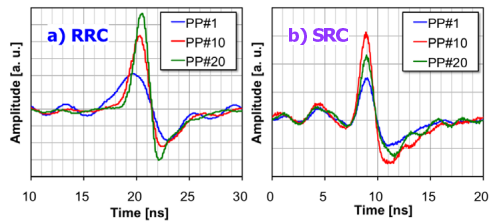

Figure 6: Bunch shape of RRC (a) and SRC (b).

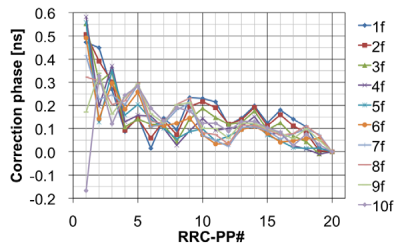

Figure 7: Correction phase depend on bunch width.

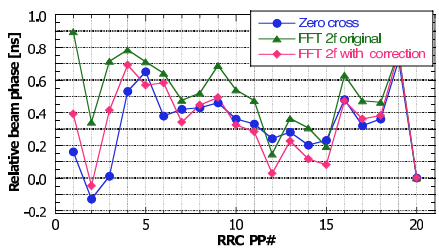

Figure 8: Comparison of isochronism of RRC before and after phase correction.

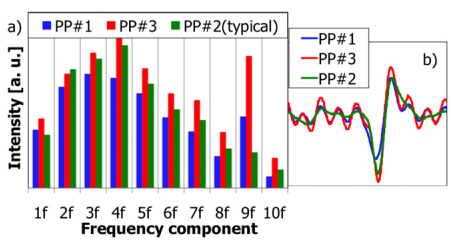

Figure 9: Frequency spectrum (a) and bunch shape (b) of PPs#1, #2 and #3 of RRC

Consistency in variation of beam-phase and intensity

Figure 10 shows the beam phase and the beam intensity of a 0.669-MeV/u $^{136}Xe^{20+}$ beam (RF: 18.25 MHz) de-

tected by PP-S71 (see Fig. 1) over a 4-h period. In this case, the 5f component of the beam-bunch signal had relatively good S/N ratio. The correlation diagrams of the LIA and OSC data presented in Fig. 10 are shown in Fig. 11, and a certain degree of linearity is observed between them.

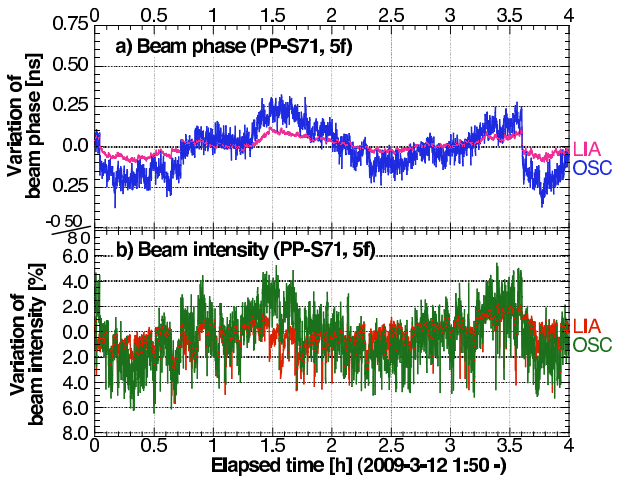

Figure 10: Beam phase and beam Intensity at PP-S71 measured using LIA and OSC systems.

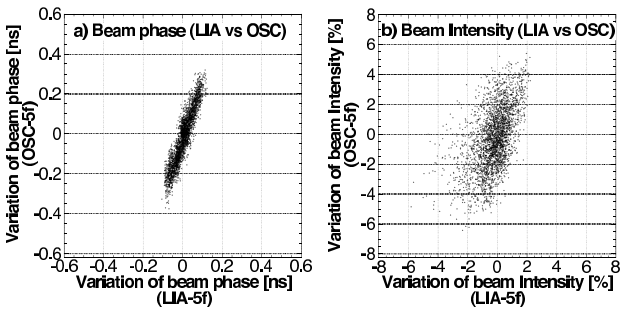

Figure 11: Correlation diagrams for LIA and OSC data presented in Fig. 10.

MEASUREMENT ACCURACY

Since the fluctuation ranges of both the beam phase and the beam intensity measured using OSC are larger than those of the beam phase and the beam intensity measured using LIA, we investigated the voltage and phase resolution of the LIA and OSC using a function generator (AFG3252, Tektronix). Figure 12a shows the phase and voltage variation measured using the LIA and OSC when the input phase and voltage from AFG3252 to them are varied by 0.01–0.10° and 0.01–0.10%, respectively, after 90 s (frequency: 18.25 MHz). Figure 12b shows 90-s average of the phase and voltage variations plotted in Fig. 12a as a function of the total increment in the input phase and voltage from AFG3252. Here, the error bars in Fig. 12b are standard deviation for measurements performed after 90 s each ($\pm 1\,\sigma$), and they represent the measurement uncertainty. We consider the voltage and phase variations, which are obtained irrespective of the error bars, as the resolution. The error margins for LIA in Fig. 12b are insignificant (smaller than the symbols), indicating high measurement accuracy in the case of LIA. The resolution and measurement uncertainty of LIA and OSC are summarized in Table 1.

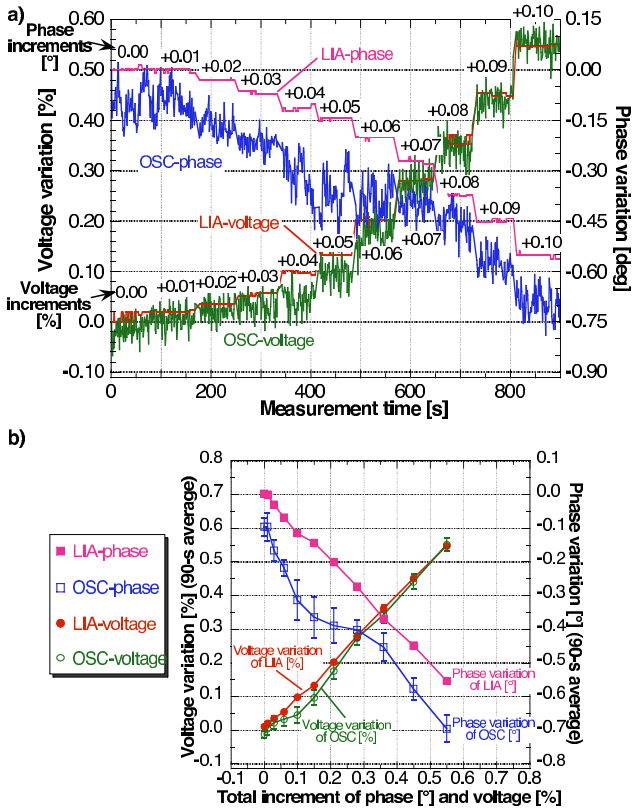

Figure 12: Phase and voltage resolution of LIA and OSC using AFG3252.

Table 1: Estimated measurement accuracy of LIA and OSC systems.

system	phase [°] ([ps])		voltage [%]	
	resolution	uncertainty	resolution	uncertainty
LIA	0.02 (3)	±0.007 (1)	0.02	±0.009
OSC	0.09 (14)	±0.06 (9)	0.05	±0.025

SUMMARY

The consistency in the isochronism measured using LIA and OSC systems is confirmed. However, it was found that some phase correction is needed when the bunch width is different on the beam orbital or some higher frequency components are superimposed on the bunch signal as in the case of RRC. Further investigation for this problem is required. The consistency in the variation of beam phase and beam intensity is also confirmed, and it was observed that LIA has a higher measurement accuracy than OSC.

REFERENCES

[1] R. Koyama et al.: RIKEN Accel. Prog. Rep. **42**, pp. xviii–xix (2009).

[2] R. Koyama et al.: Proc. of PASJ6, Tokai-mura, Ibaraki, August 2009, WOOPB03, pp. 25–29.

EXPERIMENT AND ANALYSIS: PARTIAL LOSS OF INSULATION VACUUM IN K-500 SUPERCONDUCTING CYCLOTRON CRYOSTAT

P. Bhattacharyya, A. Dutta Gupta, S. Saha, M. Ahammed, A. Mukherjee, U. Panda, U. Bhunia, A. De, S.Bandopadhaya, C. Nandi, C. Malik , R. De, S. Saha, J. Chaudhuri, R.K. Bhandari, VECC, Kolkata, India

Abstract

At higher currents in superconducting coil of the K500 superconducting cyclotron, it was found that the insulation vacuum surrounding the LHe vessel deteriorate with increasing current in the coil and finally leading to slow dump of the coil. This is a limitation for further increasing current value in the magnet coil. On the other hand, once the current value was returned to zero, vacuum reading reaches to its initial value. Experiment and analysis have been done to quantify the contribution of molecular gas conduction (FMGC) on heat load because of this partial loss of insulation vacuum. Experiment was also performed to find out how much betterment in terms of heat load is possible by incorporating an additional vacuum pump.

The cryostat safety analysis because of the loss of insulation vacuum has become very important at this new scenario. An analysis has been done to know what could be the maximum pressure rise with time in case of loss of vacuum. This data has been used to know what should be the relieving mass flow rate to avoid any pressure burst accident. Finally this data has been compared with the existing relief valve. It is found that the existing safety system can take care of total loss of insulation vacuum scenario.

INTRODUCTION

The K500 superconducting cyclotron [Figure 1] at the Variable Energy Cyclotron Centre has got its internal beam circulating up to the extraction radius of the cyclotron. The cyclotron has an 80 Ton superconducting magnet operating at about 5 T magnetic fields. The NbTi superconducting coil carries about 800 A maximum current to produce the desired magnetic field. The superconducting coils are placed in a liquid helium chamber surrounded by a vacuum insulating chamber called outer vacuum chamber (OVC).

At higher currents (>600 A) in the coils, the outer vacuum chamber (OVC) insulation vacuum reading shows deterioration, which finally leads to slow dump of the coil. The deterioration of OVC vacuum with the current in the coil is plotted in Figure 2. It is seen that at about 600 A, the slope of the pressure rise is too high to increase any amount of current. This in result increases heat load to the liquid helium chamber, thus depleting the liquid level in it and slow dump triggers as the liquid level goes below the coil top surface. This has given a tight limitation for further increasing current value in the coil. It was therefore required to determine that how much is the increase in heat load because of this phenomenon and to find out what capacity of additional vacuum pumping could make the situation better.

Figure 1: The K500 superconducting cyclotron

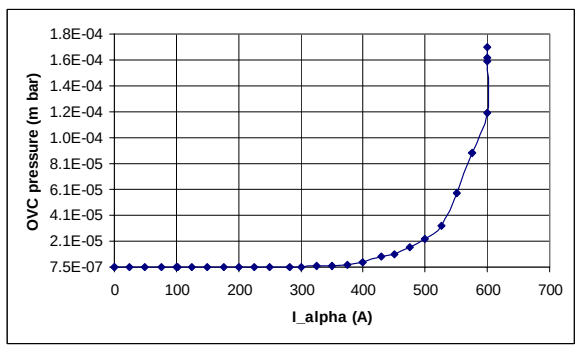

Figure 2: Vacuum reading during increase in coil current

EXPERIMENTS AND THEORETICAL EVALUATION

An experiment was done to find out the dynamic heat load which is coming only with energization of superconducting magnet. Another experiment was done to degrade the vacuum to one order by a control leak without the magnetic field on and heat load was measured. In the first experiment, heat load due to magnet energisation is found to be 100W. In the second experiment, heat load because of worsened insulation vacuum is 90 W. As is seen, the contribution of heat load as a result of degradation of vacuum is almost equal to the contribution of heat load due to magnet energisation. It can therefore be concluded that the reason for limit in the magnet coil energisation is coming from the degradation of vacuum only and an introduction of additional pumping port to improve the vacuum by nearly one order

will save a lot of heat load to the coil. A detail calculation says that the saving of heat load will be of about 70W. Details of the experiments done are given below.

Experiment to Find Out the Dynamic Heat Load

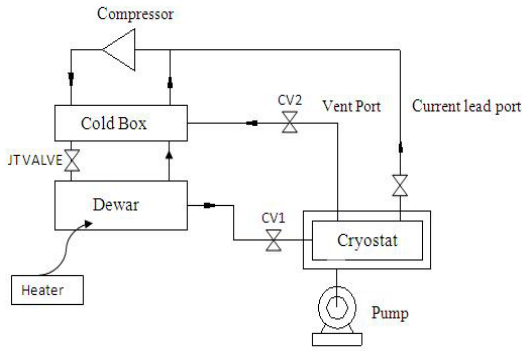

Figure 3: Experimental scheme to find out heat load due to energisation of magnet

Figure 3 shows the scheme to find out dynamic Heat load during energisation. At first, no current was given in the superconducting coil. The additional heater power of 100 W could be given to the plant dewar maintaining stable plant operation. After that, increase in the dewar heater power results in liquid level fall in both cryostat and dewar. During operating condition,when the coil current is increased above 600 A, the cryostat level starts decreasing leading to slow dump. It can therefore be concluded that a dynamic heat load of about 100W is coming at coil current 600A.

The dynamic heat load measured here comprises of free molecular gas conduction (FMGC) as a result of vacuum degradation, coil heat dissipation, current lead heat dissipation & Eddy current heating.

Experiment to Find Out the FMGC Heat Load and Comparison with Theoretical Value

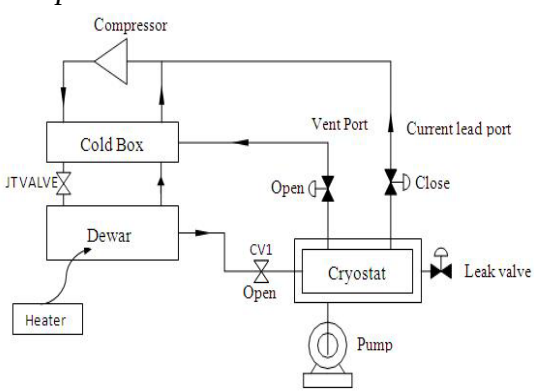

Figure 4: Experimental scheme to find out heat load due to FMGC

Figure 4 shows the experimental set up to simulate helium leak in OVC space. Different vacuum conditions have been established by means of a calibrated leak valve and corresponding maximum possible heater power was noted. Figure 5 shows the calibration graph of the leak valve.

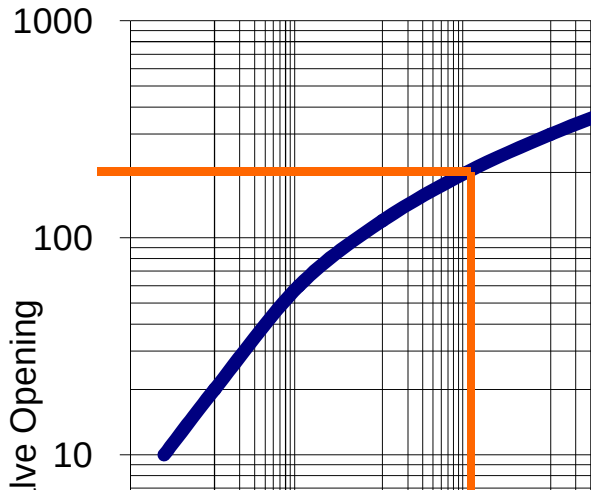

Figure 5: Leak valve calibration graph

Figure 6 shows a theoretical graph where it gives the insulation vacuum and heat load value due to FMGC. The experimental values of heat load at two vacuum values are also plotted. It can be seen that the theoretical calculation matches very well with the experimental result.

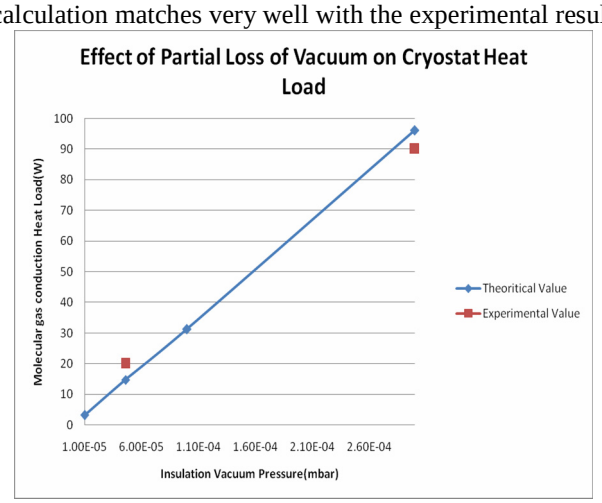

Figure 6: Comparison of theoretical and practical value of heat load.

Theoretical Evaluation of Additional Pumping

A theoretical evaluation was made to find out the vacuum value could be achieved if a standard 300 l/s turbo pump added to the OVC. The result is plotted in Figure 8. The estimated leak rate assumed at 600 A current in the coil is 0.01 mbar-l/s. At 5E-05 mbar vacuum, the estimated saving in the heat load is about 70 W at 600 A current. This saving is expected to improve the performance of the OVC and coil current can be raised to further higher value.

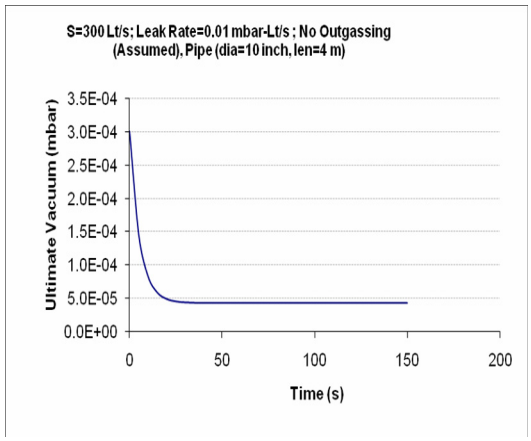

Figure 8: Calculated vacuum with additional pump

Safety Analysis for Complete Loss of Insulation Vacuum

The phenomena of increasing pressure with current in OVC raises the question about adequacy of safety system in case of accidental complete loss of insulation vacuum. The vessel was modelled as closed system. As the total mass of helium and the volume of helium chamber both are constant in case of closed system, the process is isochoric heating [1]. The pressure rise curve is dependent on initial fill up.

The loss of vacuum was assumed for air ingression into the vacuum chamber, which is the most severe case contributing to 0.6 W/cm^2 [2] heat load to the cryostat cold surface.

Below is the pressure rise curve for different initial ullage space.

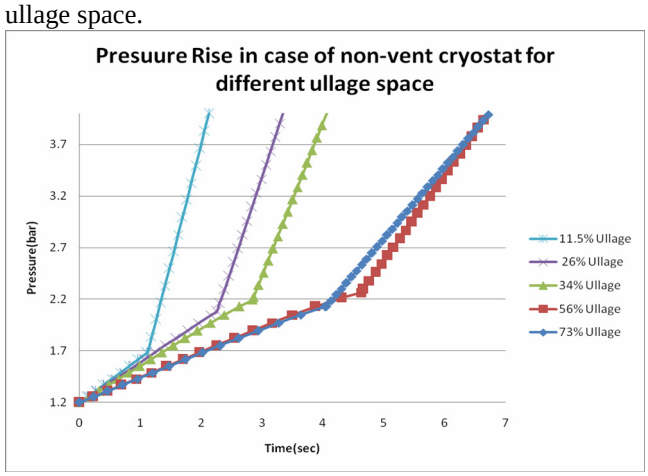

Figure 9: Pressure rise in the helium chamber in case of a total loss of insulation vacuum

The graph shows two different slopes. Initial slope is for two phase pressure rise, this line finally reaches either the saturation liquid line or saturated vapour line of two-phase dome depending upon initial fill up. The next slopes are out of the two-phase dome and describe the single phase pressure rise.

Interesting observation is that, for high liquid volume fraction(i.e. low ullage space), the liquid volume expands with the heat transferring into the liquid, and it causes the liquid to increasingly occupy more and more volume in the vessel and the gas to condense on the surface between the two phases. For low liquid volume fraction, the evaporation of the liquid is more than the volume expansion, and it causes the volume of the liquid to reduce until it vaporises completely.

To find out the relieving mass requirement, the venting process was intentionally assumed to be isobaric (at 3bar$_a$). In spite of heat addition, how much mass should be taken out to maintain the cryostat pressure at 3 bar$_a$ is calculated. For isobaric process the heat addition will be manifested as increase in enthalpy. Helium density corresponding to 3 bar$_a$ pressure and instantaneous enthalpy is found out and helium mass in the vessel is determined. By comparing this to the mass determined in the previous time step, the mass that must be removed to keep the pressure constant as the internal enthalpy is increased has been calculated. Maximum value for this particular case appears to be approximately 3 Kg/s considering normal operating condition (i.e. 11.5 % ullage). Existing rupture disc of K-500 superconducting cyclotron has maximum discharge capacity through it is 11.6 Kg/s.

CONCLUSIONS

Molecular gas conduction contributes to significant amount of heat load at current scenario where the insulation vacuum degrades with current in coil. Experiment and subsequent theoretical evaluations reveal that the reason of slow dump of the magnet is due to high heat load by molecular gas conduction. It also concludes the utility of additional pumping to reduce the heat load to cryostat. Safety analysis considering complete loss of insulation vacuum because of ingression of air reveals that present safety system can take care well of such situation.

ACKNOWLEDGEMENTS

The authors acknowledge all the people involved in the performance of the experiments and in discussion thorough out these studies.

REFERENCES

[1] Dr. Philippe Lebrun ,CERN,Lecture on “Engineering Science for cryogenic Safety” 26th DAE Safety and Occupational Health Professsional Meet.November 16-18,2009.

[2] W. Lehman and G. Zahn, “Safety Aspects for LHe Cryostats and LHe Transport Containers,” ICEC7, London, 1978.

INFLUENCE OF RF MAGNETIC FIELD ON ION DYNAMICS IN IBA C400 CYCLOTRON

Y.Jongen, IBA, Louvain-la-Neuve, Belgium
E.Samsonov, G.Karamysheva, S.Kostromin, JINR, Dubna, Russia

Abstract

Magnetic components of RF field in C400 [1] cyclotron, being under development by IBA, makes noticeable influence on ion dynamics.

In particular, increase in the dee voltage [2] along radius leads to essential phase compression of a bunch. At the same time RF magnetic field changes a central ion phase by only 2°RF.

Calculations have also shown that RF magnetic field makes visible but pretty small influence on the radial motion, while an impact of the RF magnetic field on the axial motion has not been detected.

The results are compared for the two RF magnetic field maps: (i) calculated numerically by Microwave Studio and, (ii) calculated analytically from RF electric field map by means of Maxwell' equations.

RF FIELDS COMPUTED BY MICROWAVE STUDIO

RF electric and magnetic field maps that were used in the computations corresponded to the last geometry of the dees in assumption that a dee voltage in the center is of about 80 kV. Three dimensional views of the components E_φ, E_r and B_z are shown in Fig. 1-4.

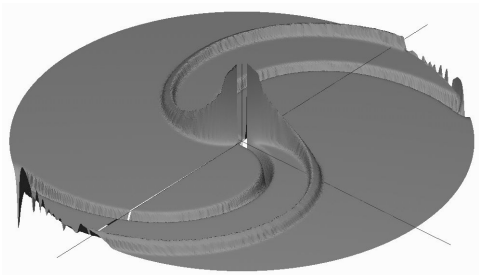

Figure 1: 3D view of E_φ component

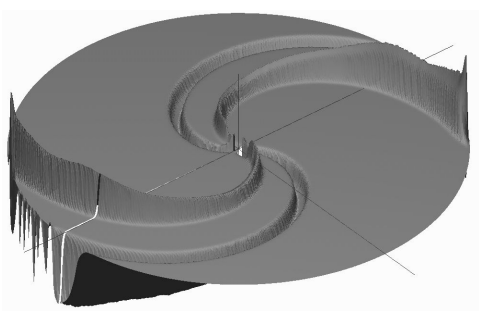

Figure 2: 3D view of E_r component.

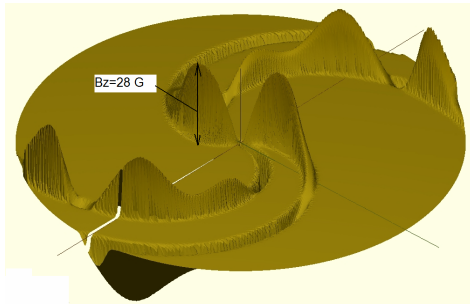

Figure 3: 3D view of the B_z(RF). Maximal positive value of B_z(RF)=28 G at radius 30 cm.

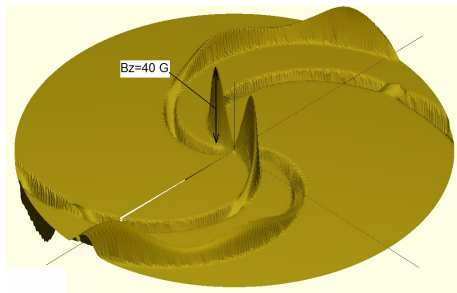

Figure 4: 3D view of the Bz(RF) through a half-period of the high-frequency oscillations in comparison with Figure 3. Maximal value of Bz(RF)=40 G at radius 22 cm.

Distribution of the maximal values of B_z(RF) along radius for two gaps of the dee is shown in Figure 5.

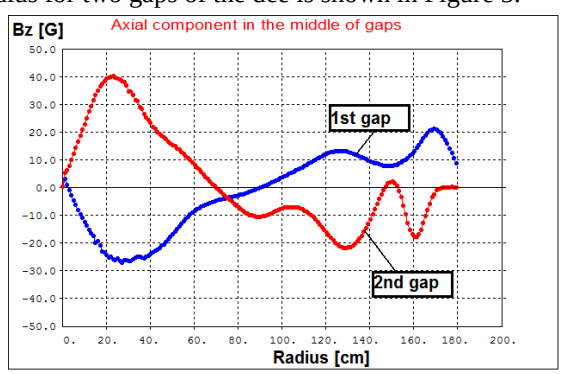

Figure 5: Maximal values of component B_z(RF) in the middle of gaps versus radius

In the case when obtaining of B_z(RF) is provided by Microwave Studio the three RF magnetic field components during acceleration are calculated by the following formulas of first approximation with respect to (z/r):

$$B_r(t) = z\frac{dB_z}{dr}\sin\psi \quad (1)$$

$$B_\varphi(t) = \frac{z}{r}\frac{dB_z}{d\varphi}\sin\psi \quad (2)$$

$$B_z(t) = B_z \sin\psi \quad (3)$$

where $\psi = 2\pi h f_{rev} t + \psi_0$ is time dependent RF phase of the ion.

Another way of RF magnetic field calculations was implemented using direct connection between electric and magnetic RF fields which is described by the Maxwell' equations. It is enough to have E_φ and E_r components in the median plane in order to compute RF magnetic field components in the vicinity of the median plane. We have derived the following formulas of first approximation with respect to (z/r):

$$B_r(t) = \left[\left(-\frac{1}{r}\frac{\partial E_r}{\partial\varphi} + \frac{\partial^2 E_r}{\partial r\partial\varphi} + \frac{1}{r}E_\varphi - \frac{\partial E_\varphi}{\partial r} - \frac{r\partial^2 E_\varphi}{\partial r^2}\right)\sin\psi\frac{1}{\dot\psi}\right]\frac{z}{r} \quad (4)$$

$$B_\varphi(t) = \left[\left(\frac{1}{r}\frac{\partial^2 E_r}{\partial\varphi^2} - \frac{1}{r}\frac{\partial E_\varphi}{\partial\varphi} - \frac{\partial^2 E_\varphi}{\partial\varphi\partial r}\right)\sin\psi\frac{1}{\dot\psi}\right]\frac{z}{r} \quad (5)$$

$$B_z(t) = \left[\frac{1}{r}\frac{\partial E_r}{\partial\varphi} - \frac{1}{r}E_\varphi - \frac{\partial E_\varphi}{\partial r}\right]\sin\psi\frac{1}{\dot\psi} \quad (6)$$

where $\dot\psi = \frac{d\psi}{dt} = 2\pi h f_{rev}$. Parameters of RF electric field maps that were used in (4)-(6) are illustrated in the Figures 6-8.

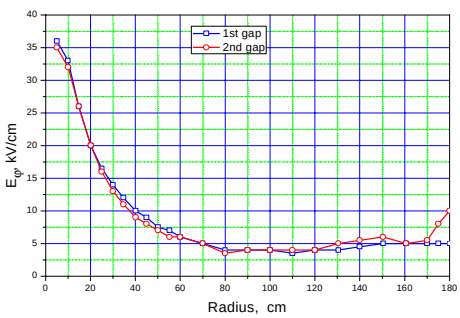

Figure 6: Maximal absolute values of component E_φ (RF) in the middle of gaps versus radius

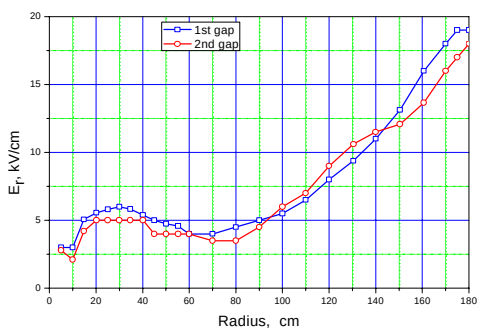

Figure 7: Maximal absolute values of component E_r (RF) in the middle of gaps versus radius

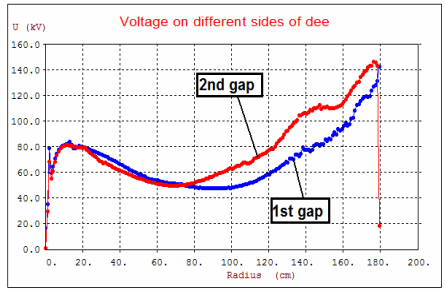

Figure 8: Radial distribution of the dee voltage along two accelerating gaps

To study influence of RF magnetic field on the ions dynamics a bunch of 200 ions was specified at radius ~4 cm, one turn after inflector. The bunch had 35°RF phase width, maximal initial value of radial oscillations was ~ 0.2 cm, initial axial amplitudes were defined by the dees axial aperture ±1 cm.

All types of computations have been done using 3 different conditions:

(1) B_z(RF) is off;
(2) B_z(RF) is on (Maxwell' formulas (4-6));
(3) B_z(RF) is on (map of B_z and formulas (1-3)).

RADIAL MOTION

Results of calculations presented in Figure 9 show that B_z(RF) field slightly improves quality of the radial motion. This is observed in the middle radii and after the structural resonance $3Q_r=4$ as well.

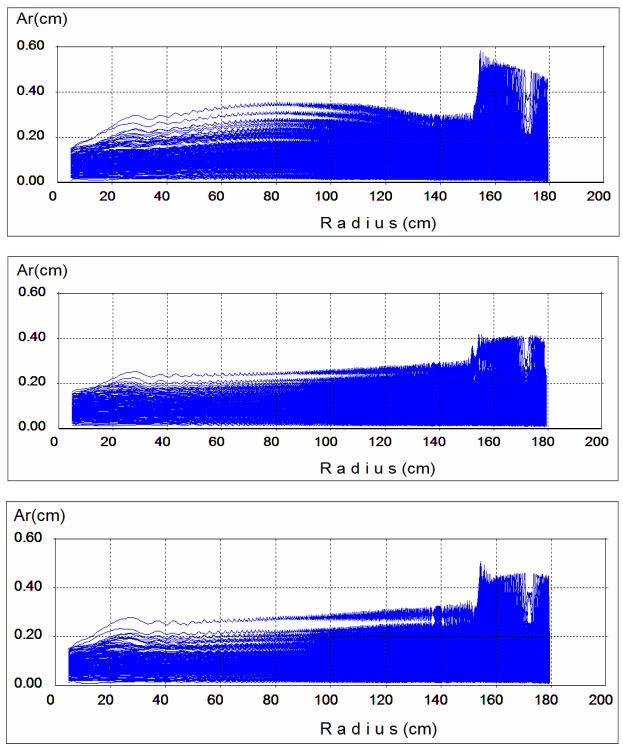

Figure 9: Radial distribution of free radial oscillations. Above - B_z(RF) is off, middle - B_z(RF) is on (Maxwell' formulas (4-6)), below - B_z(RF) is on (map of B_z and formulas (1-3).

AXIAL MOTION

Results of calculations presented in Figure 10 show that B_z(RF) field does not give noticeable effect on the axial motion.

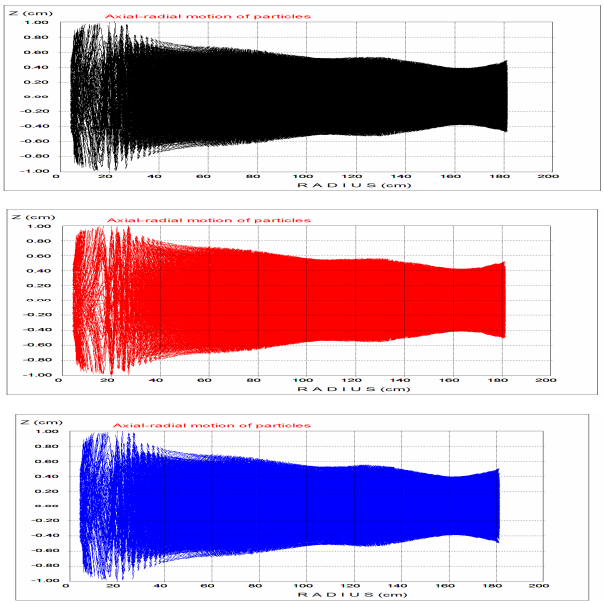

Figure 10: Axial-radial profile of the beam. Above - Bz(RF) is off, middle - Bz(RF) is on (Maxwell' formulas (4-6)), below - Bz(RF) is on (map of Bz and formulas (1-3).

PHASE MOTION

Phase motion of the bunch of ions is shown in Figure 11.

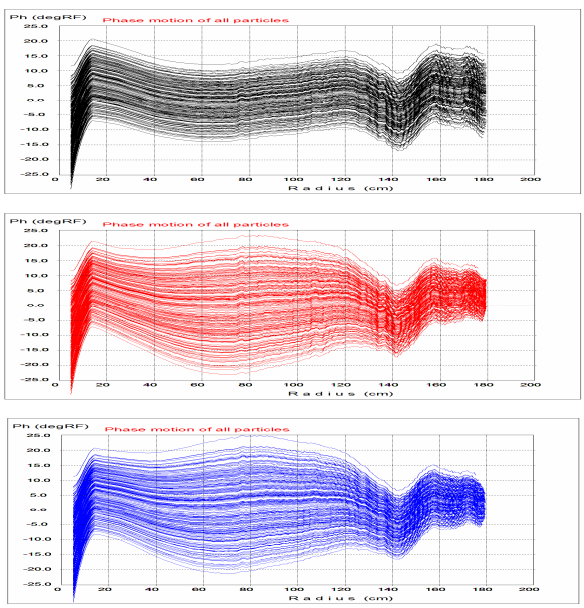

Figure 11: Phase motion of the bunch. Above - Bz(RF) is off, middle - Bz(RF) is on (Maxwell' formulas (4-6)), below - Bz(RF) is on (map of Bz and formulas (1-3)).

One can see almost full coincidence of the bunch phase motion obtained by the help of different ways of RF magnetic field calculations. Both approaches to RF magnetic field show the bunch phase width inversely proportional to the dee voltage that is predicted theoretically [3].

As it is seen in Figure 12, impact of RF magnetic field on the phase motion of central ion (having RF phase deviation inside ±5°RF during acceleration) leads to shift of the phase by not more than 2°RF. This shift is much less than one (20°RF) that has been obtained in the ACCEL cyclotron [4]. A reason of this is explained by another distribution of B_z(RF) field in C400 cyclotron, which is provided by 4 stems instead of 1 stem in ACCEL cyclotron dee.

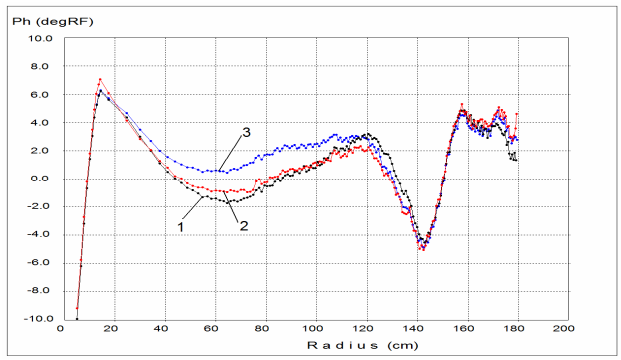

Figure 12: Phase of central ion versus average radius of orbit. 1 - no B_z(RF), 2 – B_z(RF) from Maxwell' formula (6), 3 – B_z(RF) from the map (formula (3)).

CONCLUSIONS

Bunch phase width in C400 increases and decreases inversely proportional to the dee voltage along radius.

Phase deviation of the central ion due to action of RF magnetic field is not more than 2°RF.

RF magnetic field ensures small decrease in the radial amplitudes.

No visible impact of the RF magnetic field on the axial motion has been detected.

REFERENCES

[1] Y.Yongen at al, "IBA-Dubna 400 MeV/u superconducting cyclotron for ion therapy", this conference.

[2] Y.Yongen at al, "Radio frequency system of the cyclotron C400 for hadron therapy", 18th Int. Conf. on Cyclotrons and Their Applications, Giardini Naxos, 2007.

[3] R.W.Muller, R.Mahrt, "Phase compression and phase dilatation in the isochronous cyclotron", NIM, 86(1970), p. 241-244.

[4] J.M.Schippers, D.C.George, V.Vrancovic, "Results of 3D beam dynamic studies in distorted fields of a 250 MeV superconducting cyclotron", 17th Int. Conf. on Cyclotrons and Their Applications, Tokyo, 2004.

AXIAL INJECTION BEAM LINE OF A COMPACT CYCLOTRON*

Jinquan Zhang, Mingtao Song, Xiaotian Yang, Zhiming You, Aimin Shi, Liepeng Sun, Lizhen Ma, Qinggao Yao, Xuezhen Zhang, Yun Cao, Xiaoqi Zhang, Jianhua Zhen, Haihong Song
Institute of Modern Physics, Lanzhou 730000 China

Abstract

Axial injection beam line of the compact cyclotron is presented. It is intended for transportation of the C5+ ion beam obtained in the permanent magnet ion source. The beam line is only 3.486 m from the ion source to the entrance of spiral inflector, it consists of two glasser lens, one double 90-degree bend magnet, one quadrupole and two solenoid lens. The sinusoidal buncher, Faraday cap and chopper are used respectively for increasing seizing efficiency, beam diagnostics and choice of beam utilizing time. The bend magnet and a slit collimator are used for choice of C^{5+} ion beam.

INTRODUCTION

A new compact cyclotron is designed at the Institute of Modern Physics, it is intended for acceleration of C^{5+} ions and energy 7 MeV/u at the extraction radius. The cyclotron will be used as the injector of a compact synchrotron. The overall equipment will be built for the medical application. The main parameters of the cyclotron are contained in Table 1.

Table 1 The cyclotron main parameters

Extraction radius /m	0.75
Magnetic field /T	1.168
Number of sectors	4
RF frequency /MHz	31.02
Harmonic number	4
Extraction energy /MeV/u	7.0
Z/A	0.4167(C^{5+})
RF voltage /kV	70
Number of Dees	2
Ion extraction method	Electrostatic deflector and bend

Axial injection beam line of the cyclotron is designed for transportation of the C^{5+} ion beam obtained in the permanent magnet ion source. A big vacuum box is installed in the vertical part of the beam line. A sinusoidal buncher, a Faraday cap, a slit collimator and a chopper are located in the big vacuum box. The sinusoidal bunchers are used for increasing of the injection efficiency from about 11% to 47%, it is about 1.3 m from the median plane of the cyclotron. The Faraday cap is used for the beam diagnostics and monitoring. The chopper is used for choice of the beam utilizing time, its running period is decided by the synchrotron.

*Supported by National Sciences Foundation of China (Code: 10905078)

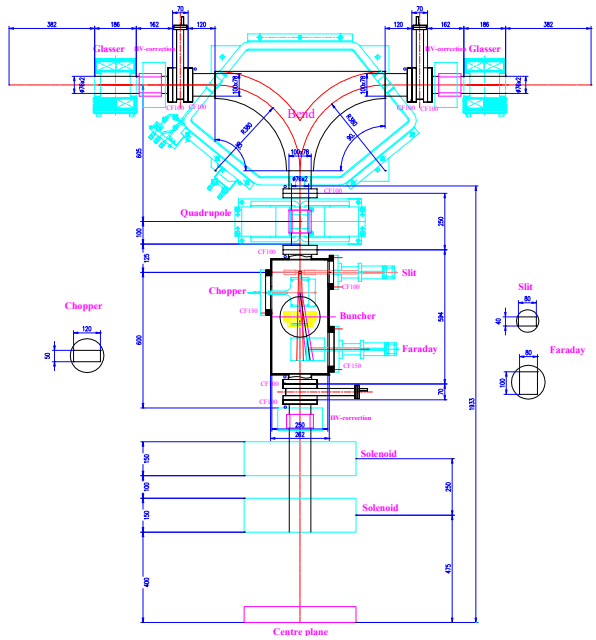

Fig.1 Beam line layout

BEAM LINE DESIGN

The C^{5+} ion beams are obtained in the permanent magnet ion source. The some parameters of beam are contained in the Table 2.

Table 2 Beam parameters

Beam intensity /eμA	200
Emittance /πmm*mrad	150
Energy /keV	100

The beam line is situated above the cyclotron magnet. It consists of the permanent magnet ion source, the double 90-degree analyzing bending magnet (DM90) and two focusing glasser lens that will be placed at the horizontal part of the beam line. A quadrupole and a buncher will be placed at the vertical part of the beam line, two focusing solenoids will be installed above the plug. The spiral inflector will transfer ion beams to the median plane of the cyclotron.

The beam line is designed with trace-3D program. The initial C^{5+} beam parameters used in the simulation are contained in Table 2. The computed C^{5+} beam envelopes along the beam line from the ion source to the entrance of the inflector are shown in Fig.2. The multi-ion simulation with 2σ gauss distribution is made for the axial injection beam line, the simulation result shows that the ion beam pass through the injection line without loss. The ion beam distributions at ion source exit and inflector entrance are shown in Fig.3.

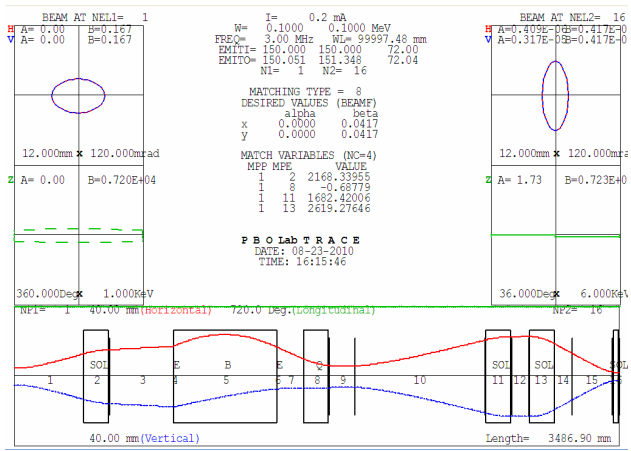

Fig.2 beam envelopes along beam line

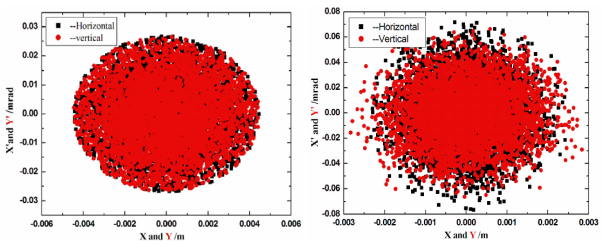

Fig.3 Ion distributions at source exit and inflector entrance

BUNCHING SYSTEM

The sinusoidal buncher is located in a big vacuum box at 130 cm from median plane of the cyclotron above the first solenoid. The longitudinal seizing efficiency of the compact cyclotron was calculated with space charge effect considered. Beam seizing efficiency, buncher voltage amplitudes and corresponding current is shown in Fig.4.

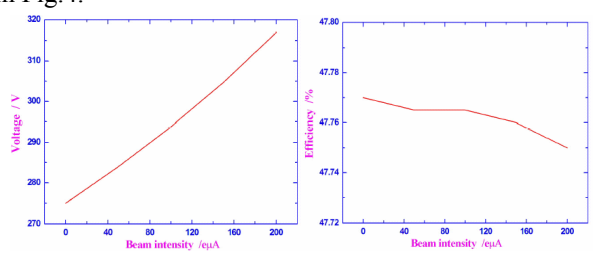

Fig.4 Beam seizing efficiency and buncher voltage amplitudes

BEAM POSITION CORRECTION

The system of the center of beam correction will consist of two two-plane dipole steering magnets, situated before and after DM90. This system gives us possibility to eliminate displacement and angle of the beam center that will appear due to cyclotron magnet fringing field.

BEAM DIAGNOSTICS

The Faraday cap is used for the beam diagnostics and ion analysis spectrum identification after the DM90. The electrostatic chopper will be used for fast interruption and modulation the beam current. All the elements will be situated in the big vacuum box below the analyzing magnet.

VACUUM SYSTEM

The horizontal part of the beam line will be pumped by two turbopumps installed at the ion source exit with the pumping speed of 700 l/s.

The vertical part will be pumped by a turbopump installed at the big vacuum box with the pumping speed of 1000 l/s.

The vacuum volume will be divided into four sections by three gate valves that will be installed before DM90 and after the big vacuum box.

The estimated average pressure in the beam line is about 10^{-7}mbar.

REFERENCES

[1] A. N. Dubrovin, E. A. Simonov, S. B. Vorozhtsov, Mermaid 3D code in ATLAS application, ATLAS Note ATL-TECH -2001-003, CERN, Geneve, (2001).

[2] O. Borisiv, B. Gikal, G. Gulbekyan, I. Ivanenko, I.Kalagin, "Optimisation of the axial injection system for U-400 cyclotron (linear buncher)", in Proc. Of EPAC2000, Vienna, Austria, pp. 1468-1470, 2000.

[3] B.N.Gikal et al. Channel of Axial Injection of DC-60 Cyclotron. JINR communication, P9-2006-39, Dubna, 2004.

[4] G.G. Gulbekyan et al. Axial Injection Channel of the DC-350 Cyclotron. Cyclotrons and Their Applications 2007, Eighteenth International Conference.

EXTRACTION SYSTEM OF A COMPACT CYCLOTRON

Huanfeng Hao, Qinggao Yao, Bing Wang, Mingtao Song, Kaidi Man,
Hongwei Zhao, Yalong Su
Institute of Modern Physics Chinese Academy of Science Lanzhou,P.R.China

Abstract

Based on the beam orbit and dynamics simulations, the extraction system of a compact cyclotron is determined, and the beam parameters of the extracted beam are calculated.

INTRODUCTION

HITFiL(Heavy Ion Therapy Facility in Lanzhou) is composed of a compact synchro- tron ,several ion beam lines ， three therapy chamber and a cyclotron injector, Fig.1. is a sketch drawing of the HITFiL. The injector of the synchrotron is a compact cyclotron ,it is now under designing at institute of modern physics Chinese academy of science, it is intended to provide carbon ion with charge number 5,the beam intensity will be more than 10 eμA,and the extraction energy is 7Mev/A.The present paper gives the designing of the extraction system of the compact cyclotron and the beam parameters of the extracted beam.

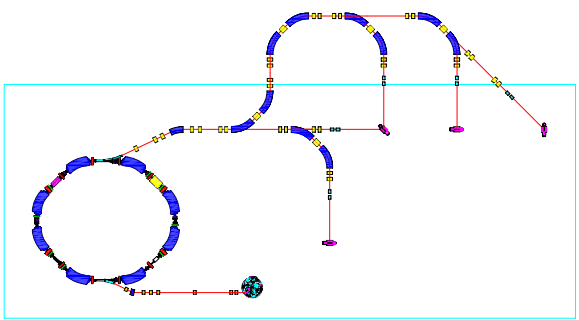

Figure 1: Layout of HITFiL

DESIGNING OF THE EXTRACTION SYSTEM

The designing of extraction system is based on the orbit calculations, the magnetic field used in beam orbit calculation was obtained by a 3D infinite element code, the electric fields used in orbit calculations is an analytical field， Fig.2. is the layout of the reference particle track and extraction elements. The whole extraction system composed of an electric deflector and a bending magnet. The electric field in the gap is 80.0kV/cm,for that its high voltage electrode will be 80kV, A bump filed be used to enhance the turn distance between extraction orbit and accelerator orbit, it is also helpful for deduce the burden of the deflector.

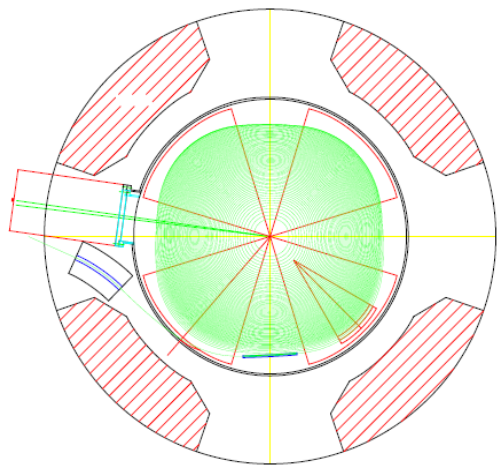

Figure 2: Overview of the cyclotron

Based on the reference particle orbit, extraction elements and it's physical parameter be determined. To obtain higher extraction efficiency and higher beam quality, multi- particle simulation was done, such calculations show that the position of the extraction elements which get from single particle calculations should be optimized.

BEAM PARAMETERS OF THE EXTRACTED BEAM

Extracted beam parameters are obtained based on multi-particle calculation, the initial conditions for such calculations is coming from the injection and center region calculations, The matching point is at the exit of the bending magnet, at this point the beam parameters are as following table, Fig.3. to Fig..5 are the 6 dimensions emittance of the beam, Fig.6.is the dispersion D and D' of the extraction beam.

Table 1：Beam parameters

	β [m]	α	ε [π mmmrad]
H	16.0	-2.77	14.24
V	3.6	-5.46	10.88

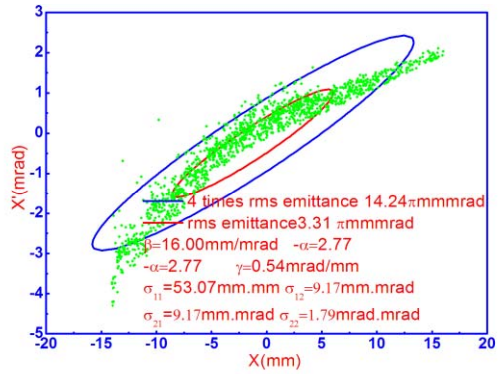

Figure 3: Horizontal emittance

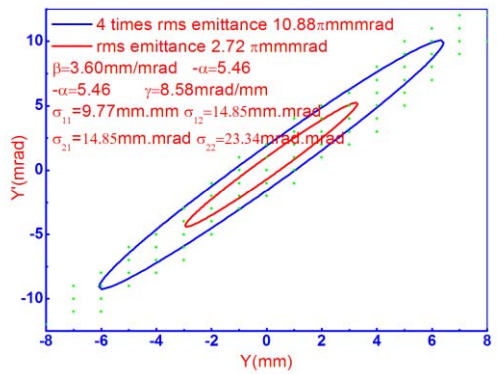

Figure 4: Axial emittance

CONCLUSION

As to now, the design and study of the extraction systems is based on the data form 3D calculations or analytical models. Because the beam is extracted through an area where the magnetic gradient is very high, and due to the strong divergence at horizontal plane and over focusing in axial plane, the beam diverged on both dimensions, but the calculations show the extraction beam may the need, both in beam intensity and beam quality.

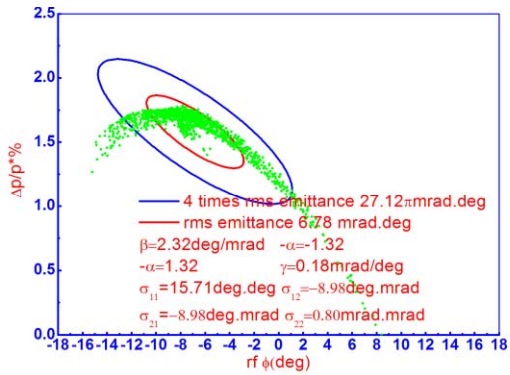

Figure 5: Longitudinal emittance

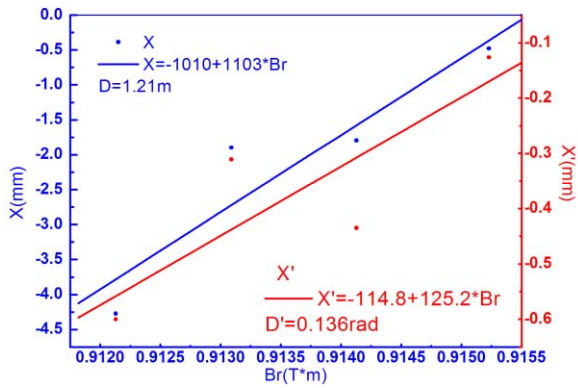

Figure 6: Dispersion at the matching point

ACKNOWLEDGEMENT

The authors wish to acknowledge the contributions made by Prof. Tianjue Zhang, Dr S.B.Vorozhtsov, V.L. Smirnov, Dr A. Goto, Dr N. Fukunishi through helpful suggestions and discussions.

REFERENCES

[1] Stanley Humphries, Jr. “Charged particle beam” Published by John Wiley & Sons Inc

[2] D.Vandeplassche et al. “Extraction simulations for the IBA C70 Cyclotron” Cyclotrons and Their Applications 2007

TRANSMISSION EFFICIENCY STUDY OF SSC

Huanfeng Hao, Hongwei Zhao, Yiping Yang, Junfeng Gao, Guohua Han, AijunWang, Shixian Wang, Xueming Su, Jianqiang Wu, Anping Li, Jingjun Yang, Qiuxian Guo, Weiqing Yang, Chunlei Xie
Institute of Modern Physics Chinese Academy of Science Lanzhou, P. R. China

Abstract

Transmission efficiency of HIRFL-SSC had been studied, found the main reasons of the lower transmission efficiency, and some advices were put forward to improve the transmission efficiency.

INTRODUCTION

HIRFL-SSC is a separated sector cyclotron at IMP(Fig.1.), it was constructed in the 1980's, the first beam extracted from SSC is 50Mev/A $^{12}C^{6+}$ in 1988, from then on SSC has been providing ion beams for 21 years, but the transmission efficiency of SSC is very lower, accelerator physicists at IMP begun to study this problems since1992, then there are four main opinions about which. The first is that the RF voltage of SSC is not reach the designing value. The second is the over trim of magnet. The third is that the designing of injection system had some problem. The forth is that the beam matching between SSC and it's injector cyclotron SFC is bad. The present paper studied those opinions by beam simulations and experiments on SSC.

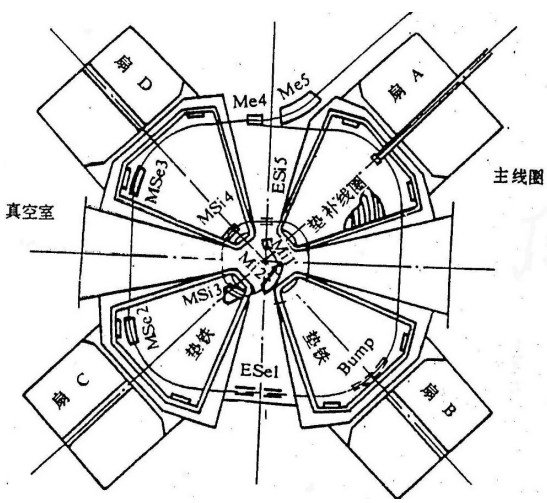

Figure 1: Layout of SSC

LOWER RF VOLTAGE OF SSC

The designing value of SSC RF voltage is 230 kV, as to now, the highest value which the SSC RF system can reach is 180. Some researchers' studies show that for high energy light heavy ions if the RF voltage below 230kV, some particle will hit on the Msi4 or Esi5 for the first accelerate turn, So they point out this is the main reason of lower transmission efficiency of SSC. The authors of the present paper did the same simulations as those researchers did, and got the same results. In our simulations, if the RF voltage is 230 kV the distance between injection beam and first accelerate beam is about 10 mm, and the beam envelope is 8 mm, so there is no beam lose in first accelerate turn, but when the RF voltage bellows 230 kV, there will have beam lost. The above situation is true just for high energy light heavy ions, for other particle beams there is no beam lose even the RF voltage lower than 180 kV. Even for high energy light heavy ions we can increase the distance between injection beam and first accelerate beam to 10 mm by change the location of Msi4 and Esi5. Experiments on SSC verified such moving have the expected effect. So lower RF voltage is not the main reason of lower transmission efficiency.

OVER TRIMMING OF SSC MAGNET

To eliminate the effects of injection elements Mi2 on the main magnet field, some iron was attached on the edge of the magnet sector B and C near Mi2(Fig.1).But the magnet field measurement showed that the iron had a little more than it was needed, such is so called over-trimming. Some researchers thought it is a main reason of the lower

transmission efficiency, they did some simulations under magnetic fields which get from soft edge approximation and included using some techniques the effects of over-trimming, the results show for the high energy light heavy ion beams some particle will lose on the Msi4 or on Esi5 because of the effects of over-trimming. As the researchers pointed out that the over-trimming effects beam patently just for special ions, so should not be the main reason of lower transmission efficiency. And the authors of the present paper use the measured magnetic field do the same simulation as those researchers did, the results show the over-trimming has no effect on beam transmission efficiency, so over-trimming is not the main reason.

DISIGNING PROBLEMS OF SSC INJECITON AND EXTRACTION SYSTEM

The injection and extraction system of SSC designed under soft edge approximation. Some researchers pointed out that the design should be modified under measured magnetic fields, and it is the tradition, also he pointed out the injection beam track is not the optimal one, and the design of Msi4 had some problem, because it sometimes use negative currents, and if the currents is negative the magnetic field inside the magnet channel would be not equality (Fig.2.). The authors agree with this opinion partly, namely the design of injection and extraction system should be modified under real magnetic field. We compared the magnetic field (Fig.2.) which from soft edge approximation or measured ones. We can find there are patent difference at injection and extraction area. And when we use the measured magnetic field do the beam simulation, we find there is a difference about 6mm of beam track between designed one and simulated one in injection, and about 20mm in extraction. We measured the beam intensity and find most beam lost at extraction. Simulations show if we move the extraction elements for property distance, we can increase the extraction efficiency from 40 percent to 80 percent.

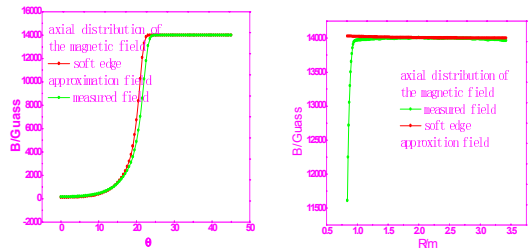

Figure 2: Main magnetic field distributions

BEAM MATCHING BETWEEN SSC AND IT'S INJECTOR SFC

Some researchers pointed out that the beam matching between SSC and SFC is bad, which may be the main reason of the lower transmission of SSC. But when we tune the beam, we found for most beams the injection and accelerate efficiency is very good, so we could not due the lower efficiency to beam matching.

CONCLUSION

The transmission efficiency of SSC is very lower, the main reason is that the injection and extraction system was designed under soft edge approximation and did not modified use real magnetic field. Now to improve the transmission efficiency of SSC, we should simulate the beam under measured magnetic field find the correct locations of the injection and extraction elements, then move the element to the right place.

ACKNOWLEDEMENT

The authors wish to acknowledge the contributions made by Pr Yifang Wang, Pr Feng Ye, Dr A. Goto, Dr N. Fukunishi through helpful suggestions and discussions.

REFERENCES

[1] Yifang Wang "Beam simulation study of SSC" internal report.

[2] Feng Ye "The main problems of HIRFL-SSC" internal report.

RESEARCH ON ACCEPTANCE OF SSC

Xiaoni Li, Youjin Yuan, Yuan He
Institute of Modern Physics, Chinese Academy of Sciences, Lanzhou 730000, China

Abstract

The injection, acceleration and extraction of SSC (Separate Sector Cyclotron） is analyzed and simulated to get the transverse and longitudinal acceptance, using two typical ions $^{238}U^{36+}$ and $^{70}Zn^{10+}$ with energy 9.7MeV/u and 5.62MeV/u respectively. In order to study the actual acceptance of SSC, the isochronous magnetic field model in coincidence with the real one is established by Kr-Kb and Lagrange methods based on the actual measurement. The transverse and longitudinal acceptance is calculated under the above isochronous magnetic field model. From the simulation results, one of the major reason of low efficiency and acceptance of SSC is the defaults in the design of MSI3. The simulation results show that the actual efficiency and acceptance of SSC can be improved by redesign the curvature of MSI3 or shim in MSI3 to change the distribution of inner magnetic field.

INTRODUCTION

SSC is the main accelerator of HIRFL (Heavy Ion Research Facility in Lanzhou). Presently higher beam intensity and quality are required to perform higher level experiments. In the view of existing conditions, the accelerator system needs to be upgraded to satisfy physical requirements, where the key issue is the SSC of HIRFL. The low beam transmission efficiency of SSC and the existing beam intensity of SSC's injector - Sector Focused Cyclotron (SFC)[1,2] limited the beam intensity of SSC. As a result from the above reasons, Institute of Modern Physics, CAS planned to build a new linear injector (SSC-LINAC) to get higher intensity beam for heavier elements.

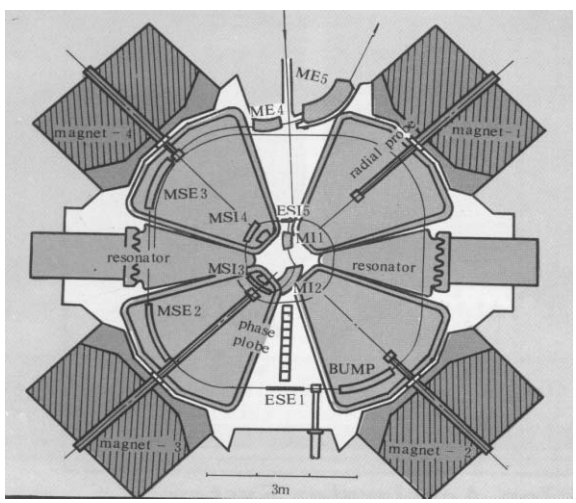

Figure 1: The overall layout of SSC.

In this paper, the transverse and longitudinal acceptance is calculated under the theoretical isochronous magnetic field model and the real one. It will provide important parameters for SSC-LINAC. In addition, the simulation results will help in machine commissioning and the upgrade of HIRFL by discussing the acceptance of SSC. Fig.1 gives the overall layout of SSC. It shows four sector magnets and the injection and extraction system of SSC, and two RF cavities.

SIMULATION RESULTS UNDER THE THEORETICAL ISOCHRONOUS MAGNETIC FIELD MODEL

The theoretical isochronous magnetic field distribution [3-5] is the hyperbola secant function. In present paper, the acceptance of SSC (the point of the injection orbit, which is 4.08m far from the centre of SSC) is calculated by tracking particles. Fig.2 and Fig.3 show the results of ions $^{238}U^{36+}$ with energy 9.7MeV/u, and $^{70}Zn^{10+}$ with energy 5.62MeV/u respectively. In Fig.2, (a), (b), (c) are radial acceptance of 13.03 π·mm·mrad, axial acceptance of 107.27 π·mm·mrad and longitudinal acceptance respectively. The energy spread is ±0.7% and the phase is from -6 to 6°.In Fig.3, (a), (b), (c) are radial acceptance of 16.43 π·mm·mrad, axial acceptance of 208.34 π·mm·mrad and longitudinal acceptance respectively. The energy spread is ±0.6% and the phase is from -10 to 10°.

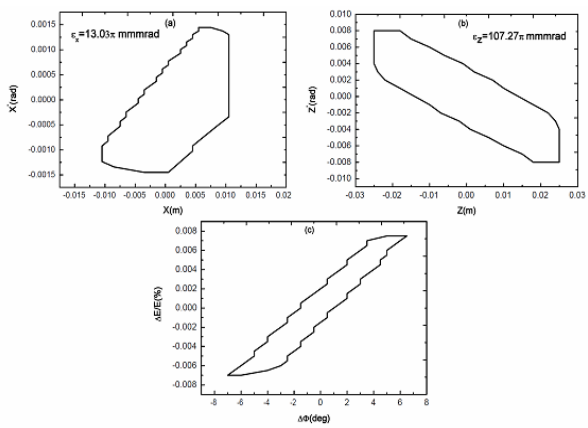

Figure 2: The results of ion $^{238}U^{36+}$ with energy 9.7MeV/u, acceptance of SSC in theoretical magnetic field (a) radial acceptance (b) axial acceptance (c) longitudinal acceptance.

*lixn@impcas.ac.cn

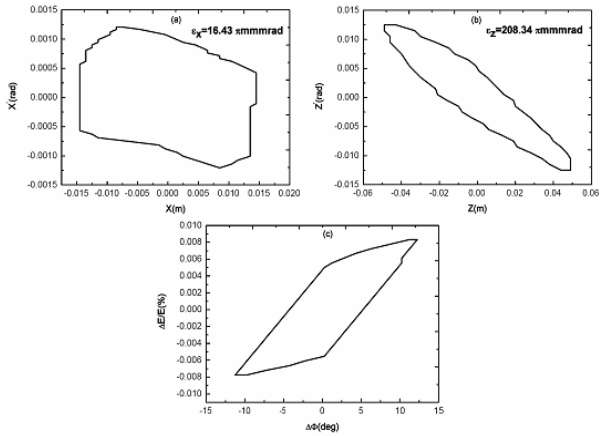

Figure 3: The results of ion $^{70}Zn^{10+}$ with energy 9.7MeV/u, acceptance of SSC in theoretical magnetic field (a) radial acceptance (b) axial acceptance (c) longitudinal acceptance.

SIMULATION RESULTS UNDER THE REAL ISOCHRONOUS MAGNETIC FIELD MODEL

The accelerator SSC was constructed twenty years ago, so now we can not measure the real isochronous magnetic field directly. However, we can build it with the existing magnetic field parameters. Here, the method we used is Kr-Kb[5-8] and Lagrange linear interpolation. Fig.4 and Fig.5 show the results of ions $^{238}U^{36+}$ with energy 9.7MeV/u, and $^{70}Zn^{10+}$ with energy 5.62MeV/u respectively. In Fig.4, (a), (b) and (c) are radial acceptance of 2.33 π·mm·mrad, axial acceptance of 41.09 $\pi \cdot mm \cdot mrad$ and longitudinal acceptance respectively. In Fig.5, (a), (b), (c) are radial acceptance of 1.54 π·mm·mrad, axial acceptance of 54.27 π·mm·mrad and longitudinal acceptance respectively.

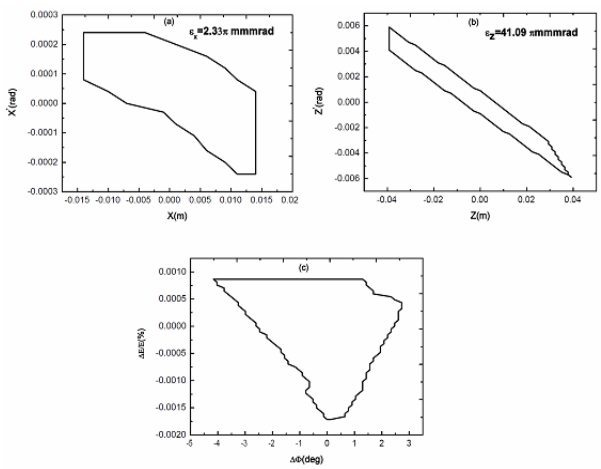

Figure 4: Acceptance of SSC in real magnetic field (a) radial acceptance (b) axial acceptance (c) longitudinal acceptance.

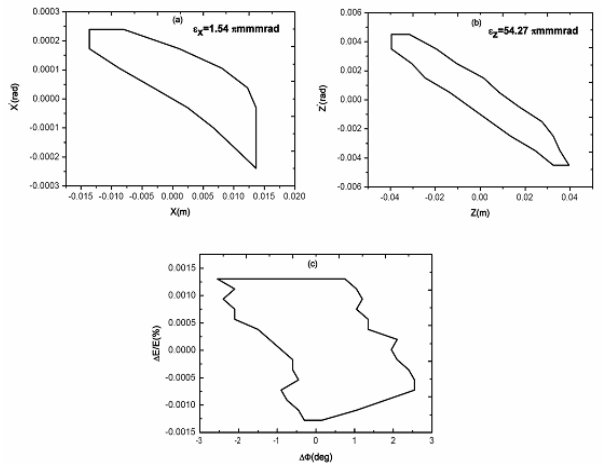

Figure 5: Acceptance of SSC in real magnetic field (a) radial acceptance (b) axial acceptance (c) longitudinal acceptance.

From the above simulation results, the acceptance under the real magnetic field model is not good. In the process of the central particle tracking, the central particle orbit in MSI3 under the real magnetic field is bad, so a lot of particles are lost in this element. Fig 6 shows the results of ion $^{238}U^{36+}$ with energy 9.7MeV/u, central particle orbit in MSI3 under the theoretical and real magnetic field.

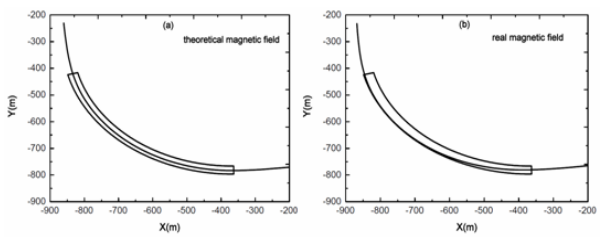

Figure 6: The results of ion $^{238}U^{36+}$ with energy 9.7MeV/u, central particle orbit in MSI3 under the theoretical and real magnetic field.

COMMISSIONING RESULTS

In the machine commissioning, the transmission efficiency is also low. Table 1 shows the transmission efficiency of three typical ions in the machine commissioning.

Table 1: The transmission efficiency of three typical ions

Particles	Matching Efficiency	Transmission Efficiency
$^{40}Ar^{14+}$18MeV/u	100%	12%
$^{20}Ne^{10+}$85.75MeV/u	50%	21%
$^{86}Kr^{26+}$25MeV/u	100%	23%

CONCLUSION

The simulation results under the real isochronous magnetic field model are worse than expected, and the transmission efficiency of SSC is also low in the machine commissioning. From the simulation results, the orbit of central particle in MSI3 is bad in measured field distribution. This might be one of the major reason of low efficiency and acceptance of SSC. The results show that the actual efficiency and acceptance of SSC can be improved by redesign the curvature of MSI3 or shim in MSI3 to change the distribution of inner magnetic field. Besides, more careful optimization in simulation and operation must be done to improve the transmission efficiency and acceptance.

REFERENCES

[1] Tang Jingyu and Yin Quanmin, Beam Longitudinal Motion at HIRFL, High Power Laser and Particle Beams, 1999, 11(6): 765-766.

[2] Tang Jingyu, Wang Yifang, Yin Quanmin, Problems of Accelerator Physics of Upgrading HIRFL, Nuclear Physics Review, 2000,17(2): 95-99.

[3] Ding Yuantao, Wang Yifang, Liu Wei, Zhu Kun. Research on Energy Acceptance Range of SSC Injection System, Nuclear Physics Review, 2001,18(1): 43-44.

[4] Wang Yifang, Injection System and Ejection System of SSC, Progress Report of Heavy Ion Research Facility Lanzhou, Beijing: Scientific Press, 1983, 2 16-25.

[5] K. Ziegler, Running of VICKSI and First Operating Experience, IEEE Trans. Nucl. Sci., Sep. 1978. No.2: NS-26.

[6] M. Barre, Main Results of the SSC，s Magnetic Field Mapping at GANIL, 9th Int. Conf. on Cyclotrons and Their Application. 1981:371

[7] Liu Wei. <<Physical Work on Separated Sector Cyclotron-raise efficiency and optimize isochronous magnetic field>>, manuscript.

[8] M. M. Gordon, Orbit properties of the isochronous cyclotron ring with radial sectors. Ann. Phys. 1968.50:571-597.

BEAM-PHASE MEASUREMENT SYSTEM FOR HIRFL

Jianhua Zheng, Wei Liu, Yanmou Wang, Weinian Ma, Yanyin, Ruishi Mao, Junxia Wu,
Tiecheng Zhao, Youjin Yuan
Institute of Modern Physics, CAS, Lanzhou 730000, China

Abstract

The beam phase measurement system in HIRFL is introduced. The system had been improved using RF-signal mixing and filtering techniques and noise cancellation method. Therefore, the influence of strongly RF disturbing was eliminated and the signal to noise rate was increased, and a stable and sensitive phase measurement system was developed. The phase history of the ion beam was detected by using 15 sets of capacitive pick-up probes installed in the SSC cyclotron. The beam phase information was necessary for tuning purposes to obtain an optimized isochronous magnetic field, where the beam intensity was increased and the beam quality was optimized. The measurement results before and after optimized isochronous magnetic field for $^{40}Ar^{15+}$ ion and $^{12}C^{6+}$ ion in SSC were given. The phase measurement system was reliable by optimizing isochronous magnetic field test, and the precision reached ±0.5°, the sensitivity of beam signal measurement was about 10nA as well.

INTRODUCTION

The heavy ion research facility in Lanzhou (HIRFL) is composed of a sector focusing cyclotron (SFC K=69), and a separated sector cyclotron (SSC K=450), which is also the injector of the cooling storage ring (CSR). As to the isochronous cyclotron SFC and SSC, it is very important in optimization of isochronous magnetic field to get the best beam quality and efficiency of beam extraction. The information of isochronous of magnetic field could be provided by the beam-phase measurement system in beam tuning. Plate capacitive phase probe was designed and installed on SFC and SSC respectively. The signal mixing filter technology was applied and the beam signal detected by the phase probes was measured using HP8508A vector voltmeter. The frequency range of the beam phase measurement could be covered by the cyclotron frequency 6.5-14.5MHz in HIRFL, and the measurement sensitivity was about 5uV. That is when beam intensity was 10nA, the signal could be identified, and the system measurement accuracy was 0.5°.

DESCRIPTION OF BEAM-PHASE MEASUREMENT SYSTEM

The beam-phase measurement system in HIRFL mainly includes phase probe for the beam signal detection, the phase measurement signal processing system, as well as computer acquirement system.

Phase Probe

Based on many international researches of accelerator labs, plate capacitive phase probe is the best choice for isochronous cyclotron. The probes are located along the centre of one hill sector on the isochronous trim coil place of the magnet with the same distance along the radius direction. The electrode is made of non-oxygen copper plate and the voltage of induction signal is proportional to the charge of the beam pulse. Two layers of shielding outside of the electrode have been designed to protect the electrode from being attacked by beam and reduce the interference of RF-frequency. To avoid any signal reflection, the probes have an impedance of 50 ohms, the beam signal detected on the probe feed through by double shielding coaxial connector SWH.1S ensure the requirement of vacuum. The 6 sets of phase probes have been installed on the centre of SFC with the size of electrode 50mm × 100mm and the distance of 35mm between upper and lower and the 15 sets of phase probes have been installed on the centre of SSC with the size of electrode 100mm × 100mm and the distance of 40mm between upper and lower. The state of isochronous of magnetic field in cyclotron could be reflected by the results of beam phase measurement fully.

Phase Measurement Signal Process

The detection signal on the phase probe is transformed to voltage by the phase measurement processing system which is related to beam phase. The beam pulse signal with the cyclotron frequency ω_d is shown:

$$u(t) = \tfrac{1}{2}\sum_{n=0}^{\infty} A_n \cos(n\omega_d t + \varphi_n)$$

While A_n and φ_n are the magnitude and phase of harmonics n respectively. Capacitive phase probes installed on the centre of cyclotron not only detect the beam signal, but also the interference of RF-frequency. Generally the signal to noise rate of the beam to RF-frequency interference increases with the adding of the harmonics, however, the intensity of beam signal decreases with the reducing of harmonics. Therefore, considering the two factors of beam intensity and signal-noise ratio, the second harmonic component is selected as the measurement signal of the beam phase:

$$u_2(t) = A_2 \cos(2\omega_d t + \varphi_2)$$

The structure of beam-phase measurement system in HIRFL is shown in Figure 1.

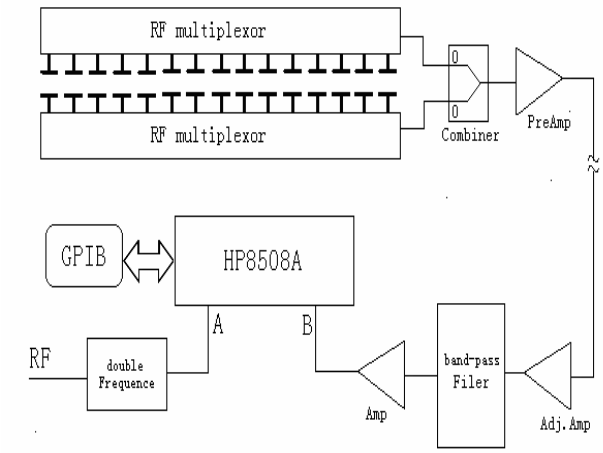

Figure 1: The diagram of beam phase measurement structure.

The signal is processed in the phase signal pre-selector including the signal combiner, noise filter, channel selection, and pre-amplification. The signal is transmitted by the double shielding coaxial cable with the equal electronics length to get the equal phase shift. The signal detected from upper and lower electrode with the same phase is added by the combiner, while the interference of RF-frequency with the contrary phase is subtracted. The coaxial switch VAS-316D with less than -70dB of crosstalk is selected to eliminate the disturbing between the channels. The signal is sent to preamplifier and filter, and then is transmitted by the 70-meter long double shielding coaxial cable to the phase measurement system located in the control room. The phase measurement system used to take the delay filter and phase meter made by self based on double balance mixer principle. However, it has been improved because of its big interference and low sensitivity. The band-pass filter has been designed to reduce the fundamental harmonic magnitude and improve the sensitivity and reliability of the system. The HP8508A vector voltmeter has been used to beam-phase measurement which is controlled by the GPIB interface. The RF-frequency voltage signal coupled on cavity of SFC and SSC is processed by doubled-frequency, which produces the RF signal with the same frequency of second harmonic of beam signal. The amplitude A_n, A_b as well as phase φ_n, φ_b are measured under the condition of with beam and without beam respectively, after calculation of vector subtraction are shown:

$$a = \tfrac{1}{2} A_2^{'} \cos\varphi_2$$

$$b = \tfrac{1}{2} A_2^{'} \sin\varphi 2$$

Therefore, the beam phase is got:

$$\varphi_{beam} = \varphi_2 = arctg\,\tfrac{b}{a}$$

SOFTWARE DESIGN OF PHASE MEASUREMENT SYSTEM

The software system is the core of beam-phase measurement, which coordinates the running of each part of the hardware. The object-oriented programming with Win 32 dynamic link library technology is used, and the human-computer interaction graphic interface is designed to accomplish the adjustment, control, and acquirement of equipment in the system. According to the principle of opening-closure, modular control software with bus structure is designed, the data is transmitted on the data bus, as well as sending messages on the control message bus, the software respond to the requirement from clients at anytime, which is not only realizes the distributed control of the system, but is also convenient to maintenance and update of the software later. The software design of the system is shown in Figure 2.

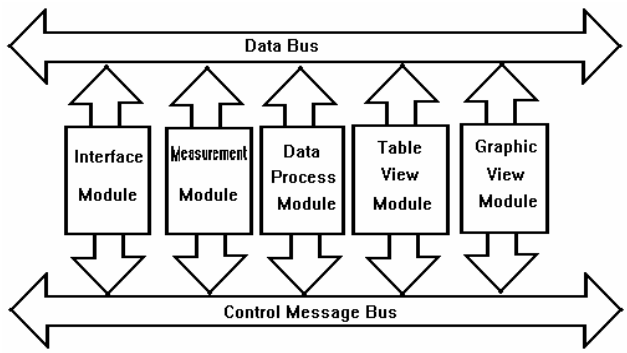

Figure 2: The diagram of system control software structure

The software has the function of automatic phase measurement of SFC, SSC and beam transport line; there is manual measurement as well as the self-check by the system. The phase information can be shown in graphs or in digitals. Generally, the system is controlled to scan all the probes getting the beam signal of phase measuring, any one of the probes can also be selected respectively. The measurement phase could be shown continuously for analysis of the isochronous of magnetic field.

MEASUREMENT RESULTS AND ANALYSIS

The beam-phase measurement system in HIRFL had been improved in the hardware and software. Various kinds of particles (Ar, C, O, N, S) had been used to the phase measurement experiment in SFC and SSC. The sensitivity of the measurement was the function of the probe size and beam intensity. The sensitivity was restricted by the interference signal caused by RF cavity to the phase probe. When the beam intensity was over 100nA, the phase accuracy was better than 0.5°. It was difficult to the absolute measurement because of many systematic errors and the weakly beam intensity. The method of background deduction was used in the software

processing, which the beam intensity from 5nA to 10nA could be measured for beam phase.

The Figure 3-1 and Figure 3-2 are the results of the beam phase measurement for $^{40}Ar^{15+}$ and $^{12}C^{6+}$ respectively.

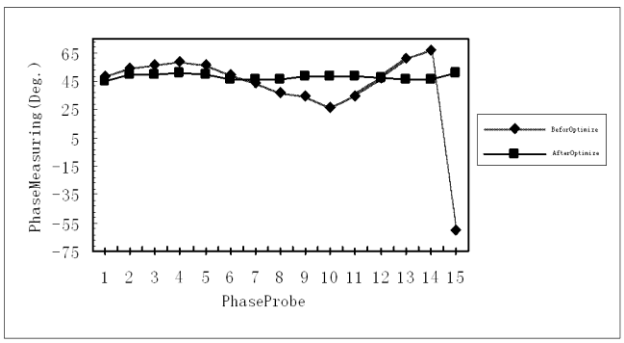

Figure 3-1: The result of the beam phase measurement for $^{40}Ar^{15+}$.

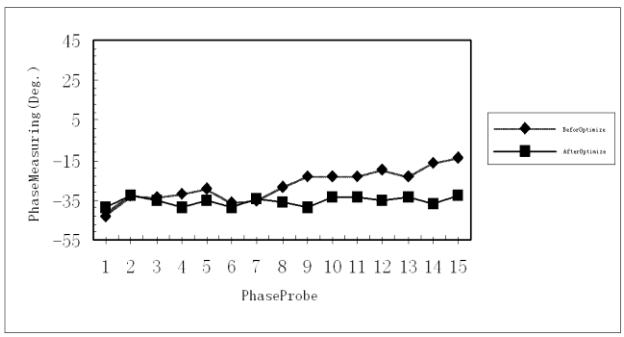

Figure 3-2: The result of the beam phase measurement for $^{12}C^{6+}$.

The results demonstrate the beam phase change before and after optimization of isochronous magnetic field on SSC. There was large difference of beam phase on 15 sets of phase probes before optimization, which showed that the isochronous of magnetic field was not better. According to the phase of measurement from each probe, changing the power current of isochronous trim coil at corresponding diameter over and over, until the difference of phase tended to be identical and the isochronous magnetic field be optimized. It could be seen from Figure 3-1 and Figure 3-2, the highest difference of phase was less than 7° . It had improved the beam intensity and the efficiency of extraction, as well as the beam quality. The total efficiency of beam intensity was over 50% when the 25 MeV/u $^{40}Ar^{15+}$ extracted from SSC in beam tuning.

CONCLUSION

At present, the beam phase measurement system in HIRFL has been put into operation; the optimization of isochronous magnetic field had been done in SSC beam tuning. The measurement data of beam phase has been proved reliability and the errors of repeated measurement less than $\pm 0.5^{o}$. The programming design is considering the integration of beam phase measurement and automatic optimization of isochronous magnetic fields to solve the problem of the human intervention when changing the isochronous trim coil, which will improve the optimizing efficiency of optimization of isochronous magnetic field and save much time for beam tuning of cyclotron.

REFERENCES

[1] W. Brautigam,et al . “Beam Phase Detection With A Fixed Intermediate Frequency System At JULIC”, IEEE Transactions on Nuclear Science Vol.NS-26.No.2,1979

[2] J.Gustafsson,… “Beam phase measurement system for the K130 cyclotron in Jyvaskyla” Nuclear Instruments and Methods in Physics Research A 335(1993)417-423

[3] Hiroro.Yamazaki, “Anti-interface Technology of Electronic Circuit”, (Publishing Campany,1989)

[4] Zheng Jianhua,… “Development of Beam Diagnostic System for HIRFL”, Proceedings of the 1997 International Conference on Accelerator and Large Experimental Physics Control Systems, Beijing Nov.3-7 1997

[5] Zheng JianHua, “Measurement based on capacitance probe”, Nuclear Electronics & Detection technology (2004,Vol.24 No.6 P.657)

A DESIGN OF SWITCH MAGNET POWER SUPPLY

Yan Huaihai, Zhou Zhongzu, Gao Yaling, Gao Daqing, Chen Youxin, Yuan Zhendong, Tang Yong, Zhang Xianlai, Feng Xiuming, Xin Junye, Yan Hongbin, Shangguan Jingbin
Institute of Modern Physics, Chinese Academy of Science, Lanzhou, 730000, China

Abstract

The paper introduces a design of power supply for switch magnet in HIRFL. The main circuit topology used Buck chopper regulator, full-bridge inverter output and power units in parallel in the power supply is introduced. The operation principle and control strategy is analyzed in this article. The power supply can be operated in DC and pulse mode, has the very good output current long-term stability, high reliability and dynamic response characteristics. Finally, some experimental data and waveforms of the power supply are shown to demonstrate the performance of the design.

SUMMARY

With construction of CSR and acceleration of proton at HIRFL, the existing beam handling system can not meet the requirements of nuclear physics experiments for more and more beam time. In order to match a new beam distribution system based on time is being constructed in HIRFL, a new switching magnet power supply is designed. Whether there is beam in CSR or not, the new beam distribution system can use the beams from SFC and SSC at the same time to do physics experiments at experimental terminals.

POWER SUPPLY PARAMETERS

- ✓ Maximum Output current: ±1050A
- ✓ Operation mode: DC/Pulse
- ✓ Maximum rise speed: (0-±1050A) /0.15s
- ✓ Maximum fall speed: 0.15s (±1050A-0)/0.15s
- ✓ Output current flat top time: 0.5s to DC
- ✓ Current stability: $<2\times10^{-4}$/8hour (±400-±1050A)
- ✓ Current ripple: $< 2\times10^{-4}$ (±400A-±1050A under 1kHz)
- ✓ Current repeat error: $<2\times10^{-4}$ (±400-±1050A)
- ✓ Current error: 0.1A
- ✓ Load parameters: Resistance: 28.2mohm, Inductance:18.7mH

The waveform of simulation work in pulse mode is shown below, the first picture shows the current waveform, and the next picture shows the voltage waveform.

MAIN CIRCUIT STRUCTURE

Main circuit structure is shown in Figure 2. The bus voltage is 200V after the diode rectifier and the bus voltage is 50V after the buck chopper. In process of rise and fall of the current, the buck chopper does not work and the bus bar voltage holds 200V so as to ensure the current change rate sufficient. When it works in a stable state, the bus bar voltage controlled by the buck chopper maintains at 50V to ensure that the duty cycle is reasonable.

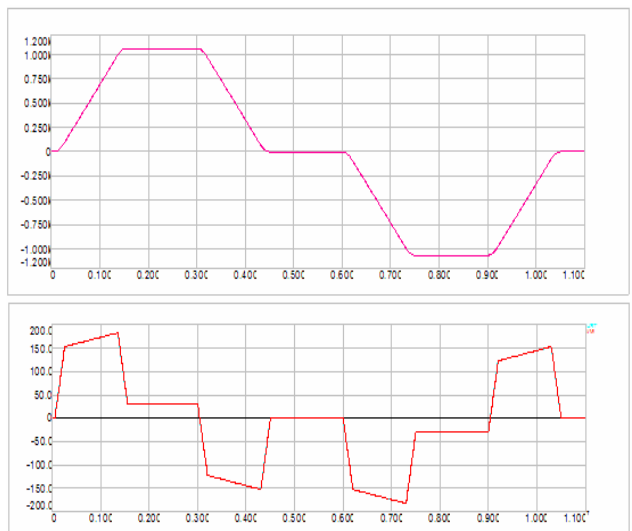

Figure 1.Waveform of power supply in pulse mode

In the power cabinet it has an input rectifier transformer and two power units, and in the control cabinet it has the control circuit for the power supply, the input and output power distribution and output filter circuit. The power supply is operated by PLC control, and displayed by a

5.5-inch touch screen. Figure2. is the main circuit structure

WORKING PRINCIPLE

The power supply system is composed of 3 parts, including input phase-shifting transformer, buck chopper regulator, and full-bridge inverter. The device from the AC network side is equivalent to 12 pulses rectifier to reduce the harmonic pollution on the grid. The power supply uses two power units in parallel as output mode.

The power supply control strategy is the outer ring current stabling flow mode and the inner current sharing mode.

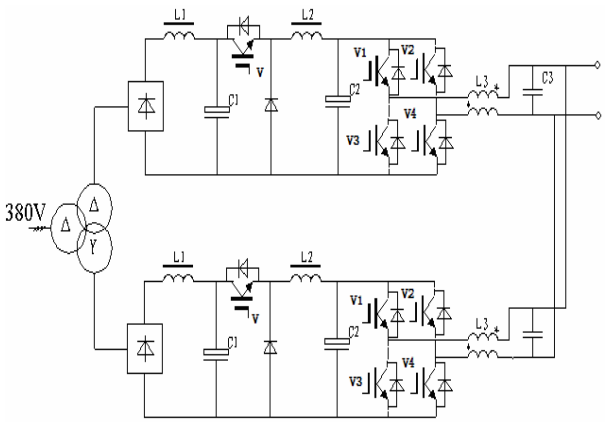

Figure 2.Main circuit structure

Buck Chopper

As the power supply works in the DC / pulse mode, it is necessary to ensure a high stability in DC mode and meet the sufficient current change rate in pulse mode. According to the load parameters, the formula: $V_0 = I_0R + L(di/dt)$, the maximum load voltage is 160.5V in pulse mode. In DC operation, the bus bar voltage controlled by the buck chopper maintains at 50V to ensure that the duty cycle is reasonable and the output current is stability. In pulse mode, the buck chopper does not work; the bus bar voltage keeps 200V to ensure the enough voltage when the current is rising.

Full-bridge Inverter

Power supply uses the full-bridge inverter output in parallel structures to improve the running reliability of power supply. Full-bridge inverter can asily meet the needs of four-quadrant operation, meanwhile it also achieves steeples output change to achieve positive and negative current output. Under controlled by the driving pulse, when the output of the power supply is positive, V1 and V4 conduct. When the output of the power supply is negative, V2 and V3 conduct. The full-bridge in parallel works in staggered phase mode.

IGBT driver use 2SD315A and PWM driver pulses transmit with the optical fiber, which make the control circuit and power circuits completely isolated.

CONCLUSION

After the switching magnet power supply put into operation, we measured the main parameters of the power supply. The output current stability is better than 2.5×10^{-5}, and the output current in pulse mode reaches the design specifications, and meet the requirements for the beam distribution system based on time. Figure 3 shows the waveform of output current 1000A rise. The waveform of power supply in pulse mode is shown in Figure 4.

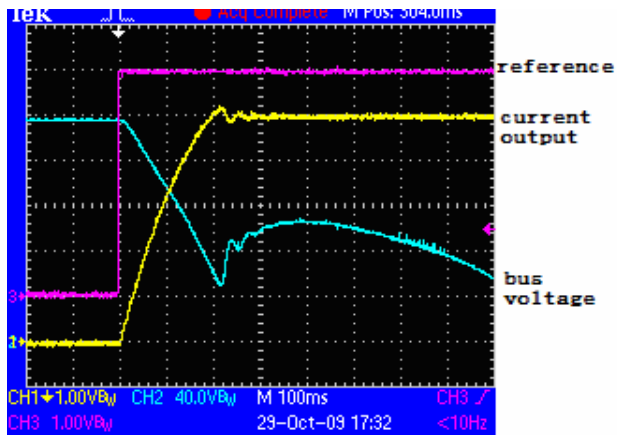

Figure3.The waveform of output current 1000A rise

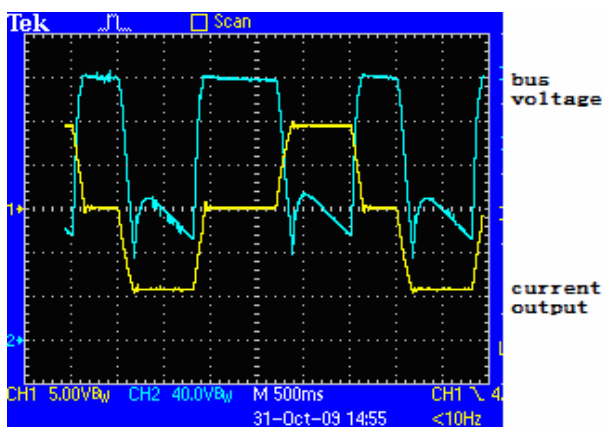

Figure 4 .Waveform of output in pulse mode.

REFERENCES

[1] ITER Joint Central Team and Home Teams. The ITER Pulsed Power Supply System[A]. in: 17th IEEE/NPSS Symposium Fusion Engineering[C]. San Diego: 1997.491-496.

[2] H Fujita. Pulse-Density-modulated Power Control of a 4kW, 450kHz Voltage-Source Inverter for Induction Melting Application [J]. IEEE Trans on. IAS. 1996,(2):279-286.

DESIGN OF HIGH ENERGY HADRON FFAGS FOR ADSR AND OTHER APPLICATIONS

B. Qin*, T. Uesugi, Y. Kuriyama, Y. Ishi, Y. Mori
Kyoto University Research Reactor Institute, Osaka, Japan
K. Okabe, Fukui University, Fukui, Japan
T. Planche, JB. Lagrange, Graduate School of Engineering, Kyoto University, Kyoto, Japan

Abstract

Design study of high energy proton FFAG accelerator has been carried out at Kyoto University Research Reactor (KURRI) for the next generation ADSR experiment where the proton beam energy covers up to 700MeV. The scaling type of FFAG with spiral sectors was employed. Details of the design issue concerning about the operational working points, lattice parameters and 3D magnet modeling / optimization are described. Also, some possibilities to apply this design to carbon therapy accelerators are presented.

INTRODUCTION

In KURRI, the first Accelerator driven sub-critical reactor (ADSR) experiment has started from March 2009, using a FFAG proton accelerator complex as a spallation neutron driver. At current phase, the output of the main ring in FFAG complex is 100MeV / 0.1nA [1]. Since the output power of the sub-critical reactor is proportional to the intensity of the neutron source, which related to the beam energy and intensity from the accelerator driver, some upgrade plans for the existing FFAG complex have been proposed and carried out [2]. One is to increase the beam intensity by replacing the current injector (Ion-beta + Booster) with a 11MeV H^- Linac injector [3]. The other way is to enhance the extraction beam energy to about 700MeV by adding a new ring. Since the number of neutrons during the nuclear spallation process has a strong dependency on the beam energy of the primary proton, the neutron multiplication rate can be increased by a factor of 30 when the proton beam energy is increased from 150MeV to 700MeV [2].

BASIC PARAMETERS FOR THE 700MEV FFAG RING

The present FFAG complex for ADSR experiment consists of one spiral injector (Ion-beta) with the extraction energy 1.5MeV, one 8-cell radial type booster and one 12-cell radial type main ring to accelerate beam energy covering 1.5MeV∼11MeV and 11MeV∼100MeV. The maximum energy of the main ring can be increased to 150MeV by changing the output energy of the injector.

The 700MeV upgrade ring will adopt the scaling type of FFAG with spiral sectors. For high energy scaling FFAG accelerators, the spiral sector is not so commonly used compared with the DFD triplets, due to the difficulty of controlling vertical tune shift. However, with the aid of 3D magnet modeling and optimization, it is possible to control the tune shift and maintain zero chromaticity. Meanwhile the compactness of the spiral sector makes it attractive.

For a given momentum ratio p_{ext}/p_{inj}, the radius excursion ΔR is related to the injection radius R_0 and field index k by the scaling law $B = B_0 \cdot (R/R_0)^k$, as Eq. 1. In case of the 700MeV ring, $p_{ext}/p_{inj} = 2.44$, when taking $R_0 = 6.9m$, ΔR is in range of 0.8m∼0.5m when changing k from 7.0 to 12.0.

$$\Delta R = ((P_{ext}/P_{inj})^{\frac{1}{1+k}} - 1) \cdot R_0 \quad (1)$$

The stable region for (k, ζ) parameter set is searched with first order matrix method, at different cell number $N = 8 \sim 16$. The main design constraints are the following: (1) Field index should be larger than 6.0, to keep a compact magnet dimension; (2) Spiral angle should be smaller than 60 degrees, for considerations on rf cavity installation etc. (3) The working point should be far away from low order normal structural resonances.

For the case of cell number $N = 14$ with the packing factor 0.4 , the working point $(\nu_x = 0.22, \nu_z = 0.14)$ is selected around parameters $(k = 7.0, \zeta = 58°)$ (see Fig. 1). The main parameters are listed in Table 1.

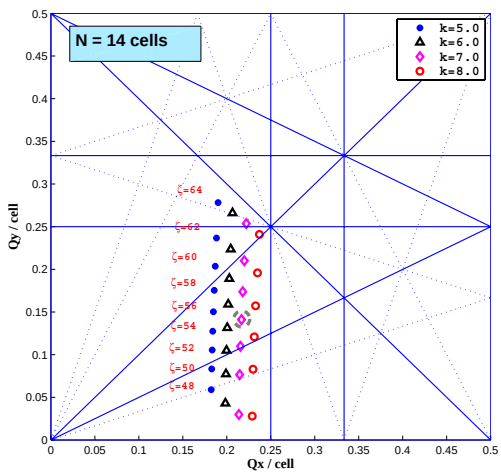

Figure 1: Working point search for $N = 14$. k is the field index, ζ is the spiral angle

The lattice was validated using Zgoubi code with FFAG-SPI procedure [4]. This procedure uses the soft enge model

* bin-qin@rri.kyoto-u.ac.jp

Table 1: Parameters of the 700MeV ring

Lattice type	spiral sector, scaling FFAG
Cell number	14
Injection / Extraction energy	150 / 700 MeV
Field index	7.0
Spiral angle	58.0 degree
Packing factor	0.4
Average orbit radius	6.9-7.7 m
B_{max}@$700MeV$	1.45T
ν_x/ν_z per cell	0.22 / 0.14
$\beta_x \quad min/max$	1.4 / 4.0 m
$D_x \quad min/max$	0.65 / 1.0 m

to simulate the realistic fringe field effect, and overall there exist a decrease for vertical tune. In realistic model, the packing factor need be decreased to compensate this vertical tune drop while keeping the same k and ζ

STUDY OF 3D TOSCA MODEL

For spiral sector FFAG, generally there exists two gap geometry formation. One is the flat pole gap, the field gradient is generated by distributed trim coils. An example is the Ion-beta in KURRI FFAG complex. The other type uses the natural variable gap shape with only main coil. Since the magnetic field flux $B(r) \propto 1/g(r)$, then the gap size $g(r)$ can be determined by $g(r) = g_0 \cdot (r_0/r)^k$, where g_0 is the gap size corresponds to r_0.

For the latter case, the coil configuration is more simple. But the vertical tune shift will be enlarged due to the decreasing fringe extend caused by the smaller gap size at higher beam energy. Some experiences such as the RACCAM prototype magnet has shown the possibility to modulate this tune shift by model optimization [5].

In general, three main methods are employed to reduce the vertical tune shift and keep zero chromaticity feature addressed by the scaling FFAGs.

1. *Introducing pole chamfer with variable width and field clamp*
2. *Effective magnetic field boundary correction based on the calculation of the field integrals* $\int B_z \cdot dl$
3. *Minute modification on local spiral angle, to compensate the vertical tune shift caused by fringe extent.*

The first magnet sector model of 700MeV spiral ring was built with OPERA/TOSCA [6], shown in Fig. 2. The chamfer width is set to be proportional to $1/g(r)$, which means larger chamfer width at larger radii. Field clamps with constant gap size is adopt to limit fringe field. The packing factor in this magnet model is reduced to 0.37 to keep the same working point in linear model.

In Fig. 4 it can be observed there exist significant vertical tune shift with $\Delta\nu_{z,cell} > 0.07$ in the initial model (model-3). The sources come from errors of the local field index,

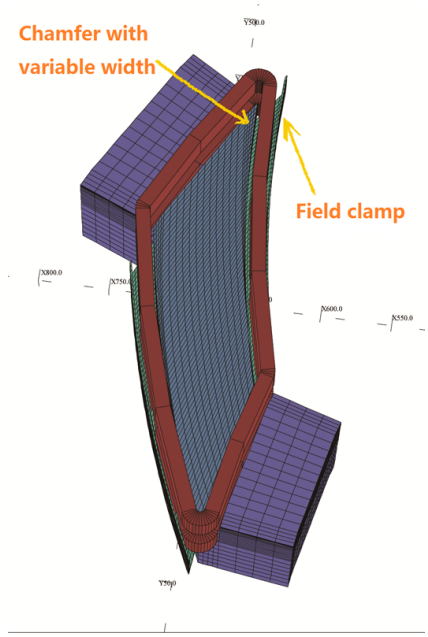

Figure 2: TOSCA magnet model with variable gap

local spiral angle and fringe field extent. The first stage to optimize the magnet model is to align the effective magnetic field boundary along the radius, using a procedure described in [5]. This is proved to be an efficient method to correct both local k and local ζ.

After some iterations, errors of the effective boundary and local spiral angle is well controlled within negligible value limited by 3D TOSCA calculations, as shown in Fig. 3. And the vertical tune shift is abbreviated especially in high energy region (blue line in Fig. 4, model-14). But obvious tune deviation still exists at lower energy (150-350MeV). Because the source of the local field index and local spiral angle have been eliminated, then the only reason is the fringe field extent, or in terms of the field flutter defined by $F = \frac{1}{N} \cdot \Sigma \frac{(B(\theta)-\bar{B})^2}{\bar{B}^2}$. The relation between ν_z and k, ζ, F can be approximately expressed by:

$$\begin{aligned} \nu_z^2 &= -k + \tfrac{N^2}{N^2-1} \cdot F \cdot (1 + 2\tan^2\zeta) \\ &\approx -k + F \cdot (1 + 2\tan^2\zeta) \qquad if\ N \gg 1 \end{aligned} \tag{2}$$

The flutter is mainly determined by magnet pole geometry and will not change when the effective field boundary is fixed. The field index k should be kept constant to ensure a stable ν_x. Then the last free parameter is the local ζ. By using the derived Equ. 3 and observed $\delta\nu_z$, the minute change of local spiral angle $\delta\zeta$ can be estimated from known numerical information.

$$\frac{d\nu_z}{d\zeta} = \frac{2F \cdot \tan\zeta}{\sqrt{-k + F(1 + 2\tan^2\zeta)} \cdot \cos^2\zeta} \tag{3}$$

This modification was applied on model-14 in range of $r < 730cm$, with $\delta\zeta < 0.03°/cm$ and max pole edge modification $\delta\theta_{max} < 0.4°$. The vertical tune of the final optimized model (model-18) is shown in Fig. 5, with a small shift about 0.01 per cell.

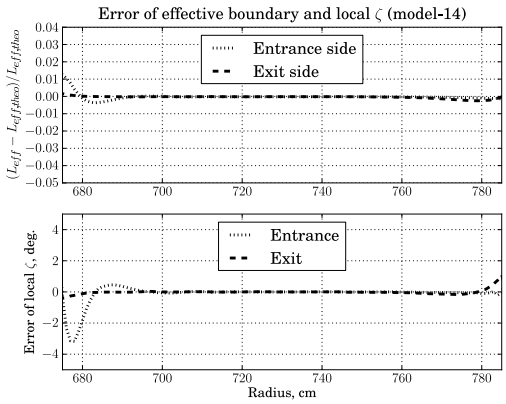

Figure 3: Errors of effective boundary and local spiral angle error after model optimization (model-14)

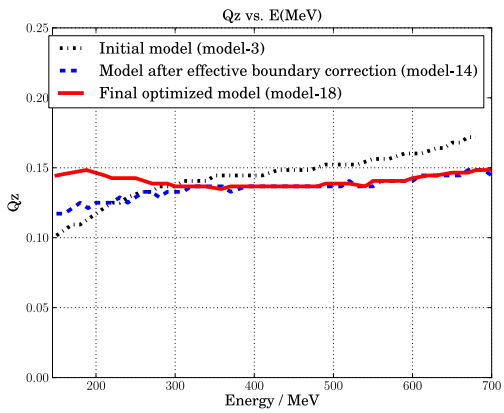

Figure 4: Evolution of the vertical tune shift, using 3D TOSCA maps. Blue:model-14 after correction of effective boundary; Red:model-18 with modification on local ζ

APPLICATION TO CARBON THERAPY

Fig. 6 shows there exists possibility to use a working point with horizontal phase advance larger than 90° and high field index, for instance $(k = 10.0, \zeta = 57^\circ)$. For applications that does not demand large acceptance, such as carbon therapy accelerators, this is an attractive scheme because the high field index makes the magnet more compact. For a scaling superconducting FFAG ring accelerates carbon ions from 12MeV/u to 400MeV/u (momentum ratio=6.35), the radius excursion can be achieved at about 0.45m with $R_0 = 2.5m$, packing factor 0.5 and maximum magnetic field 4.3T.

SUMMARY

To increase the number of neutrons during the spallation process in KURRI ADSR experiment, an energy upgrade plan is proposed to boost the beam energy of the FFAG complex to 700MeV. The scheme using spiral sector scaling FFAG was discussed. A magnet model with variable gap shape was studied with TOSCA code, and methods were employed to optimize the vertical tune shift. The possible application on carbon therapy accelerators using higher k was also discussed.

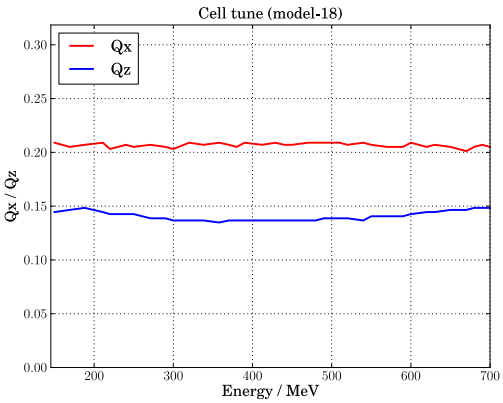

Figure 5: Horizontal and vertical tune per cell of model-18

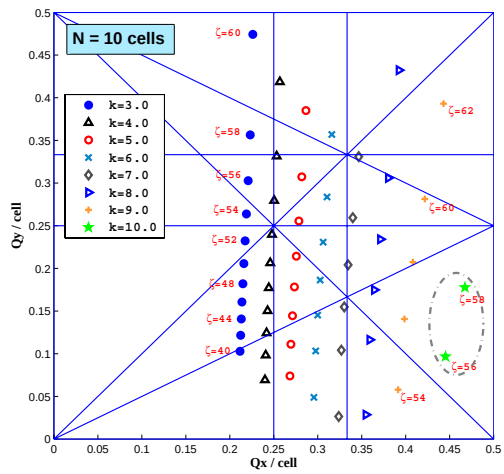

Figure 6: N=10 case, for possibilities to use high horizontal phase advance with higher k

REFERENCES

[1] T. Uesugi, et al., "FFAGS FOR THE ERIT AND ADS PROJECTS AT KURRI", Proc. of EPAC08, Genova, 2008. p. 1013.

[2] Y. Ishi, et al., "PRESENT STATUS AND FUTURE OF FFAGS AT KURRI AND THE FIRST ADSR EXPERIMENT", Proc. of IPAC10, Kyoto, 2010. p. 1323.

[3] K. Okabe, et al., "DEVELOPMENT OF H- INJECTION OF PROTON-FFAG AT KURRI", Proc. of IPAC10, Kyoto, 2010. p. 3897.

[4] J. Fourrier, et al., Nucl. Instr. Meth. A, 589 (2008) 133-142.

[5] T. Planche, et al., Nucl. Instr. Meth. A, 604 (2009) 435-442.

[6] Opera-3D User Guide,Vector Fields Limited, England.

THE DESIGN OF TRANSVERSE EMITTANCE MEASUREMENT AT HIRFL-CSR

P. Li[1, 2], J.X Wu[1], Y.J Yuan[1], Y.Q, Yang[1], S.L Yang[1]
1 (Institute of Modern Physics, CAS, Lanzhou, 730000, China)
2 (Graduate University of CAS, Beijing, 100049, China)

Abstract

HIRFL-CSR is a multi-purpose heavy ion storage ring in Lanzhou. In order to measure the transverse emittance of the injected beam on the transfer channel to the HIRFL-CSR, two kinds of emittance measurement devices which included pepper- pot and slit-grid were proposed. The pepper-pot is unique in providing an instantaneous measurement of the two-dimensional emittance of a beam. The data acquired by this method is only an image. The slit-grid is a one dimensional emittance measurement device. During the measurement, the slit, driven by the stepper motor is moved stepwise across the beam, and then the signal induced on the grid will be stored in the computer for further analysis. Because slit-grid is one dimensional device, two sets of this device are needed for transverse measurement. In this paper, we introduce the design, parameters, data acquisition and analysis of these two methods. Especially the software integration is given in this paper. Main interest is directed on the software development for emittance front-end control and data analysis such as evaluation algorithms.

INTRODUCTION

HIRFL-CSR (Heavy Ion Research Facility in Lanzhou-Cooling Storage Ring) is a multi-purpose heavy ion storage ring that consists of a main ring (CSRm), an experimental ring (CSRe) and a radioactive beam line (RIBLL2) to connect the two rings [1]. As part of the development program and to provide necessary information for HIRFL-CSR beam dynamic simulation and experiments, high quality emittance measurement are required. So in order to measure the transverse emittance of the injected beam on the transfer channel to the HIRFL-CSR, two kinds of emittance measurement devices which included pepper- pot and slit-grid were proposed. The chamber will be installed in the injection line of HIRFL-CSR which is shown as figure 1. The pepper-pot and two sets of grid-slit devices can be seen in figure 2. Two systems have already been installed in the chamber. There are also some other equipments for measurement such as CCD camera and mirror which are used for alignment in pepper-pot systems. In slit-grid system, I/U converter and DAQ card acquire beam current data for analysis.

*Work supported by HIRFL-CSR project
#lipeng@impcas.ac.cn

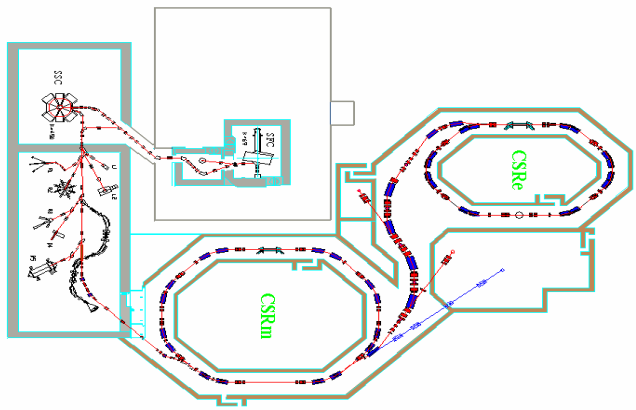

Figure 1: The layout of HIRFL-CSR

Figure 2: The chamber

SLIT-GRID SYSTEM

The slit-grid is a very popular method used for protons/heavy ions emittance measurement. The classical scheme is shown schematically in figure 3[2]. Two sets of slit-grid system with the same parameters are designed for measuring the horizontal and vertical emittance respectively. A narrow slit, driven by the stepper motor, is moved stepwise across the beam. In our slit-grid system, the width of the slit is 0.5mm. The distance between slit and grid is 300mm. There are 49 wires of which the width is 0.2mm and the spacing is 1mm in one dimension. The gird device can be seen in figure 4. During the measurement, we need two coordinates to locate the beamlets: one for the slits(x), the other for the grid(X) [3]. The wire currents are converted into reasonable voltages U using I/U converter. DAQ card is used to acquire data.

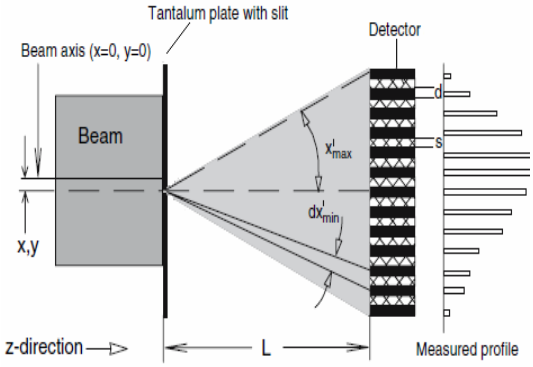

Figure 3: Scheme of slit-grid system

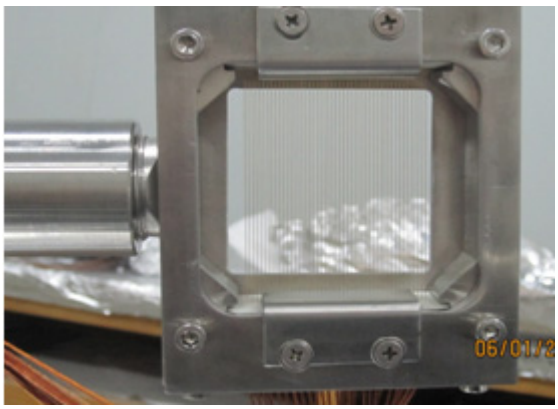

Figure 4: The grid device

PEPPER-POT SYSTEM

Due to the relatively slow movement of slit-grid systems through the beam, the measuring time becomes rather long. Although this time will be of the order some 10s up to about 5 minute for dc-beams, this can extend to some minutes for pulsed beams. The coupling effects between both transverse phase planes cannot be observed in the slit-grid system. Those drawbacks of the slit-grid system can be solved by another method called pepper-pot measurement way. The scheme of this method is shown in figure 5[2]. The beam come from left and then hit a plate with a number of small holes, arranged in the x, y-plane like the elements of lines and columns in a matrix. The sample beamlets fall on the viewing screen, where the light spots are observed by a fast PC-controlled CCD-camera system [4]. The pepper-pot screen is a 0.1mm thick tungsten foil with a square array of 27×27 holes, each 0.2mm in diameter, on a 1.5mm pitch. The beam is imaged with a quartz scintillator, 150mm from the tungsten screen, and a 1024×1344 pixel high speed camera. Data is recorded from the camera direct to a multi-image TIF file or excel file and analyzed with Matlab.

SOFTWARE SYSTEM

Two programs are used to control measurement as well as evaluate and visualize data for the two systems. Since the system may be operated by scientists and operators, who can be more or less familiar with the system parameters, the control software must be designed based graphical user interface (GUI). The software designed with Matlab consists of data acquisition, evaluation and visualization tools.

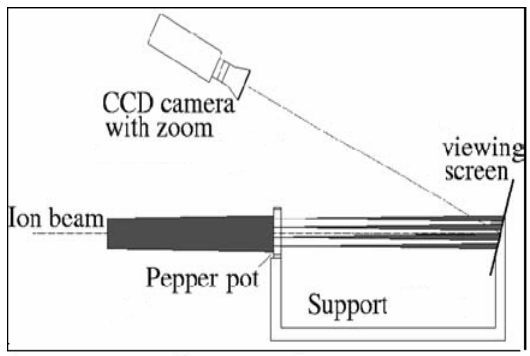

Figure 5: The scheme of the pepper-pot system

Data Acquisition

In pepper-pot system, the data is only an image acquired by a CCD-camera. The measurement process can be seen in figure 5[2]. Meanwhile accurate calibration data is crucial in converting the pepper-pot images into emittance data. The calibration data would be stored in the computer before analysis.

In slit-grid system, the data acquisition is more complicated. Because this method is a one-dimensional way to measure emittance, two slit-grid devices are needed to obtain the horizontal and vertical data. Four stepper motor are used to control the position of the slit and grid. The stepper motor is connected with the computer by RS-232 port. Meanwhile, the measured grid currents have to be converted into reasonable voltages U for digitization. The digital data is acquired by the DAQ card of NI 6224. All the data would be stored in the computer for the further analysis. Figure 6 is the scheme of measurement process in slit-grid system [2].

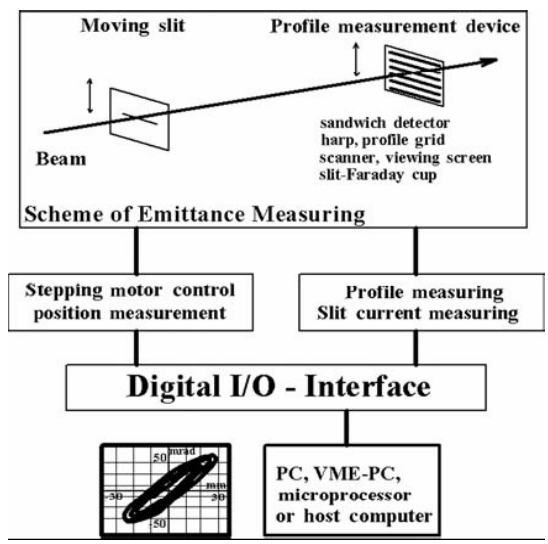

Figure 6: The scheme of measurement in slit-grid system.

Data Analysis

The root-mean-square phase space distribution parameters are calculated as a normalized sum of matrices elements. The data gathered from the pepper-pot systems is more difficult to analyse than from the slit-grid systems. But the RMS emittance can also be calculated by the following formula [5].

For one dimension:

$$V = \sum_{ix}\sum_{ix'} U$$

$$e = U / V$$

$$x_{mean} = \sum_{ix}(e_{ix,ix'} \cdot x_{ix})$$

$$x'_{mean} = \sum_{ix'}(e_{ix,ix'} \cdot x'_{ix})$$

$$\sigma_x = \sum_{ix}\sum_{ix'}(e_{ix,ix'} \cdot (x_{ix} - x_{mean})^2)$$

$$\sigma_{x'} = \sum_{ix}\sum_{ix'}(e_{ix,ix'} \cdot (x'_{ix'} - x'_{mean})^2)$$

$$M_{x,x'} = \sum_{ix}\sum_{ix'}(e_{ix,ix'} \cdot (x_{ix} - x_{mean}) \cdot (x'_{ix'} - x'_{mean}))$$

$$\varepsilon_{RMS} = \sqrt{\sigma_x \sigma_{x'} - M_{x,x'}}$$

U and e are original and normalized beam intensity. x and x' are the position and angular in horizontal dimension. Sometimes in order to improve accuracy the initial data set may be resampled. The re-sampling can use linear or cubic interpolation method [6]. Twiss parameters can be calculated according to the RMS emittance and the profile of the beam.

Geometric Emittance

The data can also be used to calculate the geometric emittance. There are many emittance subtraction modes for calculating emittance. For example, summing up all intensities $U_{x,x'}$ of the corrected data matrix defines the maximum intensity $U_{\max}$, taken as reference to calculate the percentages. Therefore, to calculate, for example, the so-called 80% emittance, a value of S = $0.2U_{\max} / n_x n_{x'}$ (n_x = number of rows, $n_{x'}$ = number of columns) has to be subtracted from each element with $U_{x,x'}$ > 0 in the data matrix. No subtraction takes places if $U_{x,x'}$ = 0. The subtraction has to be performed successively in much smaller steps as defined by S (for example S/100). Elements below zero are set to zero. Then we use the unit area $dxdx'$ and the subtracted elements to calculate the geometric emittance.

Visualization

Having finished the calculation mentioned above, the result especially the geometric emittance can be seen in an image. There is also a tool bar to adjust the contrast ratio to make a clear visualization. Furthermore, the phase space ellipses can be plotted by the RMS emittance and the Twiss parameters.

CONCLUSIONS

There are both advantages and disadvantages respectively in the two systems. The data analysis for slit-grid system is much easier than the analysis in pepper-pot system. But the measurement time in slit-grid system is longer. We can use the two systems to measure the beam parameters at the same time, and do the comparisons between the two results. The hardware and software have been designed and finished. The systems will be tested as soon as they are installed on the transfer line.

REFERENCES

[1] Yuan Y.J, XIA J.W, Zhao H.W et al. Present Status and Future Improvement of HIRFL-CSR. In: Proceeding of EPAC 2008. Genoa Italy. 2008. 388-390

[2] Measurements in Phase Spaces

[3] Min Zhang. Emittance Formula for Slits and Pepper-pot Measurement. FERMILAB-TM-1988

[4] S.Jolly, D.Lee, J.Pozimski, P.Savage.Beam Diagnostics for the Front End Test Stand at RAL. In: Proceeding of DIPAC 2007, Venice, Italy

[5] S.Y.Lee. Accelerator Physics

[6] T.Hoffmann, D.A.Liakin. Control and data analysis for emittance measurement devices. In: Proceeding DIPAC 2001. Grenoble, France 2001

TOWARDS THE 2 MW CYCLOTRON AND LATEST DEVELOPMENTS AT PSI

M. Seidel, Ch. Baumgarten, M. Bopp, J. Grillenberger, Y. Lee, D. Kiselev, A. Mezger, H. Müller, M. Schneider, A. Strinning
PSI, 5232 Villigen, Switzerland

Abstract

PSI operates a cyclotron based high intensity proton accelerator routinely at an average beam power of 1.3MW. With this power the facility is at the worldwide forefront of high intensity proton accelerators. An upgrade program is under way to ensure high operational reliability and push the intensity to even higher levels. The beam current is practically limited by losses at extraction and the resulting activation of accelerator components. Further intensity upgrades are only possible if the relative losses can be lowered in proportion, thus keeping absolute losses at a constant level. The basic upgrade path involves the reduction of space charge induced extraction losses by implementing improved RF systems and resonators in both cyclotrons. The paper describes the ongoing upgrade program, achievements that were realized since the last cyclotron conference and several operational experiences and difficulties that were observed during routine operation.

INTRODUCTION TO THE PSI FACILITY

The PSI high intensity proton accelerator generates a high power proton beam with 590 MeV kinetic energy. At full energy the relative beam losses have to be kept within the lower 10-4 range to avoid excessive activation of accelerator components in the extraction region. The PSI accelerator consists of a Cockcroft-Walton pre-accelerator and a chain of two isochronous cyclotrons, the Injector II and the Ring cyclotron. The beam is produced in continuous wave (CW) mode at a frequency of 50.6 MHz. The whole facility including the experimental areas fits in a rectangle of 120 m × 220 m. The proton beam is used to produce pions and muons by interaction with two graphite targets that are realized as rotating wheels [1]. The targets have thicknesses of 5 mm and 40 mm. Pions decay into muons that are transported in large aperture transfer lines to the experiments. Muon beam intensities up to 5·108 s-1 are achieved [2]. After collimation behind the meson production targets the remaining proton beam with roughly 1MW is then used to produce neutrons in a spallation target. The actual target consists of a matrix of lead filled Zircaloy tubes. The neutrons are moderated in volumes filled with heavy water (D2O) surrounding the target, and then transported to the 13 instruments installed in the Swiss Spallation Neutron Source (SINQ) facility. In 2010 a pulsed source for ultracold neutrons (UCN) will be brought into operation as well. The research themes at PSI cover a broad range of applications involving neutron scattering, muon spin spectroscopy and few particle physics experiments. Fig. 1 shows an overview.

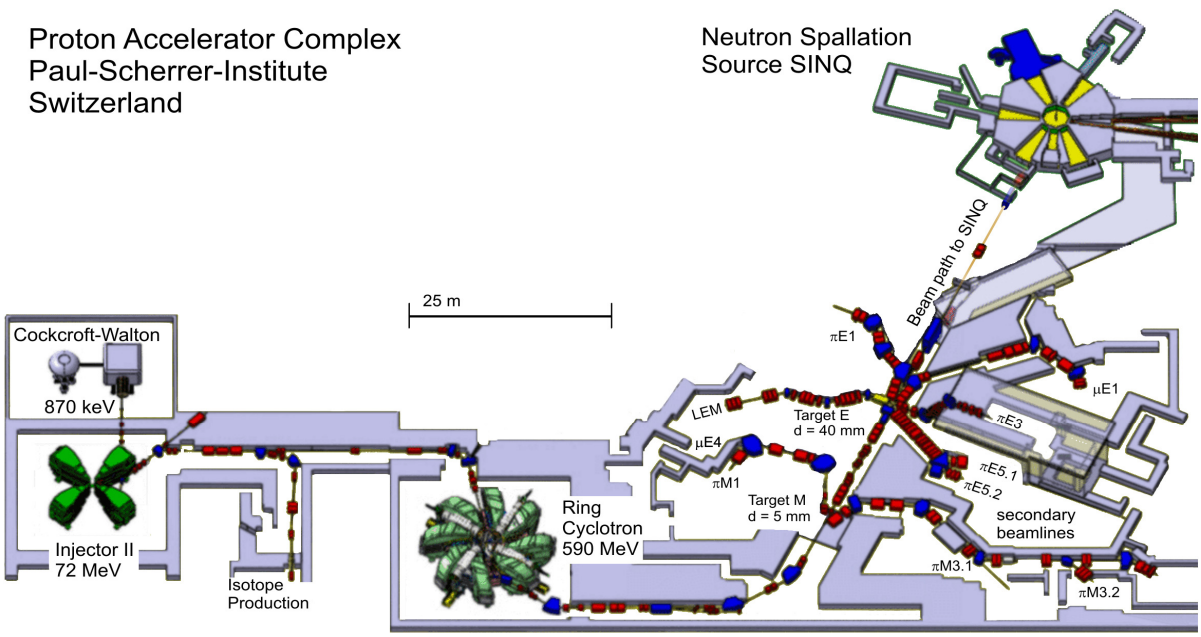

Figure 1: Overview of the PSI accelerator complex.

RECENT PERFORMANCE IMPROVEMENTS AND DEVELOPMENTS

Ring Resonators and Double Seals

The original aluminium resonators in the Ring cyclotron were successively replaced by newly designed copper resonators. The first resonator was installed already in 2004, and for some time the cyclotron was operated with both types of resonators in parallel. The new setup with all four resonators in place was completed in 2008. The new resonators can be operated at higher gap voltages, which allows reducing the number of turns in the cyclotron. In fact, because of longitudinal space charge effects the beam losses scale inversely proportional to the third power of the number of turns [3][4]. Thanks to this improvement and a new operational license a standard current of 2.2 mA, corresponding to 1.3 MW beam power, was reached in 2009. The losses at 2 mA were reduced by a factor ~2 (Fig. 2). The resonators are now operated at a voltage of 850 kV and the specification leaves room for further increases slightly beyond 1 MV. At present the limitation is given by the third harmonic resonator whose voltage cannot be raised in proportion. Because of smaller ohmic losses in the 4 copper resonators roughly 600 kW of wall plug power are saved. The efficiency of the RF system for converting wall plug power to beam power amounts to 0.32. It is obtained by multiplying the efficiencies 0.9 for AC/DC conversion, 0.64 for DC/RF conversion and 0.55 for RF to beam power. A review of resonator and RF development at PSI is given in these proceedings [5].

Together with the resonators a new type of inflatable seals was installed in the Ring cyclotron [6]. The design of these seals is critical since they need to have a relatively long length of 2.5 m. The new design incorporates two O-ring seals with an intermittent evacuated volume that also serves testing puposes (Fig. 3). After the installation practically no vacuum leaks were observed, whereas such problems occurred rather often with the old seals.

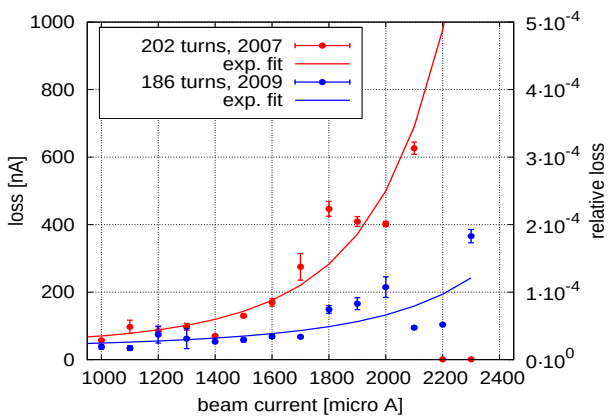

Figure 2: Loss currents under optimal conditions as a function of beam current. The turn reduction due to higher gap voltages led to a significant reduction.

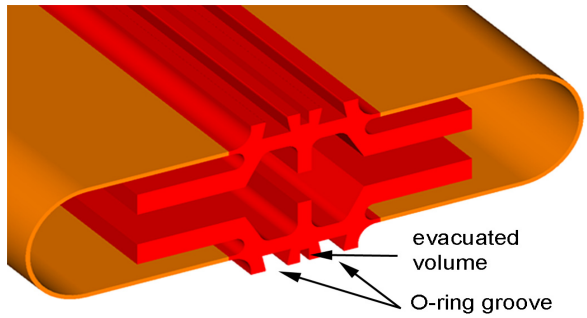

Figure 3: CAD model of the new inflatable seals that are in use to connect resonators and neighboured chambers.

ECR Proton Source

In 2010 a new ECR proton source [7][8] was brought into operation. While the old source was electrically heated with filaments that had to be replaced every two weeks, the new source employs the ECR principle and does not require regular service. At the time of writing the source was continuously in operation for 3.5 months. With RF powers between 390 W and 600 W the generated proton current is in the range of 12 mA to 18 mA. The rms beam emittance was measured to be 4.2 mm mrad and is supposedly smaller than the one of the old source. Nevertheless it took a long time to retune the accelerator in 2010 for operation at similar loss levels as with the old source in 2009. One hypothesis is that slight beam optical mismatch of source and injector II cyclotron have led to these difficulties.

10^{th} Harmonic Buncher

The 500 MHz “superbuncher” was installed delayed in fall of 2009. The buncher is situated in the 72 MeV transfer line between injector and Ring cyclotron with the goal to generate a short bunch length at injection and to establish the circular beam scheme also in the Ring cyclotron [4]. For further reduction of the turn number in the Ring the function of the buncher is critical since the voltage of the existing flattop resonator cannot be raised further. With empirical tuning of amplitude and phase a positive effect on the losses was observed at low currents of ~200 µA. At higher currents only increasing losses were observed. It is suspected that a better relative phase control for the three phases of buncher, injector and Ring cyclotron is needed. Furthermore it might be necessary to readjust the transverse optics when the buncher is operated. Because of many technical and performance problems in 2010 it was not possible to study the effect of the buncher in more detail.

OPERATIONAL EXPERIENCE

Beam Currents and Losses in 2009/10

As mentioned the turn number reduction in the Ring cyclotron of 2008 has lead in principle to a significant reduction of the losses. However, the optimal setup is fragile and minor technical problems can already result in

a strong increase of the losses and limitations of the beam current. During start-up in 2009 such problems were caused by a misaligned vertical collimator that covers the complete radius in the Ring cyclotron. The tighter vertical aperture caused enhanced scattering of the beam tails (Fig. 5). The collimator is realised as a pair of graphite sheets and was probably deformed because of heating due to stray RF waves. The original purpose of the fixed collimator was to provide a passive protection system in case of beam mis-steering. Since the loss-monitor based interlock system has been significantly improved over the years it was decided that the collimator could be safely removed. Afterwards it was easily possible to accelerate 2.2 mA. During tests a peak current of 2.3 mA was achieved without problems (Fig. 4).

In 2010 the start-up was suffering from plasma effects that were generated in the Ring cyclotron as a result of excessive stray RF amplitudes [9]. Sputtering effects caused thin coatings on the insulator surfaces of the electrostatic extraction element and it had to be replaced. But also after this problem was overcome, the facility suffered from enhanced losses at the Ring extraction which limited the maximum current to 2.0 mA till the beginning of August. Enhanced energy and beam position jitter at 50 Hz disturbed the operation. This problem was resolved as described in the next section. After careful retuning and cycling of the dipole magnets in the Injector II cyclotron the losses were finally reduced to an acceptable level and operation at 2.2 mA was resumed. It is now believed that improper optical matching of the beamline from the source to the injector cyclotron has caused the enhanced beam tails and the resulting losses. Remarkably, when the enhanced losses were present it was not possible to directly measure an enhanced emittance or detect signs of beam tails. These profile measurements were done using beam tomography methods [10] with 5 wire scanners in the horizontal plane of the 72 MeV transport line. The problems observed in 2010 demonstrate how difficult it actually is to tune the accelerator to optimum loss conditions. Many efforts are also invested to accurately simulate the beam dynamics of the high intensity beams in cyclotrons [11].

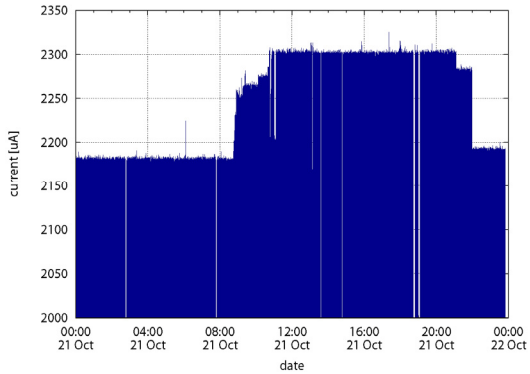

Figure 4: Example of stable operation beyond the standard current at 2.3 mA (1.36 MW) in 2009.

50 Hz Jitter Impairing the Performance of the Accelerator

After the installation of the new ECR source an enhanced 50 Hz beam jitter was observed. In the 590 MeV beamline to the meson production targets the horizontal position jitter was as large as 2 mm, corresponding to more than one rms beam width. Only little jitter was present in the vertical plane. The jitter was traced back to an energy modulation of the beam caused by 200 V peak to peak jitter of the 810 kV accelerating voltage in the Cockcroft Walton accelerator (CW). However, finally it turned out the primary reason was a beam current modulation in the proton source, whose magnitude exceeded the voltage stabilization capabilities of the CW power supply. The RF generator of the source is a filament heated magnetron. Replacement of the Magnetron power supply with a better stabilized one and an improved regulation of the CW voltage resolved the problem and led to a reduction of the jitter amplitude by a factor 3. There is still significant 50 Hz jitter present, caused by other sources. Further improvements are necessary to reduce these disturbing effects.

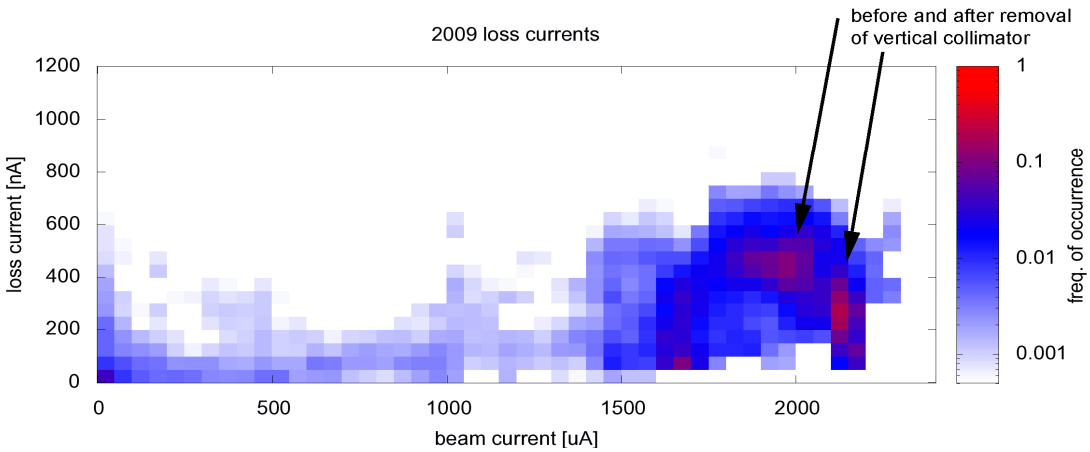

Figure 5: Distribution of extraction losses as a function of current. The colour code corresponds to the frequency of operation at the particular working point. Loss monitors were calibrated by provoking total loss of a small test current.

Beam Trip Statistics

Beam trips interrupt the user experiments and cause thermal cycles for the targets which may lead to a reduction of their lifetime. Also in view of potential ADS applications of cyclotron based high intensity accelerators the demonstration of a good trip performance is of interest. Most of the short term interruptions in the cyclotron are caused by high voltage trips of the electrostatic elements which deflect the injected and extracted beams. Other causes are occasional triggers of the interlock system by spikes in the lossrates, or trips of the RF system. In most cases the system that originated the interruption is automatically reset and the current is ramped up again within 30 seconds.

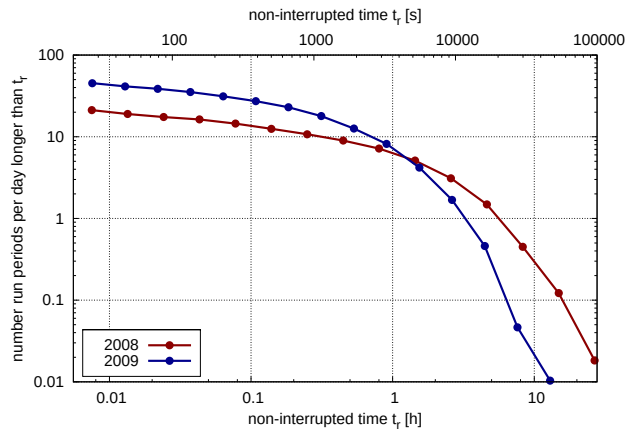

Figure 6: Distribution of durations of non-interrupted run periods in the years 08/09. The differential distribution is integrated from the right. It shows how many runs per day occur with the duration of the abscissa value or longer.

The graph in Fig. 6 shows the number of runs per day with a duration longer than the value read from the abscissa. At the very left end of the graph one can read the total number of runs (and trips) per day. On average 20 to 60 trips per day are observed and the longest uninterrupted runs have a duration of 10..20 hours. In 2009 the accelerator was run at 2.2 mA vs. 2.0 mA in 2008 and the enhanced current could be a reason for the decreased performance. In comparison the desired trip rates of planned ADS systems for transmutation or energy production are in the range 0.1-0.01 d-1 [12], i.e. 2 to 3 orders of magnitude lower.

PLANNED UPGRADE MEASURES

PSI pursues a continued upgrade program with the goal to improve the reliability of the accelerator complex and to raise the beam intensity in steps towards 1.8 MW [13].

New Resonators and RF Systems for the Injector II

The most important upgrade step for the PSI facility is the installation of two new resonators in the Injector II cyclotron. These 50 MHz resonators will replace existing 150 MHz flattop resonators, which are no longer needed because the cyclotron is operated in the circular beam regime [4]. A new resonator type has been designed and two copies are being manufactured at the French company SDMS. Fig. 8 shows a photograph of the first delivered resonator. These cavities are made from aluminium, they exhibit a sector shape and the challenges of the mechanical design lie in a good cooling concept assuring frequency stability. During operation a hydraulic tuning mechanism will regulate the frequency [14].

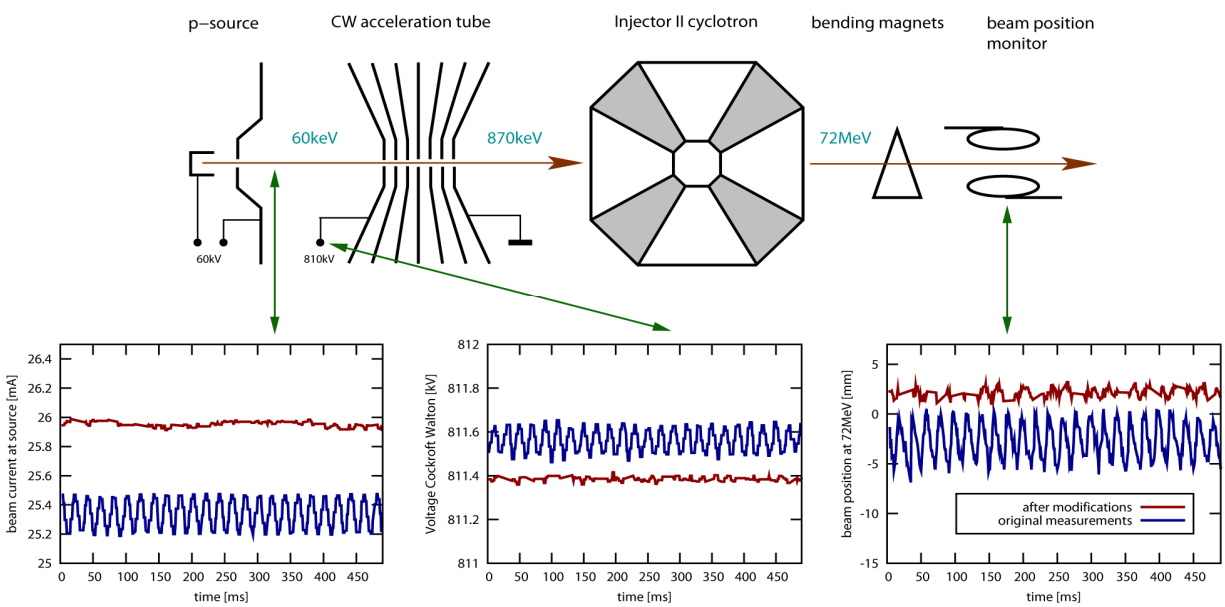

Figure 7: Illustration of the propagation of a initial 50 Hz beam current ripple at the proton source throughout the accelerator. The red curves were recorded after taking the measures described in the text.

Figure 8: The first one of two new resonators for the Injector II, delivered by the French company SDMS.

At present the first delivered resonator is undergoing high power testing at PSI. The resonator was successfully operated at specification level of 100 kW RF power for several days.

New Absorbers at the Meson Production Target

Because of scattering in the 40 mm target, a large fraction of the beam has to be collimated. Roughly 12% of the protons are lost due to nuclear reactions and the debris is absorbed by collimators behind the target. Additional 18% of the beam are collimated because the elastically scattered protons deviate too much from the ideal orbit and could not be transported to the SINQ spallation target. The first two collimators are situated close to the target and exhibit wide opening angles. They absorb secondary particles and thermal radiation. The main collimation is done with two water cooled and segmented copper collimators with a length of 30 cm each. They are installed 4.7 m downstream of the target. At a current of 2.0 mA, this collimator system is estimated to receive a total heat load of ~170 kW, and the peak temperature is calculated to reach ~650 K. After 20 years of operation the first of those collimators has received a high radiation dose. Irradiation damage corresponding to values of 12 to 35 dpa on average were estimated using different computer codes. In order to verify the intactness of the inner surface, the collimator was taken out in the shutdown 2010 and inspected in a hot-cell. Although on parts of the inner surface thin flitters of copper were found, the bulk material seems intact and no signs of swelling were found. A dose rate of ~500 Sv/h was measured on the beam axis close to the entrance into the collimator. In order to reach 3 mA with new absorbers, the deposited power has to be distributed more evenly over the two absorbers. In parallel the aperture of the collimators will be slightly opened without affecting their function to reduce the power deposition. With the help of this measure acceptable peak temperatures are expected. The application of GlidCop as a material with better strength at elevated temperatures would result in a working scheme even without opening the apertures [15]. However, brazing with GlidCop is more difficult and more testing is needed before a decision on the choice of material can be made.

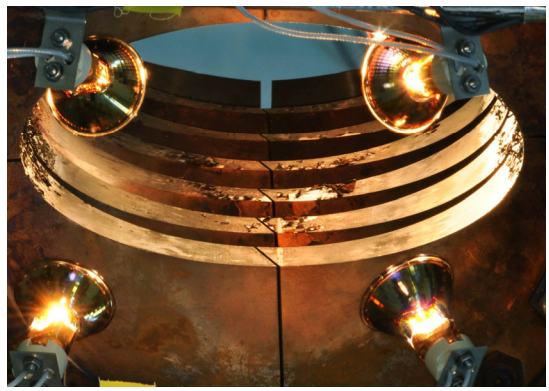

Figure 9: The inner surface of the existing collimator 2 seen from the side of the beam exit and tilted by 90°.

REFERENCES

[1] G. Heidenreich, Carbon and Beryllium Targets at PSI, Proc. AIP 642, 122 (2002)

[2] T. Prokscha et al, The new μE4 beam at PSI: A hybrid-type large acceptance channel for the generation of a high intensity surface-muon beam , NIM-A 595, 317 (2008).

[3] W. Joho, High Intensity Problems in Cyclotrons, Proc. 5th intl. Conf. on Cyclotrons and their Applications, Caen (1981).

[4] M. Seidel et al, Production of a 1.3 MW Proton Beam at PSI, IPAC10, Kyoto 1309 (2010).

[5] L. Stingelin, High Power RF Systems and Resonators for Sector Cyclotrons, these proceedings (2010).

[6] The inflatable seals were developed by U. Heidelberger in collaboration with the Swiss companies InnoRat, Wartmann and Ingenis

[7] Ch. Baumgarten et al, The New ECR-Proton Source for the PSI-Ring-Machine, ECPM Groningen (2009).

[8] P.A. Schmelzbach et al, A compact, permanent Magnet, ECR Ion Source, Proc. Cycl. and their Appl. 2007, Giardini Naxos, Italy 292 (2007).

[9] M. Humbel, Disturbance Effects Caused By RF Power Leaking Out From Cavities In The PSI Ring cyclotron, these proceedings (2010).

[10] D. Reggiani, M. Seidel, C.K. Allen, Transverse Phase-Space Beam Tomography at PSI and SNS Proton Accelerators, IPAC10, Kyoto 1128 (2010).

[11] Y. Bi et al, Towards quantitative predictions of high power cyclotrons, these proceedings (2010)

[12] Abderrahim, H.A., Cinotti, L., Giraud, B. et al., The experimental accelerator driven system (XADS). Journal of Nuclear Materials 335, 148 (2004).

[13] M. Seidel, P.A. Schmelzbach, Upgrade of the PSI Cyclotron Facility to 1.8 MW, Proc. Cycl. and their Appl. 2007, Giardini Naxos, Italy 157 (2007).

[14] L. Stingelin, M. Bopp, H. Fitze, Development of the 50 MHz Resonators for the PSI Injector II, Proc. Cycl. and their Appl. 2007, Giardini Naxos, Italy, 467 (2007). [15] Y. Lee et al, Simulation based Optimization of a Collimator System for the Beam Current Upgrade at the PSI Proton Accelerator, IPAC10, Kyoto 4260 (2010).

RELIABLE PRODUCTION OF MULTIPLE HIGH INTENSITY BEAMS WITH THE 500 MEV TRIUMF CYCLOTRON*

R. Baartman, F. Bach, Y. Bylinsky, J.Cessford, G. Dutto, D. Gray, A. Hurst, K. Jayamanna, M.Mouat, Y. Rao, R. Rawnsley, L. Root, R. Ruegg, V. Verzilov, TRIUMF, Vancouver, Canada

Abstract

In 2001, after 25 years of smooth cyclotron operation with up to 200 μA H^- acceleration, developments towards higher intensities became compelling because of the ISAC expansion. Recently the goal of reliable total proton production current up to 300 μA, within a nominal ~90% duty cycle, was routinely achieved. Beam availability was 90-94% over the last five years. Development highlights are discussed in the paper.

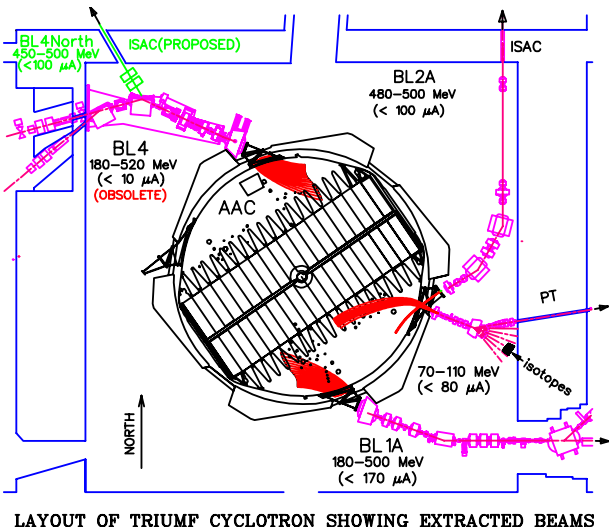

Figure 1: Layout of the cyclotron.

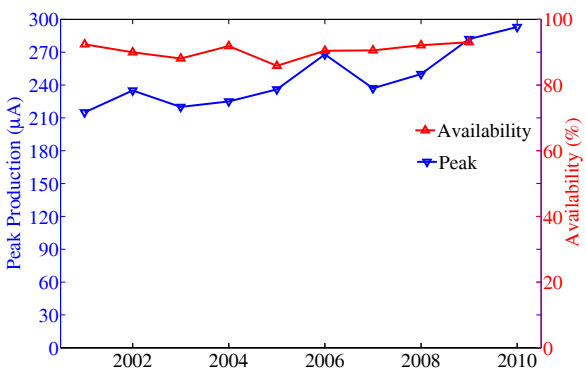

Figure 2: Peak current production and % beam availability for the last 10 years.

*TRIUMF receives funding via a contribution agreement through the National Research Council of Canada.

INTRODUCTION

The TRIUMF cyclotron delivered increasingly intense proton beams during the past 35 years. First beam was extracted at the end of 1974. At the beginning of 1978 the installation of adequate shielding allowed up to 100 μA extraction down the meson production beamline (BL1A) (see Fig. 1). Early production and milestones were summarized at EPAC88, and a one week beam delivery test at $\sim$ 200 μA was also reported [1]. Routine beam production followed during several years up to this current level. In 1995 ISAC was approved and a second high intensity beamline (BL2A) was designed & constructed to transport a 475 to 500 MeV beam to the radioactive isotope source. In order to maintain previous production levels unaltered, it was decided to increase gradually the total cyclotron extracted current from $\sim$ 200 μA to $\sim$ 300 μA, towards a goal of 100 μA for the ISAC primary beam. Higher beam stability and reliability would also be required for this beam [2]. In 2009 a 3 hour test at 290 μA total extracted current was successfully performed. A total peak current of $\sim$ 420 μA at 25% duty cycle was also reproduced. It confirmed previous predictions of a total extracted current in excess of 400 μA [1]. It should be emphasized that reliable extraction of simultaneous multiple high intensity beams hinges on the highest efficiency, reliability and stability of cyclotrons subsystems. Recent improvements to some of these systems will be described below. Peak total extracted intensities and yearly availabilities achieved during 2000-2010 are shown in Fig. 2.

ION SOURCE

Over the years TRIUMF designed H^- ion sources for different types of cyclotrons. High current cusp sources capable of delivering up to 20 mA of H^- beam within a normalized 4RMS emittance of 0.6 πmm-mrad have been first developed for commercial isotope production machines [3]. For the 500 MeV cyclotron, where the acceptance is much smaller, the cusp source is optimized for 700 μA within a normalized 4RMS emittance of 0.1 πmm-mrad. The 12 kV ion source extraction gap is followed by a pair of magnetic steering elements, an einzel lens and iron structures to shield the beam from the $\sim$ 5 gauss main cyclotron stray field. At 1.2 m from the source, a 1 m long acceleration column takes the 300 keV beam to a 34 m long electrostatic injection line. Beam emittance figures from an 'Allison' emittance scanner located at the frontend of the line are shown in Fig. 3 for a 600 μA beam.

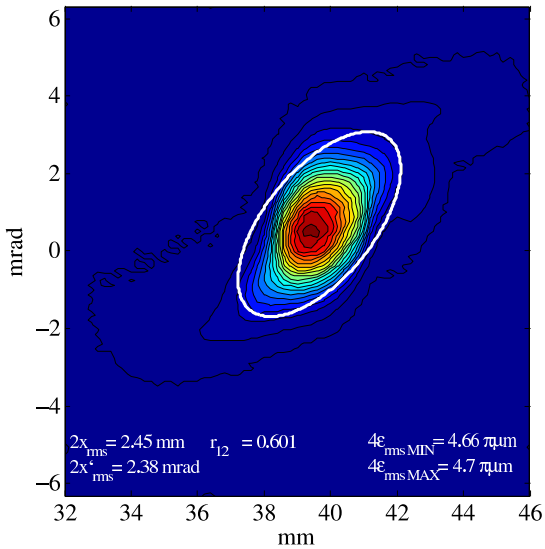

Figure 3: Emittance figure measured at 300 keV.

INJECTION BEAM LINE

The 300 keV injection line is 34 m in length and has 76 electrostatic quadrupoles. The quads are arranged in a FODO periodic lattice, with insertions for two achromatic $2 \times 45°$ electrostatic bender sections, a slit section for pulsing and matching sections to match from the ion source to the lattice, and from the lattice to the cyclotron. Diagnostics consists of 13 scanning wire profile monitors, and a number of cooled apertures and beam stops. The full $600\,\mu$A is transported to a set of slits in the periodic section, separated by $90°$ of phase advance. Adjusting the slits allows transporting zero to the full $600\,\mu$A beam current without adjusting the ion source. Besides halo-cleaning, this technique has the advantage that the emittance is the smaller, the smaller the required beam current.

For large currents, it is especially important to match the beam to the periodic section. This has been accomplished by measuring the beam profiles at a number of scanning wire diagnostic stations and fitting to find the beam's Courant-Snyder parameters. A tune for the matching section (see Fig. 4) was then calculated using the TRANSOPTR computer code [5]. The recently installed Allison-type emittance scanner has greatly simplified the matching exercise.

After a further 12 m of travel, the beam is bent downward towards the cyclotron. The vertical section is 13 m long and has only two scanning wires so matching is difficult to verify. Bunchers are needed to match the DC beam to the $40°$ cyclotron phase acceptance. These are placed 20 m from injection (partway along the horizontal section), so the $600\,\mu$A reaches a local peak current of approximately 5 mA at the end of the injection line. The large resulting space charge forces, plus the axial magnetic field from the cyclotron and lack of diagnostics make it difficult to model the beam optics accurately.

As the vertical section has operated continuously since

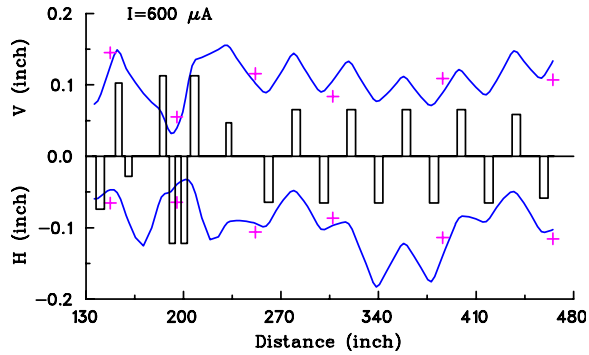

Figure 4: Calculated envelopes and measured beam sizes show good agreement in a periodic section at $600\,\mu$A. Vertical rectangles represent quadrupole focus strengths.

1975, some of the insulators of the electrostatic optics have accumulated sufficient quantity of cracked hydrocarbons and other debris that reliability is being threatened. The optic elements in question are deep inside the support structure of the cyclotron so mitigation by simply cleaning the insulators is not an option. For this reason a new vertical section has been designed and built and will be installed in Spring 2011. To design the optics, TRANSOPTR was expanded in capability to calculte beam envelopes including the effects of bunching, space charge, coupling from the axial magnetic field and the electrostatic spiral inflector, and rf acceleration in the cyclotron. Details can be found [4]. The resulting design is significantly simpler with 5 rather than 9 matching quads. As well, the new line will have 5 scanning wires and capacitive longitudinal (bunch shape) and transverse (BPM) monitors.

CENTRAL REGION

The central region was extensively studied during the cyclotron design stage [6]. This resulted in a magnetic field bump in the centre having the effect of moving the beam phase interval from negative to positive (lagging) phases during the first few turns and back to zero later. Simulations also showed a significant phase bunching effect on the first turn due to magnetic and electric field configurations. The central electric field configuration remained unaltered over the years. Beam deflecting or collimating electrodes were inserted in field-free regions. The magnetic field configuration can also be partially affected by tuning the inner trim coils: trim coil zero in particular. In order to be able to raise beam intensity and reduce losses in the central region, several systems had to be thoroughly refurbished.

These included the two low energy probes which had to be used to measure radial and vertical beam distributions. As these probes are completely inside the vacuum tank and repairs require tank lid opening, their use demands a very high level of reliability. Also, interfering rf leakage had to be reduced significantly or eliminated. Thanks to excellent work by the diagnositc and rf groups the required reliability was achieved.

The electrostatic correction-plate system [7] was also overhauled. This system and its vertical protection beam scrapers, extending radially on opposite dee segments to about 1.25 m from the centre, where vertically realigned (within $\sim$ 1 mm), to allow thermocouples to warn of small beam losses that could otherwise damage plates or wireways.

Recent additions include: (1) a cooled absorber inserted in the beam within the first quarter turn, to prevent unwanted injected ions from overheating stainless steel structural supports; (2) radial flags attached to the central vertical dee walls on the second and forth quarter (3) thermocouples on uncooled electrodes close to the beam.

Under optimal conditions transmission up to 70% has been measured between the lower end of ISIS and the total extracted current. Taking into account outer beam losses caused by vacuum and electromagnetic stripping one concludes that the centre region can accept over 75% of the ISIS beam. Extracted beams have good spot sizes at the targets and a $\sim$ 5ns time structure. We expect that the imminent installation of a new vertical injection line with optics more favourable to higher space charge will allow significant progress above 300 μA total extraction [8].

OUTER REGION

The TRIUMF cyclotron is operating with the two high energy strippers in "shadow mode". The meson production beamline (BL1A) and the radioisotope production beamline (BL2A) are one sector (60°) apart. To set up, the BL1A stripper is moved radially inward to initially extract all the beam, then the BL2A stripper is moved radially inward by steps of a fraction of a mm until the desired split ratio is obtained. Slight changes in the circulating beam orbit due to small changes in, for example, rf voltage can cause a large fluctuation of the split ratio of beam currents between BL1A and BL2A. The reason is that the radial density contains strong modulations that originate from the $\nu_r = 3/2$ resonance at 428 MeV. This modulation starts at 428 MeV and persists to 500 MeV extraction. Monte Carlo simulations and measurements with a high energy probe with a radial differential head have demonstrated such an oscillation in the beam density [9]. In principle, the modulation can be eliminated by correcting the resonance; this requires a third harmonic in the magnetic field gradient. Unfortunately, though there are harmonic coils, these were only designed to generate a first harmonic: there are 6 coils, one per sector. Powered as a third harmonic, the phase is fixed except that they can be reversed in sign for a 180° shift in phase. Thus we could only obtain a partial compensation for this resonance, reducing the beam density oscillation by $\sim$ 40%. Measurements are shown in [9].

EXTRACTION AND BEAM STABILITY

Several improvements were made to get the required higher stability for the ISAC primary beam. First, the BL2A stripper current was stabilized by installing a feedback loop between the stripper and the pulser at injection, regulating the beam's duty cycle. Decreases in the stripper current are compensated by increases in duty cycle and vice versa [10]. Second, automatic beam steering was implemented to keep the beam centred on target. Thirdly, the 2A beam line tunes were developed to image at the target the spot at the stripping foil, thereby minimizing the beam halo on target. Automatic beam steering was also implemented for all targets in BL1A.

Developments in extraction foil materials and technology have resulted in improved beam quality and stability. Highly-oriented pyrolytic graphite is now used as stripping material, mounted in a tantalum frame with a thin copper cushion. Additional heat relief features were introduced. These changes have resulted in lifetimes extended from the typical $\sim$ 65 mA-hr to over 250 mA-hr for the most recent BL1A foil, operating at 140 μA and 480 MeV with negligible release of ^{7}Be contamination. BL1A and BL2A extraction foils are now 1.5 mg/cm^2 thick instead of the previously standard 5 mg/cm^2, and are 32 mm tall by 0.25 to 16 mm in radial width for partial or full stripping extraction. BL2C utilizes carbon wire strippers as single filaments for extraction of low intensity beams for treatment of ocular melanoma, or filament curtains for high intensity operation (70 μA) for the production of radiopharmaceuticals.

REFERENCES

[1] G. Dutto et al, "The Upgrading of the TRIUMF Facility to 500 uA Operation," EPAC'88, Rome, Italy, pp. 326-328.

[2] G. Dutto et al, "Simultaneous Extraction of Two Stable Beams for ISAC," EPAC'08, Genoa, Italy, pp. 3503-3508.

[3] T. Kuo et al, "A high intensity dc H$^-$ source for low energy injection," Rev. Sci. Inst. , **73**, p. 986 (2002)

[4] R. Baartman, "Cyclotron Matching Injection Optics Optimization," Proc. PAC2009.

[5] M.S. de Jong and E.A. Heighway: "A First Order Space Charge Option for TRANSOPTR," IEEE Trans. Nucl. Sci. **NS-30**, p. 2666 (PAC1983).

[6] G. Dutto et al, "Optimization of the Phase Acceptance of the TRIUMF Cyclotron," Cyclotrons-1972, Vancouver, Canada, pp. 340-350.

[7] M.K. Craddock et al, "Effects of Axial Misalignmnet of the Dees and their Correction," Cyclotrons-1972, Vancouver, Canada, pp. 329-339.

[8] Y. Bylinsky et al, "Latest performance of the 500 MeV H$^-$ cyclotron and recent progress towards three simultaneous RIB ion beams at TRIUMF," these proceedings.

[9] Y.-N. Rao, R. Baartman, G. Dutto, L.W. Root, "Studies of the $\nu_r = 3/2$ Resonance in the TRIUMF Cyclotron," Proc. PAC2009.

[10] J.J. Pon et al, "Recent Changes in the 500 MeV Cyclotron's Central Control System to Reduce Beam Downtime and Beam On/Off Transitions". Proc. ICALEPCS2009, Kobe, Japan, pp. 179-181.

THE VARIAN 250 MeV SUPERCONDUCTING COMPACT PROTON CYCLOTRON: MEDICAL OPERATION OF THE 2nd MACHINE, PRODUCTION AND COMMISSIONING STATUS OF MACHINES No. 3 TO 7

H. Röcken#, M. Abdel-Bary, E. Akcöltekin, P. Budz, T. Stephani, J. Wittschen,
Varian Medical Systems Particle Therapy GmbH (VMS-PT), Bergisch Gladbach, Germany

Abstract

Varian Medical Systems Particle Therapy has successfully commissioned its 2nd superconducting compact proton cyclotron for use in proton therapy in 2008. The 250 MeV machine serves as proton source for treatments at the first clinical proton therapy center in Germany which opened in early 2009. Furthermore, Varian is currently commissioning and factory testing its 3rd machine.

We report on the operation and performance of the 2nd machine as well as on the successful cool-down, quench testing, and magnetic shimming of the 3rd machine.

In addition we present RF commissioning plans using a newly developed solid state amplifier, and plans for the upcoming factory beam commissioning in the new Varian cyclotron scanning nozzle test cell, scheduled for October 2010. Finally we provide a brief status and outlook on machines no. 4 to 7.

INTRODUCTION

VARIAN's superconducting compact cyclotron for use in proton therapy is an azimuthally varying field isochronous machine which delivers a 250 MeV cw beam of up to 800 nA. The use of superconduction technology with its closed cycle, zero boil-off liquid helium cryosystem allows a high induction that completely saturates the iron yoke of the compact machine. This results in a reproducible and stable magnetic field which is essential for a reliable beam operation during medical use. The initial design proposal [1] was worked out in detail by ACCEL Instruments GmbH. Some key features of this machine type are listed in Tab. 1; more details are given in our previous status report [2].

In 2007, Varian Medical Systems, Inc. bought ACCEL which had built at that time - amongst diverse advanced technology equipment for research and commercial users - two cyclotrons for use in proton therapy. In early 2009, the respective VARIAN business was re-structured and the particle therapy part is now pursued by the newly formed Varian Medical Systems Particle Therapy GmbH (VMS-PT).

#heinrich.roecken@varian.com

Table 1: Technical specifications of the VMS-PT cyclotron (engineering goals)

Beam	
Energy	250 MeV
Extracted current	800 nA (more on short term)
Emittance (hor./vert.)	< 3 / 5 π mm mrad (2σ)
Momentum spread	±0.04%
Number of turns	650
Extraction efficiency	~80%
Dynamic range for intensity modulation	1:800
Fast intensity modulation	via electrostatic deflector, >10% in 100 µs
Iron Yoke	
Outer diameter	3.1 m (3.2 m for the first two machines)
Height	1.6 m
Weight	<90 t
4 Sectors AVF SC Magnet	
Stored energy	2.5 MJ
Induction at center	2.4 T
Induction at coil	<4 T
Operating current	160 A
Rated power of cryocoolers	40 kW
RF System	
Frequency	72.8 MHz (2nd harmonic)
Voltage @ center / @ extraction radius	80 kV / 130 kV
RF power	≤115 kW

CYCLOTRONS IN OPERATION

Currently there are two VMS-PT cyclotrons in operation. The first one is located at Paul Scherrer Institute (PSI) in Switzerland as part of the PROSCAN project [3], which is treating patients since the beginning of 2007. The second one passed its commissioning phase in 2008 at the Rinecker Proton Therapy Center (RPTC) in Germany, the first and to date only European proton radiation center that provides since early 2009 a complete hospital setting for the treatment of cancer [4]. Besides the cyclotron this facility is equipped with VARIAN's proton therapy technology, like a degrader for energy adjustment, an energy selection system for the energy

filtering, a beam line for beam transportation, four rotational isocentric gantries for 360° irradiation plus one fixed beam station for head / neck treatments, delivery nozzles providing the modern pencil beam spot scanning, safety systems, treatment control software and so on. The clinical user treats patients six days per week, for eight to ten hours per day, in the three gantries that have been handed over. Work to hand over the remaining treatment rooms is ongoing. Currently, the beam commissioning required to hand over the remaining rooms is performed during nights and weekends by VMS-PT. This means that the treatment facility, including the cyclotron, is operated 24 hours per day on six to seven days per week. Service actions are typically performed every Sunday. According to the clinical user, the uptime of the whole facility for patient treatment during the first six months of operation was 97% [5]. The uptime of the cyclotron itself was even higher. The cyclotron startup, diagnostics, and performance tuning is highly automated through the dedicated control system [6]. During clinical operation normally no cyclotron operator is required.

CYCLOTRONS AND SUBSYSTEMS UNDER COMMISSIONING

In contrast to the first two machines that were assembled and commissioned at the customer's site, cyclotrons no. 3 and following will be widely assembled and tested with beam already in the customized factory near Cologne, Germany. After this pre-commissioning and factory acceptance testing (FAT), the machines will be shipped to their destinations in only two large lots each, essentially parted into the upper and the lower half. Cyclotron no. 3 is currently in the final stage of assembly and is undergoing FATs in parallel.

Cool Down, Magnet Ramping, Test Quench, and Field Mapping of 3rd Machine

In May 2010 the superconductive (sc) magnet of cyclotron no. 3 was cooled down to LHe temperature without any problems. The first ramping of the sc coil up to and beyond its nominal operating current of 160 A took place on May 18 at the first attempt. All forces on mounting suspensions of the coil and cryostat were continuously monitored and exhibited the expected magnitude.

The whole cryo- and magnet system is conservative in design. As a consequence, the obligatory factory test quench could not be forced by a fast ramping of the coil current at the limits of the power supply. Instead, it had to be triggered at full operating current by powering dedicated quench heaters that were mounted directly on the coil windings during manufacturing. The re-cooling proceeded very smoothly, and after only 5 hours the system was fully operable again. All suspension forces came back to their previous values and a detailed field map revealed that the magnet system did not alter in any way, thus proved being a stable, quench proof and also quench tolerant system.

Field mapping for fine magnetic shimming of the isochronous machine is a sophisticated task. To avoid spurious effects from the slight temperature dependence of the yoke iron's saturation magnetization we perform the mapping in a temperature stabilized cell (see Fig. 1) using a specially developed field mapping device. With this setup, a first harmonic in the 4-fold symmetrically field of up to 29 Gauss was initially determined. This was easily brought down to less than the target value of 2 Gauss by moving the coil. Releasing and tightening the suspension links a few tenth of a mm takes only a few minutes. However, some field disturbances in the order of 6 Gauss remained on outer radius and have to be shimmed locally.

Figure 1: VMS-PT cyclotron no. 3 in a temperature stabilized cell (front cover removed for photo) during FATs

Solid State RF Power Amplifier

RF power for the first two cyclotrons is provided by a 3-stage tetrode tube amplifier consisting of several electrical cabinets for power transformers and high voltage supplies. While this is an established technique, it suffers from some design drawbacks, namely the internal use of high voltages, missing redundancy, aging of tubes with high replacement costs, and less suitability for pulse operation then is desirable during cavity conditioning. Most important of these drawbacks is the redundancy issue, which has a direct influence on the potential uptime during clinical operation. Our efforts trying to resolve this potential issue raised the idea of using a transistor based "solid state" amplifier (SSA) with many identical amplification modules working in parallel. A test station with 20 modules was built in 2009 and has successfully passed a 1000 hours test at the full output power of 25 kW. First tests have shown the capability of the system to

withstand a >15% continuous power reflection. Currently a full scale SSA consisting of 120 modules for a total output power of >150 kW is finalized and undergoing FATs at VARIAN [7]. This power is much higher than the cyclotron RF operation power of ≤115 kW, and the design allows uninterrupted operation in case one or more modules fail. Through its redundancy the new amplifier features a higher availability and maintainability. This will contribute to the overall system uptime and will also have a cost reduction effect. Moreover, the digitally controlled and modularized system provides extended diagnostics capabilities.

Digital Low Level RF Electronics

The next VARIAN cyclotrons will make use of a digital low level RF control electronics (dLLRF). All modules of this new development have already passed factory performance tests [7] and the system will be used for cyclotron no. 3 commissioning in September 2010. Like the SSA, the dLLRF is designed for high redundancy with parallel signal processing of redundant pickups and automatic switchover in case of failure of a signal path. This yields a high fault tolerance and further increases system uptime. Additionally, the dLLRF is faster than the previously used system and provides more remote input and output signals.

CYCLOTRON PRODUCTION

VARIAN has converted its >4,000 m^2 production halls near Cologne, Germany into a customized cyclotron manufacturing line, suitable for the assembly and system testing of several cyclotrons per year.

Cyclotrons No. 4 to 7

All major components for the production of cyclotron no. 4 are ready in the factory. Coil winding and assembly of pole caps is underway. We expect first system tests in late 2010. The fine machined yoke iron parts for no. 5 currently undergo dimensional and other QA inspections in the factory. Assembly will start shortly. Iron for no. 6 and 7 as well as the respective long lead items are ordered. The expected cyclotron production rate is about two cyclotrons per year for the near future. This can be increased according to market needs if necessary.

Test Cell

Directly adjacent to the manufacturing line VARIAN has built a radiation shielding concrete bunker providing the complete infrastructure for cyclotron and scanning nozzle beam testing, the so-called “test cell”. Cyclotron no. 3 will be moved into the test cell after magnetic shimming. We plan to have tested all RF components, the ion source, slit systems, extractors, diagnostics, software etc. during a system integration and FAT with proton beam by the end this year. This enables the delivery of integrally factory beam tested systems.

CONCLUSION

Based on the proven design of a 250 MeV superconducting compact proton cyclotron, two machines have demonstrated remarkable performance during medical operation in the last years. The use for patient treatment started in 2007 at PSI and is a success in the PROSCAN project. A fully integrated clinical installation is operating at RPTC since 2008. VARIAN is now continuously improving the design with regard to reliability, maintainability, performance, cost reduction, and integration into the company’s radiological treatment environment. This applies to nearly all hardware and software components, ranging from specially designed components such as ion source, RF amplifier, and dLLRF to more common system components such as the vacuum and media supply systems, which appeared to be an opportunity for considerable cost reduction.

Cyclotron no. 3 is currently undergoing magnetic shimming. RF commissioning, system integration tests with beam and FATs are planned to be completed by the end of 2010. Assembly of No. 4 is advanced and no. 5 will follow shortly. Irons for no. 6 and no. 7 are currently being casted and forged. The production process has been designed so that it can be adapted to market needs.

REFERENCES

[1] H. Blosser et al., “Proposal for a Manufacturing Prototype Superconducting Cyclotron for Advanced Cancer Therapy”, NSCL internal report MSUCL-874, East Lansing, Mi USA (1993).
[2] A.E. Geisler J. Hottenbacher, H.-U. Klein, D. Krischel, H. Röcken, M. Schillo, T. Stephani, J.H. Timmer, “COMMISSIONING OF THE ACCEL 250 MEV PROTON CYCLOTRON”, Proc. of 18th Int. Conf. on Cycl. and their Appl., Giardini Naxos, Italy, p. 9-14 (2007).
[3] “The Project PROSCAN”, http://p-therapie.web.psi.ch/e/proscan.html.
[4] RPTC website, http://www.rptc.de/en.html.
[5] J. Hauffe, “Experience at Rinecker Proton Therapy Center after start of the patient treatments”, presentation at the PTCOG 48 meeting, http://www.ptcog-meeting.de/.
[6] T. Stephani, H. Röcken, U. Behrens, C. Baumgarten, “AUTOMATED OPERATION AND OPTIMIZATION OF THE VARIAN 250 MeV SUPERCONDUCTING COMPACT PROTON CYCLOTRON”, these proceedings.
[7] SSA and dLLRF provided by Cryoelectra GmbH, http://www.cryoelectra.de/

STATUS OF RIBF ACCELERATORS AT RIKEN

O. Kamigaito*, S. Arai, T. Dantsuka, M. Fujimaki, T. Fujinawa, H. Fujisawa,
N. Fukunishi, A. Goto, H. Hasebe,Y. Higurashi, K. Ikegami, E. Ikezawa, H. Imao,
T. Kageyama, M. Kase, M. Kidera, M. Komiyama, H. Kuboki, K. Kumagai, T. Maie,
M. Nagase, T. Nakagawa, M. Nakamura, J. Ohnishi, H. Okuno, N. Sakamoto, K. Suda,
H. Watanabe, T. Watanabe, Y. Watanabe, K. Yamada, H. Yamasawa, S. Yokouchi, Y. Yano
RIKEN Nishina Center for Accelerator-Based Science, Wako-shi, Saitama 351-0198 Japan

Abstract

Recent achievements and upgrade programs in the near future at RIKEN Radioactive Isotope Beam Factory (RIBF) are presented. The beam intensity and available ion species are increasing at RIBF, owing to the continuous efforts that have been made since the first beam in 2006. So far, we accelerated deuteron, helium, nitrogen, oxygen, aluminum, calcium, krypton, and uranium beams with the superconducting ring cyclotron, SRC. The extracted beam intensities reached 1,000 pnA for the helium and oxygen beams. From the operational point of view, however, the intensity of the uranium beam should be much increased. We are, therefore, constructing a new injector linac for the RIBF, consisting of a superconducting ECR ion source, RFQ, and DTL, which will be commissioned in this fiscal year. By using this injector, we also aim at independent operation of the RIBF and GARIS facility for super-heavy element synthesis.

INTRODUCTION

The Radioactive Isotope Beam Factory (RIBF)[1] at RIKEN has been constructed to produce the most intense RI beams over the whole range of atomic masses. The powerful RI beams will give us a means to access the unexplored region on the nuclear chart, far from the stability line. The scientific goals of the RIBF include establishment of a new comprehensive way to describe atomic nuclei and improvements of our understanding on the synthesis of the heavy elements in the universe. We are also promoting applications of the RI beams into various research fields such as nuclear chemistry and biological science.

The accelerator chain of the RIBF is schematically shown in Fig. 1. It consists of two injectors (heavy-ion linac: RILAC[2] and AVF cyclotron[3]), and four booster cyclotrons (RRC[4], fRC[5], IRC[6] and SRC[7]). There are three accelerating modes in the RIBF. The first one uses the RILAC, RRC, IRC and SRC for the acceleration of medium-mass ions such as calcium and krypton. The beam energy from the SRC can be changed in a wide range below 400 MeV/u by varying the rf frequency. The second one is the fixed-energy mode, which uses the fRC between the RRC and IRC. The beam energy from the SRC is fixed at 345 MeV/u, due to the fixed frequency operation of the fRC. This mode is used for the acceleration of very heavy ions such as uranium and xenon. The third mode uses the AVF cyclotron as the injector, and two boosters, the RRC and SRC. This mode is exclusively used for light ions such as deuteron and nitrogen. We can change the beam energy from the SRC below 440 MeV/u, by varying the rf frequency.

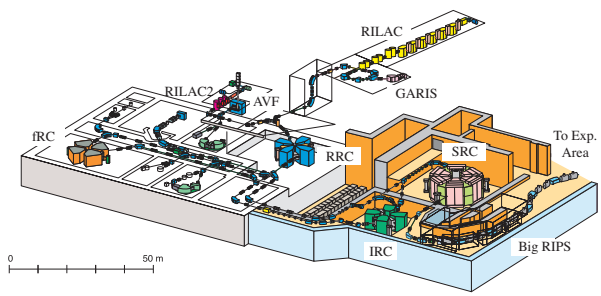

Figure 1: Birds-eye view of accelerator chain of RIBF at RIKEN. Two injectors, RILAC and AVF(K70MeV), are followed by the four booster cyclotrons: RRC (RIKEN Ring Cyclotron, K540 MeV), fRC (fixed-frequency Ring Cyclotron), IRC (Intermediate-stage Ring Cyclotron), and SRC (Superconducting Ring Cyclotron). The new injector (RILAC2), which will be commissioned in FY2010, is also indicated. The specifications of the three new cyclotrons are summarized in Table 1.

The commissioning of the three new cyclotrons, whose specifications are listed in Table 1, started in 2006, and the first beam from the SRC was extracted on December 28[8]. In 2007, two new isotopes, ^{125}Pd and ^{125}Pd, were produced in the BigRIPS spectrometer[9] using the energetic uranium beam from the SRC[10].

ACCELERATOR IMPROVEMENTS

In 2007, however, the transmission efficiency of the uranium beam was as low as 2 % excluding the charge stripping efficiency, which provided low beam intensity of 0.05 pnA at maximum from the SRC. Moreover, the stability of the beam was not good. A lot of obstacles prevented us from getting higher transmission efficiency and stability, and we improved the accelerator system in the last three

* kamigait@riken.jp

Table 1: Specifications of RIBF cyclotrons. FT stands for the flat-topping resonator.

	fRC	IRC	SRC
K-number (MeV)	570	980	2600
Number of sectors	4	4	6
Velocity gain	2.1	1.5	1.5
Number of trim coils	10	20	4+22
Number of rf resonators	2+FT	2+FT	4+FT
Rf frequency (MHz)	54.75	18-38	18-38

years[11, 12]. Several examples of the efforts are shown in the following subsections.

Beam Monitors

One of the most significant achievements was the completion of the beam-phase monitor based on the commercially available lock-in-amplifiers (SR844)[13]. It measures the beam phase at relevant positions in the beam lines as well as the beam phase in the cyclotrons, so as to maintain the stable beam delivery in the long-term experiments.

The Faraday cups used in the relevant positions along the beam lines were modified to have a stronger suppressor of the secondary electrons[12]. Calibration of the cups were also performed for various ion beams with a long, designated Faraday cup[14]. This modification made it possible to get accurate information on the beam losses and consequently help us to tune the accelerators effectively.

Radial Probes

In the early stage of the commissioning, the turn patterns in the fRC and SRC could not be measured due to the secondary electrons in the radial probes. This prevented us from adjusting the rf-phase of the flat-topping (FT) resonators precisely. Therefore, we modified the radial probes as follows[11, 12]. In the fRC, the differential electrode in the radial probe was shifted away from the integral electrode which was the origin of the secondary electrons. In the SRC, a thin tungsten ribbon was attached as a new differential electrode in front of the integral electrode at intervals of 10 mm.

Another problem was that the electromagnetic wave from the FT resonators disturbed the small beam signal in the radial probes in the IRC and SRC. We put sliding contacts in the upper gap between the probe shaft and the vacuum chamber in each of these cyclotrons; this modification made the boundary condition more symmetric, and reduced the coupling between the radiated TE_{01} wave from the FT resonator and the beam signal in the coaxial cable in the probe[12].

Finally we achieved single-turn extractions in the three new cyclotrons and obtained high quality beams, which increased the transmission efficiency.

Emittance Analysis

Intensive study has been done to evaluate the beam emittance by the beam dynamics analyses on the measured data of the profile monitors[11]. It has been found that the emittance growth was not notable in the calcium acceleration. On the other hand, significant growth of horizontal emittance was found in the uranium acceleration, which probably comes from the non-uniformity of the thickness of the first stripper between the RRC and fRC. The turn patterns in the cyclotrons were also simulated to estimate the rf voltage and phase.

Rf Systems

The monitoring system of the beam phase mentioned above is also designed to measure the rf-phase and voltage of all the rf resonators. According to the measured data, long-term stability of the first four resonators of the RILAC was not satisfactory. Therefore, the low-level circuit of these resonators have been replaced by newly designed ones. An automatic voltage regulator has been implemented at the same time for these circuits to improve the stability against the fluctuation of the commercial electric voltage. In addition, the signal dividers have been omitted, because it was found that their output phase was strongly dependent on the temperature around the dividers. The reference signal is now delivered by a directional coupler from a single cable to each low-level circuit in the RILAC[15, 16].

The rf resonators of the SRC had been suffered from heavy multipactoring in the high magnetic fields; long conditioning was required to feed the rf power after voltage breakdown in the early stage of the commissioning. The situation has been improved, owing to the experiences on the surface cleaning and rf-conditioning. Implementation of an additional cryogenic pump to each resonator also helped to reduce the conditioning time[15].

Helium Cryogenic System

The helium cryogenic system of the SRC and BigRIPS have had a serious problem since their starting time in 2005; we had to stop the helium refrigerator every two month due to gradual degradation of the refrigeration capacity in the continuous operation.

It was found in February 2008 that the origin of the degradation was the contamination of the oil from the helium compressor. Therefore, we took out the heat exchanger to wash it, and replaced the charcoal in the adsorber by a new one. At the same time, two oil separators were added in the compressor units. These modifications, which took 200 days, improved the system dramatically; no degradation has been found so far[17].

PRESENT STATUS

Owing to the efforts shown above, the beam intensity has remarkably increased, as shown in Table 3. The intensities

of light ions and medium-heavy ions are reaching our final goal of 1000 pnA.

Table 2: Maximum beam intensities extracted from SRC so far.

Ion	E (MeV/u)	I (pnA)	Achieved in
pol-d	250	120	May 2009
^{4}He	320	1000	Oct. 2009
^{14}N	250	80	May 2009
^{18}O	345	1000	Jul. 2010
^{48}Ca	345	230	Jun. 2010
^{86}Kr	345	30	Nov. 2007
^{238}U	345	0.8	Dec. 2009

The transmission efficiency through the accelerator chain has been significantly improved as well, as shown in Table 3[18]. It should be noted that the designed transmission through the RILAC is around 70 %, not 100 %, since the longitudinal acceptance is limited[19]. As shown in Table 3, 16 % of the beam is transported from the ion source to the exit of the SRC, excluding the stripping efficiency of 5 % in the uranium acceleration. The transmission efficiency from the exit of the RILAC to the exit of the SRC has exceeded 65 % in the calcium acceleration, excluding the stripping efficiency of 32 %. In the ^{18}O acceleration in 2010, the efficiency through the three cyclotrons (RRC, IRC and SRC) reached 85 %.

Table 3: Transmission efficiencies in % from ion source to exit of each accelerator. Stripping efficiencies in the charge strippers are excluded. Note that the observed currents include an error of 10 %.

	^{238}U (Nov. 2008)	^{48}Ca (Jun. 2010)
ECRIS	100	100
RILAC	40	62
RRC	30	67
fRC	35	-
IRC	23	53
SRC	16	44

Table 4: Operational statistics of RIBF accelerators from July 2009 to July 2010. MS stand for the machine study where the IRC and SRC were not used.

Beam	^{238}U	^{48}Ca	^{18}O	^{4}He	MS(U, Xe, Zn)
Time (h)	1088	1153	406	401	546

Table 4 shows the operational statistics from July 2009 to July 2010. The RIBF accelerators were operated in one of the three accelerating modes for about 3000 hours in this period. About half of the operation time is used for the experiments, and the other half for tuning. We also spent 500 hours for the machine study. The reliability index, which is defined as the ratio of an actual beam service time to a scheduled beam service time, has also increased. It exceeded 85 % in 2010, whereas it was below 70 % in 2008 and 2009[18].

Using the uranium beam in 2008, 45 new neutron-rich isotopes were created in four days in the BigRIPS spectrometer[20]. The intense calcium beams were used to study the halo structure and large deformation of neon isotopes far from the stability line[21, 22]. Thus the exploration into the nuclear extremes was really started.

FURTHER DEVELOPMENTS AND PLANS

From the operational point of view, it is clear that we need more beams from the ion source for very heavy ions such as uranium. We are planning to upgrade the intensity as shown below.

Superconducting ECR Ion Source

In order to meet the demand mentioned above, a new superconducting ECR ion source (SC-ECRIS) has been constructed, which is capable of the microwave power of 28 GHz[23, 24]. The main features of the ion source are as follows. First, the size of the ECR surface is large; it has as large plasma volume as 1100 cm^3. Second, the field gradient and surface size at the ECR zone can be changed independently to study these effects on the ECR plasma. The excitation test of the coil system was successfully performed in October 2008. After assembling the cryostat, the ion source was brought to RIKEN in December 2008.

The source was installed on the high-voltage platform of the existing Cockcroft-Walton preinjector of the RILAC, as shown in Fig. 2, in order to deliver the intense uranium beam as soon as possible[25]. Since the extraction voltage of the ion source in this scheme could be set higher than that of the RFQ-injection scheme, we expected higher beam currents and reduced emittance growth due to the suppression of the space charge effects.

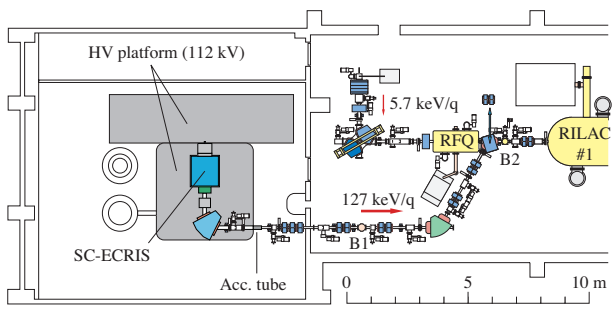

Figure 2: Preinjector for RILAC equipped with new superconducting ECR ion source. This scheme was terminated in May 2010 after the uranium beam delivery from November 2009 to April 2010.

The vacuum evacuation of the SC-ECRIS started in April 2008, and the first beam was obtained on May 11 with an existing microwave power source of 18 GHz. The construction of the medium-energy beam-transport (MEBT)

line between the high-voltage terminal and the RILAC was completed in June[26]. We performed the acceleration test of a $^{136}Xe^{20+}$ beam from the SC-ECRIS successfully with RILAC on September 11. Developments of uranium beam started based on the sputtering method at the end of October, soon after the generation tests of gold ions had been done. On November 13, we got 12.6 eμA (360 pnA) of U35+, which was six times higher than that available with the original 18-GHz ECRIS.

The maximum intensity from the SRC was, however, 72 enA (0.8 pnA), which was only twice that had been achieved in 2008 with the original ion source; the transmission efficiency was not sufficiently high. The low transmission could be partially attributed to a large emittance of the beam extracted from SC-ECRIS in the initial stage. Another reason was the lack of tuning experience for the beam from the new ion source. We also met a lot of unexpected troubles during the beam time. The developments of uranium beam have been continued after the beam time, and the maximum current from the source reached 24 eμA. The rms emittance could be made as small as 22π mm·mrad[27, 28].

New Injector (RILAC2) for RIBF

The success in the synthesis of the super-heavy element (SHE)[29] using the GARIS spectrometer in the RILAC facility strongly encourages us to pursue the search for the heavier elements. This compels us to provide a longer beam time for the SHE experiments. However, the SHE research and RIBF conflict with each other, because both of them use the RILAC. Therefore, construction of a new additional injector linac (RILAC2) has been started since 2008[25].

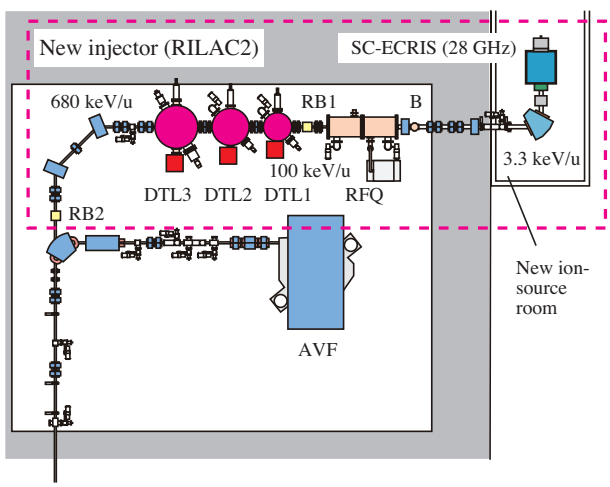

Figure 3: Schematic drawing of new injector. It is placed in the AVF cyclotron room. A prebuncher, denoted by "B", is operated at the fundamental frequency of 18.25 MHz, whereas the other resonators are operated at the second harmonic (36.5 MHz). RB1 and RB2 stand for the first and second rebunchers, respectively.

The RILAC2, placed in the AVF cyclotron room as shown in Fig. 3, is used exclusively in the fixed-frequency operation of the RIBF. It is designed to accelerate ions with a mass-to-charge ratio of 7, aiming at very heavy ions such as $^{136}Xe^{20+}$ and $^{238}U^{35+}$, up to an energy of 680 keV/u in the cw mode. The output beam will be injected to the RRC without charge stripping.

The RILAC2 consists of the SC-ECRIS, a low-energy beam-transport (LEBT) line including a prebuncher, an RFQ linac based on the four-rod structure, and three DTL resonators (DTL1 - 3). There is a rebuncher resonator (RB1) between the RFQ and DTL1 and another rebuncher (RB2) in the high-enegy beam-transport (HEBT) line after the DTL3. The rf resonators excluding the prebuncher are operated at a fixed rf frequency of 36.5 MHz, whereas the prebuncher is operated at 18.25 MHz. Strong quadrupole magnets are placed in the beam line between the rf resonators.

We modified an RFQ linac, which was originally developed by Nissin Electric Co., Ltd. in 1993[30], to be used in the RILAC2; the resonant frequency has been changed from 33.3 MHz to 36.5 MHz by putting a block tuner into every gap between the posts supporting the vane electrodes. High power tests have been done successfully in August 2010[31], using a newly constructed rf amplifier having the maximum output of 40 kW. It is now possible to accelerate ions from 3.3 keV/u to 100 keV/u without changing the vane electrodes. The design parameters of the RFQ are listed in Table 5.

Table 5: Design parameters of RFQ.

Frequency (MHz)	36.5
Duty	100 %
Mass-to-charge ratio (m/q)	7
Input energy (keV/u)	3.28
Output energy (keV/u)	100
Input emittance (mm·mrad)	200 π
Vane length (cm)	222
Intervane voltage (kV)	42.0
Mean aperture (r_0 : mm)	8.0
Max. modulation (m)	2.35
Focusing strength (B)	6.785
Final synchronous phase	$-29.6°$

The structure of the DTL resonators is based on the quarter-wavelength resonator (QWR). The dimensions of the resonators were optimized with the Microwave Studio by taking the power loss and the voltage distribution into account. The main parameters of the DTL are listed in Table 6. The inner diameter of the resonators ranges from 0.8 to 1.3 m, depending on the velocity range of the beam. The maximum electric field on the drift tubes is kept below 1.2 Kilpatrick.

In order to save the construction cost and space for the rf amplifiers, direct coupling scheme has been adopted for the rf system, as shown in Fig. 4. Detailed simulations and

Table 6: Design parameters of DTL.

Resonator	DTL1	DTL2	DTL3
Frequency (MHz)	36.5	36.5	36.5
Duty	100 %	100 %	100 %
Mass-to-charge ratio (m/q)	7	7	7
Input energy (keV/u)	100	220	450
Output energy (keV/u)	220	450	680
Length (= Diameter: m)	0.8	1.1	1.3
Height (m)	1.320	1.429	1.890
Gap number	10	10	8
Gap voltage (kV)	110	210	260
Gap length (mm)	20	50	65
Drift tube aperture (a: mm)	17.5	17.5	17.5
Peak surface field (MV/m)	8.2	9.4	9.7
Synchronous phase	$-25°$	$-25°$	$-25°$

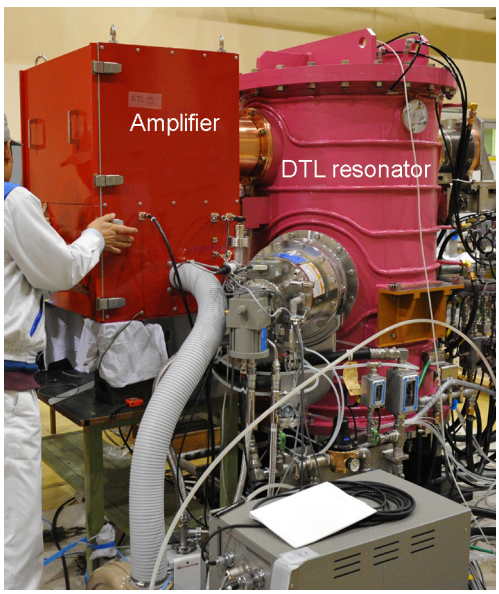

Figure 4: Photograph of DTL resonator and amplifier.

rf measurements have been done to optimize the coupling between each resonator and amplifier[32]. The maximum outputs of the amplifiers are 25 kW for the DTL1, and 40 kW for DTL2 and DTL3. High power tests have been already carried out in the AVF cyclotron room.

The LEBT line was designed by taking possible space-charge effects into account[33]. There are two sets of paired solenoids in the LEBT, that have been adopted to reduce beam envelopes without transverse coupling. Since the RFQ vanes are inclined by 45°, it is important to make the input beam symmetric in the vertical and horizontal planes. The beam matching into the RFQ will be achieved by the four quadrupoles. The analyzing magnet has been constructed according to the design by the LBNL[34]. The large pole gap of 180 mm leads to beam aberration due to fringing fields. Corrective measures have been taken by shaping the pole faces in such a manner as to introduce aberration countering sextupole moments to the beam.

The SC-ECRIS was brought to a newly constructed room from the Cockcroft-Walton terminal in June 2010. The excitation test has been performed successfully there. A dummy-load test is in preparation for the 28 GHz power source. Commissioning of the RILAC2 will be started in FY2010 with a xenon beam. We are planning to deliver the uranium beam of 5 pnA in FY2011. Figure 5 shows a photograph of the RILAC2 in the AVF cyclotron room.

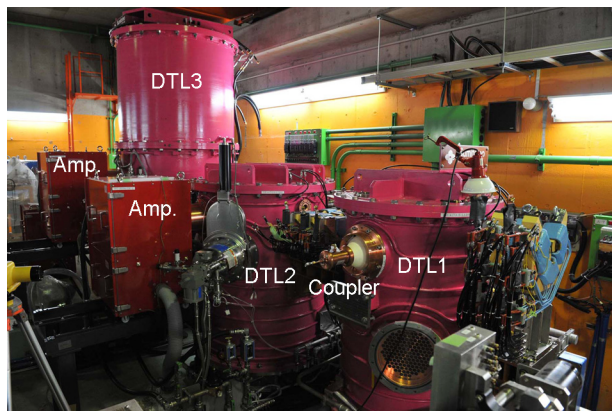

Figure 5: Photograph of DTL resonators of RILAC2 placed in AVF cyclotron room.

Charge Strippers

One of the most important issues in the acceleration of intense heavy-ion beams is the choice of the charge strippers. A carbon foil of 0.3 mg/cm^2 is currently used for the first stripper for the uranium acceleration at RIBF; it changes the charge state from 35 to 71 at 11 MeV/u after the RRC. The lifetime is, however, about 12 hours for the present beam intensity, which is far below the goal intensity of 1000 pnA. Moreover, the stripper causes emittance growth which limits the transmission efficiency, as mentioned above. In order to increase the lifetime, we have been developing polymer-coated carbon (PCC) foils [35] on the rotating-cylinder stripper system[36]. In spite of the long efforts, the lifetime had been about several minutes at the rotation speed of 100 rpm.

Recently, the rotating-cylinder system was modified to rotate very slowly, and the irradiation test of a PCC foil was carried out with the uranium beam from the SC-ECRIS. It was found that, at the rotation speed of 0.05 rpm, the foil survived for 38 hours at the beam intensity of 1.7 eμA. No significant damage was found on the foil[37]. This result shows that the mechanical stress of rotation affects the lifetime of the foils significantly. On the other hand, we found a large fluctuation of the intensity in the downstream of the stripper section, which indicated the uniformity of the foil was not sufficiently good. Further study is required to make the foils uniform enough.

We are also developing a gas stripper system as another candidate of the strippers for intense beams[38]. It was found last year that the average charge state of xenon ions

of 11 MeV/u is 40.5 in N_2 gas, which means that the xenon beam is acceptable in the fRC. Actually, acceleration test of the xenon beam in the fRC was successfully performed with the gas stripper. On the other hand, the average charge state of uranium ions was found to be 56 in the N_2 gas, far below the acceptable charge state of 69.

In April 2010, we measured cross sections of electron stripping and electron capture of uranium ions in helium gas at 11 MeV/u. The result was remarkable; the equilibrium charge state is estimated to be 66, which is close to the acceptable charge state in the fRC[17]. It implies that the helium gas stripper is a strong option for the future stripper system. Therefore, we have started a new development program to make a thick gas stripper of helium. The uranium intensity will be increased to 50 - 100 pnA when this system is operational.

ACKNOWLEDGMENTS

The accelerators in RIBF are operated by RIKEN Nishina Center and Center for Nuclear Study (CNS), University of Tokyo. The authors are grateful to the operators of SHI Accelerator Service Ltd. for their efforts and cooperation.

REFERENCES

[1] Y. Yano, Nucl. Instrum. & Methods B261 (2007) 1009.

[2] M. Odera et al., Nucl. Instrum. & Methods 227 (1984) 187.

[3] A. Goto et al., Cyclotrons'89, Berlin, Germany, p. 51 (1989).

[4] H. Kamitsubo, Cyclotrons'84, East Lansing, MI, p. 257 (1984).

[5] N. Inabe et al., Cyclotrons'04, Tokyo, Oct. 2004, 18P15, p. 200 (2004), T. Mitsumoto et al., *ibid*, 20P12, p. 384.

[6] J. Ohnishi et al., Cyclotrons'04, Tokyo, Oct. 2004, 18P14, p. 197 (2004).

[7] H. Okuno et al., IEEE Trans. Appl. Supercond. 17 (2007) 1063.

[8] A. Goto et al., Cyclotrons'07, Giardini Naxos, Sep. 2007, p. 3.

[9] T. Kubo et al., Nucl. Instrum. & Methods B204 (2003) 97.

[10] T. Ohnishi et al., J. Phys. Soc. Jpn. 77 (2008) 083201.

[11] N. Fukunishi et al., PAC'09, Vancouver, May 2009, MO3GRI01.

[12] K. Yamada et al., HIAT'09, Venezia, June 2009, MO-10, p. 16.

[13] R. Koyama et al., EPAC'08, Genoa, June 2008, TUPC052, p. 1173, R. Koyama et al., Cyclotrons'10, Lanzhou, Sep. 2010, MOPCP094.

[14] T. Watanabe et al., Cyclotrons'10, Lanzhou, Sep. 2010, WEM2CCO05.

[15] N. Sakamoto et al., Cyclotrons'10, Lanzhou, Sep. 2010, WEM2CCO02.

[16] K. Suda et al., Cyclotrons'10, Lanzhou, Sep. 2010, MOPCP068.

[17] H. Okuno, et. al., Advances in Cryogenic Engineering 55 (2010) 1410.

[18] N. Fukunishi et al., LINAC'10, Tsukuba, Sep. 2010.

[19] N. Fukunishi et al., RIKEN Accel. Prog. Rep. 41, p. 81 (2008).

[20] T. Ohnishi et al., J. Phys. Soc. Jpn. 79 (2010) 073201.

[21] T. Nakamura et al., Phys. Rev. Lett. 103 (2009) 262501.

[22] P. Doornenbal et al., Phys. Rev. Lett. 103 (2009) 032501.

[23] T. Nakagawa et al., Rev. Sci. Instrum. 79 (2008) 02A327, T. Nakagawa et al., ECRIS'08, Chicago, Sep. 2008, MOCOB01, p. 8 (2008).

[24] J. Ohnishi et al., EPAC'08, Genoa, Jun. 2008, MOPC153, p. 433 (2008).

[25] O. Kamigaito et al., HIAT'09, Venezia, June 2009, MO-11, p. 21.

[26] Y. Sato et al., IPAC'10, Kyoto, May 2010, THPEB024, p. 3939.

[27] Y. Higurashi et al., IPAC'10, Kyoto, May 2010, THPEC60, p. 4191.

[28] T. Nakagawa et al., Cyclotrons'10, Lanzhou, Sep. 2010, WEM1CIO01.

[29] K. Morita et al., J. Phys. Soc. Jpn. 78 (2009) 064201.

[30] H. Fujisawa, Nucl. Instrum. Methods A345 (1994) 23 .

[31] K. Yamada et al., IPAC'10, Kyoto, May 2010, MOPD046, p. 789, K. Yamada et al., Cyclotrons'10, Lanzhou, Sep. 2010, MOPCP025.

[32] K. Suda et al., IPAC'10, Kyoto, May 2010, THPEA023, p. 3276.

[33] Y. Sato et al., IPAC'10, Kyoto, May 2010, THPEB023, p. 3936.

[34] M. Leitner, et al., Proc. 15th Inter. Workshop on ECR Ion Sources, June 12-14, 2002, Jyväskylä, Finland.

[35] H. Hasebe et al., Nucl. Instrum. & Methods A613, (2010) 453.

[36] H. Ryuto et al., Nucl. Instrum. & Methods A569, (2006) 697.

[37] H. Hasebe et al., 25th World Conference of the International Nuclear Target Development Society, Vancouver, BC, Sep. 2010.

[38] H. Kuboki et al., Phys. Rev. ST Accel. Beams, to appear.

[39] H. Okuno et al., HB2010, Morschach, Sep. 2010.

FIRST BEAM ACCELERATION IN KOLKATA SUPERCONDUCTING CYCLOTRON AND ITS PRESENT STATUS

Chaturanan Mallik and Rakesh Kumar Bhandari (on behalf of VECC Staff)
Variable Energy Cyclotron Centre, 1/AF, Bidhan Nagar, Kolkata - 700064, India

Abstract

Major subsystems of the superconducting cyclotron at VECC, Kolkata were integrated by May 2009. After achieving the required vacuum and Dee voltage a series of internal beam trials were started. The beam was accelerated to full extraction radius on August 25th and beam confirmed by neutron measurements.

The trials were not without difficulty and several problems did crop up during the initial phase. With minor modifications vacuum of the order of 10^{-7} mbar was obtained. Major problems encountered were related to obtaining sufficient Dee voltages primarily due to ceramic insulator cracking at moderate power levels leading to vacuum breakdown. Earlier the 14 GHz ECR ion source was connected with 23 metre injection line without much difficulty.

An analogue beam was also accelerated before taking a shutdown for installation of extraction system and major augmentation of cryogenic plant. Presently extraction of the beam is being tried. It is planned to transport the beam to already installed first experimental station.

INTRODUCTION

The superconducting cyclotron magnet was functional and the magnetic field mapping and corrections were implemented by mid 2006. These developments were reported in the last cyclotron conference. Later the coil was warmed up to assemble other systems of the machine, like RF resonators, cryo-panels, 14 GHz ECR Ion source, 23 metre injection line, extraction system and augmenting main vacuum system. A significant part of the effort related to develop supervisory control and monitoring system for each subsystem incorporating present day tools.

Obtaining vacuum ~10^{-6} mbar in the beam chamber pumped by turbopumps without magnetic field and RF could be obtained relatively easily. Subsequently with magnet energised few leaks were detected and rectified. After having obtained ~10^{-6} RF conditioning was started. Several major problems cropped up in terms of 'viton o-ring' degradation and ceramic cracking at very moderate RF power levels (15 kW). Considerable time was invested in understanding the problem (being detailed later). The problem was circumvented but only partially. However a dee voltage of 45 kV was available and it was decided to try the first internal beam.

FIRST INTERNAL BEAM

It was very tempting to try the first beam as a test beam after 45 kV Dee voltage at 14 MHz was obtained and the phase was stable to provide reasonable condition for acceleration.

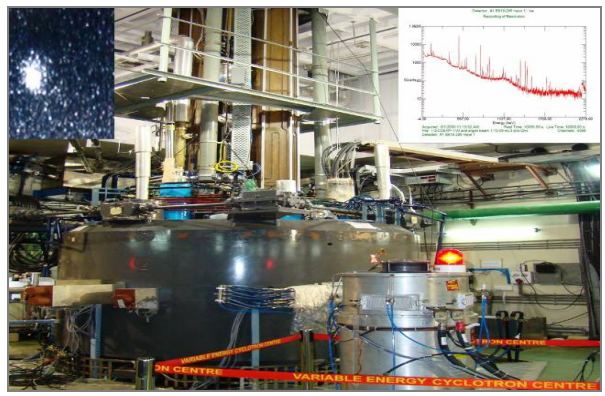

Figure 1: Superconducting cyclotron with first beam spot on left hand corner and gamma spectroscopy of the irradiated target in the right top corner

Initial plan after attempts for higher energy were shelved till suitable Dee voltages are available. And it was decided to accelerate Ne3+ in second harmonic mode at 30 kG at 14 MHz. The 14 GHz ECR Ion source was already relocated from k130 cyclotron to the superconducting cyclotron. All the diagnostics were already made functional after initial problems of measuring low currents in RF environment. In mid-august the above configuration was started as a beam test run. To our surprise it didn't take much time to obtain accelerating beam and the parameters were quite close to the calculated values. The beam was accelerated to full extraction radius on 25th August 2009. To confirm the beam an internal beam experiment with aluminium block attached to main probe was performed and all conclusive signature of beam was obtained.

Initial Observations

It was very satisfying to see that the parameters for magnetic field actually obtained during the test beam run were close to the calculated values. The dee voltages were estimated from pickup probes as the cadmium telluride based detectors are still being implemented to get fairly accurate values.

ECR Ion Source and Injection System

14.4 GHz Electron Cyclotron Resonance Ion Source was relocated from room temperature cyclotron and integrated to the superconducting cyclotron by a 28 metre injection system and a spiral inflector. The injection beam line is designed for the maximum beam rigidity of 0.058 T-m, which corresponds to ions with specific charge (η=q/A) equals to 0.12 and energy equals to (20*η) keV/nucleon, 20 kV being the maximum extraction voltage of ECRIS.

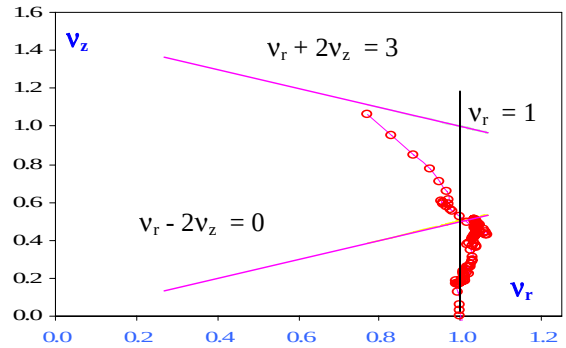

Figure 2: Tune diagram for the Test beam (Ne^{3+}, 4.5 MeV/u, B_0=30.5 kG)

Figure 3: Current vs. radius for the Ne3+ beam

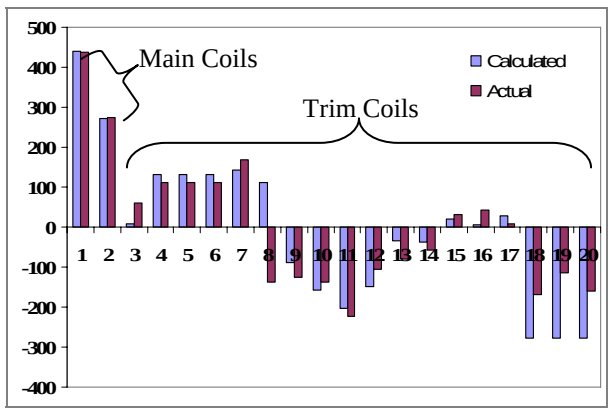

Figure 4a: Calculated and experimental value of main coil and trim coil current settings (in Amp) for Ne3+ beam at 4.5 MeV/u, B0=30.5 kG,, h=2, RF=14 MHz.

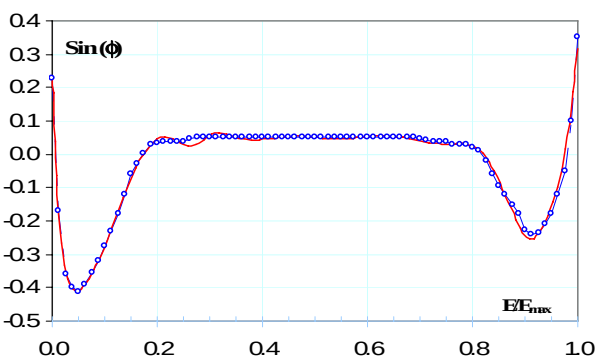

Figure 4b: Energy vs. Phase history for the Ne^{3+} beam

Operation of cyclotron with low magnetic field limited the ion beam injection voltage and due to this limitation ECR ion source was operated with low extraction voltages. With persistent operation of ECR ion source the extraction electrode was eroded due to diverging ion beam causing sputtering of electrode. This problem was overcome by changing the gap of extraction electrode from 35 mm to 25 mm. Now the ECR ion source operated with better stability as well as produces more currents. For last one year, the same electrode is under use and there is no deterioration in the performance.

Figure 5: Installed ECR Ion Source and Injection Line

Figure 6: Vertical injection line on top of yoke

SOME SYSTEM MODIFICATIONS AND IMPROVEMENTS

Radiofrequency System

The radio-frequency system of superconducting cyclotron consists of three λ/2 RF resonator cavities powered individually by 80 kW radio-frequency amplifiers (Figure-1) via three hydraulically driven Coupling Capacitor through three rigid coaxial transmission line with 50Ω characteristic impedance. The fine frequency tuning (±0.3%) of the cavity is achieved by a hydraulically driven Trimmer Capacitor. The actuators and servo valves are driven from a common power pack with computerized control system to give the Trimmer Capacitor paddle

Trimmer capacitor hydraulic drive control system was developed for fine frequency tuning of the RF resonating cavities. While conditioning the RF system, wild hunting of the hydraulic actuator was observed causing fluctuations in the Dee voltages. The problem is partially solved by tuning the hydraulic system. It has been done by adjusting the pressure and flow of oil through the servo valves. Provision for online control of gain was introduced to make the system suit to our requirement. A PC-PLC-based hydraulic drive system with precise movement (< 50 μm) has been developed indigenously for fine tuning the cavity using Trimmer capacitors and also for feeding RF power to the cavity by impedance matching through coupling capacitors.

During last year the ceramic insulators cracked several times due to excessive dielectric-heating. Each failure caused several weeks of shutdown, since changing the ceramic insulator requires dismantling of the whole RF cavity. An exhaustive thermal analysis was carried out to estimate the required air-flow rate for cooling the ceramic and analysis results were verified by simulating an off-line experimental set up. Finally the cooling was provided to the ceramics by turbine blower and improvement was observed.

During RF conditioning of the resonator cavity, there is heating in the O-ring made of viton placed with the ceramics and consequently degradation of vacuum. It is found from operational experience that silicone O-rings provides better performance in this atmosphere over viton O-ring. Therefore, all the viton O-ring, which are in a highly inaccessible zone, has been replaced by silicone O-rings.

Figure7a. Cyclotron with Zero degree Extraction Beam line, (7b) Coupling capacitor

Vacuum System

Due to the unavoidable and inherent compact geometry of the cyclotron, pumping port of beam chamber is only of 3 inch diameter. Again the turbo-scroll pumping modules are kept far apart in a position where stray magnetic field is not more than 25 gauss. These two constraints limit the conductance as well as effective pumping speed of Turbo molecular pump to a great extent. For example, though the pumping speed at the inlet port of module is ~ 500 Lt/s, net pumping speed reduces to ~ 50 Lt/s at the Beam chamber. Three numbers of cryo-panels made of OFHC copper have been used to achieve more pumping speed and better vacuum.

Detoriation of OVC (Outer vacuum chamber) vacuum is more pronounced with increasing current in small (alpha) coil. As there is no provision to find out the cold leak, extra pumping port of net conductance 150 Lt/s has been introduced in the OVC. **This has improved the OVC vacuum considerably.**

To analyze and understand various vacuum related problems, residual gas analyzer (RGA) has been used. When RF conditioning was started, the partial pressure of hydrogen gas is significant as is evident. Hydrogen outgases from metallic surface at high RF power, hence need of additional pumping for hydrogen is being realised. It is planned to use activated charcoal at the bottom surface of 10K cryo-panels so that hydrogen could be pumped out effectively by cryo-adsorption.

Extraction System

Two deflectors and nine magnetic channels including an active magnetic channel have already been installed A deflector test stand had already been setup. The deflector system has been tested there satisfactorily with more than 60 kV over 6 mm gap and less than 100 nA dark current, over several weeks.

CONCLUSION

The superconducting cyclotron at Kolkata has already accelerated the first beam. A long shut down had to be taken to augment the cryogenic plant and the extraction system along with external beam line connecting experimental station#1. Presently extraction is being tried out.

REFERENCES

[1] 'Status of K500 Superconducting cyclotron project at kolkata' Rakesh Kumar Bhandari and Bikash Sinha (for VECC Staff), International Conference on Cyclotrons and Their Applications 2007, Italy.

[2] 'Magnetic Field Mapping of Kolkata Superconducting Cyclotron': C. Mallik, et al., Proc.of the 18th Int. Conf. on Cyclotrons and Their Applications 2007, Oct. 1-5, 2007, Giardini Naxos, Italy, page 435.

[3] 'Fabrication and Installation of Radio Frequency Cavity for K500 Superconducting Cyclotron at Kolkata' paper presented at IPAC-2010(23-28 May, 2010) M. Ahammed et. al.

[4] 'Development of RF system for Superconducting cyclotron at VECC, Kolkata': S Som, et. al. Proc. of Intl. Conference on cyclotrons and their applications-2007, LNS, INFN, Catania, Italy.

[5] 'Fabrication of Extraction System for Superconducting Cyclotron", S Bhattacharyya et. Al., Proc. of Indian Particle Accelerator Conference, March, 2005, VECC, Kolkata.

COMMISSIONING OF THE JYFL MCC30/15 CYCLOTRON

P. Heikkinen, JYFL, Jyväskylä, Finland

Abstract

The new MCC30/15 cyclotron from NIIEFA, St. Petersburg, Russia, arrived at Jyväskylä on 10th of August, 2009, as a partial compensation of the Former Soviet Union debt to Finland. The cyclotron required an extension for the old experimental hall. The building of the extension started in late August, 2008, and it was scheduled to be ready by Midsummer, 2009. Both the cyclotron and the building projects took a little more time than planned. However, the delay of both projects was less than two months, and so the building was ready to host the cyclotron by the beginning of August, 2009.

The installation of the cyclotron was done by the manufacturer's (NIIEFA) specialists. Before the end of November 2009 the maximum extracted proton intensity (in pulses) was 200 μA, twice the guaranteed value, and 62 μA for deuterons, which is also more than guaranteed (50 μA). The final acceptance protocol was signed on 30th of April, 2010.

BACKGROUND

The operation of the K130 cyclotron has been very extensive. The total cyclotron operating time since 1996 has been over 6000 hours/year, the maximum being about 7500 h/year. So, there has not been much time for machine development, and also the time for maintenance has been limited. About one third of the beam time has been protons and deuterons. Thus it was a natural choice to investigate the possibility of acquiring a separate cyclotron for protons and deuterons in addition to the K130 cyclotron. The plan became a reality when a 30 MeV H^- cyclotron was approved on the list of equipment as partial compensation of the former USSR debt to Finland. An Inter-governmental Agreement between Finland and Russia was signed in 2006 to settle the old debt partially by goods and services. The Contract of the 30 MeV H^- cyclotron, MCC30/15, was approved in June 2007. The cyclotron was be built by NIIEFA, D.V. Efremov-Institute, St. Petersburg, Russia.

THE MCC30/15 CYCLOTRON PROJECT

The first negotiations on the new cyclotron started in 2004. It was already then obvious that the cyclotron should be in the debt conversion program between Finland and Russia. Finally the order could be placed in June, 2007. According to the contract the delivery time was two years from the order plus additional time of six months for installation of equipment and training the local users. There were small delays both in the cyclotron and the building projects However, the building was ready for the cyclotron to be installed in the end of July, 2009. The arrival of the cyclotron was re-scheduled to the beginning of August, 2009.

Everything else but the cyclotron magnet arrived on Friday, 7th of August, on three trucks, two days delayed due to customs problems in St. Petersburg. The Russian team together with the local people unloaded the trucks into the new experimental hall, and everything was prepared for Monday, 10th of August, to get the magnet in the cyclotron bunker. The last two trucks carrying the cyclotron magnet finally arrived at 9.20 pm and the unloading started immediately. Everything took place on the roof of the parking hall, which was supported by hundreds of steel pillars to take the heavy weight. Due to local weight limitations the lifting had to be done with extreme care. The first half of the cyclotron, weighing 24 tons, was put into its final position exactly at midnight (see Fig. 1). The second half was on its place one hour later.

Figure 1: The first half of the MCC30/15 cyclotron is being lifted into the cyclotron cave.

The Russian (NIIEFA) team started the installation of the accelerator immediately after it had arrived. Everything went smoothly and the first beam tests could be carried out in November 2009, and before the end of the month the maximum extracted proton intensity (in pulses) was 200 μA, twice the guaranteed value, and 62 μA for deuterons, which is also more than guaranteed (50 μA).

The final acceptance tests were done in April, 2010. They included maximum intensity test for maximum and minimum energies for both protons and deuterons, as well as stability tests and dual beam tests. All results reached or exceeded the guaranteed values. The maximum proton current at both 30 MeV and 15 MeV was 200 μA. The maximum deuteron current at 15 MeV was 62 μA.

The MCC30/15 Cyclotron

The contract included a fully operating cyclotron with two beamlines on opposite sides of the cyclotron up to the dipole magnets which bend the beam to the targets.

The main characteristics of the MCC30/15 cyclotron were reported in [1]. The magnet (maximum power 14 kW) is vertical thus allowing sideways opening and easy access for maintenance (Fig. 2). The field for protons and deuterons is changed using rotating shims in two opposite valleys. The shims are rotated pneumatically. The fields are shown in Fig. 3. All shims (central, rotating, 2nd harmonic compensation) are shown in Fig. 4. The fully installed cyclotron is shown in Fig. 5 and the multi-cusp ion source is shown in Fig. 6.

Figure 2: The NIIEFA team installing the matching dipole. The cyclotron magnet opens sideways on precision rails.

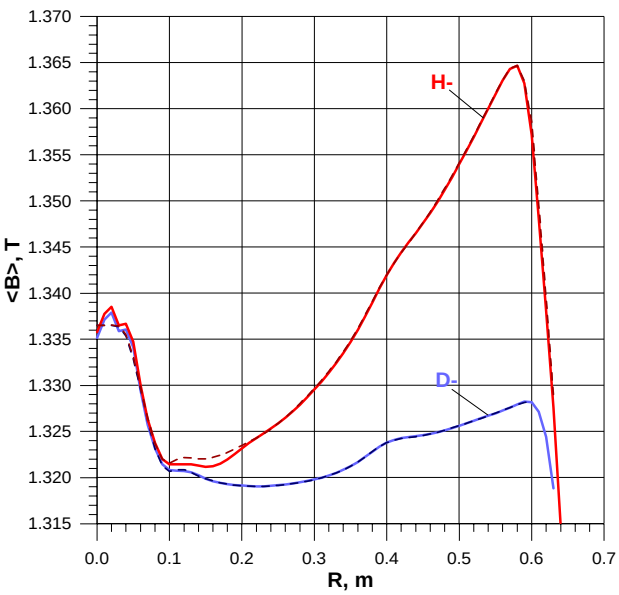

Figure 3: Simulated and required fields in the MCC-30/15 median plane. Upper curve for H^- acceleration, lower curve for D^- acceleration.

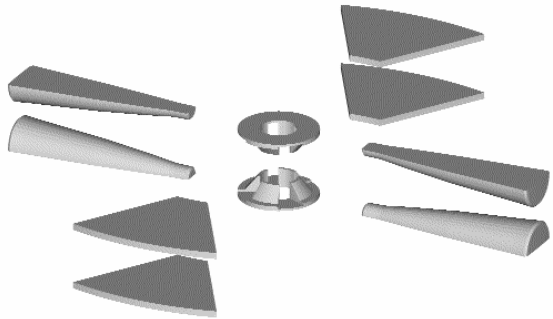

Figure 4: Set of shims for MCC30/15.

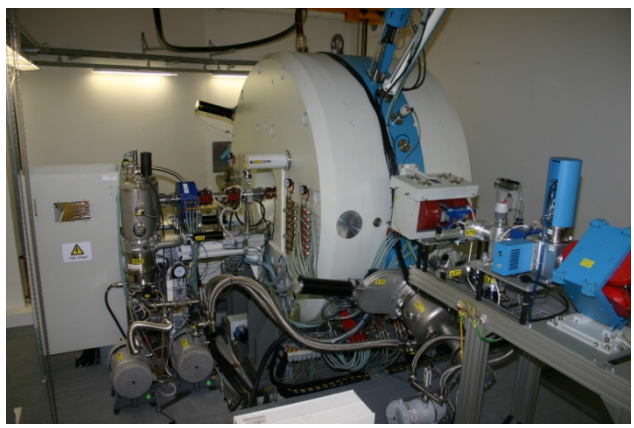

Figure 5: The fully installed cyclotron. The injection line from the ion source is seen on the left and part of the beamline to the isotope production cave on the right.

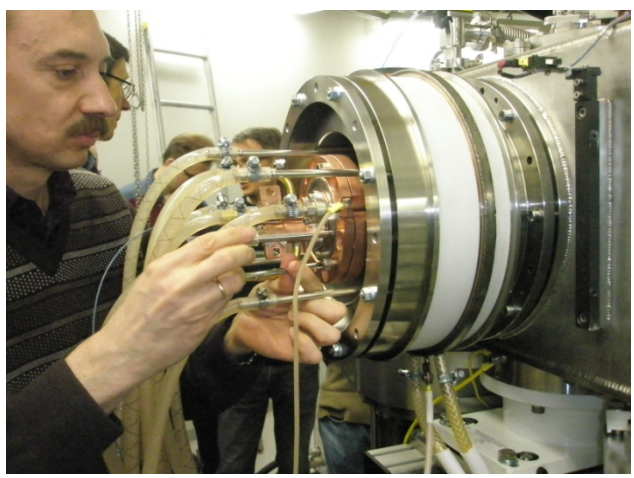

Figure 6: Sergey Grigorenko, NIIEFA, shows how to change the filament in the ion source.

The RF system consists of two dees, and the operating frequency is 40.68 MHz the RF generator output power being 25 kW, which produces a dee voltage of 40 kV.

The vacuum is pumped by two cryopumps in the cyclotron (10^{-7} mbar region) and by turbopumps in the beamlines.

Control of the cyclotron is done with a PC-based control system and PLC's. The MCC30/15 control system is coupled to the main control system of the K130 cyclotron, which controls the radiation safety of the whole laboratory.

Use of the MCC30/15 Cyclotron

The IGISOL facility [2], the main user of the proton beams, is being moved from the old experimental hall to the extension, served both by the new MCC30/15 H^- cyclotron as well as the K130 heavy-ion cyclotron. The move started in June 2010 and it is assumed to be ready during the first half of 2011. The work with IGISOL will extend the discovery potential to earlier unexplored exotic nuclei which are important in explosive nucleosynthesis scenarios. In addition, planned charge breeding of trapped ions will lead to unprecedented accuracy in mass measurements for weak interaction tests in atomic nuclei.

In addition to the scientific work with the IGISOL facility, the new MCC30/15 cyclotron is planned to be used for medical radioisotope production, mainly 123-I and 18-F. Negotiations on the isotope production are underway.

Building

An extension for the accelerator laboratory was needed to house the new cyclotron. After financial negotiations it was decided to build the extension in full size allocated in the architect's original plan, thus enabling to move the main scientific proton beam user (IGISOL) to the extension and to have the radioisotope production area also close to the cyclotron. The size of the extension is 50 x 13.5 m^2.

In conjunction with the IGISOL facility move other changes in the old experimental area lay-out were planned. The new floor plan of the laboratory is shown in Fig. 7. The area left free after IGISOL move will host the new MARA separator [3]. Some other minor modifications will be done, too. Two new dipole magnets (65 degrees and 90 degrees) have been ordered to guide the beam from the K130 cyclotron to the new IGISOL site and to the MARA separator.

REFERENCES

[1] P. Heikkinen, Proc. 18th Int. Conf. on Cyclotrons and Their Applications, Giardini Naxos, Italy, 2007, 128.
[2] J. Äystö, Nucl. Phys. A 693, 2001, p. 477.
[3] J.Sarén, et al., Nucl. Instrum. Meth. Phys. Res. B 266, 2008, p. 4196.

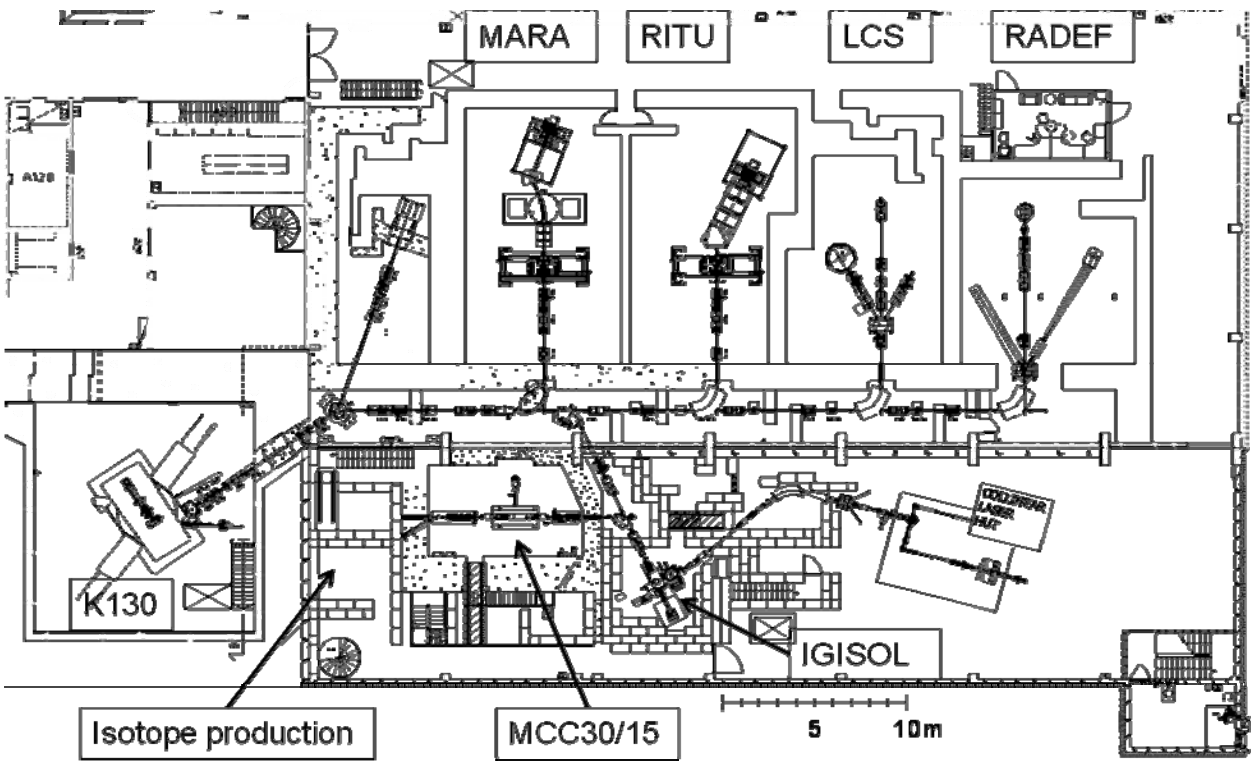

Figure 7: Layout of the JYFL Accelerator Laboratory including the planned changes. The vacuum recoil separator MARA will be installed left from the existing gas filled recoil separator RITU in the space from where IGISOL facility was moved into the extension of the experimental hall. The walls of all caves except for the proton irradiation cave left from MARA will be slightly modified in order to meet better the new needs. The extension is the 50 m long and 13.5 m wide space right from the K130 cyclotron and down from the long horizontal beam line.

A MULTI MEGAWATT CYCLOTRON COMPLEX TO SEARCH FOR CP VIOLATION IN THE NEUTRINO SECTOR

L. Calabretta, M. Maggiore, L. A. C. Piazza, D. Rifuggiato, INFN-LNS, Catania, Italy
A. Calanna, CSFN-SM, Catania, Italy

Abstract

A Multi Megawatt Cyclotron complex able to accelerate H_2^+ to 800 MeV/amu is under study. It consists of an injector cyclotron able to accelerate the injected beam up to 50 MeV/n and of a booster ring made of 8 magnetic sectors and 8 RF cavities. The magnetic field and the forces on the superconducting coils are evaluated using the 3-D code OPERA. The injection and extraction trajectories are evaluated using the well tested codes developed by the MSU group in the '80s. The advantages to accelerate H_2^+ are described and preliminary evaluations on the feasibility and expected problems to build the injector cyclotron and the ring booster are here presented.

INTRODUCTION

Recently members of the neutrino community proposed a new experiment called DAEδALUS (Decay At rest Experiment for δ_{cp} At Laboratory for Underground Science) a new approach to search for CP violation in the neutrino sector [1,2]. They proposed to utilize high power proton accelerators able to supply a proton beam with about 800 MeV, 1.5 MW average power and a duty cycle of 20% (100 msec beam on, 400 msec beam off). DAEδALUS needs three sources of neutrino; the nearest one located at 1.5 km from the underground detector must have a minimum power of 1 MW. The second source should stay at a distance of about 8 km from the detector and should supply an average beam power of 2 MW or more. The last neutrino source, 20 km far from the detector, has to be fed with a proton beam of average power higher than 5 MW. The neutrino fluxes produced by the three sources are measured by the 300 KTons Cerenkov detector filled with water doped with Gd.

The three sources have their beam time synchronised, so the detector will receive the 100 msec beam bunch from each source in sequence, while for a 100 msec all the three sources will be kept off, to allow the measure of the background.

This configuration allows to measure, how many oscillations $\bar{\nu}_\mu \rightarrow \bar{\nu}_e$ occur for each source.

Although the required average power for the first 2 sites is 1-2 MW, the 20% duty cycle has the consequence that the peak power is 5-10 MW and a peak current of about 9.5 mA is necessary. At the same time the lower beam power mitigates the problems related to thermal dissipation and activation.

At a current higher than 1 mA the space charge effects become more and more relevant both for the injection process and for the extraction process. Solutions that mitigate the spaced charge effects are advantageous, see next section.

Accelerator complexes consisting of two or three cyclotrons, one or more injector cyclotrons and a main ring cyclotron booster, have already been proposed as drivers for energy amplifier or waste transmutation plants [3,4,5]. The main constraints for these accelerator complexes are: current higher than 10 mA and energy as high as 1 GeV, minimum beam losses, high reliability and high conversion efficiency from electrical to beam power.

We believe that up to now accelerator driven systems (ADS) based on well known conventional cyclotrons accelerators are the most reliable and economical solution for a plant which requires a peak beam power of 1-5 MW[4,5]. To deliver higher peak power, i.e. 10 or more MW, the key points for the ring cyclotrons are the space charge effects, the extraction devices and the power to be dissipated in each cavity. To overcome these problems a classical solution is to increase the radius of the cyclotron and the number of cavities. But this means to increase significantly the plant cost.

An alternative solution based on the acceleration of H_2^+ molecule has been proposed [6,7]. In this case the extraction of the H_2^+ beam is accomplished by a stripper which produces two free protons breaking the molecule. Due to the different magnetic rigidity as compared to the H_2^+, the protons escape quite easily from the magnetic field of the cyclotron. Extraction by stripping does not require well separated turns at the extraction radius and allows using lower energy gain per turn during the acceleration process and/or lower radius for the magnetic sectors, with a significant reduction of thermal power losses for the RF cavities and construction cost. The extraction by stripper allows to extract beams with large energy spread (0.5÷1%) so the energy spread produced by space charge effect on the longitudinal size of the beam is not crucial in this kind of accelerator, and flattopping cavities are unnecessary.

We believe that the acceleration of H_2^+ beam, despite it needs to handle beam with magnetic rigidity two times larger, offers a remarkable advantage in terms of reliability, easier operations and lower cost.

In the past, a layout for an accelerator complex able to supply a proton beam with energy of 1 GeV and a beam power up to 10 MW was presented by some of the authors [6], in the perspective to drive a sub critical reactor. This previous proposal is now updated to fit the requirement of the MIT scientists. Moreover the number of accelerators required by the experiments, at least 4-5, forces us to minimize the accelerator cost.

The solution, here presented, consists in a two cascade cyclotrons complex. The injector cyclotron, a four sector

machine, accelerates a beam of H_2^+ up to energy of about 50 MeV/n. The beam is then extracted by an electrostatic deflector and it is injected from the injector cyclotron into an 8 sectors Superconducting Cyclotron Ring. Two stripper foils are used to extract two proton beams at the same time from the ring cyclotron. This solution allows increasing the mean life of the stripper foils and reducing greatly the design of the beam dump.

SPACE CHARGE EFFECTS

Before the injector cyclotron description, we like to underline the problems related to the space charge effects for H_2^+ vs. proton beam. The space charge produces a repulsive force inside the beam bunches, which generate detuning effects. To evaluate the strength of this effect the parameter called "generalized perveance" has been introduced [8]. The generalized perveance is defined by the following formula:

$$K \propto \frac{qI}{m \cdot \gamma^3 \beta^3}$$

Where: q, I, m, γ and β are respectively the charge, current, mass and the relativistic parameters of the particle beam. From this formula it is quite evident that the proton beam has a perveance double as compared to the H_2^+ beam when the two particles have the same speed and the same current. But if protons and H_2^+ are accelerated by the same electric field, they have the same energy but not the same speed. On the other hand a beam of H_2^+ delivers a number of protons which is double as compared to a proton beam with the same current.

In the first 3 rows of Table 1, we compare the perveance of H_2^+ beam and proton beam with a current of 5 mA and 10 mA respectively, at various energies.

The ratio of perveance values shows that, concerning the space charge effects, to accelerate a H_2^+ beam is more convenient than a proton beam with a double current. This advantage is also more evident when energy increases. The last two rows of Table 1 show the perveance values of a proton beam with a current of 2 mA and the ratio vs. the perveance of H_2^+ beam with 5 mA. Although the perveance of the 2 mA proton beam is lower at low energy, we see that if the energy of the H_2^+ beam is increased of a factor 2.3 the same perveance value of the proton beam is achieved.

Table 1: Perveance values of proton and H_2^+ beams at various energies.

	$E_p=E_{H2}$ 30 keV	$E_p=E_{H2}$ 800 MeV	E_p=30 keV E_{H2}=70 keV
H_2^+, I=5 mA	$0.881\ 10^{-3}$	$0.151\ 10^{-9}$	$0.247\ 10^{-3}$
P, I=10 mA	$1.245\ 10^{-3}$	$1.075\ 10^{-9}$	$1.245\ 10^{-3}$
K_{H2}/K_p	0.707	0.141	0.198
P, I=2 mA	$2.491\ 10^{-4}$	$2.15\ 10^{-10}$	$2.491\ 10^{-4}$
K_{H2}/K_p	3.537	0.703	0.992

INJECTOR CYCLOTRON

The injector II of the PSI and the commercial compact cyclotron designed by EBCO and IBA companies are the only kind of cyclotron accelerators which are able to deliver more than 1.5 mA of proton beam up to now.

The injector II of PSI is a conservative solution which is able to supply up to 3 mA of proton beam. It is a separate sector cyclotron with beam injection at 800 keV, final energy of 70 MeV, energy gain per turn ≅1 MeV, extraction radius of 3.3 m and single turn extraction by electrostatic deflector. Despite low voltage injection (25-30 keV) and moderate energy gain per turn (<200 keV/turn), the compact commercial cyclotrons are able to accelerate proton beams with current of 1.5-2.2 mA [9], but these accelerators use the stripper extraction to deliver the beam.

According to the above evaluation, the perveance of a H_2^+ beam with a current of 5 mA and with energy of 70 keV is similar to the perveance of a proton beam with 2 mA and energy of 30 keV.

For the previous reasons, we propose a design which is a mixing of the PSI injector II and of the compact commercial cyclotron described before. The central region of the proposed injector is a scaled up central region of the commercial cyclotron. To take account of the higher magnetic rigidity and to maintain the perveance of the H_2^+ beam similar to the perveance of the proton beam injected into a commercial cyclotron, both the injection energy and the energy gain per turn are doubled. Moreover, the energy gain per turn is supposed to increase along the radius up to the value of 1.8 MeV at the extraction radius. This value is higher than the energy gain per turn in the PSI injector to compensate for the smaller extraction radius. Although the final turn separation at the extraction is 12 mm in the solution here proposed, while for the PSI injector II the turn separation is about twice, we believe that beam losses should be lower than 0.2%. This means that expected beam losses at the extraction should be lower than 400 W for a delivered average beam power of 200 kW. Lower beam losses could be achieved increasing the voltage of the cavities at extraction. Moreover the transverse and longitudinal emittances of the beam injected into the ring cyclotron can be larger than for the PSI ring cyclotron, indeed in our solution extraction is performed by strippers which do

Table 2: Parameters of the Injector Cyclotron

Einj	35 keV/n	Emax	50 MeV/n
Rinj	41.6 mm	Rext	1.440 mm
<B> at Rinj	1.29 T	<B> at Rext	1.39 T
Sectors N.	4	Cavities N.	4
RF	30 MHz	harmonic	3rd
V at Rinj	>70 kV	V at Rext	250 kV
Injection eff.	15 %	Extraction eff.	99.8%
ΔR at Rext	11.6 mm	ΔE/turn	1.8 MeV
Δx at Rext	<3.5 mm	Turns N.	< 83
Extraction: Electrostatic Deflector + Magnetic Channels			
Deflector Gap	12 mm	Electric field	<50 kV/cm

not need a single turn extraction to achieve extraction efficiency of 99.99%.

The tentative parameters for the injector cyclotron are presented in Table 2. The beam injection through the central region is a poor efficiency process, about 15% without buncher and may be 20-25 % with buncher, so a lot of injected beam will be lost along the first turn. We estimated that along the first 3 "posts", which are used to select the proper longitudinal phase acceptance, the beam power lost will be of about 3kW at each post. Although the low energy of the beam does not produce activation anyway, the short range of the particles and the high power lost will pose serious problem of thermal cooling.

H_2^+ Ion Source

To accelerate a beam current with a peak current of 5 mA, due to the low efficiency injection, we need a source of H_2^+ able to deliver a beam current of 24 or 35 mA respectively if a buncher is used or not. Despite parasitic beam of H_2^+ is ever produced in any kind of proton source, up to now ion source able to deliver the request intensity of H_2^+ are not yet reported. Anyway at LNS in Catania [10] a compact ECR Versatile Ion Source (VIS) able to deliver up to 32 mA of proton beam has been recently developed. Tests of VIS show a parasitic beam of H_2^+ that reaches up to the 20% of the proton beam. According to the designer of VIS an optimisation of the source parameters, like position of the permanent magnets, vacuum pressure, RF power, could allow to achieve a beam current of H_2^+ higher than 20 mA. Other two important parameters of VIS are its good beam normalised emittance, about 0.1 π mm.mrad, and its extraction voltage which could be raised up to 70 kV. Both these two parameters fit with the request of the injector cyclotron. Another important feature of VIS is the moderate construction costs.

An alternative ion source much more performing that VIS is the ion source under construction for the IFMIF project [11]. This source is designed to supply Deuteron beam current higher than 100 mA at 100 keV with a normalized emittance of about 0.3 π mm.mrad.

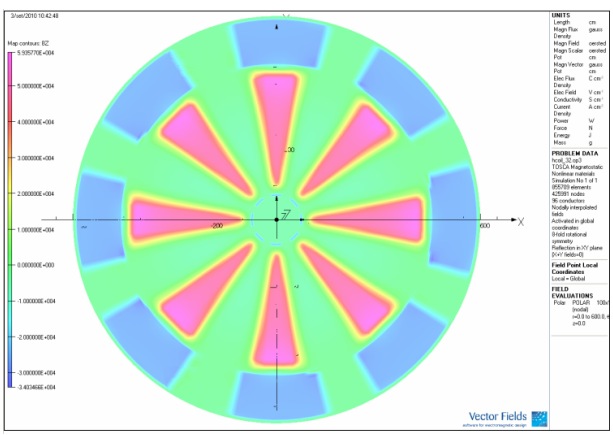

Figure 1: Magnetic field map of the ring cyclotron

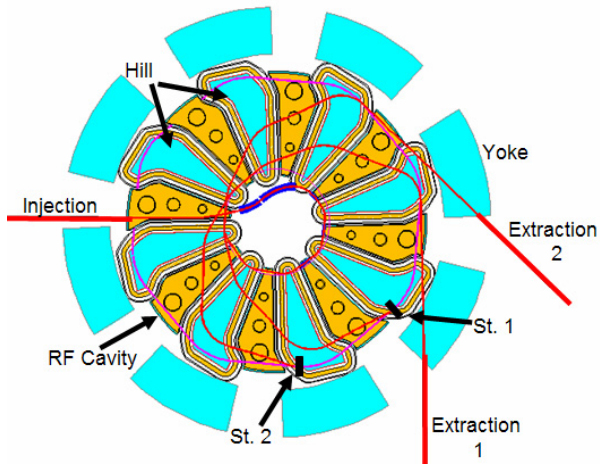

Figure 2: Layout of the ring cyclotron

Despite this is a source for deuterons the preliminary test to optimize the source optic will be performed by an H_2^+ beam, which is very similar to the deuteron beam. So this ion source prototype could be used to supply the H_2^+ beam for the injector cyclotron. Unfortunately the cost of this source is more expensive than the VIS cost.

RING CYCLOTRON

One of main constraints on the accelerator design for the DAEδALUS experiment is to reduce the construction cost. For this reason our first attempt was to design a Ring Cyclotron with extraction radius of about 4 m. In Table 3 the main parameters of this preliminary study for the Ring Superconducting Cyclotron are presented. Our preliminary study was made using straight sectors. The pattern of the achieved magnetic field is shown in Fig. 1. The simulated configuration was able to produce a magnetic field near the required isochronous one with maximum differences lower than 5%, but the vertical focusing was not acceptable for radius higher than 3.4 m. To achieve a good vertical focusing it is mandatory to spiral the magnetic field up to achieve a spiral angle near 40° at the extraction radius.

Table 3: Main parameter of the RSC

E_{max}	800 MeV/n	E_{inj}	50 MeV/n
R_{ext}	4.05 m	R_{inj}	1.44 m
<B> at $R_{ext.}$	2.28 T	<B> at R_{inj}	1.39 T
Bmax	<6.3 T	Pole gap	>50 mm
ξ_{spiral}	< 40°	Hill width	20°
Outer radius	≤6 m	Flutter	1.7÷1.27
Sector height	< 5 m	N. Sectors	8
Sector weight	< 300 tons	N. Cavities	8
Cavities λ/2	Double gap	harmonic	6th
RF	59 MHz	V	250-300 kV
ΔE/turn	3.2 MeV	RF Power	200 kW
ΔR at R_{ext}	1.5 mm	ΔR at R_{inj}	> 15 mm
Coil size	20 x 40 cm^2	Icoil	4300 A/cm^2

The magnetic field with spiralled sectors was used to evaluate both the injection and extraction trajectories, see Fig. 2. The beam envelopes along these trajectories and along the last equilibrium orbit at 800 MeV/n were also evaluated and are presented in Fig. 3. The normalised beam emittance in the transverse planes, used in the simulation, is 0.4 π mm.mrad.

The extraction by stripper was simulated simply changing the charge to mass ratio of the particles. There is a broad range of azimuth positions where it is possible to place the stripper to achieve a trajectory escaping the cyclotron field. This range starts just before the exit of the hill and ends just at beginning of the following hill. The trajectories starting in the middle of the valley pass very close to the centre of the cyclotron while the trajectories near the hill boundaries have a larger distance from the centre. These last trajectories do not cross the injection trajectory and stay inside the vacuum chamber. Like shown in Fig. 2, it is possible to use two strippers placed 45° apart one from the other to obtain two extraction trajectories. This is a good advantage because it allows doubling the mean life of the stripper foils and at the same time simplifies the design of the beam dump. Two or more beam dumps are acceptable for DAEδALUS experiment. Although the simulations are made with a preliminary field map, the results show that injection and

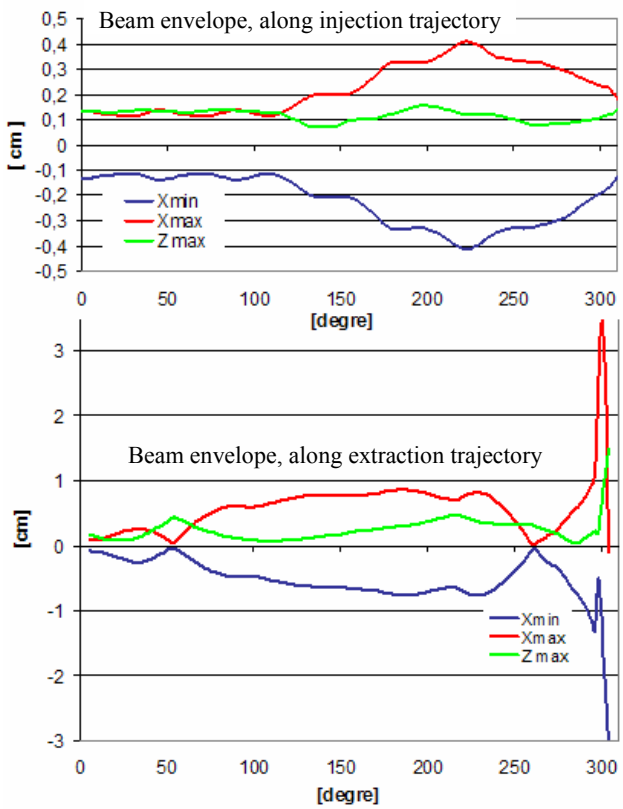

Figure 3: Beam envelope along the injection trajectory, upper, and along the extraction trajectory, lower. The 0° is the matching point on the equilibrium orbit at the injection or at the extraction radii; the 300° is outside the cyclotron.

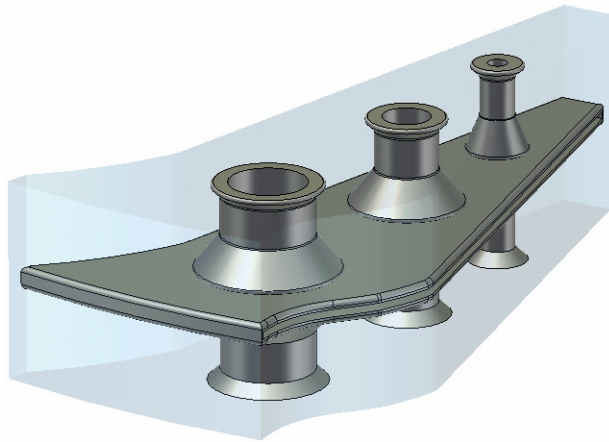

Figure 4: Layout of electrodes and stems of the proposed RF cavity. The three stems are useful for mechanical stability and to host the cryopanels to pump inside the vacuum chamber.

extraction processes are feasible. To simulate the beam envelope and the trajectories we used the computer codes developed at MSU, with some minor changes.

Unfortunately the injection trajectory simulation was limited by the integration code, which uses the azimuth angle as independent variable. So this code does not allow simulating trajectories which bend clockwise. This constraint has strongly restricted the evaluation of other more convenient injection trajectories.

However the results of our simulations demonstrate that it is possible to inject and extract the beam without interference among the stripper extractions and the injection trajectories, moreover the vertical beam size along the trajectories which stay inside the cyclotron pole are smaller than 1 cm. The beam envelope of the extraction trajectories have a significant radial blow up just near the region where the beam escapes from the cyclotron field.

It is evident that to build a coil whit spiral shape is not very easy, moreover this solution reduces significantly the room for the RF cavities, which should have also a spiral shape. Due to the small room between the sectors and the spiralled shape it is difficult to insert a single gap, pill box cavity, like the PSI one. Moreover the use of the PSI like resonators needs more room at the inner radii where the present configuration is quite full by the injection line. A preliminary RF cavity, type λ/2, double gap, which fits in the empty space between the magnetic sectors was studied and its layout is shown in Fig.4. Although the RF cavity is able to produce enough high voltage, a satisfactory energy gain per turn with a moderate power loss of 200 kW, its shape poses serious problems for the installation. Indeed the radial insertion of the cavities is not feasible. The cavities have to be inserted from the top of the ring.

A further serious problem is given by the magnetic forces on the coils. Both the hoop stress on the coils and the resulting radial shifting force are too high. For these reasons we plan to update the present design increasing

both the injection energy and the extraction radius. The preliminary results of the new simulation, with extraction radius of 4.5 m, give a flutter of 2.3, measured along a circle trajectory. The true flutter value when evaluated along the beam trajectory increases up to 3.5. This difference is due to the large scalloping of the trajectories which at the extraction radius reach up to 10 cm. The value of ν_z is now about 1 up to energy of 780 MeV/amu with completely straight sector. Work is in progress to achieve the proper isochronous field and to minimize the hoop stress on the coils and mainly to minimise the radial shifting force. Unfortunately, the maximum magnetic field on the coil in the new configuration is around 6.4 T. This high magnetic field exceeds the usual limit to use NbTi superconducting cable. We have to evaluate if it is more convenient to use Nb3Sn superconducting cable or to reduce the maximum magnetic field down to values below 6 T.

EXTRACTION BY STRIPPING

The stripping extraction is largely used in many commercial cyclotrons to deliver intense proton beam with energy of 30 MeV. This consist to accelerate the H^- beam that at extraction radius crosses a stripper foil where the two electrons are removed. Some research laboratories are also building cyclotron which accelerates H^- at higher energies, and at TRIUMF since the 1975 H^- beams are accelerated up to 520 MeV. The main limit of cyclotrons which accelerate H^- is the maximum magnetic fields usable. Indeed a charged particle moving in a magnetic field B is subject to an electric field (or Lorenz force). The equivalent electric field in the rest frame of the H^- ion is given by

$$E = 3\beta\gamma B \text{ [MV/cm]} \quad (1)$$

Where B is the static magnetic field in Tesla, $\beta=v/c$ and $\gamma=(1-\beta^2)^{-1/2}$ are the relativistic parameters of a particle with velocity v.

The probability to remove the second electron from the H^- or the lonely electron from the H_2^+ ion is given by the following formula [12]:

$$D = \frac{1}{2}\int_0^1 \exp(-\frac{\alpha}{\beta})d\mu \; ; \; \alpha = \frac{4}{3}\sqrt{2\frac{m}{h^2}}W^{\frac{3}{2}} / eE$$

Where: μ is the cosine of the angle between the electric field and the direction of the electron motion, m and e are the mass and charge of the electron, W is the binding energy of the electron in the ion (H^- or H_2^+), and E is the electric field due to the magnetic field (1).

To avoid the electromagnetic dissociation of H^-, the magnetic field has to be lower and lower when the energy increases. So to accelerate H^- up to 1 GeV the maximum magnetic field acceptable is 3 kGauss and the radius of about 19 m. The binding energy of the electron of the H_2^+ molecule is about 20 time stronger than the H^-, and consequently the use of magnetic field as high as 7 T even at energies as high as 1 GeV/amu is permitted. In Table 4 a comparison between the probability of electrical dissociation for H^- and H_2^+, for the commercial cyclotron and for the case of interest for DAEδALUS experiment are presented. The probability of electrical dissociation for commercial cyclotron was arbitrarily set to 1 and the probability for dissociation of H_2^+ accelerated at 800 MeV in an average magnetic field of 6T is 4 time less. We recall that the 30 MeV commercial cyclotrons are able today to supply a beam current up to 1.5 mA, so the amount of beam losses due to the electrical dissociation of H_2^+, with an average beam current of 5 mA, is lower than 1% the beam losses in the commercial cyclotron.

Stripper Mean Life

There are further important differences between the stripping process for H^- and H_2^+. In the H^- case both the two electrons have to be removed to extract one proton and the foil has to be thick enough to guarantee the stripping efficiency of 100% of all the particles which cross the stripper, while for H_2^+ if a molecule is not stripped at first cross through the stripper, it turns inside the cyclotron and hits once again the stripper until it is stripped. Then for H_2^+ it is possible to use a stripper with thickness thinner than for H^- and then a longer mean life is expected. According to the TRIUMF experience [13] a mean life higher than 10 hour is expected for an average beam current of 2 mA of H_2^+. This is a conservative limit. Indeed, the magnetic field to accelerate H_2^+ has reversed polarity compared to the field of H^-, so the electrons stripped in the case of H^- are bent towards the centre of the machine and hit the stripper foil after spiralling in the magnetic field, while for H_2^+ the electrons are bent towards the outer radius. So if the orbit radius of the stripped electrons is larger than 4-5 mm, an electron catcher could be installed to remove these electrons and strongly reduce the stripper damage.

If we are able to place the stripper foil in a position where the field is lower than 1 T the beam radius of the electron are larger than 4 mm. According with the measured mean life of the stripper foils in the commercial cyclotron at 30 MeV, the electron damage of the stripper foils is the main source of stripper destruction. If we are able to stop the electron produced by the stripping process the mean life of the foil should be longer than the mean life measured in the small commercial cyclotron. Indeed at higher energy the energy lost by a beam particle crossing the foil is lower than at low energy.

Table 4: Comparison of parameters relevant to evaluate the electrical dissociation for H^- and H_2^+ beams

	H^-	H_2^+
Binding energy	0.755 eV	15.1 eV
Magnetic field	<1.3> T	<2.3> T
Energy (MeV/amu)	30	800
Electric field (MV/cm)	0.998	10.8
Dissociation probability	1	0.0085

BEAM LOSSES DUE TO RESIDUAL GAS

Due to the interactions with the residual gas, ions could loose the orbital electron along the acceleration path. The fraction of particles which survives is given by [14]:

$$T=N/N_0=\exp(-3.35\ 10^{16} \int \sigma_l(E)\ P\ dl\ )$$

$$\sigma_l(E) \approx 4\pi a_0^2\ (v_o/v)^2(Z_t^2 + Z_t)/Z_i$$

Where: P is the pressure (torr), L is the path length in cm. $\sigma_l(E)$ is the cross section of electron loss, v_0 and a_0 are the velocity and the radius of the orbit of Bohr respectively, and Z_t and Z_i are the atomic number of the residual gas and of the incident ion respectively. This formula is in good agreement with experimental data. Table 5 shows a comparison of the relevant parameters for the TRIUMF cyclotron and the Ring Superconducting Cyclotron (RSC) here described. The expected losses in percent should be 10 time less, while the proton current lost should be a factor 2 smaller. The expected beam power lost along the whole acceleration path should be lower than 4.3 kW. Despite this number seems a little high, we have to consider that the particle are lost along the acceleration path so there is not a specific hot point and that 3 kW of the power loss is transported by proton particles with energy higher than 400 MeV and with a range in iron longer than 150 mm, so the power it is released in the whole volume of the iron and not in a hot spot. Of course these beam losses could be reduced if a better vacuum and/or higher energy gain per turn are achieved. The proposed high energy cyclotron here discussed is more compact and smaller than the TRIUMF one, so to achieve a better vacuum seems feasible. Moreover a better operating vacuum is useful in order to increase the reliability of the RF cavities too.

Table 5: Beam losses due to interactions with residual gases, along the acceleration path.

	E_{max} MeV	$\Delta E/\Delta n$ MeV	R_{ex} m	<I> mA	Vac. torr	I_{loss} %	I_{loss} μA
TRIUMF	520	0.34	7.8	0.4	$2\ 10^{-8}$	1.66	6.6
RSC H_2^+	800	3	4	2	$2\ 10^{-8}$	0.15	3

CONCLUSION

A lot of work has to be done to achieve the final design of an accelerator complex to deliver H_2^+ at 800 MeV/amu for the DAEδALUS experiment. The preliminary study here presented shows that it is a realistic goal. In particular the sector magnets able to produce an average magnetic fields of 2.3 T with the right magnetic field shape and the necessary coils to drive these sectors seem to be feasible even with the present technology, but the optimisation of the magnetic shape and size of the sectors to avoid the spiral shape and to reduce the magnetic forces on the superconducting coils must be completed. Significant reduction of both these problems could be achieved by increasing the extraction radius of about 10÷20%. Maybe this is the best solution which allows also for more room between the sectors where the RF cavities have to be installed. Of course the advantage to have straight sectors allows installing RF cavities similar to that built for the PSI which achieves a maximum voltage of 1 MV. The use of these cavities will reduce the number of turns in the ring cyclotron and the beam losses due the interaction with the residual gases.

Up to now the most critical point is the optimum vacuum required inside the acceleration chamber. Despite the good vacuum level achieved at TRIUMF cyclotron, the use of RF cavities to be operated at high voltage and high power, like the PSI ones, could limit this goal if not properly designed.

Cyclotrons for DAEδALUS experiment need to guarantee a high level of reliability, easy operation as well as high conversion efficiency from electrical to beam power.

We believe that extraction by stripping is a very powerful tool to increase the reliability and simplify the operation as demonstrated by the success of commercial cyclotrons.

REFERENCES

[1] J. Alonso *et al.,* "Expression of Interest for a Novel Search for CP Violation in the Neutrino Sector: DAEδALUS", Jun 2010. e-Print: arXiv:1006.0260.

[2] J. Alonso, Int. Conf. on Cycl. and their App., Lanzhou 2010, these proceedings

[3] Th. Stambach et al., Nucl. Instr. & Meth. in Phys. Res. B113(1996)1

[4] L. Calabretta, NEA Workshop on "Utilisation and Reliability of High Power Proton Accelerators", Aix-en-Provence, 1999, 163-174

[5] Y. Jongen, NEA Workshop on "Utilisation and Reliability of High Power Proton Accelerators", Aix-en-Provence, 1999, 187-198

[6] L. Calabretta et Al., EPAC'00, Vienna, June 2000, THP6B02, p. 918 (2000); http://www.JACoW.org.

[7] Calabretta et al., PAC'99, New York, March 1999, THP139 p. 3288(1999); http://www.JACoW.org.

[8] M. Reiser, Theory and Design of Charged Particle Beams, WILEY, series in "Beam Physics and Accelerator Technology"

[9] H. TsuTsui, Int. Conf. on Cycl. and their App., Lanzhou 2010, these proceedings

[10] S. Gammino et Al.," Tests of the versatile ion source (vis) for high power proton beam production", XIX ECR ion Source Workshop, Grenoble, August 2010, to be published on http://www.JACoW.org.

[11] R. Gobin et Al., Rev. Sci. Inst. 2008, 79, 02B303

[12] G. Darewych and S.M. Neamtan, Nucl. Inst. & Meth. 21(1963) 247-248

[13] Y. Bylinskii and T. Kuo, TRIUMF, private communication

[14] Betz, Rev. of Mod. Phys. Vol.44,N° 3(1972) 465

DESIGN STUDY OF K100 SEPARATED SECTOR CYCLOTRON FOR ISOL*

Ho Seung Song, Khaled Mohamed Gad, Hyun Wook Kim, Jin Hwan Oh, Byeong No Lee, Jong Seo Chai#, Accelerator and Medical Engineering Lab., SungKyunKwan University, 300 Cheoncheon – dong, Suwon Gyeonggido 440-746, Korea

Abstract

Starting from April 2010, KoRIA was launched in Republic of Korea; the main objects of this project are fundamental and applied researches, e.g. production of radioisotope beam for the basic science research, nuclear structure, material and life sciences and medical isotope production. A K=100 separated sector cyclotron will be used as a driving accelerator for ISOL, and it will provide 70-100 MeV, ~1 mA of proton beam and 35-50 MeV, ~1mA of deuteron ion beam, the SSC cyclotron will be injected by 8 MeV proton beam from 2 sector focused cyclotrons. In this paper we will describe briefly about the conceptual design of the cyclotron including the design of injector cyclotron, separated sector cyclotron.

INTRODUCTION

The purpose of this study is to design a separated sector cyclotron as ISOL driver for Korean National project, KoRIA (Korea Rare Isotope production Accelerator), which was started on April 2010 for radioactive ion beam production using both ISOL and in flight fragmentation. KoRIA will contribute to the fundamental research for basic science. Fig. 1 shows the layout of the KoRIA. [1]

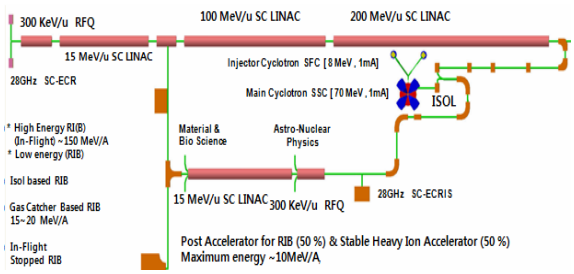

Figure 1: Layout of the KoRIA project

KoRIA facility is composed of cyclotron and superconducting linear accelerator (SC Linac). Stable and unstable ion will be accelerated with SC linac. Unstable ions, radioactive beams are produced with ISOL target bombarded by proton beams with 2 cyclotrons. Main cyclotron, separated sector cyclotron (SSC) has K100 magnet and extraction energy is 70 MeV. SSC is injected by 2 injector cyclotrons. Injection energy is 8 MeV with protons. Radioactive ion beams produced with ISOL are accelerated to 15 MeV/u post linear accelerator which is SC Linac. Accelerated radioactive beams are injected to 200MeV/u main SC Linac for getting the exotic beams.[2] For getting over 1 mA proton beams, we designed separated sector magnet cyclotron even though cost of SSC is higher than sector focus cyclotron. Beam power of protons on the ISOL target is 70kW.

Table 1: Characteristics of Cyclotrons

	SFCyclotron	SSCyclotron
Energy	8MeV	70MeV
Accelerated particles	H^- D^-	Proton Deuteron
Average field	1.155T	0.385T
Pole/extraction radius	0.4/0.35m	3.3/3.0m
Hill angle	48°	30°
Resonant frequency / Harmonics number	74.3 MHz /4th	74.3 MHz/4th
Dee Number	2	2
Dee voltage	50 kV	150kV

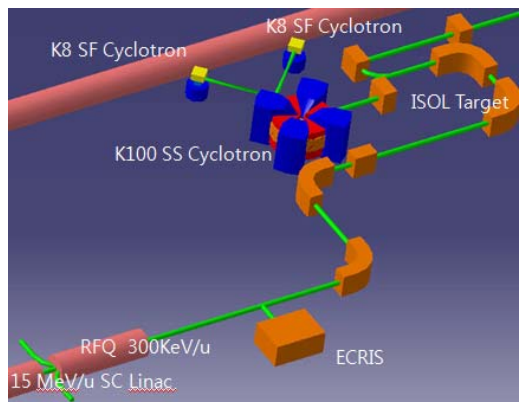

Figure 2: Layout of the cyclotron and ISOL

INJECTOR CYCLOTRON

The compact sector focus cyclotron was designed for injection of K=100 SSC. It has four magnet sectors, and maximum magnetic field is 1.92T. The magnet adopting 4th harmonics has three kinds of holes for beam injection, vacuum pumps and RF systems. Diameter of the pole was chosen to be 80cm with 50kV dee voltage and 40° dee angles. The injection system of this accelerator consists of double gap buncher, Solenoid-Quadrupole-Quadrupole (SQQ) and a spiral inflector. It will provide 8 MeV, 1mA of proton beams[3].

*This work is mainly supported by Ministry of Education, Science and Technology, Republic of Korea. Also Department of Energy Science and School of Information and Communication Engineering of SungKyun-Kwan University

#jschai@skku.edu

Magnet

SF cyclotron for injection has normal conducting magnet with 4 sectors. The diameter of magnet is 1.4m, pole is 0.4m and height is 0.76m. The top and bottom yoke of magnet has one hole at each valley (4 holes in total). Computer simulation code for magnet analysis is used OPERA 3D, TOSCA. [4] Figure 3 shows the results of designed magnet. The maximum field on the mid-plane is 1.95 T. Precise calculations of 3D field and the tunes were performed on figure 4 Also the designed isochronous field and calculated isochronous field are shown on Figure 5. [5]

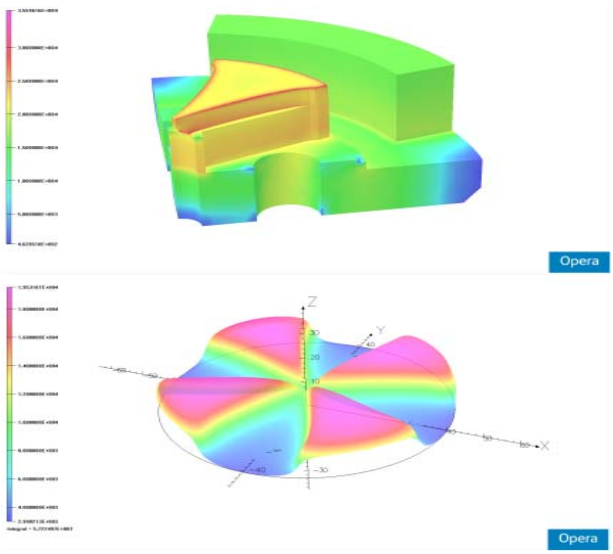

Figure 3: Simulation results of designed magnet.

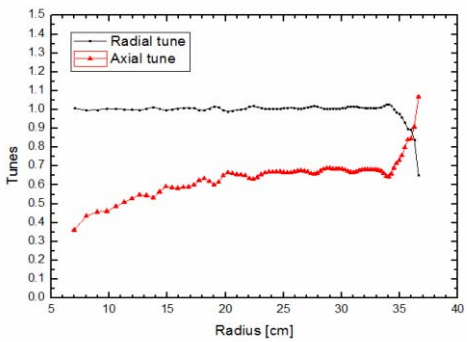

Figure 4: Radial and axial beam tunes.

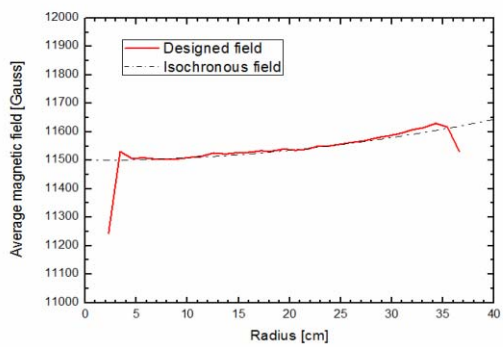

Figure 5. Average magnetic field graph of designed magnet with idle isochoronous field.

RF System

The RF system has 2 cavities with 4 vertical stems. Before designing this RF system, magnet design was preceded. Most of the parameters of whole size were decided from magnet design. Material of RF Cavity is OFHC copper to get electric conductivity better and not to affect magnetic field intensity. For the design of RF resonance cavity, CST Microwave studio is used. [6] It can show E-field and H-field in 3-dimensional. To optimize 70MHz RF frequency, various methods are used. Especially, the stem positions and shapes are primary key to decide resonant frequency and field distribution.

We suppose that the frequency is strongly influenced by the thickness of stem. Besides, it affects Q value, thus the optimization of stem thickness is very important. If thickness of stem is too much thin, the stem would be melted by RF power and Q value would be decreased.

On the contrary, the frequency becomes higher with thicker stem. RF system of Sector-focused cyclotron has resonance frequency of 74.33MHz which is based on the magnet design. λ/2 resonance mode was satisfied by optimizing stem, liner, gap of dees and so on. This 8 MeV cyclotron has 4 vertical stems in total. Dee angle is 40° and total length of each dee is about 30cm. Optimal Q value is calculated to be 5981. [7]

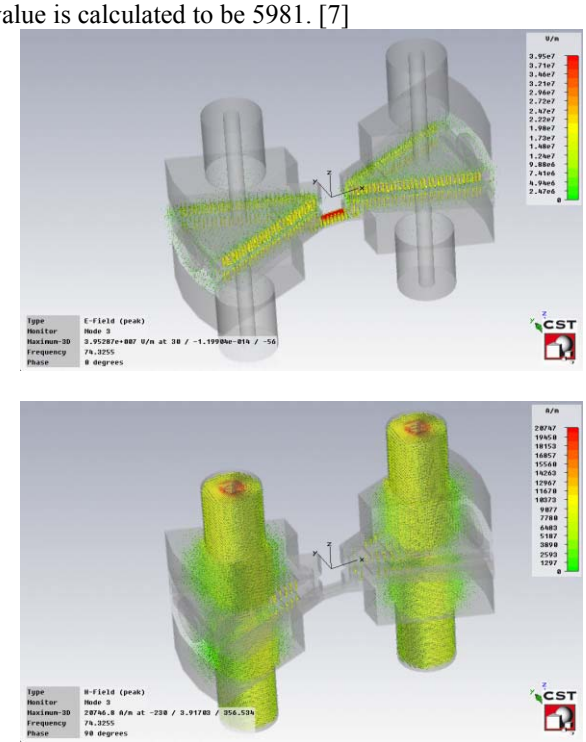

Figure 6. E-field and H-field distribution

Inflector and Central Region

To inject the pulsed beam from external ion source at dee we use the spiral inflector. It is applied 30kV DC. Figure 7 shows maps of voltage contours. We designed minimizing distortion and loss of quantity with safe arrival in the middle plane between dees including proper matching when the beam changes its orbit carefully.

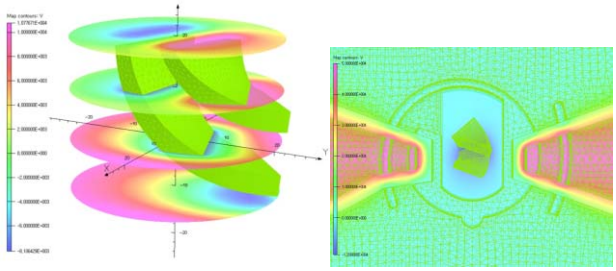

Figure 7. Inflector and central region

SEPARATED SECTOR CYCLOTRON

SSC (Separated Sector Cyclotron) was selected for accelerating high beam current about 1~2 mA. Acceleration of intense beams requires a very efficient focusing and extraction process free of beam loss. The main parameters of SSC design should satisfy the following criteria:

a) Single turn extraction: A large radial gain per turn is requested, i.e. a high energy gain per turn, in order to get an effective turn separation on the extraction radius.

b) Vertical and radial focusing: the problem of space charge effect is not fully understandable because of the very complicated nonlinearity of it. However many systems that have been designed were very successful for overcoming this problem. A deep valley sector focused cyclotrons have been designed to be an injector for separated sector cyclotron.[8]

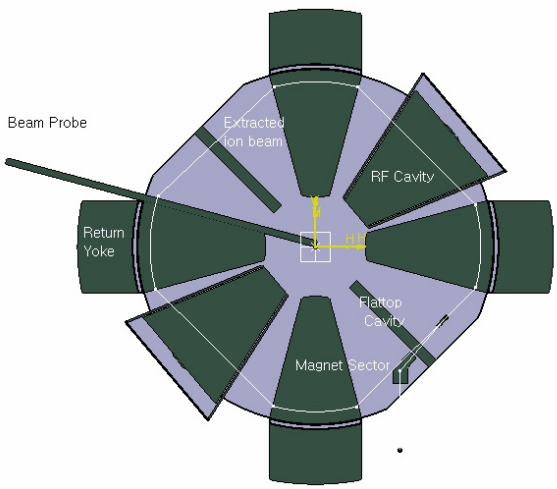

Figure 8: The layout of SSC magnet

Magnet

For accelerating high beam intensity up to 1~2mA, SSC (Separated Sector Cyclotron) was chosen. The magnet diameter is 8.8 m, injection radius is 1 m, and pole radius is 3.3m. The total weight of iron is approximately ~ 400 tons. The minimal value of 3-cm gap between sectors was defined to minimize the energy dissipation at main magnet coil. We have selected four sectors and a magnet sector angle of 30 degrees (α= 30/90=0.333). In addition, we obtained an isochronous field by using 3 groups of trim coils.

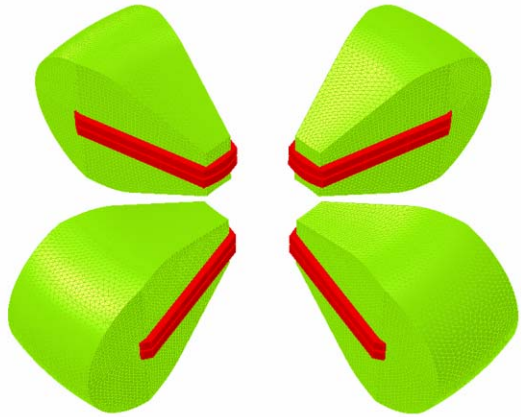

Figure 9: Meshes for magnet simulation by Opera3D

To find the total field produced by the trim coils nonlinear successive approximation technique is needed. However, in order to get a first estimate of the trim coil power requirements, linearity has been assumed. A 2D POISSON model was created consisting of a simplified azimuthally symmetric magnet with circular trim coils. [9]

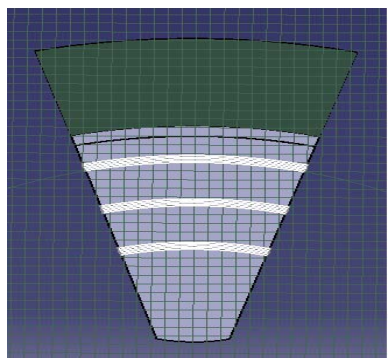

Figure 10: Trim coil position

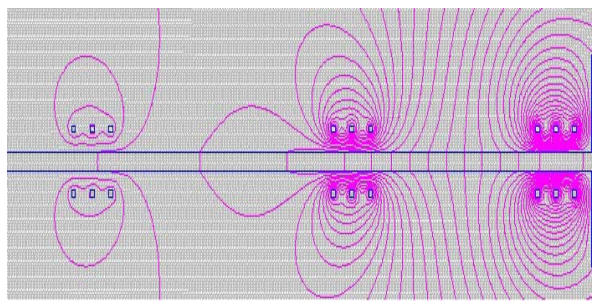

Figure 11: Trim coil simulation by POISSON

One of the first decisions to be made in the design process is the number of sectors in the magnet and the angular width of each sector necessary to achieve the final energy of approximately 70 MeV. To avoid the effects of resonances like $\nu_z = 1$ and $\nu_r = N/2$, we have selected four sectors and a magnet sector angle of 30 degrees (α= 30/90=0.333). The magnetic field of the sector magnets was studied with the finite element code TOSCA. We have adopted a minimum magnet gap of 3 cm with the

assumption that the magnet surface close to the median plane will be part of the vacuum chamber.

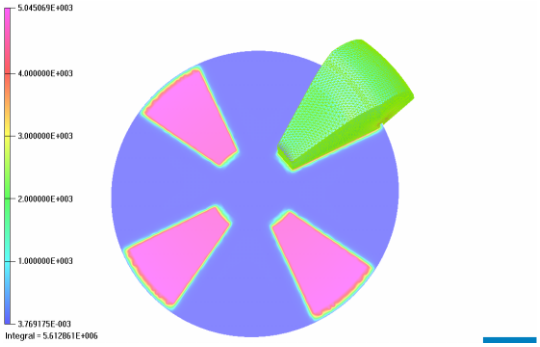

Figure 12: B-fields of simulation by TOSCA

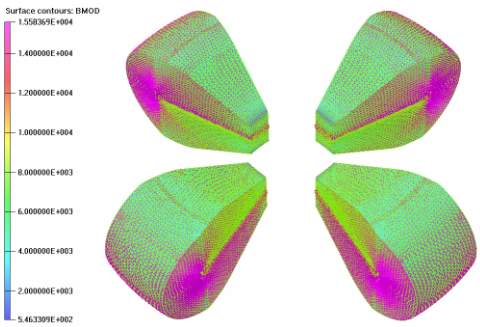

Figure 13: Flux line of simulation by TOSCA

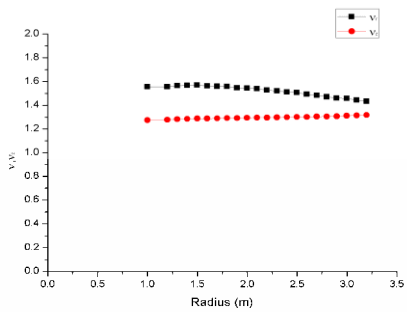

Figure 14: Beam Tunes

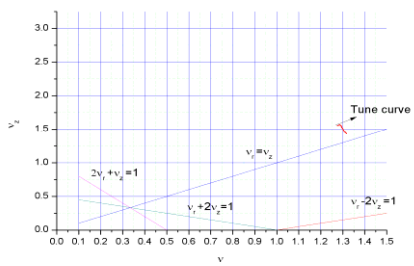

Figure 15: Tune diagram

RF System

For the design of RF system of SSC, we chose double-gap cavity with two stems. By utilizing multiple stems, voltage distribution shape is easier and power consumption is low. Resonant frequency of SSC cavity is 74.5 MHz, and it is matched with injector cyclotron as well as the magnet design. We used OFC (conductivity: 5.91e7 S/m) as a normal conductor.

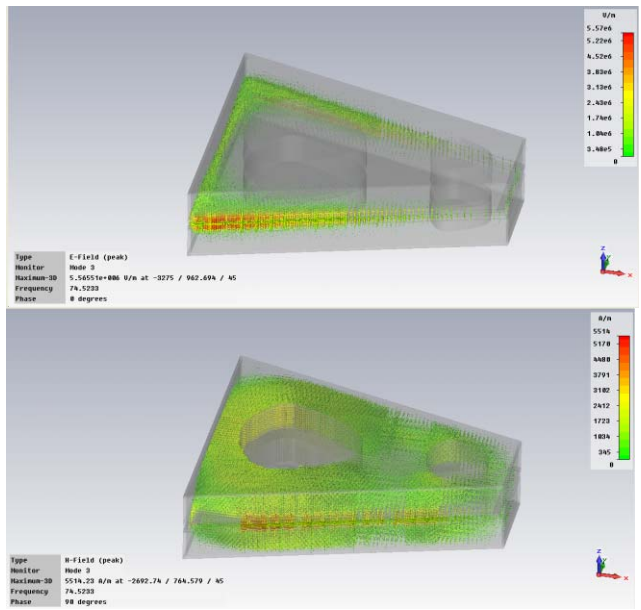

Figure 16: E-field and H-field distributions by MWS

SUMMARY

The design study of 70 MeV separated sector cyclotron is on progress. It is expected that the whole system conceptual design will be finished on November, 2010.

ACKNOWLEDGEMENT

This work was supported by Ministry of Education, Science and Technology, Republic of Korea.

REFERENCES

[1] Y.K.Kim et al, Heavyion accelerator for rare isotopes, p2-4, Physics and high technology, 18-12, 2009

[2] J.S.Chai etc, Heavy ion accelerator facility for rare isotopes, pp30-37, Physics and high technology, 18-12, 2009

[3] B.N.Lee et al, “Design study of compact cyclotron for injection K100 SSC”, 19th International conference on cyclotron and their applications, MOPCP032 (2010)

[4] Cobham, Vector Field Ltd. UK

[5] H.W.Kim et al, “Design study of AVF magnet for compact cyclotron”, 19th International conference on cyclotron and their applications, MOPCP082 (2010)

[6] CST Microwave studio manual

[7] J.H.Oh et al, “Design of RF system for compact cyclotron”, 19th International conference on cyclotron and their applications, MOPCP024 (2010)

[8] K.MH.Gad et al, “Magnet design of 70 MeV Separated sector cyclotron”, 19th International conference on cyclotron and their applications, MOPCP033 (2010)

[9] User’s Guide for the POISSON/SUPERFISH Group of Codes, LA-UR-87-115, Los Alamos Accelerator Code Group

PROGRESS ON CONSTRUCTION OF CYCIAE-100

Technology Division of BRIF, CIAE (Written by Tianjue Zhang, Zhenguo Li, Yinlong Lu)
China Institute of Atomic Energy, Beijing, 102413, P.R. China

Abstract

Beijing Radioactive Ion-beam Facility (BRIF) is being built at China Institute of Atomic Energy (CIAE). As a driving accelerator for ion beam production, CYCIAE-100 will provide proton beam of 75MeV～100MeV with an intensity of 200μA～500μA. At present, the design for each system has been accomplished and an overall progress has been made for the CYCIAE-100 project. The manufacture of the main magnet has entered into the final assembly stage. Two main magnet coils have been completed, two 100kW RF amplifiers are tested with full output power, the main vacuum chamber and main magnet lift system will be completed soon. The construction designs and suppliers surveys for other systems are finished and ready for purchase. Some key design and technology experiments are in process and significant results have been achieved in verifications. The "Central Region Model Test Stand for High Intensity Cyclotron Development" (CYCIAE-CRM) has successfully passed the formal certification held by the competent authorities. A full scale experimental RF cavity has been fabricated, on which the frequency and Q value measured coincide well with the numerically calculation. The verification test of vacuum cryo-panel structure has provided valuable information to cryo-panel structure design. The key technical problems related to CYCIAE-100 project are being solved along with the progress.

INTRODUCTION

The Beijing Radioactive Ion-beam Facility (BRIF) project being built at China Institute of Atomic Energy (CIAE) is planned for productions of intense proton and Radioactive Ion Beam (RIB) used in fundamental, applied researches and medical isotope production. In this project, a 100MeV H- cyclotron is selected as the driving accelerator to operate together with an existing HI-13 Tandem.

As a key component of BRIF project, CYCIAE-100 will provide a 75MeV - 100MeV, 200μA - 500μA proton beam. Its functions are mainly for a RIB facility, physics experiments, applied science and isotope production research. Its preliminary designs and related earlier stage work were presented at ICCAs in Tokyo of 2004 and in Italy of 2007 respectively.

The preliminary designs for all sub-systems of CYCIAE-100 were accomplished in 2006，followed by the detailed design and construction between 2007 and 2009. An overall progress has been made in design and manufacture and important results have been achieved for CRM and high power experimental RF cavity in 2009 [1]. Figure 1 shows the sketch map of CYCIAE-100.

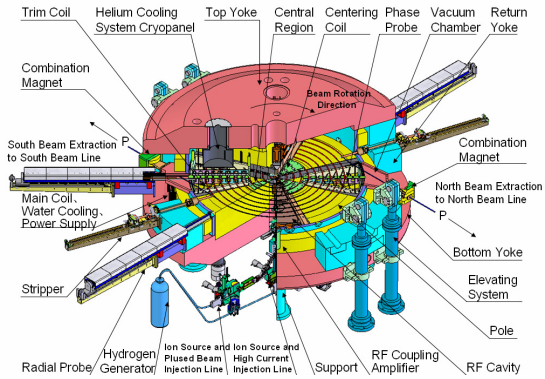

Fig. 1 Sketch map of the major parts of CYCIAE-100.

THE PROGRESS OF MAIN SYSTEMS

A lot of challenges were accepted during the period of fabrications and constructions. A significant progress has been achieved up to now. Some important results will be introduced briefly below. The latest progress of CYCIAE-100 made in recent years will be presented, among which are the final engineering design features, key component fabrication progress, construction status and their pretest specifications.

Main Magnet system

Design Optimization

Due to its large size (6.2m in diameter) and heavy weight (120 ton for one piece), the structure optimization of the main magnet is necessary before stepping into engineering process. While keeping the structure as far as convenient for fabrication, many factors, e.g. the weight, magnetic field force, vacuum force, should be considered together to evaluate its deformations at operating condition after commissioning. As a consequence, some major revisions have been made:

The top/bottom yokes adopts an uneven-height structure instead so that the magnet deformation along radius induced by the atmospheric pressure after pumping can be reduced by 41.26% compared to that of an even-height structure in previous design.

The asymmetric shimming bars are designed in a way that the limited space is best used at the outer radium (R>1200mm) between the shimming bar and the RF cavity. This design eliminates the influence from the coupling resonance on the working path at high energy end in the tune diagram. This kind of asymmetric shimming bar design is a standby solution in case the BH curve of steel is not as good as the designed specification.

Two sets of special measuring tools for main magnet are designed. One is used to measure the angle of the sector, and the other is used to measure the varying gap surface of the sector. Besides, a set of installation tool is specially designed for the shimming bar installation.

Magnet Materials Obtaining

The rough machining steel for the magnet sectors was produced by INDUSTEEL in France and transported to CIAE in April of 2008. It is consisting of 4 roughcasts for 8 sectors with a total weight of about 140 tons. The sampling and repeat test results showed that both the magnetic properties and chemical composition could satisfy the technical requirements.

For the top/bottom and return yokes, considering the large dimensions and existing industrial capablility, it has been decided to use cast steel.

The fabrication contract was signed with CITIC Heavy Machinery Co. LTD. in 2007. The casting of return yokes and experimental piece of the top/bottom yokes had been done by the end of 2007. The preliminary analysis result shows that the chemical composition of the molten steel meets the requirement of the designed specifications. All the fabrication work of the cast steel for the top/bottom yokes were accomplished in May of 2008 and the rough machining was accomplished by August.

The finished product of a top/bottom yoke weighs 129 tons with the actual molten steel of 280 tons. It is unprecedented in term of both scale and technical challenges of casting in the accelerator field and industrial capability. The finished product of each return yoke weighs 15 tons with the actual molten steel of 42 tons.

Following the completion of casting, nearly 400 samples were tested for chemical and magnetic properties under different situations including before and after the stress relief and magnetic property annealing, showing that the design requirement could be satisfied. Figure 2 shows the comparison of BH curves of the top/bottom yoke in different situations and the rough machining steel from France.

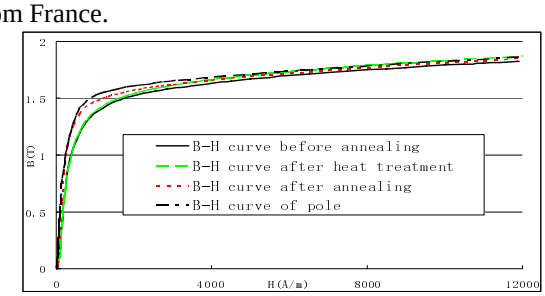

Fig.2 Measurement results of magnetic properties

The rough materials for magnet pole shimming bars and central cylinders are forged steel produced by Taiyuan Steel Company in Shanxi province, China.

Magnet machining and assembling

After the interface conditions related to the main magnet have been determined and the construction design for the fine machining of the major parts has been finished [2], the contract was signed with CITIC Heavy Machinery Co. LTD in January of 2009.

In 2009，the key parts of main magnet system were fabricated, including stress annealing of top/bottom yokes, ultrasonic flaw detection, fixture equipment machining, fine machining of top/bottom yokes, pre-fine machining of sector poles, return yokes, and shimming bars. Figure 3 shows one top yoke after pre-fine machining and the fabricated sector poles.

Fig. 3 One top yoke after pre-fine machining (left) and fabricated sector poles (right).

Up to now, all components of magnet have been fabricated. Vacuum checking for top/bottom yokes is undergoing. The magnet sectors and shimming bars have been installed together. The general installation of the whole magnet and fine adjusting the sector positions are the main tasks afterwards.

RF system

RF power source

The fabrication contract for two 100kW RF amplifiers of CYCIAE-100 was signed in 2007. By the end of June, 2008, the evaluation on the manufacturing solution to the contract was finished, entering into the fabrication stage. By the end of the year, the assembling of the driving amplifier in factory and on-site inspection has been accomplished, as seen in Figure 4.

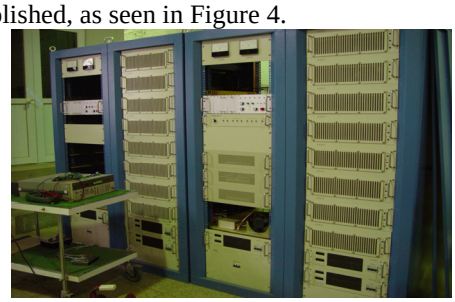

Fig. 4 The 6kW driving power amplifier and monitoring devices

All fabrications have been done in 2009. In August of 2009， the manufacture of RF power generators and transmission lines were finished. The installing and testing began in September. The check and acceptance of their specifications were completed on site in December, as shown in Figure 5. The two sets of RF power generators and transmission lines meet the design requirements both in output power, frequency and in stability, repeatability and control modes.

Fig.5 Acceptance of RF power generators and transmission lines

RF Resonance Cavity Design

Based on the preliminary design, the adjustment and optimization of RF cavity tip and Dee structure has been done and the mechanical design has been finished [3]. The RF power consumption and the numerical simulation of the temperature distribution on the cavity are calculated, and the related water cooling system is also designed. Figure 6 is the general schematics of RF cavity and the test RF cavity model installed.

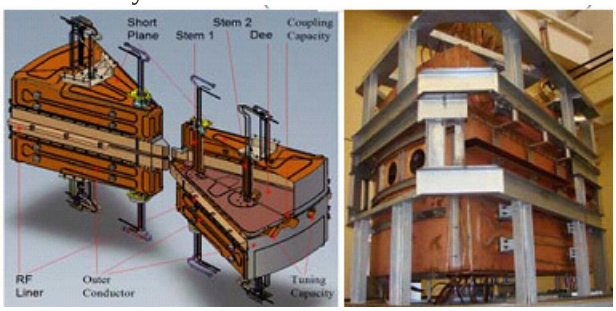

Fig.6 The schematics of RF cavity & test RF cavity model.

Main Coils System

In 2009，the construction contract for two main coils was signed with a factory in Shanghai. Meanwhile, special hanging tool used for main coil was designed. Aimed at high technical requirements with critical dimensions, the fabricating test and copper tube soldering test should be done before the formal fabricating begins.

In February of 2010, the resin pouring of two main coils was made and then the two large coils were transported to the magnet fabricating factory in Henan province for combining installation. Figure 7 shows the two completed coils on construction site.

Fig. 7 Two coils on construction site

Elevating system

Fig. 8 The components of elevating system.

The elevating system is designed to raise a weight of 180 tons with a height of 1500mm. After completing the design of both screw jacks and hydraulic elevating systems, the two solutions were compared and the 4-point hydraulic system was finally determined.

The construction contract was signed in 2009. Now the fabrication has been completed, and it will be transported to magnet manufacture factory for assembly and test with the magnet at the end of 2010. Figure 8 shows elevating system components test on construction site.

Magnetic Field Measurement System

The measurement of main magnet field is planned to be carried out under low vacuum condition in CYCIAE-100 [4]. Figure 9 shows the constructed magnetic field mapping system and 3 hall probes will rotate simultaneously with the beam. The position accuracy of the mapping system is less than 0.1mm in radius and less than 13 seconds in azimuth. At present, the fabrication of the system has been finished and is ready for the assembly and test.

In order to measure magnetic property for dipole, quadrupole, solenoid lens, ion source and switching magnet, etc., a high resolution three dimension locating platform is built at CIAE.

Fig. 9 The designed test stand of mapper.

Vacuum system

For CYCIAE-100, the vacuum of the main vacuum chamber should be better than 5×10^{-6} Pa. Considering all of the effects including the sector magnets, centering coils, beam diagnostic probes and beam extraction probes located inside the vacuum chamber, it is more difficult to obtain the required vacuum and the total pumping speed needed should be more than 140,000L/s based on outgassing load calculation.

Fig. 10 The vacuum chamber in machining process.

The final engineering design of vacuum system was fixed at end of 2009. The main vacuum chamber is a huge

aluminum cylinder of 1.27m in height and 4.08m in inner diameter and the top/bottom yokes are functioning as its covers. The fabrication contract of main vacuum chamber was signed in January of 2010. Now the soldering and stress annealing of the vacuum chamber have been finished, and the fine machining is under way. Figure 10 shows the vacuum chamber in machining process.

Standard commercial pumps could not satisfy the vacuum demands, for which large cryopanel is the only solution. Short of relevant experiences, a test stand of cryopanel structure was designed and built. The test results obtained provide useful information for the final cyopanel system design. The detail of the test is given in the section of 3.3.

Injection and Extraction System

Injection System Optimizing and Experiment

The top/bottom yokes are of uneven height and the dimension of the magnet in the axial direction is increased. Based on the new structure of the magnet, the injection line was redesigned and the calculation for the optics matching was accomplished.

The fabrication and test on the H- ion source prototype have been finished. The result from the test stand shows that when the beam intensity is above 10mA, the normalized emittance of 80% beam is 0.45 mm-mrad.

Extraction System Optimizing and Experiment

The beam transfer matrix is calculated from the stripper to the combination magnet and the dispersion effects during the beam extraction are also studied through numerical tracking [5]. The hill gap of the combination magnet is increased from 60mm to 80mm.

Since the stripping probe is a crucial device for the extraction system, specific work on the physical design and mechanical structural design of the stripping probes has been carried out. Several schemes have been researched and compared. After repetitive discussions, it has been decided that the structure of a turnable stripper foil changing in the vacuum is applied in the final design.

The structure of stripper foil exchanger was built and tested, through which the problems related to its reliability were solved, as seen in Figure 11.

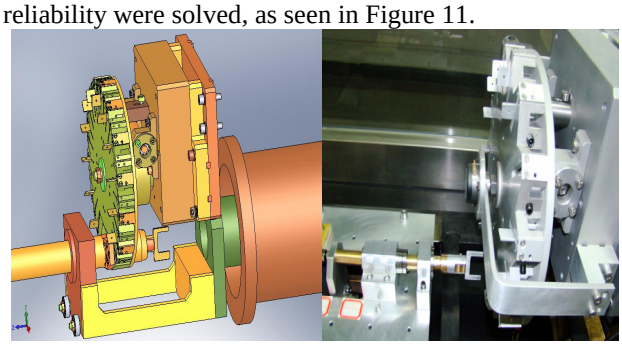

Fig. 11 The designed and real foil exchanger

Other Aspects

Beam Diagnostics System

The experimental study on the beam diagnostics system has been performed, including the data acquisition, transmission, processing, etc. The experiments on the DCCT, double wire scanner, emittance scanner have been done. The related design and fabrication has been finished as well.

The experimental phase probe, radius inserted probe, etc., have been built and tested at CRM. Their structures have been optimized and their technical feasibility has been verified through the test.

Dd26tement ose Monitoring and Safety Interlock System

The layout design of the devices for radiation monitoring and safety interlock has been completed. In the meantime, investigation on the measuring neutrons at wider energy range was done and research on fast electronics of γ detector was carried out.

The software flowchart was developed. The systematic software focuses on DSP program and its real time simulating environment was built. Purchase of the PMTs, GM tubes and PLC for radioactivity detection and control interlock is conducted. The experimental test on the preamplifier of the dose monitoring probe is under way.

Electricity and Power Supplyd26tement System

The schematic design for electricity and power supply system has been fixed. There are more than 100 power suppliers in total and can be divided into 3 types, most of which use numerical control. A new system for current stability calibration of the power suppliers has been built and tested.

In order to meet the magnetic mapping requirement, the main magnet power supply has been built with the specifications of 110A/286V in rated output and $\pm 1\times10^{-5}$/8h in stability. The photo pictures of the power supply are shown in Figure 12.

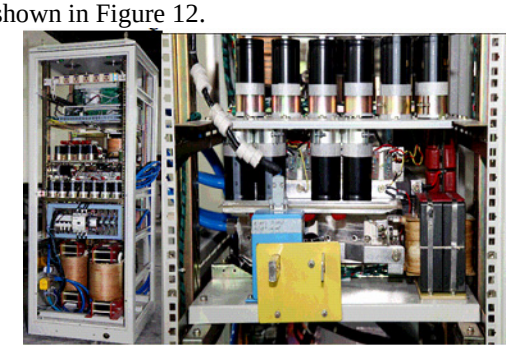

Fig. 12 Photos of main magnet power supply.

Computer Control System

EPICS system is chosen for CYCIAE-100. The control system is a middle scale, rich interlock system, which contains approximately 1,100DI/DO and 300 AI/AO

process variables, distributed in several subsystems. Figure 13 shows the general control diagram of BRIF.

The control of various power supplies is a main task of control system, the digital RS-232/485 control interface and multi-port input/output controller have been selected. Recently, an embedded EPICS IOC on Moxa DA662 computer under MontaVista Linux operating system was developed and various tests have been performed.

For low level RF(LLRF) control research, date sampling program with multi-function used on master and slave computers was developed and verified at CRM.

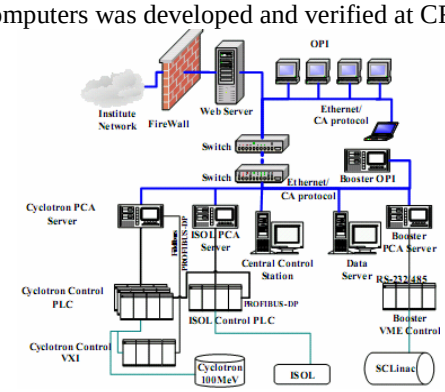

Fig. 13 General control diagram of BRIF

RESULTS OF THE KEY CERTIFICATION TESTS

Three key experimental verifications have been performed and significant progress has been achieved. They are Central Research Model (CRM), 1:1 RF Cavity Test, vacuum Cryo-panel Test.

Central Research Model

The central research model is to study the key technologies related to the CYCIAE-100 project. The model with a designed energy of 10MeV consists of all equipments of a compact cyclotron. As a comprehensive test platform, it is used to verify practically the beam dynamics calculations and the key equipments structure designs of the 100MeV machine.

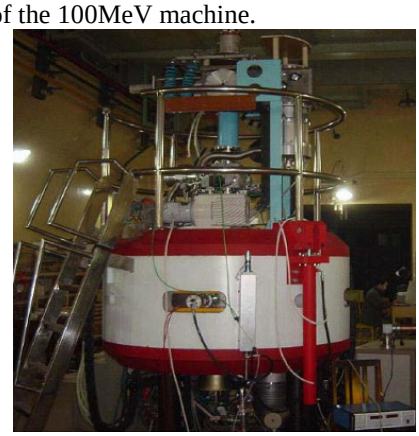

Fig. 14 Central research model

CRM has 4 straight sectors with angle of 54^o and the maximal filed of 1.75T. A 13.5kW RF amplifier drives two RF cavities with the frequency of 70.5MHz. CRM is installed in 2006 and 5.8μA beam on internal target was obtained in 2007.

In 2008, a significant progress was achieved after some improvements had been done. The internal beam intensity increased to 130μA and 5.8μA/10MeV beam was extracted [6].

In 2009, the beam specifications were upgraded further after some improvements were made. The internal beam current is up to 432μA and extraction current reaches 230μA under the condition of 64% RF duty ratio. The beam injection and acceleration efficiency is 17.7%, the 94.5% respectively, and the beam extraction efficiency is nearly 100%. Some typical beam test dada are shown in Table 1.

Table 1 Some typical beam test dada

year	Ccurrent of ion source	RF duty	Inter-current (buncher off)	Inter-current (buncher on)	Current extracted
2008	2.1mA	25%	28uA	48uA	5.8 uA
	2.1mA	70%		130uA	
2009	2.43mA	100%		32.6uA	
	2.43mA	64%			230uA

High Power RF Cavity Test

The purpose of building 1:1 scale model is to verify the final RF cavity design and to test if the key manufacture procedures are practical and reliable or not. Especially for large dimension and complicated structure of copper cavity, it is crucial how to solder and in the meantime to prevent from deformation and to keep the designed RF specifications even at high power conditions.

In 2009, 2 technological problems concerning soldering and form calibration were solved through many times of soldering experiments and equipment upgrading. So far the test RF cavity has been completed and installed. During the long period of production, useful experiences were accumulated. For example, the Dee plate welding has been done inside the furnace and heated under vacuum condition; Dee stems have got good quality through electro-beam welding, etc.

f=45.8MHz and Q=5000 come from the preliminary cold measurement at beginning. The Q value is increased to 9300 soon after polishing the cavity surface, adding contact spring sheets, necessary connectors, position tuning, etc.

Other parts, such as power coupling, frequency tuning, vacuum container are all set in place. The high RF power has been fed into the test cavity. The test stand was shown in Figure 15.

Fig. 15 High power RF cavity test stand.

Vacuum Cryo-panel test

In order to verify the cryopanel structure used to CYCOAE-100, a test stand was designed and built. A plug-in cryopump with a pumping speed of 15000 L/s was designed and tested [7]. The plug-in cryopump is mainly used to determine several key parameters, including its pumping speed, ultimate pressure, temperature distribution, etc.

Figure 16 shows the structure and appearance of the test cryopanel. It consists of half-chevron baffles, a shield, the cryopanel, a flange, an adapter, and two GM refrigerators. Gas particles are adsorbed onto the cryopanel surface and kept at a low temperature by the refrigerators. To reduce the heat load on the cryopanel, half-chevron baffle are used to block some of the incoming radiation. The entire system is surrounded with a cylindrical shield. The cryopanel heat load calculations, including the shield and baffle, have been conducted.

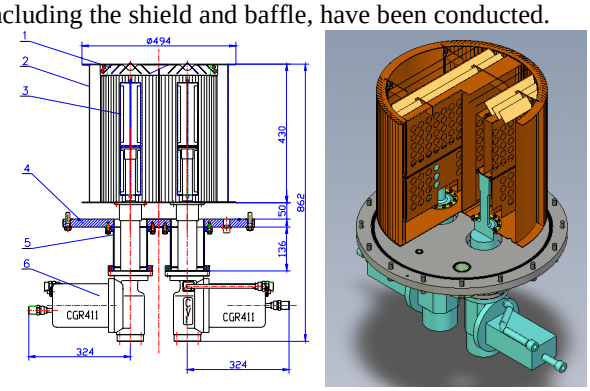

Fig.16 Structure of test Cryopanel

The design parameters and experimental results are compared and coincided well. With only the turbo-molecular pump (80L/s) operating, a pressure of 3.2×10^{-4} Pa was reached. After coating shield and baffle, the pressure dropped to 5.8×10^{-6} Pa with refrigerator after 3.5 hours of operation. The refrigerator had a power of 83W/80K at the first stage and 7.5W/20K at the second stage. The temperature on shield top reached 67.7K, and 19K on second stage of cold head. The maximum tested pumping speed was 15250L/s. Figure 17 shows the Cryopanel Test Stand.

Fig.17 Cryopanel Test Stand

The test results have provided valuable information to cryo-panel physics design and set up the foundation for cryo-panel structure design of CYCIAE-100.

CONCLUSION AND NEW SCHEDULE OF CYCIAE-100 PROJECT

In conclusion, a remarkable progress has been achieved in the past few years in the design, construction and experimental verification of CYCIAE-100. Most of the key equipments for this machine have been fabricated or will be finished by the end of this year.

Nevertheless, the schedule of BRIF as a whole project has to be postponed for some budget reasons. According to the new schedule, the construction of building for CYCIAE-100 will start in the first quarter of next year. The whole project will be completed with the first beam at the end of 2013 or the beginning of 2014.

The general outline of the new schedule is planned as follows: ①The temporary installing and testing site will be ready at end of this year. ②The fabrications of sub-systems of CYCIAE-100 are fully carried out and will be finished one by one from now on till the next year. ③In the first quarter of 2012, all equipments will be moved to the permanent positions in the CYCIAE-100 building; after final mapping of the field and installation of the relevant equipments, the sub-systems will be tested at normal conditions. ④Beam tuning is hopefully to start in the first quarter of 2013. ⑤Beam specifications are to meet required standards at end of 2013.

ACKNOWLEDGEMENTS

For the designs and constructions of CYCIAE-100, many institutes such as TRIUMF, PSI, LNS, etc. have provided substantial support in the process. The team of Technology Division of BRIF at CIAE would like to extend their cordial appreciation for their help.

REFERENCES

[1] Research Progress in High Intensity Cyclotron Technology, TianJue Zhang, MingWu Fan, ZhenGuo Li, ChengJie Chu, etc., Chinese Science Bulletin, Nov. 2009, Vol. 54, Iss 21, p3931-3939

[2] Construction Status of Main Magnet for CYCIAE-100, Zhang TianJue, IEEE in Transactions on Applied Superconductivity (MT-21, 2009).

[3] Theoretical and Practical Study on RF Model Cavity of 100MeV H- Cyclotron, JiBin, etc., Chinese Physics C, Vol.32(S1), 2008.

[4] The Design of Magnetic Field Measurements system for CYCIAE-100, Zhong JunQing, IEEE in Transactions on Applied Superconductivity, (2009).

[5] Stripping extraction calculation and simulation for CYCIAE-100，Shizhong An, etc., Chinese Physics C, 2009 33 (S2): 42—46.

[6] Test Stand Design and Construction for High Intensity Cyclotron Development, Zhang TianJue, etc., Chinese Physics C, Vol.32, P237-240 /2008.

[7] The Design and Test of Plug-In Cryopumps, Gaofeng Pan, et al., Proc. of the 23rd Particle Accelerator Conference, 4–8 May 2009, Vancouver, British Columbia, Canada.

INDUCTION SECTOR CYCLOTRON FOR CLUSTER IONS*

K. Takayama, T. Adachi, KEK, Tsukuba, Ibaraki 305-0801 Japan
H. Tsutsui, Sumitomo Heavy Industries, Ltd., Nishitokyo, Tokyo 188-8585 Japan
W. Jiang, Nagaoka University of Technology, Nagaoka, Niigata 940-2188 Japan
Y. Oguri, Tokyo Institute of Technology, Ookayama, Tokyo 152-8550 Japan

Abstract

A novel scheme of a sector cyclotron to accelerate extremely heavy cluster ions, called “Induction Sector Cyclotron (ISC)”, is described [1]. Its key feature is repeated induction acceleration of a barrier trapped ion bunch. The induction cell (transformer) is energized by the corresponding switching power supply, which is controlled by gate signals manipulated from the circulating beam signal of an ion bunch. The acceleration synchronizing with the revolution of any ion beam is always assured. A cluster ion beam such as C-60 [2] can be accelerated from an extremely low velocity to a nearly light velocity. Its fundamental concept including required key devices is described.

CONCEPT OF THE ISC

Definition

It is noted that a terminology “*sector cyclotron*” is used in the following broad sense:

- Sector magnets are employed as guiding magnets.
- A circulating orbit is varied in the radial direction in the fixed guiding fields, associated with acceleration.
- Revolution frequency of circulating ions changes in an acceleration cycle.
- Transverse focussing is resulted from edge focusing effects and field gradient in the sector magnet themselves.

In addition, the ISC is not operated in a CW mode but in a pulse mode due to an essential nature in its acceleration, as described later.

Historical Background

Historically the induction acceleration in a circular ring was invented in Europe and demonstrated in a complete manner as a betatron by Kerst. Topological modification of the betatron acceleration device was achieved. One of them was realized in a linear betatron accelerator (linear induction accelerator) and has been extensively developed [3]. Meanwhile, the concept of induction acceleration in a FFAG ring was proposed and actually demonstrated as an acceleration tool at the initial acceleration stage in the MURA 50 MeV electron FFAG [4]. This acceleration method was nothing but the original betatron acceleration, because the magnetic material cores used for the induction acceleration were excited at the acceleration cycle, yielding a small continuous induced voltage of few tens of volts. That was necessarily always less than 1 Hz; the induction device was ramped just one time during its acceleration cycle.

The induction synchrotron (IS) proposed in 2000 [5] was fully demonstrated using the KEK 12 GeV PS in 2006 [6]. Protons in the IS were accelerated and captured with pulse voltages generated by transformers known as "induction acceleration cells (IC)". The ICs were energized through the corresponding switching power supply (SPS), in which solid-state power devices such as a MOSFET are employed as switching elements and their tuning on/off state is operated through gate signals digitally manipulated from the circulating signal of an ion beam. The ICs were set and reset within a single revolution of the proton bunch in the 12 GeV PS. The ICs were operated at 1 MHz. This feature can be distinguished from any induction acceleration demonstrated in circular rings. Consequently, the acceleration synchronized with the revolution of the ion beam is always guaranteed, regardless of the type of ions and their possible charge state. In this scheme, any ions directly injected from an ion source embedded in a high voltage terminal can be accelerated from an extremely low speed almost to the speed of light. As a matter of fact, the construction of the first AIA through renovation of the existing KEK 500 MeV proton synchrotron is almost complete [7].

A similar induction acceleration of barrier trapped ions can be utilized in cyclotrons operated in a pulse mode. This idea has been proposed in the last year [1]. A sector cyclotron to accelerate cluster ions especially seems to be attractive among them, because there have been no actual methods to accelerate them to high energy in a circular accelerator so far.

Schematic View of the ISC

Figure 1 shows the principle of the ISC, where the varying cyclotron orbit is located in the inner aperture of the induction cell through the entire acceleration period. The induction cell and bunch monitor with a wide aperture are required. This feature is different from that of the induction synchrotron. An ion bunch is captured by the so-called barrier voltages, which are also generated by the other induction cell (see Fig. 2).

INDUCTION ACCELERATION OF A BARRIER TRAPPED ION BUNCH

Induction Acceleration

The concept underlying operation of an ISC is fairly simple. Conventional D-electrodes with a limited frequency bandwidth are replaced by two types of ICs, one of which is used only for acceleration (Cells A and B

*supported by Grant-in-Aid for Exploratory Research (KAKENHI No. 22265403)

in Fig.2), and the other (Cell C in the same figure) is used for confinement of ions. The induction acceleration system consists of the IC, SPS that drives the IC, and an ion bunch monitor and intelligent gate control module, where the ion bunch signal is manipulated and gate trigger signals are created in order to fire the SPS. Their essential features are the same as in the first IS and the first AIA (named "KEK digital accelerator") [8]. Cells A and B are placed symmetrically in the drift spaces between adjacent sector magnets, as shown in Fig. 2.

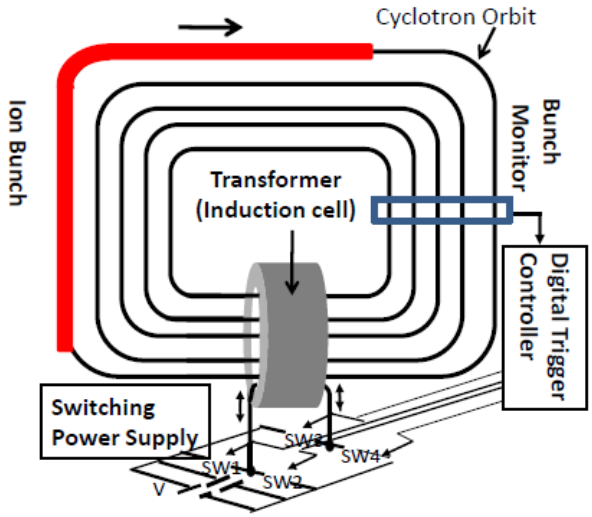

Figure 1: Principle of the ISC

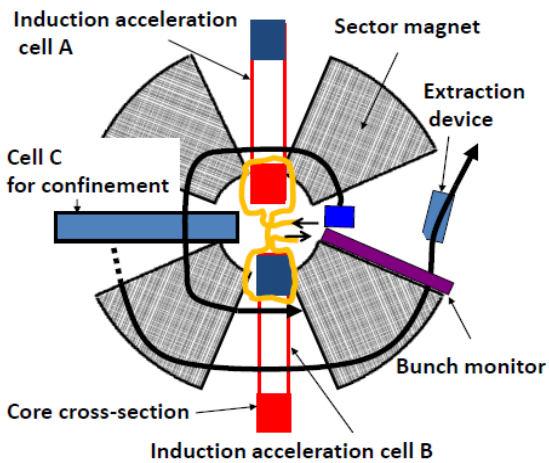

Figure 2: Concept of the ISC. Brown line indicates the exciting coil

Cells A and B are powered by a single SPS and are connected in series (primary) in such a way that the induced pulse voltages are cancelled out along the circular beam line (secondary) in Figs. 2 and 3 (top). Immediately after injection, Cell C is triggered to generate the barrier voltage, and two barrier voltage pulses are adiabatically removed in time, thus creating a long ion bunch. The length of the bunch is always maintained to be less than half a revolution period. The bunch monitor receives a passing signal from the ion bunch, based on which the respective SPSs driving Cells A/B and C are triggered through the gate trigger control module. The operational modes of Cells A/B and C are depicted with respect to time in Fig. 3 (bottom). Pulse voltages with dual polarity are generated within a single revolution period. This operation prevents the saturation of the magnetic cores in the ICs. This is a reason why the repeated acceleration is possible. The ion bunch on its circulation orbit is desirably accelerated at both acceleration gaps at every turn in accordance to the figure-8 primary winding of Cells A and B. This figure-8 winding reduces a droop in the accelerating voltage because of driving a duplicated large inductance.

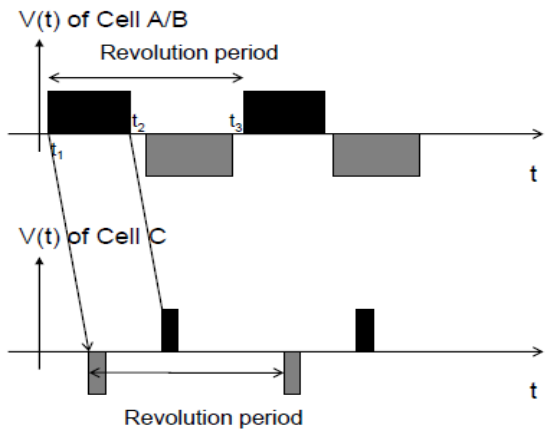

Figure 3: Induced voltage pulse profiles

Induction Cells

The induced voltage through theIC is described as $V\tau = -B_{max} S$, where V is the induced voltage, τ is the pulse width, B_{max} is the maximal flux of the swinging induction core, and S is its cross section. Here, B_{max} and S are optimized by minimizing both the heat deposited in the magnetic material and the total cost consistent with any constraints on the available space. The core is segmented into multiple bobbins. A possible core material is a nanocrystalline alloy, such as Finemet, where a thin tape 13 μm in thickness is wound in a shape resembling a race track, the inner size of which is sufficiently large to accommodate the rectangular vacuum chamber with the ceramic acceleration gap, as shown in Fig. 4a. Heat deposit inside the acceleration cell is not small. It must be removed in an efficient way similar to that in the KEK-DA. Its conceptual scheme is shown in Fig. 4b.

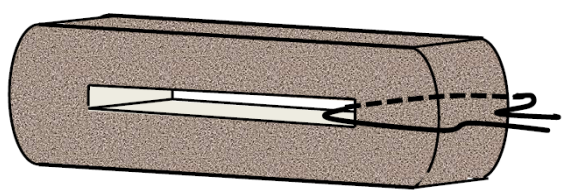

Figure 4a: Induction cell core

TRANSVERS FOCUSING

Characteristics of beam focusing in the ISC are summarized as below:

- Edge focusing of the sector magnet gives focusing in the radial direction and defocusing in the vertical direction.
- The field gradient in the F-type sector magnet takes opposite roles.
- Betatron tunes are determined by a drift length between adjacent sector magnets in addition to a balance of above focusing and defocusing effects.

Due to those properties, the present ISC may be different from a sector cyclotron in a narrow sense. A simple analysis has been given in the other paper [1] and its more details shall be given in a forthcoming full paper.

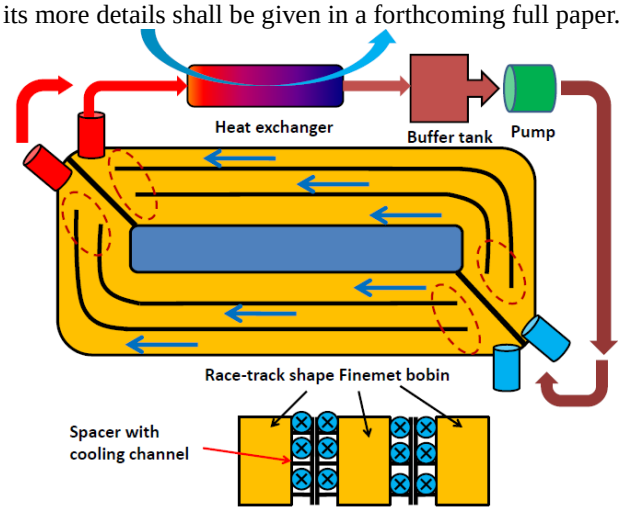

Figure 4b: Cooling system of the induction cell.

TYPICAL EXAMPLE OF THE ISC FOR C-60 LUSTER IONS

An achievable energy is given as a function of the ratio of charge state Q to mass number A of ion for different magnetic rigidity B of the sector magnet in Fig.5. Machine parameters of a typical example of the ISC for C-60, the magnetic rigidity of which is plotted with a black dot in Fig. 5, is given in Table 1.

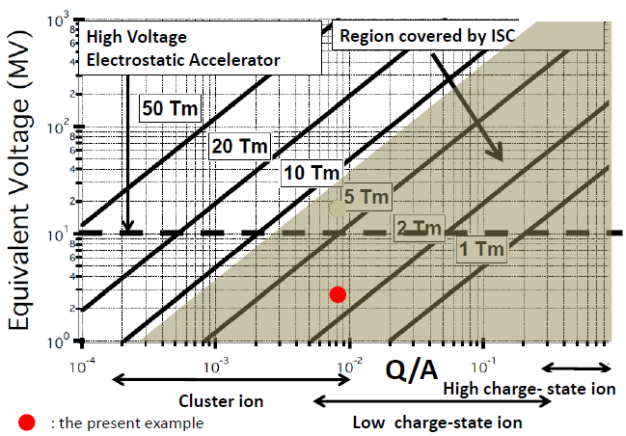

Figure 5: Achievable ion energy

SUMMARY

The present discussion is summarized as follows.

- Novel concept of induction acceleration in fixed field circular rings such as a sector cyclotron or FFAG has been proposed.
- An example of the induction sector cyclotron for C-60 has been introduced.

There are a lot of subjects remaining unsolved, such as a high charge-state cluster ion source and required good pressure and the stability of cluster ion itself under high magnetic fields. Experimental results on the life-time of cluster ions in the electro-static storage ring, which was reported by Tanabe [10], may give good suggestions to these issues.

Table 1: Machine parameters

Item	Symbol	Num. value
Mass/Charge state	A/Z	720/7
No. of sector magnets	N	4
Sector angle/Edge angle	η_0/κ[9]	$(\pi/4)/(\pi/8)$
Averaged radius at Inj/Ext	r_1/r_2	1.85/3.7 m
Bending radius at Inj/Ext	ρ_1/ρ_2	0.97/1.95 m
Flux density at Inj/Ext	$B(r_1)/B(r_2)$	0.67/1.34 Tm
Length of short straight		1.38/2.75 m
Acceleration voltage/turn	V_{acc}	30 kV
Turn number	N_{turn}	200
Rev. Freq. at inj/ext	f_1/f_2	52.8/105 kHz
Betatron tune	ν_x/ν_y	1.89/0.23

REFERENCES

[1] K.Takayama, Patent pending (applied in November 2009), K.Takayama, T.Adachi, and H.Tsutsui, submitted to *Phys. Rev. Lett.* (2010).
[2] A.E.El-Said, *Nucl. Inst. Meth.* **B267**, 953-956 (2009).
[3] K.Takayama and R.Briggs (Eds), "Induction Accelerators", (Springer, 2010) *in press.*
[4] F.LPeterson and C.L.Radmer, *Rev. Sci. Inst* **35**, 1467 (1964).
[5] K.Takayama and J.Kishiro, *Nucl. Instrum. Methods, Phys. Res.* **A 451**, 304 (2000).
[6] K.Takayama *et al*, *Phys. Rev. Lett.* **98**, 054801-4 (2007).
[7] K.Takayama, T.Adachi *et al.*, *Proceedings of IPAC2010*, MOPEC052 (2010).
[8] K.Takayama, Y.Arakida, T.Iwashita, Y.Shimosaki, T.Dixit, and K.Torikai, *J. of Appl. Phys.* **101**, 063304 (2007) and (Erratum) *J. of Appl. Phys.* **103**, 099903 (2008). Patent in Japan 3896420 (2007).
[9] J. R. Richardson, Progress in *Nuclear Techniques and Instrumentation* (North-Holland, 1965), 1-10.
[10] T.Tanabe and K.Noda, *Nucl. Inst. Meth.* **A496**, 233 (2003).

DESIGN AND CONSTRUCTION PROGRESS OF A 7MEV/U CYCLOTRON

B. Wang, H.F. Hao, J.Q. Zhang, M.T. Song, Q.G. Yao, L.Z. Ma, S.H. Zhang, X.W. Wang, A.M. Shi, Z.M. You, X.T. Yang, D.Q. Gao, X.Q. Zhang, K.D. Man, Y. Cao, H.W. Zhao
Institute of Modern Physics(IMP), Chinese Academy of Sciences, Lanzhou, 730000, China

Abstract

The 7MeV/u cyclotron accelerates carbon ions with mass number 12, 5+ charges, the extraction energy of carbon ions is 7MeV/u, and the beam current density is designed to be 10eμA. It designed as injector for the HITFiL(Heavy Ions Therapy Facility in LanZhou) synchrotron, which accelerates carbon ions to the energy 300MeV/u for tumors treatment. Computer modeling results on the axial injection, magnetic, accelerating and extraction systems of the cyclotron are given. Design of the main systems of the cyclotron and the results of beam dynamic simulations are introduced [1], [2], [3], [4]. The construction progress including the ECR ion source, the axial injection beam line, the magnet, the RF system, the vacuum system etc. will be described respectively

INTRODUCTION

The 7MeV/u cyclotron is designed as a commercial cyclotron which is operated in a hospital where the operators of the cyclotron may not be the expert in cyclotron field. At the phase of designing the cyclotron, we aimed to design a compact cyclotron to reduce the cost and a simply operational cyclotron that can be well done by staff in hospital. For these purposes, we designed the extraction average radius to be 0.75 m, the maximum magnetic induction density was about 1.9 Tesla that can be safely achieved with the pure iron material. The magnet of the cyclotron is 4 fold in azimuzal direction with 4 straight edge sectors, the sector's angle is 56 degree. The diameter of the magnet is 2.8 m and the height of the magnet is 1.6 m. We optimized the magnet pole to form the isochronous magnetic field with no trim coils to be used. In two valleys of the magnet, tow 30 degree rf Dees are located. There were eight holes in the magnet four valleys to install vaccum pumps and rf stems. The ion source was designed as a permanent magnetism ECR ion source to remove injection and extraction coils for the ECR ion source. For the axial injection line and extraction system of the cyclotron, we used as less as possible components to simplify the design and construction.

The phase of constructing the cyclotron started in December 2009. The permanent magnetism ECR ion source, the axial injection line, the rf amplifiers and rf cavity are fabricated in plants now. The schedule of the magnetic field measurement is in July 2011, the assembly of the cyclotron is in October 2011, the commissioning of the cyclotron is in December 2011.

DESIGN RESULTS

General Description

As a injector of the HITFiL synchrotron, the 7 MeV/u cyclotron was required to extract C^{5+}_{12} beam, while the beam energy was 7 MeV/u, the energy spread was less than 1%, the beam emmitance is about 20 π mm.mrad, the beam current intensity was greater than 10 eμA. The cyclotron was designed as a compact cyclotron with fixed magnetic field and rf frequency, its magnet was 4 fold symmetry with 4 straight edge sectors. The beam produced by permanent magnetism ECR ion source was injected axially into the central region, then accelerated to 7 MeV/u energy by tow 30° Dees located in the tow opposite magnet valleys, finally extracted through a electrostatic deflector(E1) and a magnetic deflector channel(M2).

ECR Ion Source

The permanent magnetism ECR ion source was designed to produce C^{5+}_{12} beam solely, the beam current was designed to be 200 eμA with 120 π mm.mrad emmitance, the extraction voltage of the ion source was 22.3kV. The configuration of the ion source is illustrated in Fig. 1.

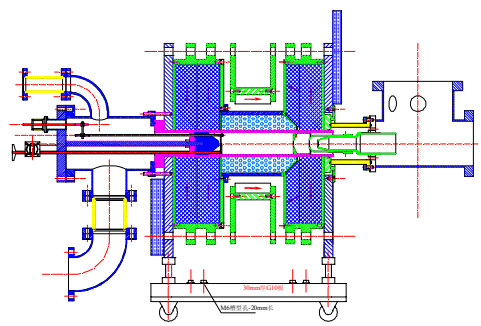

Figure 1: The configuration of the ion source

Magnet

The conceptual design of the 7 MeV/u cyclotron magnet has been performed using OPERA-3D softwar. The B-H magnetization curve of the sectors was measured on the samples, then used in the calculations. The specification of the magnet is given as following. To form the isochronous magnetic field, we cut iron on each sector's surface near the cyclotron median plane, then put a 5 mm thick cover on the sector's surface, changed the quantity of cut iron and the edge shape of cover. The 1/16 model of the magnet is shown in Fig.2. The calculated magnetic field was analysed, the difference of

average field between calculated magnetic field and the ischronous field was less than 10 Gauss in the acceleration zone, the working path of the accelerating particle didn't cross some dangerous resonances. The reults are shown in Fig. 3 and Fig. 4.

Tabel 1: magnet specifications

Outer Radius of the Magnet	1440mm
Height of the Magnet	1600mm
Radius of the Pole	840mm
Mumber of Sectors	4
Sector Angle	56°
Gap between the Hills	50mm
Gap between the Valleys	360mm
Field in Hills	1.87T
Total Weight of Iron	70 t
Ampere-Turn Number of the Main coils	70 kAT

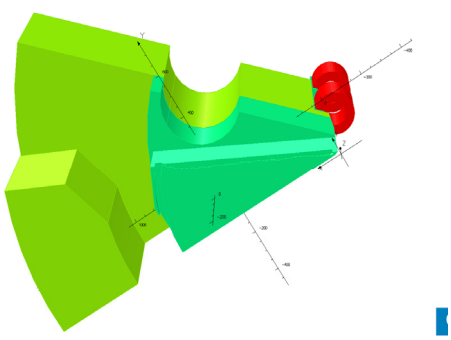

Figure 2: The 1/16 model of the main magnet

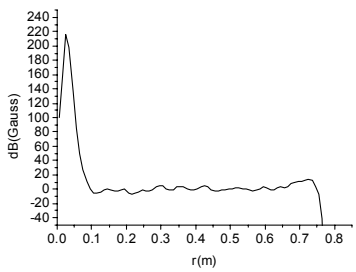

Figure 3: The difference of average field between calculated magnetic field and the ischronous field

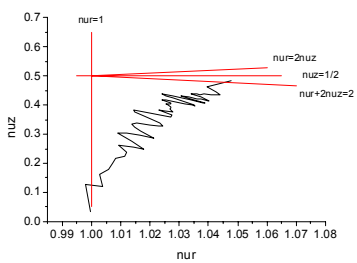

Figure 4: The resonance diagram for the acceleration of C^{5+}_{12} particle

RF System

The 7 MeV/u cyclotron operated on 4 harmonic numbers, the rf frequency of it is 31.02 MHz. The main parameters of the rf system is described in Tabel 2.

Tabel2: Parameters of rf system

rf Frequency	31.02MHz
rf Voltage	70 kV
Harmonic Number	4
Number of Dee	2
Angle of Dee	30°
Outer Radius of Dee	770 mm
Number of Cavity	2
Q Value of Cavity	7800
Dissipated Power per Cavity	18 kW

Tow half wave length cavities were installed into the valleys of the magnet, tow capacitance coupler near the outer radius of Dees imported rf power into cavities, tow 50 kW rf amplifiers connected the couplers with coaxial transmission lines respectively. Near the short plane of cavities, we installed frequency tune device and rf sampling device to tune the cavities tinily.

Fig.5 illustrates the model of one cavity of the cyclotron. The design of rf cavities used the CST Microwave Studio software.

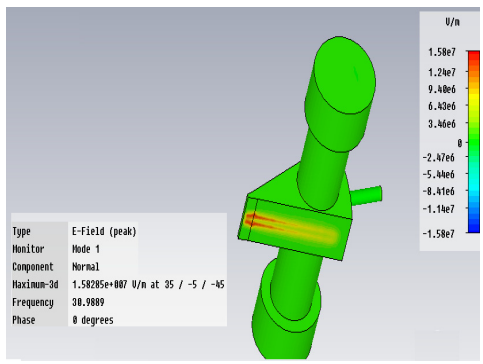

Figure 5: The model of one cavity

The calculation result indicated that the resonant frequency can changed from 30.51 MHz to 31.51 MHz with different position of short plane, the 31.02 MHz frequency could be achieved. The Dee voltage changed from outer radius to inner radius, it was 76 kV at outer radius and 64 kV at inner radius. To extract good quality beam, we requested the stability of rf system to be: rf voltage amplitude stability was $\pm 5\times10^{-4}$/24h, rf frequency stability was $\pm 1\times10^{-6}$/24h, rf phase stability was ±1°.

Vacuum System

The 7 MeV/u cyclotron used upper and lower iron yoke as vacuum seal, the principle vacuum chamber was divided into tow parts above the cyclotron medine plane. The vacuum system was composed of four cryogenic pumps of 5000l/s. The vacuum of priciple chamber was 5×10-7 mbar and the vacuum of injection line was 1×10-7mbar.

Axial Injection Line

The axial injection line was installed on the upper yoke of the cyclotron, beam extracted from ECR ion source transported downstream to the machine central region. The injection line were composed of four solenoids, a double 90º magnetic dipole, a quadrupole, a buncher and a chopper. Beam diagnostical devices contained a double direction slit and a Falady cup. A solenoid behind the ECR ion source, a double 90 º magnetic dipole, a quadrupole and a slit formed a charge analysis system. The injection line was designed by TRACE-3D code, at the entrance of spiral inflector, the emittance of the beam was waist in tow horizontal planes, where the envelope of the beam is 2.5 mm. The scheme of axial injection line is shown in Fig. 6, the beam envelope through the injection line is shown in Fig.7.

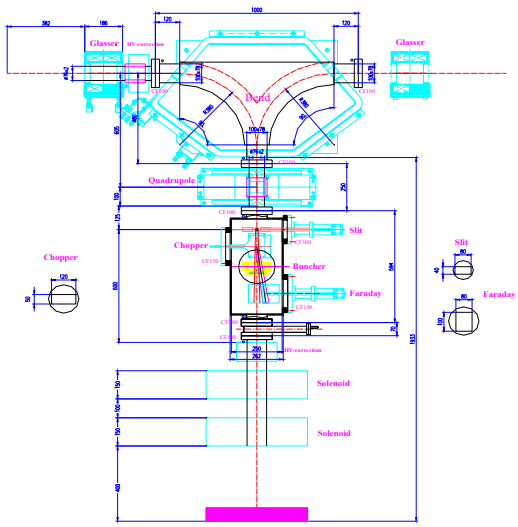

Figure 6: The scheme of axial injection line

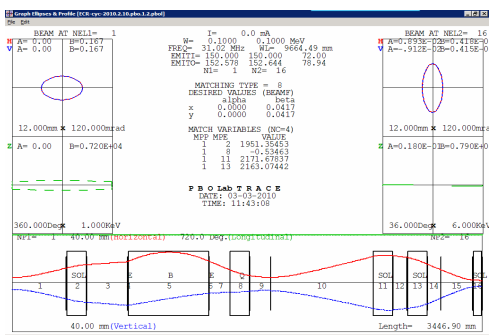

Figure 7: The beam envelope of the injection line

The Central Region

At the beginning of central region design, we found the accelerated equilibrium orbit at large radius, which could be backtraced after the first accelerating gap and matched to a special kind spiral inflector's central particle trajectory. In the calculation, we optimised the geometry of the Dee tip to get matching of energy, position and direction between the backtraced orbit and central trajectory of spiral inflector. So we defined the parameters of the spiral inflector. The chosen parameters of the inflector are described in Table 3.

Table 3: The parameters of spiral inflector

Electric bend radius	30 mm
Magnetic bend radius	27 mm
Electrod spacing	8 mm
Electrod width	16 mm
Orientation angle	-54º
Voltage of electrods	±5.5 kV

To reduce the effect of fringe field of inflector, we cut 3 degree at the exit of the spiral inflector. The electric field of the inflector was calculated by MAFIA code, the model of the inflector is illustrated in Fig.8.

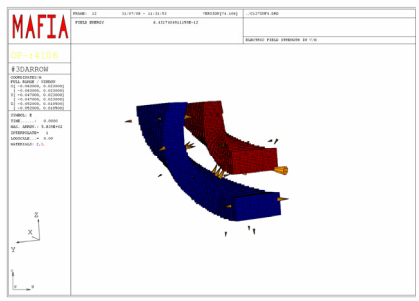

Figure 8: The model of the inflector use by MAFIA

To study beam dynamics in central region, we created 3D model of Dee tip in central region by MAFIA code, and calculated the electric field of the Dee tip. Using the data and magnetic field calculated by OPERA-3D softwar, we studied the orbit motion in the central region. Again we optimised the Dee tip model, espically for the vertical foucus of the injection beam and the centralization of the orbits. The potential lines in the medine plane of the Dee tip electric field is ploted in Fig.9. The orbits that started from inflector exit with different positions and directions, and accelerated six turns were illustrated in Fig.10.

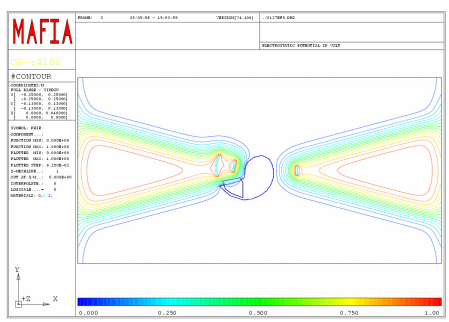

Figure 9: The potential lines in the medine plane of the Dee tip electric field

The Extraction System

The extraction system was composed of a bump coil, a electrostatic deflector(E1), and a a magnetic deflector channel(M2). We could increase the turn separation from 7 mm to 14 mm using the bump field before the entrance of E1. The maximum voltage of E1 was 85 kV with 10 mm gap. The maximum magnetic field of M2 was 1.1 T,

its direction was oppsite to the cyclotron's main magnetic field. To improve the horizontal focus of M2 and reduce its effect to sector's magnetic field in the outer radius, we optimised the M2's design to add a gradient field to it and make its yoke to be magnetic saturation. The scheme of extraction system is shown in Fig. 11.

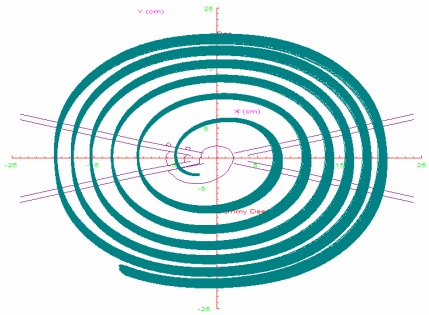

Figure 10: The orbits in the central region

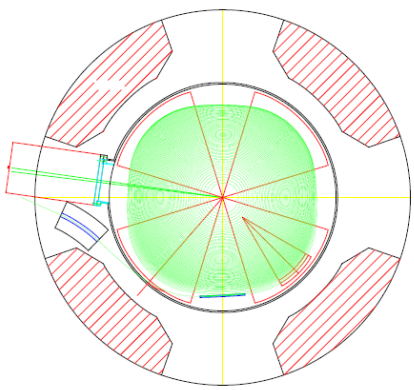

Figure 11: The scheme of extraction system

The Study of Transmission Efficiency

To realize the desiged extraction beam current intesity, we estimated the transmission efficiency of the cyclotron using multi-particles tracing method. Starting from the exit of ECR ion source, with 120 π mm.mrad emmitance beam, we traced this beam to the entrance of inflector, and produced 10,000 particles in the 4D phase space in the horizontal planes, while the energy spread of these particles was ±1%, and rf phase width was ±10° in the longitudinal plane. The calculted bucher efficiency is 45%. Then we traced the particles through inflector, and accelerated them 5 turns, the number of the particles which were not lost was 7997, the injection efficiency was 35%. These 7997 particles were accelerated to be extracted on the end of M2, the calculated extraction efficency was 20%, so the cyclotron's transimission efficency was 7%. It can be satisfy the design requirment. The emmitance of the extract beam was less than 20 π mm.mrad. The energy spread of the extract beam was ± 1%. The emmitance of the extract beam is shown in Fig.12.

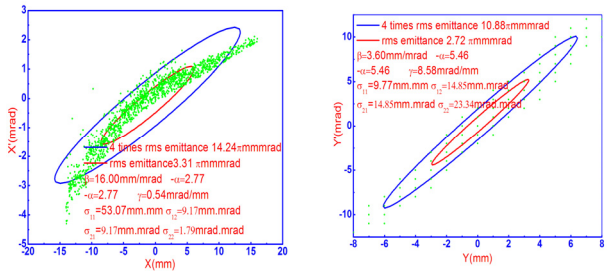

Figure 12: The emmitance of extract beam on the end of M2. Left: the emmitance in (x,x′) plane; Right: the emmitance in (y,y′) plane

CONSTRUCTION PROGRESS

ECR Ion Source

The concept design and engineering design for the permanent magnetism ECR ion source had been completed. We integrate the permanet magnetism material to form the desinged field now in institude of modern physics. The commissioning of this ECR ion source will be in December 2010.

RF System

The construction design of tow 50 kW rf amplifers had been finished. Fabrication of them will be completed in December 2010. The cavity's engineering design is conducted.

Axial Injection Line

The concept design and engineering design for injection line had been finished except the chopper. Apparatuses of the injection line were fabricated in three corporations and will be finished in December 2010.

The power supplies for the magnet coil, injection and ectraction equipments had been contracted with few corporations. The construction of other items, e.g. the magnet, the vaccum chamber, the spiral inflector, the electrostatic deflector is conducted.

CONCLUSION

The beam dynamic study of the 7 MeV/u cyclotron had been completed. From the result of beam dynamic study, the requirment from synchrotron can be achieved by the concept design. Engineering design of the cyclotron is conducted except ECR ion source and rf amplifers.

REFERENCES

[1] J.Q. Zhang et al. "Axial Injection Beam Line of a Compact Cyclotron", these Proceedings.
[2] L.Z. Ma and Q.G. Yao. "The Isochronous Magnetic Field Optimization of HITFiL Cyclotron", these Proceedings.
[3] S.H. Zhang et al. "The RF System Design of 7 MeV Cyclotron", these Proceedings.
[4] H.F. Hao et al. "Beam Extraction System of Compact Cyclotron", these Proceedings.

28GHZ SC-ECRIS AT RIBF

T. Nakagawa, Y. Higurashi, J. Ohnishi, H. Okuno, K. Kusaka, M. Kidera, E. Ikezawa, M. Fujimaki, Y. Sato, Y. Watanabe, M. Komiyama, M. Kase, A. Goto, O. Kamigaito, Y. Yano, RIKEN, Wako, Japan
T. Aihara, M. Tamura, A. Uchiyama, SAS, Ohsaki, Japan.

Abstract

The next generation heavy ion accelerator facility at RIKEN, requires an intense beam of high charged heavy ions. To meet the requirements, we constructed and tested the RIKEN new SC-ECRIS. After producing the first beam in the spring of 2009, we tried to optimize the ion source condition for maximizing the beam intensity with 18GHz microwave. We observed that the gentler field gradient and lager ECR zone size give higher beam intensity. Based on these studies, we produced 500μA of Ar^{11+} and 350μA of Ar^{12+} at the RF power of 1.8kW. We also produced highly charged U ion beam with sputtering method for RIBF. In this article, we describe the structure of the ion source, test experiment and future plan.

INTRODUCTION

Since middle of the 1990s, RIKEN has undertaken construction of new accelerator facility so-called Radio Isotope Beam Factory (RIBF) [1] and successfully produced 345MeV/u U beam (~0.4pnA on target) in 2008[2]. Using it, more than 40 new isotopes were produced with the in-flight fission reactions for only 4 days experiment.[3] It is clear that the intense U beam is strong tool to produce new isotopes in the region of medium mass nuclei and to study the mechanisms of the r-process in nuclear synthesis. For these reasons, the intense U beam is strongly demanded. To meet the requirement, we started to construct the new superconducting ECR ion source (SC-ECRIS) which has an optimum magnetic field strength for the operational microwave frequency of 28 GHz. In the end of 2008, we obtained the 102% of the designed value for the magnetic field strength. In the spring of 2009, SC-ECRIS produced first beam with 18GHz microwaves.[4] Since we obtained first beam, we made various test experiments to increase the beam intensity of highly charged heavy ions with 18 GHz microwave. During the test experiments, we tried to produce U ion beam with sputtering method and produced 0.75~2pμA for highly charged U ions (27~35+) at the RF power of ~1.2kW. In the summer of 2010, the ion source was moved from high voltage terminal to the new ion source room. From this winter, it will be used as an external ion source as a new injector system of RIBF to produce intense U and Xe ion beam[5].

DESIGN OF SC-ECRIS

Detailed structure of the ion source was described in ref. [4]. In this section, we briefly mention the structure and excitation test of the SC-coils

Sc-coils

The schematic drawing and photograph of the Sc-coils are shown in Figs.1 and 2. Inside radii of the hexapole and solenoid coils are 102 mm and 170 mm, respectively. Four coils (SL2 ~SL5) can be used for creating a flat magnetic field region between the mirrors. The hexapole magnetic field in the central region is increased by using iron poles, which is same structure as the VENUS.[6] A NbTi-copper conductor is used for coils and these are bath-cooled in liquid helium. The magnetic stored energy is 830 kJ at the design current. 3D calculations of the deformation of the coil assembly were performed with ANSYS [7]. The hexapole coils were dry-wound to work for turn transitions and was vacuum impregnated with epoxy. On the other hand, the solenoid coils were wet-wound with warm epoxy and cured. The ends of the hexapole coils were fixed with a stainless steel ring to support the large radial magnetic force acting on the current return sections. The six solenoids were assembled with stainless steel spacers and tightened with sixty-four long aluminium-alloy bolts that support a repulsive force of approximately 800 kN at the maximum.

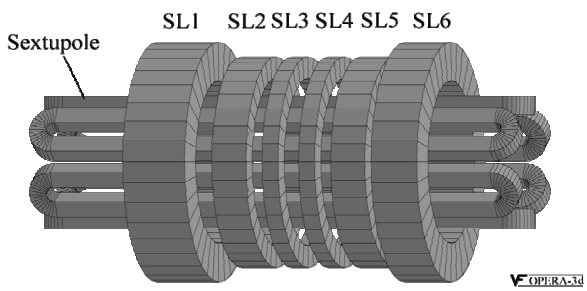

Fig.1 Schematic drawing of the Sc-coils

Using this coil configuration, we can create various shape of mirror magnetic field with six solenoid coils. This magnetic system allows us to produce both of "conventional B_{min}" and "flat B_{min}"[8] configurations. Figure 3 shows the typical axial and radial magnetic field distributions. The maximum axial magnetic fields are 3.8 T at the RF injection side (B_{inj}) and 2.2 T at the beam extraction side (B_{ext}). The maximum hexapole magnetic

field (B_r) is 2.1 T on the inner surface of the plasma chamber (r = 75 mm).

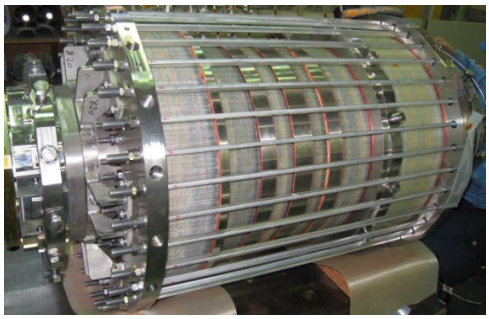

Fig.2 Photograph of Sc-coil assembly for RIKEN SC-ECRIS.

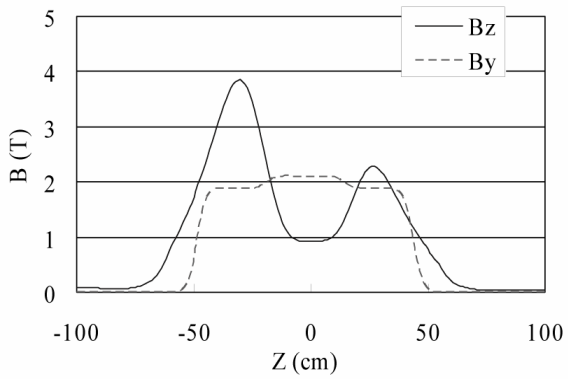

Fig.3 Axial and radial magnetic field distribution

Cryostat

Amount of the liquid-He in the cryostat is ~500 L. The cryostat is equipped with three small GM refrigerators with 4 K, 20K and 70 K stages. Figure 1 shows the schematic drawing of the system. In addition, to increase the cooling power at 4.2K, we use GM-JT refrigerators, which has a cooling power of 4.2W at 4.2K. The nine current leads made of high temperature superconducting material are used to minimize the heat load to 4 K stage. The estimated heat load to 70 K stage is 128 W caused by copper current leads, supports of a cold mass and radiation through the multi-layer insulation.

The maximum electromagnetic force between the magnetic shields and the cold mass is estimated to be 8 tons in axial direction. The cold mass is supported with the belts from an outer tank in room temperature. Four belts with a cross-section of 300 mm^2 are used for the axial direction to support the axial force up to 10 tons. On the other hand, eight belts with a cross-section of 80 mm^2 are used for each of the vertical and horizontal directions to support up to 5 tons. The six solenoids and the hexapole coils are excited individually with seven power supplies. The solenoid coils are excited through seven high temperature superconducting current leads.

Excitation Test

After the solenoid and hexapole coils were assembled, the excitation tests were performed in the cryostat. Figure 4 shows the results of the excitation test. Each solenoid coil achieved the design current without a quench. Next, the hexapole coils was tested. In the combination tests in which the hexapole and one or two of the solenoids were excited at the same time, the hexapole coils quenched in all cases. The hexapole quenched at low currents ranging from 65 A (24%) to 115 A (42%) when the SL1 and the SL2 were excited at their design currents in advance (run #3~#7). The hexapole coils also quenched similarly when the SL6 was excited in advance (run #9, #11). A cause of these quenches was presumed to be a coil motion at the ends of the hexapole coils from the voltage signals, which observed in some of these runs. In run #10, the SL6 was ramped after the hexapole coils was excited at 220 A.

In run #12 and #14~#17, the solenoids and the hexapole coils were excited simultaneously keeping a ratio of the currents. In this case the direction of the force acting on the hexapole coils did not change during the excitation. The quench current of the hexapole increased to more than 85% of the designed value in this way. It, however, was difficult to reach the design current. We have thus concluded that it is necessary to reinforce the structure at the ends of the hexapole coils. After modification, we made a same excitation test as shown in Fig.4. Finally we obtained 102% of designed value without quench.

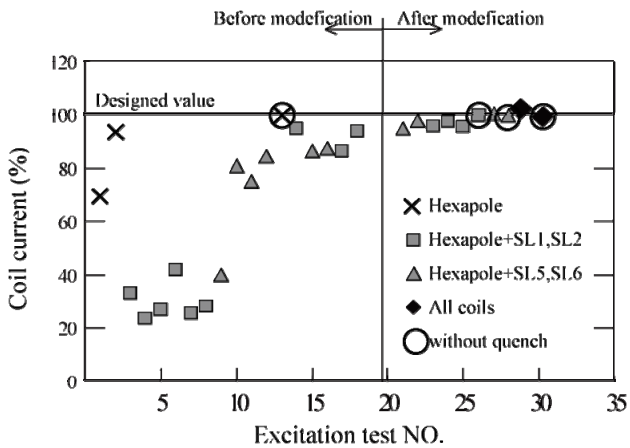

Fig.4 Results of excitation test

Plasma Chamber

Two turbo-molecular pumps (1100L/sec) are placed at the RF injection side and beam extraction side to keep the high vacuum of the plasma chamber. The position of extraction electrode is remotely controlled. The high temperature oven is inserted from the RF injection side. To set the oven on the optimum position, the position of oven is also remotely controlled. The negatively biased disc is placed in the axial direction and its position is remotely controlled with the accuracy of 0.1 mm.

The inner diameter and outer diameter of the plasma chamber are 150 and 164 mm, respectively. The chamber is made of double wall stainless steel tube with the water cooling channel in between. To keep the high voltage (40kV max), the kapton sheets (total thickness of 1.2 mm) covers the plasma chamber. Actual extraction voltage for injecting the ions into the RFQ linac is 22kV, which is lower than the maximum extraction voltage of 40kV.

LBL group demonstrated that the temperature of the cryostat increases with increasing the RF power with 28GHz.[8] It is due to the high energetic X-ray form the ECR plasma. To minimize the X-ray effect when using 28GHz microwave, the plasma chamber will be covered by Ta sheets (total thickness is ~2mm). Figure 5 shows the schematic drawing of the plasma chamber.

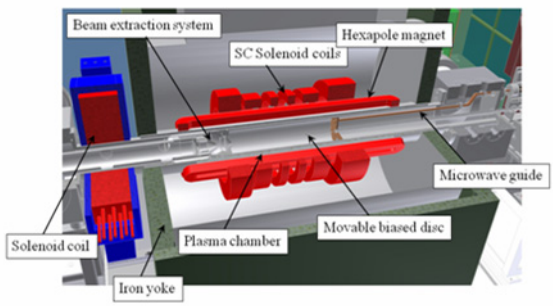

Fig. 5 Schematic drawing of the plasma chamber

LEBT

After the extraction of the beam at 22kV, the solenoid coils is used for focusing the beam. Design of the 90-degree analyzing magnet is based on the LBL one [9]. The vertical gap and bending radius are 150 mm and 510 mm, respectively. The solenoid coil is used to focus the extracted beam. The ion source, solenoid coil, and bending magnet were installed in the ion source room.

The Xe^{20+} and U^{35+} beams are injected into the RFQ linac and then new heavy ion linac for accelerating up to ~0.6 MeV/u.

EXPERIMENTAL RESULTS

Magnetic Field Configuration

To maximize the beam intensity, the optimization of the magnetic field configuration is very important. In the early stage of test experiments, we investigated the effect of the magnetic field configuration on the beam intensity of highly charged heavy ions.[4] In this sub-section, we show the part of these results.

Figure 6 a) shows the beam intensity of Xe^{24+} as a function of B_{min} at the RF power of 300W. The beam intensity gradually increased with increasing B_{min} up to ~0.5T from 15 to 60 eμA. Figure 6 b) shows the charge state distribution of Xe ions for various B_{min}. The average charge state of Xe ions increases with increasing B_{min}. This is mainly due to the effect of the magnetic field gradient at the resonance zone. The gentler field gradient gives lager kinetic energy to the electrons at the resonance zone. As a results, the average kinetic energy of the electron plasma increases with increasing the B_{min}. Therefore the mean charge state of the distribution increases with increasing the B_{min}. To evaluate it, we calculated the field gradient distribution at the resonance zone for several B_{min}. Figure 6 c) shows the field gradient distribution for several B_{min}. It is clearly seen that the field gradient increases form ~700 to ~1800G/cm with decreasing the B_{min} form 0.5 to 0.3T.

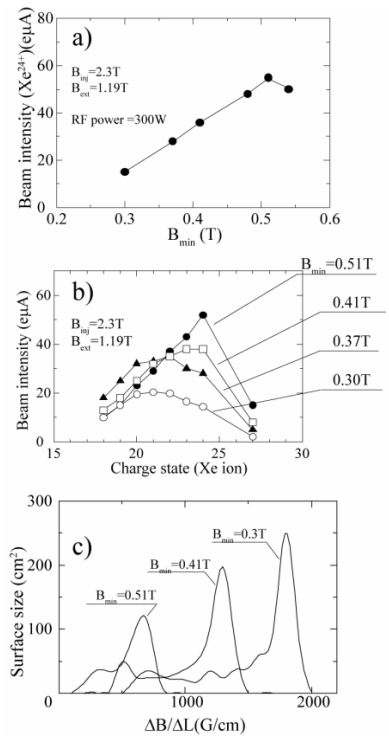

Fig.6 a) beam intensity of Xe^{24+} as a function of B_{min}, b)charge state distribution of Xe ions for several B_{min}. c)Magnetic field gradient distributions for several B_{min}

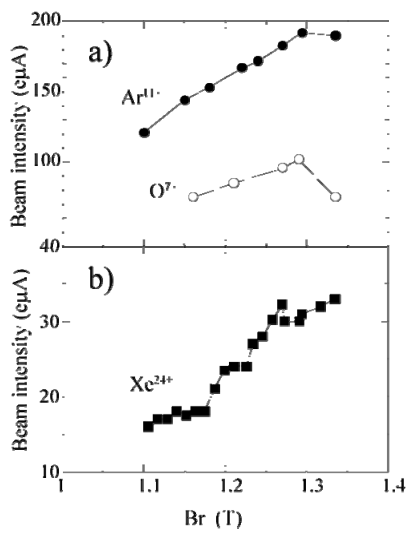

Fig.7 Beam intensity of highly charged heavy ions as a function of B_r

Figure 7 a) shows the beam intensity of Ar^{11+} and O^{7+} as a function of *B*r. The beam intensities seems to be saturated at *B*r~1.3T. On the other hand, the beam intensity of Xe^{24+} gradually increased with increasing the *B*r up to 1.32 T and is not saturated (see Fig. 7 b)). It seems that we need higher *B*r to optimize the beam intensity of highly charged heavy ions.

Effect of Field Gradient and ECR Zone Size

The strong interests for increasing the beam intensity of highly charged heavy ions are the effect of the resonance surface size and field gradient at ECR zone. As described in refs.[10-12], the lager zone size(multiple frequency heating, or broadband microwave radiation) gives higher beam intensity of highly charged heavy ions. As described in the previous section, the ion source has six solenoid coils for creating the mirror magnetic field. Using these coils, the average field gardient at resonance zone (or B_{min}) and surface size of the ECR zone can be changed, independently. It means that one can study these effects on the beam intensity cleraly.

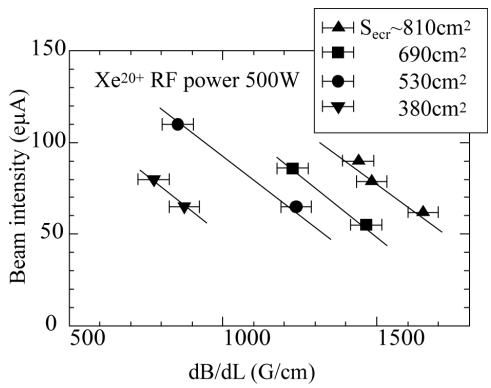

Fig.8 Beam intensity of Xe^{20+} as a function of average field gradient for several ECR zone size

Figure 8 shows the beam intensity of Xe^{20+} as a function of the average magnetic field gradient for several ECR zone sizes at the RF power of 500W. For investigating these effects, B_{inj}, B_{ext} and B_r were fixed to 2.3, 1.2 and 1.3T, respectively. It is clearly seen that the beam intensity increases with decreasing the field gradient. It seems that the beam intensity is higher for larger zone size at same field gradient.

Figure 9 a) and b) show the ratio of highly charged Xe beam intensity between two conditions. The ratio between two different field gradients increases with increasing the charge state (Fig.9 a)) on the other hand, the ratio between different zone sizes are almost constant and independent on the charge state (Fig.9 b)). It is well-known that the energy transfer from microwave to electron increases with the gentler field gradient. The electron temperature becomes higher at the gentler field gradient. For this reason, the production rate of the higher charge state Xe ions increases with increasing the electron temperature.

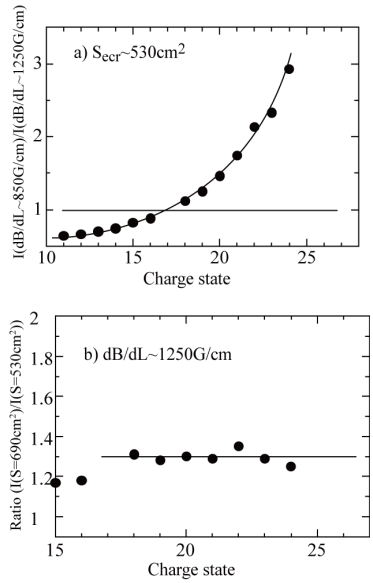

Fig.9 a)Ratio of beam intensity between two different magnetic field gradients ,b)two different ECR zone sizes.

Figure 10 shows the beam intensity of Ar^{11+} as a function of average magnetic field gradient for several ECR zone size. We can see the same tendency as Xe^{20+} case except for the beam intensity at the gentler field gradient (d*B*/d*L* < 800G/cm). Figure 11 shows the beam intensity of Ar^{11+} as a function of RF power under two conditions (A and B). The conditions (field gradient and ECR zone size) A and B are indicated in Fig.11. The beam intensity increases with increasing RF power up to 1.8kW and we obtained 500 eμA of Ar^{11+}

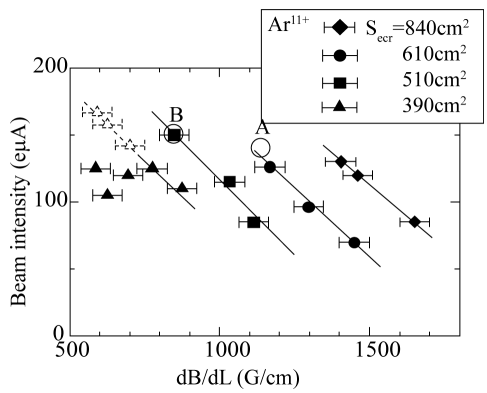

Fig.10 Beam intensity of Ar^{11+} as a function of average field gradient for several ECR zone size

We observed that the beam intensity was almost saturated at the gentler field gradient (d*B*/d*L*<800G/cm) as shown in Fig.12. The estimated beam intensities are shown as the dashed line. Simultaneously, we measured the heat load of the cryostat form the X-rays emitted from plasma. We observed that the heat load increases decreasing the field gradient. The heat load of the cryostat is strongly dependent on the X-ray energy, i.e., higher

energy X-ray gives large heat load. It means that the very high energetic electron was generated at *dB/dL*<800G/cm. We observed same tendency for Ar^{12+} and higher RF power (>1kW)(see figs. 13 and 14). It is still unclear why we do not obtain higher beam intensity in this region. To understand this phenomenon, we need further investigations.

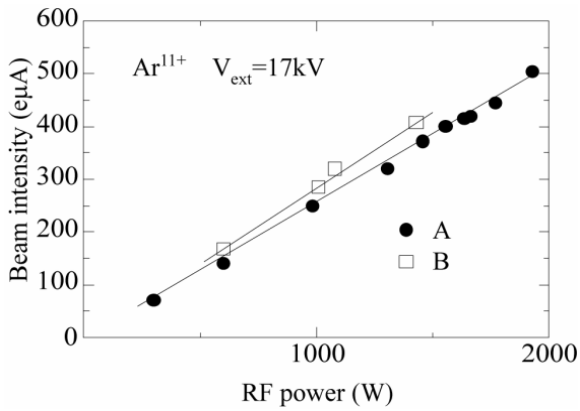

Fig. 11 Beam intensity of Ar^{11+} as a function of RF power.

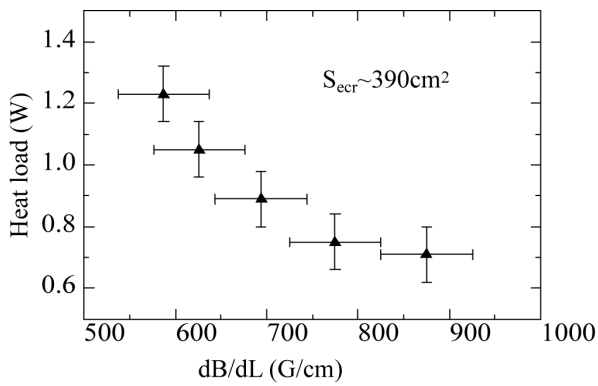

Fig.12 Heat load of X-ray as a function of magnetic field gardient.

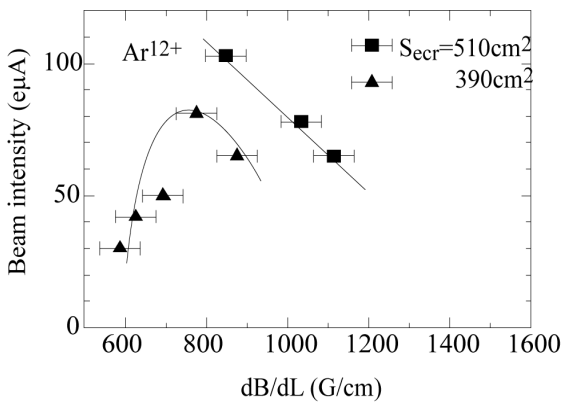

Fig.13 Beam intensity of Ar^{12+} as a function of magnetic field gradient.

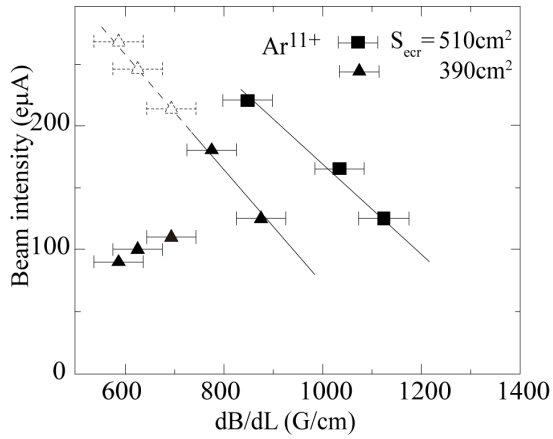

Fig.14 Beam intensity of Ar^{11+} as a function of magnetic field gradient at the RF power of 1kW.

U Beam Production

To produce highly charged U ion beam, we used the sputtering method. Figure 15 shows the beam intensity of U ion as a function of RF power(upper) and the beam intensity of highly charged U ion beam at the RF power of 1.2kW. The extraction voltage was 15kV. The beam intensity of U^{35+} was ~25eμA, which is 12 times as high as that for RIKEN 18 GHz ECRIS.

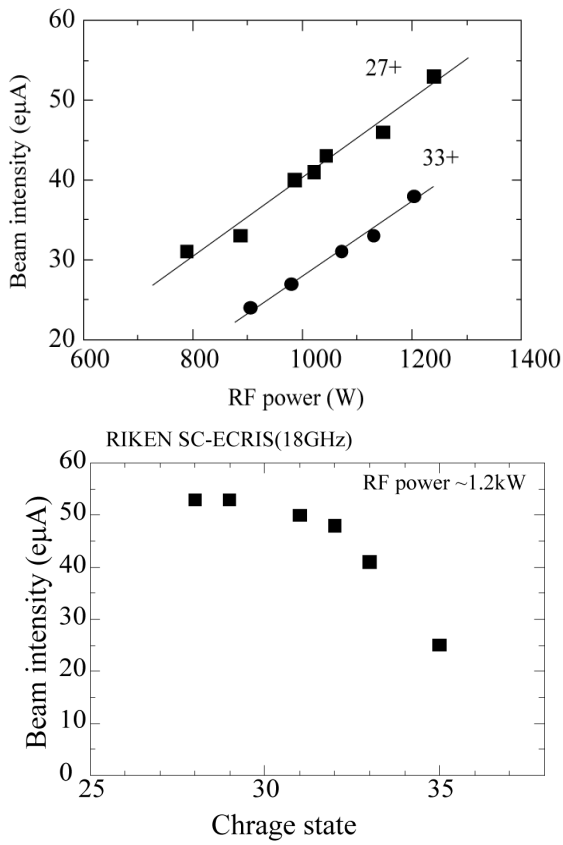

Fig.15 Beam intensity of U $^{27+ \text{ and } 33+}$ as a function of RF power(upper) and beam intensity of highly charged U ion at the RF power of 1.2kW(lower)

It is noted that the beam intensities were not saturated in this test experiment as shown in Figs.15. Because the power density of RF power in this experiment was very low (~100W/L). We may obtain higher beam intensity at the higher sputtering voltage and RF power.

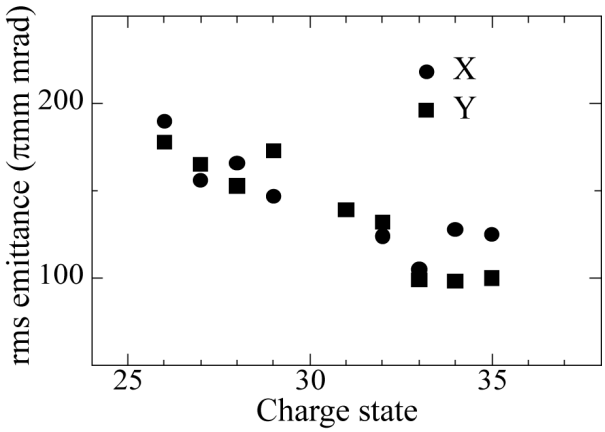

Fig.16 4rms emittance for highly charged U ion.

Figure 16 shows the X and Y emittance (4rms) for highly charged U(26~35+) ions. The emittance decreased with increasing the charge state at same extraction voltage. In this experiment, we obtained the ~ 100πmm mrad for U^{35+}. This is smaller than the acceptance of the accelerator of the RIKEN RIBF (~160 πmm mrad). It means that we can accelerate almost of the U^{35+} beam produced form RRIKEN SC-ECRIS at present.

FUTURE PLAN

It is obvious that the higher frequency gives higher beam intensity of highly charged heavy ions, if we can make optimum magnetic field distribution for higher frequency. To increase the beam intensity of highly charged U ions, we will operate the new SC-ECRIS with 28GHz microwave instead of 18GHz after moving the ion source to the ion source room for new injector system of the RIBF in the summer of 2010. The 28GHz gyrotorn was already installed and tested at RIKEN in this spring of 2010. In the winter of 2010, the test with uranium will be made to meet the requirement of the RIKEN RIB factory project

REFERENCES

[1] Y. Yano, Nucl. Instrum. Methods B261(2007)1009
[2] N. Fukunishi et al, PAC'09, Vancouver, May 2009, MO3GRI01.
[3] T. Ohnishi et al, J. Phys. Soc. Jpn. 77(2010)073201
[4] T. Nakagawa et al, Rev. Sci. Instrum. 81(2010) 02A320
[5] O. Kamigaito et al, Cyclotron'10, Lanzhou, Sept. 2010, TUM2CIO01
[6] C. Taylor et al, IEEE Trans. Applied Superconductivity, 224, 2000
[7] Ansys (http://ansysn.com)
[8] G. D. Alton, and D. N. Smithe, Rev. Sci. Instrum. 65(1994)775
[9] M. Leitner et.al, Proc. Of the 15th Int. Workshop on ECr ion sources, Jyvaskyla, Finland, 2002,p32
[10] X. Q. Xie and C. Lyneis, Rev. Sci. Instrum. 66 (1995)4218
[11] G. Alton et al, Rev. Sci. Instrum. 69(1998)2305
[12] Y. Kawai et al, Phys. Letter A371(2007)307

NEW TOOLS FOR THE IMPROVEMENT OF BEAM BRIGHTNESS IN ECR ION SOURCES *

S. Gammino1#, L. Celona1, D. Mascali1,2 and G. Ciavola1
1INFN - Laboratori Nazionali del Sud,via S. Sofia 62, 95123 Catania, Italy
2CSFNSM, Viale A. Doria 6, 95125, Catania, Italy

Abstract

According to the model that has driven the development of ECRIS in the last years, a large variation of the pumping microwave frequency (order of GHz) along with the proportional increase of the magnetic field boosts the extracted current for each charge state because of a larger plasma density. Recent experiments have demonstrated that even slight frequency's changes (of the order of MHz) considerably influence the output current, and what's more important, even the extracted beam properties (beam shape, brightness and emittance) are affected. A number of tests have been carried out in the last few years and they will be reviewed along with the results of numerical simulations which are able to explain the observed phenomena. The frequency has been systematically changed and the beam output has been recorded either in terms of charge state distributions and beam emittance. The detected bremsstrahlung X-rays are additionally analysed: they give insights about the electron energy distribution function (EEDF). An overview about the possible future improvements of ECR ion source will be given.

INTRODUCTION

Forthcoming projects aiming to radioactive beams production will be very demanding by the point of view of primary beam intensities and charge states. In this context the ion sources, being the first ring of the accelerator chain, will play roles of growing importance. ECRIS (electron cyclotron resonance ion sources) are largely used on these purpose, because of their ability to produce, in CW and pulsed operations, intense currents of multicharged ions.

However the improvement of ECRIS performances, based on the increase of either microwave frequency (it enhances the plasma density, then the output current) and mirror ratio of the magnetic trap (it confines ions for longer times in order to obtain higher charge states), is now close to saturation, limited by the reliability of the magnets and by the costs.

Concerning the generators, the limitations come not by technology but by the basic principles of plasma heating in multi-mirror devices. Experiments carried out on last generation sources, in fact, have revealed that at frequencies of the order of 28 GHz (with power levels of few kW) suprathermal electrons, with energies of the order of 1-2 MeV, are largely produced. According to theoretical and empirical estimations [1, 2], their number grows with the pumping frequency, and at 28 GHz it is already close to the limits which ensure the safety of the magnetic system. These particles in fact produce large amounts of hard X-rays, which are then partially absorbed inside the cryostat surrounding the superconducting magnets, leading to the boil-off of the liquid helium. Deterioration of the high voltage insulators was also observed. Suprathermal electrons are also useless because their ionization rate vanishes at so high energies. Their nature is still not explained by the current theories describing the ECR heating mechanism, which do not predict electron energies larger than 200-300 keV. Anyway, considering experimental data shown in [3], their production mechanism appears to be strongly related to the magnetic gradient at the ECR, and more generally to the mirror trap profile (taking into account also the distance of the resonance from the minimum field position).

ALTERNATIVE PLASMA HEATING SCHEMES

The necessity to overcome models based on semi-empirical approaches was enunciated already in the last decade of XX century by Richard Geller in order to make advances in terms of extracted currents and production of highly charged ions. For this reason several alternative heating schemes were proposed, by different teams spread over the world. The first one appeared in 1994 and it was named Two Frequency Heating (TFH): it consists in the use of two waves at different frequency instead of one [4], both carrying a total amount of power that is approximately the same of a single wave. It has been observed that the charge state distribution (CSD) peak shifts to higher charge states, and a current increase of a factor 2–4 can be obtained for the highest charge states.

Other variants on plasma ignition schemes were brought at ORNL, using a broadband generator or a flat-B field configuration [5] (i.e. shaping the magnetic field with a quasi-constant profile at the ECR position), but they did not provide remarkable benefits. In some cases they even worsen the performances, producing huge amount of hot electrons.

In the years 2001 – 2004 some controversial results were obtained at INFN-LNS of Catania [6], where the plasma was alternatively heated by TWT or Klystrons: using the first generator the current of each charge state increased considerably, and/or operations at much lower power levels than klystrons were possible, obtaining the

*Work supported by NTA – HELIOS Strategic Project and by 5th Nat. Comm. (INES experiment) of INFN.
#gammino@lns.infn.it

same performances. These results finally led to the so-called "Frequency Tuning Effect", which permits to optimize the source performance easily and in affordable way. It has been demonstrated that the different behaviour of the source when using TWT or Klystrons was due to the different -although very close – pumping frequencies used for the plasma ignition. If the pumping frequency is slightly tuned (few MHz over the several GHz used in modern devices) the average charge state and the output currents – especially for the highly charged ions– change remarkably. This effect can be also coupled to TFH, providing huge benefits to the source performances: when the TFH was tested with the SERSE source at INFN-LNS for the first time the importance of tunable frequency generators, like TWT, to fully exploit the potentialities of the double frequency heating was put in evidence.

Since 2005 several efforts have been paid to the modelling of this phenomenon, and main results are reported in [7, 8, 9, 10].

In TFH the two frequencies usually differ of about 3–4 GHz, but anyway not less than 1 GHz. It is a common idea that in the TFH mode the two frequencies have to be well separated. However, analytical calculations and numerical simulations presented in [7] showed that very close frequencies (of the order of few hundreds of MHz) could help to heat the plasma electrons more rapidly, thus improving the ionization rate, providing that a proper phase shift holds between the two waves. This effect can be denominated Two Close Frequency Heating Effect, and appropriate tests with the SERSE source of LNS is scheduled.

MODELLING OF ELECTRON AND ION DYNAMICS

We developed a numerical code implemented in MATLAB in order to follow the electron and ion dynamics by means of a MonteCarlo collisional approach. More details are available in [8, 9, 10]. We performed fully 3D collisional simulations of ECRIS plasma, splitting the electron and ion dynamics, and looking separately to their time evolution. A SERSE-like device has been implemented in our code, assuming a plasma chamber length of 45 cm, and radius 6.5 cm.

In a fully 3D MC simulation the B-min field can be correctly reproduced, in Cartesian coordinates, by using the following formulas:

$$B_x = -B_1 xz + 2Sxy$$

$$B_y = -B_1 yz + 2S(x^2 - y^2)$$

$$Bz = \begin{cases} -B_0 + B_{inj} z^2 & \forall z < 0 \\ -B_0 + B_{ext} z^2 & \forall z > 0 \end{cases}$$

The magnetic field for 14 GHz (B_{ext}=1.2 T, B_{inj}=2.2 T, B_{min}=0.3 T, B_{hex}=1.2 T) is correctly reproduced with B_0=0.3 T, B_{inj}=25 T/m^2, B_{ext}=36.5 T/m^2 and S=360. The collision probability is calculated according to a well known Monte-Carlo technique, once known the characteristic time of Spitzer collisions for particles moving at velocity v:

$$P(t) = 1 - \exp\left(-\frac{t}{\tau_{coll}}\right) \qquad \tau_{coll} = \frac{M_{i,e}^2 2\pi\varepsilon_0^2 v_{i,e}^3}{n_e z^4 e^4 \ln\Lambda}$$

Where z is the ion charge state (it is z=1 for electrons) and ln Λ the so called Coulomb logarithm. The MonteCarlo hybrid code solves the relativistic Landau equation [11] for electrons and a non relativistic equation for ions:

$$\frac{d\vec{v}}{dt} = \frac{q}{M}\left[\vec{v}\times\vec{B} + \vec{E}_s\right] \qquad (i)$$

$$\frac{d\vec{v}}{dt} = \frac{q}{m}\left(1 - \frac{v^2}{c^2}\right)^{3/2}\left[\vec{v}\times\vec{B}_S + \vec{v}\times\vec{B}_{em} + \vec{E}_{em} - \frac{1}{c^2}\left(\vec{E}_{em}\cdot\vec{v}\right)\vec{v}\right] \qquad (e)$$

where E_s the electrostatic field over the resonance surface of the plasma, which can be perturbed by eventual fluctuations of the electron density [8, 10].

The crucial assumption of our model is that the source chamber works as a resonant cavity even when filled by the plasma, which just shifts the resonance frequencies proportionally to the electron density, and introduces an absorption term in the eigen-field equation of the cavity. Experiments performed so far demonstrate that mode patterns still persist in high density absorbing plasmas [12].

THE FREQUENCY TUNING EFFECT

After the experimental evidences which confirmed the effectiveness of frequency tuning on the improvements of ECRIS performances, it was argued that the FTE was based on the coupling properties between the microwave generator and the plasma chamber. Several experiments were carried out in order to measure the reflection coefficient of the plasma chamber fed by rectangular waveguides [10, 12]. Resonant modes can be identified in correspondence to the minima of the reflection coefficient. From the experimental data generally appeared that the current signal was peaked on frequencies corresponding to modes, because of a better coupling. However this is not a strict rule: in some cases, although the matching of the microwave line with the source (cavity plus plasma) is optimal, the extracted current remains low. Therefore we must distinguish between the microwave generator-to-plasma chamber coupling and the excited mode-to-plasma coupling. In the latter case, as formerly explained in [8, 9, 10], the mode spatial structure plays the main role.In ECRIS the conditions for the electron cyclotron resonance are fulfilled over a characteristic egg-like structure defined as ECR surface. According to simulations, the heating rapidity is strongly regulated by the electromagnetic field pattern over the resonance surface. The structure of the electromagnetic field is regulated by the triplet of numbers which identifies each mode at a given frequency: $TE_{n,m,r}$ or $TM_{n,m,r}$.

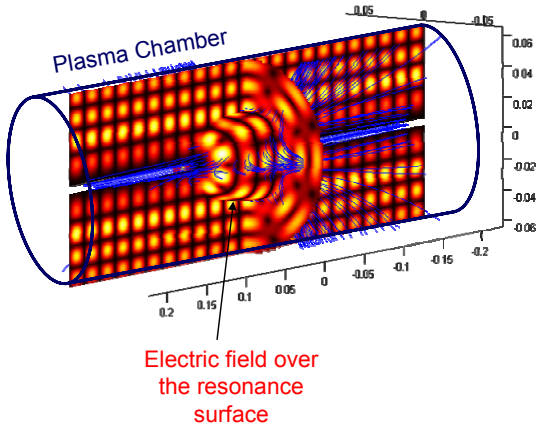

Figure 1: example of electromagnetic field distribution inside the plasma chamber for $TE_{4,4,23}$ mode excited at 14.05 GHz (light areas correspond to high field). The structure of the magnetic field lines is also shown.

Modes with high values of the triplet of integer numbers n, m, r have many maxima and minima inside the plasma chamber, and several of them intercept the resonance surface (see figure 1).

The heating process depends on the matching between areas characterized by high values of electric field with the electron fluxes, which at first approximation follow the magnetic field lines. According to simulations [9] a more or less efficient matching affects mostly the heating rapidity from the cold (1-1000 eV) to the warm (1-100 keV) population. Considering a SERSE-like device after 10-15 passages through the resonance, corresponding to about 50 ns, when the pumping frequency is varied within 50 MHz around 14 GHz, electron mean energy fluctuations are about a factor 5 to 6, (for some modes electrons reach 2-3 keV of average energy, for others up to 15-18 keV, keeping constant the RF power and the Q factor of the cavity). More recent simulations reveal that the energy gain for electrons saturates after 200-300 ns: then electrons are lost because of pitch-angle scattering into the loss cone. In order to correctly reproduce the real energy of electrons we used a high Q (10^4) factor for the cavity. Therefore the frequency tuning regulates the final temperature of the warm electron component. The suprathermal electrons are not influenced by the tuning of the frequency, as confirmed also by experimental results reported in figure 2. These measurements were done with the CAESAR source at LNS, by detecting X-rays and by collecting the corresponding Charge State Distribution at a given frequency. Note that the slope of the high energy part does not change with the frequency, meaning that the temperature of the hottest plasma component was unchanged.

Up to now we have considered the frequency tuning influence on the electron dynamics, and more specifically on the heating rapidity. However, the experimental results put in evidence that this picture is not exhaustive, and it

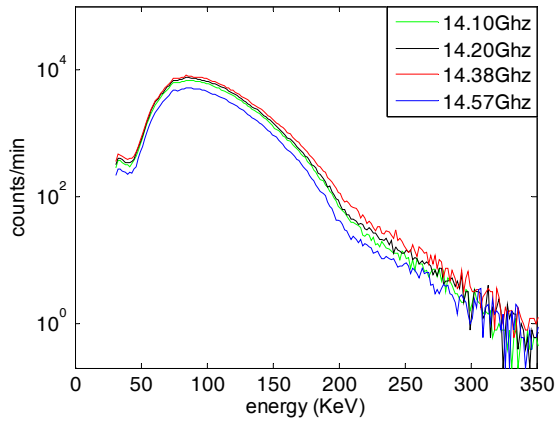

Figure 2: X-ray spectra obtained at different pumping frequency with the CAESAR source at LNS.

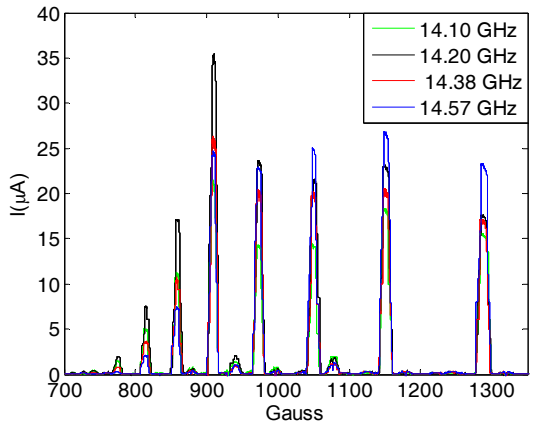

Figure 3: charge state distribution for Kr obtained at different frequencies (tests with CAESAR at LNS).

does not explain all the consequence of the heting scheme.

Figure 3 shows that the highest charge states are more influenced by FTE, as observed in previous experiments. Figure 4 shows the trend of detected X-rays integrated over fixed energy intervals, and plotted versus the pumping frequency. At 14.38 GHz the maximum number of counts was revealed, but the same frequency produces relatively low currents and even a lower mean charge state. Considering the relation $< q > \propto n_e \tau_i$, being n_e the electron density and τ_i the ion lifetime, and assuming that the number of X-ray counts is somehow linked to the electron density, the results in figure 3 and 4 can be explained only by taking into account a possible influence of FTE on the ion dynamics (τ_i changes more than n_e). Interesting data on the ion dynamics were taken already in 2008: strong variations of the beam shape were observed when changing the pumping frequency in the CAPRICE source of GSI [13]. Since then, a plenty of data have demonstrated the influence of the frequency tuning on the beam dynamics (e.g. at JYFL of 2009 and 2010 [14, 15]).

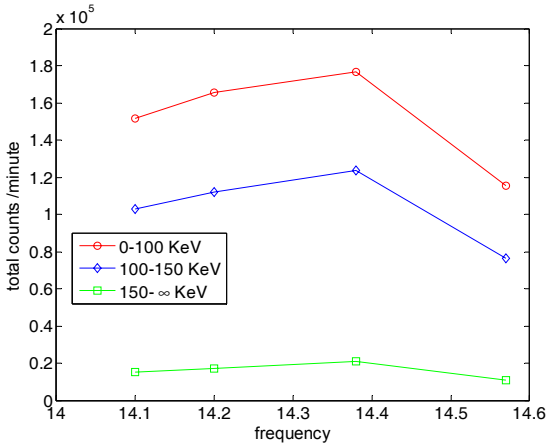

Figure 4: total counts of detected X-rays at different energy ranges versus the pumping frequency (tests with CAESAR at LNS).

The very recent experiments at JYFL have revealed that the crucial game in the next future will be played in the phase space: the transmission through the cyclotron was measured at different frequencies; it came out that the transmission coefficient depends more on the mismatch in the phase space (emittance of the source versus acceptance of the cyclotron) rather than on the beam current.

Results presented before, and largely discussed in [8, 10], put in evidence for the first time the strong relationship between electron and ion dynamics, which usually have been considered uncoupled because of the different timescales.

Several items are explained in such a way:

- ECRIS beams triangular-three arm shape can be explained assuming that the ions are magnetized in their last path towards the extraction hole, whereas they are collisional in the inner resonance region;
- The electromagnetic field pattern concerning a given excited mode changes the plasma structure in such a way that the ion motion is influenced strongly by density fluctuations.
- Inner plasma scattering mechanisms, due to non-homogeneities in the plasma structure, characterize the beam emittance.

According with our simulations, the ions are affected strongly by any fluctuation of plasma density in correspondence of the resonance surface. Looking to data presented in [10], it can be noticed that the plasma is almost completely confined inside the resonance surface. Only poorly populated fluxes of plasma particles are evident, close to the plasma chamber axis. This additional confinement provided by the electromagnetic field inside the ECR enclosed volume is due to the rapid increase of the electron perpendicular velocity (with respect to the magnetic field lines), which expels the particle from the mirror loss cone. Many of the low energy electrons reach energies on the order of keV after a single resonance crossing, then they begin to oscillate in the mirror, turning at the resonance value of the magnetic field. This mechanism has been observed also by PIC simulations: a steady state structure of the electron density appears after few tens of ns and lasts for times longer than tens or even hundreds of μs. The inner resonance plasma reaches densities at least three times larger than the outer one. More recent results [10] demonstrated that this accumulation of plasma electrons inside the ECR volume is regulated by the strength of the electromagnetic field over the resonance surface: where the electromagnetic field is higher, there will be a denser plasma. This characteristic plasma distribution influences the ion dynamics. The surface of the inner resonance plasma no longer coincides with the egg-shaped resonance area, because of density fluctuations, and the plasma surface corrugates, according to figure 5. This corrugation has remarkable consequences:

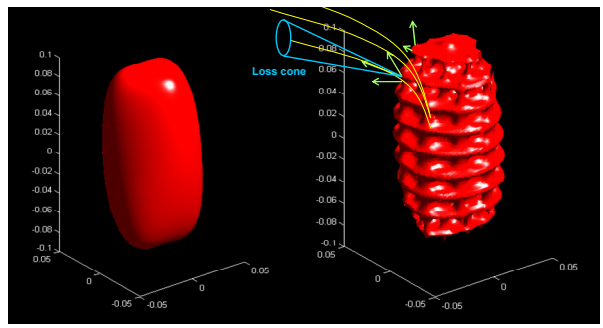

Figure 5: Smooth (left) and corrugated (right) isodensity surface of the primary plasma: the corrugation depends on the particular pattern of the electromagnetic field.

In order to preserve the quasi-neutrality, ions are accelerated when crossing the boundary between the high-density inner resonance plasma and the low density-outer resonance plasma. In fact, the electron density drops quite rapidly outside the volume enclosed by the ECR. Ions are then partially reflected, partially accelerated when passing from inner resonance plasma to the outer one, fitting the shape of the electron density distribution. Ions are dynamically confined by collisions in the inner resonance-high density plasma; in the outer-resonance plasma, because of the lower density, the number of collisions drastically decreases and the ions feel the magnetostatic field. Localization of density perturbs the ion trajectories and the plasma surface corrugation originates the ions' scattering along their path towards the extraction hole. The ambipolar electric field is directed towards the density gradients, i.e. everywhere perpendicularly to the corrugated surface (see the coloured arrows in figure 5 – right). Corrugation of the inner resonance plasma surface can introduce more or less ions into the lateral loss cones, thus decreasing the axial output current.

Therefore the following situation may be conceived: a given mode is able to rapidly move the electrons from the cold to the warm population (effect on heating rapidity – electron dynamics) but the configuration of the inner resonance density scatters the ions mostly laterally.

Therefore the number of highly charged ions in the output current will be very low and the source performances will be worse (the influence on ion lifetime is enhanced). For some other modes, the scattering may be less pronounced (thus producing high current beams) but the ions may still have large perpendicular components (with respect to the plasma chamber axis) that results in a higher emittance.
In addition, simulations put also in evidence a depletion of plasma density in the near axis region: this may be at the basis of hollow beams. The only way to reduce the around axis accumulation of plasma, flattening the density, is the excitation of modes with maxima even in the region close to x=y=0.

DISCUSSION AND PERSPECTIVES

Our modelling demonstrates that different modes excited into the plasma chamber produce different shapes of the output beam. This relationship between the mode structure and the beam emittance is confirmed by experiments on simpler devices like the microwave discharge ion sources working at 2.45 GHz. Low order modes are excited, and the extracted beam is not hollow at low currents, becoming hollow at large intensities because of space charge effects. In ECRIS, high order modes are typically excited, due to the physical size of the plasma chamber which is much higher than the operating wavelength. The main consequence is that the first two index of the excited mode are generally greater than one, resulting in electric fields having the maxima off-axis and low values in regions close to the plasma chamber axis.

Studies with the state-of-art electromagnetic simulators will start quite soon, trying to find some solutions to this problem. Non-cylindrical shapes of the plasma chamber may be tested, in order to better adapt the structure of the electromagnetic field to the resonance surface shape.

The above presented model well explains the frequency tuning effect as a consequence of the mode structure. FTE helps to improve ECRIS performances without any modification to the hardware of the source, permitting to overcome the limitations of the current semi-empirical scaling laws for the frequency (over GHz range) and the magnetic field. Therefore it could permit to fully exploit the potentialities of already existing devices, operating in a frequency range 6.4 – 28 GHz. Variable frequency microwave generators are needed; TWT amplifiers are preferable because of their versatility in changing the output frequency. For third generation sources, which make use of Gyrotrons at 28 GHz, Gyro-TWT should be employed, conjugating the requirements of high frequencies (Gyrotron) devices with the easy tuning ensured by TWT-based amplifiers.

Any further step forward, made by increasing the pumping frequency (and the magnetic field accordingly), will be possible only when problems coming from the very energetic electrons will be solved. Some tools are under investigation at LNS on this subject. Active electron donors, like carbon nanotubes based electron guns, have been successfully tested with the CAESAR source of LNS [16]: they allowed to damp the hot electron component by means of the injection of electron beams (some mA of electron currents) into the plasma.

Theoretical investigations aiming to the comprehension of the generation mechanisms of hot electrons will be continued at LNS. The magnetic field profile, and especially the gradient at the resonance point, is the main parameter affecting the electron energy distribution function (EEDF), and simulations will be improved to determine the time evolution of EEDF at different field profiles.

On this purpose, the theoretical approach will include also self-consistent interactions between electrons and ions in order to correctly determine the inner plasma ambipolar potentials. Some efforts will be devoted to the computing time: the present version of the code is really time-consuming, requiring one week of calculations for 2500 particles (ions or electrons) over 5 microseconds (for electrons) or 200 (for ions). We plan to migrate on a GRID computing environment, in order to get the availability of about 180 CPUs in the next months, taking advantages also of the code parallelization.

REFERENCES

[1] F. Jeager, A. J. Lichtenberg, and M. A. Lieberman Plasma Phys., Feb. 1973. vol. 15, no. 2, pp. 125 -150.
[2] D. Leitner et al, Rev. Sci. Instrum., Feb. 2008. vol. 79, no. 2, p. 02A 325.
[3] S. Gammino et al., Plasma Sources Sci. Technol. 18 (2009) 045016.
[4] Z.Q. Xie and C. M. Lyneis. Proc. 12th Int.Workshop ECR Ion Sources, Tokyo, Japan, 1995.
[5] G. D. Alton, Nuclear Inst. Meth. A 382, 276, 1996.
[6] L. Celona et al., Proc. 16th Int. Workshop ECR Ion Sources, Berkley, California (USA), 2004.
[7] S. Gammino et al., IEEE Transaction on Plasma Science, Vol. 36, 4, part II, August 2008.
[8] D. Mascali, Il Nuovo Cimento B, DOI 10.1393/ncb/i2010-10899-9, July 2010.
[9] D. Mascali at al., Rev. Sci. Instrum. 81, (2010), 02A334.
[10] D. Mascali, et al., Proc. 19th Int. Workshop ECR Ion Sources, Grenoble, France, August 2010.
[11] L.D. Landau, E.M. Lifshitz (1975). The Classical Theory of Fields. Vol. 2 (4th ed.). Butterworth Heinemann. ISBN 978-0-750-62768-9.
[12] L. Celona et al., accepted for publication on Eur. Phys Journal D.
[13] L. Celona et al., Rev. Sci. Instrum. 79, 2008, 023305.
[14] V. Toivanen et al. Rev. Sci. Instrum. 81, 02A319, (2010)
[15] V. Toivanen et al. Proc. 19th Int. Workshop ECR Ion Sources, Grenoble, France, August 2010
[16] F. Odorici et al., Proc. 19th Int. Workshop ECR Ion Sources, Grenoble, France, August 2010.

HIGH POWER RF SYSTEMS AND RESONATORS FOR SECTOR CYCLOTRONS

L. Stingelin*, M. Bopp, M. Broennimann, J. Cherix, H. Fitze, M. Schneider, W. Tron
Accelerator Concepts Division, Department Large Research Facilities
Paul Scherrer Institute, 5232 Villigen, Switzerland

Abstract

The Proscan cyclotron is routinely operated for medical cancer treatment and the Injector II and Ring-Cyclotron are routinely used for acceleration of a high intensity proton beam. In the framework of the high intensity upgrade, it is planned to replace two existing 150MHz resonators of the Injector II cyclotron by two new 50MHz resonators. The first prototype resonator has been manufactured by SDMS and first vacuum and RF-measurements have been carried out. Tuners, coupler and pickups have been mounted and high power RF tests are in progress on a teststand. A new building for the RF-installation has been constructed and is ready to house the power amplifiers.

INTRODUCTION

The PSI high intensity accelerator facility routinely accelerates a proton beam of about 2.2mA up to an energy of 590MeV. About 30% of protons are absorbed in the Targets M and E for meson production and 70% of the protons are used in the spallation neutron source (SINQ). This accelerator complex consists of two isochronous, fixed frequency separate sector cyclotrons. The Injector II cyclotron accelerates the proton beam up to an energy of 72MeV which is then transferred to the 590MeV Ring Cyclotron. In 2009, the overall availability of the facility reached about 90% with 8% of outages longer than 5 minutes attributed to the RF systems.

In 2004, a dedicated compact superconducting cyclotron was purchased from ACCEL Instruments GmBH. It routinely accelerates a proton beam up to 250MeV for medical cancer treatment by spot-scanning technique or for treatment of eye-melanoma.

OPERATION OF RF-SYSTEMS

Proscan

The RF-systems of the 250MeV cyclotron (COMET) for cancer treatment has been running without any major problems since 2004. Some minor problems have had to be fixed, such as a broken voltage regulation of the amplifiers. Several RF-contacts were damaged, probably because the field distribution of the dees was not sufficiently well balanced. The RF-window was covered with a metallic layer twice and had to be cleaned.

A newly developed "puller-tip" is now exchangeable and uses tungsten instead of copper to reduce the wear from sputtering.

* Lukas.Stingelin@psi.ch

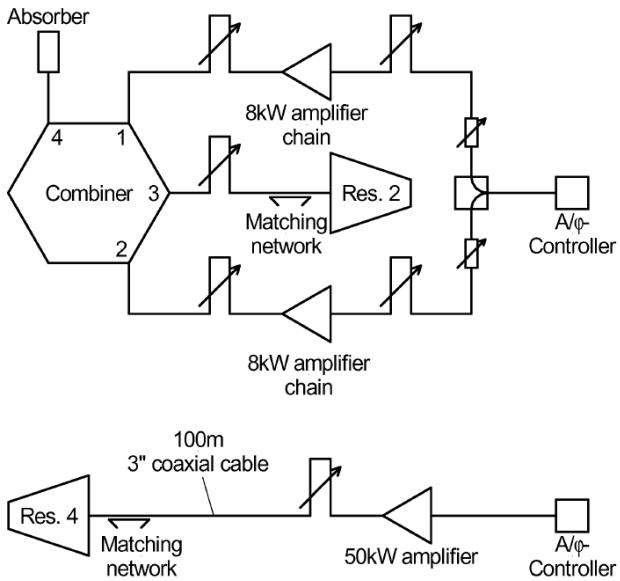

Figure 1: Power distribution in Injector II. The combiner is a 180°-Hybrid ("Rat-Race").

Injector II

The RF system of the 72 MeV Injector [1] consists currently of two double gap-acceleration resonators (50 MHz) and two smaller 150 MHz resonators, which were originally designed as flat-topping resonators. Since the proton bunches are only about 5° long, flat-topping is not efficient and the 150 MHz resonators are therefore operated in acceleration mode.

Fig. 1 shows the present power distribution in Injector II for the Resonators 2 and 4 [2]. Two 150MHz amplifiers are combined to get double power on Resonator 2. A separate power amplifier, located in a different building, is used to feed Resonator 4. This new setup was commissioned in 2003 as a temporary solution, but fortunately has been running since then without major problems. However, tuning and maintenance of the old Resonator 4 amplifier is difficult. A 3dB attenuator was inserted between driver and final amplifier in order to decouple them better and to change the operating point of the driver-amplifier.

Stability problems occurred sometimes when Resonator 4 was switched on after an interrupt. The inner surface of Resonator 4 was then coated with Aquadag [3] to prevent multipactoring by reducing the secondary electron emission coefficient of the surfaces.

590MeV Ring Cyclotron

The new copper cavities are currently operated at a gap voltage of about 850kV and leave some margin for future operation around 1MV. However, the old aluminum flat-top cavity is running at its limit. Its voltage can not be increased further because the cavity cooling is not sufficient, especially at the electrodes. Also, the pressure of the tuning-system is at its limit, as well as the high-power coaxial transmission line to the cavity and the final stage amplifier.

In order to relax the load on the coaxial transmission line, the voltage of the flat-top cavity is reduced when there is no field excited by the proton beam (zero beam current) and is ramped up when the beam-current is increased. The voltage of Cavity 1 is automatically corrected to keep the extraction energy and number of turns constant during this ramp.

The efficiency of the RF system for converting wall plug power is 0.9 for AC/DC conversion, 0.64 for DC/RF conversion and 0.55 for RF to beam power.

RF Radiation Problem in Ring Cyclotron

In 2010, the start-up suffered from plasma effects that were generated in the 590MeV Ring Cyclotron as a result of excessive RF radiation from the 150MHz flat-top cavity. The phenomenology is described also in these proceedings by Zhang et al. [4]. In order to understand the effects better,

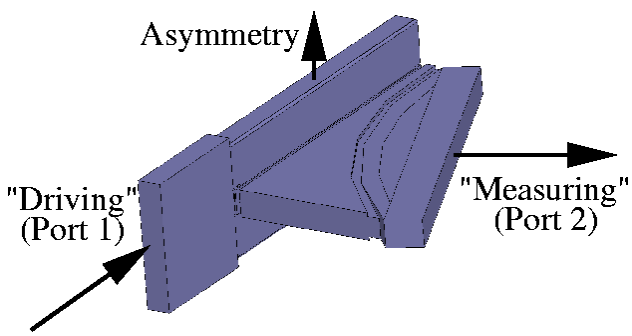

Figure 2: Geometry used for the simulation of the RF radiation from the flat-top cavity.

an attempt was made to simulate the stray RF by the HFSS harmonic solver, analogue to the the method used in 2000 for the main cavities [5]. It was found that the radiated power out of the beam-slot increases almost quadratically with offset of the upper cavity plane. The radiated power has a vertical polarization of the electric field and reaches about 2.5kW when the asymmetry of the upper to lower cavity wall is 4mm. If the flat-top cavity is perfectly symmetric, there should be almost no RF stray field and it might therefore be possible to reduce the stray field by compensating the asymmetry by the hydraulic tuning system acting on the upper and lower part of the cavity.

Since it takes some time to setup the differential tuning system, an other approach to reduce the stray field was also investigated. Unfortunately, a single bar of graphite is not sufficient to absorb the stray field well enough. Simulation and measurement showed that almost no RF power was absorbed. Only the field pattern (mode distribution at port 2) of the radiated power changed but without any benefit to reduce the plasma generation.

Preliminary simulations of a resonant "$\lambda/4$ absorber" indicate that the total radiated power could be reduced by about 5dB. However, more detailled simulations of the entire cyclotron, also with an Eigenmode solver, must be done to confirm these results.

STATUS OF RF-UPGRADE

For the future beam intensity upgrade up to 3mA [6], several RF components have already been added or modified.

- More powerful copper cavities have been installed [7] at the 590MeV Ring Cyclotron in order to increase the acceleration voltage. This increases the turn spacing at extraction of the 590MeV Ring Cyclotron and helps to reduce the turn number to overcome beam degradation due to space charge effects. Installation of the four new copper cavities in the 590MeV Ring Cyclotron was successfully completed during the shutdown 2008.

- A new 150MHz buncher cavity has been installed during the shutdown 2006 on the 870keV injection beamline of the Injector II. The new buncher configuration consists of a 50MHz main buncher followed by a low amplitude 150MHz debunching stage. Together, these two bunchers produce a long linear slope of the effective buncher voltage. Beam experiments proved that the core density of the proton beam could be substantially enhanced and allowed one to reach the nominal production beam intensity at a noticeably lower beam emittance. This results in reduced extraction losses in the Injector II, as well as in the Ring Cyclotron [8].

- A new buncher cavity, ("Super-buncher" in PSI denomination), has been installed in the 72MeV transfer line between the Injector II and the 590MeV Ring Cyclotron.

- The first prototype resonator for the Injector II cyclotron upgrade is currently tested on a high power teststand.

Super-buncher

The goal of the Super-buncher [9] is to restore the narrow phase width of the beam bunches observed at extraction from Injector II at injection into the 590MeV Ring Cyclotron [10, 11]. Since the flat-top cavity of the 590MeV Ring Cyclotron is currently running at the limit of tolerable temperatures and hydraulic pressure of the tuning system,

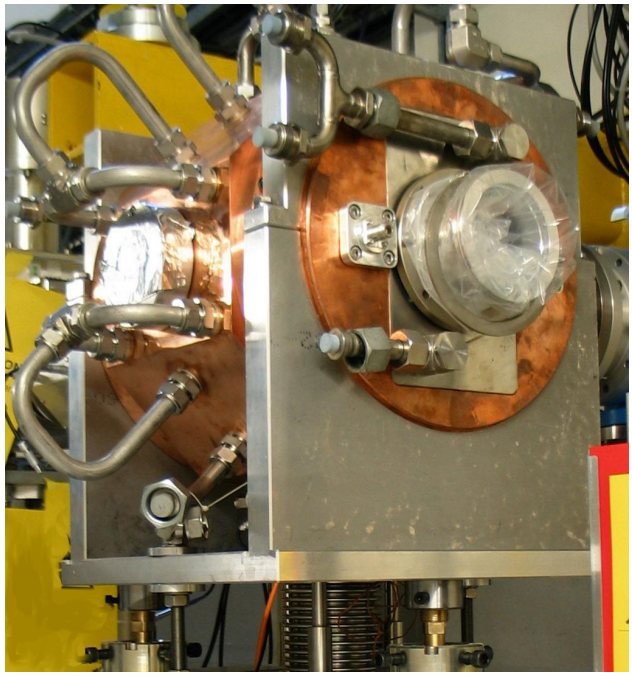

Figure 3: Installation of the Super-buncher in the 72MeV Transferline.

the Super-buncher might help to relax the flat-top cavity or even make it superfluous, as in the case of Injector II.

The Super-buncher is a two-gap drift-tube cavity, operating in the 2π mode [9]. One single stem supports the drift-tube. A standard ELETTRA-type input power coupler is used and a plunger of 6cm diameter and 6cm penetration depth is used for fine-tuning of the resonance.

Table 1: Specification of Super-buncher.

Parameter	Simulated	Measured
Resonance	506.328	
Gap Voltage [kV]	218	
Quality factor [ ]	34000	30'340
Dissipated power [kW]	10	max 20
Tuning range [MHz]	2.34	2.34
Freq. drift vacuum [kHz] [1]	**-127**	**-120**
Freq. drift thermal [kHz]	**-270**	**-260**
@ RF-Power [kW]	30	20
Max. curr. density [A/cm]	**52**	
on RF-contact @ [kW]	20	
Cavity wall material	Cu-OFHC	

Note:

1 The simulated frequency drift from air to vacuum takes only the change of dielectric constant into account. Since the structure is relatively rigid, the geometrical deformation is almost negligible for this case.

The Super-buncher has been manufactured in the PSI main workshop in 2005 from forged OFHC copper. Before the final assembly, it was screwed together, its resonance frequency measured and then fine-machined to get the exact resonance frequency. Tab. 1 shows the comparison of calculated and measured RF-parameters. Simulations have been done with ANSYS multiphysics [12]. Bead-pull measurements also showed very good agreement, within a few percent, of the electric field strength on beam axis with the calculated field distribution.

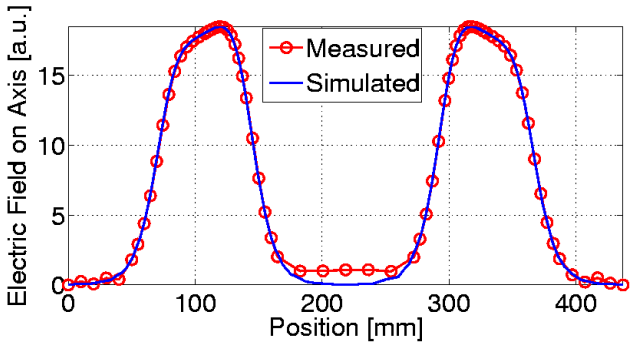

Figure 4: Comparison of simulated and measured electric field on axis by bead-pull method.

The diagram for power tests and operation is indicated in Fig. 5. Several problems had to be faced in the high power teststand:

- At 2 kW CW RF power, a small ceramic window of the inductive RF-pickup probe broke. It was found that the penetration of the pickup was too deep inside the cavity and therefore too much RF power was picked up and the probe over heated. RF pickup probes were then retracted to solve the problem.
- When the RF power was ramped up, the circulator at the output of the power amplifier broke. It is thought that the circulator had been damaged already during the transport to PSI. The circulator was then shipped back to the manufacturer for repair and installation of an arc-detector.
- After a 6h testrun at 10kW, the RF contacts of the tuning plunger were broken (partially melted due to overheating). The contact ring, made of beryllium bronze, was then silver plated and the contact force increased. Unfortunately, subsequent inspection showed scratches on the outer diameter of the plunger. The plunger was then plated with hard gold and the contact force slightly relaxed again.

After solving these problems, the Super-buncher ran successfully for many days at a power level of 15kW. It was then installed in the 72MeV transfer- line in fall 2009. Since then, several beam-dynamics experiments have been carried out with the Super-buncher. Unfortunately, it has not yet been possible to find the proper operating parameters which might allow one to run the flat-top cavity of the 590MeV Ring Cyclotron at a lower power level, or to increase the beam intensity [13]. Beam experiments also

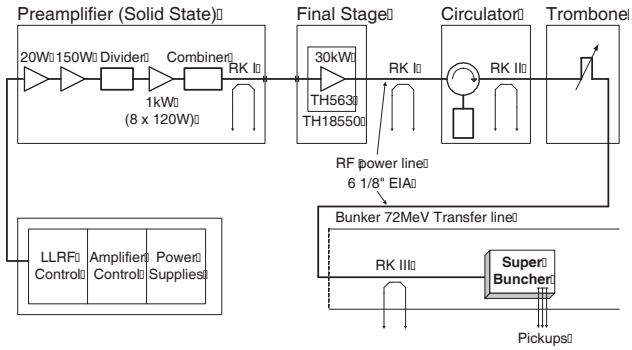

Figure 5: Schematic of Super-buncher Installation.

indicate that the phase of the Super-buncher changes with respect to the beam phase when the beam intensity is modified. In order to ease the optimization of the operation point, it is planned to install an additional phase-shifter which allows one to shift quickly the phase of the Injector II RF with respect to the Ring Cyclotron and Super-buncher.

New 50MHz Resonators for Injector II

The 72 MeV injector cyclotron has already demonstrated [13] the capability to accelerate and extract more than 2.3 mA. However, in the framework of the high intensity upgrade [7] to 3 mA, it is planned to replace the 150 MHz resonators by new, more powerful 50 MHz resonators [14]. The additional energy gain per turn will help to reduce the total number of turns and also increase the turn separation at extraction location. This will reduce the extraction losses and therefore allow the acceleration of more intense beam currents. Fig. 6 shows a 3d CAD sketch of the Injector II with new 50MHz resonators at the location of Resonator 2 and 4.

In 2007, an order was placed at the company SDMS "la chaudronnerie blanche" in France to build the two new aluminum resonators. Fig. 7 shows the prototype resonator after manufacture. Tab. 2 indicates its main parameters.

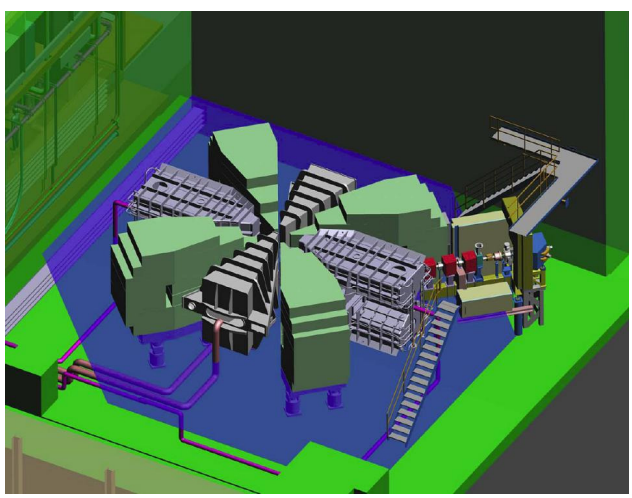

Figure 6: CAD model of Injector II with new Resonators 2 and 4.

Figure 7: LLRF-measurements of new 50MHz prototype resonators for the Injector II cyclotron at SDMS.

Resonator Design

The cavity is operated at the fundamental mode and its gap-voltage increases therefore almost linearly from 0 kV at injection to the maximum value at the extraction location [14]. In order to achieve the required maximum gap-voltage of 400kV, the cavity dissipates about 45kW of wall losses. The resonator has water cooled electrodes near the beam plane in order to reduce the transit time factor and to increase the electric field near the beam.

During the fabrication process, there were two coarse frequency adjustment possibilities of the resonator. After first measurements of the resonance frequency, the total length of the cavity was adapted for a first coarse tuning before the end-wall was welded to the cavity (-5.4kHz/mm). Later, the position of the electrodes was slightly adjusted in order to compensate the remaining fabrication tolerances and to achieve the correct initial frequency.

Two plungers of diameter 48.3 cm were installed on the end-wall, each at a distance of 61 cm from the beam plane with a maximum insertion depth of 20 cm. They are moved by hydraulic pistons and cooled by demineralized water. Their maximum tuning range is 189.3kHz.

The input power coupler is located at the end wall of the resonator, in the beam plane. It is the same inductive coupler, as used in the cavities of the 590 MeV cyclotron, but with a shorter loop length.

Conditioning and Power Tests

In 2010, the prototype resonator was installed at the high power test stand. Conditioning of the resonator went very smoothly and operation at a power of 100kW could be reached after about 3 hours. A 24 hour power test at 100kW was then successfully carried out. During conditioning and power tests, the vacuum gradually improved and reached a value of about $1.6{\cdot}10^{-7}$ mbar (a combination of turbo and cryopump is used). The maximum temperature of the resonator of about 46 to 49°C was measured at the PT100 located on the wall close to the electrodes near the center of the cyclotron and near the input power coupler.

During and after the power tests, the parameters of the quick-start electronics were optimized such that the resonator can be switched on fully automatically. The quick-start electronics uses an RF-pulse sequence to start the resonator in a short time [15].

Inspection after venting the resonator and removing the coupling loop showed scratches from the RF contacts on the plungers. After removing the plungers, it was found that some RF contacts had been bent. Therefore, the design of the RF contacts has still to be improved further. There is a also slight colouring of pickup-windows and some dark spots, probably from multipactoring during conditioning, on the lower resonator wall and the electrodes.

Table 2: Specification and comparison of simulation and measurements.

Resonance Frequency [MHz]	50.6328
Accelerating Voltage [kV]	400
Dissipated Power (for 400kV) [kW]	45
Vacuum Pressure [mbar]	$< 10^{-6}$
Material (RF walls) (support structure)	Alu. EN AW 1050 Alu. EN AW 5083
Dimensions (l,w,h)	ca. 5.3 m, 3.3 m, 3.0 m
Weight	ca. 6 t

Parameter	**Sim.**	**Meas.**
Q_0 (tuner out) [ ] [1]	28'159	24'814
Tuning range [kHz]	190	197.6
Power dissipation [kW]	100	100
Flowrate [m^3/h]	15	22
Forced convection cooling α_k $[W/m^2K]$	7'000-10'000	
Natural convection α_{kn} $[W/m^2K]$	5	
Cooling water temp [°C]	35	35.1
Ambient air temp. [°C]	25	30.8
Uniform start Temp. [°C]	25	35.1
Max. temperature (on Electrodes)	**76.5°C**	
Freq. drift vacuum [kHz] [2]	-75.2+16 **=-59.2**	(-63.9) corr. **-65.5**
Freq. drift thermal [kHz] [3]	**-32.6**	(-18.36) corr. **-30.4**

Notes:

1 If a resistance of 20mΩ is assumed per RF contact at the plunger and coupler, the simulated unloaded quality factor gets reduced to about 27'000.

2 72.2kHz correspond to geometrical deformation and 16kHz to change in dielectric. The air pressure was 976mbar in the case of measurement and 1000mbar in the case of simulation.

3 Since the uniform start temperature is 10.1°C higher in the measurement, the measured thermal frequency drift can not directly be compared to the simulated one. With a temperature coefficient of 1.195kHz/°C for aluminum, the corrected thermal frequency drift gets -32.6kHz, close to the predicted value.

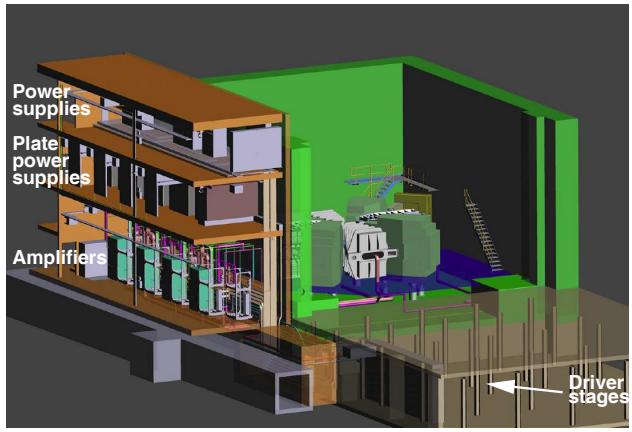

Figure 8: Layout of Injector II with new building for power amplifiers on the left.

Amplifiers, Building and Infrastructure

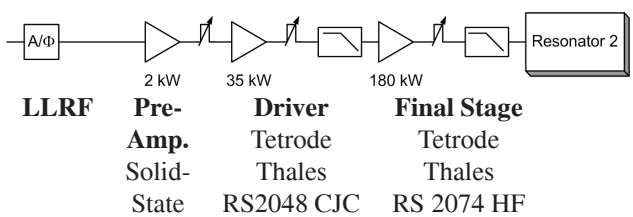

Figure 9: New amplifier chain for Resonator 2 and 4. A lowpass filter-absorber unit is inserted before the driver amplifier and the resonator to absorb higher harmonics.

A new building for the RF installation was built and completed in 2008. It will house the four final stage power amplifiers of the Injector II cyclotron, its plate, grid and filament power supplies. The driver amplifiers will be located at the place where currently the final stage amplifiers for Resonator 1 and 3 are located, in the basement of the

Injector II supply building. The new building is a metal support construction and isolated according to "Minergie" standard of Switzerland.

Fig. 8 shows a CAD drawing of the Injector II and the new building for RF power amplifiers. The layout of the new RF power amplifiers and distribution for the new Resonators 2 and 4 is indicated in Fig. 9. A 2kW solid state amplifier is chosen as pre-driver. The new 35kW tetrode coaxial cavity amplifier is currently beeing developed at PSI and will be based on a Thales RS2048CJC tube. It is planned to build the same 50MHz final stage power amplifiers as currently used for the 1MW final stage of the 590MeV Ring Cyclotron. However, a less powerful high voltage power supply will be installed. All tube-amplifiers are operated in grounded grid configuration. Higher harmonic absorbers will be installed between the driver and final stage amplifiers and the resonator. Trombones will be used to adjust the length of the coaxial lines to $n\lambda/2$ in order to avoid complex transformation of the impedances.

It is planned to install the first of the new resonators before 2013 and to have all the infrastructure ready before 2014 so as to complete the upgrade of Injector II.

CONCLUSIONS

Compared to the initial schedule [14], the upgrade program is delayed by at least 3 years.

If future beam-dynamics experiments with the Superbuncher are also not successful, a powerful flat-top cavity system for the 590MeV Ring Cyclotron might be a backup-solution for the intensity upgrade program.

Radiation of RF stray fields in the cyclotron should be investigated more in detail. This might help to improve the performance and availability of the accelerator.

REFERENCES

[1] U. Schryber et al., "Status Report on the New Injector at SIN", Proc. 9th Int. Conf. on Cyclotrons and their Applications, Caen, 1981, p. 43

[2] W. Tron et al., "Commissioning of the Injector II 150MHz RF System Upgrade", PSI Scientific and Technical Report 2003, VI, p. 43, (2004).

[3] Product name of Acheson (Henkel Corporation)

[4] H. Zhang et al., "Disturbance effects caused by RF-Power Leaking out from Cavities in the PSI Ringcyclotron", this Conference.

[5] M. Bopp et al., "Application of CAE Tools in the Design of High Power Cyclotron Cavities", Presentet at 6th International Computational Accelerator Physics Conference (ICAP2000), Darmstadt, September 2000.

[6] M.Bopp et al., "Upgrade Concepts of the PSI Accelerator RF-Systems for a Projected 3mA Operation", Proc. 16th Conf. on Cyclotrons and Their Applications 2001, East Lansing, May 2001, p. 300, (2001).

[7] H.Fitze et al., "Developments at PSI (Including New RF Cavity)", Proc. 17th Conf. on Cyclotrons and Their Applications 2004, Tokyo, October 2004, p. 67, (2005).

[8] J. Grillenberger et al., "Commissioning and Tuning of the New Buncher System in the 870keV Injection Beamline", Proc. 18th Conf. on Cyclotrons and Their Applications 2007, Giardini Naxos, October 2007, p. 464, (2008).

[9] J.-Y. Raguin et al., "500MHz Buncher for the 72MeV-Injection Line", PSI Scientific and Technical Report 2004, VI, p. 59, (2005).

[10] A. Adelmann et al., "Beam Dynamics Studies of the 72 MeV Beamline with a Super Buncher", Proceedings of EPAC 2004, Lucerne, p. 1945-1947.

[11] M. Seidel et al., "Upgrade of the PSI Cyclotron Facility to 1.8MW", Proc. 18th Conf. on Cyclotrons and Their Applications 2007, Giardini Naxos, October 2007, p. 157, (2008).

[12] http://www.ansys.com

[13] M. Seidel et al., "Towards the 2MW Cyclotron and Latest Developments at PSI", this Conference.

[14] L. Stingelin et al., "Development of the new 50MHz Resonators for the PSI Injector II Cyclotron", Proc. 18th Conf. on Cyclotrons and Their Applications 2007, Giardini Naxos, October 2007, p. 467, (2008).

[15] J. Cherix et al., "Pulsed-RF to Start the Cyclotron Cavities in a Short Time", PSI - Scientific and Technical Report 2004, VI, p. 16, (2005).

OPERATING EXPERIMENCE WITH THE RF SYSTEM FOR THE SUPERCONDUCTING RING CYCLOTRON OF RIKEN RIBF

N. Sakamoto*, M. Fujimaki, A. Goto, O. Kamigaito, M. Kase, R. Koyama, K. Suda, K. Yamada, S. Yokouchi, *RIKEN Nishina Center, Wako Saitama, Japan*

Abstract

At RIKEN RIB-factory (RIBF) an accelerator complex as an energy booster which consists of superconducting ring cyclotron (SRC), intermediate-stage ring cyclotron (IRC) and fixed-frequency ring cyclotron (FRC) provides very heavy ion beams like uranium with an energy of 345 MeV/u [1]. In December 2006, the SRC has become operational and it was succeeded to extract the first beam from SRC[2]. Since then, we have experienced various problems with the rf system for SRC and improvements have been made to achieve designed performance solving the problems one by one. This paper will discuss on our efforts to understand the source of troubles and improvements and modifications of the rf system.

RF SYSTEM FOR THE SRC

Superconducting Ring Cyclotron

The K2600 superconducting ring cyclotron (SRC) is the first superconducting separate-sector-cyclotron in the world [3]. The SRC consists of six superconducting sector magnets, four accelerating cavities and one flattop cavity (Fig.1). The rf system is frequency tunable from 18 MHz to 42 MHz so that the beam energy is variable to suite the optimum condition of secondary beam production. Up to now, a number of subjects of nuclear physics experiments utilizing beams of ^{48}Ca, ^{238}U with an energy of 345 MeV/u have been performed with high priorities. The rf frequency of 36.5 MHz for these beam has been mostly used. Designed value of the acceleration voltage is 2 MV/turn.

It was turned out that due to a strong stray field of the K2600 superconducting magnet the rf cavities suffered from very heavy multipactor. In the early stage it took long time, more than a few hours, to recover the rf voltage after breakdown.

This is one of the major problems which reduces the availability of the SRC.

Table 1: Present performance of the rf system.

	Acceleration	Flattop
Frequency [MHz]	36.5	109.5
Number of cavities	4	1
Rs [MΩ]	1.5	1.65
Unloaded Q	30000	29000
Voltage [kV/cavity]	550	-240
$P_{w.l.}$ [kW/cavity]	100	18
Vacuum [Pa]	3×10^{-6}	1×10^{-5}
Voltage Stability	±0.03%	±0.03%
Phase Stability	±0.03°	±0.09°
Availability*	92%	99%

* Here availability is defined as all of the cavities are excited.

* nsakamot@ribf.riken.jp

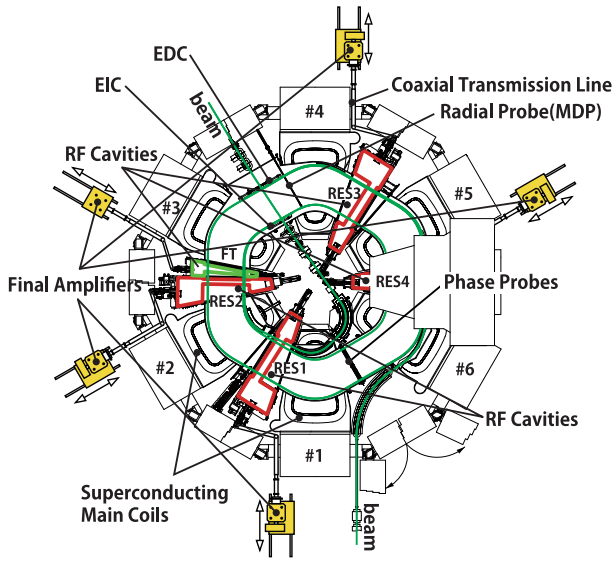

Figure 1: Schematic of the SRC.

Cavities

Design, construction, and commissioning of the rf cavities have been reported at Cyclotrons'98, -'01, and -'07 [4, 5, 6]. A present performance of the rf system is summarized in Table1.

The four acceleration cavities have an acceleration voltage of 2.2 MV/turn in total and the third harmonic cavity has a voltage of -0.24 MV with deceleration phase. The voltage of acceleration cavities were initially restricted to 450 kV, since a trouble with contact fingers which were inserted to the gap of cavity wall and the rotating capacitive tuner occurred. The gap was larger than the designed value, then lack of touching pressure made contact resistance large so that the finger got damaged. Modification of the shape of the contact finger was made to reduce the contact resistance.

Since cooling of RF shield adopted to the window of the cryogenic pump was not enough, temperature rise of cryogenic panel occurred and the vacuum pressure was abnormally raised with the cavity voltage higher than 500 kV. To solve this problem installation of water cooling channel

directly on the rf shield was done.

After these modification, finally the designed acceleration voltage of 2 MV/turn was obtained.

Amplifier and Low Level Circuit

The main rf amplifier is based on a tetrode THALES/SIEMENS RS2042SK coupled with a tetrode THALES/SIEMENS RS2012CJ with a grounded-grid circuit. This amplifier was originally designed for Riken Ring Cyclotron[7]. The SRC is energy variable machine so that the rf system is frequency tunable with a variable capacitor of input circuit, a stub with short plate, and variable output capacitor(Fig.2). Four power-amplifiers are installed and then the four acceleration cavities were excited by individual amplifiers driven by the same master oscillator. The low level system works very well owing to modifications[8] to stabilize the amplitude and the phase within 0.03% and 0.03°. The rf stability is always measured during operation by newly constructed monitor system based on the commercially available rf lock-in-amplifiers (SR844)[9]. Stabile operation of rf is crucial to realize single-turn extraction. The turn purity of 99.9 % was obtained for polarized deuteron experiment in April 2009.

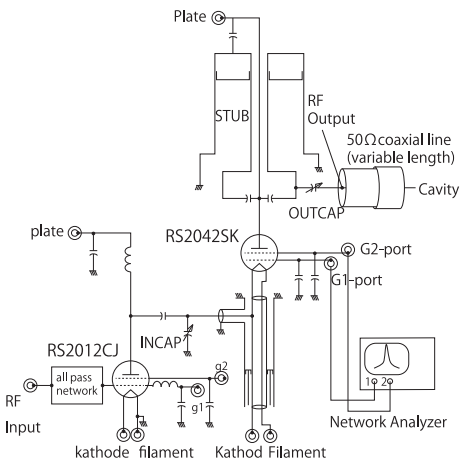

Figure 2: Simplified diagram of the amplifier circuit.

Control of Parasitic Oscillations

S_{21} from the G1-port to the G2-port($S_{21}^{G1\to G2}$) shows a helpful information on parasitic oscillations of our system(3. The setup of the measurement is indicated in Fig.2. Measurement was made using Network Analyzer (Agilent E6061A). Many peaks appear beside the resonance of fundamental mode of cavity and amplifier. The amplifier itself is known to have relatively low frequency parasitic resonances. One is the higher order mode (HOM) of input stub circuit around 55 MHz, denoted by green line in the figure, and the other is the resonance between G1-electrode and G2-electrode of the tetrode RS2042SK. Excitation of these modes causes immense damage to the amplifier.

The coaxial transmission line between the amplifier and the cavity is about 15 m long. A number of HOMs appear according to the length of transmission line as denoted by blue lines in Fig.3. Around 55 MHz, HOM of input circuit, one of the HOM of coaxial line (3) is located in the very close vicinity(yellow circle). The situation possesses considerable risk to excite the parasitic mode. Each coaxial lines is equipped with a sliding mechanism with a stroke of 1 m. By moving amplifier the length of transmission line is changed so as to avoid the coupling oscillation[10]. The measurement was made with a middle position of the stroke. For operation, the amplifier is set to the position closer to cavity by 0.5 m to avoid coupling oscillation.

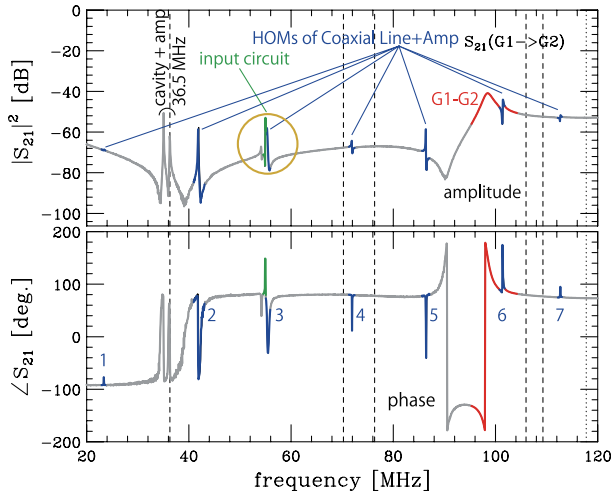

Figure 3: $S_{21}^{G1\to G2}$ measured. Dashed lines are the HOMs of the acceleration cavity.

Magnetic Field Effect to the RF System

The cavities are exposed to a very strong stray field from superconducting sector magnet. The actuators, cryogenic pumps, and turbo molecular pumps are equipped with iron shields. The strong stray field makes the situation of multipactor severe. It becomes difficult to overcome the multipactor levels. As a first step, implementation of an additional cryogenic pump(10000 l/s) to each cavity was made expecting that improvement of the vacuum condition of the cavity will help to moderate the situation of multipactor. The vacuum pressure with rf power 100 kW becomes about 3×10^{-6} Pa. The effect of stray field of 100 Gauss at the position of amplifier to the operation of power tube is negligible small.

OPERATING EXPERIENCES

RF Power Leakage

Asymmetrical excitation of rf in the cavity causes vertical component of the electric field at the median plane which propagates into beam chamber through the beam aperture. Even small portion of rf power leaks, beam

probes such as phase probes (PP) which measure the isochronous fields and a main probe and a differential probe (MDP) which measure a beam current and a beam density distribution along radial direction respectively easily malfunction because the signal level induced by circulating beam is very small. The main part of the leaked rf power comes from the flattop cavity because the operation frequency of 109.5 MHz is higher than the cutoff frequency 80 MHz of the beam aperture. To settle the problem with the beam probes, the leaking rf power should be minimized at first and then the improvement of the signal to noise ratio is anticipated to work well.

To detect the rf power leaked from the cavity a sensor which consists of a pair of capacitive pickup electrodes have been installed so as to measure the vertical component of the rf electric field[4]. Though the sensor was too sensitive to handle. On the other hand, a beam loss monitor at the electrostatic deflection channel(EDC) was turned out to be useful. The monitor is a thermometer adopted on the septum electrode of EDC and when the rf power is switched on a rise of temperature is observed according to the leak of rf. The upper and the lower frequency tuners are independently adjusted to the positions where the temperature of the beam loss sensor is minimum.

Countermeasure against RF Noise

Countermeasure against rf noise of the beam probes has been made by trial and error. Observing the noise on MDP, its level varies depending on the position in radial direction. The MDP behaved like an antenna. Therefore an electric contact was attached at the tip of MDP chassis to suppress the TE01 mode on the MDP[11]. To measure the timing of the circulating beams, a pair of electrodes located vertically is used(Fig.4). Because the beam induces monopole component of the electric field while the rf noise have dipole component, if the signals from upper and lower electrodes were combined in the same phase, rf noise is canceled in principle, without affecting the beam signal. To have larger S/N, interference filter which cancels the odd components of the signal is inserted. To measure the zero crossing timing of the beam signal, the second harmonic frequency of beam frequency is employed. Finally the probes work well without disturbance of the rf power leakage.

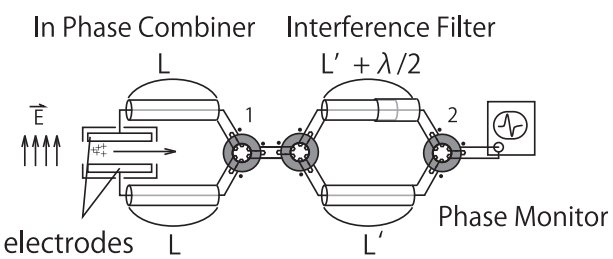

Figure 4: The noise filters for the beam phase probe(PP).

Multipactor

In the initial commissioning of the SRC, conditioning with a pulse rf power with a reputation rate of 100 Hz and the peak power of more than 100 kW was performed to overcome heavy multipactor due to the stray magnetic field. In the method conditioning started with zero magnetic field increasing the coil current step by step observing the situation of multipactor. It worked well but it took a couple of days to overcome.

In order to make the startup time shorter, conditioning with a low cw power of 10∼30 kW was tested instead of pulse and it turned out the new method successfully improved the situation. Coil current is set to the operation current first and by observing the level of the cavity pickup, the reflected power and the vacuum pressure, the rf power is increased step by step overcoming a number of multipactor levels until the cavity voltage becomes around 100 kV. Ordinary it takes only a few hours. After the conditioning with new method performed for 24 hours the recovery time after breakdown becomes as short as 5∼30 minutes during the beam tuning while in the early stage of the commissioning it took 3∼4 hours. The live time of the rf, defined by the ratio of the time when right rf voltages of all the cavity are excited to the scheduled beam bombarding time, is 92 % for the ^{48}Ca experiments in June 2010.

SUMMARY

By improving the vacuum, cooling, and surface cleaning, the designed acceleration voltage of 2 MV/turn has been realized. The beam probes, MDP and PP, work well after some modifications. Multipactor is one of the most important issues which reduce the availability of the SRC. In order to minimize the break time due to the rf breakdown, cw power conditioning has been introduced. Recovery time was 5-30 minutes during the Ca experiment in May this year. Recently conditioning at the cold start takes 1 day. The availability of the rf cavities is now more than 90% but still improvement of this number is required toward 99% which the IRC and the FRC have already achieved.

REFERENCES

[1] O. Kamigaito et al., *this conference*, TUM2CIO01.
[2] N. Fukunishi et al., PAC'09, Vancouver, (2009)M03GRI01.
[3] Y. Yano, Nucl. Instr. Meth. **B261**(2007)1009.
[4] N. Sakamoto et al., Cyclotrons'98, Caen, (1998) p.223.
[5] N. Sakamoto et al., Cyclotrons'01, Tokyo, (2001) p.342.
[6] N. Sakamoto et al., Cyclotrons'07, Giardini Naxos, (2007) p.223.
[7] T. Fujisawa et al., Sci. Papers I.P.C.R.80(1985).
[8] K. suda et al., *this conference*, MOPCP068.
[9] R. Koyama et al., EPAC'08, Genoa, (2008) p.1173.
[10] N. Sakamoto et al., HIAT'09, Venezia, (2009) p.85.
[11] K. Yamada et al., HIAT'09, Venezia, (2009) p.16.

DISTURBANCE EFFECTS CAUSED BY RF POWER LEAKING OUT FROM CAVITIES IN THE PSI RINGCYCLOTRON

D. Goetz, J. Grillenberger, M. Humbel, R. Kan, M. Schneider, L. Stingelin, H. Zhang
Paul Scherrer Institute CH-5232 Villigen PSI, Switzerland

Abstract

While commissioning the PSI high intensity proton beam facility after the shutdown 2010, direct and indirect phenomena of interaction occurred between the RF power leaking out from the cavities and the electrostatic septa at the injection and extraction region in the Ringcyclotron. As an indirect influence RF fields outside the cavities generate plasma clouds in the peripheral area of magnet poles. Accelerated plasma ions sputtered metallic atoms from the vacuum chamber wall, which then covered the insulator surface with an electrically conductive layer. The septum therefore had to be replaced. Directly, RF power dissipated from the 150 MHz flattop cavity was redirected by a beam stopper in such a way, that a linear correlation between the RF pick up signal monitored at the extraction septum (EEC) and the leakage current across the septum insulator could be observed. As an instant mending action the beam stopper, which is not permanently used, has been removed. The long term attempt to minimize these disturbing effects will be an asymmetrical setting of the hydraulic cavity tuning system and an effective RF grounding of build in components.

INTRODUCTION

In the Ringcyclotron of PSI's high intensity proton facility, the amplitudes in the RF cavities have been raised from 760 MV in 1998 to 860 MV nowadays. In lockstep with this RF upgrade the electrostatic elements had to be modified to meet the new requirements.

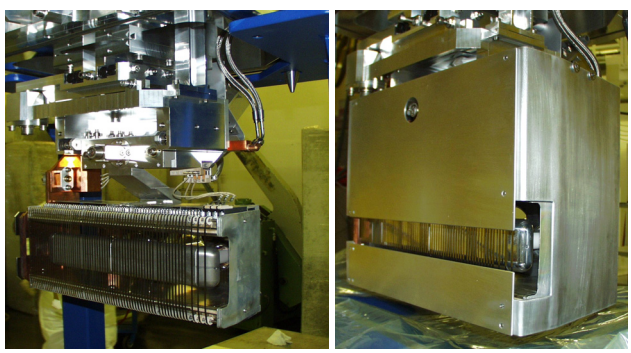

Figure 1: Electrostatic injection channel of the PSI Ring-cyclotron without shielding (left) and shielded (right).

That bundle of measures succeeded to maintain their reliable operation. As an example, the RF shielding of the electrostatic inflection channel, added in 2006, is shown in Figure 1. Despite these efforts, the septa belong to the most critical parts of the cyclotron. In particular their behaviour during the first few weeks after the annual shutdown is a cause for concern. Several times, shortly after the start up of the facility, one or even both of these elements were seriously damaged and had to be replaced.

INVESTIGATIONS IN 2010

In 2010 once more, shortly after the facility commissioning the electrostatic extraction septum EEC lost its electric field strength. The examination of the dismounted EEC septum has exhibited traces of damaging effects. The outer face of a shielding plate at the beam exit side showed a staining on its surface and one of the insulators was contaminated with a strip of conductive material.

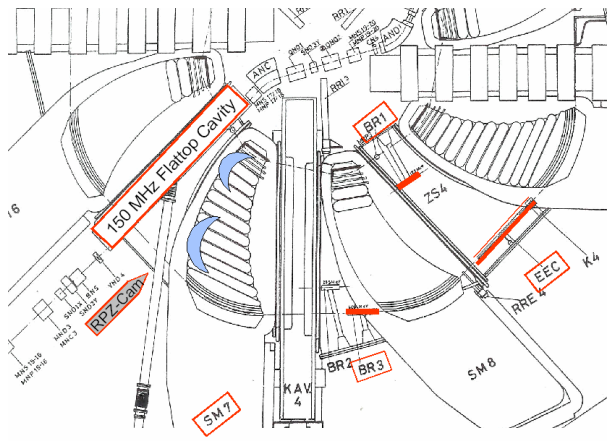

Figure 2: Layout of the PSI Ringcyclotron. The blue coloured patches represent the plasma clouds monitored by the CCD camera in the RF on, beam off state.

After the replacement, various efforts were tackled to get more insight into the damaging incidents that had happened. The scheme in Figure 2 shows coloured in red the cyclotron components involved in them. The experiments uncovered peculiar observations inside the vacuum chamber of the Ringcyclotron.

Interaction of RF with BR1, BR3 and EEC

The two beam stoppers BR1 and BR3 are used for commissioning and tuning purposes. In the beam production state of the machine they are moved out and parked off the beam path. Since years it was a well known fact, that whenever BR1 was set in beam stopping position, BR3 measured a virtual proton beam current of up to 50 µA. The current readout evidently was unreal, since no protons could transit the active stopper BR1. It instead was depending on the voltage level of the flattop cavity. While until the end of last year this fake current signal vanished when BR1 was parked, after this year's

shutdown it remained present, independent of the BR1 position. During the shutdown BR1 had undergone modifications. Its unfavourable side effect was that its carrier arm, formerly effectively RF grounded when parked, had lost its conducting connection to the ground.

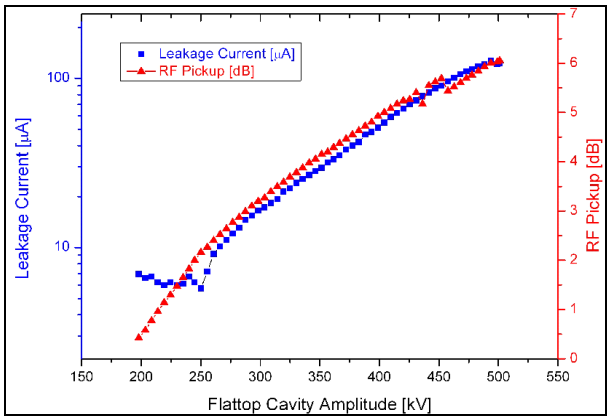

Figure 3: RF pickup and leaking current versus amplitude of the flattop cavity. The logarithmic current scale allows a direct comparison with the RF pickup in dB.

A similar impact of the flattop cavity on the EEC septum could be observed even more precisely. The EEC is protected by the control of the leakage current across the insulators and by six metal strips which collect aberrant protons. For test purposes the second strip was connected to an RF pickup device. Figure 3 displays the leakage current and the signal recorded by this device as a function of the amplitude of the flattop cavity. Above 270 kV the leakage current signal raises strictly proportional to the RF pickup, BR1 obviously acted as an RF antenna which absorbed the RF field decoupled from the flattop cavity and reemitted it radially towards the EEC septum and the stopper BR3.

Plasma Clouds Created by Flattop Cavity

A RDZ security camera, placed in front of a window in the vacuum chamber wall revealed an explicit glowing in the sector magnet SM7 near the exit gap of the flattop cavity. The ignition, shown in Figure 4, could reliably be reproduced by raising the voltage of the RF amplitude above 490 kV and expunged again by lowering the voltage below 400 kV. The ion density could be measured by means of a vacuum gauge in the cyclotron centre region. Up to 490 kV the vacuum pressure remains stable around 0.1mPa. At 490 kV, it raises sharply, indicating the dramatic ion fraction growth of the residual gas.

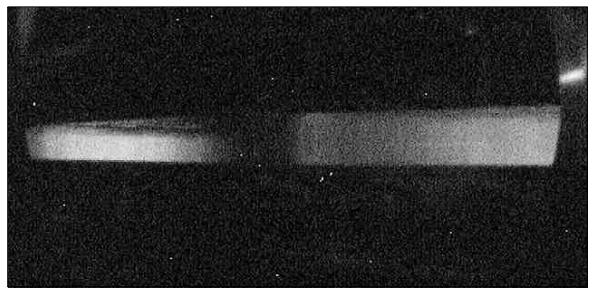

Figure 4: Plasma glowing in the pole region of sector magnet SM 7 as seen by the CCD camera.

In Figure 5 this devolution is plotted (peak A) and compared to the development of the EEC leakage current. Up to 240 kV the current stays constant. At 240 kV a splay (B) induces a sudden boost, followed by a quadratic growth as a function of the RF amplitude. The sudden increase of charged particles observed in the EEC region, is similar to the one, the vacuum gauge recorded from the plasma cloud at SM7. Though not fully proven, most probably the RF power, redirected to the EEC septum, ignites here another plasma cloud. Due to the more complicated structure of the surroundings, 240 kV RF amplitude suffice to ignite it, whereas in the almost empty region at the flattop cavity at least 490 kV are needed. Since the plasma cloud directly wraps the EEC, ions are travelling to the corresponding electrodes, yielding a rise of the leakage current proportional to the plasma concentration.

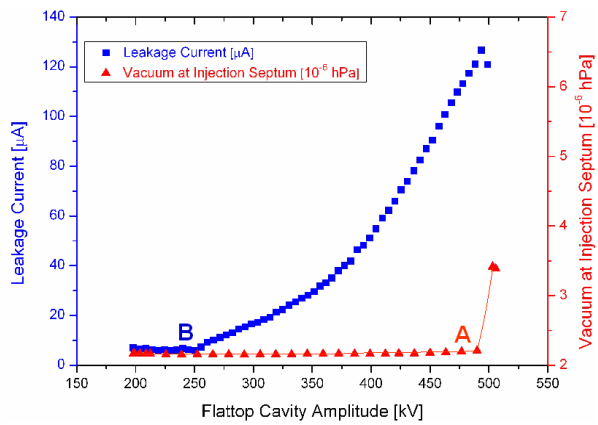

Figure 5: Residual gas pressure of the vacuum gauge and the EEC leakage current as a function of the amplitude of the flattop cavity. Plasma ignition occurs at the rib A and eventually at the splay B.

Accelerated ions sputter metallic atoms from the electrodes or the framework. These atoms then settle down on what ever surface present in the surroundings and therefore among others, on the insulators that serve as support of the EEC cathode. Sooner or later this deposition lowers their resistivity.

MENDING TASKS

It is well known, that vagabonding RF can ignite plasma clouds [1]. But these as a fact are not mandatory harmful. The presented effects show a case, where by interaction with devices, the RF field moves an existing cloud to a sensitive place or generates it there, which then deploys its destructive potential.

Short and Intermediate Term Mending

With the intent to damp the RF power decoupled from the flattop cavity, a first attempt was to install an RF absorber at the exit gap of the flattop cavity. Unfortunately the marginal effect predicted by simulation was confirmed by reality. The absorbing effect did not exceed a few percentage. By withdrawing the stopper BR1 it was possible to avoid the redirection of the RF power decoupled from the flattop cavity towards the EEC element. So both effects, the direct influence of the RF power on the stopper BR3 as well as the generation of the plasma cloud at the EEC septum were eliminated. This intervention has set the facility in the condition required for a successful beam production. Since the removal of the BR1 stopper three month ago, a proton beam of up to 2.2 mA was routinely extracted.

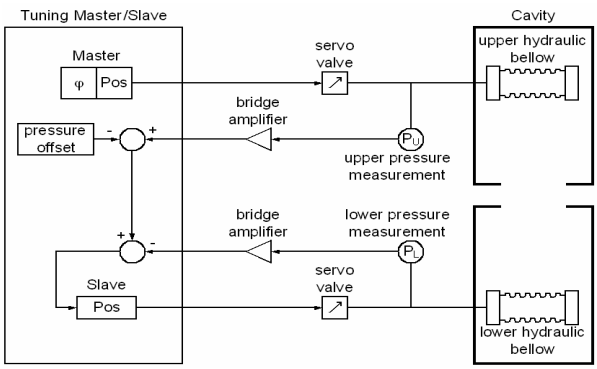

Figure 6: Block diagram of an independent pressure system for the upper and lower flattop cavity box part.

Long Term Repair of the Disturbance

This measure will nevertheless only be a short term solution, as the lack of BR1 could cause problems in case of a more complicated machine setup. As well the decoupled RF and the plasma clouds still exist in the cyclotron an may damage at another place if prospective modifications of machine elements promote it. Investigations for a low rest gas pressure and an effective RF grounding of the components inside the vacuum chamber remain important, but the minimization of the decoupled RF power became a main task. The leaking out of RF power from a cavity is known to depend on vertical asymmetry. Positioning deviations, geometrical asymmetries, or partial coating on the inside walls of the cavities may add a vertical component to the regularly horizontal oscillation plane. As a correction of the oscillations slant several compensation mechanisms are known. N. Sakamoto has presented a system with movable panels to be an efficient approach [2]. Since in the PSI cavities the resonance of the RF is tuned by a hydraulic pressure system, the approach at PSI will be the installation of a separate tuning system for the upper and the lower box part. An upgrade of the flattop cavity in this regard is under way, see Figure 6.

Clue about the Septa Reliability Cycle

Once the startup after a shutdown has succeeded, the key data of the electrostatic elements continuously improve. Some weeks after the successful first commissioning the number of voltage breakdowns drops significantly and the leakage currents reduce and get increasingly smooth. During the last quarter of the year before the annual shutdown the beam availability therefore often exceeds 95%. This observation adds another evidence for the key role decoupled RF plays in the reliability of the electrostatic elements. During the shutdown servicing and upgrading activities require an opening of the ring vacuum chamber for weeks sometimes. In this time all inner surfaces undergo contaminations with breathable air and humidity. So after the shutdown accidental partial coating of the surfaces yield a higher rest gas pressure and an enhanced amount of decoupled RF power. During production time the surface contaminations shrink bit by bit resulting in a reduction of the preconditions for ion generation and as well of decoupled RF power. Thus the irritation of the electrostatic septa is reduced.

CONCLUSIONS

In addition to a shielding of the electrostatic septa, an effective system to minimize the RF power decoupled from the cavities is mandatory to operate the Ringcyclotron reliably at a beam current up to 3 mA. The PSI approach will be an independent tuning system for the upper and the lower cavity box part.

ACKNOWLEGDEMENTS

The authors would like to thank the colleagues who have contributed to this work. In particular Mike Seidel, Stefan Mair, Anton Mezger and the operations crew for their patience during the sometimes tedious experiments.

REFERENCES

[1] M. Bopp et al. “Application of CAE tools in the design of high power cyclotron cavities”, Proc. ICAP’00, Darmstadt Germany, September 2000

[2] N. Sakamoto et al. “Construction of an RF Resonator for the RIKEN Intermediate Stage Ringcyclotron“, Proc, Cyclotrons'01, East Lansing 2001, pp 04-23

BEAM DIAGNOSTICS FOR CYCLOTRONS

R. Dölling, Paul Scherrer Institut, Villigen, Switzerland

Abstract

An overview of beam diagnostic systems for cyclotron operation and development is presented. The focus is on devices installed within the cyclotron with its special "environmental" conditions and limitations. Emphasis is placed on the requirements of high current beams, as produced by the PSI Injector 2 and Ring cyclotrons [1].

INTRODUCTION

The first operating cyclotron already used a Faraday cup to detect the accelerated beam current (Fig. 1). Since then, both cyclotrons and beam diagnostic systems have undergone several development cycles, leading to the variety of cyclotrons in operation today at a number of scientific, industrial and medical facilities [2, 3].

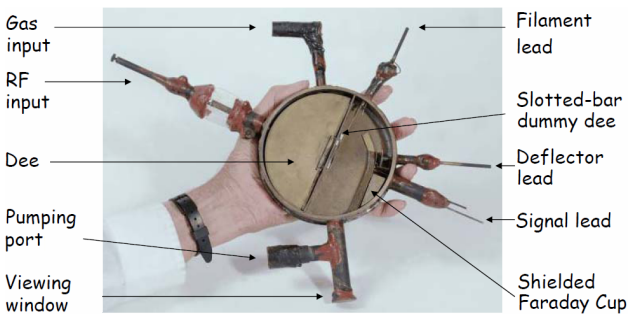

Figure 1: Lawrence & Livingston 4-inch cyclotron which delivered 80 keV protons in 1931 (picture from [4]).

Most of the beam diagnostic techniques in use today at cyclotrons were already present in the 1970s. These are reviewed in [5] and [6-9] and are further described in the proceedings of this conference series (since 1959). In addition, a wealth of detailed information on beam diagnostic techniques is available from the Proceedings of the Beam Instrumentation Workshops (BIW, since 1989) and the Beam Diagnostics and Instrumentation for Particle Accelerators Conferences (DIPAC, since 1993) and other accelerator conferences. Overviews are given in, e.g. [10-14].

Machine design and operation has profited over the years from a number of theoretical and experimental advances. These include improvements in the fields of beam dynamics and magnetic field mapping, and in the stability and reliability of machine components. The experience gained has also played a part. At the same time, requirements to beam quality and availability have also steadily increased. Beam diagnostic systems are thus called on to deliver the missing ε of information during commissioning, beam development, setup and tuning, and searches for anomalies. They are similarly required for beam stabilization and machine protection during standard operation and for the avoidance of excessive activation.

Due to the large variation in cyclotron concepts, uses and parameters, beam diagnostic systems have to adapt to many different environments. Beam current, energy and particle species and their variability, external or internal ion source, sector-focusing or not, separate sectors or compact, normal- or superconducting coils, separated or non-separated turns at extraction as well as standalone or coupled machines, unique or series cyclotron models and the different demands to the availability of the facility - all place their constraints on the requirements.

The boundary conditions within the cyclotron are especially stringent. Already the simultaneous presence of many turns, which eventually overlap, or exhibit beam halo or provide a high power beam, is in itself a complication to the 1-orbit case. The limited space, the strong magnetic field and the presence of large RF fields, beam losses and subsequent radiation, activation and perturbing particles in the direct vicinity of sensor elements, presents a formidable challenge. They hinder or make impossible the use of certain diagnostic techniques and detectors, demanding additional effort. Examples which illustrate this point are shown in Figs. 2, 3.

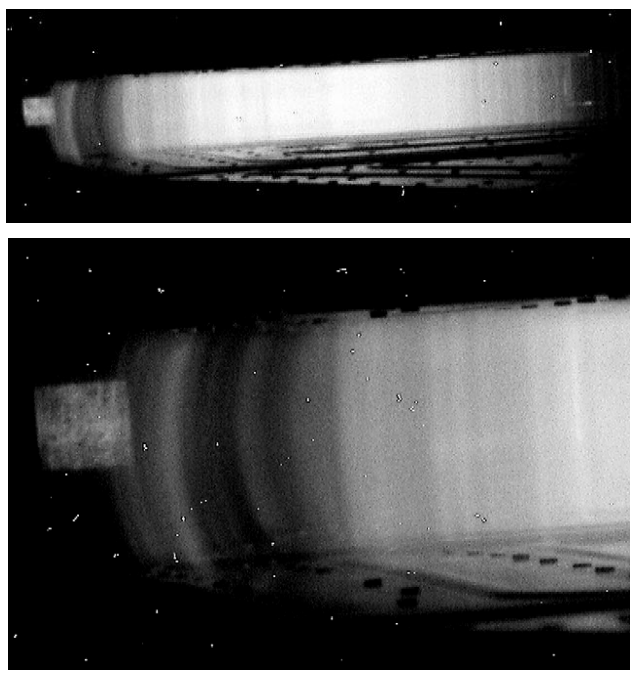

Figure 2: Radial view into the PSI Ring Cyclotron with RF and sector magnets switched on but without beam. A thin plasma is sustained at lower machine radii in the gap of the sector magnet by the RF leaking out from the nearby cavities [15]. One can imagine that the plasma (with associated currents well above the beam current) effects probe measurements.

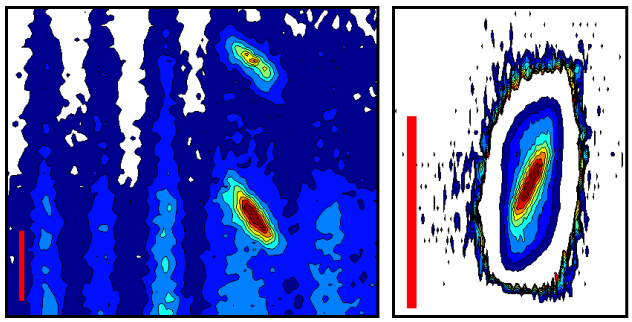

Figure 3: Time-structure measurement of the first two turns in the PSI Ring Cyclotron (left) and of the beam in the injection line (right). Bunches as seen from above move from right to left. The red bars indicate a 1 cm x 1 cm area; contour lines at every 10% (and at the right picture in addition every 10% divided by 125, single event bins are visible). The similar detectors using the same integration time were placed ~0.3 m from the beam. While the measurement in the beam line exhibits mainly shot noise, in the cyclotron a background pattern created by beam losses at other points in the cyclotron significantly decreases the resolution. (The FWHM time resolution of the detector of ~35 ps corresponds to 4 mm [16].) The few centimetres of lead shielding around the detector are not effective against the energetic stray particles.

TASKS

In the cyclotron as well as in the beam lines a fundamental task of beam diagnostics is to deliver information on the beams 6-dimensional (6D) phase space distribution, to the extent that it allows a study of differences in the beam profile/quality to that predicted by beam dynamics simulations ("knowledge aspect"). This involves matching the beam core from the ion source to the injection line, and then into the cyclotron acceptance, the beam path at injection and in the center region where current setting, beam shaping, beam centering and betatron oscillation setting are performed; the isochronism, bunch length and centering in the acceleration region, the beam path through the extraction elements, the matching to the next transport line and the efficiency of transport all along the way.

As a result the settings of magnetic and RF fields and of mechanical elements can be adjusted. Introduced into control loops this improves the beam stability ("stabilization aspect"). Also the sources of beam parameter fluctuations, e.g. magnet power supply ripples, can be traced back. Further important tasks are the prevention of thermal beam damage and the avoidance of excessive activation by monitoring the beam losses and trigger beam abort if necessary ("protection aspect").

At High Current Beams

In the case of high current beams, already a thin beam halo contributes significantly to the beam losses. The transport of the whole distribution is strongly influenced by the beam space charge and the creation of new halo by scattering at collimators. Hence, already small changes at any location along the beam path can alter the total losses strongly. This makes setup and tuning difficult and leads to a tuning method mainly determined by examining the losses of the beam along its path and "turning all available knobs" to minimize losses at a given beam current level [17]. With this concept, the diagnostics serving the "knowledge aspect" are mainly needed to see "what is different than before" in case of unexpected beam behaviour. (The "stabilization aspect" is still needed, e. g. the online beam centering for a ramping up of the beam current within a few seconds.)

Although this empirical concept is useful for finding the optimum operation for a *given* machine configuration, well-directed *changes* of the machine configuration, leading to significant improvement, cannot be initialized by it. Also it is very difficult to find hidden causes in the case of a persistently bad beam quality. To overcome this, detailed numerical simulations [18-20] of the beam transport and matching including the beam halo are required *together* with *detailed* measurements of the 6D phase space distribution. This revitalization of the "knowledge aspect" should result in an improved beam cleaning at low energies by additional slits, a matched beam core *and* halo, lower losses at higher energies, the ability to setup the whole machine in one pass and the ability to find sources of deteriorated beam by examining the beam in detail.

Since the beam transport is strongly determined by space charge, also the "knowledge aspect" diagnostics must be operable at full beam current.

On the simulations side, fitting capabilities must be included in order to find the best fitted *detailed* phase space distribution to a large set of profile and loss data.

UTILIZABLE EFFECTS

An attempt at categorizing the basic effects used by beam diagnostics of hadron beams is given in Table 1. Their use *within* cyclotrons is discussed in the following sections separately for transversal and longitudinal components.

TRANSVERSAL INFORMATION

Collimators and Radial Probes

Segmented aperture foils and fixed or movable collimators use direct current measurement at lower particle energies where the beam or a fraction of it is stopped, while at higher energies only the secondary electrons (SE) emitted from the hit surfaces contribute. They help to guide the beam by defining its path and detect beam loss. Sufficient cooling of these devices is only needed if their cutting into the beam is intended, since the switching off of the beam by interlock generation is fast enough to prevent damage.

Most beam probes as well use direct or SE current measurement. (Nevertheless temperature measurement can be a slow but low-noise alternative.) The thermal

Table 1: Categorization of effects that may be used to extract information from an ion beam. (Examples are given in [24]). Indicated are the dimensions of delivered information, approximate beam current range, whether or not the beam is destroyed, if usage within a cyclotron seems feasible (for the magnetic field separate sectors are assumed) and if realized (as far as the author is aware) and if a usage is compatible with high vacuum requirements.

information 1D: 1D-profile 2D: 2D-profile Dz: long. prof. Pos.: position E: energy C: full current	*configuration*	*usable effect/device*	*usable* A) for machine safety B) permanently C) for tuning D) at setup E) for error search F) only at commiss.	*destructive*	*able to work inside cycl.*	*alrdy. used inside cycl.*	*usabl. at good vacui*	*beam current range* (assumed DC beam at 70 MeV, 10 mm diameter, to be determined more precisely)	*common names*
		beam self fields							
Pos, Dz, C	pickups	comparison of capacitively or inductively coupled RF currents	A B C D E	no	x	x	x	nA ... A	pickup, BPM, phase probe
C, (Dz)	transformer	DC or AC current transformer, wall current monitors	A B C D E	no	?		x	nA ... A	DCCT, ACCT, wall curr. m.
1D, C, (Dz)	"wire"	electron (or ion) beam probe	B C D E	no			x	mA ... >A	electron beam probe
1D, C	residual gas	residual gas ions (with beam space charge field)	?	no			(x)	mA ... >A	[21]
		direct beam current							
1D (/+Dz), C	in full beam	probe finger: current of stopped beam fraction (/+50Ω-readout)	D E	yes	x	x	x	nA ... uA	radial probe/Faraday cup
<1D	beam edge	collimator: -"-	A B C D	"no"	x	x	x	pA ... mA	collimator
1D, C	wire	wire: -"-	C D E	~no	x	x	x	-	wire scanner
		heating of introduced solid matter							
1D, C	in full beam	probe finger: direct (or cooling water) temperature measurement	D E	yes	x	x	x	nA ... uA	calorimeter probe
<1D	beam edge	collimator: -"-	B C D	"no"	x	x	x	nA ... mA	
1D, C	wire	vibration resonance shift	C D E	~no	?		x	pA ... uA	vibrating wire scanner
1D	wire	wire: resistance	C D E	~no	x		x	uA ... mA	
E, C	in full beam	probe finger: 2 thermocouples + degrader	C D E	yes	x		x	nA ... mA	[22]
2D, C	in full beam	metal/carbon foil: thermal light emission/thermionic emission	A B F	~yes	x	x	x	uA	[23, 6]
1D	wire	wire: -"-	C D E	~no	x	x	x	uA ... mA	
		changes to introduced solid matter							
2D	in full beam	paper/Kapton/Mylar darkening, metal foil burn	F	yes	x	x		nA ... uA	foil burn
2D, C	in full beam	radiochromic film	F	yes	x	x		<pA ... nA	
2D, C	in full beam	foil activation analysis, autoradiograph	F	yes	x	x	x	pA ... uA	autoradiograph
		secondary particles from introduced solid matter							
1D, C	wire	wire: secondary emission current, direct measurement	C D E	~no	x	x	x	pA ... mA	wire scanner
<1D, C	beam edge	foil: -"-	A B C D E	"no"	x	x	x	pA ... uA	SEM foil, aperture foil
2D, C	in full beam	foil: secondary emission current + pulling + 2D-electron detector	A B C D E	~no	x		x	pA ... uA	
1D, Dz, C	wire	wire + detection of scattered or secondary particles	C D E	~no	x	x	x	nA ... mA	time structure m./wire scanner
Dz, C	in full beam	foil + detection of scattered or secondary particles	C D E	~no	x	x	x	nA ... mA	time structure measurement
2D, C	in full beam	scintillating screens + 2D-light detector	C D E	yes	x	x	x	pA ... uA	scintillator screen/viewer probe
1D, Dz, C	"wire"	scintillating fibres + (external) PMT	C D E	~no	x		x	<pA ... nA	
Dz, C	in full beam	scintillator + (external) PMT	C D E	yes	x	x	x	<pA	time structure measurement
<=2D,Dz,E,C	in full beam	silicon/diamond bulk/strip/pixel detector	C D E	yes	x	x	x	<pA/<nA	silicon strip detector
		secondary particles from introduced dense gases							
1D, C	"wire"	coaxial ionisation chamber	C D E	~yes	x		x	<pA ... uA	
1D, C	in full beam	ionisation chamber + strip-electrode readout (in beam/not)	(B) C D E	yes/~yes	x		x	<pA ... uA	strip ionisation chamber
2D, C	in full beam	ionisation chamber + pixel-electrode readout (in beam)	C D E	yes	x		x	<pA ... uA	pixel ionisation chamber
1D	in full beam	proportional chamber	C D E	~yes			x	<<pA ... nA	wire chamber
1D, 2D, C	in full beam	GEM	C D E	yes	x?		x	<<pA ... nA	GEM
		secondary particles from residual or thin gas							
2D, C	gas curtain	beam induced fluorescence + (external) light detector	A B C D E	~no				nA ... >A	gas curtain
1D, C	residual gas	beam induced fluorescence + (external) light detector	A B C D E	no	x	x	(x)	mA ... >A	BIF monitor
1D (2D), C	residual gas	res. gas ions/electrons with external fields + strip(/+energy) det.	A B C D E	~no	x	x		uA ... A	residual gas profile monitor

beam load sets limits to the use of any solid material placed in the beam. Thin carbon fibres are most resistant at higher particle energies (where the stopping power is lower and the particles pass the wire) while water-cooled tilted copper or carbon surfaces tolerate the highest beam power densities at low energies. In between can be a gap where only non-destructive methods are applicable with high current beams, in order not to be thermally damaged and to limit the activation by induced beam losses.

Different types of radial probe heads are depicted in Fig. 4. Integral probes A - D provide the beam current depending on radial position by fully stopping the beam in the thick electrodes. Differential probes C - H yield the radial beam current density. Probes B, C, G, H, I give information on the axial distribution by segmentation [7, 25] and F by a rough tomography [26]. At the thick probes A - D the radius-defining face-side must be aligned tangential to the beam direction to minimise the amount of scattered particles and protruding axial end-caps (not shown) are added to catch SE spiralling along the axial magnetic field lines. Ideally these measures should result in a probe efficiency near to 1, but this is often not the case. At probes G, I the interference of SE from different vertical segments have to be prevented by lateral off-set. In some instances the electrodes are biased or electrodes have been added for pulling away the SE [27, 7, 26]. RF fields and stray particles (as SE or residual gas ions or scattered or secondary beam particles) often disturb the measurements. A closed shielding is only possible at low beam current and at the expense of losing information at the lowest energies, and is seldom used [28].

Radial probes are used for beam centering and provide information on radial and axial coherent and incoherent betatron oscillation amplitude and frequency [5].

Thick probes are convenient tools for "pulling" the beam to larger radii at low current and directly indicate current losses. If the turns are not separated, the "shadow width" of the exchange of signal from a fixed integral probe to a moving integral probe at a different azimuth provides information on the amplitude of the incoherent radial betatron oscillation and the radial turn profile [29, 30]. The cross-over radii of both probes must be equalized for centering ("50% method" [31]). At separated turns, the radial information is more easily obtained by differential probes.

In high current beams above ~20 MeV, (if at all) only the thin probes E, F survive. They also have the added advantage that the increase to beam loss is only moderate.

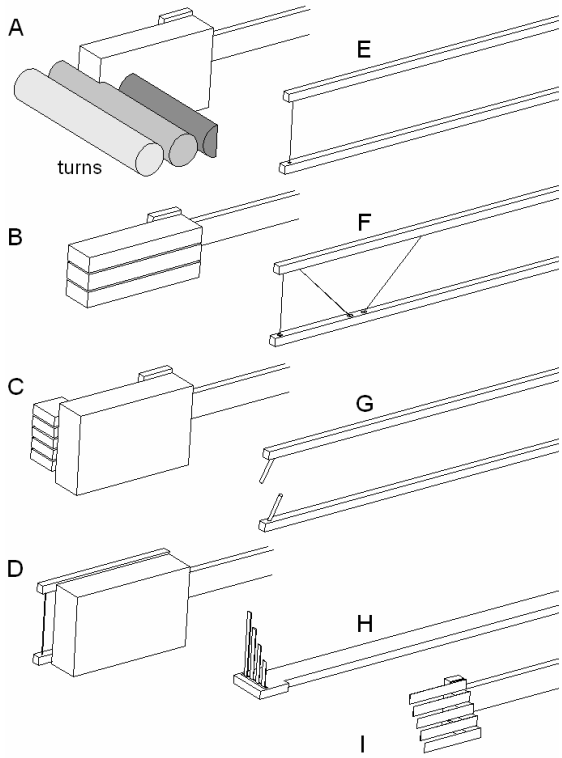

Figure 4: Schematic view of different radial probe heads.

Non-Destructive Profile Measurement

The effort for fully or nearly non-destructive methods seems only justifiable in the case of high power beams. Secondary emission monitors and residual gas ion monitors [32], which in certain configurations can deliver 2D transversal profiles [33, 34], have only occasionally been used within cyclotrons in 1D configuration [35, 36], using the cyclotron magnetic field for particle guidance, an electric pulling field and simple collecting electrodes. (In beam lines usually detectors with inherent amplification are used, but sensitivity is not an issue here and furthermore many detectors, e.g. the multichannelplate, are not usable in high magnetic fields.)

Beam-induced fluorescence profile monitors [37, 38] are in use at the 0.87 MeV injection line to the Injector 2 cyclotron at PSI [26], and may be suitably used to provide a radial profile of the inner turns in the cyclotron, which are not accessible at full beam current to the radial wire probes. Intensified CCD cameras may not be sufficiently radiation hard. Photomultiplier tubes [26, 38] can be a candidate because of their sensitivity, low noise and radiation hardness, but must be magnetically shielded (which is only possible in separate sector cyclotrons) or a relay optic must be used to transfer the image to the outside. Nevertheless the impact of stray light from perturbing effects (see Fig. 2) is not clear. In any case it will limit the dynamic range to less than ~1000.

Halo Measurement

More detailed measurements of the beam halo are of great interest for the understanding of the transport and beam losses of high current beams. With thin wire probes it is difficult to achieve the required dynamic range (of the order of 10^5 for a projected profile in the PSI facility) in the environment of the cyclotron and with the above mentioned non-destructive methods this seems even less promising. Therefore the halo should be measured separately from the beam core by moving an axial probe finger radially and axially as far as the probe heating allows. Encapsulated in the finger, a current or temperature measurement or, more sensitive, a small ionisation chamber or diamond detector [39] could provide a very large dynamic range since being shielded against RF fields and low energy stray particles.

The same technique could also be applied to beam lines by moving a finger or slit transversely into the beam. At higher energies also wire monitors with direct current measurement or detection of scattered particles seem feasible [40]. (In the 72-MeV injection line to the PSI ring cyclotron, the present thin-wire scanners are read out with logarithmic amplifiers which have a dynamic range from 50 pA to 1 mA. Nevertheless, their bandwidth at low current is too low and hence changes in the beam profile are indeed visible down to 10^{-5} levels of the maximum signal, but the local signal depends also heavily on the signal history below a 10^{-3} level.)

Image-Based Methods

For commissioning, techniques such as foil burning [6, 41] or autoradiographs, which deliver a 2D profile, are often used. They allow for the initial adjustments of the magnetic field at a minimum cost, but require the machine to be opened several times. More convenient are viewer probes which insert a scintillator screen into the beam, an image of which is recorded by an internal or external camera [42].

Very Low Current Beams

In most machines the setup is usually done with an initially low beam current, still giving sufficient signal, but limited activation. The beam current is then increased to the operation level. On the opposite for very low current radioactive ion beams an already low current pilot beam of nearly equal charge to mass ratio is used to get sufficient signal from essential monitors, before using the particle species of interest. Here sensors with inherent amplification are placed directly into the beam [14, 43].

PHASE AND TIME-STRUCTURE

The measurement of the "phase history", the radial dependency of the beam center phase with respect to the RF in the radial or spiral acceleration gap, allows to control the isochronism of the bunches and to adjust main field and trimcoils or trimrods accordingly.

The Garren-Smith method [29] measures the dependence of the bunch center phase and phase width on the

orbit radius by detuning the amplitude of the main magnetic field or the RF frequency until both the phase shift at the location of the radial probe reaches ±90° and the probe current decreases. This method is still widely in use for low current beams.

Phase probes, formed by pairs of pickups above and below the midplane coupling capacitively to the beam, can detect the bunch center phase with high accuracy. Usually ~10 probes are arranged along a machine radius, each covering several turns, but also a single radially movable probe is often used. To suppress beam unrelated RF, the probes are operated at higher harmonics or a synchronous detection of a purposely introduced modulation of the beam is used [44]. Usually both pickups of a pair are directly connected, thereby relinquishing the vertical position information. Also the time-structure of the beam can be measured with phase probes, but the resolution is limited due to the longitudinal extensions of beam self fields and pickup.

From the turn numbers dependence on radius one can determine the radial distribution of the accelerating gap voltage. With phase probes the time-of-flight through the cyclotron (or up to a certain radius [44]) can be determined, using cross-correlation and making use of a lower-frequency pulse structure [25] or the beam noise provided by the ion source [45]. This gives the number of turns in the cyclotron even when the turns are not separated.

Time-structure probes are an alternative to phase probes. At low beam currents a thick radial probe is placed in the beam, while at high beam currents a thin wire or foil is introduced and the arrival time of scattered beam particles, gammas or secondary electrons is measured by an internal or external detector with respect to the RF reference phase, e.g. multi-channel plates [46], diamond detectors [47] or scintillator-photomultiplier combinations [16] can be used as detectors. The target precisely defines the location of measurement and hence the time-structure even of short bunches can be determined with good accuracy. Although the pulse width from scintillator and photomultiplier is quite large (~2 ns), its time-resolution can be excellent due to the statistics from the many created photo-electrons. However, the level of radiation background from beam losses strongly determines the resolution and dynamic range (Fig. 3)

Using a wire target has the additional advantage, that a transversal coordinate is also determined. By moving the wire, a 2D profile can be measured (Fig. 3). Repeating this with several wire orientations, does not yield the full 3D spatial charge density distribution, but rather several 2D-projections. Hence e.g. all 9 parameters describing size and orientation of an ellipsoid representing the bunch can be determined and used in beam transport simulations. This type of measurement is under preparation for the PSI Injector 2 cyclotron, the connection beam line to the Ring cyclotron and its extraction line.

While time-structure probes need to sample over many seconds, gridded Faraday cups in 50 Ω-geometry [48] or a strip-line passed by the beam [49] can deliver the time-structure of single bunches, but are destructive.

PARTICLE ENERGY

In beam lines, beam energy and energy spread are usually determined using spectrometers, time-of-flight measurements, scattering or degrading methods. If in a cyclotron several particle species of similar charge to mass ratio are accelerated simultaneously, their separation by the cyclotron can be observed with a time-structure measurement. If the mass resolution of the cyclotron is not sufficient for a separation, the presence of different particles can still be detected by a measurement of their energy or stopping power with a thick or thin solid-state detector. The energy spread is thereby also measured. For low current beams this has been done by placing the detector directly into the beam [43].

EMITTANCE

Emittance measurements deliver start and check point information for beam transport simulations. In beam lines, the beam emittance can be determined by several direct (slit-slit, pepperpot and derived methods as e. g. Allison-scanner [50]) and indirect methods (quadrupole variation with 1 profile monitor behind, 3 profile monitors at different places without focussing in between, beam transport simulation fit to many profile monitors), with the latter suitable for high current beams.

Within the cyclotron [51] or a test stand simulating its center [52] the transversal emittance of an internal ion source has been measured directly although the limited space makes this difficult. At high beam currents, one could think of something similar for the beam halo, but for the beam core only the transport fit to radial or vertical profiles of many turns remains. Nevertheless, since beam width and angular distribution are coupled via the incoherent betatron oscillation, the emittance can also be approximately derived from beam width, orbit radius and betatron frequency.

BEAM LOSS

Collimator and aperture-foil current readings and the less sensitive comparison of full current measurements ("transmission measurement") almost directly determine beam losses. In addition, at not too low beam energies, beam losses are measured by detecting scattered beam particles or secondary particles. A variety of loss monitors are used mostly outside of the machine vacuum [53, 54].

A calibration of the sensitivity of these monitors can be established by deliberately steering a low current beam into the vacuum chamber at several locations [55]. This gives only a rough estimate, because it strongly depends on the relative position of loss and detector. Summing up the signal currents for larger machine sections, weighted also for beam energy, gives the operators an approximate but fast indication of machine performance concerning loss, activation and skyshine [56].

At PSI simple ionisation chambers filled with ambient air are in use since decades. The response is linear up to all dose rate levels of interest [57] and at excessive losses

the beam is switched off by the machine-protection system in the order of a millisecond.

Profiles measured by detecting externally the loss induced by a radial probe may be distorted due to the fact that particles, which are scattered at different parts of the probe head or at different probe positions, can be stopped at different places depending on the actual cyclotron geometry. On the other hand, losses caused purposely at known positions, e.g. from wire scanners or wire probes, can provide a cross-check for beam dynamic simulations.

CONCLUSION

Although it has been possible to measure almost any beam property of interest since many years [5], uncertainties in the beam behaviour and the beam halo nevertheless exist. Empirical tuning thus remains essential in establishing and optimizing the beam. The continued efforts in bettering beam dynamic simulations together with beam diagnostic systems will further increase our understanding of beam behaviour, ultimately alleviating the overdependence on empirical tuning. This will consequently lead to an improved machine performance, and will also suggest improvements in equipment and modes of operation or even completely new facilities.

ACKNOWLEDGEMENTS

The Author would like to thank PSI colleagues for useful discussions and M. Rohrer for the CAD drawing.

REFERENCES

[1] M. Seidel et al., "Production of a 1.3 MW Proton Beam at PSI", IPAC10, p. 1309.
[2] J.R. Richardson, "A Short Anecdotal History of the Cyclotron", CYC84, p.617.
[3] M.K. Craddock et al., "Cyclotrons and Fixed-Field Alternating-Gradient Accelerators", Rev. Acc. Sci. Tech. 1, p. 65 (2008).
[4] M.K. Craddock, Lecture "Introduction to Particle Accelerators", http://trshare.triumf.ca/~craddock/PH555/Intro-1.pdf.
[5] G.H. Mackenzie, "Beam Diagnostic Techniques for Cyclotrons and Beam Lines", CYC78, p. 2312.
[6] D.J. Clark, "Beam Diagnostics and Instrumentation", CYC66, p. 15.
[7] M. Olivo, "Beam Diagnostics Equipment for Cyclotrons", CYC75, p. 331.
[8] B. Launé, "Diagnostics for Radioactive Beams", CYC01, p. 359.
[9] J. Dietrich, "Recent Beam Diagnostic Techniques", CYC95, p. 186.
[10] P. Forck, "Lecture Notes on Beam Instrumentation and Diagnostics", JUAS 2010, http://www-bd.gsi.de/conf/juas/juas_script.pdf.
[11] U. Raich, "Instrumentation in small, low energy machines", DIPAC05, p. 1.
[12] P. Strehl, "Beam Instrumentation and Diagnostics", Springer 2006, ISBN 978-3-540-26401-9.
[13] Contributions to several CERN Accelerator Schools (CAS): e. g. many authors at CAS2008 Dourdan; R. Jones, H. Schmickler, K. Wittenburg at CAS2007 Daresbury; U. Raich at CAS2006 Zakopane; H. Koziol at CAS2000 Loutraki; http://cas.web.cern.ch.
[14] V.A. Verzilov, "Progress with Low Intensity Diagnostics at ISAC", IPAC10, p. 885.
[15] Picture from R. Kan, PSI. See also M. Humbel et al., "Disturbance Effects Caused by RF Power Leaking Out from Cavities in the PSI Ring Cyclotron", this conference.
[16] R. Dölling, "Measurement of the Time-Structure of the 72-MeV Proton Beam in the PSI Injector-2 Cyclotron", DIPAC01, p. 111.
[17] T. Stammbach, "Experience with the High Current Operation of the PSI Cyclotron Facility", CYC92, p. 28.
[18] A. Adelmann et al., "On Start to End Simulation and Modeling Issues of the Megawatt Proton Beam Facility at PSI", PAC05, p. 3319.
[19] J.J. Yang et al., "Beam Dynamics in High Intensity Cyclotrons Including Neighboring Bunch Effects: Model, Implementation, and Application", Phys. Rev. ST Accel. Beams 13, 064201 (2010).
[20] Y.J. Bi et al., "Towards Quantitative Predictions of High Power Cyclotrons", this conference.
[21] R. Dölling, "Determination of Radial Ion Beam Profile from the Energy Spectrum of Residual Gas Ions Accelerated in the Beam Potential", DIPAC99, p. 50.
[22] E. Bollmann et al., "A Simple Probe for the Relative Measurement of Beam Energies", CYC84, p. 419.
[23] H.G. Blosser, "Beam Quality Measurements and Focusing Grid Studies", CYC59, p. 203.
[24] R. Dölling, "Beam Diagnostics for Cyclotrons", Educational Session, ECPM XXXVII, Groningen, 2009. http://www.kvi.nl/~agorcalc/ECPM2009/EducationalSession/4_Doelling.pdf
[25] M.K. Craddock et al., "Properties of the TRIUMF Cyclotron Beam", CYC75, p. 240.
[26] L. Rezzonico, "Beam Diagnostics at SIN", CYC86, p. 457.
[27] W.R. Rawnsley, "A Current Mirror Circuit to Bias Beam Intercepting Pick Up Electrodes", TRI-DN-90-14, TRIUMF (1990).
[28] D.J. Clark et al., "Design and Operation of the U.C.L.A. 50 MeV Spiral-Ridge Cyclotron", CYC62, p. 1.
[29] A.A. Garren, L. Smith, "Diagnosis and Correction of Beam Behavior in an Isochronous Cyclotron", CYC63, p. 18.
[30] Y.N. Rao et al., "Calculations on LE2 Probe Head Thickness and Experimental Measurements", TRI-DN-04-8, TRIUMF (2004).
[31] H.W. Schreuder, "Shadow Measurements in a Cyclotron", NIM 95 p. 237 (1971).
[32] P. Forck, "Minimal Invasive Beam Profile Monitors for High Intense Hadron Beams", IPAC10, p. 1261.
[33] L. Badano et al., "A Real-Time Beam Monitor for Hadrontherapy Applications Based on Thin Foil Secondary Emission and a Back-Thinned Monolithic Pixel Sensor", DIPAC07, p. 352.
[34] M. Poggi et al., "Two-Dimensional Ionization Beam Profile Measurement", DIPAC09, p. 384.
[35] B. W. Allardyce et al.. "The Use of a Secondary Emission Monitor in the Extraction Channel of the CERN Synchro-Cyclotron", CYC75, p. 355.
[36] Z.B. du Toit et al., "Operating Experience with the Light-Ion Injector of the NAC", CYC86, p. 109.
[37] F. Becker et al., "Beam Induced Fluorescence Monitor & Imaging Spectrography of Different Working Gases", DIPAC09, p. 161.
[38] J. Dietrich et al., "Non-Destructive Beam Position and Profile Measurements Using Light Emitted by Residual Gas in a Cyclotron Beam Line", EPAC08, p. 1095.
[39] E. Griesmayer et al., "Diamond Detectors as Beam Monitors", BIW10.

[40] K. Wittenburg, "Halo and Bunch Purity Monitoring", CAS2008.
[41] W.C. Parkinson et al., "Modifications to the University of Michigan 83-Inch Cyclotron to Improve Beam Quality", CYC72, p. 366.
[42] F. Marti et al., "Internal Beam Dynamics Studies with a TV Probe", CYC92, p. 435.
[43] F. Chautard et al., "GANIL Status Report", EPAC04, p. 1270.
[44] T.W. Nijboer et al., "Beam-Phase Measurement in the AGOR-Cyclotron", CYC04, p. 416.
[45] F. Loyer et al, "New Beam Diagnostics at GANIL: Very Sensitive Current Transformers in Beam Lines and Counting System of Beam Turns in Cyclotrons", PAC85, p. 1938.
[46] W.R. Rawnsley et al., "The Production and Measurement of 150 ps Beam Pulses from the TRIUMF Cyclotron", CYC84, p. 237.
[47] T. Milosic et al., "Longitudinal Emittance Measurement Using Particle Detectors", DIPAC09, p. 330.
[48] F. Loyer et al, "Main Beam Diagnostics at GANIL", CYC81, p. 585.
[49] V. Verzilov et al., "A Wideband Intercepting Probe for the TRIUMF Cyclotron", TRI-DN-06-1, TRIUMF (2006).
[50] H.R. Kremers et al., "Comparison Between an Allison Scanner and the KVI-4D Emittance Meter", ECRIS08, p. 204.
[51] A.A. Arzumanov et al., "Alteration of the Ion Beam Emittance on the First Orbits in the Cyclotron", CYC81, p. 469.
[52] E.R. Forringer, "Phase Space Characterization of an Internal Ion Source for Cyclotrons", Dissertation 2004, MSU.
[53] K. Wittenburg, "Beam Loss Monitors", CAS2008.
[54] L. Fröhlich, "Beam Loss Monitors", ERL Instrumentation Workshop, Cornell Univ., 2008, http://tesla.desy.de/~lfroehli/download/ERL_instrumentation_ws_2008_BLMs.pdf
[55] U. Schryber et al., "High Power Operation of the PSI-Accelerators", CYC95, p. 32.
[56] W. Joho, "Recent and Future Developments at S.I.N.", CYC78, p. 1950.
[57] R. Dölling et al., "Beam Diagnostics at the High Power Proton Beam Lines and Targets at PSI", DIPAC05, p. 228.

BEAM DIAGNOSTICS FOR RIBF IN RIKEN

T. Watanabe*, M. Fujimaki, N. Fukunishi, M. Kase, M. Komiyama, N. Sakamoto, H. Watanabe, K. Yamada, and O. Kamigaito, RIKEN Nishina Center for Accelerator-Based Science, 2-1 Hirosawa, Wako, Saitama 351-0198, Japan
R. Koyama, Sumitomo Heavy Industries Accelerator Service Ltd., 1-17-6 Osaki, Shinagawa, Tokyo, 141-0032, Japan

Abstract

The Radioisotope Beam Factory (RIBF) at RIEKN started its operation in the end of 2006 with the aim of conducting systematic studies on the physics of radioactive isotopes. The simultaneous use of five accelerators in series necessitates precise measurement of beam properties such as beam intensities, beam energies, and bunch lengths. Hence, a beam diagnostic system plays an important role in the efficient and stable operation of RIBF. In this paper, we provide a brief summary of the conventional beam monitors used during the daily operations of RIBF. In addition, new non-destructive monitors that have been developed bearing in mind forthcoming intensity upgrades are described.

RI BEAM FACTORY

The RIBF project [1] aims to produce the world's most intense radioactive isotope beams using a four- or five-step accelerator complex. Our mission is to explore vast unknown fields of physics involving short-lived nuclei including r-process nuclei, which are required to gain an understanding of the process of nucleosynthesis in the universe. The two major acceleration schemes used in the RIBF project are illustrated in Fig. 1. The first scheme involves a variable-energy mode in which we use the RIKEN heavy-ion linear accelerator (RILAC) [2], RIKEN ring cyclotron (RRC) [3], intermediate-stage ring cyclotron (IRC) [4] and the world's first superconducting ring cyclotron (SRC) [5] in series. These accelerators are all of the variable frequency type and their beam energies can be changed. The variable-energy mode is used for ions lighter than those of krypton, and its maximum energy is 400 MeV/nucleon for ^{48}Ca and 345 MeV/nucleon for ^{86}Kr. However, an additional cyclotron, i.e. a fixed-frequency ring cyclotron (fRC) [6] should be used to accelerate ions heavier than those of xenon up to 345 MeV/nucleon, as shown in Fig. 1 (b).

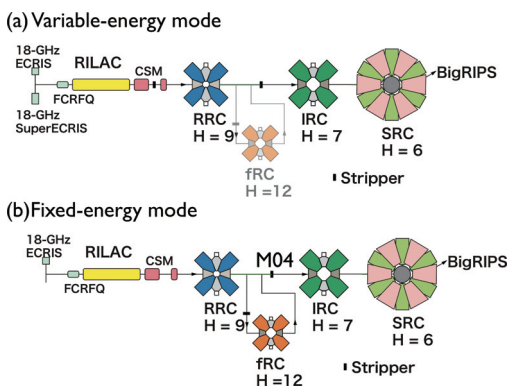

Figure 1: Acceleration schemes used in RIBF.

The beam intensities already achieved is 1 pμA, 0.23 pμA, and 1 pnA for 345-MeV/nucleon ^{18}O, 345-MeV/nucleon ^{48}Ca, and 345-MeV/nucleon ^{238}U, respectively. The total transmission efficiency of the three cyclotrons used in the variable-energy mode is nearly 85%. In contrast, the overall transmission efficiency of the four cyclotrons used in the fixed-energy mode is 40%.

CONVENTIONAL MONITORS

The beam intensities and transmission efficiency mentioned above are achieved by the use of the following conventional monitors (some of which are destructive).

Monitors Used in Beam Transport Lines

Monitors installed in beam transport lines and used in the fixed energy mode are summarized in Table 1. A Faraday cup is used to measure the beam intensity. Its design has been improved during the last three years to reduce uncertainties in the measurements. We originally adopted a compact design with a 1-kV ring suppressor and a relatively shallow cup structure. The original design allowed us to use only a single port of a beam chamber installed in beam lines. However, we found that this design overestimated beam intensities by a factor of 2 or 3 for uranium ions with energies more than 10 MeV/nucleon. The modified design employs a longer cup structure and a 72-mm suppression electrode, using which a uniform distribution of a suppression electric field can be achieved. The modified design still overestimates the beam intensity by a factor of 1.1 or 1.2, but the present overestimation is within acceptable limits for daily operations. The calibration of the beam intensity was carried out using a 40-cm long Faraday.

Table 1: Number of monitors used in beam transport lines. Abbreviations FC, PF, and PS represent a Faraday cup, beam profile monitor, and plastic scintillator, respectively.

Beam line	FC	PF	PS	Length (m)
RRC - fRC	9	12	3	81
fRC - IRC	10	25	4	119
IRC - SRC	6	13	3	64

* wtamaki@riken.jp

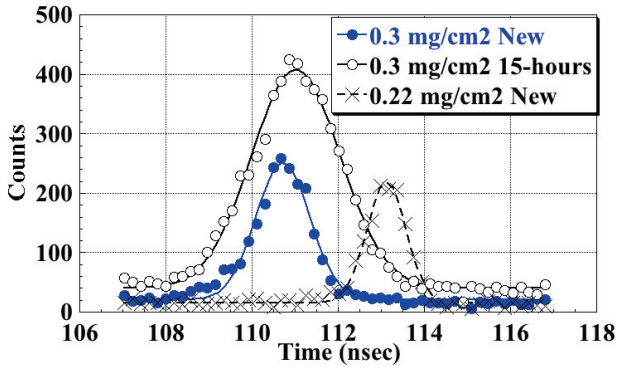

Figure 2: Longitudinal beam width measured by plastic scintillators.

We employ wire scanners as beam profile monitors. The profile monitors are used not only to check whether ions are transported according to our design but also to measure beam emittances based on the first-order ion optical theory. An example of emittance analysis can be found in Ref. [7].

Plastic scintillators are used in the time-of-flight (TOF) method to determine the beam energy. In the measurements, the beam intensity is greatly reduced (1000 cps) using beam attenuators. A mismatch in the beam energy being injected into a cyclotron causes a large-amplitude betatron oscillation of the beam centroid and results in beam loss during injection and extraction. In the case of uranium acceleration, a very thick carbon-foil is used to strip the electrons of the uranium beam, which is installed between fRC and IRC. Since a thickness error of the carbon-foil charge stripper causes the uranium beam to have the difference energy loss, the direct measurement of the beam energy is essentially important for the energy matching.

A longitudinal beam profile measured by using a plastic scintillator is also important to obtain good transmission efficiencies of the beam because the longitudinal emittance of the beams should be smaller than the longitudinal acceptance of RIBF accelerator complex. A striking example of the beam-width measurement is shown in Fig. 2. The time structure of a uranium beam were measured by using a plastic scintillator placed 38 m downstream of the charge stripper installed between RRC and fRC. When a new unused carbon-foil was used as a charge stripper, the longitudinal emittance was within the acceptance and resulted in more than 90% transmission efficiency in fRC. On the other hand, use of a charge stripper that had already been used for 15 h severely deteriorated beam quality, as shown in Fig. 2 and caused a beam loss of 50% in fRC.

Monitors Used in Cyclotrons

Phase pickup monitors and radial probes still play important roles in RIBF cyclotrons. Phase pickup electrodes are used to obtain good isochronous magnetic fields; 20, 14, 15, and 20 of these electrodes are used for RRC, fRC, IRC and SRC, respectively. In actual operation, a step-by-step optimization procedure is adopted. Starting with the values determined by magnetic-field measurements, the currents in the main and trim coils of the cyclotrons are updated to

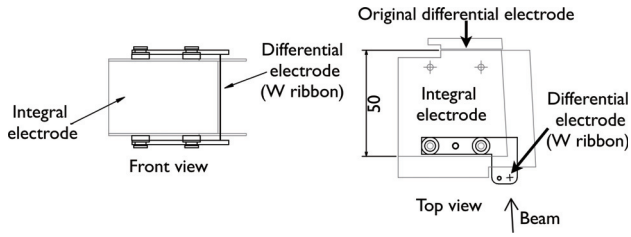

Figure 3: Modification of electrodes for SRC main radial probe. A tungsten ribbon (width : 0.3 mm) is introduced in front of the integral electrode instead of the original differential probe.

minimize a deviation from the idealistic isochronous condition by using the results of numerical simulations performed before the actual operation. Typically five rounds of updates are required to obtain the isochronous fields in which phase excursions of ions remain within a few RF degrees. In RRC, which started its operation in 1986 and is now used as an injector in RIBF, signals measured by phase pickup electrodes are pre-amplified and these signals can be monitored by using a digital oscilloscope because of a good signal-to-noise ratio. However, this is not the case with the three newly constructed cyclotrons (fRC, IRC, and SRC) because the operating acceleration voltages in these cyclotrons are twice as large as that in RRC and stray electric fields become signal-to-noise ratio worse. To overcome this problem, lock-in amplifiers and interference filters have been introduced.

A radial probe, which moves from the inner to the outer region or visa versa, measures the beam intensity and the turn pattern. The beam intensity is measured by the so-called integral electrode, whereas the turn pattern is measured by the so-called differential electrode. Both electrodes are insulated from each other. At the beam commissioning stage of RIBF, we employed similar designs as those used in RRC for the integral and the differential probes, but encountered several problems. The first problem is that a differential probe catches secondary electrons that are emitted by heavy-ion bombardment with the integral electrode The second problem is the electric noise due to stray electric fields, especially fields generated from flat-top resonators. The first problem is reduced by modifying the probe-head design, as shown in Fig. 3. To solve the second problem, the cylindrical covers of the radial probes are grounded by adding contact fingers to the upper half of the probes in addition to contact fingers already present in the lower half [8]. The differential probes are used during daily operations in order to select the optimum phases of the RF fields in the cyclotrons by comparing turn patterns. To avoid melting of the differential probes caused by the heat load, a beam chopping technique is used during the actual high-intensity operations.

NEWLY DEVELOPED MONITORS

Beam-phase and RF-phase Monitoring System

The destructive monitors described in the above section are useful for tuning a beam with a relatively low intensity

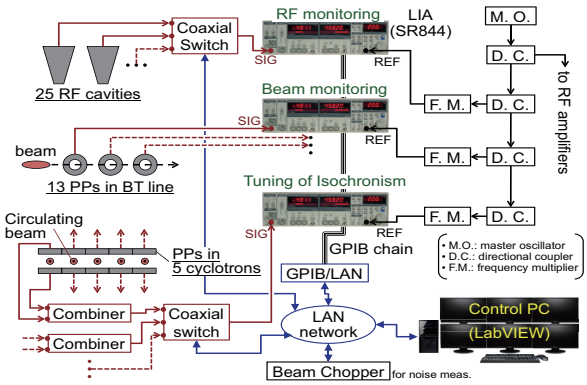

Figure 4: Block diagram of beam-phase and RF-phase monitoring system.

(less than few microamperes). However, non-destructive monitors that work continuously are required for the stable operation of RIBF. An integrated system that monitors the beam phases and RF fields of the accelerators has been developed [9]. The block diagram of this monitoring system is shown in Fig. 4. Signals induced by the passage of ions are detected by pickup electrodes. The signals are pre-amplified and continuously analyzed by a lock-in amplifier SR844 (Stanford Research Systems, Inc.). The resulting voltage and phase of the signal are displayed using a new software developed on the LabVIEW framework (National Instruments Corporation.). The target frequency of the lock-in amplifier is determined to obtain a better signal-to-noise ratio. The signals detected by the pickup electrodes installed in the RF cavities are also analyzed in a similar manner as described above. The merit of this integrated system is that we can easily understand the correlation between the fluctuations in the RF fields and the changes on the beam phases. An example of stability analysis can be found in Ref. [9]. By using the monitoring system, we found strong correlations between the measured fluctuations in the beam phase injected into RRC and the insufficient stability of the RF fields of the injector. Hence, old automatic voltage regulators were upgraded, and consequently, the stability of the beam improved.

Beam Intensity Monitor Using High-TC SQUID

A highly sensitive beam current monitor with a high-critical-temperature (high-Tc) superconducting quantum interference device (SQUID) and a high-Tc current sensor, that is, a high-Tc SQUID monitor, has been developed for use in RIBF at RIKEN [10]. In the present work, the high-Tc SQUID monitor allows us to measure the direct current (DC) of high-energy heavy-ion beams nondestructively in such a way that the beams are diagnosed in real time and the beam current extracted from the cyclotron can be recorded without interrupting the experiments performed by beam users. Both the high-Tc magnetic shield and the high-Tc current sensor were fabricated by dip coating a thin layer of Bi_2-Sr_2-Ca_2-Cu_3-O_x (2223-phase, Tc = 106 K) on a 99.9% MgO ceramic substrate. Unlike in

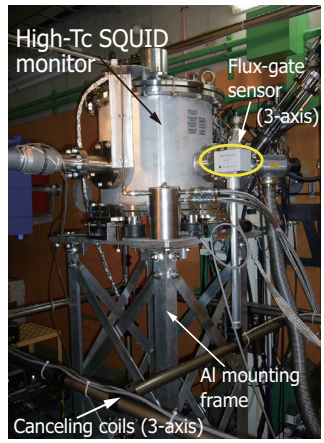

Figure 5: High-Tc SQUID monitor equipped with Al mounting frame and the noise cancellation system, which was installed in transport line between fRC and IRC.

other existing facilities, all the high-Tc devices are cooled by a low-vibration pulse-tube refrigerator in our facility, enabling us to downsize the system. Last year, to enable its practical use, the high-Tc SQUID monitor was installed in RIBF. Using the monitor, a 1-μA Xe beam intensity (50 MeV/u) was successfully measured with a 100-nA resolution. Figure 5 shows the high-Tc SQUID monitor equipped with an Al mounting frame and a noise cancellation system, which was installed in the transport line between fRC and IRC.

SUMMARY

Beam commissioning was carried out in RIBF using conventional beam instrumentation, as described above. Satisfactory performance of the beam monitors was achieved in the commissioning stage but some limitations were found, especially with regard to their destructive nature for beams. Several non-destructive monitors were developed and their effectiveness was demonstrated by using them during RIBF operation. One of the major remaining problem is to measure the time structure of a beam without reducing its intensity in order to avoid losing the space-charge effect during the measurement.

REFERENCES

[1] Y. Yano, Nucl. Instrum. Methods. B261, p. 1009 (2007), doi:10.101b/ j.nimb.2007.04.174 .

[2] M. Odera et al., Nucl. Instrum. Methods A227, p. 187 (1984).

[3] Y. Yano, Proc. 13th Int. Cyclo. Conf. p. 102 (1992).

[4] J. Ohnishi et al., Proc. 17th Int. Conf. on Cyclotrons and Their Applications, p. 197 (2004).

[5] H. Okuno et al., Proc. 17th Int. Conf. on Cyclotrons and Their Applications, p. 373 (2004).

[6] T. Mitsumoto et al., Proc. 17th Int. Conf. on Cyclotrons and Their Applications, p. 384 (2004).

[7] N. Fukunishi et al., Proc. PAC09, MO3GRI01 (2009).

[8] K. Yamada et al., Proc. HIAT09, MO-10, (2009).

[9] R. Koyama et al., Proc. EPAC08, TUPC052, (2008).

[10] T. Watanabe et al., Proc. BIW10, WEIANB02, (2010).

POST-ACCELERATION OF HIGH INTENSITY RIB THROUGH THE CIME CYCLOTRON IN THE FRAME OF THE SPIRAL2 PROJECT AT GANIL

A. Savalle, P. Bertrand, and the GANIL/SPIRAL2 staff, GANIL, Caen, France

Abstract

The cyclotron CIME is presently used at GANIL for the acceleration of SPIRAL1 radioactive beams. One of the goals of the SPIRAL2 project is to produce, post-accelerate and use in the existing experimental areas much higher intensity secondary beams induced by uranium fission like neutron-rich krypton, xenon, tin isotopes, and many others. Intensity may reach 10^{10} pps. Specific developments are needed for secondary beam diagnostics. Improvement of mass separation is also necessary, and the Vertical Mass Separator (VMS) is specially developed for this purpose.

However, the main concern is related to the high radioactivity linked to RIB high intensity. Safety and radioprotection issues will require modifications of the installation with special care for the maintenance of the cyclotron. The experience of the SPIRAL1 beams, in terms of beam losses and equipment contamination, is especially useful to define the necessary modifications.

INTRODUCTION

The SPIRAL1 facility is now operated since 9 years, so post-acceleration of radioactive beams at GANIL is now routine operation. The SPIRAL2 new facility will extend the possibilities offered to heavier radioactive beams, with much higher intensities, intense beams of neutron-rich exotic nuclei (10^6–10^{10}pps), in the mass range from A=60 to A=140 0. Extracted exotic beam will either be used in a new low energy experimental area called DESIR, or accelerated by means of the existing SPIRAL1 cyclotron (CIME). Post-accelerated beams will then be driven to existing experimental areas (figure 1).

The intense primary stable beams (deuterons, protons, light and heavy ions) will also be used at various energies for neutron-based research, nuclear physics and multi-disciplinary research, in new experimental areas called NFS and S3 0.

In what follows, we give a brief description of the main parts of the new facility, and the status of its construction. Then, in the existing facility, we develop the necessary developments concerning secondary beam diagnostics, and improvement of the mass separation.

Safety and radioprotection aspects are studied in details. Indeed, expected intensities are up to three orders of magnitude higher than with SPIRAL1, while radiological effects may be much more drastic. The experience on SPIRAL1 beams, in terms of beam losses and contamination, is studied in detail in order to decline the necessary modifications.

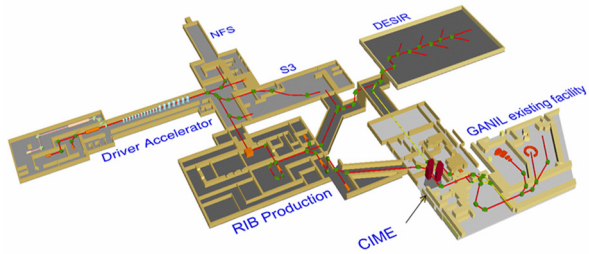

Figure 1: Layout of the SPIRAL2 project, with experimental areas and connexion to existing GANIL

SPIRAL2 DRIVER ACCELERATOR, EXPERIMENTAL AREAS AND PRODUCTION BUILDING

Beams to be Accelerated

Accelerated beams will include protons, deuterons, ions with A/q<3, and optionally ions with A/q<6. As indicated in table 1, a maximum beam power of 200kW is required for deuterons in CW mode.

Table 1: Beam Specifications

beam	P+	D+	ions	ions
Q/A	1	1/2	1/3	1/6
Max. I (mA)	5	5	1	1
Min. output W (MeV/A)	2	2	2	2
Max output W (MeV/A)	33	20	14.5	8
Max. beam power(KW)	165	200	44	48

Injector-1

The Injector-1, dedicated to protons, deuterons and ions of q/A=1/3, is mainly composed of two ECR ion sources with their associated LEBT lines, a warm RFQ and the MEBT line connected to the LINAC.

The 2.45GHz ECR source for deuterons is under test in the CEA/IRFU laboratory at Saclay, with promising results in terms of stability and reliability.

The q/A=1/3 heavy ion ECR source and its analysis beam line are installed at the LPSC laboratory (Grenoble). First beam tests give the expected results in terms of transmission, beam tuning and emittance 0.

Developed by CEA/IRFU team, the RFQ0 is a 4-vane, 88MHz 5-meter copper cavity ensuring bunching of the continuous beam, and acceleration up to 0.75Mev/u.

The first 1-meter RFQ segment is just constructed, and under mechanical and RF tests.

The MEBT line achieves the matching at entrance of the LINAC. It allows also connection of the future Injector-2, dedicated to q/A=1/6 heavy ions, and a very

clean fast chopping of the beam bunches for NFS experiments.

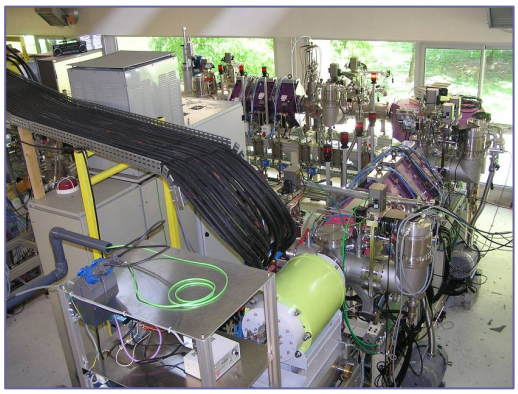

Figure 2: View of ECR source and Spiral2 LEBT1 installed at LPSC (Grenoble) for beam tests

Linac

The LINAC accelerator 0 is composed of 2 families of 88Mhz quarter-wave resonators, developed by the CEA/IRFU and the IN2P3/IPNO teams: 12 resonators with β_0=0.07, and 14 others with β_0=0.12. The transverse focusing is ensured by means of warm quadrupole doublets located between each cryomodule. These warm sections hosts beam diagnostic boxes and vacuum pumps.

All series of β_0=0.07 cavities and corresponding cryomodules shall be delivered at CEA/IRFU by September 2010 and end 2010 respectively. The production of β_0=0.12 cavities was achieved in November 2009, an tested successfully in vertical cryostat during 2010.

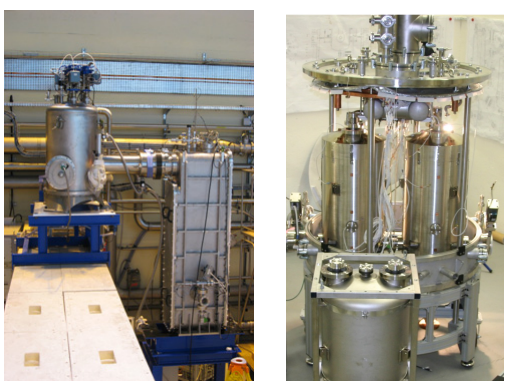

Figure 3: Tests of Crymodule A (Saclay) and assembly of Cryomodule B (Orsay)

HEBT Lines and AEL Experimental Hall

The high energy beam transfer lines transport the accelerated beam either to:

The main beam dump (200 kW) needed for the beam studies, commissioning and tuning.

- The RIB production module, located in the production building.
- The NFS experimental hall, dedicated to neutron-based research.
- The S3 experimental hall (Super Separator Spectrometer, with high mass selectivity).

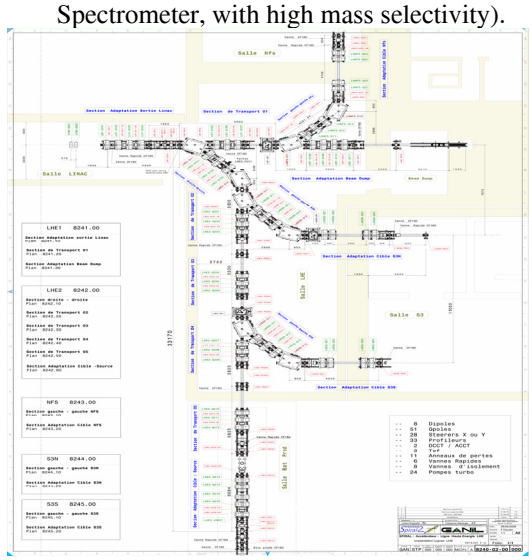

Figure 4: View of the HEBT beam lines

The Letters of Intent (LoI) for the first uses of LINAC beams in NFS or S3 have been already evaluated by the Scientific Advisory Committee (SAC). The associated detectors are in a well advanced phase of design.

Public Enquiry and Start of Construction

The public enquiry, necessary step for the authorization, was launched on June 14th, 2010. The construction of the accelerator building itself should begin by end 2010.

RIB Production and Transport

The general layout of the RIB production and beam transport scheme is presented below:

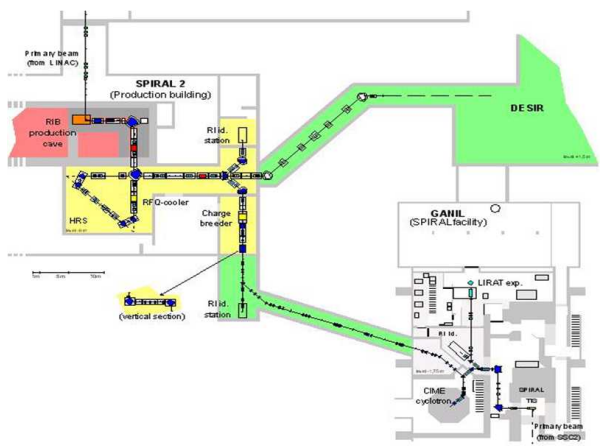

Figure 5: General layout for the RIB section

The main Target-Ion-Source (TIS) contains a rotating carbon converter for the production of neutrons using the 5mA 20A.MeV deuteron primary beam. The neutron flux produces fission reactions in a uranium carbide target. The carbon converter target is developed, in the frame of a collaboration with the LNFN/LNL laboratory. A first version is developed for a 50 kW beam power 0.

The uranium carbide target will be a high-density one (11g/cm^3) for a yield of 5.10^{13}fissions/s 0. The ionisation scheme uses four types of 1+ ion sources: ECR, FEBIAD, surface ionisation, and laser ion source.

The beam analysis line enables to select the mass of interest. Despite the use, as often as possible, of selective sources, the beam of interest will often be polluted by isobars. A selection tool is being developed, in two steps: a RFQ-cooler, developed by LPC-CAEN, to decrease the emittance to 1 π mm.mrad 0, and a High Resolution Separator (HRS), developed by CENBG 0.

Next, the 1+ transfer line, from the ion sources either to the identification station,, to the low-energy experimental area DESIR or to the charge booster, will privilege electrostatic components.

The charge booster, needed to inject the RIB into the CIME cyclotron, is of Phoenix type and developed by the LPSC laboratory 0.

The n+ beam line will transport the beam towards the CIME cyclotron, inside the existing GANIL hall.

Safety Aspects

The cave housing the production module and the 1+ analysis line will be a radiological red zone (Equivalent Dose Rate> 100 mSv/h), due to activation and to fission products. Thus, disconnection, maintenance, and TIS reconnection will be realized by a robot and master-slave manipulators.

The HRS and booster are both in a "yellow zone", accessible after decreasing of radioactivity (the access will be possible when the EDR is <2 mSv/h).

The safety requirements imply also to confine the radioactive beams. The mechanical design of the beam lines is based on independent modules with double valves, so that it will be possible to extract a module without loss of confinement. The whole vacuum system will be connected to a gas storage system, in order to release gas after a suitable radioactivity decrease period and gas analysis verifications.

Production Building

The production building, which will host the RIB production cave and the RIB transport lines, will be of nuclear type. It will contain hot cells, for the production cave (including production module, and analysis beam line), for maintenance operation on the production modules, and for nuclear waste.

Use of Radioactive Beams

The SAC will evaluate the LoI for the radioactive beams in January 2011. First requests indicate the interest of the community in SPIRAL2 beams at low energy in DESIR (40% of requests), as well as in post-accelerated beams.

ACCELERATION OF THE RIBs IN THE CIME CYCLOTRON AND USE OF THE EXISTING EXPERIMENTAL AREAS

Acceleration of RIBs in CIME Cyclotron

SPIRAL2 beams include potentially all ion isotopes from ^{6}He to ^{238}U, with two production maxima (in case of UCx fragmentation) around A=90 and A=130.

For light beams, the CIME energy range is 1.2 MeV.A (F_{RF} = 9.6 MHz, h= 6)-24 MeV.A (F_{RF} = 14.4 MHz, h= 2). For heavy ions, the maximal energy depends on the charge/mass (q/A) ratio. Examples are $^{91}Kr^{17+}$ at 9.3 MeV.A, $^{132}Sn^{20+}$ at 6.1 MeV.A.

Gas profilers will no more be convenient for heavy masses (A>100) and low energy (E<3 MeV.A), due to the thickness of the window). R&D is launched to determine how to extend the energy range of these diagnostics or to develop new ones. Preliminary, encouraging results are detailed in 0.

Another issue is the separation of the different isobars inside the cyclotron. The RIBs produced in SPIRAL2 will have higher masses, and thus will have much lower differences in Δm/m implying very small differences in phase position at extraction (Table 2).

Table 2: Possible pollutant, mass separation and phase difference at the CIME extraction for different beams

beam	Possible pollutant	d(q/m)/(q/m)	Phase shift at ejection (φ)
$^{15}O^{4+}$	$^{15}N^{4+}$	1.9 10^{-4}	48°
$^{132}Sn^{20+}$	$^{132}Xe^{20+}$	1.0 10^{-4}	35°
$^{140}Cs^{21+}$	$^{140}Ba^{21+}$	4.8 10^{-5}	16°

Using additional separation systems will thus be necessary. For this purpose, a vertical mass separator located inside the cyclotron has been developed at GANIL 0 and a prototype was tested in various configurations. The pollutants were simulated by applying a shift of the cyclotron magnetic field (ΔB/B = 10^{-4} for a pollutant with Δm/m = 10^{-4} for example).

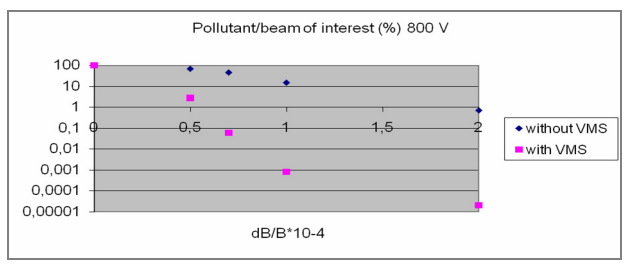

Figure 6: ratio pollutant/beam of interest in function of Δm/m

In the best case, it is possible to obtain a significant decrease of the intensity of the pollutant even when Δm/m approaches a few 10^{-5}, and to divide this intensity by a factor 10^3 when Δm/m = 10^{-4} (figure 6).

The final device is under construction. We hope to separate ^{132}Sn from ^{132}Xe, or ^{140}Cs from ^{140}Ba, or at least, to achieve a significant decrease of the pollutant intensity.

Safety Issues

The CIME cyclotron was constructed in the frame of the SPIRAL1 project, for the production of rather light ions (up to krypton) and of very short-lived elements. Thus, the problematic of radioactivity and contamination deposited inside the low-energy beam lines or in the cyclotron centre was not considered at that time.

With the SPIRAL2 project, producing beams with an important radiological impact (such as Sn beams which decays to Iodine), we must now consider the Equivalent Dose Rates (EDR) due this deposition, and also the risks of contamination. Release of radioactivity is to be avoided in case of accident leading to loss of confinement.

Hopefully, higher energy implanted atoms should be much less released than at low energy or not at all.

Experience with the SPIRAL1 Operation

In order to get a better knowledge about the way the radioactivity is deposited in the low-energy beam lines, the CIME cyclotron (figure 7), and the experimental areas, several beam tests have been realized.

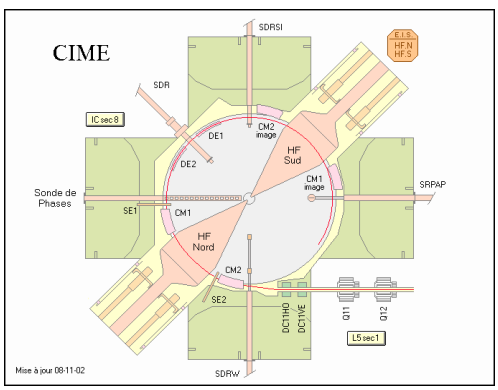

Figure 7: CIME cyclotron

First, a ^{76}Kr beam was accelerated and stopped on a tantalum plate mounted in the ejection beam line. The half-live is 14.8 hours (^{76}Kr→^{76}Br) and 16.2 hours (^{76}Br→^{76}Se).The average intensity was 2.10^7 pps before acceleration, and 5.10^6 pps after acceleration.

After 3 days of production, the beam was stopped and the cyclotron opened. EDR was measured along the beam line and inside the cyclotron. Superficial contamination was also investigated, leading to the following results:

- An EDR of 1 mSv/hour was measured at the contact of the tantalum plate. No superficial contamination was found; ions were implanted in the plate.
- An EDR of 1 mSv/hour was also measured at the contact of the inflector (entrance side), with a superficial contamination of 10 000 Bq. This corresponds to about 30% losses on inflector, with 10% superficial contamination.
- Losses were also present on the septum plate of the first exit deflector (about 15%), in the cavity extremities, and at the entrance of the second magnetic channel.
- Some losses (a few %) were also measured in the injection beam line. EDR measurements showed that the cryogenic pumps located at proximity of these beam losses were contaminated.

These results indicate the losses, thus the radiation levels to be considered in case of maintenance of specific elements. Superficial contamination must be taken into account in particular at injection (losses at low energy). Some contamination of the pumps is also to be considered in the low energy line.

During other beam tests, .the contamination of the vacuum pumps, in injection beam line as well as in ejection one, has been quantitatively determined. Beam "losses" were simulated by detuning and gamma spectrometry used to measure the contamination trapped by a cryogenic trap.

At low energy, the contamination corresponds to 10 to 20 percents of the beam losses nearby. At medium energy (> 1 MeV.A), this contamination is very low (<1%).

Consequence for the SPIRAL2 Operation and Necessary Modifications

Maintenance

Using the preceding measurements, and extrapolating to ^{132}Sn, representative of SPIRAL2, the different maintenance operations have been studied.

As an example, the EDR at 30 cm of the inflector would be around 2 mSv/hour a few days after the beam stop. Total maintenance operation lasts about 20 minutes while the operation at close proximity of the inflector lasts about 5 minutes. The total integrated dose for the operator is about 200 µSv per operation.

Considering the frequency of each maintenance operation, the annual collective dose related to SPIRAL2 beams in the existing facility is estimated to 10 man.mSv. This means that operation is possible with some optimisations, including use of spares for inflectors, deflectors, and improvement of mechanics in order to ease mounting and dismounting, and to reduce the operation time close to the equipment.

Figure 8: maintenance of the inflector

Modifications of the CIME Casemate

A particular attention will be necessary to avoid contamination of the cyclotron hall during operation maintenance. Nevertheless, taking into account an accidental contamination, a confinement will anyway be necessary. The walls will have to be sealed, and a nuclear ventilation will complete the confinement.

This study is still preliminary and the modifications are quite important (preliminary cost ~2 M€).

Vacuum

In the SPIRAL2 facility, up to the CIME cyclotron, the contamination of the pumps justifies the connection of these pumps to the storage of gases.

After ejection, the contamination of the "vacuum" gases is reduced, so that their storage is not necessary. However, they have to be collected and analyzed before release. Thus, the vacuum system has to be modified, with in particular the use of hermetic primary pumps.

Experimental Areas

The SPIRAL2 radioactive beams will be mainly used in the G1 and G2 experimental areas (figure 9). These two rooms are largely used today for SPIRAL1 beams, with in particular the gamma detector EXOGAM, and the VAMOS spectrometer in G1.

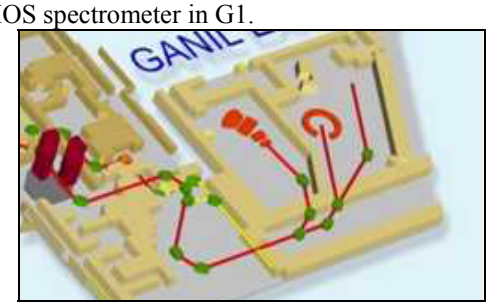

Figure 9: Cyclotron CIME connected to G1 & G2 experimental halls

The challenge of using the high intensity radioactive beams in the experimental areas is related to the high activity (up to 10^{10} Bq) close to a gamma detector. One would have to take care of:

- The incident beam (it has to be stopped away from the detector with a shielding).
- Interactions of the incident beam with residual gas resulting to halo and other causes of losses.
- Rutherford scattering on target.

A project is launched in order to modify the beam lines and experimental equipment in these two rooms. The other experimental areas will be treated in a second time.

CONCLUSION

The major SPIRAL2 accelerator components are in their phase of technical tests and/or construction, while the accelerator building is completely defined. The detailed design solution of the RIB process equipments and the production building, compatible with the safety constraints, is underway.

The necessary modifications of the existing GANIL facility have been identified, but are still to be fully validated.

At the beginning of SPIRAL2 operation with the cyclotron CIME,, the beam intensity will probably be reduced to check the hypothesis in terms of radioprotections, safety, and detection.

AKNOWLEDGEMENT

The authors address their thanks to the whole SPIRAL2/GANIL team and many French and foreign laboratories involved in the project.

REFERENCES

[1] MG Saint-Laurent on behalf of the Spiral2 project group, "Future opportunities with SPIRAL2 at GANIL", AccApp07, Pocatello, Idaho, July 30-August 2nd, 2007.

[2] P. Bertrand, MH Moscatello, "the advancement of SPIRAL2 project", Cyclotron 2007, Giardini-Naxos, Italy.

[3] J.L. Biarrotte et al., "First beams produced by the SPIRAL2 injectors", Linac 2010, Tsukuba, Japan.

[4] R. Ferdinand et al, "Spiral2 RFQ design", EPAC 2004, Luzern, Switzerland, July 2004.

[5] P.E. Bernaudin et al., "Status of the SPIRAL2 superconductiong linac", IPAC 2010, Kyoto, Japan.

[6] L.B. Tecchio, "Design of a high power Neutron converter for SPIRAL2", EMIS 2007, Deauville, France.

[7] M. Fadil, "About the production rates and the activation of the uramium carbide target in Spiral2", EMIS 2007, Deauville, France.

[8] X. Fléchard, SPIRAL2 High Intensity Cooler, http://spiral2ws.ganil.fr/2010/week/presentations/rnbT. Kurtukian Nieto, High Resolution Separator, http://spiral2ws.ganil.fr/2010/week/presentations/rnb.

[9] T.Lamy et al, "Status of charge breeding with electron cyclotron resonance ion sources", Rev. of Scient.Instrum., 11th International Conference on Ion sources (ICIS'05), France 2006.

[10] P. Anger et al,, Beam diagnostics for SPIRAL2 RNB facility, Dipac09, 25-27 May 2009, Basel, Switzerland.

[11] P.Bertrand, F. Daudin, M. Di Giacomo, B. Ducoudret, M. Duval, "improvement of the mass separation power of a cyclotron by using the vertical selection method", Cyclotron 2004, Tokyo.

ACCELERATION ABOVE THE COULOMB BARRIER – COMPLETION OF THE ISAC-II PROJECT AT TRIUMF*

R.E. Laxdal, TRIUMF, Vancouver, Canada

Abstract

The ISAC-II project at TRIUMF was proposed to boost the final energy of the radioactive ion beams of the TRIUMF ISAC facility above the Coulomb barrier. The nominal goal of 6.5MeV/u for ions with A/q=6 was recently achieved. The ISAC-II project consists of 40MV of installed heavy ion superconducting linac to broaden the energy reach and a charge state booster to broaden the mass reach. The project and commissioning is described.

INTRODUCTION

TRIUMF has operated a 500MeV H^- cyclotron since 1974. The TRIUMF facility (Fig. 1) was expanded in 1995 with the addition of a radioactive beam facility, ISAC. The radioactive species at ISAC [1] are produced by a 500MeV proton beam of up to 100μA bombarding a thick target. After production the species are ionized, mass separated and sent to either a low energy area or pass through a string of linear accelerators to feed experiments at higher energies. First beams from ISAC were available in 1998 while first accelerated beams were delivered in 2001. The initial accelerator consisted of a 4.5MV RF quadrupole and an 8.1MV Drift Tube Linac delivering beams with A/q≤30 to medium energy users at energies from 0.15-1.5MeV/u chiefly for experiments in nuclear astrophysics.

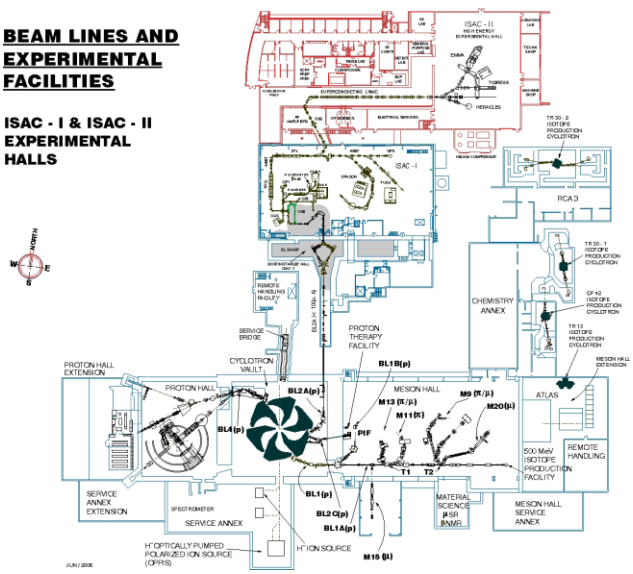

Fig. 1: The TRIUMF facility showing the 500MeV cyclotron and the ISAC-I and ISAC-II facilities.

The TRIUMF ISAC-II superconducting linac, proposed in 1999 [2], was designed to raise the radioactive ion beams above the Coulomb barrier to support nuclear physics at TRIUMF. The goal was to achieve E ≥ 6.5MeV/u for ions with mass to charge ratio of A/q ≤ 6. The first stage of this project, Phase I, commissioned in 2006, involved the addition of 20MV of superconducting linac. Phase II of the project consisting of an additional 20MV of superconducting linac has recently been installed and commissioned. In parallel an ECR ion source was installed to act as a charge state booster to raise the A/q ratio of low energy high mass beams to be compatible with acceleration through the ISAC accelerators. This paper will concentrate on the progress towards higher energies at ISAC and in particular on the recent Phase II upgrade.

LINEAR ACCELERATORS - GENERAL

Since this is a cyclotron conference a talk on a linear accelerator installation may seem somewhat out of place. TRIUMF is at its roots a cyclotron lab with a pedigree not only based on the main 500MeV cyclotron but also on the design, commissioning and operation of the commercial cyclotrons TR30 and TR13. As cyclotron builders we also have to be cognizant of other particle accelerators and their capabilities. These other machines can be used in combinations with cyclotrons either for injection or post-acceleration. The strong advantage of a cyclotron is the improved efficiency of rf utilization in cw application with the same rf system used on multiple turns. This does require a precise magnet to maintain isochronism so that the beam remains in phase with the accelerating field. Injection and extraction are complicated and beam emittance can be broadened due to the dependence of energy and radial position and particularly in cases where a variety of ions require acceleration. Cyclotron builders have imaginative ways of reducing the impact of these complications. Linear accelerators hold some advantage in certain applications. In general injection and extraction from linear accelerators is relatively straightforward and transmission high due to simplified acceleration. In particular RF quadrupoles with their strong transverse focussing and high acceptance have been used successfully in injection beamlines to take the place of large and complicated high voltage platforms that were historically used to reach the required injection energy. Drift tube linac tanks can be made with relatively few gaps (at the expense of rf efficiency) to allow some phase slip of the accelerating beam yielding straightforward ways of achieving variable energy acceleration. Superconducting hadron linacs can achieve, for very short versatile structures, significantly improved rf efficiency (~100 times) over cw room temperature linacs due to the very low resistive losses. It is relatively straightforward to accelerate beams with a normalized transverse emittance

*TRIUMF receives funding via a contribution agreement through the National Research Council of Canada

defined by the source, longitudinal emittances of 1keV/u-ns with fully variable energy and with high transmission.

ISAC-I ACCELERATORS

The accelerator chain includes a 35.4 MHz RFQ, to accelerate beams of $A/q \leq 30$ from 2 keV/u to 153 keV/u and a post stripper, 106 MHz variable energy drift tube linac (DTL) to accelerate ions of $2 \leq A/q \leq 6$ to a final energy between 0.153 MeV/u to 1.53 MeV/u. Typically 1+ beams are produced in the on-line source but recently the Charge State Booster ECR source has been commissioned to raise the charge state of the 1+ ions to produce high mass beams with charge to mass ratios compatible with acceleration.

The RFQ[3], a four vane split-ring structure, has no bunching section; instead the beam is pre-bunched at 11.8 MHz. This not only shortens the linac but reduces the longitudinal emittance at a small expense in the beam capture. The variable energy DTL[4] is based on a unique separated function approach with five independent interdigital H-mode (IH) structures, each with 0^{o} synchronous phase, providing the acceleration with quadrupole triplets between tanks and three-gap bunching cavities before Tanks 2,3,4 providing transverse and longitudinal focusing respectively. The DTL is designed to efficiently accelerate low-β heavy ions over a large operating range while maintaining high beam quality. The IH tanks consume only 63 kW of rf power to produce a total accelerating voltage of 8.1MV over the 5.6m length. To achieve a reduced final energy the higher energy IH tanks are turned off and the voltage and phase in the last operating tank are varied. Both the RFQ and DTL have been used to reliably provide a variety of radioactive and stable ions since 2001.

THE ISAC-II LINAC

The ISAC-II linac was commissioned in 2006[5] and the Phase II upgrade[6] was commissioned Apr.-Aug., 2010. The superconducting linac is composed of bulk niobium, quarter wave resonator (QWR) for acceleration, and superconducting solenoids, for periodic transverse focusing, housed in several cryomodules. The Phase-I linac consists of twenty QWRs housed in five cryomodules (SCB1-5) with four cavities per cryomodule. The first eight cavities have a geometric beta of 5.7% and the remainder a geometric beta of 7.1%. The cavities operate at 106MHz. The Phase-II upgrade also consists of twenty QWRs housed this time in three cryomodules (SCC1-3), six cavities in each module for SCC1-SCC2 and eight cavities in SCC3. These bulk niobium cavities have a geometric beta of 11% and are resonating at 141.44MHz. One 9T superconducting solenoid is installed in the middle of each of the eight cryomodules in close proximity to the cavities. The ISAC-II building is shown in Fig. 1; the SCB and SCC sections of the linac are identified.

SRF facilities at TRIUMF (Fig. 2) include a preparation room for parts cleaning, a cavity test area with overhead crane, cryogenic services and test pit, a clean assembly area, a BCP etching lab and high pressure water rinse area. The cryogenic facilities that deliver both LHe and LN2 to the linac vault are adjacent to the linac tunnel.

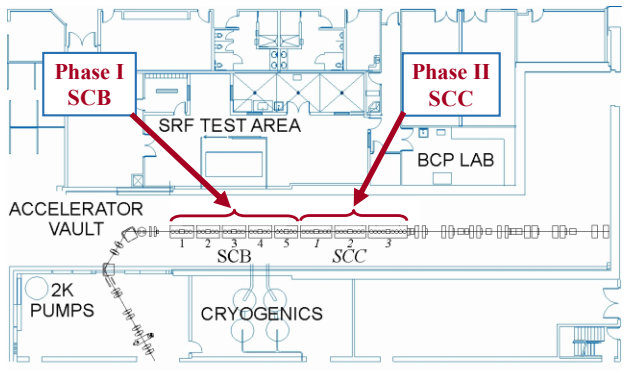

Fig. 2: The ISAC-II superconducting linac.

CAVITIES

The ISAC-II superconducting cavities are shown in Fig.3. The rf cavities are patterned after structures built for the low beta section of the INFN-Legnaro heavy ion linac. The cavities have a simple construction with a cylindrical shape, a rigid upper flange and an annular lower flange designed for mounting a removable tuning plate. The helium jacket is a cylinder of reactor grade niobium formed from two sheets and welded to the upper and lower flanges. A common outer conductor diameter of 180 mm is used for all cavities. The chief difference between the Phase I and II cavities besides the frequency (and therefore the height) is that in Phase II the inner conductor beam port region is outfitted with a drift tube. The ISAC-II performance goal is to operate cw at a gradient of 6 MV/m, as defined by the inner diameter of the outer conductor, corresponding to a peak surface field of 30MV/m and peak magnetic field of 60mT with a cavity power ≤7W.

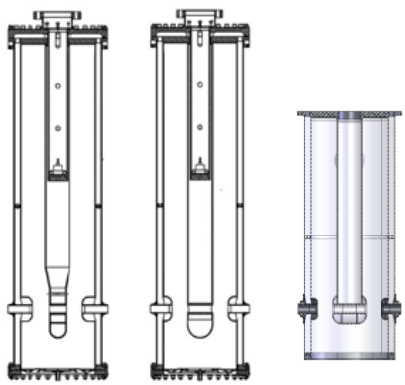

Fig. 3: From left to right: the 106 MHz β=5.7% and 7.1% QWRs for phase-I and 141.44MHz β=11% QWR for Phase-II.

The Phase I cavities were produced by Zanon in Italy and the Phase II cavities by PAVAC Industries in Canada. Cavity prototyping studies began with PAVAC Industries

in 2007. Two cavity prototypes were successfully developed and tested in 2008 [7]. Both cavities exceeded specification with an average gradient at 7W cavity power corresponding to a peak surface field of 38MV/m.

Processing and Preparation

Standard cavity processing involves visual inspection, room temperature frequency measurement, degreasing and a Buffered Chemical Polish (BCP) surface etching; 120µm in Phase I and 60-100µm in Phase II. In Phase II a number of cavities receive a custom etch where the root end (top of the cavity in Fig. 2) receives more etching to tune the frequency. An in-line chiller coil keeps the acid at 12^0C during the etching procedure. A photo of the Phase II cavity after etching is shown in Fig. 4.

The cavities are then assembled with a stainless steel top flange bolted to the niobium flange. The stainless steel flange is outfitted with a mechanical damper assembly that is inserted into the inner conductor to reduce detuning vibrations from microphonics. Pre-cool tubes of thin wall stainless steel pass through the neck of the stainless steel flange and inside the inner conductor and helium jacket to flow cold helium gas to the bottom of the cavities during cool-down.

After the assembly is complete the cavities are rinsed with high pressure ultra pure water for forty minutes and air dried in a clean room for 24 hours. Some Phase II cavities have received an additional alcohol rinse after HPWR to aid in drying. At this point the cavities are either assembled on the test cryostat for single cavity characterizations or mounted in the cryomodule for linac on-line operation. In either case the cavities are baked for 48 hours (85-90C in test cryostat, 70-75C in cryomodule) then the cryostat thermal shield is cooled with LN2. After 24 hours of pre-cool by radiation the cavity is cooled with LHe. Typical cooldown rates are 80-100K/hour between 150-50K.

Both the single cavity cryostat and cryomodule assembly take place in a clean room. In both cases there is no isolation between the thermal isolation vacuum and the rf space vacuum; cryostat and cryomodule design avoid particulate generators (MLI) and volatile lubricants, solvents, flux that could reduce cavity performance [8]. A single cold Cryoperm magnetic shield is clamped around the cavity for single cavity tests while in the cryomodule a warm µ-metal layer is fastened inside the vacuum vessel wall (1mm in SCB's and 1.5mm in SCC's). The goal is to achieve a background magnetic field of <20mG to avoid trapped flux in the superconductor that can increase surface resistance.

Production

Including the initial prototype, 21 Phase I cavities were received from Zanon. Of these one did not meet specification due to a low field quench. The others were assembled into the working linac. Single cavity characterizations gave an average single cavity performance corresponding to a peak surface field of 37 MV/m at 7W cavity power and an effective voltage of 1.3MV.

Fig. 4: Phase II cavity after etching.

Two prototypes were tested frm PAVAC Industries in 2007. Twenty production cavities were ordered from PAVAC in 2008. The planned delivery sequence of three separate batches (6+6+8 cavities) corresponded to the number of cavities to be assembled in the three cryomodules of the Phase II linac. Four cavities were rejected (#7, 8, 12, 13) due to a common fault; a vacuum leak opening up in the saddle weld joining the drift tube assembly to the inner conductor. After the weld the joint is surface polished to make a smooth transition but this step causes a thinning in the melt zone. In each case the cavity leak opened after the final etching treatment at TRIUMF of 100µm. The cavities were subsequently repaired but as a result the etch specification was reduced from 100µm to 60µm as a precaution. The rationale was as follows: all inner conductor assemblies had been completed with similar fabrication technique and due to the tight project schedule further cavity failures were deemed a high risk.

The performance tests of nineteen cavities are shown in Fig. 5. Cavity #8 is a repaired cavity. The plot shows that only two cavities (Cavity #17 and Cavity #23) are significantly under the ISAC-II specification of Ep=30MV/m@7W cavity power. The average accelerating gradient corresponds to a peak surface field of 32MV/m at 7W. We believe that the reduced performance with respect to Phase I is related to the reduced etching. This is under study. All cavities are within ~30kHz of the goal frequency of 141.44MHz within the tuning range of the flexible tuning plate.

CRYOMODULES

The Phase-II cryomodules are identical in many respects compared to the Phase I cryomodules [8]. A key design choice was to maintain the philosophy of incorporating a single vacuum space for thermal isolation and beam/rf volumes. This has been the historic choice in the low-beta community (ATLAS, INFN-Legnaro, JAERI) but recent proposed facilities in development or assembly have chosen separated vacuum systems (SARAF,

SPIRAL-II, FRIB). We have seen very little evidence of degradation in cavity performance over the first four years of operation even after repeated thermal and venting cycles. Procedures are followed to help reduce cavity degradation: 1. Initial cavity treatment and overall assembly using HPWR and clean conditions 2. Vacuum materials and components to be free from particulate, grease, flux and other volatiles 3. Maintain a LN2 cooled cold trap upstream and downstream of the linac to prevent volatiles migrating from the beamline into the cryomodule 4. Cryomodule venting with filtered nitrogen 5. Pumping and venting of modules at slow rates to avoid turbulences.

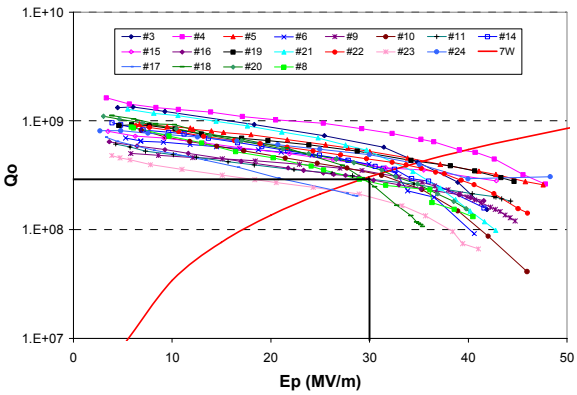

Fig. 5: Performance curves for nineteen of the Phase II cavities.

All cryomodules are assembled in a `dirty' assembly area to check the fitting of all components. Next the assembly is completely dismantled, all parts are cleaned in an ultrasound bath, rinsed with 18MΩ water at high pressure and dried in a clean room before assembly.

The cryomodules have the following features: 1. Stainless steel vacuum tank 2. The cavities and solenoid are supported from a rigid strongback that is in turn supported from the tank lid by support rods.3. LN2 thermal shield formed by copper panels with soldered copper cooling tubes and panels formed into a box. 4. Helium reservoir acts as phase separator and delivers gravity fed liquid helium at 4K to the cavities.

Because of space constraints in the clean room and available personnel only one cryomodule is assembled at a time. Each cryomodule receives at least one cold test in the SRF facility before delivery to the linac vault. The cold tests: 1. establish the repeatability of the alignment under thermal cycling, 2. provide the warm offsets required in the cold mass to achieve the prescribed alignment tolerance when cold, 3. check the performance of the cavities and the rf ancillaries, 4. determine the cryogenic performance given by the static load at 4K and the LN2 consumption and 5. confirm the integrity of the vacuum. The completed SCC1 top assembly is shown in Fig. 6 as the cold mass is lowered into the vacuum chamber prior to the first cold test. Measurements prior to the cold test confirm that the μ-metal reduces the remnant magnetic field below 20mG in the cavity region as per specification.

Fig. 6: Cryomodule SCC1 assembly prior to the first cold test

Cryogenic Performance: The cryogenic performance is established by measuring the static helium load after full thermalization. Full thermalization occurs within ~2-3 days of achieving a liquid level in the helium reservoir. The static load is measured by closing the helium supply valve and diverting the return exhaust helium through a gas meter. It is found that the static load is ~12-13 W for the phase I cryomodules and ~15-19 W for the Phase II cryomodules. The LN2 usage while thermalized is about 5 liters/hour for Phase I and 6 liters/hour for Phase II. These values match design estimations.

Alignment: A Wire Position Monitor (WPM) alignment system is used to check the stability and repeatability of the alignment during thermal cycles. Stripline monitors are attached to the cold mass using off axis alignment posts and a wire is passed along the axis of the monitors that carries a driving rf signal. The monitors pick up the signal from the wire and record the position of the wire with respect to each WPM axis. The specified alignment tolerance is ±200microns for the solenoid and ±400microns for the cavities. In addition to the WPM system optical targets are placed in the beam ports of the upstream and downstream cavities and in the upstream and downstream port of the solenoid to periodically chart the position of the cold mass in relation to the beam axis.

RF ANCILLARIES

Mechanical Tuner: Due the high cavity Q an accurate responsive tuner is required for stable cavity performance. The natural cavity bandwidth of <1Hz is broadened by overcoupling to ±15Hz. This corresponds to a motion of the lower tuning plate of ±2 microns. In both Phase I and Phase II sections the cavities are tuned by a zero back-lash lever arm that pushes against a tuner plate on the bottom end of the cavity. The lever arm is actuated by a long push rod that extends to the top of the cryomodule through a bellows to a motor. In Phase I a linear servo

motor is used. In the phase II system the linear servo motor has been replaced with a harmonic drive, brushless rotary servo motor driving a pre-loaded ball screw.

Coupling Loop: An adjustable loop coupler is used with a typical coupling β during acceleration of ~100 for a forward power of ~150W. The outer conductor is directly cooled through a LN2 cooled heat exchange block..

RF Amplifiers: Phase I utilizes 800W 106MHz tube amplifiers while Phase II utilizes 600W 141MHz solid state amplifiers. Both amplifier types provide good performance. Comparative measurements have shown that the solid state amplifier is less noisy than the tube amplifier by a factor of ~20. Both amplifiers meet specifications.

CRYOGENIC SYSTEM

The Phase II cryogenic system mirrors the Phase I system except that they share a recovery compressor. A Linde TC50 cold box feeds LHe to a 1000 liter dewar. The LHe is delivered to the cryomodules at 4K through vacuum jacketed LN2 cooled helium transfer lines with a slight overpressure in the dewar. The cryomodules are fed in parallel from a main supply manifold (trunk) through variable supply valves. The level in the cryomodules is used to control the opening of the supply valves. The vapour from the cryomodules is returned either in a warm return line direct to the compressor during cooldown or through a cold return line back to the cold box during normal operation. The measured liquefaction with LN2 pre-cool for Phase II is 240ltr/hour and the refrigeration power is 600W. The stability of the helium pressure is within ±7mBar well within the capability of the tuner.

The helium in the Phase I and Phase II systems is typically isolated. The Phase I system feeds LHe to SCB1-3 and the SRF test facility while Phase II supplies LHe to SCB4-5 and SCC1-3. Valves in the distribution system allow the cooling of the whole linac from either of the plants during maintenance periods.

PHASE II COMMISSIONING

.Phase II Schedule

The Phase II project had a very well defined time-line. TRIUMF funding for the project was scheduled to end April 1, 2010 to coincide with the start of the next five year budget cycle. In addition major initiatives proposed for the new five year cycle were politically linked to a successful conclusion of the previous five year cycle. The installation was scheduled for an extended shutdown from Sept. 2009 to March 31, 2010.

Table 1: Installation and testing schedule for Phase II linac.

Milestone	SCC1	SCC2	SCC3
Assembled	June 09	Nov 09	Mar 7/10
Test off-line	July-Sep 09	Dec 09	Mar 15/10
Install	Oct 09	Jan 10	Mar 21/10
Test on-line	Nov 09	Feb 10	Apr 7/10

Beam Commissioning

The complete linac from the downstream end is shown in Fig. 7. The final cryomodule was installed March 21. A 16O5+ beam (A/q=3.2) from the ISAC off-line (stable) source was accelerated to 10.8MeV/u just one month later on April 24. A plot of beam energy as a function of cavity number is shown in Fig. 8(a). The final energy is equivalent to acceleration of a beam with A/q=6 to 6.5MeV/u and as such demonstrated the ISAC-II goals on the first acceleration. This was achieved despite the fact that five cavities were not available for acceleration. Fig. 8(b) shows the effective voltage of each cavity during the first acceleration. Of the working cavities the average effective voltage for the Phase I linac is 1.09MV while the average effective voltage for the Phase II linac is 0.97 close to the design goal of 1.08MV. These correspond to peak surface field values of 30MV/m and 27MV/m respectively.

Fig. 7: The ISAC-II Superconducting linac.

OPERATION

First stable beam was delivered to users on April 25 just one day after commissioning and first radioactive beam was delivered one week later on May 3. Since then the linac has supported a full physics program with both stable and radioactive beams being delivered. To date stable beams of 16O5+, 15N4+, 20Ne5+ and radioactive beams (and their stable pilot beams) of 26Na, 26Al6+ (26Mg6+), 6He1+, (12C2+), 24Na5+ (24Mg5+), 11Li2+ (22Ne4+) including 74Br14+ from the charge state booster have been delivered. In addition short commissioning periods between beam delivery runs are used to characterize the machine and to satisfy licensing requirements.

Phase I Performance: The performance of the Phase I SCB cavities is monitored periodically typically during start-up after shutdown. The linac is warmed up once per year for three months as part of the site maintenance shutdown. In addition several of the cryomodules have been vented (pump replacement) and some have been taken off line for disassembly to repair internal faults (rf cable, coupling loop faults). Despite this the Phase I performance is very stable. There is some fluctuation in individual cavity performance over time but the average

accelerating gradients at 7W cavity power correspond to a peak surface field of 33±1 MV/m over the first four years of operation.

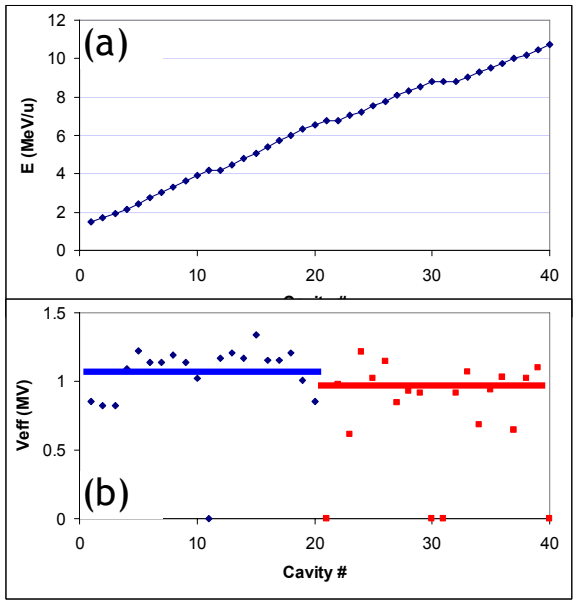

Fig. 8: Results from first acceleration of a 16O5+ beam. (a) A plot of beam energy after each cavity and (b) a plot of the effective voltage of each cavity; blue and red lines indicate the average values for Phase I and Phase II respectively.

Phase II Performance: In comparison the Phase II performance has averaged accelerating gradients corresponding to peak surface field of Ep=26MV/m at 7W in the first six months of operation. In particular the performance of cavities in SCC2 and 3 are reduced compared to single cavity test values. This is under investigation. A summary of Phase I and Phase II performance is shown in Table 2 as given by the average peak surface field for single cavity tests and on-line tests at 7W cavity power, and values for stable operation during acceleration.

Table 2: Given are the summary cavity performance values for the Phase I and Phase II linacs.

Test	Metric	SCB MV/m	SCC MV/m
Single cavity	Ep average at 7W	37	32
Acceleration	Operating Ep	30-32	27
Installed	Ep average at 7W	33	26

Operating experience: Multipacting conditioning is required for extended periods after start-up and does cause delays in initial beam tuning. Extended periods of conditioning (short pulse, low voltage) are required for 1-2 weeks after cool-down to reach a reasonable operating regime. Some degradation has been seen in cavities due to trapped flux from the solenoids. Most typically this is caused when a small interruption in helium delivery causes the cavities to warm above transition and then cool in the magnetized environment caused by the solenoid. A degaussing procedure has been developed that takes ~2 hours. The tube amplifiers have been a source of downtime due to tube aging issues causing phase drift and non-linear output affecting LLRF operation. Four cavities in Phase II remain unavailable until the next warm-up due to shorts in the rf drive lines. There is one open circuit cable in Phase I.

SUMMARY

The ISAC-II linear accelerator represents a ten year activity of research, development, prototyping, production and installation. Along the way TRIUMF has gained a core competence in superconducting rf cavity production, processing and testing. This initiative is interesting in its own right as a source of study for students and young researchers but also allows TRIUMF to consider other cutting edge accelerators such as the e-Linac project for radioactive beam production now in development. In addition we have mentored a local company, PAVAC Industries, in the fabrication of niobium resonators. Finally we have provided for our nuclear physics users an important new capability unique in the world; the ability to accelerate exotic ions from an ISOL facility to energies above the Coulomb barrier.

ACKNOWLEDGMENT

The work reported here chronicles the efforts of the TRIUMF engineering and technical teams who embraced the new technical challenge and succeeded through dedication, hard work and talent.

REFERENCES

[1] P. Schmor, et al, “Development and Future Plans at ISAC”, LINAC2004, Lubeck, Germany, Aug. 2004.
[2] TRIUMF Publication, ISAC-II – A project for Higher Energies at ISAC, TRI-99-1, Aug. 1999.
[3] R. Poirier, et al, “CW Performance of the TRIUMF 8 Meter Long RFQ for Exotic Ions”, LINAC 2000, Monterey, USA, Aug. 2000.
[4] R.E. Laxdal, et al, “Beam Commissioning and First Operation of the ISAC DTL at TRIUMF”, PAC2001, Chicago, May 2001.
[5] R.E. Laxdal, “Initial Commissioning Results of the ISAC-II Linac”, LINAC06, Knoxville, Aug. 2006.
[6] R.E. Laxdal et al, “ISAC-II Superconducting Linac Upgrade – Design and Status”, LINAC08, Victoria, Sept. 2008
[7] R.E. Laxdal et al, “Production and Testing of Two 141 MHz "Prototype Quarter Wave Cavities for ISAC-II", LINAC08, Victoria, Sept. 2008.
[8] R.E. Laxdal, et al, “Cryogenic, Magnetic and RF Performance of the ISAC-II Medium Beta Cryomodule at TRIUMF, PAC05, Knoxville, May 2005.

PROGRESS TOWARDS NEW RIB AND HIGHER INTENSITIES AT TRIUMF*

Pierre Bricault, Marik Dombsky, Peter Kunz, Jens Lassen, Friedhelm Ames and Victoire Hanemaayer, TRIUMF, Vancouver, Canada

Abstract

Over the past five years TRIUMF has operated routinely the ISAC facility at proton beam intensity up to 100 μA. A major departure from other ISOL facilities, ISAC utilizes a modular assembly for the target station. This is mainly to provide enough radiation shielding for operation at high proton beam intensity. So far ISAC was licensed to operate target materials with Z < 82. Two actinide target (UO2) tests have been performed during the past two years to assess the ISAC systems (vacuum, nuclear ventilation, personnel safety) for actinide operation. The uranium oxide target is limited to 2 μA only because of the material low operating temperature. We are now developing a uranium carbide target using similar techniques as for our other carbide targets (SiC, TiC, ZrC) operating up to 75 μA. These developments are essential for the ARIEL (Advanced Rare IsotopE Laboratory) project for which TRIUMF just received funding. This funding includes the construction of a 500 kW, 50 MeV electron superconducting LINAC and a new target hall building capable of housing two new target stations. One of these target stations is rated at 100 kW beam power from both, electrons and protons. The proton beam line utilizes a modified extraction port on the H- 520 MeV cyclotron. The other target station will be solely dedicated to the 500 kW electron beam for photo fission.

INTRODUCTION

The TRIUMF-ISAC facility was designed for rare isotope beam production using the protons from the TRIUMF H- cyclotron as the driver beam. Short-lived radioisotopes are produced in a thick target from various nuclear reactions mechanisms. The reaction products are stopped in the bulk of the target material. We operate those targets at very high temperature to enhance the diffusion of the products inside the target matrix to the surface of the grain and then the effusion process to bring the isotopes of interest to the ion source where they are ionized and extracted to form an ion beam.

In this paper we will present the resent progress in target fabrication that can withstand high power for the production of intense RI beam. Finally, we will present the AdvancE Rare Isotope Laboratory that just received funding for installation of a new superconducting electron LINAC and the building housing the tunnel, target stations and remote handling equipment.

ISOL METHOD

Beams of rare isotopes are a challenge to produce. Especially the short-lived ones, they do not exist on earth. They have to be produced artificially in the laboratory. The isotopic separation on-line or ISOL method can be described as a process where the isotope of interest is fabricated artificially by bombarding a target material nucleus with fast projectiles. In a thick target the reaction products are stopped in the bulk of the material. The target container is attached directly or indirectly to an ion source, allowing the reaction products to be quickly ionized and turned into an ion beam that can be mass analyzed and be delivered to experiments. The requirements for producing high intensity RIB are:

- A high energy driver, such as the TRIUMF H^- 500 MeV cyclotron,
- A target material inserted into a refractory oven connected to an ion source,
- An ion source at high voltage to produce an ion beam,
- A high-resolution mass separator.

To solve the problem of producing intense rare isotope beams we need to find the best target material that favors the production of the desired RIB. One more thing to consider is contamination of the ion beam by isobars; isotopes having the same mass number, A, but different atomic number, Z.

Another consideration must be the power deposited inside the target material. If the deposited power density is too high, the temperature of the target material will increase above safe operation level and then the target material will begin to evaporate. This can have disastrous effect on the ion source efficiency, especially for plasma ion sources.

To avoid excessive power deposition by the incoming beam we do not stop the primary beam in the target. This is accomplished by choosing the target length such that the energy degradation of the proton beam is only 200 to 300 MeV. A dedicated water-cooled beam dump is located just behind the target to capture the entire proton beam emerging from the target.

There are three main nuclear reactions accessible to produce rare isotope beams at our energy range. They are:

- Spallation, a breakup or fragmentation of the target material nuclei, in which the product distribution peaks a few mass units lighter than the target nucleus. Because neutron emission is energetically easier than proton emission, (due to the Coulomb barrier that the proton experiences) the production of neutron deficient nuclei is favored. A good example is the high production of Rb isotopes from Nb or Zr target.
- Fragmentation, it is the counterpart of the spallation reaction, where the product is one of the light fragments. The fragmentation method is advantageous when producing light, neutron rich products from heavier target nuclei with high

neutron to proton ratios. Because of the neutron excess in the heavy target nuclei, the fragments tend to retain a statistical memory of the neutron to proton ratio and as a result, have higher neutron to proton ratios themselves. A good example of such a reaction is the production of ^{11}Li from Ta, or the production of ^{32}Na from U targets, respectively.

Induced fission occurs when the incoming projectile deposits sufficient energy in the target nucleus to induce a breakup into two roughly equivalent mass products. Unlike neutron-induced fission, this reaction mechanism is opened to both fissile target nuclei and to heavy nuclei such as: tantalum, lead, etc. Again because of the higher neutron to proton ratio in heavy nuclei, neutron-rich products in the medium mass region can be effectively produced by this reaction mechanism.

The yield of a specific isotope can be expressed using the following equation:

$$Y = \Phi\sigma(NA/A\cdot\tau)\varepsilon_D\varepsilon_E\varepsilon_I \quad (1)$$

where: is the nuclear reaction cross section leading to this specific isotope, ϕ_p is the primary beam flux, N_t is the number of target nuclei per square cm, and the ε represents the effusion, diffusion, ionization and transport efficiencies, respectively.

Release Processes

After the isotope has been produced by one or more of the three production reactions mentioned above, it is stopped in the target material matrix because its energy is in general not sufficient to escape the target material. In order to produce a RIB the product must diffuse from the inside of the grain or foil to the surface and then effuse out of the target container to the ion source. To avoid decay losses the release and ionization must proceed as quickly as possible. To do so we generally heat the target material to the highest operational temperature. In practice if the desired isotope has a very short half-live it is preferable to have a very short target length to limit the volume from which the atoms have to escape.

The diffusion speed or efficiency is determined by the interaction of the specific diffusing isotopes moving through the target material lattice. The higher the temperature faster is the diffusion to the surface. When using metal foils we tend to limit their thickness as much as possible to speed up the diffusion process. On the other hand we cannot decrease the thickness too much, as to conserve the heat flow toward the container tube. For carbide targets we tend to make them as porous as possible and to limit the grain sizes. To reach the optimum we are mixing three different grain sizes, 1, 7 and 20 μm in equal proportion.

In the effusion process, the product atoms are in a gaseous state and randomly bounce around the target container and the target material surface until they enter the ion source. During each collision with a surface, they stick for a time before continuing in a random direction. As with the diffusion process, a high temperature is required to put the product into the gaseous state and to minimize the sticking time in order to make the product moves as quickly as possible to the exit and then to the ion source. The sticking time is a complex function of the lattice structure, temperature and desorption enthalpy between the product atom and the surface material atoms.

Ionization Process

The ionization is required to convert the desired isotope atom into a charged particle beam. Such a beam can then be guided, mass analyzed and transported to the experimental station or be further accelerated to an energy relevant e.g. for nuclear astrophysics or nuclear structure studies.

The key of the ISOL method is to achieve highest beam intensity and the highest beam purity possible. This is accomplished by passing the extracted beam through a high-resolution magnet dipole. The separation between two isotopes of the same mass number (isobars) at the image focal plane of the dipole varies with the mass difference. The larger the mass difference, the greater is the spatial separation achieved. Using a set of slits one can select the desired isotope that will be transmitted to the experiment. Unfortunately, the mass difference for heavier elements is often not large enough to ensure complete separation at the focal plane, resulting in a mixture of isotopes delivered to the experiments. The contamination level can be quite large depending to the species involved, to a point where the level of contamination makes the experiment impossible.

To limit the contamination there are some tricks that can be applied to the system to improve the selectivity. Here are some of the methods we used at ISAC to purify the rare isotope beams:

Selectively enhance the effusion of a particular species by adding a chemical product in the target container. For example, the addition of fluorine to enhance the release of Al in its molecular species Al-F. The Al-F effusion efficiency is greater than that of Al itself. The ionized Al-F$^+$ is well separated from the otherwise dominating Na contaminant because the Na-F molecule is not stable at the operating temperature.

Selectively reduce the effusion of some contaminant by cooling the transfer tube connecting the target container and the ion source. The best example of this application is for noble gasses. We have demonstrated that by cooling the transfer tube completely removed the ^{18}F contamination from the desired ^{18}Ne beam.

Selective ionization can be accomplished by laser resonant ionization. We are using routinely two or three laser frequencies to resonantly excite the electron into a level from which ionization proceeds. Resonant laser excitation is element selective. The only drawback is that the target and transfer tube are operated at very high temperature to facilitate fast release. This is sometimes enough to obtain surface ionization isobaric contaminants

– usually alkali metals. To resolve this issue we have developed a laser ion source combined with a short, segmented radio frequency quadrupole that replaces the hot transfer tube. Hence surface ionization is inhibited. Subsequently resonant laser ionization is the only remaining ionization mechanism and then the laser only ionizes the desired element. Such created ions are captured and guided by the RFQ to the ion extraction system to form a beam.

ON-LINE HIGH POWER TARGET

As we can see from equation 1 the RI yield is directly proportional to the primary beam intensity. To achieve high rare isotope beam intensity we can work on the release efficiency to a certain extend. But, rapidly we come to very strong limitation because further improvement of the release efficiency would come at the cost of destroying the target or the ion source. The only viable option is to increase the primary beam intensity. But an increase of the incoming flux requires high power targets capable of withstanding and dissipating the deposited beam power.

The ISAC on-line high power target can be described as consisting of two parts, the target material itself and the target container. Both have to sustain the high radiation dose from the primary beam. The target container has to remove the power deposition in such a way that the operating temperature of the target material can be maintained below the evaporation threshold, which in our case is the temperature corresponding to 10-6 mbar vapor pressure.

The ISAC high power target (HPT) has been described in [1]. The tantalum target container was modified to increase the effective emissivity by diffusion bonding radial Ta fins onto the standard target container. The radial fins are installed over the tantalum tube and are diffusion bonded to the target container by heating the overall system in vacuum at 1500_ C for a period of 20 hours. Off-line tests using electron beam heating show that the effective emissivity is 0.92 and the target is capable of dissipating 25 kW of power when operating at 2200_ C. Using resistive heating and beam power we can balance the temperature from 45 to 100 μA proton beam on most high power targets for both metal foil and composite carbide targets. Since we cannot rotate the proton beam on our target we must ensure that the proton beam profile is large enough to avoid puncturing the target entrance window. For a proton beam size of 7 mm FWHM we can reach routinely 75 μA and with a beam profile of 8 mm we can reach 100 μA on Ta and Nb foil targets.

Target Material

Since we operate the target material at its temperature and vapor pressure limits is important to select a target material that has the following properties:

High thermal conductivity,

Low vapor pressure.

Refractory tantalum and niobium foil metal foils and carbides are among the best candidates.

Refractory carbides are ceramic materials that have been used in commercial applications for many years, such as SiC, TiC and WC. They are mainly utilized for their hardness and abrasive properties and as high strength tooling materials. For the ISOL method targets the high operating temperature required to enhance the release processes is essential, especially, when using plasma ion sources, which are sensitive to high pressure and gas loads. At TRIUMF we have developed a production technique for target materials that combines high material porosity and easy handling [2]. In the ceramic industry this technique is known as slip casting. The ceramic powder suspended in a solvent, which contains dissolved polymers that favor the powder dispersion. This mixture in suspension is poured into a mold or onto a backing foil and then allowed to dry. The dried slip cast, which contains the ceramic powder particulates and the polymers, is easily cut into the desired shape. These carbide ceramics were used up to 40 μA. However, due to their relatively low thermal conductivity compared to metal foils, it is necessary to increase the effective thermal conductivity of the carbide ceramics in order to operate targets at higher beam intensity, above 20 μA, in our case.

We have developed a technique allowing us to pour the ceramic powders and polymers onto an exfoliated graphite foil. These composite carbide targets are capable of dissipating very high power. The ceramic layer is typically 0.25 mm thick, while the graphite layer is around 0.13 mm thick.

The same technique can be used for other target materials. For example we have tested Nb_5Si_3 backed onto a Nb foil to dissipate the heat. Normally the Nb_5Si_3 target material can only be operated at the 1 μA level. By using the Nb foil backing we were able to increase the primary beam current on this target material to 15 μA.

Another example for the use of this technique is for oxide target materials. Oxides have a very low thermal conductivity. On average, it is at least one order of magnitude lower than for carbides. The EURISOL target study group was mandated to look at the possibility of using an oxide targets for the release of a high intensity ^{18}Ne beam. A test conducted in March 2009 in collaboration between CERN and TRIUMF was meant to validate the oxide target up to 20 μA under realistic beam conditions.

Composite Al_2O_3/Nb foils were made by reactive brazing of the oxide layer onto Nb disc to enhance the low intrinsic thermal conductivity of the oxide material and to obtain a good thermal contact between the Nb foils and the tantalum tube. The prototype operated in a stable mode at nominal 25 μA proton beam current – with a peak at 30 μA – for 9 days [3].

Table 1 shows a summary of the composite carbide targets used at ISAC over the past five years and gives a comparison with metal foil targets.

Table 1 – Comparison of the primary beam intensity for the composite carbide, metal foils and oxide targets.

Target Material	Proton intensity on target
$SiC/C_{graphite}$	70 μA
$TiC/C_{graphite}$	70 μA
$ZrC/C_{graphite}$	75 μA
Ta	75 μA
Nb	100 μA
Nb_5Si_3/Nb	15 μA
Al_2O_3/Nb	25 μA

Radiation Enhancement and Associated Issues

The most striking beneficial effect we observed with increasing proton beam intensity on ISAC targets has been the observation of Radiation Enhanced Diffusion (RED) [4], [5]. The increase in diffusion or enhancement of atom mobility in an irradiated material is due to two factors: (1) enhancing the defects concentration, and (2) creating new defect species.

This can be viewed as a hidden term proportional to the incident beam flux, in the diffusion efficiency term, m can be equal to _ or 1 depending of the defect annihilation process taking place with the target material.

With intense proton beam flux the yield in equation 1 can result in a proportionality of to rather than . This effect is most remarkable for the short-lived products because most of the decay losses occur during the diffusion process. The long-lived species are less affected or enhanced since they can take longer time to diffuse to the surface having a longer half-life.

We have also observed with an Al beam that the yield increases with time. For example yield measured of ^{26g}Al and ^{26m}Al increases by a factor 10 and 7 respectively in one week, while the ^{22}Na and ^{24}Na yield remains constant. This suggests that there are cumulative irradiation induced changes to the SiC target material that affect the mechanisms of diffusion of Al in SiC. The assumption is that the lattice experiences a phase transition from α-SiC to β-SiC. The fact that Na yields do not change suggests that the Na diffusion mechanism is different from the one for Al. Na diffusion in carbides may be fast enough so the radiation-induced changes are insignificant.

The RED effect can be seen positive as it enhances the RIB intensity, at the same time it also proved to be detrimental by decreasing the target longevity. Under long time irradiation a substantial decrease in yield is observed. For example we have observed target aging effect for an ISAC high power Ta target. The target has received an integrated charge of 42000 μA-hr, corresponding to $9.4*10^{20}$ protons. The yields ratio of measurements taken 17 days apart is plotted as a function of the isotope half-life. We can see the yield has dropped by a factor 10 in some cases. On average the yields have dropped by 80% [Dom2007]. The simplest explanation for the uniform yield decreases is the loss of integrity of the target container itself. With cumulative radiation damage and buildup at the lattice boundaries, cracks open up between the crystal grains of the Ta target container. Eventually, the total area of the cracks becomes significant and allows large quantities of products to escape the target container before they have a chance to reach the ion source.

Such grain boundary cracks are observed during post-irradiation inspections of the target container.

UC_x Target Development

The physics program at ISAC demands a high power UC_x target and it is even more important for the ARIEL project that is presented in the next section. Our simulations show that the power deposition in the UC_x target for the phase one is about 22 kW for the 100 kW phase, while it is 66 kW for the 500 kW second phase [6].

At the moment the UC_x targets are in use at other ISOL facilities like, ISOLDE, HRIBF and ALTO. They are operating in the range of only few kW dissipated beam power. We have started the development of an UC_x target for the ISAC facility based on techniques similar to those used for our other carbide targets.

The difference to other carbide target materials is the fact that we cannot obtain directly the uranium carbide powder from a commercial supplier. We have prepared the uranium carbide production following these steps:

Milling UO_2 and C,
Casting the UO_2/C slurry,
Carbonization under vacuum, ($p< 10^{-4}$ mbar),
Making the target discs,
Milling the UC_x and C,
Casting the UC_x/C slurry,
Cutting the target discs from the green cast,

Conditioning and sintering the target material is done by loading the target discs into the Ta container in the green form and heating it up to 1750 _C under vacuum, ($p< 6.5*10^{-5}$ mbar).

Figure 1 shows a scanning electron microscopy (SEM) image of the sintered UC_x material. We can see that the grain sizes are quite small and the porosity is such that we obtain approximately 45% of the theoretical density. The first test of our UC_x target will take place in December 2010 at ISAC.

One of the outstanding questions regarding the usage of UC_x at ISAC is its chemical stability. This has been a longstanding question for many years. We recently, finalized tests of the UC_x chemical stability when exposed to air at different temperatures up to 400_ C and in water. The sintered UC_x discs exposed in air do not show any sign of chemical reaction and after 5 days in water at room temperature have no visible sign of chemical reaction.

We can conclude from those chemical reactivity tests in air that the UC_x is quite stable. We did not observed rapid oxidation. After 5 days we can only see a small surface discoloration. The tests in air at high temperature (400 ^{o}C) and in water show a slow oxidation.

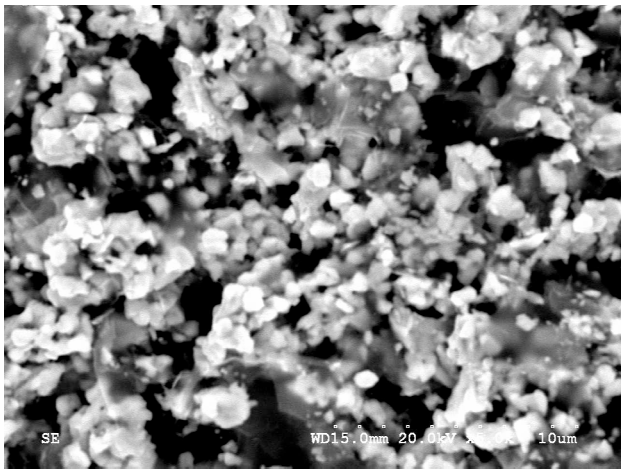

Figure 1: Scanning Electron Microscopy image of the UC_x target developed for the ISAC facility. The magnification is 5000 x.

ION SOURCES COMBINED WITH HIGH POWER TARGETS

In the previous section we saw that we were able to develop a target material and a target container capable of operating at high power. The next step in the chain for successful production of intense rare isotope beams is the ion source.

At ISAC we are using primary three types of ion sources,

Hot surface,
Resonant laser and
FEBIAD

The hot surface ion source and the laser ion source are not so much affected by the target outgas while plasma ion source are.

A Forced Electron Beam Induced Arc Discharge, (FEBIAD) [8] is one of the best plasma ion sources to operate in large range of pressure. We have developed our based on the hollow cathode developed by Sundell [9] at ISOLDE-CERN. Our FEBIAD has a smaller volume mainly constraint by the available envelope on board of our target module.

In order to satisfy the demand for isotopes for the nuclear astrophysics program we must be able to ionize with high efficiency the gaseous elements or molecules of C, N, O, F, and Ne. These elements are only ionized efficiently with an electron cyclotron resonance ion source (ECRIS). A new ECRIS capable to operate on-line with high power targets is being developed. A prototype having the following improvements is being operated at a test stand:

Improved electron confinement,
Increased operating frequency, 6 GHz,
Movable extraction electrode,
Higher throughput, increased pressure tolerance.

The new ECRIS is based on MONOBOB [10], which was developed at GANIL, where four coils made from hollow copper conductor surrounded by a ferromagnetic structure produce the desired magnetic field. The magnetic field has an axial and radial confinement. The extraction is an adjustable, three electrode system [11].

ARIEL PROJECT

The Advanced Rare IsotopE Laboratory (ARIEL) project proposed the construction of a new electron superconducting LINAC capable of delivering up to 500 kW electron beam at 50 MeV, a new proton beam line BL4N, and two new target stations combined with a high mass-resolution separator in a new building. The LINAC and the ARIEL building have been funded by the Canadian Foundation for Innovation from the Government of Canada and the Province of British Columbia provincial, representing a total funding amount of $60.7 M. Figure 2 shows the TRIUMF site layout, in blue the actual layout and the proposed ARIEL and UCN projects in red.

The ARIEL target stations and the associated equipment for servicing the area will be quite similar to the existing ISAC facility. From our experience of operating high power ISOL targets we would like to retain the following aspects:

Two-stage mass separator system, the pre-separator inside a heavily shielded hall. From our experience we have very low contamination spread in the adjacent mass separator room and beam line. The first selection slit is directly accessible by the remote handling equipment for maintenance.

The approach we use at ISAC allows us to operate ISOL targets at unprecedented beam power. We routinely operate our target at proton beam currents between 70 and 100 μA.

All non radiation resistant components are located in a low radiation field thanks to the target module-shielding plug.

On the other hand there are issues that we will address, for example:

For budget reasons when ISAC was build it was decided to build only one mass separator for the two target stations. The optics from each station merge at the pre-separator. The exit module beam optics box does not block the neutron flux back streaming from one target station to the other. This implies that we cannot service one target station while operating the other one. It reduces the flexibility in operation and forces beam off period to attend the target module for the next run.

The actual containment box at the bottom of the target module is not hermetically sealed. It creates difficulties when operating air sensitive target materials such as LaC_2. Furthermore, the target/ion source assembly cannot be pre-conditioned off-line.

All electrical, vacuum and signal connections on the top of the target module are done manually imposing long delays of at least one week and some times two weeks after beam off to allow for cool down before personnel access to the area.

Target/ion source exchanges takes from 3 to 5 weeks. This is forcing us to operate our target for much longer period than we should. We would like to speed up the process in order to reduce the target irradiation time to 2 to 3 weeks. This will reduce the impact of the yield drop due to radiation damage, metal fatigue, target sintering, etc.

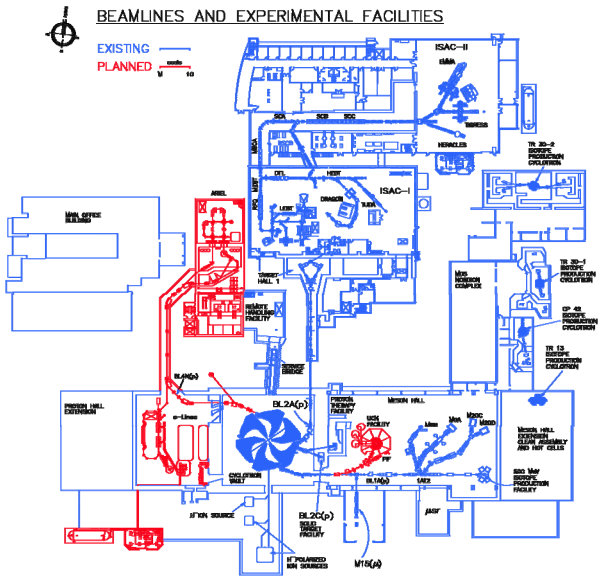

Figure 2: Layout of TRIUMF site (actual in blue), ARIEL project in red with the proposed UCN on the right of the cyclotron.

The new concept for the target module in ARIEL will be quite different than the ISAC target modules. The containment box will be a vacuum box equipped with a radiation hard valve to seal the heavy ion port.

The ARIEL facility will have a conditioning station allowing the preparation and test of the complete target module equipped with the target/ion source before it goes on-line.

The target module services will be remotely connected using a similar design as the one developed for the actual ISAC facility.

The front end beam line which houses the optics and the diagnostics and vacuum pumps is built into 1 m long sections. Each section can be disconnected and transfer to the hot cell for maintenance and repair.

CONCLUSION

We have made progress on the development of a uranium carbide target material. Using technique similar to the one used for the other composite carbide target materials we have developed an UC_x target material, which can operate up to 40 to 50 μA, depending on the thermal conductivity.

We have made tests to demonstrate the chemical stability of the UC_x. It appears that the material is quite stable when exposed to air even at high temperature (400 °C) and in water. These results give us confidence about our technique to deal with spent target in the hot-cell and long-term storage vault.

These progress on the UC_x are essential for the success of the ARIEL project, which is based on using mainly uranium target for the physics program both for the photo-fission and the spallation products like Rn and Fr for the EDM and Fr experiments.

The new ARIEL target stations have several improvements with respect of the first generation of the ISAC target station. Using new radiation resistant all metal seal gate valves and double pillow seals we have significantly simplified the vacuum system. It allows a true confinement box for the target module housing the target/ion source assembly. With the remote services connection we will have a much quicker turn around for target exchange.

Finally, once completed the ARIEL project combined with the ISAC facility will allow three RI beam users simultaneously.

REFERENCES

[1] P. Bricault, M. Dombsky, A. Dowling and M. Lane, Nucl. Instr. and Meth. B 204 (2003) 319.
[2] M. Dombsky, V. Hanemaayer, “Method of Forming Composite Targets”, U.S. Patent. No. 20060040064.
[3] T. Stora, P. Bricault, L. Bruno, S. Fernandes, F. Gröschel, I. Günther, J. Lettry, M. Loiselet, E. Noah, E. Platacis, L. Zanini, EURISOL task #3, final report, July 2009.
[4] M. Dombsky, P. Bricault and V. Hanemaayer, Nucl. Phys. A 746 (2004) 32c.
[5] M. Dombsky, P. Bricault, P. Schmor and M. Lane, Nucl. Instr. and Meth. B 204 (2003) 191.
[6] M. Lebois and P. Bricault, INPC10, (2010).
[7] K. Jayamanna, D. Yuan, M. Dombsky, P. Bricault, M. McDonald, M. Olivo, P. Schmor, G. Stanford, J. Vincent, and A. Zyuzin, Rev. Sci. Instrum. **73**, 792 (2002).
[8] R. Kirchner and E. Roeckl, Nucl. Instr. and Method 133 (1976) 187-204.
[9] S. Sundell et al., Nucl. Intr. and Methods in Physics Research B70 (1992) 160-164.
[10] C. Huet-Equilbec, P. Jardin, P. Gorel, J.Y. Pacquet, G. Gaubert, J. Cornell, M. Dubois, N. Lecesne and R. Leroy. Nucl. Instr. and Meth. B 240, Issue 4, p752-761 (2005).
[11] F. Labrecque, N. Lecesne and P. Bricault, Nucl. Instr. Meth. B 266 (2008), 4407.

STRIPPER FOIL DEVELOPMENTS AT NSCL/MSU*

Felix Marti#, Scott Hitchcock, Peter Miller, Jeffry W. Stetson, John Yurkon,
NSCL/MSU, East Lansing, MI 48824, U.S.A.

Abstract

The Coupled Cyclotrons Facility (CCF) at NSCL/MSU includes an injector cyclotron (K500) and a booster cyclotron (K1200). The beam from the K500 is injected radially into the K1200 and stripped at approximately one third of the radius at energies of approximately 10 MeV/u. Stripping is done with a carbon foil. The lifetime of the foil is very short when stripping heavy ions and does not agree with the estimates from formulas that work quite well for light ions. We will present in this paper the studies performed to understand the limitations and improve the lifetime of the foils. A foil test chamber with an electron gun has been built as part of the R&D for the US DOE Facility for Rare Isotope Beams (FRIB) project. It has been used to study different ways of supporting the carbon foils and effects of high temperature operation. Different foil materials (diamond-like carbon, graphene, etc) have been tested in the cyclotron.

INTRODUCTION

The stripper foils are mounted on a C frame with one side open, toward the large radius, where the beam will pass by in the next turn, see Figure 1.

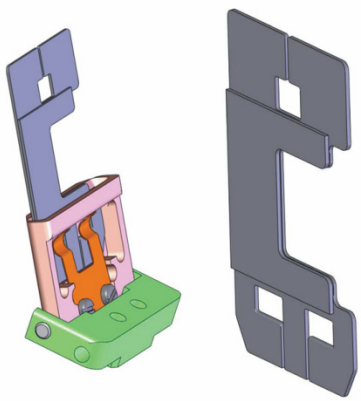

Figure 1 Stripper foil mounting frame (right) and frame holder that attaches to chain.

The lifetime of the foils for light ions is in good agreement with the estimates from Baron's formula [1]. When accelerating heavy ions (xenon and higher) the lifetime of the foils is much shorter than predicted. The foil performance decays so fast that when running high intensity uranium the extracted current has a fast decline in just fifteen minutes, making it impractical to use in regular operation.

The stripper is located inside one of the dees in the K1200 cyclotron, Figure 2. This aggressive environment (in vacuum, in a 5 T magnetic field and inside the high voltage accelerating structure) makes it difficult to install any diagnostics to observe the stripper foil.

Figure 2 K1200 cyclotron. The upper half of the dee has been removed, as well as the RF shield that covers the stripper mechanism. The platter with the chain that drags the stripper foil holders has also been removed. The water cylinders used to drive the platter and locate the platter in the correct position are shown.

To study the thermal and mechanical stresses on the stripper foils under consideration for FRIB we have built a stripper foil test chamber with an electron gun mounted on the side. This chamber allows us to have a detailed look at the foils while irradiating them with the electron beam, overcoming some of the limitations we have to observe the foils inside the cyclotron.

WHY DO FOILS FAIL?

The main reasons for foil failure are thermal and mechanical stresses and radiation damage. In the case of light ions we observe that foils usually develop a tear or the area where the beam hits the foil seems to be sputtered away.

The wrinkling of the foils is a general observation for all ions. In the case of light ions we notice that in many cases the foils detach from the supporting frames. They are mounted with aquadag or similar media. To correct this failure we are testing foil holders with pockets, see Figure 1, where the foils are inserted but not held fixed to the edges.

The failure mode for intense heavy ions (Pb, U) is different. The foil becomes thinner and thinner, moving away from the equilibrium thickness, shifting the charge state distribution toward lower charge states.

*This material is based upon work supported by the Department of Energy Office of Science under Cooperative Agreement DE-SC0000661 and NSF Grant PHY-0606007

marti@nscl.msu.edu

TEST CHAMBER STUDIES

The test chamber allows us to observe the foils with diagnostics that we do not have in the cyclotron, but being exposed only to an electron beam.

The test chamber arrangement is shown in Figure 3. An electron gun beam is focused with an einzel lens. The third electrode of the einzel lens is divided in four segments to allow different potentials to be applied and steer the beam, see Figure 4.

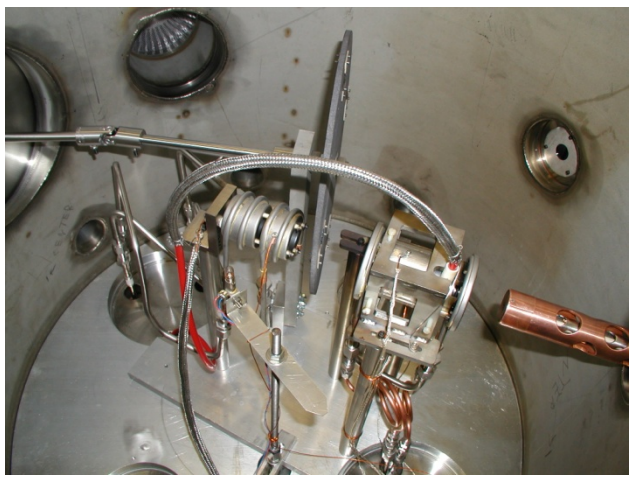

Figure 3 Photo of the inside of the stripper foil chamber showing the electron gun on the right, the einzel lens, the rotating wheels that supports the different targets and on the left the Faraday cup with the secondary electron suppression ring.

There are two observation ports where several instruments are located. We routinely use a FLIR camera that works in the long wavelength area (7-11 μm) capable of measuring temperatures between room temperature and 900°C. The port is equipped with a ZnSe viewport. In the second port a large quartz window is used and a short wavelength IR Mikron M9200 camera is located. This camera works above 900°C up to 3000°C. A fibre optic spectrophotometer (FOS) is also located in this second port as well as a standard B&W high sensitivity TV camera.

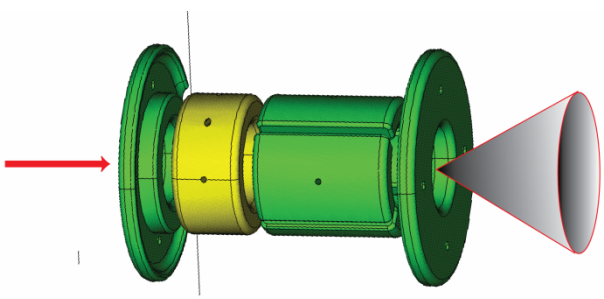

Figure 4 Einzel lens showing the high voltage electrode (yellow) and the exit electrode split in four independent components.

One of the goals of using the test chamber was to gain confidence and verify the models we use to estimate the sublimation damage. The foils can reach temperatures high enough that sublimation of the graphite is a fast process. The lifetime estimate for a 0.5 mg/cm^2 foil is shown in Figure 5. We see that temperatures close to 1900°C should be avoided to reduce the sublimation of the foils. We have modelled the thermal effects and compared with the measurements in the test chamber and found them in good agreement.

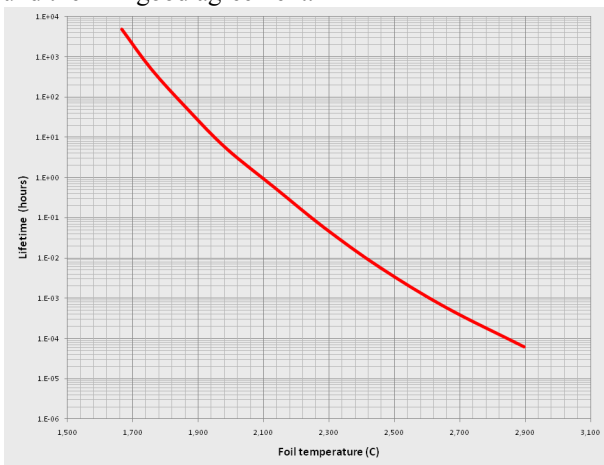

Figure 5 Lifetime of a 0.5 mg/cm^2 foil defined as loosing 20% of its thickness to sublimation, as a function of the foil temperature.

One of the issues in doing thermal imaging with IR cameras is that they expect the user to input the emissivity of the object. We used the FOS to determine the corresponding emissivity. The FOS itself was calibrated with a standard source that allowed us to determine the transmission of the whole system (window, fibre, sensor, etc). The spectra from 400 to 800 nm were used to fit a black body curve and from this we determined the temperature of the foils.

We experimented with a stationary beam and a rotating beam. The comparison of the stationary beam is shown in Figure 6.

By applying two sinusoidal voltages in quadrature the beam can be steered in a circular pattern and simulate the effect of a rotating stripper foil (one of the options considered for FRIB and used at RIKEN). These results also verified our thermal simulations.

RADIATION DAMAGE

The experience with heavy ions (Bi, Pb, U) at NSCL had shown that intense beams damaged the foils very fast after switching from tuning to running experiment mode. The extracted current could be seen decaying significantly in fifteen minutes. To study this effect in a more systematic way we loaded the stripper mechanism with foils from different manufacturers, MicroMatter, KEK and Arizona Carbon Foil (ACF). An 8.1 MeV/u Pb was accelerated in the K500 cyclotron and after stripping in the K1200 accelerated to 85 MeV/u and extracted.

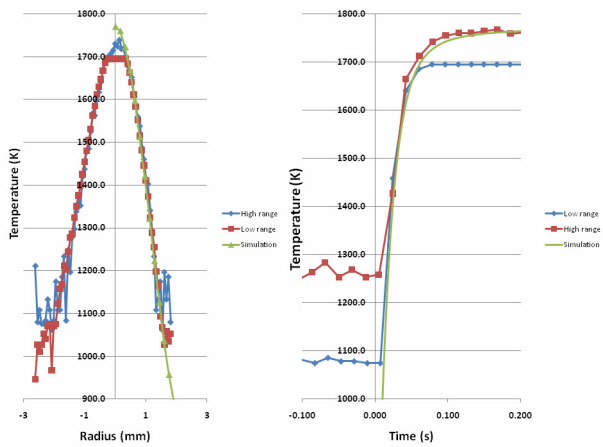

Figure 6 Comparison of the simulation with experimental results for a stationary electron gun beam. The left hand side shows the temperature vs. radius and the right hand graph shows the time dependence.

The test procedure was to inject the beam at different average power levels (20, 50 and 100%) by varying the injection line chopper duty cycle. The fraction of the ions extracted divided by the number of ions injected gave us a measure of the foil performance, without changing the tune of the cyclotrons, see Figure 7.

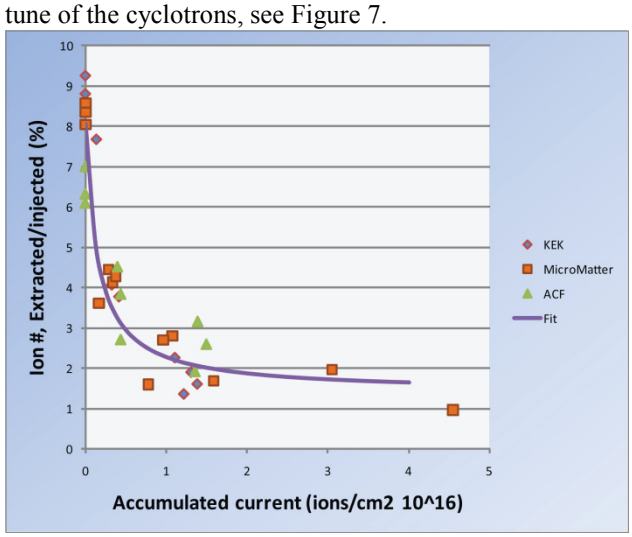

Figure 7 Fraction of ions extracted divided by the number of ions injected as a function of the beam dose for different foils.

The striking feature is the very fast decay observed in all foils. This process is so fast that it makes impractical to plan experiments at high intensities. After the experiment ended the foils were extracted from the cyclotron and examined. Many of them showed a significant growth in the transverse direction that we have not observed with light ions. At the same time a thinning of the foil was noticeable (and verified by measurements with an alpha source) in the spot where the beam was hitting it. Figure 8 shows an example of this effect.

After letting the residual activity decay for some months the foils were taken to the MSU Advanced Microscopy Laboratory and observed with a Scanning Electron Microscope (SEM). The modifications on the foil were striking as shown in Figure 9. A possible interpretation of this transverse expansion and longitudinal thinning can be found in the "ion hammering effect" described by Klaumunzer and collaborators [2]. This effect occurs above a certain threshold fluence for ions depositing a large amount of energy in the target electrons and these electrons contribute to the displacement of the target atoms.

It must be observed that the foils heated to 2000°C in the test chamber do not show this striking pattern, just the long wave wrinkling.

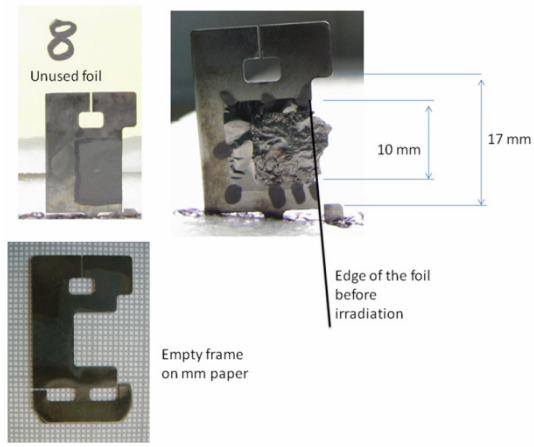

Figure 8 Upper left shows unused foil with straight edge, upper left shows the foil after irradiation with Pb beam and the growth in the transverse direction. Looking against the light a region of decreased thickness can be detected.

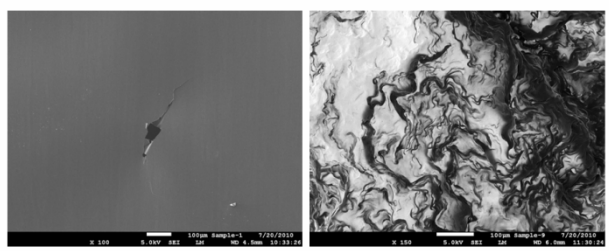

Figure 9 SEM photos showing unused MicroMatter foil on the left (100X) showing a pinhole and after irradiation with Pb beam at 8.1 MeV/u (150X).

REFERENCES

[1] E. Baron, 8th Intl. Conf. Cyclotrons, IUCF, 1979 p. 2411.

[2] A. Benyagoub and S. Klaumunzer, Radiation Effects and Defects in Solids, 1993, vol. 126, pp. 105-110

FFAG DEVELOPMENTS IN JAPAN

Y. Mori*
Research Reactor Institute, Kyoto University, Osaka, Japan

Abstract

Fixed field alternating gradient (FFAG) accelerator has been developed in many places for various applications in Japan. This paper presents the recent activities in the development of FFAG accelerators of Japan.

INTRODUCTION

Fixed field alternating gradient (FFAG) accelerator has various advantages. One is the strong focusing in 3D space where the AG-focusing is in the transverse direction and phase focusing in longitudinal direction with rf acceleration. This is just like synchrotron which brings large acceptance is 3D space. Various rf gymnastics such as bunching, stacking, coalescing,etc. become also possible. Static magnetic field gives the fast acceleration and also large repetition rate, which are useful for accelerating the short-lived particles such as muon, and also making an intense averaged beam current.

The first idea of FFAG was brought by Okawa [1], Kerst and Symon [2], and Kolomensky [3], independently, in early 1950s. In MURA project of 1960s, a couple of electron models were developed, however, the proton FFAG was not realized before the POP proton FFAG came out at KEK in 2000 [4]. Since then, development of FFAGs has been implemented in many places and several FFAGs were constructed.

Concerning the beam optics of the FFAG accelerators, there are two types:one is zero chromatic optics and the other non-zero chromatic optics. The ring with zero chromatic optics is called scaling FFAG and the other non-scaling FFAG. The scaling FFAG where the betatron tunes are always constant during acceleration, is free from the problems crossing betatron resonances. Eventually, it could have a fairly large momentum acceptance of more than +-100. On the other hand,the non-scaling FFAG where all optical elements are essentially linear changes the betatron tunes during beam acceleration, Thus, fast resonance-crossing, that is, fast acceleration is essential in the non-scaling FFAG. The orbit excursion of non-scaling FFAG is rather small compared with that of scaling FFAG, therefore, small aperture magnets become available.

* mori@rri.kyoto-u.ac.jp

BEAM OPTICS AND DYNAMICS OF SCALING FFAG

The betatron oscillation motions in cylindrical coordinates are expressed with the following equations in horizontal and vertical directions, respectively.

$$\frac{d^2X}{d\theta^2} + \frac{r^2}{\rho^2}(1 - K\rho^2)X = 0. \quad (1)$$

$$\frac{d^2Z}{d\theta^2} + \frac{r^2}{\rho^2}(K\rho^2)Z = 0. \quad (2)$$

Here, K is defined as a form with magnetic field gradient. Keeping the betatron tunes in transverse plane constant for different beam momentum, which means zero-chromaticity, the orbit similarity and constant geometrical field index must be satisfied. These conditions required for satisfying the zero-chromaticity lead the magnetic field configuration as shown in this formula.

$$B(r,\theta) = B_0(\frac{r}{r_0})^k f(\theta - \zeta ln\frac{r}{r_0}) \quad (3)$$

Leading from this magnetic field configuration in the cylindrical or circular orbit, there two types of beam optics allow to realize a zero-chromatic scaling FFAG:one is called the radial sector lattice and the other the spiral sector lattice. In the radial sector lattice, the AG focusing takes FODO with a negative bend gradient magnet. On the other hand, in the spiral sector lattice, the alternating focusing and defocusing can be realized with the edge effect.

So far the scaling FFAG lattice assumes a azimuthal symmetry, therefore, there are some disadvantages. It has relatively a large dispersion and the large orbit excursion which require a large horizontal aperture for the magnet and also for the rf cavity. Another disadvantage is that the length of the magnet-free straight section is rather small and the spaces for the injection/extraction devices and also for the rf cavity is sometimes not sufficient. Having the long straight lines keeping a scaling condition to satisfy the zero-chromaticity, reducing the dispersion and making a good match with circular scaling FFAG lattice, these difficulties can be overcome. What is a configuration of the magnetic field for scaling FFAG straight line? Obviously, it should not be presented in Eq. (3).

$$\frac{d^2X}{ds^2} + \frac{1}{\rho^2}(1 - K\rho^2)X = 0. \quad (4)$$

$$\frac{d^2Z}{ds^2} + \frac{1}{\rho^2}(K\rho^2)Z = 0. \quad (5)$$

The equations describing the betatron motions in linear coordinates are expressed in Eqs. (4) and (5). To satisfy the zero-chromatic conditions in this frame just like in the cylindrical one, the orbit curvature should be kept constant and the field index should also be constant. And these leads that the magnetic field configuration should be just an exponential form, which is different from the circular ones. [5]

$$B_z = B_0 exp[(\frac{n}{\rho})x] \quad (6)$$

A design example of the scaling FFAG straight line for the proton beam where beam energy changes from 80 to 200 MeV is shown in Fig. 1. You may clear that orbit shapes for different energies are just similar and the betatron phase advances for horizontal and vertical directions are always constant as a function of the beam energy.

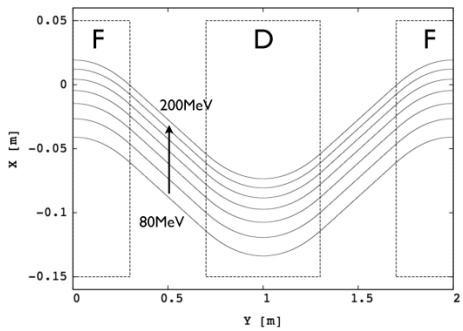

Figure 1: An example of the scaling FFAG straight line:particle is proton and energy range is 80MeV to 200MeV.

Using the scaling FFAG straight lattice, we could realize a dispersion suppressor and also matching insertion with the curved scaling FFAG lattice. For the dispersion suppressor, successive π-cells in the horizontal plane can suppress the dispersion.

$$\frac{k+1}{r_m} = \frac{n}{\rho} \quad (7)$$

The dispersion suppressor helps a lot for the accelerator design such as reducing the magnet aperture and making easier to use a high frequency rf cavity. In order to match the straight line with the circular FFAG lattice, the field configurations for both sides should equal as shown in Eq. (6), the the 1st order (linear) matching condition between two optics is expressed wit this formula. Some mismatches should occur caused by higher orders, however, the effects may not be so large.

Using a newly discovered scaling FFAG straight line, the design of scaling FFAG becomes more flexible and capable for various applications. The scaling FFAG opens a new advanced stage.

In rf acceleration, we also had an advancement in the scaling FFAG design. The beam acceleration in the scaling FFAG has some varieties because the momentum compaction is always strictly constant for different beam energies and has no higher orders. This situation takes either variable frequency of fixed frequency rf in beam acceleration. For the variable frequency rf acceleration, a broad-band rf cavity using magnetic alloys becomes feasible, which has actually been used for the world first proton FFAG (PoP-FFAG) at KEK. And, for the fixed frequency rf acceleration, the stationary bucket acceleration scheme can be useful for the relativistic high energy particle such as muon and electron.

For the fixed frequency rf acceleration, there was also a new advancement. In the strong focusing machine, the rf acceleration theory tells us that two rf buckets below and above the transition energy are interfered with some conditions, which was analyzed by Symon and Sessler in 1960s [**?**], and a serpentine acceleration path between two buckets is existed. The serpentine acceleration path was devoted to accelerate the relativistic particle in the non-scaling FFAG. [7] In the scaling FFAG, Hamiltonian describing the longitudinal particle motion can be analytically derived [8] and it shows a serpentine path accelerating either non-relativistic or relativistic particles exists as shown in Fig. 2.

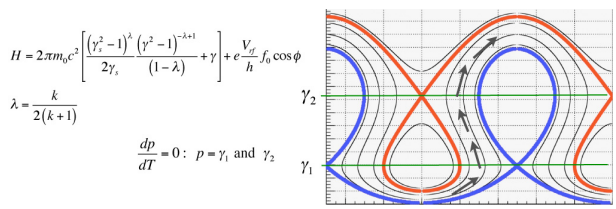

Figure 2: Serpentine acceleration in scaling FFAG.

VARIOUS ACTIVITIES IN JAPAN

Since the PoP-FFAG was developed at KEK in 2000, numbers of FFAG accelerators have been either constructed or under development for various applications in Japan.

Lepton FFAG

In Osaka University, Prof. Kuno and his group are searching for a new physics beyond Standard theory through the experiment with μ-e conversion rare events where the lower limit of branching ratio should be less than 10^{-18}. [9] To achieve this levels, the muon storage ring is essential to reduce energy spread and the pion background.

In this purpose, muon phase rotation ring with FFAG optics to reduce the energy spread of muon beam called PRISM (Phase rotation Ring for Intense Slow Muons) has been proposed. [10] The expected muon intensity is about 10^{11}-10^{12} muons/sec and the energy of muon is about 20MeV. The momentum spread of the muons can be reduced to +-2% from +-20% with this device and the pion

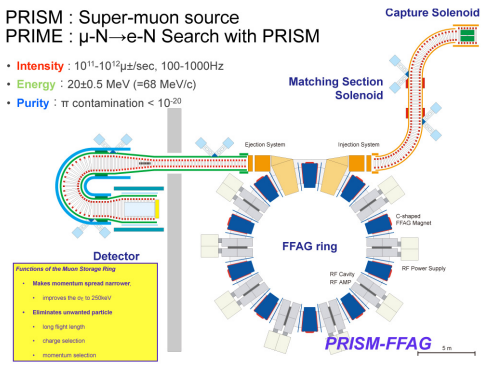

Figure 3: PRISM-FFAG for μ-e conversion in Osaka University.

background can be also reduced to less than 10^{-30} which could not be achieved with the ordinary beam line type of μ-e conversion experiment.

Before constructing full model, they have carried out the demonstration test of phase rotation for such large momentum spreading beam with α-particles. Although the number of rf cavity is just one (in real experiment, five-six rf cavities are needed), still they have clarified the phase rotation in principle, and the experimental results show a good agreement with the results predicted by the beam simulation.

They are also now thinking an advanced scaling FFAG to be used for the real stage of PRISM ring and Fig. 3 shows a schematic layout of it.

In Kyoto University, Research Reactor Institute, design and some preliminary experimental works on muon accelerators have been carried out.

The neutrino factory which devotes the lepton flavor international collaboration experiment with high energy neutrino beams is based on the muon accelerator complex with non-scaling FFAG and RLA (Recirculating Linear Accelerator) as an injector of FFAG in the present reference design. However, the RLA is a cost-driving accelerator and people is seeking more cost effective muon accelerator. As an alternative of RLA, the scaling FFAG is under consideration and being designed at Kyoto University. [11]

Figure 4 shows a design of the scaling FFAG for muon acceleration in the neutrino factory. The energy range of muon is 3.6 to 12.6 GeV and the mean radius is about 160 m. The size is almost half compared with RLA and number of rf cavities could be reduced to about 2/3 of the RLA.

The beam acceleration is one of the biggest issues in this ring. Using the stationary bucket acceleration with constant frequency rf cavity, this problem was overcome. Figure 5 shows the results of full beam tracking in 6-D phase space. The injected beam emittance in each plane is the one which is assumed in the reference design of neutrino factory. There are no beam loss and not large emittance deteriorations during the acceleration.

In collaborating with Osaka University group, a new design of PRISM-FFAG ring with advanced scaling FFAG optics is under development in Kyoto University, Research Reactor Institute, as shown in Fig. 7(a).[12] The ring uses long FFAG straight lines which make space feasible for beam injection/extraction and rf cavities.

Also, an experimental work for demonstrating the scal-

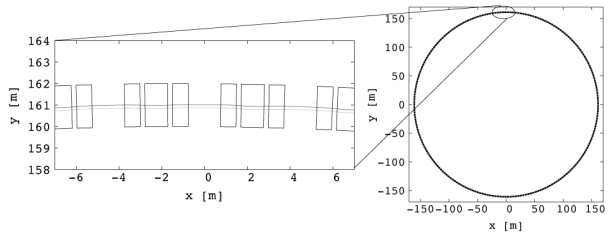

Figure 4: Design of muon FFAG accelerator for neutrino factory.

Table 1: Ring Parameters of a 3.6-12.6 GeV Muon FFAG Accelerator

Item	Parameter
Lattice type	FDF triplet
Injection/extraction energy	3.6/12.6 GeV
RF frequency	200 MeV
Number of turns	6
RF peak voltage (per turn)	1.8 GV
Synchronous energy	8.04 GeV
Mean radius	160.9 m
B_{max}(@12.6 GeV)	3.9 T
Field index k	1390
Total orbit excursion	14.3 cm
Harmonic number	675
Number of cells	225
Long drift length	1.5ṁ
Phase advance	
Horizontal	85.86 degree
Vertical	33.81 degree

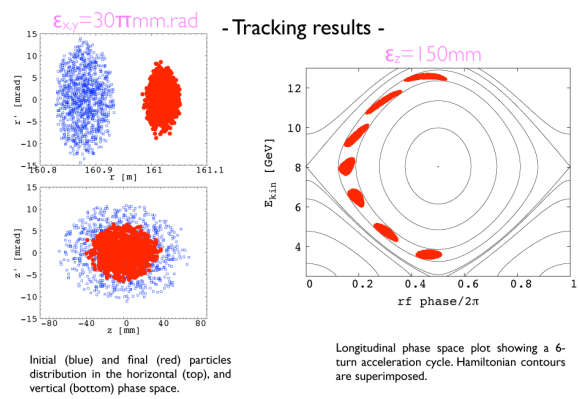

Figure 5: Simulation results of 6-D beam tracking for muon FFAG.

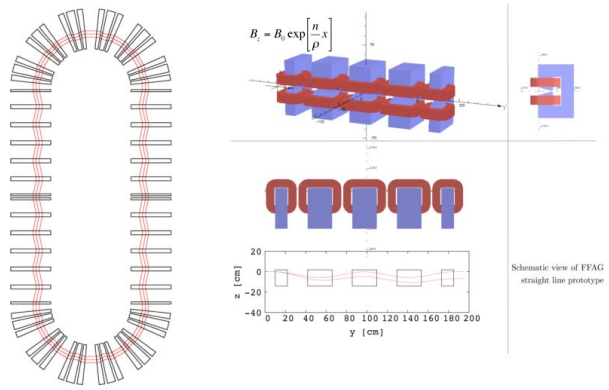

(a) (b)

Figure 6: (a)a new design of PRISM-FFAG with advanced scaling FFAG and (b)an experimental setup of scaling FFAG straight line.

ing FFAG straight line and also for clarifying the characteristics and performance of its beam optics is in progress. Figure 6(b) shows a schematic sketch of the experimental setup. In this line, the total phase advance in horizontal plane is just π.

In industrial applications, two Japanese companies have developed the FFAGs so far. NHV Co. has recently developed an electron FFAG as a prototype for various applications such as sterilization, bonding polymers, etc.[13] The beam energy is about 500keV and average beam current is about 20mA, and the diameter of the machine is 1.1 m as shown in Fig. 7. They have already completed the development and the performance is just they expected. Based on the success of the proto-type, in NHV Co., they have also started the development of a 10MeV electron FFAG. In Mitsubishi Electric Co., a very compact electron accelerator based on the complex of FFAG and Betatron has been developed as shown in Fig. 8.[14] The specifications are shown in this table. The maximum beam energy is about 6MeV and the repetition rate is 1 kHz. The average beam current of 200 μ A is expected. They have already demonstrated the operation of the machine and the performance was just as they expected.

Energy Inj. / Ext.	50 / 500keV
Orbit radius Inj. / Ext.	0.19 / 0.44m
Acceleration frequency	10kHz
Beam Current	100mA peak
Duty	20%
Outer diameter	1.1m

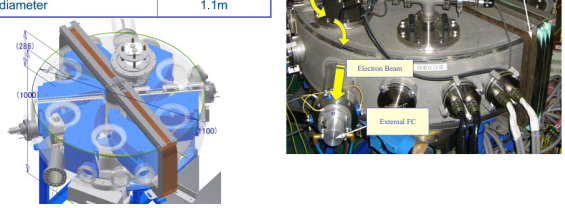

Figure 7: Electron FFAG developed at NHV Co.

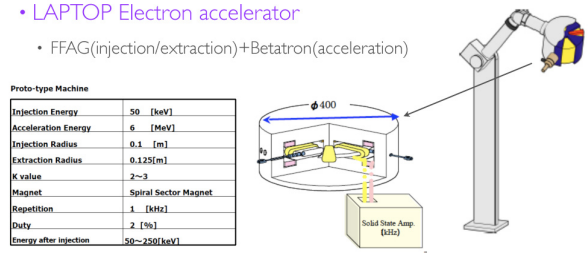

Figure 8: Electron accelerator developed at Mitsubishi Elect. Co.

Hadron FFAGs

In Kyusyu University, a 150MeV proton FFAG is now in re-installation. This machine was originally developed at KEK. [15]

This is a parameter list of 150MeV proton FFAG. The injector is a 10MeV cyclotron.

This is to be used as a multi-purpose machine for various application fields including the education of students. Among them, a unique research work regarding the AMS(Accelerator Mass Spectrometry) with Chloline 36 are being considered. This could become, if it is realized, a very powerful tool for various sciences as shown in Fig. 9. In nuclear physics and material sciences, acceleration of unstable nuclei and isomers can be very interesting. One of the problems in the acceleration of secondary particles is their large emittance, especially in the longitudinal direction. The FFAG has large acceptance, in priciple, therefore, it can be very useful for such secondary particle acceleration.

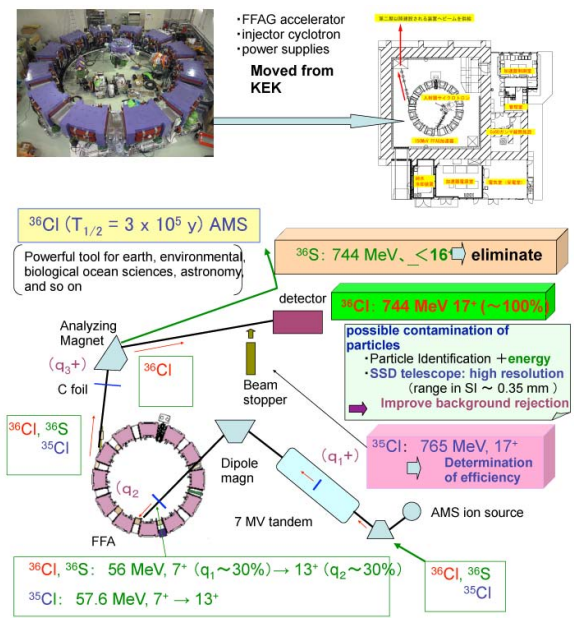

Figure 9: AMS using Chloline-36 with FFAG at Kyusyu University. (Courtesy of N. Ikeda of Kyusyu Univ.)

In Kyoto University, Research Reactor Institute(KURRI), the basic study of ADSR(Accelerator Driven Sub-critical Reactor has been carried out, combining FFAG proton accelerator and KUCA reactor. The output power of KUCA reactor is small like 100W, therefore, the requested beam power for the FFAG is about 1W. Also from the radiation safety, the beam current of the FFAG is limited less than 1nA. [16]

Figure 10 shows a schematic layout of the FFAG-KUCA system for ADSR experiment and a FFAG complex at KURRI. The 150MeV proton FFAG was installed at the newly constructed building called "Innovation Research Laboratory" and it is connected to KUCA with a long beam line, which is located just 1m below from the office ordinary people is living.

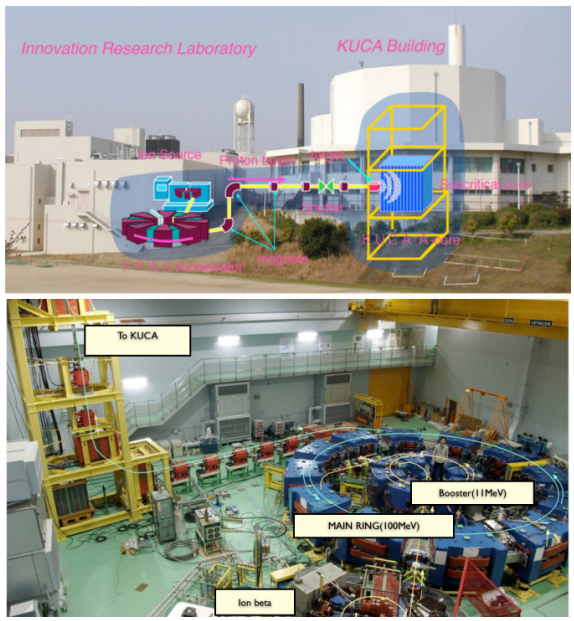

Figure 10: Schematic layout of the FFAG-KUCA system in ADSR experiment and the FFAG complex at KURRI.

The 150MeV proton FFAG, which is composed of Injector, Booster and Main Ring, and they are all FFAG rings. The beam is transported from the FFAG to KUCA through the long beam transport line.

March of last year, the first beam from the FFAG was successfully injected into the KUCA reactor and we have started the ADSR experimental studies. Since the FFAG operates with 30Hz, prompt neutrons are created in every 33msec, then, the delayed neutrons amplified by nuclear fission reactions came out depending on the reactor subcriticality as shown in Fig. 11.[17] Figure 12 presents the measured reactivity distribution in the different place of the reactor core.

The sub-criticality and their dynamical behaviors were measured and analyzed with PNM and Feynman-alfa methods, respectively. Both methods were very useful for detecting the sub-criticality of the ADSR system during operation.

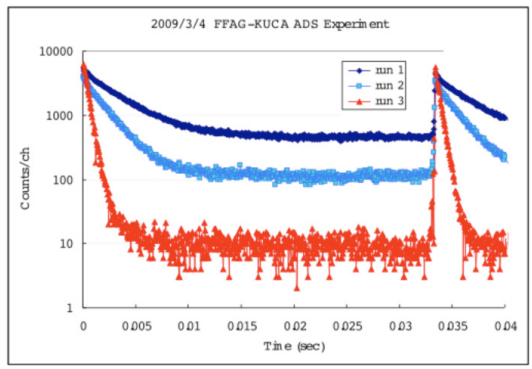

Figure 11: Time response of neutron yield for various sub-criticalities measured with the FFAG-KUCA system in ADSR experiment.

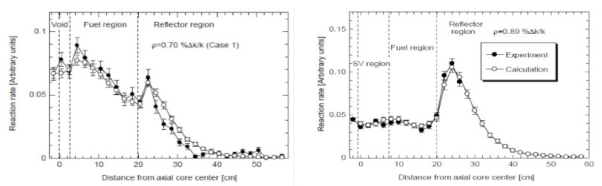

(a) (b)

Figure 12: Measured spacial distribution of the reactivity in the ADSR experiment with FFAG-KUCA system at KURRI. (a) shows the core-axial and (b) the core-horizontal directions, respectively.

In this year, another memorial ADSR experiment was realized, which is the first ADSR experiment with thorium loaded core.

The ADSR experimental study with FFAG-KUCA complex has been successful, however, the study is somewhat limited because of the low output power of KUCA. In order to proceed the next stage of ADSR experiment, not only the basic reactor physics but also the nuclear engineering study is necessary at relatively high power. Therefore, we are thinking of a new high-power sub-critical system with the neutron output power of more than 10kW. For this purpose, the beam intensity of the FFAG has to be increased to the level of more than μA. Also other applications such as nuclear data taking and material science with spallation neutron source become feasible with the beam intensity upgrade.

With charge-exchanged H^- ion beam injection to the main ring, the beam intensity can be increase up to 10 micro-ampere with 120 Hz repetition rate operation. [18] The H^- ion beam can be provided by a 11MeV H^- ion linac which has been used for the compact neutron source described below.

We are also hoping to increase the energy upgrade of the FFAG. Using a spiral type of FFAG optics, the beam energy could be increased up to 0.7-1GeV. The size of the ring is rather compact, which is about 16m in diameter and can fit

the present room. The detail design works are going on.

We have also developed a new type of compact neutron source called FFAG-ERIT(Emittance Recovery Internal Target). [19] In FFAG-ERIT neutrons are generated from the internal target placed into the proton FFAG storage ring. In order to suppress the emittance growth due to the Rutherford scattering, ionization cooling with energy recovering is adopted in this scheme.

Figure 13 shows a picture of FFAG-ERIT ring and the experimental results are also shown in the picture. The FFAG-ERIT ring has worked nicely, just as we expected and we have measured the neutron production with irradiation method and found that it had a capability of obtaining the neutron yield of more than 10^{13}n/sec with this device.

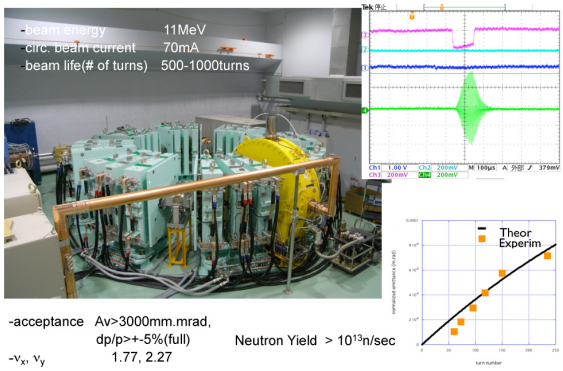

Figure 13: Picture of FFAG-ERIT and the experimental results of beam accumulation and emittance growth.

SUMMARY

Fixed field alternating gradient (FFAG) accelerator has been developed at many institutes in Japan since the first proton FFAG (PoP-FFAG) was demonstrated in 2000. This paper reviews the recent activities in the development of FFAG accelerator in Japan. In scaling FFAG accelerator, in particular, some advancements on beam optics and dynamics such as zero-chromatic straight line, dispersion suppressing and serpentine acceleration have been developed. With these developments, the FFAG accelerator could have various capabilities in many applications.

REFERENCES

[1] T. Ohkawa, Workshop at annual meeting of JPS, 1953.

[2] K.R. Symon, D.W. Kerst et al., Phys. Rev 103(1956)1837.

[3] A.A. Kolomenski, “Theory of Circular Accelerators”, 1966, p.340.

[4] Y. Mori et al., Proc. of 12th Symp. on Accelerator Science and Technology(1999), Wako, Japan.
Aiba et al., Proc. of EPAC2000(2000), Vienna, Austria, pp.581-583.

[5] J.B. Lagrange et al., Proc. of PAC’09(2009), Vancouver, Canada.

[6] K.R. Symon, A.M. Sessler, Proc. Int. Conf. High Energy Acc. (1956), p.44.

[7] S. Machida, Proc. of EPAC2006(2006), Edinburg, Scotland, pp.1541-1543.

[8] E. Yamakaw et al., Proc. of FFAG09(2009), FNAL, Chicago, USA.

[9] LOI (The PRISM Project) for Nuclear and Particle Physics Experiments at the J-PARC(2003).

[10] A. Sato et al.,Proc. of EPAC2004(2004), Edingburgh, Scotland, pp.2508-2510.

[11] T. Planche et al., Proc. of PAC’09(2009), Vancouver, Canada.

[12] J.B. Lagrange et al., Proc. of IPAC’10(2010), Kyoto, Japan, pp.4503-4505.

[13] T. Baba et al., Proc. of EPAC08(2008), Genoa, Italy, pp.3371-3373.

[14] H. Tanaka et al., Proc. of Cyclotorons 2004 (2004), Tokyo, Japan.

[15] Y .Yonemura et al., Proc. of EPAC08(2008), Genoa, Italy, pp.3523-3525.

[16] T. Uesugi et al., Proc. of EPAC08(2008), Genoa, Italy, pp.1013-1015.
Y. Ishi et al., Proc. of IPAC’10(2010), Kyoto, Japan, pp.1327-1329.

[17] C.H. Pyeon et al., Journ. of Nucl. Scie. and Tech., Vol.46 No.12, pp.1091-1093(2009).

[18] K. Okabe et al., Proc. of IPAC’10(2010), Kyoto, Japan, PP3897-3899.

[19] Y. Mori, Proc. of PAC’09(2009), Vancouver, Canada.

FIRST COMMISSIONING RESULTS FROM THE NON-SCALING FFAG ACCELERATOR, EMMA

Susan L Smith#, Daresbury Laboratory, Warrington, UK on behalf of the EMMA team

Abstract

The first results from commissioning EMMA - the Electron Model of Many Applications- are summarised in this paper. EMMA is a 10 to 20 MeV electron ring designed to test our understanding of beam dynamics in a relativistic linear non-scaling fixed field alternating gradient accelerator (FFAG). EMMA will be the world's first non-scaling FFAG and the paper will outline the characteristics of the beam injected in to the accelerator as well as summarising the results of the 4 sector 'gantry-type' commissioning which took place at Daresbury Laboratory. The paper will report on recent progress made with the full EMMA ring commissioning, giving details of tune and orbit measurements as well as their correction to the desired lattice series.

INTRODUCTION

EMMA is an accelerator currently being commissioned at Daresbury Laboratory, UK, to demonstrate the world's first operation of a new concept in accelerators called a non-scaling FFAG, (ns-FFAG) [1,2]. First conceived to provide very rapid acceleration for high energy muons, and now adopted in the baseline design of an international neutrino factory design [3], ns-FFAGs are perceived to have a wide range of potential applications ranging from cheap, simple and compact proton/carbon cancer therapy machines e.g. the PAMELA project [4], to highly reliable powerful proton accelerators producing neutrons to drive sub-critical nuclear reactors [5].

THE EMMA EXPERIMENT

EMMA's purpose is to study beam dynamics in linear ns-FFAGs. By using a high-frequency RF system, the machine will focus on dynamics that can be studied in an FFAG that accelerates rapidly. Two particular areas are of interest: the (rapid) crossing of resonances (though "resonance" might not be the best term [6]), and "serpentine" acceleration, a mode of acceleration particular to nearly isochronous linear non-scaling FFAGs [7].

The EMMA ring accelerates electrons from 10 to 20 MeV in kinetic energy. The beam is provided by ALICE (née ERLP) [8,9]. It uses the small ALICE beam to scan a significantly larger phase space (3 mm normalized transverse emittance). We can extract the beam at any point in the acceleration cycle to examine its properties in a diagnostics line.

The main ring lattice was designed to support these goals. It consists of 42 identical quadrupole doublets, where the quadrupole positions (individually) and gradients (for each family) can be varied. This permits independent control of the dipole and quadrupole gradient for each magnet type, which permits us to tune the lattice to a desired configuration, and to modify the tunes and time of flight of the lattice to study the dependence of the machines behaviour on lattice parameters [10]. Making the cells identical eliminates systematic resonances other than those associated with a single cell, preventing undesired orbit distortion and emittance growth [3].

Both the injection and extraction systems [1] consist of a septum and two kickers in successive cells. This configuration permits us to inject and extract a beam at any energy within the energy range of the machine and at any transverse amplitude of interest [11]. We can use this to measure the (fixed energy) tunes and time of flight (ToF) as a function of energy, which is essential for determining the properties of our lattice. We can also inject and extract the beam at any point in an acceleration cycle.

The ring contains 19, 1.3 GHz RF cavities which can create up to 2.3 MV of acceleration per turn [9]. The cavity frequency can be varied over a range of at least 5.6 MHz. The ability to control the RF voltage and frequency allows us to explore the parameters of the serpentine acceleration mode [4].

ENGINEERING & CONSTRUCTION

The construction methodology has been to assemble accelerator components into subsystems offline to enable integration and system testing of modules prior to installation, allowing early detection of problems and minimising assembly work within the working accelerator area. The extremely compact nature of the EMMA lattice has been very challenging for the engineering design and construction, particularly for the injection and extraction fast pulsed magnets. After a poor response from suppliers the design and construction was carried out in-house.

Seven support girders with six lattice cells each are employed to ensure the stable support of the accelerator components in an integrated way, as shown in Figure 1.

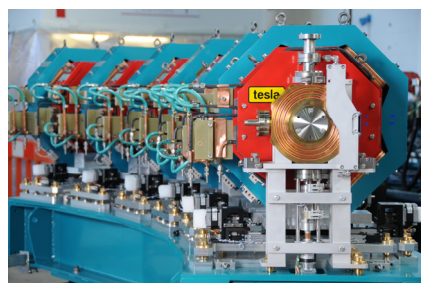

Figure 1: An EMMA girder assembly, 1/7th of the ring

The requirement to deliver close to identical magnetic

fields in every cell, places a stringent alignment tolerance of ±50 μm (1σ), ½ for transferring the magnetic centre to the local fiducials and ½ for alignment errors. This is achieved through a series of precision design, engineering and alignment control processes implemented throughout the magnet measurement, assembly and survey procedure.

COMMISSIONING OF THE RF SYSTEM

The EMMA RF system, Table 1, consists of 19 cavities, a waveguide distribution system, an amplifier and a single LLRF control system, see Figure 2, [12].

Table 1: EMMA RF Parameters

Machine Parameters	Values	Units
Frequency	1.3	GHz
Frequency range	-4.0 to 1.5	MHz
Acceleration per cavity	120	kV
Upgrade acceleration	180	kV
Beam Aperture	40	mm
RF Pulse Length	1.6	ms
Amplitude Control	0.3	%
Phase Control	0.3	Degrees

The cavities have been manufactured by Niowave Inc, USA. To distribute RF power to 19 RF cavities in such a compact ring, a novel waveguide distribution system has been designed and built by Q-Par Angus Ltd, UK. An IOT amplifier, through a cascaded network of hybrid power splitters, delivers power to each cavity. A high power phase shifter is included in each hybrid to provide independent cavity control, with reflected power being dissipated in reject loads. In acceptance tests a tuning range of 196 ° was achieved and 0.01mm, movement in the tuner motor gave a resolution of 0.1°. Isolation tests between ports showed better than 42 dB. Forward and reverse directional couplers showed a directivity of > 41 dB (spec. >40 dB). CPI's VIL409 HeatwaveTM IOT-based RF high power amplifier (RF HPA) has demonstrated up to 90 kW of pulsed power centred at 1.3 GHz over a broad bandwidth of ± 4 MHz.

Figure 2: The EMMA RF System Installation

The Instrumentation Technologies, Libera LLRF system has to synchronise with the ALICE injector, set initial cavity conditions and control the cavity amplitude/phase to ensure stable acceleration in EMMA. It has substantial diagnostic capabilities allowing it to calibrate and monitor the cavity field probe signals, forward and reflected power to each cavity, the IOT power levels before and after the circulator and control the tuner motors and phase shifters installed before each cavity input. In addition it provides closed loop control of both cavity frequency and inter cavity phase.

To cover the frequency range with respect to the ALICE carrier frequency of 1.3 GHz, requires a novel solution whereby the system synchronises itself every pulse to deal with timing jitter contributions from the photo-injector system. To set an offset frequency while maintaining synchronisation, a 'virtual reference' is created that tracks the 1.3GHz and is retimed after each timing signal. The phase relationship between the two machines is maintained even though the frequencies are effectively slipping in time.

Commissioning of the EMMA RF system has commenced. The EMMA cavity frequencies have been adjusted to 1.3008 GHz and the RF output power increased to 40 kW producing an overall accelerating voltage of just under 1 MeV/turn. With the LLRF loop closed, a global phase change has been applied to all the cavities via the LLRF system allowing the phase to each of the cavities to be adjusted from 0 to 360°.

Timing System

The timing system for EMMA is based around two eight channel Quantum Composers 9530 pulse generators. These units are aimed at providing timing and synchronisation for laser applications. A trigger pulse is received from the ALICE photoinjector 20mS before beam is generated. The timing channels have a resolution of 250pS in both delay and width and better than 50pS jitter. An EPICS interface enables remote control of the unit from the control room. The EMMA kickers, septum magnets, high power RF and LLRF are all timed in sequence and adjustable using the quantum pulse generators.

BEAM COMMISSIONING

A staged commissioning methodology has been employed. The injection line from ALICE to EMMA was commissioned with 1st beams on 26th March 2010. Initial matching of the line and diagnostic commissioning has been carried out. The primary diagnostic is a phase space tomography section, consisting of three YAG screens and two FODO cells that have already been used to make a preliminary reconstruction of the transverse phase space.

On 22nd June 2010, first injection into 4 of 7 sectors was achieved allowing an early opportunity to set up injection system and measure cell tune and the dispersion. On completion of the whole ring, on August 13th, parameters such as revolution time and closed orbit became available.

Available Diagnostics

To investigate the beam dynamics, beam position monitors are essential in measuring and understanding the orbit. For the 42 cells, a total of 81 horizontal and vertical button pickups are available. Front end processing of these turn-by-turn pickup signals takes place in the

electronics distributed along the ring, and the results are fed through individual cables into VME BPM cards. The digitised signals then go through a mapping algorithm, which calculates horizontal and vertical beam positions. This data is then made available through the EPICS control system.

In the front end electronics, pairs of button signals, e.g. left-right or up-down, are time-multiplexed onto a single cable, with a fixed time gap corresponding to a quarter of the revolution period (13.8ns). The BPM system is described in more detail in [13].

For the data reported here, the full complement of VME cards was not yet available, and the signals from the front end electronics were viewed directly on an oscilloscope in the control room. An example of a two-turn signal, showing the left and right signals in four cells from 12 to 15, is shown in Figure 3.

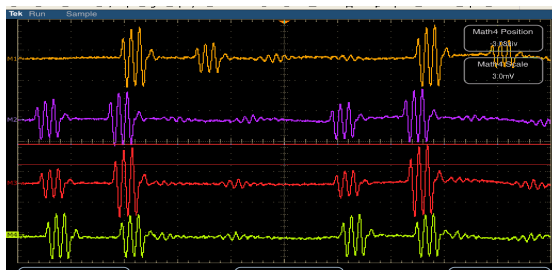

Figure 3: Left-right pickup signals for turns 1 and 2

Equivalent Beam Momentum

EMMA is designed to inject and extract a beam with energy region from 10 to 20 MeV. For commissioning at this stage, however, magnetic field is lowered to simulate a higher energy beam operation with a fixed energy beam from ALICE. Beam energy is 15 MeV and the nominal magnetic field is lowered by a factor of 15.5/18.5 to make the operation with 18 MeV equivalent energy. The operation with equivalent energy will give the same orbit and optics as that with real energy except time of flight (ToF). Slight difference of ToF due to particle speed is depicted in Figure 4.

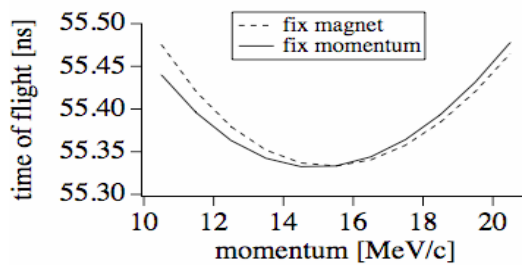

Figure 4: ToF with momentum with fixed field (dashed line) and fixed momentum 15.5 MeV/c (solid line).

Orbit at Injection Region

A beam is injected into the ring with a septum and two kickers. The septum is a quite unusual eddy-current-type devices providing a large, 65° bend angle within less than 10 cm. The septum is capable of translation (towards the machine centre and away from it) and rotation around a moving pivot point to ensure the desired beam position and angle in the entire energy range of interest. A number of tests were performed on the injection septum in the very early stages of the commissioning work.

Orbit position and angle into the septum are monitored by means of the beam position at the last quadrupoles before the septum. We can tell a deviation from the design value each time ALICE and the injection line are setup. They are always within 1 mm in horizontal and a few mm in vertical.

To make sure that position and angle after the septum is more or less repeatable, they are measured with two BPMs right after the septum. Without quadrupole excitation, beam position at two locations in free space can be measured. So far we have been unable to adjust the position and angle at the exit of the septum to the design values. The septum itself seems to be functioning as we expected. An effective magnetic length of 90.9 mm has been determined from BPM measurements of the beam angle before and after the magnet [14]. The value of the same parameter, determined from direct Faraday probe magnetic measurements is 91.4 mm, Figure 5. The good agreement shows that the septum performs as designed.

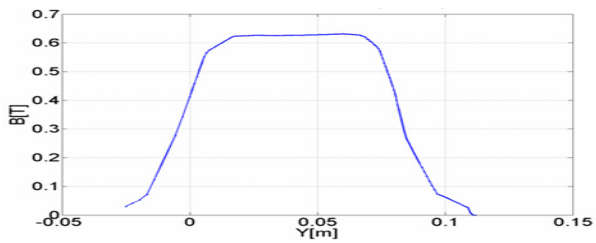

Figure 5: Septum field distribution from probe

One possible reason for miss steering is that position and angle into the septum is not as designed, although the position at the last two quadrupoles is correct. Later we will try to adjust the steering in the EMMA injection line to obtain the desired orbit values at septum exit.

At the position and angle we measured, the strength of two kickers are calculated to take the beam on to the design orbit as shown in Figure 6. The calculated kicker strength is not exactly the same as the determined values but is similar.

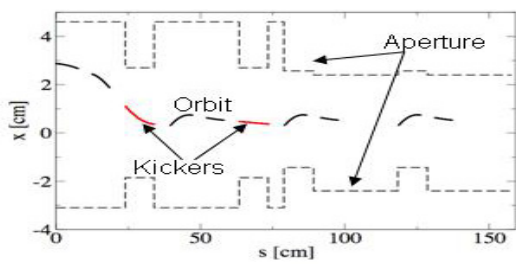

Figure 6: Injection region orbit, 2 normal cells

The kicker waveform has a large undershoot, which kicks the beam when it comes back after one turn. The waveform is adjusted such that the time difference between the first peak and the zero crossing point is around one revolution time. However, it is slightly longer.

Therefore, a beam is actually kicked before the crest with increased kicker current to avoid the second kick.

Tune Measurement

With seven BPMs consecutively located at the middle of doublet quadrupoles, we measured cell tune. One example of measured position is shown in Figure 7. The main frequency component is calculated with least square fit method and shown in Figure 8. The uncertainty in the individual BPM readings is 0.5 mm. The average chi2 per degree of freedom for the fit is 4.

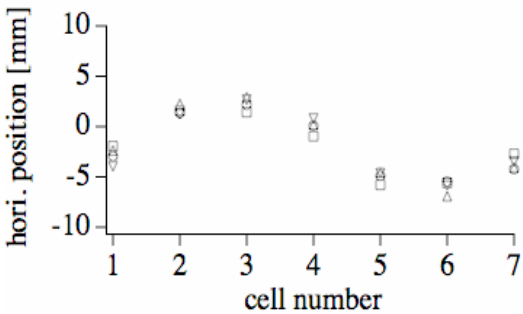

Figure 7: Beam position at seven consecutive cells

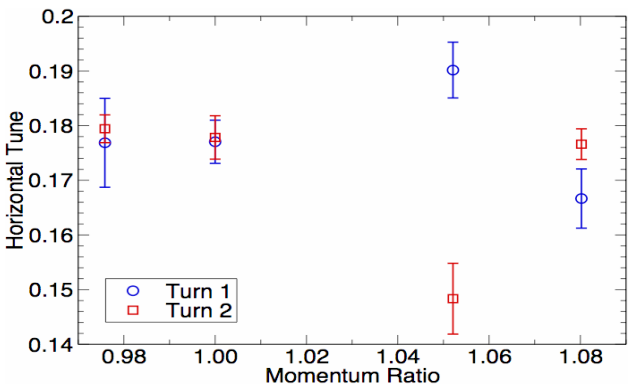

Figure 8: Tunes resulting from a fit of the data from 7 consecutive BPMs to a sinusoidal oscillation.

Dispersion Function

To avoid the complexity of retuning the injector for different energies, we change the quadruple current keeping the QD/QF ratio strength ratio constant to simulate different momentum optics whilst keeping a fixed momentum beam from ALICE.

From measuring the horizontal beam position at each of seven consecutive cells (cells 12 to 18), it was possible to fit a sine function to the betratron oscillation and deduce the mean beam position across the cells. An example of this is shown above in Figure 8. Note that seven cells approximately cover a full betratron cycle.

From the mean beam position and the effective momentum, the dispersion function could be plotted, and this is shown in Figure 9 below.

The calculated dispersion values at 100% effective momentum (15.5 MeV/c) from this data are 82mm horizontally, and 3mm vertically. These values are for the BPM positions of S=0.29m within each cell, and are consistent with the base-line EMMA model.

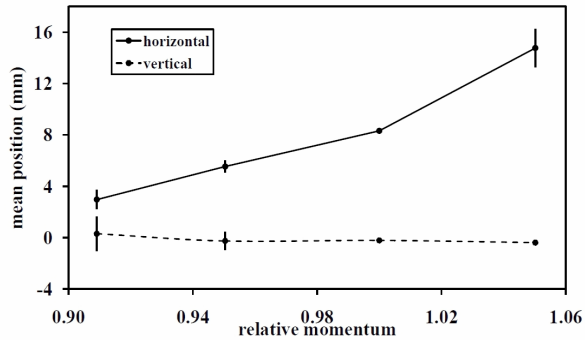

Figure 9: Mean beam position vs relative momentum

Time of Flight Measurement

Time of flight is measured as a revolution time. From differential signal of one of BPM electrode, see Figure 10 time when a bunch passing a BPM is determined and intervals of consecutive signals are obtained. The precision of the measurement is mainly determined by sampling rate of the oscilloscope, that is 50 ps. Preliminary results show the revolution time at 18.5 MeV/c, equivalent momentum is “55.3+/-0.1 ns”.

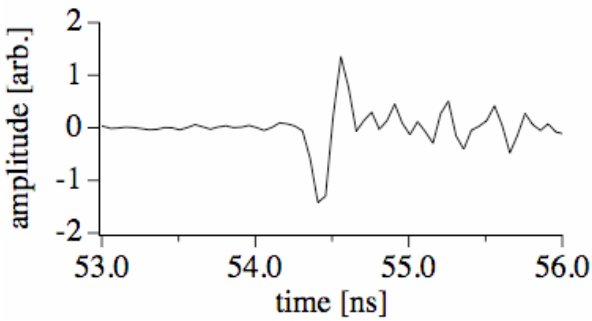

Figure 10: Beam signal to determine ToF.

Transverse Stability

Without RF, a beam is circulating for more than 1000 turns, Figure 11. The source of gradual loss is unknown. It could be initial optics mismatch, beam energy loss due to beam loading at cavity, or scattering with residual gas.

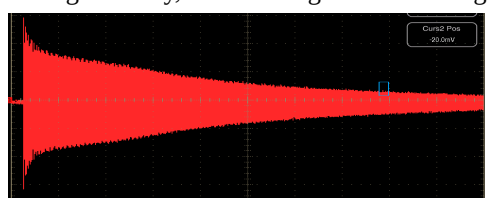

Figure 11: BPM signal with 4 μs/dev.

COMMISSIONING PLANS

Our current commissioning shifts are focussed on setting up the cavity tuning and phase to verify that the LLRF system is fully functional and capable of providing the required phase and amplitude stability, specifically at the ALICE matched frequency and over the required range of frequencies. On achieving this, it is then hoped

that a verification of successful accelerator, evidence of energy gain from acceleration inside and then outside of the bucket would follow relatively quickly.

The next steps are to get a measurement of tune and time of flight as a function of energy with the RF cavities turned off. We will initially continue on our current course of simulating different energies by using a fixed-energy beam from ALICE and scaling the magnet fields. We will set the magnet fields to simulate injecting the beam over the full energy range of EMMA (ideally in 1 MeV steps), and find the injection system parameters to inject the beam on the closed orbit for each case and allow the beam to circulate for a large number of turns. We will measure the time of flight on the closed orbit. We will then inject the beam slightly off this orbit to measure the tune. We will do this at a number of amplitudes, and measure the time of flight at those amplitudes as well. Having ~1/2 of the BPMs, i.e. those located inside the doublets, instrumented will be important for the accuracy of these measurements.

We will repeat the above process with the magnet fields fixed and varying the energy of the ALICE beam. ALICE will be tuned to supply a beam for each energy for which we generated a simulated energy in the earlier process.

The closed orbit position as a function of energy will also be used to construct a mapping from energy to position so that we can monitor the energy during the acceleration cycle without extracting the beam. We would also like to extract the beam, and we will thus find the extraction system parameters to extract the beam from the closed orbit at different energies. We will measure the energy of the extracted beam.

Once we have the tune, time of flight, and orbit position as a function of energy, we will adjust the main ring magnet parameters to bring those curves closer to the desired values, and repeat the process of finding the tune and time of flight as a function of energy.

We will set RF frequencies and phases to be synchronized with the beam at some number of energies. We can then measure synchrotron oscillations. This will also give us a time of flight measurement which can be compared to time of flight measurements made without the RF system.

We will then accelerate the beam in the serpentine acceleration mode with the RF cavities powered. We will begin with a relatively large RF voltage to have a large region of phase where we can accelerate the beam. We will using the mapping of orbit position to energy to show the bunch motion in longitudinal phase space, and will extract the beam at various turns to compare the energy measurement in the extraction line to the energy determined from the orbit position.

SUMMARY

Through innovative design, the world's first non-scaling FFAG has been realised at Daresbury as a highly sophisticated accelerator research tool. The initial ring commissioning is underway in parallel to the final system installation and testing. Next steps are the demonstration of acceleration, followed by a systematic set of experiments designed to comprehensively characterise this unique accelerator and it operation.

ACKNOWLEDGEMENTS

I acknowledge the many individuals who have contributed to the simulations, concepts and developments reported in this paper. These include the international collaboration, the members of the BASROC consortium, and the team from Daresbury Laboratory, the Cockcroft Institute and the John Adams Institute, who have designed, constructed and who are currently, very actively, taking part in commissioning of EMMA.

REFERENCES

[1] S. L. Smith, EMMA, the World's First Non-Scaling FFAG Accelerator, to appear in, Proceedings of PAC09, Vancouver, BC, Canada.
[2] R. Edgecock, in Proceedings of IPAC'10, Kyoto, Japan, p. 3593 (IPAC'10/ACFA, 2010).
[3] K. Long (Ed), "An International Scoping Study of a Neutrino Factory and Super-beam Facility", CARE-Report-2005-024-BENE, 2005.
[4] K. Peach et al, "PAMELA Overview: Design Goals and Principles", to appear in, Proceedings of PAC09, Vancouver, BC, Canada.
[5] C. Bungau, R. J. Barlow, R. Cywinski, "Reactor Design Studies for an Accelerator Driven System", to appear in, Proceedings of PAC09, Vancouver, BC, Canada.
[6] S. Machida and D. Kelliher, Phys. Rev. ST Accel. Beams 10, 114001 (2007).
[7] J. S. Berg, Phys. Rev. ST Accel. Beams **9**, 034001 (2006).
[8] C. Beard et al., "The Current Status of the ALICE Facility", FEL'09, Liverpool (2009).
[9] J.M. Garland et.al., "Characterisation of the ALICE Accelerator as an Injector for the EMMA ns-FFAG", Proceedings of IPAC'10, Kyoto, Japan.
[10] J. S. Berg, Nucl. Instrum. Methods. A **596**, p. 276 (2008).
[11] J. S. Berg, "An Injection/Extraction Scenario for EMMA,", to appear in, Proc. PAC09, Vancouver, BC, Canada.
[12] C. D. Beard, in, Proceedings of EPAC08, Genoa, Italy, p. 3377 (EPAC/EPS-AG, 2008).
[13] A. Kalinin et al, "Diagnostic System Commissioning of the EMMA NS-FFAG Facility at Daresbury Laboratory", to appear in Proceedings of IPAC'10, Kyoto, Japan.
[14] K. Marinov and S. Tzenov, internal report, an emma comm-rpt, "Septum BPM Data".

INNOVATIONS IN FIXED-FIELD ACCELERATORS: DESIGN AND SIMULATION*

C. Johnstone#, Fermilab, Batavia, IL, 60510, U.S.A.
M. Berz, K. Makino, Michigan State University, East Lansing, MI, 48224, U.S.A.
P. Snopok, University of California, Riverside, CA, 92521, U.S.A.

Abstract

The drive for higher beam power, high duty cycle, and reliable beams at reasonable cost has focused world attention on fixed-field accelerators, notably a broad class of accelerators termed Fixed-field Alternating Gradient accelerators, or FFAGs, (with cyclotrons considered a specific expression or sub-class of FFAGs). Recently, the concept of isochronous orbits has been explored and developed for the most general type of FFAG (termed non-scaling) using powerful new methodologies in fixed-field accelerator design. One application is high-intensity, in particular high-energy (GeV), proton drivers which encounter duty cycle and space-charge limits in the synchrotron and machine size concerns in the weaker-focusing cyclotrons. With isochronous orbits, FFAGs are capable of the high duty cycle, or CW operation, associated with cyclotrons. Further, their strong focusing enables smaller losses, and potential energy variability that are more typical of the synchrotron. With the cyclotron as the current industrial and medical standard, a competing CW FFAG, could potentially have broad impact on research, industrial, and medical accelerators and associated facilities. This paper reports on new advances in FFAG accelerator technology, design, and simulation, and also presents advanced tools developed for all fixed-field accelerators unique to the code COSY INFINITY[1].

INTRODUCTION

The drive for higher beam power, high duty cycle, and reliable beams at reasonable cost has focused world attention on fixed field accelerators, notably a broad class of accelerators termed Fixed-field Alternating Gradient (FFAGs). Cyclotrons can be considered a specific expression or sub-class of FFAGs which employ a predominately constant rather than gradient magnetic field. Recently, the concept of isochronous orbits has been explored and developed for the most general type of FFAG (termed non-scaling) using powerful new methodologies in fixed-field accelerator design. The property of isochronous orbits enables the simplicity of fixed RF and by inference, CW operation. By tailoring a nonlinear radial field profile, the FFAG can remain isochronous, well into the relativistic regime. One application is high-intensity, and, in particular, high-energy (GeV) proton drivers which encounter duty cycle and space-charge limits in the synchrotron and machine size concerns in the weaker-focusing cyclotrons. With isochronous orbits, the machine proposed here has the high average current advantage and duty cycle of the cyclotron in combination with the strong focusing, smaller losses, and potential energy variability that are more typical of the synchrotron. Further, compact high-performance devices like FFAG-type accelerators and cyclotrons often are operated in a regime where space charge effects become significant. The strong focussing attribute, particularly in the vertical of the FFAG, implies some degree of mitigation of space-charge effects and possible stable acceleration of higher currents.

With the cyclotron as the current industrial and medical standard, a competing CW FFAG, could potentially have broad impact on facilities using medical accelerators, proton drivers for neutron production, accelerator-driven nuclear reactors, waste transmutation, and the production of radiopharmaceuticals and open up a range of as-yet unexplored industrial applications. This paper reports on new advances in FFAG accelerator technology, design, and simulation, and also presents advanced tools developed for all fixed-field accelerators unique to the high-order code COSY INFINITY[1].

BACKGROUND

The FFAG concept in acceleration was invented in the 1950s independently in Japan[2], Russia[3] and the U.S[4] (T. Ohkawa[3] in Japan, H.S. Snyder[5] at Brookhaven, and A.A. Kolomenskij[3] in the Soviet Union). The field is weak at the inner radius and strong at the outer radius, thus accommodating all orbits from injection to final energy. Focusing is provided by an alternating body gradient (which alternately focuses in each transverse plane) or through body gradient focusing in one plane (nominally horizontal) and strong gradient-dependent edge focusing in the other (vertical) plane. An extensive discussion of the various FFAG configurations, including derivations of the formulas relating the various accelerator and orbit parameters can be found in the references[6]. The configuration initially proposed was called a radial sector FFAG accelerator. A spiral sector configuration was also invented consisting of magnets twisted in a spiral such that as the radius increases, and the beam crosses the magnet edges, it experiences alternating gradients. With no reverse-bending magnets, the orbit circumference of the spiral-sector scaling FFAG is about twice that for a circular orbit in a uniform field. These machines are the so-called scaling FFAGs (either spiral or radial-sector FFAGs) and are characterized by geometrically similar orbits of increasing radius. Direct application of high-order magnetic fields and edge focusing maintains a constant tune and optical functions during the acceleration cycle and avoids low-order resonances. The

*Work supported by Fermi Research Alliance, under contract DEAC02-07CH11359 with the U.S. Dept of Energy.
#cjj@fnal.gov

magnetic field follows the law $B \propto r^k$, with r as the radius and k as the constant field index.

The non-scaling FFAG was invented in 1997 (C. Johnstone and F. Mills) and a working lattice published in 1999[7] as a solution for the rapid acceleration of muon beams. The non-scaling FFAG proposed for muon acceleration utilizes simple, combined function magnets like a synchrotron. However, it does not maintain a constant tune and is not suitable for an accelerator with a modest RF system and a slower acceleration cycle.

Recently, innovative solutions were discovered (C. Johnstone, Particle Accelerator Corp.) for non-scaling FFAGs which duplicated the constant tune feature of the scaling FFAG without applying the scaling principle. This new non-scaling FFAG accelerator applied weak and alternating gradient focusing principles (both edge and field-gradient focusing) in a specific configuration to a fixed-field combined-function magnet to stabilize tunes [8]. Note that, stable tunes, however, do not imply isochronous orbits.

Isochronous performance is achievable only at relativistic energies in a synchrotron and predominately nonrelativistic energies in a cyclotron. In a synchrotron, the magnetic field increases proportional to momentum and therefore particles are confined about a laboratory-based reference trajectory independent of energy. Since the path-length is fixed independent of energy, the orbital frequency changes with energy. A frequency change in the accelerating RF is required except at highly-relativistic energies, so swept-frequency RF is unavoidable. In a fixed-field machine, such as a FFAG or cyclotron, the reference orbit moves outward transversely with energy so the orbital path length always changes with energy. At nonrelativistic energies the increase in path length can be scaled with momentum which is directly proportional to velocity thus keeping the orbital frequency constant and the RF frequency fixed (isochronous condition). As the energy becomes increasingly relativistic, the path length must have an increasingly nonlinear dependence on momentum which becomes increasingly difficult to engineer with a predominately dipole field.

As noted above, recently the problem of isochronous orbits has been solved for non scaling FFAG designs in the relativistic energy regime, ~a couple of GeV and below. These isochronous, compact non-scaling FFAGs lattices were discovered by tailoring an arbitrary radial field profile to both constrain tunes and confine orbits to isochronous ones using new advanced accelerator design and modelling tools. Designing and demonstrating performance, particularly for the FFAGs with their complex field profiles and edge contours required new advances in accelerator modelling which will be described in a later section.

DYNAMICS OF FFAGS

Tune is perhaps the most important optical indicator of stable particle motion, since it determines when particles in the beam, executing periodic motion around the accelerator, return to the same transverse position relative to a central, or reference orbit in the machine. In a fixed-field machine such as an FFAG or cyclotron, this reference orbit moves with energy so the tune is controlled through radial and azimuthal variations in the magnetic field as described below.

Three conventional techniques exist for controlling the beam envelope and corresponding tune, or phase advance, in a magnetic field. The first confinement technique is the weak focusing principle used in classical cyclotrons in which changes in path-length through the magnetic field as a function of transverse position focus the beam, but only in the bend plane (which is typically horizontal). Weak focusing by the dipole component of the field in the body of the magnet does not affect the vertical plane.

The second arises from the field falloff at the physical edge of a magnet. A vertically-oriented (horizontally-bending) dipole field presents either a horizontally focusing or defocusing effect or no effect depending on the on the angle through which the beam traverses the fringe field. This edge effect is essentially equivalent to a quadrupole-like element located at each magnet edge: it can be either focusing horizontally and defocusing vertically, or the reverse for a non-normal crossing angle. (A normal entrance angle has no focusing effect.) In a cyclotron, vertical control is established via edge focusing through deliberate radial shaping of the pole-tip combined with a non-normal edge-crossing angle. The use of an edge-crossing angle in a cyclotron for vertical envelope control is normally weaker than focusing from path-length differences in the horizontal plane.

The remaining technique used in synchrotrons involves application of strong-focusing, alternating gradients in consecutive ring magnets. Strong-focusing techniques are capable of focusing equally in both planes with much stronger strengths resulting in larger phase advances, shorter focal lengths, and corresponding higher machine tunes than achievable in weak-focusing machines, i.e. stronger and more versatile envelope control. Contrary to cyclotrons, edge focusing effects are kept deliberately small in large multi-cell synchrotron rings. This term becomes increasingly important for and often causes difficulties in the dynamics of small synchrotron rings.

All three principles are applied in FFAGs—scaling machines specifically require edges plus gradient fields in relatively constant strengths to achieve similar orbits and corresponding constant tunes. In the non-scaling FFAG, the different focusing principles are combined in different and generally varying composition through the acceleration cycle – the varying composition can be exploited to control the machine tune without applying the field scaling law.

In particular, and unlike a cyclotron, the strength of the edge focusing and centripetal terms can be enhanced in the presence of a gradient - importantly their strength can increase with radius and therefore with energy. Understanding the powerful interplay between gradient and the centripetal and edge focusing is critical to understanding the dynamics and potential of the FFAG accelerator.

Thin Lens Formulism

The application of the transverse focusing terms and their inter-dependence can be understood conceptually using the thin-lens approximation. This approximation provides direct insight into the transverse dynamics of both FFAGs and traditional accelerators.

The dynamics of most accelerators can be expressed and understood almost completely in terms of the three "conventional" transverse focusing principles outlined above. To understand the interplay between strong, weak and edge focusing, a simple linear, thin-lens matrix model serves as a guiding example. The approach is most easily rendered using a simple sector magnet matrix, adding a gradient term to the focusing, and then applying an edge angle to the entrance and exit. The following is the first order matrix for a horizontally-focusing sector magnet with a gradient and an edge angle, η.

$$\mathrm{M}=\begin{bmatrix} 1 & 0 \\ -\tan\eta/\rho_0 & 1 \end{bmatrix}\begin{bmatrix} \cos\Theta & \frac{1}{\sqrt{K}}\sin\Theta \\ -\sqrt{K}\sin\Theta & \cos\Theta \end{bmatrix} \quad (1)$$

where $\Theta=\sqrt{K}l$ and $K=k_0+1/\rho_0^2$ for a C.F. sector magnet. For the edge angle we adopt the sign convention to be: η>0 is outward, or away from the body of the magnet and thus it increases the net horizontal focusing. Reducing to thin lens, the matrices from the center of the gradient magnet through the edge are:

$$\begin{aligned}
&\begin{bmatrix} 1 & 0 \\ -\tan\eta/\rho_F & 1 \end{bmatrix}\begin{bmatrix} 1 & l \\ -Kl & 1 \end{bmatrix}\approx\begin{bmatrix} 1 & 0 \\ -\eta/\rho_F & 1 \end{bmatrix}\begin{bmatrix} 1 & l \\ -Kl & 1 \end{bmatrix} \\
&=\begin{bmatrix} 1 & l \\ -(k_F l+l/\rho_F^2+\eta/\rho_F) & -\eta l/\rho_F+1 \end{bmatrix} \\
&\cong\begin{bmatrix} 1 & l \\ -(k_F l+l/\rho_F^2+\eta/\rho_F) & 1 \end{bmatrix} \\
&=\begin{bmatrix} 1 & l \\ -(k_F l+\frac{(\vartheta+\eta)}{\rho_F}) & 1 \end{bmatrix}=\begin{bmatrix} 1 & l \\ -1/f_F & 1 \end{bmatrix}
\end{aligned} \quad (2)$$

since $l/\rho_F^2\cong\vartheta/\rho_F$, where ϑ is the sector bend angle and the length l is the half-magnet length. The edge angle here has been assumed small to allow the tangent function to be approximated. Note that the gradient is not necessarily linear, but this thin lens derivation applies "locally" even in the presence of a nonlinear gradient. For the case of a nonlinear gradient, the local focusing strength (B') is simply evaluated at each orbital location.

From Equation 3 for the focal length, one can immediately see that the sector angle and edge angle term increase the focusing in the horizontal plane for a positive bend angle or dipole component. The choice of dipole component – which, in the presence of a gradient, changes at each reference orbit as a function of energy – has very important consequences. If the dipole component increases with radius, then focusing increases with energy relative to injection. Both the centripetal and edge-angle term add constructively with the strong-focusing. The integrated strength of the strong-focusing term can also increase if a) the edge angle increases the path length through the magnetic field, and/or b) if the gradient itself increases with radius (for a non-constant gradient; i.e. higher or quadrupole). When the integrated strong focusing strength increases as a function of energy, it serves to stabilize the tune. Both planes are not identical, however, for in the vertical only the strong focusing and edge-angle terms contribute to a change in focusing strength.

$$1/f_F=k_F l+\frac{\vartheta}{\rho_F}+\frac{\eta}{\rho_F} \quad (3)$$

Therefore, in the vertical version of Equation 3, only the gradient, $k_D l$, and the edge term apply so two terms contribute to the vertical machine tune. The following summarizes tune and envelope control in conventional accelerators.

- *Centripetal* (Cyclotrons + FFAGs) :
  - Bend plane only, horizontally defocusing or focusing
  - Strength ∝ θ/ρ (bend angle/bend radius of dipole field component on reference orbit);
- *Edge focusing* (Cyclotrons + FFAGs) :
  - Horizontally focusing / vertically defocusing, vice versa, or no focusing,
  - Strength ∝ tan η/ρ , or ~ η/ρ for a small edge-crossing angle (edge crossing angle/bend radius of dipole field component at entrance to magnet;
- *Gradient focusing* (Synchrotrons + FFAGs) :
  - Body field components > dipole:
    $B=a+bx+cx^2+dx^3+\ldots\ B'=b+2cx+3dx^2+\ldots$
  - Constant gradient: Synchrotrons, linear-field non-scaling FFAGs (muon FFAGs)
  - Scaled nonlinear field, gradient increases with *r* or energy: Scaling FFAGs,
  - Arbitrary nonlinear field, gradient increases with *r* or energy: nonlinear, non-scaling FFAGs.

FFAG DESIGN PRINCIPLES

In a scaling FFAG, the field-scaling law predetermines that the reference beam trajectories remain parallel implying that much of the optics remain constant with energy – in particular the tunes remain fixed. The non-scaling FFAG relaxes this condition and aims only for stable beam during acceleration. If the acceleration is quick, then tune variations can be tolerated. If the acceleration is slow the tune must be more controlled (although some tune variation

can be accommodated or compensated for if the acceleration cycle is slow enough)

Non-scaling in its simplest terms implies nonparallel reference orbits in a FFAG. Although parallelism automatically implies constant tune (through fixed number of betatron oscillations), it is not a necessary condition. In the non-scaling FFAG, the different focusing terms can be varied independently to control tune and further optimize machine parameters. This last point is very important for FFAGs because it allows the field, orbit location, and important machine parameters such as tune, footprint, and aperture to be more independent and strongly controlled than in cyclotron.

The constant + linear-gradient field case serves as an instructive example. Interestingly, this case remains a valid "local" interpretation of FFAG dynamics even in the presence of a strongly nonlinear global field. The local "quadrupole" strength parameter, *k,* is simply the derivative of the field profile evaluated at the reference orbit for a specific energy. Even in the case of only linear gradient field profiles, a sextupole component [9] arises when the quadrupole body field is combined with an edge angle. The presence of higher-order field components contributes still higher nonlinear terms in combination with an edge angle. Therefore, even in the linear case, the dynamics do not obey linear optics. However, a local interpretation in terms of linear optics and dynamics remains valid and is critical to designing and understanding compact FFAG accelerators.

FFAG Lattice Design

FFAG lattices are completely periodic, like a cyclotron. Periodicity permits closed geometry and repetitive, adiabatic optical solutions over a tremendous range in momentum. However, the strong-focusing does allow stable, "long" straights to be integrated into the base unit cell. (Specialized utility insertions are under development but are nontrivial to properly match over the large dynamical momentum range of the FFAG.).

All lattices are simple, single lens structures based on the FODO cell. The maximum and minimum beam envelopes alternate between opposing planes – even in the so-called doublet and triplet FFAGs. Single lens structures are optically stable over a large range in momentum; there are no telescope-based FFAGs with any significant dynamical range.

FFAGs utilize short cells to achieve short focal lengths. The stronger the focusing and the shorter the focal length; the more adiabatic the optical functions, and the larger the stable momentum range. FFAG designs exploit combined function magnets to minimize unit cell length and optimize dynamic range. Long straights are inserted at points of reflection symmetry in the lattice (at points where the derivatives of optics functions are zero) thereby causing little disruption to the periodic optics.

Progression of the Non-scaling FFAG Design

Initial non-scaling FFAG lattices (EMMA project)[10] utilized a linear fields/constant gradient and rectangular magnets. However, it does not maintain a constant tune and is not suitable for an accelerator with a modest RF system and therefore a slower acceleration cycle. .

With tune is the strongest indicator of stable particle motion, constraining the machine tune can be sufficient to design a stable machine. In all fixed-field accelerators, the FFAG or the cyclotron, the reference orbit moves with energy. Using this property, tune can be controlled in a linear or nonlinear gradient FFAG by shaping the edges of the magnets.

All three focusing terms are impacted by the edge contour and their interaction can be used to manipulate the machine tune in the horizontal. Two terms, gradient and edge focusing, are available for tune control in the vertical. For example, use of a gradient plus an edge angle on a linear-gradient magnet enhances not only the integrated strong-focusing strength, but also weak (centripetal), and edge focusing as a function of radius (and therefore energy). Further, in a non-scaling FFAG, contributions from the different strength terms can vary with radial position and can also be independent in the F and D magnets. In a non-scaling FFAG the edge crossing angle often changes with energy resulting in non-similar orbits. This increase in strength of all the terms tracks the increase in momentum and stabilizes the tune. The result is a dramatic increase in the momentum reach of the machine, from 2-3 to a factor of 6 utilizing a simple edge contour on a constant-gradient magnet. Figures 1 and 2 below indicate the improvement in tune control in a constant-gradient non-scaling FFAG through application of a simple linear edge contour.

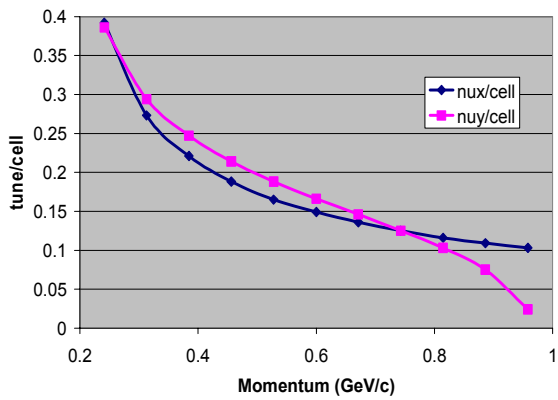

Figure 1: Variation of tune in a linear gradient, large acceptance non-scaling FFAG for rapid acceleration.

Completely stable tunes, and compact machines in footprint and aperture, however, required higher-order, field profiles tailored to reach the advanced specifications. An arbitrary field expansion has been exceptionally successful in controlling both tunes and physical attributes of a machine. An order of magnitude increase has been achieved in momentum range relative to the initial non-scaling concept (an acceleration range of a factor of 44 has been achieved in one ultra-compact nonlinear design). Even in predominately nonlinear fields, the strong focusing permits adjustment of cell tunes to produce a large dynamic

acceptance and surprisingly linear performance (elliptical phase space portraits).

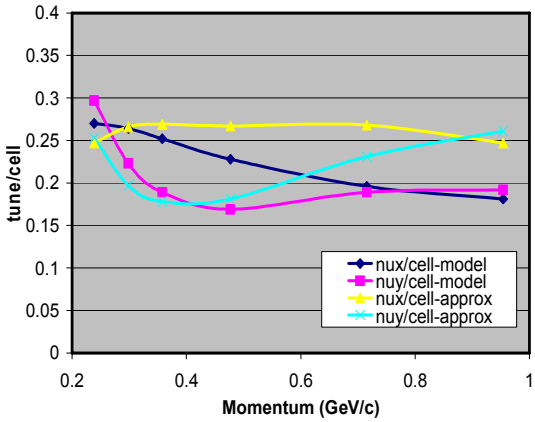

Figure 2: A constant gradient nonscaling FFAG with an edge contour to stabilize tune.

Further, isochronous orbits have been achieved in a non-scaling FFAG by applying both a nonlinear gradient and edge contour. Isochronous implies CW operation and simple rf systems.

Isochronous orbits are proportional to velocity. However, the orbital path length of a particular momentum follows the B field and thus is not necessarily proportional to velocity. At relativistic energies, momentum is an increasingly nonlinear function of velocity. Therefore, the integrated B field must be a nonlinear function of radius proportional to the relativistic velocity. A nonlinear field expansion combined with an appropriate edge angle can constrain the orbit at each momentum to be proportional to velocity and simultaneously control the tune. Unlike the cyclotron which relies on a dipole field and is therefore limited in adapting path length to match relativistic velocities, the non-scaling FFAG can maintain isochronous orbits well into strongly relativistic energy regimes as shown in Figure 3. Further, the nonlinear gradient required to achieve this decreasing change in path length with increasing momentum at relativistic energies has the advantage of providing increasing focusing in both transverse planes as a function of energy.

ISOCHRONOUS FFAG DESIGN

In general, conventional accelerator codes provide too-little flexibility in field description and are limited to low order in the dynamics; as such they cannot adequately formulate and predict FFAG accelerators, especially in the presence of the strong nonlinearities from edge contours and fields along with other high-order effects.

Powerful new methodologies in accelerator design and simulation have been pioneered using control theory and optimizers in advanced design scripts with final simulation in COSY INFINITY[1]. COSY INFINITY now has a full complement of sophisticated simulation tools to fully and accurately describe both conventional accelerators and the FFAG's complex electromagnetic fields. Specifically, new tools were developed for the study and analysis of synchrotron, cyclotron, and FFAG dynamics based on transfer map techniques unique to the code COSY INFINITY. With these new tools, closed orbits, transverse amplitude dependencies, and dynamic aperture are determined inclusive of full nonlinear fields and kinematics to arbitrary order. Various methods of describing complex fields and components are now supported including representation in radius-dependent Fourier modes, complex magnet edge contours, as well as the capability to interject calculated or measured 3D field data from a magnet design code or actual components, respectively. These new advanced tools fulfil a critical need in advanced accelerator design.

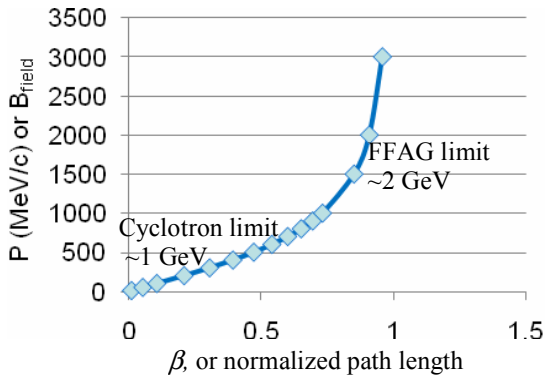

Figure 3: Momentum dependence (∝ <B> field) on velocity (or path length) to maintain isochronous condition.

High-energy Isochronous FFAG Example

The concept of isochronous orbits has been tested on a preliminary 0.25-1 GeV nonscaling FFAG designed using the new methodologies and optimizers described above.. Two options are available to extend this initial effort to a complete accelerator system: a) a two-ring system, both isochronous, with the lower energy one H^- or b) a single ring with a high-order field profile which reaches 5T at extraction to increase compactness and energy range. Use of H^- in the lower energy ring permits CW injection into the higher-energy ring through charge-changing (stripping) methods.

The design is initiated using sophisticated scripts with approximate starting machine parameters then imported into the advanced accelerator simulation code of COSY INFINITY. The ring layout and 3D field profile is given in Figure 4 and Table I gives general parameters with tracking results in Figure 5. Figure 6 shows corresponding results achieved by Craddock, et.al. [13] using the cyclotron COSY. The level of isochronous behaviour is ±3% in this preliminary design.

Table 1: General Parameters of an initial 0. 250 – 1 GeV non-scaling, isochronous FFAG lattice design.

Parameter	***250 MeV***	***585 MeV***	***1000 MeV***
Avg. Rad. (m)	3.419	4.307	5.030
Cell ν_x/ ν_y Ring ν_x/ ν_y (2π rad)	0.380/ 0.237 1.520/ 0.948	0.400/ 0.149 1.600/ 0.596	0.383/ 0.242 1.532/ 0.968
Field F/ D (T)	1.62/ -0.14	2.06/ -0.31	2.35/ -0.42
Mag. Length F D (m)	1.17/ 0.38	1.59/ 0.79	1.94/ 1.14

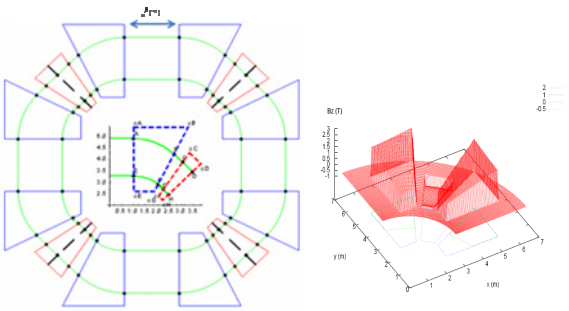

Figure 4: Ring layout and 3D field profile from COSY.

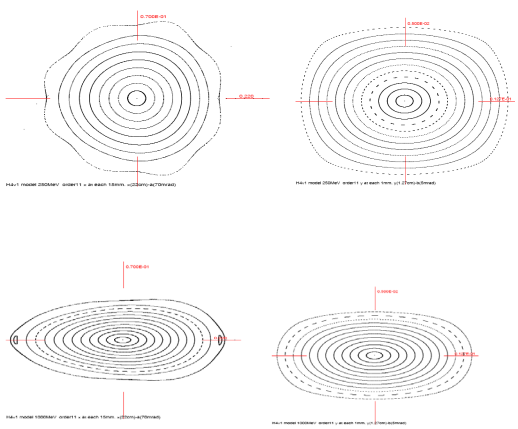

Figure 5: Tracking profiles at injection (top) and extraction (right) in horiz. (left, 1.5 mm steps) and vert. (right, 1mm steps)

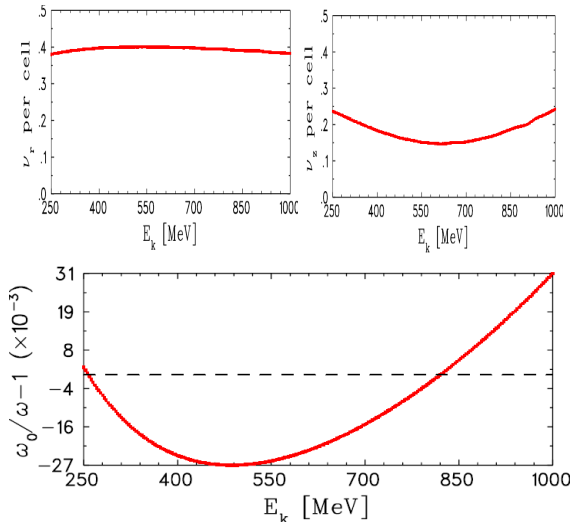

Figure 6: Results using the cyclotron code CYCLOPs {13].

REFERENCES

[1] M. Berz and K. Makino. COSY INFINITY Version 9.0 beam physics manual. Technical Report MSUHEP-060804, Department of Physics and Astronomy, Michigan State University, East Lansing, MI 48824, 2006. See also http://cosyinfinity.org.

[2] T. Ohkawa "FFAG Electron Cyclotron" Phys. Rev. 100, 1247 (1955).

[3] A.A. Kolomenskij. "A symmetric circular phasotron with oppositely directed beams" Soviet Physics, JETP, 6, p. 231-3, 1958. English version of 1957 paper in Russian.

[4] C. Prior, Editor ICFA Beam Dynamics Newsletter #43, August 2007, see http://www-bd-fnal.gov\icfabd\Newsletter43.pdf .

[5] H.S. Synder, private communication.

[6] K.R. Symon, D.W. Kerst, L.W. Jones, L.J. Laslett, and K.M. Terwilliger. Fixed-Field Alternating-Gradient Particle Accelerators. Phys. Rev. 103, pp. 1837-1859, Sept. 15, 1956.

[7] C. Johnstone, et al., "Fixed Field Circular Accelerator Designs", PAC'99, New York, P. 3068.

[8] C. Johnstone, et.al., ICFA Beam Dynamics Newsletter No. 43, July, 2007, http://www-bd.fnal.gov/icfabd/Newsletter43.pdf, pp.125-132. C. Johnstone, et. al., *Proceedings of the 2007 Particle Accelerator Conference, Albuquerque, NM, June 25-29, 2007,* pp. 2951. C. Johnstone, et. al, *Proceedings of the 2006 European Particle Accelerator Conference, Edinburgh, UK June 26-30, 2006,* pp. 2290-2292.

[9] S. Machida, Proc. U.S. Particle Accelerator Conference PAC07, Albuquerque NM, 2007.

[10] S. Smith, et. al. see these proceedings.

[11] M. Craddock, et. al., see these proceedings.

CYCLOTRON AND FFAG STUDIES USING CYCLOTRON CODES

M.K. Craddock*, University of British Columbia and TRIUMF#,
Y.-N. Rao, TRIUMF, Vancouver, B.C., Canada

Abstract

This paper describes the use of cyclotron codes to study the beam dynamics of both high-energy isochronous cyclotrons using AG focusing and non-scaling (NS) FFAGs. The equilibrium orbit code CYCLOPS determines orbits, tunes and period at fixed energies, while the general orbit code GOBLIN tracks a representative bunch of particles through the acceleration process. The results for radial-sector cyclotrons show that the use of negative valley fields allows axial focusing to be maintained, and hence intense cw beams to be accelerated, to energies >5 GeV. The results for FFAGs confirm those obtained with lumped-element codes, and suggest that cyclotron codes will prove to be important tools for evaluating the measured fields of FFAG magnets.

INTRODUCTION

FFAGs are members of the fixed-magnetic-field or cyclotron family [1] and may be thought of simply as ring synchrocyclotrons with sectored magnets providing AG focusing. Nevertheless, cyclotrons and FFAGs have been developed by two different communities, which have sometimes taken different approaches in their work. The studies described here bridge this gap to some extent by applying orbit codes developed for isochronous cyclotrons to FFAGs, and some FFAG ideas to cyclotrons.

In recent years FFAG designs have generally been developed using synchrotron lattice codes – or adaptations of them – perhaps because their designers have mostly come from a synchrotron background. But synchrotron codes are poorly adapted for use in accelerators with fixed magnetic fields, where the central orbit is a spiral rather than a closed ring, and the magnetic field must be characterized over a wide radial range. Special arrangements must therefore be made to deal with momentum-dependent effects accurately.

Here, we report studies made with the cyclotron orbit code CYCLOPS [2], which tracks particles through magnetic fields specified on a polar grid and determines the equilibrium orbits (E.O.) at each energy and their optical properties. This has the advantages of:

- being designed for multi-sector machines with wide aperture magnets;
- allowing simultaneous computation of orbit properties at all energies;
- having the capability of tracking through measured magnetic fields.

In our initial studies [3, 4] we found good agreement with the orbit parameters determined by J.S. Berg [5] for his F0D0-2 10-20 GeV muon FFAG, and by Johnstone and Koscielniak [6] for their "tune-stabilized" FFAG for cancer therapy with 18-400 MeV/u carbon ions. (Both are of "linear non-scaling" or "LNS" design, where the magnets have constant field gradients.) But in the latter case, non-radial hard magnet edges proved tricky to model with a polar grid, even with a very fine mesh, leading to noisy results. To eliminate the noise, we smoothed the field's hard edges by introducing a sinusoidal field variation – an approximate but effective procedure. A variation extending over 4 grid spacings proved sufficient.

We report studies of three very different FFAG lattices and some cyclotrons. In one case CYCLOPS's sister code GOBLIN [7] has also been used to study accelerated orbits.

ISOCHRONOUS MUON FFAG

Rees [8] has proposed an isochronous radial-sector FFAG design (IFFAG) for accelerating muons from 8 to 20 GeV. This employs a novel five-magnet "pumplet" 0doFoDoFod0 lattice cell (from the Welsh word pump, pronounced pimp, for five), where the d magnets (and Fs at low energy) are reverse bending, and the d, F and D magnets each have special field profiles *B(r)*. With long drift spaces between the d magnets, and 123 cells, the circumference is 1255 m.

Méot *et* al. [9] have used the ray-tracing code ZGOUBI (originally developed for the study and tuning of mass spectrometers and beam lines.) to follow muons through a simulated field grid and confirm the orbit properties Rees predicts: good isochronism, and tunes that rise gently with energy, though ν_z exhibits some deviations (Figure 1). To achieve isochronism and vertical focusing at such high energies is not possible in regular FFAGs or isochronous cyclotrons with only two magnets per cell. By using more magnets, Rees gains additional free parameters.

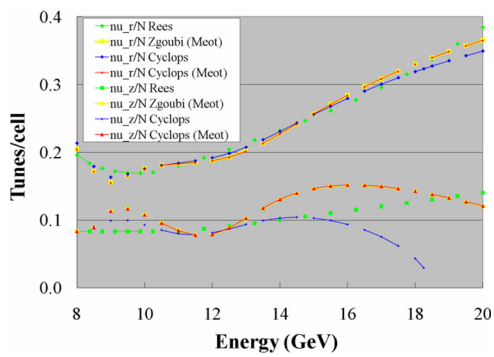

Figure 1: Betatron tunes in the isochronous IFFAG, as computed by Rees, Méot and CYCLOPS.

With CYCLOPS, sinusoidal edges were again needed to suppress noise. The tunes initially obtained [4] agreed

*Work supported by the National Sciences and Engineering Research Council of Canada through grant SRO 328338-05.
#TRIUMF receives federal funding under a contribution agreement through the National Research Council of Canada.

moderately well with those published by Rees and Méot, though the values for ν_z diverged above 15 GeV. Subsequently we learnt that the latter's studies were made after some small adjustments in magnet position and field profile. With these adjustments included, the CYCLOPS results are almost identical to those of ZGOUBI (Figure 1).

REVERSE-BEND CYCLOTRONS

In the past, designs have been presented for isochronous ring cyclotrons to accelerate protons from 0.5 to 3.5 GeV and from 3.5 to 10 or 15 GeV [9-11], to provide cw, and therefore high-intensity, beams at these energies. The high spiral angles ε needed, however, lead to various practical problems: strong distorting forces on the magnet coils (particularly if these are superconducting), restricted space for rf cavities and injection and extraction equipment, and strong radial kicks during acceleration.

In view of these difficulties (and of Rees's intriguing results), it seemed interesting to explore how far the energies of radial-sector cyclotrons could be raised by using reverse-bend magnets to increase the flutter. This being an exploratory study, we made the simplest possible assumptions: N radial sectors, hard-edge magnets, no drift spaces, and equal but opposite hill and valley fields:

$$B_h = -B_v = \gamma B_0$$

To achieve optimum flutter, the field strength must of course be constant along the scalloped orbits – not along a circle. For maximum magnetic field B_m = 5 T, N = 15 sectors, and various values of the hill fraction h and "cyclotron radius" R_c, the tunes computed from a lumped-element model are shown in Figure 2 (in agreement with a CYCLOPS run for h = 0.60). The strong AG focusing pushes both ν_r and ν_z to the half-integer stopband $N/2$ = 7.5 at high energies – by 2.4 GeV for h = 0.6. This can be mitigated by increasing the width of the hills, h = 0.65 giving stable orbits up to 3 GeV with R_c = 6.5 m.

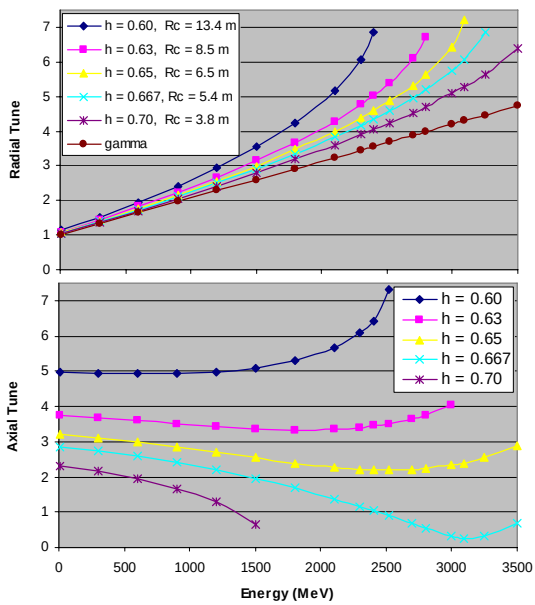

Figure 2: Tunes in a reverse-bend cyclotron with constant fields on orbit (N = 15, h and R_c as shown).

A more powerful way to reach higher energies is to increase the number of sectors. With N = 30 and the original h = 0.6 the ν_r = 15 resonance is raised above 5.5 GeV, with R_c = 14.9 m. The tunes computed by CYCLOPS are shown in Figure 3. Note the increasing deviation of ν_r and ν_z from the approximate formulae as the small-angle approximations for phase advance become increasingly invalid.

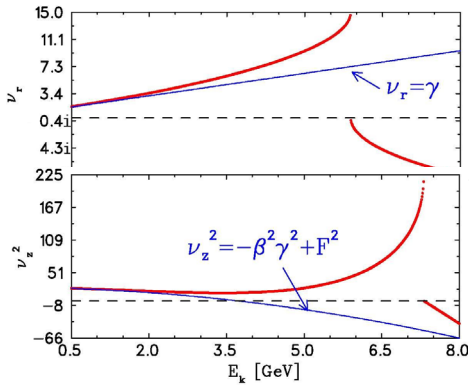

Figure 3: Tunes in a reverse-bend cyclotron with constant fields on orbit (N = 30, h = 0.6, R_c = 14.9 m).

PROTON FFAG FOR ADSR

C. Johnstone [11] has proposed a 2-stage proton FFAG, operating at fixed frequency, to drive a sub-critical reactor. We have studied the second (250-1000 MeV) stage, softening the hard-edge field minimally with an Enge function. The CYCLOPS results agree well with those from COSY, and are more extensive. (Figure 4).

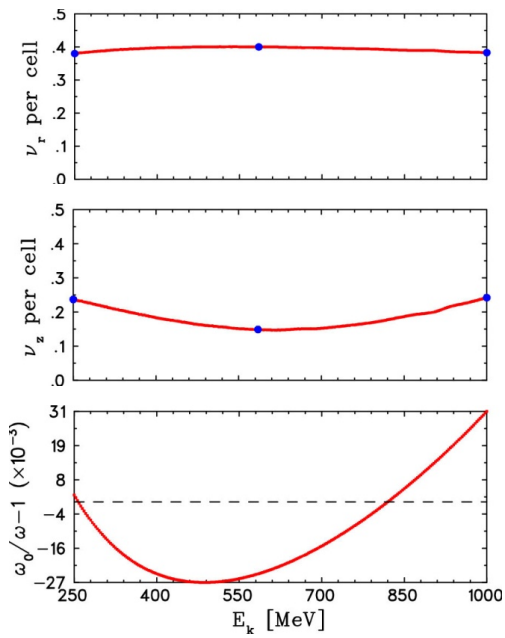

Figure 4: Betatron tunes and orbit time variation in the 250-1000 MeV FFAG for ADSR (•••• CYCLOPS, • COSY).

ELECTRON MODEL FFAG "EMMA"

EMMA [12] is a 10-20 MeV model of a 10-20 GeV muon LNS-FFAG for a neutrino factory, and is currently being commissioned at Daresbury. The lattice consists of 42

doublet cells, where the offset quadrupoles provide both bending and a linear field gradient.

CYCLOPS has been run both on the design "Baseline" hard-edge field [13], and on the measured combined field of the two quadrupole magnets. The results are shown in Figure 5 along with those of Giboudot [14] using other codes and Berg for the Baseline field. Agreement is good for the horizontal tune but less so for the vertical. In the case of flight time only relative values are plotted, so the vertical positions of the curves are of no significance. But there are real differences in the estimates for the energy of the minimum, for reasons unknown.

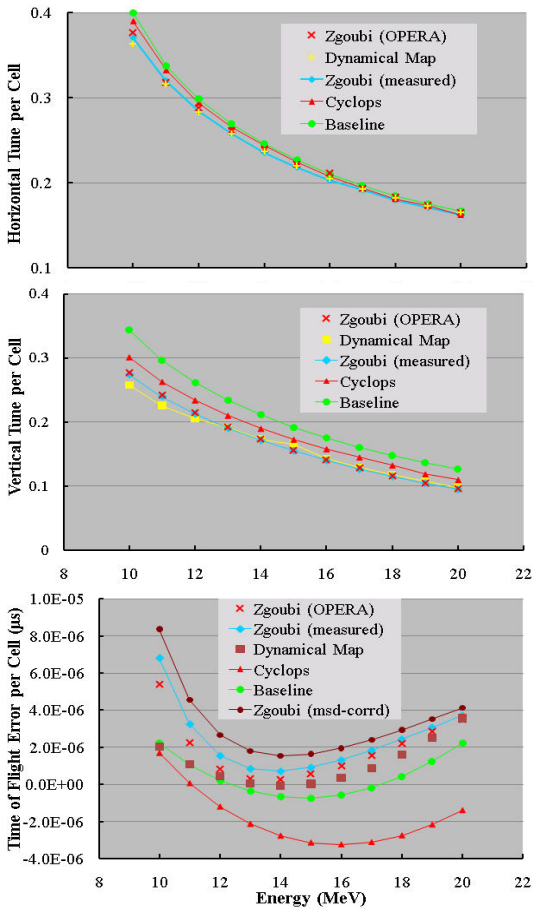

Figure 5: Tunes and time of flight error per cell in the measured EMMA field, as determined by various codes.

Accelerated Orbits

We have also run accelerated orbits in both the Baseline and measured fields using the GOBLIN code. A 4.3π eV-μs electron bunch was tracked over 5 turns through 21 evenly spaced 89-kV cavities. The initial phase was chosen midway between the two cusp trajectories (calculated by integrating the time-of-flight errors from CYCLOPS). Fig. 6 shows snapshots taken after passage through 0, 20, 41, 62, 83, 104 and 125 cavities. For the Baseline field the two upper plots show development of the bunch for radial emittances ε_x = 250π and 1400π μm, similar to that presented by Méot [15]. For the measured field (bottom plot) the bunch distortion is greater and the beam gains less energy.

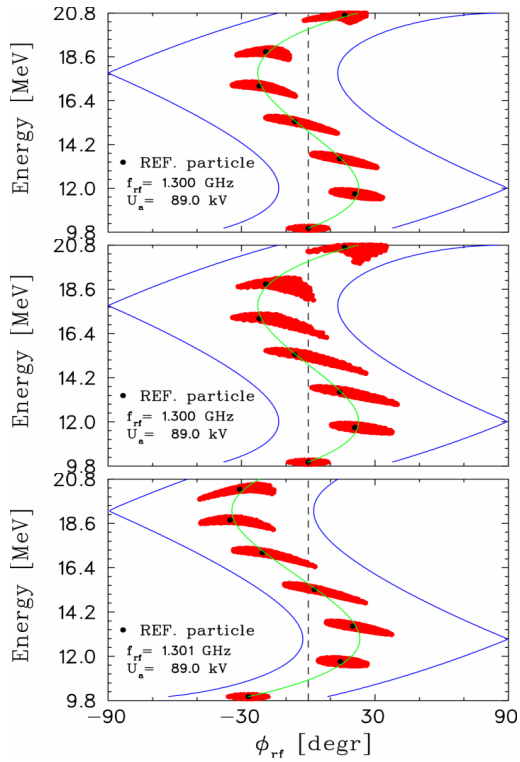

Figure 6: Energy-phase plots: (top) Baseline field, ε_x = 250π μm; (middle) Baseline field, ε_x = 1400π μm; (bottom) measured field, ε_x = 250π μm.

ACKNOWLEDGEMENTS

We are indebted to Drs. J.S. Berg, Y. Giboudot, C. Johnstone, E. Keil, S. Machida, F. Méot, and G.H. Rees for kindly making their data available to us.

REFERENCES

[1] E.M. McMillan, Particle Accelerators, in Experimental Nuclear Physics, III, 639-786 (Wiley, 1959)
[2] M.M. Gordon, Part. Accel. 16, 39 (1984)
[3] M.K.Craddock, Y.-N.Rao, Cyclotrons'07, 370 (2007)
[4] M.K.Craddock,.Y.-N.Rao, PAC'09,.FR5REP114 (2009)
[5] J.S. Berg, FFAG Workshop, BNL, October 2003, http://www.cap.bnl.gov/mumu/conf/ffag-031013/Berg3.pdf
[6] C. Johnstone, S. Koscielniak, PAC'07, 2951 (2007)
[7] M.M. Gordon, T.A. Welton, ORNL-2765 (1959)
[8] G.H. Rees, FFAG04 Workshop, KEK (2004) http://hadron.kek.jp/FFAG/FFAG04_HP/plenary/
[9] F. Lemuet, F. Méot, G. Rees, PAC'05, 2693 (2005)
[10] K. Symon, D.Kerst, et al., Phys. Rev. 103, 1837 (1956)
[11] C. Johnstone, FFAG09 Workshop, Fermilab (2009). http://conferences.fnal.gov/ffag09/
[12] T.R. Edgecock, THXMH01, these proceedings
[13] J.S. Berg, NIM, A596, 276 (2008)
[14] Y. Giboudot, FFAG09 Workshop, Fermilab (2009)
[15] F. Méot, EPAC06, 2080 (2006)

REVIEW ON CYCLOTRONS FOR CANCER THERAPY

Yves Jongen#, IBA, Louvain-la-Neuve, Belgium

Abstract

The science and technology of proton and carbon therapy was initially developed in national and university laboratories. The first hospital based proton therapy facility was built at Loma Linda University with the help from Fermilab. After this initial phase, and starting with the tender for the proton therapy system at MGH, many proton and carbon beam facilities have been ordered from industry and built. Industrially made proton and carbon therapy facilities represent today the vast majority of the installed base.

INTRODUCTION: THE HISTORY OF PROTON THERAPY SYSTEMS

Robert Wilson was the first to point out the possibilities offered by the Bragg peak in the field of the radiotherapy of cancer in a paper published in 1946 (1).

A few years later, tests were conducted at Lawrence Berkeley Laboratory to verify Bob Wilson's predictions, and in 1954 protons started to be used on patients in Berkeley.

Similarly, proton treatments were started in Uppsala in Sweden in 1957.

Harvard cyclotron Laboratory (HCL) had a 160 MeV synchrocyclotron. In 1961, Dr. Ray Kjellberg started to use the proton beams at HCL to do radio-surgery of brain malformations. Then, in 1972, Dr. Herman Suit, from Massachusetts General Hospital (MGH), helped by Michael Goitein, started to apply the proton beams of HCL to do fractionated radiotherapy of cancer. A lot of what is today considered as standard proton therapy technology was developed between 1970 and 1990 by Herman Suit, Michael Goitein, and a team of talented physicists at HCL: Andy Koehler, Bernie Gottschalk, and later Miles Wagner, Skip Rosenthal and Ken Gall.

But as successful as HCL was in proton therapy, it quickly became clear that a proton therapy facility located directly within the hospital campus was a much better option. In 1983, the institutions doing or planning to do proton therapy got together to form an informal group named the Proton Therapy Cooperative Group or PTCoG.

One of the first tasks of the PTCoG was to reach a consensus on a set of desirable specifications for an in hospital proton therapy facility. These specifications are still today the bible of those who plan to design a proton therapy system.

Unexpectedly, the first group which succeeded to raise the funds needed to build the first hospital based PT facility was not MGH or Berkeley, but the team led by Dr. James (Jim) Slater at Loma Linda University Medical Center (LLUMC) in California. Jim Slater was a friend of Herman Suit, and they had worked together as interns at MDACC. LLUMC requested the help of the Fermi National Laboratory to design and build the required proton accelerator. The accelerator was designed and built by a group of experienced accelerator physicists from Fermilab and, not surprisingly, the accelerator technology selected by this group was a small, compact synchrotron. The gantry design and construction was subcontracted to SAIC. A private company initially named today Optivus, was established in Loma Linda, CA by Jim Slater to maintain and develop the system at LLUMC. The company is led by Jon Slater, the son of James Slater. Optivus is trying to sell a PT system that essentially is based on the design of the LLUMC system. Although Optivus is probably the oldest company in the PT field, it is the only one that has not designed nor built a PT system. Some members of the company, however, were associated with the development and testing of the LLUMC PT system, first at Fermilab and then at the Loma Linda site.

In the mid-1970s at the Catholic University of Louvain (UCL) in Louvain-la-Neuve, Belgium, Professor Andre Wambersie and Yves Jongen developed a close collaboration to build a fast neutron therapy facility, which was used to treat a large number of patients. In 1986, Jongen left UCL to start the Belgium-based company Ion Beam Applications s.a. (IBA). Wambersie met Jongen in 1989 and suggested that IBA start the design of a cyclotron-based proton therapy facility. The following year, IBA presented the initial design of its PT system based on an isochronous cyclotron and compact, scanning-only, gantries at the Particle Therapy Co-Operative Group (PTCOG) XII meeting in Loma Linda.

In 1991, IBA and Sumitomo Heavy Industries (SHI) in Japan signed a 10-year collaboration agreement to jointly develop a PT system based on the IBA concept. Though this collaboration ended in 2001, it explains why the PT systems developed by IBA and SHI share many common features.

The first official tender to acquire a commercially built PT facility was launched by the Massachusetts General Hospital (MGH) in 1992. Several companies responded, but the competition finally narrowed to three groups: Maxwell-Brobeck, in association with Varian, offered a synchrotron-based system; Siemens offered two versions: one based on a synchrotron and another based on a superconducting isochronous cyclotron (the isochronous cyclotron was designed by Pierre Mandrillon from CERN and CAL, Nice); and IBA, in association with General Atomics, offered a system based on a resistive isochronous cyclotron. The tender process took a long time, but finally the contract was awarded to the IBA-GA team in April 1994.

* yves.jongen@iba-group.com

The development of the MGH PT facility was very challenging. The specifications were new and demanding and the budget available to MGH was only $20 million for a two-gantry facility. At the time of the contract, an experienced observer drily commented: "Unfortunately, this tender will probably mean the death of three good accelerator companies. Perhaps the two companies who did not win the contract, but certainly the company who got it."

He was partly right, and came close to being entirely right. Shortly after the MGH contract was signed, the Brobeck division of Maxwell was disbanded and the special project group of Siemens was sold to its management. The group restarted business under the name of ACCEL Instruments and later returned to proton therapy.

IBA also met serious problems in the development of the MGH PT system. Although the new cyclotron, the beam lines and the isocentric gantries were developed and delivered in time and within budget, IBA had badly underestimated the effort and the methodology needed to develop the complex software needed to control a PT facility. The project was seriously delayed and the first patient finally was treated at the Northeast Proton Therapy Center in Boston in November 2001. IBA's financial loss on the MGH project was huge and might have killed the company if IBA had not had other, more profitable, activities.

In 1995, the National Cancer Center in Japan launched a tender for the construction of a PT center in Kashiwa. The contract was signed the following year with SHI, who built the system in close collaboration with IBA. Knowing the difficulties IBA had with developing software for MGH's PT system, SHI selected a simpler and more pragmatic approach in the design of the control system, which proved robust and effective but limited in its functionalities. As a result, NCC Kashiwa's PT center treated its first patient in November 1998, three years ahead of MGH.

After 2000, the commercial activity and the number of competitors in the field of proton therapy began to increase dramatically. From 1994 to 2010, 37 proton therapy facilities, representing a total of 96 treatment rooms were contracted to industrial companies (fig. 1). In Japan, the government funded the construction of several PT facilities. Hitachi and Mitsubishi Electric introduced synchrotron-based PT facilities. In Germany, ACCEL Instruments teamed up with Pr. Henry Blosser to propose a PT system based on a 250 MeV superconducting isochronous cyclotron.

Over the last five years, radically new concepts have appeared on the PT market. The company Still River Systems (SRS) was founded in Boston by a group of medical physicists who had shared the proton therapy experience of HCL and MGH. They started the company to develop and commercialize a single-room PT system based on a very high magnetic field superconducting synchrocyclotron mounted on a gantry that rotates around the patient. PROTOM International Inc., based in Flower Mound, TX was founded to commercialize a very simple and inexpensive synchrotron developed in Russia by Professor V. Balakin. At the Lawrence Livermore National Laboratory, the concept of the Dielectric Wall Accelerator was developed by Georg Caporaso and his team and will be commercialized by Compact Particle Acceleration Corporation, a spin-out of Tomotherapy Inc.

Finally, several research institutions in the world work actively on the acceleration of protons by laser beams.

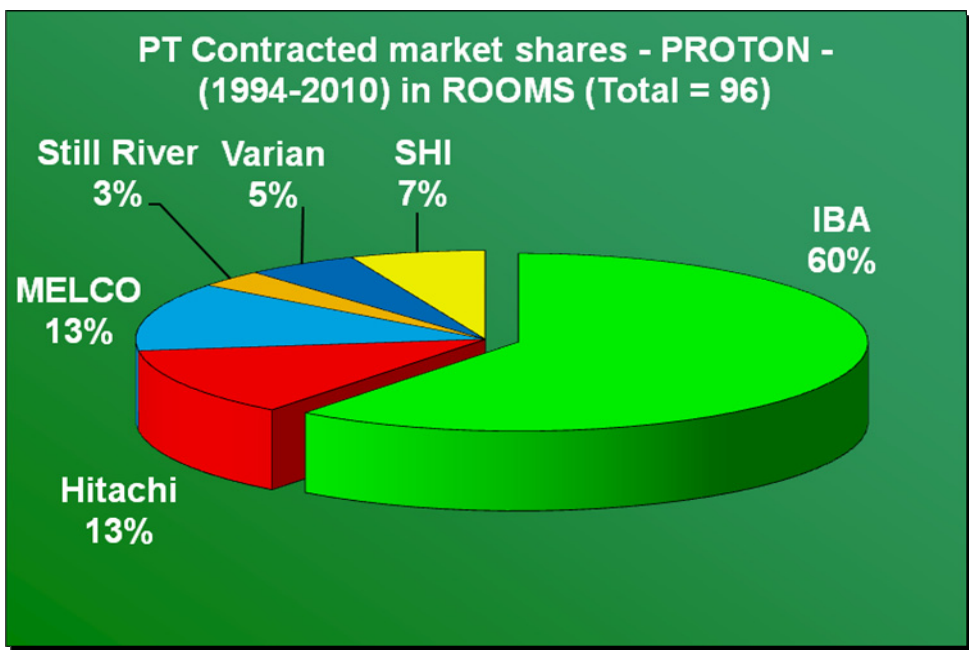

Figure 1: Commercial Proton Therapy Systems Sales - market shares - (1994-2010) in ROOMS

COMMERCIAL PROTON BEAM THERAPY SYSTEMS

The IBA Proteus® 235 Proton Therapy System

IBA's Proteus 235 is without doubt the system which enjoyed the largest commercial success so far. The cyclotron uses a fixed field resistive magnet, a fixed frequency RF system, and accelerates protons to a fixed energy of 230 MeV . The cyclotron's magnet (Fig. 2) is 4.34 meters in diameter, 2.1 meters high, weighs 220 tons, and the coils power is 175 kW. The RF system uses 2 30° dees located in opposite valleys and connected at the center. The dees operate at 106 MHz, on the 4th harmonic of the protons' orbital frequency. The beam extraction is made by an ESD located in one of the valleys without RF cavities. The beam extracted at 230 MeV is then adjusted to the energy required for the treatment by the use of a variable energy degrader made of graphite, followed by a magnetic analyzer to select the required energy width. The system formed by the degrader and the magnetic analyzer is named the Energy Selection System or ESS

Figure 2. IBA 230 MeV resistive cyclotron for proton therapy

Figure 3. Gantry Treatment Room of the IBA Proteus Proton Therapy System

The energy of the beam extracted from the cyclotron is 230 MeV and is fixed. The beam extracted from the cyclotron is then focused into a small spot into a variable energy degrader made of graphite, followed by a magnetic analyzer. This energy selection system allows precise tuning of the continuous proton beam, from 60 MeV to 230 MeV, in under a second.

Most often, proton therapy is delivered in rooms equipped with isocentric gantries. The IBA isocentric gantry has 370 degrees of rotation with 0.4 mm radius precision, and a gantry rolling floor. Each gantry room includes a patient positioning system featuring a robot-controlled patient couch. The robot allows three orthogonal linear motions, rotation around the vertical axis, and ±3 degrees of pitch and rolling of the patient couch. 17 of the 35 commercial PT systems sold to date were designed and built by IBA. The 9 systems named in bold are already treating patients. The others are under construction or installation.

- **The Francis H. Burr Proton Therapy Center** at Massachusetts General Hospital, Boston, MA
- **Midwest Proton Radiotherapy Institute**, Bloomington, IN (Gantries only on an existing cyclotron)
- **Wanjie Proton Therapy Center**, Zibo, China
- **University of Florida Proton Therapy Institute**, Jacksonville, FL
- **National Cancer Center**, Ilsan, Korea
- **Roberts Proton Therapy Center**, University of Pennsylvania Health System, Philadelphia, PA
- **Procure Proton Therapy Center**, Oklahoma City, OK
- **Centre de Protonthérapie de l'Institut Curie**, Orsay, France
- Westdeutsches Protontherapiezentrum, Essen, Germany
- **Hampton University Proton Therapy Institute**, Hampton, VA
- Central DuPage Hospital (a Procure Center), Warrenville, IL
- ATreP Proton Therapy Center , Trento, Italy
- PTC Prag, University Hospital Bulovka, Czech Republic
- Somerset Procure Proton Therapy Center, Somerset, NJ
- Seattle Procure Proton Therapy Center, Seattle, WA
- Krakow proton therapy center (Krakow, Poland)

Sumitomo Proton Therapy System

The proton therapy system proposed by Sumitomo Heavy Industries (SHI) of Japan is very similar to the system proposed by IBA because initially the two companies shared a common development. However, since 2001, the two systems have undergone separate developments.

SHI has only one system currently treating patients, built in collaboration with IBA, but it was the first commercial system to do so. Its proton therapy facility at the National Cancer Center East, in Kashiwa, Japan has been treating patients since 1998. The company reports that firm contracts have been signed for three systems, one in Taiwan, one in the United States and a compact system in Japan. Although construction of the Taiwan system is underway, installation has not yet begun.

Hitachi PROBEAT Proton Therapy System

Hitachi proposes a proton therapy system based on a synchrotron, which has been sold to four institutions. The first one, at the Proton Medical Research Center (PMRC) at the University of Tsukuba in Japan, began treating patients in 2001. The second, at the University of Texas M.D. Anderson Cancer Center in Houston, went into operation in 2006. These systems are based on a slow-cycle synchrotron that provides 70-250 MeV protons. Hitachi proton therapy systems have also been sold to the Wakasaka Wan Energy Research Center in the Fukui prefecture in Japan, and more recently at the Nagoya City proton Center, in Aichi prefecture, Japan.

Mitsubishi Proton Beam Treatment System

Mitsubishi Electric is marketing a PT system powered by a synchrotron that delivers 70 – 250 MeV protons to up to six treatment rooms.

Two of the PT systems are now in clinical use, one at the Shizuoka Cancer Center and the other at the Southern Tohoku Proton Therapy Cancer Center in Fukushima, Japan. Two additional systems are under construction at the Fukui Prefecture Proton Therapy Center and at the Medipolis Medical Research Institute, in Kagoshima, Japan

Varian Proton Therapy System

Varian's proton therapy system is based on a isochronous superconducting cyclotron, providing 250 MeV. Unlike the IBA and SHI isochronous cyclotrons, the ACCEL-Varian cyclotron is equipped with 4 RF cavities to maximize the energy gain per turn and the extraction efficiency. Here again, a graphite variable energy degrader is used to adjust the proton energy between 70 and 250 MeV. The 3-meter diameter, 1.6 meter-high cyclotron weighs 90 Tons

In 2007, Varian bought ACCEL, who designed and was in the process of building the PT system at the Rinecker Proton Therapy Center in Munich, Germany. Varian took over the project, which began treating patients in March 2009. So far, no other sales have been officially confirmed by Varian, but several cyclotrons are under construction.

Still River Systems Monarch 250 TM Proton Therapy System

Still River Systems (SRS) has developed a very original concept for a single room proton therapy system. The SRS system uses a very high field synchrocyclotron mounted on a gantry and rotating around the patient (Fig. 6). The very high field synchrocyclotron, initially developed by Tim Antaya at MIT has a central field of 9 T

and uses coils made of Nb-Sn superconductor. To support the large mechanical forces encountered in this magnet, the coils are placed inside a stainless steel bobbin and are conduction cooled at 4°K by cryocoolers. The SRS magnet does not use liquid helium: a dry cryostat is indeed very desirable for a gantry-mounted magnet.

The beam of the SRS cyclotron is extracted at 250 MeV, in the direction of the patient. Range shifting is done at the exit of the cyclotron.

The Monarch 250 system includes a gantry that rotates 190 degrees and a treatment couch that turns 270 degrees so all clinically required beam orientations can be achieved.

The development of the very high field cyclotron magnet took quite longer than expected, but finally the prototype of the Monarch 250 has produced its first extracted beam in June of this year, and should be delivered to the first customer end of 2010 or early 2011.

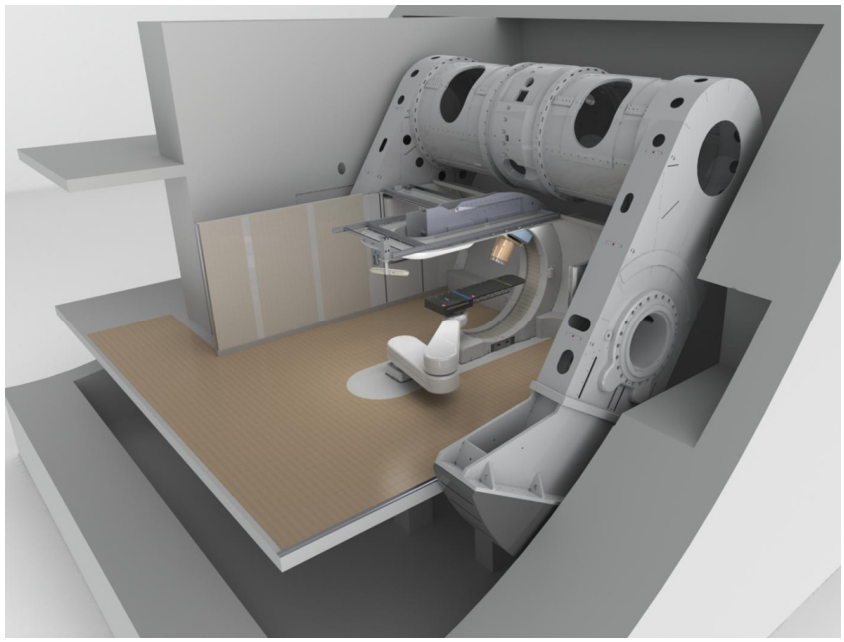

Figure 6. Still River Systems Monarch 250 Proton Therapy System

COMMERCIAL CARBON BEAM THERAPY SYSTEMS

Synchrotron Based Carbon Therapy Systems

The development of carbon beam therapy started in national laboratories. The first treatments of patients with heavier ions were made at the LBNL, at the Bevalac facility in Berkeley in the 1980's. After LBNL, heavy ion therapy was developed in Chiba (Japan) at the National Institute for Radiological Sciences (NIRS), on the HIMAC accelerator system. It can be said that the bases of modern hadron therapy were really developed at NIRS. Among other findings, NIRS demonstrated that carbon ions were probably the ions offering the best compromise in the conflicting demands of hadron therapy of cancer.

After NIRS, the scientists at GSI in Darmstadt started to study the radiobiology of carbon ions, and soon after started to build at GSI a facility for the clinical research of the potential advantages of carbon beam therapy.

The work at GSI brought a lot of new knowledge and understanding in the field of the interaction between carbon beams and living tissues. The group of Pr. Gerhard Kraft at GSI developed the now famous "local effect model" which is today the standard reference in calculating the relative biological efficiency of hadron beams. In the field of technology, the group at GSI was also the first to develop an efficient, fast and safe method to deliver the carbon beam to the patient by spot scanning.

There were limits to the possibility to do clinical research into a facility intended for basic physics research like GSI. So the GSI team, under the leadership of Thomas Haberer, started to develop the design of a more compact, hospital based, carbon therapy facility. This system is based on a large (27 m diameter) carbon synchrotron, able to accelerate carbon ions to 4.8 GeV, or 400 MeV/u. The 4+ carbon ions are produced in an ECR ions source, pre-accelerated by a RFQ, then by a DTL, and injected into the synchrotron after stripping to the 8+ charge state.

The prototype of this facility was built by GSI in collaboration with Siemens in Heidelberg, at the German Cancer Research Center (DKFZ), and started treating patients in 2009.

Siemens Medical Systems acquired the rights of the GSI design, and sold similar carbon therapy facilities in Marburg and in Kiel (Germany) and in Shanghai (China)

In a similar way, NIRS developed the design of a compact, hospital based carbon therapy facility based on a synchrotron. The prototype of this facility is installed in Gunma University (Japan) and started treating patients this year. The Gunma design is now proposed industrially by Japanese industries such as SHI, MELCO or Hitachi.

IBA's C-400 Hadron Therapy System

IBA has designed a compact superconducting isochronous cyclotron for carbon therapy in collaboration with scientists from Dubna, Russia.

The C-400 can accelerate Q/M = 0.5 ions such as hydrogen (as H2+ molecule), helium, lithium-6, boron-10, carbon-12, nitrogen-14, oxygen-16, and neon-20 ions. All ion species will be accelerated to 400 MeV/u except for hydrogen, which will be accelerated in the form of H2+ to achieve the desired Q/M, then split and extracted at 260 MeV/u. Live ion sources for hydrogen, helium, and carbon will be located under the cyclotron, allowing to switch very rapidly from one ion to another. This cyclotron is described more extensively in another paper of this conference presented by Nikolay Morozov (2)

Figure 7. The IBA C-400 cyclotron

CONCLUSIONS

Proton therapy and carbon beam therapy were initially developed in national or university laboratories. The initial experiments were conducted at LBNL. At Harvard, the HCL played a key role in the development of proton therapy technology. In carbon beam therapy, the role of NIRS in Japan was also essential.

After the contract of the MGH facility awarded to IBA in 1994, more than 40 proton and carbon therapy facilities have been ordered from industry. Half of these are built and treat patients. The other half is under construction or being installed.

In 1991, after the development of the first hospital based proton therapy facility at LLUMC, the synchrotron was generally considered the choice accelerator technology for proton therapy.

Then in 1992, IBA came with an efficient cyclotron design. Other manufacturers followed, and the cyclotron technology was finally selected in 75% of the proton therapy facilities built since that time.

Today, in carbon beam therapy, the synchrotron technology has been selected for every facility. But IBA has introduced the design of a compact, superconducting cyclotron for carbon beam therapy. It is possible that, in the future, cyclotrons will be preferred in carbon beam therapy as they are today in proton therapy.

BIBLIOGRAPHY

[1] Robert Wilson "The radiological use of fast protons" (Radiology 1946-47 487-91)

[2] Nikolay Morozov "IBA-JINR 400 MeV/u superconducting cyclotron for hadron therapy" (this conference, paper FRM1CIO03")

IBA-JINR 400 MEV/U SUPERCONDUCTING CYCLOTRON FOR HADRON THERAPY

Y. Jongen, M. Abs, A. Blondin, W. Kleeven, S. Zaremba, D. Vandeplassche, IBA, Belgium
V. Aleksandrov, S. Gursky, O. Karamyshev, G. Karamysheva, N. Kazarinov, S. Kostromin,
N. Morozov, E. Samsonov, G. Shirkov, V. Shevtsov, E. Syresin, A. Tuzikov, JINR, Dubna, Russia

Abstract

The compact superconducting isochronous cyclotron C400 [[1, 2, 3, 4] has been designed by the IBA-JINR collaboration. It will be the first cyclotron in the world capable of delivering protons, carbon and α ions for cancer treatment. The cyclotron construction will start probably this year within the framework of the ARCHADE project [5] (Caen, France). $^{12}C^{6+}$ and $^{4}He^{2+}$ ions will be accelerated to 400 MeV/u and extracted by the electrostatic deflector. H_2^+ ions will be accelerated to the energy of 265MeV/u and extracted by stripping. The magnet yoke has a diameter of 6.6 m; the total weight of the magnet is about 700 t. The designed magnetic fields are 4.5 T and 2.45 T respectively in the hills and in the valleys. Superconducting coils will be enclosed in a cryostat. All other parts and subsystems of the cyclotron will be warm. Three external ion sources will be mounted on the switching magnet on the axial injection line located below the cyclotron.

The main parameters of the cyclotron, its design, the current status of the development work on the cyclotron systems are presented.

INTRODUCTION

Today, cancer is the second highest cause of death in industrial countries. Its treatment still presents a real challenge. Protons and light ions allow depositing the radiation dose more precisely in a cancer tumor, reducing greatly the amount of dose received by healthy tissue surrounding the tumor as compared with electrons. But in addition to the ballistic accuracy of protons, light ion beams, like carbon beams, have an extra advantage in radiation therapy: they have a different biological interaction with cells and are very effective even against some type of cancerous cells which resist usual radiations. That is why in the last years an increasing interest in the particle therapy based on $^{12}C^{6+}$ ions has been seen.

IBA, the world's industrial leader in equipment of the proton therapy centers, and the team of accelerator physicists from JINR have developed a superconducting C400 cyclotron based on the design of the current proton therapy C235 cyclotron.

BASIC CONCEPT OF CYCLOTRON

Most of the operating parameters of the C400 cyclotron are fixed: fixed final kinetic energy, fixed magnetic field and fixed RF system frequency (small main magnetic field and RF frequency changes are necessary to switch between different accelerated ions). The cyclotron is relatively small and cost effective.

The most important parameters of the 400MeV/u superconducting cyclotron are listed in Table 1. The view of the cyclotron is presented in Fig.1.

Table 1: Main parameters of the C400 cyclotron

General properties	
accelerated particles	H_2^+, $^{4}He^{2+}$(α), ($^{6}Li^{3+}$), ($^{10}B^{5+}$), $^{12}C^{6+}$
injection energy	25 keV/Z
final energy of ions, protons	400 MeV/u 265 MeV/u
extraction efficiency	~70 % (by deflector)
number of turns	~2000
Magnetic system	
total weight	700 t
outer diameter	6.6 m
height	3.4 m
pole radius	1.87 m
valley depth	0.6 m
bending limit	K = 1600
hill field	4.5 T
valley field	2.45 T
RF system	
number of cavities	2
operating frequency	75 MHz, 4th harmonic
radial dimension	1.87 m
vertical dimension	1.16 m
dee voltage: center extraction	 80 kV 160 kV

Three external ion sources are mounted on the switching magnet on the axial injection line located below the cyclotron. $^{12}C^{6+}$ ions are produced by a high-performance ECR at current 3 μA, α particles and H_2^+ ions are also produced by a simpler ECR source. All species have a charge to mass *q/m* ratio of 1/2 and all ions

are extracted at the same voltage 25 kV, so the small retuning of the RF system frequency and a very small magnetic field change achieved by different excitation of 2 parts of the main coil are needed to switch from H_2^+ to α or to $^{12}C^{6+}$ ions. The expected time to switch between species will be no longer than two minutes, like the time needed to retune the beam transport line between different treatment rooms.

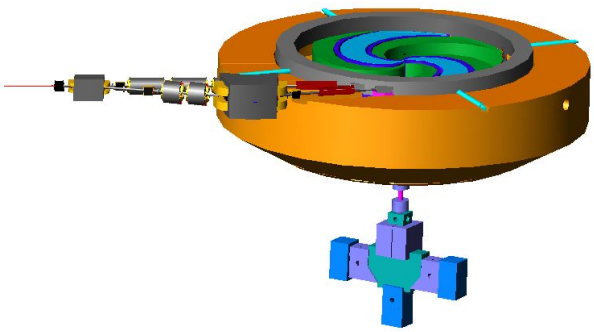

Figure 1: View of the median plane in the C400 superconducting cyclotron

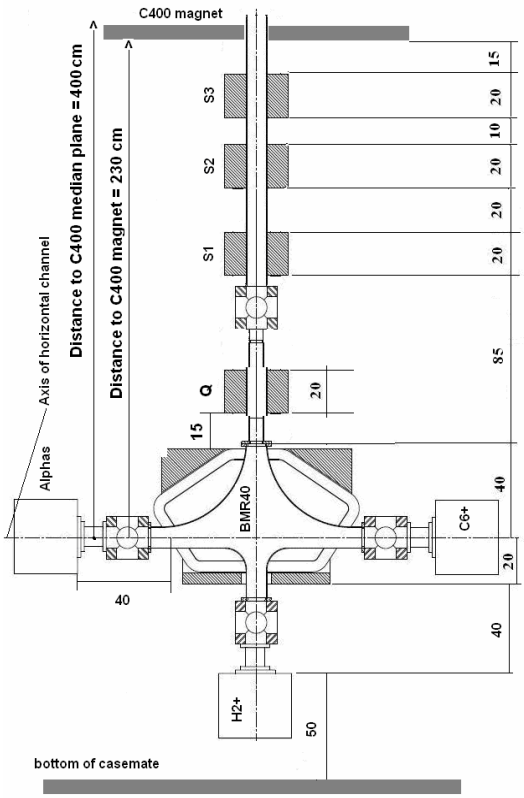

Figure 2: Scheme of the injection beam line

Focusing in the axial injection channel (Fig.2) is provided by three solenoid lenses (S1, S2, S3), the rotational symmetry of the beam is reestablished with the help of the quadrupole Q placed immediately downstream the dipole bending magnet BMR40. This 90º bending magnet has two horizontal and one vertical entrances and the common exit for all ion beams. The bending radius of the BMR40 magnet is 400 mm. The maximum magnetic field is 0.075 T and the gap height is 70 mm. The maximum magnetic field of the solenoids is below 0.3 T, a good field region is 80 mm. The maximum quadrupole lens gradient is below 10 mT/cm.

The main feature of the axial injection system is the presence of the strong stray magnetic field not only in the vertical part of the channel but also in its horizontal part. For this reason, ion sources, the switching magnet and the quadrupole of the axial injection beam line have to be shielded. Beam transport line calculations indicate that for all types of ions the beam diameter at the spiral inflector entrance is smaller than 2 mm.

A model of the dee tip geometry at the cyclotron center with the inflector placed inside the housing was developed (see Fig. 3). Dee tips have the vertical aperture 12 mm in the first turn and 20 mm in the second and further turns. On the first turn the gaps were delimited with pillars reducing the transit time. The azimuthal extension between the centers of the accelerating gaps was chosen to be 45º. The electric field in the inflector was chosen to be 20 kV/cm. Thus, the height (electric radius) of the inflector is 2.5 cm. The gap between the electrodes is 6 mm, and the tilt parameter k′=0.1. To reduce the fringing field effects, the aspect ratio of the electrode width to the gap between electrodes is 2. The electric potential distribution simulation of the central region was performed.

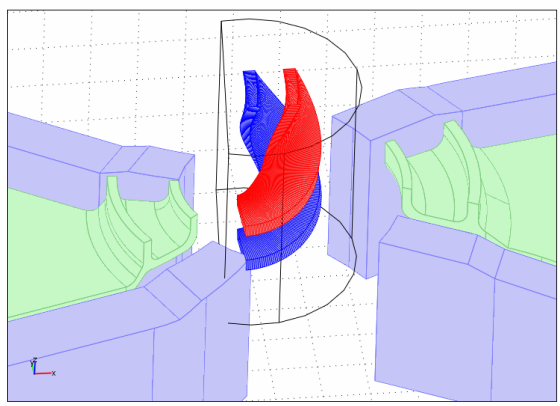

Figure 3: Central region with the spiral inflector model

The magnetic field bump (about 200 G) in the central region does not provide sufficient magnetic axial focusing. The electric axial focusing plays the main role during first turns.

Beam simulations has shown that using two phase selection slits, the injection efficiency is about 12% for ions with amplitudes of radial oscillations smaller than 4 mm. The use of the buncher will increase the beam intensity at least by a factor of two.

The possibility of modulating the beam intensity by changing voltage of inflector electrodes was tested. Particles have been tracked through the inflector with decreasing voltage. It is necessary to decrease voltage by about 12% to lock the beam. Results indicate that this

method of intensity modulation has one disadvantage – radial displacement of the beam – but it is smaller than 1 mm.

MAGNETIC SYSTEM

The simulation and design of the C400 magnetic system was based on its main characteristics: four-fold symmetry and spiral sectors; the deep-valley concept with RF cavities placed in the valleys; the elliptical pole gap is 120 mm at the center decreasing to 12 mm at extraction; magnetic induction inside the yoke is below 2.2 T; the main coil current is 1.2 MA. An elliptical gap between the spiral sectors provides stable beam acceleration up to 10 mm from the pole edge. Keeping the last orbit as close as possible to the pole edge facilitates extraction. The main parameters of the cyclotron magnetic system were optimized by computer simulation using the well known Vector Fields OPERA-3D software package.

The view of the magnet with spiral sectors is given in Fig. 4. The sectors have the following parameters: the initial spiral parameter Nλ=77 cm with increasing spiral angle to the final radius with the parameter Nλ~55 cm; the sector azimuthal length varies from 25º at the cyclotron center to 45º at the sector outer edge; the axial profile is an ellipse with the 60 and 1874-mm semi-axes. At large radii the axial profile of the ellipse is cut by planes at the distance z= ± 6 mm from the median plane.

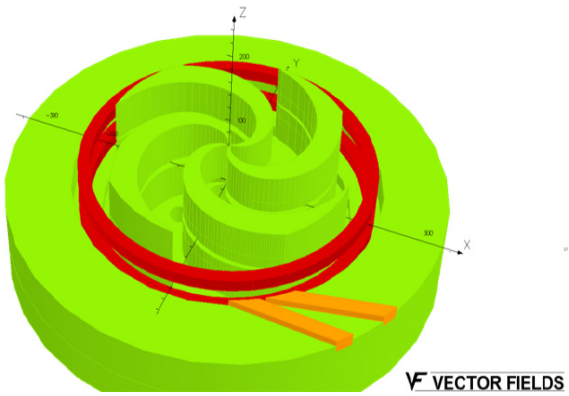

Figure 4: OPERA-3D simulation of the C400 magnetic system

The average magnetic field and amplitudes of the basic number Fourier harmonics as a function of radius are shown in Fig. 5. The required isochronous magnetic field was shaped by profiling the azimuthal length of sectors.The accuracy of the average magnetic field at the shaping simulation is ±10 G in the middle and end regions of the beam acceleration. The optimized sector geometry provides axial betatron oscillation frequency (vertical tune) Q_v~ 0.4 in the extraction region (see Fig. 6) to decrease the vertical beam size and to minimize effects of field imperfections.

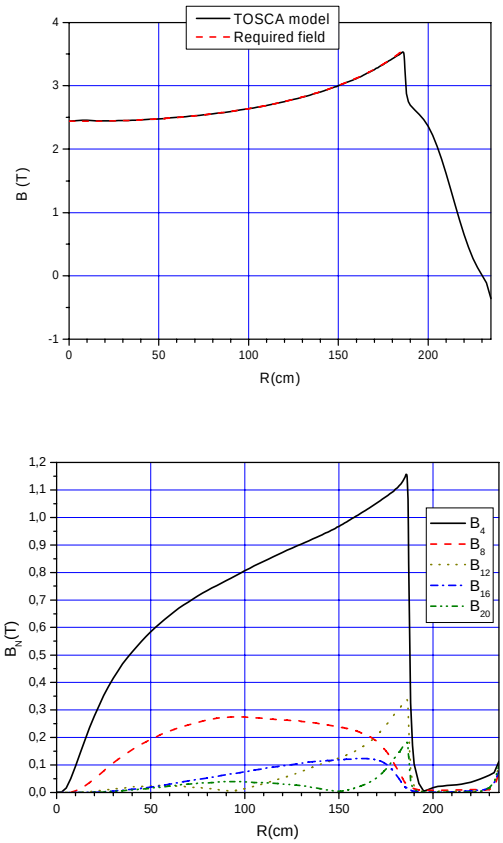

Figure 5: Up: average magnetic field; down: amplitudes of Fourier harmonics of the cyclotron magnetic field as a function of radius

During the magnet simulation the following design goals were achieved:

- Optimization of the magnet sizes
- Avoiding dangerous resonances
- Realization of the vertical tune Q_z ~ 0.4 in the extraction region
- Keeping the optimal value of the spiral angle of the sectors (minimize total sector phase angle change)
- Average magnetic field shaping by variation of the sector azimuth width
- Last orbit kept as close to the pole edge as possible (~10 mm)
- Minimization of iron weight, keeping the stray field at an acceptable level
- Optimal solution for the SC coil design
- Optimal design solution for the trimming of the magnetic field change from carbon to H_2^+ ions :
  a) RF frequency change by 0.6%,
  b) main coil consisting of two parts,
  c) excitation current redistribution in two parts of the main coils by means of additional small current (60 A) power supply.

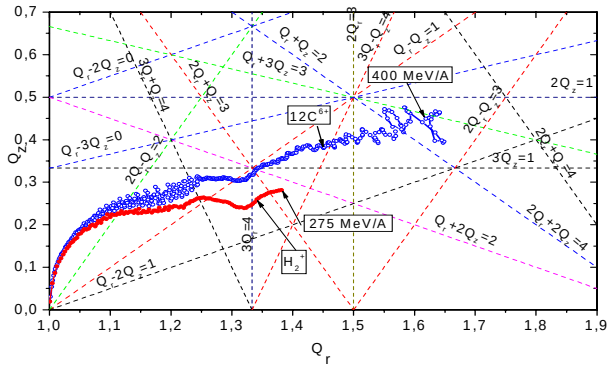

Figure 6: Working diagram of the cyclotron

ACCELERATING SYSTEM

Acceleration of the beam will occur at the fourth harmonic of the orbital frequency, i.e. at 75 MHz, and will be obtained through two normal conducting cavities [6] placed in the opposite valleys.

The geometric model of the double-gap delta cavity housed inside the valley of the magnetic system of the C400 cyclotron was developed in the CST Microwave Studio [7]. The finally chosen geometry is presented in Fig.7. The depth of the valley permits using the cavity with the total height 1160 mm. The vertical aperture of the dee was 20 mm. The accelerating gap width was 6 mm in the center increasing to 80 mm at radius R=750 mm and remaining constant up to the extraction region .

Cavities have a spiral shape complementary to the shape of the sectors. The sector geometry permits azimuthal extension of the cavity (between the middles of the accelerating gaps) equal to 45° up to the radius of 1500 mm then decreasing to 32° in the extraction region. Four stems were inserted with different transversal dimensions in the model. Different positions of the stems were studied to insure increasing voltage along the radius of the accelerating gap, which should range from 80 kV in the central area to 160 kV in the extraction region. It is important to have a high value of the voltage approximately from the radius R=1500 mm before the crossing of the resonance $3Q_r=4$.

Thickness of the dee was 20 mm. The edges of the dees were 10 mm thick and have a rounded form.

Calculations of the created model were performed using the eigenmode JD lossfree solver (Jacobi Division Method) in the CST MICROWAVE STUDIO and the Block LANCZOS solver in ANSYS. The half-structure model of the cavity was used where the vertical symmetry is presented.

Shaping of the radial voltage distribution is obtained by adjustment of stems positions. The variation of the horizontal dimensions of all stems by one percent changes the frequency by about 300 kHz. The value of the voltage along the radius does not change noticeably while the frequency is shifted less than 1 MHz.

Simulations show that the frequencies from both codes are similar when the number of mesh cells is 7 millions for CST and 3 millions for ANSYS:

F_{rf} =75.02 MHz, CST Microwave Studio

F_{rf} =74.80 MHz, ANSYS

The accuracy of the calculations for the cavity frequency is better than 0.3%. One can see in Fig. 8 that the difference between the acceleration gap voltage profiles in two codes is negligible.

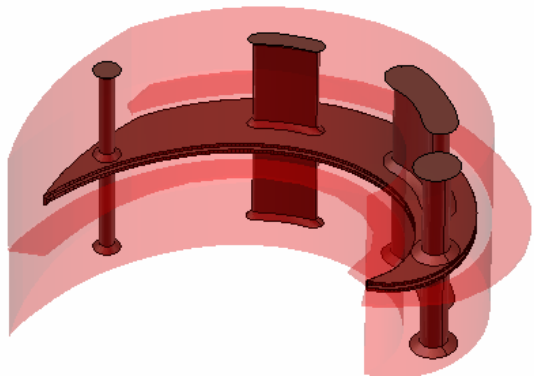

Figure 7: View of the cavity model

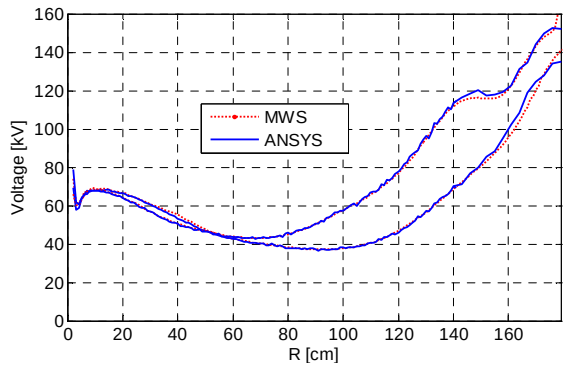

Figure 8: Voltage distribution along radius on both sides of dees calculated using two independent methods

Power dissipation in the model was calculated with the assumption that the wall material is the copper with conductivity $\sigma=5.8*10^7$ 1/(Ω*m). The quality factor was about 14000 and power losses of the model were as follows:

For the stored energy 1 J the voltage in the center is 65 kV and the average losses are 35 kW.

For the stored energy 1.5 J the voltage in the center is 80 kV and the average losses are about 50 kW.

Each cavity will be powered by a 75 MHz, 100 kW tetrode-based amplifier (as used in the current C235). The cavities will be excited with the RF generator through a coupling loop (which should be rotated azimuthally within small limits (± 30 degrees). The active tuning system must be designed to bring the cavities to the frequency initially to compensate for detuning because of temperature variations due to RF heating and to provide frequency difference 450 kHz for $^{12}C^{6+}$ and H_2^+ ions acceleration. It was found that the best position for the tuner is at the radius R=1200 mm (between the second and third stems).

It was demonstrated that it was possible to fit the resonant frequency of the cavity by varying diameter of

the fourth stem. The frequency difference per diameter difference is about 100 kHz/mm.

ION DYNAMICS

Detailed beam dynamics simulations were performed to be sure that the resonances crossed during acceleration would not cause significant harmful effect to the beam. During a whole range of acceleration the carbon beam crosses the lines of 15 resonances up to 4th order (Table 2). The working diagrams presented in Fig. 6 were computed via the analysis [8] of small oscillations around the closed orbits. All resonances can be subdivided into two groups. The first group consists of 6 internal resonances ($nQ_r \pm kQ_z = 4$, n, k=0, 1, 2, 3, 4, $n+k \leq 4$) having the main 4th harmonic of the magnetic field as a driving term. The second group includes 11 external resonances ($nQ_r \pm kQ_z = m$, m=0, 1, 2, 3) that could be excited by the magnetic field perturbations.

The analysis of dangerous resonances defines limits of acceptable magnetic field imperfections. All these limits can be achieved in practice.

Table 2: List of resonances up to 4th order

Resonance, (Level of danger)	Radius (cm) (Driving Term)	Description, tolerances
$Q_r = 1$ (Yes)	2-10 (B_{z1})	Increase in radial amplitudes B_{z1}< 2-3 G
$4Q_r = 4$ (Not)	2-10 (B_{z4},φ_{z4})	Weak influence on radial motion at acceleration
$2Q_r - Q_z = 2$ (Not)	110 (B_{z2}, B_{r2})	Increase in axial amplitudes B_{z2}< 200 G, B_{r2} < 50 G
$3Q_r + Q_z = 4$ (Not)	131 (B_{z4}, φ_{z4})	No influence up to A_z, A_r=5-7 mm
$Q_r - Q_z = 1$ (Yes)	145 (B_{r1})	Increase in axial amplitudes B_{r1} < 5-7 G
$3Q_r = 4$ (Yes)	154 (B_{z4}, φ_{z4})	Increase in radial amplitudes beginning with A_r=1.5 mm. Can be corrected by average field perturbation.
$2Q_r + Q_z = 3$ (Not)	157 (B_{r3})	Increase in axial amplitudes B_{r3}<10 G
$Q_r + 2Q_z = 2$ (Not)	162 (B_{z2})	Increase in axial amplitudes B_{z2}<20 G
$3Q_z = 1$ (Not)	167 (B_{r1})	Increase in axial amplitudes B_{r1}<20 G
$3Q_r - Q_z = 4$ (Not)	167 (B_{z4}, φ_{z4})	Increase in radial amplitudes. No influence if no axial amplitudes increase on resonance $3Q_z = 1$ due to B_{r1}.
$2Q_r = 3$ (Not)	172 (B_{z3})	Increase in radial amplitudes. B_{z3}<10 G
$Q_r + Q_z = 2$ (Not)	177 (B_{z2}, B_{r2})	Increase in radial and axial amplitudes. B_{r2}<10 G
$2Q_r + 2Q_z = 4$ (Not)	177 (B_{z4}, φ_{z4})	No influence
$Q_r + 3Q_z = 3$ (Not)	179 (B_{z3})	Increase in axial amplitudes B_{z3}<10 G
$2Q_r - Q_z = 3$ (Not)	180 (B_{z3})	Increase in axial amplitudes B_{z3}<10 G
$2Q_r + Q_z = 4$ (Not)	181 (B_{z4}, φ_{z4})	Increase in axial amplitudes. Requires proper deflector positioning.
$2Q_z = 1$ (Yes)	181 (B_{z1}, B_{r1})	Increase in axial amplitudes. B_{r1}<10 G, dB_{z1}/dr<1 G/cm

EXTRACTION

Extraction of protons will be done by means of the stripping foil. It was found that 320 MeV is the possible minimum kinetic energy of protons that can be extracted during one turn downstream the stripping foil passage and 265 MeV is the minimum energy of protons for 2-turn extraction (Fig. 9). The second solution was chosen because the energy of extracted protons is closer to the usually applied energy for the proton beam treatment. The stripper foil is at the radius of 1634 mm, the azimuth is 56° in the chosen coordinate system.

Electrostatic deflection extraction will be used for carbon and α beam. The single electrostatic deflector located in the valley between the sectors will be used with the electric field about 150 kV/cm. The extraction efficiency was estimated about 73% for the septum with increased (0.1 - 2) mm thickness along its length**.** The extraction of the carbon and proton beams by the separate channels and their further alignment by the bending magnets outside the cyclotron was chosen as the acceptable solution. A plan view of both extraction beam lines is shown in Fig. 10. The passive magnetic elements (correctors) will be used inside the cyclotron and the active elements (quadrupole lenses and bending magnets) outside the yoke. The system for carbon ion extraction consists of the electrostatic deflector, two passive magnetic correctors MC1-2, three quadrupole lenses CQL1−3 and two steering dipole magnets CSM1-2. The proton beam extraction system consists of the stripping foil, magnetic corrector PMC1, two bending magnets BM1-2, two quads PQL1-2 and two steering magnets PSM1-2.

Both beams have a spot with $\sigma_{x,y}$<1 mm at the degrader entrance, located 675 cm from the cyclotron

center.. Transverse emittances are (10π mm·mrad, 4π mm·mrad) and (3π mm· mrad, 1π mm· mrad) for the extracted carbon and proton beams, respectively.

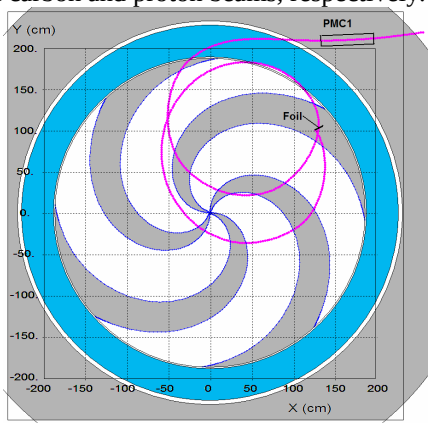

Figure 9: Two-turn extraction of protons with energy 265 MeV

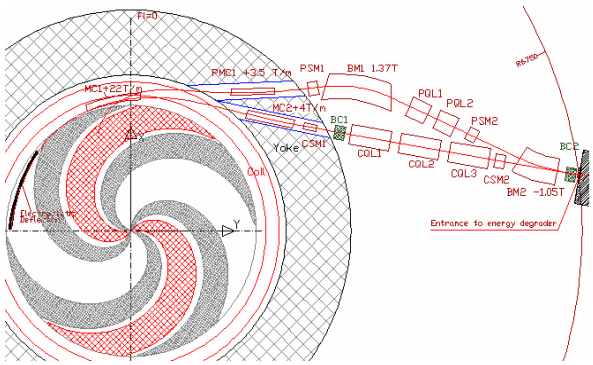

Figure 10: Layout of the C400 cyclotron with two extraction lines

VACUUM REQUIREMENTS

Numerical simulations of the beam transmission efficiency dependent on the charge exchange of H_2^+ and C^{6+} ions with the residual gas have been carried out for the future cyclotron. The loss of the beam intensity due to collision breakup with the residual gas molecules is determined by the cross sections for the losses process over a wide energy range and depends on the pressure distribution. A uniform pressure in the cyclotron was assumed because external injection is used. Nitrogen was assumed as a residual gas.

Different methods were used for cross section estimation for H_2^+ and C^{6+} ions. Losses in the axial injection line were estimated from experimental data on cross sections for the fixed projectile energy. The theoretical approach crosschecked by some experimental data for given energies was used for cyclotron vacuum chamber volume.

Vacuum requirements in the injection line are determined by $^{12}C^{6+}$ ions and beam losses are about 2 % for the pressure $2*10^{-7}$ torr.

Losses of H_2^+ ions during acceleration due to electron stripping were estimated using Bohr's formula [9].

The vacuum requirements in the cyclotron are determined by H_2^+ ions. For the pressure the 10^{-7} torr estimated losses will be 2-5 %; for the pressure $2*10^{-7}$ torr, 4-10 %. Losses of C^{6+} ions will not exceed 1% for the pressure $2*10^{-7}$ torr.

CONCLUSIONS

Computer modeling of the main systems and detailed simulations of the beam dynamics in the C400 cyclotron have been performed.

The results show that the energy range up to 400 MeV/amu (K = 1600) can be achieved with the compact design similar to that of the existing IBA C235 cyclotron. Transmission of carbon ion beam between the ion source and the beam extraction foil was estimated as 13%.

The C400 cyclotron will also provide a proton therapy beam with energy 265 MeV. Losses of protons due to the charge exchange with the residual gas during acceleration will not exceed 10% and extraction will be without losses.

Design of different cyclotron subsystems is presently in progress.

REFERENCES

[1] Y. Jongen et al., "Design studies of the compact superconducting cyclotron for hadron therapy", X EPAC 06, Edinburg. Scotland , 2006.

[2] Yves Jongen et al, "IBA C400 Cyclotron Project for Hadron Therapy", The 18th International Conference on Cyclotrons and their Applications Cyclotrons 2007, Laboratori Nazionali del Sud, Giardini Naxos, Italy 2007.

[3] Y.Jongen at al, "Current status of the IBA C400 cyclotron project for hadron therapy", XI EPAC08, p.1806-1809, Italy, 2008.

[4] Y.Jongen at al, "Simulation and design of the compact superconducting cyclotron C400 for hadron therapy", Proc. 11 Internal Heavy Ion Accelerator Technology, D9, Italy, 2009.

[5] http://archade.fr/.

[6] Yves Jongen et al, "Radio Frequency System of the Cyclotron C400 for Hadron Therapy", The 18th International Conference on Cyclotrons and their Applications Cyclotrons 2007, Laboratori Nazionali del Sud, Giardini Naxos, Italy 2007. http://felino.elettra.trieste.it/cyc07/papers/TUPPRA05.pdf.

[7] CST STUDIO SUITE http://www.cst.com.

[8] Y. Jongen et al., "Numerical study of the resonances in superconducting cyclotron C400", in Proc. of Cyclotrons 2007, p. 382.

[9] Franzke B. "Interaction of stored beams with the residual gas".

FAST SCANNING TECHNIQUES FOR CANCER THERAPY WITH HADRONS – A DOMAIN OF CYCLOTRONS

J.M. Schippers, D. Meer, E. Pedroni,
Paul Scherrer Institut, 5234 Villigen, Switzerland

Abstract

In protontherapy fast 3D pencil beam scanning is regarded as the most optimal dose delivery method. The requirements to apply this treatment technique and to obtain the maximum possible benefit have a big impact on the accelerator concept. Routinely a very stable, reproducible and adjustable beam intensity is needed, which can be set at a few percent accuracy within a millisecond. Quick changes of maximum intensity from the cyclotron are also needed when changing treatment room. Rescanning the tumour volume at high speed to prevent motion artefacts, needs beam energy variations within 50-80 ms.

It will be shown that a cyclotron offers the most advantageous possibilities to achieve this ambitious performance.

INTRODUCTION

The high spatial accuracy potentially obtainable by hadron therapy has increased the interest for radiation therapy with protons and carbon-ions considerably during the last years. Although in several groups developments are taking place on new accelerator concepts, to date all existing hadron therapy facilities that are in operation or in construction, use a (synchro) cyclotron (protons only) or a synchrotron (protons only or any particle between protons and carbon ions). Protons are accelerated to 230-250 MeV and carbon ions to 400-450 MeV/nucl. Both types of machines have proven to work accurately and safely in a programme of daily patient treatments and show excellent reliability figures.

With regards to beam delivery techniques, most treatments performed today are using passive beam spreading techniques to spread the dose over the tumour volume. However, there is an increasing interest in the possibilities of pencil beam scanning, a technique which is currently in clinical use at PSI Switzerland, HIT and RPTC in Germany and in Houston and Boston, USA. This technique, developed at PSI and GSI [1,2], has shown more possibilities to reduce the dose in healthy tissue than the passive techniques could offer.

The recent developments in accelerator concepts are mainly focussed on scale reduction, with an affordable single room treatment facility as final goal. However, the consequences for the quality of the dose delivery have not been elaborated in all cases. Furthermore, several important specifications of the accelerator and beam delivery system depend on the chosen beam delivery technique.

In this review the relation between accelerator specifications and the quality and type of the dose delivery method will be discussed, followed by a detailed description of the implications for the design and the experience with the cyclotron and beam lines at PSI, where the a fast 3D pencil beam scanning system is being developed for proton therapy.

DOSE DELIVERY TECHNIQUES

Dose Spreading in Depth

The energy of the particle determines its penetration depth in the patient. One should distinguish two purposes of beam energy change: a modulation of the energy to spread the dose in depth over the thickness of the tumour or just to set the maximum penetration depth. Modulation must be done at a much faster time scale and requires much more different energies than a setting of the maximum range in a field. The energy is set at the correct value either when extracted from the accelerator, or in an adjustable degrader in the beam line, or in the nozzle, just before the patient.

In case of a synchrotron the maximum energy needed in a certain treatment is set by the accelerator and can be selected at each spill. In case of a cyclotron, a degrader is used in the beam line, typically just outside the cyclotron. At both accelerator types all magnets in the beam transport system must be set according to the (degraded) energy of the beam. The energy modulation is typically performed just in front of the patient, in the nozzle of the beam transport system. A wheel with an azimuthally varying thickness that rotates in the beam, plates that can be inserted or retracted or plates with a variation in thickness (“ridge filters”) are used to give the desired energy spread. A novel approach has been developed at PSI, where the degrader and the following beam transport system have been optimized for speed, to allow fast energy modulation by the degrader at the exit of the cyclotron [3, 4].

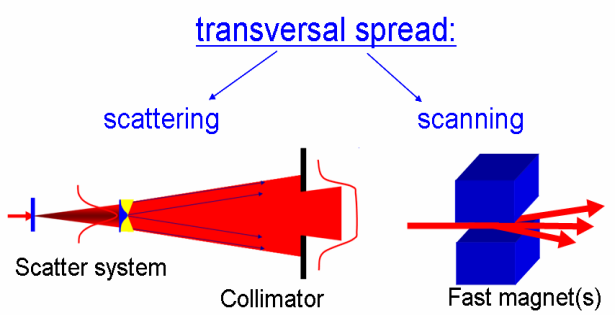

Figure 1: Passive scattering and pencil beam scanning: the tow methods to spread the beam in the transverse plane.

Transversal Dose Spreading

The most commonly used method to distribute the beam particles in the lateral direction is passive scattering (fig. 1) at which the beam is broadened by multiple scattering in foil(s). Just before the patient, the broadened beam is collimated to match the tumour shape. For large tumour cross sections or when heavy ions are used, beam wobbling is often added to the system to enlarge the covered cross section of the beam.

The best coverage of the target volume in combination with the lowest dose in the surrounding normal tissue is obtained with the pencil beam scanning technique (Figs. 1,2). Here fast steering magnets ("scanning magnets") are used to aim the beam sequentially at volume elements (voxels) in the target volume and at each location a specific dose is deposited. To date this is done on a discrete grid (spot scanning; "step and shoot") [1]. At PSI a faster method is in development [5,6], by which the pencil beam is moved along a certain trajectory within the target volume (continuous or raster scanning, fig. 2).

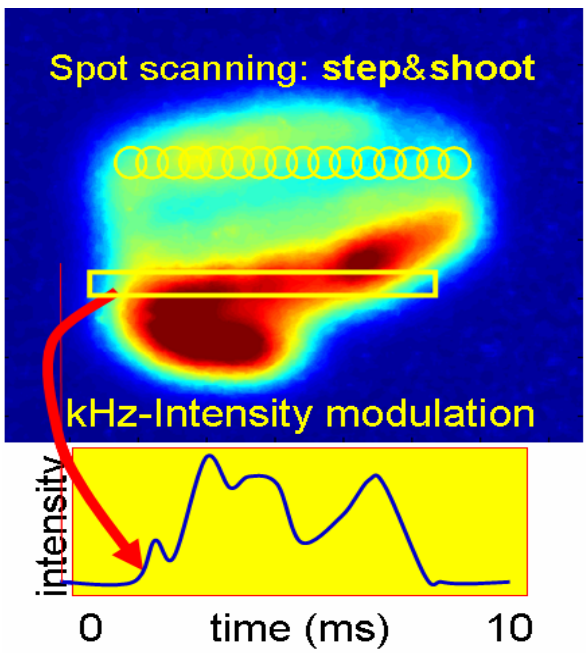

Figure 2: Pencil beam scanning can be applied by aiming at discrete spots (spot scanning) or by sweeping over the tumour and varying the beam intensity accordingly. Mind the short time needed for one line.

Continuous scanning techniques can be *time driven* or *event driven*. In the time driven system the pencil beam moves with a prescribed fixed speed in the transversal plane and the beam intensity is varied as a function of the position of the pencil beam. In event driven systems the beam intensity is fixed or just taken as it comes from the accelerator. The speed of the pencil beam motion is adjusted according to the necessary voxel dose, eventually corrected for the actual beam intensity. The treatment time will be a bit longer than in a time driven system.

An important problem for the application of pencil beam scanning, is motion of the tumour and/or critical healthy tissue during the dose administration e.g. due to breathing [7]. Different (combinations of) strategies are being pursued to deal with this problem. The first one is beam gating [8-10], the second one is to perform continuous scanning in a very fast way [7,11] to rescan the tumour many times during one treatment fracion. One might also apply an on-line correction of the beam position, the intensity and the energy to "follow" the motion (tumour tracking or adaptive scanning) [12].

CONSEQUENCES FOR THE ACCELERATOR

The passive beam spreading techniques and modulation of the energy in the nozzle can be equally well performed by means of a (synchro)cyclotron and a synchrotron. The only aspect to take care of, is the risk of interference of time structures in the beam with periodic changes in the dose application devices. For example when beam wobbling is used, one should investigate how the periodic movement of the beam might interfere with a pulsed beam, otherwise the dose distribution could be distorted. This also implies that accelerators delivering a pulsed beam with a low (<0.5-1 kHz) repetition rate are not so suitable to be used in combination with the "classical" passive dose delivery techniques.

For spot scanning the specifications of the accelerator are rather relaxed if the beam is switched off when one moves to the next spot. This is an event driven system: the dose is applied to a certain spot until the required dose is reached and then the beam is switched off and aimed at the next spot. In this case the "only" specification of the accelerator is that the beam intensity should be sufficient. When the beam is not switched off in between the spots (e.g. at HIT in Heidelberg [13]), the allowed intensity fluctuations and their time scale should be considered in relation with the speed of the movement to the next spot. In all cases the beam positioning must be fast and typically correct within a millimetre. For a cyclotron this is no serious effort, but with a synchrotron applying resonant slow extraction, one must take care of a possible change in beam position during extraction.

Most of the currently developed new accelerator concepts are based on pulsed accelerators (synchrocyclotron, FFAG, linac based systems, DWA, laser driven systems). In the application proposals these are often considered to be appropriate for spot scanning. However, pulse repetition rate and accuracy of the dose per pulse are important issues to be considered with such machines. Considering that one needs to apply typically 8000 spots in a volume of 1 litre within a reasonable time of the dose delivery, a minimum pulse rate of a few hundred Hz is necessary for a single coverage of the tumour and at least a few kHz are necessary when rescanning is desired. Further, in the proposed systems the dose rate during the dose application in a spot is usually very high. Therefore the event driven approach in

which the beam is intercepted when the required dose has been reached, cannot be used. In this case the dose per spot is determined by an intensity pulse from the ion source. The phase (width) of the pulse should match the phase acceptance window of the accelerator. Much attention should be given to the achievable accuracy in the dose per pulse (1%) and whether this dose can be varied at least a factor 20 from pulse to pulse.

If time driven techniques are used in continuous pencil beam scanning, the intensity of the beam must be adjustable within a fraction of a millisecond (depends on scanning speed) and set to the desired value with an accuracy of a few percent. Unexpected fluctuations or interruptions in the beam intensity or a pulsed beam are not desired. The requirements are related to the maximum allowed difference between obtained and expected dose distributions and with the speed of the pencil beam motion. At PSI the beam intensity fluctuations must be less than 2% (1 s.d.) at a band width of 10 kHz and the beam can be switched on or off within 40 µs. At the moment such requirements can only be achieved with a cyclotron.

When an event driven technique is applied, the stability of the beam intensity is less critical, although too large or too fast fluctuations are difficult to compensate by the speed of the scanning magnets. Cyclotrons operating with a less stable beam or synchrotrons with optimized beam stability are eligible for this technique.

RESULTS

At the Centre of Proton Therapy at PSI, a program is running to develop fast continuous scanning techniques. The new techniques will be applied in Gantry-2 [11], and tests of several aspects of the scanning technology are in progress [5,6]. In this section details of the applied methods will be described and some of the achieved results will be presented.

Energy

The possibility for a fast change in energy at any moment in time is of advantage to reduce treatment time (range shifter), to reduce the switching time between areas (cycling and new setting) and to allow energy modulation. Therefore the magnets in the beam line and Gantry-2 are laminated [14], the power supplies are capable of making fast current changes and the control system sends the new beam line settings to all power supplies at the same moment in time. Figure 3 shows that it takes 80 ms to make an energy step equivalent to a range change of 5 mm in water. This time is limited by decay of eddy currents in the fringe field of the last (90 degr.) bending magnet of the gantry [14]. Improvements are still possible to 50 ms: the time it takes for the degrader and the other beam line magnets.

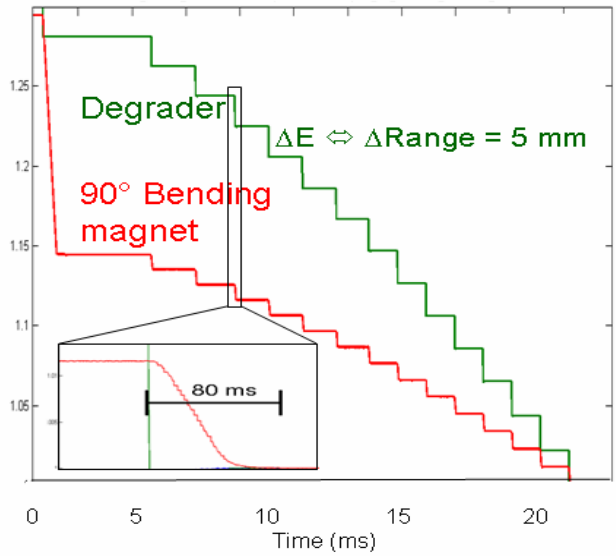

Figure 3: Recorded sequence of degrader settings and the current in the 90° bending magnet of Gantry-2 for range steps of 5 mm in water. The insert shows that the time to make this step is 80 ms.

The degrader system at PSI is followed by two stacks of collimator holes, so that the transmitted emittance can be selected. Due to multiple scattering and nuclear interactions the transmission through the degrader and the following collimators is strongly dependent on the final energy (fig. 4). This has been modelled in a detailed study [4], in which also the possible advantage of beryllium in stead of carbon as degrader material has been investigated. This is especially of interest for treatments of eye melanoma, which needs a high dose rate (~15 Gy/min) and a low energy (70 MeV). As can be seen in fig. 4, a gain with a factor 1.3 may be possible by using beryllium.

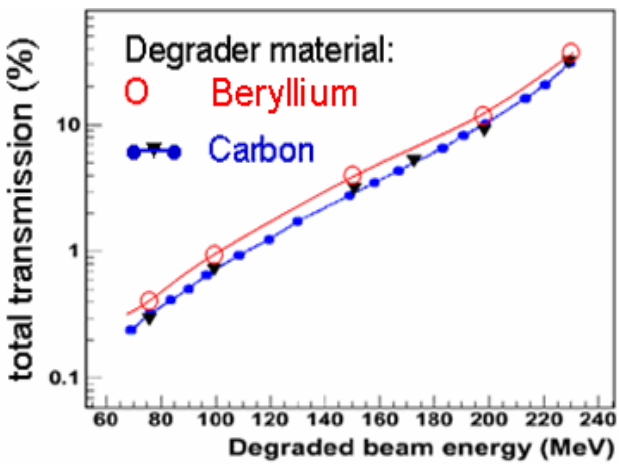

Figure 4: The transmission through the degrader and collimators at PSI as a function of the degraded energy. The calculation model has been validated with measurements (triangles) and used to estimate the transmission in case of a beryllium degrader.

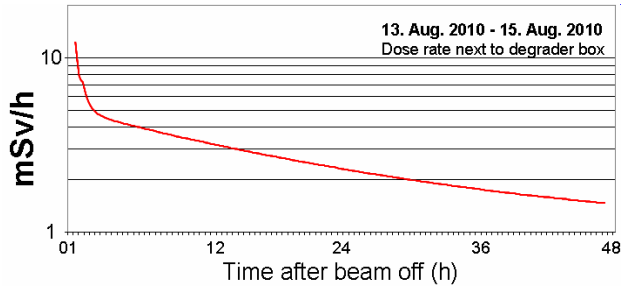

Figure 5: Dose rate next to the degrader after switching off the beam

The radioactivity caused by the 90-99.5% beam loss is often mentioned as an important disadvantage of cyclotron based systems. However, the activation can be limited by selecting specific materials in the degrader system. An ample use of graphite for stopping the protons yields a rapid decrease of the dose rate to an acceptable level for service and maintenance after beam switch off, as shown in fig. 5. Furthermore the volume of materials with long living isotopes will be very limited. At the PSI degrader system it has been demonstrated that this "disadvantage" of a cyclotron based system can be dealt with adequately, if the limitation of activation is integrated in the design of the degrader system.

Intensity

At PSI each treatment room has specific requirements with respect to beam intensity. Gantry-1 (spot scanning) needs < 0.5 nA and a fixed energy for each patient between 100 and 200 MeV. Gantry-2 will need intensity variations between 0 and several nA at any energy between 70 and 230 MeV. The eye treatment facility OPTIS2 needs a few nA at 70 MeV. The intensity of the beam at the patient is set by different processes. First of all the intensity is set by the ion source in the centre of the cyclotron. It has been shown, however, that a sufficiently stable operation of the source requires a minimum fixed intensity (arc current). Therefore a fixed arc current is used for the day, which is high enough to deliver all necessary beam intensities. Coarse adjustment of the intensity of the beam is done by means of two phase slits mounted at small radius in the cyclotron. The adjustable aperture of these slits determines I_{max}, the maximum extracted intensity needed for a certain field or for a patient. A change of I_{max} takes a few seconds. At the morning setup the slit settings corresponding to the typically needed I_{max} values are saved for the day and used when a switch between treatment areas is performed. Figure 6 shows the first time this feature has been used at PSI by switching between patient treatments at Gantry-1 and OPTIS2. The figure shows the beam intensity and the treatment room to which the beam is sent (which has "Mastership") during a period of 1 h. A change of Mastership occurs within a few seconds. The short periods of zero beam intensity reflect the effective area-switching times of 10-30 sec. The high intensity for OPTIS2 and the ~100 nA for Gantry-1 are set as soon as the patient is ready.

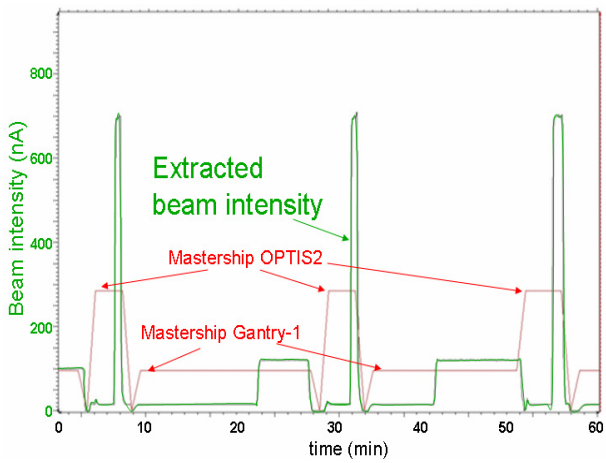

Figure 6: The extracted beam intensity and the treatment area to which the beam is going ("master area") during one hour. The intensity is set according to the need at the master area. The time that the beam intensity is 0, reflects the time needed for the switch between the areas.

I_{max} is chosen about 10% higher than needed. The actually obtained extracted beam intensity is set by a DC voltage between electrodes in the centre of the cyclotron (Fig. 7, top). The electric field between these electrodes deflects the beam out of the median plane into the vertical direction, so that the beam is partially intercepted by a vertically limiting aperture. The extracted beam intensity can thus be set between zero and I_{max} within a few tens of µs. For operation at Gantry-1 and OPTIS2 a slow (Hz) feedback on the deflector voltage controls the current to a stable value, as shown in fig. 7, bottom.

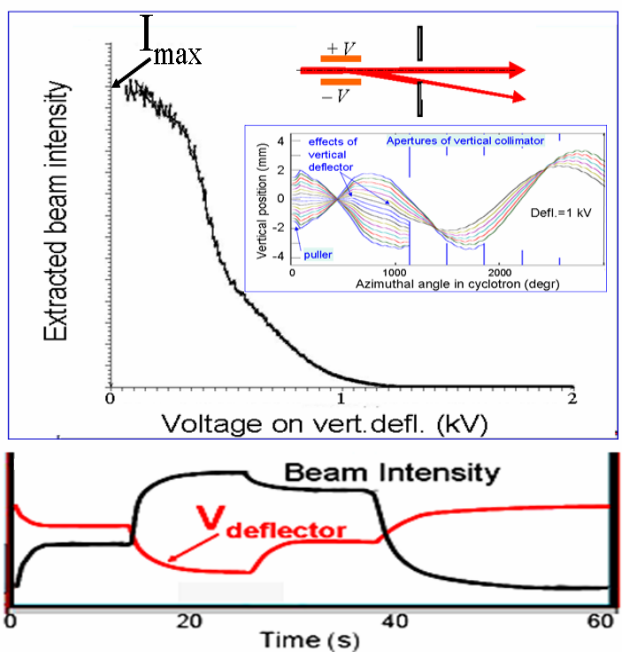

Figure 7: By means of a vertical deflection of the beam in the centre of the cyclotron and a collimator which intercepts a beam fraction that depends on the deflector voltage, the intensity can be controlled very fast between 0 (Vdefl > 1.5-2 kV) and I_{max} (Vdefl ≈ 0).

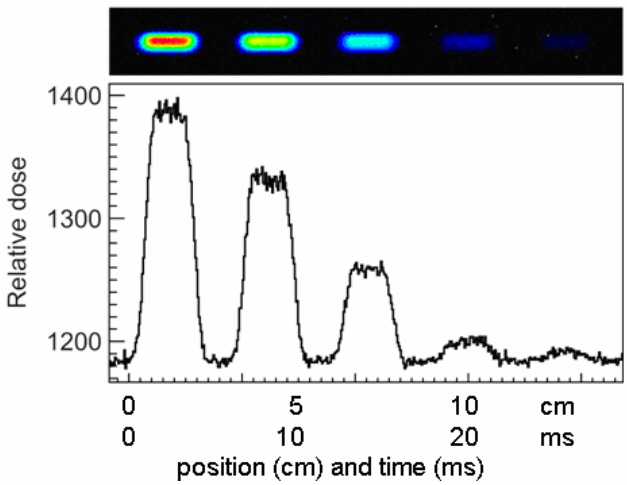

Figure 8: Dose pattern along a line of 15 cm length, from an intensity modulated sweep of the pencil beam during 30 ms.

However, the deflector is especially suitable to perform fast intensity variations during continuous scanning in Gantry-2, see Figure 8. To obtain sufficient speed, the reference characteristic of the beam intensity as a function of deflector voltage is used together with a fast (>10 kHz) feedback control loop.

The transmission through the degrader system varies a factor 50 if the energy is changed between 70 and 230 MeV. When scanning at large depth, i.e. at high energies, one would not like to regulate the beam intensity within the lower 5% of the deflector's dynamic range, with the additional risk of a sudden too high dose rate in case of a deflector failure. Furthermore, for precise dose monitoring an energy independent proton current at the isocenter of the gantry is advantageous. Therefore it is necessary to adjust I_{max} as a function of degrader setting.

Since a change in phase slit aperture would be too slow for energy modulation, two additional concepts to match I_{max} to the beam energy have been developed. The first concept is a brute force method, at which, as a function of beam energy, a fraction of the beam is intercepted in the beam line. This is performed by defocusing the beam at two collimators mounted in the beam line to Gantry-2, as shown in Fig. 9.

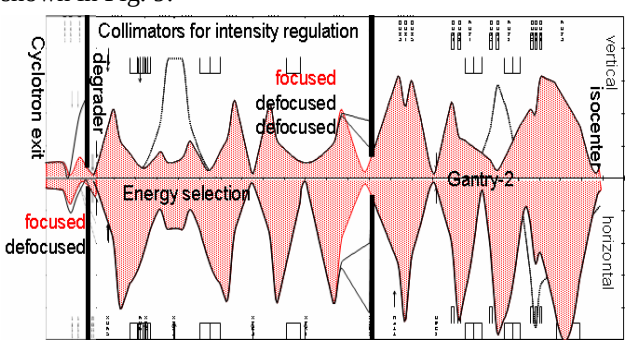

Figure 9: Calculated beam envelopes of focused and defocused beams, partly intercepted at collimators before the degrader and behind the energy selection system.

The first collimator is located just before the degrader, where an increase of beam loss from e.g. 90% to 97% is no problem and the second collimator is located behind the energy selection system, where the absolute beam intensity is already only a few nA. Since the obtained intensity decrease has shown to be very reproducible, the defocused setting has become an integrated part of the standard beam line setting to Gantry-2.

The second concept for fast regulation of I_{max} is still in development and is based on a reduction of the Dee voltage, without spoiling the good extraction efficiency. As shown in Figure 10, a decrease in Dee voltage can already reduce the beam intensity by a factor two, while maintaining a constant and a high extraction efficiency. A lower Dee voltage does reduce the intensity, but undesired losses occur at extraction. By adding slits in the central region, we expect to increase the Dee-voltage window with high extraction efficiency and be able to use this method for a fast and "clean" regulation of I_{max}.

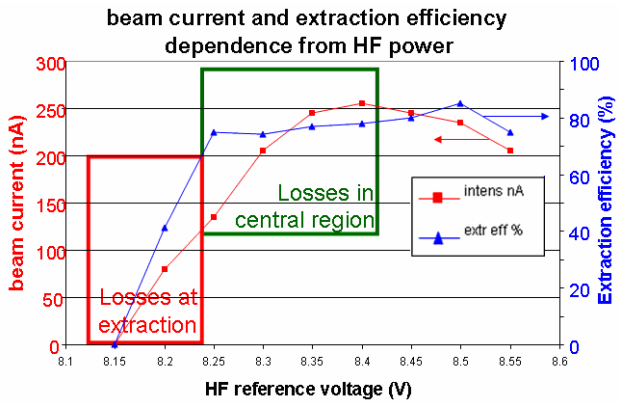

Figure 10: Extracted beam intensity and extraction efficiency as a function of the Dee voltage. The intensity can be decreased partly by decreasing the Dee voltage without loss of extraction efficiency. Lower Dee voltages reduce the extraction efficiency.

CONCLUSIONS

In order to exploit the advantages of 3D pencil beam scanning, the scanning process must be performed as fast as possible. This allows different strategies to prevent dose errors due to tumour/organ motion. A reliable application of fast 3D scanning necessitates firm specifications on the accelerator: a CW beam, with an intensity that must be stable, quickly and accurately adjustable over a large dynamic range as well as a fast and accurate energy modulation. Currently the combination of these specifications is not possible to achieve with pulsed machine operation at repetition rates below 0.5-1 kHz. It has been demonstrated, however, that compact cyclotrons can comply with the above mentioned specifications for fast 3D scanning, and at the same time provide a reliable and safe operation during routine patient treatments with protons. Since this yields that cyclotron based systems would also be of advantage in carbon ion therapy, several types of such systems are currently being developed [15-17].

ACKNOWLEDGEMENTS

We would like to acknowledge our colleagues at the Centre of Proton Therapy and those involved at the proton therapy accelerators at PSI.

REFERENCES

[1] E. Pedroni et al, Med. Phys. 22 (1995) 37-53
[2] Haberer T et al., Nucl. Instr..Meth. A 330 (1993) 296–305
[3] J.M. Schippers et al., Nucl. Instr. and Meth. B 261 (2007) 773-776
[4] M. J. van Goethem et al., Phys. Med. Biol. 54 (2009) 5831-5846
[5] D. Meer et al., Scientific Report PSI (2006) 58-59
[6] S. Zenklusen et al., subm. for publ. in Med. Phys.2010
[7] M H Phillips et al., Phys. Med. Biol. 37 (1992) 223-233
[8] K. Hiramoto et al., Nucl. Instr. Meth. B 261 (2007) 786–790
[9] S. Yamada et al, Proceedings, Asian Particle Accelerator Conference 1998, KEK Proceedings 98-10
[10] Y. Tsunashima et al., Phys. Med. Biol. 53 (2008) 1947-1959
[11] E. Pedroni et al., Z. Med. Phys. 14 (2004)25-34
[12] N. Saito et al., Phys. Med. Biol. 54 (2009) 4849-4862
[13] T.Haberer et al., Radiother. Oncol. 73 S186–90
[14] M. Negrazus, et al., IEEE Trans. Appl. Supercond., (2006) 228-230
[15] Archade project http://archade.fr/
[16] L. Calabretta et al., Nucl. Instr. and Meth. A562 (2006) 1009
[17] J.M. Schippers, et al., Proc. HIAT09, Venice (It) TU11 (2010)

ADVOCACY FOR A DEDICATED 70 MEV PROTON THERAPY FACILITY

A. Denker*, C. Rethfeldt, J. Röhrich, Helmholtz-Zentrum Berlin#, Germany
D. Cordini, J. Heufelder, R. Stark, A. Weber, BerlinProtonen am Helmholtz-Zentrum Berlin

Abstract

Since 1998 we treated more then 1500 patients with eye tumours at the HZB cyclotron with a 68 MeV proton beam.

The 5 years follow up shows a tumour control rate of more then 96%. The combination of a CT/MRT based planning and excellent physical beam conditions like 2 nA in the scattered proton beam, a 0.94 mm distal dose falloff and a dose penumbra of 2.1 mm offers the opportunity to keep side effects on a lowest level.

However all new medical proton facilities are equipped with accelerators delivering beams of 230 MeV and more. While this is needed for deep seated tumours, a lot of physical and medical compromises have to be accepted for the treatment of shallow seated tumours like eye melanomas.

Hence, we suggest a 70 MeV proton therapy facility. It should be equipped with a horizontal beam line and can have optionally a vertical line for more complicated cases under anaesthetics or for biological experiments. By the use of PBO-Lab and MCNPX beam line concepts and a radio-protecting architecture are designed.

MOTIVATION

Experiences from Berlin

Treatment of ocular melanomas at our cyclotron started in 1998. Since then, more than 1500 patients have been treated. In the past years, the number of patients per year increased to more than 200 [1]. The therapy planning and treatment system includes, among others:

- CT and/or MRI-based modelling and planning with the tool OCTOPUS [2,3] (see fig. 1)
- digital image guided patient positioning using TREAT [4]
- use of retractors to avoid irradiation of the eye lids

By far the most of the indications were uveal melanomas, followed by iris melanomas. The subgroup of large uveal melanomas increased. In order to prevent toxic reactions due to the inactivated tumour mass, the irradiation is followed by surgical removal of the tumour (endoresection or transscleral resection) [5]. Peculiar cases were the treatments of small children under anaesthesia, as they were not able to cooperate in the positioning process: Two children (5 and 7 months old) with retinonablastomas and a 5 year old child with an osteoma were treated.

The protons are accelerated by a 5 MV van-de-Graaff generator in combination with a k132 isochronous cyclotron giving a quasi DC, 68 ± 0.3 MeV proton beam. Regarding the depth dose profile, a distal falloff 90 - 10% of 0.94 mm is achieved. A simple single scattering technique provides a beam diameter of 40 mm with a penumbra of 80 - 20% of 2.1 mm.

All required therapeutic beam intensities can be delivered from the cyclotron with a dose rate of at least 15 Gy/min.

Side effects could be minimized due to the properties of our proton beam. The sharp distal dose falloff is often crucial for preventing high dose irradiation of sensitive structures essential for sight (optic nerve, papilla, macula). Furthermore, the sharp lateral penumbra and sharp distal falloff enabled us to spare the bones of the children's skull completely in a frontal irradiation approach.

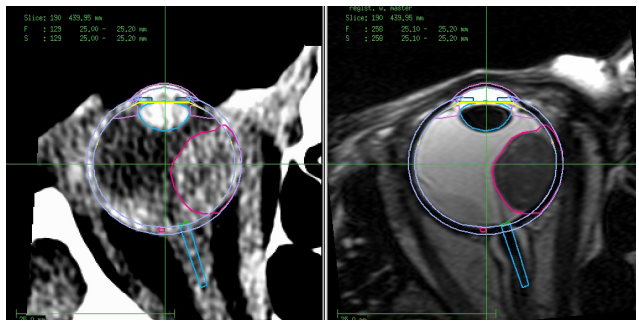

Figure 1a: CT (left) and MRI (right) slice of a right eye with delineated eye ball and lens (blue), papilla (green) on top of optic nerve (cyan), macula (magenta), and tumour (red). These slices are used for treatment planning.

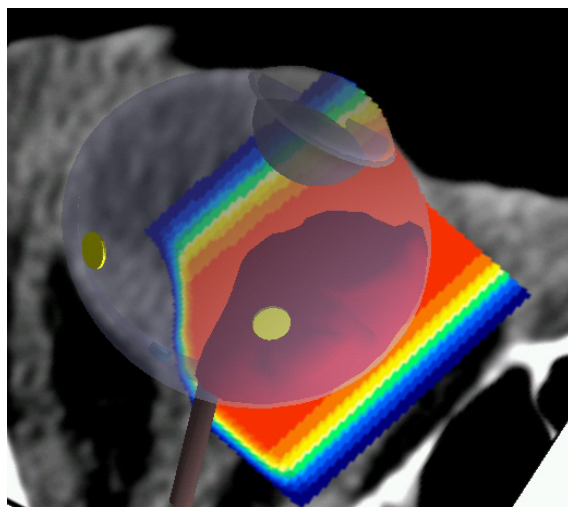

Figure 1b: Dose distribution calculated with OCTOPUS.

New Facilities

So far, 60000 patients have been treated with protons, among them more than 17000 with ocular tumours. Since 1990, an increase of medical proton facilities replacing therapy units at research facilities is observed world-wide. End of July 2010, the particle therapy co-operative group

(PTCOG) lists 19 new facilities under construction [6]. However, the 11 projects building cyclotrons are equipped with an accelerator delivering at least 230 MeV.

Hence, for the treatment of ocular melanomas, they all need to degrade the proton beam to the desired energy of about 70 MeV. The resulting large energy spread or very low beam intensity means that ocular tumour therapy has to accept compromises regarding side effects or requires an extremely sophisticated beam shaping technique as at the Paul Scherrer Institute new eye facility OPTIS2 [7]. A dedicated facility would provide a proton beam with the desired properties and allow a patient workflow taking into account the special needs of eye patients.

A 70 MeV DEDICATED FACILITY

The requirement for an accelerator dedicated for eye tumour therapy is the provision of a quasi-DC beam with the following properties:

- energy of extracted beam: 72 MeV
- intensity of extracted beam ~ 100 nA
- dE/E ≤ 0.4%
- half beam extent, x, y: 2 mm • 4 mm
- half beam divergence x' • y': 4 mrad • 3 mrad

With these properties, it is possible to provide a sharp distal falloff and a sharp penumbra (see below). 72 MeV have been chosen as this energy will allow the treatment of all ocular tumours, even in the case of optic nerve infiltration.

A small cyclotron would fulfil these needs well, with the benefit of comparable low costs.

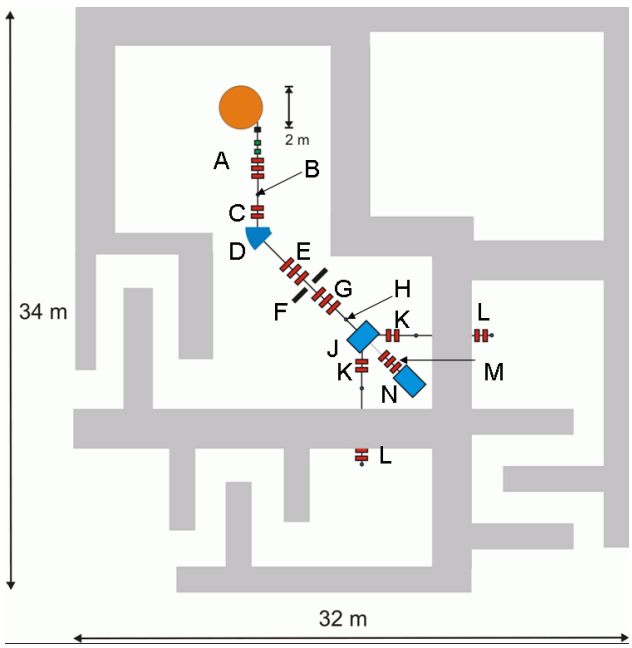

Figure 2: Layout of the proposed facility. An energy selections system permits the definition of energy as well as energy spread. Two horizontal beam lines and one vertical line are suggested. For details see text.

Layout of the Beam Lines

Fig. 2 depicts the layout of the beam lines. Two horizontal beam lines, with identical properties, permit preparation of the patients in one room, while the other room is used for treatment or physics experiments. It is possible to treat anesthetized children on a horizontal beam line. However, the handling of anesthetized children would be much easier on a dedicated vertical beam line would. In addition, this room may be used for irradiation of cell cultures.

Calculations for the beam lines have been performed using TRANSPORT within the PBO-Lab Package [8] and Graphics TURTLE [9].

After the cyclotron, the beam is first focused on a slit system (A,B). An energy selection system, consisting of a quadrupole doublet (C), a 45° dipole(D), two quadrupole triplets (E,G) with the energy slits (F) in between, allows the definition of the energy as well as the energy spread.

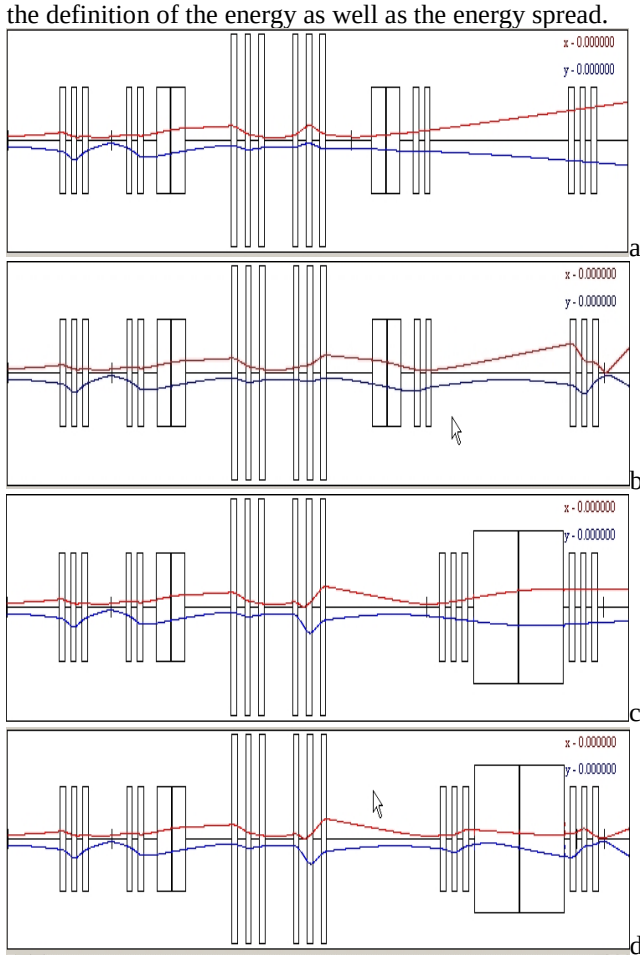

Figure 3: Beam envelopes for the beam lines, from top to bottom: horizontal line: broad beam, sharp beam, vertical line: broad beam, sharp beam.

At this point, the energy spread is reduced to 0.2% in order to provide a distal falloff of less than 1 mm in the therapy rooms, which is close to the physical limit. The advantage of this layout compared to a mere energy shift by using a range shifter is that the energy spread and thus the width of the Bragg peak are kept small. This is of

interest for the treatment of tumours lying close to sensitive structures, e.g. macula, papilla, and optic nerve. The dipole K switches between the two horizontal rooms, while dipole N transfers the beam to the vertical room.

For all beam lines, two different ways of focusing are foreseen:

- focusing on a simple scattering foil after the energy selection system (fig. 3a, 3b): Two foils will be necessary on different positions (H): one for the horizontal lines, one for the vertical line. The last active quadrupole will then be the quadrupole G, focusing on a 50 µm Ta scattering foil. This proven technique will provide a beam spot of at least 40 mm at the isocentre (see fig. 4).
- sharp focus in the treatment room. Thus, the penumbra 80 - 20% is reduced from 2.0 to 1.5 mm. In this case, the quadrupoles K and L are active.

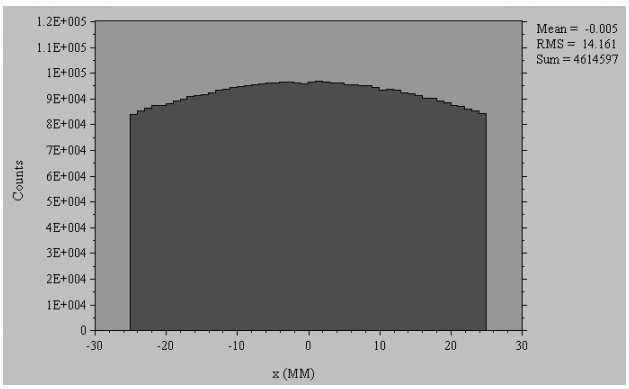

Figure 4: Turtle histogram of the horizontal broad beam behind the exit window. The beam intensity is sufficiently homogenous over more than 40 mm diameter.

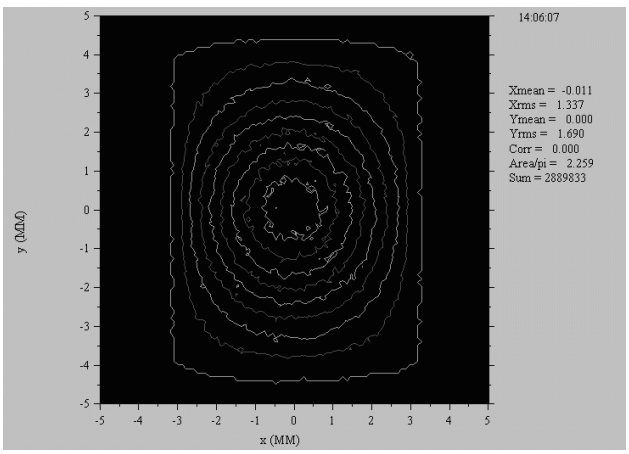

Figure 5: Turtle histogram of the horizontal sharp beam providing a well-defined beam spot in the treatment room.

For further neutron dose calculations, the transmission of the protons has been evaluated, assuming an extraction efficiency of 80%, hence, an extracted beam intensity of 100 nA. The resulting beam intensities are listed in table 1. For the sharp focusing, higher beam intensities are achievable in the rooms, which may be useful for experiments. First estimations of the neutron dose have been performed and used in the layout of the walls and mazes of the facility. More exhaustive calculations using FLUKA as well as MCNPX will be used for a detailed design.

Table 1: Transmission of the proton beam for the different focusing versions.

Place	Broad Beam	Sharp Beam
cyclotron exit	100 nA	100 nA
collimator 1 m behind exit	60 nA	60 nA
energy slits	30 nA	30 nA
collimator behind scattering foil	6.5 nA	
beam in treatment room	2.5 nA	30 nA

SUMMARY AND PERSPECTIVES

From our experience, the treatment of ocular melanomas requires special features from the accelerator, like matching energy and energy spread, as well as sufficient intensity. The positioning process is time consuming, and not well predictable, as it requests active cooperation of the patient, thus restricting the workflow in the overall patient throughput. Albeit it is possible to treat children under anaesthesia at a horizontal line, a vertical beam line would ease the process.

This proposal for a dedicated 70 MeV proton therapy facility for ocular melanomas is based upon our experiences gathered in more than 10 years of treatment. The achievable distal falloff, close to the physical limit, and sharp penumbra provide best therapeutic potential for patients with ocular tumours.

Detailed calculations of the neutron doses are in progress.

In Germany we see a definite necessity for a single low energy facility which guarantees the excellence of proton therapy for the need of 80 million people.

ACKNOWLEDGEMENTS

The authors would like to thank K. Ott from the HZB radiation safety department for fruitful discussions.

REFERENCES

[1] A. Denker et al., these proceedings
[2] B Dobler and R Bendl, Phys. Med. Biol. 47 (2002) 593
[3] K. Pfeiffer and R. Bendl, Phys. Med. Biol. 46 (2001) 671
[4] R. Stark, et al. Biomedizinische Technik 50 [Suppl. 1, Pt. 1] (2005) 346-347
[5] N.E. Bechrakis, M.H. Foerster, International Ophthalmology Clinics 46 (2006) 95-107
[6] http://ptcog.web.psi.ch/newptcentres.html
[7] J. Heufelder, M. Schippers, personal communication
[8] G.H. Gillespie, et al., Proc. 15th Inter. Conf. Cyclotrons and Their Applications (1999) 532-535
[9] http://people.web.psi.ch/rohrer_u/turtcomp.htm

REVIEW OF CYCLOTRONS USED IN THE PRODUCTION OF RADIO-ISOTOPES FOR BIOMEDICAL APPLICATIONS

P. W. Schmor, AAPS Inc., TRIUMF, 4004 Wesbrook Mall, Vancouver, BC, Canada

Abstract

Cyclotrons are the primary tool for producing the shorter-lived proton-rich radio-isotopes currently used in the biosciences. Although the primary use of the cyclotron produced short-lived radio-isotopes is in PET/CT and SPECT diagnostic medical procedures, cyclotrons are also producing longer-lived isotopes for therapeutic procedures. Commercial suppliers are responding by providing a range of cyclotrons in the energy range of 3 to 70 MeV. The cyclotrons generally have multiple beams servicing multiple targets. This paper provides a comparison of some of the capabilities of the various current cyclotrons. The use of nuclear medicine and the number of cyclotrons providing the needed isotopes is increasing. In the future it is expected that there will be a new generation of small 'table top' cyclotrons providing patient doses on demand.

INTRODUCTION

Cyclotrons have become the tool of choice for producing the short-lived. proton-rich radio-isotopes used in biomedical applications [1]. Industry has responded with a variety of cyclotrons to address the particular needs of different users groups. Most of these machines have been installed in hospitals, institutes for academic research, and commercial facilities specializing in producing and selling of radio-isotopes. Cyclotrons for biomedical radionuclide production are generally compact, accelerate light ions (proton, deuteron or helium) and are primarily used to produce short-lived, proton-rich radio-nuclides. The main use of these unstable isotopes is for diagnostics and therapy in biomedicine. Other fields using radio nuclides as tracers include agriculture (bio-kinetics in plants and soil), biology (bio-chemical and toxicological studies), ecology (pollution, environmental impact, and ecology studies), Geology (migration of elements in soils and waters) and pharmacology (metabolic studies). The use and need of radio-active isotopes for biomedical applications continues to increase worldwide. However, the list of radio nuclides and the applications have not changed significantly over the past 20 years [2].

Five years after demonstrating the first cyclotron in 1931 [3], G. Lawrence was producing phosphous-32 with by an accelerator and for injection into a patient with chronic leukaemia. Other isotopes generated by his cyclotron also had important applications in medicine. However, his vision to develop a radiopharmaceutical industry at the Radiation Laboratory to help sustain accelerator physics in the late 1930s was an idea ahead of its time. In 1941 the first cyclotron dedicated to the production of radioisotopes was installed at Washington University, St Louis and was used to produce isotopes of phosphorus, iron, arsenic and sulphur. In the mid 1950s a group at Hammersmith Hospital in London put into operation a cyclotron wholly dedicated to radionuclide production. Scanditronix was founded in 1961 as a private company to commercialize cyclotrons for use in the medical field.

Radioactive isotopes have both diagnostic and therapeutic applications in Nuclear Medicine. PET (positron emission tomography), PET/CT and SPECT (single photon emission computed tomography) are the main diagnostic procedures in nuclear medicine. Radioactive isotopes for biomedical applications are produced in reactors and with accelerators. Of particular importance for PET are the short-lived positron emitters, 11C, 13N, 15O and 18F. Carbon, nitrogen and oxygen represent basic constituents of organic matter and this characteristic permits the labelling of a great variety of radio-pharmaceuticals. SPECT uses medium-lived radio-nuclides that are single photon emitters. This is a technique in which a gamma camera rotates around the patient taking ‘pictures’ which a computer uses to form a cross-sectional tomographic image. Therapeutic applications prefer to use radionuclides that have a high linear-energy transfer associated with their decay products and that can be chemically attached to a biologically active molecule which preferentially attaches to a tumour site. Table 1 contains a list of the main radioisotopes produced by cyclotrons along with some of the reactions that are used to produce the radioisotopes. The production yields come from a variety of sources but primarily from a review article by Ruth et al, vary considerably depending on target design and the chemical form of the radioisotope molecule that is being used for measured the yields and in some cases from calculations [4].

The principle advantage of accelerator produced radioisotopes is the high specific activity (SA) that can be obtained via the nuclear reactions that produce an isotope that is chemically different from the target element. Another significant advantage is the smaller amount of radioactive waste generated in particle reactions compared to reactor produced radioactive isotopes. (SA is a measure of the number of radioactive decays from an isotope of interest per unit weight of an irradiated sample). Most of the reactions used are of the form (p,n), (p,2n), (p,), (p,xn) and to a lesser extent reactions involving D, 3He and 4He as the projectile. Measured cross sections for many of these reactions along with references for the measurements can be found in an IAEA report titled “Cyclotron produced radio-nuclides: Physical Characteristics and production methods” [5]. For proton/deuteron acceleration the negative ion is preferred in order to reduce activation around the cyclotron whereas for helium acceleration, the positive ions must be accelerated.

In 2005, an IAEA report estimated that, worldwide, there were about 350 cyclotrons that were primarily used

for the production of radio-nuclides [6]. Nearly 50% of these were in the 10-20 MeV energy range and about 75% of the cyclotrons were being used to produce ^{18}F for FDG.

Medical Isotope	Life-time $T_{1/2}$	Use	Nuclear Reaction	Target Abun-dance (%)	Energy Range (MeV)	Production Yield (mCi @ sat)	Typical Dose (mCi)
^{11}C	20.4m	PET	^{11}B(p,n)	80.3	8 - 20	40/μA	
^{11}C	20.4m	PET	^{14}N(p,α)	99.6	12	100/μA	
^{11}C	20.4m	PET	^{10}B(d,n)	19.7	7	10/μA	
^{13}N	9.96m	PET	^{13}C(p,n)	1.1	5 - 10	115/μA	
^{13}N	9.96m	PET	^{12}C(d,n)	98.9	2 - 6	50/μA	
^{13}N	9.96m	PET	^{16}O(p,α)	99.8	8 - 18	65/μA	
^{15}O	2m	PET	^{15}N(p,n)	0.36	10 - 15	47/μA	
^{15}O	2m	PET	^{16}O(p,pn)	99.8	>26	25/μA	
^{15}O	2m	PET	^{14}N(d,n)	99.6	8 - 6	27/μA	
^{18}F	109.8m	PET	^{18}O(p,n)	0.20	8 - 17	180/μA	5 - 20
^{18}F	109.8m	PET	^{20}Ne(d,α)	90.5		82/μA	
^{64}Cu	12.7h	SPECT	^{64}Ni(p,n)	0.93	5 - 20	5/μA	
^{67}Cu	61.9h	SPECT	^{68}Zn(p,2p)	19.0	>40	0.02/μA	
^{67}Ga	78.3h	SPECT	^{68}Zn(p,2n)	19.0	20 – 40	4.5/μA	10
^{82}Sr/^{82m}Rb	25d/5m	PET	^{85}Rb(p,4n)^{82}Sr Produces Rb	72.2	50 -70	0.18 /μAh	
^{99m}Tc	6h	SPECT	^{100}Mo(p,2n)	9.7	19	14/μAh	20
^{103}Pd	17.5d	Therapy	^{103}Rh(p,n)	100	10 -15	0.52/μAh	
^{111}In	67.2h	SPECT	^{112}Cd(p,2n)	24.1	18 - 30	6/μAh	3
^{123}I	13.2h	SPECT	^{124}Xe(p,2n)^{123}Cs →^{123}Xe→^{123}I	0.10	25 - 35	27/μAh	
^{123}I	13.2h	SPECT	^{123}Te(d,2n) ^{123}I	0.89	10 - 15	20/μAh	
^{124}I	4.1d	PET	^{124}Te(p,n)	4.7	10 - 18	0.1/μAh	
^{124}I	4.1d	PET	^{124}Te(d,2n)	4.7	>20	0.15/μAh	
^{186}Re	90.6h	Therapy /SPECT	^{186}W(p,n)	28.4	18		
^{201}Tl	73.5h	SPECT	^{203}Tl(p,3n)^{201}Pb →^{201}Tl	29.5	27 - 35	0.7/μAh	4
^{211}At	7.2h	Therapy	^{209}Bi(α,n)	100	28	1/μAh	0.05-.01

Table 1: This table lists commonly used Cyclotron-Produced Isotopes, some of the possible nuclear reactions used to produce the isotopes, typical production yields and some key physical properties for the target and production isotopes.

It is convenient to categorize the cyclotrons into three broad (proton) energy ranges based on their primary function [7]. (For reasons based on efficiency and cost considerations, some facilities/manufacturers have chosen accelerators and reactions that also use deuterons and helium as a projectile.) These proton energy ranges are:

- Cyclotrons with proton energy less than 20 MeV are primarily used for producing positron emitting radio-nuclides. These PET isotopes tend to have short half-lives and the cyclotrons are located in regional centres/hospitals determined by the yield loss due to the delivery time from cyclotron to patient. Many of the cyclotrons have the capability of being shielded with close-packed steel and thereby reduce the need for the user to provide a heavily shielded bunker. The delivery time of the

radio-isotope, the patient dose requirement and the number of doses required per day lead to a cyclotron providing up to 50 μA per target. Many of the current cyclotrons have the capability of using multiple targets on each of two or more extracted beams.

- Cyclotrons with proton energies between 20 to 35 MeV are primarily used to produce many of the gamma-emitting radioisotopes (commonly used as imaging radio-isotopes for SPECT) as well as the production of several PET isotopes. The SPECT isotopes have medium half-lives and production generally takes place in dedicated facilities. The longer half-lives permit isotope delivery to more distant users and this leads to dedicated production facilities with high power targets and larger throughput.
- Cyclotron providing protons with energies of greater than 35 MeV are used in the production of a number of the isotopes used for radio-therapy. The primary need is for high current cyclotrons with currents in the 1mA range.

CYCLOTRON DESIGN CONSIDERATIONS

For the customer, the primary cyclotron specification is given by a minimum target yield for a given radio-isotope in the form of a particular molecule within a specified irradiation time. For the cyclotron designer, this user provided specification leads to a decision on the nuclear reaction to be used, the target material, the accelerated particle, the target chemistry, the energy and the cyclotron current on target. The accelerated particles must have adequate energy for the chosen nuclear reaction and adequate current to provide the required yields at that energy. Secondary specifications include; the number of targets, the target dimensions, the number of extracted beams (ports), shielding (facility) requirements, activation, and operating costs. Invariably, compromises are needed in order to arrive at a manageable facility budget.

Table 2 lists some of the important characteristics of the cyclotrons offered by many of the current industrial suppliers. The most common choice for the magnet is a conventional room temperature coil. Most manufacturers have the option of self-shielding for the cyclotrons when the maximum energy is less than 15 MeV. The customer must choose between vault (concrete) shielding versus the more expensive but compact arrangement of close packing steel around the cyclotron and targets. Earlier generations of cyclotrons accelerated mostly positive ions. Today, most of the cyclotrons accelerate H- and/or D- because of the ease of extracting multiple beams into targets that are separately shielded by steel or concrete. The choice of either internal or external targets impact the footprint of the system and also the radiation exposure for personnel servicing the cyclotron. For H- currents less than 200 μA an internal PIG ion source is the preferred cost effective choice. If H- currents greater than about 200 μA are required, then an external (Cusp) ion source is required. With internal targets and H+ acceleration, high currents are easily achievable with internal PIG type ion sources. Extraction of intense H+ beams invariably lead to severe component activation in the cyclotron.

CYCLOTRON SUPPLIERS

Commercial companies have responded to the varied user specifications with a number of basic cyclotrons with optional add-ons in an attempt to satisfy each particular need and budget. What follows is a list of several companies, arranged alphabetically and their key product specifications. A short comparative summary can be found in Table 2.

Advanced Cyclotron Systems Inc (ASCI)

ACSI fabricates and sells 14 MeV, 19 MeV (fixed and variable energy) 24 MeV and 30 MeV cyclotrons. Simultaneous dual extraction is available in each of the models. The 14 MeV cyclotrons are available in self- shielded and unshielded configurations. A new product line is the TR24 providing high-current, variable-energy extracted proton-beams in the energy range 15 to 24 MeV to partly bridge the energy gap between their 19 and 30 MeV models. The TR30 offers variable-energy extraction (15-30 MeV) with currents exceeding 1,200 A and simultaneous dual beams. The TR30 (TR30/15) can also be configured to provide dual-particle acceleration.

Advanced Biomarkers Technology (ABT)

ABT has recently introduced a new low power, small 'table-top' cyclotron with internal targets. The company website notes that the accelerator has an on-off switch, a target selector switch and a beam current switch. The cyclotron accelerates H+ from an internal ion source. The accelerator has a fixed-energy of 7.5 MeV, a target volume of 15 micro-litres and is designed to provide single-patient doses (millicuries) of 18F and 11C. At 1 A and 7.5MeV, 1 millicurie/minute of 18F is produced. Currents are in the range of 1 to 5 A. With shielding the total weight of the accelerator is 10.8 ton and only occupies about 2 square metres.

Best Cyclotrons Systems Inc (BSCI)

BSCI is bringing three new cyclotron models to market [8]. They are fabricating a fixed-energy 14 MeV H- cyclotron with internal ion source, having a total extracted current of up to 100 μA into four external beams. Their 35 MeV cyclotron has an external CUSP type ion source, two simultaneous extracted beams with energy variable from 15-35 MeV and an advertised maximum extracted current greater than 1.5 mA. A 70 MeV model accelerates H- from an external ion source, has simultaneous variable-energy extraction from 35-70 MeV into two external beam lines.

China Institute of Atomic Energy (CIAE)

CIAE is presenting, at this conference, details of their plans for 14 MeV and 70 MeV cyclotrons for the production of medical isotopes [9, 10, 11]. Both have external ion H-/D- ion sources. The CYCIAE-70 provides 700 A of extracted H+ at 35 - 70 MeV and 40 A of D+ at 18 - 33 MeV. The CYCIAE-14 is designed to provide two dual extraction ports servicing 4 different targets. It is a fixed-energy cyclotron providing up to 400 A at 14 MeV.

Efremov (NIIEFA)

The Efremov Institute supplies a cyclotron that accelerates negative hydrogen and deuterium ions, in a vertical plane, to energies of 18 and 9 MeV, respectively. The cyclotron uses a CUSP type external ion source and provides extracted currents of H/D at 100/50 A [12].

EuroMeV

EuroMeV offers the ISOTRACE superconducting cyclotron (based on the OSCAR-12 initially developed by Oxford Instruments). This cyclotron provides an extracted beam current up to 100 A at a fixed energy of 12 MeV. The cyclotron weighs only 3.8 tonnes and has a total operating power consumption of 40 kW.

GE Healthcare

GE Healthcare has two cyclotron products for PET, namely, MINItrace and PETtrace. MINItrace accelerates H- in a vertical oriented cyclotron that provides 50 A at a fixed-energy of 9.6 MeV. The PETtrace also accelerates in a vertical plane either H- /D- up to a fixed-energy of 16.5/8.6 MeV with extracted currents of 100/65 A. The MINItrace cyclotron features integrated shielding and fully automated operation during start-up, tuning and operation.

IBA

IBA markets cyclotrons at 3 (D), 10/5 (H/D), 11 (H), 18/9 (H/D), 30 (H) and 70/35 (H/D) MeV. Cyclone 3D is described at this conference [13]. Cyclone 3D was originally marketed to address the need for 15O in the early 90s. The original 4 pole geometry has been replaced by three poles to provide additional vertical focussing. Cyclone 10/5 is a fixed energy cyclotron with four extraction ports. Cyclone 11 is a new product line that features a fixed-energy, self-shielded cyclotron that accelerates H- up to 11 MeV [14]. The design is based on the Cyclone 10/5 cyclotron. Cyclone 18/9 is a fixed-energy cyclotron that accelerates H- up to 18 MeV and D- up to 9 MeV. Cyclone 18 Twin is a fixed-energy cyclotron that accelerate H- up to 18 MeV and that improves uptime and reliability by using two independent ion sources. Cyclone 30 is a fixed-energy cyclotron that accelerates H- up to 30 MeV and can extract two independent beams. Cyclone 30 XP is another new product line that accelerates proton, deuteron and alpha beams up to 30 MeV. Protons and deuterons are accelerated as negative ions and extracted by stripping and at variable energy. The alpha beam is accelerated as He++ and extracted with an electrostatic deflector [15]. Cyclone 70 is a multi-particle, fixed-energy cyclotron that accelerates H- up to 70 MeV as well accelerating alpha beams. The specifications for the Cyclone 70 installed in Arronax had the H- at variable energy from 35-70 MeV with a maximum current of 750 A, D- from 17-25 MeV at 50 A, He++ at 70 MeV and A and H2+ at a fixed 35 MeV and maximum current of 50 A.

KIRAMS

The Cyclotron Application Laboratory (KIRAMS) has developed two cyclotrons for radioisotope production. The KIRAMS-30 accelerates H- from an external ion source up to 30 MeV. The cyclotron extracts protons of up to 500 A into through two ports at energies from 15 – 30 MeV [16]. The KIRAMS-13 accelerates H- from an internal PIG ion source up to 13 MeV and extracts currents of up to 80 A through two ports.

Siemens

Siemens markets the Eclipse brand cyclotrons which were initially developed by CTI and sold under the RDS label. The Eclipse cyclotrons accelerate H- up to a fixed energy of 11 MeV. The Eclipse HP provides 60 A into each of two beam lines and onto a carousel that holds up to 2 targets whereas the RD provides 40 A on a carousel that holds up to 8 targets in each of two beam lines. The Eclipse ST is a self-shielded HP.

Sumitomo

Sumitomo has built a series of cyclotrons under the names HM-7, HM-10, HM-12S, HM-12 and HM-18. Each accelerates both H- and D-. The HM-7 is a fixed energy cyclotron that has a self-shielding option and provides H/D at an energy of 7/3.5 MeV. The HM-10 is also a fixed-energy cyclotron that accelerates H-/D- to 9.6/4.8 MeV, can be equipped with 5 targets and has a self shielding option. The HM-12 cyclotron accelerates H-/D- up to 12/6 MeV, has two extraction ports that can each be equipped with up to 4 targets. The HM-12S is the shelf-shielded version of the HM-12. The HM-18 cyclotron is also a fixed energy cyclotron accelerating H-/D- up to 18/10 MeV, has two extraction ports each accommodating four targets. All of the Sumitomo cyclotrons use internal PIG ion sources.

Others

There are numerous facilities still using cyclotrons that were manufactured by companies that no longer offer cyclotrons for sale. These cyclotrons include products originally manufactured and sold by Scanditronix (MC series cyclotrons), The Cyclotron Corporation (TCC series cyclotrons), Japan Steel Works (JSW/BC series cyclotrons), and Computer Technology and Imaging Inc (CTI with their CTI-RDS, Radio Isotope Delivery System cyclotrons).

Company Name	Cyclotron Model	Particles	Energy (MeV)	Beam Current (μA)	Ion Source Type	Peak Field (T)	Hill Valley ratio	RF Freq. (MHz)	Plane Of Accel	Cyc. Weight (t)	Shield Weight (t)	Power (kW)
ACSI	TR14	H-	14	>100	Cusp	2.1		74	V	22	40	60
ACSI	TR19/(9)	H-/(D-)	19/(9)	>300/100	Cusp	2.1		74/37	V	22		65
ACSI	TR24	H-	24	>300	Cusp	2.1	4	83.5	H or V	84		80
ACSI	TR30/(15)	H-/(D-)	30/(15)	1500/400	Cusp	1.9			H	56		150
ABT	TableTop	H+	7.5	5	PIG	1.2		72	H	3.2	7.6	10
Best	BSCI 14p	H-	14	100	PIG			73	H	14		60
Best	BCSI 35p	H-	15-35	1500	Cusp			70	H	55		280
Best	BSCI 70p	H-	70	800	Cusp	1.6		58	H	195		400
CIAE	CYCCIAE14	H-	14	400	Cusp							
CIAE	CYCCIAE70	H-	70	750	Cusp							
NIIEFA	CC-18/9	H-/D-	18/9	100/50	Cusp			38.2	V	20		60
EUROMEV	Isotrace	H-	12	100	Cusp	2.36	(SC)	108	V	3.8		40
GE	MINItrace	H-	9.6	>50	PIG	2.2	~2	101	V	9	40	35
GE	PETtrace	H-/D-	16.5/8.6	>100/65	PIG	1.9	~1	27.2	V	22	47	70
IBA	Cyclone 3	D+	3.8	60	PIG	1.8	1	14	H	5		14
IBA	Cyclone 10/5	H-/D-	10/5	>100/35	PIG	1.9	~5	42	H	12	40	35
IBA	Cyclone 11	H+	11	120	PIG	1.9	~5	42	H	13	52	35
IBA	Cyclone 18/9	H-/D-	18/9	150/40	PIG	1.9	~5	42	H	25		50
IBA	Cyclone 30	H-/(D-)	30 /(15)	1500/?	Cusp	1.7	14		H	50		180
IBA	Cyclone 70	H-/α										
IBA	Cyclone 70 (Arronax)	H-/D- /H_2^+/He^{++}	30-70/15-35 /17.5/70	2x350/50 /50/35		1.7	14	66/30	H	125		350
KIRAMS	KIRAMS-30	H-	15-30	500	Cusp	1.9	8	64	H			
KIRAMS	Kotron-13	H+	40372	100	PIG	2	2	77.3	H	20	80	18?
Siemens	Eclipse RD	H-	11	2x40	PIG	1.9	~13		H	11	39	35
Siemens	Eclipse HP/ST	H-	11	2x60	PIG	1.9	~13	72				35
Sumitomo	HM-7	H-/D-	7.5/3.8						V		30	
Sumitomo	HM-10	H-/D-	9.6/4.8						V		52	
Sumitomo	HM-12/S	H-/D-	12/6	>60/30	PIG	2	~5	45	V	11	56	45
Sumitomo	HM-18	H-/D-	18/10	>90/50	PIG	2	~4	45	H	24	86	55

Table 2: This table lists current manufactures of cyclotrons used in radioisotope production for medical applications, their cyclotron models, and compares some key cyclotron specifications.

FUTURE

The total number of cyclotrons producing radionuclides is gradually growing to meet the expanding needs of nuclear medicine. In some regions, physicians now require a PET/CT scan before setting up a treatment protocol for certain diseases. This growth that has been observed in the past decade is expected to continue. New cyclotron models adapted to current needs are being designed.

The recent shortage of reactor produced 99- molybdenum used in 99m-techecium generators, has revived interest in the possibility of accelerator production. 99Mo is currently produced in older research reactors using highly enriched uranium (HEU). Both the security issue surrounding the safe storage of the HEU and also the expected lifespan of these older reactors has given urgency to pursuing alternate production methods. Approximately 80% of nuclear medicine procedures currently use 99mTc. The molybdenum isotope of mass 100 (100Mo) bombarded with ~15 - 19 MeV protons could be used to supply regional amounts of 99mTc directly through the (p, 2n) reaction [17, 18]. High-current cyclotrons are needed to meet the demand and to avoid the build-up of ground-state contamination, but the high-power target technology will be challenging.

The primary PET isotopes are 11C and 18F. In most cases the cyclotrons producing these isotopes run in batch mode producing 10s of curries per run. Patient doses on the other hand tend to be a factor of 1000 smaller; i.e.; 10s of millicurries. Hospital clinical users have expressed interest in small machines that provide single patient doses with the touch of a button. Visionaries are suggesting that we will soon have small 'table-top' accelerators with targets using micro-fluidics to carry out the chemistry on a 'chip', providing the radio-pharmaceuticals in patient doses prior to each procedure. One supplier (Advanced Biomarkers Technology, USA) has already developed a ‘table top’ cyclotron which promises to provide patient doses on demand.

REFERENCES

[1] B. F. Milton, 'Commercial Compact Cyclotrons in the 90’s', proceedings of the 14th International Conference on Cyclotrons, World Scientific Pulblishing Co., (1996)
[2] C Birattari et al, Biomedical applications of cyclotrons and review of commercially available models, Journal of Medical Engineering & Technology, Volume 11, Number 4, pages 166-167 (1987)
[3] Ernest O. Lawrence and M. Stanley Livingston, 'The Production of High Speed Light Ions Without the Use of High Voltages', Phys. Rev. 40, 19-35, (1932)
[4] T J Ruth et al, Radionuclide Production for the Biosciences, Nucl. Med. Biol. Vol 16, No 4, pp 323-336 (1989)
[5] Cyclotron Produced Radionuclides: Physical Characteristics and Production Methods, IAEA Technical Report No. 468, Vienna (2009)
[6] Directory of Cyclotrons used for Radionuclide Production in Member States 2006 Update, IAEA Technical Report IAEA-DCRP/2006, Vienna (2009)
[7] Cyclotron Produced Radionuclides: Principles and Practice, IAEA Technical Report No. 465, Vienna (2008)
[8] R. R. Johnson et al, 'New High Intensity Compact Negative Hydrogen Ion Cyclotrons', these proceedings
[9] J Zhong et al, 'The Physics Design of Magnet in CYCIAE-14', these proceedings
[10] S. An et al, 'Physics Design and Calculation of the CYCIAE-70 Extraction System', these proceedings
[11] M Li et al, 'The Injection Line and Central Region Design of CYCIAE-70' these proceedings
[12] P. V. Bogdanov et al, 'New Compact Cyclotron CC-18/9 Designed and Manufactured in NIIEFA, proceedings of RuPACC 2006, Novosibirsk, Russia, pp 70-72
[13] S Zaremba et al, 'Upgrade of the IBA Cyclone 3D Cyclotron', these proceedings
[14] V Nuttens et al, 'Design of IBA Cyclone 11 Cyclotron Magnet', these proceedings
[15] E Forton et al, 'Design of IBA Cyclone 30XP Cyclotron Magnet'. these proceedings
[16] K Kang et al, 'Status of KIRAMS-30 Commissioning', these proceedings
[17] A. Mushtaq, Medical Isotope Production, the Non Proliferation Review, vol 16, # 2, pp 285-292, (2009)
[18] B. Scholten et al, 'Excitation functions for the cyclotron production of 99mTc and 99Mo, Applied Radiation and Isotopes, 51, 60-80, (1999)

MEDICAL CYCLOTRON AND DEVELOPMENT IN CHINA

Mingwu Fan, Huazhong University of Science and Technology, Wuhan, P.R.China
Tianjue Zhang, China Institute of Atomic Energy, Beijing, P.R.China
Jiawen Xia, Institute of Modern Physics, Chinese Academy of Sciences, P.R. China

Abstract

The first medical cyclotron CYCIAE-30 in China has been designed and constructed by China Institute of Atomic Energy (CIAE), and its construction was finished in 1995. Since then, medical cyclotron got developed in China, several cyclotrons had been constructed, and some medical experiments and practice had been done with those cyclotrons. Now medical cyclotron develops even quickly in China, several medical cyclotrons are under design and construction. Meantime, a compact cyclotron virtual prototyping was developed to help the cyclotron design and reduce cyclotron R & D cost.

INTRODUCTION

Cyclotron, especially medical cyclotron had a slow development in China in the past few decades, up to now ,there are just a few cyclotrons in China which had be designed and constructed by Chinese accelerator groups themselves, the main medical cyclotrons or cyclotrons on which medical research or practice be done are the CYCIAE-30 and the HIFRL, CYCIAE-30 is a high intensity medical cyclotron which affiliate to China Institute of Atomic Energy (CIAE), The HIFRL is the two-cyclotron complex at Institute of Modern Physics, Chinese Academy of Science (IMP). Recent years medical cyclotron has a quick development, a 10MeV high intensity cyclotron synthesis experimental platform be constructed in CIAE in 2009, several medical cyclotrons are been under designing or construction. Also the technology of cyclotron had gotten development in China especially the Virtual Prototyping was adopted and developed at Huazhong University of Science and technology [1].

MEDICAL CYCLOTRONS AT CHINA INSTITUTE OF ATOMIC ENERGY

There are two cyclotrons at CIAE, one is the CYCIAE-30 (fig.1) which was designed and constructed by Chinese and has been operated since 1995, and it is the first high intensity medical cyclotrons used for accelerated mass production of isotope. Fig 2 shows the total yearly beam times at the first several years.

The other one is a compact cyclotron [2] (fig.3), it is the main part of a high intensity cyclotron experimental platform (CYCIAE-CRM), and it is also the first compact cyclotron which China has Independent Intellectual Property Rights. The main beam parameters of the machine are show in table 1:

Figure 1: CYCIAE-30

Table 1: main parameters of CYCIAE-CRM

Parameters	Value
Accelerated particle	H^-
Extraction energy	10Mev
Internal beam intensity	430μA
Accelerate efficiency	94.5%
Extraction efficiency	99.87%

The success of this machine is a significant affair, it can be used for the developing of PET-cyclotrons which be used for diagnose of cancer and other diseases, this region in China was monopolized by foreign companies in the past.

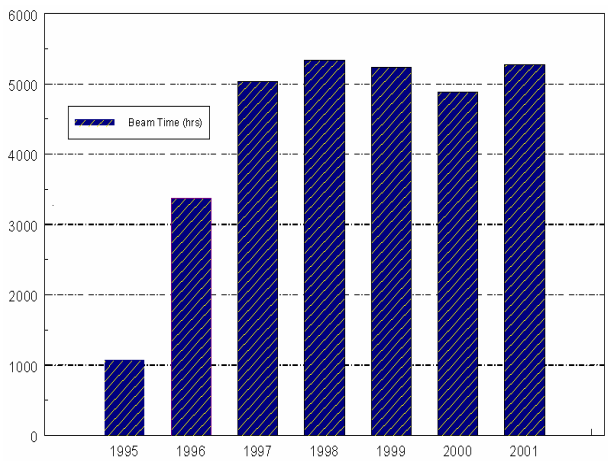

Figure 2: beam time of CYCIAE-30

Figure 3: CYCIAE-CRM cyclotron

Now a PET cyclotron prototyping CYCIAE-14 (fig.4) is under construction at CIAE [3], it will be finished in the next 2 years, it can product not only the normal PET particles 11C, 15O, 13N, 18F but also the isotopes 64Cu, 124I, 99mTc. The main parameters of the machine are show in table 2.

Table 2: Parameters of CYCIAE-14

Parameter	value
Particle accelerated	H-
Final energy	14.6MeV
Bmin/Bmax	2.0kGs/18.5kGs
Radius of sector magnet	500mm
Sector angle	52o
Hill gap	23-26mm
Valley gap	318mm
Outer radius of magnet	880mm
Height of Magnet	1066mm
Dee Voltage	50kV
RF frequency	73.02MHz
Harmonic mode	4
Extracted particle	Proton

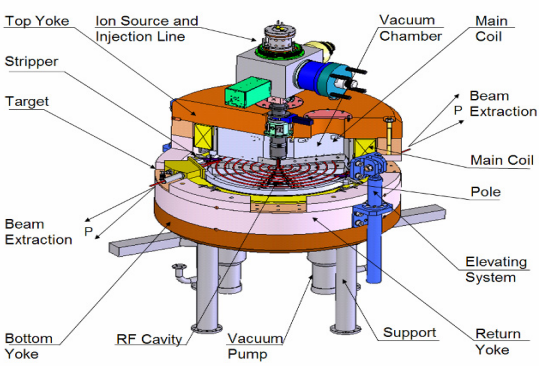

Figure 4: The sketch of CYCIAE-14

MEDICAL RESEARCH AND PRACTICE ON THE CYCLOTRONS AT IMP

Comparison to CIAE cyclotron technology development, IMP did a lot of works on biomedical research and practice using the cyclotron system - HIRFL (fig.5), HIRFL consists of two ECR ion source (one is a normal ECR source, and the other is a superconductive ECR source), two cyclotrons (The injector is a sector focus cyclotron, it is an upgrade of a classical cyclotron, the energy constant is K=69. The main accelerator is a separate sector cyclotron which energy constant is K=450.) , and several beam transport lines.

The biomedical research begun in middle of the 1990's at IMP, the aim is focus on:

(1) Understanding the biological effects induced by heavy ions.

(2) The mechanisms of the action between heavy ions and biological material.

(3) The application of heavy-ion irradiation in medicine and biology.

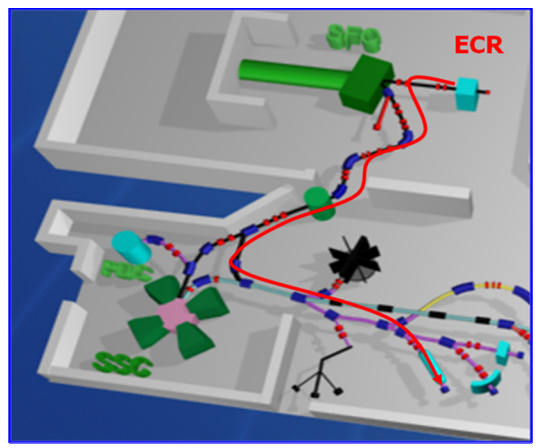

Figure 5: Layout of HIRFL

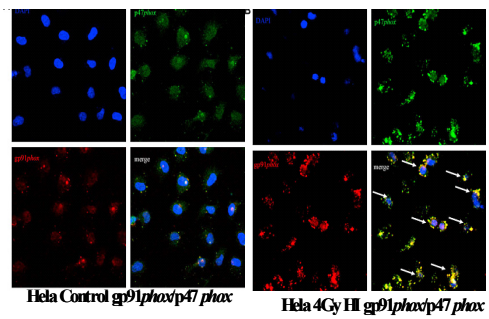

Figure 6: The effect of NADPH oxidise-mediated generation of reactive oxygen species on cancer cell DNA injure induced by heavy-ions

Basic Researches on Biomedical Related to Heavy Ion Irradiation

Biomedical group at IMP have been doing a series researches to understand the biological effects induced by heavy ions and the mechanisms of the action between heavy ions and biological material, fig.6 to fig.10 show some results of those researches and the results.

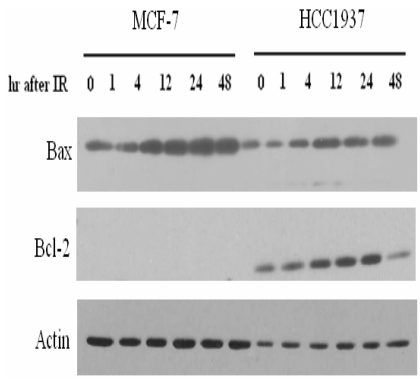

Figure 7: BRCA1 answers for the cancer cell death induced by heavy-ion irradiation by adjusting Bcl-2 protein

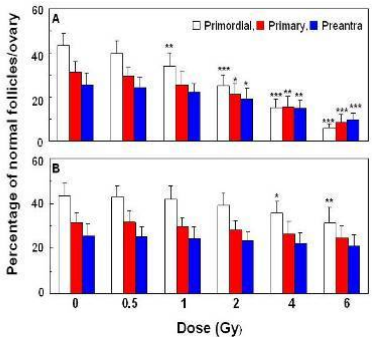

Figure 8: Affections of heavy-ion irradiations on procreating cells and genetics

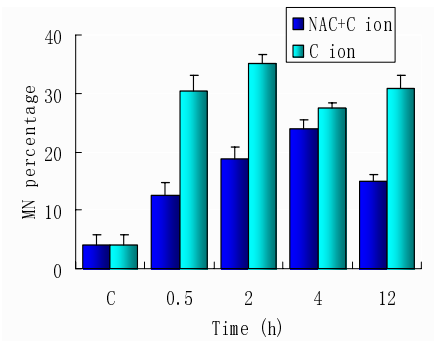

Figure 9: affections of heavy-ion irradiations on the immunity system of mice

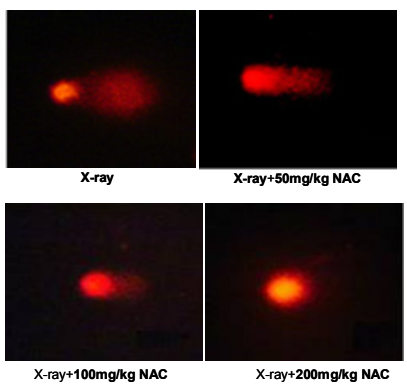

Figure 10: conservation of antioxidant of injure induced by heavy ions

Fig.6 and fig.7 show the cell injure induced by heavy-ions and their corresponding mechanisms. Fig.8 shows the affections of heavy-ion irradiations on procreating cells and genetics. Fig.9 and fig.10 show the affections of heavy-ion irradiations on the immunity system of mice, conservation of antioxidant of injure induced by heavy ions.

Basic Researches on Heavy-Ion Tumour Therapy

Some techniques had been adopted by IMP medical group about heavy-ion tumour therapy researches, such as siRNA and the protein group method, fig.11 to fig.15 show the techniques and the results.

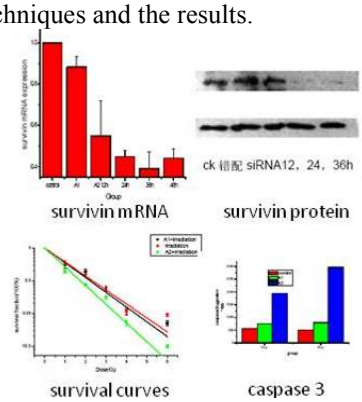

Figure 11: siRNA restraints the answer of surviving protein

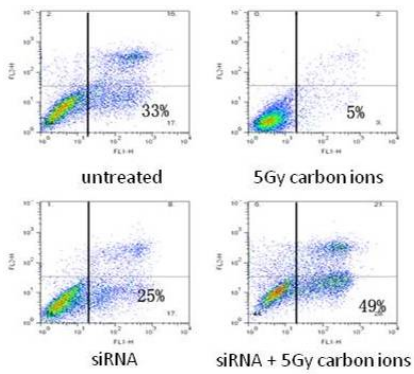

Figure 12: siRNA increase sensitivity of tumor cell to heavy-ion irradiaton

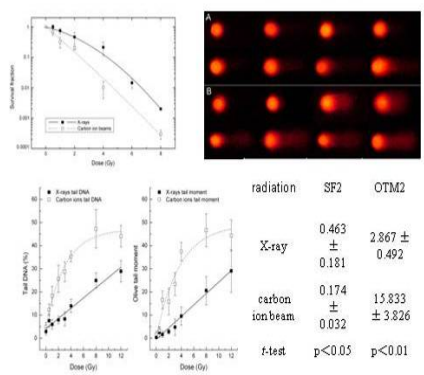

Figure 13: The affection of heavy ion irradiation in mammal cell DNA injure

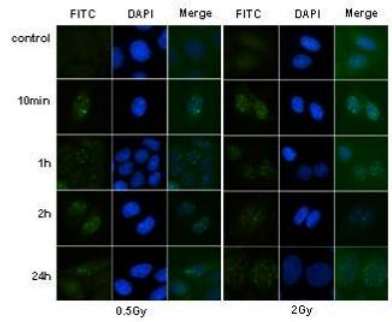

Figure 14: The affection of heavy ion irradiation in mammal cell DNA repair

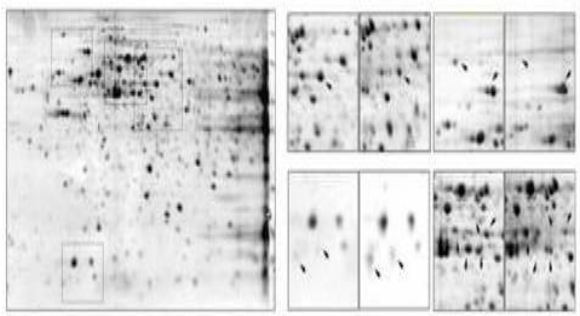

Figure 15: The protein group method in ion irradiation cancer biomedical

Practice of Tumour Therapy at IMP

Up to now, there are 103 patients who has a superficial tumour had been treated at IMP. Fig.16 and fig 17 show some results of the therapy.

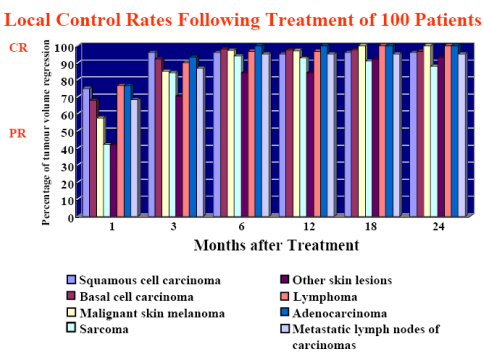

Figure 16: Local control rate

Figure 17: Some typical patient

In these figures the horizontal coordinate is the month after therapy, the bars are squamous cell carcinoma of skin, Basal cell carcinoma of skin, malignant skin melanoma, Sarcoma, Other skin lesions, Lymphoma, Breast cancer and Metastasis lymph nodes of carcinomas

MEDICAL CYCLOTRONS UNDER CONSTRUCTION AT IMP

Now IMP is designing a cancer therapy machine, it consists a injector cyclotron and a main accelerator synchrotron, the sketch (fig.18) and some parameters (table.3) of the injector cyclotron are show below.

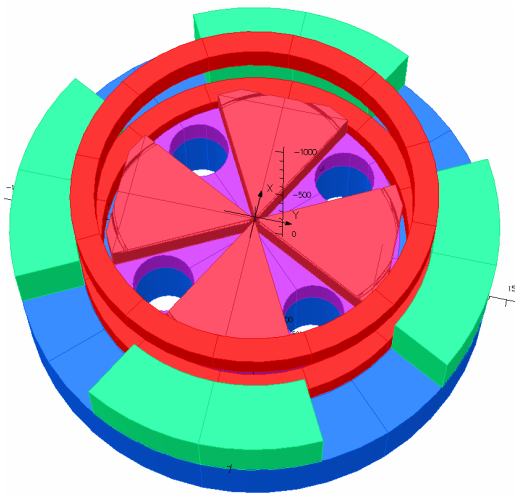

Fig.18: Sketch of the injector cyclotron

Table.2: parameters of the injector cyclotron

Accelerated Ion Species	$^{12}C^{6+}$
Extraction Energy	7Mev/u
Ex-Beam Intensity (C)	10euA
Energy Spread	±1%
Emittance	20-25 π mm.mrad
Frequency	31.02MHz
Accelerating Voltage	70KV
Degree of Dees	30°
Dee Number	2
Stability of Phase	±1°
Stability of Voltage	$\pm 5\times10^{-4}$/24hour
Stability of Frequency	$\pm 1\times10^{-6}$/24hour
Power Source Number	2
Power	50KW

PROGRESS IN VIRTUAL PROTOTYPING FOR DESIGN OF COMPACT CYCLOTRON

Virtual Prototyping (VP) has been developed since 1990s with the strong demand for products to short R&D period and to reduce cost, the virtual prototyping technology had be adopted and made progress at Huazhong University in China.

CVPP is the development of VP, the primary goal is to provide an integrate environment for multi-domain design or analysis components covering beam dynamics, the cyclotron magnet, the RF cavity etc. In CVPP, the design, theoretical analysis, manufacture, assemble, operation and maintenance could be studied and adjusted by an interactive way, thus the complete machine can be optimized from a top view.

Under the integrate design environment CVPP, a compact cyclotron had been studied at Huazhong University. The pictures from fig.19 to fig.22 are the virtual prototype model and main parts of the 10 MeV internal ion source cyclotron - CYCHU-10.

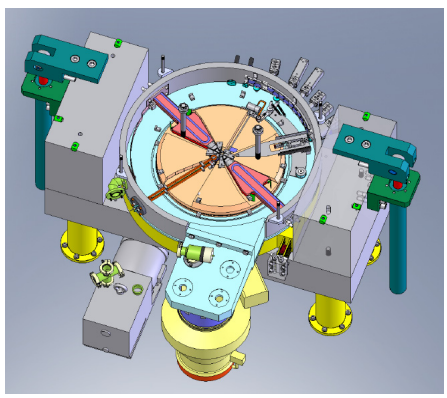

Figure 19: The virtual prototype model of CYCHU-10

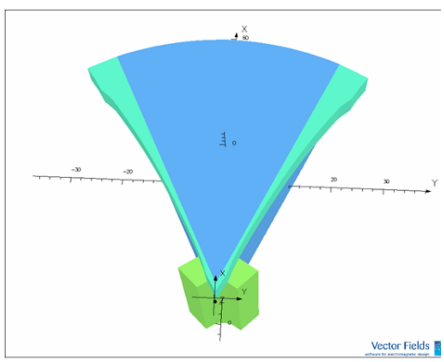

Figure 20: Optimized one sector magnet pole model

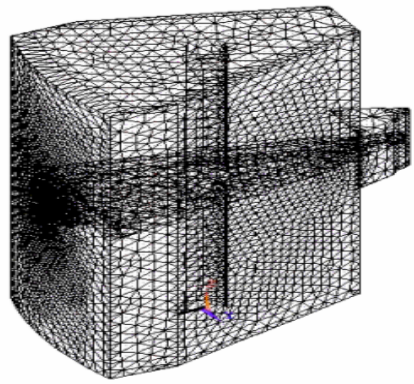

Figure 21: The FEM model of a 65MHz cavity

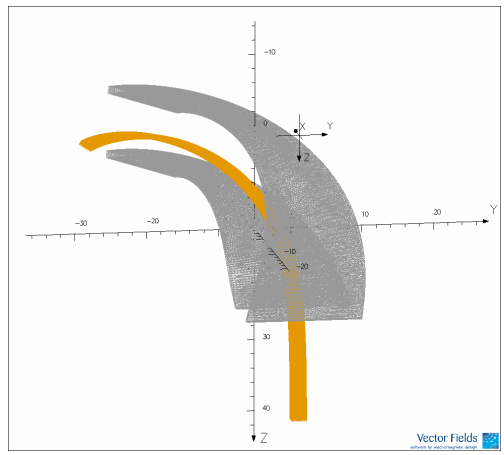

Figure 22: The spiral inflector FEM model and beam trajectories

ACKNOWLEDGEMENTS

The authors acknowledge with thanks the help and support provided by Dr Qiang Li, Dr XinGuo Liu.

REFERENCES

[1] Fan Ming-Wu, Qin Bin, Xiong Yong-Qian et al, Chinese Physics C 32 S1 (2008) 234.

[2] Zhang Tian-Jue, Li Zhen-Guo, Chu Cheng-Jie, et al, Chinese Physics C 32 S1 (2008) 237.

[3] Tianjue Zhang, Yinlong Lu, Zhiguo Yin, et al., Overall Design of CYCIAE-14, a 14MeV PET Cyclotron, the 10th European Conference on Accelerators in Applied Research and Technology (ECAART10 - ATHENS, SEPT. 13-17, 2010).

BNCT SYSTEM USING 30 MEV H- CYCLOTRON

T. Mitsumoto, K. Fujita, T. Ogasawara, H. Tsutsui, S. Yajima, Sumitomo Heavy Industries, Ltd., Tokyo, Japan
A. Maruhashi, Y. Sakurai, H. Tanaka, Kyoto University Research Reactor Institute, Osaka, Japan

Abstract

Kyoto University and Sumitomo Heavy Industries, Ltd. (SHI) have developed an accelerator-based neutron source for Boron Neutron Capture Therapy (BNCT) at the Kyoto University Research Reactor Institute (KURRI). In order to obtain 10^9 n/cm^2/sec epithermal neutrons for cancer treatment, a newly designed 30 MeV H- AVF cyclotron named HM-30 was constructed and is being operated. With newly developed spiral inflector, the beam current in the central region can exceed 2 mA. The cyclotron is operated stably at 1 mA. Extracted proton beam is expanded by two scanner magnets in order to moderate heat concentration on the beryllium target, which is directly cooled by water to endure 30 kW heat load. Fast neutrons are emitted from the target, and moderated to epithermal region by a moderator which consists of lead, iron, polyethylene, etc. Thermal neutron flux in a water phantom is measured by gold wire, which is consistent with the calculation using MCNPX. Preclinical studies are being carried out with 10B-p-Borono- phenylalanine (BPA).

INTRODUCTION

In BNCT [1], ^{10}B is selectively taken into the malignant tissues by suitable boron delivery agent such as BPA and sodium borocaptate (BSH). Exposure of thermal neutron flux generates energetic alpha particles and ^{7}Li nuclei, which kill the malignant tissues at the cellular level.

For clinical research of BNCT, thermal neutrons have been provided mainly by nuclear reactors [2,3]. Since it is inappropriate to install nuclear reactors in hospitals, many kinds of accelerator based neutron sources have been considered [4,5,6].

One approach is combination of a high current (~100 mA) low energy (~2.5 MeV) proton accelerator and a lithium target [4]. With this combination, fast neutron yield in the target is 1×10^{14} n/sec, for irradiating 2×10^9 n/cm^2/sec thermal neutrons in tumor.

A serious problem of this approach is that the heat load in the lithium target (~250 kW) is too high. Using a lower beam current (~2.8 MeV, ~20mA) has been proposed [5,6]. This approach sacrifices the neutron yield, nevertheless the heat load is still around 60 kW, and it is too high for the lithium target.

Another approach is to use a middle energy (10~50 MeV) high current (1~3 mA) proton cyclotron and a beryllium target. With a 30 MeV proton cyclotron, 1.9×10^{14} n/sec fast neutrons can be obtained at 1 mA, but the heat load is only 30 kW.

KURRI and SHI started developing the accelerator based neutron source for BNCT in 2007. In order to get high flux neutrons, we selected a combination of the 30 MeV proton beam and the beryllium target. A new AVF cyclotron named HM-30 was designed to generate 30 MeV proton beam with the maximum current of 2 mA.

At the same time, an irradiation system was also designed. Since the thermal neutron does not reach the inner part of a human body, the application of epithermal neutron (0.5 eV ~ 40 keV, in our definition) is more preferable. An epithermal neutron irradiation system optimized for the 30 MeV proton beam was designed with MCNPX [7].

The BNCT system was installed at KURRI in the southern part of Osaka prefecture in 2008. The facility layout is shown in Fig. 1. It is composed of a HM-30 cyclotron, a beam transport system, an irradiation and treatment system with auxiliary systems.

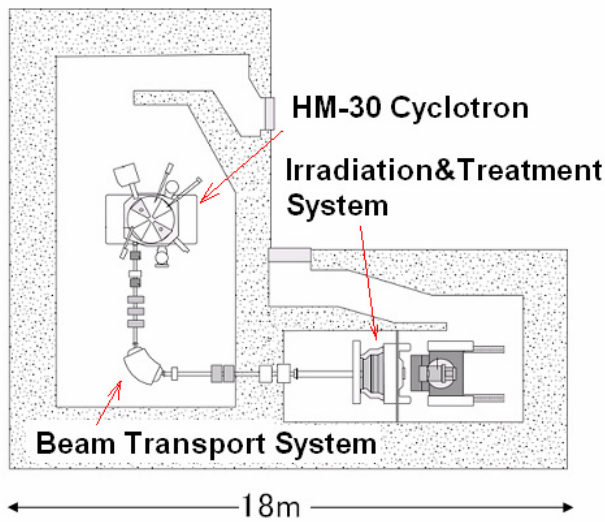

Figure 1: Layout of the cyclotron BNCT system at KURRI.

HM-30 CYCLOTRON

The HM-30 cyclotron, shown in Fig. 2, accelerates H- to 30 MeV. The proton beam is extracted by a carbon foil stripper. Main specifications are listed in Table 1.

Injection

A volume cusp type H- ion source (30 keV, 15 mA DC) is used, since it provides high beam current. The normalized effective emittance is around 1 π mm-mrad. The low energy beam transport line consists of two solenoid coils and one buncher. The full beam size at the entrance of the inflector is 6 mm by simulation.

Table 1: Main specifications of HM-30 cyclotron

Particle	Negative hydrogen ion
Injection Energy	30 keV
Injection method	Axial injection
RF frequency	73.1 MHz
RF accelerating voltage	200 kV/turn
Harmonic number	4
Extraction method	Foil stripping
Extraction energy	30 MeV
Extracted beam current	1 mA (2 mA is possible)
Size	W 3.0m × D 1.6m × H1.7m
Weight	60 tons

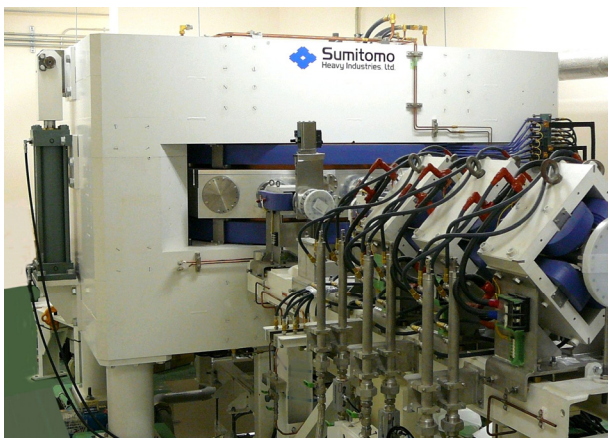

Figure 2: HM-30 cyclotron.

Acceleration

The H^- beam is axially injected via a spiral inflector. Parameters of the inflector and the position of RF accelerating gaps were optimized for maximizing the beam transmission and minimizing the precession of the beam orbit. For optimization, the magnetic field of the sector magnet was calculated with TOSCA [8] and was also measured with a Hall probe. Electric fields in the spiral inflector and in the first four RF accelerating gaps were calculated with TOSCA. Beam tracking was done with Runge-Kutta code. As a result, the beam off-center value is less than 2 mm.

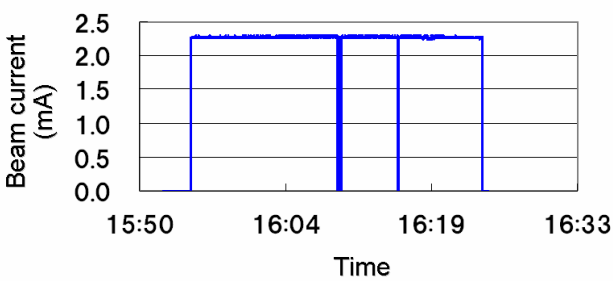

Figure 3: Beam current at center region (R=50 mm).

The beam current measured at the central region with a movable probe is 2.3 mA, as shown in Fig. 3. Since the beam is stable in 30 minutes, it is possible to operate it for medical treatment. There are some short stops by sparks at the cyclotron cavity. But the operation restarts automatically within a few seconds.

No significant beam loss is observed with the movable probe after three turns of the beam acceleration, which indicates the magnetic field error is within the tolerance.

Extraction

The proton beam is extracted by the carbon foil stripper. Although the cyclotron is designed to generate 2 mA proton beam as a maximum, the operating beam current is limited to 1 mA due to the limitation of the facility. As shown in Fig. 4, the cyclotron is stably operated in 1 hour at 1 mA, which suffices the requirement for the medical treatment.

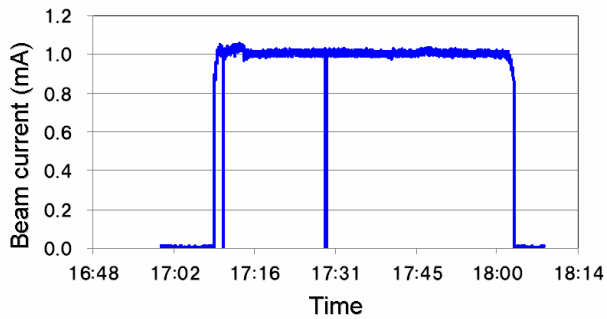

Figure 4: Beam current measured with DCCT just before the beryllium target. In this case, the current at the ion source is 6mA, and the RF buncher is off.

BEAM TRANSPORT SYSTEM

The 30 MeV beam transport system has one 90 degree bending magnet for analyzing energy and five quadrupole magnets for beam focusing.

Proton beam is expanded by two scanner magnets in order to avoid heat concentrating on the target.

Beam current is monitored by DCCT, and integrated to adjust the irradiation time. This is one of the advantages of the beam accelerators over the nuclear reactors.

IRRADIATION AND TREATMENT SYSTEM

The irradiation and treatment system is shown in Fig. 5.

The target is 190 mm diameter beryllium. It is directly and effectively cooled by water to endure ~30 kW heat load.

The neutron yield by $^9Be(p,n)^9B$ reaction is 1.9×10^{14} n/sec/mA^{-1}, by ENDF/B-VII proton data [9]. The neutron spectrum from the target has a peak around 1 MeV and

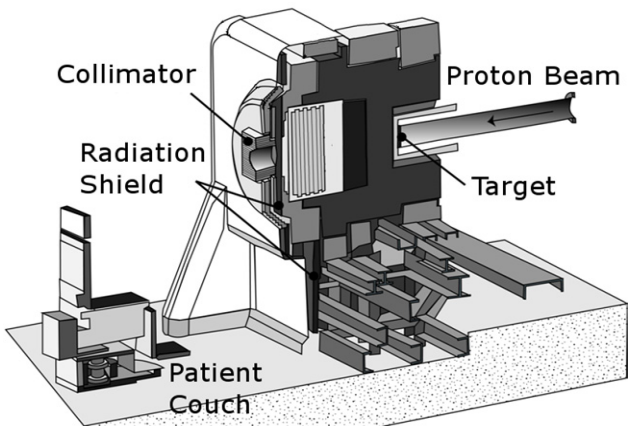

Figure 5: Irradiation and treatment system.

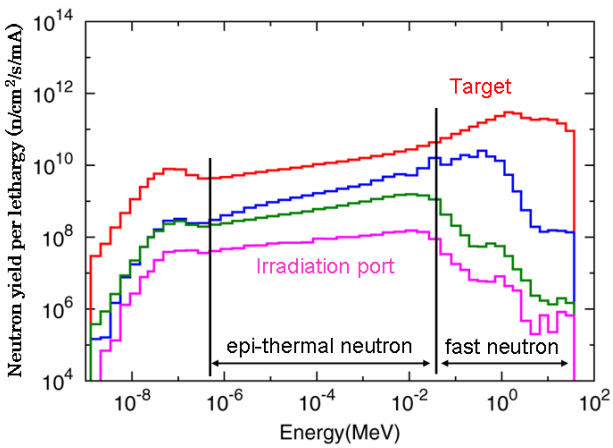

Figure 6: Neutron spectra calculated with MCNPX. Red, blue, green, pink lines are in the target, iron, calcium fluoride, and irradiation port, respectively.

long tail, as shown in Fig. 6. Fast neutrons are moderated to epithermal neutrons by lead, iron, aluminum and calcium fluoride. A neutron collimator made of polyethylene including 50% lithium fluoride is placed near the patient. The patient couch can be used as both a bed and a chair.

The thermal neutron flux in a water phantom is measured by an activation method. As shown in Fig. 7, the peak flux in the phantom is 1.8×10^9 neutron/cm^2/sec at 20 mm from the surface. The measured distributions are in good agreement with the calculated distributions by MCNPX and ENDF/B-VII. Using this neutron beam, mouse and human cell irradiation tests have been performed since July 2009.

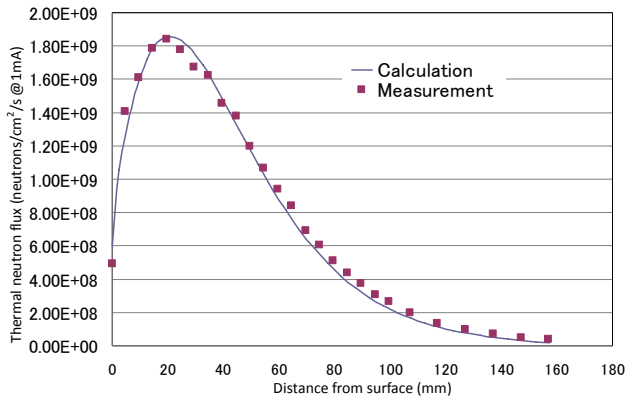

Figure 7: Thermal neutron flux in a cylindrical phantom, as a function of the distance from surface of the phantom.

SUMMARY AND FUTURE PLAN

The accelerator based neutron source for BNCT has been constructed. The proton beam of 30 MeV-1 mA by a newly developed cyclotron produces the thermal neutron flux of 1.8×10^9 neutron/cm^2/sec in the phantom. Preclinical studies have been carried out with ^{10}B compounds.

Now we are working for obtaining approval of medical product registration in FY2012.

REFERENCES

[1] G. L. Locher, Am. J. Roentgenol. 36 (1936) 1.
[2] http://www.rri.kyoto-u.ac.jp/en/
[3] http://sangaku.jaea.go.jp/3-facility/04-facility/13-jrr4.html , in Japanese.
[4] O. A. Anderson et al., EPAC1994 (1994) 2619.
[5] E. Forton et al., Appl. Radiat. Isot. 67 (2009) S262.
[6] D. A. Swenson, LINAC08 (2008) 220.
[7] D. B. Pelowitz, LA-CP-05-0369 (2005).
[8] http://www.vectorfields.co.uk/
[9] M. B. Chadwick et al., Nucl. Data Sheets, 102 (2006) 2931.

List of Authors

Bold papercodes indicate primary authors

Institutes List

AEC
Chiba, Japan
- Kamiya, T.
- Okada, T.
- Takahashi, Y.

Agricultural, Medical & Industrial Research School
Gohadasht, Iran
- Sadeghi, M.

ALTEK
San Gregorio (CATANIA), Italy
- Longhitano, A.

ASD
Garden Bay, Canada
- Gelbart, W.Z.

ASIPP
Hefei, People's Republic of China
- Hu, C.D.
- Jiang, C.C.
- Liang, L.Z.
- Liu, S.
- Wei, J.L.
- Xie, Y.H.
- Xie, Y.L.

ATOMKI
Debrecen, Hungary
- Kormány, Z.

BCSI
Vancouver, BC, Canada
- Du, D.
- Gyles, W.
- Johnson, R.R.
- Sabaiduc, V.
- Suthanthiran, K.

CAEP/IFP
Mainyang, Sichuan, People's Republic of China
- Zhang, K.

CASIC
Beijing, People's Republic of China
- Wei, S.D.
- Xiao, H.C.
- Xie, Y.
- Yu, C.J.

Charite
Berlin, Germany
- Cordini, D.
- Heufelder, J.
- Stark, R.
- Weber, A.

CIAE
Beijing, People's Republic of China
- An, S.
- Bi, Y.J.
- Fei, K.
- Guan, F.P.
- Hu, W.P.
- Ji, B.
- Jia, X.L.
- Li, M.
- Li, P.Z.
- Li, Z.G.
- Lin, J.
- Liu, G.S.
- Lu, Y.L.
- Pan, G.F.
- Song, G.F.
- Wang, C.
- Wang, Z.H.
- Wei, S.M.
- Wen, L.P.
- Xie, H.D.
- Xing, J.S.
- Yang, F.
- Yang, J.J.
- Yao, H.J.
- Yin, Z.G.
- Zhang, S.P.
- Zhang, T.J.
- Zhao, Z.L.
- Zhong, J.Q.

CYRIC
Sendai, Japan
- Sakemi, Y.

DAE/VECC
Calcutta, India
- Ahammed, M.
- Ahmed, M.
- Bandyopadhyay, S.
- Bhandari, R.K.
- Bhattacharjee, T.
- Bhattacharya, S.
- Bhattacharyya, P.
- Bhattacharyya, T.
- Bhunia, U.
- Chakraborty, P.S.
- Chaudhuri, J.
- Das, T.

- De, A.
- Debnath, J.
- Dey, M.K.
- Dey, R.
- Dutta Gupta, A.
- Dutta, A.
- Gangopadhyay, P.
- Goswami, A.
- Hemram, B.
- Kumar, Y.
- Mallik, C.
- Mandal, A.
- Mandal, B.C.
- Mandal, N.
- Manna, B.
- Mukherjee, A.
- Murali, S.
- Nandi, C.
- Naser, Z.A.
- Pal, G.P.
- Pal, S.P.
- Pal, S.
- Panda, U.
- Pandit, V.S.
- Paul, S.
- Pradhan, J.
- Prasad, J.S.P.
- Raj, P.R.
- Rao, Y.E.
- Rashid, M.H.
- Roy, S.
- Saha, S.
- Sarma, P.R.
- Seth, S.
- Sing Babu, P.
- Som, S.S.
- Sur, S.
- Thakur, S.K.
- Tiwari, T.P.

Fermilab
Batavia, USA
- Johnstone, C.

FZJ
Jülich, Germany
- Brings, R.
- Dietrich, J.
- Felden, O.
- Gebel, R.
- Hölzle, R.
- Maier, R.

GANIL
Caen, France
- Bertrand, P.
- Chautard, F.
- Savalle, A.

HUST
Wuhan, People's Republic of China
- Chen, D.Z.
- Chen, Z.
- Fan, M.
- Hu, X.
- Li, D.
- Liu, K.F.
- Qin, B.
- Xiong, Y.Q.
- Yang, J.
- Yu, T.

HZB
Berlin, Germany
- Denker, A.
- Rethfeldt, C.R.
- Röhrich, J.R.

IBA
Louvain-la-Neuve, Belgium
- Abs, M.
- Blondin, A.
- Delvaux, J.L.
- Deprez, S.
- Forton, E.
- Jongen, Y.
- Kleeven, W.J.G.M.
- Medeiros-Romao, L.
- Mehaudens, M.
- Nactergal, B.
- Neuvéglise, D.
- Nuttens, V.
- Peeters, F.
- Pinchart, M.
- Servais, T.
- Vandeplassche, D.
- Vanderlinden, T.
- Verbruggen, P.
- Zaremba, S.

IMP
Lanzhou, People's Republic of China
- Cai, X.H.
- Cao, Y.
- Chen, Y.X.
- Feng, X.M.
- Gao, D.Q.
- Gao, J.F.
- Gao, Y.L.
- Guo, Q.X.
- Han, G.H.
- Hao, H.F.
- He, Y.
- Li, A.P.
- Li, P.
- Li, X.N.
- Liu, W.
- Ma, L.Z.

- Ma, W.
- Ma, X.
- Man, K.D.
- Mao, R.S.
- Meng, J.
- Shangguan, J.B.
- Shi, A.
- Song, M.T.
- Su, X.M.
- Su, Y.L.
- Su, Y.W.
- Sun, L.P.
- Tang, Y.
- Tu, X.L.
- Wang, A.J.
- Wang, B.
- Wang, S.X.
- Wang, X.W.
- Wang, Y.
- Wu, J.X.
- Xia, J.W.
- Xie, C.L.
- Xin, J.Y.
- Xu, H.S.
- Xu, Z.
- Yan, H.B.
- Yan, H.H.
- Yang, J.C.
- Yang, J.J.
- Yang, W.Q.
- Yang, X.D.
- Yang, X.T.
- Yang, Y.P.
- Yang, Y.Q.
- Yao, Q.G.
- Yin, Y.
- You, Z.M.
- Yuan, P.
- Yuan, Y.J.
- Yuan, Z.D.
- Zhang, J.H.
- Zhang, J.Q.
- Zhang, S.H.
- Zhang, W.
- Zhang, X.L.
- Zhang, X.Q.
- Zhang, X.Z.
- Zhao, H.W.
- Zheng, J.H.
- Zhou, Z.Z.

INFN/LNL
Legnaro (PD), Italy
- Galatà, A.

INFN/LNS
Catania, Italy
- Calabretta, L.
- Caruso, A.C.
- Celona, L.
- Ciavola, G.
- Consoli, F.
- Gammino, S.
- Maggiore, M.M.
- Mascali, D.
- Piazza, L.A.C.
- Rifuggiato, D.
- Spartà, A.

iThemba LABS
Somerset West, South Africa
- Anthony, L.S.
- Botha, A.H.
- Conradie, J.L.
- Crombie, M.A.
- de Villiers, D.
- De Villiers, J.G.
- Delsink, J.L.G.
- Duckitt, W.
- Fourie, D.T.
- Hogan, M.E.
- Kohler, I.H.
- Lussi, C.
- McAlister, R.H.
- Mostert, H.W.
- Ntshangase, S.S.
- Pilcher, J.V.
- Rohwer, P.F.
- Sakildien, M.
- Stodart, N.
- Thomae, R.W.
- Van Niekerk, M.J.
- van Schalkwyk, P.A.

JAEA/QuBS
Takasaki, Japan
- Taguchi, M.

JAEA/TARRI
Gunma-ken, Japan
- Ishibori, I.
- Ishizaka, T.
- Kashiwagi, H.
- Kurashima, S.
- Miyawaki, N.
- Nara, T.
- Okumura, S.
- Yokota, W.
- Yoshida, K.
- Yuri, Y.
- Yuyama, T.

JINR/DLNP
Dubna, Moscow region, Russia
- Karamyshev, O.
- Shishlyannikov, P.
- Smirnov, V.L.

JINR
Dubna, Moscow Region, Russia
- Aleksandrov, V.
- Borisov, O.N.
- Glazov, A.A.
- Gulbekyan, G.G.
- Gurskiy, S.
- Karamysheva, G.A.
- Kazacha, V.I.
- Kazarinov, N.Yu.
- Kostromin, S.A.
- Morozov, N.A.
- Samsonov, E.
- Shevtsov, V.
- Shirkov, G.
- Syresin, E.
- Tuzikov, A.
- Vorozhtsov, S.B.

JYFL
Jyväskylä, Finland
- Aho, V.P.
- Ärje, J.
- Heikkinen, P. M.T.
- Kalvas, T.
- Kauppinen, J.A.
- Koivisto, H. A.
- Kommpula, J.P.
- Ropponen, T.
- Tarvainen, O.A.
- Toivanen, V.A.

KEK
Ibaraki, Japan
- Adachi, T.
- Sato, Y.
- Takayama, K.

KT Science Ltd.
Akashi, Japan
- Kawaguchi, T.

KURRI
Osaka, Japan
- Maruhashi, A.
- Mori, Y.
- Planche, T.
- Qin, B.
- Sakurai, Y.
- Tanaka, H.

KVI
Groningen, The Netherlands
- Beijers, J.P.M.
- Brandenburg, S.
- Hevinga, M.A.
- Hofstee, M.A.
- Kremers, H.R.
- Mironov, V.
- Mulder, J.
- Nijboer, T.W.
- Saminathan, S.
- Sen, A.
- van Goethem, M.J.
- Vorenholt, J.

Kyoto ICR
Uji, Kyoto, Japan
- Fujisawa, H.

LBNL
Berkeley, California, USA
- Alonso, J.R.
- Casey, P.W.
- Ferracin, P.
- Hodgkinson, A.
- Kireeff Covo, M.
- Leitner, D.
- Lyneis, C.M.
- Phair, L.
- Pipersky, P.
- Prestemon, S.
- Sabbi, G.L.
- Sessler, A.
- Todd, D.S.
- Wan, W.
- Yoshiki Franzen, K.

MIT
Cambridge, Massachusetts, USA
- Alonso, J.R.

MSU
East Lansing, Michigan, USA
- Berz, M.
- Makino, K.

Nagaoka University of Technology
Nagaoka, Niigata, Japan
- Jiang, W.

NCC, Korea
Kyonggi, Republic of Korea
- Kim, J.-W.

NCC
Goyang, Kyeonggi, Republic of Korea
- Park, Y.-H.

NIRS
Chiba-shi, Japan
- Hojo, S.
- Honma, T.
- Kanazawa, M.
- Miyahara, N.

- Muramatsu, M.
- Noda, K.
- Sakamoto, Y.
- Sugiura, A.
- Tashiro, K.

NSC/KIPT
Kharkov, Ukraine
- Barankov, D.Y.
- Irzhevskyi, D.O.
- Petrusenko, Y.T.
- Shkyryda, S.M.

NSCL
East Lansing, Michigan, USA
- Cole, D.G.
- Doleans, M.
- Hitchcock, S.
- Machicoane, G.
- Marti, F.
- Miller, P.S.
- Poe, D.R.
- Ropponen, T.
- Stetson, J.W.
- Sun, L.T.
- Wu, X.
- Yurkon, J.

PAC sprl
Dion Valmont, Belgium
- Conard, E.P.

PPRC
Tehran, Iran
- Saidi Bidokhti, P.

PSI-LRF
Villigen, PSI, Switzerland
- Amrein, B.
- Frey, P.
- Humbel, J.M.
- Kostezer, M.
- Schmidt, A.
- Steen, G.

PSI
Villigen, Switzerland
- Adelmann, A.
- Baumgarten, C.
- Bopp, M.
- Broennimann, M.
- Cherix, J.
- Dölling, R.
- Fitze, H.
- Humbel, J.M.
- Joho, W.
- Kiselev, D.C.
- Lüscher, R.
- Morath, O.
- Schippers, J.M.
- Schneider, M.
- Seidel, M.
- Stingelin, L.
- Tron, W.
- Wohlmuther, M.
- Zhang, H.

RCNP
Osaka, Japan
- Fukuda, M.
- Hatanaka, K.
- Kibayashi, M.
- Morinobu, S.
- Nagayama, K.
- Saito, T.
- Tamura, H.
- Yorita, T.

RIKEN Nishina Center
Wako, Japan
- Arai, S.
- Dantsuka, T.
- Fujimaki, M.
- Fujinawa, T.
- Fujisawa, H.
- Fukunishi, N.
- Goto, A.
- Hasebe, H.
- Hemmi, M.
- Higurashi, Y.
- Ikegami, K.
- Ikezawa, E.
- Imao, H.
- Kageyama, T.
- Kamigaito, O.
- Kase, M.
- Kidera, M.
- Komiyama, M.
- Koyama, R.
- Kuboki, H.
- Kumagai, K.
- Maie, T.
- Nagase, M.
- Nakagawa, T.
- Nakamura, M.
- Ohnishi, J.
- Okuno, H.
- Sakamoto, N.
- Suda, K.
- Watanabe, H.
- Watanabe, T.
- Watanabe, Y.
- Yamada, K.
- Yano, Y.
- Yokouchi, S.

SHI
Tokyo, Japan
- Fujita, K.
- Mitsumoto, T.
- Ogasawara, T.
- Tsutsui, H.
- Yajima, S.

SKKU
Suwon, Republic of Korea
- Chai, J.-S.
- Gad, Kh.M.
- Kim, H.W.
- Lee, B.N.
- Oh, J.H.
- Park, J.A.
- Song, H.S.

STFC/DL/ASTeC
Daresbury, Warrington, Cheshire, United Kingdom
- Smith, S.L.

Tehran University, Faculty of Medicine
Tehran, Iran
- Shirazi, A.

Texas A&M University Cyclotron Institute
College Station, Texas, USA
- May, D.P.
- Tribble, R.E.

Texas A&M University, Cyclotron Institute
College Station, USA
- Abegglen, F.P.
- Chubaryan, G.
- Derrig, G.J.
- Kim, G.J.
- Tabacaru, G.

TIT
Tokyo, Japan
- Oguri, Y.

TRIUMF, Canada's National Laboratory for Particle and Nuclear Physics
Vancouver, Canada
- Ames, F.
- Baartman, R.A.
- Bach, F.W.
- Bricault, P.G.
- Bylinskii, I.V.
- Cessford, J.F.
- Dombsky, M.
- Dutto, G.
- Fong, K.
- Gray, D.T.
- Hanemaayer, V.
- Hurst, A.
- Jayamanna, K.
- Koscielniak, S.R.
- Kunz, P.
- Lassen, J.
- Laverty, M.P.
- Laxdal, R.E.
- Mouat, M.
- Rao, Y.-N.
- Rawnsley, W.R.
- Root, L.W.
- Ruegg, R.
- Schmor, P.
- Verzilov, V.A.
- Zheng, Q.

Tsinghua University
Beijing, People's Republic of China
- Bi, Y.J.

TSL
Uppsala, Sweden
- Gajewski, K.J.
- Gålnander, B.
- Lundström, B.
- Pettersson, M.
- Prokofiev, A.V.
- van Rooyen, D.

TUB
Beijing, People's Republic of China
- He, X.
- Tang, C.-X.

UBC & TRIUMF
Vancouver, British Columbia, Canada
- Craddock, M.K.

UCR
Riverside, California, USA
- Snopok, P.

UniDo/IBS
Dortmund, Germany
- Böhme, C.

University of Fukui, Faculty of Engineering
Fukui, Japan
- Okabe, K.

University of Washington Medical Center
Seattle, USA
- Banerian, S.P.
- Douglas, J.G.
- Emery, R.C.

- Kalet, I.J.
- Laramore, G.E.
- Reid, D.D.
- Risler, R.

VINCA
Belgrade, Serbia
- Beličev, P.
- Dobrosavljević, A.S.
- Jocić, V.
- Nešković, N.
- Trajić, I.M.
- Vujović, V.
- Vukosavljević, Lj.

VMS-PT
Bergisch Gladbach, Germany
- Abdel-Bary, M.
- Akcoeltekin, E.M.
- Behrens, U.
- Budz, P.
- Röcken, H.
- Stephani, T.
- Wittschen, J.C.

Participants list

— A —

Andreas Adelmann
PSI
Switzerland

Hossein Afarideh
Amirkabir university of technology
Iran

Jose Alonso
MIT
USA

Dong Hyun An
KIRAMS
Korea

Shizhong An
CIAE
China

Timothy Antaya
MIT/PSFC
USA

— B —

William Beeckman
SIGMAPHI S.A.
France

Jason Beirne
Siemens
Germany

Patrick Bertrand
GANIL
France

Rakesh Kumar Bhandari
DAE/VECC
India

Oleg Borisov
JINR
Russia

Sytze Brandenburg
Kernfysisch Versneller Instituut
The Netherlands

Pierre Bricault
TRIUMF
Canada

Juergen Bundesmann
Helmholtz-Zentrum Berlin fuer Materialien und Energie
Germany

Iouri Bylinskii
TRIUMF
Canada

— C —

Xiaohong Cai
IMP
China

Luciano Calabretta
INFN-LNS
Italy

Yun Cao
IMP
China

Antonino Caruso
INFN-LNS
Italy

Luigi Celona
INFN/LNS
Italy

Jong seo Chai
SKKU
Korea

Anwar Chaudhri
GMX
Germany

Frederic Chautard
GANIL
France

Greg Chubaryan
Texas A&M University
USA

Jacobus Conradie
iThemba LABS
South Africa

Michael Craddock
TRIUMF
Canada

— D —

Carlo De Martinis
Universita' degli Studi di Milano & INFN
Italy

Andrea Denker
Helmholtz-Zentrum Berlin fuer Materialien und Energie
Germany

Malay Kanti Dey
DAE/VECC
India

Aleksandar Dobrosavljevic
Vinca Institute of Nuclear Sciences
Serbia

Rudolf Doelling
PSI
Switzerland

David Du
BCSI
Canada

Louis Dumez
GLD
France

Juergen Duppich
PSI
Switzerland

Gerardo Dutto
TRIUMF
Canada

— F —

Mingwu Fan
HUST
China

Yucheng Feng
IMP
China

Eric Forton
IBA
Belgium

Dennis Friesel
PartTec, Ltd.
USA

Mitsuhiro Fukuda
RCNP Osaka University
Japan

Toshimitsu Furuya
Kyocera Corporation
Japan

— G —

Daqing Gao
IMP
China

Gabriel Gaubert
PANTECHNIK
France

Ralf Gebel
FZJ
Germany

Mitra Ghergherehchi
Amirkabir university of technology
Iran

Akira Goto
RIKEN Nishina Center
Japan

Georgy Gulbekyan
JINR
Russia

Xiaohong Guo
IMP
China

— H —

Huanfeng Hao
IMP
China

Kichiji Hatanaka
RCNP Osaka University
Japan

Xiaozhong He
CAEP/IFP
China

Yuan He
IMP
China

Pauli Heikkinen
JYFL
Finland

Yasuo Hirao
NIRS
Japan

Satoru Hojo
NIRS
Japan

Zhengguo Hu
IMP
China

Martin Humbel
PSI
Switzerland

— J —

Vinder Jaggi
TRIUMF
Canada

Holger Jensen
Copenhagen University Hospital
Denmark

Carol Johnstone
Fermilab
USA

Yves Jongen
IBA
Belgium

In Su Jung
KIRAMS
Korea

— K —

Osamu Kamigaito
RIKEN Nishina Center
Japan

Mitsutaka Kanazawa
NIRS
Japan

Joonsun Kang
KIRAMS
Korea

Kun Uk Kang
KIRAMS
Korea

Galina Karamysheva
JINR
Russia

George Kim
Texas A&M University
USA

Hyun wook Kim
SKKU
Korea

Jong-Won Kim
Biomedical Engineering
Korea

Achim Kleinrahm
ZAG Zyklotron AG
Germany

Hannu Koivisto
JYFL
Germany

Richard Kriske
University of Minnesota
USA

Satoshi Kurashima
JAEA/TARRI
Japan

— L —

Arnaud Lancelot
SIGMAPHI S.A.
France

Jean-Luc Lancelot
SIGMAPHI S.A.
France

Robert Laxdal
TRIUMF
Canada

Byung No Lee
SKKU
Korea

Jinyu Li
IMP
China

Peng Li
IMP
China

Xiaoni Li
IMP
China

Zhenguo Li
CIAE
China

Qiang Liang
IMP
China

Marc Loiselet
UCL
Belgium

Claude Lyneis
LBNL
USA

— M —

Hongyi Ma
IMP
China

Lizhen Ma
IMP
China

Xinwen Ma
IMP
China

Guillaume Machicoane
MSU
USA

Chaturanan Mallik
DAE/VECC
India

Abdel-Bary Mamdouh
VMS-PT
Germany

Lijun Mao
IMP
China

Ruishi Mao
IMP
China

Felix Marti
MSU
USA

Donald May
Twxas A&M University
USA

Luis Medeiros-Romao
IBA
Belgium

Mamdouh Mohamed
Abdel-Bary Dewidar
VMS-PT
Germany

Yoshiharu Mori
Kyoto University
Japan

Akihiro Morita
Sumitomo Heavy Industries, Ltd.
Japan

Nikolay Morozov
JINR
Russia

— N —

Takahide Nakagawa
RIKEN Nishina Center
Japan

Vincent Nuttens
IBA
Belgium

— O —

Jin Hwan Oh
SKKU
Korea

Junichi Ohashi
Thamway Co.Ltd
Japan

— P —

Emma Pearson
IBA
Belgium

Leandro Piazza
INFN-LNL
Italy

Edward Pozdeyev
BNL
USA

— Q —

Bin Qin
Kyoto University
Japan

— R —

Yinong Rao
TRIUMF
Canada

Rudolf Risler
University of Washington
USA

Heinrich Röcken
VMS-PT
Germany

— S —

Vasile Sabaiduc
BCSI
Canada

Naruhiko Sakamoto
RIKEN Nishina Center
Japan

Evgeny Samsonov
JINR
Russia

Asushi Sasagawa
Kyocera Corporation
Japan

Alain Savalle
GANIL
France

Jacobus Maarten Schippers
PSI
Switzerland

Paul Schmor
TRIUMF
Canada

Hermann Schweickert
ZAG Zyklotron AG
Germany

Mike Seidel
PSI
Switzerland

Zhandos Seksembayev
Eurasian national
University
Kazakhstan

Thomas Servais
IBA
Belgium

Andrew Sessler
LBNL
USA

Yong Shang
IMP
China

Jingbin Shangguan
IMP
China

Vladimir Shevtsov
JINR
Russia

Aimin Shi
IMP
China

Sergii Shkyryda
NSC/KIPT
Ukraine

Susan Louise Smith
STFC/DL/ASTeC
UK

Fenyuan Song
Kyocera Corporation
Japan

Ho-seung Song
SKKU
Korea

Mingtao Song
IMP
China

Thomas Stephani
VMS-PT
Germany

Jeffry Stetson
MSU
USA

Lukas Stingelin
PSI
Switzerland

Kenji Suda
RIKEN Nishina Center
Japan

— T —

Ken Takayama
KEK
Japan

Isao Tanihata
RCNP Osaka Univ
Japan

Shuji Tatsumi
Sumitomo Heavy Industries,
Ltd.
Japan

Sajjan Thakur
DAE/VECC
India

Ville Toivanen
JYFL
Finland

Hiroshi Tsutsui
Sumitomo Heavy Industries,
Ltd.
Japan

— V —

Daniel van Rooyen
TSL
Sweden

Antonio Villari
PANTECHNIK
France

— W —

Bin Wang
Chang Feng B&C
China

Bing Wang
IMP
China

Jinchuan Wang
IMP
China

Xianwu Wang
IMP
China

Zihua Wang
IBA
Belgium

Nobuhiro Watanabe
Kyocera Corporation
Japan

Tamaki Watanabe
RIKEN Nishina Center
Japan

Shidong Wei
Chang Feng B&C
China

Adam WenLei
Sigmaphi China
China

Jürgen Christian Wittschen
VMS-PT
Germany

Junxia Wu
IMP
China

Xiaoyu Wu
MSU
USA

— X —

Jiawen Xia
IMP
China

Guoqing Xiao
IMP
China

Daniel Xie
IMP
China

Hushan Xu
IMP
China

Zhe Xu
IMP
China

— Y —

Kazunari Yamada
RIKEN Nishina Center
Japan

Huaihai Yan
IMP
China

Jiancheng Yang
IMP
China

Xiaodong Yang
IMP
China

Xiaotian Yang
IMP
China

Xiaotian Yang
IMP
China

Yipping Yang
IMP
China

Yasushige Yano
RIKEN Nishina Center
Japan

Qinggao Yao
IMP
China

Zhiguo Yin
CIAE
China

Tetsuhiko Yorita
Osaka University
Japan

Ken Yoshiki Franzen
LBNL
USA

Youjin Yuan
IMP
China

Takahiro Yuyama
JAEA/TARRI
Japan

— Z —

Simon Zaremba
IBA
Belgium

Albert Zeller
MSU
USA

Wenlong Zhan
IMP
China

Hui Zhang
PSI
Switzerland

Jiexi Zhang
MIT/PSFC
USA

Jingquan Zhang
IMP
China

Junhui Zhang
IMP
China

Kaizhi Zhang
CAEP/IFP
China

Shenghu Zhang
IMP
China

Tianjue Zhang
CIAE
China

Wei Zhang
IMP
China

Xiaoqi Zhang
IMP
China

Xuezhen Zhang
IMP
China

Hongwei Zhao
IMP
China

Huanyu Zhao
IMP
China

Jianhua Zheng
IMP
China

Qiwen Zheng
TRIUMF
Canada

Tong Zhou
SKKU
Korea

Zhongzu Zhou
IMP
China